

INTERNATIONAL SYMPOSIUM ON GIS APPLICATIONS IN GEOGRAPHY & GEOSCIENCES



PROCEEDING BOOK

18 - 21 October, 2017

Canakkale, Turkey

EDITORS

**Suha Ozden, Cengiz Akbulak, R. Cüneyt Erenoglu,
Oznur Karaca, Faize Saris and Mustafa Avcioğlu**



**INTERNATIONAL SYMPOSIUM ON GIS APPLICATIONS
IN GEOGRAPHY & GEOSCIENCES**

Editors

Süha ÖZDEN, Department of Geological Engineering, COMU

Cengiz AKBULAK, Department of Geography, COMU

R. Cüneyt ERENOĞLU, Department of Geomatics Engineering, COMU

Öznur KARACA, Department of Geological Engineering, COMU

Faize SARIŞ, Department of Geography, COMU

Mustafa AVCIOĞLU, Department of Geological Engineering, COMU

Published with support of:

Çanakkale Onsekiz Mart University

Published date: December 2017

Web Site: <http://isggg2017.comu.edu.tr>

ISBN : 978-605-4222-54-4



COMMITTEES

Honorary Chair

Prof. Dr. Yücel ACER, Rector of Çanakkale Onsekiz Mart University

Executive committee

Süha ÖZDEN, Co-Chair, Çanakkale Onsekiz Mart University
Cengiz AKBULAK, Co-Chair, Çanakkale Onsekiz Mart University
Hasan ÖZDEMİR, İstanbul University
Tolga GÖRÜM, İstanbul University
Öznur KARACA, Çanakkale Onsekiz Mart University
R. Cüneyt ERENOĞLU, Çanakkale Onsekiz Mart University
Faize SARİŞ, Çanakkale Onsekiz Mart University
Mustafa AVCIOĞLU, Çanakkale Onsekiz Mart University

Organizing Committee

Süha ÖZDEN, Çanakkale Onsekiz Mart University
Cengiz AKBULAK, Çanakkale Onsekiz Mart University
Nebiye MUSAĞLU, İstanbul Technical University
Levent GENÇ, Çanakkale Onsekiz Mart University
Kaan Şevki KAVAK, Cumhuriyet University
Hasan ÖZDEMİR, İstanbul University
R. Cüneyt ERENOĞLU, Çanakkale Onsekiz Mart University
Tolga GÖRÜM, İstanbul University
Öznur KARACA, Çanakkale Onsekiz Mart University
Faize SARİŞ, Çanakkale Onsekiz Mart University
Salem KHALAF, Çanakkale Onsekiz Mart University
Zahide ACAR DENİZ, Çanakkale Onsekiz Mart University
Canan Zehra ÇAVUŞ, Çanakkale Onsekiz Mart University
Mustafa AVCIOĞLU, Çanakkale Onsekiz Mart University

Scientific Committee

Zahide ACAR DENİZ, Çanakkale Onsekiz Mart University, Turkey
Cengiz AKBULAK, Çanakkale Onsekiz Mart University, Turkey
Özgün AKÇAY, Çanakkale Onsekiz Mart University, Turkey
Ertuğrul AKSOY, Uludağ University, Turkey
Gustavo A.M. de ALMEIDA, Southampton University, UK
Niyazi ARSLAN, Çukurova University, Turkey.
Nurettin ARSLAN, Çanakkale Onsekiz Mart University, Turkey
Mustafa AVCIOĞLU, Çanakkale Onsekiz Mart University, Turkey
E. Özgür AVŞAR, Çanakkale Onsekiz Mart University, Turkey
Fusun BALIK ŞANLI, Yıldız Technical University, Turkey
Constanza BANADONNA, University of Geneva, Switzerland
Arzu BAŞARAN UYSAL, Çanakkale Onsekiz Mart University, Turkey
A.Melih BAŞARANER, Yıldız Technical University, Turkey
Paul BATES, Bristol University, UK
Cihan BAYRAKDAR, İstanbul University, Turkey
Martin BEDNARIK, Comenius University in Bratislava, Slovakia
Tolga BEKLER, Çanakkale Onsekiz Mart University, Turkey
Süha BERBEROĞLU, Çukurova University, Turkey
Deanne BIRD, University of Iceland, Australia
Fabiana CALÒ, National Research Council (CNR) of Italy, Italy
Tülay CENGİZ TAŞLI, Çanakkale Onsekiz Mart University, Turkey
Canan Zehra ÇAVUŞ, Çanakkale Onsekiz Mart University
M. Ali ÇULLU, Harran University, Turkey
Mehmet Fatih DÖKER, Sakarya University, Turkey
Aşlı DOĞRU, Boğaziçi University, Turkey
Marian DRUSA, University of Zilina, Slovakia
Oya ERENOĞLU, Çanakkale Onsekiz Mart University, Turkey

R. Cüneyt ERENOĞLU, Çanakkale Onsekiz Mart University, Turkey
Aksel ERSOY, Oxford Brookes University, UK
Cem GAZİOĞLU, İstanbul University, Turkey
Levent GENÇ, Çanakkale Onsekiz Mart University, Turkey
Tolga GÖRÜM, İstanbul University, Turkey
Erdem GÜNDOĞDU, Çanakkale Onsekiz Mart University, Turkey
Muhammet KAÇMAZ, Sakarya University, Turkey
Öznur KARACA, Çanakkale Onsekiz Mart University, Turkey
Kaan Şevki KAVAK, Cumhuriyet University, Turkey
Şinasi KAYA, İstanbul Technical University, Turkey
Cem KINCAL, Dokuz Eylül University, Turkey
Özlem KOCAHAN YILMAZ, Namık Kemal University, Turkey
Tolga KOMUT, Çanakkale Onsekiz Mart University, Turkey
Ahmed M. KOTB, Al Azhar University, Egypt
Hansjörg KUTTERER, Federal Agency for Cartography and Geodesy, Germany
Plamen MALDJANSKI, University of Architecture, Civil Engineering and Geodesy, Bulgaria
Georgi MILEV, Bulgarian Academy of Sciences, Bulgaria
Nebiye MUSAOĞLU, İstanbul Technical University, Turkey
M. Kirami ÖLGEN, Ege University, Turkey
Hasan ÖZCAN, Çanakkale Onsekiz Mart University, Turkey
Hasan ÖZDEMİR, İstanbul University, Turkey
Süha ÖZDEN, Çanakkale Onsekiz Mart University, Turkey
Haluk ÖZENER, Boğaziçi University, Turkey
Muhammet Zeynel ÖZTÜRK, Ömer Halisdemir University, Turkey
Elena PENEVA, University of Architecture, Civil Engineering and Geodesy, Bulgaria
Khamarrul Azahari RAZAK, Universiti Teknologi, Malaysia
Bülent SAĞLAM, Artvin Çoruh University, Turkey
Faize SARİŞ, Çanakkale Onsekiz Mart University
Guy SCHUMANN, Bristol University, UK
Dursun Zafer ŞEKER, İstanbul Technical University, Turkey
Şermin TAĞIL, Balıkesir University, Turkey
Orhan TATAR, Cumhuriyet University, Turkey
Mohamed Magdy TORAB, Damanhour University, Egypt
Hüseyin TUROĞLU, İstanbul University, Turkey
Tarık TÜRK, Cumhuriyet University, Turkey
Aylin YAMAN KOCADAĞLI, İstanbul University, Turkey
Cengiz YILDIRIM, İstanbul Technical University, Turkey
Tahsin YOMRALIOĞLU, İstanbul Technical University, Turkey
İsmail YOUSSEF İSMAİL, Menofia University, Egypt
Mehmet Ali YÜCEL, Çanakkale Onsekiz Mart University, Turkey

PREFACE

The International Symposium on GIS Applications in Geography and Geosciences (ISGGG) was held in Çanakkale Onsekiz Mart University during 18-21 October 2017. The symposium brought together various researchers in different fields and enabled participants to share and discuss their ideas and research results.

Approximately 270 people attended to the symposium, which organized as keynote lectures, oral and poster presentations and also "UAV for GIS" certificate program.

There were five keynote lectures covering the different areas of the symposium: Prof. Dr. Paul Bates (University of Bristol, UK) talked on "*Using GIS to Build Global Flood Hazard Models*", Prof. Dr. Tahsin Yomralıoğlu (Istanbul Technical University, Turkey) on "*Geographical Information Paradigm*", Prof. Dr. Magdy Torab (Damanhour University, Egypt) on "*Some Applications in The Usage of GIS in Geoearchaeological Researches*", Prof. Dr. Haluk Özener (Bogazici University, Turkey) on "*Earthquake and Tsunami Information System at KOERI*" and Dr. Fabiana Calò (National Research Council of Italy, Italy) on "*SAR-based Remote Sensing for Natural Hazards Analysis*".

This book contains the full papers those submitted by their authors following the symposium. Papers were organized according to the symposium topics. The editorial board checked only the format of the papers and necessary arrangements have been made. Therefore, authors have complete responsibility for the content of the papers.

We would like to thank all the contributors and attendees. We were honored by your support and participation to the ISGGG 2017.

ISGGG
2017

Editorial Board

Contents

Presentation Title	Page No
AGRICULTURE AND FORESTRY	1
Evaluation of Different GPS Types On Forest Road Network In Turkey	2
Use of GIS For Timber Extraction Systems: A Case Study	9
Use of GIS to Evaluate the Organochlorine Pesticide Accumulations in Soil of Seydisuyu Plain (Eskişehir, Turkey)	15
ARCHAEOLOGY	20
Photogrammetrical Applications and GIS Analyses of Ancient Agricultural Terraces in Bozburun Peninsula	21
Determination of Potential Clay Beds with GIS Based Approach In the Kerküşti Höyük and Its Vicinity	33
ENVIRONMENTAL MANAGEMENT	42
Conservation of wetland based on ecological sensitivity analysis: A case study of Kızılırmak Delta	43
Study of the coastal wave energy propagation using GIS and hydrodynamic model	55
Mapping of arsenic and boron pollution in the intense mining catchment of Mustafakemalpaşa stream - Northwestern Turkey	64
GEOLOGY, GEOPHYSICS AND GEOMORPHOLOGY	74
A Research for the Characterization of Coastal Sands in East Mediterranean (Between Samandağı and Narlıkuyu) and TRNC by ArcGIS	75
Imaging of Spectral Properties of Opal Mineral using Sensor Data, Yenice District, North-Western Turkey	85
Relationship Investigation Between Roughness and Temperature Of Rock Surfaces	97
Discrimination and Classification of the Rock-type with Multispectral Sensing	104
Comparison of Surface Morphology determined with Terrestrial LIDAR Method and Underground Geometry determined with GPR: Kamara (Denizli/Turkey) Fissure Ridge-type Travertine	111
Determination of Fault Types by GIS Applications according to Earthquake Depths	122
Modeling of Soil Parameters Obtained by Geophysical Methods Using GIS: A case Study in Trabzon	128
Planar failure determination of the slopes along the Bağarası-Foca state highway with the help of Geographical Information Systems	135
Crustal Structure of Golbasi-Celikhan Segment, Eastern Anatolia, Turkey	146
Crustal Structure and Geothermal Exploration in Western Anatolia of Turkey using Local Earthquake Tomography	150

GEOMATICS	154
Comparing the Performance of Reverse Geocoding Services: Google and Bing Maps	155
An Application Development for Use of Borehole Data on iOS Based Mobile Devices	162
Investigating The Accuracy Analysis of Single Baseline RTK	171
Evaluations on Digital Elevation Model Generation by Using Airborne LIDAR Technique in West of Turkey	182
Analysis on the Quality of High-Resolution Global Digital Terrain Models (DTM) using GPS/leveling Data in Turkey	192
Modelling Land Registry and Cadastre Transactions with UML: A Case of Turkey	202
Strip Adjustment of Mobile Mapping Point Clouds: Case Study in Istanbul Technical University (ITU) Ayazaga Campus	209
GIS & Three-Dimensional Modelling for Cultural Heritages	219
The Distribution of the total Scale Factor in Large Scale Mapping in Turkey by Map Projection and Topography	229
Validation of Bernese-Derived Precise Orbits for GRACE Satellites	235
Python GIS Application and SQL Usage	244
GNSS	247
Investigation of The Relationships of Discrete Wavelet Transform Components in GNSS Time Series	248
Description of Behaviors of GNSS Stations By Signal Processing Methods in Konya Closed Basin	259
Multipath Mitigation Using The Bandpass Filter Technique For GPS Applications	272
The Impact Of Different GPS/GNSS Parameters On Landslide Monitoring	283
Evaluation of The Height Accuracy of Some Levelling Techniques	292
Estimation of Crustal Deformations in Marmara Region Using Continuous GNSS Stations' Observations	304
HUMAN GEOGRAPHY	312
Determination of Trekking Routes in Gökçeada (Imbros) with GIS	313
The Assessment of Subjective Well-Being Map Of Turkey	323
Overcapacity of Lower-Level Municipalities In Metropolitan Region: Case Of Bağcılar	333
HYDROLOGY	342
Evaluation of the trace-element in Goksu Delta Using GIS techniques	343
Flood Inundation Mapping for Tathçay (Çankırı)	349
Performance Analyses With LiDAR Data in Flood Modelling Using Remote Sensing and GIS in Artvin City	355
TERKOS-Canal İstanbul Saltwater Intrusion Using Hybrid Geographic Information System-Analytical Solution	365

LAND USE	377
Assessment And Mapping of Spatial Variation of Soil Quality Around The Gulf of Edremit, Turkey	378
A Case Study on Comparison of the Classifiers provided by Google Earth Engine for Land Cover Identification	390
Investigation of Normalized Difference Vegetation Index and Land Surface Temperature Using Remote Sensing Techniques for 20 years of Diyarbakir Province	402
Designing Land Administration Data Infrastructure Supporting the Interoperability between Applications: Land Valuation Example for Turkey	409
Identification of Future Land-Use Conflict and Landscape Pattern in Denizli, Turkey	419
Preparation of Preliminary Survey Report with GIS in Land Consolidation Projects	430
A Study on Determination of Optimum Parcel Size in Land Consolidation	439
METEOROLOGY AND CLIMATOLOGY	444
Trend Analysis Of The Zenith Tropospheric Delay (ZTD) Time Series	445
Comparison of Areal Precipitation Estimation Methods in Akarcay Basin, Turkey	456
Evaluating the impact of agricultural drought using MODIS sensor: A Case of Study over the Aegean Region	467
Temperature extremes in summer and winter seasons over the Mediterranean Coastlines of Turkey	475
NATURAL HAZARDS AND MANAGMENT	487
Development of GIS-based Building Management Model for Natural Disasters	488
Monitoring Natural Disasters Using Geographical Information Systems: A Case Study of Kayseri	496
Applying GIS and Multi Criteria Evaluation in Forest Fire Risk in Bakırçay Basin	502
UAV-assisted Landslide Activity Monitoring: Applications and Open Issues	514
An Assessment of Disaster Management from the Viewpoint of Geographical Information System	523
REMOTE SENSING	531
Biodiversity Mapping Using Landscape Complexity and Bird Species as Indicators by Remote Sensing and GIS	532
Comparison of PCA and NLPCA Methods for Band Reduction of Hyperspectral Images	539
Texture Based Classification of Hyperspectral Images with Support Vector Machines Classifier	548
Assessment of Transparency and Water Quality in the Bay of Bou-Ismaïl from Landsat Satellite Imagery	558
Wetland Mapping Using Sentinel-1 SAR Data	570
SPATIAL ANALYSIS	579
Modeling of Urban Transportation Network by Linear Programming	580
Site Selection of Solid Waste Landfill Using Geographical Information System: A Case Study for Artvin City Center	588

A GIS-Based Landfill Site Selection Approach Using Spatial Multi-Criteria Decision Making Methods	599
Design and Development of an Spatial Advertisement Tax System	607
Determining Parameters Affecting Residential Real Estate Value and Their Significance Level Using AHP Method: The Case of Artvin	618
Spatial Analyses of Accessibility of Urban Transportation Network for Istanbul	630
URBAN AND REGIONAL PLANNING	638
Analysis of Landscape Changes for a Sustainable Urban Decision Making	639
Development of a New Silhouette Analysis Tool for Urban Planning Applications	647
Recognising Building Patterns in Topographic Maps with HDBSCAN Clustering Algorithm	658
An Overview of Mobile LIDAR Systems and Their Usability in Corridor Mapping Studies	668
Use of GIS in Some Issues of Landscape Planning	677
Use of SENTINEL-1 Data in Oil Spill Surveillance and Modeling	686





AGRICULTURE AND FORESTRY

Evaluation of Different GPS Types on Forest Road Network in Turkey

Erhan Çalışkan¹

¹Department of Forest Engineering, Faculty of Forestry, Karadeniz Technical University, 61080, Trabzon-Turkey, E-mail: erhan_caliskan@yahoo.com

ABSTRACT

Forest roads are essential for forest management by providing corridors for transportation, haul routes for forest products, access for recreation and education, and infrastructure for fire protection. In the past two decades, surveying procedures improved in term of speed, accuracy and simplicity mostly due to use of computers and technical development in general. The aim of this study was to assess accuracy of different GPS - types and their range of application with emphasis the examination of its suitability for forest road surveys. For this purpose, Çaykara (Trabzon-Turkey) district forest road network, three different locations were selected with three completely different terrain configurations. At each location, 220 meters of a forest road were measured and from these measurements the site plan and the longitudinal profile for the measured road section were obtained. The measurements were performed using four different instruments: of handheld GPS, DGPS, CORS and Total Station devices. We want to compare the accuracy between different geodetic techniques on various terrains and to examine the rationality of the use of different surveying methods. The data obtained by the GPS device analysis accuracy by comparing with the data obtained was performed with a total station instrument. Finally the measurements accuracy with GPS in the reference to the forest road was calculated, the suitable results were brought and the relative suggestions for its indicated forest application in Turkey.

INTRODUCTION

Forest roads are among the most important infrastructure facilities for forestry operations which are also renewable natural resources. Forestry operations are forest road design and slope stability, analysis of harvesting systems for economic efficiency and site protection, and planning and scheduling of harvests and transportation systems.

Global positioning system (GPS) receivers are frequently useful for engineering activities in the forest environment and for forest inventory and road inventory (Evans et al. 1992 and Abdi et al. 2012 and Kosmos et al. 2007), topography and cadastral forest surveys (Soler et al. 1996, Yoshimura et al. 2002), geographic information system (GIS) forest applications (Wing and Bettinger 2003), resource and spatial area management (Wing & Kollegg 2004), and forest area and perimeter estimation (Tachiki et al. 2005).

Global Positioning System (GPS) technology is now widely used for navigation and surveying. GPS is also essential for supporting logistics in forestry. Despite removal of Selective Availability (SA) in May 2000, there is the error in GPS positioning without a differential GPS is 10-20 m (Tsuchiya and Tsuji 2001). which could be temporally larger due to signal degradation and multipath.

It is well known that forest canopy adversely affects GPS positional accuracy due to signal attenuation when GPS is used inside forests. Many studies have been conducted to determine the performance of GPS positional accuracy under different canopy conditions. Mori and Takeda (2000) showed the effects of SA removal on positional accuracy of the DGPS. Kobayashi et al. (2001) evaluated five GPS receivers' performance by comparing the positional accuracy of the autonomous GPS, real-time DGPS and carrier phase GPS.

Using known methods of surveying and photogrammetry requires time and money, while satellite ones give a general geographic information, while they have not confirmed a good accuracy. The use of different types of GPS from a relatively low cost (GPS handheld) to more expensive differential DGPS (two receivers and one, two or three frequencies) leads to sufficient accuracy to capture a few meters to a few centimeters. There are techniques as differential global positioning system (DGPS) that improve precision and accuracy under tree canopies. Hasegawa and Yoshimura (2003) achieved a mean error of a 1 to 30-min observation varied between 0.029-0.226 m (without closed tree canopies) and it was 0.415-0.894 m (with closed tree canopies), using Dual-frequency GPS receivers by carrier phase DGPS static surveying. Sawaguchi and others (2003) using DGPS got mean CEP95=2.80 m for deciduous broadleaved trees and 4.99 m for conifers. Erdem,(2011) DGPS CORS type GPS is the most accurate one for allthree habitat types. It was most accurate in open habitat as the error margin in dense foliage was 3,41 m in horizontal and 3,88 m in vertical; 0,06 m in horizontal and 0,05 m in vertical for open habitat; 0,62 m in horizontal and 1,16 m in vertical for timber line habitat.

The objective of this study is an attempt to examine and compare the performance of different GPS receivers at three different locations of forest road network in Trabzon(Çaykara) forest region of Turkey.

MATERIALS AND METHODS

Study area

Trabzon Province(Çaykara) is situated between longitude $39^{\circ} 30''$ and $40^{\circ} 30'$ E and latitude $40^{\circ} 30'$ to $41^{\circ} 7'$ N in the middle of the east Black Sea region of Turkey.

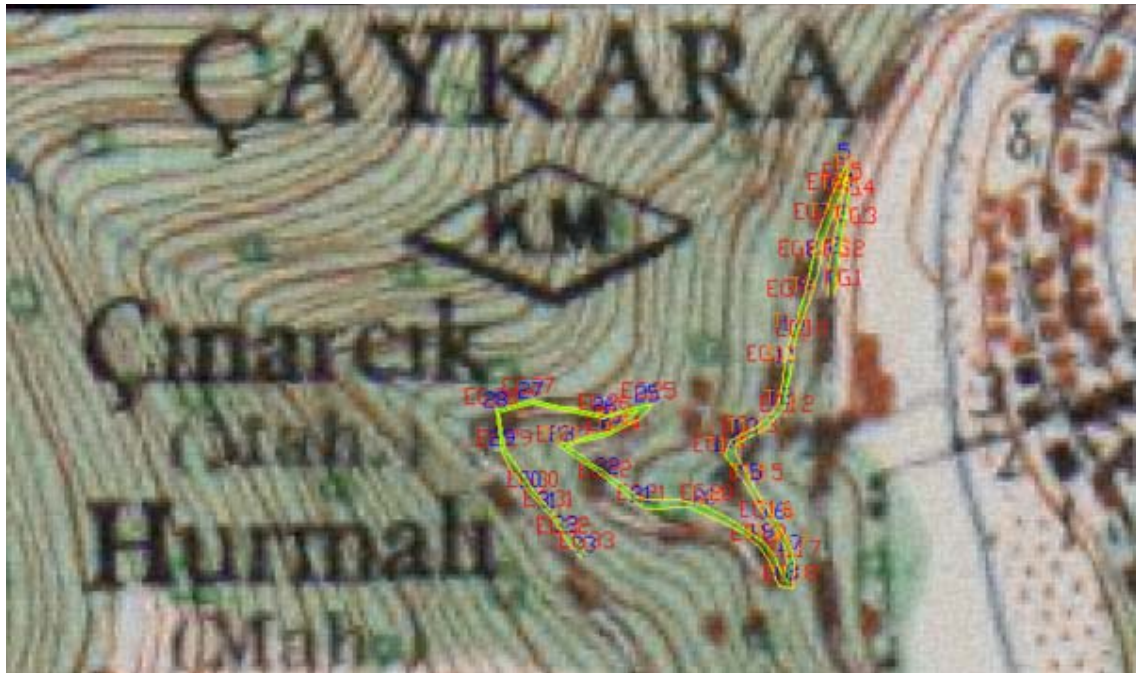
The study area were forest road on three different locations. At each location section 220 m long of forest road was chosen as a research object with intersections 20 m. Measurements for the field test were taken at the eleven positional points. The first location is an open flat field. It is without any disturbing elements like hills, forests, villages. The second location is a forest road which provides access to the forest. The road has many curves and steep longitudinal inclination. The surrounding area is completely overgrown with mixed forest, tree canopies forest road. The third location is a forest road located in the valley.



Figure 1. Satellite view of study area (1:5000)

We tested the usefulness of four different methods of recording situations, and three locations:

- ✓ Garmin GPS Map 76 Csx handheld GPS ,
- ✓ Topcon GMS-2 DGPS
- ✓ Trimble PGA-1 DGPS (CORS)
- ✓ Total Station devices (Pantex W-823NX)



Method

During field trials, care was taken to ensure that all measurements were made simultaneously, in the sense that the satellite distributions were in the same conditions. During the measurements performed with 4 different devices, it is set up in succession on the point to keep all variables as same as possible and it is aimed to decrease the time between measurements to the minimum.

Topcon Link program, which is the data transfer and post- processing software that this company produced for Topcon brand devices, was used to transfer the obtained data to the computer environment. The data obtained with the Garmin handheld GPS receiver is transferred to the computer environment using Map Source software. Transformations of the data transferred to the computer environment were made using Topcon Link, ArcGIS and NetCAD software.

RESULTS AND DISCUSSION

Radiation measurements were first performed on the points installed in the field by means

of the total station device. Static measurements were performed with CORS-compliant DGPS receivers at selected two points before each station was measured with a total station device. This measurement data is transferred to the total station device and used as reference point coordinates in the measurements.

The parametric transformations of the obtained data were first performed and transformations were made to the UTM European Datum 1950 Zone 39 coordinate system in line with the parameters used in our country.

The "RMSE - Root Mean Square Error" quantities were calculated with reference to the coordinates measured with the total station device of each point to determine the error amounts of the point data obtained in the field studies.

Quadratic Mean Error amounts for each point are calculated. The RMS error is the difference between the desired output coordinates and the actual coordinates of the control point when transformed by a point transformation matrix and is calculated by the following formula;

$$RMSE = \sqrt{(xr - xi)^2 + (yr - yi)^2}$$

xr = Total station with measured x coordinates

xi = GPS device with measured x coordinates

yr = Total station with measured coordinates

yi = GPS device with measured y coordinates

Table 1. Accuracy of the GPS – types by the forest road network

	Location 1 RMSE(m)	Location2 RMSE(m)	Location 3 RMSE(m)
GPS handheld	3.5	4.60	9.69
DGPS	2.5	4.10	7.87
CORS	0.06	0.74	3.89

Location 1, according to the measurements made;

With CORS receiver system, RMSE values of 0,06 m, DGPS receiver system with 2,50 m and handheld GPS receiver system with 3,56 m have been reached.

Location 2, according to the measurements made;

With CORS receiver system, RMSE values of 0,74 m, DGPS receiver system with 4,10 m and handheld GPS receiver system with 4,60 m have been reached.

Location 3, according to the measurements made;

With CORS receiver system, RMSE values of 3,89 m, DGPS receiver system with 7,87 m and handheld GPS receiver system with 9,69 m have been reached.

In total, this study was carried out in a forest road network of 660 m. Measurements were made every 20 m.

As a result of the planning, working hours were determined as 8.00-13.00. At these times, the number of satellites was at least 6, mostly 7, and a total of 13 different satellites were used. The PDOP and GDOP values ranged from 2 to 3, which are desirable features for good GPS measurement (Seeber, 1993; Wells, 1986; Domingue, 1993).

According to these results, it is considered appropriate to use a hand-held GPS receiver in studies such as the creation of wildlife life maps that do not require high sensitivity in forest areas and the determination of fire border lines. It is thought that the choice of DGPS and CORS systems will be economical from the point of view of accuracy and time when studies such as determination of the locations of the forested construction structures requiring high accuracy, determining the boundaries of the site area, and making forest road applications are considered.

ACKNOWLEDGMENT

I would like to thank the IV class students Abdullah Ergün and Mustafa Şahin. Due to the contribution of the field work, KTU Forest Faculty, Department of Forestry Engineering.

REFERENCES

- Abdi, E., Sisakht, R., Goushbor, L., Soufi, H., 2012. Accuracy assessment of GPS and surveying technique in forest road mapping. *Ann. For. Res.* 55(2): 309-317, 2012.
- Domingue, J. 1993. Measuring Silvicultural Operations with a Global Positioning System, Minister of Supply and Services Canada, Project, Quebec.
- Erdem, R., 2011. *Orman Mühendisliğinde GPS (küresel yer belirleme sistemi) Ölçmeleri*, Yüksek Lisans tezi, s.97 .İstanbul.
- Evans D., Carraway R., Simmons G., 1992. Use of global positioning system (GPS) for forest plot location. *Southern Journal Applied Forestry* 16(2), 67-70.
- Mori, A. & Takeda, H. 2000. The effects of released S/A on accuracy of DGPS surveying inside the forest (in Japanese with English summary). *Journal of Japanese Forestry Society* Vol 82: 393–396.
- Kosmas A.G. Vasileios J. G, Anastasia S. 2007. The applicability of different gps - types with the survey of forest road networks in Greece. FORMEC'07: Meeting the Needs of Tomorrows' Forests – New Developments in Forest Engineering, October 7 – 11, 2007, Vienna and Heiligenkreuz – Austria
- Kobayashi, H., Yada, Y., Chachin, T., Okano, K., Nogami, Y. & Torimoto, H. 2001. Evaluation of GPS receivers' performance inside and outside forests (in Japanese with English summary). *Journal of Japanese Forestry Society*, 83: 135-142.
- Tachiki Y., Yoshimura T., Hasegawa H., Mita T., Sakai T., Nakamura F., 2005. Effects of polyline simplification of dynamic GPS data under forest canopy on area and perimeter estimations. *Journal of Forest Research* 10(6): 419-427.

- Tsuchiya, J. and Tsuji, H. (2001) *New plain GPS surveying* (in Japanese), 449 pp, Japanese Association of Surveyors, Tokyo (in Japanese).
- Sawaguchi, I., Nishida, K., Shishiuchi, M., and Tatsukawa, S. 2003. Positioning precision and sampling number of DGPS under forest canopies. *Journal of Forest Research* 8, 133–137.
- Seeber. G. 1993. *Satellite Geodesy : Foundations, methods, and applications*, Walter de Gruyter Berlin; New York ;USA
- Wells. D. 1986. Guide to GPS Positioning, Canadian GPS Associates, CANADA
- Wing M.G., Ettinger P., 2003. GIS: An updated primer on a powerful management tool. *Journal of Forest Research* 101(4): 4-8.
- Wing M.G., Kellogg L.D., 2004. Locating and mobile mapping techniques for forest applications. *Geographical Informormation Science* 11(1): 87-95.
- Yoshimura T., Gandaseca S., Gumus S., Acar H., 2002. Evaluating the accuracy of GPS positioning in the forest of the Macka region. *2nd National black sea forestry Congress*, Turkey, Artvin, pp. 62-69.
- Yoshimura, T. and Hasegawa, H. (2003): Comparing the precision and accuracy of GPS positioning in forested areas. *Journal of Forest Research* 8, 147–152.



Use of GIS for Timber Extraction Systems: A Case Study

Erhan Çalışkan¹

¹Department of Forest Engineering, Faculty of Forestry, Karadeniz Technical University, 61080, Trabzon-Turkey, E-mail: erhan_caliskan@yahoo.com

ABSTRACT

Forestry operations in Turkey are carried out at different parts of the country under different conditions. Only the best forest road networks can provide conditions for working in wide, scattered and difficult mountainous areas. The forest areas found in mountainous lands with harsh slopes in Turkey makes timber extraction systems more problematic and more complex. The aim of this study was to determine timber extraction system using Geographical Information Systems (GIS) Trabzon Regional Directorate of Forestry in Turkey. In the work done for this, it has been decided that the most suitable method of extraction by taking into account the slope, the distance of skidding, the age of the stands, development stage, canopy and the direction of extraction. Before deciding on extraction methods, the roads on the land were planned to be built in places that were drawn and inadequate using satellite imagery in the GIS program. It is planned to have a maximum slope of 12% in the planning of new roads. Our total area is 6003 ha. The general road density is 18 m / ha, the actual road density is 19 m/ha and the opening ratio is 83%. During the removal process, new systems with low cost can be developed by taking advantage of technological improvements so that youth and forest are not damaged.

INTRODUCTION

Turkey has 22.7 million ha of naturally managed forest area making up for 27% of its total. Approximately 46% of the total area is on steep land with slopes greater than 40%. Hence, harvesting in mountainous regions has always played a significant role. (GDF, 2013). Forestry operations in Turkey are carried out at different parts of the country under different conditions. Only the best forest road networks can provide conditions for working in wide, scattered and difficult mountainous areas. Approximately 18 million m³ logs are transported via forest roads in Turkey, each year. Previous studies developed forest road networks via manual methods, while in the last few years computer software and hardware have been used extensively and effectively for solving complex problems in forest areas, especially in developed countries (Akay 2003; Rogers 2005; Demir 2007). Today, concepts such as digital map, GIS and land information systems have gained importance in the design of road networks (Akay, 2003; Aruga, 2005; Gümüş, 2008; Çalışkan, 2013).

Most of the research today is based on strategic and tactical level of planning timber harvesting and forest opening (Bumber 2011, Eichrodt and Heinimann 2001, Enache 2013, Enache et al. 2013, Lepoglavec 2014, Lubello 2008, Kühmaier and Stampfer 2010)

The aim of this study was to determine timber extraction system using Geographical Information Systems (GIS) Trabzon Regional Directorate of Forestry in Turkey.

MATERIAL AND METHODS

Trabzon Forestry District Directorate Macka Forest Management on the topographic map of the road network was planned, taking into consideration the types of stands and dividing slopes transport issues were discussed. The planning of the road network is based on an average road density of 20 m/ha. When planning, it was started from the existing main forest roads, gradually passed to other roads, and care was taken that these roads had a reverse slope. A road network plan has been drawn up taking into account that the transportation of forest products on the roads will be made downwards. The current roads are also drawn in the 'current road' layer with satellite images. For places that are not suitable for roads and are suitable for construction, they are drawn under the name of 'new road' layer with max. 12% slope by means of equal curves.

The timber extraction types, transport facilities, land structure and road planning criterias were considered together at each stage and the solution form was adapted to the existing land structure.

Determination of Timber Extraction Methods

Timber extraction by man power

The slope is around 0-30%, the development of the development age is in the era, and the development with 30-50% slope can be applied with the downward controllable slope and the slope with 50% slope.

Timber extraction by animal power

The animal power average slope is% 25 and the mean skidding distance is 250 meters. The choice of the removal method with animal power has been preferred because of the low slope of the ground due to the small diameter of the wood to be trafficked and the lack of youth that may damage the soil surface and the ability to transport the ground on the soil surface.

Timber extraction by forest tractor

Because the average slope is% 45, that is, the steep terrain and the mean running distance are 125 m, and at the same time the product quantity is small and thin, it is possible to use a pulling method with a forest tractor and pulling it out by a cable.

Timber extraction by Cable Yarding System

Cable yarder systems are preferred due to the fact that the average slope is $>51\%$ and the average distance of the runway is 500 m, which means that the ground is rocky. Because the floor is rocky, it does not allow the product to be moved and shifted over the ground.

Timber extraction with the Monorail Technique

This system has no tilt problem. He can work up to 100 degrees. It facilitates the extraction process especially in the steep and circulating regions. This method has been chosen with the reason that the products to be transported are small in diameter.

Timber extraction with Log Chutes System

These systems can be safely used in 20% to 50% inclined land. This method is preferred so that the land slope is 40% and the distance is 500 m and the new youth on the soil is not damaged. Another reason why this method is preferred is that the trees are thin. Timber extraction systems and technical limits are given in Table 1.

Table 1. Timber extraction systems and their technical limits

Timber Extraction Methods	Slope(%)	Development Stage	Canopy	Skidding Distance	Extraction Direction
Man power	0-30 transport, 30-50 cont. shift., 50< noncont. shift	0-30 b (8-19 cm)	No restriction	300	From up to down
Animal power	0-33	No restriction	No restriction	500	From up to down
Forest Tractor	0-50 skidding, 50< cable pull	c, d (20-33, 34<)	2, 3	500 skidding, 150 m cable pull	from top to bottom
Cable Yarding S.	50<	c, d (20-33, 34<)	2, 3	Short 300 middle 300-800, long 800-2000	Both directions
Monorail S.	0-100	a,b,c	1, 2	500	Both directions
Log Chute S.	30-60	b, c (8-19 cm, 20-33 cm)	No restriction	500	From up to down

RESULTS AND DISCUSSIONS

The areas, slopes, lengths of the roads and the distance between the tracks were determined with the ArcGIS software in the field study and also the methods of dividing the roads are determined. With the ArcGIS program in the field study, areas, slopes, lengths of the roads and the distance between the tracks were determined and the methods of timber extraction the roads were determined.

The area of operator was calculated in ArcGIS environment and found 6003 ha. The operator is measured on the existing road-intensive map to determine that it is 30 km and the required road length for catching the 20 m/ha road density is determined. The total road length required for 20m / ha road density in a 6003 ha wide forest operation is 120km. (6000ha x 20m / ha = 120 000m). Thus, the length of the road to be drawn on the map at the first stage was determined as 90 km. The distance of the road is 500 m depending on

the road density ($YY \times YA = 10000$, ie $YA = 10000/20 = 500$ m). When opening a forest with a road network, the opening rate is used to determine the success status. Since the rate of opening to operation is a measure of the distribution of the roads throughout the forest area, the area open to the operation of the plotted 93 km road lanes is calculated to be approximately 5000 ha. According to this, it is determined that the ratio of opening to the operation is very good with 83%.

The study area is 6003 ha total forest area. There is a road of 30 km on it. In this project, it is planned to construct a new road of 90 km and it is determined that the road will be 120 km long. Accordingly, the general road density is 18 m / ha and the actual road density is 19 m / ha (Figure 1).

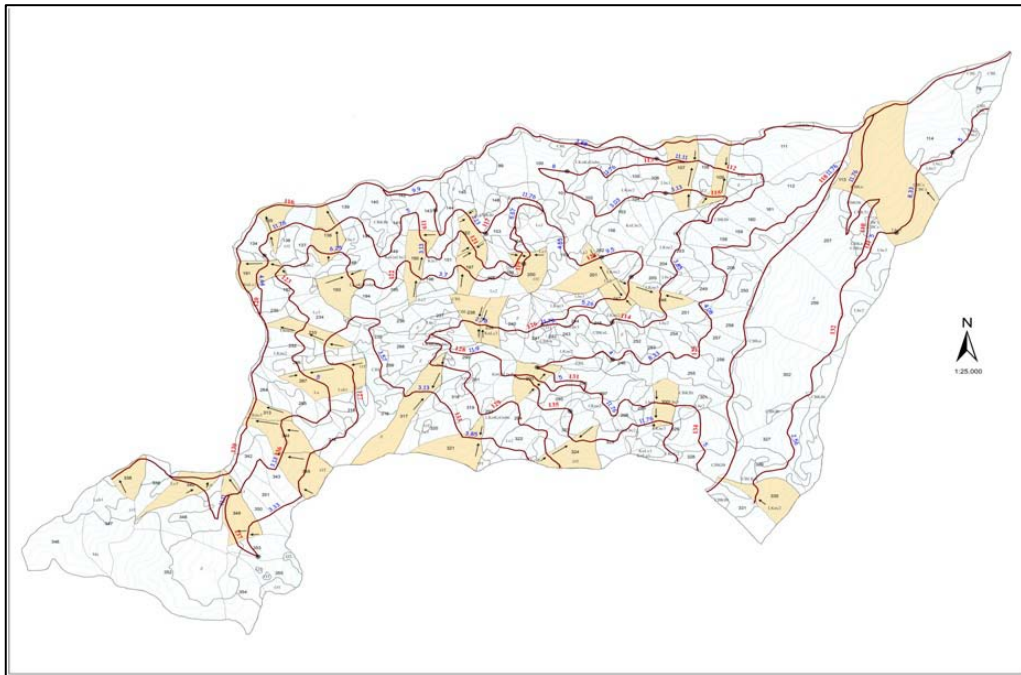


Figure 1. Existing forest road network and planning forest road network in study area

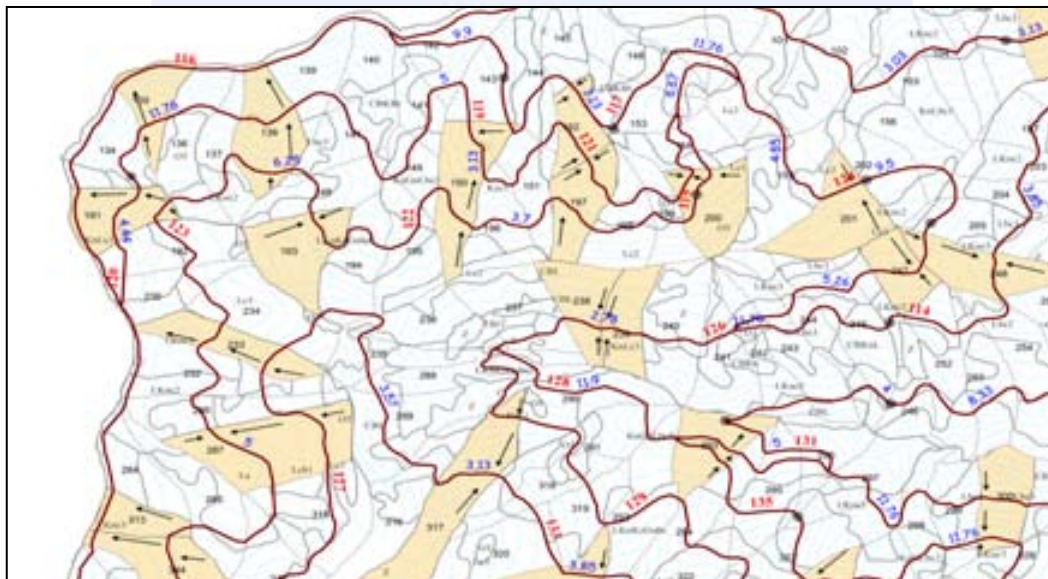


Figure 2. Timber extraction direction

Table 2. Timber extraction systems and stand type

Compartment Number	Stand Type	Slope (%)	Timber extraction method
107	Lbc3	63	112 coded road up to 150 m tractor pull 112 coded road up to 460 m cable yarder s. 115 coded road up to 330 m cable yarder s.
109	Lc3	62	112 coded road down to 470 m cable yarder s 112 coded road up to 150 m tractor pull 114 coded road down to 100 m controll. Scrol.
113	Lc3	44	111 coded road 340 down log chute
135	LKnKzGnbc2	63	116 coded road down to 400 m monorail sys. 119 coded road down to 350 m monorail sys
138	LKnKzGnbc2	76	122 coded road down to 180 m monorail sys 119 coded road down to 170 m monorail sys
150	Kzc1	64	119 coded road down to 480 m cable yarder s 121 coded road down to 400 m cable yarder s
152	LKnKzGnbc2	64	121 coded road down to 300 m cable yarder s 117 coded road up to 150 m tractor pull
191	Lc3	48	116 coded road down to 150 m forest tractor 123 coded road down to 200 m log chute
193	LKnKzGnbc2	60	122 coded road down to 500 m cable yarder s 122 coded road down to 250 m monorail sys.
197	LKnKzGnbc2	54	119 coded road down to 400 m cable yarder s 121 coded road down to 250m cable yarder s 121 coded road up to 250 m monorail sys.
200	Lbc2	55	119 coded road down to 350 m log chute 121 coded road down to 90 m log chute 121 coded road up to 180 m tractor pull
201	Lc3	38	124 coded road down to 400 m log chute 124 coded road up to 150 m tractor pull
233	Lc3	48	127 coded road down to 500 m cable yarder s 123 coded road down to 400 m cable yarder s 116 coded road down to 350 m log chute
238	Lc3	41	126 coded road down to 450 m cable yarder s 126 coded road up to 330 m cable yarder s
239	Lc2	45	126 coded road down to 500 m cable yarder s 126 coded road up to 150 m tractor pull
247	LKnc3	53	124 coded road down to 300 m log chute 124 coded road up to 320 m cable yarder s
248	LKnc3	65	114 coded road down to 250 m cable yarder s 124 coded road down to 500 m cable yarder s 124 coded road down to 500 m monorail sys.

REFERENCES

- Akay A.E. (2003). *Minimizing total cost of construction, maintenance, and transportation costs with computer-aided forest road design*. PhD thesis. Oregon State University, Corvallis, Oregon. 229 p.
- Aruga, K. (2005). Tabu search optimization of horizontal and vertical alignments of forest roads, *Journal of Forest Research*, 10: 275–284.
- Çalışkan, E., (2013). Planning of Forest Road Network and Analysis in Mountainous Area, *Life Science Journal*, 10(2), 2456–2465.
- Demir M. (2007). Impacts, management and functional planning criterion of forest road network system in Turkey. *Transportation Research Part A*, 41 (1): 56–68.
- Eichrodt, A.W., Heinemann, H.R., 2001: Mobility of Timber Harvesting Vehicles. Proceedings »Appalachian Hardwoods: Managing Change«, Council on Forest Engineering (COFE), July 15–18, 2001, Snowshoe, USA, 1–6.
- Enache, A., 2013: *Decision support system for locating forest roads in Romanian mountain forests*. PhD Thesis, Transilvania University of Braşov, Romania, 1–230.
- Enache, A., Kühmaier, M., Stampfer, K., Ciobanu, V.D., 2013: An integrative decision support tool for assessing forest road options in a mountainous region in Romania. *Croat. j. for. eng.* 34 (1): 43–60.
- Gumus S., Acar H.H., Toksoy D. (2008). Functional forest road network planning by consideration of environmental impact assessment for wood harvesting. *Environmental Monitoring and Assessment*, vol. 142 (1–3): 109–116.
- Kühmaier, M., Stampfer, K., 2010: Development of a Multi-Attribute Spatial Decision Support System in Selecting Timber Harvesting Systems. *Croat. j. for. eng.* 31(2): 75–88.
- Lubello, D., 2008: *A rule based SDSS for integrated forest harvesting planning*. Dottorska disertacija, Università degli studi di Padova, Padova, 1–213.
- Rogers L.W. (2005). *Automating Contour- Based Route Projection for Preliminary Forest Road Designs using GIS*. Ms.C. thesis. University of Washington. 87 p.

Use of GIS to Evaluate the Organochlorine Pesticide Accumulations in Soil of Seydisuyu Plain (Eskişehir, TURKEY)

Arzu Çiçek¹, Cem Tokatlı^{*2}, Esengül Köse³

¹Anadolu University, Applied Environmental Research Centre, Eskişehir, Turkey

²Trakya University, Ipsala Vocational School, Edirne, Turkey, E-mail: tokatlicem@gmail.com

³Eskişehir Osmangazi University, Osmangazi Vocational School, Eskişehir, Turkey

ABSTRACT

Seydisuyu Plain is located in the Central Anatolia Region of Turkey and contains very significant agricultural lands. In this study, the total organochlorine pesticide accumulations in soil of Seydisuyu Plain were investigated by determining Alfa HCH, HCB, Beta HCH, Gama HCH, Aldrin, Cis Heptachlorepoxide, Trans chlordane, Cis chlordane, Dieldrin, 44DDE, Endrin, 44DDD, 44 DDT, Metoxychlor and pesticides with Endosulfan in soil samples and the detected data were evaluated by using the Geographic Information System (GIS) in order to make a visual explanation by presenting distribution map of organochlorine pesticide accumulations in soil of Seydisuyu Plain. For this purpose, soil samples were collected seasonally (Summer 2011 – Summer 2013) from 47 stations selected on the Seydisuyu Plain. According to data observed, the organochlorine pesticide accumulations in soil of Seydisuyu Plain were determined between the ranges of 51 – 276 ppb.

INTRODUCTION

Soil is a major reservoir for many pollutants like pesticides and it is a secondary emission source of pollutants to groundwater, surface water, and the atmosphere (Zhang et al., 2011; Tao et al., 2008). Although they are known as very harmful for environment and human health, organochlorine pesticides (OCPs) are being used commonly in agricultural activities against pests all over the world (Nair and Pillai, 1992; Kaushik et al., 2012).

Seydisuyu Plain is located in the Central Anatolia Region of Turkey in Eskişehir Province and contains very large and productive agricultural lands. The aim of this study was to evaluate the OCPs concentrations in soil of Seydisuyu Plain by using GIS technology.

* Corresponding Author

MATERIAL AND METHOD

Seydisuyu Plain, which is one of the most significant agricultural lands of Turkey, is located in the Eskişehir Province between the locality of 38.0851 – 39.0361 north latitude and 30.0161 – 31.0071 east longitudes (Çiçek et al., 2013).

Soil samples were collected seasonal periods in summer 2011 – summer 2013 from 47 stations located on the plain. Coordinates and localities of stations are given in Table 1.

Table 1. Coordinate information of investigated stations

Name of Station	Coordinates		Latitude (m)
	N	E	
Akin	39° 20' 16.9"	30° 31' 04.3"	1046
Aksaklı	39° 36' 46.9"	30° 44' 41.2"	924
Aslanbeyli	39° 27' 03.8"	30° 36' 46.9"	1069
Ayvalı	39° 28' 46.5"	30° 37' 23.9"	1039
Bardakçı	39° 19' 53.7"	30° 47' 31.7"	1028
Beşsaray	39° 26' 02.4"	30° 31' 54"	1272
Beykışla	39° 41' 49.6"	30° 81' 57.3"	938
Büyükdere	39° 35' 07.8"	30° 45' 07.5"	930
Büyükyayla	39° 10' 52.3"	30° 33' 25.6"	1135
Cevizli	39° 21' 58.4"	30° 43' 58"	1167
Çatören	39° 19' 28.2"	30° 36' 31.9"	1120
Çukurağıl	39° 30' 0.4"	30° 46' 06.2"	931
Çukurca	39° 13' 53.3"	30° 42' 12"	1210
Çürüttüm	39° 20' 39.7"	30° 25' 10.6"	1275
Değişören	39° 33' 28.5"	30° 40' 20.4"	978
Doğançayır	39° 32' 02.6"	30° 49' 50"	919
Fethiye	39° 13' 49.2"	30° 32' 17.4"	1070
Gemiç	39° 20' 50.3"	30° 29' 55.5"	1109
Göcenoluk	39° 20' 38.1"	30° 22' 24.3"	1248
Gökbahçe	39° 09' 36.7"	30° 25' 10.6"	1106
Gökçeğüney	39° 12' 00.5"	30° 41' 23.6"	1223
Göknebi	39° 24' 30.8"	30° 32' 16.6"	1193
Gümüşbel	39° 44' 25.3"	30° 81' 41.8"	934
İdrisyayla	39° 23' 13"	30° 25' 06.4"	1272
İkizoluk	39° 18' 19.8"	30° 24' 49.4"	1275

Karacalık	39° 29' 26.7"	30° 31' 59.9"	1193
Karaören	39° 13' 54.2"	30° 34' 31.7"	1054
Kesenler	39° 20' 39.7"	30° 25' 10.6"	976
Kırka	39° 16' 53.2"	30° 31' 43.9"	1043
Kümbet	39° 12' 35.1"	30° 36' 20.9"	1078
Numanoluk	39° 18' 33.3"	30° 35' 42.4"	1199
Oynaş	39° 10' 16.7"	30° 37' 41.7"	1110
Örencik	39° 24' 22.1"	30° 39' 54.2"	1038
Salihler	39° 16' 34.4"	30° 27' 00.2"	1066
Sancar	39° 23' 46.1"	30° 44' 41.2"	1037
Sandıközü	39° 23' 17.6"	30° 21' 30.4"	1219
Sarayören	39°33'19.25"	30°36' 23.47"	1092
Sarıcaılyas	39° 20' 59.1"	30° 40' 17.1"	1187
Şükranlı	39° 16' 32.4"	30° 40' 35.6"	1313
Taşlık	39° 32' 24.7"	30° 37' 50.4"	1062
Üçsaray	39° 27' 07.3"	30° 30' 15.6"	1248
Yapıldak	39° 10' 16.8"	30° 39' 19.1"	1142
Yarbasan	39° 16' 56.5"	30° 34' 22.5"	1136
Yazıdere	39° 29' 41.8"	30° 44' 09.5"	940
Yenikent	39°34'19.47"	30°44' 30.16"	929
Yeşiltepe	39° 22' 23.9"	30° 37' 07.8"	1074
Yukarısöğüt	39° 27' 20"	30° 34' 52.6"	1096

The presence and amount of organochlorine pesticides residues in soil samples were determined by extraction with the Shimadzu brand QP2010 Plus model GC / MS (EPA Method 8081a, 1996).

The distribution map of OCPs on the Seydisuyu Plain was made by using Geographic Information System (GIS) by using the “ArcGIS” package program.

RESULTS AND DISCUSSIONS

The total organochlorine pesticide (OCPs) concentrations by determining Alfa HCH, HCB, Beta HCH, Gama HCH, Aldrin, Cis Heptachlorepoxide, Trans chlordane, Cis chlordane, Dieldrin, 44DDE, Endrin, 44DDD, 44 DDT, Metoxyclor and pesticides with Endosulfanin were investigated in soil of Seydisuyu Plain seasonally and the annual averages of detected OCPs accumulations in soil samples are given in Figure 1.

According to results of this study, the OCPs concentrations in soil of Seydisuyu Plain were recorded between the values of 51 – 276 ppb. The highest concentrations of OCPs were determined in Cevizli, Yapıldak, Fethiye, Sandıközü, Üçsaray and Gemiç Villages.

In a study performed in Taihu Lake Region in the Yangtze River Basin, where is known as a significantly contaminated area in China, OCPs concentrations in most soil samples were detected in the range of 100 – 200 ppb (Wang et al., 2007). Although Seydisuyu Plain Region is not as contaminated as Taihu Lake Region, the specified values in China are similar to data detected in the present study.

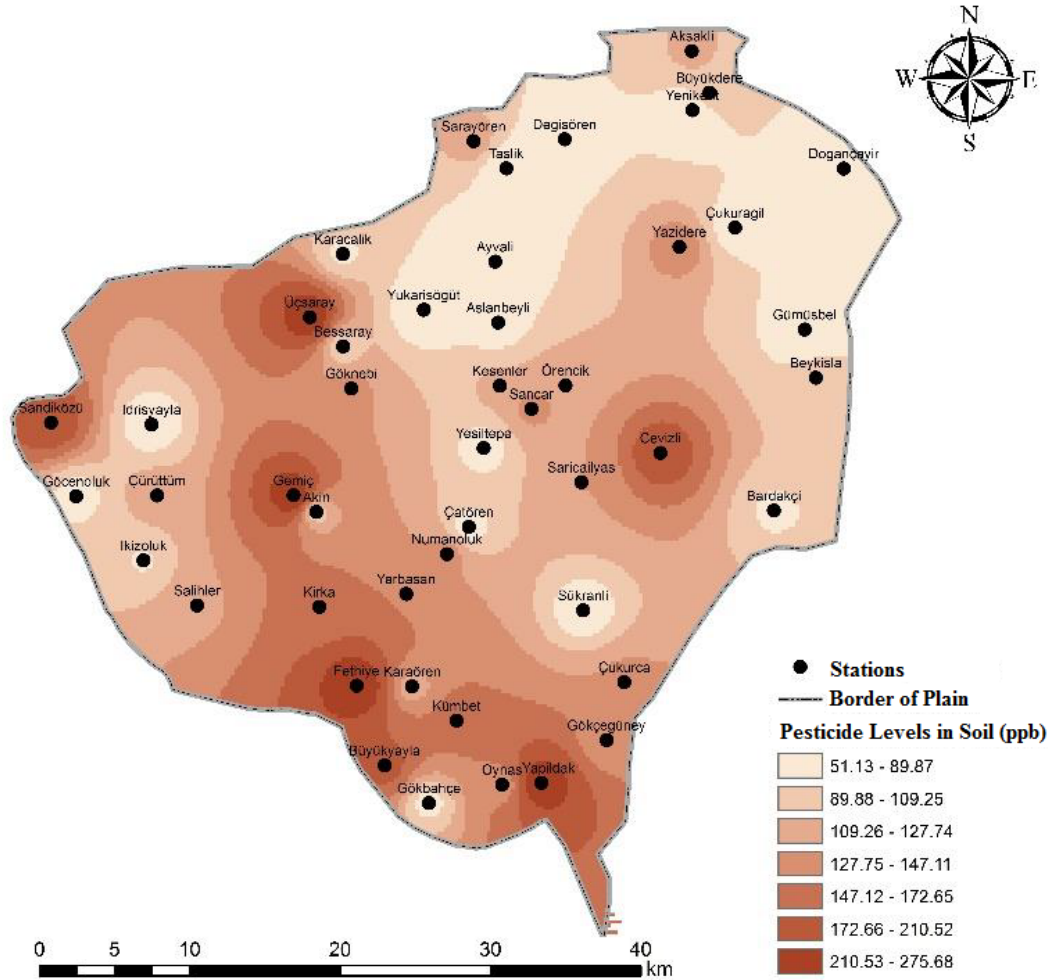


Figure 1. Distribution map of OCPs on the Seydisuyu Plain

CONCLUSIONS

The use of organochlorine pesticides has been banned in Turkey and in many countries on the world. However, studies have shown that even though they are banned, such pesticides are still being produced illegally and their non-controlled use continues. The unconscious use of pesticides causes major problems over time and it is an obligation to take necessary precautions to keep the accumulation of pesticides to the minimum level. Use of pesticides that can decompose in a short time instead of pesticides that have high accumulation properties in foods is a necessary to minimize this significant problem.

ACKNOWLEDGMENTS

The authors would like to thank for the financial and technical supports supplied by Anadolu University, Turkey. This investigation has been supported by the project numbered as 1101F011 accepted by Anadolu University, Commission of Scientific Research Projects.

REFERENCES

- Çiçek, A., Bakış, R., Uğurluoğlu, A., Köse, E., Tokatlı, C., 2013. The Effects Of Large Borate Deposits On Groundwater Quality Of Seydisuyu Basin (Turkey). *Polish Journal of Environmental Studies*, 22 (4): 1031-1037.
- EPA Method 8081a (1996), Organochlorine pesticides by gas chromatography.
- Kaushik, C.P., Sharma, H.R., Kaushik, A., 2012. Organochlorine pesticide residues in drinking water in the rural areas of Haryana, India. *Environ Monit Assess*, 184: 103–112.
- Nair, A., Pillai, M.K.K., 1992. Trends in ambient levels of DDT and HCH residues in humans and the environment of Delhi, India. *The Science of the Total Environment*, 121, 145–157.
- Tao, S., Liu, W.X., Li, Y., Yang, Y., Zuo, Q., Li, B.G., Cao, J., 2008. Organochlorine pesticides contaminated surface soil as reemission source in the Haihe plain, China. *Environ. Sci. Technol.*, 42, pp. 8395–8400.
- Wang, F., Jiang, X., Bian, Y., Yao, F., Gao, H., Yu, G., Munch, J.C., Schroll, R., 2007. Organochlorine pesticides in soils under different land usage in the Taihu Lake region, China. *Journal of Environmental Sciences*, Volume 19, Issue 5, Pages 584–590.
- Zhang, A.P., Liu, W.P., Yuan, H.J., Zhou, S.S., Su, Y.S., Li, Y.F., 2011. Spatial distribution of hexachlorocyclohexanes in agricultural soils in Zhejiang Province, China, and correlations with elevation and temperature. *Environ. Sci. Technol.*, 45, pp. 6303–6308.



ARCHAEOLOGY

Photogrammetrical Applications and GIS Analyses of Ancient Agricultural Terraces in Bozburun Peninsula

Volkan Demirciler¹

¹*Department of Archaeology, Canakkale Onsekiz Mart University, Terzioğlu Campus, 17020, Turkey.
(volkandemirciler@comu.edu.tr)*

ABSTRACT

This paper examines the ancient agricultural terraces of the Bozburun Peninsula which were surveyed in the field works conducted in 2009-2012. The study area, which encompasses about 16.000 hectares, was limited to Turgut Village in the north and the beginning of Loryma ancient site in the south. In antiquity, this sub-region where terrace agriculture was practiced in a systematic manner, was under the control of the Island of Rhodes and a part of the ancient trade network. The application of Geographical Information Systems (GIS) and photogrammetry techniques revealed possible relationships between the agricultural terraces of the region and morphology (elevation, slope, aspect and soil types). The results display that the environmental conditions were highly considered in the process of terrace construction and their deployment. Through intensive and successful terracing activities in the Peninsula, a surplus accumulation must have been achieved far beyond a subsistence economy.

INTRODUCTION

Understanding the dynamics of the countryside and its relations to the urban sites in antiquity has accelerated in Landscape Archaeology. In this respect, the *chora* and ancient agricultural systems have become quite popular subjects for the scholars (e.g. Osborne, 1987; Rich and Wallace-Hadrill, 1991; Wells, 1992). The agricultural terraces in Bozburun Peninsula (hereinafter the “Peninsula” in SW Turkey), which were controlled by the Island of Rhodes in antiquity, deserves to be investigated within the same context. Considering the prosperous Rhodian economic history (e.g. Rice, 1999; Reger, 1999; Gabrielsen, 2001) it would not be irrational to pose that the agricultural terraces of the Peninsula (the “terraces”, from here below) could have been much more exploited during late Classical and early Hellenistic periods when the hands of the Rhodians were simply there.

The text below attempts to investigate the terraces of the Peninsula, preferably under a quantitative approach. It is discussed that the terraces of the Peninsula were constructed according to some basic parameters among which elevation, slope, aspect and soil types of the terrain take the foremost seats. The paper also suggests that despite the physical disadvantages of the Peninsula, the terraces were managed successfully and a considerable amount of surplus was achieved through intensive cultivation and production.

Turgut Village in the north and the beginning of the ancient site of Loryma in the south specify the scope area (Fig. 1) that covers ca. 16.000 hectares. The space falling to between the mentioned sites, but also extending to the southern tip of the Peninsula and toward the north nearing Physcus (modern Marmaris), was an important part of the agricultural trade network of the Rhodian State, during the Hellenistic period (Fraser and Bean, 1954; Van Bremen, 2007).

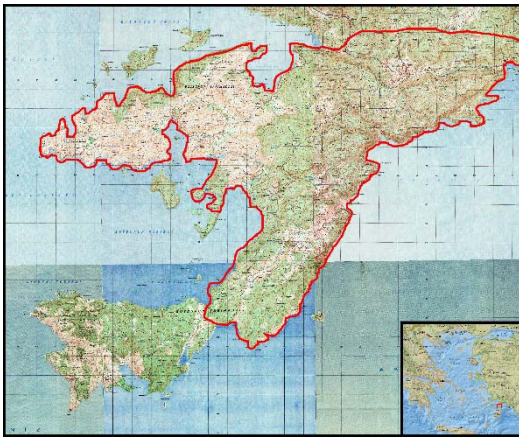


Figure 1. Location map of the study area

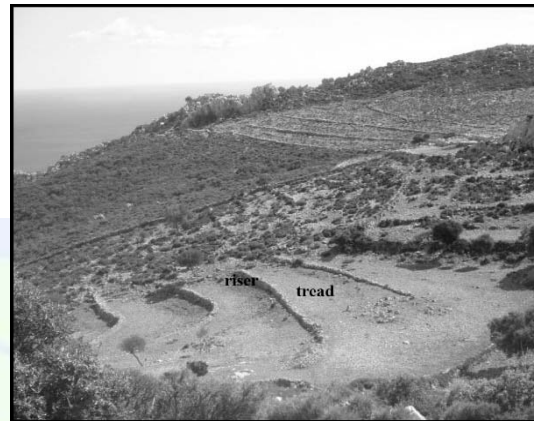


Figure 2. Parts of agricultural terraces

The problem of dating the ancient terraces has long been discussed in archaeology (e.g. Rackham and Moody, 1992; Foxhall, 1996; Price and Nixon, 2005). New interdisciplinary techniques have recently been applied for absolute dating (e.g. Bevan et al., 2013; Kinnaird et al., 2017), however are often useful to date single terraces in small-scale areas. In our case, the study area is so wide that an absolute dating of all the terraces is hardly possible. The basic assumption is that, the terraces, which were detected both at the field and via photogrammetry tools, were operated during the Hellenistic period.

AGRICULTURAL TERRACES

Agricultural terraces displaying contour shaped platforms are constructed in order to minimize the soil erosion in the sloped areas and make these lands suitable for cultivation. They often consist of a vertical wall named as “riser”; a level surface extending behind this “riser” which is called a “tread” (Fig. 2). These generally help improve soil, water or crop management in agriculture (Hudson, 1992: 152).

Based on their geomorphic formations, functions, morphologies or construction techniques, the agricultural terraces can be classified in various ways. Donkin (1979) suggests three types of terraces according to their geomorphic formations as “cross-channel”, “contour” and “valley-floor” terraces whereas Morgan (1986: 226) labels them with reference to their functions as “diversion”, “retention” and “bench” terraces. “Diversion” terraces are constructed to prevent landslide and create land suitable for cultivation. Those in the “retention” group are built to stop and keep the water flowing into

the soil. With “bench” terraces, the aim is to make cultivation on the lands where the slope degrees are high.

Rackham and Moody (1992: 123-125) distinguish three main types (“stepped”, “braided” and “pocket”) by looking at their shapes. The “stepped” terraces are contour shaped ones which do not have special functions but rather form cultivable lands. The “braided” category relates to those built in the form of zigzags. There are interspaces between the neighbouring terraces. The intention is here to plough the soil easily. Finally, the “pocket” terraces which are constructed for olive and vine cultivation, take the half-moon shape.

In the ancient Mediterranean world, the accumulation of surplus could be attained by increasing the yields of three major agricultural crops: simply olive, vine and grain. Different from the cereals, olive and vine could well be cultivated on the marginal lands where soil was often infertile for grain cultivation and/or slopes were very steep. During the Hellenistic era, the marginal lands were incorporated to the agricultural systems, particularly via terracing. Olive and vine became valuable crops in the agricultural economy and surplus accumulation accelerated at the end (Renfrew, 1972: 480-482).

METHOD OF THE STUDY

The main method of the study was field survey which was conducted in the years between 2009-2012 with the permissions given by the Ministry of Culture and Tourism of the Turkish Republic. Aerial techniques (basically photogrammetrical applications) and GIS were additionally utilized to map all of the terraces of the study area and seek the factors behind their construction process.

Below given are the three map types used in the study:

1. Raster Maps: 1/25.000 scale topographical maps were obtained from the General Command of Mapping and 1/5000 scale cadastral maps were obtained from the General Directorate of Land Registry and Cadastre. These maps were used before and during the field survey.
2. Digital Maps: 1/25.000 scale digital contour map was obtained from the General Command of Mapping and used for generating the Digital Elevation Model of the study area. 1/25.000 scale digital soil maps were obtained from the Ministry of Agriculture and used in the GIS analyses of the agricultural terraces.
3. Aerial Photographs: 1/15.000 scale stereo pair aerial photographs in printed versions (dated 1972) were obtained from the General Command of Mapping and carefully examined prior to the field works, in order to determine the survey areas which revealed an archaeological potential. Recent digital aerial photographs were also used for creating the orthophoto which was used as a base map for vector drawing of the terraces.

GIS ANALYSES AND RESULTS

Basically, three data sets were used in the course of GIS analyses: Vector Data, Topographic Data (Elevation, Slope and Aspect) and Soil Data. All of these analyses were completed by using ESRI-ArcGIS Desktop (10.0) software.

Vector Data: All the terraces and flat fields were drawn as polygons and the relevant vector map was created (Fig. 3). It was seen that the total study area measures ca. 15.873,64 ha. The areal calculations, which were made by using the vector map, showed that 20,78 % of it (3.297,82 ha) was terraced. The flat areas that are suitable for cultivation (without terracing) covers only 544 ha (corresponds to 3,43 % of the total area) (Tab. 1).

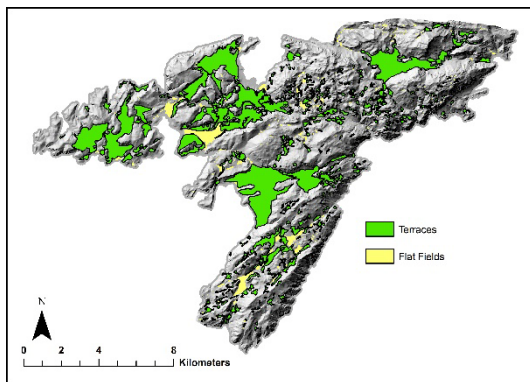


Figure 3. Agricultural terraces and flat fields in the study area

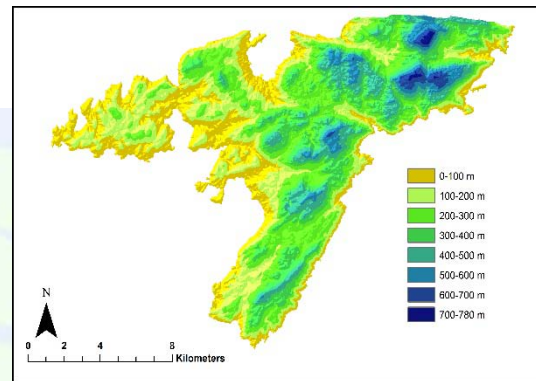


Figure 4. Elevation map of the study area

Table 1. Distribution of agricultural terraces and flat fields

Total Area (ha)	Terraces (ha)	Terraces / Total Area (%)	Flat Fields (ha)	Flat Fields / Total Area (%)
15.873,64	3.297,82	20,78	544	3,43

Topographic Data: As per the topographic analyses, elevation, slope and aspect maps of the study area were created. The results are explained as below:

Elevation: The elevation map of the study area (Fig. 4) shows that elevation values range between 0-780 m. The average value is 236,04 m (Tab. 2). As is visible in Tab. 3, values were classified in 100 m intervals. According to the table, 84,72 % of the study area presents elevation values ranging between 0-400 m.

Table 2. Elevation values of the total area

Total Area (ha)	Min. Elevation (m)	Max. Elevation (m)	Mean Elevation (m)
15.873,64	0,00	780,00	236,04

Table 3. Elevation intervals of the total area

Elevation Interval (m)	Total Area (ha)	Percentage (%)
0-100	3.551,57	22,37
101-200	3.522,96	22,19
201-300	3.650,97	23,00
301-400	2.724,65	17,16
401-500	1.547,40	9,75
501-600	626,85	3,95
601-700	206,58	1,30
701-800	42,67	0,27

The elevation values of the terraced areas were obtained by overlapping the elevation map of the study area and the vector data of the terraced areas (Tab. 4). As the table shows, the values of the terraced areas range between 0-662,21 m while the average elevation value is 191,91 m. Tab. 5 shows the classified elevation values of the terraced areas in 100 m intervals. Accordingly, the elevation values of the terraced areas range between 0-400 m and the terraced areas located in this interval constitute the 97,03 % of all the terraced areas in the study area. The elevation difference histogram of the terraces (Fig. 5) was obtained by subtracting the elevation percentages of the terraced areas from the elevation percentages of the total area. Looking at the positive sector of the histogram it is seen that the percentages of the terraces are greater than the percentages of the total area. Understandable from the histogram, elevation intervals of 300-400 m and 400-500 m were the most preferred intervals for terrace construction. However, elevation intervals in the negative sector of the histogram suggest that these elevation intervals were not preferred for terrace construction.

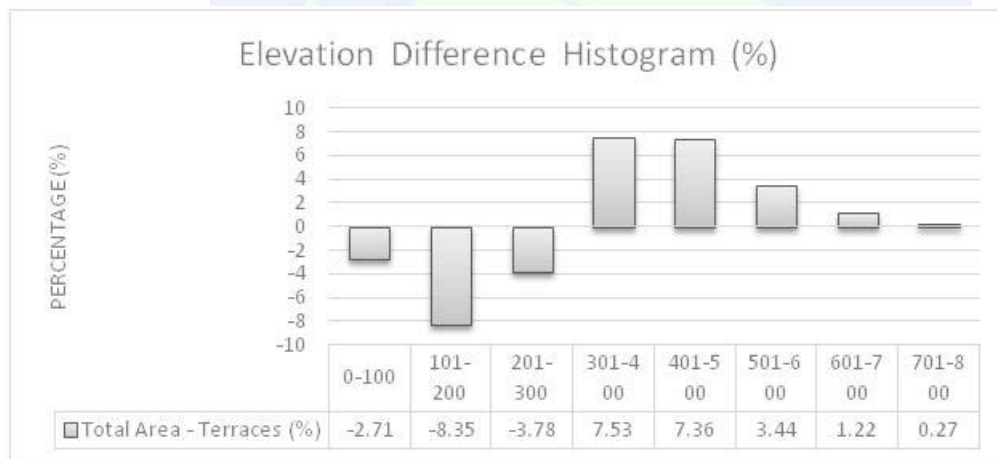


Figure 5. Elevation difference histogram of the terraces

Terraces (ha)	Min. Elevation (m)	Max. Elevation (m)	Mean Elevation (m)
3.297,82	0,00	661,21	191,91

Elevation Interval (m)	Terraces (ha)	Percentage (%)
0-100	991,88	30,08
101-200	1.007,12	30,54
201-300	883,18	26,78
301-400	317,68	9,63
401-500	78,78	2,39
501-600	16,67	0,51
601-700	2,51	0,08

Slope: The slope map of the study area was created in order to understand the relationship between agricultural terraces and slope (Fig. 6). The slope values of the total study area

range between 0-85,99 degrees and the average slope value is 22.21 degree (Tab. 6). The values were classified in intervals (Tab. 7). It is clear that 79,44 % of the total area has slope values over 12 degree.

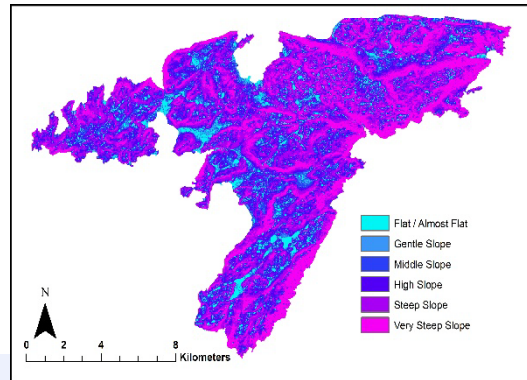


Figure 6. Slope map of the study area

Table 6. Slope values of the total area

Total Area (ha)	Min. Slope (degree)	Max. Slope (degree)	Mean Slope (degree)
15.873,64	0,00	85,99	22,21

Table 7. Slope intervals of the total area

Slope Interval (degree)	Meaning	Total Area (ha)	Percentage (%)
0-2	Flat or Nearly Flat	1.186,54	7,47
2-6	Slight-Slope	551,97	3,48
6-12	Middle-Slope	1.525,75	9,61
12-20	High-Slope	3.604,32	22,71
20-30	Steep-Slope	4.974,68	31,34
>30	Very Steep-Slope	4.030,38	25,39

Table 8. Slope values of the terraces

Terraces (ha)	Min. Slope (degree)	Max. Slope (degree)	Mean Slope (degree)
3.297,82	0,00	72,08	14,82

Table 9. Slope intervals of the terraces

Slope Interval (degree)	Meaning	Terraces (ha)	Percentage (%)
0-2	Flat or Nearly Flat	342,33	10,38
2-6	Slight-Slope	207,93	6,31
6-12	Middle-Slope	662,96	20,10
12-20	High-Slope	1.129,60	34,25
20-30	Steep-Slope	834,89	25,32
>30	Very Steep-Slope	120,11	3,64

On the other hand, the slope values of the terraced area range between 0-72.08 degrees and the average slope value is 14,82 degree (Tab. 8). The slope values of the terraced areas

were also classified in Tab. 9. The slope difference histogram of the terraces (Fig. 7) was obtained by subtracting the slope percentages of the terraced areas from the slope percentages of the total area. Looking at the positive sector of the histogram it is seen that the percentages of the terraces are greater than the percentages of the total area. Obviously, the areas which have slope values over 20 degree were preferred for terrace construction. The most preferred areas for terrace constructions have slope values over 30 degree. Negative sector of the histogram indicates that areas which have slope values under 20 degree were not preferred for terrace construction.

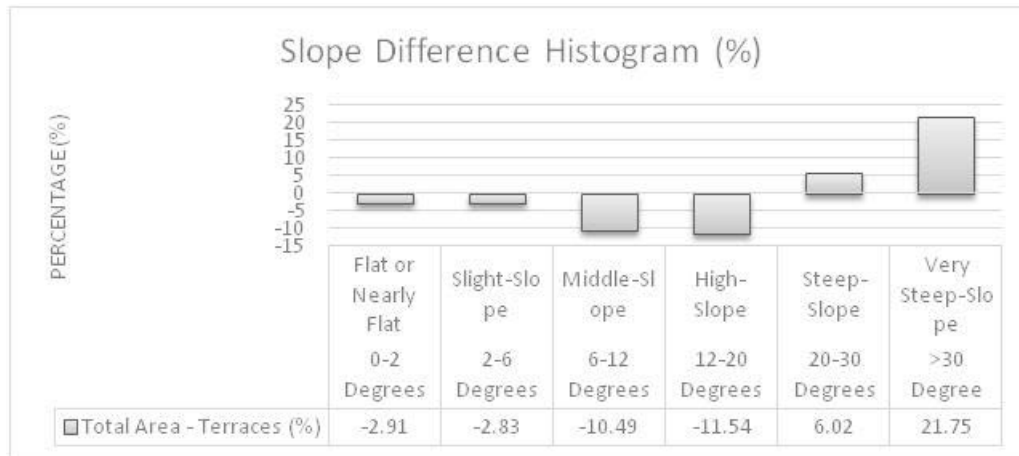


Figure 7. Slope difference histogram of the terraces

Aspect: The aspect map of the study area (Fig. 8) was created to see if there is a relationship between terrace construction and aspect. By overlapping the aspect map and vector map of the terraces we get the aspect results of the total area (Tab. 10) and the aspect results of the terraced area (Tab. 11). Aspect difference histogram of the terraced areas (Fig. 9) was obtained by subtracting the direction percentages of terraces from the direction percentages of the total area, in a similar manner. The directions in the positive sector of the histogram (south, south-east and east) were preferred for terrace construction. The most preferred direction for terrace construction appears to be the south-east category but the most avoided direction is north-west.

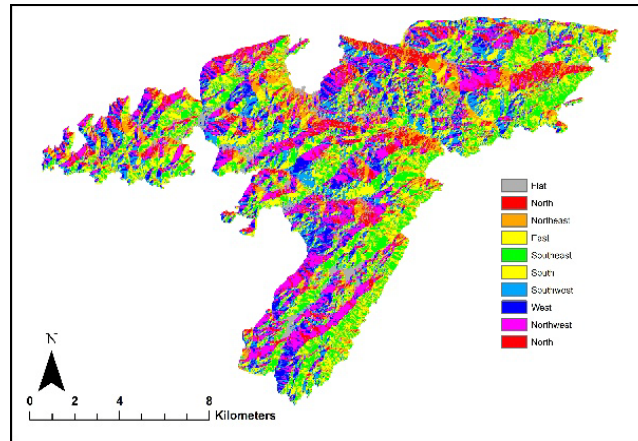


Figure 8. Aspect map of the study area

Table 10. Aspect results of the total area

Aspect (direction)	Total Area (ha)	Percentage (%)
Flat	1.007,18	6,34
North	1.931,61	12,17
North-East	1.343,46	8,46
East	1.439,58	9,07
South-East	2.326,73	14,66
South	2.221,74	13,40
South-West	1.696,56	10,69
West	1.622,07	10,22
North-West	2.284,71	14,39

Table 11. Aspect results of the terraces

Aspect (direction)	Terraces (ha)	Percentage (%)
Flat	292,14	8,86
North	388,85	11,79
North-East	285,54	8,66
East	265,36	8,05
South-East	389,89	11,82
South	417,81	12,67
South-West	372,30	11,29
West	365,86	11,09
North-West	520,07	15,77

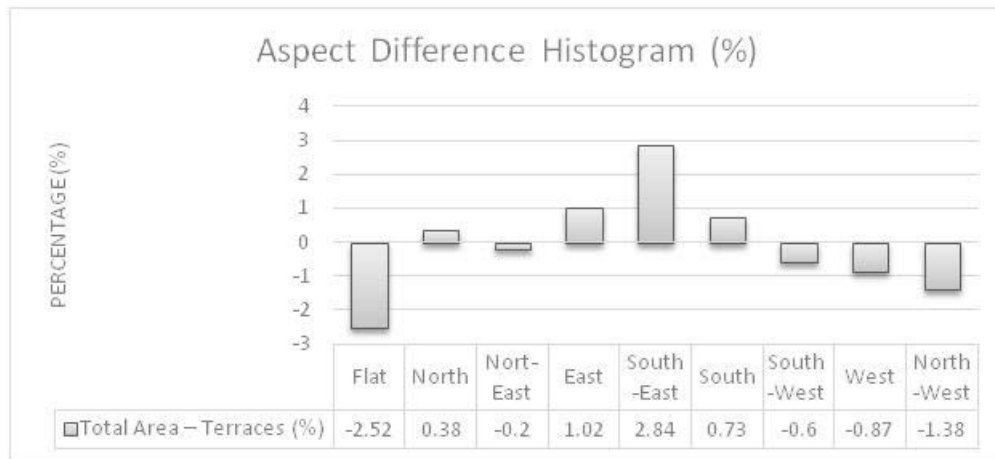


Figure 9. Aspect difference histogram of the terraces

Soil Data: Soil map of the study area (Fig. 10) shows the distribution of the major soil types. The Red-Brown Mediterranean soil covers 39,24 % of the total area whereas Terra Rosa soil constitutes 44,59 % of the major soil types in the study area (Tab. 12). Red-Brown Mediterranean soils are composed of hard calcareous, granites, mudstone and various kinds of metamorphic crystal rocks. They belong to humid and sub-humid climatic zones and can be seen in the areas which have 400-1000 mm annual rainfall rates. Terra Rosa type of soil is dark red soil and mainly composed of hard calcareous. It is very specific for the Mediterranean climate regions and can be seen in the areas which have 600 mm or more annual rainfall rates (T.C. Köy Hizmetleri Genel Müdürlüğü, 1998: 20). Red-Brown Mediterranean soil covers 68,22 % and Terra Rosa type of soil makes up 23,31 % of the terraced area (Tab. 13). Major soil types difference histogram of the terraced areas (Fig. 11) was, for the fourth time, created by subtracting the major soil types percentages of the terraced areas from the major soil types percentages of the total area. According to this histogram, the soil type in the positive sector of the histogram (Terra Rosa) was preferred for terrace construction.

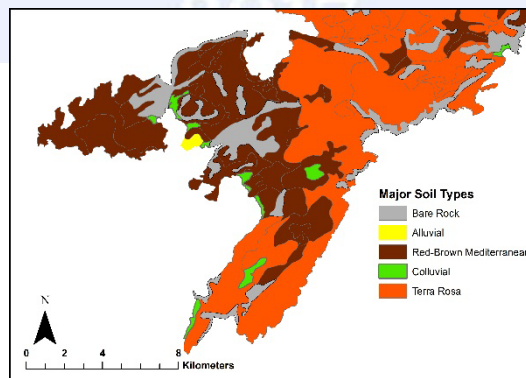


Figure 10. Soil map of the study are

Table 12. Major soil type distribution of the total area

Major Soil Types	Total Area (ha)	Percentage (%)
Bare Rock	2.215,34	13,96
Alluvial	58,45	0,37
Red-Brown Mediterranean	6.228,59	39,24
Colluvial	292,45	1,84
Terra Rosa	7.078,81	44,59

Table 13. Major soil type distribution of the terraces

Major Soil Types	Terraces (ha)	Percentage (%)
Bare Rock	0	0
Alluvial	157,78	4,78
Red-Brown Mediterranean	2.249,76	68,22
Colluvial	121,51	3,68
Terra Rosa	768,77	23,31

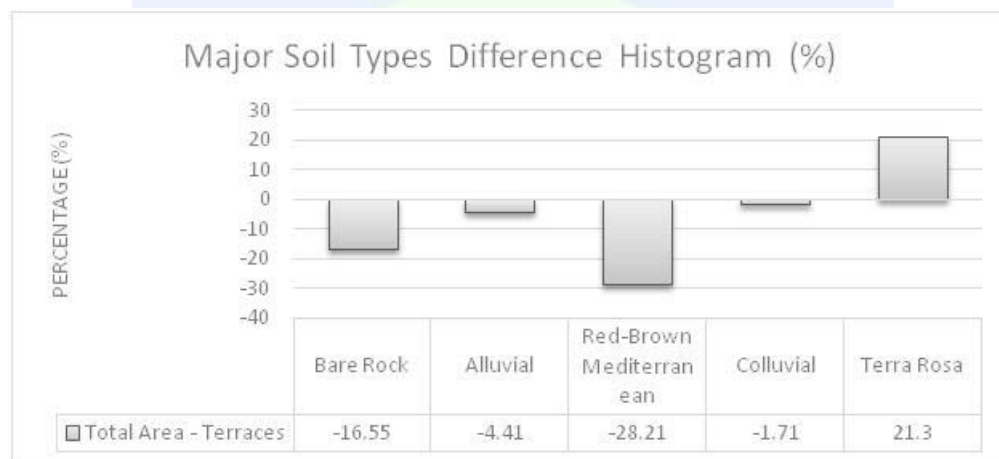


Figure 11. Major soil types difference histogram of the terraces

CONCLUSION

GIS analyses of the study area have shown that about 85 % of the total area has elevation values ranging between 0-400 m. and that, about 97 % of agricultural terraces were constructed in this elevation interval. The most preferred areas chosen for terrace construction are in the elevation intervals of 300-400 m and 400-500 m and have slope values over 30 degrees. In order to get the maximum benefit from the positive effects of solar radiation (especially for vine cultivation), agricultural terraces were built in south, south-east and east directions. The reason of not-preferring terrace construction in north-west directions can be explained by avoiding the negative effects of the northern winds on agricultural productions. Even though the terraces are widespread all over the study area, the difference histogram of the major soil types indicates that the most preferred type was Terra Rosa. From here onwards, it can be suggested that the morphological character of the study area must have affected the construction of the terraces which determined the agricultural system of the Peninsula in antiquity. GIS analyses that were made by using the vector data of the terraces and flat fields have proven that out of 15.873 ha of the total

study area, 3297,82 ha of land were terraced (20,77 % of the total area). However, only 3,43 % of the study area (544 ha) seems to be suitable for agriculture without terracing. Accepting that flat fields were reserved for cereal cultivation and terraces for olive and vine, we can make some production estimations, to understand whether the Peninsula was able to create a surplus or not.

Turning an eye to the Athenian tribute lists (of the Classical period), Tuna (1978: 170-171) suggested that population of the Carian Chersonesos (the acknowledgement of the former Peninsula in the 5th century B.C) should be maximum 2000 people. Assuming that, on average, 750 kg/ha grain was produced for the good and bad years (Oğuz-Kırca 2015: 476), we can suggest that 408.000 kg grain (544 ha x 750 kg/ha) could have been produced on the flat fields, annually. Taking a consumption figure of 200 kg. grain per capita, the population that the Peninsula could have fed can be speculated to 2040 people (408.000 kg/ 200 kg). However, basing the estimations solely on potential grain production can never suffice, particularly over the flat fields. Hence, we can barely talk about a significant surplus accumulation in the Peninsula.

Relevant to the terraced land or the land used for viticulture; Tuna (1990: 350) suggests that 1.603.411 lt. of wine could be produced potentially in ancient Knidos. He reached his results on wine by taking the unit- “iugerum” (1/4 hectare) which yielded around 20 amphorae per annum. Oğuz-Kırca (2015: 475-476) takes 25 lt. as the mean capacity of a Rhodian amphora in the Hellenistic period. Accordingly, the potential of wine production is calculated as 6.595.640 lt (20x4x25x3297,82) which is a remarkable figure for the Peninsula especially comparing to the agricultural production potential of ancient Knidos.

The abovementioned figures propose something never echoed for the Bozburun Peninsula before. Presumably, it was the wine with which a significant amount of surplus accumulation was attained in the Peninsula.

In conclusion; When examined in a holistic manner and in light of the newly applied aerial and quantitative techniques- (basically photogrammetry and GIS) in the region we have been operating, the agricultural terraces in the Bozburun Peninsula have still many to disclose in the name and about the agricultural memory of the Mediterranean environments. The results presented above have shown that the terraces, making up the most marginal spaces of the region, were constructed in a systematic way and considering the environmental conditions (basically taking into account the elevation, slope, aspect and soil types criteria). The amount of agricultural land that can be cultivated without terracing in the region is far from being able to create a self-sufficient economy. It appears that they were the agricultural terraces which must have made it possible to create a surplus accumulation in antiquity, rather than serving for a subsistence production.

REFERENCES

- Bevan, A, et al 2013. “The Long-Term Ecology of Agricultural Terraces and Enclosed Fields from Antikythera, Greece” *Human Ecology* V.41: 255-272.
- Donkin, R. A. 1979. *Agricultural Terracing in the Aboriginal New World*. Arizona.

- Foxhall, L. 1996. "Feeling the Earth Move: Cultivation Techniques on Steep Slopes in Classical Antiquity." In *Human Landscapes in Classical Antiquity*, edited by G. Shipley and J. Salmon. 44-67. Routledge.
- Fraser, P. M., Bean, G. E. 1954. *The Rhodian Peraea and Islands*. Oxford.
- Gabrielsen, V. 2001. "The Rhodian Associations and Economic Activity." In *Hellenistic Economies*, edited by Z. H. Archibald et al. 163-184. Routledge.
- Hudson, N. 1992. *Land Husbandry*. London.
- Kinnaird, T., Bolos, J., Turner, A., Turner, S. 2017. "Optically-Stimulated Luminescence Profiling and Dating of Historic Agricultural Terraces in Catalonia (Spain)" *Journal of Archaeological Science* No. 78: 66-77.
- Morgan, R. P. C. 1986. *Soil Erosion and Conservation*. London.
- Oğuz-Kırca, E. D. 2015 "The Ancient Population of a Chersonessian Heir: Phoinix" *Tarih Araştırmaları Dergisi* (34) No. 58: 445-488.
- Osborne, R. G. 1987. *Classical Landscapes with Figures: The Ancient Greek City and its Countryside*. London.
- Price, S., Nixon, L. 2005. "Ancient Greek Agricultural Terraces: Evidence from Texts and Archaeological Survey" *American Journal of Archaeology* No. 109(4): 665-694.
- Rackham, O., Moody, A. 1992. "Terraces." In *Agriculture in Ancient Greece: Proceedings of the Seventh International Symposium at the Swedish Institute in Athens, 16-17 May, 1990*, edited by B. Wells, 123-130. Stockholm.
- Reger, G. 1999. "The Relations Between Rhodes and Caria from 246 to 167 B.C." In *Hellenistic Rhodes: Politics, Culture and Society*, edited by V. Gabrielsen, 76-97. Aarhus.
- Renfrew, C. 1972. *The Emergence of Civilisation: The Cyclades and the Aegean in the Third Millennium B.C.* London.
- Rice, E. E. 1999. "Relations Between Rhodes and the Rhodian Peraea." In *Hellenistic Rhodes: Politics, Culture and Society*, edited by V. Gabrielsen, 45-54. Aarhus.
- Rich, J., Wallace-Hadrill, A. 1991. *City and Country in the Ancient World*. Routledge.
- T.C. Köy Hizmetleri Genel Müdürlüğü. 1998. *Muğla İli Arazi Varlığı*. Ankara.
- Tuna, N. 1978. *Antik Devir Batı Anadolu Kıyı Yerleşmelerinde Mekansal Örgün*. M.Sc., M.E.T.U., Ankara.
- Tuna, N. 1990. *Datça Yarımadası'nda Hellenistik Dönem Amphora Üretim Merkezleri, Türk Tarih Kongresi Bildirileri (10) I*. Ankara.
- Van Bremen, R. 2007. "Networks of Rhodians in Karia" *Mediterranean Historical Review* No. 22(1): 113-132.
- Wells, B. 1992. *Agriculture in Ancient Greece: Proceedings of the Seventh International Symposium at the Swedish Institute in Athens, 16-17 May, 1990*. Stockholm.

Determination of Potential Clay Beds with GIS Based Approach at the Kerküşti Höyük and Its Vicinity

Savaş Sarialtun^{1,2}

¹Department of Geography, Canakkale Onsekiz Mart University, Terzioğlu Campus, Turkey

²Préhistoire et Technologie, Université Paris Nanterre, France (e-mail:savassarialtun@gmail.com)

ABSTRACT

The main purpose of this study was to determine clay beds with GIS analysis within the 10 km radius of the surroundings of Kerküşti Höyük, which is located in the district of Derik/Mardin in south-eastern Turkey. The site was mainly occupied during the Halaf Period. The clay characterization and morphology of Halaf wares at Kerküşti Höyük are presented. Comparing Geographical Information System (GIS) database with existing archaeometric analysis, this article aims to identify the geographical borders of the area with favourable clay sources for pottery production in 6000 BCE. In this study some modeling and thematic mapping for understanding clay sources choice and their mobility activity using Geographic Information Systems (GIS). Particularly, geological and hydrological databases are very helpful for slope and/or surface curvature in this modelling. The potential clay deposit model using a 5 m Digital Elevation Model (DEM) and combination of derivatives such as slope, surface curvature defined, and slope location classification was based on a case-based reasoning approach. In this disquisition, it would be provided a case study that contributes to our understanding of Halaf communities fulfil the need for pottery production.*

INTRODUCTION

Kerküşti Höyük, which is located in the district of Derik/Mardin in south-eastern Turkey, was dug in 2005-2006 as rescue excavations. The site which was inhabited from the Early Halaf until almost the end of the Middle Halaf period between 5900 to 5700 BC, is geographically located at the center of the Halaf world. The site was abandoned probably as the result of flooding and was not reoccupied until the Late Chalcolithic Age. The Halaf period of the site preliminarily yields two main phases (Va and Vb). Its location at the transition point of zones of different environmental settings (mountainous area and steppe zone) not were only suitable for different life styles (permanently and seasonally) and different subsistence strategies (agriculture and husbandry) but also enabled the people of Kerküşti to communicate with different regions.

* According to UTM Zone 37 Central Meridian 39 (ED50) the site is situated between 604.523, 7mE / 4.118.073, 8mN to 604.663, 1mE / 4.118.532, 7mN.

Geographically, the site lies in the middle of the northernmost extent of the Northern Mesopotamian plain, just southeast of the Mardin-Midyat Threshold. The plain is cut by intermittent tributaries of the Khabur River. Outcrops of the southernmost limits of the Karacadağ basalt intrusions (Yıldırım and Karadoğan 2010:121) are visible in various parts of the plain. Kerküşti Höyük lies on the west bank of an intermittent stream named Kocadere that flows in a basalt intrusion.

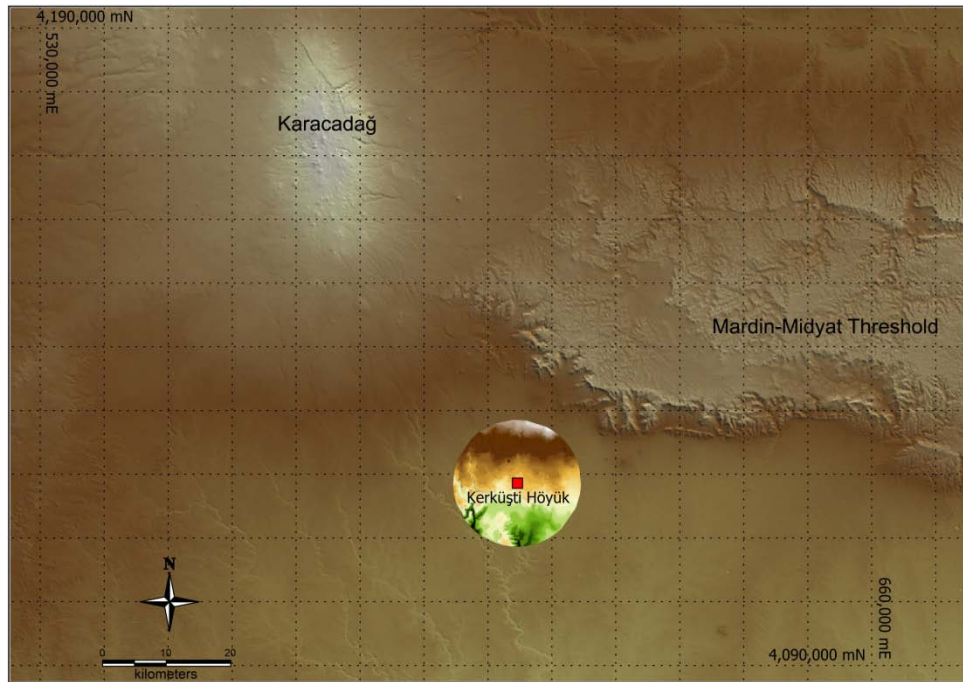


Figure 1. The location of the study area

HALAF POTTERY of KERKÜŞTİ HÖYÜK

The Halaf pottery of Kerküşti does not differ in fabric and decoration from that of the other Halaf sites. There are, however, four pieces that do not show a local character, probably imports. Two of them were found in Subphase Vb1 and the others in Subphase Vb2. The decoration on a bowl showing a row of seated gazelles is similar to a sherd from Tell Halaf (Schmidt 1943: Taf. V.2). Moreover, there are three decorated pieces that were painted with bitumen. Basically the pottery of Kerküşti Höyük comprises seven ware types according to fabric, paste and surface treatments. Vessels were mainly handmade. Molding and coiling/ slab manufacture were also observed.

Standard Painted Ware and Standard Plain Ware are wares, whose fabric, paste and surface treatment are fine. The inclusions in their paste, mainly calcium carbonate particles and sand, were either intentionally added, or were naturally present in the clay. Apart from this, dominant wares in Phase Va are Orange Painted and Orange Plain Ware that are mainly used in thick-walled handmade jars and conical bowls. Except for five sherds in Subphase Vb1, they disappeared in the following subphases. Orange Painted and Plain Wares were made of coarse clay with rough calcium carbonate, chamotte and grit inclusions. Some of

them have pitted surfaces. Although the Dark Faced Burnished Painted Ware is only represented in Phase Va, Dark Faced Burnished Ware (DFBW) is found in all phases. The ones in Phase Va and Subphase Vb1 are of better quality than later ones. Both wares are made of coarse clay tempered with grit and calcium carbonate and/or (rarely) sand and mica. Their outer surfaces and interior at the rims are slipped and burnished. The forms of DFBW are horizontal necked globular body jars and hole mouth vessels. DFBW was decorated with thick bands and triangles. Coarse Ware displays vegetal temper and is plain and moderately or badly fired. It was found mainly in Phase Vb and has no characteristic forms. There are three basic vessel shapes: Bowls in ten different variations, jars in six and plates in five subtypes.

METHODOLOGY

Prognosticative analytic and thematic modeling are an important subject tool that allows specialist to make survey and research decisions. In other words, predictive modeling does more than reduce the time, and effort of field survey. A survey of the geographical and/or archaeological study includes many possible cultural and ecological variables for site-locations. Our study combines both archaeological and geomorphological research methods for some recommendations.

Table 1. Scales for the comparisons method from the slopes

Value	Intensity of Importance	Gradient ratio (%)	Definition	Code
1	Extreme importance	≤ 1	Flattest	TD
2	Very strong importance	1 - 2	Flat	D
3	Strong importance	2 - 5	Wavy Flat	DD
4	Moderate importance	5 - 10	Sloping Slope	AY
5	Insignificant	10 - 20	Dip slope	EY
6	Insignificant	20 - 40	Steep slope	DY
7	Insignificant	$40 \geq$	Very Steep Slope	CDY

An area of 10 km radius was chosen as a study area for the determination of potential clay beds in the surroundings of Kerküşti Höyük. The subject area is used by digitizing N44a3, N44a4, N44b4, N44c1, N44d1, N44d2 and N44d3 topographic map points of 1/25000 scale. Hydraulic model studies were carried out using slope, lithology and GIS techniques. DEM maps were created using digital elevation data of the study area. In addition, TIN terrain models were produced with an irregular triangular mesh. After this stage, the slope map has been removed by DEM map and slope map raster data was converted vector data. Finally, thematic modeling and analyzes were done based on the data. The spatial analysis of the corresponding digital map with the help of MapInfo 15 GIS software has revealed possible clay deposits and characteristic features as a result of slope, lithology and hydraulic model studies. The slope intervals and definitions were taken from the article published by Oguz Erol in 1993 (Erol, 1993: 26 Figure.6).

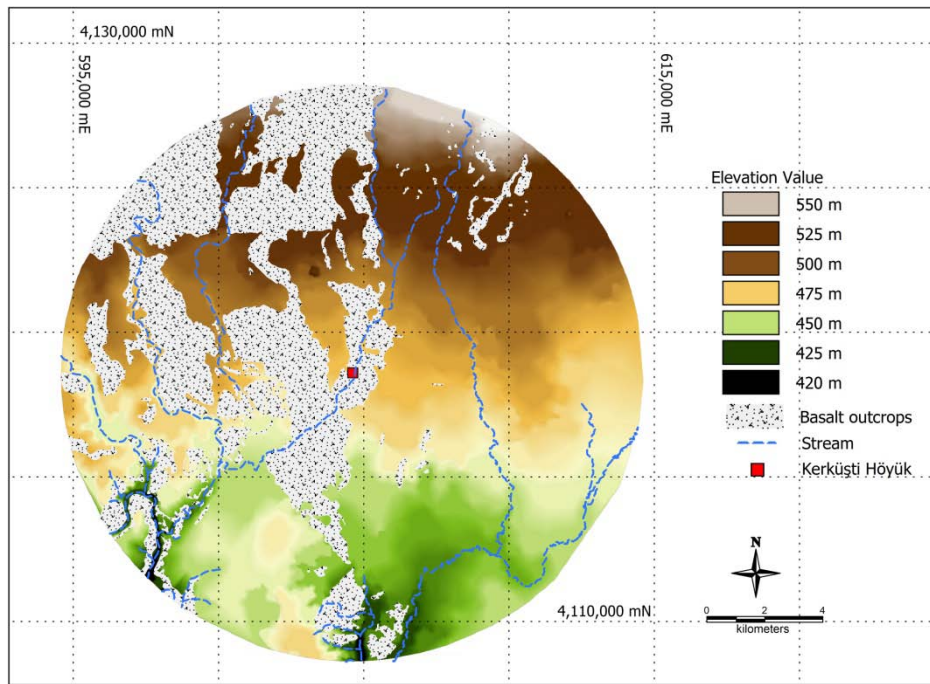


Figure 2. DEM modeling of the study area (10km radius)

Petrographic thin section and EDX / SEM analyzes of the pottery samples that were collected in the archaeological layers were carried out. The obtained results were evaluated mutually and the clay characterization of the material subject to work was determined. The element and micro-morphological compositions of pottery samples were examined by using a Phillips XL-30S FEG Scanning Electron Microscope equipped with EDX detector. The analyses were carried out at İzmir Institute of Technology, Center for Materials Research (IZTECH-MAM).

I have to emphasize that, this offered modeling is a “passive” geographical method, since “active” methods include intensive surveys as well as micro morphological examinations of the collected samples from potential clay sources.

DATA AND ANALYSIS

Several of the possible model parameters were found to have no significant correlation to clay source location decisions in the study area. These parameters were based on the shortest distance to Kerküşti Höyük as well as the shortest distance to the streams.

Looking by 10km radius, the study area is occupied: Flattest Slopes (0-1%) 51.33%, Flat Slopes (1-2%) 29.11, Wavy Flats Slopes (2-5%) 15.30%, Sloping Slopes (5-10%) 1.05%, Dip Slopes (10-20%) 0.38%, Steep Slopes (20-40%) 0.11 and Very Steep Slopes (40% and more) 0.05% of the area. The slope feature of the study area is a basin property where the slopes are less and the plains cover more than 95%. If the basalt outcrop is considered, the variation of the statistical data is changed, even though the slope and the plain equations are the same. The analyzed parameters are presented in Table 1 and Table 2.

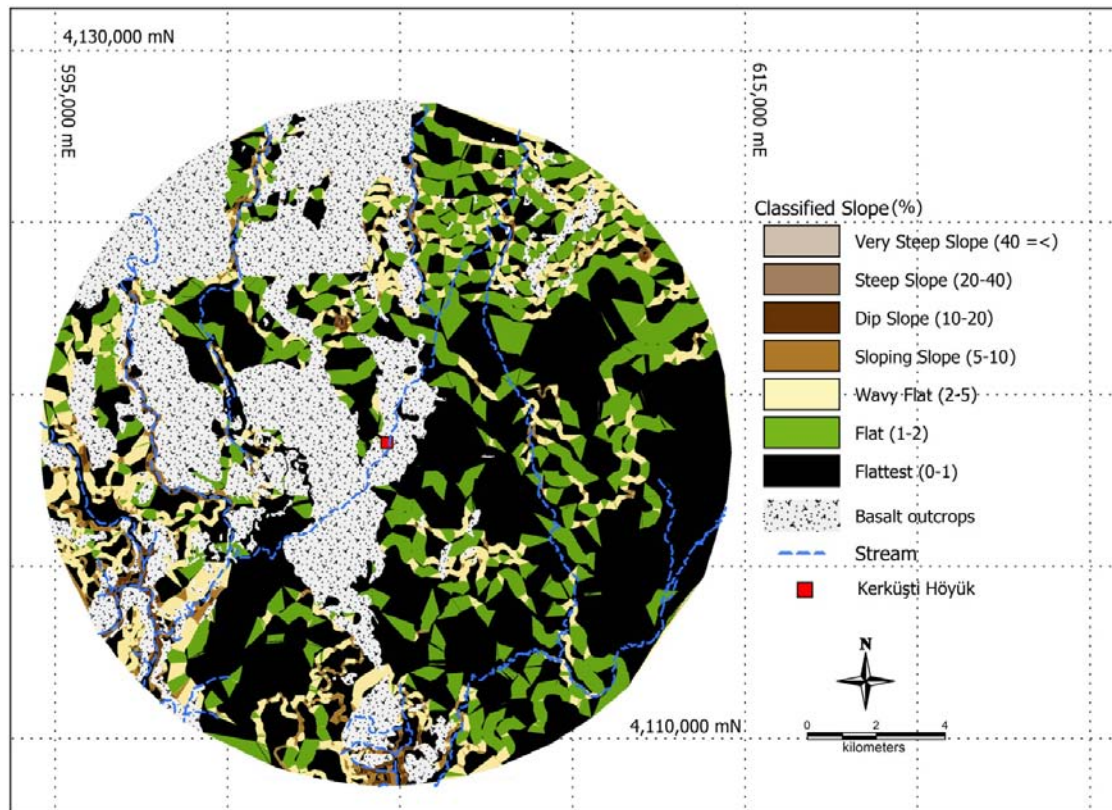


Figure 3. Classified slopes of the study area.

Table 2. Parameters: Attribute is the description of the measurements in the study area.

Without Basalt Outcrops						With Basalt Outcrops					
Radius	Code	Gradient	Area	Pct. (%)	m2	Radius	Code	Gradient	Area	Pct. (%)	m2
1km	TD	Flattest	6242	64.70	624200	1km	B	Basalt Outcrop	31156	76.36	3115600
	D	Flat	3069	31.81	306900		TD	Flattest	6242	15.30	624200
	DD	Wavy Flat	306	3.17	30600		D	Flat	3069	7.52	306900
	AY	Sloping Slope	30	0.31	3000		DD	Wavy Flat	306	0.75	30600
	EY	Dip slope	0	0.00	0		AY	Sloping Slope	30	0.07	3000
	DY	Steep slope	0	0.00	0		EY	Dip slope	0	0.00	0
	CDY	Very Steep Slope	0	0.00	0		DY	Steep slope	0	0.00	0
			9647	100.00	964700		CDY	Very Steep Slope	0	0.00	0
									40803	100.00	4080300
Radius	Code	Slope	Area	Pct. (%)	m2	Radius	Code	Gradient	Area	Pct. (%)	m2
2km	TD	Flattest	41822	77.40	4182200	2km	B	Basalt Outcrop	108369	66.73	10836900
	D	Flat	10521	19.47	1052100		TD	Flattest	41822	25.75	4182200
	DD	Wavy Flat	1662	3.08	166200		D	Flat	10521	6.48	1052100
	AY	Sloping Slope	31	0.06	3100		DD	Wavy Flat	1662	1.02	166200
	EY	Dip slope	0	0.00	0		AY	Sloping Slope	31	0.02	3100
	DY	Steep slope	0	0.00	0		EY	Dip slope	0	0.00	0
	CDY	Very Steep Slope	0	0.00	0		DY	Steep slope	0	0.00	0
			54036	100.00	5403600		CDY	Very Steep Slope	0	0.00	0
									162405	100.00	16240500
Radius	Code	Slope	Area	Pct. (%)	m2	Radius	Code	Gradient	Area	Pct. (%)	m2
5km	TD	Flattest	297973	57.77	29797300	5km	B	Basalt Outcrop	488224	48.63	48822400
	D	Flat	156159	30.28	15615900		TD	Flattest	297973	29.68	29797300
	DD	Wavy Flat	53610	10.39	5361000		D	Flat	156159	15.55	15615900
	AY	Sloping Slope	5422	1.05	542200		DD	Wavy Flat	53610	5.34	5361000
	EY	Dip slope	1939	0.38	193900		AY	Sloping Slope	5422	0.54	542200
	DY	Steep slope	582	0.11	58200		EY	Dip slope	1939	0.19	193900
	CDY	Very Steep Slope	86	0.02	8600		DY	Steep slope	582	0.06	58200
			515771	100.00	51577100		CDY	Very Steep Slope	86	0.01	8600
									1003995	100.00	100399500
Radius	Code	Slope	Area	Pct. (%)	m2	Radius	Code	Gradient	Area	Pct. (%)	m2
10km	TD	Flattest	1184744	51.33	118474400	10km	B	Basalt Outcrop	1691893	42.30	169189300
	D	Flat	671997	29.11	67199700		TD	Flattest	1184744	29.62	118474400
	DD	Wavy Flat	353106	15.30	35310600		D	Flat	671997	16.80	67199700
	AY	Sloping Slope	65404	2.83	6540400		DD	Wavy Flat	353106	8.83	35310600
	EY	Dip slope	24583	1.07	2458300		AY	Sloping Slope	65404	1.64	6540400
	DY	Steep slope	7164	0.31	716400		EY	Dip slope	24583	0.61	2458300
	CDY	Very Steep Slope	1109	0.05	110900		DY	Steep slope	7164	0.18	716400
			2308107	100.00	230810700		CDY	Very Steep Slope	1109	0.03	110900
									4000000	100.00	400000000

Table 3. The listed parameters of the site location relative to its west and east areas. (with basalt outcrop)

Western side of the settlement						Easternside of the settlement					
Radius	Code	Gradient	Area	Pct. (%)	m2	Radius	Code	Gradient	Area	Pct. (%)	m2
1km	B	Basalt Outcrop	13626	64.56	1362600	1km	B	Basalt Outcrop	17530	88.99	1753000
	TD	Flattest	4094	19.40	409400		TD	Flattest	2148	10.90	214800
	D	Flat	3049	14.45	304900		D	Flat	20	0.10	2000
	DD	Wavy Flat	306	1.45	30600		DD	Wavy Flat	0	0.00	0
	AY	Sloping Slope	30	0.14	3000		AY	Sloping Slope	0	0.00	0
	EY	Dip slope	0	0.00	0		EY	Dip slope	0	0.00	0
	DY	Steep slope	0	0.00	0		DY	Steep slope	0	0.00	0
	CDY	Very Steep Slope	0	0.00	0		CDY	Very Steep Slope	0	0.00	0
			21105	100.00	2110500				19698	100.00	1969800
Radius	Code	Gradient	Area	Pct. (%)	m2	Radius	Code	Gradient	Area	Pct. (%)	m2
2km	B	Basalt Outcrop	60310	75.58	6031000	2km	B	Basalt Outcrop	48059	58.18	4805900
	TD	Flattest	12856	16.11	1285600		TD	Flattest	28966	35.07	2896600
	D	Flat	5189	6.50	518900		D	Flat	5332	6.45	533200
	DD	Wavy Flat	1413	1.77	141300		DD	Wavy Flat	249	0.30	24900
	AY	Sloping Slope	31	0.04	3100		AY	Sloping Slope	0	0.00	0
	EY	Dip slope	0	0.00	0		EY	Dip slope	0	0.00	0
	DY	Steep slope	0	0.00	0		DY	Steep slope	0	0.00	0
	CDY	Very Steep Slope	0	0.00	0		CDY	Very Steep Slope	0	0.00	0
			79799	100.00	7979900				82606	100.00	8260600
Radius	Code	Gradient	Area	Pct. (%)	m2	Radius	Code	Gradient	Area	Pct. (%)	m2
5km	B	Basalt Outcrop	330974	65.35	33097400	5km	B	Basalt Outcrop	157250	31.61	15725000
	TD	Flattest	86369	17.05	8636900		TD	Flattest	211604	42.53	21160400
	D	Flat	60503	11.95	6050300		D	Flat	95656	19.23	9565600
	DD	Wavy Flat	23358	4.61	2335800		DD	Wavy Flat	30252	6.08	3025200
	AY	Sloping Slope	3022	0.60	302200		AY	Sloping Slope	2400	0.48	240000
	EY	Dip slope	1614	0.32	161400		EY	Dip slope	325	0.07	32500
	DY	Steep slope	567	0.11	56700		DY	Steep slope	15	0.00	1500
	CDY	Very Steep Slope	86	0.02	8600		CDY	Very Steep Slope	0	0.00	0
			506493	100.00	50649300				497502	100.00	49750200
Radius	Code	Gradient	Area	Pct. (%)	m2	Radius	Code	Gradient	Area	Pct. (%)	m2
10km	B	Basalt Outcrop	1150904	57.12	115090400	10km	B	Basalt Outcrop	540989	27.25	54098900
	TD	Flattest	382147	18.97	38214700		TD	Flattest	802597	40.43	80259700
	D	Flat	220540	10.95	22054000		D	Flat	451457	22.74	45145700
	DD	Wavy Flat	188824	9.37	18882400		DD	Wavy Flat	164282	8.28	16428200
	AY	Sloping Slope	46597	2.31	4659700		AY	Sloping Slope	18807	0.95	1880700
	EY	Dip slope	18617	0.92	1861700		EY	Dip slope	5966	0.30	596600
	DY	Steep slope	6210	0.31	621000		DY	Steep slope	954	0.05	95400
	CDY	Very Steep Slope	1084	0.05	108400		CDY	Very Steep Slope	25	0.00	2500
			2014923	100.00	201492300				1985077	100.00	198507700

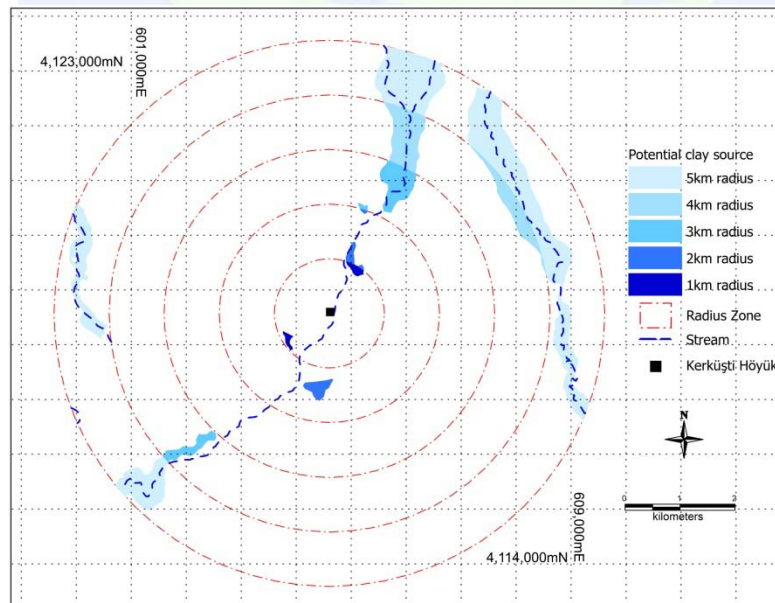


Figure 4. Potential clay source of the study area (in 5km radius)

According to the classification given by considering all the data, the potential clay sources likely to be picked up in the immediate vicinity of the settlement have been determined. So that, the potential clay sources in the 1 km radius 0.069km² (1.10%), in 2 km radius 0.170 km² (2.71%), in 3 km radius 0.390 km² (6.23%), in 4 km radius 1.206 km² (19.27%) and in 5 km radius 4.425 km² (70.69%) are covered of the selected zone.

Considering the quantities of pottery ware used and/ or manufactured at the Kerküsti Höyük during the Halaf Period and potential clay sources, it can be argued that the obtaining raw material was in middle-range zone (2-5km radius).

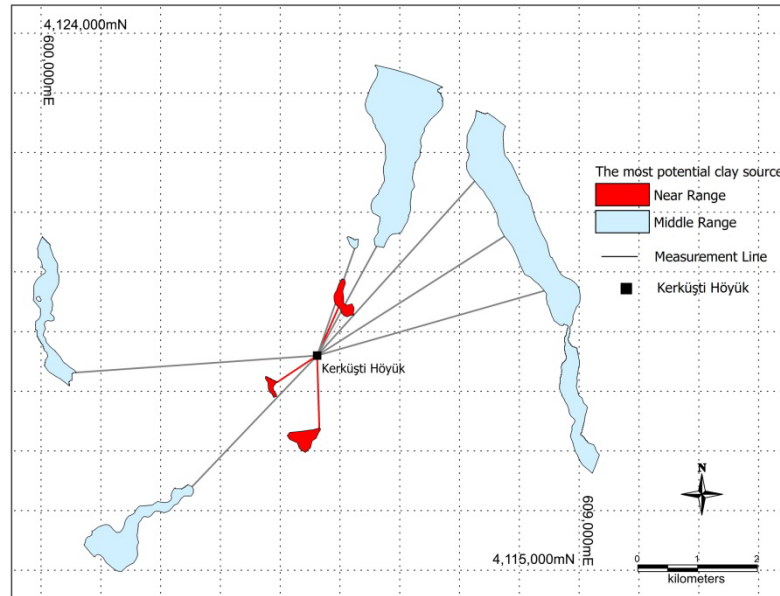


Figure 5. The most potential clay source of the study area (in 5km radius)

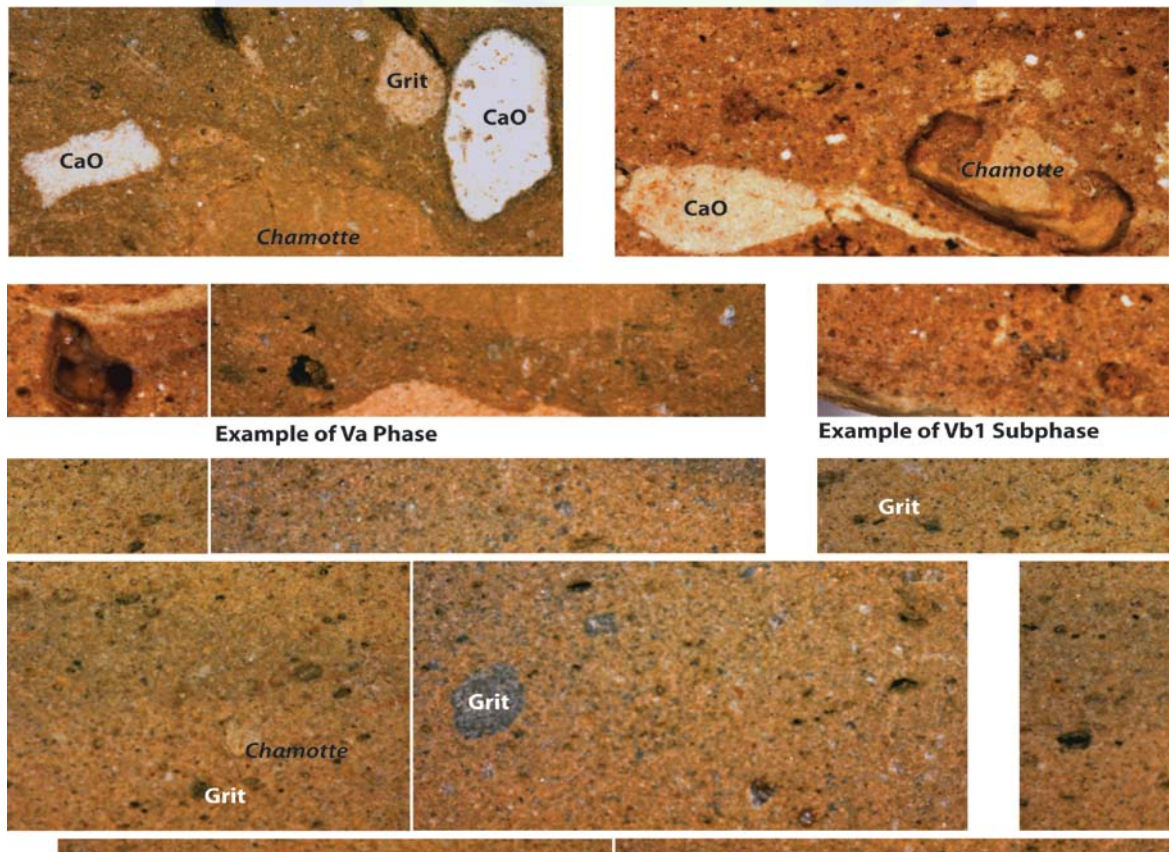


Figure 6. Thin section microphotograph (50x) of pottery from phases Va-Vb.

Based on EDX/SEM analyses data show that the pottery production at Kerküşti is pointed to various geological units. In the first subphases (Va-Vb1), the amount of lime particles in the pottery paste is much more and the size is more apparent. However, with the subphase Vb2, this rate is the opposite. Despite this decrease in lime fractions, both in the subphase Vb2 and the succeeding phases, iron mineral in the pottery paste increased in both quantity and size as compared to the ones of the first two subphases (Va-Vb1). Both field observations and SEM images show that these samples have different grain size and also different mineralogical compositions.

Frankly, EDX analyses of the sherds from the first two subphases (Va and Vb1) demonstrate predominance of O (37,11%), Ca (31,24%), C (18,83%) and Fe (3,35%). In spite of that, the mineral composition of the ones in the later subphases (Vb2 and Vb3) is as follows: O (26,06%), Ca (7,59%), C (6,08%) and Fe (35,75%). Beside these minerals, there are also some other minerals in less amount.

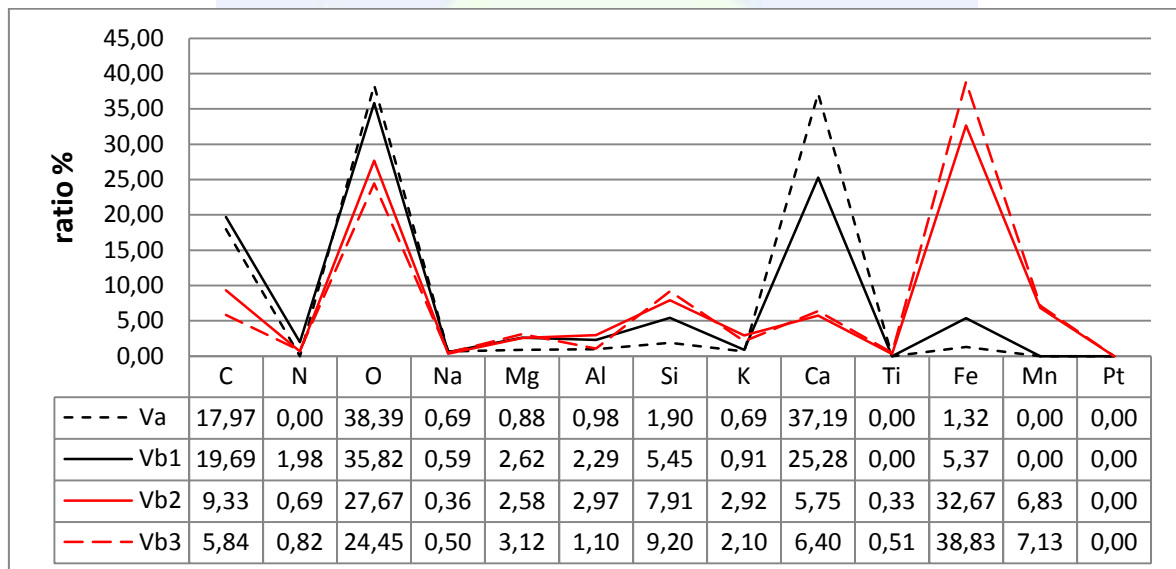


Figure 7. Element distribution of each subphase from Halaf pottery.

CONCLUSIONS

This investigation shows both the validity and the necessity of further research of the potential clay sources in the study area. This case study, which has been implemented through the use of GIS technologies, is applicable to other settlements of the Halaf period. It should be noted that the above-mentioned methods and approaches can be used in such activities, and the use of GIS should be made effective by making it widespread.

Taking into account the limitations of all data: great amount of large calcium carbonate (CaCO_3) particles can be detected in the paste of the pottery of subphases Va and Vb1 whereas the paste used during the subphases Vb2 and Vb3 has less amount of tiny calcium carbonate particles. This striking difference in the combination of paste/clay may have

been explained as a choice of different clay sources and/or of different techniques comes through various contacts.

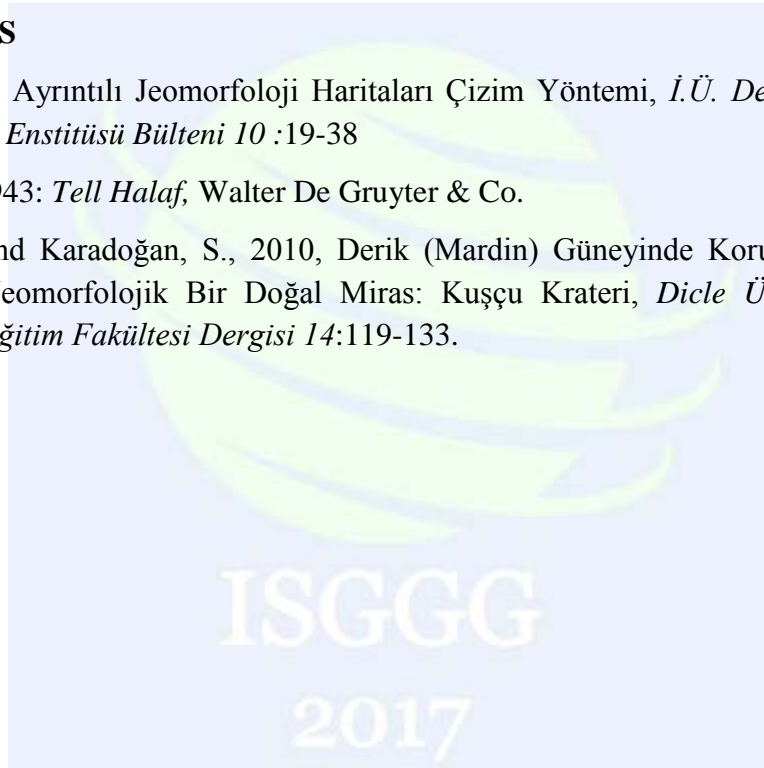
According to GIS data; the possibility of exploiting clay sources from the immediate vicinity (5km radius) of the settlement for pottery manufacturing especially from the eastern part of the Kerküşti Höyük, is very high.

ACKNOWLEDGMENTS

First and foremost, I would like to thanks Fatih SUCU, Zeynep KEZER and Kadriye TOY form Başarsoft for they patience and good advice. Besides, thanks to Assoc. Prof. Dr. Aslı ERİM ÖZDOĞAN for allowing me to use of her original site records.

REFERENCES

- Erol, O., 1993, Ayrıntılı Jeomorfoloji Haritaları Çizim Yöntemi, *İ.Ü. Deniz Bilimleri ve Cografya Enstitüsü Bülteni 10* :19-38
- Schmidt, H., 1943: *Tell Halaf*, Walter De Gruyter & Co.
- Yıldırım, A. and Karadoğan, S., 2010, Derik (Mardin) Güneyinde Korunması Gereken Jeolojik-Jeomorfolojik Bir Doğal Miras: Kuşçu Krateri, *Dicle Üniversitesi Ziya Gökalp Eğitim Fakültesi Dergisi 14*:119-133.





Conservation of Wetland Based on Ecological Sensitivity Analysis: A case Study of Kizilirmak Delta

Kemal Ersayin¹, Sermin Tagil^{*2}

¹Department of Geography, Gaziosmanpasa University, Tasliciftlik Campus, 60250, Turkey e-mail: kemal.ersayin@gop.edu.tr

²Department of Geography, Balikesir University, Cagis Campus, 10145, Turkey e-mail: stagil@balikesir.edu.tr

ABSTRACT

Wetlands that are natural museum are important part of the earth with natural richness and economic importance. At the same time, wetlands have ability to become a part of cultural heritage by influencing the tradition around them. For these reasons, the conservation of wetlands is an significant issue nowadays. In conservation activities that aimed to establish a balance between human and nature, ecological sensitivity analysis is an effective method determining the priority areas for protection since the regional eco-environmental components are assessed holistically. Geographic Information System (GIS) technologies are important tool that increase the effectiveness and scientific value of ecological sensitivity analyzes with powerful spatial data and computational capability. Kizilirmak (Halys) Delta, which is a case study area, is a very important wetlands with many different and important habitats. Also, it is a area where strong competition between human and nature owing to economic attractive. For these reasons, Kizilirmak Delta is choosed as a case study area. The aim of the study in this context; find out ecosystem areas which have high level ecological sensitivity depending on natural and anthropogenic factors and make suggestion for sustainable use of these areas. In the study, ecological sensitivity was tried to be determined using a multi-parameter model. First, factors having an impact on ecological sensitivity has been determined with literature review and field works. These factors considered in the study; elevation, land use, soil, water systems, population density, settlements and roads. The weights of this factors in multi-parameter model has been determined with Analytic Hierarchy Process (AHP) method. Sensitivity and risk values which obtained are classified as; extremely sensitivity and risky, highly sensitivity and risky, moderately sensitivity and risky, light sensitivity and risky, non-sensitivite and risk. It has been determined that 11% of the delta is extremely and highly sensitivity and risky zone.

* Corresponding Author

INTRODUCTION

Wetlands are defined differently according to their purposes by the countries, scientists or different organizations. Scientifically, wetlands are defined as the ecosystems which constantly or periodically have surface waters or where hydrophytes can grow because hydric soil is always available (Cagırankaya and Koyluoglu, 2013). Wetlands, accepted as the natural wealth museums of the world due to their biodiversity, constitute one of the most important ecosystems of the earth by their natural functions. Their contributions to the physical environment include feeding and storing the underground water, adjusting the water regime by flood control, coastal stabilization, microclimate stabilization, supporting the food chain by retaining and delivering the nutrients, and increasing the water quality by trapping the residues and toxic substances. If sustainable and well-planned, their economic contributions include salt production, aquaculture, straw, timber, grazing, drinking, utility and irrigation water, transportation and tourism (Erdem, 2013). All these functions clearly reveal the importance of the wetlands. With their economic attractions and opportunities, wetlands constitute the fields where human activities become denser and this lead to a human-wildlife conflict in wetlands. This conflict points out the need to protect the wetlands which also constitutes the problem of the study.

Recently, there are important increases in the methods where ecological conditions and integrity are assessed to protect the wetlands. In parallel to this increase, studies assessing the methods used are also carried out (Abbruzzese and Leibowitz, 1997; Carletti, Leo and Ferrari, 2004; Fennessy, Jacobs and Kentula, 2007). The basic purposes of the wetland monitoring and assessment studies include reporting the ambient condition of the wetland resources, trying to influence the decision-makers by directing the management activities and making a positive contribution to the protection activities. The most effective way to make this contribution is to define the ecological risks and the reasons of ecological sensitivity, and accordingly, to develop a map consisting of wetland zones. In short, it is necessary to make an ecological planning for wetlands.

In ecological planning, ecological sensitivity analyses are the most effective methods for assessing the regional eco-environmental components to determine the environment with protection priority (Liang and Li, 2012). The importance of the ecological sensitivity analyses in protecting the wetlands are examined in Kizilirmak Delta example in this study. In addition to its rich biodiversity created by its wetlands, the dense anthropogenic pressure in Kizilirmak Delta was an effective factor in selecting this area.

MATERIAL AND METHOD

Study Area

Study area covers Kizilirmak Delta being the largest delta plain of the Black Sea region and the third largest one of Turkey. The total area surface is 52779 ha (Figure 1).

Coexisting habitats of several ecological characters such as sea, river, lake, reed bed, swamp, meadow, pasture, forest, dune and agricultural areas, richness in nutrients and favorable climate conditions have enabled the delta area to accommodate a very rich

biodiversity (Yavuz, 2011). For all these reasons, Kizilirmak Delta is an important area both nationally and internationally. It was declared as one of 122 important plant areas of our country due to its rare plant species. It is also internationally important in terms of ornithology. More than 320 bird species (75% of the known bird species in Turkey) use this area for reproduction, wintering and migration (Hustings and Dijk, 1992). For all this richness, different parts of the delta are protected under 3 different statuses (Ramsar, Natural Site and Wildlife Improvement Area).

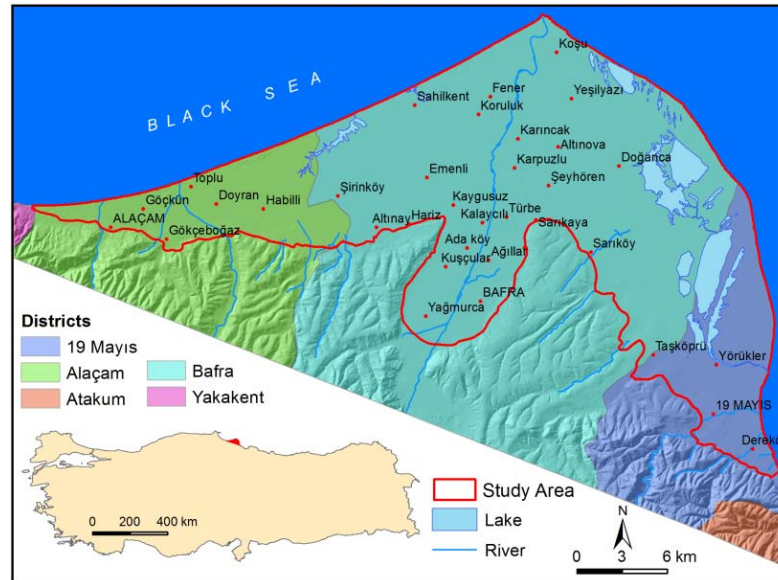


Figure 1. Study area.

Table 1. Data sources and features.

Parameters	Source	Features
Elevation	Military	1/25.000 scale digital topography map
Land Use	Bafra-Forest Management Institution, 2005 Landsat ETM+	Land use map was produced with forest management map. Verification was made from satellite images.
Soil	Ministry of Food, Agriculture and Livestock	1/25.000 scale soil map. Major soil groups was considered.
Water surfaces	Bafra-Forest Management Institution, 2005 Landsat ETM+, Esri Basemap	Stream network, channels and lakes data were collected and corrected from different sources.
Population density	TÜİK, Esri Basemap, Google Earth vb.	The amount of population was obtained from Turkish Statistical Institute. According to the function, settlements divided into rural and urban areas.
Settlements		
Transportation density	Bafra-Forest Management Institution, Esri Basemap	Road data was obtained from forest management map. Also deficiencies of this map was fixed using Esri Basemap. Classified as asphalt, soil and stabilized.

Material

In this study assessing the ecological sensitivity to protect the wetlands, firstly the parameters affecting the sensitivity were specified considering the study area. Literature was taken into account in this stage. Field studies were also considered based on the fact that they control on-site sensitivity. As stated by Zhang et al., (2009) several factors lead to regional ecological and environmental problems and these factors vary from region to region. Land surveys were carried out in 2015 August and April. In addition to the land

observations, methods of meeting and interview both with the academics and volunteers working in the field and with the local people, and information on the area was collected by open-ended questions. As a result, seven parameters affecting the ecological sensitivity in the delta area were determined: elevation (1), land use (2), soil (3), water surfaces (4), population density (5), settlements (6), transportation density (7). Parameter data and their resources are provided in Table 1.

UTM (Universal Transverse Mercator) WGS 84 UTM Zone 36 N coordinate system was used in the study. The resolution of 15×15m was used when converting all numerical maps into raster format.

Method

The ecological sensitivity analysis that can serve as an important basis to protect the wetlands has some stages. The first one of them is to determine the parameters and parameter class weights in a study assessing the ecological sensitivity with a multi-parameter model. This is difficult because there are complicated relations between the parameters and these relations are not the same everywhere. Each parameter class should be weighted based on its importance. The weights given are responsible for the accuracy of the results (Liang et al., 2007; Wang et al., 2011). The most suitable way to clear this hurdle is to use the Analytic Hierarchy Process (AHP) among the "Multi-Criteria Decision Making" methods (Cai et al., 2011; Gao and Zhang, 2011). By this method, objective and subjective decision criteria can be compared and a ranking can be obtained as a result of the weighting based on different decision criteria (Saaty, 1980). In this context, the weights of the parameters obtained in the study and their sub-classes are provided in Table 2.

Table 2. Classes and weights of assessment parameters.

No	Parameters	Classes of parameters		Weights of classes		Weight of Parameters
1	Elevation (m)	0-3		0,51	0,34	
		3-5		0,29		
		5-10		0,11		
		10-15		0,06		
		>15		0,03		
2	Land Use	Swamp		0,39	0,16	
		Coastal dune		0,23		
		Stream bed		0,15		
		Bare land		0,07		
		Forest		0,11		
		Agricultural		0,03		
		Settlement		0,02		
3	Soil	Hydromorphic		0,64	0,24	
		Coastal dune		0,28		
		Alluvium		0,08		
4	Water surfaces	Rivers and channels (m)	< 50	0,64	0,40	0,11
			50-100	0,26		
			100-200	0,11		
			>200	0,00		
		Lake (m)	< 50	0,64	0,60	
			50-100	0,26		
			100-200	0,11		
			>200	0,00		

Table 2. continued						
5	Population density (person/km ²)	0		0,51		0,07
		0-40		0,26		
		40-70		0,13		
		70-120		0,07		
		> 120		0,03		
6	Settlements	Urban (m)	< 250	0,56	0,70	0,05
			250-500	0,26		
			500-1000	0,12		
			1000-2000	0,06		
			> 2000	0,00		
		Rural (m)	< 250	0,56	0,30	
			250-500	0,26		
			500-1000	0,12		
			1000-2000	0,06		
			> 2000	0,00		
7	Transportation density	Soil and stabilized road (m)	< 200	0,57	0,30	0,03
			200-600	0,28		
			600-1200	0,11		
			1200-2000	0,04		
			> 2000	0,00		
		Asphalt road (m)	< 200	0,57	0,70	
			200-600	0,28		
			600-1200	0,11		
			1200-2000	0,04		
			> 2000	0,00		

While AHP has a special advantage in assessing many factors or criteria, it is not able to show the spatial distribution of these factors or criteria. In the study, Geographical Information Systems (GIS) completed this lack of the AHP with its strong spatial analysis function. The spatial distribution of the sensitivity on and around Kizilirmak Delta wetland was determined by applying the weighted superposition method to the parameters classified in GIS environment before and whose sub-class weights were given. The following formula was used when assessing the ecological sensitivity:

$$S_{ij} = \sum_{k=1}^n W(k) C_{ij}(k) \quad (1)$$

In the formula (1), S_{ij} reflects the ecological sensitivity value in each cell. $k=1, 2, \dots, n$ are the parameters effective on the ecological sensitivity. $W(k)$ means the importance weight of the ecological parameters. $C_{ij}(k)$ corresponds to the sensitivity level in each level of the factors (Gao and Zhang, 2011; Li et al., 2010; Wang, Tian, and Cui, 2009). The weight values given in table 2 were used in the formula.

RESULTS AND DISCUSSIONS

Elevation Change

Despite the absence of an important elevation difference, the existing small elevation differences may lead to the influences such as altered ground water level, limited drainage, injectability of the sea water, wetland formation and habitat change. The delta was classified from the most ecologically sensitive areas to the least sensitive ones with the help of Kizilirmak Delta's conditions and the literature, and their weights were determined (Table 3). The areal distribution of these areas were also specified (Figure 2a).

Table 3. Spatial distribution of parameters and weights of classes

Parameter classes	Area		Weight of Class	Parameter classes	Area		Weight of Class
	km ²	%			km ²	%	
Elevation (m)				Population density (person/km ²)			
0-3	187,18	37,75	0,51	0	60,39	12,18	0,51
3-5	108,42	21,87	0,29	0 - 40	156,82	31,63	0,26
5-10	108,1	21,8	0,11	40 - 70	113,75	22,94	0,13
10-15	50,03	10,09	0,06	70 - 120	83,99	16,94	0,07
> 15	42,11	8,49	0,03	> 120	80,85	16,31	0,03
Rivers and channels (m)				Lakes (m)			
0-50	22,59	4,56	0,64	0-50	9,69	1,96	0,64
50-100	22,08	4,45	0,26	50-100	8,7	1,76	0,26
100-200	43,1	8,69	0,11	100-200	14,47	2,92	0,11
> 200	407,99	82,29	0	> 200	462,91	93,37	0
Urban settlements (m)				Rural settlements (m)			
0-250	33,04	6,66	0,56	0-250	69,41	14	0,56
250-500	7,35	1,48	0,26	250-500	52,58	10,61	0,26
500-1000	11	2,22	0,12	500-1000	110,6	22,31	0,12
1000-2000	23,48	4,74	0,06	1000-2000	145,59	29,37	0,06
> 2000	420,92	84,9	0	> 2000	117,61	23,72	0
Asphalt roads (m)				Soil-Stabilized roads (m)			
0 - 200	63,82	12,87	0,57	0 - 200	211,02	42,56	0,57
200 - 600	87,09	17,57	0,28	200 - 600	175,61	35,42	0,28
600 - 1200	88,82	17,92	0,11	600 - 1200	59,93	12,09	0,11
1200 - 2000	83,44	16,83	0,04	1200 - 2000	26,56	5,36	0,04
> 2000	172,62	34,82	0	> 2000	22,68	4,57	0
Land Use				Soil			
Agriculture	325,75	65,1	0,03	Alluvium	416,85	84,01	0,08
Swamp	78,74	15,7	0,39	Hydromorphic	60,85	12,26	0,64
Settlement	44,32	8,9	0,02	Coastal dune	18,48	3,73	0,28
Coastal dune	18,47	3,7	0,23				
Bare land	12,65	2,5	0,07				
Forest	12,02	2,4	0,11				
Stream bed	8,49	1,7	0,15				

The ground water level is very high under the elevation of two meters on the delta area, and studies showed that it approximated to the surface for up to one meter in rainy periods (Arslan, 2007). At the same time, the halophytes that can survive with a high salt concentration spread over the low parts of the delta area. All these reasons increase the ecological value and sensitivity of the lowest parts of the area.

Land Use Differentiation

Being sensitive to the changes in the circle of the natural events and to the human activities, wetlands may easily deteriorate and lose many ecological and economic functions. This also leads to the extinction of the habitats and occurrence of irreversible changes. Kizilirmak Delta is also an area under the intensive pressure of human activities due to its richness. The sub-classes of the land use parameter on the delta area, their weights and areal ratio (Table 3) as well as the land use map (Figure 2b) were generated. When assessed in terms of sensitivity, swamps having the highest sensitivity with their richness and forming the heart of the wetlands constitute the sub-class with the highest sensitivity value. The dunes surrounding the delta area and particularly the lagoon lakes like a shield constitute the sub-class with the second highest sensitivity.

Soil Differentiation

Despite being considered as the inanimate elements of the ecosystem, it is one of the important parts of the system as it accommodates thousands of living beings. The hydromorphic land in Kizilirmak Delta constitutes the sub-class with the highest sensitivity within the soil parameter due to its biodiversity created by being a product of the watery environment and richness in organic substances (Table 3). When considered on the study land scale, the alluvial lands with heavy intensive agriculture represent the class with the least natural sensitivity. The dunes, which ecologically surround not only the accommodated rare habitats but also the wetland behind them (Figure 2c) and serve as a kind of protector of these areas, can be quickly affected by the external factors and damaged. Therefore, dunes were also included in the assessment as one of the sub-classes effective on the ecological sensitivity within soil parameter

Distance to Water Systems

The close surroundings of the aquatic systems that are ecologically important due to their biodiversity are also sensitive areas because of the conditions occurring there. These areas should also be emphasized in terms of ecological integrity (Vaughan et al., 2009). When the wetland ecosystem and its formation mechanism are considered, the importance of the water systems and their close surroundings on the natural environment and ecology at the area is very clear. Four different zones were created around the water systems based on the literature both on the land conditions and the sensitivity assessment (Wang et al., 2011; Wu, Wang, and Mao, 2013) (Figure 2d). The sub-class weights and their area coverage are provided in Table 3.

Population Density

The population increases the pressure on the surrounding natural resources, creates excess demand and leads to destruction with the desire to meet the basic needs such as nutrition and accommodation (Jonhson, 1984). Kizilirmak Delta is also an area with population pressure due to its attractions. This controls the ecological sensitivity in the delta through the accompanied environmental problems. Increased population density makes the protection activities and strategies difficult. Whereas, the most significant purpose of creating protection areas is to minimize the human effect there. Considering all these

matters and that it reflects the spatial difference in Kizilirmak Delta, the sub-classes of population density were determined and they were distributed spatially (Table 3; Figure 2e).

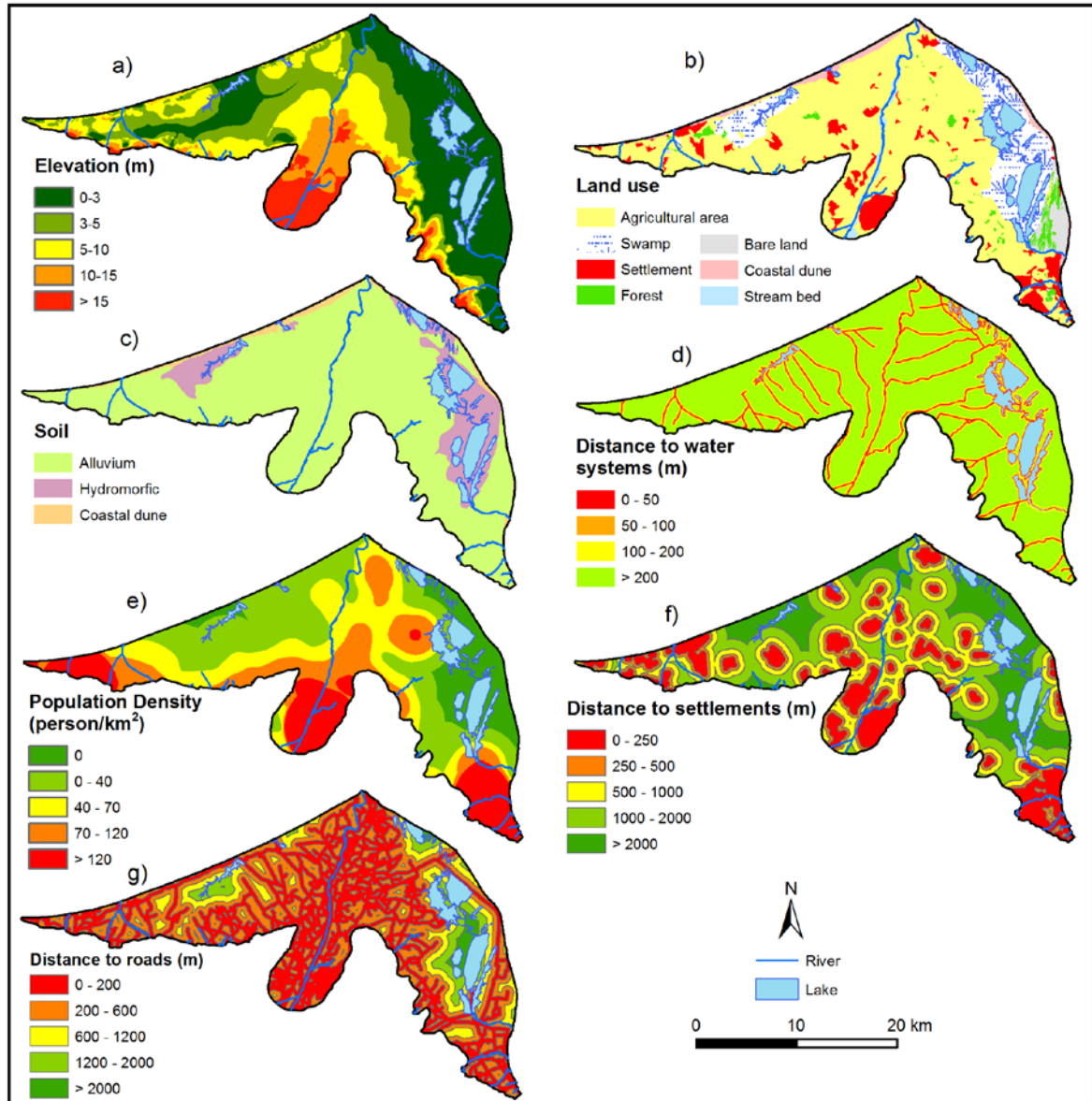


Figure 2. Ecological sensitivity and risk parameters.

Settlement Distribution

People settle on a space in two different ways, i.e. rural and urban. Urban areas are more active in increasing the risk level and ecological sensitivity in the natural environment. Therefore, the sensitivity weight of the urban settlements were taken into account so as to be higher than that of the rural settlements in the study (Table 2). Settlements create ecological sensitivity and risk not only within their area coverage but also on the surrounding areas (Radeloff et al., 2005). Considering this and the studies performed (Wang et al., 2011; Wu et al., 2013), tampon regions were created around the settlements

(Figure 2f). The class weights of the tampon regions were determined based on the assumption that the one being nearest to the settlements created more ecological risks (Table 3). The settlements in Kizilirmak Delta are generally accumulated around the town centers and between the lagoon lakes and Kizilirmak River (Halys). Secondary residences within the borders of the protection areas in the delta constitutes an important problem in the context of settlements. Summer residence areas are increasingly spreading around Dereköy located at the east of the delta and they continue to develop inside the delta.

Distance to Roads and Paths

Roads constitute an anthropogenic element which emerges with the existence of two parameters (population and settlement) emphasized previously and has varying densities and effective areas based on these two parameters. Ecologically, roads influence the natural environment with the results such as decreased plant and animal populations, limited movements of the species, creating avoidance behavior on the fauna, pollution in water systems, impaired erosion and sediment balance, chemical pollution in the atmosphere, impaired natural vegetation due to the introduction of the exotic species, habitat fragmentation and reduction (Develey and Stouffer, 2001; Forman and Alexander, 1998). The negative effects caused by the roads may be observed with a distance of several meters to several kilometers from the road within the ecosystem. These areas are defined as “road effect zone”. Zoning was performed around the roads on the area considering this study aiming to protect the Kizilirmak Delta wetlands and the literature (Table 2). Additionally, two sub-classes including asphalt roads and stabilized-soil roads were created based on the information that the roads with larger traffic volume cause bigger habitat and population problems (Forman, 2000). The weights and proportional distributions of these sub-classes and road effect zones are provided in Table 3. The fact that the roads spread on almost the entire area in Kizilirmak Delta cause increased sensitivity. The total length of the roads in the delta amounts to 783 km. The road density equals to 1581 m/km^2 .

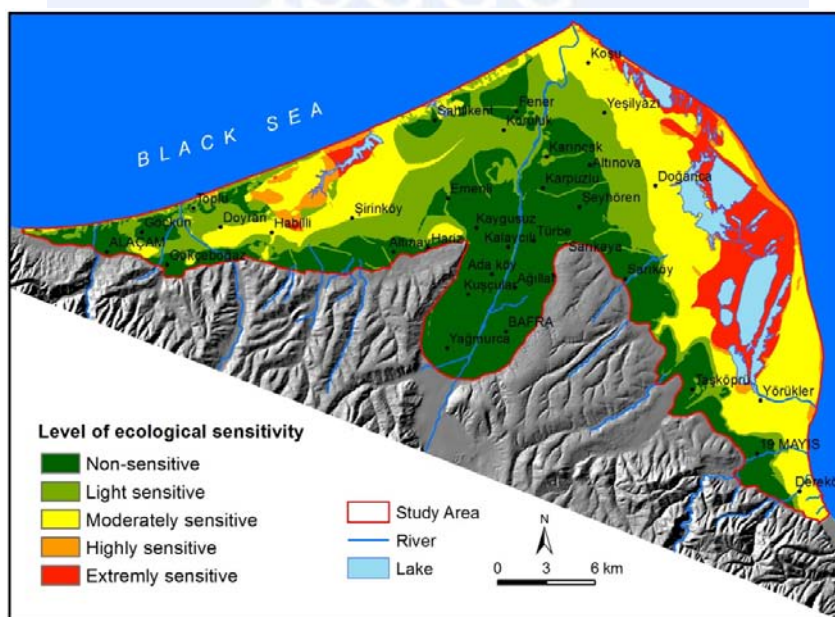


Figure 3. Ecological sensitivity and risk zones.

Ecological Sensitivity and Risk Zones

The sensitive regions were determined as a result of the comprehensive assessment made using the seven parameters described above (Figure 3). The parameters of elevation, soil and land use were more determinative than the other parameters as they had a higher importance weight (Table 2). If the protection of a wetland which has been already formed by river accumulation, the parameter of elevation has a determinative quality itself.

As a result, the eastern coasts of the delta were determined to have areas with a higher level of sensitivity. On the western coasts, the relatively lower part surrounding Karabogaz lake is observed to be an area with high ecological sensitivity. Particularly at the entire delta area, the lakes located near the sea level and the soil created around them as well as the land use type turn them into areas with a high ecological sensitivity. The ecological sensitivity was determined to be extremely on the area of 44.83 km² (%9) at and around the lagoon lakes. A high sensitivity was determined on the area of 16.99 km² (%3.4) the majority of which corresponded to the dunes around the delta area. Moderately sensitivity areas were determined to be 141.75 km² (29%), light sensitivity and risk areas were determined to be 113.66 km² (22.97%), and no sensitivity areas were determined to be 177.66 km² (35.88%).

CONCLUSION

Wetlands are multi-functional complex systems; therefore, it is more beneficial to assess them as an integrated ecosystem in area or basin basis rather than individual parts of it (Turner et al., 2000). In this study aiming to serve as a basis to protect the wetlands in Kizilirmak Delta, the study area covered not the borders of the wetlands, but the complete delta area. This shows that the ecological sensitivity assessment can be applied integratively to the area.

Time and cost constitute the major problem in the methods used to assess the wetlands (Carletti et al., 2004). The time advantage of the ecological sensitivity analysis, its cost efficiency, simplicity and ability to be directed for different purposes puts forth that it is an important method in protecting the wetlands.

An important aspect of the wetland management is to define the ecological risks affecting the region and develop a wetland zoning map based on these risks (Malekmohammadi and Blouchi, 2014). The ecological sensitivity analysis showing the areas with different ecological sensitivity in regional basis by using the GIS technologies also provides an advantage in wetland management from this aspect.

REFERENCES

- Abbruzzese, B. and Scott G. L., 1997. Environmental Auditing: A Synoptic Approach for Assessing Cumulative Impacts to Wetlands. *Environmental Management* 21(3): 457–75.
- Arslan, H., 2007. Assessment of groundwater quality in Bafra plain for irrigation. *Jour. of*

Tekirdag Agr. Fac. 4: 219-226

- Cagırankaya, S. and Koyluoglu, F., 2013. The concept of wetland, what is wetland ? and classification of wetlands. pp. 7–38 in *Wetlands*. Ministry of Forestry and Water Management: Ankara.
- Cai, Z., Zhong, S., Jiang, W. and Lei, M., 2011. A Schema of Ecological Environment Sensitivity Evaluation Based on GIS. *2011 International Conference on Multimedia Technology* 5250–55. Retrieved
- Carletti, A., Giulio, L. and Ferrari, I., 2004. A Critical Review of Representative Wetland Rapid Assessment Methods in North America. *Aquatic Conservation: Marine and Freshwater Ecosystems* (14):103–13.
- Develey, P. F. and Stouffer P. C., 2001. Effects of Roads on Movements by Understory Birds in Mixed-Species Flocks in Central Amazonian Brazil. *Conservation Biology* 15(5):1416–22.
- Erdem, O., 2013. Importance, function and values of wetlands. pp. 67–80 in *Wetlands*. Ministry of Forestry and Water Management: Ankara.
- Fennessy, M. S., Jacobs, A. D. and Kentula, M. E., 2007. An Evaluation of Rapid Methods for Assessing the Ecological Condition of Wetlands. *Wetland* 27(3):543–60.
- Forman, R. T. T., 2000. Estimate of the Area Affected Ecologically by the Road System in the United States. *Conservation Biology* 14(1):31–35.
- Forman, R. T. T., and Alexander, L. E., 1998. Roads and Their Major Ecological Effects. *Annual Review of Ecology and Systematics* 29:207–31.
- Gao, C. and Zhang, J., 2011. Ecological Sensitivity Analysis in Wuhan City Based on RS and GIS. *2011 International Conference on Remote Sensing, Environment and Transportation Engineering* 251–54.
- Hustings, F. and Dijk, K., 1992. Bird Census in the Kizilirmak Delta, Turkey, in Spring 1992.
- Jonhson, B., 1984. Nufus Artısı ve Cevreyle İlgili Beklentiler. Pp. 98–119 in *Yerlesim ve Cevrebilim Sorunları*, edited by R. Keles. Turk Sosyal Bilimler Dernegi.
- Li, J., Hu, Y., Liu, Z. and Liu, M., 2010. Ecological Suitability Evaluation for Eco-Tourism in Qipanshan Area. *2010 International Conference on Web Information Systems and Mining* 112–19. Retrieved November 3, 2014
- Liang, C. and Li, X., 2012. The Ecological Sensitivity Evaluation in Yellow River Delta National Natural Reserve. *Clean - Soil, Air, Water* 40(10):1197–1207.
- Liang, T., Cai, C. X., Liu, M. and Peng, X. L., 2007. Study on Methodolgy of Ecological Suitability Assessment of Urban Landscape, an Example of Pingxiang. *Geographical Research* 27:782–88.
- Malekmohammadi, B. and Blouchi, L., 2014. Ecological Risk Assessment of Wetland Ecosystems Using Multi Criteria Decision Making and Geographic Information

- System. *Ecological Indicators* 41:134–44. Retrieved
- Radeloff, V., Hammer, R. B., Stewart, S. I., Fried, J. S., Holcomb, S. S. and McKeefry, J. F., 2005. The Wildland-Urban Interface in the United States. *Ecological Applications* 15(3):799–805.
- Saaty, T. L., 1980. *The Analytical Hierarchical Process*. New York, USA: J. Wiley.
- Turner, R. K., Jeroen, C. J. M., Bergh, V. D., Söderqvist, T., Barendregt, A., Straaten, J., Maltby, E. and Ierland, E. C., 2000. Ecological-Economic Analysis of Wetlands: Scientific Integration for Management and Policy. *Ecological Economics* 35(1):7–23.
- Vaughan, I. P., Diamond, M., Gurnell, A. M., Hall, K. A., Jenkins, A., Milner, N. J., Naylor, L. A. Sear, D. A., Woodward, G. and Ormerod, S. J., 2009. Integrating Ecology with Hydromorphology: A Priority for River Science and Management. *Aquatic Conservation: Marine and Freshwater Ecosystems* 19:113–25.
- Wang, D., Wang, M., and Liu, J., 2011. Ecological Sensitivity Assessment in Taierzhaung Based on '3S' technology. *Remote Sensing, Environment and Transportation Engineering (RSETE), 2011 International Conference* 255–58.
- Wang, K., Tian, G. H. and Cui, L., 2009. Ecological Sensitivity Analysis in Tongshan Scenic Spot Based on GIS and RS. *Journal of Northeast Forestry University* 37:200–203.
- Wu, X., Wang, Y. and Mao, W., 2013. GIS Based Construction Land Layout in Ecological Area. *International Journal of Computer Science Issues* 10(1):25–30.
- Yavuz, K. E., 2011. Onemli Bir Doga Alanı: Kizilirmak Deltasi. *Samsun Sempozyumu* 2011.
- Zhang, L., Liu, L. Q., Hu, H. B. and Dong, Y. W., 2009. Eco-Sensitivity and Countermeasures Based on Regional Development - a Case Study of Qinzhou City. *Journal of Ecology and Rural Environment* 25(3):16–20.

Study of the Coastal Wave Energy Propagation Using GIS and Hydrodynamic Model

Amarouche Khalid¹, Bachari Nour-El-Islam^{*2} and Houma Fouzia¹

¹ The Marine and Coastal Ecosystems Laboratory at the National School of Marine Sciences and Coastal Management (ENSSMAL/ Campus Dely Ibrahim Bois des Cars, Algiers, Algeria. (e-mail: amarouchekhalid@gmail.com).

² The Spatial Oceanography Laboratory, Faculty of Biological Sciences, University of Science and Technology of Houari Boumedien (USTHB), PO Box 32, El Alia, Bab Ezzouar, 16111 Algiers, Algeria. (e-mail: bacharinouri@gmail.com).

ABSTRACT

The monitoring and study of the wave energy propagation along the coast presents a very difficult task, account of the significant daily variation of the sea states. In this study, we have developed a GIS for the analysis, processing and monitoring of the Wave energy propagation along the coast under these different form. The large number of results led us to carry out a spatial analysis using raster calculator tool, which allowed us to better present and interpreted the SWAN output (simulation wave near-shore model). In order to classify coastal zones with high-energy potential we carried out a spatial multicriteria analysis which allowed us to select three zones in the near-shore with an average wave power greater than 35kW/m on stormy days.

INTRODUCTION

Currently more than 40% of the Algerian population is on the coastal strip, which constitutes 1.8% of the country (Kateb, 2003). This high concentration near the coastline is related to considerable economic activity in various sectors (Magnan, 2009), also the climate change and the high human exploitation in these coastal areas make them more exposed to natural hazards (Simav et al., 2013). Our study area (BouIsmaïl Bay) is located 15 km west of Algiers; it represents an important economic and tourist zone with a coastline of 65 km. Account of the absence of wave and current measuring instruments in this bay, the hydrodynamic regime is unknown. The wave propagation measurements is a fairly expensive and difficult (Bass, 2013; Castelle, 2004) and the number of wave measuring instruments that can be installed in a given period remains limited for economic reasons (Aydoğan et al., 2013). Therefore, we are based on the SWAN model (Simulating Waves Nearshore) version 40.41; a discrete spectral model Based on the wave action balance equation (Booji et al., 1999) add to the meteorological database of 14 years of the weather station located at 36 ° 46 ' N and 03 ° 04' E. Several cases of SWAN model evaluation studies in different regions of the world and with different input data sources have shown the good precision of its output results with an underestimation of significant-heights and periods in some cases (Akpınar et al., 2012; Bottema and Beyer, 2002; Dragani

* Corresponding Author

et al., 2008; Dykes et al., 2002). This underestimation may be related to the input data accuracy (Akpınar et al., 2012).

This study aims to develop a methodology that allows us to study the propagation of the wave energy along the coast and selected areas with high-energy potential. These energies can be destructive or constructive; it may constitute a risk to navigation, mooring, swimming, and erosion, as it may be a favorable resource for the renewable marine energy. The methodology developed is based on a combination between the Swan hydrodynamic model and GIS tools that allows us to represent, communicate and clarify the output data information (Loubersac et al., 2000). GIS allows the storage of multidisciplinary data and allows to inspect the relationships between them in different scales and in a digital format (Szlafrstein & Sterr, 2007). The large amount of numerical information of the input and output data from the hydrodynamic model requires to be stored in a tabular Geodatabases, also a spatial statistical analysis using raster calculator tools has allowed us to better present and interpret our results. To classify the coastal areas with high-energy potential we carried out a spatial multicriteria analysis, which make us to select three station with an average wave power (Et) greater than 35kW/m on stormy days.

Two Geodatabases have resulted from this work, the first includes the input, output data of the hydrodynamic model SWAN, and the second database contains the data processed and analyzed. These data are indicators and tools for decision-making in coastal management projects and for the safety of maritime navigation.

METHODOLOGY

The methodology developed for monitoring the propagation of wave energy along the coast and for the selection of zones with high energy potential can be summarized in two steps:

- 1- The hydrodynamic modeling: Six offshore wave conditions from the N, NNE, NE, E, NW, and W directions were modeled. These six conditions represent the six most violent storms recorded during 14 years by the weather station of the ONM (National Weather Office) (Table.1). The results of the wave energy propagation on stormy days allow us to better observe their behavior even in the most sheltered areas.

Table 1. Condition of the modeled stormy days

Stormy days	14/01/2010	18/02/2015	06/03/2010	21/04/2015	21/10/2011	10/12/2014
Wind speed	>14	>14	>17	>14	>15	>14
Persistence	9h	18h	>15h	15h	9h	12h
Wind direction	280°	360°	100°	22°	40°	330°
Wave height	2.3 m	3.5 m	4.5 m	4 m	3.2 m	2.8 m
Wave periode	6.7 s	9 s	9.5 s	10 s	8.3 m	8 s

- 2- Development of a GIS under ArcGIS10.3 for the processing of results and for the classification of areas with high hydrodynamic potential. This part of our work is summarized in three steps:
 - Creation of the spatial tabular Geo-database and mapping of model results
 - Spatial analysis: It is a spatialized statistical analysis of data (Bachouche et al., 2016). In this section, we calculated the averages, variances, and maximum wave power along the coast using the GIS tool raster calculators.

- •Spatial multi-criteria analysis; to select the nearshore areas with high wave power, whatever the conditions of the offshore wave.

DATA COLLECTION AND PROCESSING

The data used in this study are the wave generating forces and the modifying forces including the winds, the sea level variation and the geostrophic Velocities. Synoptic wind data recorded between 2002 and 2016 were processed to filter out the six most violent storms that blew in six different directions opposite to the coastline. Sea level and current data have been downloaded from the Aviso+ web database in NetCDF format.

RESULTS AND DISCUSSIONS

Numerical modeling of wave energy propagation based on the Swan model allowed us to obtain several results concerning the spatial and temporal variations of the wave physical characteristics in the nearshore whose significant heights, the set-up, the orbital current velocity, the wave energy per area unit and the wave power in Kw/ m. All these results have been mapped and located in the tabular geo-database.

These wave power maps (Figure 1) indicate a significant variation in the wave energy dissipation near the coast. This variation depends mainly to the offshore waves and winds direction. The maximum energies that reach the coastline are observed with storm winds from the northeast sector. According to the National Coast Guard Service (SNGC) the most part of the vessels sinking near the Bouismail Bay was recorded with the winds of North and North-East Sectors.

ISGGG
2017

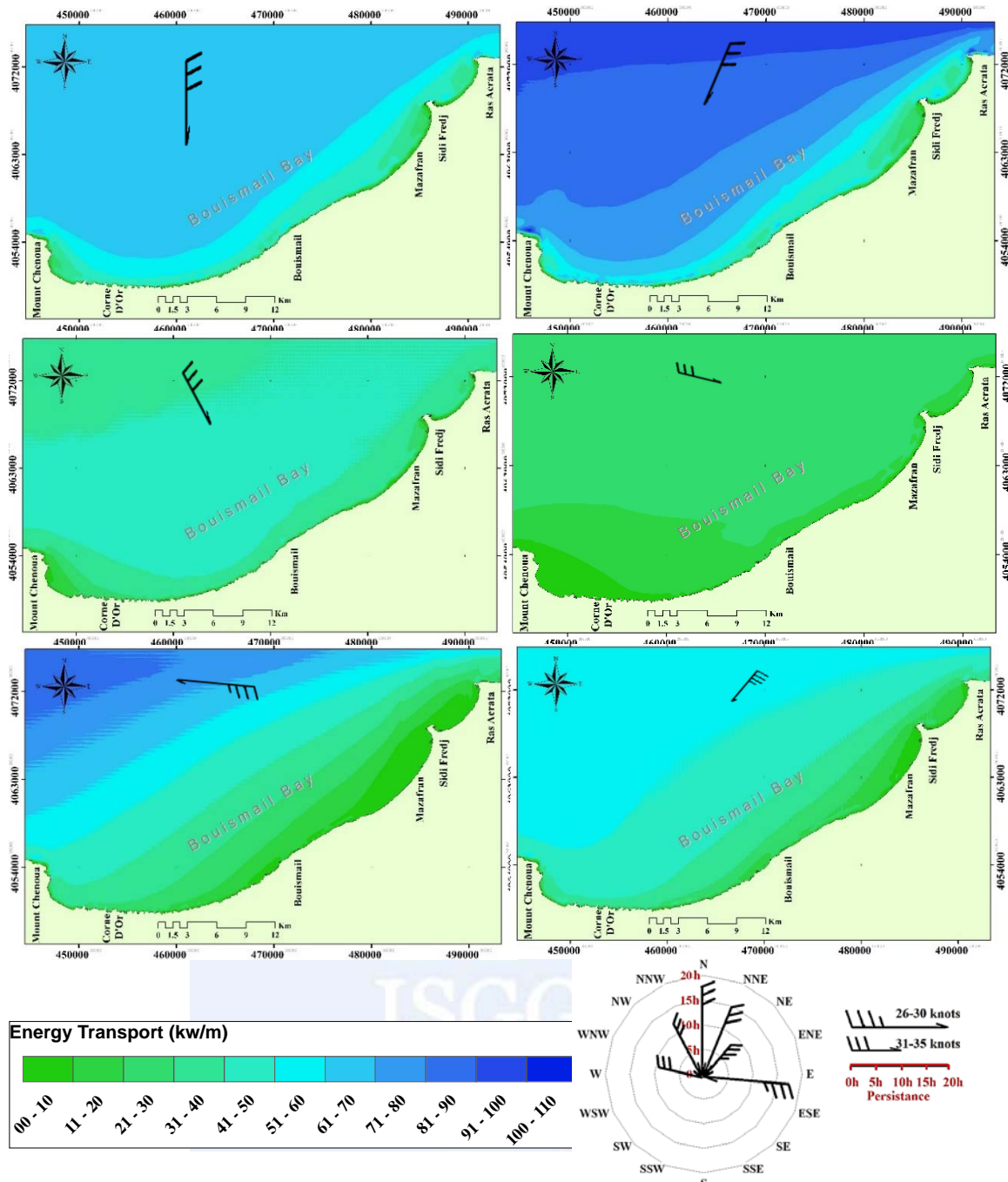


Figure 1. Wave Power Propagation maps of Six Stormy days recorded during the previous 14 years

- Spatial Analysis Results

In order to interpret the large number of results obtained after modeling the six most violent storms recorded since 2002 from six different directions, we calculated the mean and the maximum wave power recorded along the bay that can be observed during a storm. These results allow us to give a first estimation of the zones with high-energy potential and thus estimate the probable coastal risk during the decennial storm.

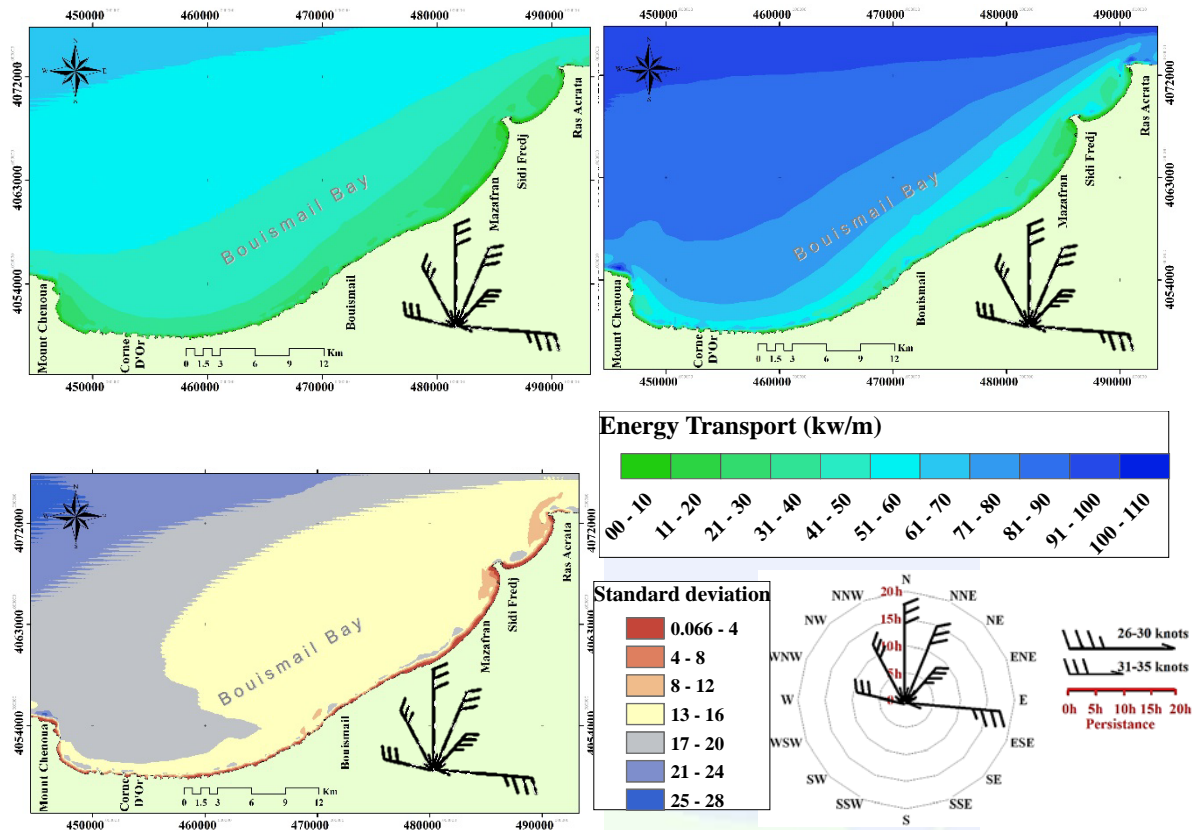


Figure 2. maps of mean and maximum wave powers on storm days and standard deviations

The highest wave power average near the coast was recorded in the western part of the bay and in the Sidi-fredj beach (Figure 2.). Thus, there is an important correlation between the maximum and average energies. The standard deviations map allows us to estimate the zones whose energies recorded during the storm are close to the calculated mean whatever the direction of the offshore waves, to the other hand, the zones with a high standard deviation value have energies that varies greatly according to the conditions of the offshore wave.

The strong energies recorded in the shallow water represent a significant advantage for the wave energy recuperators whereas it is easier to install, maintain and tighten it closer to the electricity grids (Shin 2013). Our objectives are to locate the zones with the highest energy potential whatever the conditions of the offshore swell, ensuring that these zones are close to the coast. To do this we passed to the third step of our studies, which is the multicriteria analysis. Three criteria were the subject of this analysis:

1. Wave power average greater than 25 kw/m, > 30kW/ m and > 35kW/ m
2. A low standard deviation value (<12)
3. A maximum depth of 20 m.

Results of the multicriteria analysis

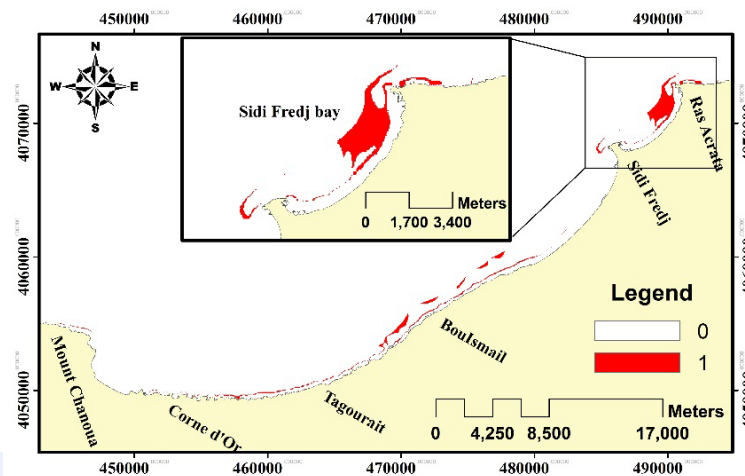


Figure 3. Results of the first multicriteria analysis: $E_t > 25 \text{ kW/m}$ & $\sigma < 12$ & depth < 20

This map indicate the zones with an wave power average greater than 25 kW/m, a standard deviation less than 12, and a depth water less than 20 m. The most remarkable zone for its length and area is located in the eastern part of the small bay of Sidi Fredj (Figure 3). This zone has experienced very high coastal erosion during the last decade (Aini & Boutiba, 2014). In order to make the protection of this area more profitable, the implanted of a breack water equipped with a wave energy recuperator (SSG Slot-Cone Generator) can be evaluated by this result; The SSG wave energy collector was optimized during the EMACOP project for a maximum hydraulic efficiency of approximately 27% frome the total wave energy (Hardouin, 2016).

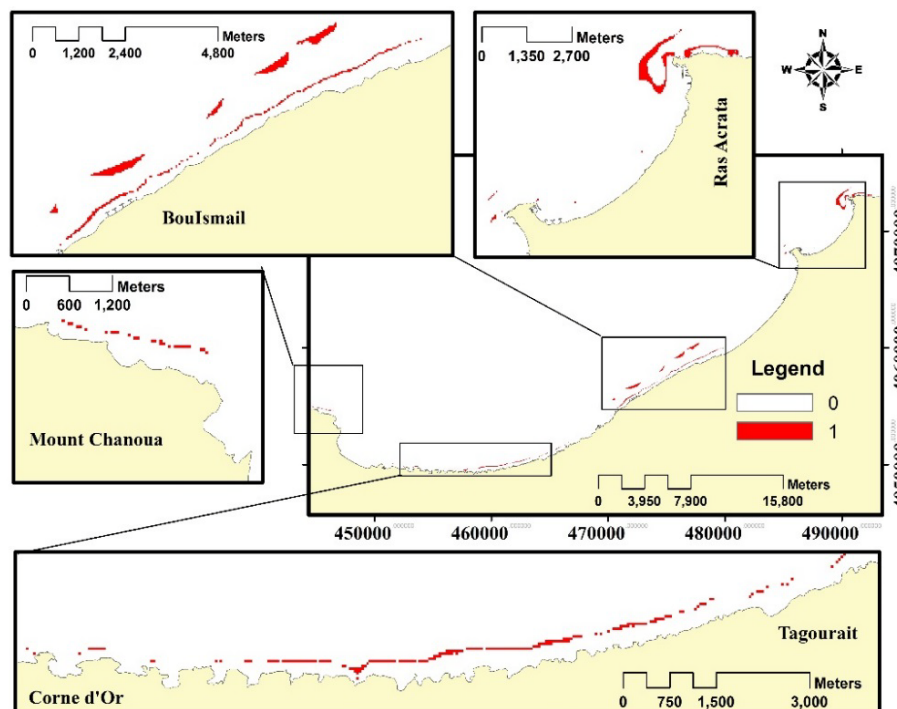


Figure 4. Results of the second multicriteria analysis: $E_t > 30 \text{ kw/m}$ & $\sigma < 12$ & depth $< 20 \text{ m}$

The map below (Figure 4) indicate the zones with an wave power average greater than 30kW/m, a standard deviation of less than 12 and a depth of less than 20m. This result enabled us to select the regionally high-potential areas of renewable marine energy, also it allows us to locate areas with high risk of navigation or high risk of erosion. The area that has the highest interest for energy recovery was observed in BouIsmaïl zone, of which four Breakwaters with a length of 450 m are exposed to a considerable and omnipresent energy.

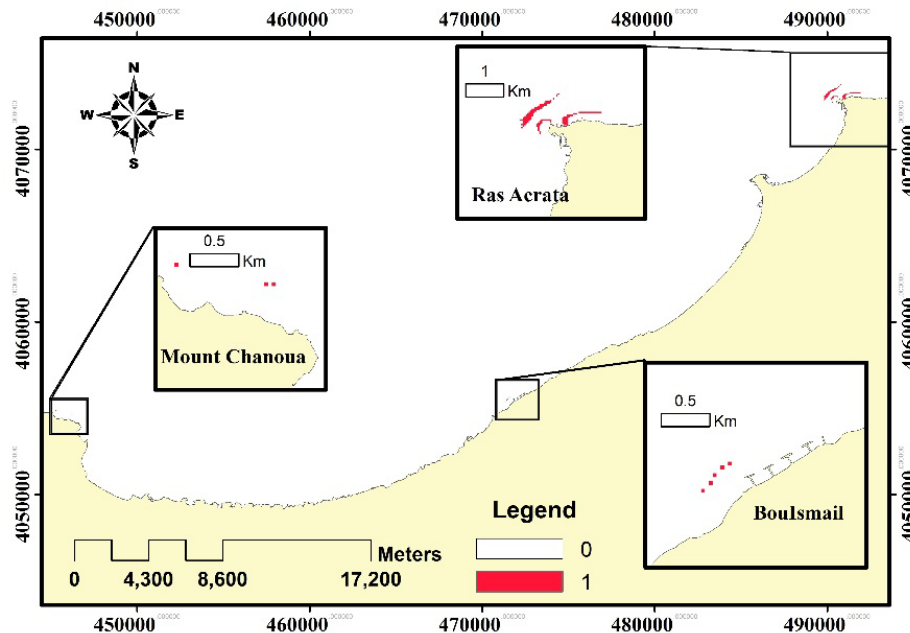


Figure 5. Results of the third multicriteria analysis: $E_t > 35 \text{ kW/m}$ & $\sigma < 12$ & depth $< 20 \text{ m}$

The last results of the multicriteria analysis (Figure 5) aims to filter even more the zones that mark the strongest marine energies. Three zones were located with a wave power average on storm days greater than 35 kW/m and a standard deviation less than 12 in depths less than 20m. The most notable area among them is Ras Acrata with a length that exceeds 2 km along the coast, or 70 megawatt of energy. The maximum energy recorded in this zone is 80kW/m with a NNE wind of a speed greater than 14m/s and a persistence of 12hour.

CONCLUSIONS

The coastal areas of BouIsmaïl Bay do not have the same energy potential; the variation of this energy depends on several factors including coastal and underwater morphology. The wave power transmitted to the coast generally depends on the direction of the offshore wave's propagation; the phenomenon of diffraction and refraction causes a high dissipation of this energy. The use of GIS for geospatial analysis and multicriteria analysis of the hydrodynamic model results (SWAN) allowed us to select the coastal areas exposed to the highest marine energy with a low dependence to the offshore wave direction. These areas can be exposed to a high risk of erosion and presents very dangerous areas to navigation. The installation of breakwaters occupied by wave energy recuperators in the case of a coastal protection project in these areas may be more cost-effective and economical. The

geodatabase developed during this study allows us to optimize the choice of the most favorable zones and the most profitable for the development of renewable marine energies. as well this geodatabase it constitute a decision support tool for the ICZM projects, the coastal vulnerability studies and the coastal safety services.

ACKNOWLEDGMENTS

The authors wish to thank the researchers of The Spatial Oceanography Laboratory, University of Science and Technology of Houari Boumedien, for sharing their invaluable insights and experiences.

REFERENCES

- Aini, A., Boutiba, M., 2014. Morphodynamique de la zone côtière Est de la presqu'île de Sidi-Fredj (Ouest Alger). *Phd Thesis*. University of Science and Technology Houari-Boumedienne. Alger.
- Akpınar, A., van Vledder, G. P., Kömürcü, M. İ., & Özger, M. (2012). Evaluation of the numerical wave model (SWAN) for wave simulation in the Black Sea. *Continental Shelf Research*, 50, 80-99.
- Aydoğan, B., Ayat, B., & Yüksel, Y., 2013. Black Sea wave energy atlas from 13 years hindcasted wave data. *Renewable energy*, 57, 436-447.
- Bachouche, S., Houma, F., and Belkessa, R., 2016. Risk assessment of heavy metal in surface sediments from Algiers harbor (Algeria). *Int. J. Science & Knowledge*; Vol, 5(1), 32-40.
- Bass, S.J., 2013. Ambient noise and wave breaking on a sandy beach: energy dissipation estimates, *Journal of Coastal Research*, Vol 65 No 2.
- Booij, N., Ris, R. C., and Holthuijsen, L. H., 1999. A third generation wave model for coastal regions: 1. Model description and validation. *Journal of geophysical research: Oceans*, 104(C4), 7649-7666. <https://doi.org/10.1029/98JC02622>.
- Bottema, M., and Beyer, D., 2002. Evaluation of the SWAN wave model for the Dutch IJsselmeer area. In *Ocean Wave Measurement and Analysis*, 580-609.
- Castelle, B., 2004. Modélisation de l'hydrodynamique sédimentaire au-dessus des barres sableuses soumises à l'action de la houle, *Phd Thesis*, University of Bordeaux I.
- Dragani, W. C., Garavento, E., Simionato, C. G., Nuñez, M. N., Martín, P., and Campos, M. I., 2008. Wave simulation in the outer Rio de la Plata estuary: evaluation of SWAN model. *Journal of waterway, port, coastal, and ocean engineering*, 134(5), 299-305.
- Dykes, J. D., Hsu, Y. L., and Rogers, W. E., 2002. SWAN evaluation in the northern Gulf of Mexico. In *7th Int. Workshop on Wave Hindcasting and Forecasting*.

- Hardouin, A., 2016. La synthèse des travaux réalisés dans le cadre de la tranche 2 du Projet National EMACOP est désormais disponible. Synthesis. Institute for Applied Research and Experimentation in Civil Engineering – IREX
- Kateb, K., 2003. Population et organisation de l'espace en Algérie. *L'Espace géographique*, 32(4), 311-331.
- Loubersac, L., Salomon, J. C., Breton, M., Durand, C., and Gaudineau, C., 2000. Perspectives offertes par la communication entre un modèle hydrodynamique et un SIG pour l'aide au diagnostic environnemental : caractérisation de la dynamique et la qualité des masses d'eaux côtières. In *CoastGIS'99-Geomatic and coastal environment*. 9-11 September 1999, Brest.
- Magnan, A., 2009. *Le tourisme littoral en Méditerranée*, The Institute for Sustainable Development and International Relations (IDDRI), 48p.
- Shin, S., Lee, K. H., Kim, D. S., Kim, K. H., and Hong, K., 2013. A study on the optimal shape of wave energy conversion system using an oscillating water column. *Journal of Coastal Research*, 65(sp2), 1663-1668.
- Simav, Ö., Şeker, D. Z., and Gazioğlu, C., 2013. Coastal inundation due to sea level rise and extreme sea state and its potential impacts: Çukurova Delta case. *Turkish Journal of Earth Sciences*, 22(4), 671-680.
- Szlafsztein, C., Sterr, H., 2007. A GIS-based vulnerability assessment of coastal natural hazards, state of Pará, Brazil. *Journal of Coastal Conservation*, 11(1), 53-66.

Mapping of arsenic and boron pollution in the intense mining catchment of Mustafakemalpaşa stream - Northwestern Turkey

Philip Isaac Omwene, Salim Oncel, Meltem Çelen, Mehmet Kobya

Department of Environmental Engineering, Gebze Technical University, 41400 Gebze-Kocaeli.

ABSTRACT

This study was aimed at mapping the spatial distribution of Arsenic and Boron Pollution in Mustafakemalpaşa catchment area using measured field data and considering the discharge of small tributaries. Arsenic (As) and Boron (B) are the most common water pollutants in northwestern Turkey. Literature studies suggest that mining activities and the geology of this region are responsible for these pollutions. Water samples were seasonally collected from 50 sampling points in the basin. Samples analyzed for the boron and arsenic pollution using inductively coupled plasma optical emission spectroscopy (ICP-OES). Inverse Distance Weighted (IDW) interpolation technique in ArcGIS 10.4.1 toolbox was used for pollution mapping. The results show, significant variation of both arsenic and boron concentration among the sampling points, however no significant seasonal variations for both boron and arsenic levels was noted. The obtained pollutant values are above World Health Organization (WHO) drinking water limits. The distribution of both arsenic and boron along the course of the streams is found to be closely related to mining activities in the area.

INTRODUCTION

Arsenic (As) been described to be a toxic metalloid and therefore endangering public health if consumed at high levels (Hindmarsh and McCurdy 1986). Schwartz 1997, reported that prolonged consumption of water contaminated with over 50 µg/L of arsenic may cause internal cancers, the WHO guide line for As in drinking water is 10 ug/L. Arsenic is mostly found as inorganic arsenite (⁺³) and arsenate (⁺⁵) oxidation states in water (Dove and Rimstidt, 1996). At oxic conditions and thermodynamic equilibrium, arsenic is dominated by arsenate oxyanions (H₂As(V)O₄⁻ or (H₂As(V)O₄)²⁻ depending on the pH. At reducing conditions and over a wide range of pH, the uncharged arsenite species ((H₃AsO₃)⁰) predominates (Carbonell-Barrachina et al.1999). From the environmental risk point of view, exploration of certain natural resources can lead to significant environmental pollution, such activities include; geothermal fields, mining operations in sulphide bearing ores with high arsenic content such as arsenopyrite (FeAsS), arsenian pyrite (Fe (S, As)₂), realgar (AsS) and orpiment (As₂S₃). Its reported that up to

4% As levels are present in the mineral deposits of Kutahya -Emet region (Baba and Sozbilir, 2012).

On the other hand, Boron mainly occurs as orthoboric acid in most volcanic spring waters and as borate minerals such as borax ($\text{Na}_2\text{B}_4\text{O}_7 \cdot 10\text{H}_2\text{O}$), colemanite ($\text{Ca}_2\text{B}_8\text{O}_{11} \cdot 5\text{H}_2\text{O}$) and ulexite ($\text{NaCaB}_5\text{O}_9 \cdot 8\text{H}_2\text{O}$), (Gemici et al. 2008). Although boron is an essential nutrient for plants and many organisms, its reported to be toxic to aquatic and terrestrial organisms above certain thresholds (Emiroğlu et al. 2010). Over 70% of the world boron reserves are in Turkey with major deposits in Kütahya province in northwestern turkey (Helvacı, 2005). The existing borate deposits in the region are mined by surface or underground methods (Helvacı 2004). Geogenic sources such as geothermal discharges, leaching of rocks among others may cause boron pollution in the environment. In addition, anthropogenic sources of boron pollution may include municipal wastewaters, and industrial residues, boron pesticides and fertilizers among others (Dotsika et al. 2006).

Studies focusing on smaller tributaries in the catchment area are limited in literature and this is a draw back in identifying the pollutant input routes. Spatial mapping of pollution based on the real field data can help the local community, water resources managers and all the relevant stakeholders in quarantining unsafe zones and identifying the pollution sources. This study was aimed at; (1) determining arsenic and boron contents in Mustafakemalpaşa stream and its tributaries (Emet and Orhaneli) and comparing with the national and international water quality standards, (2) Identifying the most polluted tributaries based on arsenic and boron pollution, which are main sources of pollution input into the catchment and finally (3) serve as an approach to guide to policy makers in making informed decisions in regards to water pollution in the catchment area.

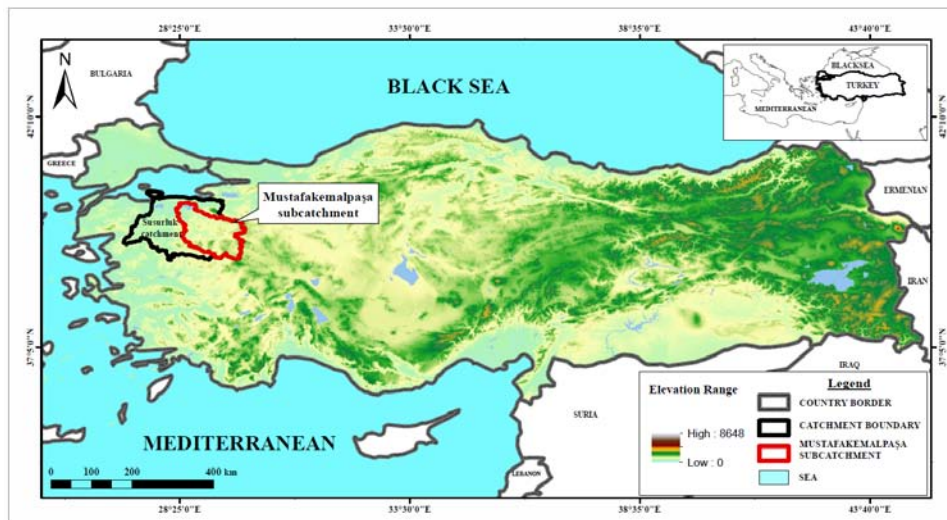


Figure 1. Location of Mustafakemalpaşa catchment area.

MATERIALS AND METHODS

Study region

Mustafakemalpaşa catchment is located within the boundaries of Bursa, Balıkesir and Kütahya provinces in the 25° 45' to 25° 74' N and 84° 10' to 84° 55' E geographic

coordinates with a total catchment area of 10,622 km², an area characterized by intensive mining of Boron, Chromium, Lignite and Iron. The drainage network in the catchment discharges into Lake Ulubat and finally into the Marmara Sea through Susurluk river. The climate in the region is a typical transitional climate of that between the Mediterranean and the Black Sea climates. With the highest precipitation received in winter and the least precipitation received in summer. According to data obtained from Turkish state metrological service, the average annual temperature in the catchment is 13.2°C. Annual precipitation in the basin ranges between 40 mm and 65 mm.

Data collection

Data for this study was obtained from 55 designated GPS coordinate sampling points in the catchment area in October 2016, March 2017 and July 2017. In October, the weather is characterized by rainy but warm conditions with an average flow rate of 17.4 m³/s, in the main Mustafakemalpaşa stream. In March, the weather is rainy and foggy with an average stream flow rate of 115.1 m³/s, in July the weather is hot and dry with a flow rate of 19.1 m³/s. Water samples were collected using sterilized polyethylene bottles and analyzed within 5 days of sampling. All the sampling and analysis procedures were performed in accordance with the Standard Method for the Examination of Water and Wastewater (AWWA). The location of sampling points used in this study are shown in Figure 2 below.

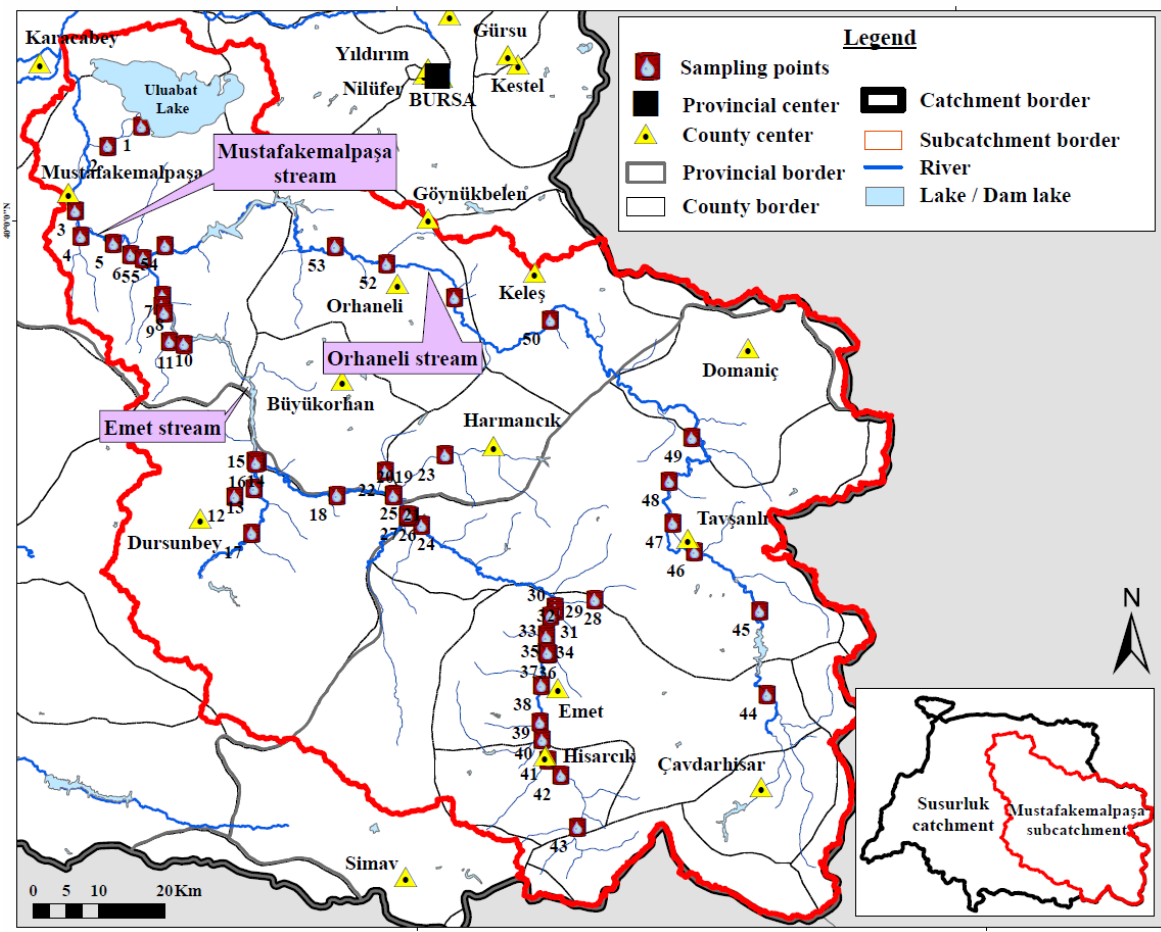


Figure 2. Water and sediment Sampling points used in this study.

Chemical and Physicochemical Analysis

The analyses on temperature, pH, salinity, and conductivity were performed in-situ using a “Mettler Toledo sevengo” device. Prior to analysis, all the water samples were filtered through 0.45µm filter. The total arsenic and boron concentrations was measured using inductively coupled plasma optical emission spectroscopy (ICP-OES), a reliable method for arsenic measurements (Rahman et al. 2002). All analysis recorded as a mean of triplicate measurements.

Spatial mapping tool

The spatial mapping tool used in this study was the geo-statistical, Inverse Distance Weighting Method, based on ArcGIS 10.4.1 software. Equations (1) and (2) summarizes the IWD formulae (Chen et al.2012).

$$C_p = \sum_{i=1}^N W_i C_i \quad (1)$$

$$W_i = \frac{d_i^{-\rho}}{\sum_{i=1}^N d_i^{-\rho}} \quad (2)$$

where C_p is the unknown pollutant concentration; C_i is the pollutant concentration at known point; N is the total number of amount of sampling points; W_i is the weighting of each point; d_i is the distance from each sampling point to the unknown site; ρ is the power function, the default value of $\rho = 2$ was used in this study.

RESULTS AND DISCUSSION

Large variations in both arsenic and boron levels at different points in the water samples was seen (Figure 2 and Figure 3). Average dry season concentrations (June to August) were 0.423 mg/L and 24.93 mg/L for arsenic and boron respectively, whereas the wet season (Feb-April) average concentrations was 0.460 mg/L and 53.66 mg/L for arsenic and boron respectively.

As can be seen from Figure 3, the variation in arsenic and boron values measured from Emet stream are similar. The lowest values are seen in the upstream points, about 200-220km distances from the Uluabat lake. After this point, a striking increase is seen in both the arsenic and the boron parameters at a distance of about 180 km from the lake. This can be explained by the dense presence of boron mines in the area. As it is clearly seen from the figure after the confluence of Orhaneli stream, arsenic and boron values reach the lake at relatively low values through Mustafakemalpaşa stream.

From Figure 4 the average annual arsenic pollution at the upstream sampling points, about 230-250 km from Ulubat lake, along Orhaneli stream were observed to be below the WHO guide line (10µg/L) hence suitable for human consumption. However, as the flow continued downstream, an increase in arsenic pollution is observed this may be due to inflows from polluted tributaries. The maximum arsenic pollution level (103µg/L) along

Orhaneli stream noted at about 97 km from Ulubat lake. The high arsenic pollution value at this point could be due to lignite mining activities and thermal power plant in the region.

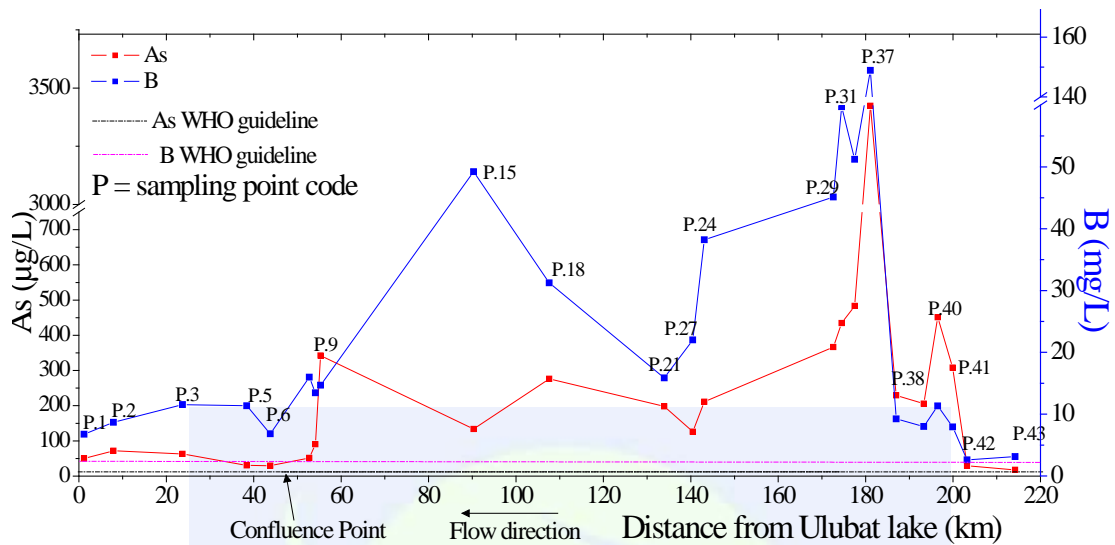


Figure 3. Annual average concentrations of arsenic and boron in the water of Mustafakemalpaşa and Emet streams, Data based on three field campaigns (October, March and July).

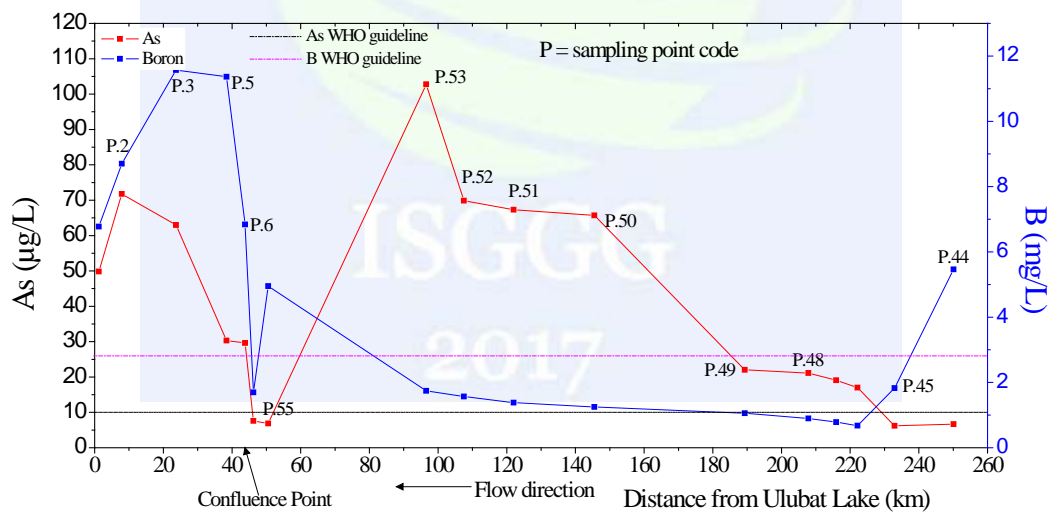


Figure 4. Annual average concentrations of arsenic and boron in the water of Mustafakemalpaşa and Orhaneli streams, Data based on three field campaigns (October, March and July).

Pollution maps

The pollution maps shown in Figure 5 and 6 were generated from ArcGIS 10.4.1 software, using the Inverse Distance Weighting (IDW) tool box. These maps clearly illustrate the arsenic and boron polluted regions of the catchment and can easily be interpreted.

As presented in Figure 3 the values below 10 μ g/L which is suitable for human consumption according to WHO guide line only can be found upstream of Orhaneli stream and some small tributaries of Emet and Mustafakemalpaşa streams. The values change between 10-50 and 50-100 μ g/L predominantly along the other parts of the streams. The values between 100-300 μ g/L can be seen at the Tavşanlı city on Orhaneli stream. Considering the Emet stream the values between 100-300 μ g/L can be found in the section of the Emet stream beginning from Hisarcık to the point where it confluence with Orhaneli stream. The highest values (above 400 μ g/L) were measured only north of the Emet county.

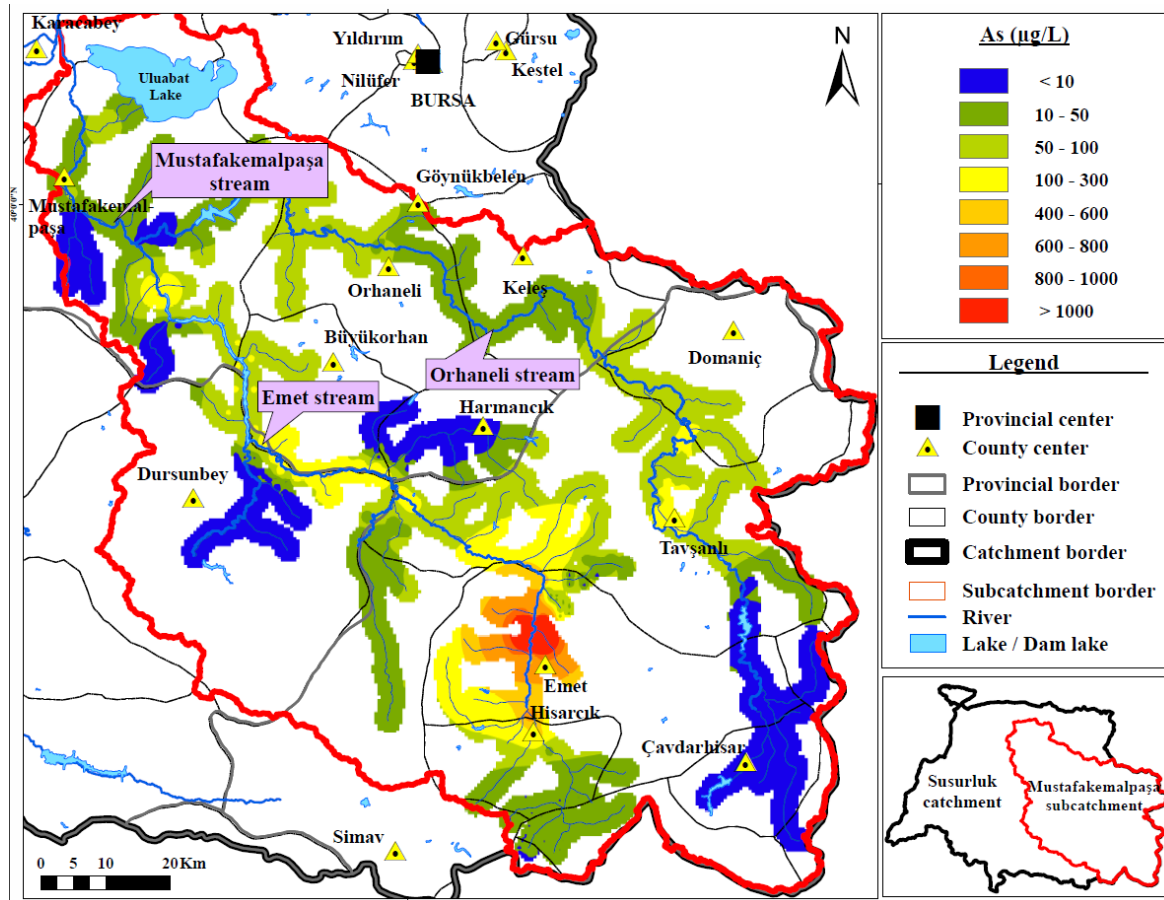


Figure 5. Map of arsenic concentration.

The map of boron pollution is given in Figure 6. The most spectacular characteristic of the boron pollution in the basin is that the values in the Orhaneli stream are below 2.4 mg / L which is the allowed value for human consumption according to the WHO guide lines. Besides these low values are observed in some tributaries in the middle and northern part of Emet stream. Similar to arsenic pollution map the highest concentrations of boron were detected in areas close to the Emet and Hisarcık counties. As it can be seen from the map that despite the clean water coming from Orhaneli stream, the boron values along Mustafakemalpaşa stream have relatively high values.

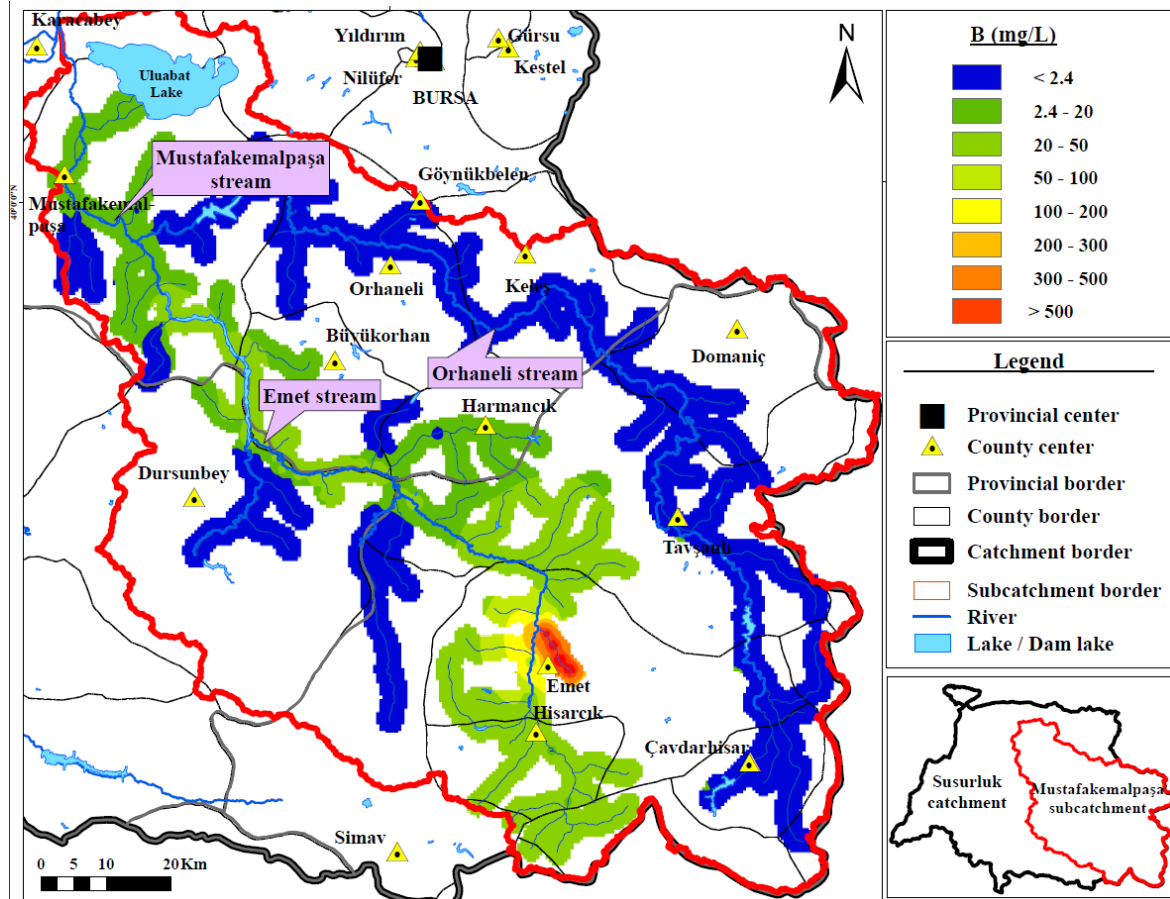


Figure 6. Map of Boron concentration.

The maps represented in Figure 6 and Figure 7 were prepared in order to compare the concentration distribution of arsenic and boron with the distribution of the minefields based on subcatchments. Thus, it is aimed to better analyze the effect of minefields in the basin on pollution distribution.

As it is clearly seen from Figure 5 the subcatchment numbered 6 has the highest mean As concentration (905.42 $\mu\text{g/L}$). This subcatchment has the most dense mining areas in the study site. The boron mines are located in the southern and central parts of the basin, and lignite mines are located intensively on the northern boundary of the basin. The subcatchments numbered 4 and 2 have the second and third highest mean arsenic concentration values respectively. These high values can be expressed by the presence of lignite mining areas and effect of subcatchment numbered 6. The subcatchments numbered 3 and 5 have the lowest As concentration 8,01 $\mu\text{g/L}$ and 13,47 respectively. These two subcatchments have no boron or lignite mining areas. The subcatchment numbered 7 is the subcatchment of Orhanlı stream has a mean value of 34.65 $\mu\text{g/L}$ As. There are numerous mining areas in the subcatchment numbered 7 but the effect of these areas on As pollution is limited. This can be explained by geochemical characteristics of minerals in the rocks. Additionally, the technological level of mining activities in this region may be attributed to the relatively low pollution concentration. The subcatchment numbered 1 is representing the Mustafakemalpaşa stream and has a mean value of 42.09 $\mu\text{g/L}$.

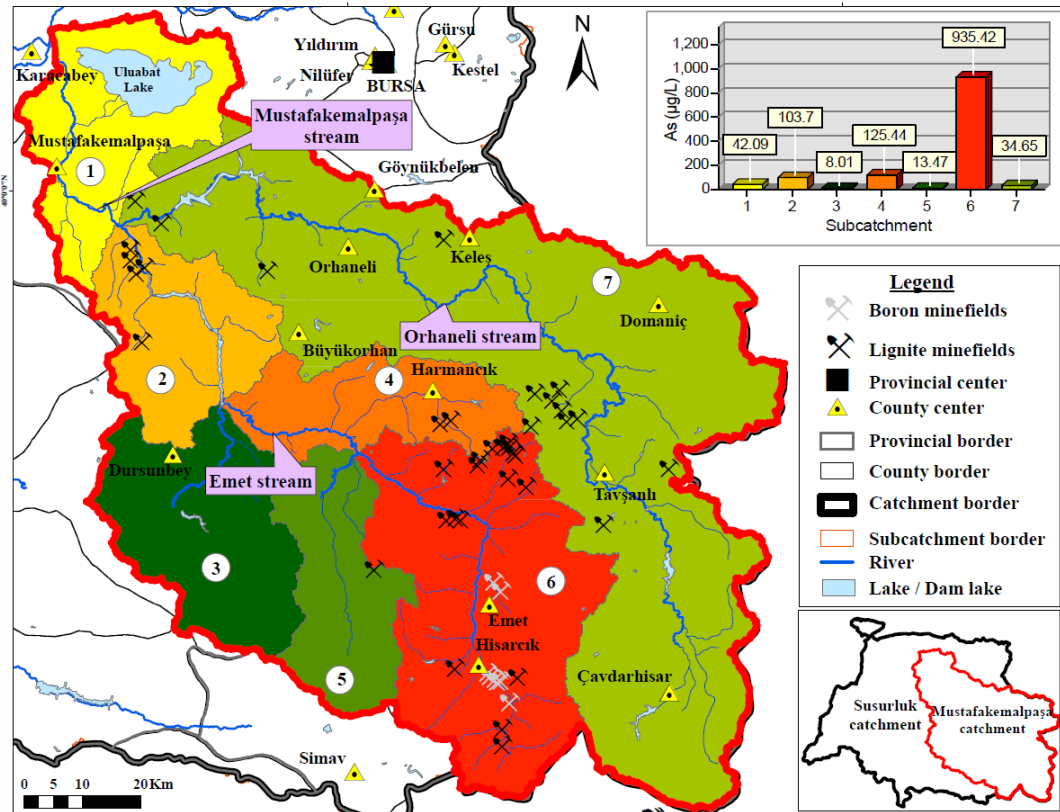


Figure 7. Map of Annual average concentration distribution of arsenic in the subcatchments.

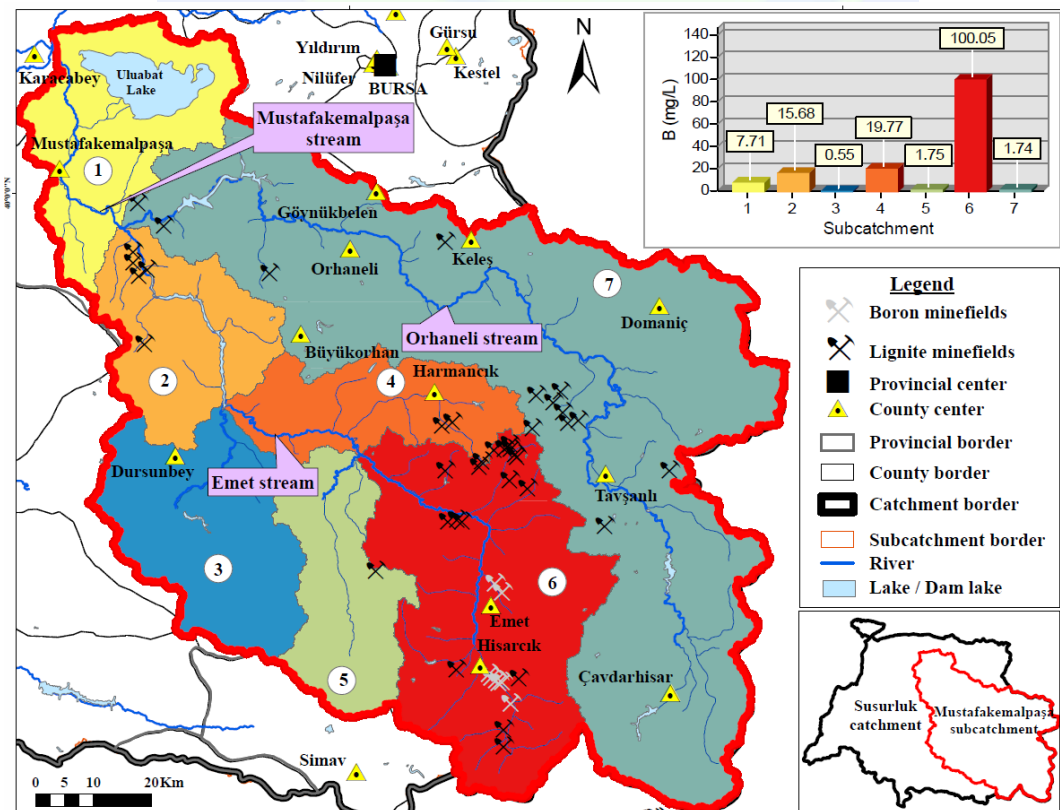


Figure 8. Map of Annual average concentration distribution of boron in the subcatchments.

The Figure 8 below shows the mean boron concentration distribution of the subcatchments. The variation of the boron pollution of the subcatchments are very similar to the as pollution distribution given in Figure 7.

CONCLUSIONS

The concentrations of both arsenic and boron in many areas of Mustafakemalpaşa catchment is found to exceed the maximum allowable limits (10 µg/L for As and 2.4 mg/L for B) set by national and international standards for drinking water. Sampling Points 8, 35 and 41 were identified as the main polluted points (hotspots) in the catchment area, these are near points of wastewater discharges from mining sites; point 35 is a discharge point from boron mining sites. Point 41 is upstream of Hisarcık town, the high boron and arsenic pollution at this point is attributed to the mining sites located in southern part of Hisarcık town. It is noted that a significant reduction of both arsenic and boron concentration occurs downstream after pollutant input from these contaminated tributaries (wastewaters), this could be due to dilution by the less polluted water from other tributaries downstream and the pollutant retention by the water impoundment structures located in the stream. Although previous studies mainly seem to support the argument that As enrichment in the stream waters of this region is predominantly controlled by weathering of already As-rich underlying rocks (Özkul. et al. 2015). This study clearly points out that another major cause of arsenic in the streams are point discharges from mining waste as indicated by the high pollution levels in samples taken down stream of discharge points (hotspots). Continuously monitoring of boron and arsenic pollution from the mining wastewater discharges should be carried to avoid contaminating the entire catchment area.

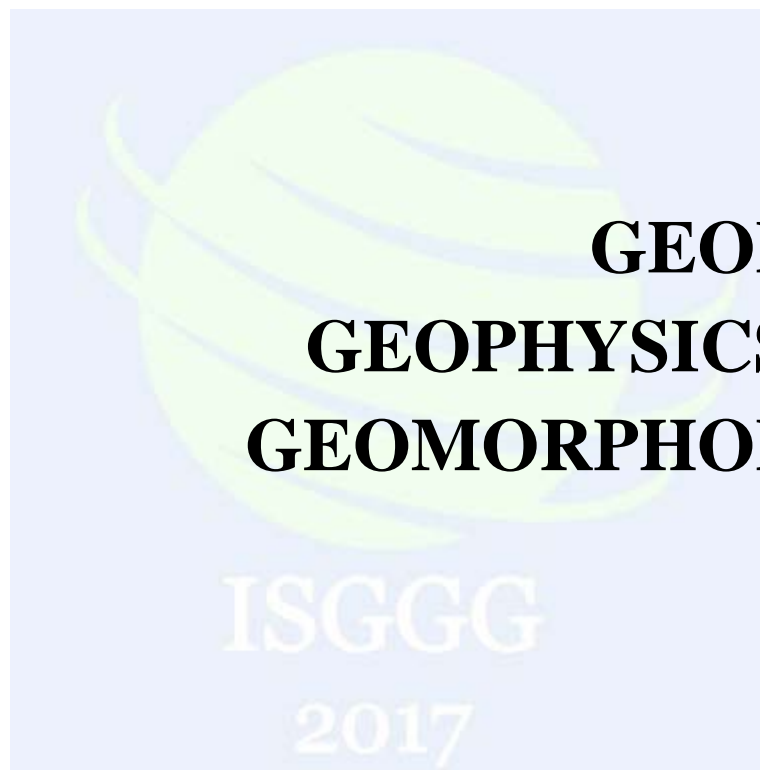
ACKNOWLEDGMENTS

This research was carried out as part of masters of science thesis study entitled “Assessment of Water and Sediment Quality in Mustafakemalpaşa Stream and its tributaries using Statistical Techniques and Geographical Information System Analyses” with financial support from Gebze Technical University under project number 2017-A101-07.

REFERENCES

- Hindmarsh J.T., McCurdy R.F., 1986. Clinical and environmental aspects of arsenic toxicity. *Crit Rev Clin Lab Sci* 23, 315–347
- Rahman M.M., Mukherjee D., Sengupta M.N., Chowdury U.K., Lodh D., Chanda C.N., Roy S., Selim M., Quamruzzaman Q., Milton A.H., Shadullah S.M., Rahman M.T., Chakraborti D., 2002., Effectiveness and reliability of arsenic field testing kits: are the million dollar screening projects effective or not? *Environ Sci Technol* 36, 5385–5394
- Schwartz R.A., 1997. Arsenic and the skin. *Int J Dermatol* 36, 241–250

- WHO, 2005. Water sanitation and health. Guidelines for drinking water quality. 3rd edn. World Health Organization.
- Baba, A. and Sozbilir, H., 2012. Source of arsenic based on geological and hydrogeochemical properties of geothermal systems in Western Turkey', *Chemical Geology*. 334, 364–377. doi: 10.1016/j.chemgeo.2012.06.006.
- Gemici Ü., Tarcan G., Cahit C., Somay A.M., 2008. High arsenic and boron concentrations in groundwaters related to mining activity in the Bigadiç borate deposits (Western Turkey), *Applied Geochemistry* 23(8): 2462–2476. doi: 10.1016/j.apgeochem.
- Helvacı, C., 2005. Borates. In: Selley, R.C., Cocks, L.R.M., Plimer, I.R. (Eds.), *Encyclopedia of Geology* 3, 510–522.
- Helvacı, C., Mordog an H., Colak M., Gundogan I., 2004. Presence and distribution of lithium in borate deposits and some recent lake waters of west-central Turkey. *Int. Geol. Rev.* 46, 177–190.
- Dotsika, E., Poutoukis, D., Michelot, J.L., Kloppmann, W., 2006. Stable isotope and chloride, boron study for tracing sources of boron contamination in groundwater: boron contents in fresh and thermal water in different areas in Greece. *Water Air Soil Pollut* 174, 19–32
- Emiroğlu O., Çiçek A., Arslan N., Rüzgar S.M., 2010. Boron concentration in water, sediment and different organisms around large borate deposits of Turkey, *Bulletin of Environmental Contamination and Toxicology* 427–431. doi: 10.1007/s00128-010-9961-8.
- Dove, P.M. and Rimstidt, J. D., 1996. The solubility of scorodite, $\text{FeAsO}_4 \cdot \text{H}_2\text{O}$, *Amer. Mineralog* 70, 838–844
- Carbonell-Barrachina, A. A., Jugsujinda, A., Burlo, F., Delaune, R. D. and Patrick, W. H., 1999. Arsenic chemistry in municipal sewage sludge as affected by redox potential and pH, *Water Res.* 34(1): 216–224.
- Chen, F. W. and Liu, C. W., 2012. Estimation of the spatial rainfall distribution using inverse distance weighting (IDW) in the middle of Taiwan, *Paddy and Water Environment* 10(3): 209–222. doi: 10.1007/s10333-012-0319-1.



**GEOLOGY
GEOPHYSICS AND
GEOMORPHOLOGY**

A Research for the Characterization of Coastal Sands in East Mediterranean (Between Samandağı and Narlıkuyu) and TRNC by ArcGIS

Emine Demirel^{*1}, Soner Top¹, Nil Yapıcı¹

¹Department of Mining Engineering, Çukurova University, 01330, Adana, Turkey (e-mail: eminedemirell@hotmail.com)

ABSTRACT

In this study, determining the heavy metal contents of coastal sands of selected locations of Turkish east Mediterranean (between Samandağı and Narlıkuyu) and TRNC (Turkish Republic of Northern Cyprus) was investigated. 32 samples were taken from appropriate locations. The samples whose coordinates were determined by GPS were pinned on the map with 1/100.000 scale. Controls of formations of the area were performed and informations about the region were saved. Photographes of the sample locations were taken. Chemical and heavy metal compositions of the materials were determined by ICP/ICP MS chemical analysis in Canada (in ACME laboratories). Two samples of each location were sent to the analysis. Arithmetic means were calculated and showed in this paper. Besides, the particle size distributions were detected by wet sieve analysis and the cumulative passing curves were plotted. The chemical analysis and the particle size (d50 and d80) results of the samples were graphed by running ArcGIS 10.1 computer software. The research reveals that Mersin coasts have significant grade of chromium (2 %), Karataş coasts have considerable grade of zirconium and Hatay coasts have important grade of nickel.

It is thought that this research dealing with the characterization of Turkish coastal sands will contribute positive feedbacks to the literature. The research can be used a source for determining of the origin of these useful elemental contents in the East Mediterranean Coastal Sands.

INTRODUCTION

0.04% of Turkey is covered with sand dunes. There are a total of 290.000 decare beach sand beaches in Turkey, with 73.500 decares in the Black Sea Region and 216.500 decares in the Mediterranean Region. It is important that the current reserves of all heavy elements in coastal sands of Turkey must be contributed to the economy to create added value (Aykol ve Gültekin, 1992; DPT, 2016; Kozlu et al., 2002; Demirel, 2017). This study is

^{*} Corresponding Author

aimed to determine the characteristics of the coastal placers of Eastern Mediterranean and TRNC.

METHODS

Experimental Studies

Samplings were made from east to west in Samandağ-Narlıkuyu (Turkey) on 26 locales and Dipkarpaz-Girne (KKTC) on 6 location lines. A total of 32 locations were surveyed. The samples whose coordinates are determined by GPS are marked on a map with the scale of 1 / 100.000. After opening a 10 cm deep slit on the beach, samples were taken with plastic gloves and heavy metal and mineral contents were determined after the representative samples were dried and reduced by quartering (Figure 1).

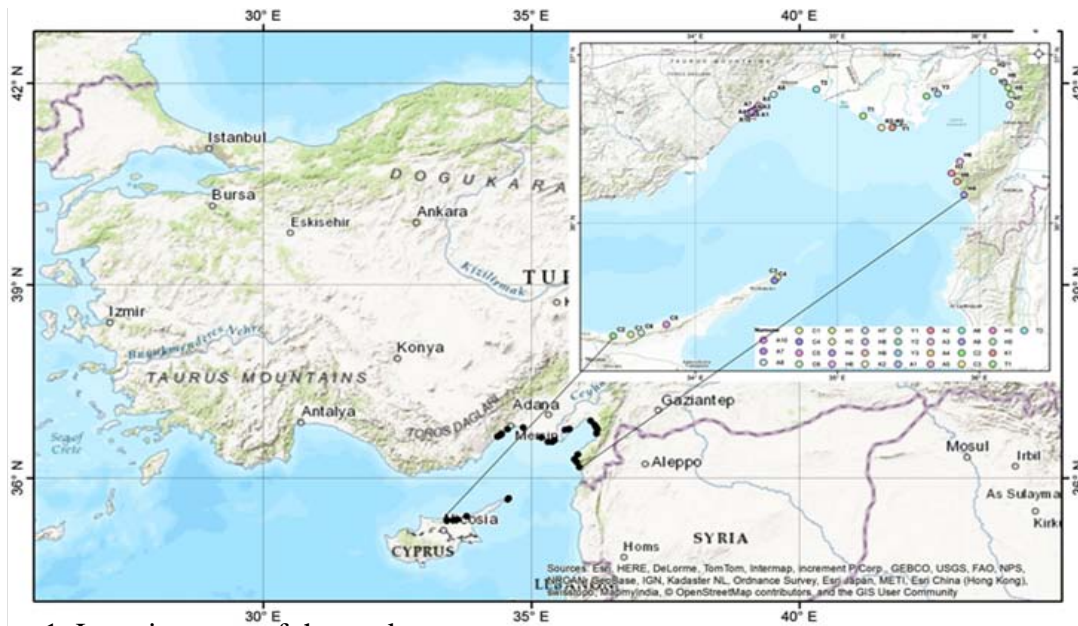


Figure 1. Location map of the study

Chemical Analyses

The samples were sent to Canada via Acme Analitik Laboratuvar Hizmetleri Ltd. Şti. in order to determine the contents of sands.

Table 1. Dimension values of d50 and d80 of receiving samples (mm).

	A-1	A-2	A-3	A-4	A-5	A-6	A-7	A-8
d50	0,40	0,80	0,64	0,27	0,40	0,26	1,00	0,30
d80	0,70	4,00	1,40	0,78	0,70	0,40	12,50	0,41
	A-9	A-10	K-1	K-2	T-1	T-2	Y-1	Y-2
d50	0,50	0,36	0,23	0,25	0,50	0,25	0,25	0,50
d80	3,80	0,56	0,30	0,35	0,72	0,40	0,41	0,85
	Y-3	H-1	H-2	H-3	H-4	H-5	H-6	H-7
d50	0,20	0,37	0,53	0,55	0,57	0,25	0,32	0,43
d80	0,60	0,75	0,71	0,75	0,83	0,70	0,78	2,20
	H-8	H-9	C-1	C-2	C-3	C-4	C-5	C-6
d50	2,00	0,50	0,25	0,26	0,22	0,36	0,50	0,31
d80	7,50	0,75	0,40	0,48	0,28	0,45	1,00	0,47

Sieve Analysis

Particle size analyzes were carried out by taking a minimum of 250 grams of dried samples. Dry-sieving were performed in the mining engineering laboratory of Cukurova University Mining Engineering Department.

Based on the sieve analysis graphs of coastal sands, the d50 and d80 values, which are the grain sizes of 50% and 80% of the sand, are found and are shown in Table 1. Accordingly, H8 and A7 are coarse-aggregate aggregates and the others are fine-sized aggregates.

Distribution Graphs of the Contents by ArcGIS Program

The chemical analysis values and grain size distributions obtained from the sample were mapped using the ArcGIS 10.1 computer program (Figure 2-11).

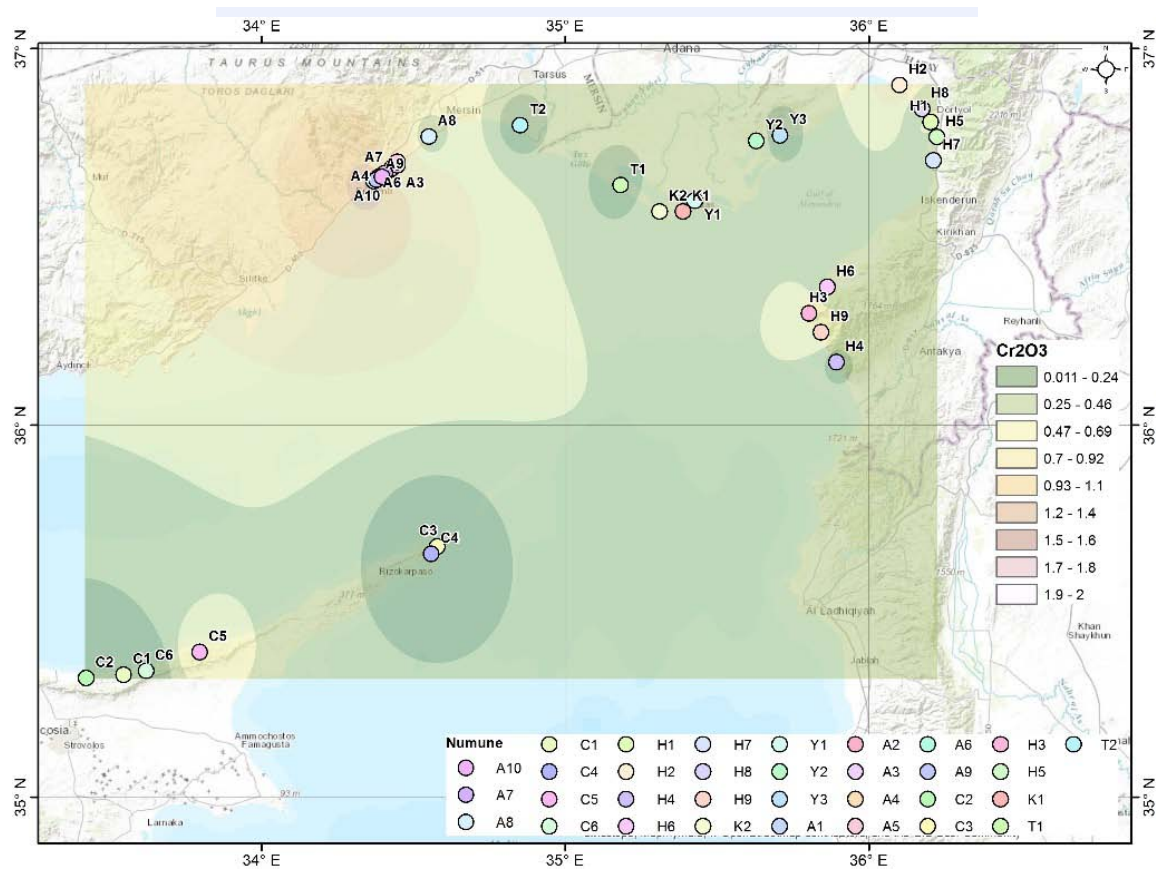


Figure 2. Cr_2O_3 distribution graph (%).

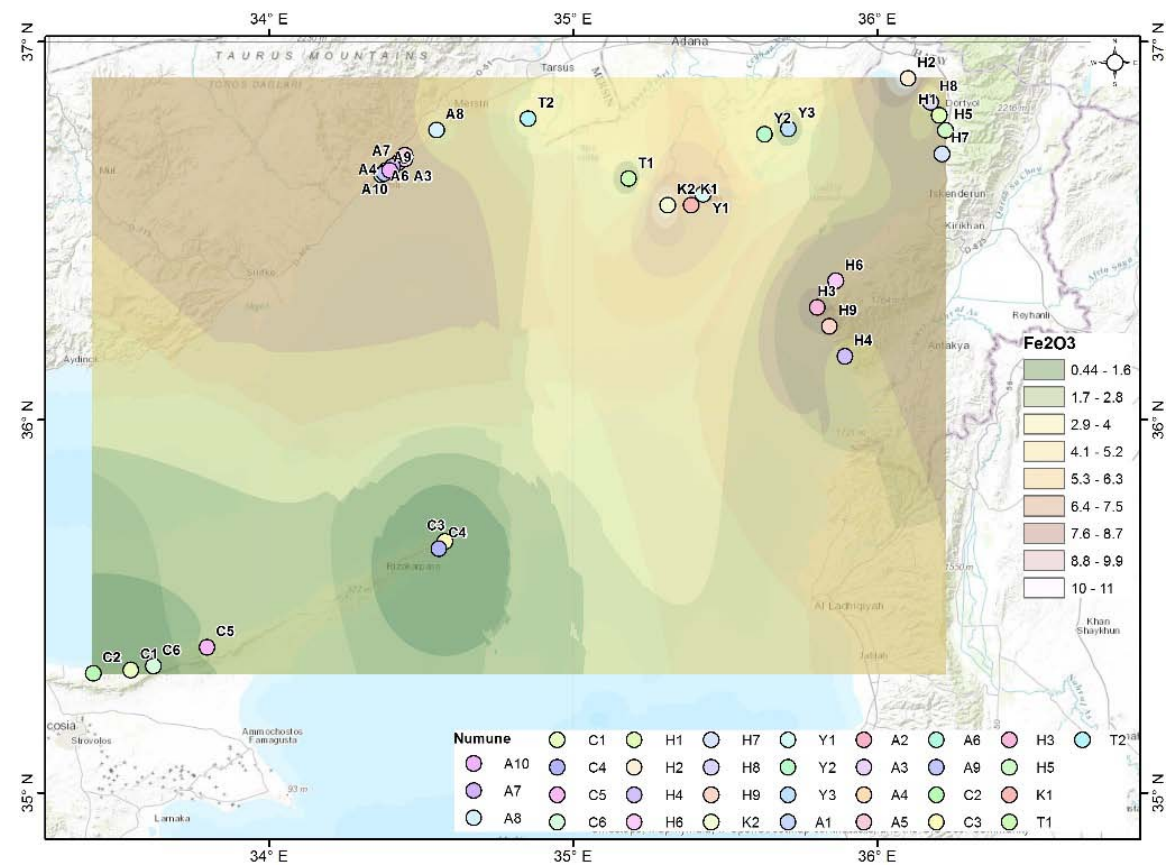


Figure 3. Fe₂O₃ distribution graph (%).

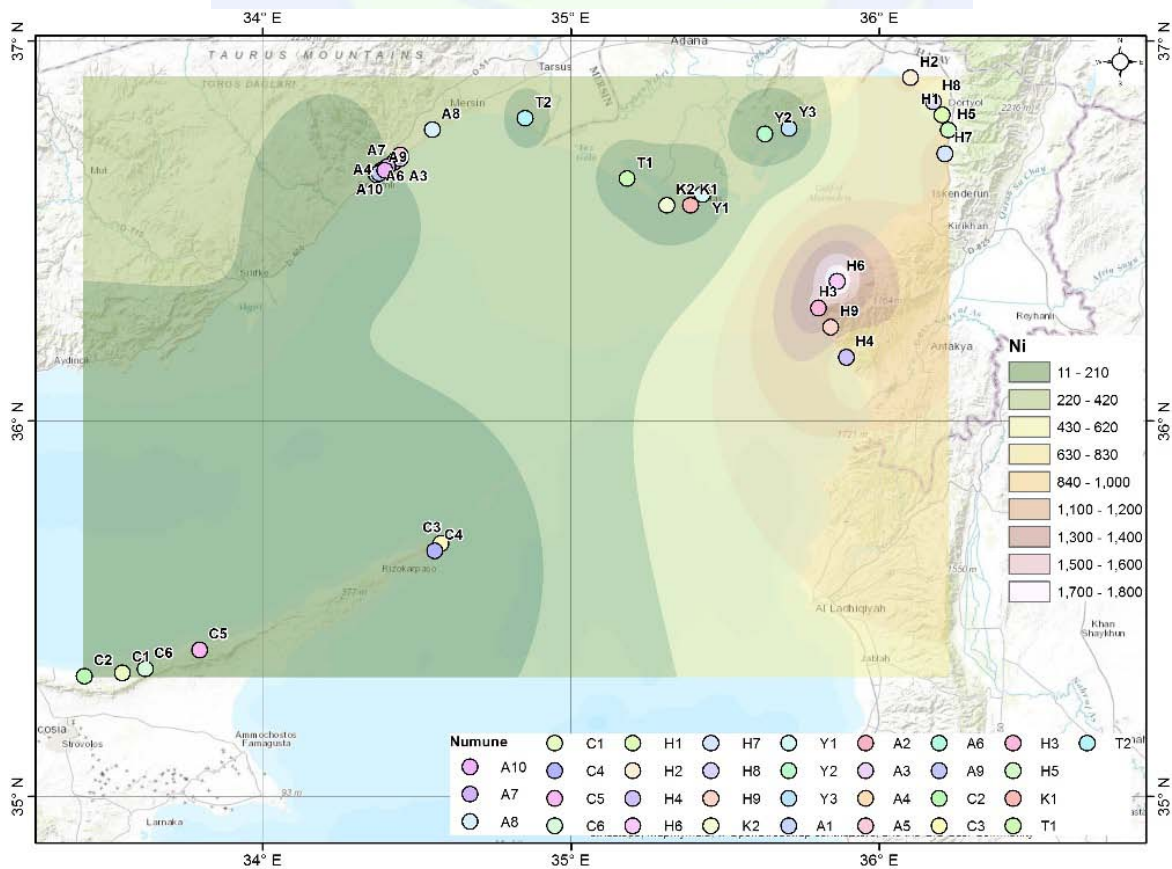


Figure 4. Ni distribution graph (ppm).

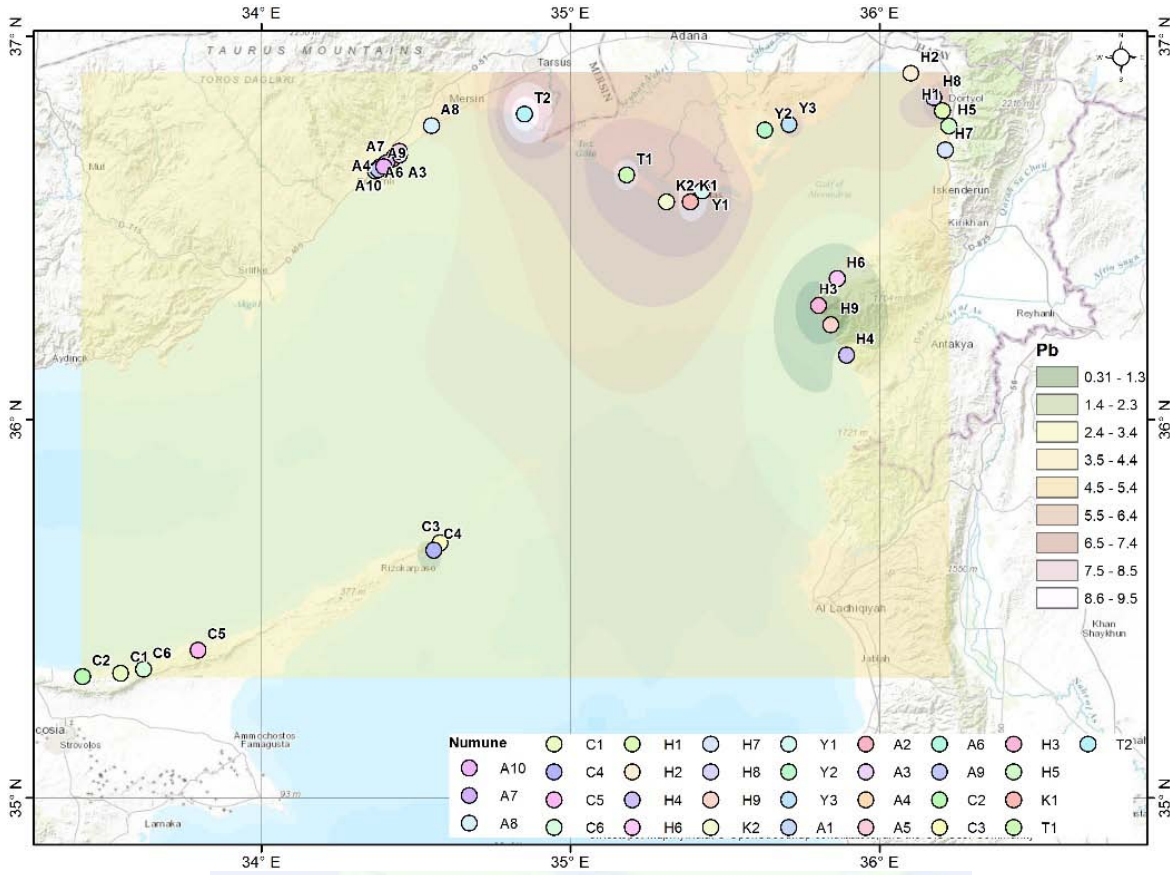


Figure 5. Pb distribution graph (ppm).

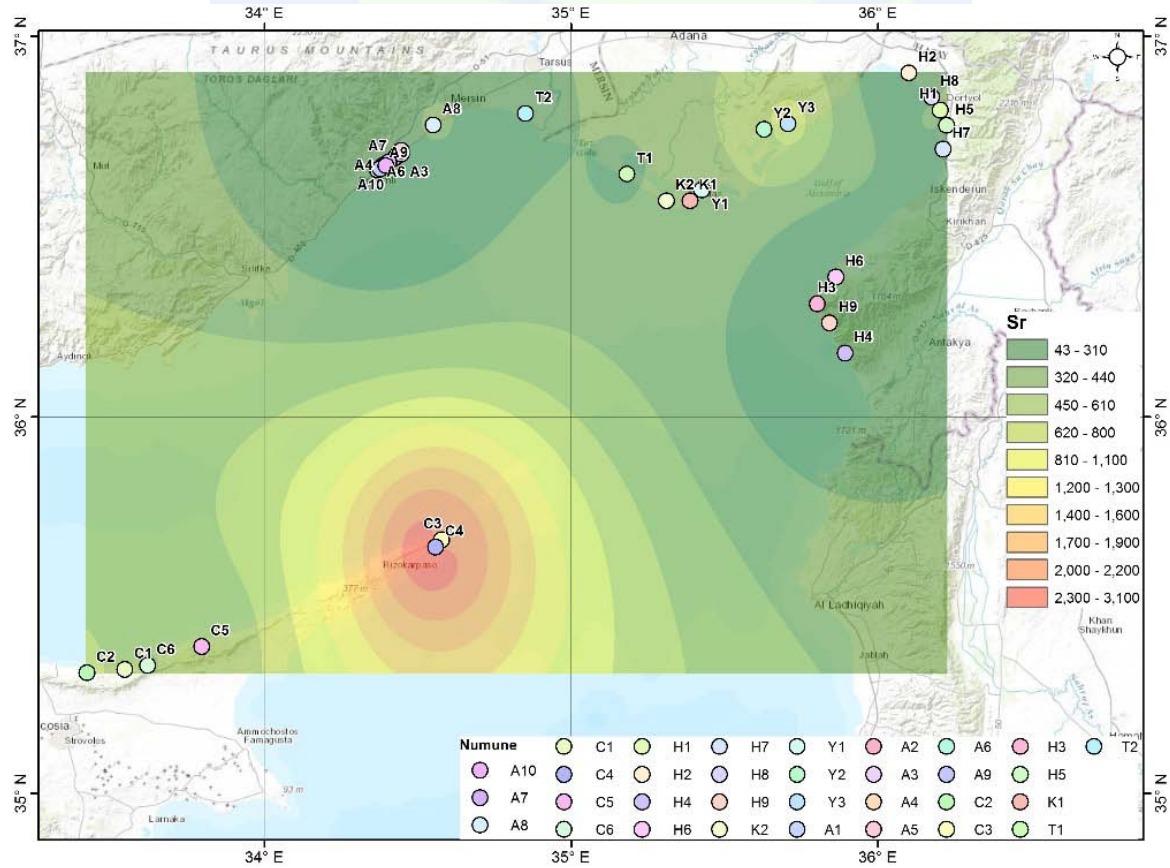


Figure 6. Sr distribution graph (ppm).

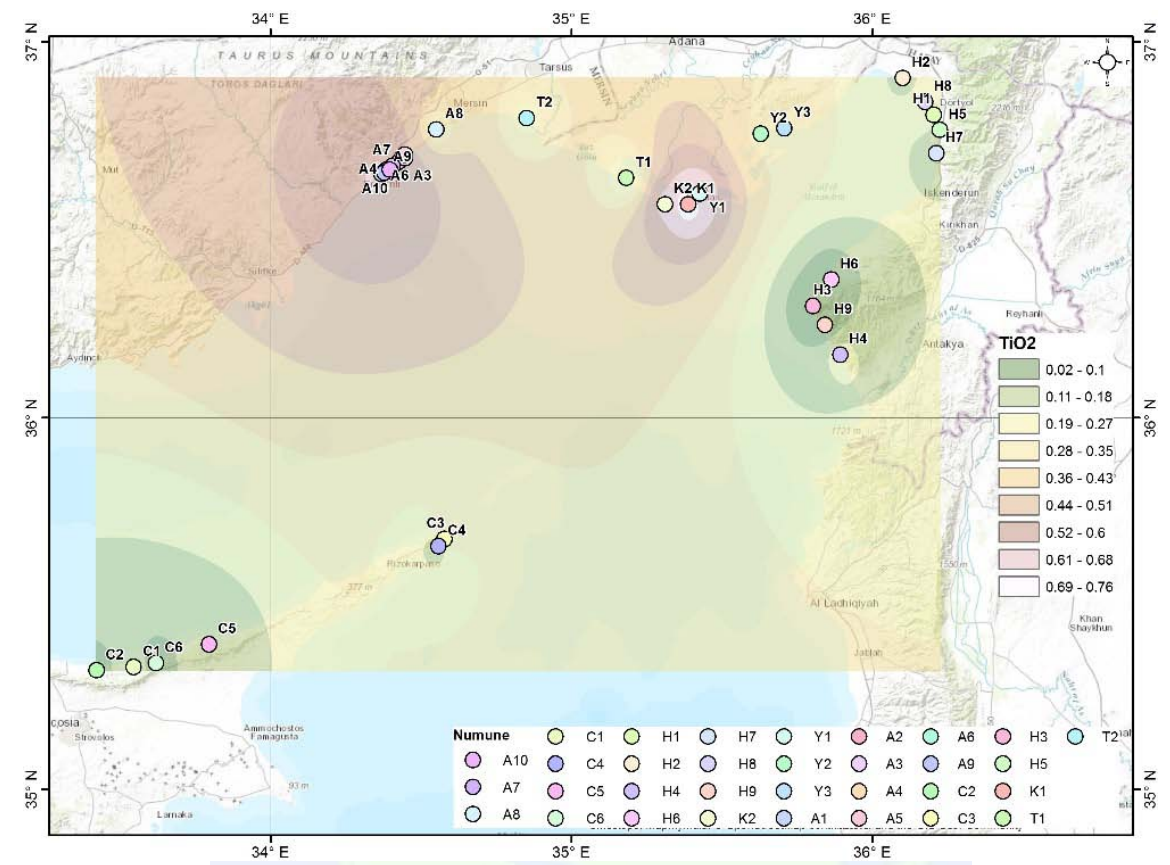


Figure 7. TiO_2 distribution graph (%).

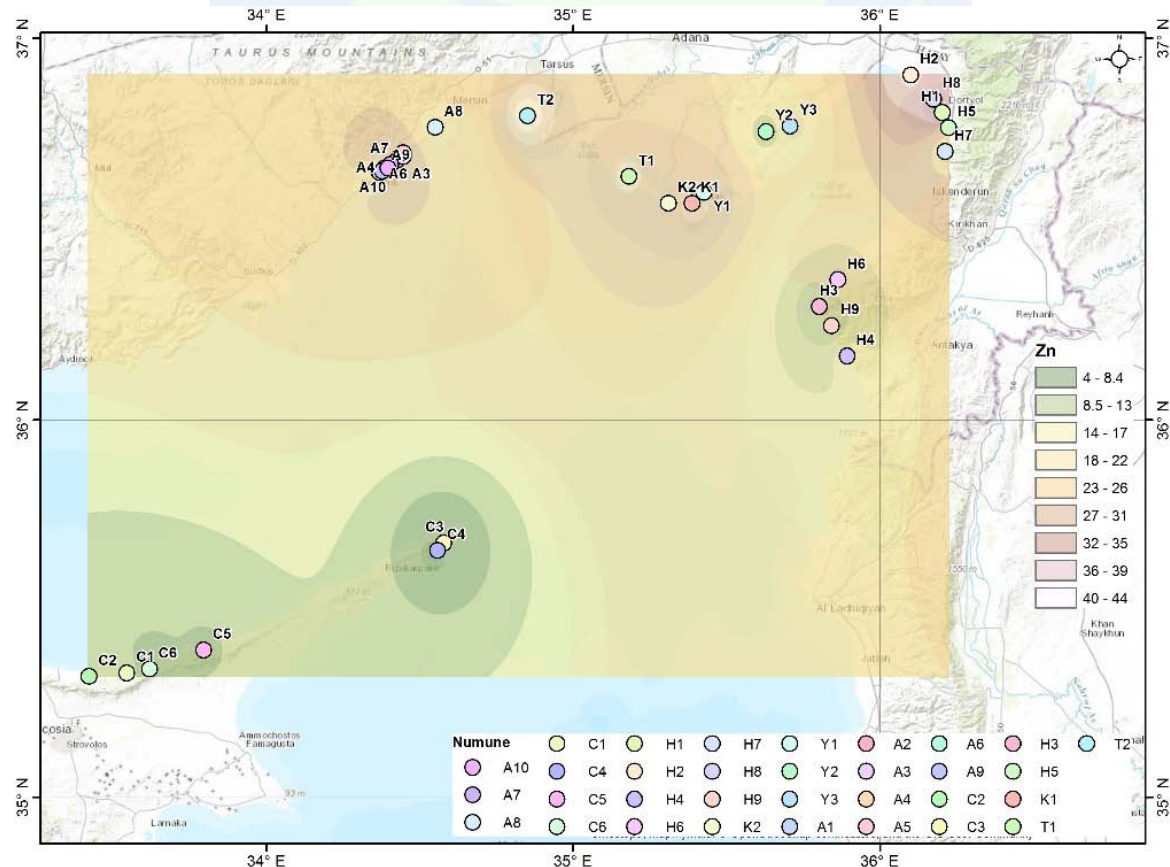


Figure 8. Zn distribution graph (ppm).

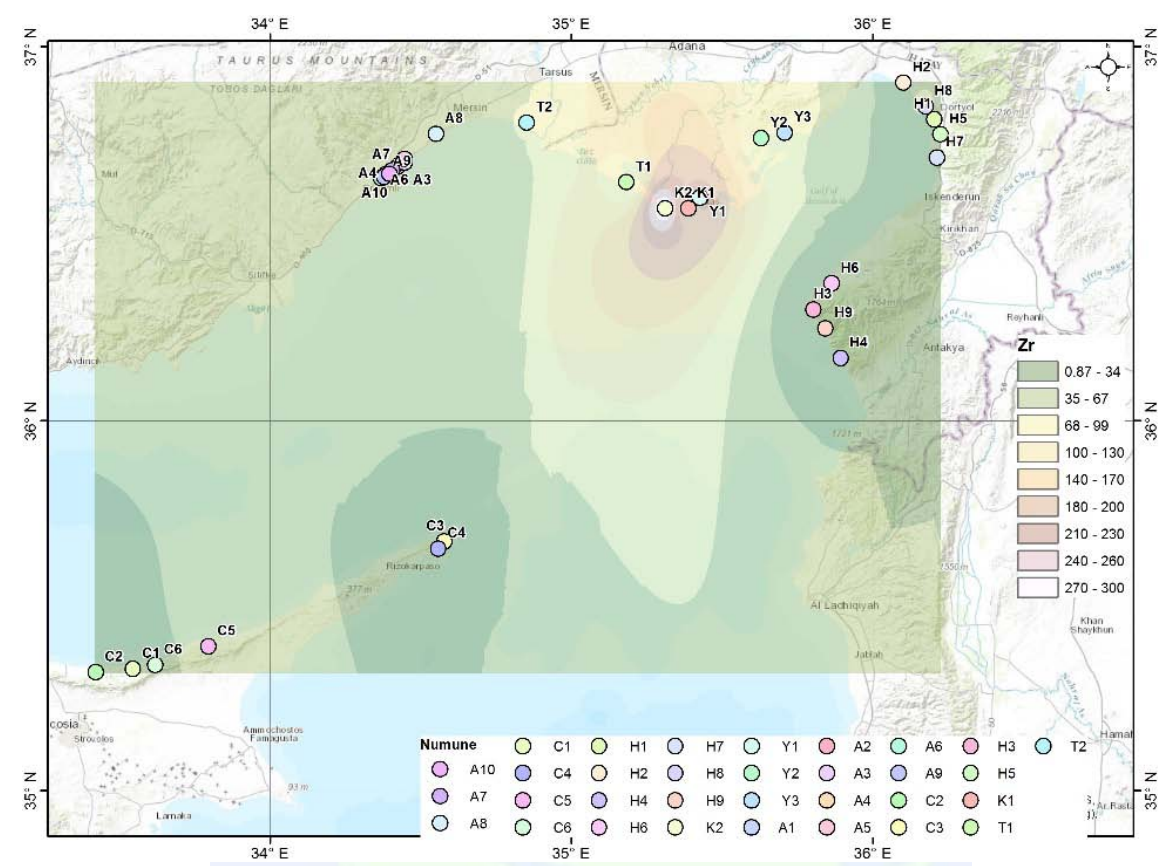


Figure 9. Zr distribution graph (ppm).

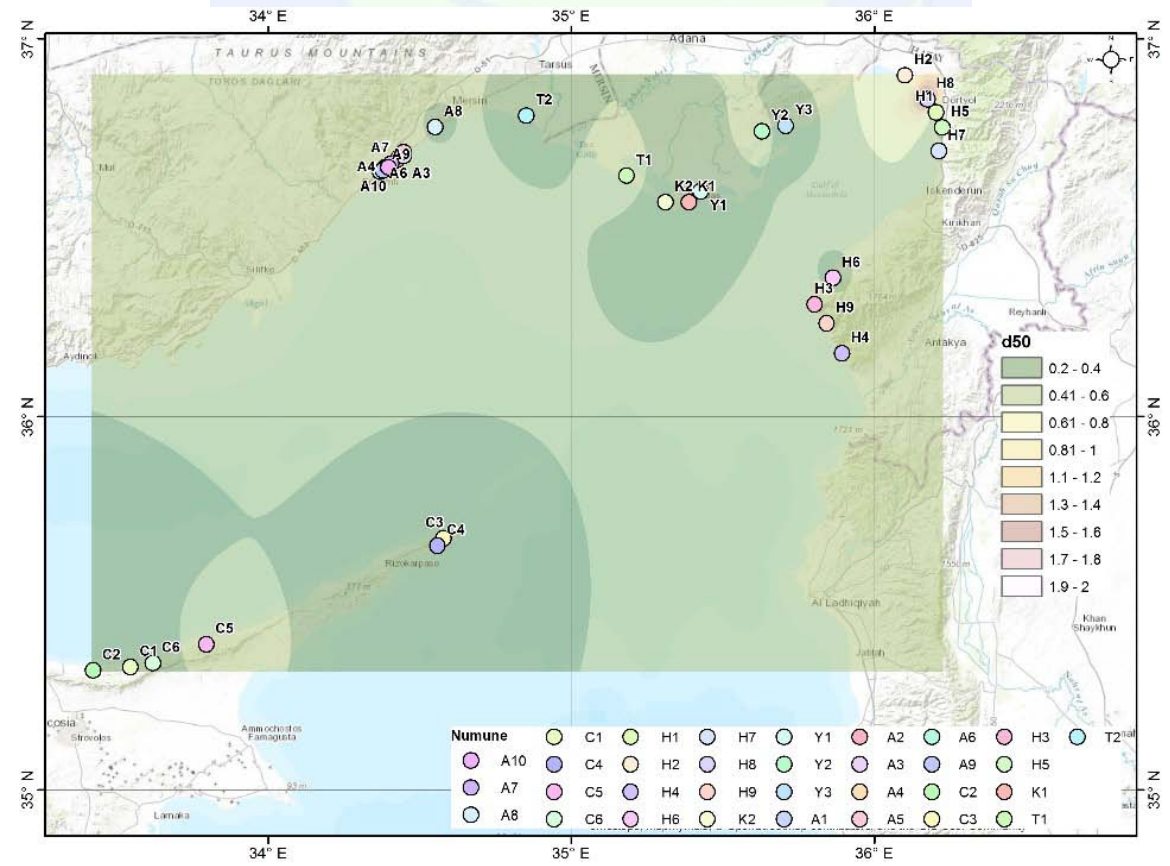


Figure 10. The d50 value distribution chart of all samples (mm).

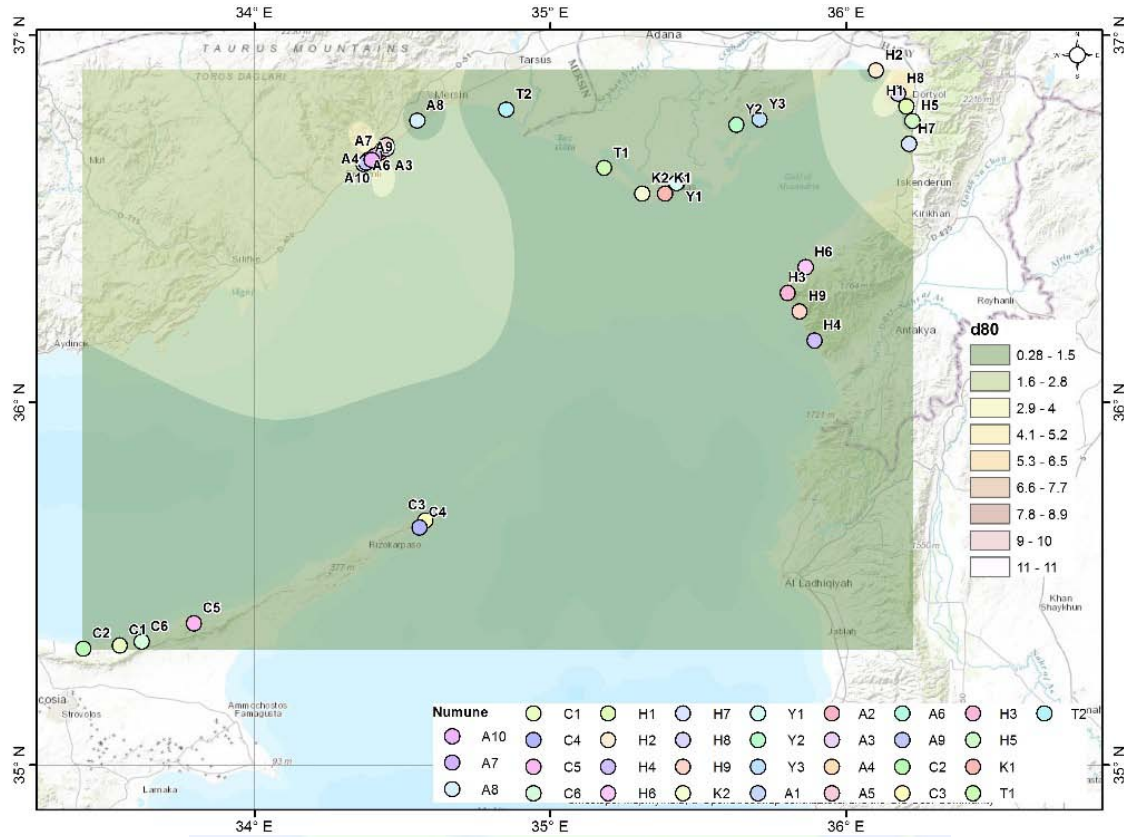


Figure 11. The d80 value distribution chart of all samples (mm).

RESULTS AND CONCLUSIONS

In this study, samplings were made from east to west in Samandağ-Narlıkuyu (Turkey) at 26 locational locations and Dipkarpaz-Girne (KKTC) at 6 location lines. A total of 32 locations were surveyed. The samples whose coordinates are determined by GPS are marked on a map having 1 / 100.000 scale. Formations in the region were inspected, information about the area was recorded, and photographs were taken. This study has revealed the inventory of concentrates which can be considered important in Eastern Mediterranean coasts. The concentrations and the mineral contents determined at the location points are given below.

A: The rates of Fe_2O_3 (6,48-8,66%), MgO (5,92-11,71%) and CaO (14,36-21,94%) are high in the sand. These ratios are due to ophiolitic rocks in accordance with the geology of the region. The ratio of CaO increases because of the limestones in the region. The cobalt ratio is still high because of the regional rocks. The abundance of TiO_2 (0,50-0,70%), Ni (123-442 ppm) and Cr (% 2) is also due to ultrabasic (Peridotite, serpentinite) rocks.

T: High rate of silicon (55-60%), Fe_2O_3 (2% average), MgO (4% average), CaO (12% average) It indicates that there is a serious sandstone sedimentation in the region. There is an increase in concentration in Ba, Sr ratios.

K: Fe_2O_3 (4,5%), TiO_2 (0,22% average), Ba (ppm 409) in sand are not different in other elements. It can be evaluated due to the concentration of Zr element in K2 sample.

Y: Ca is high (27% average). The Sr ratio is around 600 ppm.

H: Fe₂O₃ (3,44-11,04%), MgO (13,72-39,14%), CaO (2,64-20,92%), TiO₂ (0,03-0,17%), Ni (ppm 444-1845), Cr (0.19-1.011%) are remarkable. The high proportion of Ni bound to the ultrabasic rock units suggests that this region can be assessed.

C: There is a significant increase in CaO (33-42%). The limestones in the region have increased the rate.

XRD and microscopic analyzes were performed to obtain more detailed information about the structure of the sampleS. Mineral contents were determined. Mineral paragenesis of each region is revealed. XRD peaks and stereo microscope studies support each other. The contents are as follows.

A: Amorphous quartz, pink quartz, crystal quartz, hematite, magnetite, goethite, calcite, feldspar, chromite, organic material.

T: Quartz, orthoclase, calcite, biotite, opal, olivine, hematite.

K: Crystal quartz, opal, calcite.

Y: Calcite, quartz, feldspar, magnetite, hematite, organic material.

H: Olivine, quartz, calcite, hematite, magnetite, organic material, pyroxene, dentritic opal, little citrin.

C: Calcite, crystal quartz, opal.

The following suggestions can be made regarding future works on the region:

- The chromite concentration (around 2%) in the Mersin provinces, especially in the operable grades, is in question. Further research on this area can be made in the future.
- The zircon concentration in Karataş coasts is considerably higher. As one of the commercial methods of obtaining zircon is coastal placers, feasibility studies can be done for zircon from here.
- Nickel contents were found high in Hatay. Additional work can be done for this circumstance. Moreover, this region can be evaluated because olivine (forsterite) ratio is high especially in H3 region.
- This study can be used to investigate the origins of economically feasible mineral/elemental contents in Turkish coastal sands.
- It is proposed to extend the scope of this study which includes Eastern Mediterranean and Cyprus coasts and to investigate more detailed sampling of mineral/heavy metal contents of the coasts with more sampling.

REFERENCES

- Aykol, A., Gültekin, A.H., 1992. *Plaser Yatakları*, İstanbul Teknik Üniversitesi Vakfı.
- Demirel, E., 2017. Doğu Akdeniz (Samandağı-Narlıkuyu arası) ve KKTC sahil kumlarındaki ağır metal/mineral içeriklerinin araştırılması. Çukurova Üniversitesi, *Yüksek Lisans Tezi*.
- DPT, http://plan9.dpt.gov.tr/oik41_madencilik/41madencilik.pdf, (Erişim Tarihi: 10.06.2016).
- Kozlu H., Goncuoglu C. M., Sarmiento G.N. ve Gul, M.A., 2002. Mid-Ordovician (Late Darriwilian) conodonts from the South-Central Taurides, Turkey: geological implications. *Turkish Journal of Earth Sciences* 11, 1–14.



Imaging of Spectral Properties of Opal Mineral using Sensor Data, Yenice District, North-Western Turkey

**Ayten Çalık^{*1,6}, R. Cuneyt Erenoglu², Oya Erenoglu³, Emin Ulugergerli⁴
and Niyazi Arslan⁵**

¹Department of Geological Engineering, Canakkale Onsekiz Mart University, Terzioğlu Campus, 17020, Canakkale, Turkey, e-mail: aytençalik@comu.edu.tr

²Department of Geomatics Engineering, Canakkale Onsekiz Mart University, Terzioğlu Campus, 17020, Canakkale, Turkey.

³ Department of Geography Education, Canakkale Onsekiz Mart University, Anafartalar Campus, 17020, Canakkale, Turkey.

⁴Department of Geophysics Engineering, Canakkale Onsekiz Mart University, Terzioğlu Campus, 17020, Canakkale, Turkey.

⁵ Department of Geomatics Engineering, Cukurova University, Ceyhan Campus, 01950, Ceyhan, Adana, Turkey.

⁶Canakkale Onsekiz Mart University, Earth Science and Natural History Museum, Terzioğlu Campus, 17020, Canakkale, Turkey

ABSTRACT

In this study, opal mineralization from Yenice district, northeast of Bayramic village are selected for imaging of spectral properties of opal mineral using remote sensing.

Based on the field observations and the result of the XRD and SEM analyses of Yenice opals have been formed by low - T silica- rich hydrothermal solutions in the dacitic volcanic rocks. As a follow up, the region was also analyzed using ASTER remote sensing data. Different band ratios and spectral reflectance values of the region were computed by using different ASTER bands for three days.

Joint evaluation of both methods provides multiple outputs; delineation of the surface coverage of the exposed mineralization, possible extension of the zonation through the morphology and possible internal zonation of mineral accumulation.

INTRODUCTION

Locating mineral occurrence is the first step of the academic and commercial evaluation of the precious and semiprecious gems. Traditionally, as an initial step, both geological maps and tectonic history of the target region pinpoint the possible exploration area. Then, earth

^{*} Corresponding Author

surface needs to be searched by the experts to find possible exposed minerals, if exist any. Next step is to delineate the boundaries of the zone and to define the geological strikes, if possible, associated with the mineralization. As a next step, non-invasive geophysical surveys over and surrounding of the outcrops usually suit for the purpose and image the subsurface geology depending of the physical characterization of the minerals-host relation. Before employing detailed subsurface imaging methods and invasive methods (e.g mechanical drilling or excavation), we propose a quick and efficient approach in this study; joint evaluation of the spectral decomposition remote sensing data, X-ray diffraction(XRD) and scanning electron microscopy (SEM) analyses.

This approach provides information about the surface coverage of the mineral deposition. Although subsurface imaging still needs additional survey, proposed approach leads the decision makers about required additional examination on quality of gems and geophysical survey planning.

XRD has been the principal method for mineral discrimination since the early 1920s (e.g. Westgren and Phragmén 1925) and its application is subject to many Nobel prize in various science. The method relies on the fact that, when a beam of incident X-rays applied, the crystalline atoms diffract it into many specific directions. Diffraction angles and intensities are characteristic to the material and a various other information can be determined. SEM produces images of topography and composition of a sample by scanning the surface of it with a beam of incident electrons. Reflections produce various signals that contain information about the scanned surface. On the other hand, remote sensing detects and classifies objects on the earth surface using reflectivity of the propagated electromagnetic waves.

A common point of the three methods is to explore reflectance of the various electromagnetic fields. It is good to hold that there is a distinct scale difference between the methods. Previous ones are in micro-scale while last one can detect macro-scale surface features. We expected that comparison of the results may present some kind of relation between different method and all can be used for mineral exploration.

We tested our approach over the opal out crop found at the south of Yeniköy district, northeast of Bayramiç village, Çanakkale Turkey (Figure 1). Mineralogical analyses of the opal samples were carried out by X-ray Diffraction (XRD) methods. The samples were analyzed using JEOLJSM-7100F scanning electron microscope (SEM) at different magnifications up to 50000X for texture of samples and major element analyze. X-ray Diffraction was performed on a PanalyticalX'pert Pro MPD operating at 40 kV and 30 mA using Cu-K α radiation. Diffraction patterns were recorded between 3 and 70° theta with step size: 0, 0167 and time per step: 40. The XRD analyses were carried out in Kale Seramik R&D Center - Çanakkale. The samples were analyzed using JEOLJSM-7100F scanning electron microscope (SEM) at different magnifications up to 50000X. The SEM investigations were carried out in Çanakkale Onsekiz Mart University, Science and Technology Application and Research Center.

Furthermore, the ASTER data in AST_L1T format was used for the area between upper left latitude 39° 36' 00" and longitude 26° 08' 40", lower right latitude 39° 33' 00" and

longitude 26° 13' 26". The specification of AST_L1T data was defined in WGS84 datum and UTM Zone 35. The data was selected for minimum cloud coverage, less than % 5, as the thermal bands are adversely influenced from clouds. In order to carry out band ratios, all the SWIR and TIR bands were converted to 15 m of pixel size for spatial resolution and all bands combined with each other by layer stacking.

According to the preliminary results, time-resolved multispectral imaging enables characterizing and classifying some features like minerals more efficiently and in less time. The additional data obtained from multispectral imaging over opal mineral provides new opportunities for feature measurements.

GEOLOGICAL SETTING

The opals, which are the subject of the work, are located in the central part of the Biga Peninsula in Northwest Anatolia and in the south-east of the Yenice Village on the Çan-Bayramiç highway (Fig. 1a).

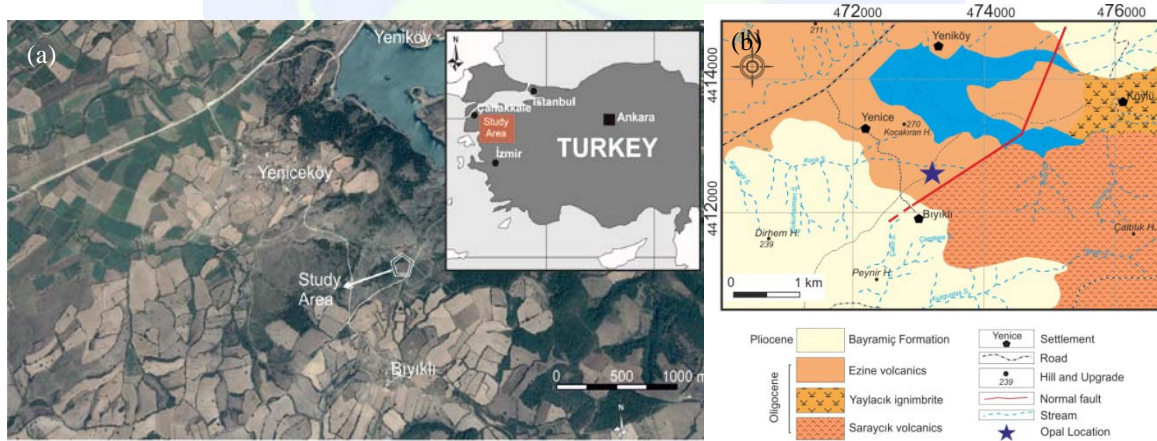


Figure 1. Study area and its geological map.

The area where the Opals are located contains geologically different rock units consisting of magmatic and sedimentary rocks. The volcanic community, which is widespread during the Oligocene period, has been distinguished as three different map units, Saraycık volcanics, Yaylacık ignimbrite and Ezine volcanics due to their lithological differences and stratigraphic locations. After the active magmatism, sediments belonging to the Bayramiç Formation deposited in the Pliocene and later regions are located. (Fig.1b).

In the study area, Saraycık volcanics consist of basic compound rocks. The outer surfaces of Saraycık volcanic units are brownish yellow, clean surfaces gray, dark gray basalt and basaltic andesite (Fig. 2a).

Yaylacık ignimbrites generally consist of yellowish, white colors rhyolites. On the clean surfaces of the rocks with light gray, beige-colored altered surfaces, there is a clear flow of dough and minerals (Fig. 2b). The ignimbrite rocks in the region are overlain by Saraycık volcanics, overlain by Ezine volcanics and the sediments of the Bayramiç Formation.

In the study area, Ezine volcanics are mostly seen as andesitic and dacitic lava flows. Fresh surfaces of lavas are usually gray and pink in color. It is observed in porphyritic and

abundant fractured and cracked. (Fig.2c). The opals in the region are seen in Ezine volcanics. They have different color tones like cream, yellow, and orange, burgundy. This coloration shows the effect of the element of iron found in the bodies. They have a fragile, cracked, fragile texture (Fig. 3). The position of the Opals in the volcanics should probably be related to a fault zone in the immediate vicinity. This fault might have served as a fracture system that provided pathways for the circulation of low-T silica - rich hydrothermal solutions in the region.

Bayramiç formation consists of red-brown conglomerate, light yellowish carbonated sandstone and mudstones (Fig. 2d). Conglomerates and sandstones are massive or roughly layered. Mudstones are generally massive.



Figure 2. a) Basaltic andesite units of Saraycık volcanics, b) The ignimbrites observed around the village of Köylü, c) Overview of andesitic lavas of Ezine volcanics, d) Carbonated sandstones of Bayramic Formation.



Figure 3. Some snapshots from the opals.

MORPHOLOGY AND MINERALOGY OF THE YENICE OPALS

The opals occur as veins in Oligocene dacite host rock where outcrops at the south of Yeniköy district, northeast of Bayramiç village. Macroscopically, opals are beige, yellowish – beige to sub translucent red and brown coloured (Fig. 4a). The opal veins are fractured and more altered to clay minerals near the surface (Fig. 4b).

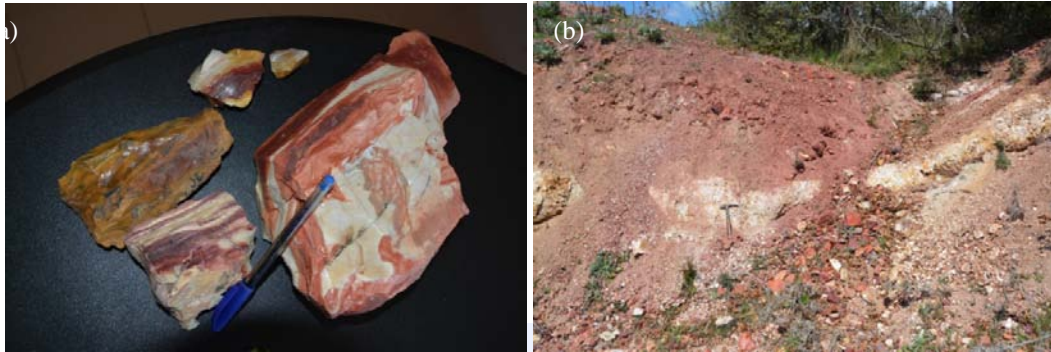


Figure 4. (a) Beige, yellowish – beige to sub translucent red and brown coloured Yenice opals. (b) Yenice opal veins are fractured and more altered to clay minerals near the surface.

The XRD analyses revealed that Yenice opals are composed of opal – CT, opal – C and alpha quartz– moganite (Fig. 5).

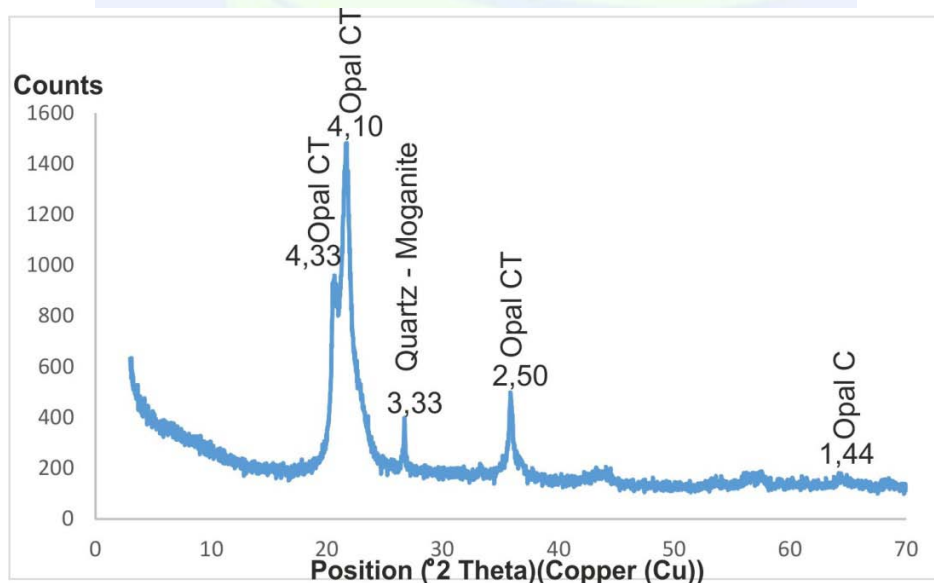


Figure 5. The XRD pattern of the Yenice opal.

MICROSCOPY AND GEOCHEMISTRY OF THE YENICE OPAL

SEM images of the fresh crack surface of the Yenice Opals (beige, yellowish- beige and red body coloured opals), which were taken at 50000x magnification. SEM images show that the internal structure of the Yenice opals consists mainly of spherulitic texture (Fig. 6). The opals are made up of tiny spheres that can be observed with SEM. There is a large variations sphere in size.

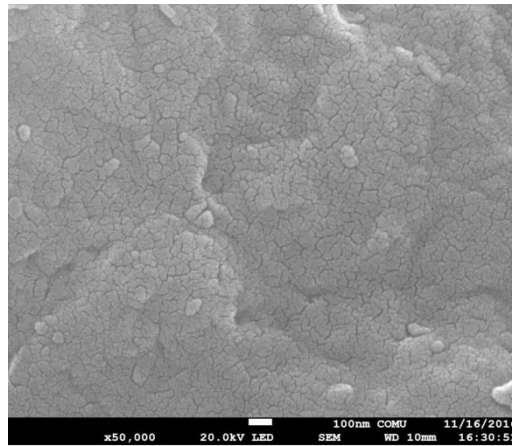


Figure 6. Electron microscope image of the Yenice opals (50000X magnification).

The major element composition of the opal by SEM reveals that opals are mainly composed of silica. Al, Fe and Ca are also present as the main impurities. The red opal has higher concentration of Fe element than the beige, yellowish - beige opals. Cu and Ti also present in the red opal (Fig. 7). These transition elements might give red colour to the opals.

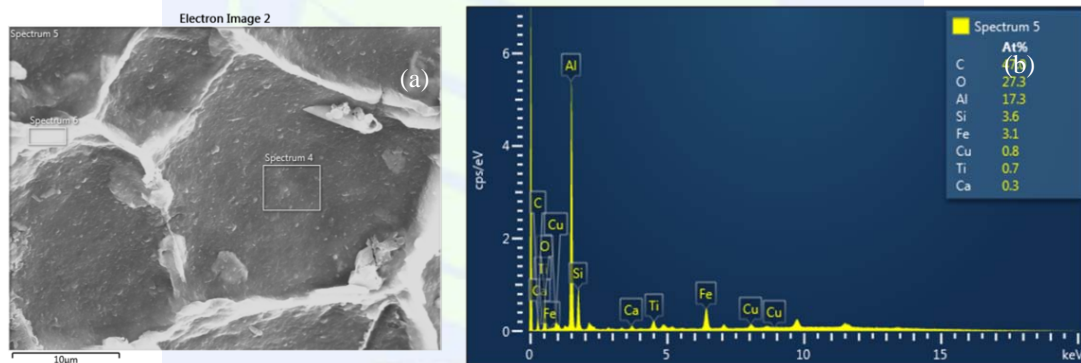


Figure 7. (a) SEM image of the Yenice opal (red colour), (b) Major – element composition of the opal sample by SEM.

REMOTE SENSING RESULTS

In this study, Yenice opals were selected for imaging of spectral properties of opal mineral. The opals occur as veins in the dacite host rock where outcrops at the south of Yeniköy district, the northeast of Bayramiç village. Macroscopically, opals are beige, yellowish – beige to sub translucent red and brown colored. The opal veins are fractured and more altered to clay minerals near the surface. The XRD analyses revealed that Yenice opals are composed of opal – CT, opal – C and alpha quartz. The major element composition of the opal by SEM reveals that opals are mainly composed of silica. Al, Fe and Ca are also present as the main impurities.

Remote sensing is a reliable and widely used method for studies related with Earth. The ASTER AST_L1T data in WGS84 datum and UTM Zone 35N was used for the area between upper left latitude 39° 52'24"N and longitude 26° 39' 51"E, lower right latitude 39° 50' 57"N and longitude 26° 42' 24"E. Two different days were selected at 09:18:10 on

20.09.2000 and 09:14:58 on 11.09.2003, respectively. The center of the opal mineral zone with the $39^{\circ} 51' 44''$ N latitude and $26^{\circ} 41' 06''$ Elongitude is represented by black circle and extended area with the black rectangles in all the Figures. VNIR, SWIR and TIR bands were used in the computation arranging spatial resolution of 15m, 30m and 90m, respectively, to 15m pixel size.

Remote sensing satellites can efficiently be used for mineral exploration equipped with different satellite sensors. These satellite sensors sensitive to radiant energy that is reflected or emitted by an object interacting with atmosphere designed in different wavelength. Each object has a special reflectance and emittance characteristic with respect to the shape, size, and physical, chemical attributes.

In geology, band ratios can be used for spectral enhancement of the images that were implemented to variety of bands in order to highlight different mineral composition. This is the simple and efficient approach to have an idea about the studied region spectral behavior. The band ratio can be obtained by dividing radiance image of one band to the other recorded with Digital Numbers (DNs). Each material has its own spectral feature mentioned as spectral reflectance. In band rationing high reflectance values in spectral reflectance curve is divided into low reflectance values using band absorption feature of the material.

There are several band ratio index generally used in geological studies that approved its efficiency for mineral exploration (Goetz et al., 1983; Kruse et al., 1993; Rowan et al., 2003; Ramadan and Kontny, 2004; Ninomiya and Cudahy, 2005; Amer et al., 2010; Gabr et al., 2010; Sadeghi et al., 2013). In the first step of the study, variety of band ratios were used as Band3 divided into Band2 ($3/2$) for vegetated area, Band4 divided into Band6 ($4/6$) for clay, Band 13 divided into Band 11 ($13/11$) for opal, sum of Band5 and Band 7 divided into Band 6 ($(5+7)/6$) for AlOH, and sum of Band 5 divided into Band 3 and Band 1 divided into Band 2 ($(5/3)+(1/2)$) for ferrous iron, respectively. In the second step, independent component analysis was applied to six SWIR bands in order to highlight spectral separability of different minerals. Independent component analysis is a multivariate statistical method to find undefined features in a set of random variables.

Figure 8a and 8b depicts the study area in VNIR bands for Red (Band 3), Green (Band 2) and Blue (Band 1) color composite at 09:18:10 on 20.09.2000 and at 09:14:58 on 11.09.2003, respectively. The ratio of band 3 to band 2 ($3/2$) were applied to radiance image defining vegetated area that can cause misinterpretation of the selected area for mineral exploration. In Figures 8c and 8d, the values vary from 0.63 to 1.80 and 0.62 to 2.08 at 09:18:10 on 20.09.2000 and at 09:14:58 on 11.09.2003 for the band ratio ($3/2$), respectively. Figures 8e and 8f show the content of clay mineral using ratio of band 4 to band 6 ($4/6$). The values change from 1.07 to 1.57 and 1.21 to 1.72 at 09:18:10 on 20.09.2000 and at 09:14:58 on 11.09.2003, respectively. If we exclude the vegetated area using vegetation index ($3/2$), clay index ($4/6$) take values about 1.40 and 1.45 in the intersection of a circle and square (Fig. 8e). Circled area shows the opal mineral region with the extent of square. In Figure 8f, the values are between 1.35 and 1.45 around the circle. Vegetated areas show high values as red color in all figures. Opal mineral can be found in

quartz related region. Quartz mineral enclosed by clay and hydroxyl-bearing minerals (Zhang et al, 2016). All these minerals spectrally contribute to absorbance properties of the material resulting in different reflectance values. The spectral reflectance curves of opal and quartz shows similar patterns. The opal index can be calculated by dividing the ASTER band 13 to band 11. Figures 9c and 9d show opal index (13/11) between 1.22 and 1.28 at 09:18:10 on 20.09.2000 and 1.25 and 1.29 at 09:14:58 on 11.09.2003, respectively. In these Figure, opal index takes values about 1.25 in a square around the circle. The presence of AIOH mineral can be obtained by $(\text{Band } 5 + \text{Band } 7) / \text{Band } 6$ band ratio that is given at 09:18:10 on 20.09.2000 (Fig. 9e) and at 09:14:58 on 11.09.2003 (Fig. 9f). The values changes between 1.69 and 2.12 (Fig. 9e) and 1.62 and 2.18 (Fig. 9f). In Figures 9e and 9f, AIOH index takes values between 1.90 and 2.00 depict the presence of AIOH mineral content in a square around the circle.

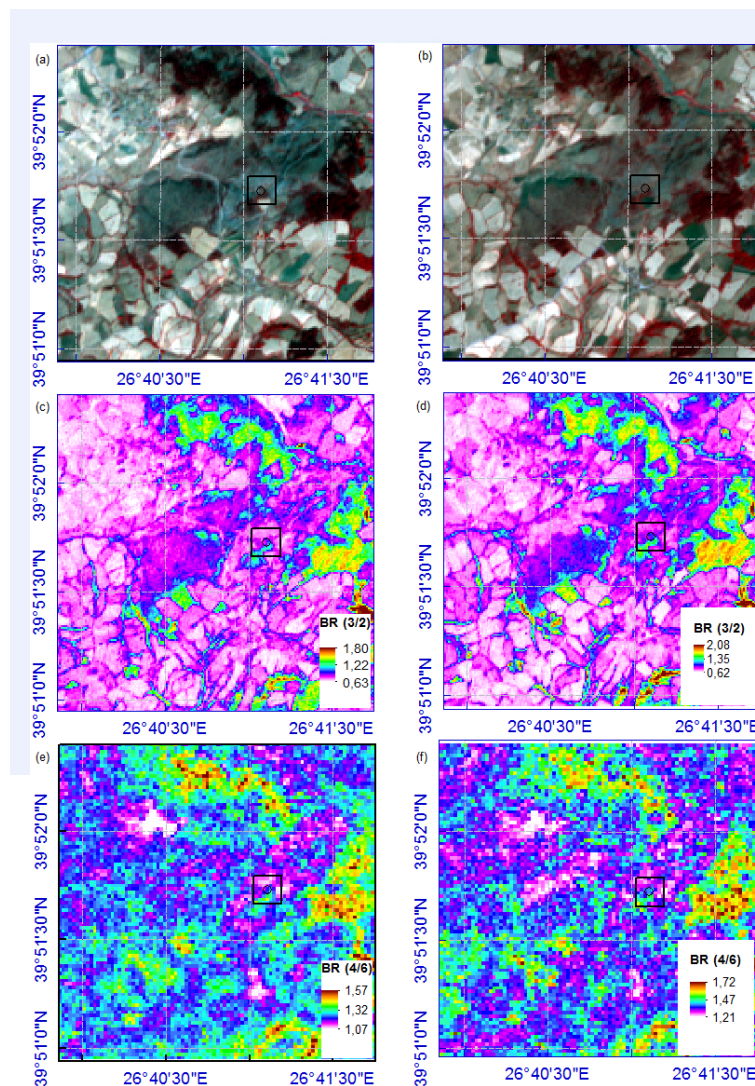


Figure 8. Red (Band 3), Green (Band2) and Blue (Band1) band combination of three ASTER bands: **a.** at 09:18:10 on 20.09.2000, **b.** at 09:14:58 on 11.09.2003; Band ratios of the ASTER bands: **c.** Band 3 to Band 2 at 09:18:10 on 20.09.2000, **d.** Band 3 to Band 2 at 09:14:58 on 11.09.2003, **e.** Band 4 to Band 6 at 09:18:10 on 20.09.2000, **f.** Band 4 to Band 6 at 09:14:58 on 11.09.2003.

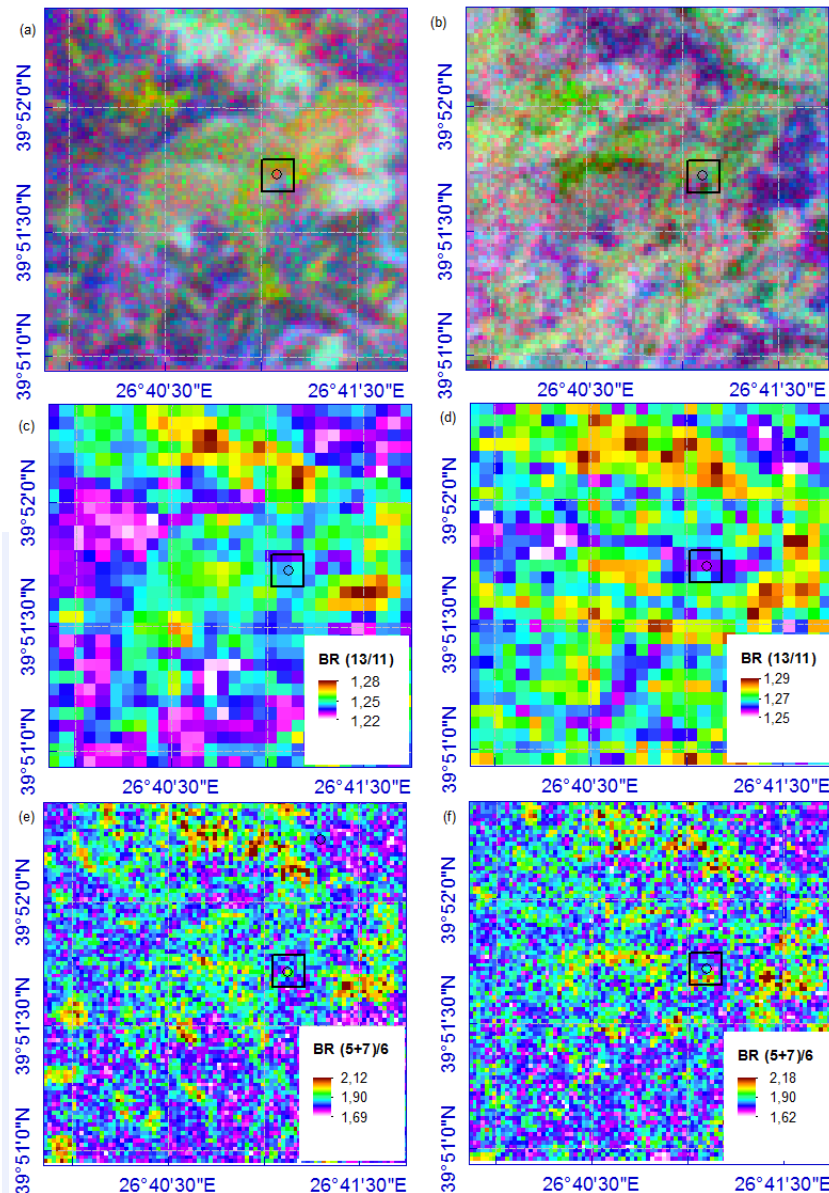


Figure 9. Color composite of independent component analysis in Red (ICA 3), Green (ICA 2) and Blue (ICA 1): **a.** at 09:18:10 on 20.09.2000, **b.** at 09:14:58 on 11.09.2003; Band ratios of the ASTER bands: **c.** Band 13 to Band 11 at 09:18:10 on 20.09.2000, **d.** Band 13 to Band 11 at 09:14:58 on 11.09.2003, **e.** (Band 5+ Band 7) / Band 6 at 09:18:10 on 20.09.2000, **f.** (Band 5+ Band 7) / Band 6 at 09:14:58 on 11.09.2003

In Figures 9a and 9b, color composite of independent component analysis results are given at 09:18:10 on 20.09.2000 and at 09:14:58 on 11.09.2003, respectively. In the center of the circle red color shows exact point of the opal mineral (Fig. 9a). Color composite of independent component analysis successfully demonstrate the location of this mineral that was suppressed. When the Figure 9b is examined, similar findings can be found in the center and bottom of the circle.

The selected area is analyzed for iron mineral as the opal mineral includes minerals such as iron. Figure 10 shows ferrous iron index (Band 5/Band 3)+(Band1/Band2) for the selected

days. The values range between 1.42 and 2.16 and between 1.28 and 2.30 respectively. There are maximum values about 2.16 (Fig. 10a) and 2.30 (Fig. 10b) in red color around the circles that shows high iron content.

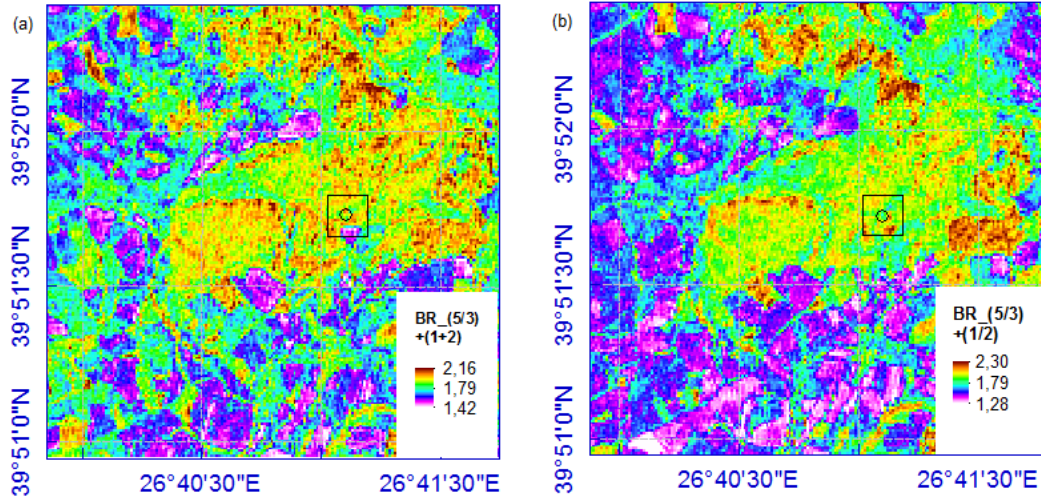


Figure 10. Band ratio of the (Band 5/Band 3)+(Band1/Band2)a. at 09:18:10 on 20.09.2000, b. at 09:14:58 on 11.09.2003.

CONCLUSIONS

Geological mapping using remote sensing data is very important for pre-field geological mapping of an area, especially where it is not easily accessible. Remote sensing data used for this study are freely available. Therefore, pre-field geological mapping and property extraction using these data sets has great advantage in reducing cost, time and human labor. The approach over the opal out crop found at the south of Yeniköy district, northeast of Bayramiç village, Çanakkale Turkey. The opal samples were mineralogically analyzed by XRD methods. According to the XRD results, the major element composition of the opal by SEM reveals that opals are mainly composed of silica. For remote sensing processing, the ASTER data in AST_L1T format was processed using different band combinations and independent component analysis for a geological classification. We evaluated the applicability of the ASTER data for obtaining geological information on lithological mapping associated with opal mineral, using the selected image-processing methods. The ASTER data yielded spectral information that allowed identification of vegetated area, clay mineral, opal mineral and AlOH. This investigation demonstrates the implications for geologists of ASTER data for opal mineral exploration.

ACKNOWLEDGMENTS

This study was supported by Canakkale Onsekiz Mart University, Scientific Research Projects Coordination Unit (FHD-2016-987).

REFERENCES

- Amer, R., Kusky, T. and Ghulam, A., 2010. Lithological Mapping in the Central Eastern Desert of Egypt Using ASTER Data. *J. Afr. Earth Sci.* 56, 75–82.
- AST, 2015. Advanced Spaceborne Thermal Emission and Reflection Radiometer (ASTER) Level 1 Precision Terrain Corrected Registered At-Sensor Radiance Product (AST_L1T), AST_L1T Product User's Guide. Version 1.0, USGS, EROS Data Center Sioux Falls, South Dakota.
- Dai, F.C., Lee, C.F. and Zhang, X.H., 2001. GIS-based geo-environmental evaluation for urban land-use planning: a case study. *Engineering Geology* 61, 257–271.
- Gabr, S., Ghulam, A. and Kusky, T., 2010. Detecting Areas of High-Potential Gold Mineralization Using ASTER Data. *Or. Geol.* 38, 59–69.
- Goetz, A.F.H., Rock, B.N., Rown, L.C., 1983. Remote Sensing Exploration an Overview. *Econ. Geol.* 78, 573–590.
- Herrmann, S. and Osinski, E., 1999. Planning sustainable land use in rural areas at different spatial levels using GIS and modelling tools. *Landscape and Urban Planning* 46 (43): 93-101.
- Kruse, F.A., Lefkoff, A.B., Boardman, J.B., Heidebrecht, K.B., Shapiro, A.T., Barloon, P.J. and Goetz, A.F.H., 1993. The Spectral Image Processing System (SIPS) - Interactive Visualization and Analysis of Imaging Spectrometer Data. *Remote Sens. Environ.* 44, 145–163.
- Ninomiya, Y.F.B. and Cudahy, T.J., 2005. Detecting Lithology with Advanced Spaceborne Thermal Emission and Reflection Radiometer (ASTER) Multispectral Thermal Infrared Radiance-at-Sensor Data. *Remote Sens. Environ.* 99, 127–139.
- Ramadan, T.M. and Kontny, A., 2004. Mineralogical and Structural Characterization of Alteration Zones Detected by Orbital Remote Sensing at Shalatein District, SE Desert. *Egypt. J. Afr. Earth Sci.* 40, 89–99.
- Rowan, L., Hook, S.J., Abrams, M.J. and Mars, J.C., 2003. Mapping Hydrothermally Altered Rocks at Cuprite, Nevada, Using the Advanced Spaceborne Thermal Emission and Reflection Radiometer (ASTER), a New Satellite-Imaging System. *Econ. Geol. Bull. Soc. Econ. Geol.* 98(5), 1019–1027.
- Sadeghi, B., Khalajmasoumi, M., Afzal, P., Moarefvand, P., Yasrebi, A.B., Wetherelt, A., Foster, P. and Ziazarifi, A., 2013. Using ETM+ and ASTER Sensors to Identify Iron Occurrences in the Esfordi 1: 100000 Mapping Sheet of Central Iran. *J. Afr. Earth Sci.* 85, 103–114.
- T. Zhang, G. Yi, H. Li, Z. Wang, J. Tang, K. Zhong, Y. Li, Q. Wang and X. Bie, 2016. Integrating Data of ASTER and Landsat-8 OLI (AO) for Hydrothermal Alteration Mineral Mapping in Duolong Porphyry Cu-Au Deposit, Tibetan Plateau, China. *Remote Sens.*, 8, 890.

Westgren A; Phragmén G (1925). "X-ray Analysis of the Cu-Zn, Ag-Zn and Au-Zn Alloys". Phil. Mag. 50: 311.



Relationship Investigation between Roughness and Temperature of Rock Surfaces

Abdullah Harun Incekara^{*1}, Dursun Zafer Seker², Celil Serhan Tezcan²
Erkan Bozkurtoglu³, Bulent Bayram⁴

¹ Gaziosmanpasa University, Department of Geomatics Engineering, 60150 Tasliciftlik, Tokat, Turkey

e-mail: abdullah.incekara@gop.edu.tr

² Istanbul Technical University, Department of Geomatics Engineering, 34469 Maslak, Istanbul, Turkey

e-mail: seker@itu.edu.tr

³ Istanbul Technical University, Department of Geological Engineering, 34469 Maslak, Istanbul, Turkey

e-mail: erkan@itu.edu.tr

⁴ Yıldız Technical University, Department of Geomatics Engineering, 34210 Esenler, Istanbul, Turkey

e-mail: bayram@yildiz.edu.tr

ABSTRACT

Roughness properties of rock structures have a significant impact on surface reaction to some processes like weathering. In this study, relationship between roughness and temperature of rock surface which is located in Istanbul Technical University Ayazaga Campus was investigated. Size of selected object is approximately 3 m x 1 m and areas that are rougher than their surroundings are clearly identifiable by visual interpretation. 3D model of rock surface was produced with the help of photographs and 12 control points which were homogeneously distributed on the object. Temperature values of all ground control points were measured by infrared thermometer. These values were used as basic data to produce temperature map of the rock surface. Temperature distribution map was produced by using IDW interpolation method in a commercial GIS software. On the rock surface, the temperature distribution in the regions that can be clearly seen as rough was examined. The temperature map was evaluated together with the 3D model produced by thermal photographs for the same surface. Obtained results presented that there is a strong relationship between roughness and temperature of the rock surfaces.

INTRODUCTION

Rock is a mineral mass or a mineral-like solid which consists entirely of a single mineral as well as the accumulation of multiple minerals. A small number of rocks are composed of non-mineral substances like solid organic residues (Ocakoglu, 2014). Measurements are

^{*} Corresponding Author

usually made in contact with the surface in order to determine the existing characteristics of the rock. Photogrammetric methods may be preferred in situations where the geological methods may be dangerous and ineffective due to the location of the object. In the photogrammetric method, it is possible to analyze on the 3D model produced with the help of photographs to determine and interpret the rock structure properties such as discontinuity, roughness and weathering. The fact that the 3D model realistically reflects the object is the most important factor that provides this advantage.

The structural disorder and fractures that break the physical connections in the rock structure are called discontinuities (Schultz and Fossen, 2008) and the measure of fluctuations in small scale due to angular changes on the discontinuity surfaces is defined as roughness (Poropat, 2009).

In this study, it has been investigated whether the roughness of the rock structures has a relation with the temperature or not. The behavior of rough surfaces against temperature compared to smooth surfaces has been analyzed. In this way, it has been examined that interpreting the rock surface characterization with the help of temperature distribution is possible or not.

STUDY AREA

Rock surface located in Istanbul Technical University Ayazaga Campus shown in Figure 1 was selected in order to investigate the relationship between roughness and temperature. Selected object has approximately 3 m x 1 m dimensions. It is necessary to form sections with a certain interval on the produced model for the surfaces where the rougher region is not clearly visible, to calculate the roughness angles by means of the fracture angles, and to compare the results with certain standards such as JRC (Avsar et al., 2016). For the selected object, the areas where the roughness is more can be clearly determined by visual interpretation.



Figure 1. Study area

DATA and METHODOLOGY USED

Applied methodology shown in Figure 2 consists of two steps as field study and evaluation of the data obtained in field study. Field study covers the measuring coordinates and

temperature of control points and taking the photographs for surface. The integration and comparison of the obtained data with each other is the second step.

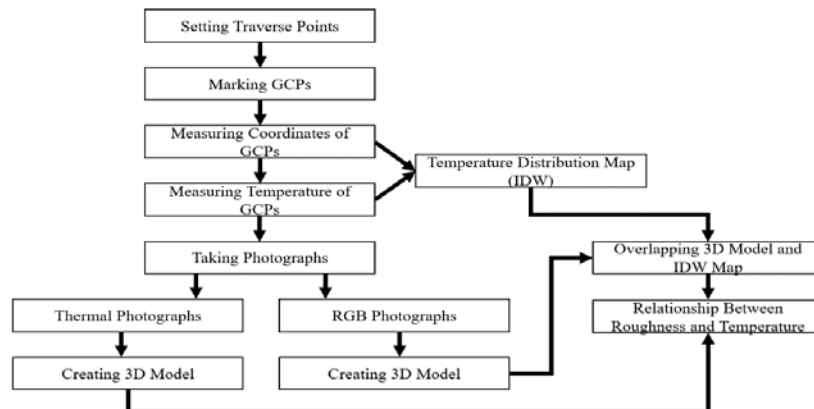


Figure 2. Applied methodology

The target papers prepared for the control points were placed in a homogeneous distribution on the object. Two traverse points in the local coordinate system were used to determine the 3D coordinates of the control points. The averages of the values obtained from both traverse points were taken into account. RGB photographs were taken by mirrorless Sony a600 digital camera with 6000 x 4000 maximum resolution and 24 mm x 16 mm sensor size, which corresponds to approximately pixel pitch of 4 μm . Thermal photographs were obtained by using FLIR thermal camera by controlling with the android software on the phone. It is possible to reflect the surface with different color combinations during the shooting of thermal photographs. Regions warmer than their surroundings are represented by a brighter color such as white and other regions are darker. The color combinations representing the temperature differences can be changed to red and purple instead of white and gray later on.

The temperature values were measured by BENETECH GM300 infrared laser contactless thermometer from the middle of the target papers, which is the part measured by total station, used for the ground control points. There were 17 control points marked during the field study but only 12 of them on the front face which we thought that they were exposed to sunlight under equal conditions were evaluated. The temperature distribution map is only produced for the front face of the rock surface because the incidence angle of the sun rays on the front face of the rock and on the upper side will be different. Thermal photograph example for surface and thermometer used to measure temperatures were shown in Figure 3.

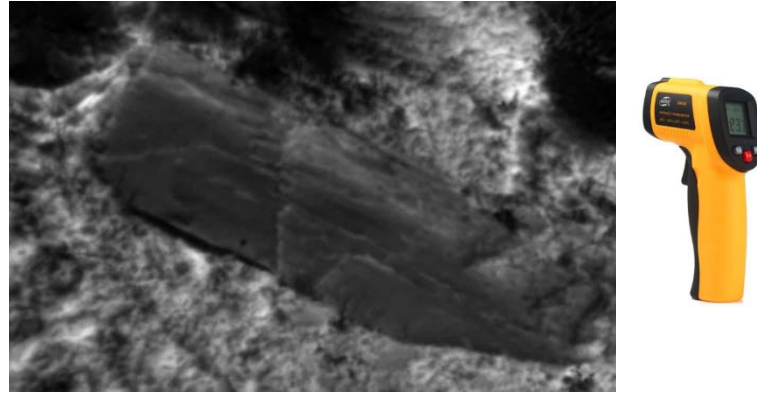


Figure 3. Infrared thermometer used and a thermal image taken

Table 1. Temperature value of ground control points

GCP Number	Temperature Value (°C)
1	36.5
2	36.5
3	36.6
4	37.2
5	32.5
6	34.8
7	32.6
8	32
9	34.7
10	36.8
11	34.5
12	34.9

Intermediate values were estimated with reference to 12 control points where temperature values were measured on the rock. Intermediate value estimation, also called interpolation, is the process of finding the attributes of the unknown points with the help of attribute values of known points. In this step, temperature value of GCPs are attribute data used during interpolation. Inverse Distance Weight (IDW) method which is one of the most commonly used interpolation methods was preferred in order to produce temperature distribution map. The principle of the IDW method is based on the following formula given below. The measured values are used to estimate the value of the unmeasured location. The measured value closest to the estimating region has more effect on the predicted value than the other measured values. So, the IDW method assumes that every measured point has a decreasing effect with distance. In other words, IDW is inversely proportional to distance. While more weight is given to the nearest point, less weight is given to the far point.

$$P_j = \frac{\sum \frac{P_i}{d_{i,j}^n}}{\sum \frac{1}{d_{i,j}^n}} \quad (1)$$

where P_j = Estimated value

P_i = Measured value

$d_{i,j}$ = Distance between measured and unmeasured point

n = Power factor

Discontinuity and roughness regions are shown as 1, 2, and 3 on the 3D model in **Figure 4**. There is a breakup fracture in regions 1 and 3. In region 2, fracture type is cutting fracture. The breakup fracture develops from the weak zone of the rock. In region 1, discontinuity is the breakup fraction developed depending on the compression in the environment and cutting fracture in region 2. Therefore, on the surface of this fracture, rock surface has more roughness than its surroundings. This is the case in region 1. The breakup fracture of the region 3 differs from region 1. In this region, there is a breakup fracture developed during slope down movement of fallen block of the rock. This situation is different from natural discontinuity but as a result the surface is still rough. These regions were evaluated both in the temperature map produced by the IDW method and in the model produced by using thermal photographs.

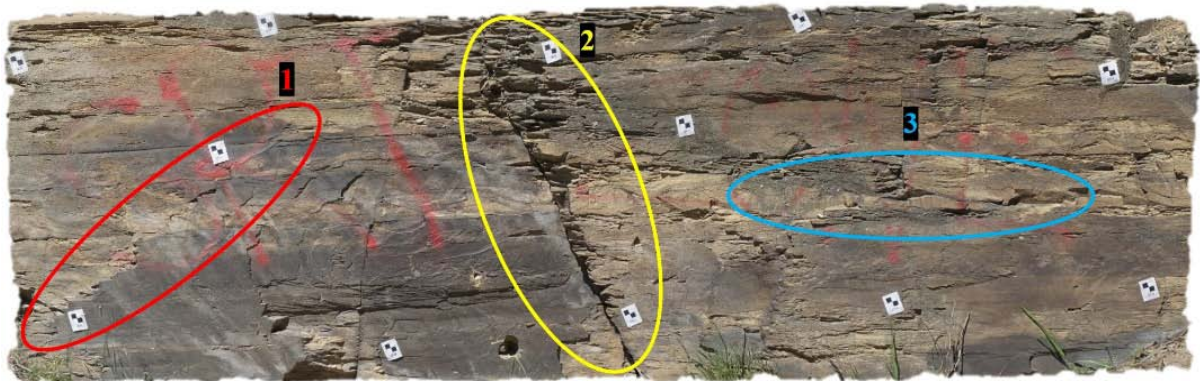


Figure 4. 3D rock surface model and rough areas

RESULTS AND CONCLUSIONS

Using the 3D coordinate information and temperature values of the 12 control points, a temperature distribution map was produced by the IDW method. The temperature distribution map (IDW) were overlapped on the 3D surface model later on. **Figure 5** shows the temperature distribution in different regions of the surface and **Figure 6** depicts the appearance of the same surface obtained with the help of thermal photographs. The upper part of the rock is seen as the hottest area in Figure 6 but this area is not included in the comparison and interpretation in terms of making the evaluation on equal conditions because it is exposed differently to the sunlight according to the front surface of the rock.

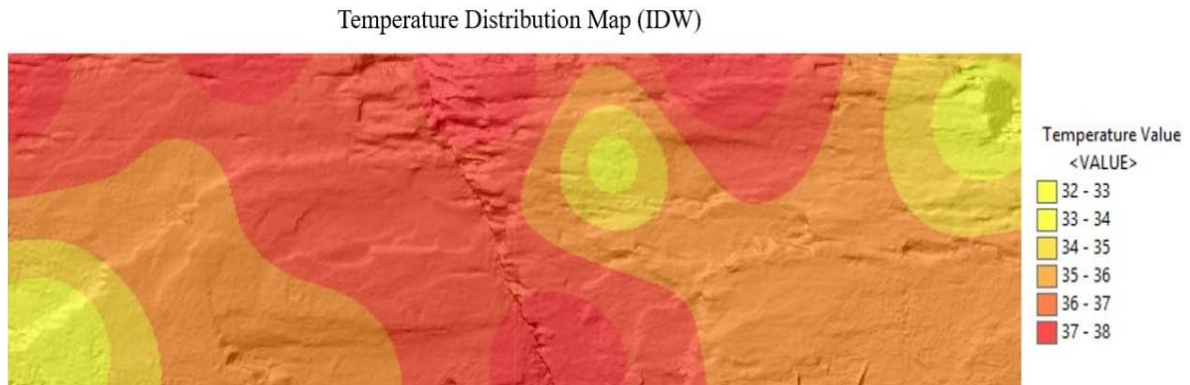


Figure 5: Surface temperature variations

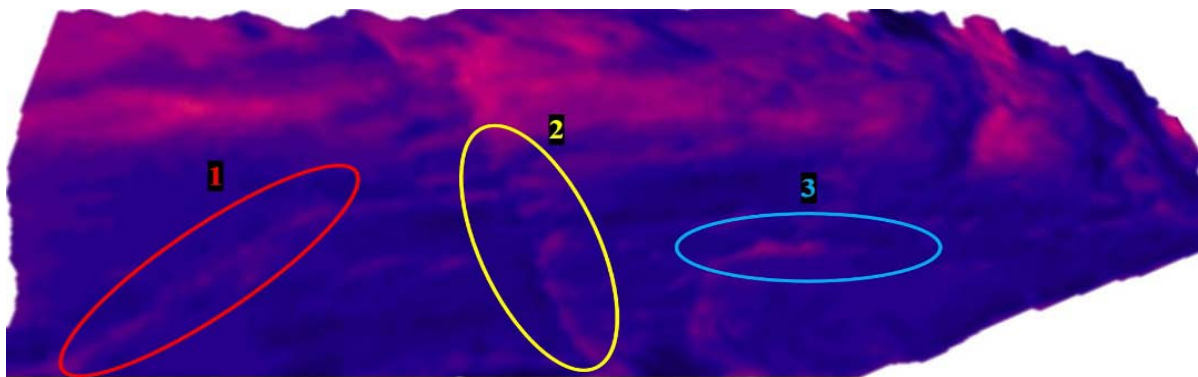


Figure 6: 3D model created by using thermal photographs and roughness regions

3D model produced by using thermal photographs were accepted as reference data to evaluate relationship between roughness and temperature of the rock surface. The reason of this acceptance is completely realistic reflectance of the surface temperature without intermediate value estimation. When 3D model showed in Figure 6 is considered, it is observed that regions which have more roughness are warmer than regions with less roughness under equal conditions. It is clear that the color of the model turns red when regions 1, 2, and 3 are examined. This means that rough areas absorb more sunlight. Temperature distribution of the surface created by means of temperature of control points is partly compatible with thermal model. Region 2 with quite fracture is warmer than its surroundings according to map produced by IDW method. It is not possible to say this completely for regions 1 and 3.

Used thermal camera has not capacity for discrimination of radiometric differences. Also, resolution of thermal photographs is considerably lower than that of digital RGB photographs. Even if these areas have more temperature, it cannot be seen differences among themselves in terms of temperature. A radiometric thermal camera will give a more detailed and correct temperature variation.

Both RGB and thermal photographs of the surface were taken afternoon and the temperature of the control points were also measured simultaneously with the photographing. Therefore, temperature values were between 32° C and approximately 37°

C. Measurements to be made at different times of the day, especially when the surface is not exposed to direct sunlight, will also confirm the relationship between surface roughness and temperature.

The reason why the temperature change on the surface showed by the interpolation map generated by the IDW method does not show similarity in some regions with thermal model may be derived from temperature measurement principle of infrared thermometer. the incident angle of the laser beam to the surface may have caused the measured temperatures to deviate from the actual values.

As a result of the study, it was reached that there is a strong relationship between temperature and roughness. Also, it was seen that obtaining information about rock surface without using thermal camera is possible. It is likely to improve the application in this way in a GIS software which can be used a study to be made rock surface.

REFERENCES

- Avsar, E.O. Bozkurtoglu, E. Aydar, U. Seker, D.Z. Kaya, S. & Gazioglu, C., (2016). Determining roughness angle of limestone using optical laser scanner, *International Journal of Environment and Geoinformatics (IJECEO)*, Vol 3(3), pp. 57-75
- Ocakoglu, F., (2014). Genel Jeoloji-1, Osmangazi Üniversitesi, Jeoloji Mühendisliği Bölümü, Şubat 2014, Eskişehir
- Poropat, G.V., (2009). Measurements of Surface Roughness of Rock Discontinuities, *Proceedings of the 3rd CANUS Rock Mechanism Symposium*, May 2009, Toronto
- Schultz, R.A. & Fossen, H., (2008). Terminology for structural discontinuities, *The American Association of Petroleum Geologists (AAPG)*, Vol 92(7), pp. 853-867

Discrimination and Classification of the Rock-type with Multispectral Sensing

Oya Erenoğlu ^{*1} and R. Cüneyt Erenoğlu²

¹Department of Geography Education, Canakkale Onsekiz Mart University, Anafartalar Campus, 17100, Turkey e-mail: o_turkdonmez@comu.edu.tr

²Department of Geomatics Engineering, Canakkale Onsekiz Mart University, Terzioğlu Campus, 17020, Turkey.

ABSTRACT

This study contains the possibility of separating and classifying remotely-sensed multispectral data from different geological rock-type groups and proposes the use of a low-cost handy sensor, a calibrated multispectral camera. The spectral data was recorded by an ADC II micro multispectral camera mounted on a field-based platform in the spectral range of 520nm to 920nm for the recognition of different geological formations. The software also enables users to convert the green, red and invisible NIR bands captured by the camera as a monochrome image into blue, green and red respectively.

The study area was selected in the southwest of the Biga Peninsula (NW Turkey) to analyze the discrimination potential of this camera for rock types and close-range remote sensing applications. The region consists of Pliocene conglomerates, sandstones and mudstones sediments and Miocene rhyolitic tuffs and ignimbrites intercalated with them. After proper strategy of corrections and data processing, a supervised classification of the multispectral data was performed to distinguish sedimentary and volcanic rocks. The obtained results confirmed that the used multispectral camera can be efficiently exploited to map differences in geological formations.

INTRODUCTION

Photogrammetry makes scientific measurements by the central projection imaging from various types of sensors, particularly for recovering the 3D positions of studied points. Digital photogrammetry has been employed to obtain high accuracy for 3D models of different research areas (Erenoğlu et al., 2017; Yastıklı, 2007; Yılmaz et al., 2007). Modern close-range remote sensing introduced the potential of high-sensitive imagery. The photogrammetric survey has advanced its own traditional acquisition and processing method with the help of developed technology (Remondino et al., 2011; Colomina and Molina, 2014).

* Corresponding Author

The ADC Micro extends the power of advanced multi-spectral imaging to small sized systems. In so doing, Tetracam's smallest multi-spectral imaging marvel makes this powerful technology once only accessible via satellites practical for use by agricultural, industrial and scientific users located around the world. For example, multi-spectral data of the plant surface was successfully used to determine the location of sick leaves on the 3D model (Furbank and Tester, 2011). Multi-spectral data on 3D objects was captured to produce visual images with high quality in computer graphics (Kim et al., 2012). For the production of 3D-models and orthorectified images SLR and high-quality compact cameras are commonly used. For data processing software packages of the conventional imagery as well as computer vision are used (Gehrke and Greiwe, 2013).

This study contains the possibility of separating and classifying remotely-sensed multispectral data from different geological rock-type groups and proposes the use of a low-cost handy sensor, a calibrated multispectral camera. The software also enables users to convert the green, red and invisible NIR bands captured by the camera as a monochrome image into blue, green and red respectively.

The study area was selected in the southwest of the Biga Peninsula (NW Turkey) to analyze the discrimination potential of this camera for rock types and close-range remote sensing applications.

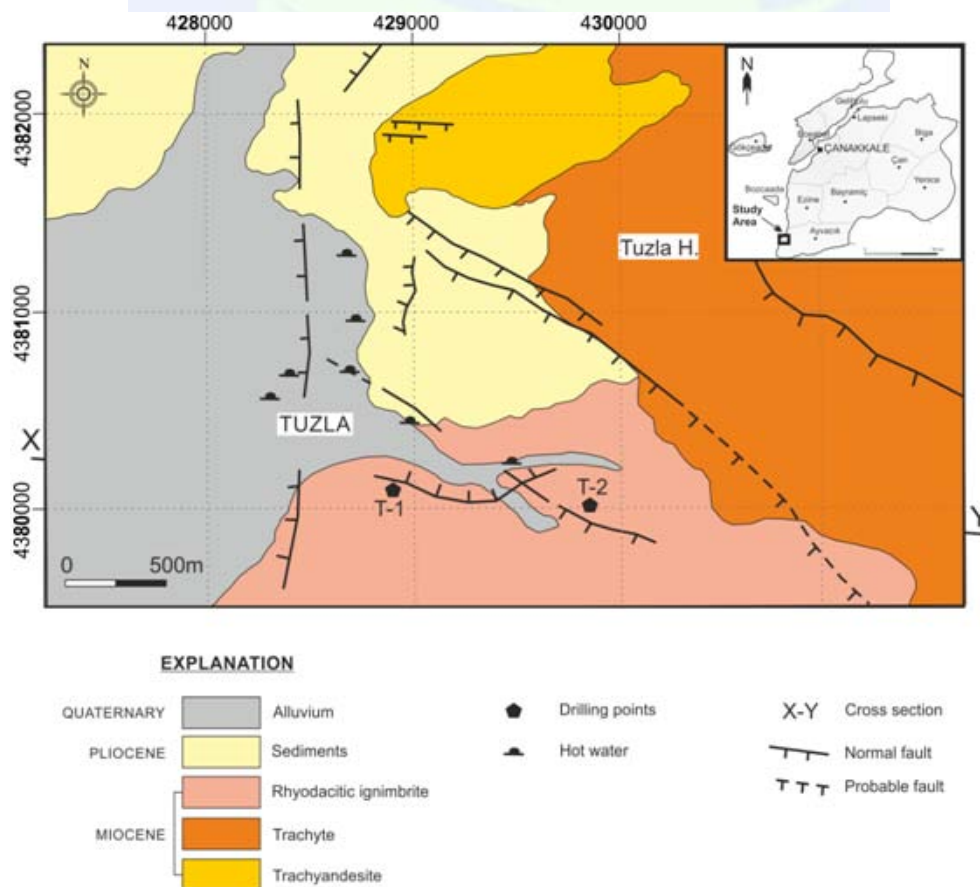


Figure 1. Geological map and geological cross-sections of the study area (Modified from Karamanderesi, 1986).

GEOLOGICAL SETTING

Geological units in the region are represented by the presence of metamorphic, magmatic and sedimentary rocks (Figure 1). The basement rocks of the study area consist of Paleozoic aged metamorphic rocks including gneiss, calcschists and quartzschists. The metamorphic are observed by marble, dolomitic and recrystallized limestone. Oligocene-Lower Miocene aged a granodiorite pluton intruded into these units in the region. This pluton is firstly called as Kestanbol (Tuzla) Pluton by Gözler et al., (1983) and Ercan et al., (1984). The pluton show less range in composition and are generally composed of granodiorite and/or monzogranite and quartz monzonite.

In the study area, the Kestanbol pluton and the volcanic rocks are widely located. The volcanism starting with rhyolitic volcanic tuffs and agglomerates in the area continued trachytic-trachyandesitic lava and then finally rhyolitic tuffs and ignimbrites. In all Miocene, the volcanism has been active for several phases. From the detailed study about Miocene volcanics, Öngör (1973) expressed that the volcanic activity are grouped in three volcanic centers including volcanoes of Behram, Ayvacık and Babakale (Assos). Ayvacık volcano is of andesite, latites, trachyandesite types of lava breccias. Babakale volcano is of numerous lava and volcanic breccias. Behram (Assos) volcano is the center having the highest explosion index. When the early events were latites, dacite and rhyodacite types of lava eruptions, a large number of ignimbrite eruption occurred and these eruptions are spread over a wide area during the second event. The upper Miocene-Pliocene sediments are located on the ignimbrites that are the latest product of volcanism. Quaternary alluvial materials are uncomfortably covered all units in Tuzla plains.

MATERIAL AND METHOD

The development and improvement of various types of sensors, data processing methodologies and multi-resolution 3D representations contribute considerably to identify the different type of rocks in geological works. In this study, the uses of three band multi-spectral camera covering the Near Infra-Red (NIR), Red Green (RG) (spectral range: 0.52-0.92 μ m), and typical digital camera producing an image in the visible spectrum (spectral range: 0.4-0.7 μ m) are proposed to discriminate the type of rocks. Table 1 shows spectral features of the sensors used in this study. In addition, Figure 2 shows the photographs of the multispectral camera.

Table 1. The spectral features of the sensors of the multispectral and digital camera systems

Camera	System	Band number	Spectral range(μ m)	Pixel size (μ m)
Canon 650D	Blue Green Red	3	0.4-0.7	4.3 x 4.3
ADC Micro	Near IR Green Red	3	0.52-0.92	3.2 x 3.2



Figure 2. The multispectral camera used in this study.

Camera Calibration

Numerical estimates of camera interior orientation are requested by focal length, location of the principal point, sensor parameters, and coefficients of lens distortions are identified. During production of ortho-rectified image mosaics, geo-referencing software may use these parameters to produce mosaics with high positional precision. White Teflon Calibration Plate (AKA Calibration tag or Software Calibration Tile) was successfully used to perform the camera calibration (Fig. 3).

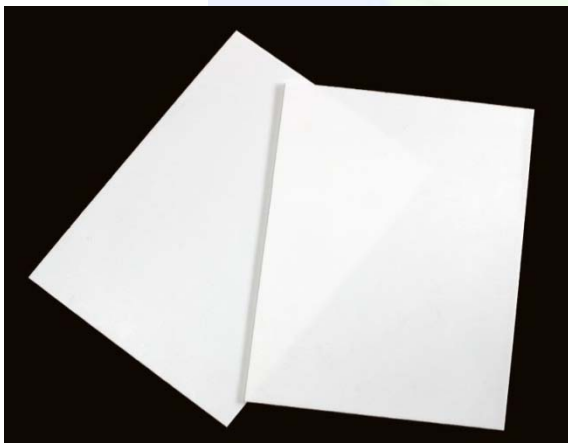


Figure 3. White Teflon Calibration Plate.

ANALYSIS AND RESULTS

The workflow of the procedure used in this study is as follows:

- Digital and multi-spectral imagery acquisition,
- Camera calibration using Tetracam PixelWrench 2 x64 software,
- Feature detection,
- Structure-from-motion,

- Three dimensional point clouds by dense image matching,
- Digital and multi-spectral orthomosaic,
- Spectral indices and supervised classification from the models,
- Rock detection and classification.

First of all, we studied on the image given in Figure 4 in order to extract different lithological units such as ignimbrite (volcanic rock), conglomerate and sandstone (sedimentary rock). For this purpose, the NIR-G filtering was applied on multispectral image. According to the results from the analysis, the volcanic rocks are observed as dark colors while sedimentary rocks are in light colors.

In the figure 5, the faults which are one of the structural unit in the region, were successfully identified using the Green NDVI and the NIR-G processes. Furthermore, in the NIR-G processing provides different lithological units among the sedimentary rocks (conglomerate in red color and sandstone in gray and beige colors). Finally, the salt layers developed around the hot water sources were easily distinguishable using the NIR-G processing of the multispectral analysis (Figure 6).

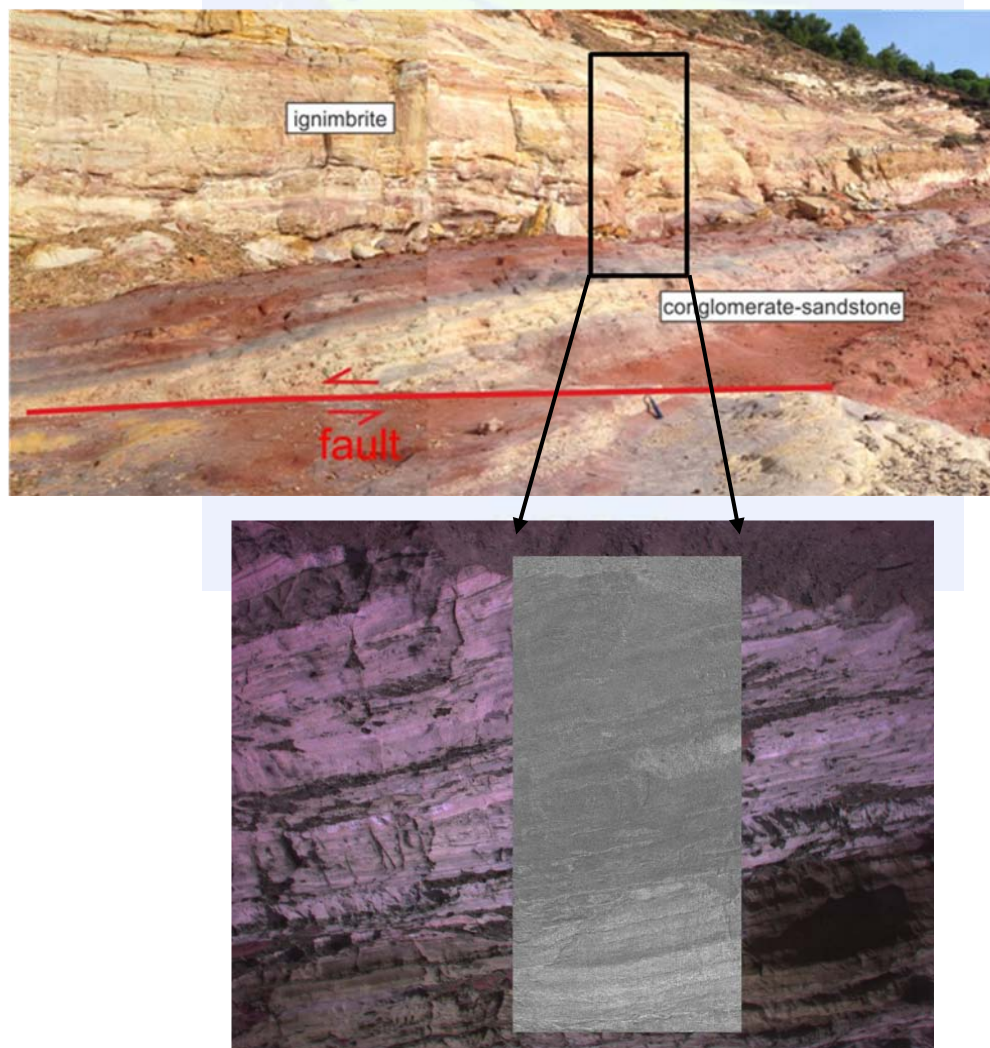


Figure 4. Various lithological units in the study area and multispectral analysis.

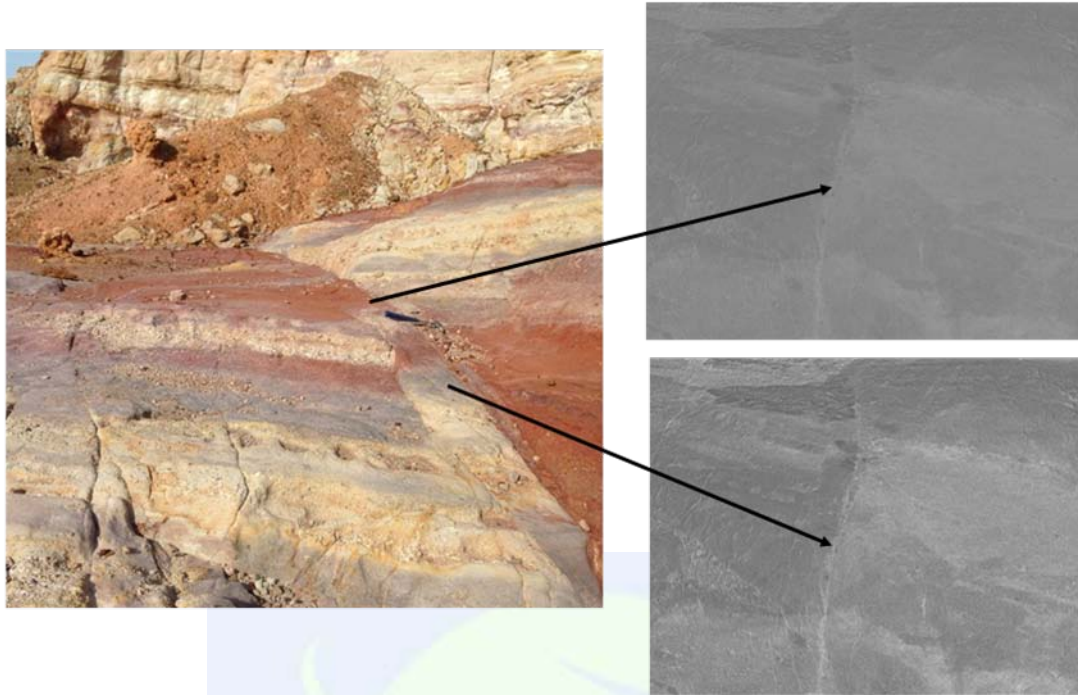


Figure 5. Multispectral analysis results of the fault

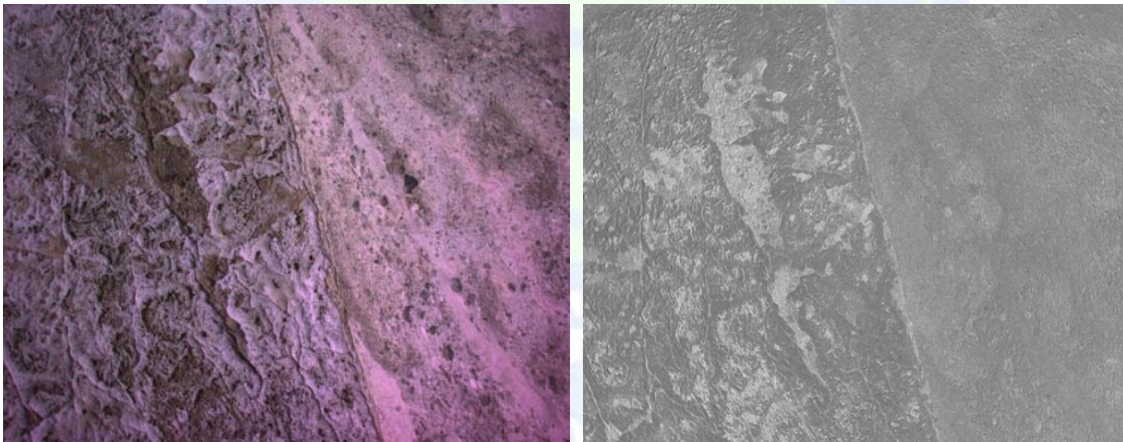


Figure 6. The result of multispectral analysis of rock-salt.

CONCLUSIONS

The study can be briefly concluded as follows:

- A visible-very near infrared multispectral camera was tested and analyzed in a field campaign.
- According to the results above, the sedimentary rocks and ignimbrite were classified using NIR-G process. In addition, some structural elements such as faults and cracks can be determined by Green NDVI and NIR-G process.

- Finally, the salts on the rocks were successfully identified using raw images and NIR-G filtering. The obtained results confirmed that the used multispectral camera can be efficiently exploited to map differences in geological formations.

REFERENCES

- Colomina, I. and Molina, P., 2014. Unmanned aerial systems for photogrammetry and remote sensing: A review, *ISPRS Journal of Photogrammetry and Remote Sensing* 92 (2014) 79–97.
- Ercan, T., and Türkecan, A., 1984, Batı Anadolu-Ege adaları-Yunanistan ve Bulgaristan'daki plutonların gözden geçirilişi: *Türkiye Jeoloji Kurumu Ketin Simpozyumu Kitabı*, 189-208, in Turkish.
- Erenoğlu, R.C., Akçay, Ö., Erenoğlu, O., 2017. An Uas-Assisted Multi-Sensor Approach for 3D Modeling and Reconstruction of Cultural Heritage Site, *Journal of Cultural Heritage*, vol.22, pp.1-12, 2017.
- Furbank, R. and Tester, M. 2011. Phenomics technologies to relieve the phenotyping bottleneck. *Trends in Plant Science* 16(2011) 635–644.
- Gehrke, R. and Greiwe, A., 2013. Multispectral image capturing with foveon sensors. *International Archives of the Photogrammetry, Remote Sensing and Spatial Information Sciences*, Volume XL-1/W2, Rostock, Germany.
- Gözler, M.Z., Ergül, E., Akçören, F., Genç, Ş.C., Akat, V. and Acar, Ş., 1983. Çanakkale boğazı doğusu - Marmara denizi güneyi - Bandırma-Balıkesir-Edremit ve Ege denizi arasındaki alanın jeolojisi ve kompilasyonu: *MTA Rap.*, 7430 (unpublished), in Turkish.
- Karamandereci, I. H. 1986. Hydrothermal Alteration in Well Tuzla T-2, Canakkale, Turkey. Report 3: *Geothermal Training Programme in Iceland UNU G.T.P.*,
- Kim, M.H., Harvey, T.A., Kittle, D.S., Rushmeier, H., Dorsey, J., Prum, R.O. and Brady, D.J., 2012. 3D imaging spectroscopy for measuring hyperspectral patterns on solid objects, *ACM Transactions on Graphics* 4(2012) 1-11.
- Öngür, T. 1973. “Volcanology and geological report of Canakkale Tuzla geothermal area”, *MTA report*, (unpublished).
- Remondino, F., Barazzetti, L., Nex, F., Scaioni, M. and Sarazzi, D., 2011. UAV photogrammetry for mapping and 3D modelling—current status and future perspectives, in: *Proceeding of ISPRS – Int. Arch. Photogramm. Remote Sens. Spatial Inform. Sci.*, 2011, pp. 25–31.
- Yastıklı, N., 2007. Documentation of cultural heritage using digital photogrammetry and laser scanning, *Journal of Cultural Heritage* 8 (2007) 423-427.
- Yılmaz, H.M. Yakar, M. and Gulec, S.A., 2007. Dulgerler, Importance of digital close-range photogrammetry in documentation of cultural heritage, *Journal of Cultural Heritage* 8(2007) 428–433.

Comparison of Surface Morphology Determined with Terrestrial LIDAR Method and Underground Geometry Determined with GPR: Kamara (Denizli/Turkey) Fissure Ridge-type Travertine

Cahit Çağlar Yalçiner^{*1}, Erdem Gündoğdu², Süha Özden³, Erhan Altunel⁴,
Yunus Can Kurban⁵

¹Çanakkale Onsekiz Mart Univ., Çan Vocational Sch., Department of Mining and Mineral Extraction;
e-mail: yalciner@comu.edu.tr

²Çanakkale Onsekiz Mart Univ., Çan Vocational Sch., Department of Mining and Mineral Extraction

³Çanakkale Onsekiz Mart Univ., Faculty of Engineering, Department of Geological Engineering

⁴Eskişehir Osmangazi Univ., Faculty of Engineering, Department of Geological Engineering

⁵Eskişehir Osmangazi Univ., Graduate School of Natural and Applied Sciences, Depart. of Geological Eng.

ABSTRACT

Fissure-ridge type travertines are an important tectonic element and with surface topography and definition of underground geometry very important for our ability to understand formation of travertines. Extensional fractures developing linked to local extension in the upper crust are structural elements allowing hydrothermal fluids to move within the crust. Hot water reaching the surface through these fractures is rich in calcium carbonate and may cause travertine formation with different morphologies at the surface. Among travertines, the type with clearest morphology is fissure ridge type travertines. The general surface morphology of ridge-type travertines is in the form of a lens. This morphological shape varies in dimension and appearance linked to the formation process and rate. The high resolution 3-dimensional terrestrial scanning device LIDAR can clearly reveal the topography formed by ridge-type travertines at the surface. With the surface shape allowing access to detailed information about travertine structure, the underground situation allows us to access details about formation. This study mapped the Kamara (Denizli) travertine structure determining topographic characteristics with terrestrial LIDAR method in 3-dimensions at the surface and investigated the underground geometry with the GPR (ground penetrating radar) method. By modeling the obtained GPR profiles, the 3-dimensional underground image of the mass of the Kamara travertine was obtained. When this image is investigated, asymmetric thickness variation was observed toward both sides from the central axis of the fracture. The asymmetry observed in surface investigations was in accordance with the underground image. This compliance shows that the geometric shape of the travertine during formation is preserved at the surface.

^{*} Corresponding Author

INTRODUCTION

Travertine deposits (Ford and Pedley, 1996; Capezzuoli et al., 2014) are continental carbonate bodies closely connected to mainly Ca^{2+} and HCO_3^- saline fluids discharging from thermal springs linked to deep carbonate geothermal reservoirs.

In addition to areas with thermal springs along with rising and circulation of fluids, there is a tight control by brittle structures affecting the upper crust in areas characterized by geothermal anomalies and general active extensional tectonics (Curewitz and Karson, 1997; Rowland and Sibson, 2004; Bense et al., 2013). Basically, travertine deposits are accepted as a sign of tectonic activity. Study of travertines may contribute to defining the geometry of the related main structure(s), age and kinematics (Altunel and Hancock 1993a, 1993b; Faccenna et al., 1993; Çakır, 1999; Hancock et al., 1999; Martinez- Diaz and Hernandez-Enrile 2001; Brogi, 2004; Mesci et al., 2008; Brogi and Capezzuoli 2009; Temiz and Eikenberg 2011).

With the aim of contributing to better understanding of the role of faults in controlling travertine deposition and the growth of travertine fissure ridges, field geology, geophysics, seismology, geochemistry and geochronology were studied within an integrated approach. Within the Kamara geothermal field (Fig. 1) located in the northwest section of the Denizli basin (West Anatolian extensional region; Bozkurt, 2001a, 2001b, 2003), the majority of the fissure ridges and some travertine bodies formed due to common active hydrothermal circulation (Alçiçek et al., 2015) and active and seismogenic regional extensional structures (Şimşek 1984; Sun 1990; Westaway, 1990; 1993; 1994; Alçiçek et al., 2007, McClusky et al., 2000) have been largely documented. This area has also been considered a key example to define the interaction between basal layer subsidence and gravity collapses encouraging and controlling development of travertine fissure ridges (De Filippis et al., 2012).

The aim of the study is to examine the relationship between active faults and travertines in the Kamara region of the Pamukkale travertines, and to determine the effect of tectonism on fissure ridge-type travertine formations. In this way, geophysical measurements were completed in light of geologic data (Fig. 2).

The main results of the study show that travertine deposition and hydrothermal circulation developed under tight control of possibly still-active late Quaternary faults. This is within the framework of the tectonic evolution of the Denizli Basin and western Anatolia dominated by NW- and NE-striking normal and transfer faults (Alçiçek et al., 2013).

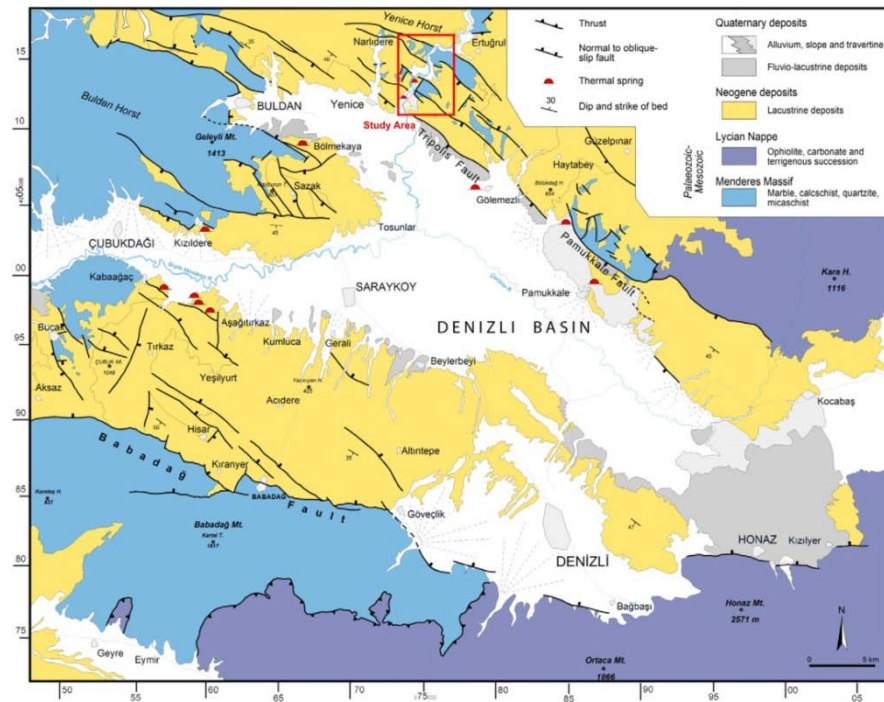


Figure 1. Geological sketch-map of the Denizli Basin (based on Sun, 1990, after Alçiçek et al., 2007, Brogi vd., 2016) and location of the study area.

Uranium series age dating of Pamukkale travertines show that the travertines were deposited in different locations from 400,000 years ago to the present. The extensional fractures allowing water forming the travertines in the region to reach the surface open at a rate of 0.02-0.1 mm/year perpendicular to strike, with nearly 20 mm/year extension along strike. In the Pamukkale region over the last 200,000 years, opening has occurred in a NE-SW orientation at rates of 0.23-0.6 mm/year (Altunel, 1996).

Due to reasons such as being a tectonically active zone, with common lithologic units like limestone and marble and suitable climatic conditions, Turkey is rich in terms of travertine locations. Travertines in Turkey generally formed in the Plio-Quaternary. Thin-layered, very hard, laminated travertine deposits forming due to hot water discharging at the surface along fractures are commonly found on the North Anatolian, East Anatolian and West Anatolian Fault systems. The porous, loose, sponge-like structure formed by cold and warm spring waters containing plant and animal remains of tufa deposits develop around karstic and tectono-karstic springs. Additionally in some areas travertine and tufa deposits are found intercalated together.

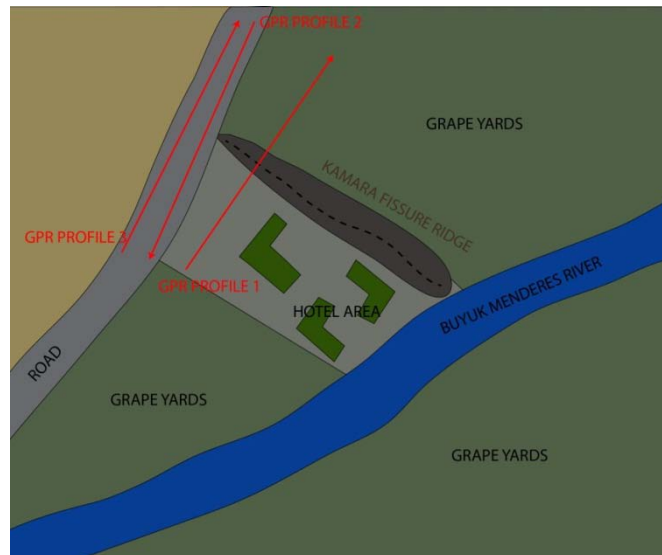


Figure 2. Location of applied GPR measurements

METHODOLOGY

GPR (Ground Penetrating Radar) Method

The ground penetrating radar (GPR) method is a method that has begun to be commonly used in active tectonic studies in recent years (Audru et al., 2001; Bano et al., 2000; Meghraoui et al., 2001; Yalçiner, 2009). The GPR method has many areas of use from researching subsurface active faults to determining damage to buried ancient cities, to researching buried natural structures (like canals, terraces) and human-built modern structures (roads, walls, etc.). In this study the GPR method will determine the location of buried fault lines. The GPR method is based on the principle of observing echoes reflected from surfaces by transmitting very high frequency EM waves (radio waves) into the ground with a horizontal electric field vector (TE: transverse electric) transmitting antenna (Conyers, 2004). With this method, the signal coming back or changing due to reflection/dispersion on the edges of layers and/or buried objects is recorded as a function of the time taken to be received by the antenna (Balkaya and Göktürkler, 2016) (Fig 3a). If there is a contact between rocks with different dielectric properties underground, the electromagnetic waves will reflect and transmit from this interface. For the waveform, continuous electromagnetic traces or electromagnetic traces lasting a few nanoseconds called CHIRP are used. Frequencies 50% above and below the chosen central frequency for the source wave are used. For example, a 100 MHz central frequency uses the interval from 50 MHz to 150 MHz. GPR was first developed to measure the thickness of ice (Cook, 1960). Studies in normal ground environments using seismic methods and processing with data processing techniques obtained research depths from 10-20 m. Currently the GPR method is commonly used for shallow ground research and archeometry studies (Conyers, 2006). A simple GPR setup is formed of a computer, recording device CU (control unit), transmitting and receiving antennae. The obtained radar data are presented in sections similar to seismic methods. If there are parallel measurement lines, time level mapping may be made. The amplitude values for all measurements with a certain time value are

removed and processed as measurement points on the map (Conyers, 2004). One of the most important sections of GPR studies is to obtain the most appropriate visuals for the target by using a variety of filter parameters and techniques in the data processing stage (Leucci and Negri, 2006). A sample application from the filter stage is given in Figure 3b.

Terrestrial Lidar Method

For high resolution modeling of the true appearance of structures above ground on the travertine ridges in a computer environment, the terrestrial Lidar method working with laser scanning was applied in the field. Previous computer models based on photographic determination did not always reach sufficient resolution.

The terrestrial Lidar equipment used in this study was Optech ILRIS-3D brand, class 1 1500 nm wavelength laser and combined integrated digital camera system. The device scans 2500 points per second and the study interval is determined as from 3 m to 1500 m. The full device setup includes a tripod carrying the Lidar, portable computer, power unit and battery system supporting this unit (Fig 3c).

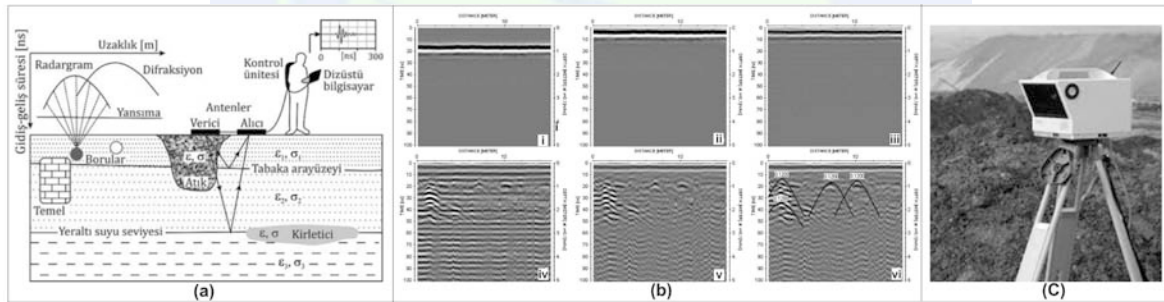


Figure 3. (a) Schematic GPR setup (adapted from Blindow, 2007; taken from Balkaya and Göktürkler, 2016) (b) Example GPR profile (i) raw data, (ii) first time filter, (iii) direct current filter, (iv) energy filter, (v) environment cleaning filter and (vi) rate analysis (c) Optech ILRIS-3D Lidar

RESEARCH FINDINGS AND FIELD DATA

In this study the development of ridges in the shape of lenses was researched, with the aim of determining the factors involved in hydrothermal fluid flow and travertine deposition in the Kamara region.

With this aim, the GPR method was applied to the region, and a fault zone buried by the newest travertine structure in the region was identified (Fig. 4). Additionally, seismic activity recorded in recent years, and the correlations between thermal spring activity and the chemical-physical properties of the fluids were evaluated. When results of previous studies are assessed, it appears that the fluids depositing travertines in the past are correlated with current chemical and physical characteristics.

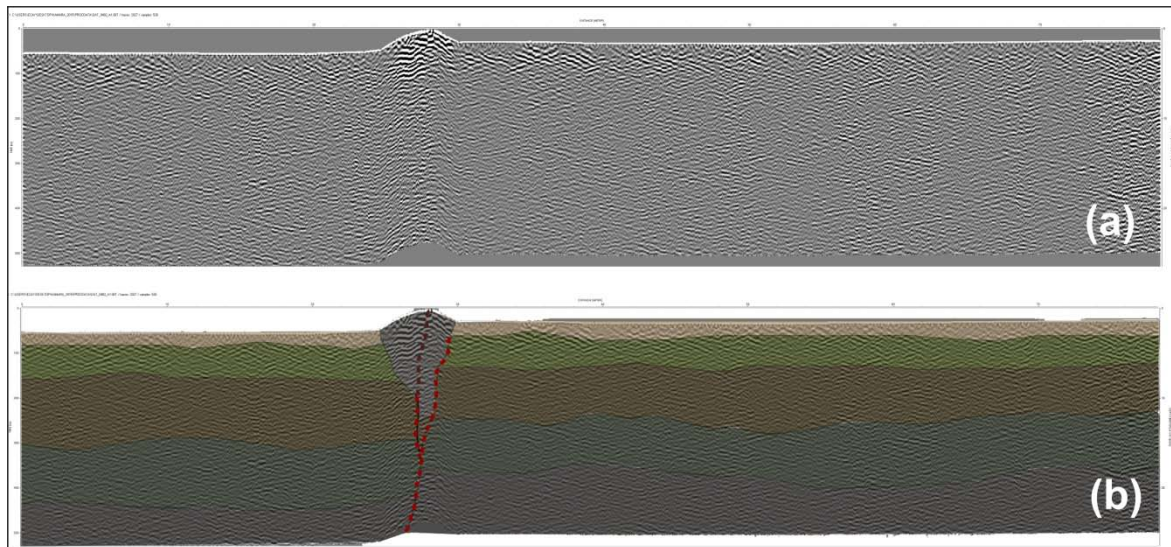


Figure 4. Sample GPR profile from Kamara. (a) processed GPR data and (b) modeled GPR data (colored areas are layers, dotted red lines show fissure)

DISCUSSION

Formation of Kamara travertines

To understand the general tectonic properties of the formation of the Kamara travertine and surroundings, it is necessary to investigate the regime forming southwestern Anatolia. Studies by Alçiçek et al., 2013 and Noten et al., 2013 explained the tectonics of this regime forming NW- and NE-striking Neogene and Quaternary basins. Kinematic measurements from current studies show the Kamara region was shaped by normal faults with northeast strike beginning activity in the late Miocene-Pliocene period (Brogli et al., 2016). At the same time northwest-oriented normal faults related to these faults have been active from the Miocene to the present day and were effective in the current state of the region (Ten Veen et al., 2009).

Current state of Kamara Travertines

The thermal output at the Kamara travertine was active until the years 1996-1997. Later, drilling was used to bring thermal waters to the surface in the region (depth nearly 145 m). This change in the thermal source was determined in the article by Alçiçek et al., 2016 investigating temperature and electrical properties. All these results clearly reveal the correlation between earthquakes formed by the tectonic regime currently active in the region and the Kamara travertine. Chemical measurements described by Brogli et al., 2016 determined that the Kamara travertine is a syn-tectonic formation.

Shallow geophysical studies were performed to determine the location and show the underground extension and relationship of the effective tectonic structures with the fissure ridge travertines of the Kamara travertines. Faults that are still effective in the region were identified with shallow geophysical studies (Fig. 5).

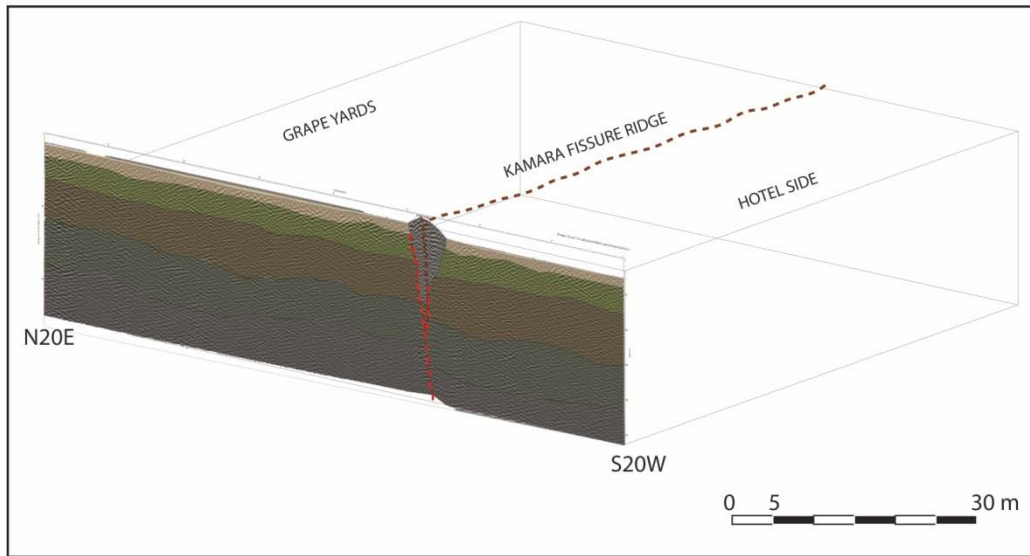


Figure 5. Schematic block diagram of the model obtained from GPR data (colored areas are layers, dotted red line shows fissure)

CONCLUSION

The thermal springs of the Kamara travertine and in the region formed with the effect of northeast and northwest striking normal faults (Alçiçek et al., 2013; Van Noten et al., 2013). With thermal activity continuing since the Middle Pleistocene, the correlation of this system with active faults was determined by geochemical, tectonic and kinematic studies. Earthquakes forming on these control mechanism faults affected the water routes and depths in the thermal system which affected travertine formation. Thus understanding the faults under the surface becomes important in this interactive system in terms of understanding the whole system.

Previous studies have openly revealed the correlation with tectonism in this region, describing the importance of understanding the underground structure of the Kamara travertine. The determination of the underground geometry of active faults with surface geometry that we could trace with high resolution shallow geophysical methods adds a new dimension to active tectonic studies as well as filling in a missing piece.

While the GPR data obtained reveal the location on the fault of thermal water routes ensuring formation of the travertine structure, ERT measurements allow a cross section of geologic structures to be seen. The Kamara travertine is an ideal environment to interpret ERT geophysical anomalies and presents clear traces of water levels and geologic levels.

Investigation of these types of tectonic structures found in western Anatolia with field observations, geochemistry, and kinematic studies along with support by shallow geophysical methods will be beneficial for future studies. Considering the success of the GPR method in previous studies, with very comprehensive areas of use, it has a large effect on investigating the relationship of tectonic structures to travertines by allowing

creation of underground block diagrams. Future studies are necessary to use block diagrams formed by these types of measurements to create 3 dimensional sections.

ACKNOWLEDGMENTS

This study was supported by the ÇOMÜ-BAP project numbered FBA-2015-491 called “Research into sub-surface geometry of fissure ridge-type travertines with GPR”.

REFERENCES

- Alçıçek, H., Varol, B., Özkul, M., 2007. Sedimentary facies, depositional environments and palaeogeographic evolution of the Neogene Denizli Basin of SW Anatolia, Turkey. *Sediment. Geol.* 202, 596–637.
- Alçıçek, M.C., Brogi, A., Capezzuoli, E., Liotta, D., Meccheri, M., 2013. Superimposed basins formation during the Neogene–Quaternary extensional tectonics in SW-Anatolia (Turkey): insights from the kinematics of the Dinar Fault Zone. *Tectonophysics* 608, 713–727.
- Alçıçek, H., Wesselingh, F., Alçıçek, M.C., 2015. Palaeoenvironmental evolution of the late Pliocene-early Pleistocene fluvio-deltaic sequence of the Denizli Basin (SW Turkey). *Palaeogeogr. Palaeoclimatol. Palaeoecol.* 437, 98–116.
- Alçıçek, H., Bülbül, A., Alçıçek, M.C., 2016. Hydrogeochemistry of the thermal waters from the Yenice Geothermal Field (Denizli Basin, southwestern Turkey). *J. Volcanol. Geotherm. Res.* 309, 118–138.
- Altunel E and Hancock P L 1993a Morphology and structural setting of Quaternary travertines at Pamukkale, Turkey *Geol. J.* 28 335–46
- Altunel E and Hancock P L 1993b Active fissuring and faulting in Quaternary travertines at Pamukkale, Western Turkey. Neotectonics and active faulting *Z. Geomorphol.* NF 94 285–302
- Altunel E and Hancock P L 1996 Structural attributes of travertine-filled extensional fissures in the Pamukkale plateau, *Western Turkey Int. Geol. Rev.* 38 768–77
- Audru J.-C., Bano M., Begg J., Berryman K., Henrys S. and Nivière B., 2001. GPR investigations on active faults in urban areas: the Georisc-NZ project in Wellington, New Zealand. *Earth and Planetary Science*, Volume 333, Number 8, 31 October 2001 , pp. 447-454(8).
- Balkaya, Ç. ve Göktürkler, G. 2016. “Karşılıklı kuyu yer radarı verilerinin modellenmesi”, *Pamukkale Üniversitesi Mühendislik Bilimleri Dergisi*, 22(6), 581-596.
- Bano, M., Marquis, G., Nivière, B., Maurin J.-C., and Cushing M., 2000. Investigating alluvial and tectonic features with ground-penetrating radar and analysing diffraction patterns. *J. Appl. Geophys.* 43, pp. 33–41.
- Bense, V.F., Gleeson, T., Loveless, S.E., Bour, O., Scibek, J., 2013. Fault zone

- hydrogeology. *Earth-Sci. Rev.* 127, 171–192.
- Blindow, N., Eisenburger, D., Illich, B., Petzold, H. ve Richter, T. 2007. *Environmental Geology*. Editors: Knödel K, Lange G, Voight H-J. Ground Penetrating Radar, 283–335, Hannover, Germany, Springer Berlin Heidelberg New York.
- Bozkurt, E., 2001a. Late Alpine evolution of the central Menderes Massif, western Turkey. *Int. J. Earth Sci.* 89, 728–744.
- Bozkurt, E., 2001b. Neotectonic of Turkey—a synthesis. *Geodin. Acta* 14, 3–30.
- Bozkurt, E., 2003. Origin of NE-trending basins in western Turkey. *Geodin. Acta* 16, 61–81.
- Brogi, A., Liotta, D., Ruggieri, G., Capezzuoli, E., Meccheri, M., Dini, A., 2016. An overview on the characteristics of geothermal carbonate reservoirs in southern Tuscany. *Ital. J. Geosci.* 135, 17–29.
- Brogi, A., Capezzuoli, E., 2009. Travertine deposition and faulting: the fault-related travertine fissure-ridge at Terme S. Giovanni, Rapolano Terme (Italy). *Int. J. Earth Sci. (Geol. Rundsch.)* 98, 931–947.
- Brogi, A., 2004. Faults linkage, damage rocks and hydrothermal fluid circulation: tectonic interpretation of the Rapolano Terme travertines (southern Tuscany, Italy) in the context of the Northern Apennines Neogene–Quaternary extension. *Eclogae Geol. Helv.* 97, 307–320.
- Capezzuoli, E., Gandin, A., Pedley, H.M., 2014. Decoding tufa and travertine (freshwater carbonates) in the sedimentary record: the state of the art. *Sedimentology* 61, 1–21
- Conyers, L. B. 2004. “Ground-penetrating Radar for Archaeology”, *Altamira Press*, Walnut Creek, California.
- Conyers, L. B. 2006. “Innovative ground-penetrating radar methods for archaeological mapping”, *Archaeological Prospection*, 13(2), 139–141.
- Cook, J. C. 1960. “Proposed monocyple-pulse, VHF radar for airborne ice and snow measurements”, *AIEE Trans. Commun. and Electron*, 79 (2), 588–594.
- Curewitz, D., Karson, J.A., 1997. Structural settings of hydrothermal outflow: fracture permeability maintained by fault propagation and interaction. *J. Volcanol. Geotherm. Res.* 79, 149–168.
- Cakir Z 1999 Along-strike discontinuity of active normal faults and its influence on Quaternary travertine deposition; examples from Western Turkey. *Turk. J. Earth Sci.* 8 67–80.
- De Filippis, L., Faccenna, C., Billi, A., Anzalone, E., Brilli, M., Ozkul, M., Soligo, M., Tuccimei, P., Villa, I., 2012. Growth of fissure ridge travertines from geothermal springs of Denizli basin, western Turkey. *Geol. Soc. Am. Bull.* 124, 1629–1645.

- Faccenna, C., Funiciello, R., Montone, P., Parotto, M., Voltaggio, M., 1993. Late Pleistocene strike slip tectonics in the Acque Albule basin (Tivoli, Latium). *Mem. Descr. Carta Geol. d'Italia* 69, 37–50.
- Ford, T.D., Pedley, H.M., 1996. A review of tufa and travertine deposits of the world. *Earth- Sci. Rev.* 41, 117–175.
- Hancock P L, Chalmers R M L, Altunel E and Çakır Z 1999. Travertine: using travertine in active fault studies *J. Struct. Geol.* 21 903–16
- Leucci G and Negri S 2006 Use of ground penetrating radar to map subsurface archaeological features in an urban area *J. Archaeol. Sci.* 33 502–12.
- Martinez-Diaz, J.J., Hernandez-Enrile, J.L., 2001. Using travertine deformations to characterise paleoseismic activity along an active oblique-slip fault: the Alhama de Murcia fault (Betic cordillera, Spain). *Acta Geol. Hisp.* 36, 297–313.
- McClusky, S., Balassanian, S., Barka, A., Demir, C., Ergintav, S., Georgiev, I., Gurkan, O., Hamburger, M., Hurst, K., Kahle, H., Kastens, K., Kekelidze, G., King, R., Kotzev, V., Lenk, O., Mahmoud, S., Mishin, A., Nadariya, M., Ouzounis, A., Paradissis, D., Peter, Y., Prilepin, M., Reilinger, R., Sanli, I., Seeger, H., Tealeb, A., Toksoz, M.N., Veis, G., 2000. Global Positioning System constraints on plate kinematics and dynamics in the eastern Mediterranean and Caucasus. *J. Geophys. Res.* 105 (B3), 5695–5719.
- Meghraoui, M., Camelbeeck, T., Vanneste, K., Brondeel, M. and Jongmans D., 2001. Active faulting and paleoseismology along the Bree fault, lower Rhine graben, Belgium. *J. Geophys. Res.*, 105(B6), 13,809–13,841.
- Mesci B L, Gürsoy H and Tatar O 2008 The evolution of travertine masses in the Sivas area (central Turkey) and their relationships to active tectonics *Turk. J. Earth Sci.* 17 219–40.
- Rowland, J.V., Sibson, R.H., 2004. Structural controls on hydrothermal flow in a segmented rift system, Taupo Volcanic Zone, New Zealand. *Geofluids* 4, 259–283
- Sun, S., 1990. Denizli-Uşak Arasının Jeolojisi ve Linyit Olanakları (Geology and Lignite Potential of Denizli-Uşak Region). *Mineral Research and Exploration Directorate of Turkey (MTA)*, Scientific Report No: 9985, Ankara (in Turkish), p. 92.
- Şimşek, Ş., 1984. Denizli-Kızıldere-Tekkehamam-Tosunlar-Buldan-Yenice alanının jeolojisi ve jeotermal enerji olanakları (Geology and Geothermal Energy Potential of the Denizli-Kızıldere-Tekkehamam-Tosunlar-Buldan-Yenice Area). *General Directorate of Mineral Research and Exploration (MTA) Report*, No. 7846, Ankara (unpublished) (In Turkish).
- Temiz, U., Eikenberg, J., 2011. U/Th dating of the travertine deposited at transfer zone between two normal faults and their neotectonic significance: Cambazlı ridge travertines (the Gediz graben, Turkey). *Geodin. Acta* 24, 95–105.

- Ten Veen, J.H., Boulton, S.J., Alçiçek, M.C., 2009. From palaeotectonics to neotectonics in the Neotethys realm: the importance of kinematic decoupling and inherited structural grain in SW Anatolia (Turkey). *Tectonophysics* 473, 261–281.
- Van Noten, K., Claes, H., Soete, J., Foubert, A., Özkul, M., Swennen, R., 2013. Fracture network and strike-slip deformation along reactivated normal faults in Quaternary travertine deposits, Denizli Basin, Western Turkey. *Tectonophysics* 588, 154–170.
- Westaway, R., 1990. Block rotations in western Turkey: 1. Observational evidence. *J. Geophys. Res.* 95, 19857–19884.
- Westaway, R., 1993. Neogene evolution of the Denizli region of western Turkey. *J. Struct. Geol.* 15, 37–53.
- Westaway, R., 1994. Present-day kinematics of the Middle and Eastern Mediterranean. *J. Geophys. Res.* 99, 12071–12090.
- Yalciner, C.C., Bano, M., Kadioglu, M., Karabacak, V., Meghraoui, M., Altunel, E., 2009. New temple discovery at the archaeological site of Nysa (Western Turkey) using GPR method. *J. Archaeol. Sci.* 36, 1680–9.



Determination of Fault Types by GIS Applications according to Earthquake Depths

Kaan Hakan ÇOBAN¹ and Nilgün SAYIL¹

¹ Department of Geophysical Engineering, Karadeniz Technical University, Trabzon, Turkey.

e-mail: h.coban@ktu.edu.tr, sayil@ktu.edu.tr

ABSTRACT

Geographic information systems (GIS) are used in geophysical engineering as well as in many fields. It is used in applied geophysics and seismology, which is different disciplines of geophysical engineering. Also in applied geophysics, the GIS applications are used to create contour maps according to geophysical measurements, to 3D map of the data and to evaluate the results. In seismology, GIS applications are used to map the epicentral distributions of earthquakes and the location of the faults. It is very important to make an evaluation according to fault type (normal fault, reverse fault or strike-slip fault) because of the high destruction effect of strike-slip fault types, especially at the points where the earthquakes are close to the surface. In this study, it was aimed to map the earthquakes with magnitude $M > 5.0$, which occurred on different types of faults between 1900 and 2016 in selected region. Also the database was created by modeling the depths of the earthquakes with the help of GIS applications. The fault types were tried to be determined by investigating the depths of the earthquakes with the help of the created database. Thus, the database can be used in works where the earthquake effects should be reduced (for example, the determination of living areas, the design of buildings, etc.) In addition, GIS applications will provide significant contributions to large-scale earthquake risk studies with more detailed databases.

INTRODUCTION

Researchers have done many research on earthquakes in literature. Definitions of earthquakes according to this research; Mallet (1859) stated that "rocks are broken with earthquakes and that other rocks are compressed". Gilbert (1883) said that earthquakes were associated with faults. Reid (1911) developed the modern earthquakes description "Elastic Rebound Theory". It is defined as an earthquake that spreads energy from a point due to breaks in the Earth's crust as seismic waves and shakes the environments where these waves pass (Stein and Wyssession, 2003). It is called seismology in the field of

science, which explores how earthquakes occur, how earthquake waves spread in the earth, measuring instruments and methods, evaluation of records, and other issues related to earthquakes.

Earthquakes should be investigated because Turkey is located on the active Alp-Himalaya earthquake zone and include the active North Anatolian Fault Zone and East Anatolian Fault Zone. Seismology, which is a discipline of Geophysical Engineering, is studied about earthquakes. Earthquake stations are being established in order to observe earthquakes in the direction of these studies. The earthquakes locations, depth information, and what type of fault the earthquake has caused are devastating effects of earthquakes. It is very important to make an evaluation according to the fault type (normal fault, reverse fault, or strike-slip fault) and depths, since earthquakes are particularly susceptible to destruction in strike-slip fault types at points close to the surface.

In this study, it is aimed to show how GIS applications can be used in the seismology and the importance of using GIS applications especially in earthquake risk studies and classification of fault types according to earthquake depth models by creating epicentral maps. In this context, earthquakes with magnitudes $M > 5.0$, which occurred (1900 - 2016) on different types of faults, were mapped with the help of GIS applications and the depths of the earthquakes were modeled and analyzed according to fault types.

GIS APPLICATIONS ACCORDING TO EARTHQUAKE DEPTHS AND FAULT TYPES

The point at which the earthquake occurs is called the focus. The focus point is where the energy emerges. This point is defined as the focal point (Hypocentral) or the inner center. In reality, the place where energy emerges is an area, but it is accepted as a point in practical applications. It is the point on the ground that is closest to the focus point. At the same time, it is the point where the earthquake is most damaged or felt the strongest. The focus point of the focal point on the earth is called the epicenter (Fig-1).

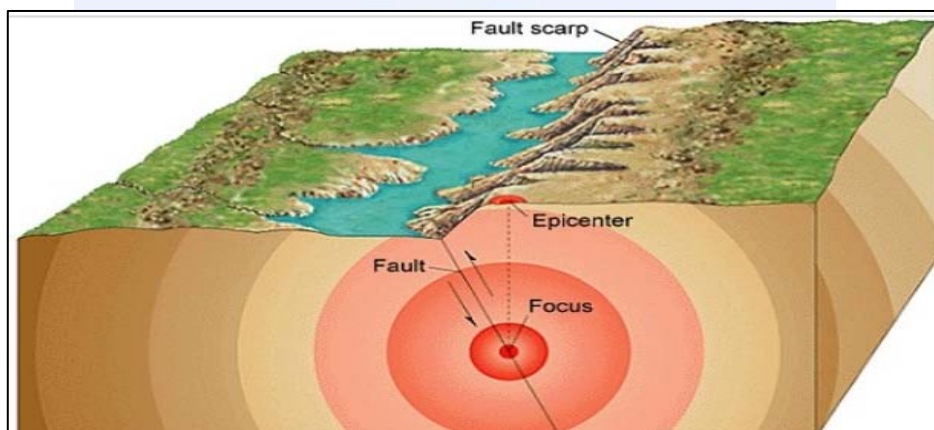


Figure 1. The model of earthquake focus (URL-1)

The fault is to move to different sides of the blocks along the rock breaks after the earthquakes (Evison, 1963). The different types of faults are shown in Fig-2. The faults are defined in three types:

- 1- Normal Fault; the moving block moves downwards.
- 2- Inverse Fault; moving block moves upwards.
- 3-Strike Slip Fault; In this type of fault, the blocks move sideways relative to each other

The moving block is called the right direction if it moves to the right with respect to the fixed block, and it is called the left direction strike-slip fault when it moves to the left.

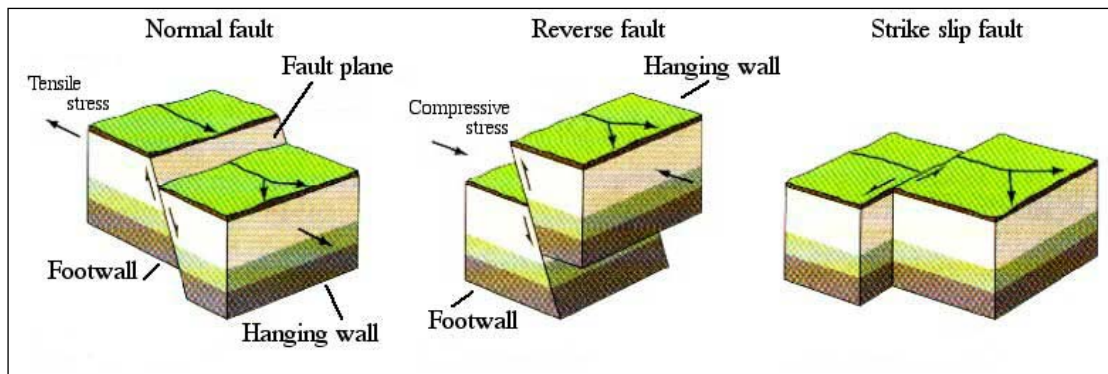


Figure 2. The model of the faults types (URL-2)

The devastating effects of earthquakes vary according to their depth and fault types. Especially, the destructive earthquakes near the surface are observed in the strike-slip fault types because of that the depths of earthquakes should be evaluated in the safe zone selection.

The study area is defined as between $35.8 \leq \text{LAT} \leq 41.5$ and $25 \leq \text{LONG} \leq 32$ coordinates. The area was chosen to include various types of faults earthquakes. The earthquakes of magnitude ($M > 5.0$), which occurred between 1900 and 2017, were taken from Bogazici Kandilli Observatory and Earthquake Research Institute web site (URL-1). The epicenter maps of earthquakes were created with the help of GIS applications (Fig-3).

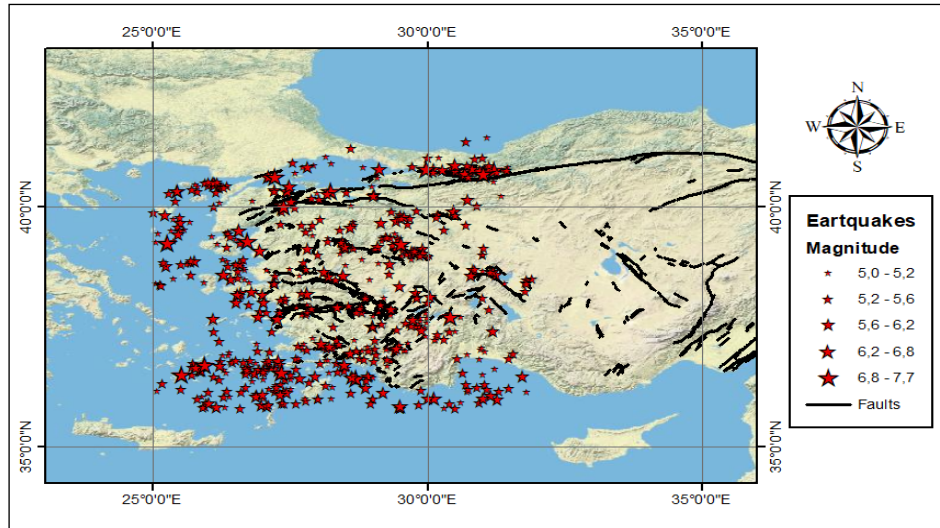


Figure 3. The epicentral distribution of the earthquake data (URL-1)

Contour maps were created according to depth data with the help of GIS applications to the depth information of earthquakes. (Fig-4).

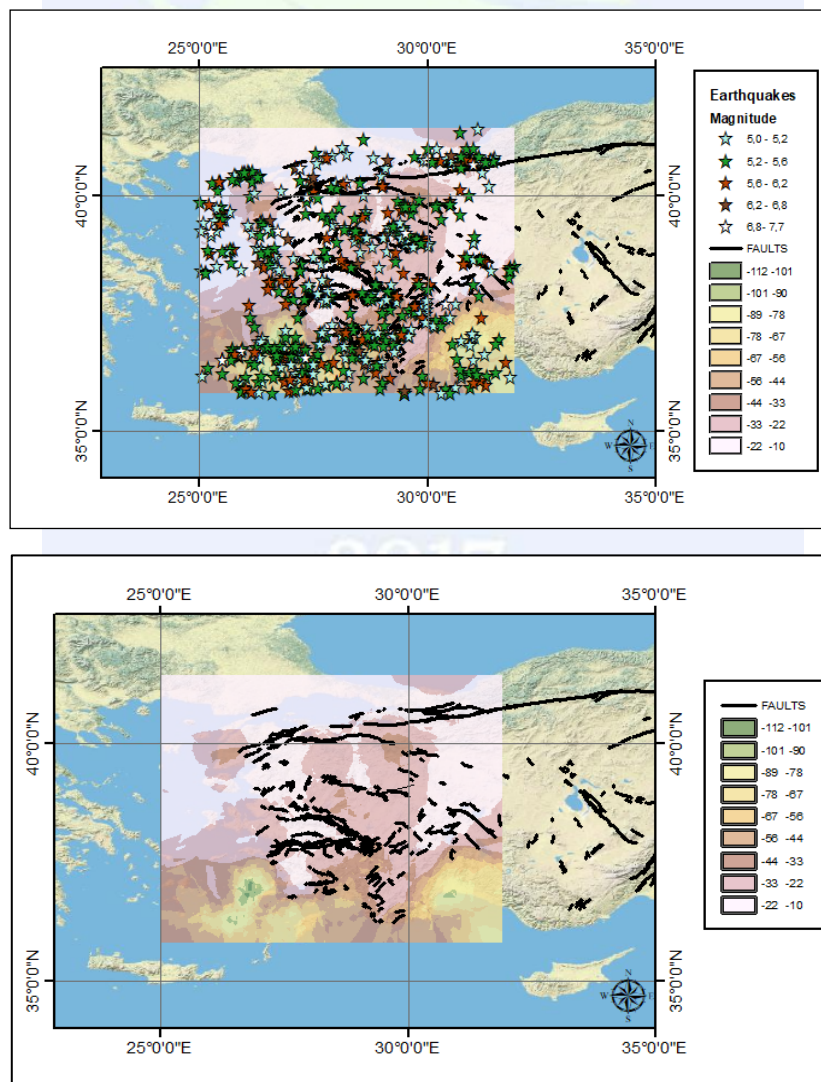


Figure 4. a)-b)The contour maps of earthquakes depth

According to the created contour maps, depth sections in 3 different points in different fault types were taken with the help of GIS applications (Fig-5).

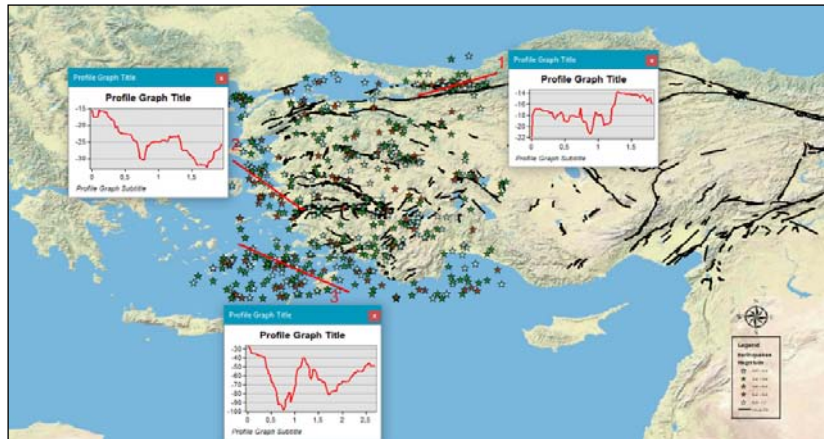


Figure 5. The graph of earthquakes depth according to profiles

Using the database, the depths of the earthquakes are modeled in 3D with the GIS applications (Fig-6). The depth model can be associated with the profiles (in Fig-5) and the maps (in Fig-4)

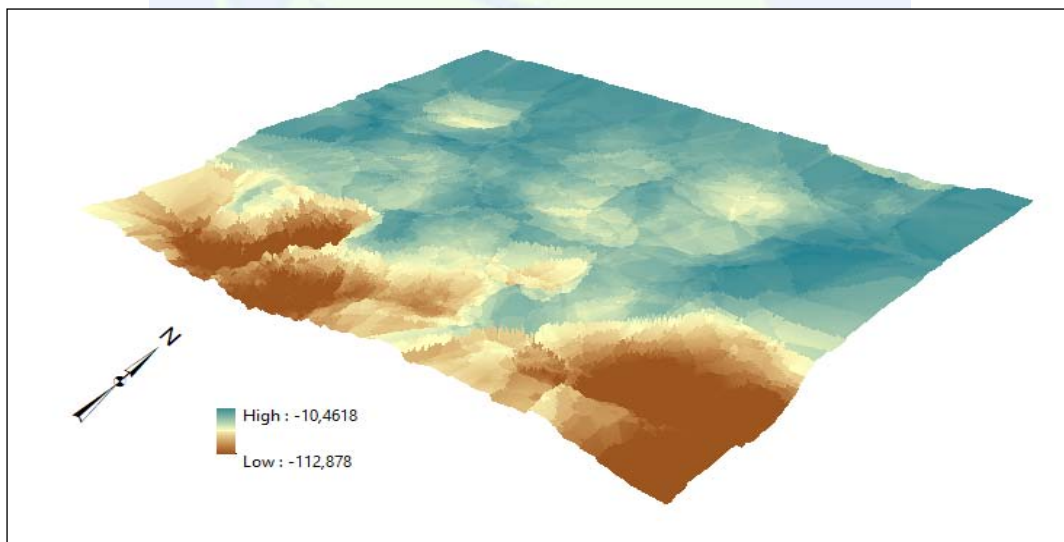


Figure 6. 3D earthquakes depth model (High means Min-depth; Low means Max-depth)

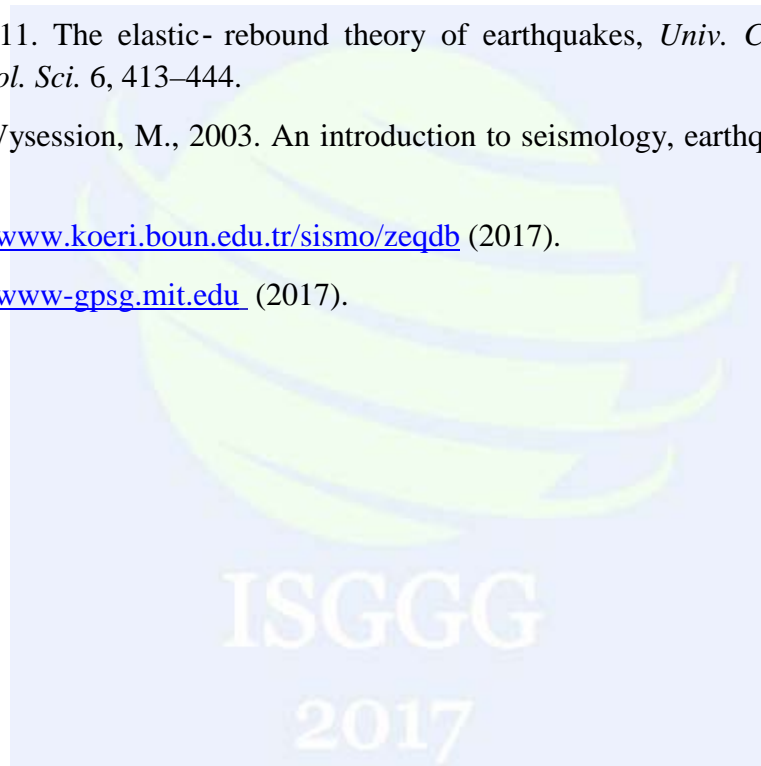
CONCLUSIONS

GIS applications in the seismology should be used effectively in earthquake research studies. In this study, it is aimed how GIS applications can be used in seismology and an application study on earthquakes. In this context, a data base was constructed from earthquakes with different magnitude ($M > 5.0$) between 1900 and 2017 which occurred in different fault types selected as application fields. The location of earthquakes is mapped with the created database. According to the depth information of the earthquakes, contour maps were created with the help of GIS applications, depth sections and 3D depth model were created and fault types were investigated. It will provide effective solutions in the

selection of safe zone with databases to be constructed with GIS in earthquake risk assessment studies.

REFERENCES

- Evison, F. F., 1963. Earthquakes and faults. *Bulletin of the Seismological Society of America* 53:873-891.
- Gilbert, G.K., 1884. A theory of the earthquakes of the Great Basin, with a practical application. *American Journal of Science*.
- Mallet, R., 1859. Report to the Royal Society of the Expedition into the Kingdom of Naples to Investigate the Circumstances of the Earthquake of the 16th December 1857. *Proc. R. Soc. Lond.* 1859-1860 10, 486-494.
- Reid, H. F., 1911. The elastic-rebound theory of earthquakes, *Univ. Calif. Publ. Bull. Dept. Geol. Sci.* 6, 413-444.
- Stein, S. and Wysession, M., 2003. An introduction to seismology, earthquakes, and earth structure.
- URL-1 <http://www.koeri.boun.edu.tr/sismo/zeqdb> (2017).
- URL-2 <http://www-gpsg.mit.edu> (2017).



Modeling of Soil Parameters Obtained by Geophysical Methods Using GIS: A case Study in Trabzon

Kaan Hakan ÇOBAN^{*1}, Özgenç AKIN¹ and Nilgün SAYIL¹

¹Department of Geophysical Engineering, Karadeniz Technical University, Kanuni Campus, 61080, Turkey.
(h.coban@ktu.edu.tr)

ABSTRACT

The models obtained as a result of the use of geographic information systems (GIS) provide a better understanding of the results in geophysical data as well as in many areas. In this study, bedrock depth, average S wave velocity (V_s) up to 30m (V_{s30}) and dominant period values were obtained by geophysical measurements in Trabzon and the results were modeled by GIS. Single Station Microtremor Records (SSMR) were used to obtain the predominant periods. V_s values were obtained by using Multichannel Analysis of Surface Waves (MASW) and Refraction Microtremor (ReMi) methods. When the results are examined, the ground predominant periods obtained with SSMR varies between 0.1-0.37s. According to Kanai and Tanaka (1961), these values indicate that the ground consisted of "rocks-dense sandy pebbles". The average bedrock depth was calculated from SSMR is 24m. V_s values obtained from MASW&ReMi methods range from 162-2263m/s. V_{s30} values calculated by using V_s values range from 428-817m/s. As a result the ground class determined as C (Very dense soil&soft rock) (NEHRP) and B (Very dense sand-gravel, very stiff clay) (Eurocode 8) class.

INTRODUCTION

The best approach for obtaining ground parameters is through direct observation of seismic ground motions, but such studies are restricted to areas with relatively high rates of seismicity. Because of these restrictions non-reference site methods have been applied to site response studies such as using single station microtremor recordings in the last decades. In this study Nakamura Method was applied to SSMR data and the predominant periods were obtained. Also, the bedrock depth was calculated with an equation (Kanai, 1983) by using the predominant frequencies obtained by Nakamura method. This method is widely used, especially for determining the predominant period of the soil for the purpose of seismic microzonation. In recent years, this method became the preferred method for obtaining resonance frequencies of soft sediments and determining the sediment thickness. Through the Nakamura H/V spectral ratio method, the natural predominant frequencies of the soil of the study area can be revealed more accurately.

^{*} Corresponding Author

Shear-wave velocity (V_s) is an essential parameter for determining the dynamic properties of soil, but it is quite difficult and expensive to derive by using conventional geophysical techniques. That's why Surface Wave Methods (SWM) have been developed in last decades and it has been used extensively in seismic site characterization studies. The popularity of surface wave testing continues to grow as data collection and analysis packages are being marketed around the globe as easy-to-use systems (Cox and Wood, 2010).

SWM are based on the study of the dispersion of surface seismic (mainly Rayleigh) waves and can be split up as active source and passive source methods. Active source methods generally use a linear array of sensors to measure the phase velocity of waves emanating from a known source (typically located in-line with the array) and propagating past the receivers. Traditionally, passive source methods have employed two-dimensional (2D) sensor arrays to measure the phase velocity of microtremors (passive environmental noise) emanating from an unknown source(s) (Tokimatsu *et al.* 1992). However, due to the desire to simplify sensor layout and speed up field data collection, passive methods have been introduced that employ linear arrays of receivers to estimate phase velocity (Louie 2001, Park and Miller 2008).

Active source methods are generally capable of resolving shorter wavelengths (higher frequencies) than passive methods because the source and receiver array can be tailored to the desired frequency range needed to resolve near-surface layers. On the other hand, passive methods can generally resolve longer wavelengths because microtremors typically contain significant low frequency energy, while a specialized active source is required to actively generate low frequency (< 3 Hz) waves with significant energy (Yoon and Rix 2004, Park *et al.* 2005).

In this study, MASW and ReMi methods have been conducted as active and passive source methods to obtain the ground V_s values. According to these values the bedrock depth was defined and average V_s up to 30m (V_{s30}) values were calculated. The ground was classed by using NEHRP and Eurocode 8 classifications by V_{s30} values. The aim of this study is to create an example model that will allow easier interpretation of geophysical data by using GIS.

DATA AND METHOD

In this study, SSMR were collected at 88 points and MASW&ReMi profiles were measured at 11 points in Trabzon (Figure 1). SSMR data were evaluated with "Geopsy" program and the spectra results were used in Nakamura Method. According to Nakamura (1989), vertical components of noise vibrations are not influenced from the ground layers. However, the horizontal components are acquired to major amplifications depending on ground layers with low velocity and density. Consequently, the ground transfer functions were obtained by divided of the horizontal components spectrum to vertical components spectrum (Figure 2 and Equation 1).

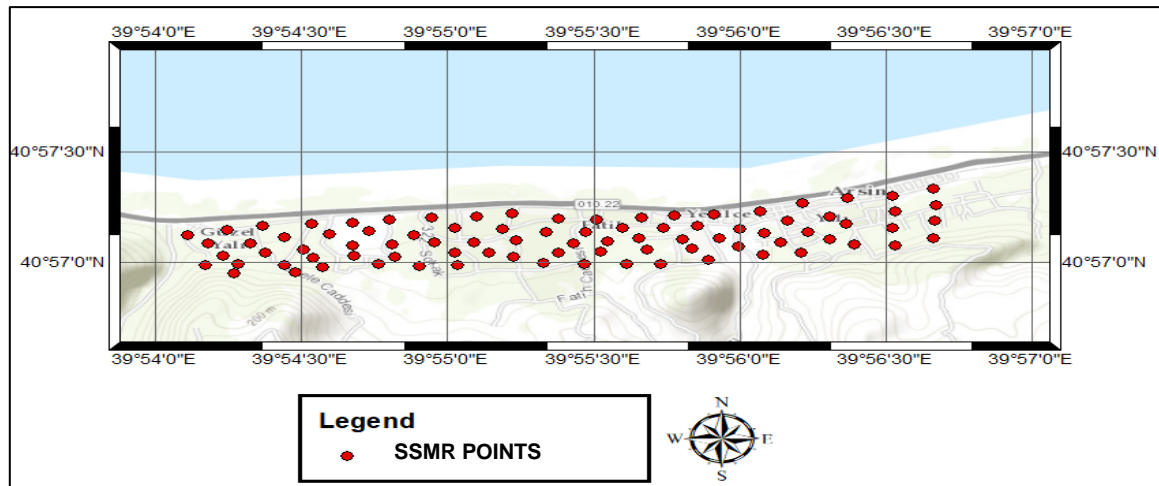


Figure 1. Study area and collected data points.

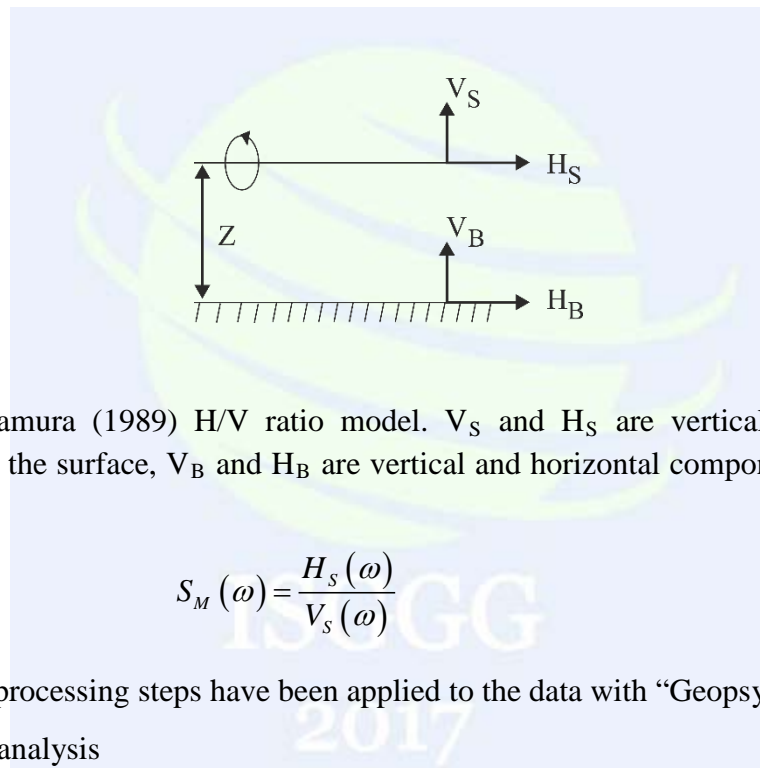


Figure 2. Nakamura (1989) H/V ratio model. V_S and H_S are vertical and horizontal components on the surface, V_B and H_B are vertical and horizontal components in depth of Z .

$$S_M(\omega) = \frac{H_S(\omega)}{V_S(\omega)} \quad (1)$$

The following processing steps have been applied to the data with “Geopsy”;

- Trend analysis
- Tapered 5% by using Konno-Ohmachi window
- Filtering (Butterworth filter)
- Divided into the windows width 25 sec.
- Fast Fourier Transform (FFT)
- H/V ratio

After these steps, the predominant frequencies have been determined by comparing with the spectra of the three components. An example evaluated datum has been shown in Figure 3.

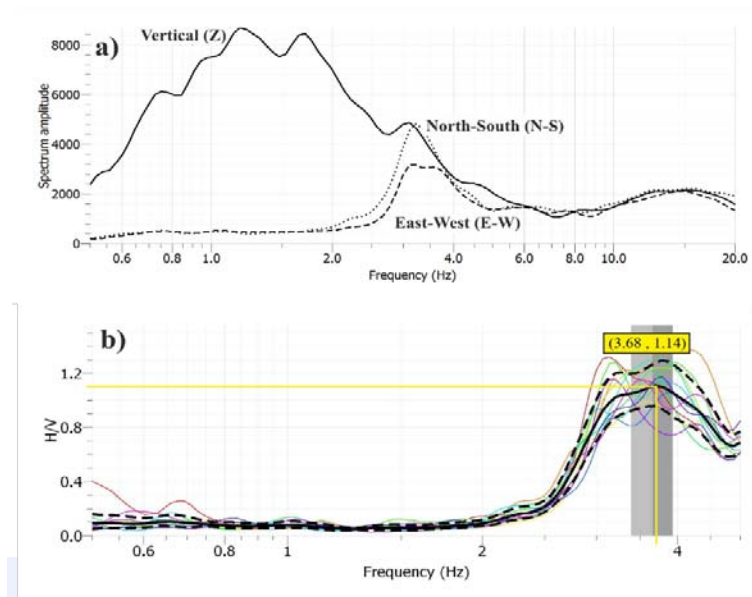


Figure 3. An example microtremor measurement evaluated with Geopsy praogram a) the spectra of three components, b) the result of predominant frequency (or period) and H/V ratio.

Multi-channel analysis of surface wave (MASW) and Refraction Microtremor (ReMi) methods were used to obtain V_S values in this study. These methods developed to estimate S-wave velocity profile from surface wave energy under cover of dispersion. In these methods multiple detectors are used to record the seismic signals. Since Rayleigh wave of a particular frequency can propagate at multiple velocities, multiple dispersion curves are produced. The dispersion curve with the lowest velocity is called the fundamental mode, and all others are the overtones. Because of the multiple modal nature of dispersion, it is necessary to identify unambiguously data points associated with the fundamental mode dispersion in surface wave surveys. It is well known, all surface wave analysis technique involve three steps; data acquisition, determining Rayleigh dispersion curve and inversion. While, same techniques can be used in 2nd and 3rd step for ReMi and MASW, first step is different because target depth. We try to explain data acquisition differences for both methods in Table 1.

Table 1. Acquisition differences between ReMi and MASW methods.

	ReMi	MASW
Geophone frequency	4.5 - 14 Hz	4.5 Hz
Source	Passive any urban noise	Active hammer or weight drop
Recording time	> 30-50 s	0.5-1 s
Sampling Time	1-2 ms	0.5-1 ms
Vertical stack	> 5	Depends on noise
Spread length	Default of refraction	2-3 times target depth
Offset	-	Equal target depth

The data have been evaluated by SeisImager/Pickwin program and fundamental mode dispersion curves obtained from MASW and ReMi methods have been combined (Figure 4). In this way, while two methods overlap their blind side; low frequency band of MASW, high frequency band of ReMi, meaningless S-velocity contrasts in single inversions changes with more reliable and comprehensible velocity propagation. Thereby using the combined dispersion curve, the beginning model parameters were selected and 1D S-wave velocity-depth models computed by inversion (Figure 5).

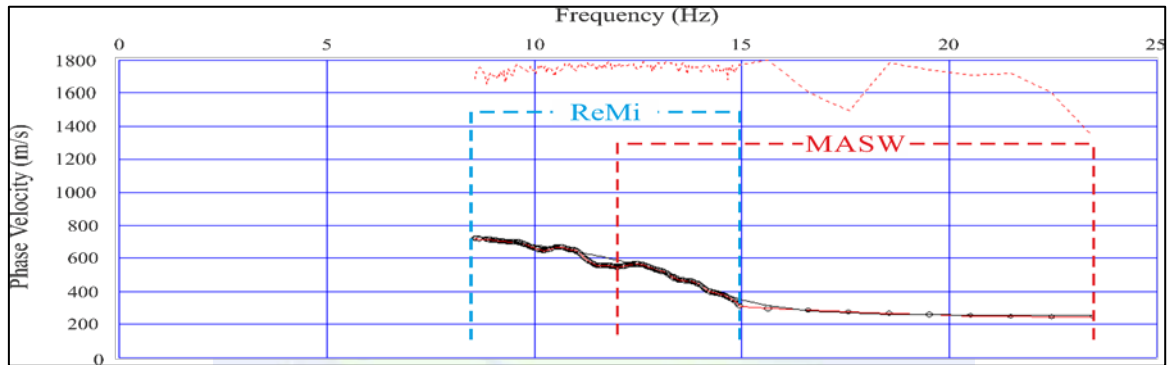


Figure 4. Combination of the dispersion curves obtained from MASW (red line) and ReMi (blue line) methods.

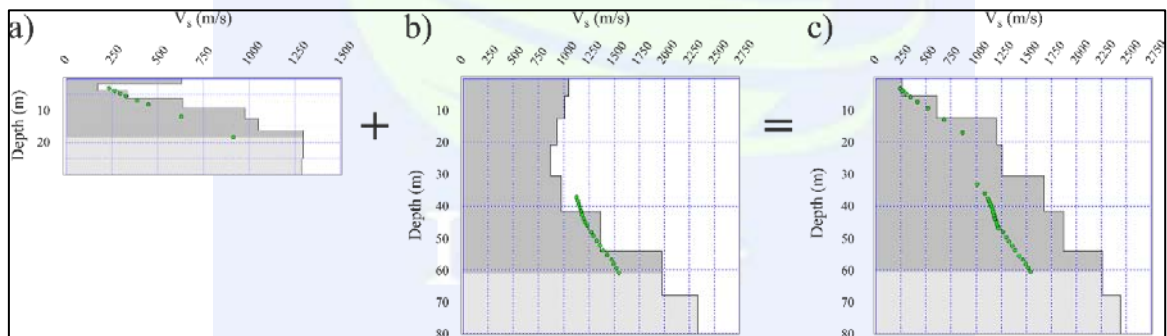


Figure 5. 1D S-wave velocity-depth models a) obtained from MASW method b) obtained from ReMi method and c) obtained from combined dispersion curves (MASW+ReMi).

CONCLUSIONS

In this study, the bedrock depth has been calculated from the geophysical methods that explained in details before in the text. The ground predominant periods obtained with SSMR methods varies between 0.1-0.37s. and Vs values obtained from MASW&ReMi methods at 11 profiles range from 162-2263m/s (Figure 6). Kanai and Tanaka (1961) ground classification is express that the ground consisted of "rocks-dense sandy pebbles". V_{S30} values calculated by using Vs values range from 428-817m/s. As a result the ground class determined as C (Very dense soil&soft rock) (NEHRP) and B (Very dense sand-gravel, very stiff clay) (Eurocode 8) class.

The average bedrock depth was calculated from Kanai (1983) formula by using calculated V_s values from MASW&ReMi and predominant frequency obtained by SSMR method. The map of bedrock depth has been prepared by GIS application (Figure 7).

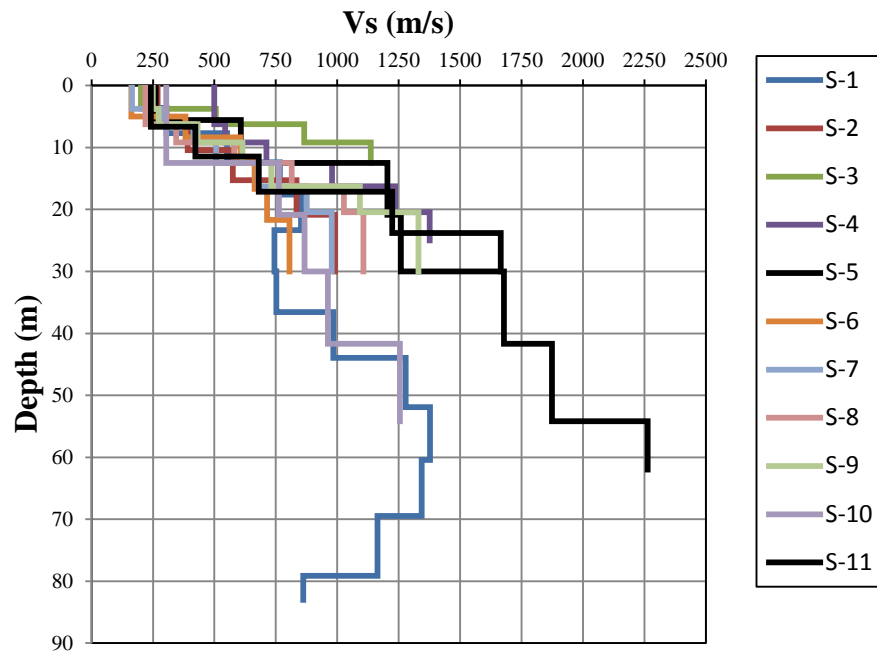


Figure 6. V_s values obtained from MASW&ReMi methods.

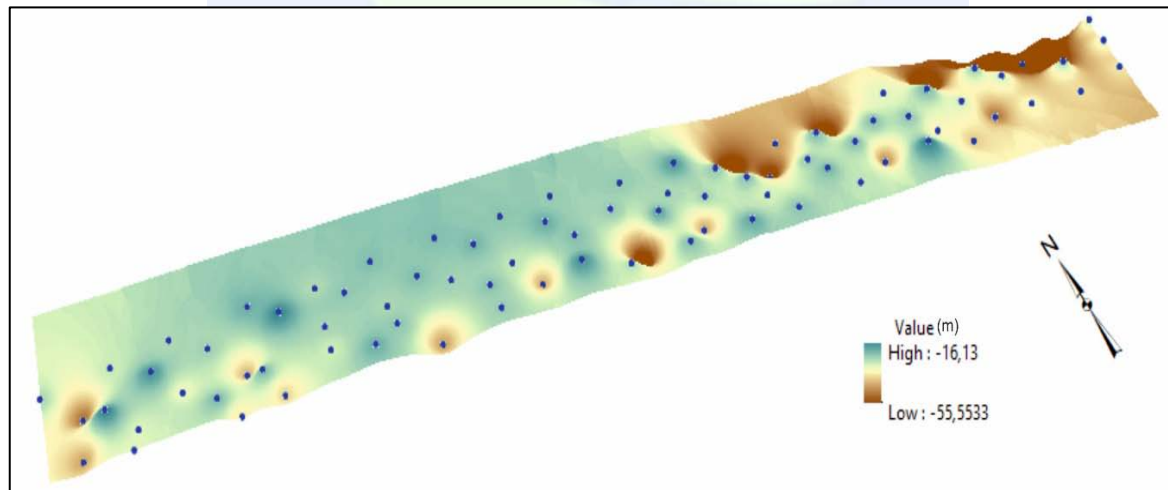


Figure 7. The bedrock depth of the study area.

REFERENCES

- Cox, B. R. and Wood C. M. 2010. A Comparison of Linear-Array Surface Wave Methods at a Soft Soil Site in the Mississippi Embayment, GeoFlorida 2010: *Advances in Analysis, Modeling & Design*, pp. 1369-1378.

- Kanai, K. and Tanaka, T., 1961. On Microtremors, VII, *Bulletin of the Earthquake Research Institute*, 39, 97-114.
- Kanai, K., 1983. *Engineering Seismology*, 251, University of Tokyo, Japonya.
- Louie, J. N. 2001. Faster, better: shear wave velocity to 100 meters depth from refraction microtremor arrays. *Bulletin of Seismological Society of America* 91, 347-364.
- Nakamura, Y., 1989. A method for dynamic characteristics estimation of sub-surface using microtremor on the ground surface, *Quarterly Report of Railway Technical Research Institute*, 30, 1, 25-33.
- Park, C.B, Miller R.D., Ryden, N., Xia, J. and Ivanov, J. 2005. "Combined use of active and passive surface waves" *Journal of Environmental & Engineering Geophysics*, 10, 323-334
- Park, C.B. and Miller, R.D. 2008. "Roadside passive multichannel analysis of surface waves (MASW)" *Journal of Environmental & Engineering Geophysics*, 13, 1-11.
- Tokimatsu, K., Shinzawa, K., and Kuwayama, S. 1992. Use of short-period microtremors for Vs profiling. *Journal of Geotechnical Engineering* 118, 1544-1558.
- Yoon, S., and Rix, G. 2004. Combined active-passive surface wave measurements for near-surface site characterization. Proc., *Symposium on the Applications of Geophysics to Engineering and Environmental Problems*, Vol. 17, Denver, CO:1556-1564.

Planar failure determination of the slopes along the Bağarası-Foca state highway with the help of Geographical Information Systems

Mawuko Luke Yaw Ankah¹ and Cem Kınca²

1 The Graduate School of Natural and Applied Sciences, Applied Geology, Dokuz Eylül University, Tinaztepe Campus, 35160, Izmir, Turkey. E-mail : mawuko.ankah@yahoo.com

2 Geological Engineering Department, Engineering Faculty, Dokuz Eylül University, Tinaztepe Campus, 35160, Izmir, Turkey. E-mail : cem.kincal@deu.edu.tr

ABSTRACT

Slope stability analysis is critical to investigate the mass movements along the highway road-cuts. Planar and wedge type of failures are commonly observed along the Bağarası-Foça route. The major factors of slope stability include lithology, slope angle, slope aspect and discontinuity orientation. A database is formed by discontinuity orientation data, slope positions and lithology. Lithic and vitric tuff units outcrop along the route. Three discontinuity joint sets are recorded.

MapInfo Professional software was used to prepare digital thematic maps which are;

- Geological map (lithological data)*
- Slope map (strike, dip and dip direction data)*
- Discontinuity map (covering three discontinuity sets)*

Planar-type slope failure hazard map is prepared using the lithology information, slope and discontinuity orientations. GIS-based overlay technique was used while preparing the hazard map.

Taking precautions are important to prevent mass movements which may cause slope failures to the highway. This study will present the potential planar-type mass movement along the Bağarası-Foça state highway and some precautions to prevent further slope failures.

INTRODUCTION

Slope failures are geologic hazards. Slope failures could result in blocking roads/highways, destruction of engineering structures and even burial of cities (Hunt, 2005). In mines, slope failures could lead to production loss and potential ore reserve losses. Urbanized areas stand to suffer greater consequences from slope failures because even small slides can damage buildings and block access to traffic (Transportation Research Board, 1996). Slope stability assessment is therefore important to preserve lives and property.

Ulusay (2013) identified five important factors which form the foundation of rock slope assessment. These factors are lithology, structure, state of deterioration, hydrogeological conditions prevailing in rock slopes and correct selection of rock mass geomechanical parameters. One other important factor which was identified is external forces, such as dynamic loading due to earthquakes for slopes found at earthquake-prone regions.

Geographical Information Systems (GIS) are useful in slope stability determination (kinematic analysis) and monitoring. Kinematic analysis generally involves analyzing discontinuity data with the aid of stereonet. Park et al. (2016), however, identified a limitation of kinematic analyses using stereonet. The authors noted that in areas where rock slope orientations are not uniform and slopes are dispersed over a large area, GIS tools yield better kinematic analysis results compared to stereonet because GIS has efficient data analyzing capabilities.

Many researchers have successfully used GIS to conduct slope stability assessment. Oztekin et al. (2006) assessed the degradation and stability of a highway cut slope in Ankara, Turkey. GIS tools were employed in the study. GIS tools were used to estimate the possibility of failure recurring in areas which had experienced failure previously.

Yilmaz et al. (2011) conducted research on GIS-based kinematic slope instability and Slope Mass Rating (SMR) maps using a railway route in Turkey as a case study. Various discontinuity orientation measurements were taken in the field and the data was input into ArcGIS software. Analysis was then conducted for plane and wedge failures. The results showed that planar and wedge failure was likely to occur at some sections of the route. Slope Mass Rating (SMR) was used to classify the slopes. The authors noted that the SMR results agreed with and validated the results of the kinematic analysis.

Irigaray et al. (2011) suggested a method of slope stability analysis that combined GIS technology and probabilistic analysis. Technological tools employed in the study were DIPS 5.0, ArcGIS 9.3, RocPlane 2.0 and Swedge 5.0. Kinematic analysis was done with the aid of DIPS 5.0 and ArcGIS 9.3 software while Factor of Safety and Probability of Failure were calculated using RocPlane 2.0 and Swedge 5.0 software. A high degree of accuracy was found (90% of the slopes) when the results of the analyses were compared to field observations.

Shaban et al. (2001) successfully conducted research on the instability of a road slope in Lebanon using GIS tools. Field studies, aerial photographs and Global Information System (GIS) tools were employed in the study. Hazard assessment maps were generated which indicate the level of risk of various sections of the slope.

Location of the Study Area

The study area (Figure 1) is located in Izmir, Turkey, on the Aegean coast between the towns of Bağarası and Foça at about 69 km (43 mi) northwest of Izmir city center. The study area has a Mediterranean climate, which is typically associated with shrubs. Near the settlement areas, olive farming and horticulture are common. The most important rivers in

the region are SW flowing Reşitbey Stream, NE flowing Karaman Stream, SW flowing Foça Stream, and the south flowing Mersin Stream.



Figure 1. Location of the study area (Google Earth, 2016).

GEOLOGY OF THE STUDY AREA

The study area falls within the western coast of the Aegean region. Akay (2000) and Akay & Erdogan (2004) identified three different suites of volcanic rocks in the Foca region. These are (from youngest to oldest):

- The Foça alkaline volcanic rocks,
- Foca volcanic rocks, and
- The Yuntdag volcanic rocks.

The lithological units in the area are andesitic lithic and vitric tuffs, rhyolitic lithic and vitric tuffs, basalt, rhyolite and alluvion. The oldest lithological unit in the study area is the vitric tuff, which is overlain by the lithic tuff. Basalt dikes intruded the vitric and lithic tuffs. The rhyolite unit occurs as domes within the volcanic tuffs.

The general geological map of the study area is presented in Figure 2.

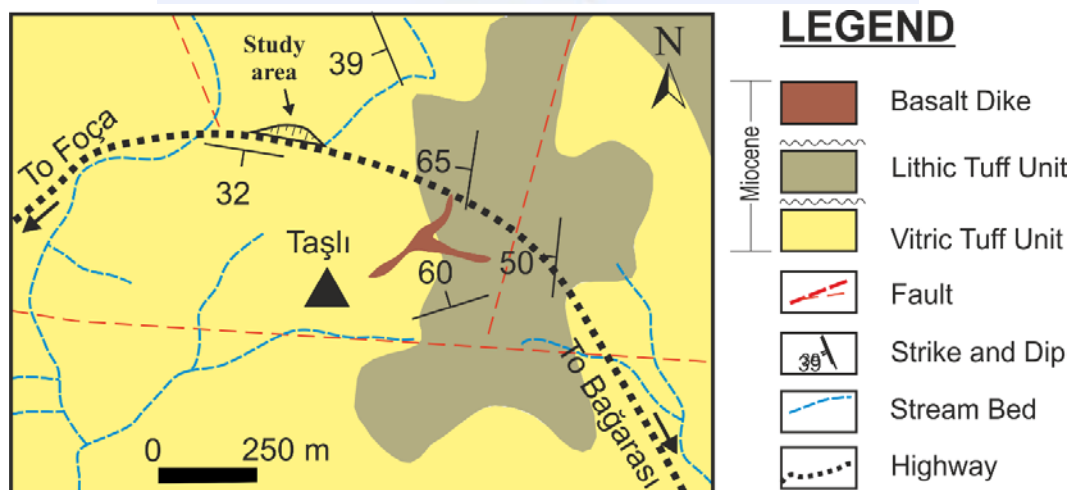


Figure 2. General geological map of the study area

METHODOLOGY

The lithologies in the study area were carefully studied and mapped. Detailed discontinuity data collection was also conducted in the field (scanline mapping of discontinuities). Block samples of HW-SW rocks were collected from the between the Bağarası-Foça (Izmir) State highway slope. Laboratory tests were conducted to determine the saturated and dry unit weight, porosity and compressive strength of the rock materials.

MapInfo Professional software and its GIS tools were employed in the study to conduct the potential of planar and wedge failures. Prior to conducting the analyses, the data obtained from the field (discontinuity orientation data, slope positions and lithology) were used to create a database. Digital thematic maps (geological map, slope map and discontinuity map) was prepared using MapInfo software. The geological map was prepared using the lithological mapping data while the discontinuity data (strike, dip and dip direction) were used to prepare the slope map. Three discontinuity sets were used to prepare the discontinuity map. Planar failure and wedge failure potential hazard maps were prepared with the aid of GIS-based overlay techniques.

Lithology data as well as slope and discontinuity orientation data were used for the hazard map preparation.

“RocLab” developed by Hoek, Torres and Corkum (2002) was used to estimate the rock mass properties of the volcanic tuffs. The results obtained from the GIS-based kinematic analyses were validated with kinematic analysis using Dips 5.1.

ENGINEERING GEOLOGY

The main types of mass movements in the Foca-Bağarası (Izmir) districts and its surroundings are planar, wedge and toppling type failures, as well as complex combinations of all these types.

Planar failure (Figure 3) occurs when the strike of the plane on which sliding occurs is within $\pm 20^\circ$ of the strike of the slope. In addition, for planar failure to occur, the failure plane must dip at an angle lesser than that of the slope face, and the internal angle of friction for the discontinuity must be less than the dip angle of the discontinuity (Hoek and Bray 1981).

Wedge type failures are commonly observed in road cuts with high slopes, which is composed of tuff geological unit. Weathering of volcanic tuffs causes slope stability problems in road-cuts. Gravity also plays a major role in the occurrence of wedge and planar failures. Wedge failures (Figure 4) mainly occur due to gravitational falls of wedge blocks defined by the intersection of the discontinuities with other structural features which act as release surfaces (Marinos and Hoek, 2001). The main type of wedge failure observed in the study area involves sliding along the line of intersection of two planar and/or nearly planar joint surfaces.



Figure 3. Planar failure observed in the field.



Figure 4. Potential wedge failures observed in the field.

Stereographic projection methods (Figure 5 and 6) are useful for conducting kinematic analyses when assessing the stability of a rock slope. The techniques were originally developed by Markland (1972), and have been successfully used by many authors (Goodman, 1976; Hoek and Bray, 1981; Matherson, 1988; Kaya et al., 2015, Qi et al., 2016) in conducting slope stability analyses.

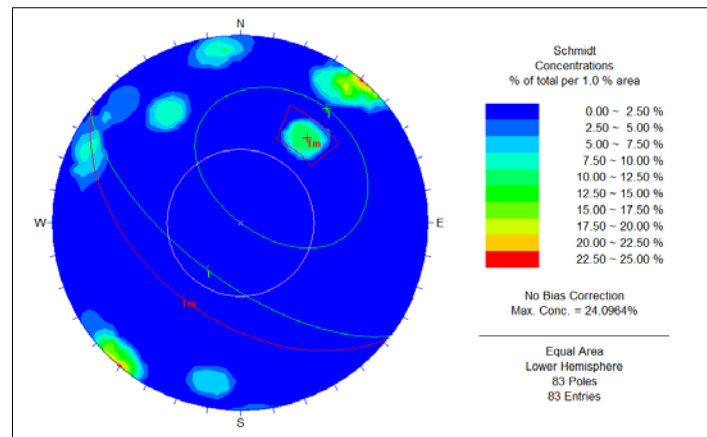


Figure 5. Planar failure analysis

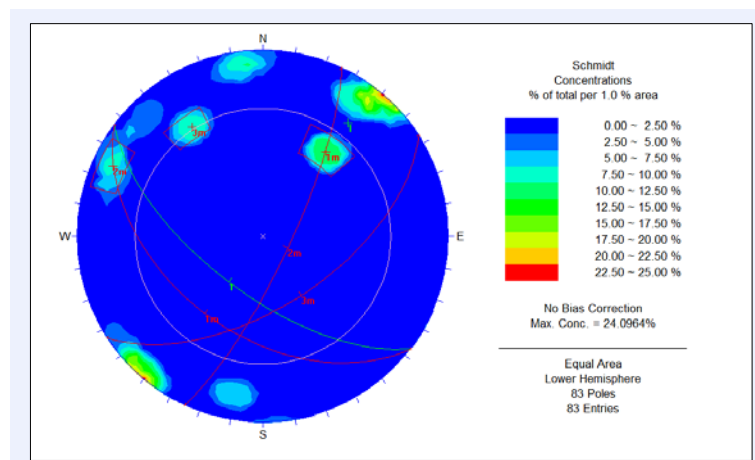


Figure 6. Wedge failure analysis

Generally, wedge sliding along the line of intersection of two discontinuity planes (planes A and B) is possible when the plunge angle of this line is less than the dip angle of the slope face (Hoek and Bray, 1974).

Average trend and plunge estimation of intersection lines in wedge failures is essential in engineering geology, especially when there are undulations in the discontinuities. Hoek and Bray (1974) suggested a method of probable sliding direction estimation based on the assumption that the wedge forming discontinuity planes are planar.

Shear strength tests

A major contributing factor to instability in volcanic tuffs is smooth discontinuity surfaces. As such, direct shear strength tests were conducted to determine the shear strength parameters (c' and ϕ') of the discontinuity surfaces. Average ϕ' obtained was 32° with no cohesion.

Shear strength parameter determination is essential in rock slope stability assessment (Barton, 1976). The friction angle (ϕ') of the discontinuities in the volcanic tuff unit was

used in the kinematic analyses. Environmental factors such as softening due to water along the discontinuities weaken discontinuities and rock masses rock masses, and lowers their physico-mechanical properties (Mimuro et al., 1991; Ulusay and Yoleri, 1993).

Probable wedge sliding direction based on Hoek and Bray (1974) was found to be in the NE-SW direction.

GIS Applications

Investigated slope face is found from Googleearth and digitized using related tool and is saved in KML/KMZ format. Then, slope face which is in vector format is opened in Global Mapper software and exported as MapInfo Professional TAB/MAP format (Figure 7).

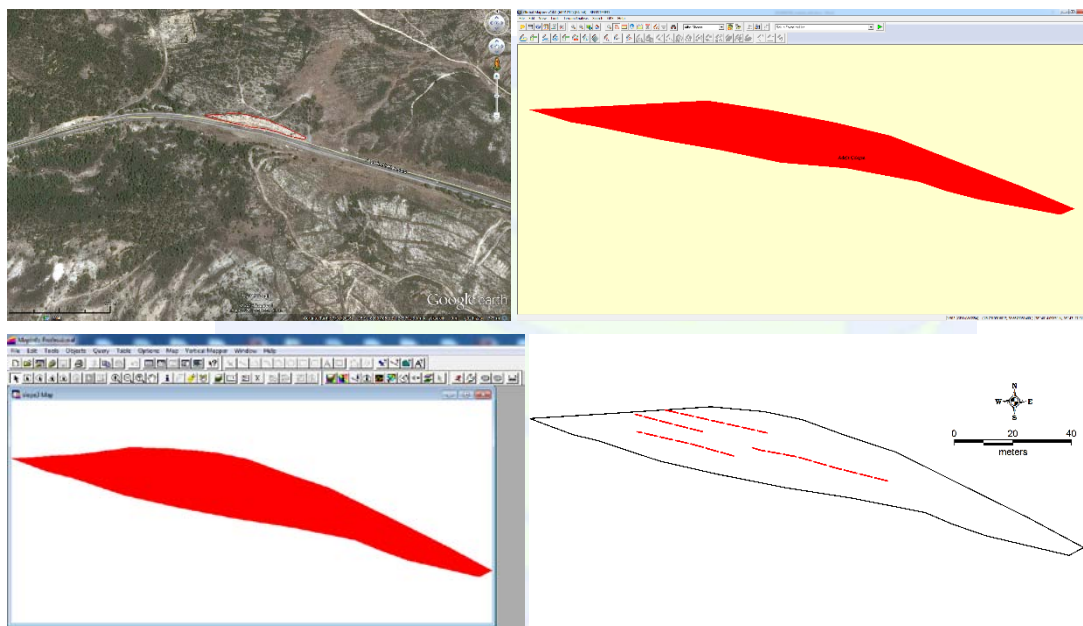


Figure 7. Slope digitization process

Later, panoramic view of the slope is registered using MapInfo's command, Raster → Modify Image Registration. The coordinates of the digital image saved in MapInfo format were used during the geocoding process. Discontinuity data were then digitized with the help of field investigations and screen digitizing (Figure 8).

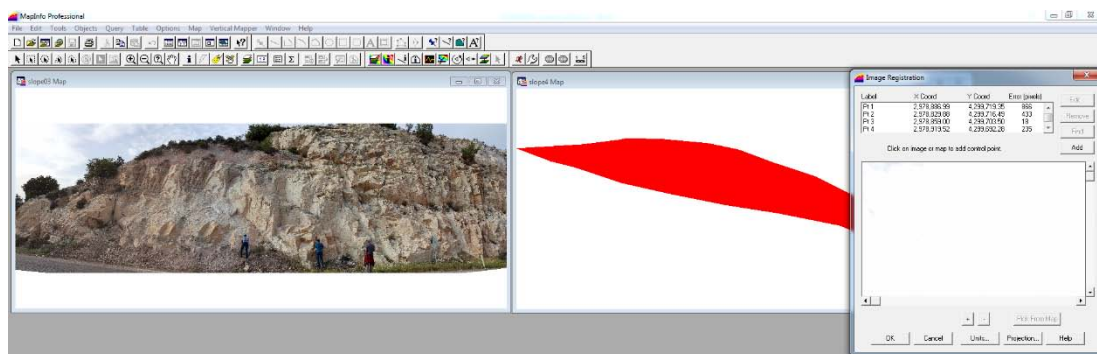


Figure 8. Slope image registration.

The slope geometry was digitized and using overlay techniques, the discontinuity data was superimposed on the digitized slope. Risky discontinuity orientations which could cause potential planar and wedge failures when kinematically possible were identified. Plane failure potential GIS map and wedge failure potential GIS maps were prepared based on the field data. Field investigations and observations were considered in preparing the maps. Planar failure analysis is presented in Figure 9a and 9b. Discontinuities forming potential planar failures from field investigations are shown in red dash lines.

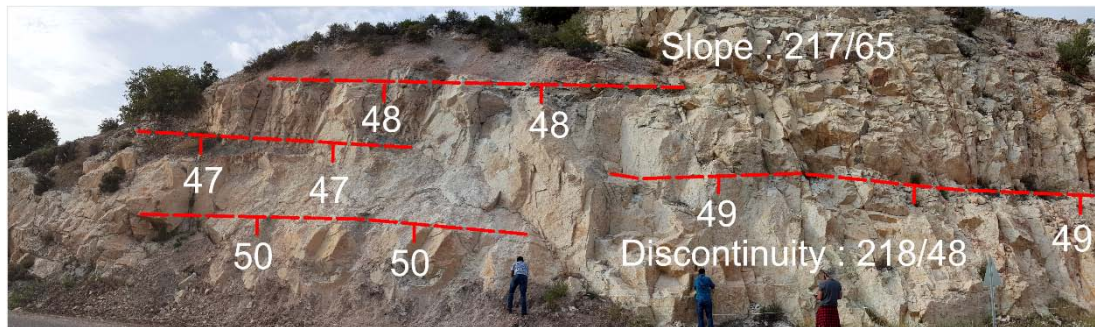


Figure 9a. Discontinuities forming potential planar failures.

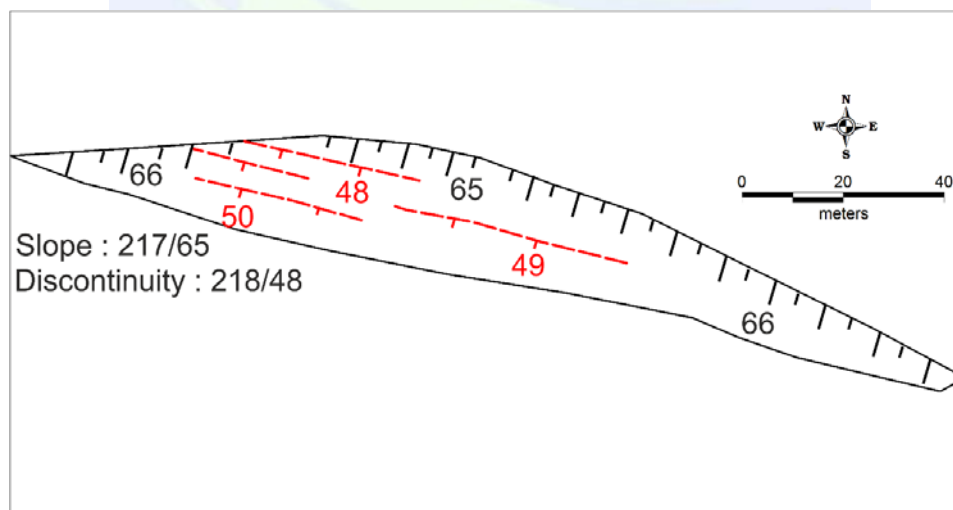


Figure 9b. Planar failure potential GIS hazard map of the investigated slope

The results of the wedge failure analysis is presented in Figure 10a and 10b. The sets of discontinuities forming potential wedge failures from field investigations are shown in white dash lines. The combined potential planar and wedge failure GIS hazard map of the vitric tuff is presented in Figure 11.

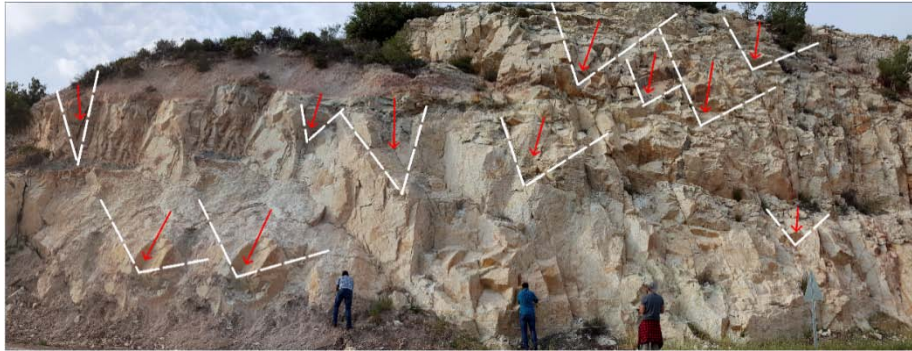


Figure 10a. Discontinuities forming potential wedge failures (Red arrows represent intersection line of wedge block which is the direction of sliding).

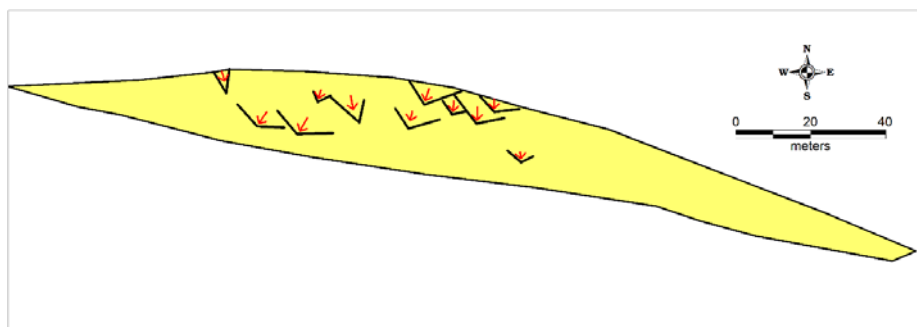


Figure 10b. Wedge failure potential GIS hazard map overlaid on geological map of the investigated slope (Yellow color represents vitric tuff units).

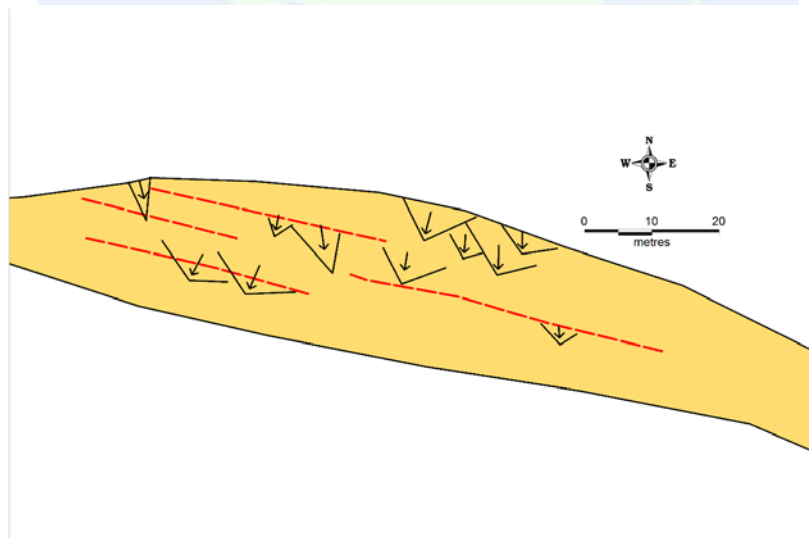


Figure 11. Combined potential planar and wedge failure GIS hazard map of the vitric tuff unit

CONCLUSIONS

The main lithology in the study are is vitric tuffs. Results of the GIS-based kinematic analysis of planar and wedge failures in the vitric tuffs corresponded with the results of the

kinematic analysis conducted using Dips 5.1. Potential planar and wedge failures were identified along the Bağarası-Foca (Izmir) state highway. The wedge failures are mainly controlled by discontinuities in the volcanic tuffs.

PRECAUTIONS

The most economical ways of maintaining the stability of the slope is presented in order below:

- a. Regular monitoring of the state highway slopes should be conducted to identify weak zones.
- b. Drainage ditches should be constructed to prevent surface run-off water from accumulating at the top and toe of the slope.
- c. Benches should be constructed to reduce the slope angle and height
- d. Loose rock materials on the slope face should be removed.
- e. Retaining walls should be constructed to protect traffic from danger caused by falling blocks.
- f. Wire meshing should be done on the slope face to prevent falling rock blocks.

REFERENCES

- Akay, E., 2000. *Magmatic and tectonic evolution of the Yuntdağ volcanic complex (Western Anatolia)*. PhD Thesis, Dokuz Eylül University, İzmir [unpublished].
- Akay, E., Erdoğan, B. 2004. Evolution of neogene calc-alkaline to alkaline volcanism in the Aliğa-Foça region (Western Anatolia, Turkey). *Journal of Asian Earth Sciences* 24(3): 367-387.
- Goodman, R.E., 1976. *Methods of Geological Engineering in Discontinuous Rocks*: West Publishing Company, St. Poul, MN, 170-207.
- Hoek E., Bray, J.W., 1974. *Rock Slope Engineering*. London: Instn Min. Metall.
- Hoek, E., Bray, J.W., 1981, *Rock Slope Engineering*, the Institution of Mining and Metallurgy, Stephen Austin and Sons Ltd., London, 3rd edition, 385 p.
- Hoek E, Carranze-Torres C, Corkum B., 2002. Hoek–Brown failure criterion-2002 edition. In: *Proceedings of the North American rock mechanics society meeting*, Toronto, July 2002. p. 267–73.
- Hunt, R. E., 2005. *Geotechnical engineering investigations handbook*. (Second Edition). UK. CRC Press.
- Oztekin, B., Topal T., Kolat C., 2006. Assessment of degradation and stability of a cut slope in limestone, Ankara-Turkey. *Engineering Geology*, 84(1-2):12-30.
- Irigaray, C., El Hamdouni, R., Jiménez-Perálvarez, J. D. Fernández, P., Chacón, J., 2012. Spatial stability of slope cuts in rock massifs using GIS technology and probabilistic analysis. *Bulletin of Engineering Geology and the Environment*. 71:569–578.

- Kaya, A., Akgün, A., Karaman, K., Bulut, F., 2016. Understanding the mechanism of slope failure on a nearby highway tunnel route by different slope stability analysis methods: a case from NE Turkey. *Bulletin of Engineering Geology and the Environment* 75 (3):945-958.
- Marinos, P., Hoek, E., 2001. Estimating the geotechnical properties of heterogeneous rock masses such as flysch, *Bull. Eng. Geol. Env.*, Springer-Verlag, 60:85-92.
- Markland, J.T., 1972. *A useful technique for estimating the stability of rock slopes when the rigid wedge sliding type of failure is expected*, Imperial College Rock Mechanics Research Report, No.19, 10p.
- Matherson, G.D., 1988, The collection and use of field discontinuity data in rock slope design, *Q.J. Engineering Geology*, 22, 19-30.
- Mimuro, T., Yamauchi, M., Watanabe, K., Denda, A., 1991. Deterioration of mechanical properties of Neogene sedimentary soft rocks. *International Congress on Rock Mechanics, ISRM*, vol. 1, pp. 299 – 302.
- Park, H., Lee J., Kim K., Um J., 2016. Assessment of rock slope stability using GIS-based probabilistic kinematic analysis. *Engineering Geology* 203, 56–69.
- Qi, C., Wu J., Liu J., Kanungo, D.P., 2016. Assessment of complex rock slope stability at Xiari, Southwestern China. *Bulletin of Engineering Geology and the Environment*, 75 (2): 537-550.
- Shaban., A., Khawlie M. R., Kheir R. B., 2001. Assessment of road instability along a typical mountainous road using GIS and aerial photos, Lebanon - Eastern Mediterranean. *Bulletin of Engineering Geology and the Environment* 60(2):93-101.
- Transportation Research Board, 1978. *Landslides Analysis and Control*. Special Report 176, R. L. Schuster, and R. J. Krizek (Eds.), National Academy of Science, Washington, D.C., p. 234.
- Ulusay, R., 2013. Harmonizing engineering geology with rock engineering on stability of rock slopes. In X. Feng, J.A. Hudson & F. Tan (eds). *Rock Characterisation, Modelling and Engineering Design Methods*, 11-13. Proceedings of the 3rd ISRM Sinorock Symposium, Tongji University, Shanghai, China. UK: Taylor & Francis Group.
- Ulusay, R. and Yoleri, M.F., 1993. Shear strength characteristics of discontinuities in weak, stratified, clay-bearing coal measures encountered in Turkish surface coal mining. *Bulletin International Association Engineering Geology*, 48, 63-71.
- Walker, B.F. and Fell, R. (eds.), 1987. Soil slope instability and stabilization. *Proc. of an Extension Course on Soil Slope Instability and Stabilization*, Sydney. A.A. Balkema, Rotterdam, 1-231.
- Yilmaz I, Marschalko M, Yildirim M, Dereli E, Bednarik M., 2011. GIS-based kinematic slope instability and slope mass rating (SMR) maps: application to a railway route in Sivas (Turkey). *Bulletin of Engineering Geology and the Environment*, 71:351–357.

Crustal Structure of Golbasi-Celikhan Segment, Eastern Anatolia, Turkey

Caglar Ozer^{1,2}, Mehmet Ozyazicioglu³, Elcin Gok¹ and Orhan Polat^{*1}

¹Department of Geophysical Engineering, Dokuz Eylul University, Tinaztepe Campus, Izmir, Turkey. e-mail: (orhan.polat@deu.edu.tr)

²Department of Geophysical Engineering, Ataturk University, Erzurum, Turkey e-mail: (caglaroz@atauni.edu.tr)

³Department of Civil Engineering, Ataturk University, Erzurum, Turkey e-mail: (mehmetoz@atauni.edu.tr)

ABSTRACT

We announce a new seismic crustal model in Golbasi-Celikhan fault segment where based on the East Anatolian Fault Zone (EAFZ) using the Local Earthquake Tomography method. In order to conduct the tomographic calculation, we have selected more than 2000 events from 2011 to 2017 by 35 recorders. The seismic network was installed by the Earthquake Department of the Disaster and Emergency Management Authority (AFAD). We showed that low Vp and low Vp/Vs represent the gas content which associated with geothermal origin beneath the Guzelyurt, Olgunlar, Akcadag, Sofular and Karlik regions, which are mostly connected with fault zone. Dominant high P- velocity values are observed beneath the subduction zone that is located at 30-40 km depths in nearly all depth cross section. Conrad discontinuity is detectable in 20 km depth. Our consequences proposed that the Moho depth is located at ~35 km and varying from 30 to 40 km in the Eastern Anatolia, Turkey.

INTRODUCTION

The Golbasi-Celikhan fault segment (Fig. 1) is characterized by ~20 km long parts displayed active left lateral strike-slip characteristic. The drainage connection is offset by a few meters to 0.5 km in Holocene age sediments. The last biggest earthquake caused by big surface rupture is Ms 7.2, 1893 earthquakes (Duman & Emre 2013).

In this study, we used Local Earthquake tomography (LET) method to compute the crustal thickness variations and possibility of geothermal resources in the Golbasi-Celikhan fault segment using LOTOS code (Koulakov 2009) which is freely available. The use of the LOTOS code that presents the first usage of this algorithm in the Eastern Anatolia authorized us to get high-resolution tomograms mainly decreasing the grid spacing with respect to previous investigations applied in the region, and also to interpret a detailed Vp/Vs model not previously available for the study area.

* Corresponding Author

DATA

We used to travel times recorded by permanent three-component digital seismometer network, which was operated by AFAD from 2011 to 2017 in an area of about $5^{\circ} \times 4^{\circ} \text{ km}^2$ and centered in the Eastern Anatolia. There were 15.000 local earthquakes ($M_L \geq 2.0$) that were recorded in a period of nine years about 35 instruments in the region between 36 and 40N latitude and 36-41E longitude at the continent-continent collision of the Arabian and Eurasian plates.

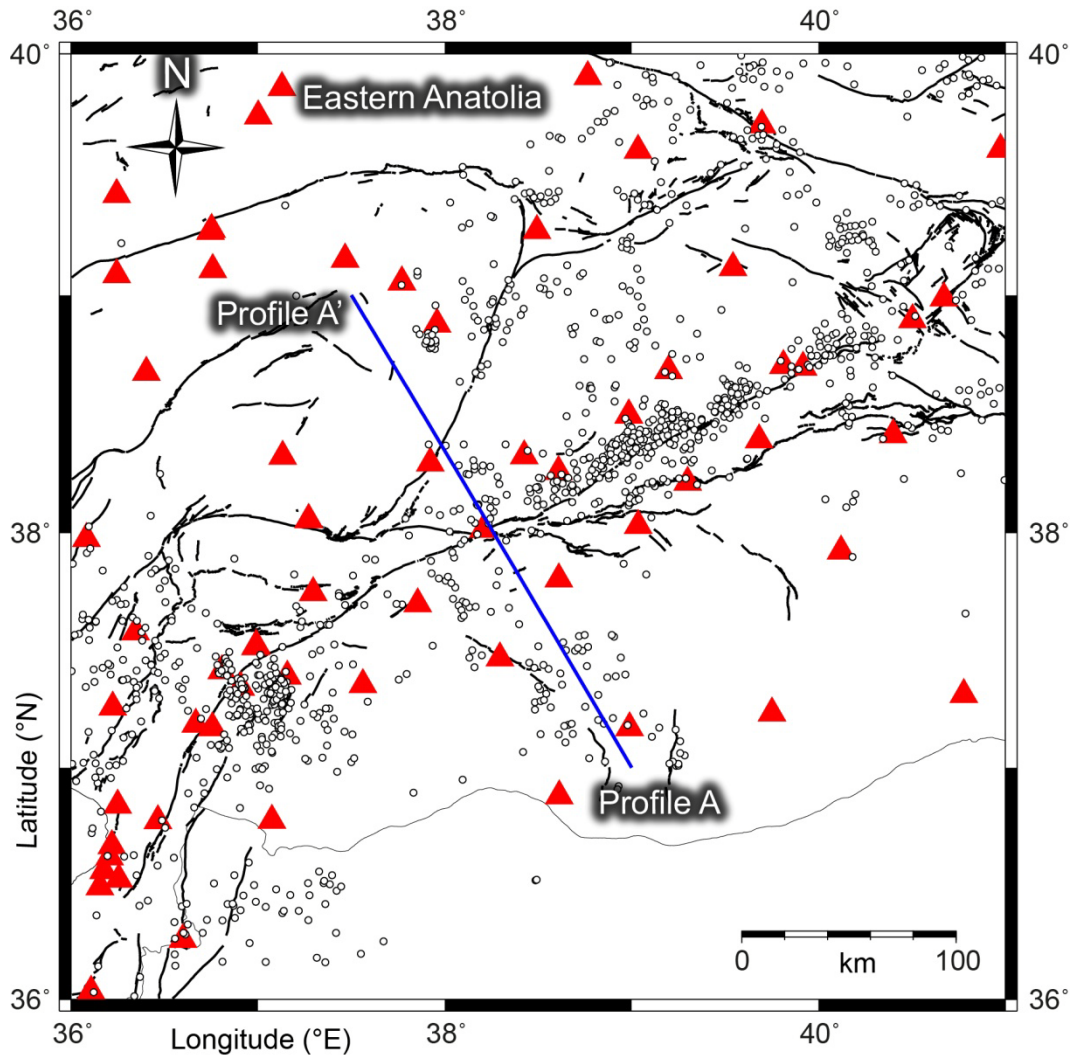


Figure 1. Location of selected 2000 events (hand-picked, $M \geq 2.0$) recorded between 2011 and 2017 in the eastern Anatolia. Stations are represented by filled red triangles and thin black lines show fault traces (digitized after Emre, et al. 2013).

TOMOGRAPHY RESULTS

The LET algorithm is often preferred in many studies since it reveals crustal seismic variations by performing 3-D joint inversion for hypocentral parameters and velocities. The velocity perturbations have close relations with lithological changes, petrological

characteristics of rocks, fluid-rich and high-pore-pressure sub-areas, regional tectonics, and the structure and geometry of faults (Ozer and Polat 2017a, b, c).

Tomographic inversion results of P- wave velocity structure and Vp/Vs ratio at vertical section are shown in Fig. 2. The absolute velocities are layered nearly horizontally and the tomogram show good correlation with the known tectonic and geological characteristics of the study area. Our tomographic models illustrate P-wave velocities from 3.0 to 9.0 km/s between 0 and 40 km in the crust.

The intrusive shape high-velocity part of the upper mantle to upper crust at the beginning of seismic layer, which is probably to symbolize a thrust fault zone effect, forms a thick zone from the deepest part to 10 km. The motion between the Arabian and the Anatolian plates have been clearly detectable as a high Vp velocities at the beginning of the profile. We found that the average crustal P- wave velocity structure beneath the Eastern Anatolia divided four seismic parts helping the tomographic images (Fig. 2). Furthermore, we estimate Conrad and Moho discontinuities at ~20 km, ~35 km; respectively.

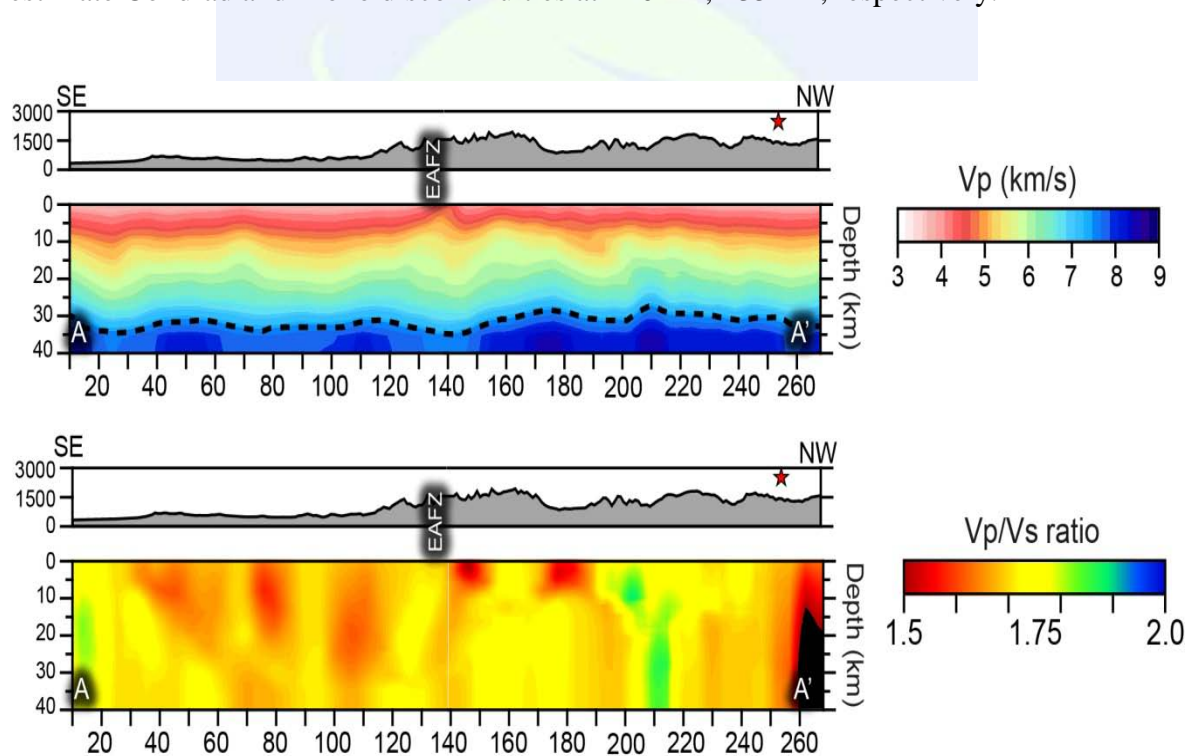


Figure 2. Vertical sections of absolute P-wave velocity and Vp/Vs ratio models. Red Star: Geothermal area. Dashed black line show predicted Moho discontinuity depth.

CONCLUSIONS

This study offers the first Local Earthquake Tomography (LET) application in eastern Anatolia and ensures important perspective about crustal structure and some new potential/target geothermal reservoirs that have not been investigated in detail yet. P- wave seismic velocity and Vp/Vs ratio of depth cross-section get an important acknowledgement to appear the lithological and petrological structure of the study area. We finalized that four main crustal seismic layers are determined down to 40 km beneath Golbasi-Celikhan

fault segment in the upper crust (~0-8 km depth; $V_p \leq 4.6$ km/s), middle crust (~8-18 km depth; $4.6 < V_p \leq 5.8$ km/s), lower crust (~18-32 km depth, $5.8 < V_p \leq 7.4$ km/s) and upper mantle layer (> 32 km depth, $V_p > 7.4$ km/s); respectively.

ACKNOWLEDGMENTS

This study is supported by DEU (Nr. 2016.KB.FEN.013). We appreciate to the AFAD (Ankara, Turkey) for providing us the data. Thanks to Ivan Koulakov for providing the latest LOTOS modules. Calculations were performed in SeismoLab (Seismological Laboratory) of the Geophysical Engineering Department of Dokuz Eylul University, Izmir, Turkey. Travel grant was funded by the Earthquake Engineering Association of Turkey (TDMD). We also thank the General Directorate of Mineral Research and Exploration (MTA) for the fault data which digitizing in its website.

REFERENCES

- Duman, T.Y. and Emre, O., 2013. The East Anatolian Fault: geometry, segmentation and jog characteristics, *Geological Society, London, Special Publications* 372 (1), 495-529.
- Emre, O., Duman, T.Y., Ozalp, S., Elmaci, H., Olgun, S. and Saroglu, F., 2013, 1/1.125.000 Olcekli Turkiye Diri Fay Haritasi, *Maden Tetkik ve Arama Genel Mudurlugu Ozel Yayinlar Serisi*, Ankara, Turkiye.
- Koulakov, I., 2009. LOTOS code for local earthquake tomographic inversion: Benchmarks for testing tomographic algorithms, *Bulletin of the Seismological Society of America* 99 (1), 194-214.
- Ozer, C., and Polat, O., 2017a. Determination of 1-D (one-dimensional) seismic velocity structure of Izmir and surroundings. *Journal of science and engineering*, 19 (55), 147-168.
- Ozer, C., and Polat, O., 2017b. 3-D crustal velocity structure of Izmir and surroundings. *Journal of the Faculty of Engineering and Architecture of Gazi University*, 32 (3), (accepted).
- Ozer, C., and Polat, O., 2017c. Local earthquake tomography of Izmir geothermal area, Aegean region of Turkey. *Bollettino di Geofisica Teorica ed Applicata*, 58 (1), 17-42.

Crustal Structure and Geothermal Exploration in Western Anatolia of Turkey using Local Earthquake Tomography

Caglar Ozer^{1,2}, Elcin Gok¹ and Orhan Polat^{*1}

¹*Department of Geophysical Engineering, Dokuz Eylul University, Tinaztepe Campus, Izmir, Turkey. (orhan.polat@deu.edu.tr)*

²*Department of Geophysical Engineering, Ataturk University, Erzurum, Turkey e-mail: (caglaroz@atauni.edu.tr)*

ABSTRACT

This study reveals initial results of the crustal structure of Western Anatolia from the Local Earthquake tomography (LET). Study area spans 26-30°E longitudes and 37.5-39.5°N latitudes. Based on tomographic images, crustal structure generally reveals low Vp and low Vp/Vs beneath geothermal areas. We suggest Aliaga, Bigadic, Denizli, Doganbey, Kosk and Menemen areas as low Vp, low Vp/Vs anomalies which are an indicator of steam, CO2 or mixture of them. Low Vp, high Vp/Vs models which propose geothermal fluids, are clearly visible near Buharkent, Kosk, Kuyucak, Saraykoy and Suzbeyli region. We also report that Candarli, Kalekoy, Ortakoy, Saruhanli, Yelki regions might be good candidate for new potential geothermal resources.

INTRODUCTION

The seismic velocity structure in the upper crust beneath the western Anatolia, Turkey, is investigated by using simultaneous inversion technique of P- and S- wave travel times from local earthquakes. We conduct a local earthquake tomography (LET) technique to illustrate the crustal structure by using 10203 P- and 8654 S- wave arrivals from 1586 earthquake recorded between 2010 and 2015 by the Earthquake Department which belongs to the Disaster and Emergency Management Presidency (AFAD) of Turkish Republic (Figure 1).

CRUSTAL STRUCTURE OF WESTERN ANATOLIA FROM THE LET

The Local Earthquake Tomography (LET) is effective seismological tool to identify geological and tectonic structures, geothermal resources, petrological properties of rocks, monitoring the volcanoes, etc. (Ozer and Polat 2017a, b, c). Studies on the crustal structure and geothermal potential of western Anatolia emphasize that different perspective of the studies still need in the study area. Therefore we conduct LET to understand crustal structure and geothermal potential of the Aegean region of Turkey.

^{*} *Corresponding Author*

We report from our initial study that geothermal areas located in the Western Anatolia are represented by the low V_p and low V_p/V_s ratio for most cases. Previous studies (e.g.; Hauksson 2000; Kaypak and Gokkaya 2012) report that this anomaly is related with saturated rock, high gas pressure and CO_2 content. At the same time, few areas also exhibit low V_p and high V_p/V_s ratios which can be also interpreted the existence of geothermal liquids. We report 4 main seismic layers with different P-wave values down to 30 km. The Moho discontinuity is observed at around 29 km depths as undulated shape (Figure 2 and Figure 3).

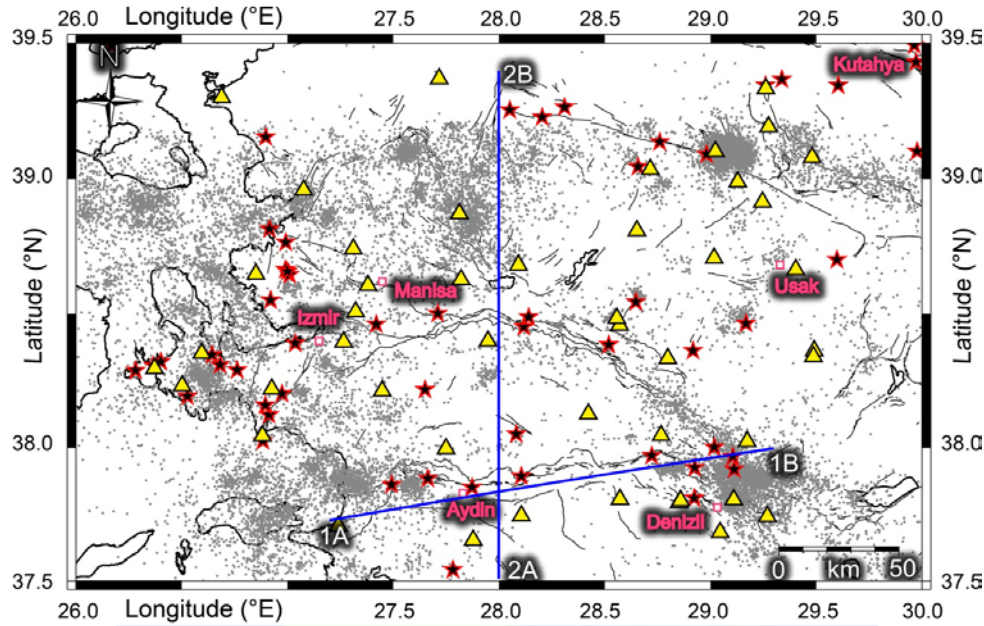


Figure 1. Map of the study area displaying main tectonic characteristic in western Anatolia of Turkey. Triangles are seismic stations, stars represent geothermal areas. Faults and profiles (e.g.; 1A-1B, 2A-2B) are indicated with thick lines

Also Ozer and Polat (2017c) reported for Izmir region, the upper crust mainly comprises Neogene sediments and Quaternary alluvial deposits showing low velocities. The middle layer exhibits velocities typical of the gabbro and other Lithospheric crystalline rocks. A sharp increase in velocities is evident at the lower crustal layer revealing the Bornova Flysch zone. We report at 27 km of depth an undulated transition at the crustal-mantle boundary.

From local tomography, we identify four main seismic layers at variable depths from the surface to the lower crust. The lower crust/mantle discontinuity is found at approximately 27 km of depth. This transition is characterized by an undulated shape, and intrusive bodies are imaged beneath the main geothermal systems (Ozer and Polat, 2017c).

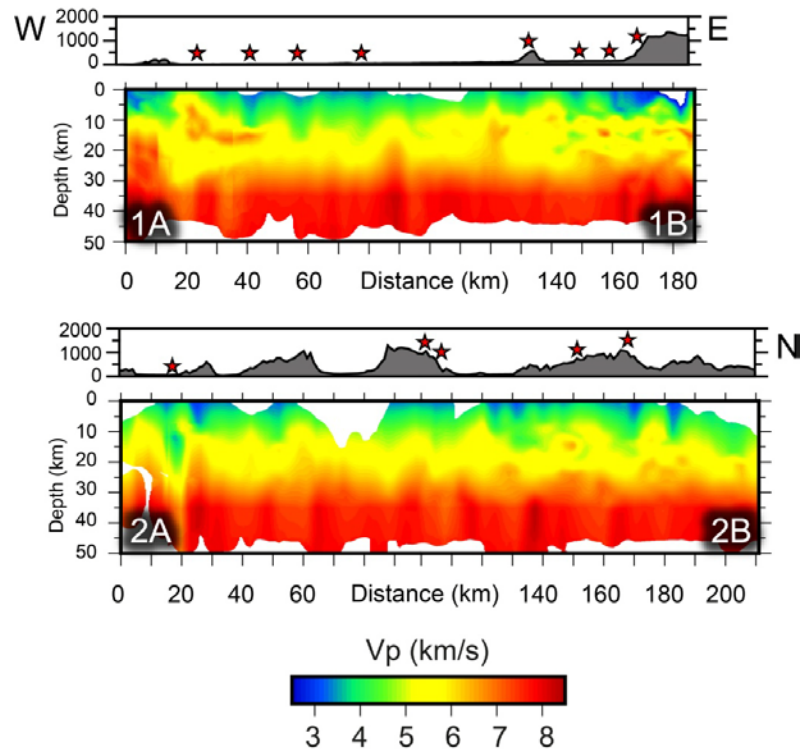


Figure 2. Cross-sections along two profiles for the V_p velocity anomalies model of tomogram along Büyük Menderes, Kucuk Menderes and Gediz grabens

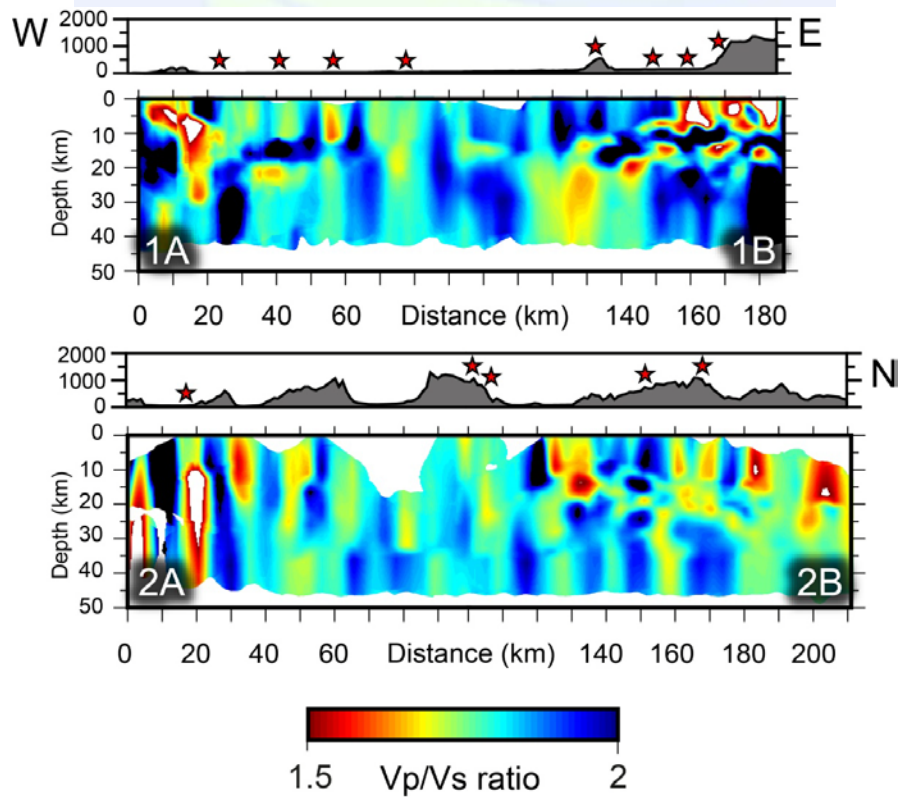


Figure 3. V_p/V_s values of cross-section tomogram along Büyük Menderes, Kucuk Menderes and Gediz grabens

CONCLUSIONS

This research presents the first LET study to better understand the crustal velocity structure of western Anatolia and provides significant insights for the future potential geothermal areas which have not been yet drilled in the region. We have identified four main crustal layers based on P-wave seismic velocity anomalies which range from 3.5 to 8.5 km/s. Features deeper than 40 km depths are not well-calculated due to the insufficient number of recorded earthquakes. The lowest Vp velocity (<3.5 km/s) in shallow areas (<3-5 km) are identified as quaternary alluvium. Furthermore, we used Vp/Vs ratio to interpret petrological features such as geothermal gas, fluid contents beneath present or potential geothermal areas.

ACKNOWLEDGMENTS

This study is a part of the PhD thesis of Caglar Ozer at Institute of Natural and Applied Sciences in DEU, Izmir-Turkey. It is supported by DEU (Nr. 2016.KB.FEN.013). We appreciate to the AFAD (Ankara, Turkey) for providing us the data. Thanks to Ivan Koulakov for providing the latest LOTOS modules. Calculations were performed in SeismoLab (Seismological Laboratory) of the Geophysical Engineering Department of Dokuz Eylul University, Izmir, Turkey. Travel grant was funded by the Earthquake Engineering Association of Turkey (TDMD). We also thank the General Directorate of Mineral Research and Exploration (MTA) for the fault data which digitizing in its website.

REFERENCES

- Hauksson, E., 2000. Crustal structure and seismicity distribution adjacent to the Pacific and North America plate boundary in southern California. *J Geophys. Res* 105 (B6), 13875-13903.
- Kaypak, B. and Gokkaya, G., 2012. 3-D imaging of the upper crust beneath the Denizli geothermal region by local earthquake tomography, western Turkey. *J Volcanol Geoth Res* 211-212, 47-60.
- Ozer, C., and Polat, O. (2017a). Determination of 1-D (one-dimensional) seismic velocity structure of Izmir and surroundings. *Journal of science and engineering*, 19 (55), 147-168.
- Ozer, C., and Polat, O. (2017b). 3-D crustal velocity structure of Izmir and surroundings. *Journal of the Faculty of Engineering and Architecture of Gazi University*, 32 (3), (accepted).
- Ozer, C., and Polat, O. (2017c). Local earthquake tomography of Izmir geothermal area, Aegean region of Turkey. *Bollettino di Geofisica Teorica ed Applicata*, 58 (1), 17-42.



GEOMATICS

Comparing the Performance of Reverse Geocoding Services: Google and Bing Maps

Batuhan KILIÇ^{*1} and Fatih GÜLGEN²

¹ Department of Geomatic Engineering, Yildiz Technical University, Davutpasa Campus, 34220, Turkey. e-mail: batuhank@yildiz.edu.tr

² Department of Geomatic Engineering, Yildiz Technical University, Davutpasa Campus, 34220, Turkey. e-mail: fgulgen@yildiz.edu.tr

ABSTRACT

Nowadays, it is possible to achieve in detailed geographic information rapidly using mobile devices over the location based services (LBS). The point features on digital maps, which refer to points of interest (POI) for people, have an important role in LBS. A point of interest on a map is positioned with a coordinate pair, such as latitude and longitude values in geographic coordinate system. Addresses are one of the fundamental means by which people conceptualize location in the modern world. In this context, the inverse geocoding process (i.e. reverse geocoding) is also needed in the extraction of textual information, such as a name or an address, from geographic coordinates.

The objective of this study is to examine the quality of online reverse geocoding that is provided by Google and Bing services in Turkey and USA. The quality of each reverse geocoding service is evaluated with address similarity metric. Address similarity reveals the relationship between two addresses using Levenshtein distance algorithm. The results in Fatih district are approximately 60% similar to reference data and each other. In Miami Beach, Google service produces better Levenshtein values, and both services present highly compatible results.

INTRODUCTION

The increase of mobile devices and social networks enables users to acquire geographical information in detail and rapidly. At the base of geographical data, the point features take up an important place. Point features that refer people to their destination and indicate their location on digital maps are known as point of interest (POI) which is gathered from land using various systems and devices or is obtained by volunteering participants from social networks. POIs are presented to the users through map services. In a map service, the location of POI is defined by their latitude and longitude values, which depend on the geographic coordinate system. However, each of POI has address information in real world

^{*} Corresponding Author

and a bridge between its geographic coordinates and address needs to be established. This situation can be solved with geocoding and reverse geocoding process.

With the rapid developments in internet and Geographic Information Systems, reverse geocoding associated with geocoding has become one of the main preprocess steps for many application areas, such as vehicle tracking, location based services, market research, provision of public utilities, work of emergency services etc. (Ratcliffe 2001, Kounadi vd. 2013). In this study, the results of two freely available reverse geocoding services have been examined and compared on urban areas in two different countries. Methodology is elaborated in two experimental testing regions in Turkey: Fatih district of Istanbul province and United States: Miami Beach of Florida State. In the preprocessing step, the address data of accommodation places in both regions were collected by means of scraping software from the *Booking.com* web site. Some accommodation buildings were accepted as reference POIs and their geographic coordinates were obtained and verified employing the land surveying. In the second stage, the postal addresses are derived by means of programming codes developed for Google and Bing's reverse geocoding. They were compared with the each other and the reference data using the Levenshtein distance utilized by internet search engines.

GENERATION OF REFERENCE DATA AND PREPROCESSING

In this study, the quality of online reverse geocoding is examined individually. The addresses used for testing belong to accommodation facilities in Turkey and the United States. The point features used for testing belong to addresses of accommodation facilities in them. Two areas were selected as the testing region where the hotels are concentrated. The first study area includes the ones within the borders of the Fatih district of Istanbul (Figure 1). The second area contains the hotels within Miami Beach boundaries of Florida state (Figure 2).

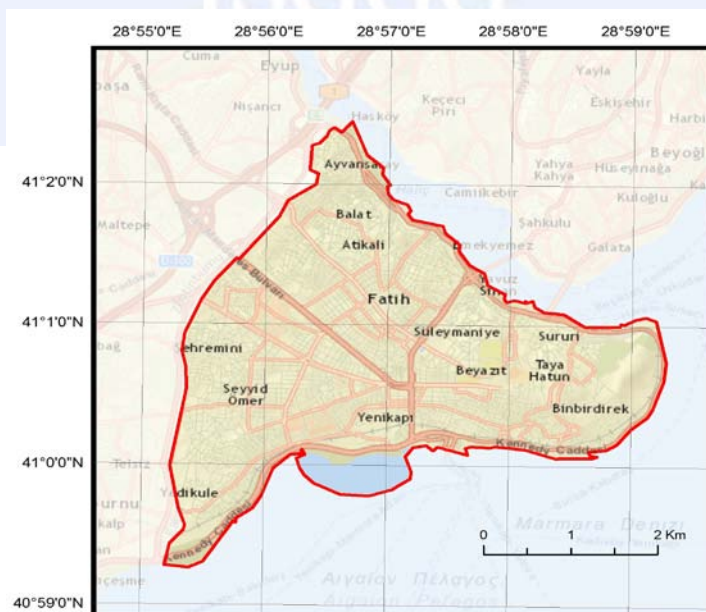


Figure 1. Fatih district in Istanbul

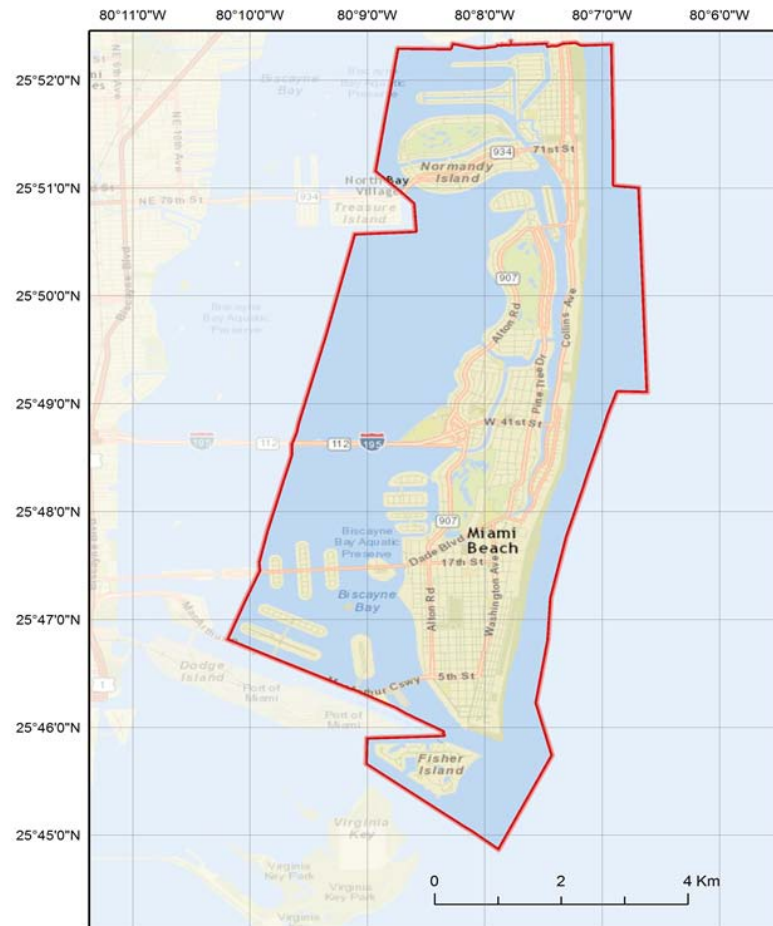


Figure 2. Miami Beach region in Florida

The accommodation facilities' name and their addresses which are the basis for the study, have obtained through a website known as *www.booking.com*. A *web scraping* process has been performed to collect hotel information through this website. Web scraping is a data scraping process used to gather standard information on specific sections of websites. Although web scraping is not a new term, in years past the practice has been more commonly known as screen scraping, data mining, web harvesting, or similar variations (Mitchell, 2015). There are various commercial web scraping software such as Visual Web Ripper, Web Content Extractor, Web Scraper Plus+ and many more (Rodrigues, 2010). In this scope, in order to collect the accommodation data, Web Content Extractor V.8.4 software developed by Newprosoft Company was used (Figure 3).

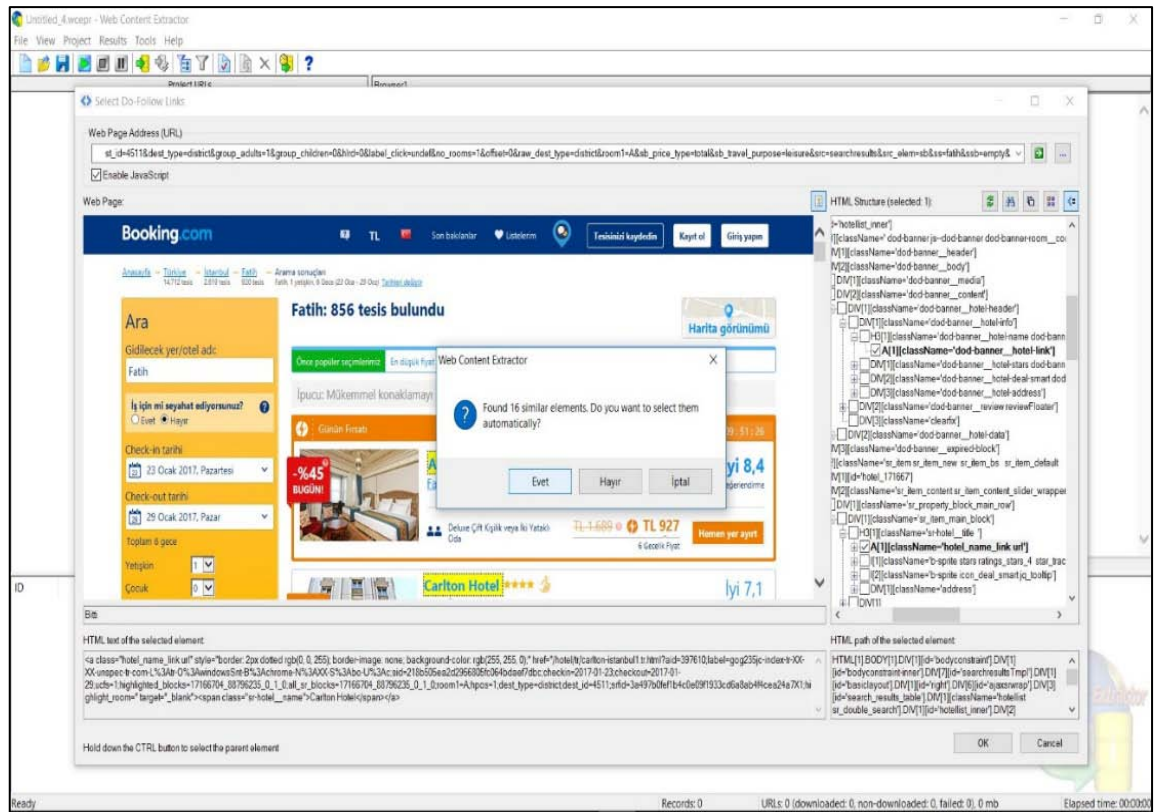


Figure 3. Web Content Extractor v.8.4 interface

When the hotel information of both regions is examined, once the collection process, it is understood that there are repeated addresses. Along with the cleaning of information on these hotels, remaining hotels were considered as points of interest and their approximate locations were calculated via Google and Bing maps by using facility names. Then, perspective street views are analyzed and locations of 74 hotels in Fatih and 82 hotels in Miami Beach are verified by reading the advertising signboards of the accommodation facilities (Figure 4a and Figure 4b). These hotels are digitized via ArcGIS World Street Map service as to form a building polygon in WGS84 datum. Point features, that form the reference for reverse geocoding, were derived from centroids of polygons and stored as points of interest in geographical data sets of Fatih and Miami Beach (Figure 5a and Figure 5b).



Figure 4. Perspective views of reference hotels in two study areas

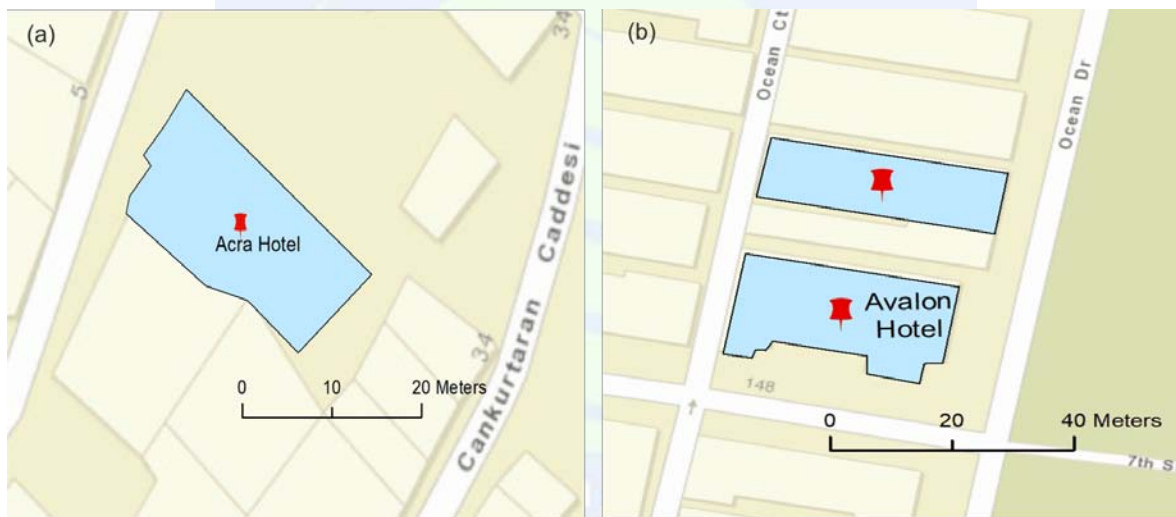


Figure 5. Map views of reference hotels in two study areas

REVERSE GEOCODING PROCESS AND ADDRESS SIMILARITY

After obtaining the geographic coordinates of the centroids of all the building polygons in both study areas, the address information are derived from the both services by reverse geocoding over the Python programming language using geographic coordinates. The reference addresses in both study areas and standard addresses obtained from Google and Bing Maps are compared using an algorithm known as 'Levenshtein distance'. Also, the similarity between the standard addresses of the services is determined for both regions (Table 1 and 2). Levenshtein is known as an algorithm used in information theory, computer science and mathematics. In practice, the Levenshtein distance between two words is the minimum number of single-character edits (insertions, deletions or substitutions) required to change one word into the other (URL-1).

Table 1. Similarity average between the addresses in Fatih

		Reference		<i>Google maps</i>
		<i>Google maps</i>	<i>Bing maps</i>	<i>Bing maps</i>
Similarity (%)	Fatih	62.7	62.8	62.5

Table 2. Similarity average between the addresses in Miami Beach

		Reference		<i>Google maps</i>
		<i>Google maps</i>	<i>Bing maps</i>	<i>Bing maps</i>
Similarity (%)	Miami Beach	70.5	62.9	88.2

According to Table 1 and 2, Similarity of the addresses derived from Google and Bing services in Fatih with reference data and each other is approximately similar. In Miami Beach, similarity of the services with each other is higher than their consistency with the reference addresses. Difference between the address formats used is the main reason for percentage values obtained in Fatih being lower than those in Miami Beach.

CONCLUSIONS

In this work, reverse geocoding process was reviewed comparatively through Google Maps and Bing Maps services. The applications realized in two different study areas show that they have different reverse geocoding capabilities in Turkey and USA. In Fatih, similarities of addresses obtained by reverse geocoding are similar for both services. On the other hand, it seems that the address similarity obtained from Google maps in the Miami Beach area are better than Bing. When the compatibility of both services is examined, the similarity values between the addresses obtained with the reverse geocoding of both services in Table 1 and 2 have significant differences of approximately 25% for Fatih and Miami Beach.

Any point within the boundary of a building polygon may be selected for reverse geocoding as the main input data. If the centroid of the building polygon is closer to the other road instead of the one used in the address information, reverse geocoding may be worked incorrectly. Therefore services should, generally, place the address point as to the front entrance of a building in accordance with the actual status in spite of that they have not done yet in especially navigation maps. This will in particular improve the quality of route finding, transportation and, last but not least, reverse geocoding.

REFERENCES

- Kounadi, O., Lampoltshammer, T.J., Leitner, M. and Heistracher, T., (2013). "Accuracy and privacy aspects in free online reverse geocoding services", *Cartography and Geographic Information Science*, 40: 140-153.

- Mitchell, R., (2015). *Web Scraping with Python: Collecting Data from the Modern Web*, "O'Reilly Media, Inc.", United States of America.
- Ratcliffe, J.H., (2004). "Geocoding crime and a first estimate of a minimum acceptable hit rate", *International Journal of Geographical Information Science*, 18: 61-72.
- Rodrigues, F., (2010). *POI Mining and Generation*, PhD Thesis, Faculty of Sciences and Technology (FCTUC) Department of Informatics Engineering - University of Coimbra, Portugal.
- URL-1, Levenshtein distance, Wikipedia – The Free Encyclopedia, https://en.wikipedia.org/wiki/Levenshtein_distance, [Accessed 09 March 2017].



An Application Development for Use of Borehole Data on iOS Based Mobile Devices

Furkan Özoğlu^{*1}, Türkay Gökgöz²

¹ Directorate of Geographic Information Systems, Istanbul Metropolitan Municipality, Kasımpaşa, 34440, Istanbul, Turkey. e-mail: furkan.ozoglu@ibb.gov.tr

² Department of Geomatics Engineering, Yıldız Technical University, Davutpaşa Campus, 34220, Istanbul, Turkey. e-mail: gokgoz@yildiz.edu.tr

ABSTRACT

Borehole data is widely used in underground and aboveground field works. However, attributes of borehole data kept in created borehole databases, access methods to such data and ability to use these map-based data are of great importance. In some studies; in addition to desktop and web-based applications working on computers, especially together with the spread of mobile devices in recent years, borehole data can also be viewed on map-based mobile applications in mobile devices such as telephone and tablets. In this study, the aim is to store, manage and maintain data centrally outside mobile device through the use of cloud-based database management system rather than a local database management system. An application has been developed in Swift programming language that can show both semantic and geographical borehole data on map in compliance with several iOS-based mobile devices. When developing the application, built-in Global Navigation Satellite System (GNSS) receivers and Model View Controller (MVC) software architecture of devices were used. Consequently, it was shown that both geometric and semantic data of boreholes stored in a cloud database can be effectively used even in smart mobile devices with small screen.

INTRODUCTION

Together with the development of mobile devices, mobile-based applications are also developed. Mobile application development has been spread to many fields, especially in the field of cartography. Since mobile devices include GNSS receiver, especially map-based mobile applications provide great advantages to users. In addition, web-based map applications are gradually designed and developed as mobile applications that can run on mobile devices.

In this study, the aim is to manage geological data (i.e.borehole data) as a cartography practice. In the literature, there are several studies and developed applications that have been realized for various platforms in which management of borehole data is carried out.

^{*} Corresponding Author

SedLog is a desktop software that can show underground graphically, in which data can be added in Comma Separated Values (CSV) format and in which printouts can be taken in PDF, Scalable Vector Graphics (SVG) and JPEG formats (Zervas *et al.*, 2009). SedMob is the mobile application of SedLog software. In this application, data is received in CSV format from a server. Since it is hybrid, it can run in mobile platforms such as iOS and Android (Wolniewicz, 2014).

A web-based geographical information systems (GIS) application has been developed to show ten thousand borehole points and other geological data in Seoul, South Korea, an application that includes functions such as statistical analysis (Chang, Park, 2004). Using augmented reality technology and map library, a mobile application (BoreholeAR) has been developed suitable to borehole data structure of local institutions in Seoul, South Korea and that runs on iPad devices (Lee, Suh, Park, 2014).

Istanbul Geological and Geotechnical Information System (ZeBiS) has been developed by Selçuk and Gökğöz (2001). In this desktop GIS application, data sets consist of borehole data, and base maps are three-dimensional topographical maps. Software components of the system are AutoCAD Map, Access, RockWorks and an interface program written with AutoLISP and running under AutoCAD Map. Functions performed by the application are finding a destination (for example a building land) on a map via site and street name queries, displaying borehole(s) the nearest to or in a certain distance from destination, displaying data of a selected borehole and preparing an ASCII file in the file format of RockWorks99 by the data of selected boreholes.

Borehole data consists of data about underground and aboveground and these are usually shown in tabular form. Besides, to interpret borehole data geologically, they should be considered in conjunction with spatial data.

In this study, a mobile application was developed that runs in iPhone devices in iOS platform. It is named 'iZemin'. It will be referred with this name in the study. Besides, unlike other studies, a cloud-based database management system was used rather than device-based database management system. Thus, central management of borehole data was ensured. Moreover, it was compatible with operations of local institutions in Istanbul.

DESIGN OF APPLICATION

A fast and stable database is required for visualizing and managing borehole data. Details of development environment of the system and libraries used in this study are explained in detail below.

Application Development Platform

Development on Apple iOS system is possible with xCode (8.3.3) software. iZemin mobile application was developed with the swift programming language. Besides, together with testing on iPhone 7, designs were optimized in a way to run on all iPhone models. These devices have a Global Navigation Satellite System (GNSS) receiver. Other hardware specifications of the device are given in Table 1.

Table 1. iPhone 7 Hardware specifications

System-on-chip	Apple A7
Memory	2048 MB LPDDR3 RAM
Screen resolution	750x 1334 pixels (326 ppi)
GNSSa	A-GPS, GLONASS
Accelerometer	3-Axis accelerometer
Gyroscope	3-Axis Gyroscope

Mobile Libraries

During the process of developing mobile application, it is necessary to add required libraries to the project to use sensors and GNSS receivers on mobile device. There are a large number of libraries, but to keep application size small, only libraries to be used in developed application are added to the project.

In iZemin application, a total of five libraries was used. Four of these libraries are built-in and one of them is external. In Table 2, libraries used in iZemin application and their specifications are given.

Positional data in GNSS are processed and provided the user through Corelocation library. With Mapkit library, 2D map is shown, and a support for layers to be opened on this map is established. Besides, satellite image is provided to user with this library. Since Foundation and Ulkit libraries contain basic functions, they come as attached to the project. With these two libraries, basic functions found in iOS platform can be used and design processes can be carried out. Firebase library was used as external library in the application, and thus communication of the application with cloud database was ensured. Detailed explanations related to this library are given below.

Table 2. Libraries used in development of iZemin application.

Library	Classification	Usage	Detail
Corelocation	On-Board	Map	GPS sensor
Mapkit	On-Board	Map	2D maps and satellites
Firebase	External	Database	Cloud based database
Foundation	On-Board	iOS application basics	iOS basic functions and design
Ulkit	On-Board	iOS application basics	iOS basic functions and design

DEVELOPMENT OF APPLICATION

Database Module

Together with the development of cloud database technology, data storage opportunity is offered to web or mobile-based application developers either free or paid. In particular, there are many databases established especially with the support of technology companies such as Google and Amazon. Firebase used in this study is a service powered by Google.

Since borehole data is not user-specific data, and real-time view in all devices is one of the aims of this study, rather than a local database such as SQLite, a cloud-based database management system was preferred in iZemin application. Firebase iOS library, a widely used database platform spread in mobile and web environment, were used. Thus, desired edits can be made on data through the web interface shown in Figure 1.

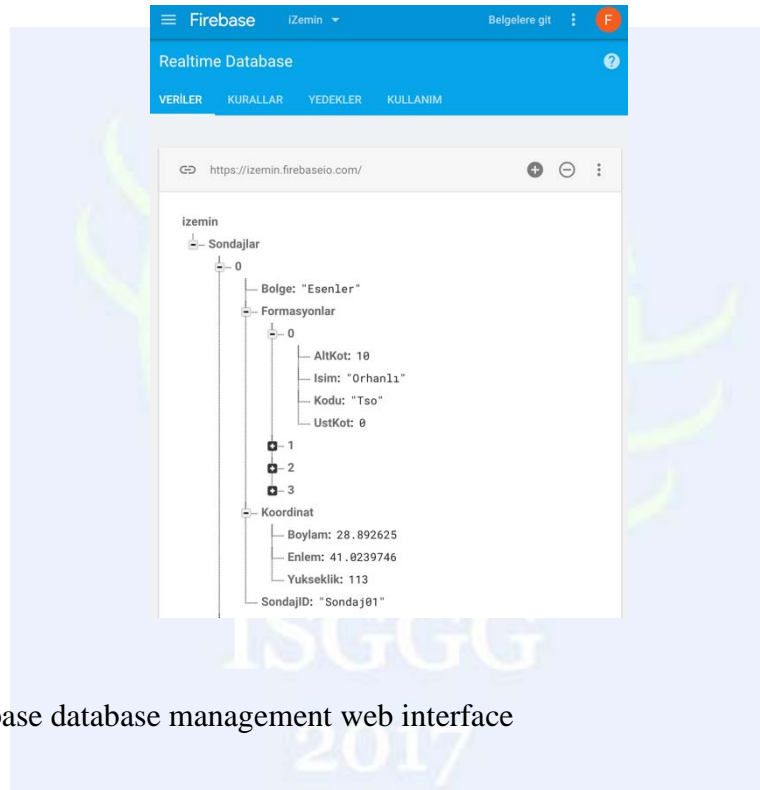


Figure 1. Firebase database management web interface

NoSQL has been developed as an alternative solution to relational database systems. Together with the increase in Internet speed, increasing number of users taking active role in systems is an important reason. In a database kept as relational tables, it is necessary to update current structure (table and relationships) that is not defined in tables. Therefore, an additional cost emerges. However, since there are no tables and columns in a NoSQL database system, an additional cost is not required to establish structure later or only a very little cost is necessary. However, it has some disadvantages especially in sectors such as banking, the concept of transactions applied in database is not found in NoSQL database system, data loss may occur.

An original database structure was designed for iZemin in this study considering the database structure of template data used by Istanbul Metropolitan Municipality. It is kept on Firebase database management system in JavaScript Object Notation (JSON) format

(Figure 2). Variable types of borehole data in the database are automatically created by the database management system of Firebase. Borehole data and corresponding data types are given in Table 3.

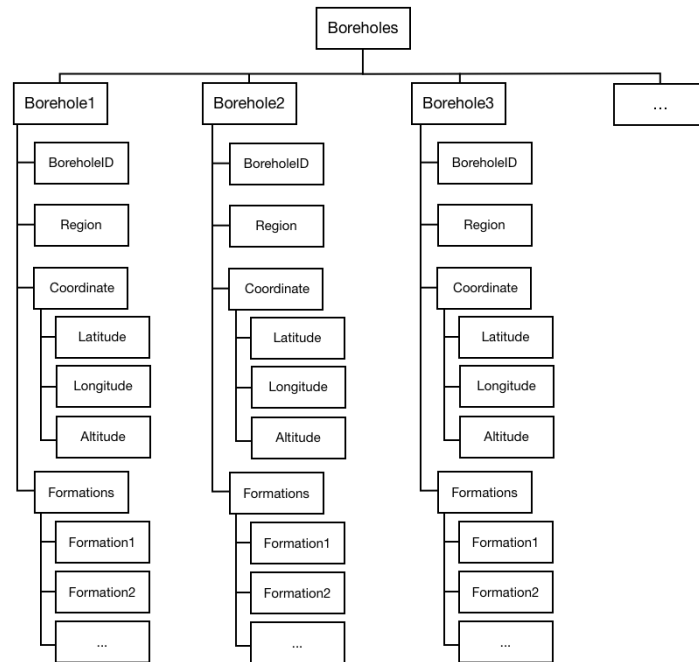


Figure 2. Borehole data structure in web interface database management system of Firebase

Table 3. Borehole data types in database

Items	Data Type
Boreholes	Array
Borehole	Dictionary
BoreholeID	String
Region	String
Formations	Dictionary
Lower Elevation	Double
Upper Elevation	Double
Name	String
Short Code	String
Coordinate	Dictionary
Latitude	Double
Longitude	Double
Altitude	Double

Map Module

In iZemin mobile application, 2D map library (Mapkit) offered to developers free of charge by Apple company was used. Satellite image found in this library is offered to users as an option in the application. This library was chosen since it is the most stable library running in iOS platform. There are no limitations related to usage of Mapkit library. Map data is located with geographic coordinates in Web Mercator projected coordinate system. Therefore, data to be used in the application was prepared in accordance with this system. In the case of use of data in different systems, data conversion would be required.

Location information for moving mobile device is shown with a blue icon on the base map (Figure 3a). This presentation is possible with co-operation of GPS receiver of mobile device and Corelocation library used in development platform. Thus, real-time position of mobile device is reflected on map dynamically. In the event that location of mobile device is outside borders of screen, the map is relocated to ensure that device location is again in the center of screen. Borehole List and Search Screen is shown in Figure 3b. Locations of borehole points queried are shown with a green pin in relevant screen of iZemin (Figure 3c). With date box placed on pin, it is possible to pass to the screen where borehole data is provided (Figure 3d).

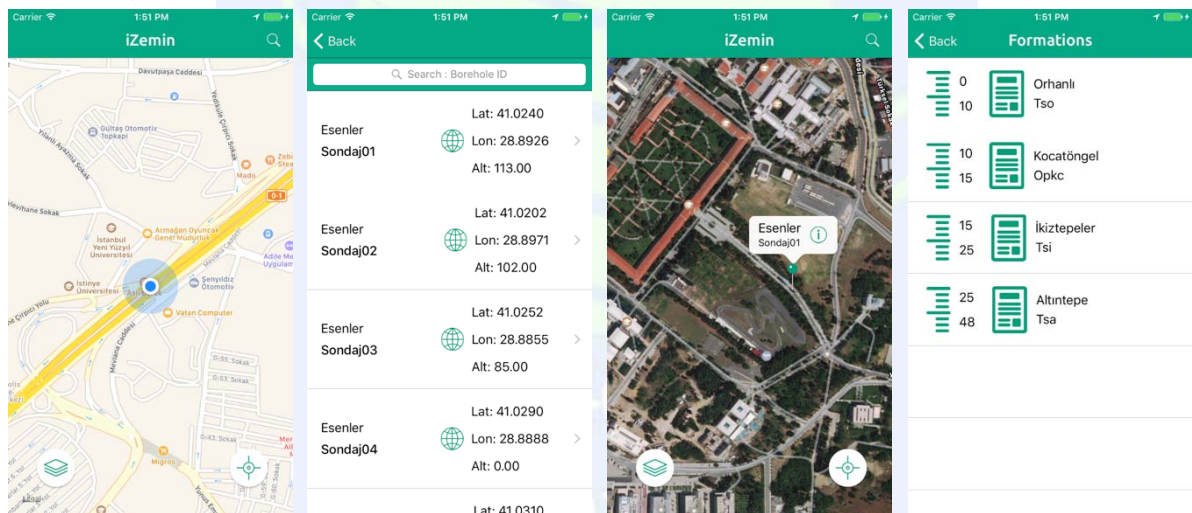


Figure 3. Screens of iZemin: a) Base map, b) Borehole list and search, c) Borehole location and data display, and d) Formation

Model View Controller Architecture

Model View Controller (MVC) is a software architecture that prevents mixing of modules with different roles in the application and that separates user interface from each other in a business logic. With this architecture, it is possible to separate structures of the code serving for different purposes from each other, and the software code can be easily developed and tested. In Figure 4, data interface controlling architecture is shown.

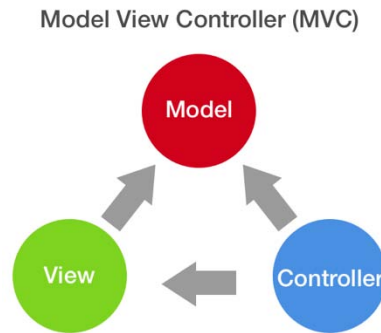


Figure 4. Model view controller (MVC)

Model section is used to determine how data is processed. View section refers to visual interface where user is in interaction. MVC architecture is applied in different programming platforms. Within iOS application development platform in which iZemin application is developed, UIView objects correspond to interface and UIViewController objects correspond to controllers. Controllers manage attached interface objects depending on their behaviors.

There are four controllers in iZemin application. While three of them represent the base of application, one of them controls switching between screens. In Figure 5, relationships of used libraries with controller classes are shown.

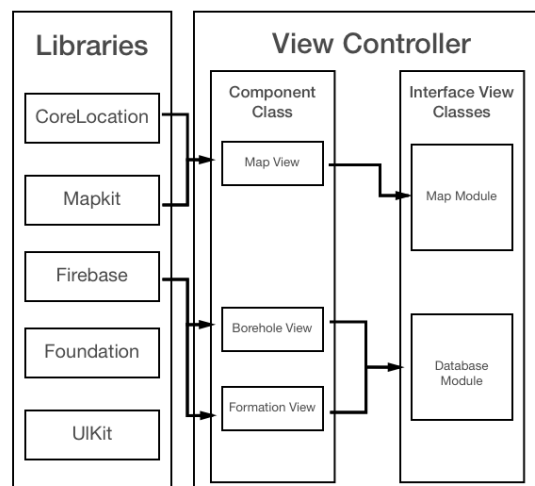


Figure 5. Relationship diagram of libraries used in iZemin application with interface classes

In Figure 6, interfaces and controllers in XCode development environment developed for iZemin application are shown. Among these controllers, there is a main interface object and in this interface object; there are button, list, figure and map objects. IBAction and IBOutlet link classes establish a bridge between interface and controller.

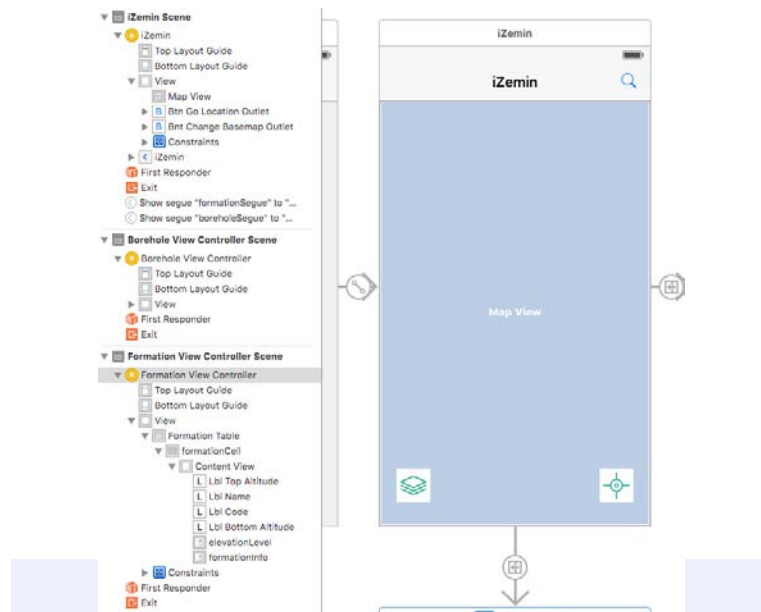


Figure 6. Data interface controller architecture (MVC)

CONCLUSIONS

Together with improving smart mobile devices, number of mobile applications also increases. Today, there are applications available that use all specifications of smart mobile devices. Some of these applications are related to cartography. However, cartography-related applications are generally applications that are of interest to general users. Applications specific to public institutions and organizations are very few. With iZemin mobile application developed in iOS platform in this study, it is possible to show borehole locations and data stored in a cloud database. Consequently, it was shown that both geometric and semantic data stored in a cloud database can be effectively used even in smart mobile devices with small screen.

iZemin application can be also adapted to tablet devices, specifications of which are close to mobile phones. In addition, spatial queries such as “search for near boreholes” and “search for borehole based on certain criteria” can be added to this application. Thanks to internal GNSS receiver found on device, a route can be drawn to desired borehole point. An easy use can be provided in vehicle with navigation applications.

REFERENCES

- Lee, S., Suh, J., & Park, H. D., 2015. BoreholeAR: A mobile tablet application for effective borehole database visualization using an augmented reality technology. *Computers & Geosciences*, 76, 41-49.
- Wolniewicz, P., 2014. SedMob: a mobile application for creating sedimentary logs in the field. *Computers & Geosciences*, 66, 211-218.

- Zervas, D., Nichols, G. J., Hall, R., Smyth, H. R., Lüthje, C., & Murtagh, F., 2009. SedLog: A shareware program for drawing graphic logs and log data manipulation. *Computers & Geosciences*, 35(10), 2151-2159.
- Chang, Y. S., & Park, H. D., 2004. Development of a web-based geographic information system for the management of borehole and geological data. *Computers & Geosciences*, 30(8), 887-897.
- Selçuk, M., & Gökgöz, T., 2001, April. Geological and Geotechnical Information System for Istanbul. Fourth Turkish-German Joint Geodetic Days. Berlin, Germany.
- Apple, iOS Developer Library Documentation MVC,
<https://developer.apple.com/library/ios/documentation/General/Conceptual/CocoaEncyclopedia/Model-View-Controller/Model-View-Controller.html>, online, accessed 20-Aug-2017.
- Apple, iOS Developer Library Documentation,
<https://developer.apple.com/library/ios/navigation/>, online, accessed 20-Aug-2017.
- Firebase, Firebase Developer Library Documentation,
<https://firebase.google.com/docs/libraries/>, online, accessed 20-Aug-2017.



Investigating The Accuracy Analysis Of Single Baseline RTK

Ercenk Ata^{*1}, Atınc Pırtı²

¹Department of Geomatic Engineering, Yıldız Technical University, Davutpasa Campus, 34220, Turkey. e-mail: ata@yildiz.edu.tr

²Department of Geomatic Engineering, Yıldız Technical University, Davutpasa Campus, 34220, Turkey. e-mail: atinc@yildiz.edu.tr

ABSTRACT

This paper presents the initial results of RTK/OTF satellite measurements made using TCP/IP internet data transmission. One permanent reference station (TVSN) belonging to Tavsanlı Municipality, Kütahya Turkey was used for test measurements. As a result of measurements taken at eight measurement points situated about 1 kilometre to 35 kilometres from the reference station (TVSN) the accuracies of up to a few centimetres were obtained for points situated in the open terrain. The accuracies obtained at the point with numerous covers in the form of tree branches and leaves ranged from several centimetres to almost 10 centimetres, which is characteristic for GPS measurements taken under conditions of limited availability of satellites.

INTRODUCTION

The RTK concept is based upon the principle that the errors that affect the calculation of the absolute position in GPS can be considered the same in a certain geographical area in which one is working. Those mistakes are caused by the effects of the ionosphere, troposphere, and orbits of the GPS satellites, oscillators of the satellites and of the receivers, multipath, among others. With these working conditions, the coordinates obtained by the GPS receivers in absolute positioning method, range from 1 to 10 metres, according to the geometry of the visible satellites at the precise moment of the acquisition of the GPS data. For us to work with centimetre accuracy or better two hypotheses exist; one of them is the execution of the post-processing of the GPS data using specific software with precise orbits of satellites (available sensibly after 15 days of the observation of the data), which is a long time for the great majority of the GPS users and it needs added knowledge, and the other is the positioning technique RTK. Currently the satellite positioning method RTK is the technologically most advanced kinematic method for determining coordinates of points in real time. That method allows obtaining precise coordinates in real-time thanks to which it finds wide application in numerous areas,

^{*} Corresponding Author

including: land, water and air navigation, hydrography, road safety and first of all land survey measurements (Pirti et al., 2009; Vollath et al., 2002; Wolf and Ghilani, 2002).

RTK rovers traditionally receive RTK data from a single RTK reference station. The reference station may be permanently setup (e.g. on the roof of the office) or it might be temporarily set up in the field. In both cases the principle is the same. Recent advances in RTK algorithms allows the rover to successfully and repeatedly work at distances of up to 50 km from the RTK reference station. As the distance increases between the reference and the rover the accuracy of the rovers computed position decreases. This decrease in accuracy is due to distance dependent errors-mainly atmospheric errors. Essentially, as the distance between the rover and the reference station increases; the atmospheric conditions at the rover and reference station will become increasingly different. This decreases the accuracy and makes it more difficult for the rover to fix the ambiguities (Lachapelle et al., 2001; Landau et al., 2002; Snay, 2008; Vollath, 2000).

DATA AND METHOD

The work was performed in Tavşanlı, Kutahya, Turkey, and see Figure 1. In order to test the performance of single baseline RTK, two different test configurations are considered, both within the borders of city of Kütahya, which is situated 300 km south of İstanbul. Eight arbitrary points were selected in the Tavşanlı district in the city of Kutahya to test the positions obtained from single baseline RTK, whether or not they are internally and externally precise. Figure 5 illustrates the distribution of points used in these two cases. Two surveys (RTK and static) were performed, one using a Topcon GR3 RTK field unit and single baseline reference station (TVSN) with a TCI/IP link and the other using a Topcon GR3 static unit. The point TVSN on the roof of the Tavşanlı Municipality building, which is depicted in Figure 3, is taken as reference station for these tests. The distances between the test points in the outside of Tavşanlı and the reference point (TVSN) vary approximately from 1 km to 35 km. The TVSN unit provides up to 35 kilometres of coverage with the TCI/IP link. In test 1, the internal accuracy of RTK results is tested, while in test 2 the external accuracy is investigated. Two different cases are investigated in test 1, namely different satellite configuration and same reference station, and in test 2 namely static surveys versus single baseline RTK survey, so as to observe internal and external accuracies of the RTK method. Since the test field is densely populated with urban structures and densely covered with trees, as can easily be seen from the Figures 1 and 3, the tests carried out make it possible to observe how precise results the method of the single baseline RTK will produce, especially in the unobstructed and obstructed (urban and forest) environments (Gürel and Erkaya, 2010; Bahşi and Hoşbaş, 2010).

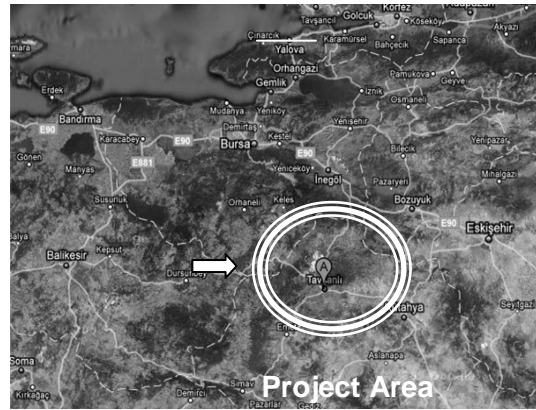


Figure 1. Project area

As explained above, two tests were carried out in order to evaluate the performance of the single baseline RTK method for the project area. For RTK and static surveys, the single reference point (TVSN) was used as reference station in the project area (TVSN, see Figure 3). For this purpose, the static survey was conducted in order to determine the coordinates of these eight points in the project area. The measurements in these test points were performed with at least 3 hours of observation times on 18 November 2008. The minimum elevation cut-off angle and the sample rate were 10 degrees and 10 seconds, respectively.

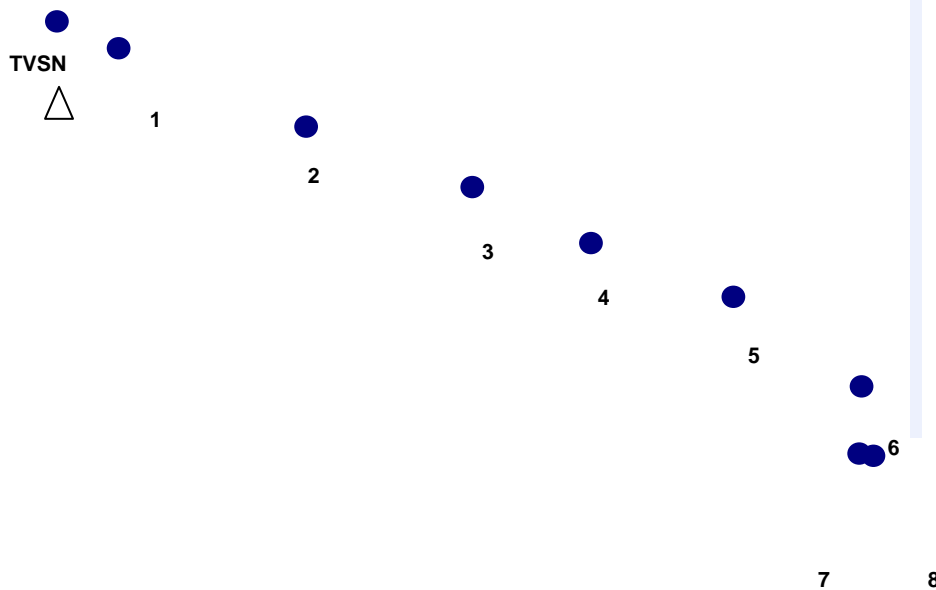


Figure 2. The distribution of the test points in the project area

The data processing and network adjustments were conducted using the Topcon Pinnacle Software. In the adjustment procedure, the ITRF 2000 coordinates of TVSN were held fixed (Table 1). In all static measurements are conducted using two Topcon GR3 dual frequency receiver with standard hardware and software and observing visible 6-9 satellites throughout the whole sessions and PDOP values 1.3-3.2 (Gürel and Erkaya,

2010; Bahşı and Hoşbaş, 2010). The objective of the tests was to assess the single baseline RTK achievable accuracy and to check the repeatability of the results under different satellite configurations by using the same reference point (TVSN). The accuracy and repeatability assessment of the single baseline RTK survey was carried out by comparing the coordinates of a group of points (8 points), marked on the ground. The specifications of the eight test points in the project area are explained in Table 2 (Gürel and Erkaya, 2010; Bahşı and Hoşbaş, 2010).



Figure 3. TVSN reference point and eight test points (Gürel and Erkaya, 2010; Bahşı and Hoşbaş, 2010).

Table 1. Coordinates and their standard deviations of the eight points in static mode

Point	X_{ITRF}	Std.(mm)	$Y_{ITRF}(m)$	Std (mm)
TVSN	4379000.189		456279.660	
1	4380120.024	1	454506.420	1
2	4383555.266	6	449434.017	6
3	4386587.094	5	445324.140	5
4	4388737.431	7	441701.182	7
5	4393683.987	10	432218.997	10
6	4391353.218	7	438213.159	7
7	4393927.422	11	427685.152	11
8	4393665.228	8	427799.640	8
	$h_{ITRF}(m)$	Std (mm)		
TVSN	894.057			
1	863.989	2		
2	901.019	11		
3	1023.072	8		
4	1022.255	10		
5	840.421	16		
6	891.265	13		
7	710.399	19		
8	693.319	20		

Table 2. The specifications of the eight test points in the project area

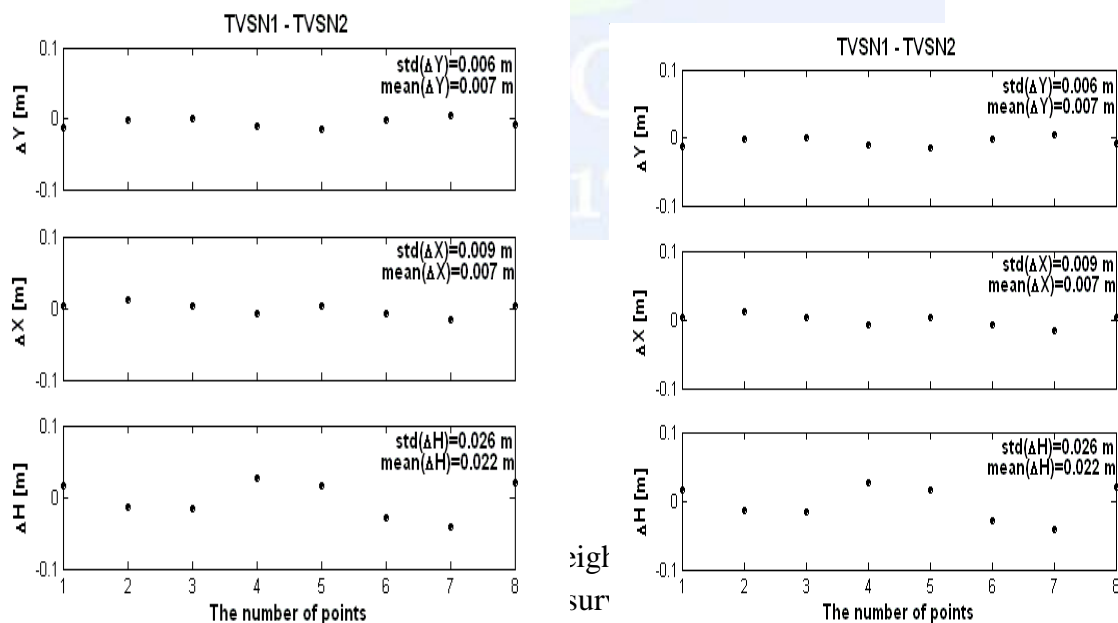
Point	Specifications
1	<i>the clear line of sight</i>
2	<i>under tree</i>
3	<i>the clear line of sight</i>
4	<i>under the forest</i>
5	<i>the clear line of sight</i>
6	<i>under tree</i>
7	<i>close to the urban environment</i>
8	<i>the clear line of sight</i>

RESULTS

This test was aimed at observing whether the single baseline RTK method produces precise results at different times with different satellite configuration. Two sets of observations were carried out using the same test points and the same reference station (TVSN), but at different observation times with different satellite configurations, which was accomplished by choosing the second period of observation two days later than the first one at an arbitrary observation time. The intent with this was to study the effect of satellite configuration on the single baseline RTK results (Gürel and Erkaya, 2010; Bahşi and Hoşbaş, 2010).

To evaluate the single baseline RTK repeatability, two independent RTK surveys using a reference point (TVSN) was carried out, each time occupying all of the test points. The surveys were conducted on two days and at different times of the day from TVSN (15 November 2008, 9:00 – 12:30 h local time (LT)), TVSN (17 November 2008, 12:40 – 16:30 h) with changed satellite configurations to ensure the independence of the results. The reference station TVSN was about maximum 35 km away from the project site, about minimum 1 km, see Figure 5. The satellite visibility was 6-9 GPS satellites in the project areas and the recorded PDOP average values were between 1.5 and 3.8 on both days. A total of 16 point observations for the 8 test points were obtained over the two days. In the analysis step, the differences of the coordinates of the eight test points obtained from TVSN1, TVSN2 were calculated, such as TVSN1 - TVSN2. Table 1 shows the differences and their means and standard deviations for the eight points. The analysis of the two tests for the single baseline RTK results shows that the discrepancies of the horizontal coordinates are a few mm to 2 cm. The discrepancies of the height coordinates were a few centimetres to about 4 cm (Table 1) (Gürel and Erkaya, 2010; Bahşi and Hoşbaş, 2010).

As explained above, four points (Points 2, 4, 5, and 7, see Table 2) were marked very close to the obstructed areas (tree, forest and buildings environments). The ambiguity resolution time was approximately 210 minutes for these four points on both days. The differences for the horizontal coordinates of these four points were greater than 1 cm for the RTK measurements of the first, second day, see Figure 3. The second day's measurements yielded the greatest coordinate differences of the two days. This may be partially due to the fact that the measurements were taken in the afternoon of 17 November 2008, when the satellite configuration was not favourable, resulting in a poor accuracy of these four points in the obstructed areas (Gürel and Erkaya, 2010; Bahşi and Hoşbaş, 2010).



All 8 points are also used for technical tasks, which often require a high accuracy of the H coordinate. An analysis of the first, second day measurements at the project area clearly demonstrates that the differences are ~ 3-4 cm for the vertical coordinates for the four

points, see Figure 7. For the other points, the height differences were at the level of a few centimetres, see Figure 7 (Gürel and Erkaya, 2010; Bahşi and Hoşbaş, 2010).

With this we can conclude that the test for different time with the different satellite configuration shows that RTK produces internally precise positions. In studying the differences in Figure 4, it can be seen that 1 cm mean difference is obtained for the X and Y coordinate components while there is about 3 cm of the mean difference in the vertical direction (Gürel and Erkaya, 2010; Bahşi and Hoşbaş, 2010).

For static measurements, a receiver is set up at a specific point. Points are determined over a relatively long period of time, and the mean average is derived from the sum of these measurements, possibly after extreme values have been filtered out. Such static measurements have the advantage that the variations in the positions determined, can be levelled out because the probability is high that a sufficient number of satellites can be tracked for determining the position (Vollath, 2000). In this step of the test, the RTK derived coordinates of the test points were compared to their coordinates as precisely determined using static method is chosen since in literature it is proven to produce the most accurate positions which can be obtained from GPS measurements. The static survey was carried out to check the performance of the single baseline RTK. A study of how much these differences vary is illustrated in terms of minimum and maximum differences, mean values of these differences and standard deviation values in Figure 5. As can be seen from Figure 5, the standard deviation values computed from the positioning differences obtained from the test tend to be below 7 cm (Gürel and Erkaya, 2010; Bahşi and Hoşbaş, 2010).

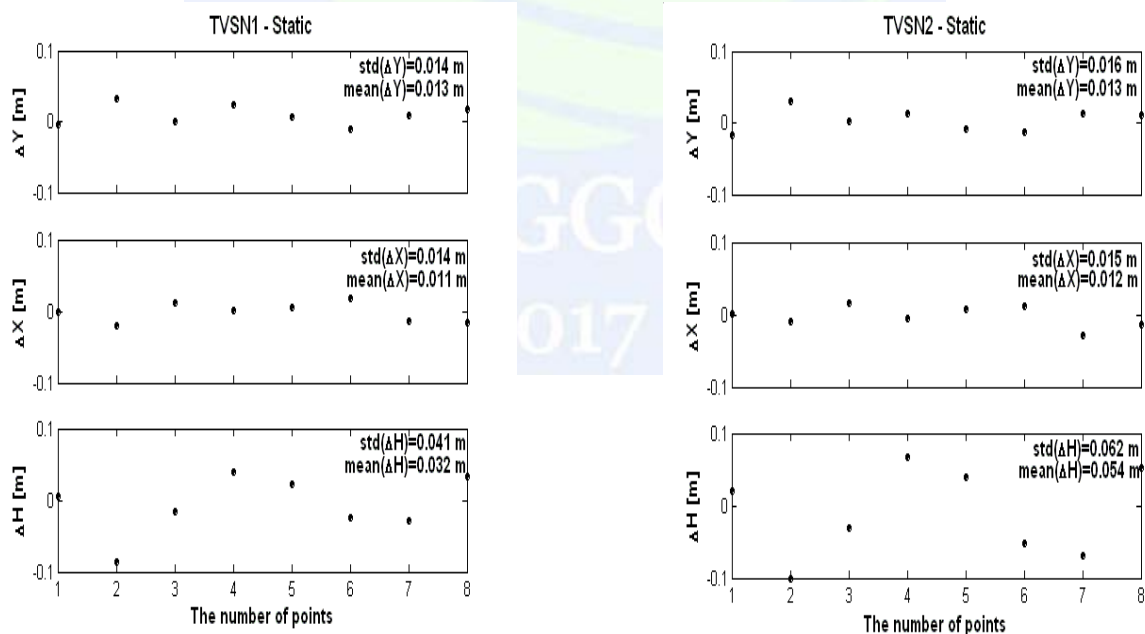


Fig. 5. Comparison of the coordinates of the eight points in the project area between static GPS and two days of RTK (TVSN (15.11.2008), TVSN (17.11.2008)) surveys

In this test, the accuracy and repeatability assessment of the single baseline RTK survey was carried out by comparing the coordinates of a group of points (8 points) obtained from TVSN with the coordinates determined by the static survey from TVSN. The comparison

of the results of the RTK and static surveys shows that the variations were greater in height and smaller in horizontal coordinates, see Figure 5. The standard deviation of the horizontal coordinate differences was about 1-2 cm on the first day and 1-2 cm on the second day. The standard deviation of the height differences was 3-4 cm on the first day, 6-7 cm on the second day. As shown in Figure 5, the two-day differences between the RTK survey and the static survey were less than 2 cm for the horizontal coordinates and less than 7 cm for the vertical coordinates. The maximum variations were about 4 cm in the X-Y coordinates and about 10 cm in the H coordinates, see Figure 5. From these results it is clear that RTK method can produce positions almost as accurate as the static approach, except for the densely built-up and forest areas.

GPS job specifications often require that baseline measurements be taken between fixed control stations. The benefit of making these measurements is to verify the accuracy of both the GPS measurement system, and the control being held fixed. Obviously the smaller the discrepancies between measured and known baseline lengths, the better. If the discrepancies are too large to be tolerated, the conditions causing them must be investigated before proceeding further. Table 3 shows the computed baseline vector data from a GPS survey of the network of Figure 5. Note that eight fixed baseline (between TVSN and Points 1, 2, 3, 4, 5, 6, 7, and 8) was measured by static surveys on 18 November 2008. The analysis of fixed baselines is as follows (Gürel and Erkaya, 2010; Bahşi and Hoşbaş, 2010; Wolf and Ghilani, 2002).

- 1) Compute the coordinate differences between stations TVSN and 1 as

$$\Delta X_{TVSN1} = -1119.835 \quad \Delta Y_{TVSN1} = 1773.240 \quad \Delta H_{TVSN1} = 30.068$$

- 2) Compute the absolute values of differences between the measured and fixed baselines as

$$dX = |1119.835 - 1119.837| = 0.002, \quad dY = |1773.240 - 1773.236| = 0.004, \quad dH = |30.068 - 30.074| = 0.006$$

- 3) Compute the length of baseline as

$$TVSN1 = \sqrt{(1119.835)^2 + (1773.240)^2 + (30.068)^2} = 2097.454 \text{ m}$$

- 4) Express the differences, as computed in Step 2, in parts per million (ppm) by dividing the difference by the length of the baseline computed in Step 3 as

$$\Delta X\text{-ppm} = 0.002 / 2097.454 \times 1000000 = 0.95$$

$$\Delta Y\text{-ppm} = 0.004 / 2097.454 \times 1000000 = 1.91$$

$$\Delta H\text{-ppm} = 0.006 / 2097.454 \times 1000000 = 2.86$$

- 5) Check the computed values for the ppm against a known standard. Typically, the FGCS standard given in the following section is used.

The Federal Geodetic Control Subcommittee (FGCS) has published the document entitled “Geometric Geodetic Accuracy Standards and Specifications for Using GPS Relative Positioning Techniques”. The document specifies seven different orders of accuracy for GPS relative positioning and provides guidelines on instruments and field and office procedures to follow active them. Table 4 lists these orders of accuracy (Wolf and Ghilani, 2002).

The FGCS document also make recommendations concerning categories of surveys for which the different orders of accuracy are appropriate. Some of these recommendations include: order AA for global and regional dynamics and deformation measurements; order A for “primary” networks of the National Spatial reference System (NSRS), and regional and local geodynamics; order B for “secondary” NSRS networks and high-precision engineering surveys; and the various classes of order C for mapping control surveys, property surveys, and engineering surveys. The allowable error ratios given in these standards imply the extremely high accuracies that are now possible with GPS (Gürel and Erkaya, 2010; Bahşı and Hoşbaş, 2010; Wolf and Ghilani, 2002).

Table 3. Observed baseline vectors and ppm values

Observed Baselines	dX ₁ dY ₁ dH ₁ [m]	dX ₂ dY ₂ dH ₂ [m]	Baseline [m]	(ppm) ₁	(ppm) ₂	Observed Baselines	dX ₁ dY ₁ dH ₁ [m]	dX ₂ dY ₂ dH ₂ [m]	Baseline [m]	(ppm) ₁	(ppm) ₂
TVSN-1	0.002	0.001	2097.454	0.95	0.48	TVSN-5	0.005	0.008	21885.97	0.23	0.37
	0.004	0.017		1.91	8.11		0.006	0.008		0.27	0.37
	0.006	0.021		2.86	10.01		0.023	0.039		1.05	1.78
TVSN-2	0.021	0.009	8222.628	2.55	1.10	TVSN-6	0.018	0.011	28187.45	0.64	0.39
	0.033	0.030		4.01	3.65		0.010	0.013		0.35	0.46
	0.086	0.100		10.46	12.16		0.024	0.053		0.85	1.88
TVSN-3	0.012	0.016	13326.71	0.90	1.20	TVSN-7	0.013	0.028	32034.59	0.41	0.87
	0.001	0.002		0.08	0.15		0.008	0.012		0.25	0.37
	0.015	0.031		1.13	2.33		0.028	0.069		0.87	2.15
TVSN-4	0.002	0.006	17531.75	0.11	0.34	TVSN-8	0.016	0.013	32256.81	0.50	0.40
	0.023	0.013		1.31	0.74		0.018	0.010		0.56	0.31
	0.040	0.067		2.28	3.82		0.032	0.052		0.99	1.61

As seen Table 3, real-time solution via internet is suitable for environments with reasonably good satellites tracking conditions (limited obstructions, multipath, and radio frequency noise) and with reliable communication from the GPS base to the rover. The results in the obstructed environment obtained directly from real-time solution via the

internet measurements show a slightly lower precision than the results from post-processing. Modern GPS systems have improved satellite tracking technology such that weaker signals can be observed under trees with moderate foliage (Note that dense foliage will still cause cycle slips, foliage and tree density increases, artillery survey with GPS under foliage will become increasingly difficult. Satellites will be lost, resulting in poorer DoPs). Despite this advanced tracking capability, the signals are noisier, weaker and therefore more likely to be subject to multipath and diffraction. The surveyor should be aware that positions may not be accurate despite quality indicators showing good solutions.

Table 4. GPS Relative Positioning Orders of Accuracy

Order	Allowable Error Ratio	Parts-Per-Million (ppm)
AA	1:100 000 000	0.01
A	1:10 000 000	0.1
B	1:1 000 000	1.0
C-1	1:100 000	10
C-2-I	1:50 000	20
C-2-II	1:20 000	50
C-3	1:10 000	100

CONCLUSIONS

Data transmission from the single baseline RTK reference stations using the internet provides significant benefits in RTK solutions, like much less cost, better secure transmission and extension of the RTK range, reduced initial costs for RTK surveying since only a single rover receiver is necessary, increased productivity since no temporary RTK base station is needed. The NTRIP protocol is an efficient tool in comparison with the usual radio-based RTK systems. The positioning accuracy in the unobstructed environment found was very impressive and competitive against post-processing methods even for baselines up to some tens of kilometres. Real-time solution via the internet can be very accurate and productive in many geodetic surveying and GIS applications. Real-time solution via the internet is very efficient in difficult situations we are going to encounter certain accuracy problems. Buildings and forest environments should also be classified under difficult situations. To raise measurement reliability there, results from different resolutions of ambiguities should be used on each point. This would enhance measurement reliability and accuracy. Nevertheless, it appears that forest and urban measurements with 1 cm accuracy cannot be guaranteed on all occasions, since difficult situations may lead to greater errors.

ACKNOWLEDGMENT

I would like to thank the staff of Topcon Company and Tavsanlı Municipality in Kütahya, Turkey for their helps.

REFERENCE

- Bahşi, N Hoşbaş R.G., 2010. *Evaluating the singla bseline RTK GPS in the clear environment, March*, Msc. Thesis, Nisan, Yıldız Technical University, İstanbul, Türkiye.
- Gürel, N Erkaya, H (2010). *Evaluating the single baseline RTK system in the urban and trees environment*), Msc. Thesis, Nisan, Yıldız Technical University, İstanbul.
- Lachapelle, G. Fortes L.P. Cannon, M.E. Alves, P. Townsend, B. (2001). RTK Accuracy Enhancements with a Reference Network-Based Approach, *The Third International Symposium on Mobile Mapping Technology*, January 3-5, Cairo, Egypt
- Landau H., Vollath, U. and Chen, X (2003). Virtual Reference Stations versus Broadcast Solutions in Network RTK – Advantages and Limitations, *Proceedings of GNSS 2003–The European Navigation Conference*, April 22-25, Graz, Austria.
- Landau, H. Vollath, U. and Chen, X (2002). Virtual Reference Station Systems, *Journal of Global Positioning System*, Vol. 1, and No. 2.137–143.
- Pirti, A (2008). Accuracy Analysis of GPS Positioning near the Forest Environment, *Croatian Journal of Forest Engineering*, Volume 29, Issue 2, pp.189-201, Zagreb.
- Rizos, C. (2007). Alternative to current GPS-RTK services and some implications for CORS infrastructure and operations, *GPS Solution*, 11(3): pp. 151-158.
- Snay, Richard A. (2008). Continuously Operating Reference Station (CORS): History, Applications, and Future Enhancements. *Journal of Surveying Engineering* 134(4)
- Vollath U., Deking, A. Landau, H., Pagels, C.,Wagner, B. (2000). Multi-Base RTK Positioning using Virtual Reference Stations, *Proceedings of the 13th International Technical Meeting of the Satellite Division of the Institute of Navigation*, Utah, USA, September.
- Vollath U., Landau, H., and Chen, X., (2002). Network RTK – Concept and Performance, *Proceedings of the GNSS Symposium*, November, Wuhan, China.
- Wolf, P. R., Ghilani, C. D. (2002). *Elementary Surveying, An Introduction to Geomatics*, 10th Edition, Prentice Hall Upper Saddle River, New Jersey, 887 pages
- URL1: <http://www.hh.se/download/18.7dcf486b1244904a0e2800041/lecture9.pdf>

Evaluations on Digital Elevation Model Generation by Using Airborne LIDAR Technique in West of Turkey

Fırat KOÇ^{*1}, R. Alper Kuçak¹, Serdar Erol¹, Bihter Erol¹

¹ Department of Geomatics Engineering, Istanbul Technical University, Ayazaga Campus, 34469, Turkey. e-mail: kocfi, kucak15, erol, bihter@itu.edu.tr

ABSTRACT

Digital Elevation Models (DEMs), an important data source for geographical information systems, can be produced by classical measurement techniques as well as by LIDAR (Light Detection and Ranging) system. Because of the three-dimensional data generated by the combination of the Global Navigation Satellite System (GNSS), the Inertial Navigation System (INS) and the laser scanning device, LIDAR is more useful than the conventional methods. LIDAR systems have recently encountered frequently in many areas of geomatics applications. The density of the point cloud data obtained with this technology that differs according to the used laser system and the flying altitude. This directly affects the quality of the models to be obtained in the point cloud according to the application. DEMs are successfully used in 3D (3 dimension) urban information systems, disaster applications, military applications, engineering and architectural studies and also in various 3D visualization studies such as restoration. The accuracy of the produced DEM also has a great importance for many applications. Therefore, evaluating the accuracy of the generated models is essential in practice. In this study, point cloud data in different densities obtained from LIDAR measurements at two different flying altitudes (1200 m and 2600 m) are analyzed. Before these analyses are performed, filtering procedure is applied to remove noises on the raw data with Cloud Compare open source software. The resulting products (DEMs, DSMs, buildings, energy transmission lines and trees) from the point cloud diluted by filtration are obtained from Envi software for the rural area under consideration. The results are compared each other in order to clarify superiorities and weaknesses for the data obtained from the different flying altitudes and LIDAR systems. We acknowledge General Command of Mapping of Turkey for providing Airborne LIDAR data.

INTRODUCTION

DEM is a model which expresses the position and altitude information of the earth as 3D. These models are divided into digital terrain model (DTM) and digital surface model (DSM). DTM is a model in which objects on the land are ignored, only the earth is numerically transferred. DSM is also a model that includes natural and artificial objects on

^{*} Corresponding Author

land (Çam et al., 2013). DEMs can be obtained with LIDAR systems, as well as with many other calculated measurement techniques. Lidar is a technology which is used to produce 3D spatial information with high accuracy and high precision. Lidar systems can make quick measurements on the ground with an average of 150,000 pulses per second. As a result of these measurements, a 3D geographically referenced point cloud is obtained. Lidar is a system formed by the integration of laser scanner, GPS and IMU systems. Accuracy of measurement impressed by the position and orientation accuracy of the GPS-IMU systems and the deviation of laser beam. When the flight altitude is increasing, accuracy is decrease (Kraus, 2003).

During data collection, Lidar has a large amount of data that needs to be classified because of its ability to collect data from different areas. For this reason, the raw point cloud must be filtered before the DEM is created. In the classification phase, information about the land (height, density, multiple turns, etc.) is extracted to determine whether the data belong to the land. This process is called "filtering". In the second step, DEM is produced using surface points obtained by filtering (Meng et al., 2010).

DEMs have specific accuracy. When this accuracy is calculated, measurements with a certain accuracy are used. For this reason, the accuracy of DEMs is expressed with relative accuracy instead of absolute accuracy. When a new surface is compared with a known surface of measurement accuracy, the differences of the relative heights in the corresponding points of these surfaces are calculated. RMS of the obtained values are used to define the surface accuracy. The formula used as follows:

$$\text{RMS} = \pm \sqrt{(\sum \Delta h^2 / (n - 1))} \quad (1.1)$$

Another way of statistically expressing accuracy is to calculate standard deviation values. The standard deviation is calculated using the following formula:

$$\text{Standart Deviation} = \pm \sqrt{(\sum \Delta h^2 / n) - \overline{\Delta h}^2} \quad (1.2)$$

$\overline{\Delta h}$: algebraic average, n: correspondence points (Saygılı, 2008)

DATA AND METHODOLOGY

This application was built by HGK in Izmir Bergama. In this application, Lidar point cloud data obtained by making test flights from 1200 and 2600 meters height to two different companies were used. Pegasus HA-500 lidar system from Optech and Riegl LMS-Q1560 lidar system were used in the test flights.

Table 3: Parameters of test flights of Optech Pegasus HA-500 and Riegl LMS-Q1560

Flight Altitude	Angle +/-	Speed (knots)	Density (point/m ²)	Number of colon	overlapping
2600 m	20	150	≥ 2	18	%50
1200 m	35	150	≥ 8	32	%25
2600 m	30	150	≥ 2	11	%30
1200 m	35	150	≥ 8	32	%25

The application area was chosen as agricultural land. The area of the area with a length of 300 m and a width of 175 m is 52500 m².



Figure 2. The selected area for application

Firstly, SOR (Statistical Outlier Removal) filtering was performed on the data using the Cloud Compare program. SOR filter; calculates the average distance between each point in the point cloud and the neighbouring points in the determined number. The standard deviation is multiplied by the boundary multiplier value and added to the calculated average distance. In this way the maximum distance value for the points is calculated. This removes points outside the distance (URL 1).

Maximum distance= Average distance + nsigma * standard deviation

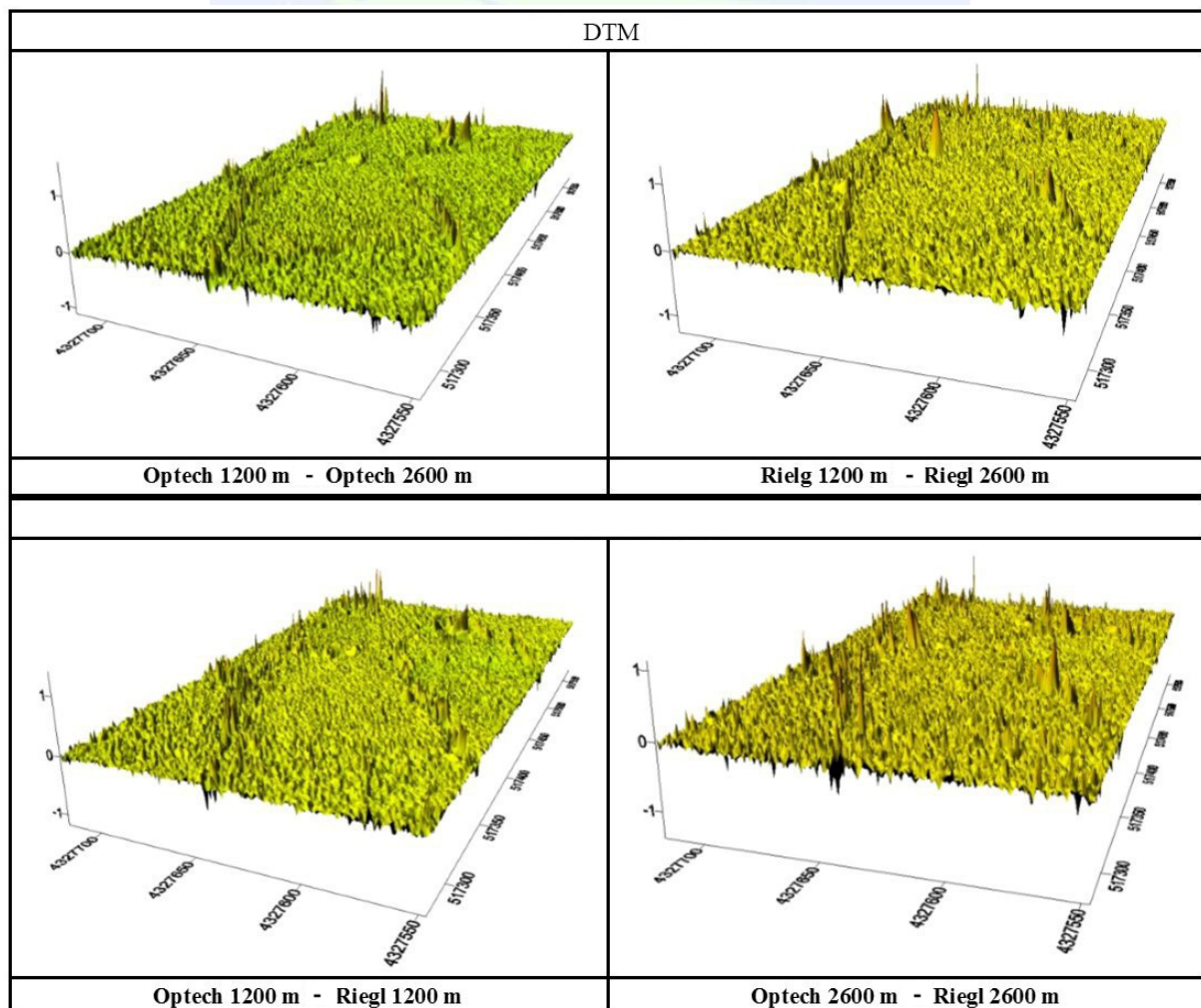
As a result of these operations, the raw data produced on the common area were filtered and the noises were removed. Point cloud data is recorded in LAS format and prepared for DTM and DSM production.

The Envi Lidar program was used to generate DSM and DTM from spot cloud data recorded in LAS format. Projection systems were selected as UTM, datums as WGS84 and UTM zones as 35N in Bergama district of İzmir province. Density maps are interpreted to fine tune the parameters before switching to process.

In order to create Digital Surface and Digital Terrain models, we used some Process parameters. These parameters;

- **Grid Resolution:** On the whole of the data analyzed, there are an average of 4 points per square meter. The Grid Resolution value is set to 1 for the algorithm to give a precise result.
- **Near Terrain Classification:** This parameter is used to classify objects such as buildings, trees, energy transmission lines that are not part of the model after the DEM is created. The default value of 50 cm has been used for precise classification.
- **Height and radius values for trees:** For the classification of the trees in the region, the minimum height of the tree is 130 cm and the maximum height is 5000 cm. Radius values are defined as minimum 200 cm and maximum 600 cm.
- **Height and area values for buildings:** The minimum building area used to identify the buildings was defined as 10 m² and the near floor filter width was defined as 30 cm
- The recording types and locations of the products to be obtained after the parameter values are determined are defined.

Analysis of generated models is divided into 2 categories. First one is Analysis of DTMs. The DTMs generated by the process were compared with the Surfer 13 program.



The DTMs which are produced with the Envi Lidar program was compared by using the Surfer 13 program. When looking at the difference maps, it is determined that the regions where the differences are overrepresented are similar. The following table appears when statistical comparison is made.

Table 4. DTM Analysis

Surfer	DTM				
	Avg.	Median	Std.Dev	Min.	Max.
Optech 1200-2600	0.044	0.050	0.075	-1.105	1.576
Optech1200Riegl1200	0.016	0.020	0.072	-1.181	1.396
Riegl 1200-2600	-0.005	-0.005	0.066	-1.262	1.272
Optech2600Riegl2600	-0.033	-0.035	0.085	-1.397	1.143

When the difference analyzes were examined, it was seen that the standard deviation was between 0.07 m and 0.09 m. The mean height differences were found not to exceed 0.04 meters. But in some regions it seems that this difference is more. The difference maps have been created in Arcsene program for further analysis.

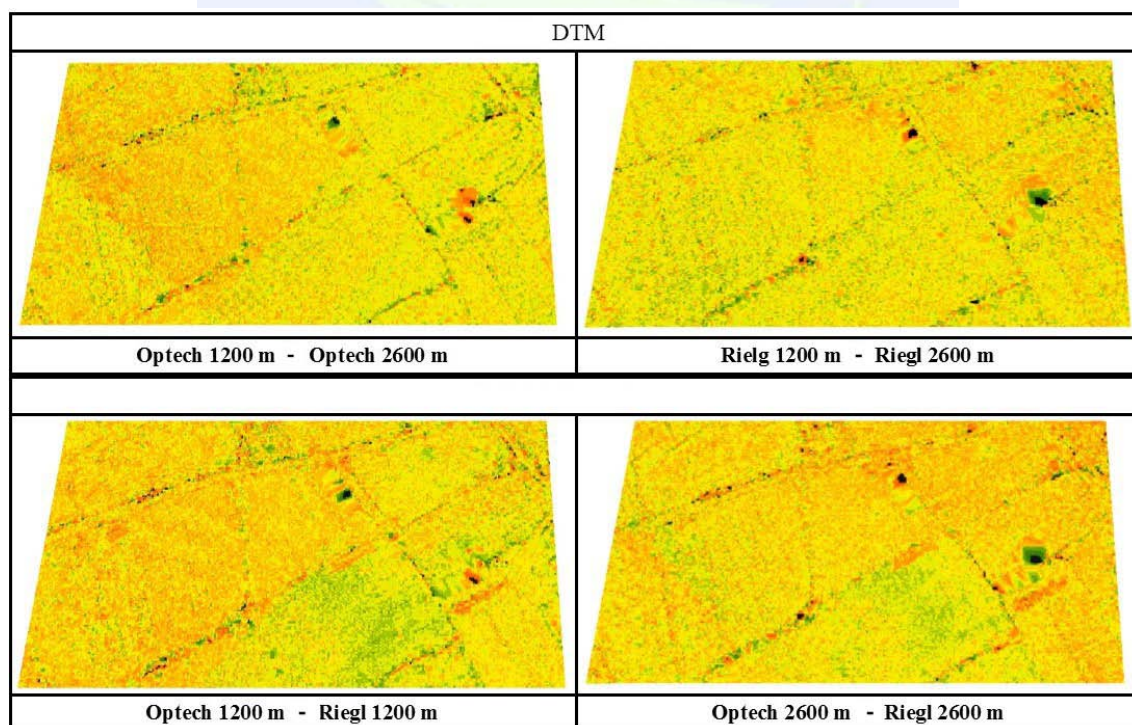


Figure 1. DTM map (ArcScene).

Table 5. DTM analysis (ArcScene).

ArcScene	DTM			
	Avg.	Std. Dev.	Min.	Max.
Optech 1200-2600	0.043	0.074	-1.105	1.576
Optech 1200-Riegl1200	0.015	0.071	-1.180	1.396
Riegl 1200-2600	-0.005	0.066	-1.261	1.271
Optech 2600-Riegl2600	-0.033	0.085	-1.397	1.143

When the difference analyzes obtained from the ArcScene program were examined, it was determined that the mean difference values and the standard deviations corresponded to the values obtained from the Surfer 13 program. When we look at the difference maps obtained from ArcScene program, the differences in the areas indicated by black color. Gradually decreasing in red and green regions and approaching zero in yellow regions. Judging from the maximum and minimum difference values, it is understood that there are rough errors in black regions. In these regions, satellite images have been looked at in order to better analyze what kind of topography is on the ground.



Figure 2. Display of places where too many differences are detected.

The yellow squares shown in Figure 4 display where the differences are greater than 0.30 meters. It is understood that there are buildings in these regions.

Second is analysis of DSM. DSMs generated after process operations were compared using Surfer 13 and ArcScene programs. The processes applied in the DSM analysis were applied in the same way.

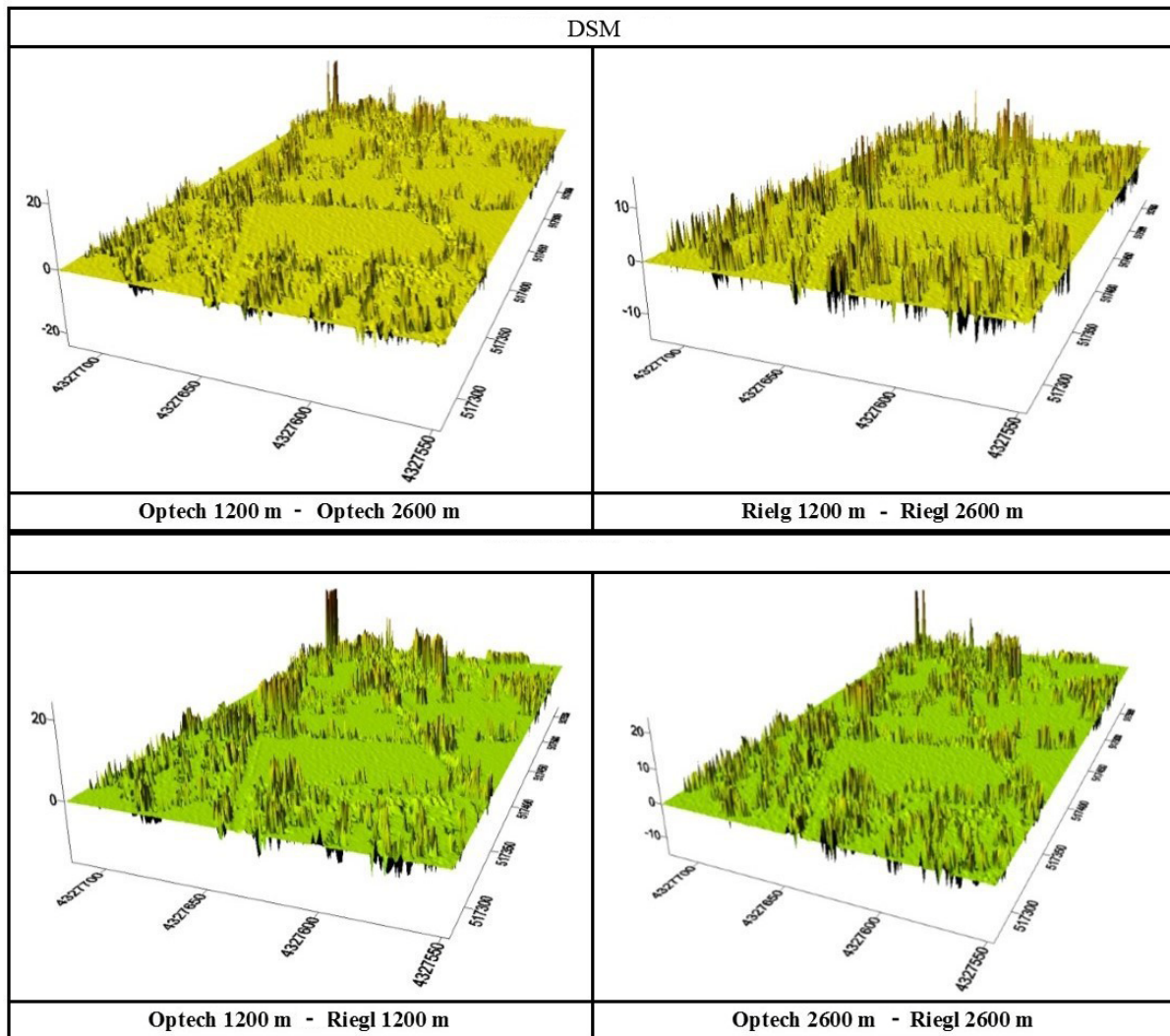


Figure 3. DSM maps (Surfer 13)

Table 6. DTM Analysis

Surfer	DSM				
	Avg.	Median	Std.Dev.	Min.	Max.
Optech 1200-2600	0.062	0.020	1.352	-24.120	24.308
Optech 1200 Riegl1200	0.194	-0.018	1.421	-15.699	24.33
Riegl 1200-2600	0.079	0.039	1.129	-14.917	15.727
Optech2600-Riegl2600	0.212	-0.001	1.446	-15.271	24.287

When the DSM difference analysis was performed, the mean difference values were found between 0.06 m and 0.20 m. It has been determined that the standard deviation values reach 1.5 meters. When the minimum and maximum difference values are taken into account, there are big differences from 14 meters to 25 meters. These differences indicate

that the models have rough errors in certain areas. In order to better analyze where the coarse faults occur, the difference maps were created from ArcScene program.

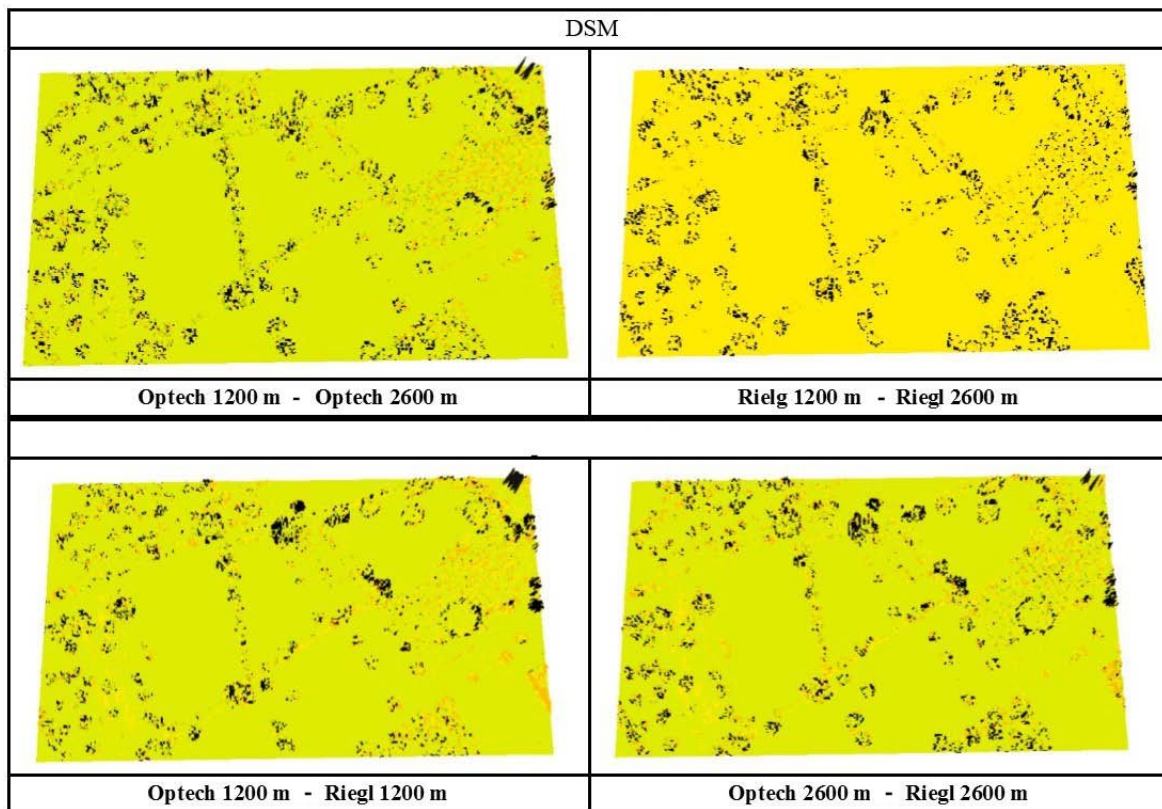


Figure 4. DSM map (ArcScene).

Table 7. DSM analysis (ArcScene).

ArcScene	DSM			
	Avg.	Std. Dev.	Min.	Max.
Optech 1200-2600	0.062	1.352	-24.120	24.308
Optech 1200-Riegl1200	0.194	1.421	-15.699	24.329
Riegl1200-2600	0.079	1.129	-14.916	15.727
Optech2600-Riegl2600	0.212	1.446	-15.270	24.287

When the difference analyzes obtained from the ArcScene program were examined, it was determined that the mean difference values and the standard deviations corresponded to the values obtained from the Surfer 13 program. When you look at the black areas, the edges of the trees are striking. Satellite images have been viewed to examine the topography in this area.



Figure 5. Display of the region where the gross error was detected.

When we look at the satellite image, it is determined that there is an electric pole in this area. Therefore, an error due to classification and filtering during the process has caused this height difference to occur.

CONCLUSIONS

Lidar point cloud data obtained by test flights made by Optech and Riegl firms in İzmir Bergama district were filtered, processed, DEM, DSM, plant cover and buildings were created. All of the models created from the data belonging to the same company were compared within themselves. When DTM difference maps are examined, it is determined that the differences are within the range of meters in certain areas. When these regions are examined, it is seen that the differences are usually high in places where buildings are located. When DTM is created, objects on the topography such as buildings, trees are filtered. For this reason, the differences are more frequent in the places where the buildings are located, indicating that the situation is caused by filtering errors.

The DSM was created and compared using the same techniques used in DTM production from the data sets. As a result of comparison the average error in Optech and Riegl is 0.07 m. However, in some regions it has been determined that the differences have reached 25 m.

It is understood that these areas are generally surrounded by buildings and wood edges. The differences in the perimeter of the buildings and the edges of the trees are also in the average tree or building size. It shows that the differences in the surroundings of buildings and trees are in the average tree or building size. Comparisons without conjugate points in areas where buildings and trees are located can lead to faults. Therefore it is thought that DTM and DSM can also be related to the method used during the creation. These errors may be due to the different scanning scans of the Lidar system, flight plan, coordination or filtering operations. In future Lidar applications, comparisons by measuring conjugate points will be useful for clarifying the relative accuracy of the two systems.

REFERENCES

- Çam, A., Fırat, O., Yılmaz, A., (2013). Harita Genel Komutanlığında Ortofoto ve Sayısal Yüzey Modeli Üretimi Faaliyetleri [Orthophoto and Digital Surface Modeling Activities in the General Command of Mapping.]. *Paper presented at TMMOB Coğrafi Bilgi Sistemleri Kongresi*. Retrieved from http://www.hkmo.org.tr/resimler/ekler/00360d17e5981e4_ek.pdf
- Kraus K., 2003. *Photogrammetry I (Fotoğraflardan ve Lazer Tarama Verilerinden Geometrik Bilgiler)*, Yedinci Baskı [Photogrammetry I (Geometric Information from Photographs and Laser Scanning Data), Seventh Edition]. Translators: Altan O., Külür S., Toz G., Demirel H., Duran Z.
- Meng, X., Currit, N., & Zhao, K. (2010). Ground filtering algorithms for airborne LIDAR data: a review of critical issues. *Remote Sensing Journal*, 2(3), 833- 860. doi:10.3390/rs2030833
- Saygılı, A. (2008). *SRTM (shuttle radar topography mission) verilerinden elde edilen sayısal yükseklik modellerinin doğruluğunun incelenmesi [Examination of the accuracy of digital height models obtained from SRTM data]*. (Master's Thesis), Yıldız Teknik Üniversitesi/Fen Bilimleri Enstitüsü, İstanbul, Türkiye.
- URL1: http://pointclouds.org/documentation/tutorials/statistical_outlier.php



Analysis on the Quality of High-Resolution Global Digital Terrain Models (DTM) using GPS/leveling Data in Turkey

Mustafa Serkan Işık^{*}, Bihter Erol and Serdar Erol

Istanbul Technical University, Civil Engineering Faculty, Department of Geomatics Engineering, 34469 Maslak, Istanbul, Turkey. (e-mail: isikm@itu.edu.tr)

ABSTRACT

The topographical heights are required in practice for a number of engineering applications. Beside of their practical use, the specific correction terms to the gravity observations, carried out on the Earth surface, which are typically the terrain corrections, downward continuation corrections etc., are also calculated using the topographical heights for Geoid modeling and Geophysical exploration purposes. Using a high resolution Digital Terrain Model (DTM) is the most practical and economical way for obtaining the height data nowadays. However, whatever its generation method is, these models are generated relying on the observational data and naturally they include errors that are not uniformly distributed. So, it is important to clarify the accuracy of the DTM in the study area before using its data. In general, validating the DTMs using independent point-wise data such as GPS and leveling heights provide an overall accuracy measure in terms of root means square error of the DTM derived heights. In this study three high resolution digital elevation models ASTER (Advanced Space-borne Thermal Emission and Reflection Radiometer), SRTM (Shuttle Radar Topography Mission) and Turkey Digital Topographic Data DTED2 are assessed using GPS/leveling data. Using three different sets of GPS/leveling data in validations it is aimed to clarify the role of distribution of the ground-control points as well as the region's characteristics, such as roughness of topography, land-cover etc., in the validation results.

INTRODUCTION

Height information is of great importance for many disciplines that benefits geo-information such as geodesy, geophysics and hydrology. In this context, the proper definition of physical heights and its accuracy should meet the current needs of the geosciences, especially in international and global applications. Of course, this requires the detailed knowledge of Earth's true shape (geoid) under the effect of its gravity field.

The definition of vertical datum is always made by analyzing tide gauge observation to calculate the mean sea level. This comes from the fact that the true shape of geoid was known to be coincided with the mean sea level; though, in fact, it is not. It is known that

^{*} Corresponding Author

mean sea level changes everywhere on Earth, thus cannot be used as a reference for heights. The variations between geoid and mean sea level can reach up to ± 2 meters. Besides, different data periods in the determination of vertical datum also causes significant offsets among countries. Thus, international and global projects suffer from this contradictory situation in practice. In that case, the solution is either to connect the vertical datum of countries via traditional levelling, which is time consuming and rather expensive, or to use a Digital Elevation Model (DEM) whose vertical datum is a geoid model calculated from a global geopotential model. But the latter is also not a solution for every project, because of the limitations in vertical accuracies of globally distributed DEMs.

Most frequently used digital elevation models are Shuttle Radar Topography Model (SRTM) (NASA JPL., 2013; Farr and Kobrick, 2000) and Advanced Spaceborne Thermal Emission and Reflection Radiometer Global Digital Elevation Map (ASTER GDEM) (NASA JPL, 2009). The accuracy of these models varies regionally and should be validated for each study area in order to clarify the performance of the model. There have been some studies to clarify the performance of DEMs globally and regionally (Rodriguez et al., 2006; ASTER Validation Team, 2009; Hirt et al., 2010). In Turkey, local validation of the models can be found in Bildirici et al. (2008) and Feizabadi and Erol (2014).

In this study, it is aimed to investigate the performance of commonly used global DEMs ASTER GDEM and SRTM as well as the Turkey Digital Topographic Data DTED2 using three different sets of GPS/Levelling data located in north-west side of the Turkey. Both 1 arc-second (30 meter) and 3 arc-second (90 meter) resolution ASTER GDEM and SRTM data sets are validated in order to clarify the contribution of higher resolution products.

CASE STUDY

Study Area and Data Used

The study area is the north-west side of the Turkey, mainly covered by Marmara region within the latitudes 39°N-42°N and longitudes 28°E-32°E (see Fig.1). The study is conducted with three different GPS/Levelling data sets located in north-west side of the Turkey. The first data set includes 75 GPS/Levelling benchmarks and covers the Turkey between the latitudes 39°N-42°N and longitudes 28°E-32°E. The benchmarks belong to Turkish National Fundamental GPS Network (TNFGN-TUTGA), which is B-order geodetic network. The distribution of the points is shown with the topography of Turkey from SRTM data in Fig.2. The second data set is Istanbul GPS Triangulation Network (IGNA) which includes 1204 GPS/Levelling benchmarks co-located in Istanbul city (see Fig.3). IGNA network is quite homogenous and dense considering the size of the area covered. The third and final one is Sakarya GPS/Levelling data set which includes 109 co-located benchmarks (see Fig.4). Sakarya network is also homogenous; however, the density of network in the mountainous areas is sparse. The description of GPS/Levelling data sets are given in Table 1.

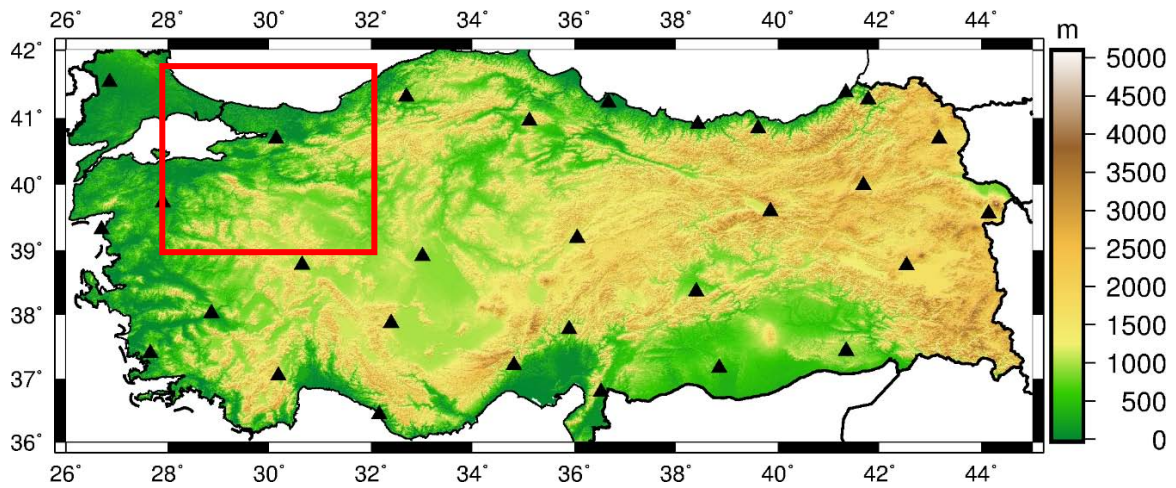


Figure 1. Study area (red rectangle) and the topography of Turkey.

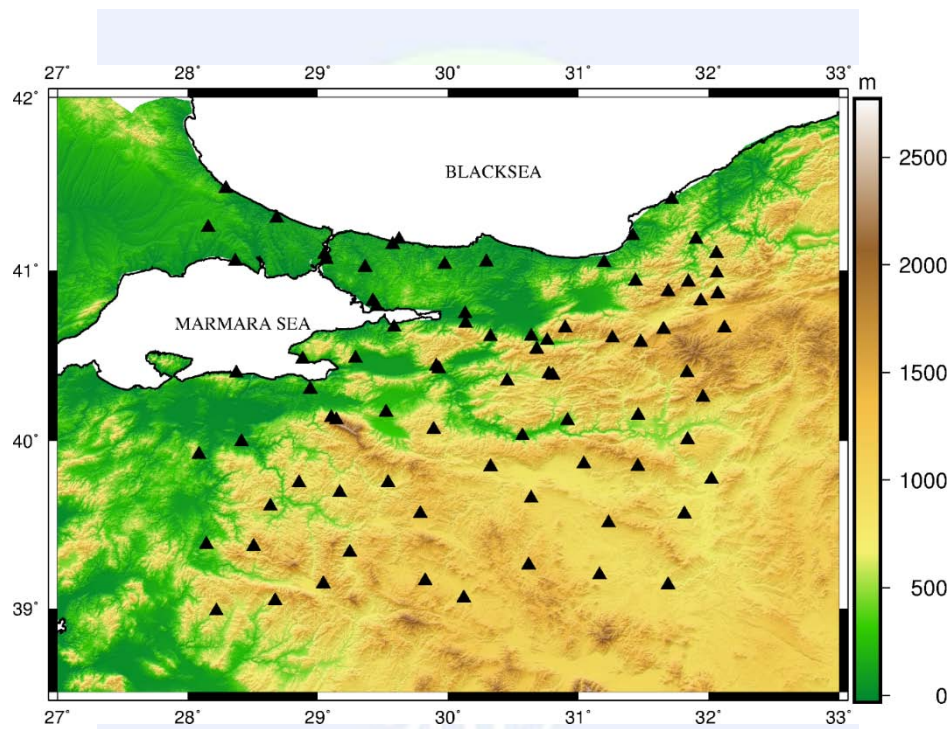


Figure 2. Distribution of 75 TUTGA GPS/Levelling data set.

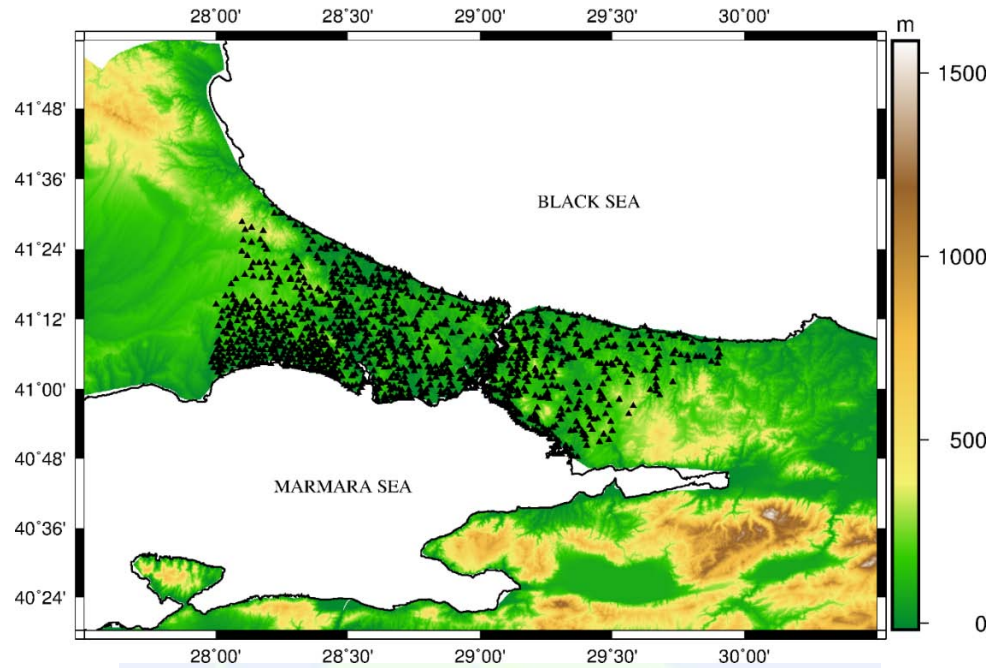


Figure 3. Distribution of 1204 IGNA GPS/Levelling data set.

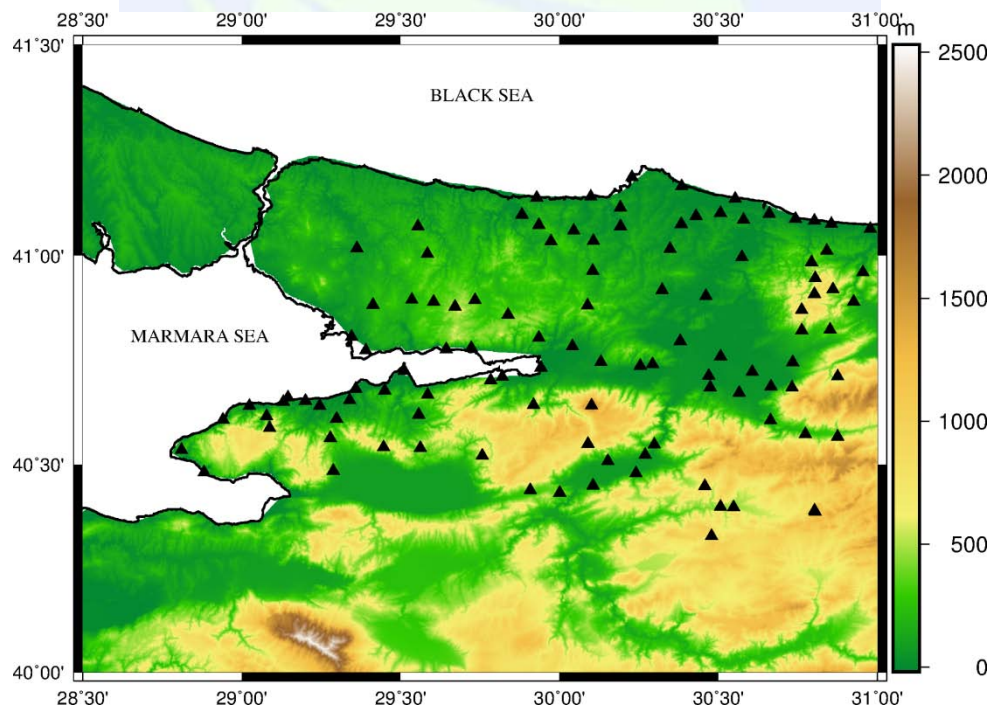


Figure 4. Distribution of 109 Sakarya GPS/Levelling data set.

DEMs that are used within the study are ASTER GDEM, SRTM and Turkey Digital Topographic Data DTED2 (hereafter it will be shortened as DTED2). ASTER GDEM is a joint project of NASA and Japanese Ministry of Economy, Trade and Industry (METI) and it is released in 2009 (NASA JPL, 2009). The SRTM mission is a joint project of National Geospatial-Intelligence Agency (NGA), NASA and National Imagery and Mapping Agency (NIMA) that aimed the collection of elevation data between the latitudes 60°N and 56°S (NASA JPL, 2013).

Table 1. Description of GPS/Levelling data sets.

Data Set	TUTGA	IGNA	Sakarya
size of area	3° x 4°	1° x 2°	1° x 1.5°
number of BMs	75	1204	109
BM density	1 BM / 45 km	1 BM / 5 km	1 BM / 13 km
the distribution of BMs	homogenous and sparse	homogenous and dense	homogenous and mixed
Horizontal datum	ITRF96	ITRF96	ITRF96
Vertical datum	TUDKA99	TUDKA99	TUDKA99
Topography	0-2500 m	0-500 m	0-1800 m
Reference	Ayhan et al. (2002)	Ayan et al., (2006)	Çelik et al. (2001)

Until 2014, SRTM 1 arc-second resolution data was only available for US territories. Recently, 1 arc-second resolution SRTM data have been released globally. DTED2 model is produced by General Command of Mapping from 25K topographic maps with 10 m intervals. DTED2 model is a restricted data that can be obtained from General Command of Mapping at charge. The characteristics of these models are summarized in Table 2.

Table 2. Description of DEM data sets.

Data Set	ASTER	SRTM	DTED-2
Coverage	Global	Global	Turkey
Resolution (arc-second)	1" – 3"	1" – 3" – 30"	1"
Acquisition Type	Stereo-pair images	RADAR	25K topographic maps
Horizontal datum	WGS84	WGS84	WGS84
Vertical datum	EGM96	EGM96	TUDKA99
Projection	Geographic	Geographic	Geographic
Reference	NASA JPL (2009)	NASA JPL (2013)	HGK (2017)

Methodology

In order to assess the performance of DEMs, the orthometric heights of GPS/Levelling benchmarks and corresponding orthometric heights which are interpolated from the models are compared (Eq.1).

$$dH = H_{GPS/Levelling} - H_{model} \quad (1)$$

In this equation, dH is the orthometric height difference between GPS/Levelling benchmarks and model, $H_{GPS/levelling}$ is the orthometric height of the benchmarks and H_{model} is the orthometric height interpolated from the models using bi-linear interpolation method (Han, 2013). Throughout the study, all interpolation computations are carried out using Generic Mapping Tools (GMT5) software (Wessel et al., 2013).

Aside from the orthometric heights obtained by traditional levelling, ellipsoidal height of the benchmarks is used to evaluate the performance of models (Eq.2).

$$dH = H_{GPS/EGM96} - H_{model} \quad (2)$$

In this equation, $H_{GPS/EGM96}$ is the orthometric height calculated using ellipsoidal height of the benchmarks and corresponding geoid heights N derived from EGM96 global geopotential model (see Fig.5).

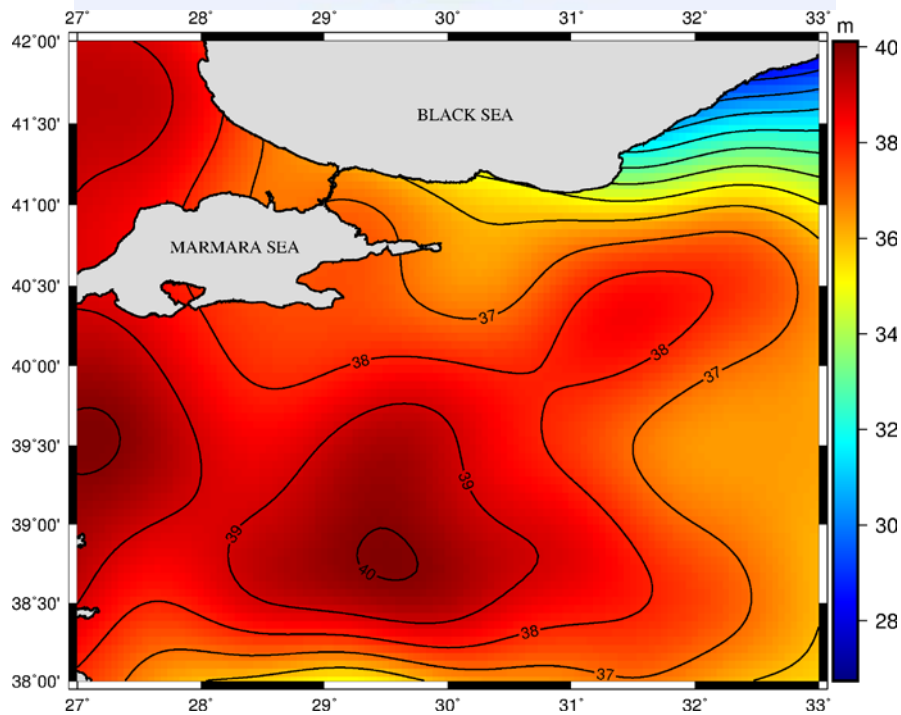


Figure 5: Geoid heights in the study area derived from EGM96.

Numerical Results

The statistical results of the analysis using orthometric heights from levelling are given in Table 3, 4 and 5. The statistical results of the comparison using ellipsoidal heights from GPS observations and geoid heights from EGM96 are given in Table 6, 7 and 8. Both comparison methodologies show quite similar results. SRTM 3" model performs worse than all models in terms of standard deviation. It can be seen that DTED2 model is better than the other models in general. SRTM 1" data shows better agreements than SRTM 3" and ASTER GDEM models at all GPS/levelling data sets in meter level. The difference between DTED2 and SRTM 1" data at IGNA benchmarks is insignificant, both performs with an accuracy about ± 3.9 m in Istanbul.

The standard deviations of all models at IGNA data set are significantly smaller compared to the Sakarya and TUTGA. This can be attributed to the topographic features of the GPS/Levelling data sets, since the topography of the region covered by IGNA is relatively smoother than the others. This is also visible in the mean values of residual heights at IGNA benchmarks which are smaller than TUTGA and Sakarya (see Table 4 and 7).

Table 3. Statistics of residual heights ($H_{GPS/Levelling} - H_{model}$) at TUTGA GPS/Levelling Benchmarks.

Model Name	Min	Max	Mean	Standard Dev.
ASTER 3"	-4.413	36.328	9.758	7.494
ASTER 1"	-8.225	37.255	7.794	7.830
SRTM 3"	-19.602	37.140	10.145	9.752
SRTM 1"	-8.355	23.634	6.711	6.555
DTED2 1"	-5.446	22.462	5.162	4.475

Table 4. Statistics of residual heights ($H_{GPS/Levelling} - H_{model}$) at IGNA GPS/Levelling Benchmarks.

Model Name	Min	Max	Mean	Standard Dev.
ASTER 3"	-19.158	26.189	2.632	5.404
ASTER 1"	-24.021	24.633	1.826	5.215
SRTM 3"	-26.619	32.230	4.101	5.617
SRTM 1"	-14.923	30.948	2.891	3.934
DTED2 1"	-58.077	33.058	3.491	3.944

Table 5. Statistics of residual heights ($H_{GPS/Levelling} - H_{model}$) at Sakarya GPS/Levelling Benchmarks.

Model Name	Min	Max	Mean	Standard Dev.
ASTER 3"	-6.731	25.194	5.853	6.807
ASTER 1"	-11.808	34.199	4.415	6.658
SRTM 3"	-15.011	35.503	8.628	8.166
SRTM 1"	-8.974	32.840	5.583	6.106
DTED2 1"	-10.118	21.138	4.737	4.299

Table 6. Statistics of residual heights ($H_{GPS/EGM96} - H_{model}$) at TUTGA GPS/Levelling Benchmarks.

Model Name	Min	Max	Mean	Standard Dev.
ASTER 3"	-3.911	36.583	9.974	7.504
ASTER 1"	-7.724	37.510	8.002	7.806
SRTM 3"	-18.532	38.361	10.364	9.847
SRTM 1"	-7.286	24.194	6.919	6.609
DTED2 1"	-6.438	23.683	5.340	4.769

Table 7. Statistics of residual heights ($H_{GPS/EGM96} - H_{model}$) at IGNA GPS/Levelling Benchmarks.

Model Name	Min	Max	Mean	Standard Dev.
ASTER 3"	-19.378	25.900	2.660	5.409
ASTER 1"	-24.240	24.344	1.816	5.239
SRTM 3"	-26.570	32.016	4.119	5.642
SRTM 1"	-14.874	30.658	2.881	3.962
DTED2 1"	-57.970	33.376	3.482	3.945

Table 8. Statistics of residual heights ($H_{GPS/EGM96} - H_{model}$) at Sakarya GPS/Levelling Benchmarks.

Model Name	Min	Max	Mean	Standard Dev.
ASTER 3"	-7.124	25.328	5.914	6.863
ASTER 1"	-11.370	34.333	4.461	6.696
SRTM 3"	-14.900	35.724	8.707	8.193
SRTM 1"	-8.161	33.061	5.629	6.099
DTED2 1"	-9.305	21.331	4.783	4.336

CONCLUSIONS

In this study, the performance of ASTER and SRTM DEMs with 1" and 3" resolutions and Turkey Digital Topography Model DTED2 are evaluated at three different GPS/Levelling data sets located in Marmara region of Turkey. In the comparison, both orthometric heights from levelling and ellipsoidal height from GPS observations together with geoid model calculated from EGM96 model are used. Both comparison methods show statistically similar results. The standard deviation of DTED-2 model is significantly smaller compared to others at TUTGA and Sakarya GPS/Levelling data sets. However, there is no significant difference between the standard deviation of DTED-2 and SRTM 1" models, which is ± 3.9 m, at IGNA GPS/Levelling data set. In conclusion, DTED-2 model is found to be the superior to 3" and 1" resolution ASTER GDEM and SRTM DEMs and the accuracy of the model is about ± 4 m in the north-west of Turkey.

ACKNOWLEDGMENTS

This study is carried out as a part of scientific research project financially supported by TUBITAK under contract with the number of 114Y581. USGS The Land Processes Distributed Active Archive Center (LP DAAC), NASA and METI are gratefully acknowledged for the availability of ASTER GDEM and SRTM data sets.

REFERENCES

- Ayan, T., Deniz R., Arslan E., Çelik R.N., Denli H.H., Akyılmaz O., Özşamlı C., Özlüdemir M.T., Erol S., Erol B., Acar M., Mercan H. and Tekdal E., 2006. *İstanbul GPS Nirengi Ağı (İGNA) 2005-2006 Yenileme Ölçü ve Değerlendirmesi*, Scientific Technical Report, Istanbul Technical University, Geodesy Division, Istanbul, Turkey. (in Turkish)
- Ayhan, M. E., Demir, C., Lenk, O., Kılıçoğlu, A., Aktuğ, B., Açıkgoz, M., Firat, O., Şengün, Y. S., Cingöz, A., Gürdal, M. A., Kurt, A. I., Ocak, M., Türkezer, A., Yıldız, H., Bayazit, N., Ata, M., Çağlar, Y. and Özerkan, A., 2002. Turkish National Fundamental GPS Network–1999 Report. *Map Journal*. Special issue-16 (in Turkish)
- ASTER Validation Team, 2009. ASTER global DEM validation summary report. ASTER GDEM Validation Team: METI, NASA and USGS in cooperation with NGA and other collaborators. <https://lpdaac.usgs.gov> (accessed 8 September 2017)
- Bildirici İ.Ö., Üstün A., Uluğtekin N., Selvi H.Z., Abbak R.A., Buğdaycı İ., Doğru A.Ö. 2008. *Yerel Yükseklik Bilgileriyle Desteklenmiş SRTM Verileri Kullanılarak Türkiye için 3''x3'' çözünürlüklü Sayısal Yükseklik Modelinin Oluşturulması*, TÜBİTAK Projesi Raporu, No. 106Y130, Türkiye. URL: <http://www.tsym3.selcuk.edu.tr> (08.09.2017)
- Çelik, R. N., Ayan, T., Erol, B., 2001. *MERLIS (Marmara Earthquake Region Land Information System) Jeodezik Altyapı çalışmaları için Geoit Modeli Belirleme*,

- Technical Report, Istanbul Technical University, Project No. 2002/06/209. (in Turkish)
- Farr, T. G., and Kobrick, M., 2000. Shuttle Radar Topography Mission produces a wealth of data. *Eos, Transactions American Geophysical Union*, 81(48), 583-585.
- Feizabadi, M., Erol, B., 2014. Assessment of High-Resolution SRTM and ASTER based Digital Terrain Models in Turkey, *XXIV International Symposium: Modern Technologies, Education and Professional Practice in Geodesy and Related Fields*, November 6-7, Sofia, Bulgaria.
- Han, D., 2013. Comparison of commonly used image interpolation methods. In *Proceedings of the 2nd International Conference on Computer Science and Electronics Engineerings (ICCSEE)* (pp. 1556-1559).
- Hirt, C., Filmer, M. S., and Featherstone, W. E., 2010. Comparison and validation of the recent freely available ASTER-GDEM ver1, SRTM ver4. 1 and GEODATA DEM-9S ver3 digital elevation models over Australia. *Australian Journal of Earth Sciences*, 57(3), 337-347.
- HGK 2017. Harita Genel Komutanlığı Ürün Portalı, URL: <http://www.hgk.msb.gov.tr/urun-50-dted-2.html> (8.9.2017).
- IDEM 2016. International Digital Elevation Model Service, <http://www.cse.dmu.ac.uk/EAPRS/iag/>.(26.04.2016)
- Lemoine, F.G., Kenyon, S.C., Factor, J.K., Trimmer, R.G., Pavlis, N.K., Chinn, D.S., Cox, C.M., Klosko, S.M., Luthcke, S.B., Torrence, M.H., Wang, Y.M., Williamson, R.G., Pavlis, E.C., Rapp, R.H., Olsen, T.R., 1998. *The development of the joint NASA GSFC and the National Imagery and Mapping Agency (NIMA) geopotential model EGM96*. NASA Technical Paper NASA/TP-1998-206861, Goddard Space Flight Center, Greenbelt.
- NASA JPL., 2009. ASTER Global Digital Elevation Model [Data set]. NASA JPL. <https://doi.org/10.5067/aster/astgtm.002>
- NASA JPL., 2013. NASA Shuttle Radar Topography Mission Global 1 arc second [Data set]. NASA LP DAAC. <https://doi.org/10.5067/measures/srtm/srtmg1.003>
- Rodriguez, E., Morris, C. S., and Belz, J. E., 2006. A global assessment of the SRTM performance. *Photogrammetric Engineering & Remote Sensing*, 72(3), 249-260.
- Wessel, P., Smith, W. H., Scharroo, R., Luis, J., and Wobbe, F., 2013. Generic mapping tools: improved version released. *Eos, Transactions American Geophysical Union*, 94(45), 409-410.

Modelling Land Registry and Cadastre Transactions with UML: A Case of Turkey

Zeynel Abidin Polat^{*1}, Hicret Gürsoy Sürmeneli¹ and Mehmet Alkan¹

¹ Department of Geomatic Engineering, Yildiz Technical University, Davutpaşa Campus, 34220, Turkey. e-mail: zapolat@yildiz.edu.tr

ABSTRACT

Many institutions (Eg. Municipality, notary, court) and documents (Eg. real estate value statement, certificate of inheritance, warrant of attorney) are involved in the transactions carried out in the land registry and cadastral directorates. The process step and the required documents can be changed in each land registry and cadastre transactions. In this context, there is a need for a systematic modeling approach that will manage the land registry and cadastral procedures necessary for the implementation of sustainable land management

Unified Modeling Language (UML) is used in general-purpose visual modeling language for the determination of system components for the visualization and documentation. Today, UML has taken standard language version both designing conceptual object-oriented software and many other applications. This language can be used to modeling the structural diagram of a data model conceptual level. UML is frequently used in the design followed and supported models which reflects the real world by the system designers and agencies. In this context, It is a useful modeling language to model the requirements of internal and external information systems in terms of both data and functional. UML is a suitable model to define the relationships between cadastre and land management components when considered in terms of design of information systems and development business processes.

In this study, the use of UML in the modeling of land registry and cadastral transactions has been examined. In this context, it can be demonstrated that using of UML in land registry and cadastre transactions modeling effectively with modeling some land registry and cadastre transactions process using UML diagrams.

INTRODUCTION

Cadastral system is a complicated system, consisting of many sub-systems including many activities and procedures. However, it is directly related to legal, economic and technical issues to designate human life. Therefore, a systematical modelling approach is required for analysis and decision making procedures. Eliminating any gaps within cadastral

^{*} Corresponding author

system, this modelling approach must be applied so as to arrange the relation between cadastral components.

While the use of modelling language ensures comprehension of complicated systems, it also provide several conveniences in terms of land registry and cadastral transactions:

- Ensures a perspective to determine user requirements by reviewing performance process and services of land registry and cadastral performance procedures.
- Provides a base for an integrated planning by dealing with corporate functions and performance procedures with a reverse engineering approach.
- Ensures transformation between geographical data formats (e.g., GML) (Aydinoğlu and Tastan, 2015).

UNIFIED MODELLING LANGUAGE (UML)

This is a modelling language, developed by UML Grady Booch, James Rumbaugh and Ivar Jacobsen (Tuladhar, 2002). It was acknowledged as a standard in 1997 by Object Management Group (OMG). Modelling not only the application structure, behaviour and architecture but also performance processes and data formations, Unified/Integrated Modelling Language is a method, which is most widely used by OMG (Çoruhlu et al., 2015).

UML language is a common language, which is developed in order to be used in software development processes and that is used by different disciplines (Page-Jones, 2002; Fowler, 2003; Inan et al., 2010; Egenhofer and Frank, 1992; Çoruhlu et al., 2015). In view of Inan (2010);

today, solutions with respect to these issues can be ensured through the use of object oriented data modelling. These include the following:

- Ability to represent real world geometries,
- Ability to represent the same data at different conceptual levels in different details,
- Management of the backgrounds and versions of objects, and
- Management of measures with different sensitivity and accuracy together.

The consideration that the world consists of objects, which interact with each other in certain forms has been the source of inspiration for the emergence of object-oriented design concept (Çoruhlu et al., 2015). And the interaction between the objects is identified as holding them together thanks to direct or straight-forward relation and commands. Objects are classified based on the common commands likely to be applied to the objects (i.e., operations and procedures) or the common responds of objects to the commands (Inan, 2010). Today, this approach is also applicable to the design of object-oriented data modelling (Inan, 2010; Uçar and Kuşak, 2002; Çoruhlu et al., 2015).

In our country and the world, object-oriented modelling is intensely used a lot on the basis of land management practices (Aydinoğlu, 2009). In object-oriented data modelling, four

basic abstraction concepts (i.e., classification, generalisation/specialization, association, aggregation) are used (Egenhofer and Frank, 1992).

Packet diagram is used in UML, in order to reveal the structure of a performance system in a plain and comprehensible manner. Basically, UML covers the following diagram types:

Class Diagrams: Class is the common definition of community of objects with the same functions, same relations and same meaning. Classes are used to identify the fixed structure of the software.

Object Diagrams: Object is an example of the class. In this type of diagrams, objects formed from each class are included instead of the class.

State Diagrams: These are the diagrams to model the state of the real objects in any time and how such state has changed within time. In general, state diagrams are created not only for all objects but for the objects which are only complicated and behaviour of which diversify also according to the current state as well as the messages sent itself.

Sequence Diagrams: Class and object diagrams model the static information. However, the states, which change within time in real time systems are not indicated with these diagrams. In order to specify this type of states, which change in time, sequence diagrams, which deal with the communication of objects with each other based on time, are used.

Activity Diagrams: State of an object can be changes in time either by the user or the internal functions of the object itself. This order of change is indicated with activity diagrams.

Use Case Diagrams: Review of the habit of a program with the eye of the user is performed by means of use case diagrams. These diagrams are of capital importance in a system, which will be used by people in the real world.

Collaboration Diagrams: In the projects, which consist of many parts, it is essential that all parts fulfil their functions completely so that a procedure operates in accordance with its objective. Relation between these parts is indicated through collaboration diagrams.

Component Diagrams: Especially in the full-size projects, in which a great many people are employed, it is required to decompose the project. It must be ensured through correct modelling of the system that components work individually. This type of modelling is carried out via component diagrams.

Deployment Diagrams: Deployment diagrams are used at the stage in which it is planned how to deploy the software. These diagrams perform the physical examination of the system. Any and all details such as connections among the computers, machines on which the program will be installed, network and printer connections within the system are indicated through deployment diagrams.

Package Diagrams: Package diagrams are the diagrams that indicate the interaction between the systems in cases where there are sub-software or interacted side-systems to constitute the system in big software, and that briefly outline package side of system architecture.

UML use-case diagram in Figure 2 regarding the sales operation provides response to following questions such as; "which users make use of the states in some performance items" and "which states are included in assigned position of which organizations."

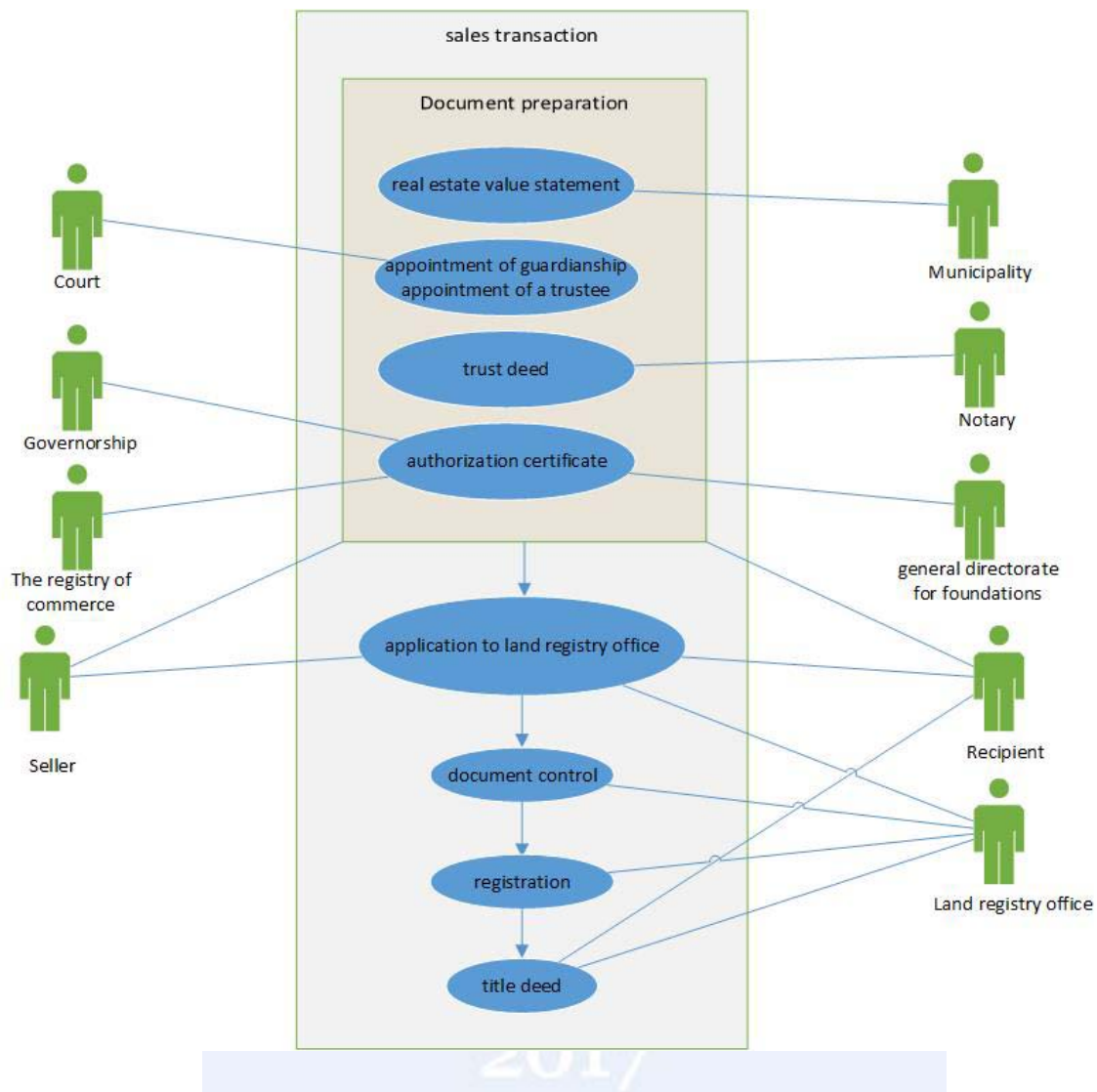


Figure 2. Visualization of sales operation with UML use-case diagram

Class diagrams in Figure 3 indicate the classes to represent the objects, required to be included in the system to develop the software regarding the sales operation and the relationship among these classes. Class diagrams are static. That is to say, they can only show the interaction of the classes with each other, it doesn't indicate what happens following these interactions. Among these classes; it is designated how the sales operation should be thanks to their relationship with each other either through the data, produced by GDTC or the data, produced by other organizations.

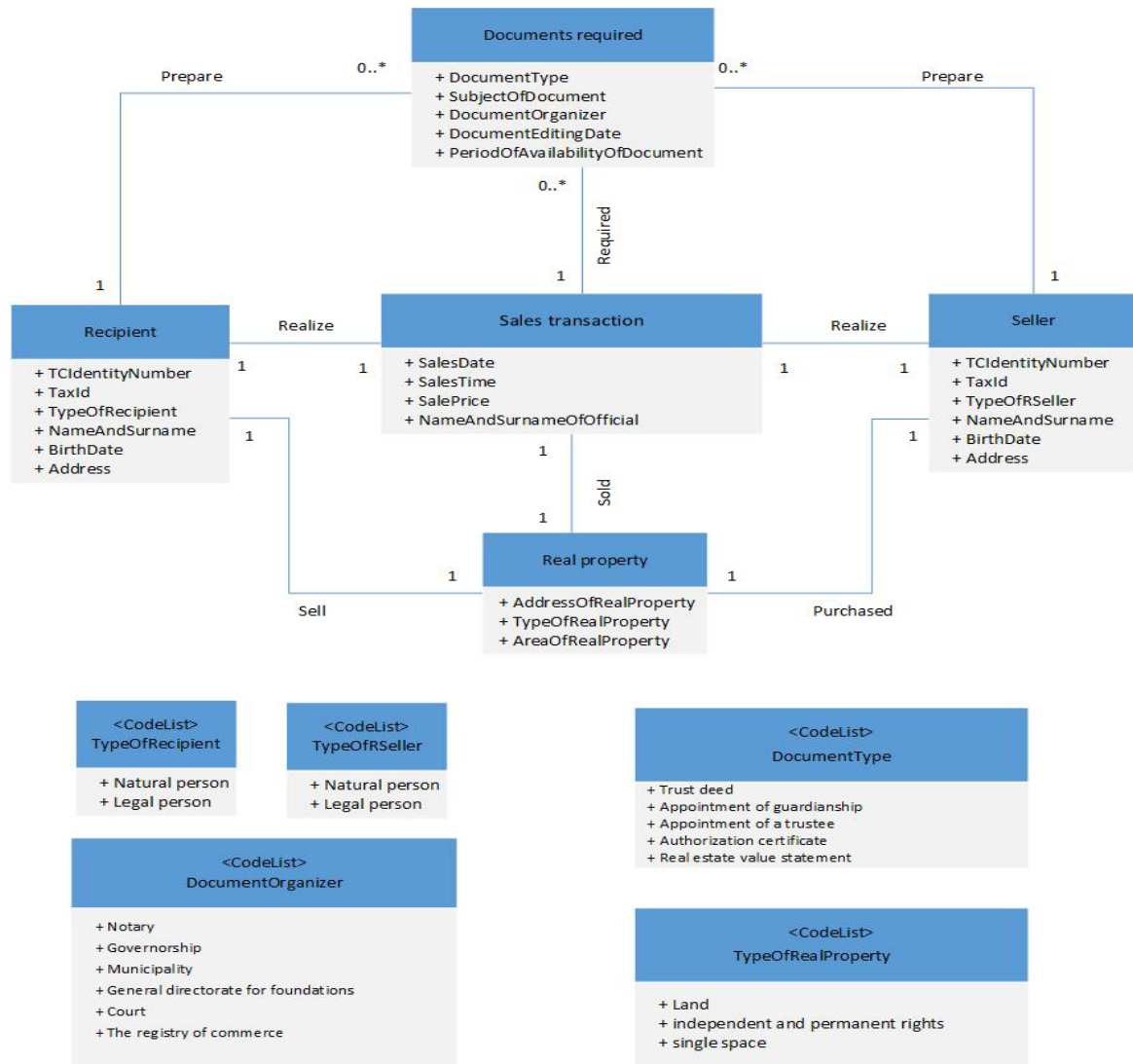


Figure 3. Visualization of sales operation with UML class diagram

CONCLUSIONS

In recent years; UML is actively used in different occupational disciplines especially in object-oriented software development. In this respect, the use of UML in property-based applications as well, and thus the design of geographic data base design has been easier. Thanks to this study in which UML diagrams are prepared for the users of UML, it makes it possible to understand the system and working principle of the system as it deals with the whole of the designed diagrams without a need to know the process, carried out in the directorates of land registry and cadastre.

REFERENCES

- Aydinoglu, A. Ç., Tastan, B., (2015), Developing Interoperable Geographic Data Model for the Mitigation Phase of Disaster Management, *FIG Working week 2015*, 17-21 May 2015, Sofia, Bulgaria.
- Çoruhlu, Y.E., İnan, H.İ., Yılmaz, H., Demir, O., (2015), Geographic Data Model of Foundation Immovable , *Sigma J Eng & Nat Sci* 33 (4), 539-559.
- Inan H.İ. (2010), “*Arazi İdare Sisteminin Tarım Bileşeni Olarak Konumsal Veri Modeli Geliştirilmesi*”, Doktora Tezi, Fen Bilimleri Enstitüsü, KTÜ.
- Uçar, D., Kuşak, L., (2002), Nesneye Dayalı Veri Modelinin Coğrafi Bilgi Sistemi Tasarımındaki Yeri, *Selçuk Üniversitesi Jeodezi ve Fotogrametri Mühendisliği öğretiminde 30. Yıl Sempozyumu*, 16-18 Ekim 2002, Konya.
- Tuladhar A.M., (2002) – “Why is Unified Modeling Language (UML) for Cadastral Systems?”, *International Institute for Geo-Information Science and Earth Observation*.
- Fowler, M., (2003) “*UML Distilled: A Brief Guide to the Standard Object Modeling Language* (3rd Edition)”, Boston, ISBN: 0-321-19368-7.
- Page-Jones, M., (2002) “*Fundamentals of Object-Oriented Design in UML*”, Addison-Wesley, Dorset House Publishing, New York, ISBN 020169946X.
- Inan, H.I., Sagris V., Devos W. ve diğerleri, (2010). “Data model for the collaboration between land administration systems and agricultural land parcel identification systems”, *Journal of Environmental Management*, vol.91, no.12, 2440-2454.
- Egenhofer, M. J. ve Frank, A. U., (1992). “Object-Oriented Modeling for GIS”, *URISA Journal*, 4, 2, 3-19.

ISGGG
2017

Strip Adjustment of Mobile Mapping Point Clouds: Case Study in Istanbul Technical University (ITU) Ayazaga Campus

R. Alper Kuçak^{*1}, Serdar Erol¹

¹ Department of Geomatics Engineering, Istanbul Technical University, Ayazaga Campus, 34469, Turkey. e-mail: kucak15@itu.edu.tr, erol@itu.edu.tr

ABSTRACT

Mobil LIDAR (Light Detection and Ranging) systems include several laser scanners and multi-view cameras, IMU (Inertial Measurement Unit) and GNSS (Global Navigation Satellite System) systems. All of these systems work cooperatively to generate the point clouds in three dimensional (3D) geodetic coordinate system. The point clouds, obtained from multiple scans, are overlapped. Especially, the LIDAR systems having multiple laser scanners may suffer from noise and other error sources such as inertial drift, GNSS error sources, rigid platform calibration etc. The measurements with multiple scanners in Mobile mapping require calibration in order to overcome the disadvantages by high noise rates as well as the overlapping problem in strips. The calibration process is proceeded between Laser and IMU, CCD (Charge Coupled of Device) Camera and Laser Scanner or GNSS receiver and carried out along the scanning boresight. After the calibration steps, CCD Camera and Laser scanners can become ready to use. However, the calibration may not be sufficient to eliminate all errors and provides an appropriate point cloud for modelling. In such situations, registration between LIDAR point clouds, which is called “strip adjustment” is applied. The strip adjustment is a critical process for generating a useable point clouds. In this paper, we focus and aim to solve strip adjustment problem for point cloud registration. For this reason, a case study is carried out in the Ayazaga campus of Istanbul Technical university (ITU). The point clouds of Ayazaga campus are produced using Riegl VMX-450 Mobile Mapping System. Using Cloud Compare and Matlab platforms, the point clouds are registered in different regions for the unique case study area. In conclusions, the preliminary results are evaluated by means of feasibility and the potential of the approach for strip adjustment is clarified. Koyuncu Harita ve Mühendislik Company is acknowledge for providing the mobile mapping systems to the study.

INTRODUCTION

Mobil LIDAR (Light Detection and Ranging) systems include several laser scanners and multi-view cameras, IMU (Inertial Measurement Unit) and GNSS (Global Navigation

^{*}Corresponding Author

Satellite System) systems. All of these systems work cooperatively to generate the point clouds in three-dimensional (3D) geodetic coordinate system. The point clouds, obtained from multiple scans, are overlapped. Especially, the LIDAR systems having multiple laser scanners may suffer from noise and other error sources such as inertial drift, GNSS error sources, rigid platform calibration etc. The measurements with multiple scanners in Mobile mapping require calibration in order to overcome the disadvantages by high noise rates as well as the overlapping problem in strips. However, the calibration may not be sufficient to eliminate all errors and provides an appropriate point cloud for modelling. In such situations, registration between LIDAR point clouds, which is called “strip adjustment” is applied.

MLS is a product of the latest technology towards low cost and fast acquisition of 3D spatial data. It is not an obvious issue that is the boresight alignment accuracy of MLS systems. However, this may be the lack of calibration for the realization of appropriate and effective practice workflows in existing systems on the market. These misalignments frequently appear in MLS system and are derived from the axes of the single units cannot be mechanically aligned and structural errors of every mechanical installation. (Rieger, P., et al., 2010)

In Mobile LiDAR Systems (MLS), the planar surfaces scan at least some times at different angles to each other, routed through buildings. For example, MLS vertically aligned according to the driving direction, the street of facades and the roofs on the left side scans the left as shown in the sketch (Figure 1). After completing the first strip scan, the 3D laser scanner is rotated 180 degrees and the axis of the frame of the vehicle is being driven in the reverse direction to perform a second strip scanning. Thus, the left side of the street, scanned again as shown in Figure 1. This process is the picture on the right as shown in the drawing, the laser at different angles both on the street and in the direction of driving of the strip can be repeated several times. (Rieger, P., et al., 2010)

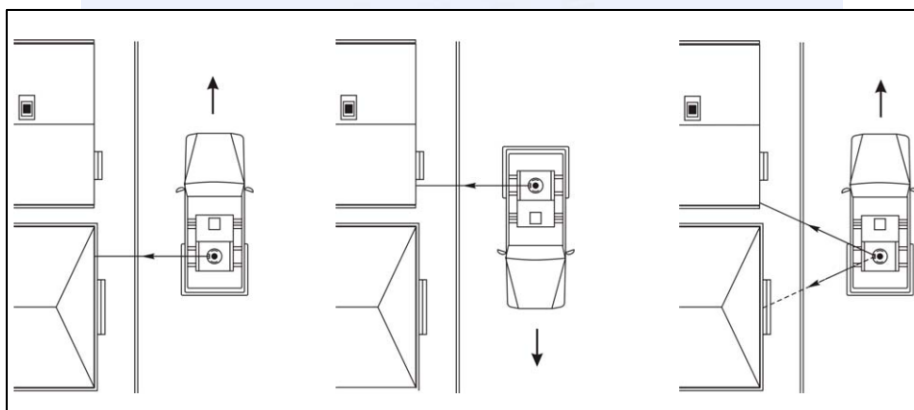


Figure 1. Mobile scanning of facades from different driving- and scanning directions (Rieger, 2010).

The strip adjustment methods are based on a 3D transformation for point cloud datasets. The well-known Iterative Closest Point (ICP) algorithm (Besl and McKay, 1992) has evolved a lot in recent years and are increasingly used in computer vision for registering 2D/3D curves and range images. It can provide robust solutions, if the surface details appropriate the case in strip adjustment. The ICP algorithm finds the best transformation by calculating three-dimensional rigid body translation and rotation parameters of the transformation again and again, by selecting correspondences between the sets. (Toth, C. K. 2009).

In this paper, we focus and aim to solve strip adjustment problem for point cloud registration. For this reason, a case study is carried out in the Ayazaga campus of Istanbul Technical university (ITU). The point clouds of Ayazaga campus are produced using Riegl VMX-450 Mobile Mapping System. Using Cloud Compare and Matlab platforms, the point clouds are registered with 3D Helmert transformation and ICP in different regions for the unique case study area. In conclusions, the preliminary results are evaluated by means of feasibility and the potential of the approach for strip adjustment is clarified.

DATA and METHOD

The Study Area

ITU (Istanbul Technical University) Yılmaz Akdoruk Student Dormitory were selected as study area which is located in Ayazaga Campus of ITU in Turkey. But, All of The Campus was scanned with Riegl VMX 450 Lidar System (Figure 2).



Figure 2. Yılmaz Akdoruk Student Dormitory



Figure 3. ITU Ayazaga Campus Riegl VMX 450 Scanning

Mobile Mapping Data was determined by “Riegl VMX 450 Lidar System” which can get 1,000,000 points per second with 8 mm accuracy until 50 m and measure with impulse method (Figure 3).

3D Similarity Transformation

3D Similarity Transformation is known as the Helmert transformation often used in geodesy (Figure 4). It refers to the transformation involved in changing the coordinates of a point set with respect to one reference system to make them transform to another reference system and this process involves rotation, scaling and translation. It is named after Professor Dr. Friedrich Robert Helmert, who lived from 31 July 1843 to 15 June 1917. He was director of the geodetic institute in Potsdam, Germany, from 1886 to 1917, and a Professor at the University of Berlin. He is known as the founder of the mathematical and physical theories of modern geodesy (URL 1). Helmert transformation is consisted of the fundamental of ICP Algorithm for registration. Also, it is used for the initial registration process of point clouds. The registration of point clouds involves the estimation of the 3D Helmert transformation parameters (i.e., scale factor, three translations, and three rotation angles) relating the combination of the different point clouds (Al-Durgham and Habib 2014). Depending on the accuracy of the estimated transformation parameters, registration processes are classified coarse or fine registration techniques (Matabosch et al. 2005). Initial registration techniques are preferred to establish rough alignment between the different point clouds. Fine registration, on the other hand, starts from coarsely initial registration to achieve more accuracy registration of the point clouds (Fangning and A.Habib, 2016).

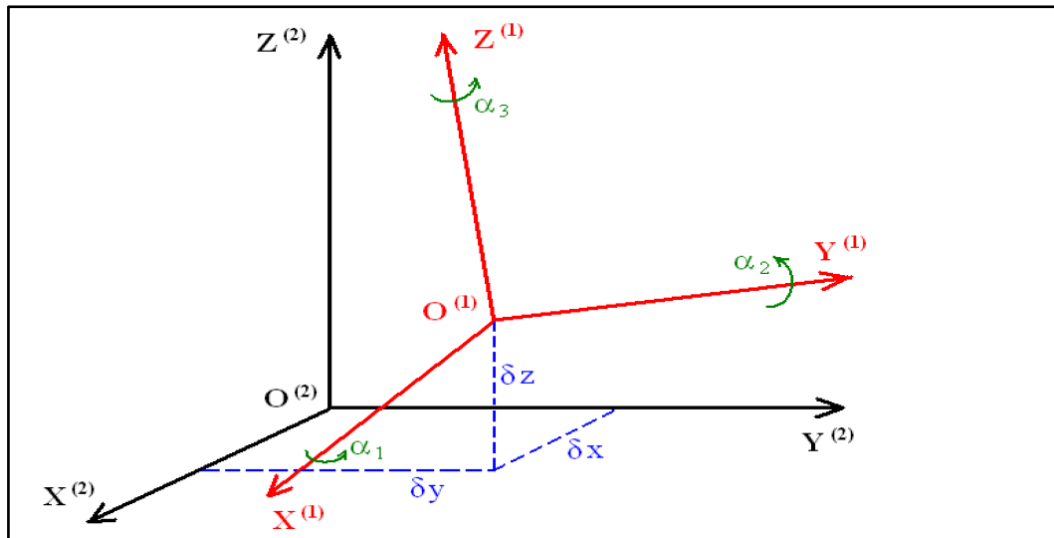


Figure 4. 3D Similarity Transformation

Especially, the entitled seven-parameters Helmert transformation applies to point sets p_i , q_i , $i=1\dots n$. So we can write as for points Equation 1 and Helmert Transformation process is done by the following mathematical model (Equation 2).

$$p_i = X_i^2, Y_i^2, Z_i^2 \quad \text{and} \quad q_i = X_i^1, Y_i^1, Z_i^1 \quad (1)$$

$$\begin{bmatrix} X_i^2 \\ Y_i^2 \\ Z_i^2 \end{bmatrix} = \begin{bmatrix} \delta_x \\ \delta_y \\ \delta_z \end{bmatrix} + s \cdot R(\alpha_1, \alpha_2, \alpha_3) \cdot \begin{bmatrix} X_i^1 \\ Y_i^1 \\ Z_i^1 \end{bmatrix} \quad (2)$$

Transformation parameters are a scale (s), three rotations R and three translations (T_δ). As a result, the seven parameters are s, R^3, T_δ^3 (Equation 2). If the rotation matrix (R) is orthogonal, its inverse is equal to its transpose. After terms of the matrix q_i multiply with a scale factor s and R rotation matrix by using this rule, translations T (δ_x, δ_y and δ_z) are added to translate to a new coordinate system (Watson, 2006).

ICP (Iterative Closest Point)

The iterative closest point (ICP) algorithm is adaptable for sets of points, sets of line segments, sets of parametric curves, sets of implicit curves, sets of triangles, sets of parametric surfaces. In the description of the algorithm, a "data" shape P is registered to be in best alignment with a "model" shape X . The data shape and model can be represented in one of the allowed formats. If the form has already been determined, the data path should be decomposed into a set of points. The points to be used for triangle and line sets are the vertices and the endpoints, and if the data shape comes in a surface or curve form, then the vertices and endpoints of the triangle/line-approximation are used. The curve and surface

closest-point evaluators implemented in our system require a framework of lines or triangles to yield the initial parameter values for the Newton's iteration; therefore, the number N is still relevant for these smooth entities but varies according to the accuracy of the approximation (Besl & McKay, 1992).

The distance “d” between an single data point \vec{p} and a point cloud model X is shown as below(3).

$$d(\vec{p}, X) = \min_{\vec{x} \in X} \|\vec{x} - \vec{p}\| \quad (3)$$

The closest point in X that yields the minimum distance is represented \vec{y} such that $d(\vec{p}, \vec{y}) = d(\vec{p}, X)$ where $\vec{y} \in X$. After calculating the closest point is O (Nx), the nearest points are calculated for each point in P, that process is O (Np, Nx). Let Y represent the resulting set of closest points and let C be the closest point operator (4):

$$Y = C(P, X) \quad (4)$$

Given the resultant corresponding point set Y, the least squares registration is computed as described above:

$$(\vec{q}, d) = Q(P, Y) \quad (5)$$

The positions of the data shape point set are then updated via $P = \vec{q} P$ (5) which means apply the registration vector to the point set P. The iteration is initialized by adjusting $P_0 = P$, The registration vectors are defined according to the initial points P_0 so that the final registration represents the complete transformation.(Besl & McKay, 1992)

The algorithm proceeds as follows (Figure 5):

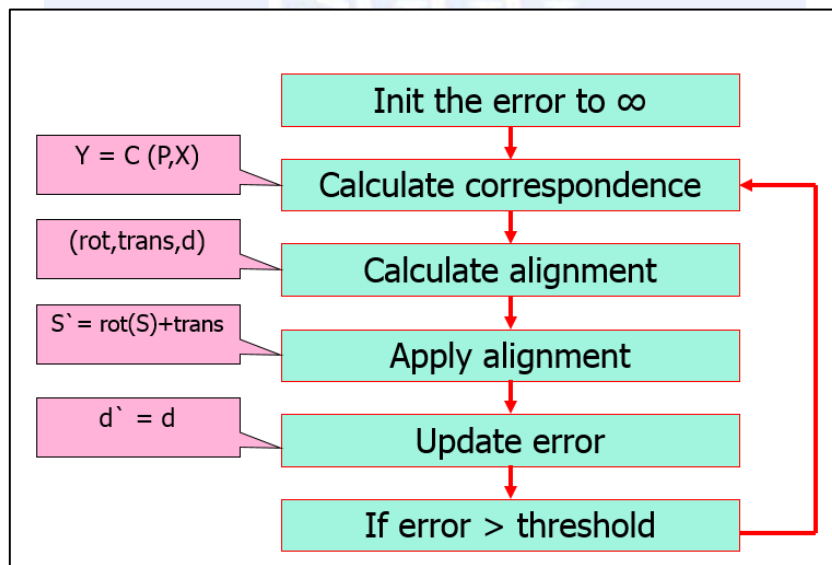


Figure 5. ICP algorithm proceeds (URL 2)

When the average square error change falls below a predetermined threshold ($\tau > 0$), it ends the iteration to indicate the desired sensitivity of the recording: $d_k - d_{k+1} < \tau$. If a zero-dimensional threshold is accepted, one can replace $\tau \sqrt{\text{tr}(\sum x)}$ where the square root of the trace of the covariance of the model shape indicates the rough size of the model shape. (Besl & McKay, 1992)

RESULTS

In this case study, mobile mapping data strip adjustment problem was solved with ICP Algorithm. As shown in Figures 6 and 7, there are a number of reasons for the differences between the forward and backward scans in mobile mapping data. We can eliminate the scan differences of these same surfaces with the ICP algorithm. 5-6 cm difference between the scans is combined with registration accuracy below 1 cm RMS by selecting a scan reference and the accuracy within the model is always preserved. This is a good solution for point cloud modelling.

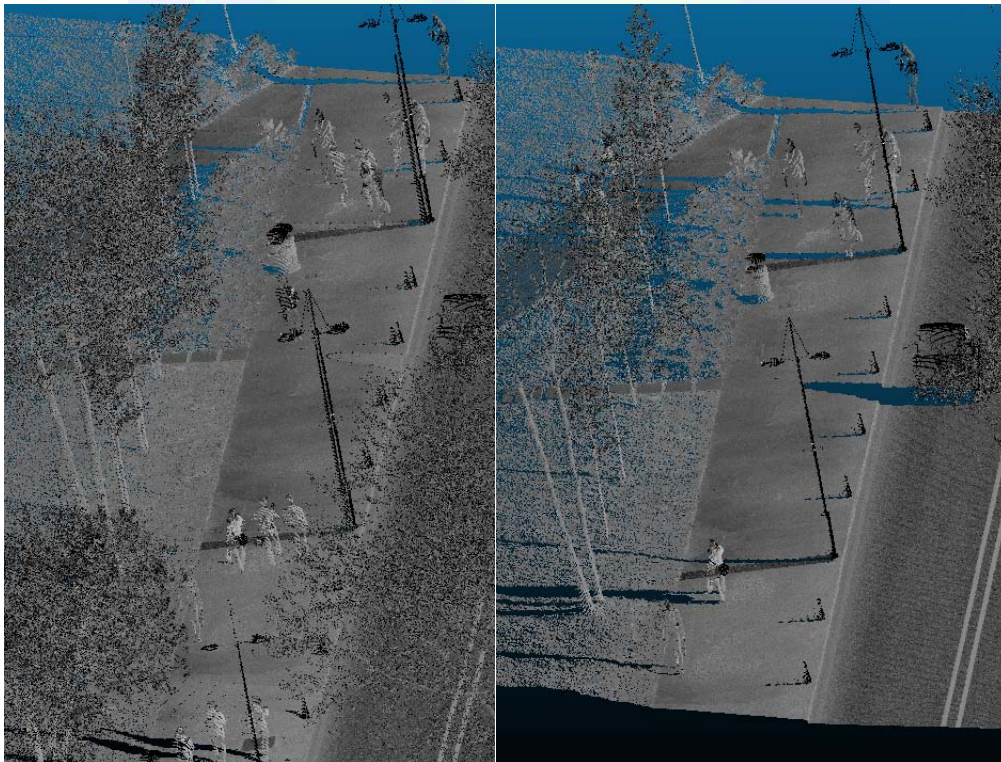


Figure 6. ICP(Besly and McKay,1992) Before and After ITU Street

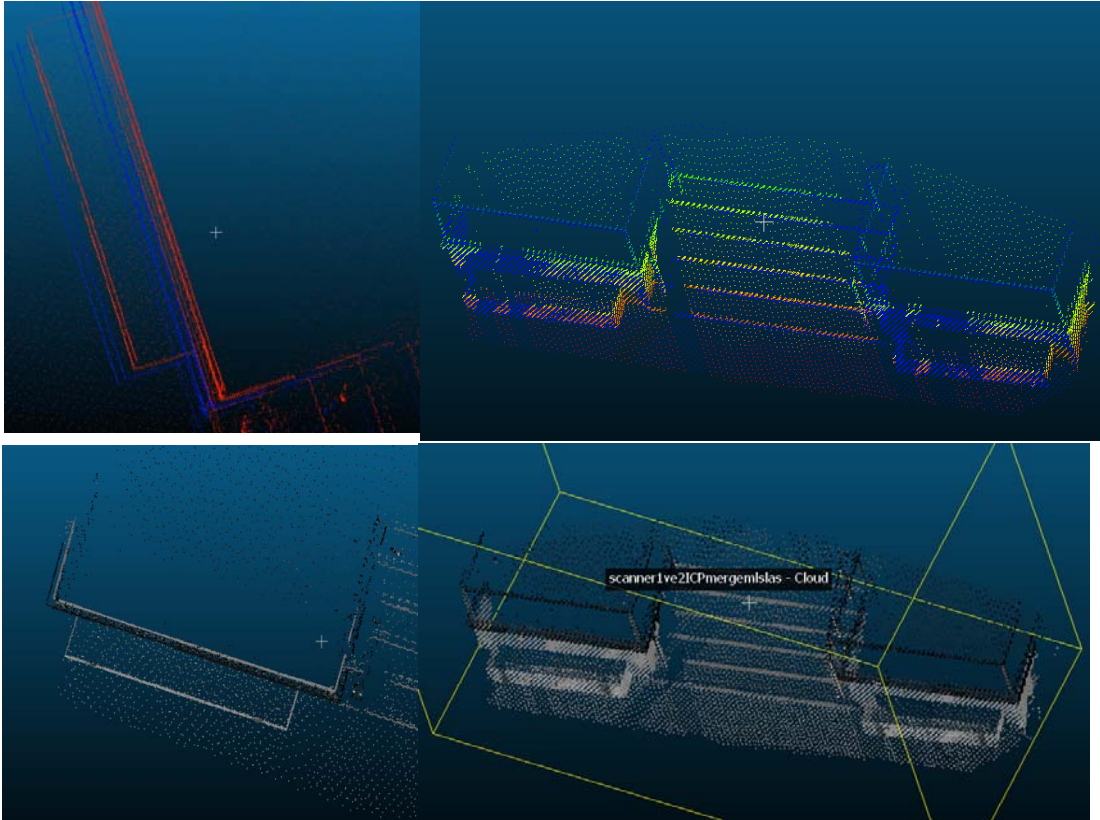


Figure 7. ICP (Besly and McKay,1992) Before and After (Yılmaz Akdörük Dormitory Stairs)

As shown in Figures 8, ICP Algorithm can register point cloud strips easily, but it is important that when ICP apply the data, initial alignment is very important for fine registration.

ISGGG
2017

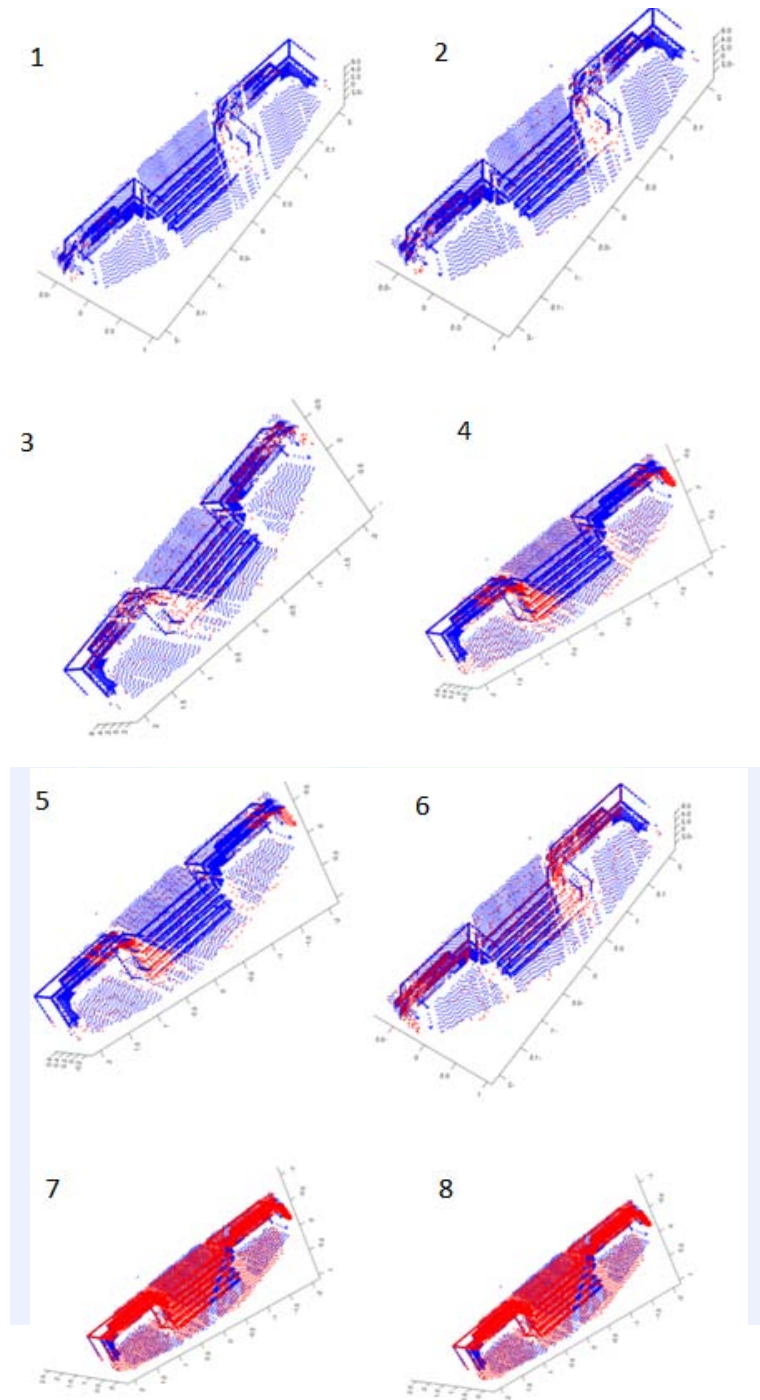


Figure 8: Step by step ICP Registration with MATLAB

After the initial registration had applied, the fine registration was done with ICP Algorithm. Hence, RMS value was found 0.01 m. These values are acceptable results for ICP registration.

CONCLUSIONS

In this paper, ITU (Istanbul Technical University) Yılmaz Akdoruk Student Dormitory were selected as study area. It is located in Ayazaga Campus of ITU in Turkey. It was

scanned with MLS systems. On the other hand, 3D Helmert transformation was used for initial registration process. Computed transformation parameters were used for the initial Registration Process and the performance of point cloud fine registration is given statistically and visually to compare the results.

After transformation parameters had been estimated, the fine registration was done with ICP Algorithm. 0.05 – 0.06 m differences between strips reduced until 0.01 m for the point cloud data of Yılmaz Akdoruk Student Dormitory stairs. These values are acceptable results for ICP registration.

Current research about ICP Registration process helps us to understand the existing problems in Strip Adjustment.

ACKNOWLEDGMENTS

Koyuncu Harita ve Mühendislik Company is acknowledge for providing the mobile mapping systems to the study.

REFERENCES

- Al-Durgham, K., and Habib, A. (2014). "Association-matrix-based sample consensus approach for automated registration of terrestrial laser scans using linear features." *Photogramm. Eng. Remote Sens.*, 80(11), 1029–1039.
- Besl, P. J., & McKay, N. D. (1992). Method for registration of 3-D shapes. Paper presented at the Robotics-DL tentative.
- Habib, A. F., and Alruzouq, R. I. (2004). "Line-based modified iterated Hough transform for automatic registration of multi-source imagery." *Photogramm. Rec.*, 19(105), 5–21.
- Matabosch, C., Salvi, J., Fofi, D., and Meriaudeau, F. (2005). "Range image registration for industrial inspection." *Electronic Imaging 2005*, International Society for Optics and Photonics, San Jose, CA, 216–227.
- Rieger, P., et al., 2010. "Boresight alignment method for mobile laser scanning systems." *Journal of Applied Geodesy*, 13-21.
- Watson, G. (2006). Computing helmert transformations. *Journal of Computational and Applied Mathematics*, 197(2), 387-394.
- Toth, C. K. (2009). "Strip adjustment and registration" *Topographic Laser Ranging and Scanning-Principles and Processing*, 235-268.
- URL 1: <http://www.w-volk.de/museum/memori02.htm>
- URL 2: <http://www.slideshare.net/PankajGautam28/iterative-closest-point-algorithm-analysis-and-implementation>

GIS & Three-Dimensional Modelling for Cultural Heritages

Murat Yakar^{*1} and Yusuf Doğan²

¹Department of Geomatics Engineering, Mersin University, Ciftlikköy Campus, 33343, Turkey. (e-mail: myakar@mersin.edu.tr)

²Institute of Science, Selcuk University, Alaaddin Keykubat Campus, 42003, Turkey.

ABSTRACT

Cultural heritages are history of the nations and history forms identity of the nations. Therefore, protection of cultural heritages means protection of history and identity of the nations. Identification of current status of cultural heritages is important for documentation, preservation and using as a base for restoration. Documentation studies need robust and scientific methods. GIS and photogrammetry is the most commonly used scientific methods to documenting cultural heritages recently. In the documentation studies, processing information of historical monuments on computer according to GIS and documenting in three-dimensional with digital terrestrial photogrammetry is one of the main methods.

In this study for documentation, all data of forty-six historical monuments located in Silifke/Mersin were collected and transferred to database so it is made queryable. Some of those heritages were reconstructed as 3D model by using photogrammetric technics. Finally, 3D Models were integrated into the system for presentation.

INTRODUCTION

Cultural Heritage (CH) structures play an important role in sustaining the relationship between man and his past. In order to preserve cultural heritage assets for the next generations, fast and accurate documentation of structures and their surrounding areas based on scientific techniques need to be developed (Kivilcim & Duran, 2016). Cultural heritages are history of the nations and history forms identity of the nations. Therefore, protection of cultural heritages means protection of history and identity of the nations. Identification of current status of cultural heritages is important for documentation, preservation and using as a base for restoration. The topic of the documentation and conservation of the cultural heritage is well established in the contemporary society (Lezzerini et al., 2016). Correct documentation is necessary not only for posterity but also in functionality in contemporary usage and re-evaluation of the historical buildings. Photogrammetry uses only photographs and mathematical equations. These are important in view of correct and accurate measurement of cultural heritage (Yilmaz, Yakar, Gulec, &

^{*} Corresponding Author

Dulgerler, 2007). Digital photogrammetry can significantly cut the time spent developing the documentation and conservation plans (Waas & Zell, 2013).

Traditional survey and conventional architectural representation are typically 2D visualizations of an object that consists of plans, sections, profiles and rectified images. To understand the object comprehensively, one has to extract 2D information and to build a 3D geometry simulation in their mind (Hanan, Suwardhi, Nurhasanah, & Bukit, 2015). A series of photos from an object can be sufficient for constructing a 3D model of the object. The technique for such reconstruction, called photogrammetry, has been used profusely in graphical and numerical documentation in cultural heritage, particularly in historical buildings (Reinoso, Moncayo, & Barrera, 2014). Photogrammetry is an independent method in the documentation process. This method is based on at least two images with overlapped data, which guarantee the triangulation process. The aim of digital close-range photogrammetry is making the process of recording and processing data simpler and faster. This method is an accurate technique for documenting color and texture, and providing metric data of objects with different size and complexity in a relatively short time. This technique can be used when the access to the object is limited, or when the direct measuring on the object would threaten it (Hassani, 2015).

GIS includes software and hardware tools, and a group of procedures elaborated to facilitate the capture, edition, administration, manipulation, analysis, modelling, representation and the exit of spatial referenced and semantic data, to solve any type of planning, administration, storage, and further information concerning the problem. GIS technology greatly facilitates the inventory, evaluation, preservation, and documentation of archaeological sites and historical structures. As heritage conservation becomes more holistic and historic sites are steadily becoming integrated with the surrounding landscapes, GIS has been recognized as a critical component in the development of virtual historic collections and archives (Toz & Duran, 2004).

The history of Silifke dates back to ancient times. Despite the fact that various societies were known to exist around Silifke 8000 years ago, there is no exact information about the identity of these early societies. There were many nation that lived around the Silifke from these ancient times to present day (Bakar & Demir). All those nations have left various heritages but especially from Roman and Byzantine period there are much more heritages.

This paper presents a study about documentation of cultural heritage of Silifke where is rich in CH and integration to GIS. In documentation study inventory has been created as attribute data and spatial data has been produced (point, line, and polygon). Finally, 3D model of some CHs have been generated and all data integrated to the GIS.

MATERIALS AND METHODS

In the scope of this study, the following activities were performed:

- Data acquisition
- Design of GIS
- Photogrammetric works

Data acquisition

Before the acquiring data in the field, the study area has been detected as Silifke/Mersin in Turkey. The information of Cultural Heritages of this city such as position, age, and historical information etc. were researched from different sources (web sites, local government, museum, books and citizens etc.). In the light of this research 46 CHs have been detected and route plan has been prepared. Canon PowerShot SX 220 HS digital compact camera, Topcon GPT 3007 Total Station and Magellan SporTrak Pro hand-held GPS device have been provided to collect data from the field. All the CHs were visited according to route plan and photographs were taken while coordinates were in ED50 Datum by hand-held GPS device. It is seen in the investigation and detection studies that CHs of Silifke are mostly from the Hellenistic, Roman and Byzantine periods. The monumental tombs built at that time were better able to withstand and reached to daylight than the other heritages. Ancient cities are a ruin and a pile of stones view right now.

Design of GIS

The information system we want to create has been designed by ArcGIS software the Silifke district boundary has been digitized with polygon tool, all the roads have been digitized with polyline tool and all the settlements and villages have been positioned with point tool since it will be based on analysis of information such as location, transportation information of CHs. Acquired coordinates of CHs from the field have been imported into the system. All those data have been inputted to an excel table to create a database.

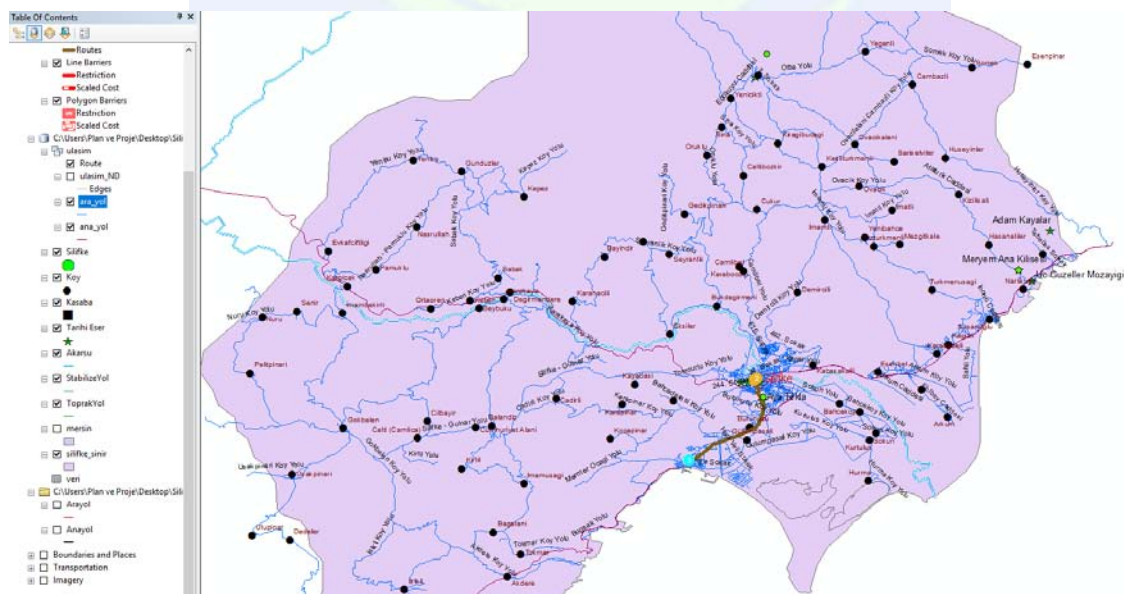


Figure 1. Digitized boundary, roads, streams and settlements

Table has been formed with these columns; ID, CH name, settlement, UTM coordinates, geographic coordinates, elevation, datum, period, year, century, architecture, restoration

age and restorer (Figure 3). Network Dataset has been created to solve the shortest way to CHs from any point. Street names, types and directions (one way or double) have been inputted one by one to 3757 polylines for accurate navigation. The system was made operational by using a lot of network analyze test in different query probabilities. In addition, every digital object created with database table. Having multiple tables prevents duplicating information in the database, because you store the information only once in one table (ESRI, 2017). Database tables have been related to each other to pull the data together in meaningful ways.

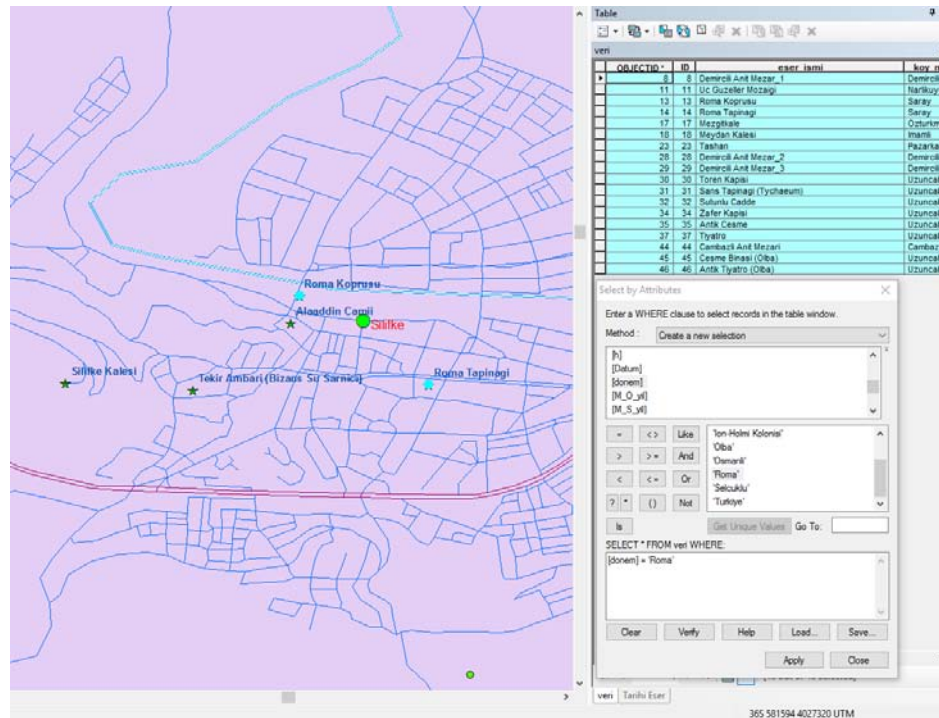


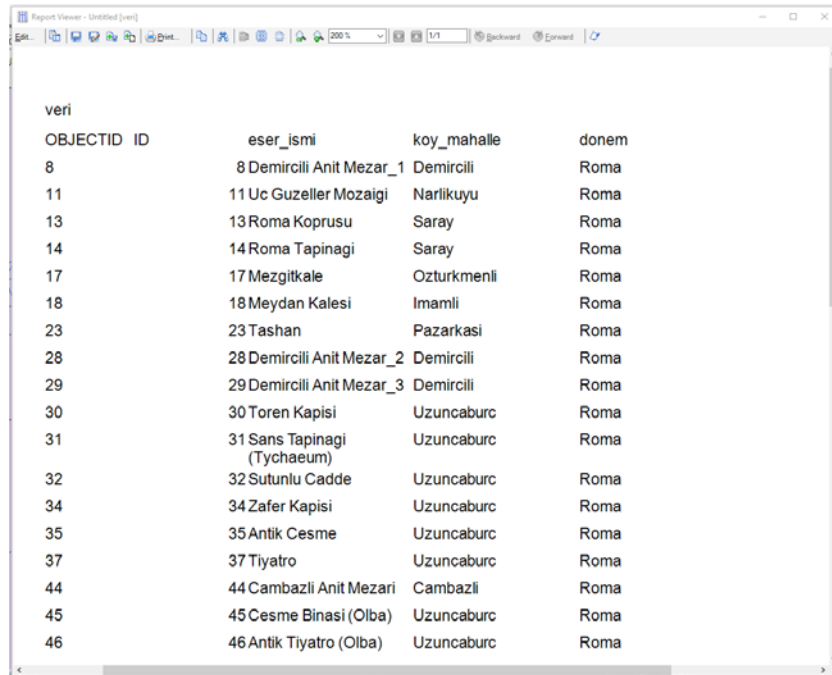
Figure 2. Query of Roman Period CHs by Using Select by Attributes Menu

OB	ID	eser_ismi	koy_mahalle	Y 3	X 3	Y 6	X 6	phi	lamda	h	Datum	dönem
1	1	Meryem Ana Kilisesi	Narlıkuyu	59900	403459	59896	403297	36° 26' 12".87	34° 6' 15".14	196.38	WGS84	Bizans
2	2	Aya Tekla	Mukaddem	58357	402627	58354	402466	36° 21' 48".30	33° 55' 52".45	110.62	WGS84	Bizans
3	3	Aphrodisias Antik Kenti	Yesilovacik	56213	400323	56210	400163	36° 9' 26".85	33° 41' 25".67	59.16	WGS84	Ion-Holmi Kolonis
4	4	Cambazli Kilisesi	Cambazli	59248	404981	59244	404820	36° 34' 29".22	34° 1' 59".72	975.15	WGS84	Bizans
5	5	Karakabakli Antik Kenti	Karadedeli	59110	403380	59106	403219	36° 25' 50".23	34° 0' 57".48	446.44	WGS84	Bizans
6	6	Kulesir	Karadedeli	58913	403625	58910	403464	36° 27' 10".46	33° 59' 39".61	601.41	WGS84	Bizans
7	7	Isikkale Antik Kenti	Karadedeli	59035	403480	59031	403319	36° 26' 22".92	34° 0' 27".79	508.43	WGS84	Bizans
8	8	Demircili Anit Mezar_1	Demircili	58597	403545	58594	403383	36° 26' 45".29	33° 57' 32".25	761.44	WGS84	Roma
9	9	Uzuncaburç (Dokaisereia) Antik Kenti	Uzuncaburç	58285	405071	58281	404909	36° 35' 1".40	33° 55' 32".68	1246.19	WGS84	Helenistik
10	10	Olba Antik Kenti	Uzuncaburç	58638	405081	58635	404919	36° 35' 3".42	33° 57' 54".97	1244.16	WGS84	Helenistik
11	11	Uc Guzeller Mozaigi	Narlıkuyu	59975	403358	59971	403196	36° 25' 39".90	34° 6' 44".74	59.39	WGS84	Roma
12	12	Tekir Ambari (Bizans Su Sarnici)	Pazarkasi	58266	402761	58262	402599	36° 22' 32".03	33° 55' 16".19	94.60	WGS84	Bizans
13	13	Roma Koprusu	Saray	58302	402800	58299	402639	36° 22' 44".82	33° 55' 30".90	69.59	WGS84	Roma
14	14	Roma Tapinagi	Saray	58351	402764	58348	402603	36° 22' 32".92	33° 55' 50".58	80.59	WGS84	Roma
15	15	Silike Kalesi	Pazarkasi	58230	402766	58227	402605	36° 22' 34".05	33° 55' 2".05	205.60	WGS84	Olba
16	16	Tokmar Kalesi	Tokmar	56925	401428	56922	401267	36° 15' 23".57	33° 46' 14".04	512.92	WGS84	Selcuklu
17	17	Mezgitkale	Ozturkmenli	59206	403787	59203	403625	36° 28' 1".81	34° 1' 37".91	544.36	WGS84	Roma
18	18	Meydan Kalesi	Imamli	58741	404101	58737	403939	36° 29' 45".24	33° 58' 32".24	848.33	WGS84	Roma
19	19	Gokburç	Ovacik	59040	404238	59036	404076	36° 30' 28".74	34° 0' 32".94	978.29	WGS84	Bizans
20	20	Resadiye Camii	Saray	58369	402773	58365	402612	36° 22' 35".82	33° 55' 57".56	79.59	WGS84	Osmanli

Figure 3. Database Table about CHs

Once the whole system has been designed, network analyze, query by feature, exporting scale maps, integration with hyperlink the documents such as photographs, inventory and 3D models has been completed.

In the above figures, Roman period CHs have been detected and network analyze has been created among these heritages.



veri	OBJECTID	ID	eser_ismi	koy_mahalle	donem
	8		Demircili Anit Mezar_1	Demircili	Roma
	11		Uc Guzeller Mozaigi	Narlikuyu	Roma
	13		Roma Koprusu	Saray	Roma
	14		Roma Tapinagi	Saray	Roma
	17		Mezgitkale	Ozturkmenli	Roma
	18		Meydan Kalesi	Imamli	Roma
	23		Tashan	Pazarkasi	Roma
	28		Demircili Anit Mezar_2	Demircili	Roma
	29		Demircili Anit Mezar_3	Demircili	Roma
	30		Toren Kapisi	Uzuncaburc	Roma
	31		Sans Tapinagi (Tychaeum)	Uzuncaburc	Roma
	32		Sutunlu Cadde	Uzuncaburc	Roma
	34		Zafer Kapisi	Uzuncaburc	Roma
	35		Antik Cesme	Uzuncaburc	Roma
	37		Tiyatro	Uzuncaburc	Roma
	44		Cambazli Anit Mezari	Cambazli	Roma
	45		Cesme Binasi (Olba)	Uzuncaburc	Roma
	46		Antik Tiyatro (Olba)	Uzuncaburc	Roma

Figure 4. Report for Roman CHs as a Result of Query

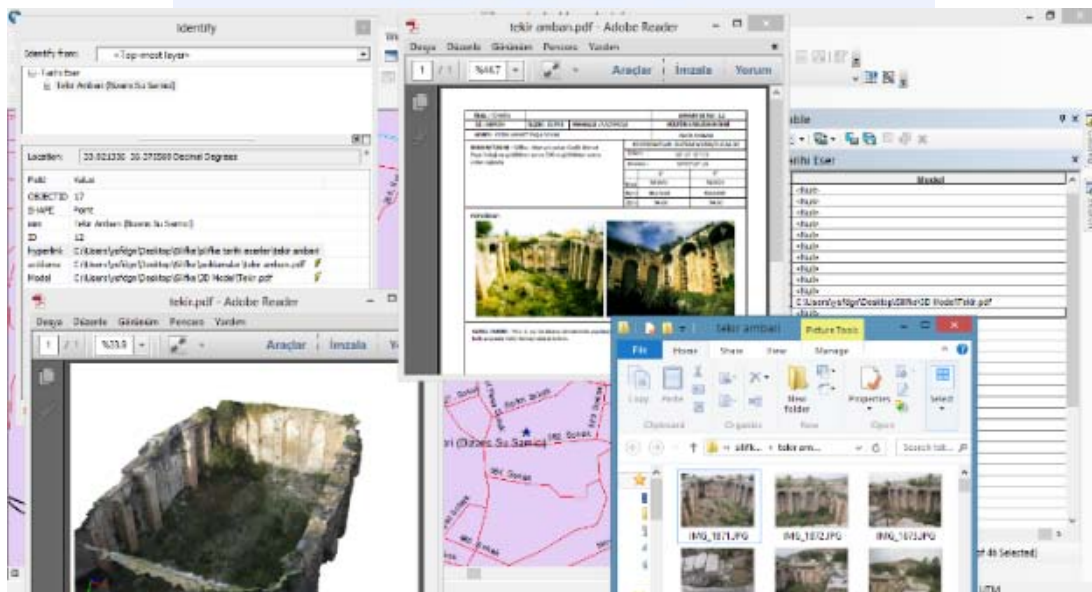


Figure 5. Calling Data Integrated with Hyperlink

Photogrammetric Works

Photogrammetric works are carried out in two places; field and office. The field step of the works aims to obtain data belong to structure by photogrammetric methods. These data consist of surveying techniques based on geodetics and photographs taken by photogrammetric methods.

In this study we surveyed three monumental tomb in Silifke; Mezgitkale, Öterkale and Korinth style Imbriogion monumental tombs. Polygon points were set up as closed traverse on different places where each façades of structures could be seen and they were facing each other. So that the surveying of each side could be possible. Measurement was carried out by Total Station on every single point in local coordinate system that we defined, then point coordinates were calculated by closed traverse calculation. The coordinates of about ten points on each façade were measured by using marker sheet taped on the structure or specific details on the wall of structure.

Attention was paid to make the photographs overlapped each other by taking plenty of photographs from all around the structure. The photographs high rated overlapped are quite successful to generate more quality and detailed 3D model.

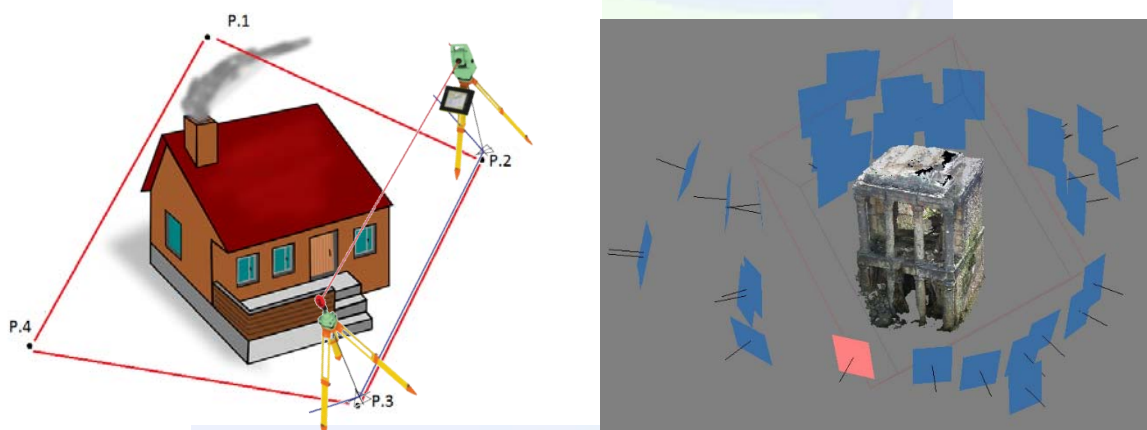


Figure 6. Setting up Closed Traverse and Positions of Camera during data acquisition

The calibration of the Canon SX220 HS digital camera was accomplished using PhotoModeler and several images of calibration sheet supplied by the software. The photographs and the reference points acquired were imported into the software. Reference points were marked on the structure which taped in the field works. Referenced photographs were oriented and adjusted to measure and to draw on the photographs. 3D models of structures were generated by drawing corners and specific details on the photographs.

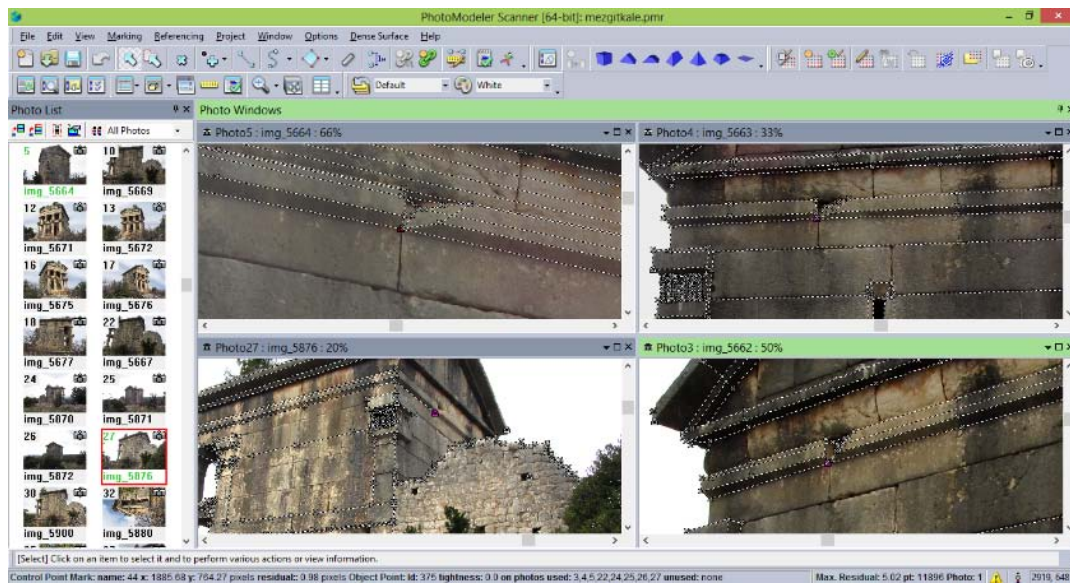


Figure 7. Drawing details from photographs

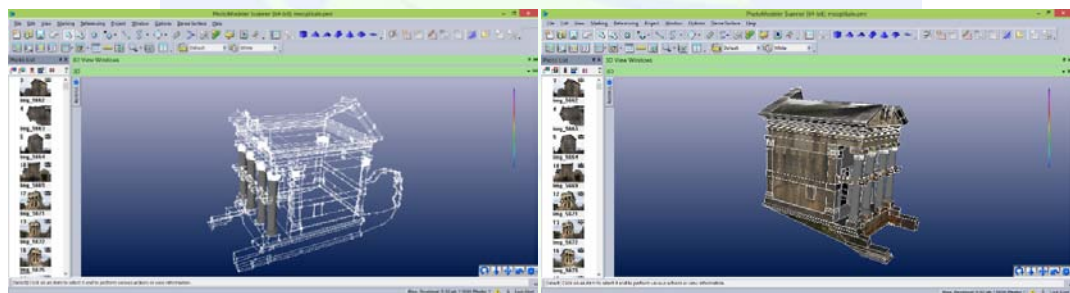


Figure 8. 3D wireframe model of Mezgitkale and 3D textured model of Mezgitkale

The other photogrammetric software to generate 3D model we used is AgiSoft PhotoScan. This is a software that generates point cloud from images. It has a quite usable interface and generates 3D model in several simple step. The software also need camera calibration but it is not necessary pre-calibration even it is available to process the photographs. Because camera calibration parameters can be solved when photographs are aligned in the first step. As a result of aligning photos sparse point cloud were generated. Reference points acquired were marked on the aligned photographs and the following steps were performed; building dense point cloud, mesh and texture.

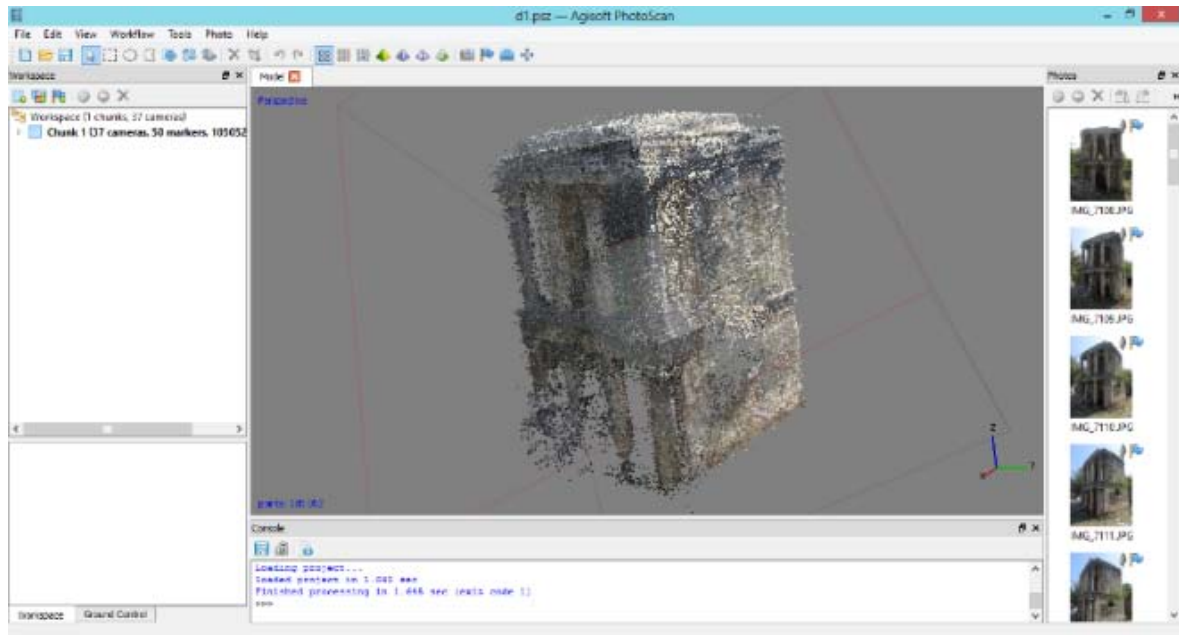


Figure 9. 3D point cloud of Öterkale Imriogion

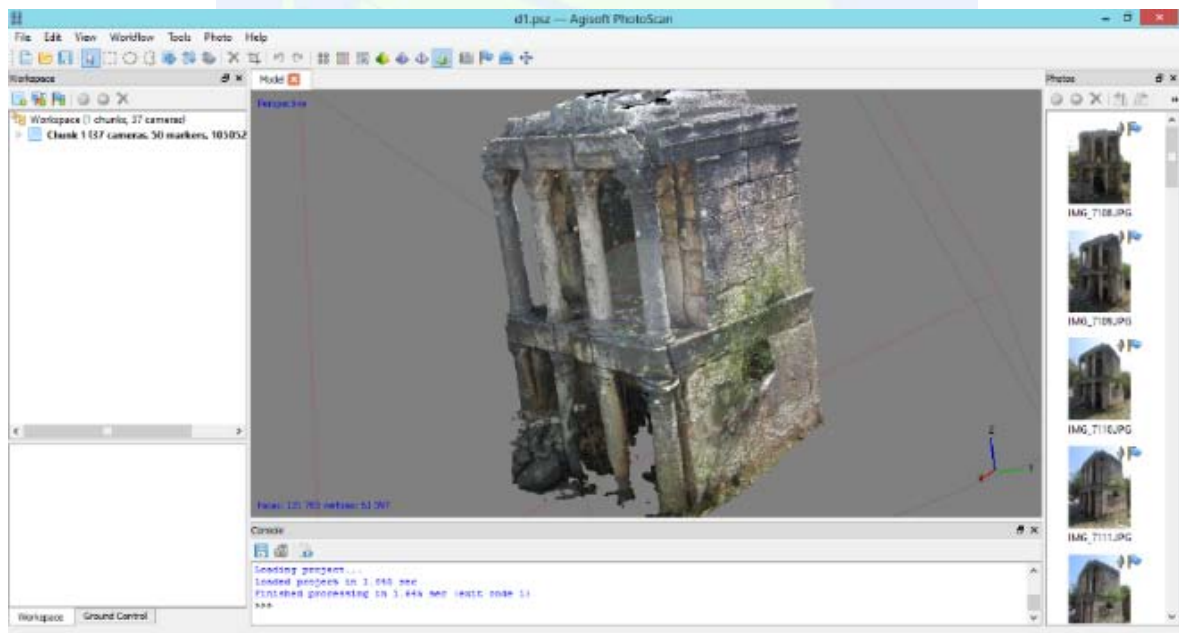


Figure 10. 3D textured model of Öterkale

A lot of data e.g. images, coordinates, information about 46 heritages have been collected from the field and different sources. Inventory of all those heritages have been created using that data acquired.

Generated 3D models have been exported in 3D pdf format from PhotoScan software. So it is available for all computers that the software is not installed.

Inventory and exported 3D models have been integrated by using Hyperlink in ArcGIS software. Therefore, it is available to present information, inventory and 3D model of Cultural Heritages (Figure 5).

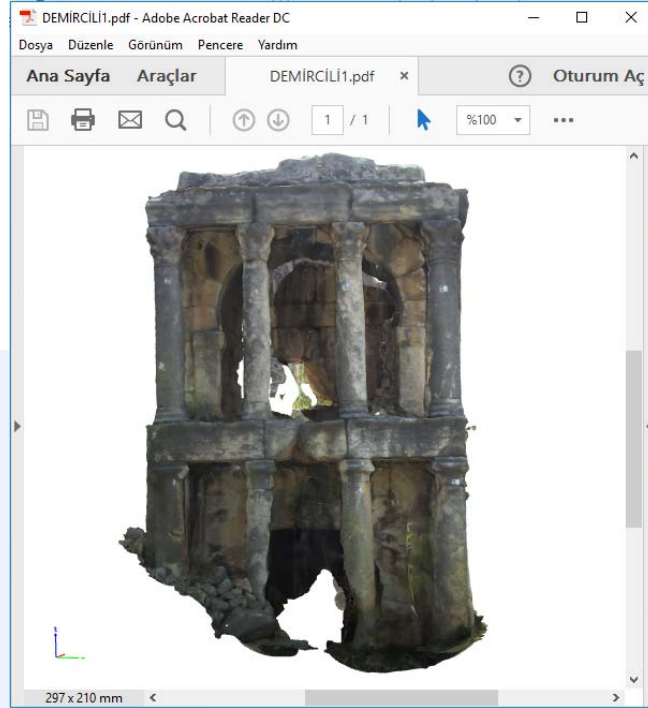


Figure 11. Exported 3D model as pdf format

CONCLUSION

Geographic Information System is the most talented tool for documenting, storing and presenting of cultural heritages. It is also significant to be source for restoration and restitution works. As known restoration and restitution works require considerable costs. Deciders have to make the right decision to manage their investment to avoid the prodigality. However, our fundamental aim is to protect the cultural heritage and ensure its sustainability, but we are also thinking that we are bringing a strong base to state agencies and private companies as a result of this study. System may facilitate and accelerate to access the information about cultural heritages. So important decisions could be made quickly and accurately. We believe that this system would benefit to every sector i.e. from tourism to architectural, from economy to sociology.

As a result of this study, Silifke is a city with a deep-rooted and rich history that has numerous cultural heritage such as theaters, aqueducts, fountains, king and commercial roads, mausoleum, mint and castles etc. Therefore, Silifke has been a very efficient workplace for us. The heritage has been documented and integrated to the information system and digital archive has been designed to quick access. 3D models have been generated with two different software and methods but with the same survey technics.

It is obvious that cultural heritage documentation is a requirement to protect and integration to GIS to make an accurate decision to use the sources right. It plays a significant role to develop the country in a regular plan created by GIS.

REFERENCES

- Bakar, N., & Demir, Ö. Tarihi Yapıların Tarih, Kültür ve İnanç Turizmine Etkileri: Silifke Örneği.
- Hanan, H., Suwardhi, D., Nurhasanah, T., & Bukit, E. S. (2015). Batak Toba Cultural Heritage and Close-range Photogrammetry. *Reflections on Creativity: Public Engagement and the Making of Place*, 184, 187-195. doi:10.1016/j.sbspro.2015.05.079
- Hassani, F. (2015). Documentation of Cultural Heritage Techniques, Potentials and Constraints. *25th International Cipa Symposium 2015*, 45(W7), 207-214. doi:10.5194/isprsarchives-XL-5-W7-207-2015
- Kivilcim, C. O., & Duran, Z. (2016). A Semi-Automated Point Cloud Processing Methodology for 3d Cultural Heritage Documentation. *XXIII ISPRS Congress, Commission V*, 41(B5), 293-296. doi:10.5194/isprsarchives-XLI-B5-293-2016
- Lezzerini, M., Antonelli, F., Columbu, S., Gadducci, R., Marradi, A., Miriello, D., . . . Lazzeri, A. (2016). Cultural Heritage Documentation and Conservation: Three-Dimensional (3D) Laser Scanning and Geographical Information System (GIS) Techniques for Thematic Mapping of Facade Stonework of St. Nicholas Church (Pisa, Italy). *International Journal of Architectural Heritage*, 10(1), 9-19. doi:10.1080/15583058.2014.924605
- Reinoso, J. F., Moncayo, M., & Barrera, D. (2014). Close-range photogrammetry applied to the documentation of cultural heritage using telescopic and wide-angle lenses. *Imaging Science Journal*, 62(7), 387-394. doi:10.1179/1743131x14y.0000000077
- Toz, G., & Duran, Z. (2004). *Documentation and analysis of cultural heritage by photogrammetric methods and GIS: A case study*. Paper presented at the XXth ISPRS Congress. Istanbul, Turkey.
- Waas, M., & Zell, D. (2013). *Practical 3D photogrammetry for the conservation and documentation of Cultural Heritage*. Paper presented at the International Conference on Cultural Heritage and New Technologies, Vienna.
- Yilmaz, H. M., Yakar, M., Gulec, S. A., & Dulgerler, O. N. (2007). Importance of digital close-range photogrammetry in documentation of cultural heritage. *Journal of Cultural Heritage*, 8(4), 428-433. doi:10.1016/j.culher.2007.07.004
- ESRI. (2017). <http://desktop.arcgis.com/en/arcmap/10.3/manage-data/tables/about-joining-and-relating-tables.htm> (21.08.2017)

The Distribution of the Total Scale Factor in Large Scale Mapping in Turkey by Map Projection and Topography

İbrahim Öztuğ Bildirici^{*1}, Mustafa Berber² and Ali Kılıç¹

¹Selcuk University Engineering Faculty, Department of Geomatics Engineering, Selcuklu, Konya, bildirici@selcuk.edu.tr, alikilicharita@gmail.com

²Department of Civil & Geomatics Engineering, California State University, Fresno, CA, USA 93740, muberber@csufresno.edu

ABSTRACT

Due to map projection distortions and topography, horizontal distances on the terrain differ from the distances derived from the projection coordinates. This scale change is called scale factor. In this paper, scale factors caused by map projection and topography have been examined. Gauss-Krüger projection is selected for analyses because it is the official map projection for large scale mapping activities in Turkey. The variation and geographical distribution within Turkey are investigated. A web application is also presented, with which regional analyses and point based queries can be performed. Results show that the scale factor values are above acceptable limits for large scale mapping in some parts of the country.

INTRODUCTION

A map projection is systematic way of representing all or a part of the Earth on a projection surface such as a plane map surface. A curved 2D surface is transformed to a flat 2D surface, with a resulting scale factor, that increases or decreases with the size and the location of the area being projected.

In Turkey, Gauss-Krüger projection system has been used in 3° zones according to official regulations for 1:5000 scale and large-scale mapping activities (HKMO, 2008). This is a transverse cylindrical-conformal projection. The reference surface is GRS80 ellipsoid. Because it is an interrupted system, the whole country is divided into 7 zones, each having an individual coordinate system. The differential scale increases away from the central meridian, on which the scale is true.

Another fact that affects the scale is the topography, i.e., the height above sea level. The total scale factor is the multiplication of both factors caused by projection and topography. The total scale factor on a point depends on the height and distance to the central meridian, accordingly. Because of varying topography across Turkey, the total scale factor can reach up to 700 ppm that is a high value for large scale mapping activities. In this study, the scale factors by projection and height are calculated on a grid with 30" resolution. The extreme

^{*} Corresponding Author

values are determined and their distribution is depicted by using thematic maps. The results show that the scale factors are far beyond the acceptable limits. This fact highlights the importance of corrections for horizontal distances due to topography and projection. Furthermore, we created a map mash-up that calculates scale factor on a point selected by the user, which is a web-based tool that is publicly available. The distribution on a desired area can also be visualized. With help of this tool, Geomatics Engineers can determine the effect of the scale factor in any area within Turkish territory.

A similar analysis has been performed in Macedonia by Idrizi (2014).

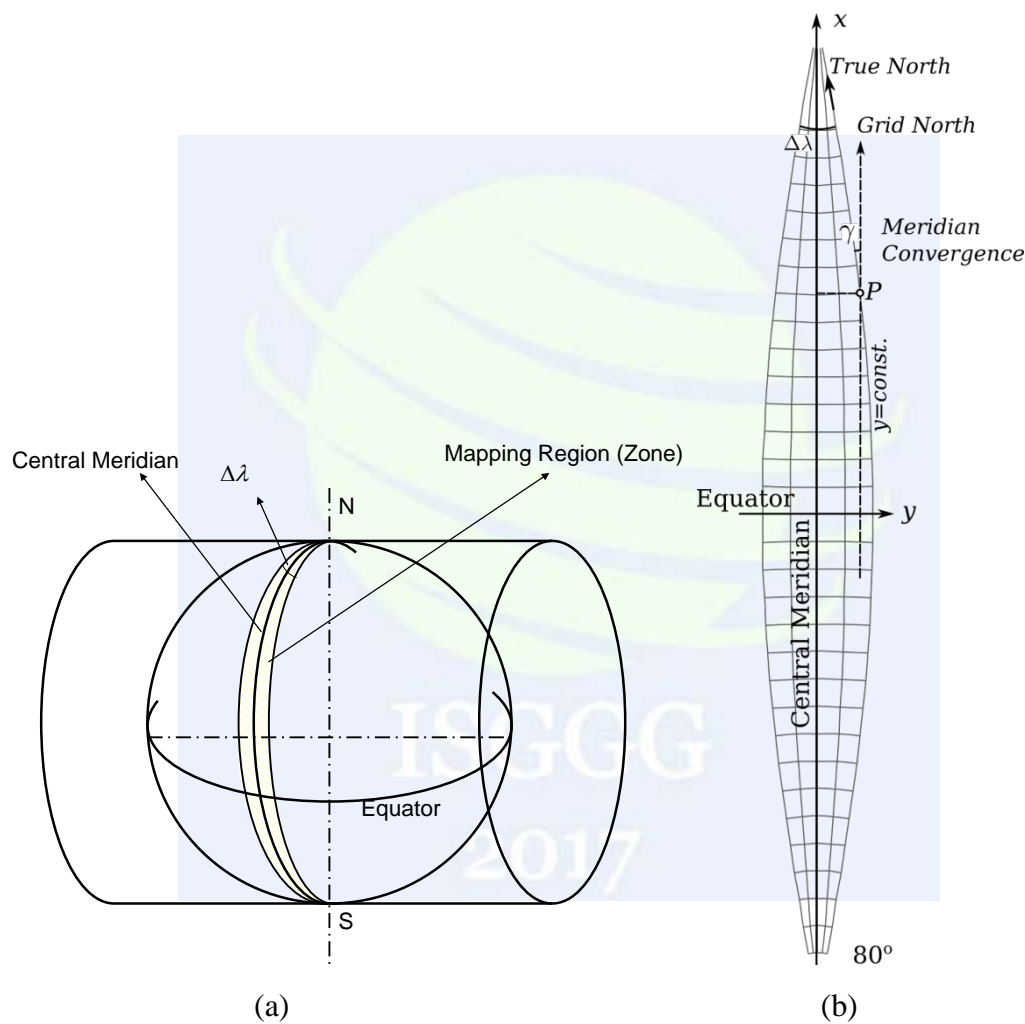


Figure 1. a) The projection principle of Gauss-Krüger Projection, b) The plane coordinate system within a zone.

MATERIAL AND METHOD

Gauss-Krüger projection has been used in large-scale mapping activities for a long time in Turkey according to the large-scale mapping regulation (Article 10, HKMO 2008). It is the well-known Mercator projection in transversal aspect. Here, ellipsoid surface is projected to a cylinder that is tangent to the ellipsoid through a meridian. The projection is

conformal, and causes scale change. That is why it is implemented in zones. In large-scale mapping the size of the zones is 3° in longitude difference (Fig. 1). The scale changes are maximal at the edges of the zones, which causes serious length differences between the projection surface and the reference surface (ellipsoid). In other words, the distance between two points on the ellipsoid differs from the corresponding distance in projection plane. In order to diminish the scale change the projection coordinates are multiplied by a standard scale factor (m_0). In large-scale mapping the coefficient is taken as unity, in medium-scale mapping (in UTM system) as 0.9996 where the zones are 6° wide.

The projection coordinates are calculated from geographical coordinates by using following equations (Grossmann 1976, Üstün&Demirel 2013,). For ellipsoidal parameters see Appendix A.

$$y = N \left\{ \Delta\lambda \cos \varphi + \frac{\Delta\lambda^3 \cos^3 \varphi}{6} (1 - t^2 + \eta^2) + \frac{\Delta\lambda^5 \cos^5 \varphi}{120} (5 - 18t^2 + t^4) + \dots \right\} \quad (1)$$

$$x = G + N \left\{ \frac{\Delta\lambda^2}{2} \sin \varphi \cos \varphi + \frac{\Delta\lambda^4}{24} \sin \varphi \cos^3 \varphi (5 - t^2 + 9\eta^2 + 4\eta^4) + \dots \right\} \quad (2)$$

G denotes the meridian arc distance from equator to the point of interest.

$$G = \alpha\varphi - \beta \sin 2\varphi + \gamma \sin 4\varphi - \delta \sin 6\varphi + \dots \quad (3)$$

$\alpha, \beta, \gamma, \delta$ are the coefficients that depend on the ellipsoid. For numerical values for GRS80 refer to Demirel &Ustun (2013) or Grossmann (1976).

The differential scale around a point can be calculated by using the following equation.

$$m_p = m_0 \left(1 + \frac{1}{2} \cos^2 \varphi (1 + \eta^2) \Delta\lambda^2 + \frac{1}{24} \cos^4 \varphi (5 - 4t^2 + 14\eta^2 + 13\eta^4 - 28t^2\eta^2) \Delta\lambda^4 + \dots \right) \quad (4)$$

m_0 is the standard scale factor that is mentioned above. This is taken as unity in 3° zone implementation.

In order to interpret the numerical values easily, scale factor can be expressed in part per million (ppm).

$$(m_p)_{PPM} = (m - 1)10^6 \quad (5)$$

Meridian convergence is the angle between the grid north and the geographical (true) north, and is denoted by γ (Fig. 1)

$$\gamma = \sin \varphi \Delta\lambda + \sin \varphi \cos^2 \varphi (1 + 3\eta^2 + 2\eta^4) \frac{\Delta\lambda^3}{3} + \dots \quad (6)$$

Due to the average terrain height, the horizontal distance in the terrain is larger than the one on the ellipsoid. According to Fig. 2 the scale factor by topography (m_T) can be calculated assuming that the ellipsoid is represented by a sphere.

$$D_e = D_t \frac{R}{R+h} \quad (7)$$

The scale factor by topography:

$$m_T = 1 + \frac{R}{R+h} \quad (8)$$

It can also be expressed in part per million.

$$(m_T)_{PPM} = \frac{R}{R+h} 10^6 \quad (9)$$

Here, ellipsoid can be represented by Gauss' sphere by using average latitude within the region of interest.

$$R_G = \frac{c}{1 + e'^2 \cos^2 \varphi} \quad (10)$$

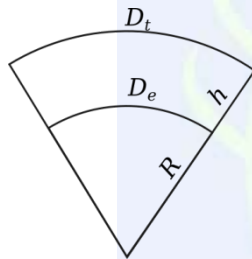


Figure 2. The horizontal distances on the ellipsoid and the terrain.

The total scale factor by map projection and topography is the multiplication of both.

$$m = m_T m_p \quad (11)$$

There are studies, in which special coordinate systems are proposed to keep the scale factor small enough. This is necessary in engineering projects such as railway and highway projects (Iliffe 2017).

APPLICATION

Analysis of the Total Scale Factor within Turkey

In order to show the total scale factor along the Turkish Territory, a grid is formed by using SRTM30 DEM. The total scale factor is calculated in ppm. The values range from 200 ppm to -700 ppm. For large scale mapping, these values seem to be high (Iliffe 2017). The results are depicted in a thematic map. Since the Gauss-Krüger system is interrupted, the results are shown in Mercator Projection. In the map, central meridians of Gauss-Krüger system are also depicted (Figure 3).

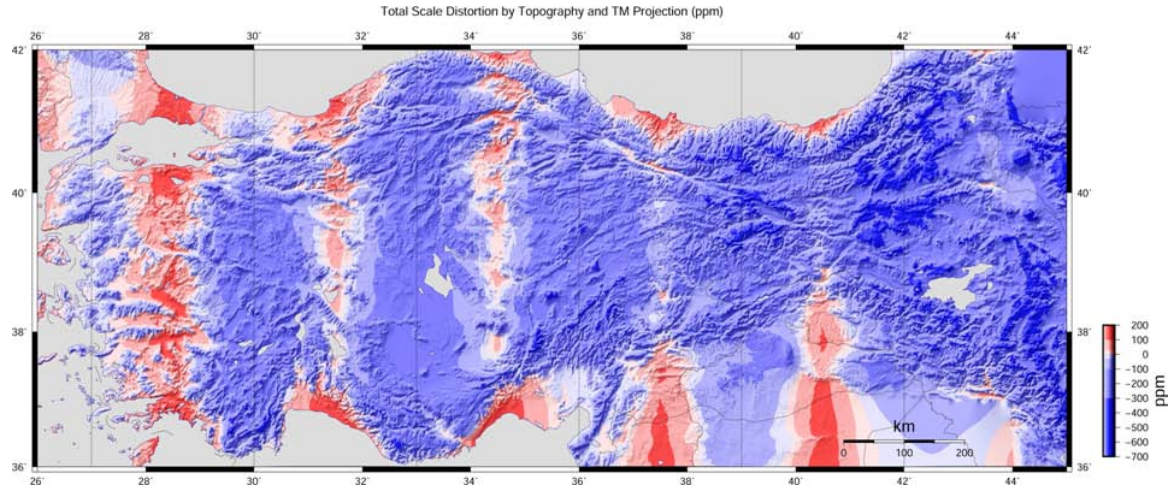


Figure 3. Distribution of the total scale factor in Turkey.

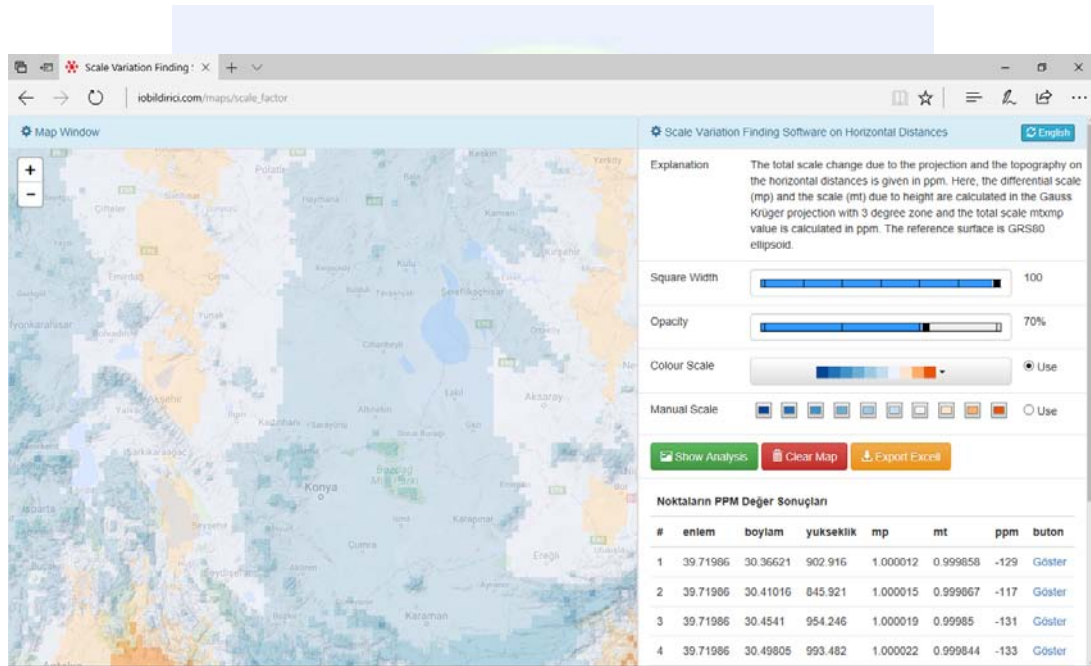


Figure 4. Web application (http://www.iobildirici.com/maps/scale_factor).

Web Application

In order to show the total scale factor at any point, a web application is developed. It is developed by using Leaflet (URL1) Mapping Library with JavaScript programming language. It is available at http://www.iobildirici.com/maps/scale_factor.

The application is capable of showing scale factor values for a selected region by using isopleths, in which cell size and colors are customizable. Users can also query the values of individual points. The main screen is shown in Fig. 4.

CONCLUSIONS

In this paper, the scale factor of horizontal distances is focused on. The analysis show high ppm values that are marginally acceptable for large scale topographic mapping activities.

This fact highlights the importance of scale factor that must be taken into account when measuring horizontal distances on the terrain.

In this study, the variation and the geographical distribution of the scale factor within Turkey is shown. A web application is also available, with which users can create isopleths and see the geographical distribution in a certain region. The scale factor values for any point can also be taken from the application.

REFERENCES

- HKMO, 2008. Açıklamalı-Örnekleme Büyük Ölçekli Harita ve Harita Bilgileri Üretim Yönetmeliği, HKMO (Chamber of Surveying Engineers), Ankara
- Demirel, H., Üstün, A., 2013. *Matematiksel Jeodezi*, unpublished lecture notes, <http://atlas.selcuk.edu.tr/1205429/dokumanlar/jeodezi2013.pdf>
- Grossman, W., 1976. *Geodatische Rechnungen und Abbildungen in der Landesvermessungen*, 3. Auflage. Konrad Wittwer, Stuttgart.
- Iliffe, J. C., 2017, The development and analysis of quasi-linear map projections, *Cartography and Geographic Information Science*, DOI:10.1080/15230406.2017.1325332
- URL1: <http://leafletjs.com/> accessed August 2017.
- Idrizi, B. 2014. Length Differences between Topography Surface and Map Projections; Case Study: Country Area of Macedonia, *5th International Conference on Cartography and GIS*. June 15-20, 2014, Riviera, Bulgaria ISSN: 1314-0604, Eds: Bandrova T., Konecny M.

APPENDIX A

Ellipsoidal parameters

φ, λ	Geographical latitude and longitude
a, b	Semi-major and semi-minor axes of the ellipsoid
$c = \frac{a^2}{b}$	Polar radius of curvature
$e^2 = \frac{a^2 - b^2}{a^2}$	First eccentricity
$e'^2 = \frac{a^2 - b^2}{b^2}$	Second eccentricity
$\eta^2 = e'^2 \cos^2 \varphi$	Intermediate parameter
$t = \tan \varphi$	Intermediate parameter
$N = \frac{c}{\sqrt{1 + e'^2 \cos^2 \varphi}}$	Radius of curvature orthogonal to Meridian

Validation of Bernese-Derived Precise Orbits for GRACE Satellites

Sureyya Ozgur Uygur^{*1}, Cuneyt Aydin¹, Niyazi Arslan² and Orhan Akyilmaz³

¹Department of Geomatic Engineering, Yildiz Technical University, Davutpasa Campus, 34220, Turkey.
(ouygur@yildiz.edu.tr)

¹Department of Geomatic Engineering, Yildiz Technical University, Davutpasa Campus, 34220, Turkey

²Department of Surveying Engineering, Cukurova University, Ceyhan Campus, 01950, Turkey

³Department of Geomatic Engineering, Istanbul Technical University, Ayazağa Campus, 34469, Turkey

ABSTRACT

Precise orbit determination of satellites is an important issue for geodetic community, especially for gravity field missions like GRACE (The Gravity Recovery and Climate Experiment). GRACE is a twin satellite system equipped with a dual-frequency BlackJack GPS onboard receiver, a SuperSTAR accelerometer, a star tracker, a K-band ranging (KBR) system and a satellite laser ranging (SLR) retroreflector. The data related to those scientific instruments are provided to users through the Information System and Data Center (ISDC). Also International GNSS Service's or Center for Orbit Determination in Europe's (CODE) data products (GPS precise sp3 orbits and high-rate clock corrections) are used.

In this study, daily GRACE Level-1B data were used to estimate the kinematic and reduced-dynamic orbits of GRACE satellites using Bernese 5.2 Processing Engine (LEOPOD.PCF). The accuracy of orbits is assessed using several validation procedures. These can be classified into two groups: Internal validation method and external validation methods. Internal validation method consists of the comparison of kinematic and reduced-dynamic orbits estimated by the user. External validation methods consist of KBR validation, independent validation of the orbit quality with SLR and the comparison with GNV1B orbit of Jet Propulsion Laboratory (NASA/JPL).

Daily orbit estimations were performed for one month and the results were validated using above-mentioned methods. Results were analyzed and interpreted.

INTRODUCTION

Satellites in the Low Earth Orbit (LEO) are defined as the Earth orbiting satellites with altitudes of 300-1500 km above the earth's surface. Especially for global gravity field determination problem, LEO satellites have great importance. The information of the Earth's gravity field and the geoid, derived from the classical methods is deficient. To overcome this deficiency and to provide high-resolution gravity field determination from space techniques, three fundamental criteria for any satellite gravity mission has to be

^{*} Corresponding Author

considered: Uninterrupted tracking in three spatial dimensions, measurement or compensation of the effect of non-gravitational forces and orbit altitude as low as possible [Rummel et al., 2002]. In order to fulfill these requirements, three missions have been realized. These are CHAMP (CHALLENGING Minisatellite Payload), GRACE (Gravity Recovery and Climate Experiment) and GOCE (Gravity field and steady-state Ocean Circulation Explorer) missions. Only GRACE mission is subjected to this study.

The Gravity Recovery and Climate Experiment (GRACE) satellites were launched in 2002 into a near polar orbit. The satellites are equipped with; a KBR system to continuously track the changes in the inter-satellite distance, onboard GPS receivers providing data in order to determine satellite orbits and time synchronization of KBR measurements, accelerometers to measure non-gravitational accelerations and the star cameras to determine satellite attitudes. The main purpose of the GRACE mission is the determination of the time-varying part of the Earth's gravity field with unprecedented accuracy from GPS, accelerometer, and inter-satellite K band range observations [Tapley et al., 2004]. To achieve this goal, the orbits of GRACE satellites are needed to be precisely determined.

PRECISE ORBIT DETERMINATION

Precise orbit determination (POD) is of importance for at least two reasons [Liu, 2008]: Firstly, POD is needed to locate the data in three dimensional space. Secondly, the orbit is mainly as a result of the Earth's gravitation.

The orbit determination strategies are classified into two groups by [Bock, 2003]. One is kinematic strategies and the other is dynamic and reduced-dynamic strategies. Kinematic orbit determination is a geometric approach and any dynamic information of satellite is not necessary. In this procedure satellite positions are estimated epoch by epoch based on GPS observations. For this reason the accuracy of the kinematic orbit depends on the accuracy of the GPS observations, on the GPS satellite constellation and on the quality of the GPS orbit and clock products. The orbit is sensitive to data gaps. On the other hand, dynamic and reduced-dynamic strategies is based on the numerical integration of the equation of motion and the variational equations to obtain the orbit itself, as well as the partial derivatives with respect to the orbital parameters [Švehla and Janáček, 2006]. For dynamic strategies, mathematical models of forces acting on a LEO satellite and the knowledge of physical properties of the satellite are required. The missing physical information and the model errors are the weaknesses of dynamic strategies. In order to reduce the effect of these errors, empirical parameters such as stochastic pulses, are introduced into the system. Such an orbit determination process is called as reduced-dynamic or pseudo-stochastic orbit modelling. This method makes use of both the geometric strength of the GPS observations and the fact that satellite trajectories are particular solutions of a deterministic equation of motion [Jäggi et al. 2006]. The detailed mathematical models of related orbit determination processes followed in this study are given in [Bock, 2003], [Bock et al., 2005], [Jäggi et al., 2006] and [Jäggi, 2007].

For kinematic orbit determination, zero-difference processing of GPS data is performed. This means that there are no ground stations used. The satellite coordinates and the clock corrections are kept fixed. The final precise GPS orbits, 5 sec high-rate GPS clock corrections [Bock et al, 2009] and the Earth Rotation Parameters (weekly ERP files) from the Center for Orbit Determination in Europe (CODE) are used.

The pseudo-stochastic orbit modeling technique in (Jäggi et al., 2006) is used in this study to determine reduced-dynamic LEO orbits in a batch least-squares adjustment from undifferenced (zero difference) ionosphere-free GPS carrier phase data at 30 s intervals [Jäggi et al., 2007]. Piecewise constant accelerations in predetermined directions (radial, along-track and cross-track) are used in every 6 minutes with the a priori constraints set to $5 \times 10^{-9} \text{ m/s}^2$. Both kinematic and reduced-dynamic orbits have a length of 24 hours.

LEO Level-1B data (including GPS, star camera, accelerometer, KBR...) is available from the GFZ (German Research Centre for Geosciences)'s data center, Information System and Data Center (ISDC). For GRACE, the files are in mission-specific binary format and they have to be converted into ASCII format. GPS RINEX data (version 2.20) with 10 sec interval and star camera data are used in the orbit determination stage. The orbit determination process is performed with Bernese GPS Software [Dach et al., 2015].

ORBIT VALIDATION

In order to validate the orbit solutions, several comparison processes were performed. The resulting orbits were compared to each other (internal validation) and compared to the publications of different institutes and foundations (external validation). This is a 3D Helmert coordinate transformation process and the differences between the solutions are given in Figure 1, Figure 2 and the root mean square error of the orbit differences are given in Figure 3. For the external validation Jet Propulsion Laboratory's post-processed precise (GNV1B) orbits with a sampling rate of 5 s were used.

These comparisons show that the internal accuracy of the Bernese-derived reduced-dynamic orbit is within 2 to 3 centimeters for GRACE-A, 2 to 4 centimeters for GRACE-B and the external accuracy of the Bernese-derived reduced-dynamic orbit is on the level of 1,5 cm for GRACE-A, on the level of 1 cm for GRACE-B. As clearly seen GNV1B and Bernese-derived reduced-dynamic orbit are the same type of orbits and they both have a 3D accuracy of nearly 2,5 cm.

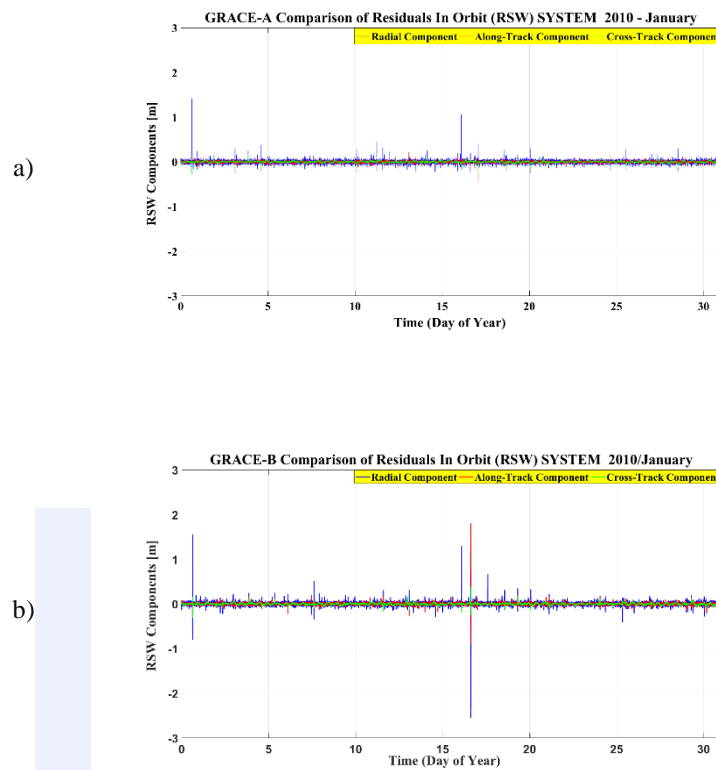


Figure 1. Comparison of reduced-dynamic orbits to kinematic orbits; a) for GRACE-A and b) for GRACE-B

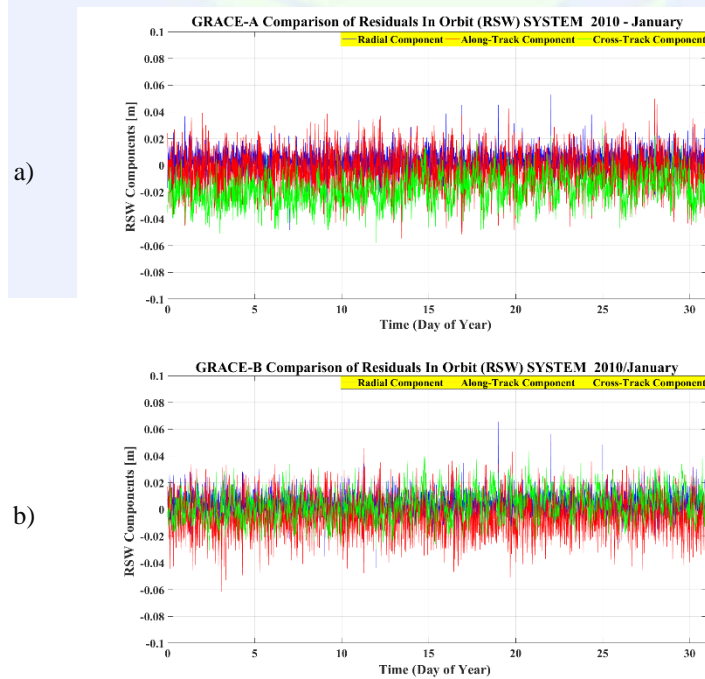


Figure 2. Comparison of reduced-dynamic orbits to GNV1B orbits; a) for GRACE-A and b) for GRACE-B

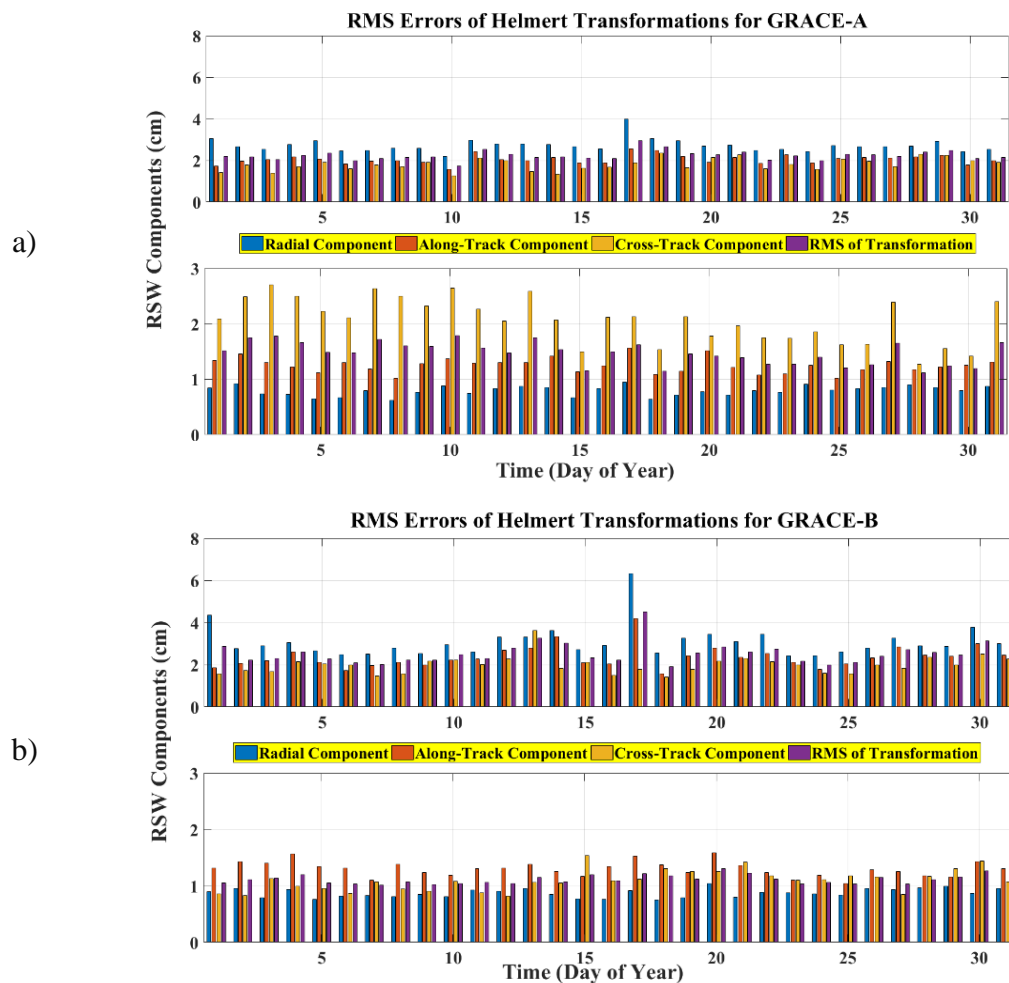


Figure 3. RMS error values of Helmert Transformation between the orbits RD-KIN (on top) and RD-GNV1B (below) ; a) for GRACE-A and b) for GRACE-

SLR ANALYSIS

SLR is one of the space-geodetic techniques used for precise positioning, for determination of the Earth's gravity field, and for measurement of geodynamical phenomena. SLR is also an independent validation tool for orbit determination in an absolute sense. Theoretical background of SLR analysis is briefly described in (Sośnica, 2014).

GRACE satellites are equipped with laser retro-reflector arrays in order to allow SLR measurements. The only disadvantage of the SLR tracking of GRACE satellites is the discontinuity of the observations. Apart from that SLR observation informs of 3D orbit quality.

The normal point data is provided to the user by International Laser Ranging Service (ILRS) data centers and SLR analyses were processed via Bernese 5.2 software. The RMS error values and the residuals of SLR observations were presented in Figure 4 and Figure 5.

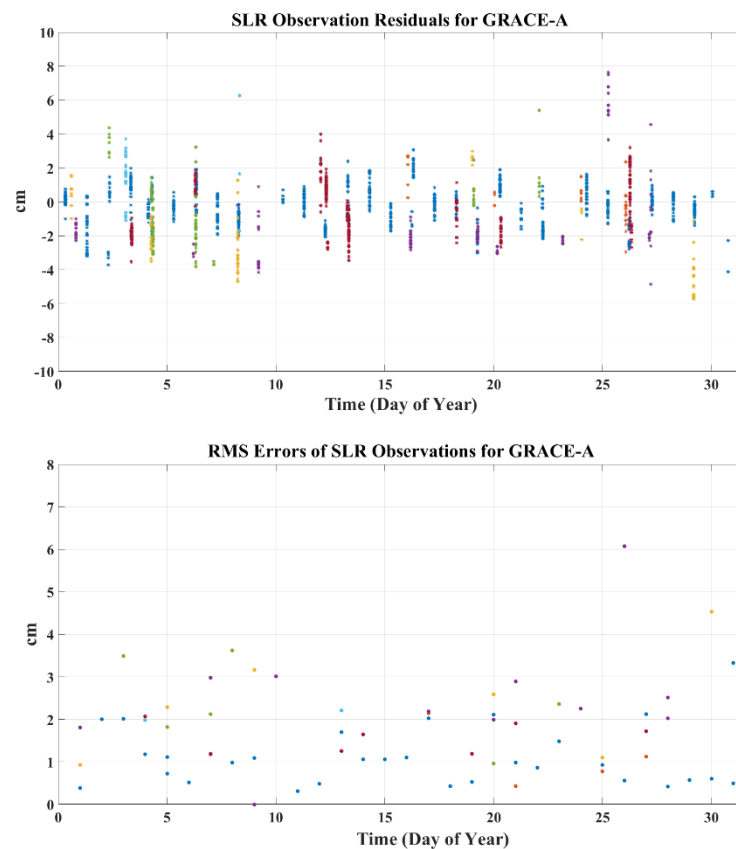


Figure 4. GRACE-A SLR observation residuals (on top) and RMS errors (below)

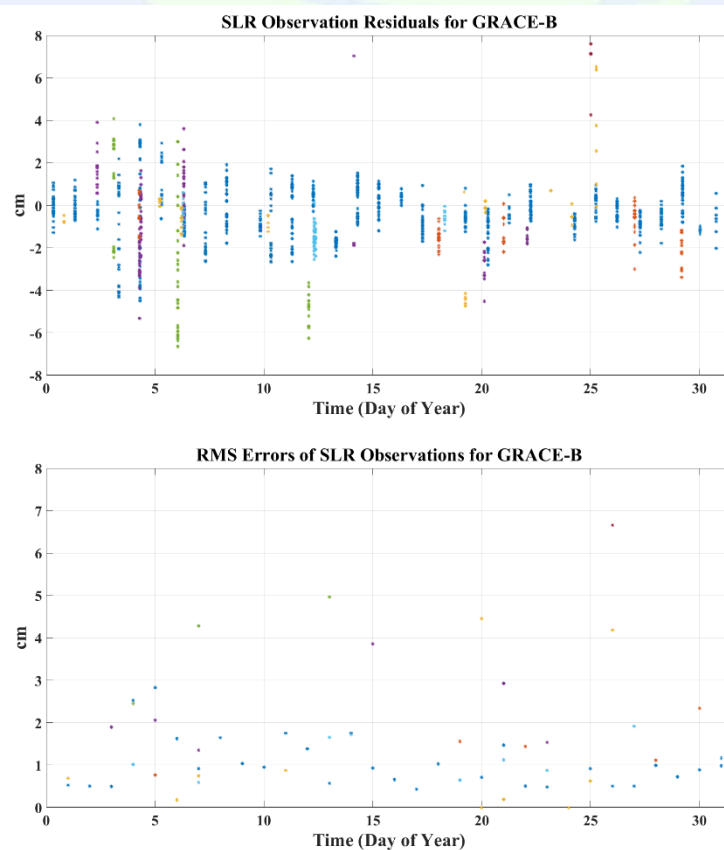


Figure 5. GRACE-B SLR observation residuals (on top) and RMS errors (below)

When the graphs are analyzed, it is seen that the root mean square error values are generally in the range of 0-3 cm. Unfortunately, SLR measurements to GRACE satellites are usually sparse. As a consequence, this situation may cause increasing RMS values.

KBR VALIDATION

The low-low satellite to satellite tracking technique has been put into practice using K-band microwave ranging (KBR) system. The KBR system provides ultra-precise measurements of the biased range (line of sight distance) between both satellites on the K/Ka Band links with systematic phase variations being as low as 10 μ m (Jäggi, 2007). KBR Level 1B data (KBR1B) is provided to the user through ISDC and includes biased range, range-rate, range-accelerations and correction terms (light time and geometric corrections). The KBR measurements is a unique tool to validate the change of the relative GRACE orbit positions in the line of sight direction.

Relative reduced-dynamic orbit velocities (Equation 1) were compared to corrected KBR range-rates (the comparisons were performed for both Bernese-derived and GNV1B orbits) and the results were presented in Figure 6.

$$V_{AB} = (\dot{r}_B - \dot{r}_A) \frac{r_B - r_A}{|r_B - r_A|} \quad (1)$$

As Figure 6 examined, it is clearly seen that the biggest amplitude of the differences belong to reduced-dynamic orbit. If the coordinates and velocities of reduced-dynamic orbit is corrected using the KBR data as described in [Tangdamrongsub, 2012], the resulting range-rate differences almost coincide with GNV1B and the KBR range-rate differences.

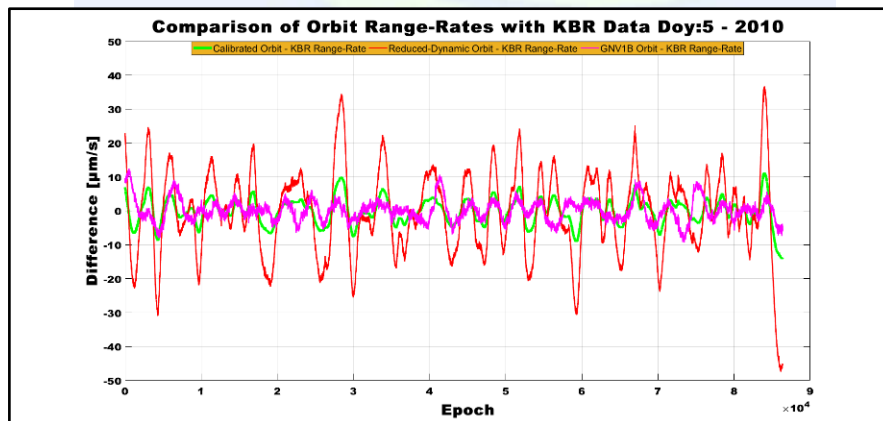


Figure 6. KBR validation of relative velocities

CONCLUSIONS

In order to analyze the precision of our reduced-dynamic and kinematic orbit solutions, we performed 3-D Helmert transformations. Our results indicate that the RMS values; for the differences between kinematic and reduced-dynamic solutions are characterized by means

and RMS of 2.72 ± 0.31 , 2.04 ± 0.22 , 1.81 ± 0.40 cm and for the differences between GNV1B and reduced-dynamic solutions, 0.79 ± 0.09 , 1.25 ± 0.13 , 2.06 ± 0.40 cm.

SLR is a high accuracy, independent validation tool for LEO satellite orbits. As a consequence of the SLR validation of our GRACE reduced-dynamic orbits, the overall RMS errors of SLR stations range between 0.5 and 3.5 cm for both GRACE satellites.

K-band data provide a precise and independent validation of GRACE relative orbit positions and velocities. In this study, only GRACE relative velocities were compared to KBR range-rates. No range comparison were performed. The differences generally range between ± 20 $\mu\text{m/s}$. By using KBR data together with the reduced-dynamic orbit relative position and velocity vectors in the energy balance approach (neglecting potential terms), the resulting range-rate differences show significant improvement.

REFERENCES

- Bock, H., 2003. *Efficient Methods for Determining Precise Orbits of Low Earth Orbiters Using the Global Positioning System*. PhD thesis, Institut für Geodasie und Photogrammetrie, Geodatisch-geophysikalische Arbeiten in der Schweiz. ISBN:3-908440-08-4.
- Bock, H., Hugentobler, U., Jäggi, A., ve Beutler, G., 2005. Precise orbit determination for champ using an efficient kinematic and reduced-dynamic procedure. In Reigber, C., Lühr, H., Schwintzer, P., and Wickert, J., editors, *Earth Observation with CHAMP-Results from Three Years in Orbit*, number ISBN 3-540-22804-7, pages 157–162. Springer Verlag Berlin Heidelberg, Germany.
- Bock, H., Dach, R., Jäggi, A. et al. J Geod., 2009. 83: 1083. <https://doi.org/10.1007/s00190-009-0326-1>
- Case, K., Kruizinga, G. and Wu, S.C., 2010. *GRACE Level 1B Data Product User Handbook*, Jet Propulsion Laboratory, California Institute of Technology.
- Dach, R., S. Lutz, P. Walser, P. Fridez (Eds); 2015. *Bernese GNSS Software Version 5.2. User manual*, Astronomical Institute, University of Bern, Bern Open Publishing. DOI: 10.7892/boris.72297; ISBN: 978-3-906813-05-9.
- ISDC, 2016. Information System and Data Center. Last Access: 15.06.2017, <http://isdc.gfz-potsdam.de/>.
- Jäggi, A., Hugentobler, U. and Beutler, G. J Geodesy, 2006. 80: 47. <https://doi.org/10.1007/s00190-006-0029-9>.
- Jaggi, A., 2007. *Pseudo-Stochastic Orbit Modeling of Low Earth Satellites Using the Global Positioning System*. PhD thesis. Institut für Geodasie und Photogrammetrie, Geodatisch-geophysikalische Arbeiten in der Schweiz. ISBN:3-908440-17-8.

- Jäggi A, Hugentobler U, Bock H, Beutler G., 2007. Precise orbit determination for GRACE using undifferenced or doubly differenced GPS data. *Adv Space Res* 39(10): 1612–1619. doi:10.1016/j.asr.2007.03.012.
- Liu, X., 2008. *Global Gravity Field Recovery From Satellite to Satellite Tracking Data With The Acceleration Approach*, PhD Thesis, Technical Report Publications on Geodesy 68, Netherlands Geodetic Commission, The Royal Netherlands Academy of Arts and Sciences, Delft, ISBN: 978-90-6132-309-6.
- Sośnica, K.. 2014. *Determination of Precise Satellite Orbits and Geodetic Parameters using Satellite Laser Ranging*. PhD thesis of the Faculty of Science of the University of Bern. ISBN: 978-83-938898-0-8.
- Švehla D., Földvály L., 2006. From Kinematic Orbit Determination to Derivation of Satellite Velocity and Gravity Field. In: Flury J., Rummel R., Reigber C., Rothacher M., Boedecker G., Schreiber U. (eds) *Observation of the Earth System from Space*. Springer, Berlin, Heidelberg.
- Tangdamrongsub, N., C. Hwang, C. K. Shum, and L. Wang, 2012. Regional surface mass anomalies from GRACE KBR measurements: Application of L-curve regularization and a priori hydrological knowledge, *J. Geophys. Res.*, 117, B11406, doi:10.1029/2012JB009310.
- Tapley, B., S. Bettadpur, J. Ries, P. Thompson, and M., Watkins, 2004. GRACE *Measurements of Mass Variability in the Earth System*. *Science*, 305, 503-505.

Python GIS Application and SQL Usage

Ümran Köylü^{*1}, Abdurrahman Geymen¹ and Fehim Köylü²

¹Department of Geomatics Engineering, Erciyes University, 15 Temmuz Campus, 38280, Kayseri Turkey. (e-mail umrank@erciyes.edu.tr, ageymen@erciyes.edu.tr)

²Department of Computer Engineering, Erciyes University, 38039, Kayseri, Turkey e-mail: fehimkoylu@erciyes.edu.tr

ABSTRACT

Geographic Information Systems (GIS) is a system that provides a cooperative organization of spatial data and non-spatial data. Spatial and non-spatial data are stored in databases together. Getting help from a programming language is necessary to organize the data used in the GIS analysis easily and to overcome the transaction intensity. Python is an open source language, is easy to write and understand. It has comprehensive and extensive libraries. The use of the Python software language in GIS analysis and data management will enable faster and more efficient operation. In GIS applications it is possible to define task arrays with a script in python language. Geoprocessing tools can be imported Python scripts. In addition to running analyzes with Python scripts, database modules are called and the database can be edited with cursor. The cursor is a line area in databases. Together with the cursor, you can navigate through the tables in the relational databases to make changes and edits. Thanks to these features of the Python software language, making GIS analysis is fast and efficient.

INTRODUCTION

Geographic Information Systems (GIS) is a system that enables the collection, storage, management and analysis of geographic and relevant attribute data which are developed in accordance with the purpose (Shekhar and Xiong 2007; Worboys 1995). The process of organizing and processing data in GIS applications leads to work intensity. One of the most important stages is to use of time efficiently and to access results of the analysis quickly and safely. The use of software languages will facilitate this process. Python language, which is easy to use and code-producing, is quite common in GIS applications. The use of Python in GIS applications is quite common among scientists (Brown 2014; Etherington 2011; Karssenberget al. 2007; Koylu and Geymen 2016; Roberts et al. 2010).

The Python is free, open source and object-oriented, powerful scripting language (Bird et al. 2009; Lutz 2013; McKinney 2012). It has many built-in functions and comprehensive library and can import modules. Repetitive analysis can be easily operated in the Python scripts.

^{*} Corresponding Author

In GIS, attribute data is stored in tables in relational databases in conjunction with geographic data. Python scripts can be manipulated database by cursor method. In the Python the scientific calculations and analyzes can be done by translating the tables into array in order to process the numerical values in the tables.

PYTHON SCRIPT TOOLS

Python scripts can be produced in different formats. This can be generated in three ways: editing the existing script, automating it through the ArcGIS model builder, or creating and saving the script in the Python window. The Python script is saved as *.py extension files.

The modules to be used in Python are called with the import function. The working folder is set. GIS property classes can be defined as variables, files are opened with these variables. Geoprocessing tools and analysis functions can be run with invoked modules. Geoprocessing tools can be imported in python scripts by arcpy module. Parameters values can be provided by users. Complex tasks can be automated by python scripts and some result objects can be used as input objects for other geoprocessing tools (Figure 1). Errors checking can be done with the troubleshooting feature. Feature classes can be opened and used with looping in script file. Python scripts written with these properties can be converted to script tools and added to GIS programs. The generated script tools can be used again by editing the inputs and outputs and shared to other users (Zandbergen 2015).

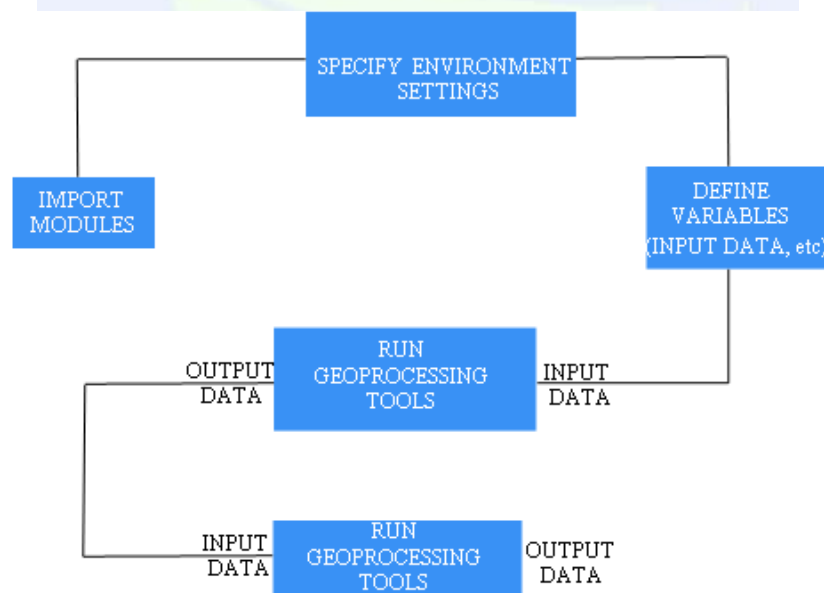


Figure 1. Flow diagram of Python script file for geoprocessing analysis

Arcpy module has cursor function. The cursor function provides ease of operation in databases. Manipulating database files with Python script files has the same logic as the operation steps of running geoprocessing commands. Cursor functions are used to manipulate the database. Structured Query Language (SQL) clauses can be used when performing these edits. The results are retrieved with SQL commands and the files are

closed after the edits in the file. Also, with Python, numerical calculations can be done by translating tables into numerical array (McKinney 2012; Nelli 2015).

CONCLUSIONS

In GIS analysis, complex and repetitive tasks can be automated by python scripts. Thanks to this, time can be used efficiently and effectively and intensive workload will be reduced by means of specially produced tools. Python scripts can be converted to tools. The tools can easily be shared with others. Produced tools can be used again by renewing the inputs and outputs.

REFERENCES

- Bird, S., Klein, E. and Loper, E., 2009. *Natural Language Processing with Python: Analyzing Text with the Natural Language Toolkit*. O'Reilly Media.
- Brown, J.L., 2014. SDMtoolbox: a python-based GIS toolkit for landscape genetic, biogeographic and species distribution model analyses. *Methods in Ecology and Evolution*, 5, 694-700. 10.1111/2041-210X.12200.
- Etherington, T.R., 2011. Python based GIS tools for landscape genetics: visualising genetic relatedness and measuring landscape connectivity. *Methods in Ecology and Evolution*, 2, 52-55. 10.1111/j.2041-210X.2010.00048.x.
- Karssenbergh, D., de Jong, K. and van der Kwast, J., 2007. Modelling landscape dynamics with Python. *International Journal of Geographical Information Science*, 21, 483-495. 10.1080/13658810601063936.
- Koylu, U. and Geymen, A., 2016. GIS and remote sensing techniques for the assessment of the impact of land use change on runoff. *Arabian Journal of Geosciences*, 9484 10.1007/s12517-016-2514-7.
- Lutz, M., 2013. *Learning Python: Powerful Object-Oriented Programming*. O'Reilly Media.
- McKinney, W., 2012. *Python for Data Analysis: Data Wrangling with Pandas, NumPy, and IPython*. O'Reilly Media.
- Nelli, F., 2015. *Python Data Analytics: Data Analysis and Science using pandas, matplotlib and the Python Programming Language*. Apress.
- Roberts, J.J., Best, B.D., Dunn, D.C., Treml, E.A. and Halpin, P.N., 2010. Marine Geospatial Ecology Tools: An integrated framework for ecological geoprocessing with ArcGIS, Python, R, MATLAB, and C plus. *Environmental Modelling & Software*, 25, 1197-1207. 10.1016/j.envsoft.2010.03.029.
- Shekhar, S. and Xiong, H., 2007. *Encyclopedia of GIS*. Springer US.
- Worboys, M.F., 1995. *GIS: A Computer Science Perspective*. Taylor & Francis.
- Zandbergen, P.A., 2015. *Python Scripting for ArcGIS*. Esri Press.



GNSS

Investigation of The Relationships of Discrete Wavelet Transform Components in GNSS Time Series

Osman Oktar^{*1}, Hediye Erdoğan²

^{1,2}Department of Geomatic Engineering, Aksaray University, 68100, Turkey (osmanoktar@aksaray.edu.tr; hediyeerdogan@aksaray.edu.tr)

ABSTRACT

In this study, we investigated 788 days of spatial behaviors of AKHR, BEYS, CIHA, KAMN, YUNA, AKSI and KNYA GNSS stations of CORS-TR network in located in the Central Anatolia Region of Turkey. Observations recorded from stations were evaluated and discrete wavelet transform (DWT) were applied to coordinate time series. Decomposition level for DWT was chosen 9, so 9 detail components (D1-D9) and 9 approximation components (A1-A9) were obtained. Then, cross correlation analysis were performed between original signal and these components. It was determined that cross correlation values between original signal and approximations is going to be weakened from A1 to A9. For North and East series, D8 and D7 had the highest values and they were 0.5. For Up series, D2, D3, D4, and D5 had the highest values and they were about 0.5. As a result of the assessments, the Approximation components of the North, East and Height time series were very strong in relation to the time series but weak with the detail components. While the results of the analysis for the North and East time series for the same station in the detail components were similar, the results obtained in the Up time series differ from those of the two coordinate components. In the cross-correlation analysis, the main series and the component series were considered as two different variables, but the component time series were obtained from the main series.

INTRODUCTION

A satellite navigation or SAT NAV system is a system of satellites that provide autonomous geo-spatial positioning with global coverage. It allows small electronic receivers to determine their location (longitude, latitude, and altitude) to within a few meters using time signals transmitted along a line-of-sight by radio from satellites. Receivers calculate the precise time as well as position, which can be used as a reference for scientific experiments. A satellite navigation system with global coverage may be termed a Global Navigation Satellite System (GNSS) [URL1].

^{*} Corresponding Author:)

The original motivation for satellite navigation was for soldiers and military vehicles, planes, and ships in accurately determining their locations world-wide. Today, the uses of GNSS have extended to include both the commercial and scientific worlds. Commercially, GNSS is used as a navigation and positioning tool in airplanes, boats, cars, and for almost all outdoor recreational activities such as hiking and fishing. In the scientific community, GNSS plays an important role in the earth sciences. Meteorologists use it for weather forecasting and global climate studies (Ahmed, 2010), and geologists can use it as a highly accurate method of surveying and in earthquake studies to measure tectonic motions during and in between earthquakes. Also, GNSS is used in determination of geodetic datum, creating a reference system, geophysical-geodynamic studies, sea-level determination, cadastral and mining surveying and precision agriculture studies.

Such practices caused national cartography institutions in countries, local institutions and the private sector to set up GNSS networks created by stable GNSS stations which provide continuous and real-time observations. Particularly, for tectonic studies, GNSS based geodynamic projects were developed at a regional level. We can refer the works from in the California region (Larsen et al., 1992), (Straub et al., 1995) and (Reilinger et al., 1997) in the Mediterranean area and (Feigl et al., 1993) and (Miyazaki et al., 1996) in Japan and (Erdoğan et al., 2009). A nationwide GNSS infrastructure network known as CORS-TR was established in Turkey by Istanbul Kültür University (IKU), General Command of Mapping and General Directorate of Land Registry and Cadastre during 2006–2009. Spatial analyses of CORS stations, development of campaign type measurements with surface deformations, determination of linear plate movement etc. will help studies being carried out more accurate and realistic.

In this study, 788 days of GNSS observations using 7 CORS-TR stations (1.10.2008–26.11.2010) in Konya Closed Basin of Turkey were processed with GAMIT/GLOBK program package. Then, trend analysis, continuous wavelet transform (CWT) and discrete wavelet transform (CWT) are applied to coordinate time series.

WAVELET ANALYSIS OF GNSS COORDINATE TIME SERIES

Wavelet Transform (WT) was developed about three decades ago. WT was first applied to analyze seismic waves in geophysics studies (Torrence et al., 1998). Then, wavelet analysis has gained huge popularity among scientists and engineers who are interested in analyzing the time-frequency characteristics of signals. Dividing the signal into different frequencies and researching each component in terms of scale is the main idea of WT. The WT breaks up the signal into its “wavelets”, which are scaled and shifted versions of the “mother wavelet”. The two basic criteria for a function $\psi(t)$ to be considered a wavelet function are (1) that the average value of the wavelet must be zero and (2) that it must have unit energy. The criteria can also be written mathematically as follows (Calais, 1999):

$$\int_{-\infty}^{+\infty} \psi(t) dt = 0 \quad (1)$$

$$\int_{-\infty}^{+\infty} \psi^2(t) dt = 1 \quad (2)$$

A number of wavelet functions, which have different features, have been identified such as Haar, Daubechies, Symlets, Morlet, and Mexican Hat etc. Different wavelets may be used depending on the application. A couple of mother wavelet as shown in Figure 1 also they were used in this study.

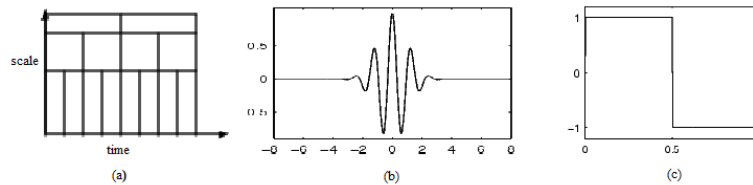


Figure 1. a) Wavelet Transform, b) morl wavelet, and c) db1 wavelet.

WT use a time-scale region as shown in Figure 1, so we can detect when specific events occur. WT can be classified in two types: The Continuous Wavelet Transform (CWT) and The Discrete Wavelet Transform (DWT). CWT is a result of multiplication between analyzed time series and scaled and shifted versions of wavelet function at all time. For the original signals $x(t)$ and wavelet function $\psi(t)$ CWT is defined as (Leon, 2008):

$$CWT(a, b) = \frac{1}{\sqrt{a}} \int_{-\infty}^{\infty} x(t) \psi\left(\frac{t-b}{a}\right) dt \quad (3)$$

$CWT(a, b)$ is the coefficients as a result of transition, a is the scale (dilation) parameter of the wavelet, b is the translation parameter of the wavelet, and t is time. CWT requires lots of time and memory because of calculating wavelet coefficients at every possible scale. Therefore, discrete values, which are depended on powers of two, of scale and positions are chosen in the discrete wavelet transform (DWT). Mallat (1989) developed an effective method, which utilizes filters, to apply this template. For the discrete signal $x(k)$ and the wavelet function $\psi(n)$, the DWT is defined as (Leon, 2008):

$$DWT(m, n) = \frac{1}{\sqrt{a_0^m}} \sum_k x(k) \psi(a_0^{-m}n - k) \quad (4)$$

The DWT filtering process effectively separates the low and high frequency components. From the point of resolution, the low frequency components will have a large scale and the high frequency components will have smaller scale. The low frequency components called as approximations and the high frequency components called as details. Approximations contain main features of the original signal. Noise is generally in detail components.

STUDY FINDINGS AND DISCUSSION

The time series analysis was carried out using the CORS positions from 7 GNSS stations including AKHR, BEYS, CIHA, KAMN, YUNA, AKSI, and KNYA of the CORS-TR network (national GNSS network), located in the Konya Closed Basin of Turkey (Figure 2).



Figure 1. The CORS-TR stations in the Konya Closed Basin of Turkey.

For the time series analysis, 788 days (1.10.2008–26.11.2010) of GNSS observations of the CORS-TR stations were first processed with GAMIT software and produced daily time series of CORS-TR stations (Gülal et al., 2013). After the signal processing, 27 time series were obtained from 7 stations. Because of data loss in AKSI and KNYA time series, they were divided into two separate time series including AKSI1, AKSI2, KNYA1, and KNYA2. Thus, 27 time series for 7 stations were obtained. These time series show the changes in the signals in the north, east, and up directions of stations according to coordinate system of the GNSS. The time series of the CIHA, AKSI1 and KNYA1 stations are shown in Figure 3. In Figure 3, the signal change $S(t_i)$ of the time series was acquired assuming that $S(t_1) = 0$ for the time initiation of t_i ($i = 1$). In this case, the signal change at any time point during the time series is in relation to the initiation time of the signal.

A filtering procedure, *Third-order Floating Weighted Average (FWA)*, was applied to the series to partially eliminate the noise effect, also big outlier data in the raw time series. The raw and filtered time series of the CIHA, AKSI1 and KNYA1 stations are shown in Figure 3. After the filtering procedure, Details and Approximations are obtained with DWT.

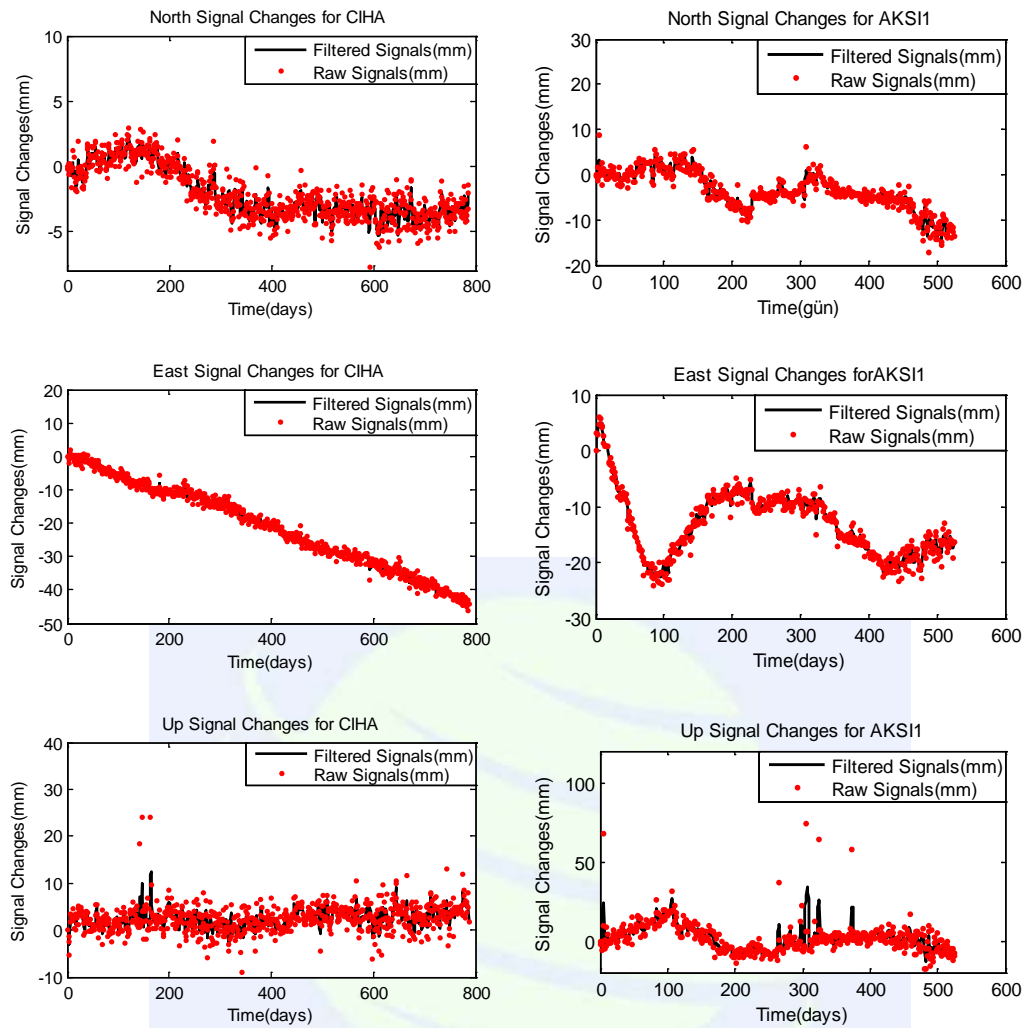


Figure 2. Time series of CIHA and AKSI1 stations for raw and filtered signals.

DWT was carried out to GNSS coordinate time series of North, East, and Up coordinates components of stations with multiresolutional analysis. For translation, db1 wavelet from Daubechies wavelet family was chosen because it is practicable to DWT. Considering the number of data, decomposition levels were set 9 for AKHR, BEYS, CIHA, KAMN, YUNA, and AKSI1, 6 for AKSI2, 7 for KNYA1, and 8 for KNYA2. In this way, approximations and details were obtained with DWT applied for all series. Approximations (a) and Details (b) of Station YUNA for UP Signals are shown in Figure 6.

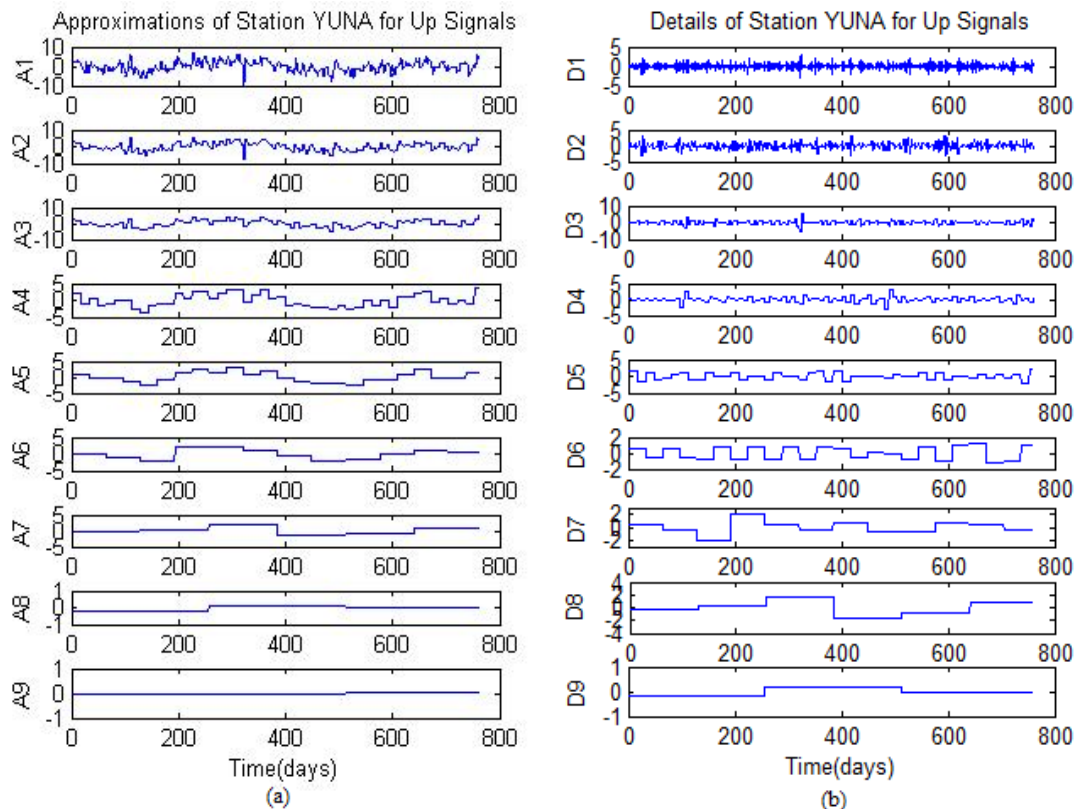


Figure 3. (a)Approximations of Station YUNA for UP Signals, (b)Details of Station YUNA for Up Signals.

Figure 3 (a) shows that A1 has a high correlation with the original signal while A9 has a low correlation. In this case correlation between the original signal and approximation decreases from A1 to A9. Besides, A8 and A9 have very low correlation with the original signals. Figure 3 (b) shows that D1 and D2 (especially D1) have vibrations caused from noise at 0. Also, these components have the highest frequency changes of the original signal. D1 has the highest frequencies and it decreases from D1 to D9. Furthermore, it is clearly seen that D9 has low correlation with the original signal.

Then the cross-correlations between detail-approximation components and the original time series were calculated and graphs of the obtained results are given. With these graphs obtained, correlations between A-D components and original signals and the delays were investigated. In graphs, delays are given horizontally and correlations are given vertically.

Because of the large number of graphs obtained, only graphs related to AKHR station are given in this section. For AKHR North series, Figure 4 shows that the highest values were obtained in D8 and D7. The correlation value for both components is approximately 0.5. This shows that the correlations between the D8-D9 components and the original time series is higher and the activities, which have the annual period, are important on the coordinate characteristic of the station.

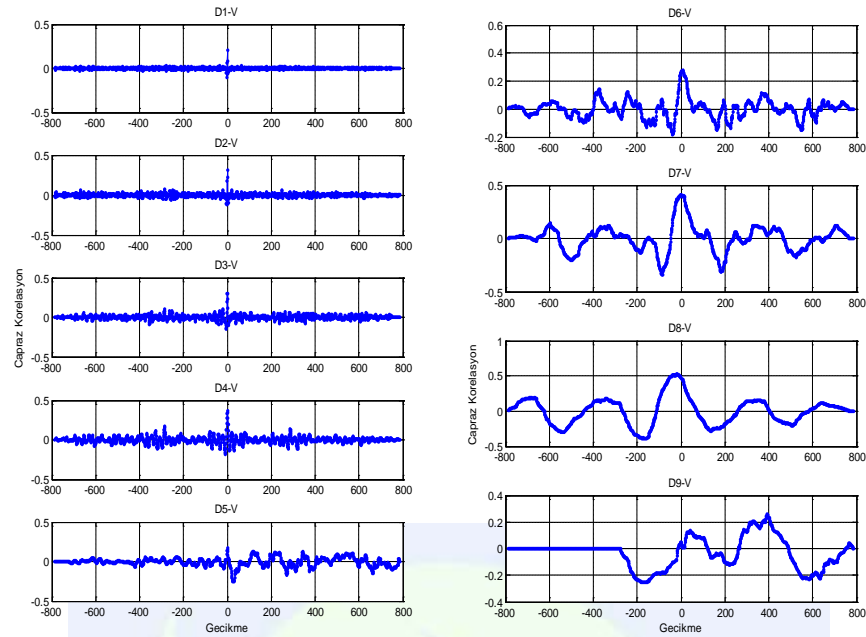


Figure 4. Cross correlations of AKHR North (D1-D9)-V.

Figure 5 shows that while A1 has the highest value (approximately 1), A9 has the lowest value (0.2). Furthermore, correlation value between the original signal and approximation decreases from A1 to A9 and especially A8 and A9 have very low correlation with the original signal.

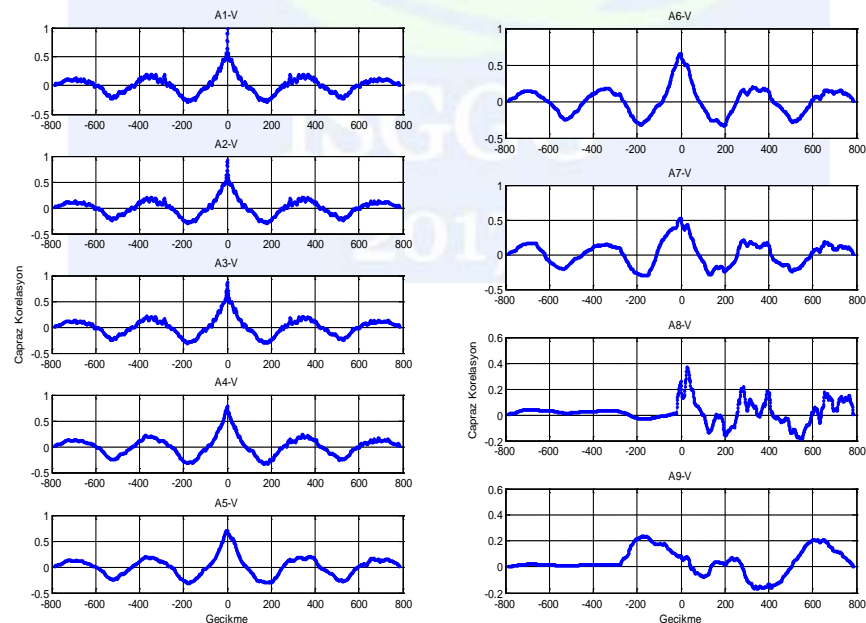


Figure 5. Cross correlations of AKHR North (A1-A9)-V.

For AKHR East series, Figure 6 shows that the correlation of the first 5 detail components is close to 0, so that the correlation of these components with the main time series is very low. However, D8 and D7 have the highest correlation values (0.5) and these results are similar to AKHR North results.

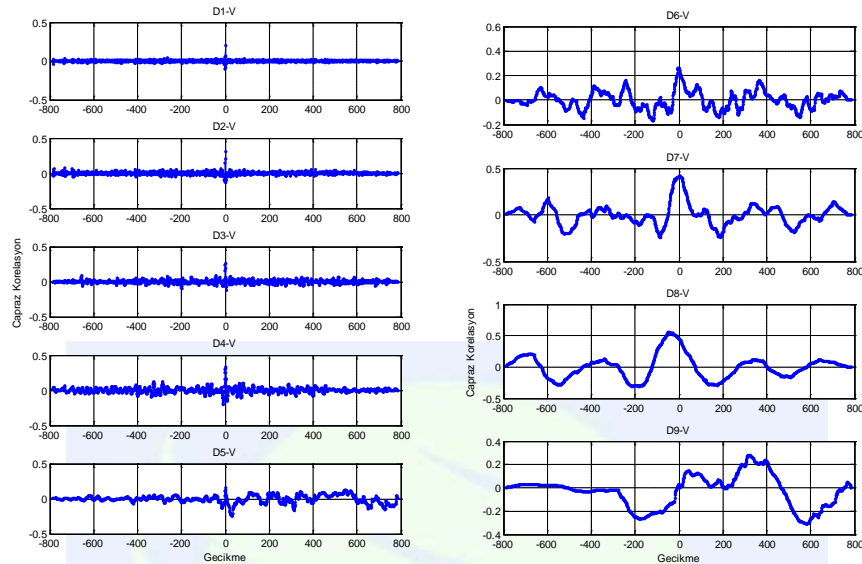


Figure 6. Cross correlations of AKHR East (D1-D9)-V.

Figure 7 shows that while A1 has the highest value (approximately 1), A9 has the lowest value (0.2). Furthermore, correlation value between the original signal and approximation decreases from A1 to A9 and especially A8 and A9 have very low correlation with the original signal. These results are similar to AKHR North results.

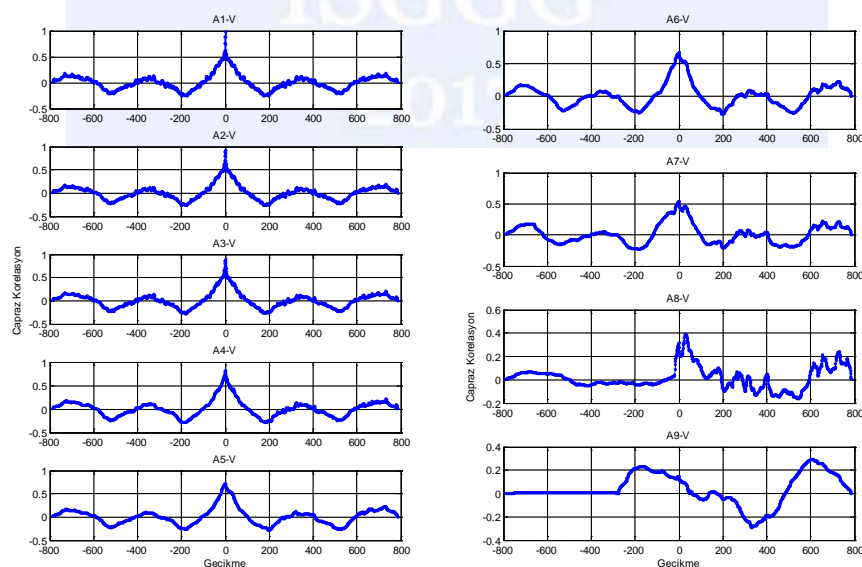


Figure 7. Cross correlations of AKHR East (A1-A9)-V.

For AKHR East series, Figure 8 shows that the highest correlation values are obtained in D2, D3, D4, and D5 and the values are approximately 0.5. These results are not similar to AKHR North and AKHR East.

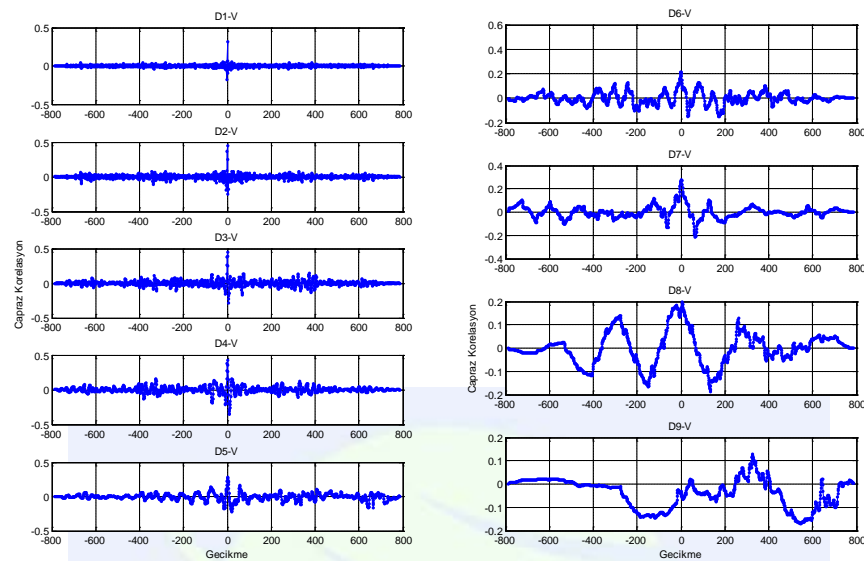


Figure 8. Cross correlations of AKHR Up (D1-D9)-V.

Figure 9 shows that while A1 has the highest value (approximately 1), A9 has the lowest value (0.1). Furthermore, correlation value between the original signal and approximation decreases from A1 to A9. These results are similar to AKHR North and AKHR East. However, correlation values of A7 is 0.2 and this result is different from AKHR North and AKHR East.

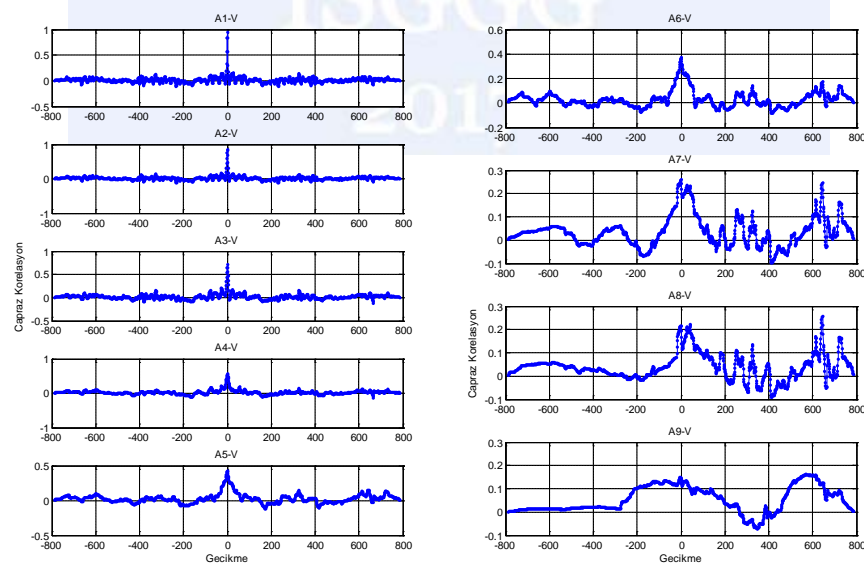


Figure 9. Cross correlations of AKHR Up (A1-A9)-V.

In conclusion, while correlations of approximations of North, East, and Up time series are very strong, correlations of details of North, East, and Up time series are generally very weak. For North and East series D7 and D8 have the higher correlation values. However, this situation differs from station to station in Up series. The analysis results for the North and East time series for the same station in the detail components are similar.

In the cross-correlation analysis, the main series and the component series are considered as two different variables, but the component time series are obtained from the original series. In this case, it is not possible to mention about delay.

CONCLUSIONS

In this paper, 788 daily GNSS time series were obtained using GAMIT software to process the GNSS observations from seven stations of CORS-TR network, located in Konya Closed Basin of Turkey.

DWT was carried out to GNSS coordinate time series of North, East, and Up coordinates components of stations with multiresolutional analysis. For translation, db1 wavelet from Daubechies wavelet family was chosen because it is practicable to DWT. Considering the number of data, decomposition levels were set 9 for AKHR, BEYS, CIHA, KAMN, YUNA, and AKSI1, 6 for AKSI2, 7 for KNYA1, and 8 for KNYA2. In this way, approximations and details were obtained with DWT applied for all series.

The cross-correlations between Approximations-Details obtained with DWT and the original time series were calculated and graphs of the obtained results are given. while correlations of approximations of North, East, and Up time series are very strong, correlations of details of North, East, and Up time series are generally very weak. For North and East series D7 and D8 have the higher correlation values. However, this situation differs from station to station in Up series. The analysis results for the North and East time series for the same station in the detail components are similar. In the cross-correlation analysis, the main series and the component series are considered as two different variables, but the component time series are obtained from the original series. In this case, it is not possible to mention about delay.

ACKNOWLEDGMENTS

We would like to thank to Assoc. Dr. I. Tiryakioglu for GNSS data processing.

REFERENCES

- C. Straub, H.G. Kahle, 1995, Active crustal deformation in the Marmara Sea region, NW Anatolia, inferred from GPS measurements, *Geophysical Research Letters*, 22, pp. 2533–2536.
- E. Calais, Continuous GPS measurements across the Western Alps 1996–1998, 1999, *Geophysical Journal International*, 138(1), pp. 221–230.

- F. Ahmed, 2010, *Evaluation of GNSS as a tool for monitoring tropospheric water vapour*, MSc thesis, Department of Earth and Space Sciences, Chalmers University of Technology, Göteborg, Sweden.
- Gülal E., Erdoğan H., Tiryakioğlu İ., 2013, Research on the stability analysis of GNSS reference stations network by time series analysis, *Digital Signal Processing*, 23(6), pp. 1945–1957.
- K.L. Feigl, D.C. Agnew, Y. Bock, D. Dong, A. Donnellan, et al., 1993, Space geodetic measurement of crustal deformation in central and southern California, 1984–1992, *Journal of Geophysical Research*, 98(B12), pp. 1677–1712.
- Leon, J., 2008, “A system level implementation of wavelet based filtering for GNSS signals”, Theses and dissertations. Paper 174. Ryerson University.
- Mallat, S., 1989, "A theory for multiresolution signal decomposition: the wavelet representation", *IEEE Pattern Anal. and Machine Intell.*, 11(7), pp. 674–693.
- R.E. Reilinger, S.C. McClusky, M.B. Oral, R.W. King, M.N. Toksoz, A.A. Barka, I. Kinik, O. Lenk, I. Sanli, 1997, Global Positioning System measurements of present-day crustal movements in the Arabia–Africa–Eurasia plate collision zone, *Journal of Geophysical Research*, 102 (B5), pp. 9983–9999.
- URL1-SatelliteNavigation, http://en.wikipedia.org/wiki/Satellite_navigation, retrieved 2011-12-30.
- S. Erdogan, M. Sahin, I. Tiryakioğlu, E. Gülal, A.K. Telli, 2009, GPS velocity and strain rate fields in Southwest Anatolia from repeated GPS measurements, *Sensors* 9(3) 2017–2034.
- S. Larsen and R. Reilinger, 1992, Global Positioning System measurements of strain accumulation across the Imperial Valley, California: 1986–1989, *Journal of Geophysical Research*, 97(B4), pp.8865–8876.
- S. Miyazaki, H. Tsuji, Y. Hatanaka, Y. Abe, A. Yoshimura, K. Kamada, K. Kobayashi, H. Morishita, Y. Iimura, 1996, Establishment of the nationwide GPS array (GRAPES) and its initial results on the crustal deformation of Japan, *Bull. Geogr. Surv. Inst. (Jpn.)* 42, pp. 27–41.
- Torrence, C., and G. P. Compo, 1998, A Practical Guide to Wavelet Analysis, *Bulletin of the American Meteorological Society*, 79(1).

Description of Behaviors of GNSS Stations By Signal Processing Methods In Konya Closed Basin

Hediye Erdoğan¹, Osman Oktar^{*2}

^{1, 2} Department of Geomatic Engineering, Aksaray University, 68100, Turkey. (osmanoktar@aksaray.edu.tr
hediyeerdogan@aksaray.edu.tr)

ABSTRACT

In this study, the effects of underground water level changes measured from Konya Closed Basin wells to the positions of stationary GNSS stations in this region were investigated by analysis of time series and cross-correlation function. As a result of trend component analyses of time series it was determined that horizontal positions of stations in this region were moving in the Northeast direction (18.88 mm/year). For Up coordinates, while ANRK, KLUU, and NIGD have movements (0.56 mm/yıl) in up direction, the other stations have movements in down directions. Vertical movement of KNY1 station that have 560-day data is in down (-) direction, its annual movement is 70.96 mm and this movement or velocity is the maximum compared to vertical movements of stations in this region. As a result of trend analysis of 19 wells for underground water level changes, linear changes were obtained in down direction and the mean value is -39.22 cm/year. The decrease in the water level of the wells in the Konya Closed Basin is statistically significant by majority, and at meter level in some wells. As a result of the cross correlation analysis between GNSS stations and groundwater level time series, there is a negative correlation between both north and east coordinates of the GNSS stations and underground water levels. In contrast, there is positive correlation between up (Up) coordinates and the underground water levels.

INTRODUCTION

With the help of GNSS stations that continuously collect data, it is possible to examine changes in position information as a function of time. These data are generally used to observe the slip movements of earth crust and to estimate slip velocity of ground (Langbein and Johnson 1997, Williams et al. 2004). It is assumed that GNSS signal fits a model. This model includes components such as linear slip, semi-annual and annual oscillations, post-earthquake logarithmic oscillation and a starting point, as well as a noise component. The correct estimation of the model parameters depends on modeling the data appropriately, and the appropriate modeling depends on the estimation of what kind of

* Corresponding Author

noise the residual signal (difference between model and data, modeling or observation error) is. It is expressed that the noise in GNSS data is the combination of the time independent White noise and time dependent colored noise (Langbein and Johnson 1997, Williams et al. 2004). (f is frequency and its unit is Hz) While the white noise component is caused by measurement errors, the color $1/f$ noise component is caused by the ambiguity of the position of the GNSS receiver (Langbein and Johnson, 1997; Mao et al., 1999).

In addition, there are many parameters that affect the position accuracy of GNSS stations. These parameters are minimized in stages such as device selection, measurement method, measurement time, software selection and process of measurements. Also, the selection of station locations is one of the important factors affecting position accuracy. Because GNSS stations have areas of usage needing very high accuracy, station locations should be as stable as possible in terms of tectonics, on solid rock or on hard-ground areas, and ground point should be monument (Calais, 1999). All these reasons and requirements are important in terms of examining the time-dependent changes in the position information of stationary GNSS stations within the cause-and-effect relationship. Determining position information of GNSS stations accurately, continuously, fast, and economically with reliable methods is important in terms of providing to users who work on commercial or scientific studies based on position information.

In this study, daily position informations (North, East, Up) of 16 stationary GNSS (CORS-TR) stations in and around Konya plains were used. Daily position data (North, East, Up) of 15 stations that have 6 years data (2008-2014) and KNY1 station that has 560 day data (2014-2015) depending on time were obtained, and time series of these stations were created. Linear behavior and size of linear behavior of the stations were determined by trend analysis of these time series obtained for the stations. In addition, groundwater changes have been studied in this study since drought in the working area over the last decade, due to global climate change, and reduction in groundwater causing from excess water use.

METHOD

Excluding artificial or co-seismic and post-seismic slip, time series $Y(t_i)$ obtained from GNSS measurements at t_i ($i=1, 2, 3, \dots, N$) can be separated to three components generally (Gülal vd.,2013).

$$Y(t_i) = T(t_i)_{\text{Trend}} + P(t_i)_{\text{Periodic}} + S(t_i)_{\text{Stochastic}} \quad (1)$$

In the analysis of time series, firstly the time-axis graph of the series is drawn and the unusual measurements (example: gross errors) are eliminated and general interpretation of the series can be made. A suitable low-pass filtering operation (example: Five-order Floating Weighted Average) is applied to the series for particularly eliminating the noise effect in the series and in order to reveal trend and periodic components more clearly. Then it is determined whether the series has a trend component, and it is defined as below;

$$T(t_i)_{Trend} = \sum_{k=1}^m c_k t_i^{k-1} \quad (2)$$

In this equation, c_k ($k = 1, 2, \dots, m$) are the parameters depending on the order of the polynomial function. Changes (velocities) in increasing or decreasing direction of GNSS stations linearly are defined by taking $m=2$. The test size determined for each parameter is compared to the determined $1-\alpha$ confidence level and $\pm t_{f, 1-\alpha/2}$ confidence limit of t -distribution depending on f degrees of freedom. As a result of comparing, if the parameters are significant, there is a linear movement in the time series.

RESEARCH FINDINGS AND DISCUSSION

In this study, the linear movements (velocities) of GNSS stations continuously measuring in the Konya Closed Basin (Figure 1b) and the changes of underground water level causing these movements (expecially vertical movement) are investigated. For this reason, the periodic and stochastic components of time series analysis were not analyzed in this study.

Study Area: Konya Plain is located in the central and southern part of Central Anatolia Region. The field is surrounded by Bozdağ and Obruk Plateau in north and northwest; the inner slopes of Toros arc starting from Sultan Mountains to the South of the Karaman Province in south; Ereğli Plain in east; Takkeli Mountain, Gevele Mountain, and Loras Mountain in west (Figure 1a).

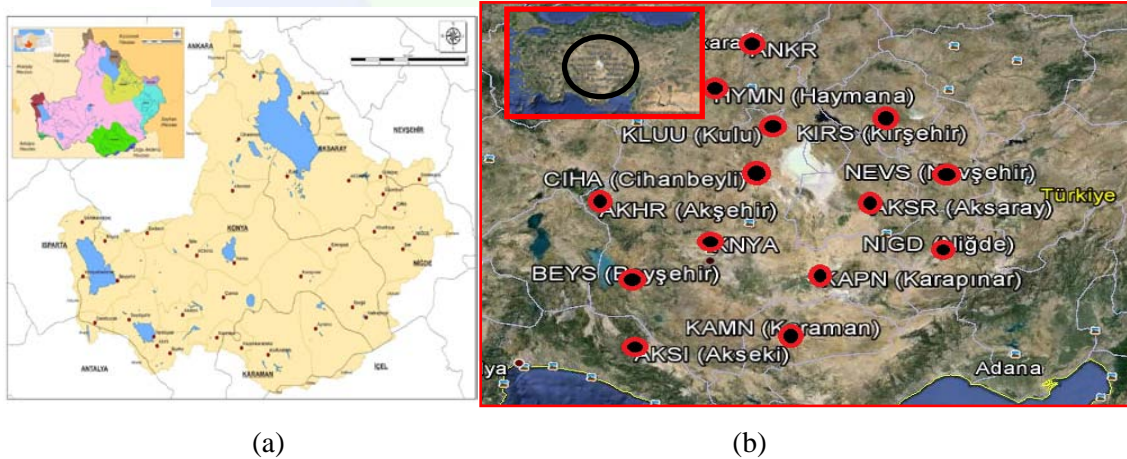


Figure 1. (a) Konya Closed Basin political map (Tübitak, MAM, 2009), (b) CORS-TR station positions.

In addition, it has been observed that the formation of sinkhole has increased in recent years in and around Konya Plain. It is estimated that there is a relationship between the occurrence of these current sinkholes and the decrease in underground water level. From past to present, concrete examples of decrease of underground water level are seen in Akgöl (Ereğli), Acıgöl (Karapınar), Meke Tuzla (Karapınar), and Timraş Sinkhole (Göçmez et al., 2004).

GNSS Stations

Daily position informations (North, East, Up) of 16 stationary GNSS (CORS-TR) stations in and around Konya plains were used. Daily position informations (North, East, Up) of 15 stations that have 6 years data (2008-2014) and KNY1 station that has 560 day data (2014-2015) depending on time were obtained, and time series of these stations were created (Figure 2 and Figure 3). The data were obtained from the General Command of the Mapping, and ITRF08 fixed was taken in data process. Time series in north and east directions of KAMN, KAPN, KNYA and KNY1 stations from 48 (16.3 = 48) time series obtained for 16 stations are given in Figure 2 and Figure 3. Figure 2 shows that the linear movements and equations of the series. Figure 4 also shows up time series, linear changes, function of linear change and frequency spectrum of the same stations. Because there is high number of stations, time series graphs of other stations are not given. However, linear functions and station speeds (annually) are given as table (Table 1 and Table 2). It can be seen that the time series in north and east directions of the stations show a linear increase in the north and east directions (Figure 2). The same results were obtained in the time series of the other stations not given as figures. In addition, pulse movement is seen at marked points in KNYA north and east time series and the last part of the series. This situation was seen in up coordinate values more prominently.

Trend component analysis

It was determined that whether time series in North, East and Up directions of GNSS stations contain any linear movement or not by the use of the proposed function in the Eq. (2). c_1 and c_2 parameters of the linear function generated by taking $m=2$ and standard deviations of these parameters were estimated by LSM.

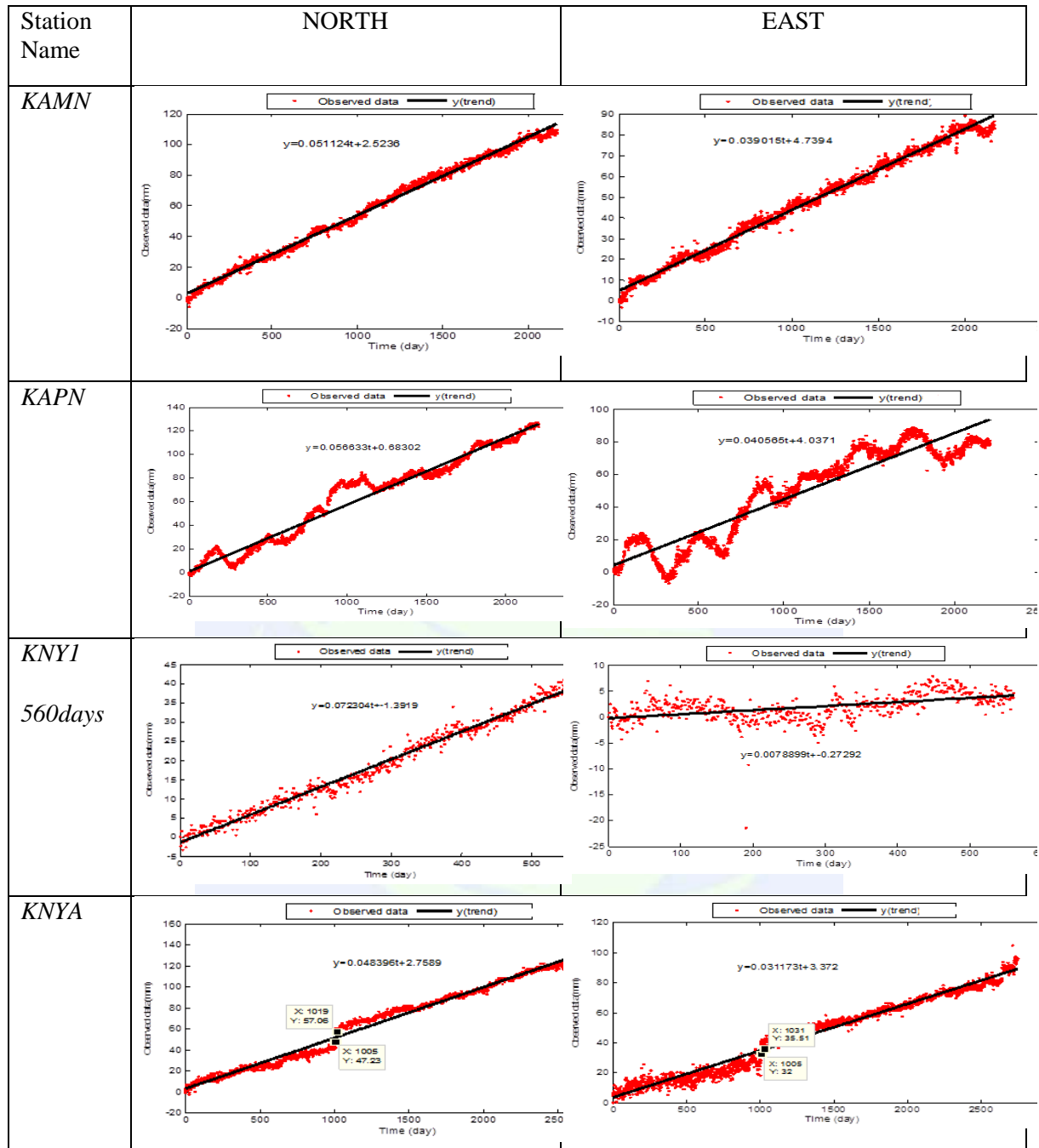


Figure 2. Coordinate time series, linear movements, and linear functions of KAMN, KAPN, KNYA, and KNY1 stations in North and East directions.

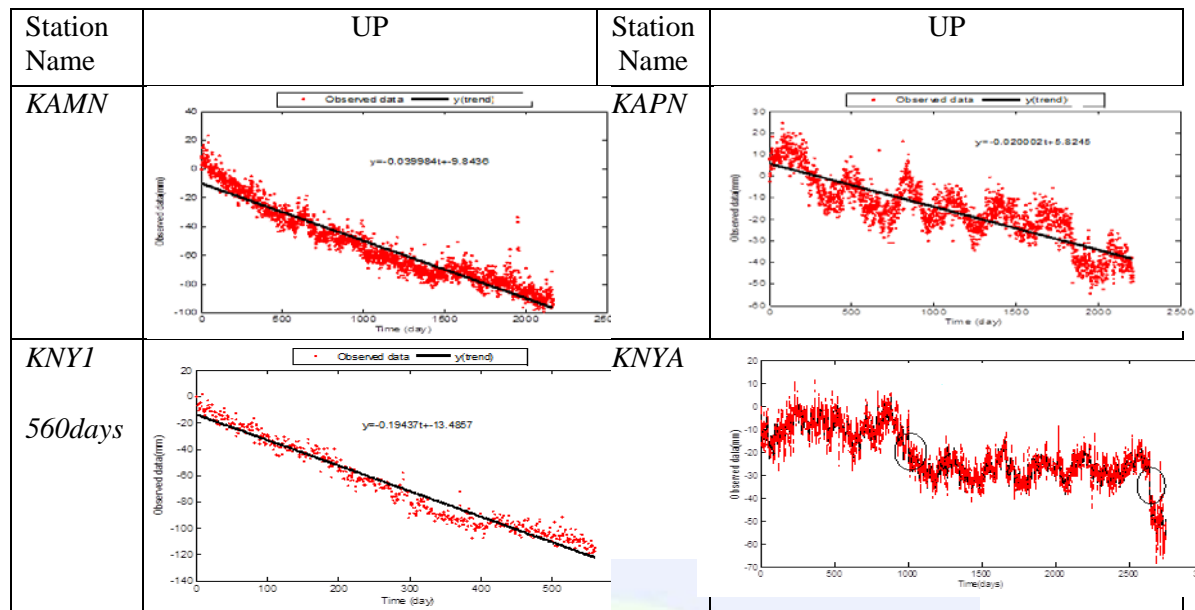


Figure 3. Linear changes in up coordinate time series of stations.

Whether the deviations of the calculated parameters from the "0" value are significant or not is determined by $\alpha=0.05$ error possibility according to t-distribution (for $f>200$, $t_{f,1-0.05/2}=2$ and for $f>500$, $t_{f,1-0.05/2}=1.96$). As a result of the trend component analysis of GNSS stations, it was determined that the time series of north and east coordinates of all stations showed a statistically significant linear movement in the positive (increasing) direction. Linear movements and linear functions are given in Figure 2. Table 1 shows statistically significant linear movements (linear models) and annual linear changes (velocities) of all stations. The " c_2 " parameter in trend function indicates stations' daily (+) increasing or (-) decreasing direction of linear change. With this parameter, linear changes or movements of the stations can be detected at desired time.

Table 1. Linear functions and annual velocities of GNSS stations (North and East).

Station	North Linear Functions ($Y=c_2t+c_1$)	Linear Changes (mm/year)	East Linear Functions ($Y=c_2t+c_1$)	Linear Changes (mm/year)	Resultant Changes (mm/yil) Directions
AKHR	$Y(trend)=0.0245t+1.7226$	8.94	$Y(trend)=0.0113t+1.6671$	4.12	9.84/northeast
AKSI	$Y(trend)=0.0302t+14.0774$	11.02	$Y(trend)=0.0406t+0.0612$	14.82	18.47/northeast
AKSR	$Y(trend)=0.0513t-0.7534$	18.72	$Y(trend)=0.0229t+1.3993$	8.36	20.50/northeast
ANRK	$Y(trend)=0.0427t+1.2507$	15.59	$Y(trend)=0.0115t+1.6134$	4.20	16.15/northeast
BEYS	$Y(trend)=0.0313t+1.5188$	11.42	$Y(trend)=0.0283t+3.0769$	10.33	15.40/northeast
CIHA	$Y(trend)=0.0418t-2.7231$	15.26	$Y(trend)=0.0191t-2.8808$	6.97	16.78/northeast
HYMN	$Y(trend)=0.0361t+4.5038$	13.18	$Y(trend)=0.0148t-0.9256$	5.40	14.24/northeast
KAMN	$Y(trend)=0.0511t+2.5236$	18.65	$Y(trend)=0.0390t+4.7394$	14.24	23.46/northeast
KAPN	$Y(trend)=0.0566t+0.6830$	20.66	$Y(trend)=0.0406t+4.0371$	14.82	25.43/northeast
KIRS	$Y(trend)=0.0490t+7.9869$	17.89	$Y(trend)=0.0192t-1.0199$	7.01	19.21/northeast
KLUU	$Y(trend)=0.0435t+5.2655$	15.88	$Y(trend)=0.0196t+1.2331$	7.15	17.42/northeast
NEVS	$Y(trend)=0.0535t+1.2779$	19.53	$Y(trend)=0.0256t+1.7963$	9.34	21.65/northeast
NIGD	$Y(trend)=0.0550t-0.6508$	20.08	$Y(trend)=0.0334t+1.1063$	12.19	23.49/northeast
YUNK	$Y(trend)=0.0314t+0.6469$	11.46	$Y(trend)=0.0135t-2.7270$	4.93	12.48/northeast
KNY1(560 days)	$Y(trend)=0.0723t-1.3919$	26.39	$Y(trend)=0.0079t-0.2729$	2.88	26.55/northeast
KNYA	$Y(trend)=0.0484t+2.7589$	17.67	$Y(trend)=0.0312t+3.3720$	11.39	21.02/northeast

As shown in Table 1, GNSS stations in this region have linear movements in northeast

direction (ITRF08 fixed). Annual mean movement or velocity of stations is 18.88 mm. The stations having annual velocity greater than 2 cm are; AKSR, KAMN, KAPN, NEVS, NIGD, KNY1, and KNYA. Maximum velocity is 26.55 mm/year and it is obtained in KNY1 station. Minimum velocity is 9.84 mm/year and it is obtained in AKHR. Linear movements and linear functions of up coordinate time series of GNSS stations (KAMN, KAPN, KNYA VE KNY1) are shown in Figure 3. In addition, statistically significant linear movements (linear models) and annual linear changes (velocities) of stations are given in Table 2.

Table 2. Linear functions and annual velocities of GNSS stations (Up).

Station	Up Linear Functions ($Y=c_2t+c_1$)	Linear Changes (Velocities) (mm/year)
AKHR	$Y(trend)=-0.0143t+14.3868$	-5.22
AKSI	$Y(trend)=-0.0063t+22.6557$	-2.30
AKSR	$Y(trend)=-0.0102t-1.5357$	-3.72
ANRK	$Y(trend)=0.0023t-8.4197$	0.84
BEYS	$Y(trend)=-0.0025t+5.2138$	-0.91
CIHA	$Y(trend)=-0.0035t+3.5352$	-1.28
HYMN	$Y(trend)=-0.0037t-0.1510$	-1.35
KAMN	$Y(trend)=-0.0400t-9.8436$	-14.60
KAPN	$Y(trend)=-0.0200t+5.8245$	-7.30
KIRS	$Y(trend)=-0.0023t-8.6258$	-0.84
KLUU	$Y(trend)=0.0018t-5.7144$	0.66
NEVS	$Y(trend)=-0.0007t+5.2945$	-0.26
NIGD	$Y(trend)=0.0005t+10.1856$	0.18
YUNK	$Y(trend)=-0.0026t+2.009$	-0.95
KNY1(560days)	$Y(trend)=-0.1944t-13.4857$	-70.96
KNYA	$Y(trend)=-0.0106t-6.9657$	-3.87

It is determined that up coordinate time series of all stations have statistically significant linear movements in positive and negative direction. Considering linear movement in Up direction of KNY1, the mean value of linear movements in negative direction for Up coordinates is -8.74 mm/year as shown in Table 2. Annual Vertical movement of KNY1 stations that has 560-day data is 70.96 mm in down (-) direction and this is the highest value of vertical movements of stations in this region. KNY1 is the new GNSS station set up in 2014 because of the fact that there is peak (Figure 2 and Figure 3) in KNYA station time series. The cause of the maximum change in KNY1 is decrease in groundwater level in this region (Özdemir, 2016). Unless annual velocity of this station is considered, the mean value of vertical changes in negative direction is -3.55 mm/year. Vertical movements of ANKR, KLUU, and NIGD stations are in up direction and mean annual movement is 0.56 mm (Table 2). Except for KNY1 station, annual velocities of stations for Up coordinates are sufficiently small values. With -1.5 cm/year velocity, KAMN has the second highest velocity among the stations studied for this region (Table 2).

Underground Water Level Changes

In this study, 19 wells were measured monthly in order to determine the underground water level changes of Konya plain. The wells in this region have at least 11 year data and

at most 49 year data (for 19 station). The time-dependent changes (monthly) of the 2 wells used to determine groundwater level changes are given in Figure 4. As in the trend analysis of GNSS stations, trend analysis was performed for 19 wells. Linear functions and annual changes are given in Figure 5 and Table 3. As a result of the analysis, linear changes such as mean = -39.22 cm/year for 19 wells, mean = -15.56 cm/year for 3 wells in Konya-Cihanbeyli field, mean = -63.48 cm/year for 4 wells in Konya-Selçuklu field, mean = -68 cm/year for 6 wells in Karaman field, and mean = -19.50 cm/year for 2 wells in Niğde field in decreasing direction are obtained. It is seen that the annual change in KONYA-SELÇUKLU-MEYDAN, KARAMAN-AYRANCI-HUYUKBURUN, and KARAMAN-MERKEZ-SUDURAĞI wells according to the well data is over 1 m (Table 3). However, the linear function of KONYA-KULU and KONYA-SEYDİŞEHİR well data shows insignificant linear change at 95% confidence level. In addition, a linear increase (69.72 cm/year) was detected in the KONYA-BEYSEHİR-DOĞANBEY well.

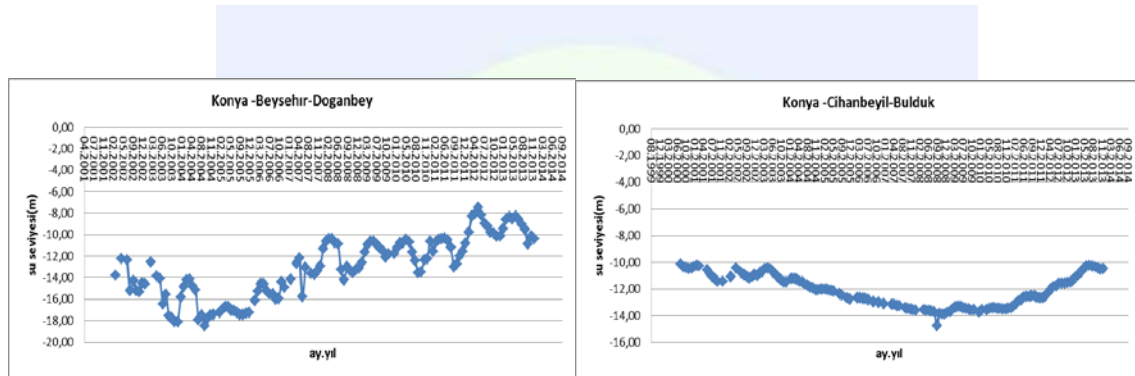


Figure 4. Time series of Doğanbey and Bulduk stations (wells).

Table 3. Linear functions and annual changes of well observations.

Name of Well	Linear Functions $y(\text{trend})=c_2t+c_1$	Linear Changes (velocities) (cm/year)	Results
KONYA-BEYSEHİR-DOĞANBEY	$y(\text{trend})=0.0581t-17.0946$	69.72	significant
KONYA CİHANBEYLİ BULDUK	$y(\text{trend})=-0.0109t-11.2754$	-13.08	significant
KONYA-CİHANBEYLİ-KARTAL	$y(\text{trend})=0.0046t-24.4201$	5.52	significant
KONYA-CİHANBEYLİ-SIGIRCIK	$y(\text{trend})=-0.0326t-22.3711$	-39.12	significant
KONYA-KARAPINAR-GULFET-YAYLA	$y(\text{trend})=-0.0520t-10.6263$	-62.40	significant
KONYA-KULU	$y(\text{trend})=-0.0039t-11.3281$	-4.68	insignificant
KONYA-SELÇUKLU	$y(\text{trend})=-0.0363t-5.4342$	-43.56	significant
KONYA-SELÇUKLU-MEYDAN	$y(\text{trend})=-0.1098t-7.4969$	-131.76	significant
KONYA SELÇUKLU-SARICALAR	$y(\text{trend})=-0.0257t+0.1759$	-30.84	significant
KONYA SELÇUKLU TUTUP	$y(\text{trend})=-0.0398t+2.1481$	-47.76	significant
KONYA-SEYDİŞEHİR	$y(\text{trend})=-0.0003t-2.2111$	0.36	insignificant
KARAMAN- AYRANCI -HUYUKBURUN	$y(\text{trend})=-0.0933t-66.2993$	-111.96	significant
KARAMAN- KAZIMKARABEKİR-MERKEZ	$y(\text{trend})=0.0024t-7.8545$	2.88	significant
KARAMAN -CENTER -AKCASEHIR	$y(\text{trend})=-0.0585t-33.6459$	-70.20	significant
KARAMAN -CENTER -EMİNLER	$y(\text{trend})=-0.0379t-2.9531$	-45.48	significant
KARAMAN -CENTER -KOCASOYUK	$y(\text{trend})=-0.0610t-0.9697$	-73.20	significant
KARAMAN- CENTER -SUDURAĞI	$y(\text{trend})=-0.0922t-23.1213$	-110.64	significant
NIGDE- ALTINHISAR- CENTER	$y(\text{trend})=-0.0256t-7.9697$	-30.72	significant
NIGDE -BOR -BAHCELİ	$y(\text{trend})=-0.0069t-1.8532$	-8.28	significant

The majority of the water level of the wells in this region has statistically significant decrease, and it is in meter level in some wells. Climate, geologic and geomorphological factors have influenced the changes in the level of groundwater in the Konya Plain. Changes in groundwater level occur both within the year and between years. There is a decrease in the June-September period, which characterizes the dry season within the year, and an increase in the rainy season in January-May. Indeed, it is observed that there is a significant decrease of up to 1 m. in groundwater levels in 30-40 year water wells distributed in the region (Göçmez and İşcioğlu, 2004; Doğdu et al., 2007; Üstün et al., 2007). At some stations monthly water level data have been recorded since 1960. The decrease in underground water level of relevant 24 wells is observed in study of Üstün and his friends (2007). As a result of examining the time series of wells, it is determined that the decrease in most wells is not linear, in other words the decrease velocity increases in time. Doğdu and his friends (2007) examined the meteorological records of Konya Closed Basin (KCB) from 1929 to the present day, and they have found significant rainfall reduction in basin since the early 1980s. It was determined that the decrease in underground water levels for 11 wells that observed long-term (>30 year) consistent with this (Üstün et al., 2007). The underground water level of the wells around Karapınar is 16.9 m in September 1970 and 31.2 m in September 2003. It has been determined by Göçmez et al. (2004) that there is a decrease of 14.3 m in the level of underground water in 33 year period. Narrowing/constriction (press) in the aquifer systems due to underground water drawdown can create a vertical deformation (downfall) in the floor over these systems. Given similar examples elsewhere in the world, it is likely to encounter such a situation for KCB. Some examples of partial downfall events of the earth crust and more detailed information about monitoring with geodetic methods of these components are can be found in studies such as Phienweij et al., (2006), Abidin et al., (2007), Galloway and Hoffman (2007), and Üstün et al., (2007).

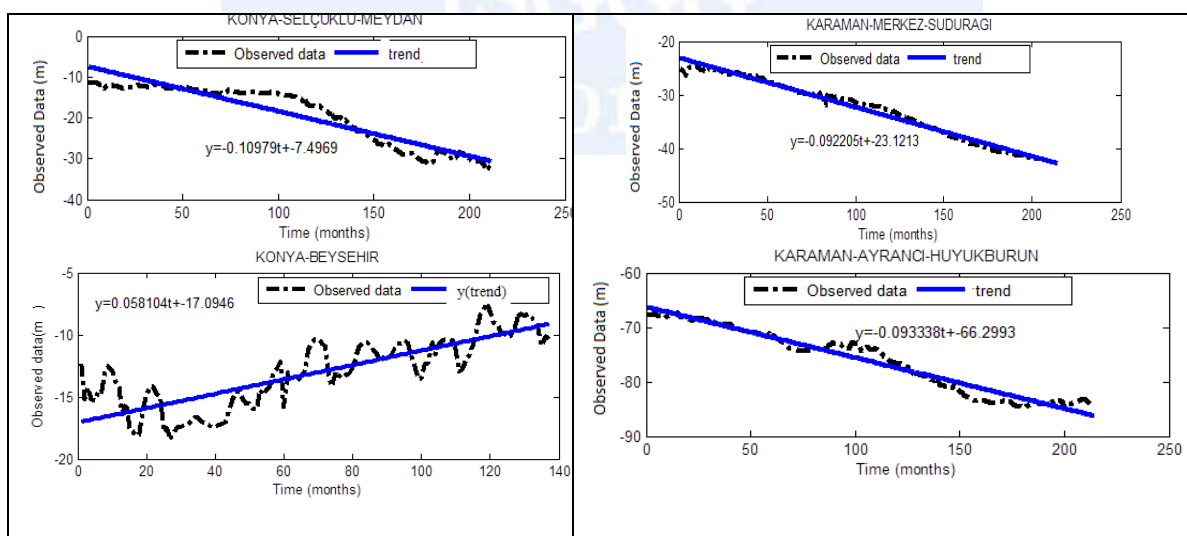


Figure 5. Linear functions and power spectrums of well observations in Konya and Karaman.

As a result of linear analysis of well data in KCB, it can be stated that at the underground water level in this region, especially in the last decade period, there is a decrease resulting from the drought that result of the global climate change and excess water use.

Cross-Correlation

A cross-correlation analysis was performed between KAMN, KAPN and KNYA time series (North, east, up) and water level changes obtained from Karaman-Center-Akçaşehir, Karaman-Center-Eminler, Karaman-Center-Kocahüyük, Karaman-Center-Sudurağı, Konya-Karapınar-Gülfet, Konya-Selçuklu-Center wells, which are close to these stations and where the underground water level is greatly decreased. Results of the cross-correlation analysis are given in Table 4 and Figure 6 (four of them). As a result of cross-correlation analysis between KAMN up coordinates and Karaman-Center-Akçaşehir underground water levels, correlation is maximum ($r_{\text{cross}}=0.77$) for lag=0. In addition, the correlation between the variables is negative and the correlation for the first 13 lag is significant. Similar results were obtained as a result of the cross correlation analysis between the east coordinates of the same station and the same well (the maximum correlation is -0.79 for lag=0). Correlation between up coordinates of the same station and same well is positive, correlation is significant for first 13 lag, the maximum correlation is 0.74 for lag=0.

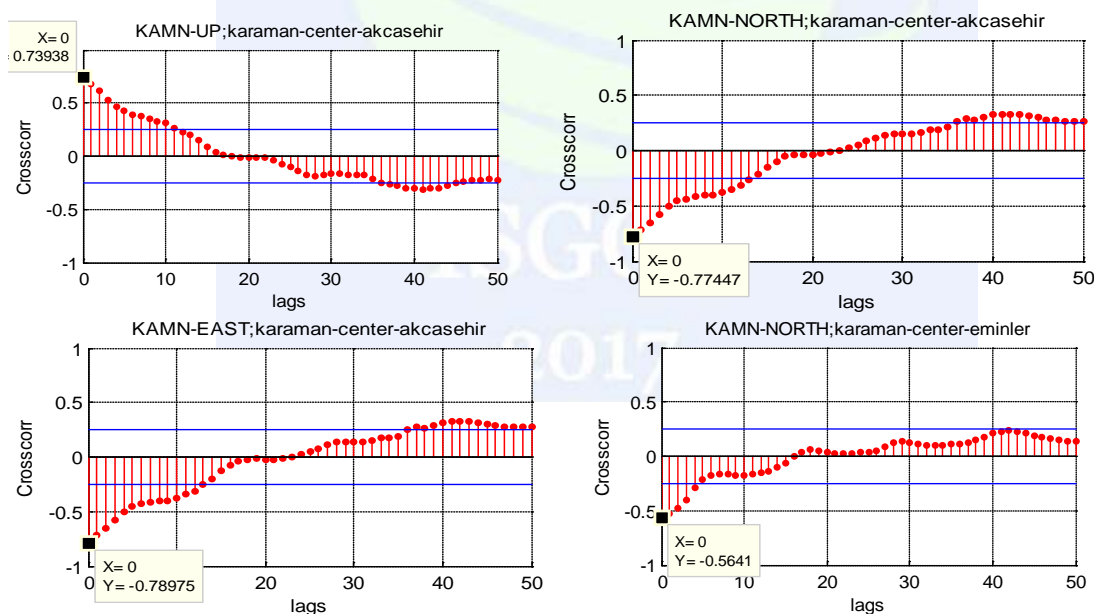


Figure 6. Some of cross-correlation analysis results.

As can be seen in Table 4, while there is a negative correlation between north and east coordinates of GNSS stations and well data, there is a positive correlation between up coordinates of GNSS stations and well data. In this case we can say that the decrease in underground water levels effect horizontal positions of GNSS stations in positive directions; however, the decrease in underground water levels effect vertical position of

GNSS stations in negative direction. In addition, it is determined that correlation is high between KAMN station coordinates and Karaman-Center-Akçaşehir/Karaman-center-Sudurağı. Correlation between KAMN station coordinates and Karaman-Center-Kocahüyük is low (mean=0.5). Correlation between KAPN and Konya-Karapınar-Gülfet is 0.7. Correlation between KNYA station and Konya-Selçuklu-Center is insignificant. Correlation between KAMN station coordinates and Karaman-Center-Sudurağı data (rcross=0.99) is very high (Table 4). Also, lag values are high for data that have high correlation. Since the data are monthly, there is a correlation for approximately one year of data for the first 13 lag.

Table 4. Results of cross-correlation analysis between GNSS stations and underground water level data obtained from wells closed stations.

GNSS station	Coordinate component	Name of well	Lag/ Maximum correlation/direction	Lag value of significant correlation
KAMN	North	Karaman-Center-Akçaşehir	0/-0.77/negative	First 13
	East	Karaman-Center-Akçaşehir	0/-0.79/negative	First 13
	Up	Karaman-Center-Akçaşehir	0/0.74/positive	First 15
	North	Karaman-Center-Eminler	0/-0.56/negative	First 5
	East	Karaman-Center-Eminler	0/-0.58/negative	First 5
	Up	Karaman-Center-Eminler	0/0.53/positive	First 4
	North	Karaman-Center-Kocahüyük	0/-0.48/negative	First 5
	East	Karaman-Center-Kocahüyük	0/-0.48/negative	First 5
	Up	Karaman-Center-Kocahüyük	0/0.49/positive	First 5
	North	Karaman-Center-Sudurağı	0/-0.99/negative	First 16, 30-50
	East	Karaman-Center-Sudurağı	0/-0.99/negative	First 16, 33-50
	Up	Karaman-Center-Sudurağı	0/0.98/positive	First 14, 31-50
KAPN	North	Konya-Karapınar-Gülfet	0/-0.73/negative	First 11,
	East	Konya-Karapınar-Gülfet	0/-0.67/negative	First 10
	Up	Konya-Karapınar-Gülfet	0/0.68/positive	First 11
KNYA	North	Konya-Selçuklu-Center	nsignificant	
	East	Konya-Selçuklu-Center	nsignificant	
	Up	Konya-Selçuklu-Center	insignificant	

RESULTS

The following results have been obtained for the analysis of time series of North, East, and Up coordinates of stationary GNSS stations and time series of underground water levels.

- In horizontal, GNSS stations in Konya Closed Basin have linear movements in northeast direction (ITRF08 fixed) and annual mean movement or velocity of these stations is 18.88 mm. Moreover, while vertical movements of ANKR, KLUU, and NIGD stations are in up direction and mean annual movement is 0.56 mm, other stations have movements in down direction. Annual vertical movement of KNY1 stations that has 560-day data is 70.96 mm in down (-) direction and this is the highest value of vertical movements of stations in this region.
- As in the trend analysis of GNSS stations, trend analysis was performed for 19 well observations. As a result of the analysis, it is obtained that 19 stations have linear movements in down direction and mean = -39.22 cm/year. It is seen that the annual change in KONYA-SELÇUKLU-MEYDAN, KARAMAN-AYRANCI-HUYUKBURUN, and KARAMAN-MERKEZ-SUDURAĞI wells according to the well data is over 1 m. However, the linear function of KONYA-KULU and KONYA-

SEYDİŞEHİR well data shows insignificant linear change at 95% confidence level. A linear increase (69.72 cm/year) was detected in the KONYA-BEYSEHİR-DOĞANBEY well data. The majority of the water level changes of the wells in this region has statistically significant decrease, and it is in meter level in some wells. It can be stated that linear decrease that is -70.96 mm/year in up coordinates, which have 560 days (quite little time), of KNY1 GNSS stations is generally caused by the decrease in underground water level in this region.

- A cross-correlation analysis was performed between KAMN, KAPN and KNYA time series (North, east, up) and water level changes obtained from Karaman-Center-Akçaşehir, Karaman-Center-Eminler, Karaman-Center-Kocahüyük, Karaman-Center-Sudurağı, Konya-Karapınar-Gülfet, Konya-Selçuklu-Center wells, which are close to these stations and where the underground water level is greatly decreased. While there is a negative correlation between north and east coordinates of GNSS stations and well data, there is a positive correlation between up coordinates of GNSS stations and well data. In this case we can say that the decrease in underground water levels effect horizontal positions of GNSS stations is in positive directions; however, the decrease in underground water levels effect vertical position of GNSS stations is in negative direction.

ACKNOWLEDGMENTS

This study was supported by Aksaray University Scientific Research Projects Coordination Unit. Project Number: 2015-064. We would like to thank Aksaray University for their support, General Command of Mapping for GNSS data, and General Directorate of State Hydraulic Works for observations of underground water level in Konya Closed Basin.

REFERENCES

- Langbein, J. and Johnson, H. 1997. Correlated Errors in Geodetic Time Series: Implications for Time-Dependent Deformation, *Journal of Geophysical Research*, 102, 591–604.
- Williams, S. D. P., Bock, Y., P. Fang, P. J., Nikolaidis, R.M., Prawirodirdjo, L., Miller, M. and Johnson, D. J. 2004. Error Analysis of Continuous GPS Position Time Series, *Journal of Geophysical Research*, 109(B03412).
- Mao, A., Harrison, C. G. A., Dixon, T. H., (1999). Noise in GNSS Coordinate Time Series. *Journal of Geophysical Research* 104 (B2), 2797–2818.
- Calais, E., (1999). Continuous GNSS Measurements Across the Western Alps, 1996–1998. *Geophysical Journal International*, 138 (1), 221–230.
- Gülal E., Erdoğan H., Tiryakioğlu İ., (2013). Research on the stability analysis of GNSS reference stations network by time series analysis, *Digital Signal Processing* 23 (2013) 1945–1957.

- TÜBİTAK MAM Çevre Enstitüsü (ÇE), Proje Adı: *Havza Koruma Eylem Planlarının Hazırlanması – Konya Kapalı Havzası Raporu* s, 113 / 473/ÇYGM-2009).
- Göçmez G., Eren Y., Aydın Y., ve Söğüt A. R., (2004). Karapınar Çevresinde Yeni Oluşan Obruk, *Karapınar Sempozyumu Bildiri Kitabı*, s.305-316.
- Özdemir, S., (2016). TUSAGA ve TUSAGA-Aktif İstasyonlarının Hassas Koordinat ve Hızlarının Hesaplanması Üzerine, *Harita Dergisi*, sayı 155.
- Göçmez G. ve İşçioğlu A., (2004). Konya Kapalı Havzasında Yeraltı Suyu Değişimleri, *I. Yeraltı Suları Ulusal Sempozyumu (23-24 Aralık, Konya) Bildiriler Kitabı*, s.19-28.
- Doğdu, M. Ş., Toklu, M. M., Sağnak, C. (2007). Konya Kapalı Havzası'nda yağış ve yeraltı suyu seviye değerlerinin irdelenmesi, *I. Türkiye İklim Değişikliği Kongresi–TİKDEK 2007*, 11–13 Nisan 2007, İstanbul.
- Üstün, A., Tuşat, E., Abbak , R.A., (2007). Konya Kapalı Havzasında Yeraltı Suyu Çekilmesi Ve Olası Sonuçlarının Jeodezik Yöntemlerle İzlenmesi, *3. Mühendislik Ölçmeleri Sempozyumu 24 -26 Ekim, Selçuk Üniversitesi – Konya*.
- Phienweij,N., Giao P. H., Nutalaya, P., (2006). Land subsidence in Bangkok, Thailand, *Engineering Geology*, 82: 187–201.
- Abidin, H. Z., Andreas, H. Djaja, R., Darmawan, D. Gamal, M., (2007). Land subsidence characteristics of Jakarta between 1997 and 2005, as estimated using GPS surveys, *GPS Solutions*, DOI 10.1007/s1029100700610.
- Galloway, D. L. ve Hoffmann, J., (2007). The application of satellite differential SAR interferometry derived ground displacements in hydrogeology, *Hydrogeology Journal*, 15: 133–154.

Multipath Mitigation Using The Bandpass Filter Technique For Gps Applications

Atınç Pırtı

Department of Surveying Engineering, Yildiz Technical University, Davutpasa Campus, 34220 Esenler, Istanbul – Türkiye. e-mail: atinc@yildiz.edu.tr

ABSTRACT

Global Positioning system (GPS) is designed to serve both civilian and military applications. However, the GPS performance suffers from several errors, such as ionosphere delay, troposphere delay, ephemeris error, and receiver noise and multipath errors. Among these errors, the multipath is one of the most unpredictable error sources in high-accuracy navigation. In this study analysed the multipath characteristics of each station using a quality-checking software package called TEQC. In addition, this paper applies a band pass filter to reduce code multipath errors in GPS.

INTRODUCTION

In recent years GPS has become a useful tool for applications such as navigation, tracking and mapping and in many such applications it is now considered to be indispensable. A satellite navigation system positioning device functions by measuring the time taken to receive signals from various satellites. From these measurements the distance from each satellite to the device is calculated and hence the location of the device is determined. However, depending on the location of the device, there may be obstacles which cause unwanted reflections of the satellite signals. For example, signals can reflect off a building. This means that the device will receive reflected signals that have not come directly from the satellite. Such reflected signals cause errors in the position calculation of the device. An incorrect location may be calculated, for example because the reflected signal taking longer to arrive at the device than the direct signal is interpreted as a direct signal from a device location further from the satellite than the true location. It is also possible that signals are disregarded, resulting in no location at all being shown. This phenomenon is known as multipath and the received signal comprising a direct and a reflected signal is known as a multipath signal. For most applications of satellite navigation systems, it is preferable for as accurate a location as possible to be output with as little interruption as possible. To achieve this it is necessary to detect and deal with multipath errors. Various methods have been used to attempt to deal with the multipath problem, such as code carrier divergence methods. These methods rely on monitoring differences between time delays and phase changes. However, they have not been very successful as the measure of

multipath is noisy and leads to ambiguity and false alarms. It is difficult to distinguish multipath fading from changes in signal amplitude arising from other causes such as gain in the receiver and fading through the atmosphere and therefore it is difficult to accurately correct for the fading. Because the method of the present invention determines if a signal is a multipath signal by monitoring for a characteristic change in a fading frequency of the signal over time to determine if the first signal is a multipath signal, the method is sensitive and stable and detects persistent reflected signals that would cause a systematic error in a positioning solution. (Axelrad 1994), (Hannah 1998), (Parkinson 1996), (Hoffmann 2000), (Rabbany 2006), (Sleewaegen 1997). The two techniques of mitigating multipath by choke ring antenna and by signal processing are two complimentary techniques and one cannot substitute for the other. Choke ring antenna can mitigate multipath signals reflected from objects below the antenna. It has no effect on multipath signals reflected to the antenna from objects above the antenna (e.g. tall buildings or trees). Signal processing techniques to mitigate the effect of multipath have little effect when the multipath distance (the difference in distance between the direct signal and the reflected signal) is less than few meters, irrespective of whether the reflected signal comes from objects above or below the antenna. Fortunately most of the reflected signals from objects above the antenna (that cannot be mitigated by choke ring) have multipath distances of more than several meters which can be mitigated by signal processing techniques (Deng 2013), (Hoffmann 2000), (Li 2015), (Parkinson 1996), (Qi 2012), (Rabbany 2006), (Young 2012).

Signal processing techniques have also previously been developed for reducing the effect of multipath errors on the tracking loops. These techniques include methods that apply temporal filtering of the multipath errors, multipath correction from site calibration or correlation shape correction using multiple digital correlators. While many of these methods have proven successful in reducing the effect of multipath on the code tracking loops, temporal filtering and multi-correlator signal processing have no effect on the multipath carrier phase errors (Hannah 1998), (Mora Castro 1998), (Parkinson 1996). The band pass filter design described in this paper minimizes the multipath effect on the code tracking loops within the GPS receiver.

BAND PASS FILTER

A band pass filter can be implemented in any one of several technologies. Passive analogue filters utilize resistors, capacitors, and inductors to achieve the desired frequency response. Active filters add one or more operational amplifiers to prevent a signal from becoming too attenuated by the passive components and to exaggerate or to minimize a particular response by controlled feedback. A bandpass filter has symmetric characteristics when transmission zeros are symmetrically disposed about a centre frequency of a filter's usable bandwidth. In contrast, a bandpass filter has asymmetric characteristics when transmission zeros are placed asymmetrically about the filter's pass band. The latter is useful for satisfying desired out-of-band amplitude and/or in-band group delay asymmetric specifications. Band pass filters are often second-order or biquadratic. The bandwidth of such filters is directly the coefficient of the first-order term in the denominator polynomial

of the second-order filter transfer function. Band pass filters operating at microwave frequencies generally use coupled resonant cavities, made of waveguide sections provided with appropriate coupling irises. The interior volume of the cavities depends on the operating wavelength and it increases as the desired resonance frequency decreases. In the band pass filter constituted by many resonators, types of filter characteristics to be realized are determined by a value given to each coupling between the resonators. The bandwidth of a filter can be described by its quality factor (Q) and its centre frequency ω_0 . Q is a measure of the sharpness of the peak of the bandwidth response function. Another measure of the filter performance is the noise figure, which is the signal to noise ratio of the applied input to the signal to noise ratio at the output. It is desirable that the noise figure be low to preserve dynamic range. Changing the characteristics of a band pass filter involves altering the electrical and/or magnetic characteristics. Both band pass Q and insertion loss depend to some extent on the electrical length L of a resonant cavity, and band pass Q depends on the characteristics of dielectric substances present in the cavity. In microwave band pass filters, the frequency band of the signal of the filter is a function of the resonant frequency of resonators that are incorporated within the filter and respective coupling coefficients between each of these resonators. In order to achieve a specific precise bandwidth, the resonators are longitudinally spaced in a sequential manner (Deng 2013), (Li 2015), (Lyons 2004), (Qi 2012), (Scharf 1991), (Weng 2012), (Young 2012), (Zhang 2013) [URL 1].

ANALYSIS TOOLS

TEQC

TEQC was designed and developed and is maintained by the University Navstar Consortium (UNAVCO) Facility. The program is named after its three main functions: Translation, Editing and Quality Checking (Estey and Meertens 1999). With TEQC, one can extract a variety of information from a RINEX file. Some of the information we get are: the receiver clock slips, receiver cycle slips, site multipath, satellite elevation and azimuth angle, receiver clock drift, and receiver signal-to-noise ratios. A key parameter in describing the signal quality in radio transmission applications is the signal-to-noise power S/N ratio, measured at the output of the receiver system. Actually, the quality of the signal (the accuracy of the data) is better, the higher the S/N, where the S/N, is a function of the carrier-to-noise ratio C/N, measured at the input to the receiver system. The multipath and SNR report files are especially important for the assessment of site-specific (environmental and instrumental) errors. Using linear combinations of pseudorange and carrier phase observations. TEQC can also compute pseudorange multipath, ionospheric phase effects, and the rate of change of the ionospheric delay. The program is designed to call external MATLAB functions, for example, for fast Fourier transform (FFT) computations, bandpass filtering and geographic plotting. In this study, closely investigating the most severely affected sites, both by examining photographs and by analyzing multipath variations with respect to elevation angle and azimuth, has helped lead to a better understanding of the kinds of factors contributing to pseudorange multipath at a site. My

main tool for calculating the variation of the L1 and L2 pseudorange multipath at each site was the TEQC software. It computes the MP1 and MP2 linear combinations using both pseudorange and carrier phase data to eliminate the effects

of station clocks, satellite clocks, tropospheric delay, and ionospheric delay (Estey 1999), (Hilla 2003), (Hilla 2002), (Hoffmann 2000), (Ogaja 2007).

$$\begin{aligned} \text{MP1} &\equiv P_1 - \left(1 + \frac{2}{\alpha - 1}\right)L_1 + \left(\frac{2}{\alpha - 1}\right)L_2 = \\ M_1 + B_1 - \left(1 + \frac{2}{\alpha - 1}\right)m_1 + \left(\frac{2}{\alpha - 1}\right)m_2 \end{aligned} \quad (1)$$

where $B_1 \equiv -\left(1 + \frac{2}{\alpha - 1}\right)n_1\lambda_1 + \left(\frac{2}{\alpha - 1}\right)n_2\lambda_2$, and $\alpha = \frac{f_1^2}{f_2^2}$

$$\begin{aligned} \text{MP2} &\equiv P_2 - \left(\frac{2\alpha}{\alpha - 1}\right)L_1 + \left(\frac{2\alpha}{\alpha - 1} - 1\right)L_2 \\ &= M_2 + B_2 - \left(\frac{2\alpha}{\alpha - 1}\right)m_1 + \left(\frac{2\alpha}{\alpha - 1} - 1\right)m_2 \end{aligned} \quad (2)$$

where $B_2 \equiv -\left(\frac{2\alpha}{\alpha - 1}\right)n_1\lambda_1 + \left(\frac{2\alpha}{\alpha - 1} - 1\right)n_2\lambda_2$

In Eqs. (1) and (2) P_1 and P_2 represent the dual-frequency pseudorange observations, L_1 and L_2 represent the dual-frequency carrier phase observations, and m_1 and m_2 represent the dual-frequency carrier phase multipath. The MP1 and MP2 quantities vary in time mostly due to M_i and B_i , where M_i is the pseudorange multipath for frequency $i = 1, 2$ and B_i is a bias related to the L1 and L2 integer carrier phase ambiguities, n_1 and n_2 . TEQC carefully monitors cycle slips and their effect on the bias terms B_i . In practice, the constant part of MP1 and MP2 is removed so what TEQC actually reports is the root mean square (RMS) variation of MP1 and MP2 for each satellite, as well as a mean RMS for all satellites. In MP1 and MP2, there remains the effects of pseudorange noise ($\prec 50$ cm), carrier phase multipath ($\prec 7$ cm), and carrier phase noise ($\prec 2$ mm) but these are much smaller in size compared to the pseudorange multipath (which can be as large as 10 to 15 m at low elevation angles) (Estey 1999), (Hilla 2002), (Hoffmann 2000), (Ogaja 2007), (Leland 2005), (Scharf 1991).

MATERIAL AND METHODS

Two experiments are designed to show the multipath effect of an increasing relative distance on a forest canopy as well as quantifying the magnitude of multipath effect. These two experiments were performed in the Samandira area of Istanbul, Turkey, see Figure 1. The GPS (static) measurements were taken (30 July 2003 – Day of year (DOY) 211) before and after the forest was cut off (16 September 2003– DOY 259), see Figure 2. To study signal multipath and diffraction effects on static GPS baselines due to forest, three stations (P1, P2 and P3) were located at the distances of 0 m, 5 m and 10 m from the forest

environment including 8-10 m tall pine trees, see Figure 2a. P1 was the starting point and the second point P2 was located about 5 m and the third one P3 was located about 10 m away from the starting point and those three stations were observed by using GPS method. In the first step of this study, GPS measurements were carried out both before and after the trees were cut off (Pirti 2008), (Pirti 2005).

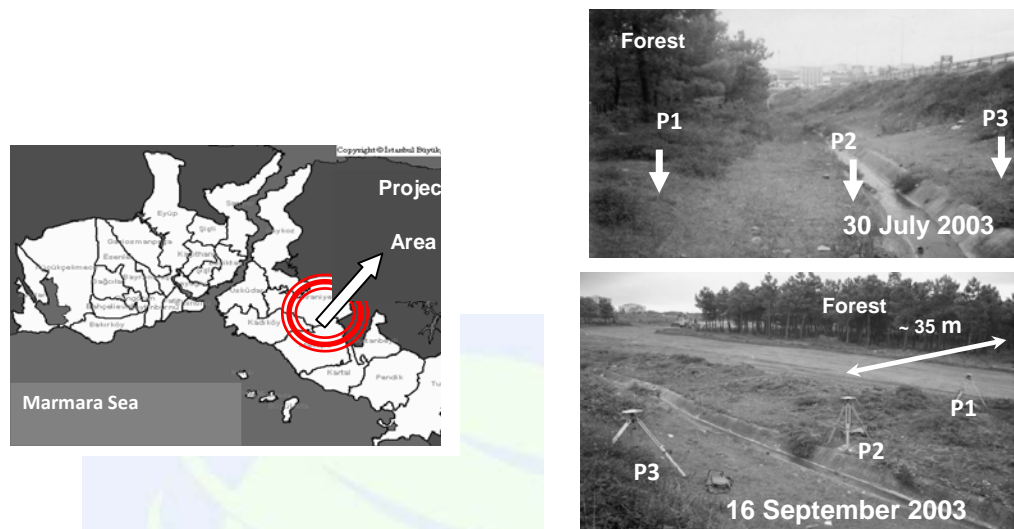


Figure 2. The three points in the project area (near the forest) a. on DOY 211 (with forest) and b. on DOY 259 (without forest) (Pirti 2008)

The data were recorded at three stations by static GPS measurements 6 hours for both days. Three Ashtech Z Surveyor receivers and Ashtech geodetic antennas were used for the static GPS measurements. Because every site has the same kind of receiver, we can objectively evaluate the data quality based on the multipath indices (MP1 and MP2). The reason is because values of MP1 and MP2 are dependent on the receiver and the receiver firmware. In addition, those sites equipped with the same kind of antenna should be equally affected by phase centre variations are dependent on the antenna type. The coordinates of the three points were determined in two GPS sessions (with forest and without forest) with 5 second intervals; elevation cut-off angles for two days were 15 degrees (Pirti 2008), (Pirti 2005).

RESULTS

As explained above, three GPS antennas at these three stations are located near the forest environment. Hence, it is important to detect and separate high-frequency multipath from the GPS receiver noise and other patterns in the GPS time series. This is due to the fact that high frequency oscillations in the time series can be caused by a variety of other factors such as forest and antenna pole movements. Here, we use TEQC-generated L1 and L2 pseudo range multipath to supplement the analysis and add further confidence to the results. The results of this study are described here in this section. The section will discuss the pseudo range multipath indices MP1 and MP2 (Estey 1999), (Ogaja 2007), (Mora Castro 1998), (Scharf 1991).

ANALYSIS OF GPS MEASUREMENTS ON 30 JULY 2003 AND ON 16 SEPTEMBER 2003

POINT 1 (P1-(30 JULY 2003))

Figure 3a is the L1 multipath traces for P1 showing the satellite specific pattern on 30 July 2003. The impact of the trees on the signal quality during this period is clearly seen from Figure 3a. These plots (Figure 3a and 4a) were created using the epoch-by-epoch multipath variations found in the *.mp1 and *.mp2 plot files output by TEQC. Generally this is not well behaved site, the maximum value of the L1 and L2 pseudo range multipath being about 5 m. For a general analysis, it was calculated the average values of MP1 and MP2 RMS of the point P1 on 30 July 2003 are 0.433 m and 0.547 m respectively (Figures 3a and 4a).

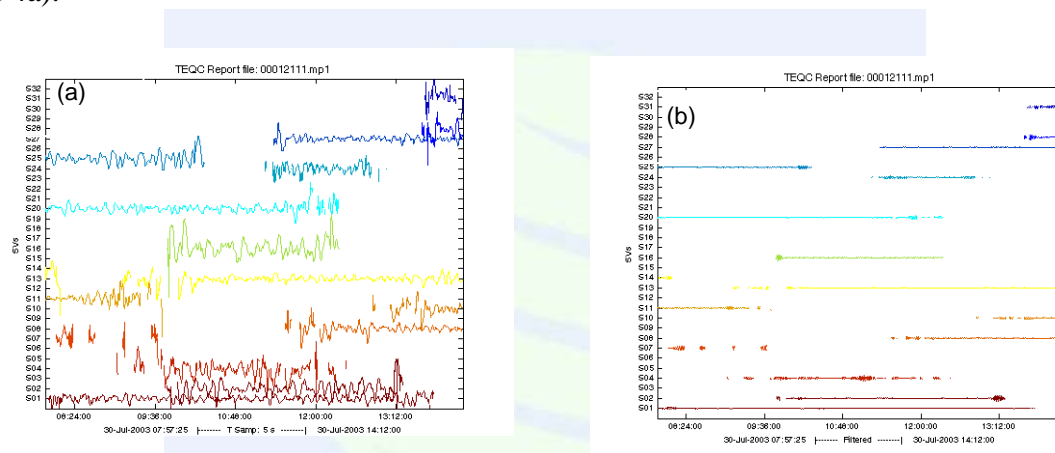


Figure 3. L1 multipath at point (P1) on 30 July 2003 (a) satellite specific patterns), traces of -0.055 Hz (bandpass filtered) multipath (b)

Figure 4a is the L2 multipath traces for P1 showing the satellite specific pattern on 30 July 2003. The impact of the tree on the signal quality during this period is clearly seen from Figures 4a. As shown the average values of MP1 and MP2 RMS values on 30 July 2003, the forest environment tends to be much more affected in MP1 than in MP2 for P1 on this day in this study. The low and medium elevation of the satellites generally affected much more MP1 values than MP2 RMS values in the multipath environment. The multipath noise patterns are well correlated with the satellite elevation data (low elevation satellites have noisier multipath signals compared to high elevation angles). Bandpass filter is applied to the multipath time series in order to extract multipath at the frequency of interest. Figures 3b and 4b show the traces of L1 and L2 multipath as extracted from the original time series using a second order Butterworth bandpass filter (lower and upper cut-off frequencies set at 0.05 Hz and 0.06 Hz, respectively).

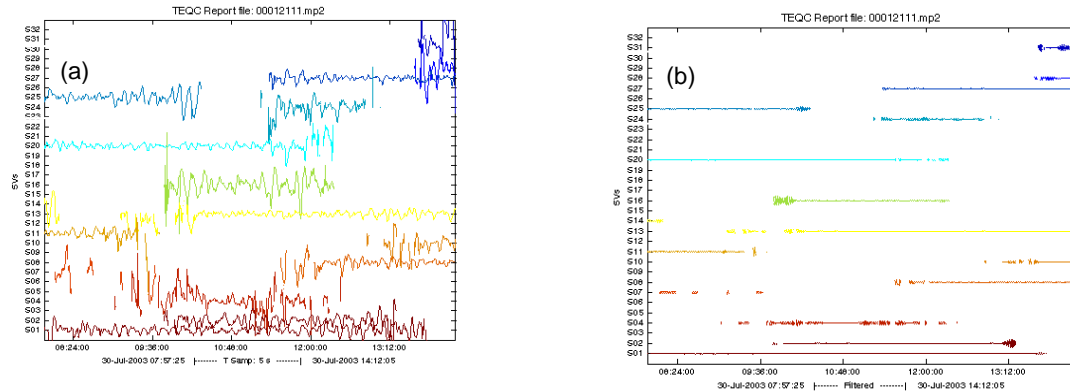


Figure 4. L2 multipath at point (P1) on 30 July 2003 (a) satellite specific patterns), traces of -0.055 Hz (bandpass filtered) multipath (b)

POINT 2 (P2-(30 JULY 2003))

Band pass filter is applied to the multipath time series in order to extract multipath at the frequency of interest. Figures 5b and 6b show the traces of L1 and L2 multipath as extracted from the original time series using a second order Butterworth bandpass filter (lower and upper cut-off frequencies set at 0.05 Hz and 0.06 Hz, respectively).

Figures 5a and 6a are the L1 and L2 multipath traces for P2 showing the satellite specific pattern on 30 July 2003, respectively. For a general analysis, it was calculated the average values of MP1 and MP2 RMS of the point P2 on 30 July 2003 are 0.837 m and 0.894 m respectively. The impact of the trees on the signal quality during this period is clearly seen from Figures 5a. As shown the average values of MP1 and MP2 RMS values on 30 July 2003, the forest environment tends to be much more affected in MP2 than in MP1 for P2 on this day in this study.

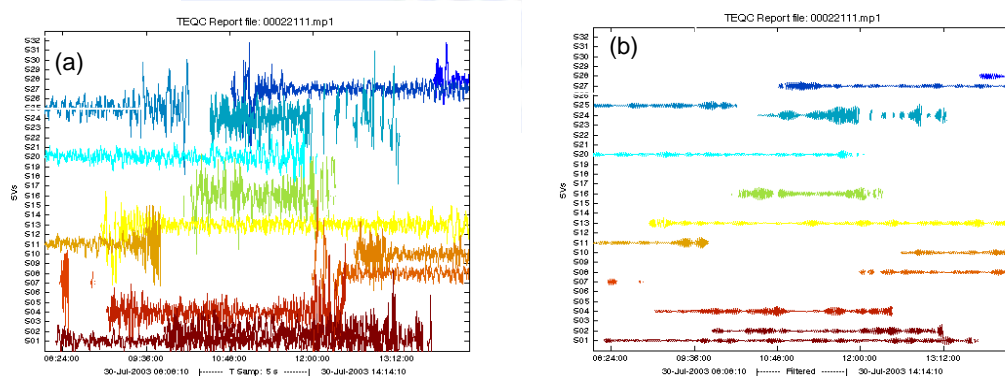


Figure 5. L1 multipath at point (P2) on 30 July 2003 (a) satellite specific patterns), (b) traces of -0.055 Hz (bandpass filtered) multipath

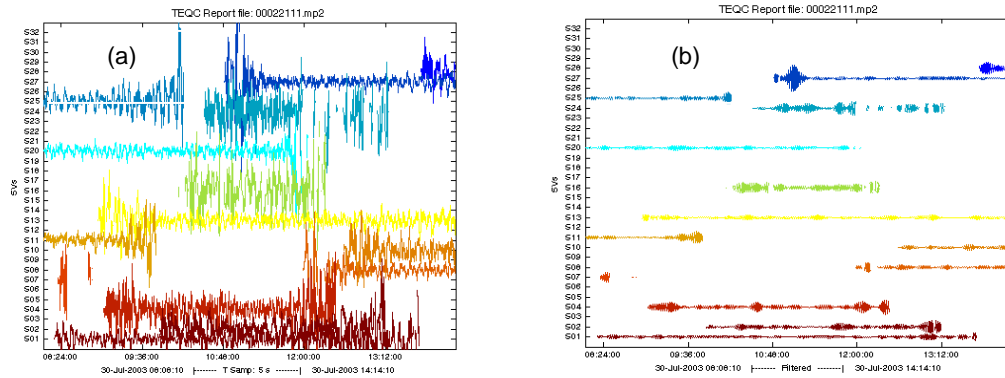


Figure 6. L2 multipath at point (P2) on 30 July 2003 (a) satellite specific patterns), traces of -0.055 Hz (bandpass filtered) multipath (b)

POINT 3 (P3-(30 JULY 2003))

Figures 7a and 8a are the multipath traces for P3 showing the satellite specific pattern on 30 July 2003. For a general analysis, it was calculated the average values of MP1 and MP2 RMS of the point P3 on 30 July 2003 are 0.674 m and 0.674 m respectively.

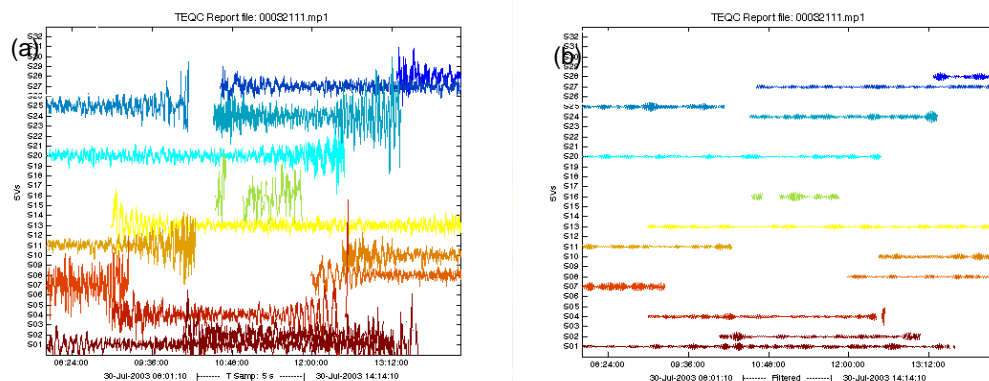


Figure 7. L1 multipath at point (P3) on 30 July 2003 (a) satellite specific patterns), traces of -0.055 Hz (bandpass filtered) multipath (b)

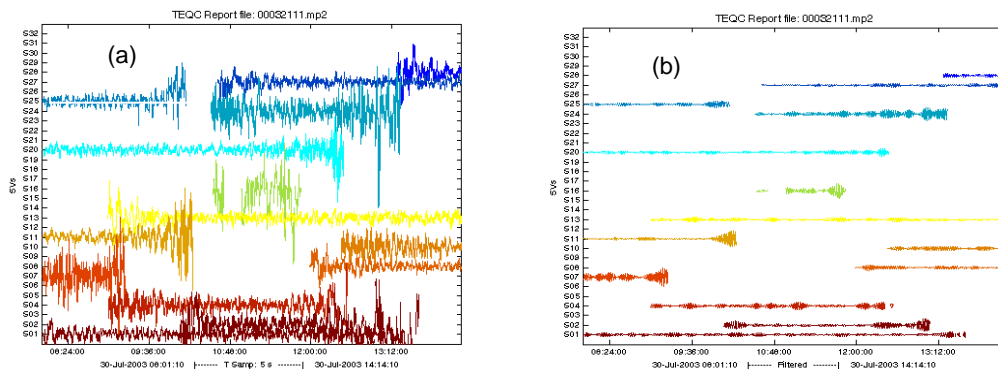


Figure 8. L2 multipath at point (P3) on 30 July 2003 (a) satellite specific patterns), traces of -0.055 Hz (bandpass filtered) multipath (b)

Band pass filter is applied to the multipath time series in order to extract multipath at the frequency of interest. Figures 5b and 6b show the traces of L1 and L2 multipath as extracted from the original time series using a second order Butterworth bandpass filter (lower and upper cut-off frequencies set at 0.05 Hz and 0.06 Hz, respectively).

Figures 3, 4, 5, 6, 7 and 8 show the examples of the range of multipath errors that can be found in the three points on 30 July 2003. Looking closely at the photograph in Fig. 2 for points P1, P2 and P3 have been placed nearby the forest environment. Photographs obtained for this study clearly show how some sites can become problematic when GPS antennas are placed in close to the forest. Figure 2 shows that on the point (P2) close to the multipath environment, the effect of the multipath is greater than points P1 and P3. Figures 5a and 6a clearly show that the severely affected GPS site in this study, Point 2 (P2). Figure 5a shows that P2 station; exhibit much larger MP1 and MP2 numbers than any other points.

The plots of both the unfiltered and filtered multipath time series are shown in Figs. 3, 4, 5, 6, 7 and 8 for the time span 08:00:00-14:14:10. The plot of filtered multipath for P2 on 30 July 2003 (Fig. 5b) is especially important –it shows that the high-frequency multipath is strongest. This information can be related to the environment surrounding the GPS antenna on the ground. The multipath caused by satellites at P2 is of short wavelength/high frequency; hence it supports the argument that the obstructed environment is a distinct object, possibly located near the forest.

CONCLUSION

The bandpass filter technique for minimizing or eliminating the effect of multipath signals in a receiver processing pseudorandom (PRN) code signals, such as in a global positioning system (GPS) receiver. The presence of multipath signals adversely affects both code measurements and carrier phase measurements of received PRN signals. One aspect of the invention provides for improved code tracking in the presence of multipath signals, by applying the bandpass filter the received code with a multipath mitigation that reduces or eliminates the multipath effects.

ACKNOWLEDGMENTS

I am grateful to Dr. C. Ogaja for providing the codes for multipath analysis.

REFERENCES

- Axelrad P., Comp C. J., Macdoran P. F. 1994. Use of Signal-To-Noise Ratio for Multipath Error Correction in GPS Differential Phase Measurements: Methodology and Experimental Results. In: *Proceedings of ION GPS-94*, Salt Lake City, September 20-23, pp. 655-666.

- Deng, H.-W., Zhao, Y.-J.; Fu, Y., et al. 2013. Compact and high performance microstrip diplexer for GPS and WLAN application, *Microwave And Optical Technology Letters*, Volume:55, Issue:6, Pages: 1233-1237 Published: JUN 2013
- Estey I.H., Meertens C.M. 1999. TEQC: the multi-purpose toolkit for GPS/GLONASS data, *GPS Solutions* 3 (1):, pp. 42-49
- Hannah B., Walker R., Kubik K. 1998. Towards a Complete Virtual Multipath Analysis Tool. In: *11th International Technical Meeting of the Satellite Division of the Institute of Navigation, ION GPS-1998*, Nashville, September 15-18, pp. 1055-1063.
- Hilla S. 2002. A new plotting program for Windows-based TEQC users. *GPS Solution* 6(3):2002, p. 196-200
- Hilla S., Cline M. 2003. Evaluating pseudo range multipath effects at stations in the national CORS network, *GPS Solutions* 7(4):2003, p. 253-267
- Hoffmann-Wellenhof B., Lichtenegger H., Collins J. 2000 *GPS Theory and Practice*, Fifth Revised Edition, Wien New York, Springer-Verlag: 382 pages
- Leland, B. J. 2005. *Digital Filters and Signal Processing*. Kluwer Academic Publisher, 3. Edition
- Li J., Hickie, M., Psychogiou, D., et al. 2015. A Compact L-Band Bandpass-Filter with RF MEMS-Enabled Reconfigurable Notches for Interference Rejection in GPS Applications IEEE Microwave Magazine, Volume: 16 Issue: 1 Pages: 81-88 Published: JAN-FEB
- Lyons R. G. 2004. *Understanding Digital Signal Processing*, Second Edition, Prentice Hall, March 15, 688 pages.
- Mora-Castro E. J., Carrascosa-Sanz C., Ortega G. 1998. Characterization of the multipath effects on the gps pseudorange and carrier phase measurements. In: *proceedings of ion gps-98*, September 15-18.
- Ogaja C., Hedfords K. 2007. Teqc multipath metrics in Matlab, *GPS Solutions* 11(3), p. 215-222, Springer
- Parkinson B. W., Spilker J. J. 1996. *Global Positioning System, Theory and Applications*. Stanford University and Telecom, Stanford, California, AIAA (America Institute of Aeronautics&Ast) Publisher:, pages 793
- Pirti A. 2008. Accuracy analysis of GPS positioning near the forest environment. *Croatian Journal of Forest Engineering*, 29(2): pp. 189-199.
- Pirti A. 2005. Using GPS near the forest and quality control. *Survey Review*, 38: p. 286-298
- Qi, N., Xu, Y., Chi, B., et al. 2012. A Dual-Channel Compass/GPS/GLONASS/Galileo Reconfigurable GNSS Receiver in 65 nm CMOS With On-Chip I/Q Calibration IEEE *Transactions On Circuits And Systems I-Regular Papers* Volume: 59 Issue: 8 Pages: 1720-1732 Published: AUG

- Rabbany, A. 2006. *Introduction to GPS*. 2nd Edition, New York, USA, Artech House Publishers: pages. 230
- Scharf, L. 1991. *Statistical Signal Processing*. New York: Addison-Wesley
- Sleewaegen J. 1997. Multipath Mitigation, Benefits from using the Signal-to-Noise Ratio. In: *Proceedings of ION GPS-97*, Kansas City, September 16-19, pp. 531-540.
- Weng M. H, Chen W. Y. and Chang S. J. 2012. A new tri-band bandpass filterbased on stub-loaded step-impedance resonator, *IEEE Microw. Wireless Compon. Lett.*, vol. 22, no. 4, pp.179 -181
- Young, K. 2012. GPS and Wireless LAN Bandpass Filter based on LTCC, *The Journal of Korea Navigation Institute* Volume: 16 Issue: 2 Pages: 227-233 Published: 2012 Volume: 16 Issue: 2 Pages: 227-233
- Zhang S., Zhu L. 2013. Compact tri-band bandpass filter based on $\lambda/4$ resonators with U-folded coupled-line", *IEEE Microw. Wireless Compon. Lett.*, vol. 23, no. 5, pp.258 -260
- URL1:<http://www.electronics-manufacturers.com/info/rf/microwave-electronics/bandpass-filter.html>, 10.11.2008



The Impact of Different GPS/GNSS Parameters on Landslide Monitoring

Deniz Güngördü^{*1}, R.Cüneyt Erenoğlu²,

¹Department of Geomatics, Canakkale Onsekiz Mart University, Terzioğlu Campus, 17020, Turkey. e-mail: denizgungordu@comu.edu.tr

²Department of Geomatics, Canakkale Onsekiz Mart University, Terzioğlu Campus, 17020, Turkey e-mail: ceren@comu.edu.tr

ABSTRACT

Landslides are one of the most dangerous types of natural disasters. In last decades, the Global Positioning System (GPS/GNSS) technology has shown that it is capable to monitor sub-centimeter landslide deformations. In this study, it is aimed to observe an active landslide area with the help of a micro-geodetic GPS/GNSS network and to determine statistically significant point deformations. In addition to this purpose, it is aimed to develop an optimum measurement and evaluation strategy for effective monitoring of active landslides by studying some parameters such as observation time, baseline lengths and altitude differences depending on the selected GPS/GNSS measurement technique. In this context, a micro-geodetic GPS/GNSS network was established after the geodetic network optimization. GPS/GNSS measurements were performed in three periods with static, rapid static and RTK methods. In the evolution of GPS/GNSS data, academic research software were used. The data obtained from the field were divided into subgroups and the effect of observation period, multipath effect, phase shift, atmospheric effects were investigated. As a result, it was determined that deformation occurred at some points of the landslide area.

INTRODUCTION

Global Positioning System/Global Navigation Satellite System (GPS/GNSS) has become an alternative to conventional methods such as terrestrial surveys and geometric levelling (Gili et al., 2000). Today GPS/GNSS systems are widely used to monitor crustal movements. Continuous GPS methods have also been established for this purpose, i.e. International GNSS Service (IGS) (Mao et al., 1999; AmiriSimkooei et al., 2007).

There are two approaches for monitoring landslides using GPS/GNSS: campaign type of observations and continuous monitoring. Both approaches require site or station establishment on solid grounds to determine movement. As an example of monitoring the

^{*} Corresponding Author

landslides with campaign GPS/GNSS measurements, it can be shown in Gili et al. (2000) and Moss et al. (1999). Particularly in the campaign measurement approach, it is desirable that the measurements carried out in each period are of equal accuracy. Various measurement methods are applied in determining position by GPS/GNSS and static, rapid static, real time kinematic GPS/GNSS and Continuously Operating Reference Station (CORS) are frequently used in this area (Stewart and Rizos, 2002; Featherstone et al., 1998).

Static GPS/GNSS observations have become a tradition to solve the great crustal movements. But recently, scientist are working on real-time observations and increasing the quality of rapid static GPS based on constantly working reference stations (Akarsu et al. 2015; Crowell et al., 2012; Hastaoglu and Sanli, 2011; Wang and Soler, 2012). The duration of the rapid static method is much longer than the RTK method. This time varies from 1 to 30 minutes. Rapid static is shorter than the static method because the technique utilizes algorithms that provide fast ambiguity resolution using some statistics (Frei, E., and Beulter, G. 1990). The accuracy in cm level is obtained from rapid static and RTK observations. However, due to long observation period, the static positioning provides the most precise results (Table 1). 8-24 hourly observation is carried out with this method. This method yields a 2-4 mm accuracy in the horizontal component and 7-13 mm for the vertical component. The shorter observation period, the lower accuracy. (Hastaoglu and Sanli, 2011; Eckle et al. 2001).

According to Sanli and Kurumahmut (2008), the accuracy of GPS/GNSS position varies according to the duration of the session for large height differences. It is useful to know the accuracy, because in many engineering applications involving large height differences such as bridges, high buildings, landslides and dams, campaign GPS is still required when economy is concerned (Brunner 2005, Lovse et al. 1995, Schon 2007).

In this study, it is aimed to observe active landslide area with the aid of established micro-geodetic GPS / GNSS network and to determine statistically significant point deformations. In addition to this purpose, it is designed to develop an optimum measurement and evaluation strategy for monitoring a case study of active landslide by examining certain parameters such as observation time.

Table 1. Main characteristics of RTK and FS GPS methods compared with static method. (Gili et al., 2000)

Method	Observed time	Post-process	Baselines	Typical baseline planimetric error
Static	One to several hours	Yes	50-100 km	5-1 mm + 1-0.1 ppm
Rapid Static	8-20 min	Yes	15-20 km	5 mm + 1 ppm
RTK	1-10 s	No	10 km	10 mm + 2 ppm

STUDY AREA

As a study area, Şevketiye landslide (Figure 1) was selected in Lapseki province of Çanakkale (Figure 2).



Figure 1. Şevketiye landslide.



Figure 2. Şevketiye region.

The city of Çanakkale, located in the northwestern part of Turkey known as Biga Peninsula is tectonically a very active region and comprises a mosaic of various kinds of metamorphic, igneous, and sedimentary rocks (Figure 3). For the years 1981–2016, the average rainfall was measured to be 616,1 mm/year (MGM 2017) (see Figure 4). In addition to intense rainfall, the study area is prone to moderate-to-high magnitude earthquakes. Both earthquakes and rainfalls trigger landslides in the region (Coşkun, N. et al. 2016).

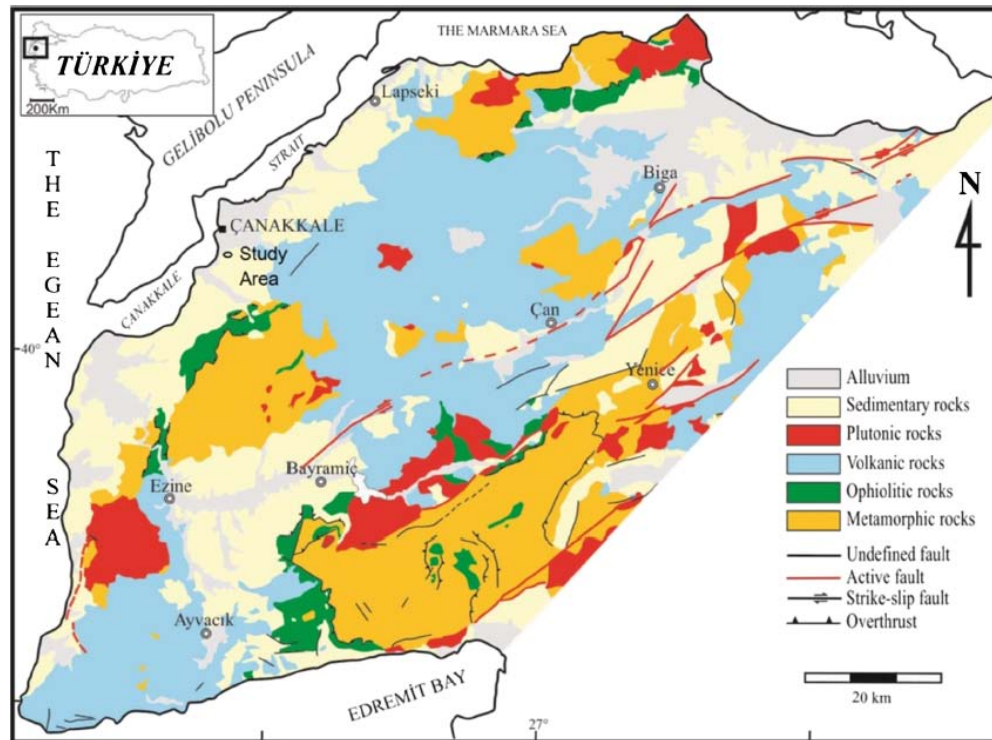


Figure 3. Geological map of the Biga Peninsula (adapted from MTA 2002).

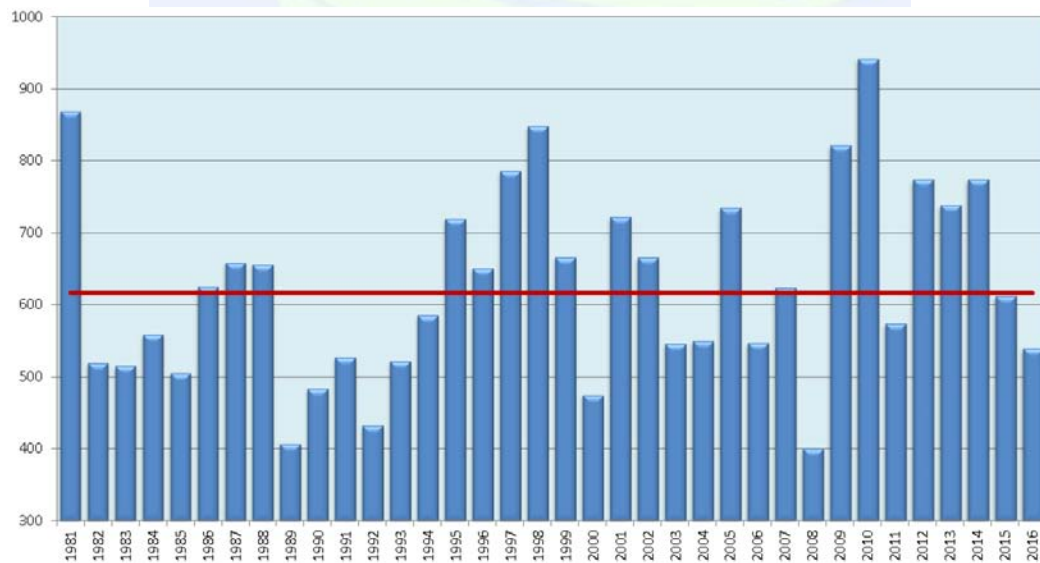


Figure 4. Annual precipitation rates for Çanakkale between 1981 and 2016.

METHOD

In this study, the evaluation of the established geodetic network was carried out by free network adjustment which all network point coordinates have been selected as unknown.

$$V_{\Delta} = A_{\Delta}x - \ell_{\Delta} \quad P_{\Delta} = K_{\Delta}^{-1} \quad (1)$$

$$V_{\Delta}^T P_{\Delta} V_{\Delta} + x^T x = \min. \quad (2)$$

The number of points in the network is p and G matrix:

$$G^T = \begin{bmatrix} \frac{1}{\sqrt{P}} & 0 & 0 & \frac{1}{\sqrt{P}} & 0 & 0 & \frac{1}{\sqrt{P}} & 0 & 0 & \dots & \frac{1}{\sqrt{P}} & 0 & 0 \\ 0 & \frac{1}{\sqrt{P}} & 0 & 0 & \frac{1}{\sqrt{P}} & 0 & 0 & \frac{1}{\sqrt{P}} & 0 & \dots & 0 & \frac{1}{\sqrt{P}} & 0 \\ 0 & 0 & \frac{1}{\sqrt{P}} & 0 & 0 & \frac{1}{\sqrt{P}} & 0 & 0 & \frac{1}{\sqrt{P}} & \dots & 0 & 0 & \frac{1}{\sqrt{P}} \end{bmatrix} \quad (3)$$

Normal equations are obtained by minimizing the Lagrange Function and normal equations;

$$\begin{bmatrix} N & G \\ G^T & 0 \end{bmatrix} \begin{bmatrix} x \\ k \end{bmatrix} - \begin{bmatrix} n \\ 0 \end{bmatrix} = \begin{bmatrix} 0 \\ 0 \end{bmatrix} \quad (4)$$

As a result of solving the normal equations, unknown parameters, corrections, adjusted measures and their variance-covariance matrices are obtained. The inverse weight matrix of the unknown;

$$Q_{xx} = N^{-1} = (N + GG^T)^{-1} - GG^T \quad (GG^T = I) \quad (5)$$

$$x = Q_{xx}n \quad (6)$$

$$X = X^0 + x \quad (7)$$

$$V_{\Delta} = A_{\Delta}x - \ell_{\Delta} \quad (8)$$

$$m_0 = \pm \sqrt{\frac{V_{\Delta}^T P_{\Delta} V_{\Delta}}{n_{\Delta} - u_{\Delta} + d_{\Delta}}} \quad (9)$$

$$K_x = m_0^2 Q_{xx} \quad (10)$$

$$Q_{\bar{\ell}} = A_{\Delta} Q_x A_{\Delta}^T \quad (11)$$

$$K_{\Delta} = m_0^2 Q_{\Delta} \quad (12)$$

$$Q_v = Q_{\ell} - Q_{\bar{\ell}} \quad (13)$$

Where, x is the unknown parameters; X, adjusted coordinates of points; V_{Δ} , corrections; m_0 , average error of unit measurement; K_x , variance-covariance matrix of adjusted coordinates; $Q_{\bar{\ell}}$, variance-covariance matrix of adjusted measurements; K_{Δ} , average errors of adjusted measurements; Q_v , covariance matrix of corrections and p is the number of

points; n_{Δ} , number of coordinates (coordinate differences); u_{Δ} , the number of unknown coordinates and d_{Δ} is the number of datum parameters. In three-dimensional geodetic networks, the number of datum parameters (d_{Δ}) equal to 3 and corresponds to the displacement elements (Kurt, O., 2001).

Bardaa's Test Method

In Baarda method, the global test is applied first. In this way, it is decided whether the established mathematical model is correct or not. For this, a priori and a posteriori variance (s_0^2) are compared. If the test value,

$$T = \frac{s_0^2}{\sigma_0^2} > F_{f, \infty, 1-\alpha} ,$$

then it is assumed to be an error in the model. It is believed that this error originates from a gross error of some measure and the research begins with the test described below.

Various test methods have been developed to detect gross error. The difference among these methods is designed on the use of different variances for the standardization of corrections. In this study, we utilized the Baarda's data snooping method which is using a priori variance (σ_0^2). Standardized normal distribution test value:

$$V_{i,B} = |V_i|/\sigma_0\sqrt{Q_{vivi}} \sim N(0,1)$$

Baarda's method assumes that the all measurements are suspicious. If $V_{max} = \max(V_i; 1, 2, \dots, n)$ is greater than confidence level $V_{max,B} > u_{1-\alpha_0/2}$ then it is decided that measurement with the highest standardized correction is outlier. u confidence limit/level is considered from the distribution charts or is calculated from significance level (α_0) and degree of freedom (f). If we determine the source of the error, the related observation is omitted and re-measured. Otherwise it is excluded from the bulk of data. Using remain the observations, Baarda's test will be continued until no outlier in the data (Demirel, H. 2003).

RESULTS

This paper evaluates the appropriate GPS technique for monitoring the landslide behaviors. We established a geodetic GPS/GNSS network with nineteen points and carried out campaign type of observations. Academic software was used to evaluate GPS/GNSS data. In addition to academic GPS / GNSS data Bernese v. 5.0 (Dach et al., 2007) software, Matlab software was used for all mathematical operation. Sensitive orbital information is obtained from International GPS Service (IGS) in SP3 (Standard Product 3) format, SOPAC (Scripps Orbit and Permanent Array Center). Each campaign is evaluated according to ITRF2008. 16 stations from the IGS global monitoring network were included in the evaluation. These stations are ANKR, ARTU, BOR1, BRUS, BUCU, GRAS, GRAZ, IRKT, ISTA, JOZE, KIT3, KOSG, MADR, MATE, METS, NICO, NSSP, NYAL,

ONSA, ORID, SOFI, TRAB, TUBI. After the process, horizontal and vertical velocity fields (Figure 5) were obtained. The points in the landslide zone indicate the fall movement especially in the east of the region. According to the Figure 5, the points at the east of the region are displaced in the northwest direction, and the points at the west are displaced in the northeast direction and values of the velocity components of the points are given in the Table 2.

Table 2. Site velocity vectors.

Site Velocity Vectors (cm/year)			
Site ID	V-north	V-east	V-up
SV01	-1.26	-0.96	-7.16
SV02	-2.04	-1.92	-6.57
SV03	2.30	-2.24	-2.94
SV04	8.60	-0.82	-3.44
SV05	2.70	-4.09	-1.55
SV06	-6.56	6.00	-12.89
SV07	2.16	2.90	-5.88
SV08	6.26	4.32	-5.19
SV09	4.66	-1.95	-3.84
SV10	7.58	-7.83	-1.49
SV11	2.26	2.80	-1.00
SV12	-2.73	2.05	-1.77
SV13	-1.26	-4.07	-4.88
SV14	-9.94	-2.30	-6.16
SV15	3.38	-10.33	-2.78
SV16	1.16	5.00	-10.32
SV17	-5.21	-2.49	-6.86
SV18	-3.43	-2.03	-6.15
SV19	-7.85	4.82	-0.60

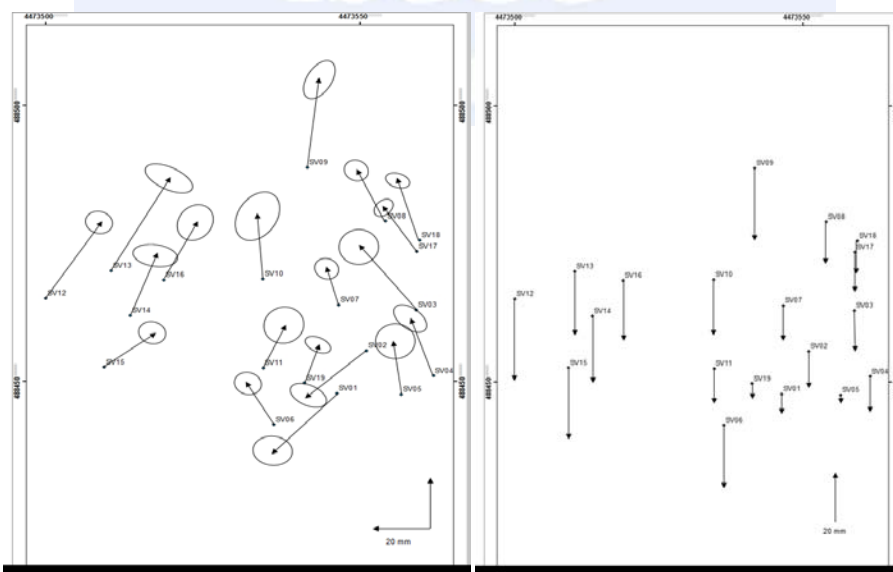


Figure 5. Horizontal and vertical velocity fields of the micro deformation network during the working period.

CONCLUSIONS

Within the scope of GPS / GNSS monitoring studies, the points in the landslide zones give similar geometric responses to the impact loads. Horizontal and vertical speeds tend to be similar, but they appear in different sizes. Landscape horizontal mass movements in the Landscape of Sevketiye, which is in the immediate vicinity of the highway, are usually formed in a vertical direction to the highway.

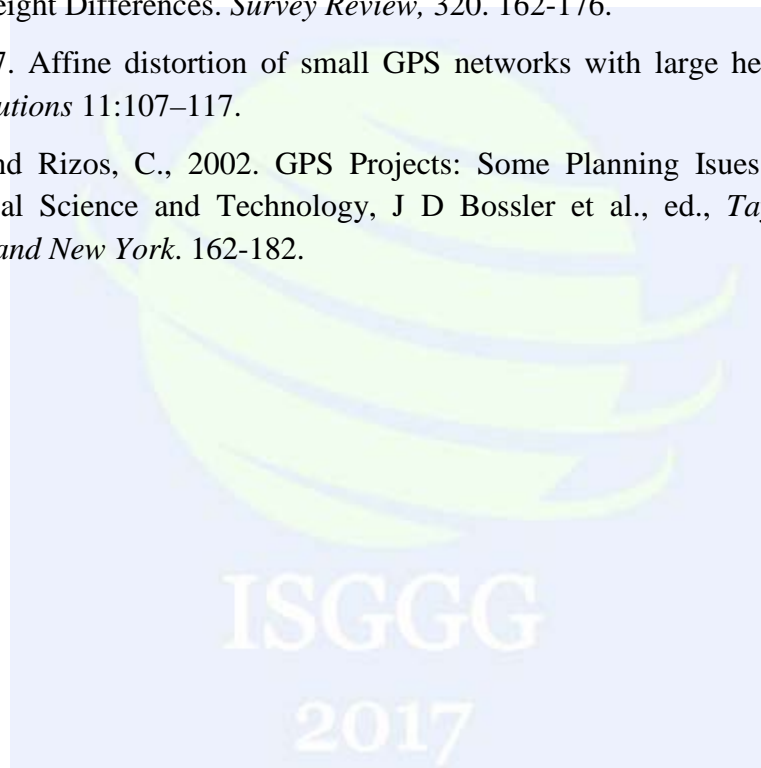
ACKNOWLEDGMENTS

This research project, FYL-2016-1018, supported by Canakkale Onsekiz Mart University Scientific Research Projects Coordination Unit.

REFERENCES

- Amiri-Simkooei, A.R., Tiberius, C.C. J.M and Teunissen, P.J.G.: 2007, Assessment of noise in GPS coordinate time series: Methodology and results. *J. Geophys. Res., Solid Earth*, 112.
- Akarsu, V., Sanli, D. U., and Arslan, E. 2015. *Accuracy of velocities from repeated GPS measurements. Nat. Hazards Earth Syst. Sci.*, 15, 875–884.
- Brunner, F.K., 2005. Bridge monitoring: external and internal sensing issues. In: Ou JP, Li H, Duan ZD Structural health monitoring and intelligent infrastructure. *Balkema*, 693-698.
- Coşkun, N., Çakır, Ö., Erduran, M. et al. 2016. A potential landslide area investigated by 2.5D electrical resistivity tomography: case study from Çanakkale, Turkey.” *Arabian Journal of Geosciences* 9: 6.
- Dach et al., 2007. Bernese GPS software version 5.0. , Astronomical Institute, University of Berne, Switzerland.
- Demirel, H. 2003. *Dengeleme Hesabı*. Yıldız Technical University, Istanbul.
- Eckl, M. C., Snay, R. A., Soler, T., Cline, M. W. and Mader, G. L., 2001. Accuracy of GPS-derived Relative Positions as a Function of Inter-station Distance and Observing-session Duration. *Journal of Geodesy*, 75: 633-640.
- Featherstone, W. E. and Stewart, M. P., 2001. Combined Analysis of Real-time Kinematic GPS Equipment and Its Users for Height Determination. *Journal of Surveying Engineering*, 127(2): 31-51.
- Frei, E., and Beulter, G. 1990. Rapid static positioning based on the fast ambiguity resolution approach ‘FARA’: Theory and first results. *Manuscr. Geod.*, 15, 326–356.
- Gili JA, Corominas J, Rius J, 2000. Using global positioning system techniques in landslide monitoring. *Engineering Geology* 55:167–192

- Hastaoglu, K. O. and Sanli, D. U., 2011. Monitoring Koyulhisar landslide using rapid static GPS: a strategy to remove biases from vertical velocities. *Nat Hazard*, 58:1275–1294.
- Kurt, O., 2001. GPS Ağlarının Dengelenmesi (Adjustment of GPS Networks). *Zonguldak Karaelmas University, Zonguldak*.
- Lovse, J.W., Teskey, W.F., Lachapelle, G., Cannon, M.E., 1995. Dynamic deformation monitoring of tall structures using GPS technology. *Journal of Surveying Engineering*, 121(1):35-40.
- Mao, A., C. G. A. Harrison, and T. H. Dixon, 1999. Noise in GPS coordinate time series, *J. Geophys. Res.*, 104, 2797 – 2816.
- Sanli, D. U. and Kurumahmut, F., 2008. Accuracy of GPS Positioning in the Presence of Large Height Differences. *Survey Review*, 320. 162-176.
- Schon, S. 2007. Affine distortion of small GPS networks with large height differences. *GPS Solutions* 11:107–117.
- Stewart, M. and Rizos, C., 2002. GPS Projects: Some Planning Issues. In: Manual of Geospatial Science and Technology, J D Bossler et al., ed., *Taylor & Francis, London and New York*. 162-182.



Evaluation of The Height Accuracy of Some Levelling Techniques

Atınç Pırtı, Ercenk Ata

*Yildiz Technical University, Department of Surveying Engineering, Davutpasa, 34220 Esenler, Istanbul –
Turkiye, e-mail: atinc@yildiz.edu.tr*

ABSTRACT

Applications in geodesy and engineering surveying require the determination of the heights of the vertical control points in the national and local networks using different techniques. These techniques can be classified as geometric, trigonometric, barometric and Global Positioning System (GPS) levelling. The purpose of this study is to analyse height differences obtained from these three of these four techniques using precise digital level and digital level (geometric levelling), total station (trigonometric levelling) and GPS which collects phase and code observations (GPS levelling). The accuracies of these methods are analysed. The results obtained show that the geometric levelling is more stable and reliable than the other two methods. The results of the three levelling methods agree with each other within a few millimetres.

INTRODUCTION

Levelling is the general term applied to any process by which elevations of points or differences in elevation are determined. It is a vital operation in producing the necessary data for mapping, engineering design and construction. Differences in elevation have traditionally been determined by digital levelling, trigonometric levelling, barometric levelling and GPS levelling. Vertical control surveys are generally carried out by direct digital levelling or trigonometric levelling. The method selected depends primarily on the accuracy required, although the type of terrain over which the levelling is done is also a factor. Geometric levelling can produce the highest order of accuracy. In spite of the fact that trigonometric levelling produces a somewhat lower order of accuracy than digital levelling, the method is still suitable for many projects such as establishing vertical control for topographic mapping or for lower order construction setting-out. It is particularly convenient in hilly or mountainous terrain where large differences in elevations are encountered. Both methods are subject to systematic and random errors. The primary systematic errors include earth curvature, atmospheric refraction and calibration of the surveying tools. Barometric levelling serves to determine approximate differences of elevations. In surveying with the aid of a barometer; used especially for large areas. The Global Positioning System (GPS) can be used for low-order vertical control surveys. To get accurate elevations using this method, the geoidal undulations in the area must be known and applied. The ellipsoidal heights obtained from GPS cannot be used directly for

practical surveying. The ellipsoidal heights have to be transformed to orthometric heights, being the distance measured along the plumb line between the geoid and a point on the Earth's surface and taken positive upward from the geoid. The difference between the ellipsoidal and the orthometric height is defined as the geoid height or geoid undulation. With the knowledge of the geoid (quasigeoid), it is possible to derive orthometric or normal heights from ellipsoidal heights. The most recent and advanced levelling approach is GPS levelling which is the combination of the GPS derived ellipsoidal heights and the geoid information in order to determine orthometric heights. The studies relating to the GPS technique need ellipsoidal heights with centimetre or sub-centimetre accuracy which are obtained from the GPS solution. This will only be possible with an interconnected network or reference stations (Ayan 2001), (Ceylan 2008), (Assuming the PDL data as error free for the time being and equal weight of all sections (all sections assumed to be 250 m long), (Erol 2008). In this study, accuracy of the height determination techniques has been compared the twenty vertical control points were marked in the project area. In order to determine of height differences between these 20 points, three methods were used and analysed, namely, GPS levelling, reciprocal and simultaneous short range trigonometric levelling, and geometric (digital and precise digital levelling) levelling. The procedures and obtained results are explained in this paper.

DIGITAL LEVELLING

Recent advances in electronics now enable surveyors to perform digital levelling with an electronic (digital) level. The development of this type of level has become possible due to the advances in microchip technology and image processing. The attributes of self-levelling instrumentation coupled with digital array photography and electronic image processing have generated a digital level, which is very much close to being truly automatic. The digital level processes an electronic image of a bar coded staff for the determination of heights and distances with automatic recording of the data for future processing on a computer. The digital level is an automatic level (with a pendulum compensator) capable of normal optical levelling with normal graduated staffs. The level can also be used with the bar coded staff and rod readings obtained digitally with output to a display on the instrument. The measuring system of the digital levelling consists of a level comprising optics and compensator, a bar code scale mostly on an invar band fixed into a rod frame, a CCD linear array and software controlling all operations, procedures and processes of the digital level (Anderson 1998), (Ingesand 1999), (Kahmen 2000), (Rüeger 2000), (Wolf 2002), (Woschitz 2002).

PRECISE DIGITAL LEVELLING

Precise digital levelling may be used in certain instances in construction such as in deformation monitoring, the provision of precise height control for large engineering projects like long-span bridges, dams and hydroelectric schemes and in mining subsidence measurements. Precise digital levelling staffs have an invar bar code kept under constant

tension on the face. Invar has a very low coefficient of expansion, and the staffs are calibrated to an exact length. They have scales graduated on invar strips, which are only slightly affected by temperature variations. Precise digital level rods are equipped with rod levels to facilitate plumbing, and special braces aid in holding the rod steady. Cloudy weather is preferable for precise levelling, but an umbrella can be used on sunny days to shade the instrument and prevent uneven heating which causes the bubble to run. Automatic levels are not as susceptible to errors caused by differential heating. Precise work should not be attempted on windy days. For best results, short and approximately equal backsight and foresight distances are recommended. The maximum sight distances are (50 m, 60 m, 90 m) and allowable differences between backsight and foresight lengths (2-4 m, 5-10 m, 10-10 m) for first-second, and third-order levelling respectively. Rod persons can pace or count rail lengths or highway slab joints to set sight distances. Precise levelling demands good-quality turning points. Lines of sight should not pass closer than about 0.5 m from any surface, e.g., the ground, to minimise refraction. Readings at any set up must be completed in rapid succession; otherwise, changes in atmospheric conditions might significantly alter refraction characteristics between them (Assuming the PDL data as error free for the time being and equal weight of all sections (all sections assumed to be 250 m long), the(Featherstone 1998), (Assuming the PDL data as error free for the time being and equal weight of all sections (all sections assumed to be 250 m long), (Federal Geodetic Control Committee 1984), Federal Geodetic Control Committee 1988).

SHORT RANGE SIMULTANEOUS RECIPROCAL TRIGONOMETRIC LEVELLING

Trigonometric levelling is the method of obtaining height differences using measured slope distances and zenith angles. The targets in trigonometric levelling can always be placed at the same height above the ground. Thus, the sighting distances are not limited by the inclination of the terrain and systematic errors, e.g. refraction, because the back and foresight lines pass through similar layers of air. By extending the sighting distances to a few hundred metres, the number of set-ups per kilometre is minimised. The accuracy of trigonometric levelling mostly depends on the earth's curvature and refraction which directly affect the zenith angle and distance observations. Usually, the surveyor measures the reciprocal zenith angles and slope distances from both ends of the baseline. Besides, the surveyor should then use the mean value of the computed height difference in order to correct for earth curvature and refraction. However, this is not always practical and warranted. It should be remembered that in order to minimise the errors introduced by curvature and refraction, the distances between the instrument set-ups should be shorter than 250 m. The influence of the earth's curvature and refraction is given by $c \& r = 0.0675 K^2$ metres, where K is the distance in kilometres. For 0.5 km the effect of $c \& r$ is 16.8 mm, for 0.2 km it is 2.7 mm, and so on (Anderson 1998). Figure 1 illustrates the short range trigonometric levelling with reciprocal and simultaneous measurement of zenith angles and slope distances. Field tests show that standard deviations of $\leq 2 \text{ mm} / \sqrt{\text{km}}$ are achievable, even along inclined terrain, at speed of 10 km/day when using sights no greater than 250 m

for the reciprocal method (Ceylan 2008), (Assuming the PDL data as error free for the time being and equal weight of all sections (all sections assumed to be 250 m long), (Chrzanowski 1985), . The electronic total stations were set up on the 20 marked points of the 5 km run. The instruments were set up on the marks and the heights of instrument (i_A and i_B) were measured three times from the centre of the telescope (horizontal axis) above the station mark in the field, see Figure 1. The height difference between two points, namely, A and B can be written as,

$$\Delta H_{AB} = \sum_A^B \Delta h_{ij} + t_A - t_B \quad (1)$$

where ΔH_{AB} is the height difference between the terminals A and B, Δh_{ij} are the individual height differences, t_A and t_B are the height of the target at A and B from ground to the total station. The observations have been made reciprocally and simultaneously between two points (Figure 1). The zenith angles (Z'_{AB} and Z'_{BA}) and slope distances (C_{AB} , and C_{BA}) were measured for the test scenario. The height difference between A and B points (ΔH_{AB}) are computed using the following section (Anderson 1998), (Ceylan 2008), (Kuntz 1986), (Wolf 2002).

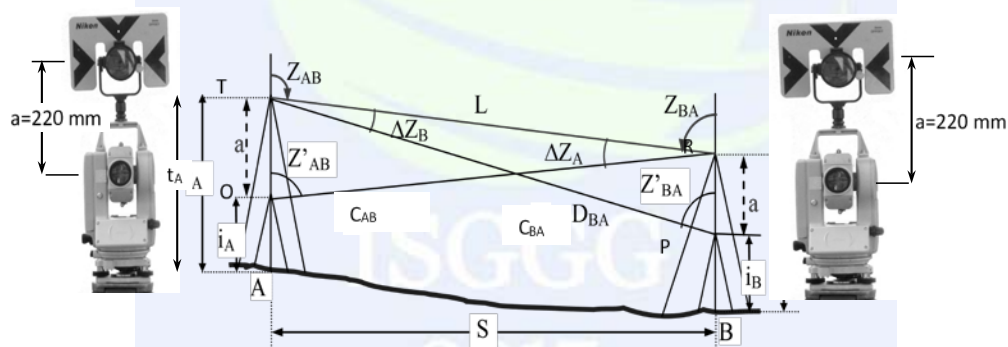


Figure 1. Model of the reciprocal and simultaneous short range trigonometric levelling

GPS LEVELLING

The geoid is defined as the gravity equipotential surface which best approximates mean sea level over the entire Earth. It has been defined as the datum for the orthometric height system. The irregular shape of the geoid, however, does not allow for an easy computation of the horizontal positions of points. Therefore, a reference surface of regular shape, usually a biaxial ellipsoid, is selected to best approximate the geoid either locally or globally. The geometric relationship between the geoid and the reference ellipsoid surface can be fully described by their separation and the slope of the geoid with respect to the reference ellipsoid. The former is known as the geoidal height (N), and the latter is known as the deviation of the vertical (θ). The deviation of the vertical is defined as the spatial angle between the ellipsoid normal and the actual gravity vector. In geodetic computations,

geoid parameters are needed for coordinate transformations and for reducing the actual surveying measurements made on the surface of the Earth to an appropriately chosen reference frame, for instance, the surface of a reference ellipsoid, or a projection plane, etc. There is a variety of methods for geoid modelling. (Ceylan 2008). Parameters describing the Earth's gravity field are most often used to determine the general shape of the geoid over a large area. For the purpose of geodetic control in a small area covered by an engineering survey requiring high precision, however, local variations in the Earth's gravity field must be considered. With a large number of monuments where both the GPS ellipsoidal heights and the orthometric heights from digital levelling have been observed, the geoidal heights at these points can be approximated by using the following simple relation

$$N = h - H$$

(2)

where N is the geoidal height, h is the ellipsoidal height from GPS surveys, and H is the orthometric height from digital levelling (Zilkoski 1997), (Ayan 2001), (Erol 2008), (Featherstone 1998).

THE UNITED STATES FEDERAL GEODETIC CONTROL SUBCOMMITTEE (US FGCS) ACCURACY STANDARDS

The FGCS established accuracy standards and specifications for various orders of levelling. The (US) Federal Geodetic Control Subcommittee (FGCS) established accuracy standards and specifications for various orders of geometrical levelling. The FGCS recommends the following formula to compute the allowable misclosures (tolerances):

$$T_{\text{Misc}} = \pm m \sqrt{K} \text{ mm,}$$

(3)

where T_{Misc} is the allowable loop or section misclosure, in millimetres; m is a constant; and K is the total length levelled in kilometres. For loops (circuits that begin and end on the same bench mark), K is the total perimeter distance. The FGCS specifies the constants (m) of 4 (first-order class I), 5 (first-order class II), 6 (second-order class I), 8 (second-order class II), and 12 mm (third-order) for five classes of levelling. It is important to point out that meeting the FGCS misclosure criterion alone does not guarantee that a certain order of accuracy has been met (Assuming the PDL data as error free for the time being and equal weight of all sections (all sections assumed to be 250 m long), the (Featherstone 1998), (Assuming the PDL data as error free for the time being and equal weight of all sections (all sections assumed to be 250 m long), (Federal Geodetic Control Committee 1984), (Federal Geodetic Control Committee 1988).

DESCRIPTION OF THE EXPERIMENT

The experiment was conducted in the Samandira region of Istanbul, see Fig. 2. The GPS and terrestrial surveys (geometric and short range trigonometric levelling) were performed on a levelling route of about 5 kilometres length. In order to minimise the errors introduced by earth curvature and refraction, distances between the tests points had to be restricted to about 250 m. Figure 3 illustrates the distribution of the selected points in the project area. The digital levelling (both digital and precise digital levelling) was carried out in order to assess the accuracy of the short range trigonometric levelling and the GPS levelling (Telci 2006). The height differences between the 20 points were determined by geometric levelling performed as double run levelling. The instrument used for the precise digital levelling was a Leica DNA 03 precise digital level, together with two bar coded invar staffs of three metres length and the staffs were stabilised with struts. The Leica DNA 03 precise digital level provides rapid, accurate solutions for a wide range of levelling applications, from topographic and construction surveys to first-order levelling and monitoring. It provides 0.3 mm accuracy on a 1 km double run line with an invar staff and is ideal for first and second order levelling and high precision measurements. The levelling routine was performed double observance (BFFB, aBFFB) to increase the reliability of the measurement and to reduce possible errors caused by the staff sinking. Applying alternating observations procedures (aBFFB = BFFB FBBF) to eliminate horizontal tilt (residual error of the automatic compensator) (Assuming the PDL data as error free for the time being and equal weight of all sections (all sections assumed to be 250 m long), (Assuming the PDL data as error free for the time being and equal weight of all sections (all sections assumed to be 250 m long)). The instrument used for the digital levelling was a Topcon DL 102 digital level (0.8 mm/km with fibre glass staff) and with the two bar-coded aluminium rods of five metres length. The levelling routine was performed observance (BFFB). Minimum ground clearance of 0.5 m required to refractionary influences of ground proximity. Limit target distance, < 30 m. Levelling staffs with adjustable brace poles provide good stability. The staffs were stabilised with struts. Include equal backsights and foresights, maintaining a line of sight >0.5 m above the ground and levelling the instrument to minimise any errors due to the obliquity of horizon problem. All these precautions were taken during the survey. Maximum allowable staff reading is 3 m. Four persons were performed in double run digital levelling. It took 6.5 hours on 5 km double run levelling. In the short range trigonometric levelling, the distances were measured by using two Nikon DTM 330 total stations with the (3 mm + 2 ppm) distance specification and 4.5'' zenith angle accuracy. The zenith angles and slope distances were reciprocally and simultaneously measured by using the same instruments four times in two faces. The heights of instruments, prisms, and targets for all points were measured three times to obtain mm level accuracy, see Fig. 2. The instruments were only set up on the 20 mark points. The instrument uses dual-axis compensation, and electronic level sensors, and it applies collimation, vertical index, and trunnion axis corrections automatically. Auto dual-axis compensation can ensure the accurate levelling of total station (Automatic dual-axis compensator with working range $\pm 3'$ (± 55 mgon)). In the compensation range $3'$, although the instrument is tilt, the horizontal and zenith angle can be measured precisely.

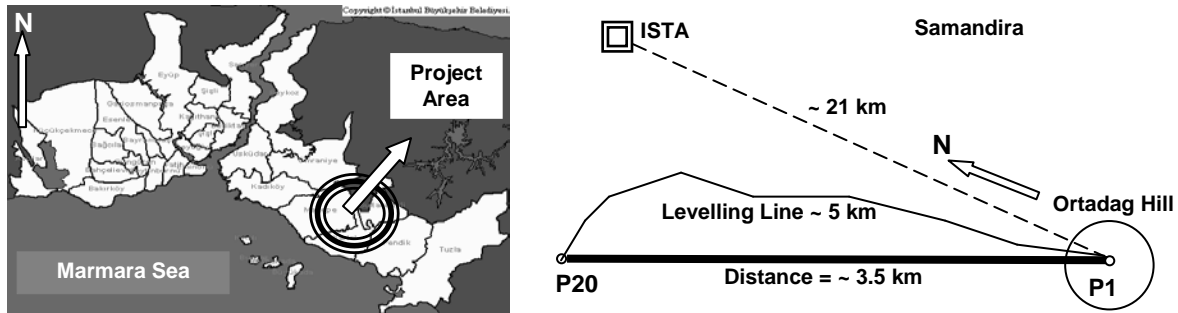


Figure 2. Project Area and GPS Network

The GPS surveys were carried out in order to determine the ellipsoidal heights of the 20 points along a levelling route (~ 5 km). The GPS measurements were taken with four Ashtech Z Max GPS receivers using the static method. The GPS data were recorded in seven sessions. These sessions were measured on 10 May 2006 between 8:00-18:30h (Local time). During this period, the satellite visibility varied between 6 and 9 satellites, and the PDOP values between 2.8 and 1.5. The GPS data were collected in 10 seconds epoch intervals. The station occupation time was ten hours and thirty minutes for the reference point (P1) and about sixty minutes for the remaining points. The reference station (P1) suffered no sky obstructions and was set up on Ortadag Hill which is the highest point in the project area, see Fig. 4. The GPS data processing and adjustment for the reference point (P1) was conducted using the Bernese Software 4.2. In the adjustment procedure, the ITRF 2000 coordinates of ISTA (IGS (International GPS Service) Station) were held fixed. The GPS data for the rest of the points were processed by the Ashtech Solutions 2.60 Software using the reference point (P1) as fixed. The horizontal and vertical (height) positioning precision of the points is obtained, on average, as 1 mm and 5 mm, respectively. These results show that the GPS measurements are quite accurate and consistent (Telci 2006).

COMPARISON OF HEIGHT DIFFERENCES FROM DIFFERENT METHODS

In order to compare the results of the levelling methods, the height differences between the points were separately determined, as are shown in Table 1. In these tables, ΔH_{Back} is backward levelling; ΔH_{Fore} is the forward levelling; ΔH_{Mean} is the mean of the backward and forward levelling; ΔH_{Trig} is the height difference from reciprocal and simultaneous short range trigonometric levelling and ΔH_{GPS} is the GPS levelling height differences between the points. Precision in levelling is increased by repeating measurements, making frequent ties to established benchmarks, using high-quality equipment, keeping it in good adjustment, and performing the measurements carefully. No matter how carefully the work is executed, however, errors will exist and will be evident in the form of misclosures. To determine whether or not work is acceptable, misclosures are compared with permissible values on the

Figure 3. The distribution of the test points in the project area

Table 1. Comparison of height differences obtained from different methods (Note: GPS data are corrected with the geoid undulations) (Telci 2006)

	<i>Precise Digital Levelling</i>		<i>(Ordinary) Digital Levelling</i>		<i>Trigonometric Levelling</i>	<i>GPS Levelling</i>
	ΔH_{Back} ΔH_{Fore}	ΔH_{Mean}	ΔH_{Back} ΔH_{Fore}	ΔH_{Mean}	ΔH_{Trig}	Δh_{GPS}
$\Sigma \Delta H$	-105.88519 105.88706	-105.88614	-105.8903 105.8837	-105.8873	-105.878	-105.882
	Misclosure	$= \pm 1.87 \text{ mm}$	Misclosure	$= \pm 6 \text{ mm}$		
$T_{Misc} = 4\sqrt{K} = \pm 9 \text{ mm}$ (FGCS First Order Class I) $T_{Misc} = 6\sqrt{K} = \pm 13 \text{ mm}$ (FGCS Second Order Class I)						

ACCURACY ANALYSIS OF HEIGHT DETERMINATION TECHNIQUES

This section covers the basics of the statistical theory used to determine the level of accuracy for a survey. The standard deviations and the differences between paired observations for precise digital levelling and ordinary digital levelling are illustrated in Table 2. The precise digital levelling measurements were processed for the 5 km double run levelling; the standard deviation of a single run measurement of 250 m is $\pm 0.25 \text{ mm/km}$; the standard deviations of double run levelling of 1 km is $\pm 0.17 \text{ mm}$. The ordinary digital levelling measurements were being processed for about 5 km back and fore levelling range; the standard deviation of one measurement in 250 m is $\pm 1.20 \text{ mm/km}$; the standard deviation of double run levelling in 1 km distance levelled is $\pm 0.85 \text{ mm/km}$. The height differences determined by precise digital levelling were assumed as true values for the comparison of the height differences derived from digital, GPS and reciprocal and simultaneous short range trigonometric levelling method. In Table 2, the d values could be considered the corrections (residuals) of the DL, TL, and GPS (corr.) data

to the PDL data taken a reference deviation of the differences between precise digital levelling value and digital levelling value. After that, we calculated the absolute t-value.

Table 2. Accuracy analysis of two height determination methods (precise digital levelling with Leica DNA03 and (ordinary) digital levelling with TOPCON DL-102) and accuracy analysis and testing all height determination methods (Note: GPS data corrected with geoid), (Telci 2006)

	ΔH_{PL}	ΔH_{DL}	ΔH_{TL}	Δh_{GPS}	d_{PL-DL} [mm]	d_{PL-TL} [mm]	d_{PL-GPS} [mm]
1-2	-40.56827	-40.5695	-40.566	-40.565	1.23	-2.27	-3.27
2-3	-17.79039	-17.7892	-17.788	-17.787	-1.19	-2.39	-3.39
3-4	-18.65703	-18.6574	-18.658	-18.660	0.37	0.97	2.97
4-5	-0.34028	-0.3403	-0.339	-0.344	0.02	-1.28	3.72
5-6	-0.93113	-0.9311	-0.933	-0.939	-0.03	1.87	7.87
6-7	-0.74409	-0.7447	-0.742	-0.741	0.61	-2.09	-3.09
7-8	-1.12021	-1.1204	-1.120	-1.122	0.19	-0.21	1.79
8-9	-1.5715	-1.5714	-1.573	-1.575	-0.1	1.5	3.5
9-10	-3.82522	-3.8254	-3.822	-3.820	0.18	-3.22	-5.22
10-11	-1.79897	-1.7994	-1.796	-1.795	0.43	-2.97	-3.97
11-12	-13.39333	-13.3934	-13.391	-13.391	0.07	-2.33	-2.33
12-13	-9.63998	-9.6397	-9.641	-9.642	-0.28	1.02	2.02
13-14	-5.35411	-5.3538	-5.352	-5.347	-0.31	-2.11	-7.11
14-15	2.77112	2.7711	2.768	2.767	0.02	3.12	4.12
15-16	-1.42499	-1.4249	-1.425	-1.426	-0.09	0.01	1.01
16-17	-0.17022	-0.1706	-0.170	-0.172	0.38	-0.22	1.78
17-18	2.59111	2.5912	2.594	2.588	-0.09	-2.89	3.11
18-19	4.36295	4.3632	4.361	4.369	-0.25	1.95	-6.05
19-20	1.71840	1.7184	1.715	1.720	0	3.4	-1.6
	-105.88614	-105.8873	-105.878	-105.882			
				$\sum Pd^2 =$	14.43	362.22	1144.63
			$\sigma_{1KM} =$		± 0.62 mm	± 3.09 mm	± 5.50 mm
			$\sigma_{5KM} =$		± 1.38 mm	± 6.86 mm	± 12.21 mm

<i>Line</i>	<i>Length</i>	<i>Weight</i>	<i>Precise Digital Levelling</i>	<i>(Ordinary) Digital Levelling</i>
	<i>K [km]</i>	<i>P (1/km)</i> <i>(1 / K)</i>	<i>d</i> [mm]	<i>d</i> [mm]
$\Sigma =$	4.934 km	$\sum Pd^2 =$	2.31 (mm ² /km)	54.09 (mm ² /km)
Single run 1 km precision ± 0.25 mm ± 1.2 mm Double run 1 km precision ± 0.17 mm ± 0.85 mm Double run 5 km precision ± 0.55 mm ± 2.65 mm				

$t = \frac{0.85}{\sqrt{0.55^2 + 2.65^2}}$	$t = \frac{8.15}{\sqrt{0.55^2 + 6.86^2}}$	$t = \frac{4.15}{\sqrt{0.55^2 + 12.22^2}}$
=0.314	=1.180	=0.340
$T\{\alpha = 0.05, f = 38\}$	2.024	

CONCLUSION

In this study, four different levelling methods are compared. Geometric levelling is usually accepted as being more accurate than the other methods. The discrepancy between geometric levelling and short range trigonometric levelling is at the level of 8 millimetres. The accuracy of the short range trigonometric levelling is due the reciprocal and simultaneous observations of the zenith angles and slope distances over relative short distances of 250 m. The difference between the ellipsoidal height differences obtained from the GPS levelling used without geoid and the orthometric height differences obtained from precise geometric levelling is 4 millimetres. The geoid model which is obtained from a fifth order polynomial fit of the project area is good enough in this study. The discrepancy between the precise geometric and GPS levelling (with geoid corrections) is 4 millimetres over 5 km. This shows the necessity of an appropriate geoid model which for the study area. It was seen that the short range trigonometric levelling and the GPS levelling techniques give sufficiently accurate results when compared to geometric levelling. This study presented some practical solutions towards determination of the heights of vertical control points in engineering surveying applications using different techniques.

REFERENCES

- Anderson, J. M.; Mikhail, E. M. (1998). *Surveying, Theory and Practice*, 7th edition WCB/McGraw-Hill, Boston.
- Ayan, T. (2001) Geodetic Network Densification in Istanbul, IGNA (Istanbul GPS Network), *IV. Turkish-German Joint Geodetic Days*, Berlin.
- Ceylan, A., Baykal, O. (2008) 'Precise height determination using simultaneous-reciprocal trigonometric levelling', *Survey Review*, 40 (308), pp. 195-205, April, DOI: <http://dx.doi.org/10.1179/003962608X290997>.
- Chrzanowski, A., Greening, T., Kornacki, W., Second, J., Vamosi, S., Chen, Y.Q. (1985) Applications and limitations of precise trigonometric height traversing. *Third International Symposium on the North American vertical Datum*, Rockville, Maryland, U.S.A.
- Colorado Procedure 14-03, Standard Practice for F and t-test Statistical Method for HBP Voids Acceptance, 2007, <http://www.dot.state.co.us/designsupport/Field%20Materials%20Manual/2007/CP%2014.pdf>
- Erol B., Erol S. and Çelik R. N. (2008) "Height Transformation using regional geoids and GPS/levelling in Turkey", *Survey Review*, 40 (307), pp. 2-18, January, DOI 10.1179/003962608X253394

- Featherstone, W.E., Dentith, M.C., Kirby, J.F. (1998) "Strategies for the Accurate Determination of Orthometric Height from GPS", *Survey Review*, 34 (267), pp. 278-296, 1998, DOI: 10.1179/sre.1998.34.267.278.
- Federal Geodetic Control Committee (FGCC). (1998) *Geometric Geodetic Accuracy Standards and Specifications for Using GPS Relative Positioning Techniques*, Version 5.0, U.S. Department of Commerce, May 11, 1988, reprinted with corrections, August 1.
- Federal Geodetic Control Committee. (1984) *Standards and Specifications for Geodetic Control Networks*, U.S. Department of Commerce, September
- Hoffmann-Wellenhof, B.; Lichtenegger H.; Collins J. (2000) *GPS Theory and Practice* 5th revised edition, Springer-Verlag, Wien-New York.
- Ingensand, H. (1999) The evolution of digital leveling techniques-limitations and new solutions. In Lilje, M. (ed.) *the Importance of Heights*. FIG, Gävle, Sweden, pp. 59-68.
- Kahmen, H. (2000) *Vermessungskunde*, 20. völlig neu bearbeitete Auflage, Walter de Gruyter, 2000.
- Kotsakis C. (2008) Transforming ellipsoidal heights and geoid undulations between different geodetic reference frames. *Journal of Geodesy*, 82: 249-260, DOI 10.1007/s00190-007-0174-9.
- Kuang S., Fidis C., Thomas F. (1996) Modelling of local geoid with GPS and levelling: a case study. *Surveying and Land Information Systems* 56 (2), 75-88.
- Kuhar M., Berk S., Koler B., Medved K., Omang O., Solheim D. (2011) The quality role of height system and geoid model in the realization of GNSS heighting. *Geodetski Vestnik* Vol. 55/ No. 2 (226-234), DOI: 10.15292/geodetski-vestnik.2011.02.226-234
- Kuntz, E., and Schmitt, G. (1986) Precise Height Determination by Simultaneous Zenith Distances, *The Symposium on Height determination and recent vertical crustal movements in Western Europa*, Hanover, Germany, September 15-19.
- Rüeger, J. M., Brunner F. K. (2000) On System Calibration and Type Testing of Digital Levels. *Zeitschrift für Vermessungswesen* 4.
- Rüeger, J.M., Brunner, F. K. (1982) EDM Height Traversing Versus Geodetic Levelling, *The Canadian Surveyor*, 36, pp.69-81.
- Schofield, W., Engineering Surveying (2001) *Theory and examination problems for students*, 5th Edition, Butterworth-Heinemann, Linacre House, Jordan Hill, Oxford, 521 pages
- Telci, G., Gürel, N., Bahşi, N. M., Hames, F. A., Uzun, I. A., Inel, A. (2006) *GPS Heightening (GPS ile Yükseklik Tayini)*, Thesis, Yildiz Technical University, Istanbul –Turkey, 57 pages (in Turkish)

- Wolf, P. R.; Ghilani, C. D. (2002) *Elementary Surveying, An Introduction to Geomatics, 10th Edition*, Prentice Hall Upper Saddle River, New Jersey, 887 pages
- Woschitz, H., Brunner, F. K. System (2002) Calibration of Digital Levels – Experimental Results of Systematic Effects. Reprint of paper published in: *INGEO2002, 2nd Conference of Engineering Surveying*. Kopacik A and Kyrinovic P (eds), Bratislava, November: pp 165-172
- Zilkoski, D., D’Onofrio J.D., Frakes S.J. (1997) *Guidelines for Establishing GPS-Derived Ellipsoidal Heights [standard: 2 cm and 5 cm]*, Version 4.1.1. National Geodetic Survey.



Estimation of Crustal Deformations in Marmara Region Using Continuous GNSS Stations' Observations

M. Fahri Karabulut^{*1}, V. Engin Gülal² And İbrahim Tiryakioğlu³

¹Department of Geomatic Engineering, Yıldız Technical University, Davutpaşa Campus, 34220, Turkey
e-mail : mfahri@yildiz.edu.tr

²Department of Geomatic Engineering, Yıldız Technical University, Davutpaşa Campus, 34220, Turkey.

³Department of Geomatic Engineering, Afyon Kocatepe University, Ahmet Necdet Sezer Campus, 03200, Turkey.

ABSTRACT

Some of information, such as the structure of the faults, age, seismic motion and the speed of the blocks have a great importance for the interpretation of earthquakes that occur on the faults. When you look at the history of the Marmara Region, there are many devastating earthquakes on the area (especially the North Anatolian Fault). For this reason, the speeds of the GNSS stations, which are continuously monitored by different institutions and organizations, are estimated using the GAMIT / GLOBK program, in order to learn about the faults in the area and to monitor their behavior. For the data evaluation and speed estimation, five days of data were taken every month since the stations started to work. Strain analysis was performed using the velocities of the stations obtained. As a result of the strain analysis, it is seen that the region generally has wider values of extension. Consequently, the speeds of the selected stations were calculated with higher accuracy than the campaign types. Besides the advantage of speed estimation with high accuracy, the low density of the stations is a major disadvantage.

INTRODUCTION

The North Anatolian Fault zone, which is one of the most important strike-slip faults in the world, has a remarkable precaution to understand the tectonics of the Eastern Mediterranean as well as its remarkable high seismic activity. The length of the NAF, starting from Karlioava to the borders of Greece, is about 1500 m (Barka A.A.).

Since 1900, the fact that there are no major earthquake in the Sea of Marmara except for two major earthquakes has not made it possible to explain and support the models related to the Sea of Marmara (Kalafat D.).

Active faults are the main parameters used in the evaluation of earthquake hazard. Therefore active faults' type, geometry, kinematic function, depth, size, age, amount of slip

* Corresponding Author

and direction, whether produces earthquakes in historical and prehistoric times, the size of the generated earthquake, the recurrence interval of earthquakes and rate of annual slip has to be determined correctly (Dirik K.).

Determination of slip velocity is one of the main topics of geodesy. When looking at the literature, the velocities of plates with very small values can be determined with mm accuracy using several different methods. Satellite and space based positioning methods such as VLBI, SLR and GPS are the methods used for speed determination.

DATA AND METHOD

In this study, data of 34 continuous GNSS stations in the Marmara Region were used. 10 stations belonging to National Positioning System (UKBS) established and operated by İstanbul Water and Sewerage Administration (İSKİ), 10 stations belonging to CORS-Tr, 7 stations belonging to BUSKİ Permanent GNSS Network (BUSAGA) established and operated by Bursa Water and Sewerage Administration, 5 stations belonging to Nature Movement Research Association (DOHAD), 1 station belonging to YTU and 1 station belonging to Geomatics Group (Figure 1).

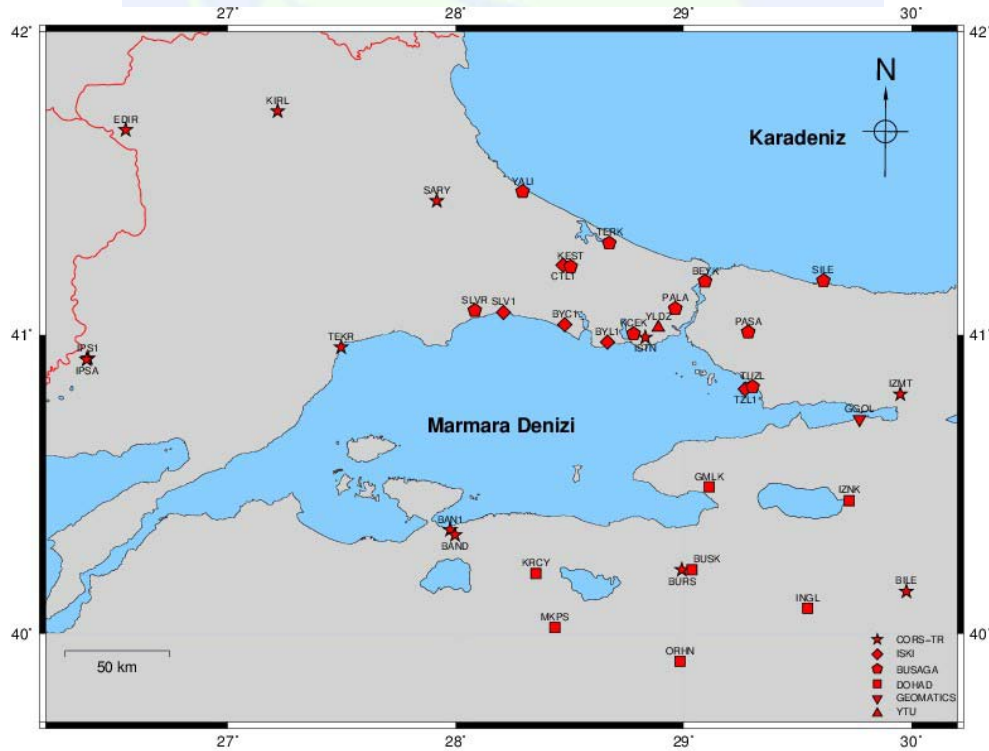


Figure 1. Distribution of stations

Some stations belonging to CORS-Tr located in Marmara Region were not used. Considering the stability and performance of the station, it is not included in the work at the KARB and SLEE stations (Tiryakioğlu İ.). A data set was obtained by collecting all the data in the range from the first days of recording to the working stations until 08.10.2016.

From this data set, the data for the days remaining between the 15th and 20th day of each month were selected and evaluated. Thus, both speeds have achieved sufficient accuracy

(Larson K. M., Zhang J. et al., Mao A. et al., and Blewitt G. and Lavalée D.) and the data evaluation period has been shortened by at least a few months.

The obtained data were processed with the GAMIT/GLOBK software package. 22 IGS stations with good performance were selected within the 2000 km diameter around the Marmara Region. for the processing data and the estimation velocities of stations.

After the velocity estimation, The deformations occurred in the Marmara Region were obtained by using the Grid Strain software package prepared by geologists who is from the University of Padova and Italy National Institute of Geophysics and Volcanology.

Stations that are very close together (BAND, BUSK, IPSA, ISTN, TZL1 and YLDZ), EDIR station with local deformation, CTL1 and GGOL stations whose data is less than 1 year, PALA station not relied on for speed due to having the same name as IGS station during the evaluation phase and IPS1 station located too far away considering the distribution of points were subtracted from the analysis.

RESULTS

The Eurasia fixed velocities of stations are given in the table 1 and velocity vectors are given following figure 2.

Table 1. Velocity values of stations

İstasyon Adı	Doğu (mm/y)	Kuzey (mm/y)	Yukarı (mm/y)	İstasyon Adı	Doğu (mm/y)	Kuzey (mm/y)	Yukarı (mm/y)
BAN1	-20.48	-4.43	1.49	KCEK	-1.09	-1.38	0.24
BAND	-18.80	-5.74	3.11	KEST	0.42	-0.35	2.60
BEYK	0.44	-2.15	0.52	KIRL	0.71	-0.72	0.43
BILE	-22.47	-3.83	0.25	KRCY	-20.98	-4.80	-1.32
BURS	-21.12	-3.67	-1.01	MKPS	-21.54	-6.79	2.36
BUSK	-21.12	-3.67	-1.01	ORHN	-21.41	-5.17	1.18
BYC1	-1.46	-1.34	-2.79	PALA	-0.71	-1.49	15.85
BYL1	-2.86	-2.03	-4.28	PASA	-2.42	-1.18	0.37
CTL1	6.58	-6.20	-2.78	SARY	0.52	-1.29	0.28
EDIR	2.21	-0.41	-2.34	SILE	0.49	-1.78	0.61
GGOL	-11.66	-0.09	-7.38	SLV1	-1.31	0.27	5.23
GMLK	-18.72	-2.10	-2.41	SLVR	-0.02	-0.94	0.68
INGL	-21.80	-10.31	-2.07	TEKR	-0.66	-2.97	0.79
IPS1	-1.02	-1.81	0.34	TERK	0.01	-0.82	0.34
IPSA	-1.02	-1.81	0.34	TUZL	-3.23	-0.89	0.03
ISTN	-0.89	-1.14	-0.01	TZL1	-4.41	-1.21	5.34
IZMT	-4.71	-1.64	0.50	YALI	0.38	-1.20	0.73
IZNK	-20.98	-3.08	-0.33	YLDZ	-1.41	-1.45	1.75

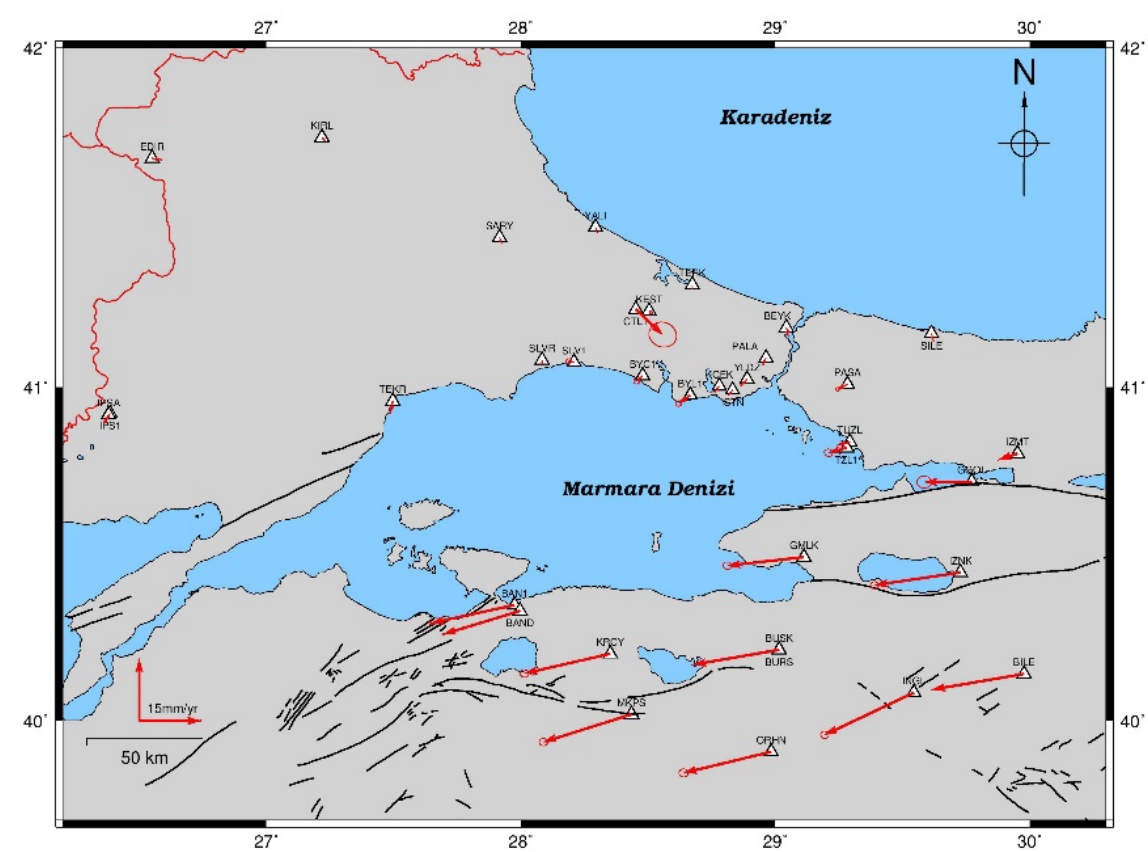


Figure 2. Eurasia fixed velocities

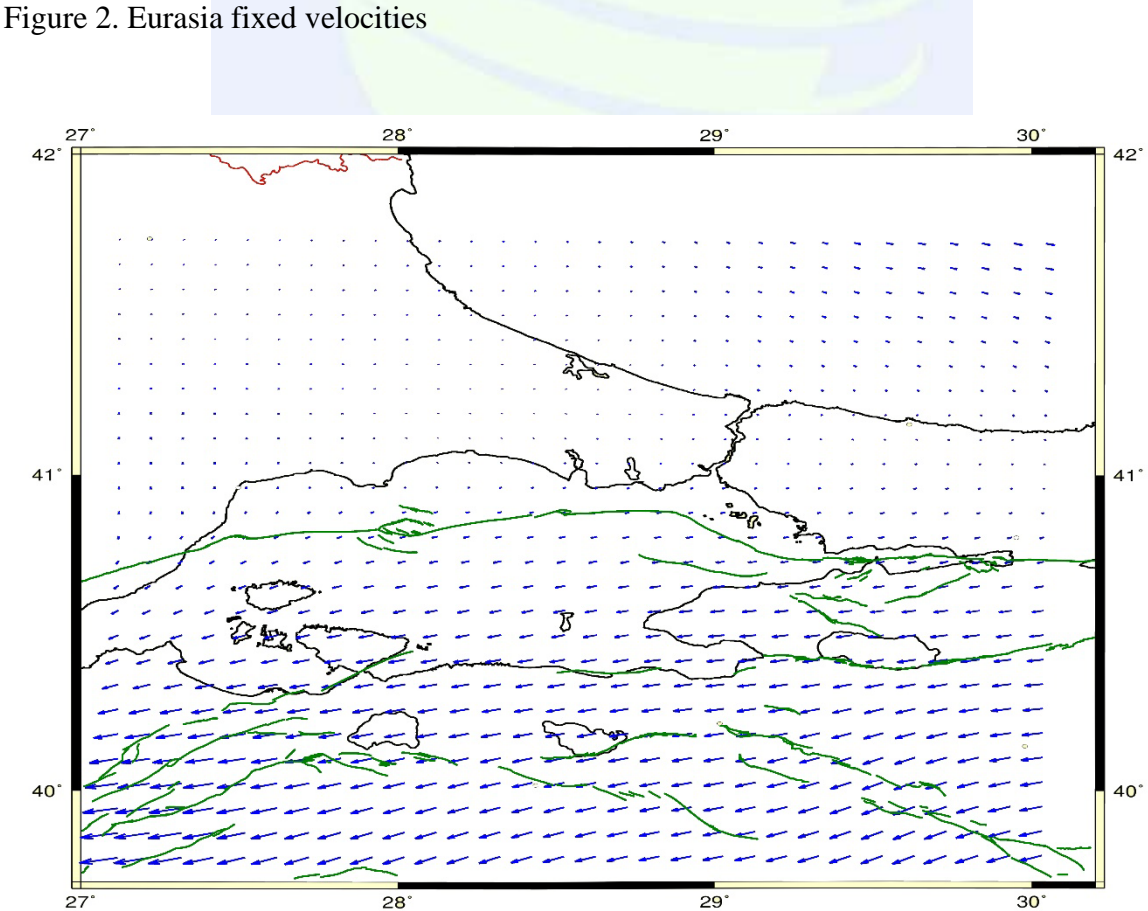


Figure 3. Translation map (Maximum translation:41 mm/y)

As a result of the strain analysis, it is observed that the region extending from the area between İzmit and Yalova-Gölcük to the west from the Marmara Sea towards the Çanakkale, is compression in the northwest-southeast direction and extension northeast-southwest direction. İzmit and Yalova-Gölcük sections extension are dominant values while the eastern sections of the Çanakkale compression are dominant. Compression and extension values in the Marmara Sea are approximately equal and lower than in the other two regions. The region south of the Marmara Sea is dominated by extension and there is only extension in around Bursa. When this extension is in the West of Bursa with high values in the direction of northeast and southwest, when the approach towards Bursa, this expansion becomes north-south direction and the value approaches zero. When the direction of Bursa goes to the east, the extension that takes place here shows the same character as the west of Bursa. It is estimated that the values in the northern parts of the Marmara Sea are very small.

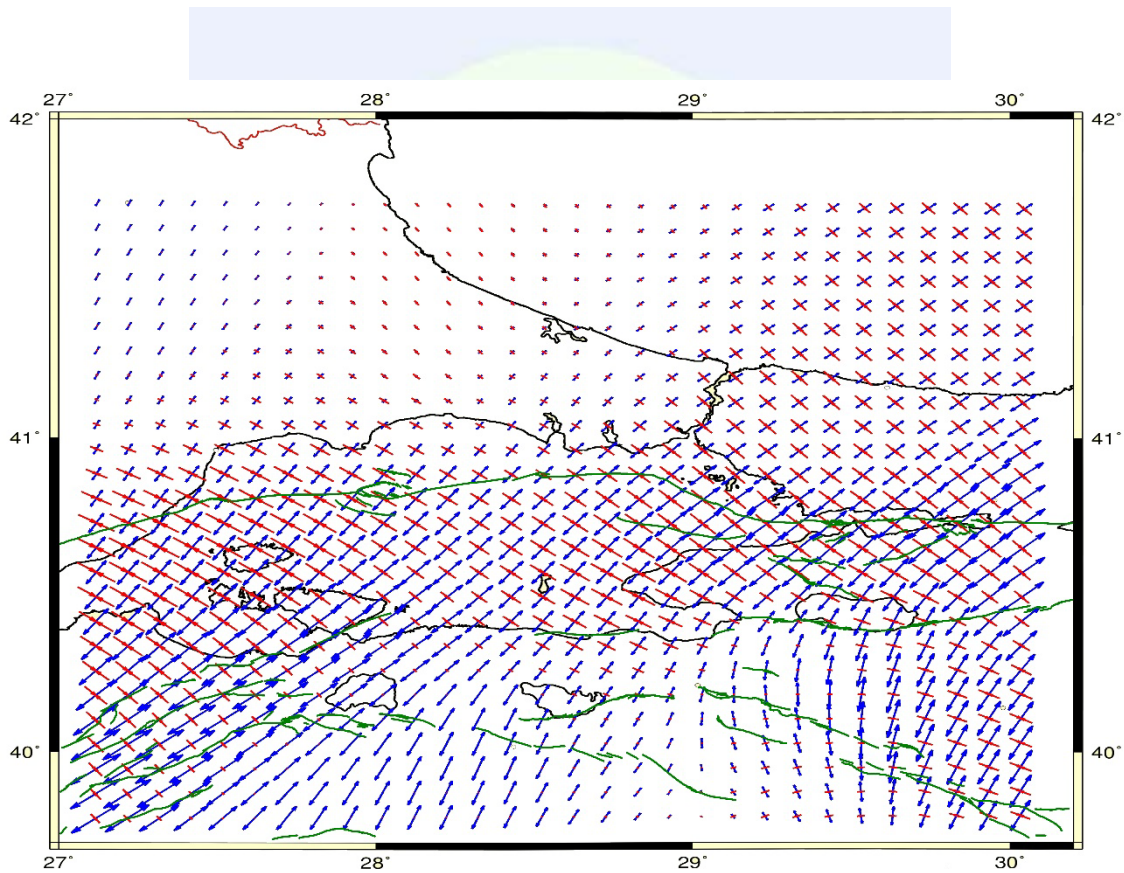


Figure 4. Map of strain (The red arrows show compression, the blues show extension. Maksimum strain:210 nanostrain/yr)

There is about 120 nanostrain/yr compression in the northwest-southeast direction and about 180 nanostrain/yr extension in the northeast-southwest direction and the maximum shear strain is about 290 nanostrain/yr on the Yalova and Gölcük sides. Deformation is observed in the regions between İzmit, Bilecik, İnegöl, between Karacabey-Mustafakemalpaşa and Gemlik-Yalova where the extension is dominant at about 160, 130 and 90 nanostrain/yr, respectively, and the maximum shear strain values were calculated to be approximately 220, 160 and 150 nanostrain/yr respectively. In the Prince Islands and

Kumburgaz parts on the northern arcs called the Main Marmara Fault of the NAF zone, extension is about 120 nanostrain/yr and compression at 100 nanostrain/yr. In these regions, the maximum shear strain values obtained as 220 nano-strain/yr.

It has been observed that the extension movement changes direction by turning anti-clockwise from north to south and the compression motion is in the northwest-southeast direction in general.

In the studies were done by Ergintav S. et al., Schmittbuhl J. et al., Hergert T. et al. and Şengör A. M. C. et al., were carried out on the arm called Main Marmara Fault which is the north line of the NAF. The kinematics of the fault was created by dividing this arm into four segments (Figure 5, Çınarcık (Prince Islands), Kumburgaz, Center and Tekirdağ segment) and the probable earthquake predictions were made by examining potential energy, velocity and seismic activity accumulated in these segments. According to the results obtained, Çınarcık (Prince Islands) segment is expected to have an earthquake of about 7 and over. According to comments made to the Kumburgaz segment, whether or not there will be any breakage in the near future has become a controversial issue. Seismic activities of the remaining two segments indicate that they will not be broken yet due to major earthquakes in recent years.

In this study, the results obtained around Çınarcık segment and Kumburgaz segment are not similar to these studies. As a result of the analysis, Çınarcık and Kumburgaz segments show slip rates of about 4 mm/yr and 6 mm/yr, respectively. However, these values were obtained as 16 mm/yr and 2 mm/yr in the literature. We can say that the differences in the values found in the literature are due to the analysis by ignoring the kinematics and structure of the fault.

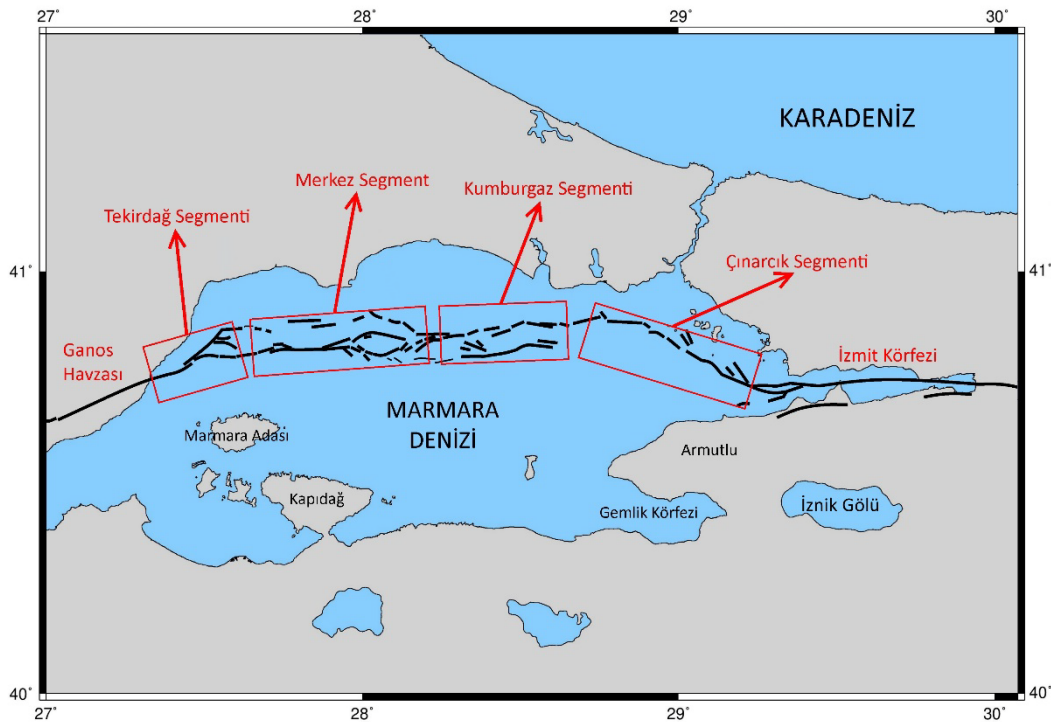


Figure 5. Segments of the Main Marmara Fault

CONCLUSIONS

According to the obtained velocities, when the Eurasian plate was taken constantly, it was observed that the Anatolian plate moved westward at a speed of about 25 mm/yr. These values are similar to those in the literature.

In the analysis using Grid Strain software, the station density should be higher in the vicinity of the fault line. However, the obtained strain values are distributed homogeneously and do not give proper values to the fault geometry.

In the future studies kinematic analyzes can be made on the Çınarcık and Kumburgaz segments according to the existing network. In addition to these two segments, in order to be able to work for the Central segment and the Tekirdağ segment, it is necessary to increase the stations in the southern and northern parts of the existing network.

ACKNOWLEDGMENTS

We would like to thank İSKİ, CORS-Tr, BUSKI, DOHAD, YTÜ and Geomatics Group institutions for the use of the stations' data.

REFERENCES

- Barka A.A., 1992. The North Anatolian Fault Zone. *Annales Tectonicae*, 4:164-195.
- Kalafat D., 2011. Marmara Bölgesi'nin Depremselliği ve Deprem Ağının Önemi, *1. Türkiye Deprem Mühendisliği ve Sismoloji Konferansı*, 11-14 Ekim 2011, Ankara.
- Dirik K., Jeoloji Mühendisliğine Giriş: Genel Jeoloji, http://yunus.hacettepe.edu.tr/~kdirik/Jeol156_KD.pdf , 1 Ağustos 2016.
- Tiryakioğlu İ., 2015. Bireysel Görüşme, Afyon Kocatepe Üniversitesi, Afyonkarahisar.
- Larson K. M., 1991. Application of the Global Positioning System to Crustal Deformation Measurement: 1. Precision and Accuracy, *Journal of Geophysical Research*, 96:16,547-16,565.
- Zhang J., Bock Y., Johnson H., Fang P., Williams S., Genrich J., Wdowinski S., ve Behr J., 1997. Southern California Permanent GPS Geodetic Array: Error Analysis of Daily Position Estimates and Site Velocities, *Journal of Geophysical Research*, 102:18,035-18,055.
- Mao A., Harrison C. G. A. ve Dixon T. H., 1999. Noise in GPS Coordinate Time Series. *Journal of Geophysical Research*, 104:2797-2816.
- Blewitt G., and Lavalée D., 2002. Effect of Annual Signals on Geodetic Velocity. *Journal of Geophysical Research*, 107:2145.
- Ergintav S., Reilinger R. E., Çakmak R., Floyd M., Cakir Z., Dogan U., King R. W., McClusky S. ve Özener H., (2014). İstanbul's Earthquake Hot Spots: Geodetic

Constraints on Strain Accumulation Along Faults in The Marmara Seismic Gap.
Geophysical Research Letters, 41 (16):5783-5788.

Schmittbuhl J., Karabulut H., Lengline O. ve Bouchon M., (2015). Seismicity Distribution and locking Depth Along The Main Marmara Fault, Turkey. *Agü Publications Geochem. Geophys. Geosyst*, 17: 954-965.

Hergert T. ve Heidbach O., (2010). Slip-Rate Variability and Distributed Deformation in The Marmara Sea Fault System. *Nature Geoscience*, 3: 132-135.

Şengör A. M. C., Grall C., İmren C., Le Pichon X., Görür N., Henry P., Karabulut H. ve Siyako M., (2014). The Geometry of The North Anatolian Transform Fault in The Sea of Marmara and Its Temporal Evolution: Implications for The Development of Intracontinental Transform Faults, *Can J. Earth Sci.*, 51:222-242.





HUMAN GEOGRAPHY

Determination of Trekking Areas in Gökçeada (Imbros) with GIS

Canan Zehra Çavuş^{1*}, Tülay Cengiz Taşlı², and Cengiz Akbulak¹

^{1,3}Department of Geography, Canakkale Onsekiz Mart University, Terzioğlu Campus, 17020, Turkey. E-mail: cekrem@comu.edu.tr[†], cakbulak@comu.edu.tr¹

² Department of Landscape Architecture, Canakkale Onsekiz Mart University, Terzioğlu Campus, 17020, Turkey. E-mail: cengiztulay@comu.edu.tr

ABSTRACT

Gökçeada, known as Imbros in antiquity, is the largest island of Turkey with a surface area of 289 km². The island's unique flora and fauna features, variable topographic structure, local products, architectural structure and historical richness constitute an important potential in terms of tourism diversity. Ecotourism and trekking routes within this scope are also in these diversities. In this study, it was aimed to determine suitable routes for trekking in Gökçeada. The trekking area were determined using evaluation factors such as slope, aspect, elevation, current land use, distance to water sources, land use capability class and distance to road. The evaluation factors used in the study and the value ranges of these factors are based on field observations, expert opinions and literature. After giving the suitability score for the range of values of the assessed factors, the weight points were determined considering the importance of the factors according to each other. In the process of determination for the weight points, the Analytical Hierarchy Process (AHP) method, which is one of the multi-criteria decision making techniques, is used. The thematic maps created by giving the scores of the appropriateness and weight to the evaluation factors were interrogated by GIS and the appropriate routes were determined spatially using the overlay method. The analyses revealed that 0.4% (122.2 ha), 16.6% (4668.5 ha), 74.2% (2095.5), and 7.4% (374.2 ha) of Gökçeada (i.e. Imbros) were highly, moderately, marginally suitable, and unsuitable for trekking, respectively.

INTRODUCTION

The ongoing industrialization and urbanization in the world and people's increasing workload turned trekking into a special activity. Over time, a particular group of urban people has formed who like to get away from the city even for a short while and to walk in the natural environment. Thanks to naturalism having emerged in the 19th century, people started to regularly go out to the nature to explore and learn, as a result of which trekking groups and clubs were formed (Bekiroğlu, 2008). With the advent of informatics revolution following the industrial revolution and since trekking equipment has become

* Corresponding Author

lighter and more comfortable, trekking has reached a larger population of people who wish to get away from modern life. Trekking once referred to individual or group activities of nature lovers to be in and with nature. But as from the 1980s it turned into a sports activity which could be performed by everyone. Today it has acquired an economic dimension under the name of alternative tourism and has become a growing sector (Gülbahar, 2009).

Trekking is referred to as an activity in which hourly, daily and annual walking trips are taken in the countryside and mostly in rugged areas (WiseGEEK, 2017). Trekking, the common term for walks in nature, can be categorized as day hiking, regular hiking, and backpacking, and also as forest trekking, desert trekking, mountain trekking, canyon trekking, field trekking, stream bed trekking and winter trekking without predetermined routes (Geneletti and Dawa, 2008). Nature walks can be taken as an individual activity or along with other activities (hunting, mountaineering, etc). Broadly speaking, trekking refers to time-restricted walks appealing to any age group in the rugged parts of a region, where mountaineering techniques are not required without entering arduous and steep areas, following narrow paths in environmental conditions with certain difficulties and properties.

At the present time, areas suitable for trekking are determined by various methods. Particularly the overlay technique, developed by Ian L. Mc Harg (1969), is a prominent one. As computers and remote sensing techniques have become more advanced, the overlay has come to be employed with computers. The employment of Analytic Hierarchy Process (AHP), one of the Multi-Criteria Decision-Making (MCDM) methods, is a prevailing practice to determine suitable areas (Yaralıoğlu, 2004). Spatial Multi-Criteria Analysis (SMCA), which allows for the simultaneous use of AHP and GIS, is a powerful approach to be deployed for a systematical and comprehensive analysis along with GIS data. This approach substantially compensates for the shortcomings of the combination of subjective values and choices and geographical characteristics (Jankowski, 1995; Cengiz, 2003; Bunruamkaew and Murayama, 2011; Çavuş, 2014). The integration of GIS and AHP merges the powerful visualization and mapping skills with decision-oriented methodologies. The present study aims to determine potential trekking areas in Gökçeada by using GIS and AHP.

GENERAL GEOGRAPHICAL FEATURES OF STUDY AREA

Gökçeada is located between Semadirek (Samothrace), Limni (Limnos) and the Gallipoli Peninsula in the Northern Aegean Sea. The island has a surface area of 289.5 km², which makes it the largest island in Turkey. Gökçeada marks the westernmost point of Turkey and it is a town in Çanakkale province (Fig. 1).

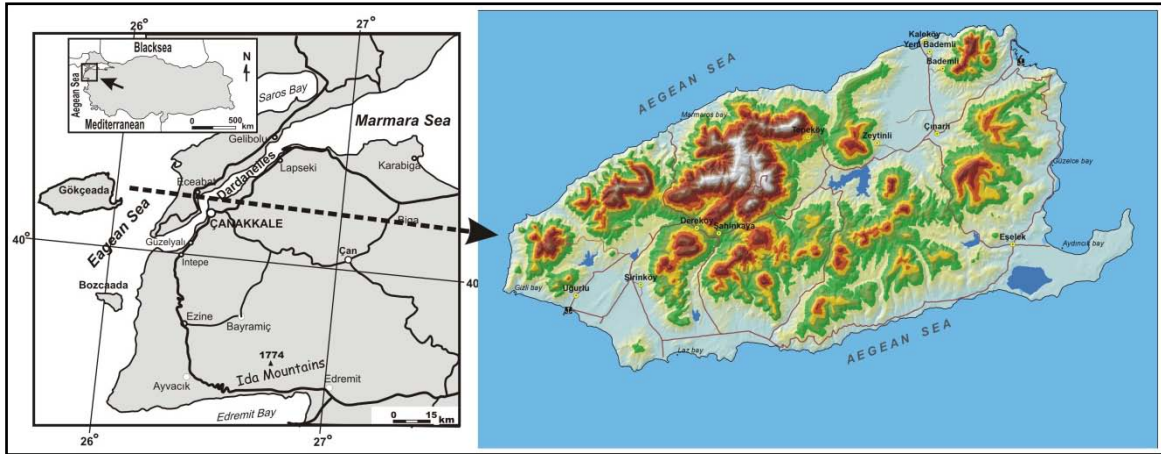


Figure 1. Location map of Gökçeada

Doruk Tepe (Doruk Hill) (673 m) is the highest elevation point on the island, which is majorly covered with hills and mountains. 40% of the surface area of the island has a grade of 30% or more. While the northern part of the island has steep and cliffed shores, south and southwestern coasts have relatively low altitudes and beaches (Özden et al., 2008). The Aydıncık Peninsula, Aydıncık Gulf and the Salt Lake in the southern region apart from the prominent plains in different sections mark different morphological units. Evaluation of the aspect features of the island's topography revealed the highest ratio on the northwestern and northeastern sides.

Gökçeada remains in the Mediterranean climate zone and also in “the Marmara Transition Climate” (Öztürk, 1989). Average annual temperature is 15.1 °C (based on 32-year figures between 1975 and 2006), average annual precipitation amounts to 740.3 mm, and the prevailing wind direction is N-NE (MGM, 2008). Majority of the island is covered by a Mediterranean vegetation type, i.e. maquis. While the higher elevations are covered by Turkish pine (*Pinus brutia*), broad-leaved species, such as oak trees, can be observed too. The island is rich in water resources thanks to its suitable shape and rock structure. The Gökçeada Dam is the most important potable water source on the island. Moreover, there are 4 dams allocated for irrigation.

Thanks to its advantageous location, settlements were established in various historical periods. The archaeological research shows that settlements date back to 3000-2000 BC (Neolithic - Old Bronze Age) (Erdoğan, 2012). It is known that several peoples and empires have ruled on the island till the present day. Studies revealed that Pelasgians were the first people to inhabit the island. The traces of Ionians, Achaeans, Dorians, Romans, Byzantines, Venetians, the Genoese and Turks could be found in the following periods. The island was renamed from Imbros to Gökçeada on 29 July 1970 by the Decree 8479 of the Council of Ministers (Hüryılmaz, 2006).

The settlement patterns in Gökçeada consisting of the town center and 9 villages have been shaped by Greek and Turkish culture. Rural settlements seem to partially maintain the authentic architectural structure. Kaleköy (Kastro) Village, Tepeköy (Agridia) Village, Dereköy (Shinudi) Village, Zeytinliköy (Aya Theodori) Village, Bademli (Gliky) Village

are among the old villages reflecting the Greek culture. Şirinköy, Yeni Bademli, Uğurlu, and Eşelek Villages are the settlements founded after 1980 by the Resettlement Law 2510 (Uçar, 2010). In 2016, populations of the town center and villages were counted to be 6354 and 2422, respectively. Over the last decade, while the population in the city center has decreased, the rural population has increased (TSI, 2017).

The economy in Gökçeada relies on agriculture, animal husbandry, fishing, and tourism. Besides, viticulture and olive growth have always been common agricultural practices. However, they do not play a notable part in the island's economy. The island has a great potential for trekking thanks to the visual characteristics resulting from its biodiversity, monumental trees, forests, water resources, cultural structure, authentic island life, settlement history, and ruins. The island was declared a Cittaslow (slow city) in 2011, which makes it the one and only slow city on an island. The diversity of tourism types expected to invigorate the island economy could also cause harm to natural, historical, and cultural elements peculiar to the island. Therefore, membership in the Cittaslow organization has a vital role in the protection of Gökçeada's local identity and characteristics.

MATERIAL AND METHODOLOGY

Maps from various resources were used for the purpose of the study (Table 1). The data and maps were imported to the virtual media via Arc-GIS 10 software program.

Table 1. List of data and their original sources

Data	Scale	Source	Map
Topography map	1/25 000	General Command of Mapping	-Digital Elevation Model -Slope -Aspect -Elevation
CORINE (2012)	Level III	Ministry of Forestry and Water Affairs	-Landuse
Soil map	1/100 000	General Directorate of Rural Services	-Land Capability Classes

Evaluation factors and value intervals were obtained from the related literature, field research and the specialists of assorted disciplines. Weight assignment was performed based on the AHP technique, developed by Saaty (1980). AHP, relying on the creation of a hierarchy in the analysis of multi-criteria complex problems, involves scoring according to Saaty's evaluation scale and the formation of a pairwise comparison matrix (Saaty, 1980). Suitability points were assigned for value spacing according to a 1-5 scale. The points for value spacing and weights for evaluation factors were assigned by specialists. They were standardized according to weights and suitability values. The pixel size was assigned to be

10 m x 10 m in consideration of the size of the research field and performability of the analyses. The obtained results were categorized as highly suitable (4), moderately suitable (3), marginally suitable (2) and not suitable (1) (Table 2).

RESULTS

Different evaluation factors were considered for the determination of the trekking areas in Gökçeada. The highest weight point (33.1%) of all the evaluation factors belongs to the existing land use status. The highest suitability concerning land use status was obtained from forest areas (3497 ha; 12.4% of the total area). These areas prevail the central and northwestern parts of the island. The second highest score (23.1%) was yielded from the slope evaluation factor. The areas with 0-5% grades were discovered to have the highest slope suitability (7.2%), and the ones with 30% and more inclination to have the lowest (18.6%). The northern sections from Eski Kaleköy to Gökçeada city center and the areas around Uğurlu Village in the south and the south of Şahinkaya Dam Lake are the most suitable spots for trekking. In the third place is the elevation evaluation factor (15.6%). The value interval from 0 to 200 m was found to yield the lowest suitability (18784 ha; 66.7% of the total area) for trekking, while the elevation of 600 m and higher exhibited the highest suitability (68 ha; 0.2%). Aspect evaluation factor is in the fourth place in terms of weighs (10.7%). The northern slopes yielded the highest score of suitability values. On the other hand, the lowest (13.2%) was produced by the southern slopes. The distance to water resource factor had a weight of 7.1%. While the value interval of 0-300 m was calculated to represent the lowest suitability (13.2% of the total area), the highest was observed for the elevation between 300 and 1000 m (23.4%). In terms of land use capability which was in the sixth place (4.8%), class I-II lands were revealed to exhibit the lowest suitability (8.8%), whereas class VII lands had the highest score (53.6%). In the seventh place (3.3%) was the distance to road factor. The distance from 0 to 1000 m was calculated to produce the highest suitability score (53.6%), while the lowest was obtained from the distance of 5000 m and higher (5.4%). The distance to settlement factor was placed in the last slot (2.4%) in consideration of weights. The highest suitability level was obtained from the distance between 0 and 500 m (10.8% of the total area). (Table 2; Fig. 2)

Table 2. Factors and criteria in land suitability analysis for ecotourism

Factors	Weight
Slope (%)	0.231
Aspect	0.106
Elevation (m)	0.156
Land use	0.331
Distance to water source (m) (walking distance)	0.071
Land Use Capability	0.048
Distance to main road (m) (walking distance)	0.033
Distance to settlement (m) (walking distance)	0.024

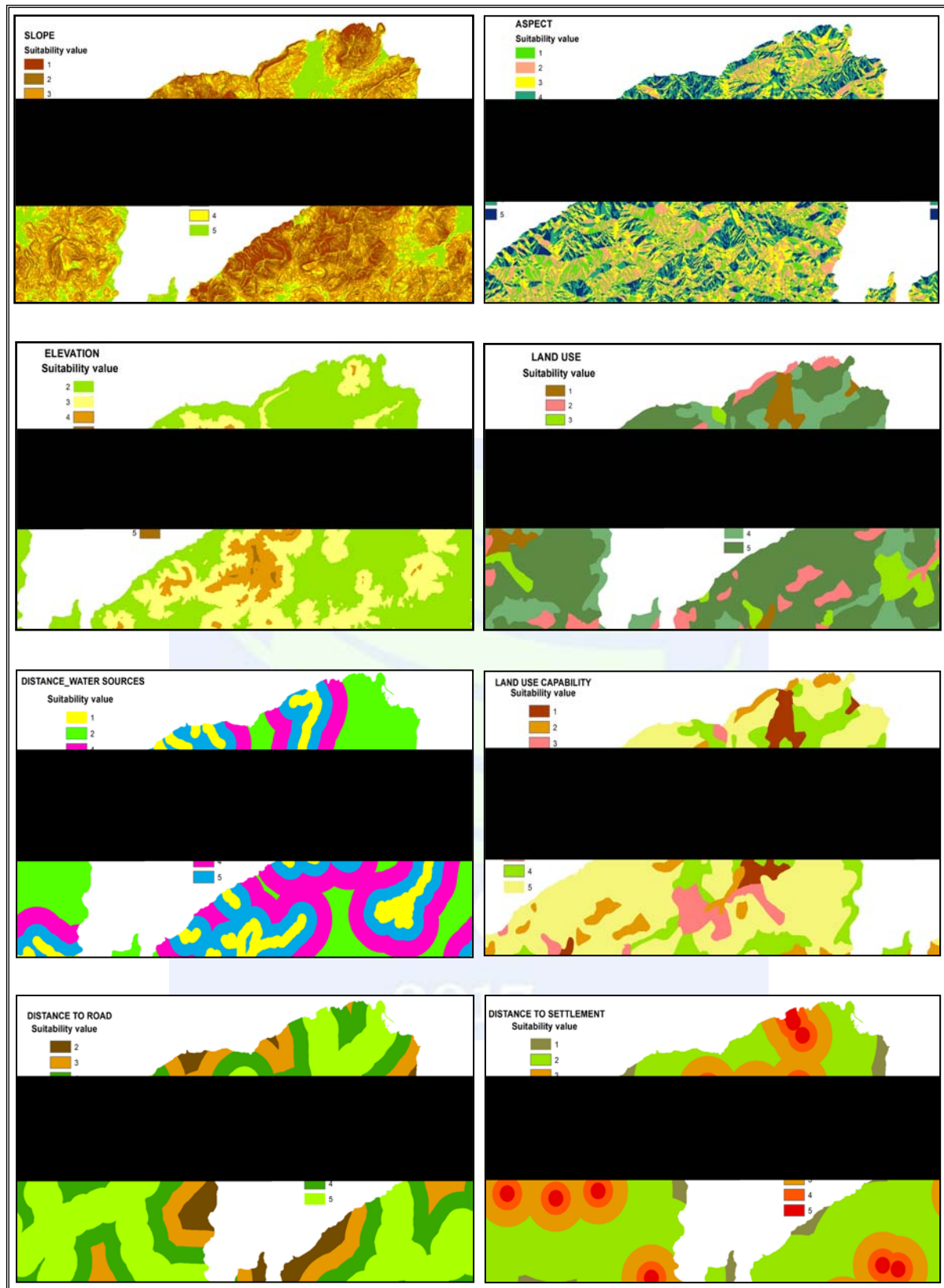


Figure 2. Suitability classes and suitability maps for trekking areas

Trekking suitability map of Gökçeada was produced by merging weights and suitability scores of the evaluation factors in GIS (Fig. 3). The suitability analysis results showed that

the most suitable areas for trekking accounted for 0.4% of the total surface area. On the other hand, the unsuitable areas cover 7.4% (Table 3).

Table 3. Suitability classes for Gökçeada trekking areas

Suitability class	Area (ha)	%
Higly suitable	122.2	0.4
Moderetaly suitable	4668.5	16.6
Marginally suitable	20875.7	74.2
Not suitable	2095.5	7.4
Lake, dam	374.2	1.3
Total	28136.1	100

The most suitable areas were determined to be the vicinity of Uğurlu Göleti in the west, the north of Şirinköy Dam Lake, the environs of Şahinkaya Village and the area between Eşelek and Zeytinli Villages. It is noticeable that these areas display a linearity typical of stream valleys, they are plain or slightly sloping, their relative distance to water resources is minimum 300 m, and they are forest areas facing north and northwest. Areas unsuitable for trekking are majorly located between Kaleköy and Kuzu Limanı. It is the one and only underwater national park in Turkey. Moreover, this area, also covering the Peynir Kayalıkları (The Cheese Rocks) situated in the vicinity of the Kaşkaval Headland, is not suitable for trekking. Furthermore, there are some areas along the coastline in the south of the island, which are unsuitable for trekking (Fig. 3). It is striking that areas highly suitable for trekking are not generally close to settlements. The distance of trekking areas from settlements can be considered preferable to culturally and architecturally protect the inhabited areas.

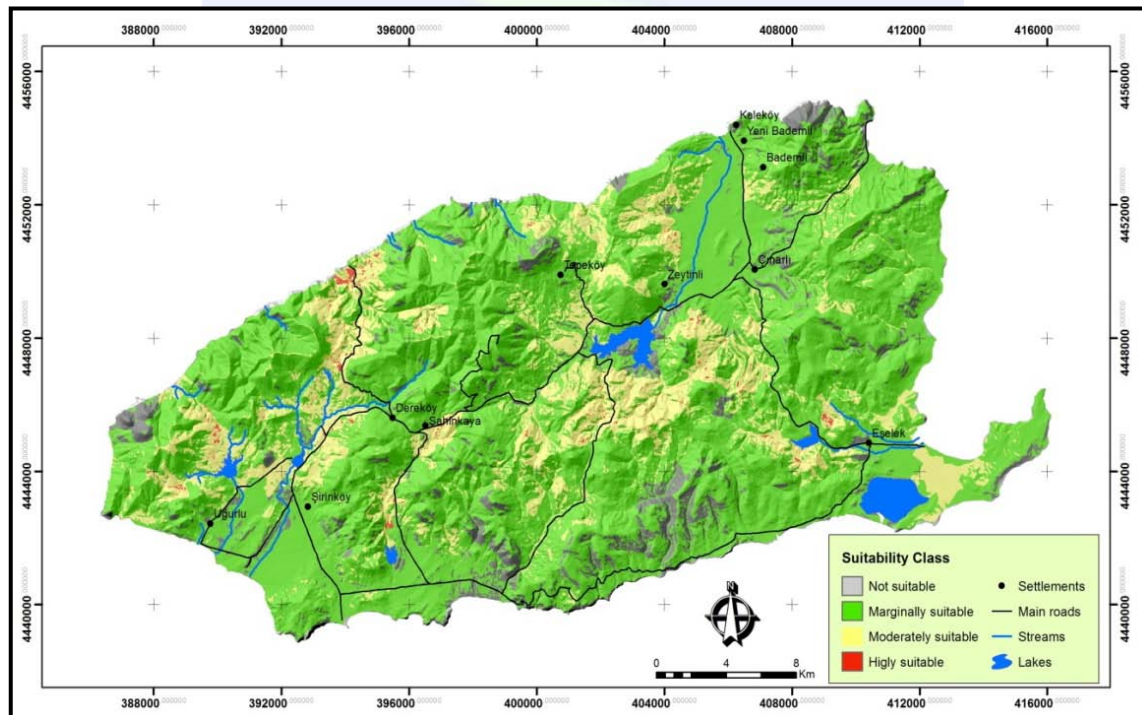


Figure 3. Suitability map for Gökçeada trekking areas

DISCUSSION AND CONCLUSION

Today, tourism and recreational activities have become more diversified. Among these activities is trekking appealing to various age groups and done for assorted purposes, in different areas, and for varying durations. Areas suitable for trekking activities, which lend themselves to the protection of natural resources, support sustainable use and are in harmony with the socio-cultural structure (Koçak and Balcı, 2010; Çakır and Çakır, 2012; Turgut et al. 2014). Various suitability analyses are carried out to this end (Kliskey, 2000; Geneletti and Dawa, 2009). Suitability analyses have complex processes. Many of the previous studies have proved that AHP effectively serves for the solution of sophisticated problems (Akbulak, 2010; Cengiz, 2003; Çavuş, 2014) and for the designation of trekking areas (Bunruamkaew and Murayama, 2011). AHP, developed by Saaty (1980), shows that subjective judgments might yield useful results employable in the decision-making and planning phases. Yet it can be asserted that suitability values obtained by means of AHP alone fall short of accounting for spatial differentiation. To this end, the combined employment of GIS and AHP, being important tools of suitability analyses and using spatial data, play a crucial part in spatial decision-making (Ying et al., 2007; Akbulak, 2010). GIS also allows for the presentation of analysis results on maps.

The present study aims to determine Gökçeada's suitability for trekking by employing GIS and AHP methods. In this context, evaluation factors were determined based on the island's characteristics, specialists' views, and literature review. Weights and suitability points assigned to evaluation factors were overlaid in GIS to produce a trekking suitability map of Gökçeada.

The obtained results showed that a great majority of Gökçeada's land was marginally suitable for trekking, which is followed by moderately suitable, unsuitable, and suitable areas. Half of Gökçeada's land is under protection in a different status. The results on trekking areas revealed that heed should be paid to the social and natural structure of the island while taking recreation-related decisions. It is imperative that the results of the present study should be taken into account at both decision and application stage.

REFERENCES

- Açıksöz, S., Topay, M., and Aydın, H., 2006. Bartın Arıt Beldesi trekking potansiyelinin belirlenmesi, *ZKÜ Bartın Orman Fakültesi Dergisi* Cilt 8 Sayı 10, s: 78-87.
- Akbulak, C., 2010. Analitik Hiyerarşi Süreci ve Coğrafi Bilgi Sistemleri ile Yukarı Kara Menderes Havzası'nın Arazi Kullanımı Uygunluk Analizi. *Uluslararası İnsan Bilimleri Dergisi*, Cilt:7, Sayı:2, 559-576.
- Bekiroğlu, M., 2008. *Uçmaktüre'nin doğal ve kültürel özelliklerinin ekoturizm açısından değerlendirilmesi*. Yüksek Lisans Tezi (Basılmamış), NKÜ, Fen Bilimleri Enstitüsü, Peyzaj Mimarlığı Anabilim Dalı, Tekirdağ.

- Bunruamkaew K., and Murayama Y., 2011. Site Suitability Evaluation for Ecotourism Using GIS & AHP: A Case Study of Surat Thani Province, Thailand. *Procedia Social and Behavioral Sciences* 21, 269–278.
- Cengiz, T., 2003. *Peyzaj Değerlerinin Korunmasına Yönelik Kırsal Kalkınma Modeli Üzerine Bir Araştırma: Seben İlçesi (Bolu) Alpağut Köyü Örneği*. Doktora Tezi (Basılmamış), AÜ Fen Bilimleri Enstitüsü, Ankara.
- Cengiz T., Akbulak C., Özcan H., Beytekin H., 2013. Gökçeada’da Optimal Arazi Kullanımının Belirlenmesi. *Tarım Bilimleri Dergisi*, 149-162
- Çakır, G., Çakır, A., 2012, İğneada Longoz Ormanları ve Çevresinin Rekreatif Faaliyetler Açısından Değerlendirilmesi, *KSÜ Doğa Bilimleri Dergisi (Özel Sayı)* 281-286.
- Çavuş, C.Z., 2014. *Çanakkale Boğazı Doğusunda Arazi Kullanımı Uygunluğunun Yerleşme İçin Değerlendirilmesi*. Doktora Tezi (Basılmamış), ÇOMÜ Sosyal Bilimler Enstitüsü, Çanakkale.
- Emekli, G., 2005, Avrupa Birliği’nde turizm politikaları ve Türkiye’de kültürel turizm, *Ege Coğrafya Dergisi*, 14 (1-2),100-107.
- Erdoğan, B., 2012, “Uğurlu-Zeytinlik: Gökçeada’da Tarih Öncesi Dönemlere Ait Yeni Bir Yerleşme”, *Trakya Üniversitesi Edebiyat Fakültesi Dergisi* 2/4 : 1-16
- Geneletti, D. and Dawa, D., 2009. Environmental impact assessment of mountain tourism in developing regions: a study in Ladakh, Indian Himalaya. *Environmental Impact Assessment Review* 29(4): 229–242.
- Gülbahar, O., 2009. 1990’lardan günümüze türkiye’de kitle turizminin gelişimi ve alternatif yönelimler, *SDÜ İktisadi ve İdari Bilimler Fakültesi Dergisi*, 14(1), 151-177.
- Hüryılmaz, H., 2006. *Kuzeydoğu Ege Denizi’nin Rüzgarlı Bahçesi:Gökçeada*, Editör: Bora Uysal, ISBN: 975-92501-1-X.
- Jankowski, P., 1995. Integrating Geographical Information Systems and Multiple Criteria Decision-Making Methods. *International Journal of Geographical Information Systems* 9-3, 251-273.
- Kliskey, A.D., 2000, Recreation terrain suitability mapping: a spatially explicit methodology for determining recreation potential for resource use assessment, *Landscape and Urban Planning* 52, 33-43.
- Koçak, F., Balcı, V., 2010. Doğada Yapılan Sportif Etkinliklerde Çevresel Sürdürülebilirlik, *Ankara Üniversitesi Çevre Bilimleri Dergisi* 2(2), 213-222.
- Köy Hizmetleri Çanakkale İl Müdürlüğü, 1999. *Çanakkale İli Arazi Varlığı*, Köy Hizmetleri Genel Müdürlüğü Yayınları, İl Rapor no:17, Ankara
- Özden, S., Ateş, Ö., Şengün, F., Tunç, İ.O., Türkdönmez, O., Şanlıyüksel, D., Avcıoğlu, M. and Ertekin, C., 2008, Gökçeada’nın jeolojik özellikleri, *Çanakkale İli Değerleri*

- Sempozyumu 25-31 Ağustos 2008, *Gökçeada Değerleri Sempozyumu Bildiriler Kitabı*, 47-58.
- Öztürk, B.,1989. Gökçeada'nın İklimi. *İÜ. Deniz Bilimleri ve Coğrafya Enst. Bülten*, Sayı:6/6,
- Malczewski, J., 2004. GIS-Based Land-Use Suitability Analysis: A Critical Overview. *Progress in Planning* 62, 3–65.
- The International Tourism Society, <http://www.ecotourism.org/book/how-ecotourism-different-nature-tourism-sustainable-tourism-responsible-tourism>. Erişim Tarihi: 13.09.2017.
- Topay, M., 2003. *Bartın Uluyayla peyzaj özelliklerinin rekreasyon-turizm kullanımları açısından değerlendirilmesi üzerinde bir araştırma*. Doktora Tezi (Basılmamış), AÜ Fen Bilimleri Enstitüsü, Peyzaj Mimarlığı Anabilim Dalı, Ankara.
- Tozar, T., 2006. *Doğal kaynakların sürdürülebilirliği için geliştirilen ekolojik planlama yöntemleri*, Yüksek Lisans Tezi (Basılmamış),YTÜ Fen Bilimleri Enstitüsü, İstanbul.
- TUİK, 2017. <https://biruni.tuik.gov.tr/medas/?kn=95&locale=tr> Erişim Tarihi: 10.09.2017
- Turgut, H., Yavuz Özalp, A., Akıncı, H., 201. Determination of the Physical Characteristics of the Trekking Tracks in Hatila National Park through GIS, *Pensee Journal*, Vol 76/ 3, 67-83.
- WiseGEEK, <http://www.wisegeek.org/what-is-trekking.htm>. Erişim Tarihi: 10.08.2017.
- Yalçınlar, İ., 1980. Gökçeada'nın Jeomorfolojisi, *İ.Ü. Coğrafya Enstitüsü Dergisi*, Sayı 23, 239-256.
- Yaralıoğlu, K., 2004. *Uygulamada Karar Destek Yöntemleri*, İlkem Ofset, İzmir.
- Yaşar, O., 2006. Turizm Coğrafyası Açısından Bir Araştırma: Gökçeada (İmroz). *Fırat Üniversitesi Sosyal Bilimler Dergisi*, Cilt: 16, (1).
- Ying, X., Guang-Ming, Z., Gui-Qia, C., Lin, T., Ke-Lin, W., Dao-You, H. (2007). Combining AHP with GIS in synthetic evaluation of eco-environment quality- A case study of Hunan Province, *China Ecological Modelling* 209, 97-109.
- Yücel, T., 1966. İmroz'da Coğrafya Gözlemleri, *Coğrafya Araştırmaları Dergisi*, No: 1, 65-108.

The Assessment of Subjective Well-Being Map of Turkey

Erdal Karakaş¹ and Öznur Akgiş²

¹Department of Geography, Bilecik Şeyh Edebali University, Turkey. e-mail: erdal.karakas@bilecik.edu.tr

²Department of Geography, Bilecik Şeyh Edebali University, Turkey. e-mail: oznur.akgis@bilecik.edu.tr

ABSTRACT

Edward Soja says that people are as spatial as social, the space is socially produced and therefore changed by socially. Accordingly, whatever your area of research is, if you do not acquire a spatial perspective, your work will not be qualified enough.

From this point of view the aim of this study is to determine the level of subjective well-being of the provinces in Turkey and to determine spatial distribution of subjective well-being throughout the country. The data set of the study constitutes the results of the 2013 Life Satisfaction Survey conducted by the Turkish Statistical Institute (TURKSTAT). 25 variables were evaluated in this study, including income, education-health, access to public services and social networks, which are assumed to be components of subjective well-being. Principal Component Analysis (PCA) analysis is applied. Accordingly, it is determined that 4 principal components explain 76.6% of the total variance. The first principal component alone is the key component with the highest variance explanatory rate, accounting for 51.9% of the variance. For this reason, using the first principal component, the level of subjective well-being was determined by multiplying the value of the variable used and the value of the principal component.

According to the findings, there are significant differences in the spatial distribution of subjective well-being in Turkey. In the western part of the country, the level of subjective well-being is higher, whereas in the eastern part of the country it is very low. In addition the variables with the highest degree of relationship with subjective well-being are those related to public services. As a result, it is possible to say that inequality of subjective well-being is another social problem in addition to the problem of spatial inequality in income and consumption which represents the material aspect of wealth in the whole country.

INTRODUCTION

Traditionally, well-being was defined as a material process determined by considering the income variable (Conceição and Bandura, 2008). However, income does not cover much of human life, and it has now been recognized that new methods need to be applied. In this context, the use of subjective data is of great importance for development researchers and

is increasingly used by social scientists in many studies (Akgiş, 2015; Easterlin, 2006; Van Praag et al., 2003; Camfield and Esposito, 2014, Kahneman, 2003).

Well-being is a very difficult concept to define, but its measurement is much more difficult. Empirical analyzes on well-being are examined under two categories. These are objective and subjective measurements (Conceição and Bandura, 2008). Subjective well-being is recognized by some researchers as synonymous with the concepts of "happiness" and "life satisfaction". However, psychology states that the concept of happiness has a narrower concept than subjective well-being, and therefore does not adequately explain subjective well-being (Conceição and Bandura, 2008). Although these two concepts are different from each other, many researchers consider happiness and life satisfaction as a measure of subjective well-being (Easterlin 2004).

There are three components of subjective welfare. These include: Life evaluation, Affect and Eudaimonic well-being. Life evaluations reflect a general assessment of a person's life or a particular aspect of it. Pavot and Diener et al. (1991) describes the process of making such an assessment, including the individual who creates a "standard" that they perceive to be appropriate for them, by comparing living conditions to that standard. One of the best documented measures of life assessment, the Personal Welfare Index, consists of eight questions involving dissatisfaction with life in eight different ways, and they are collected using equal weights to calculate a general index (International Wellbeing Group, 2006). Similarly, panel data obtained from the German Socio-Economic Panel of Van Praag et al. (2003) show six general life satisfaction (job satisfaction, financial satisfaction, home satisfaction, health Satisfaction, leisure time satisfaction and environmental satisfaction) it controls the individual personality effect.

Affect is the term psychologists use to describe one's feelings. Impact criteria can be thought of as the measure of certain emotions or emotional states, and are usually measured at a particular time. These measures capture how they have experienced how people remember their lives (Kahneman and Krueger, 2006). The affect has at least two different hedonic dimensions: a positive effect and a negative effect (Diener et al., 1999), while capturing a general assessment of life in a single measure. Positive effect, happiness, joy and satisfaction, such as positive affects catches. The negative effect, on the other hand, involves the experience of unpleasant emotional situations such as sadness, anger, fear and anxiety.

Eudaimonia includes some definitions of subjective well-being in the psychological literature, as well as other aspects of a person's psychological processes, in addition to the life evaluations and influences that focus on one's experiences (present or remembered). In particular, there is an important literature that focuses on the concept of good psychological function, sometimes referred to as "developing" or "eudaimonic" well-being (Huppert et al., 2009). Eudaimonic well-being focuses on the functioning and fulfillment of one's potential, beyond the reflective evaluation of the participant and emotional situations. Eudaimonia's measurement is based on both the psychological and humanistic literature, which defines fundamental universal "needs" or "goals", a useful answer to criticism that subjective well-being is based on "happiness" or only hedonistic philosophy.

And at the same time it harmonizes with the perceptions that many people consider important to value in life.

Edward Soja says that people are as spatial as social, the space is socially produced and therefore changed by socially. Accordingly, whatever your area of research is, if you do not acquire a spatial perspective, your work will not be qualified enough. Nevertheless, perhaps the least explored issue within the economic geography studies is the prosperity issue. Even though it is assumed that poor individuals tend to concentrate in certain areas, and therefore poverty and well-being are a spatial characteristic (Henninger and Snel, 2002), studies on this subject are very limited.

Well-being research from a geographical point of view is of great importance for expressing the spatial distribution of the problem in terms of the causes of poverty and the measures to be taken in combating poverty (Henninger and Snel, 2002, Hyman et al., 2005). In particular, the maps to be prepared on the issue of poverty give clues as to where the resources should be transferred, since it expresses where the poverty is concentrated (Fujii, 2008).

Advantages of well-being maps can be listed as follows. It allows social, economic or environmental data obtained by surveys or satellite images to be evaluated together. For example, spatial differences in income distribution help to compare data on different levels of education, access to services, or wealth. It allows the creation of a spatial framework and allows for the creation of new alternatives for analysis. The creation of spatial models with poverty maps gives new perspectives in understanding the causes of poverty. The distribution of resources can be made more efficient. At the same time, these maps are guiding the application areas of preventive policies. It has been shown that geographically determining the target is effective in increasing wealth (Baker and Grosh, 1994). Well-being maps are highly valued in the strategic planning and decision-making stages of international development organizations in terms of ensuring consistent and consistent visibility in international research. For this reason, it can be said that the well-being maps are more than cartographic works.

The issue of working in this context is the distribution of subjective well-being in Turkey. The aim of the work is to determine areas where the subjective well-being is low and intensive, and to guide policy makers in priority areas. The study basically consists of three parts. In the first part, the concept of subjective development and the importance of geographical point of view in development researches are discussed. In the second part, information about the data used in the study, the scale used for measuring subjective welfare and the analysis of basic components are given. The third section contains the findings and conclusions obtained.

DATA AND METHODS

Data

This research is an applied study and quantitative analysis methods were used. The results of the Life Satisfaction Survey prepared by the Turkish Statistical Institute (TURKSTAT)

were used in the study. These surveys were first applied in 2003 and are regularly carried out since that date. The surveys were first applied in 2013 at the provincial level. The survey was conducted face-to-face with 125,720 households and 196,203 people over the age of 18 in the country. The survey includes detailed information on many topics such as public services, health, education, social networks. Those made after 2013 are less detailed. For this reason, in this study, 25 variables of the year 2013 including public service, health, education and life satisfaction were used.

Table 1. Descriptive statistics of the variables used in the study

	N	Min.	Max.	Mean	Std. Deviation
Satisfaction with judicial services	81	28,7	84,4	55,1	13,09
Satisfaction with relatives	81	77,6	96,0	88,0	3,97
Satisfaction with education	81	26,7	80,3	52,7	10,70
Satisfaction with friends	81	83,7	97,2	92,9	2,36
Satisfaction with public service	81	58,8	94,8	84,2	7,15
Satisfaction with monthly household income	81	21,7	69,8	44,8	9,49
Satisfaction with wages in working life	81	41,1	91,3	73,4	8,09
Satisfaction with job	81	63,9	91,6	78,7	6,47
Satisfaction with the number of doctors and health personnel	81	12,3	64,0	41,3	10,16
Satisfaction with educational services	81	48,1	88,8	74,0	8,46
Satisfaction with pensions	81	1,4	20,9	10,2	4,34
Satisfaction with marriage	81	86,9	97,2	94,2	1,98
Satisfaction with medicine prices	81	1,8	25,4	7,37	3,86
Satisfaction with medicine supply	81	25,2	78,7	42,7	11,17
Satisfaction with personal health	81	59,1	80,7	71,9	4,44
Satisfaction with health care	81	54,5	89,1	77,4	7,30
Satisfaction with social life	81	21,5	80,8	54,0	11,27
Satisfaction with transportation services	81	50,1	94,2	78,1	8,79
Satisfaction with garbage and waste services	81	33,1	86,5	66,5	12,70
Satisfaction with sewerage services	81	28,8	82,6	65,0	12,31
Satisfaction with network water services	81	30,6	86,8	64,	12,87
Satisfaction with public transport services	81	23,5	78,8	58,3	11,58
Satisfaction with the amount of green space	81	22,5	82,3	53,8	14,74
Satisfaction with disability services	81	14,5	71,3	42,4	12,13
Satisfaction with services for the sick and the poor	81	15,3	73,4	48,6	12,59
Valid N (listwise)	81				

Development of Scale

In recent years, it has become very important to scientifically quantify the emotions, attitudes, behaviors, likes, social, economic, health and educational characteristics of individuals that are not observable but who feel their presence and lead our life. In this sense, scales are an important research tool in many areas of social sciences. In this research, first of all, the subjective welfare scale was developed by using the variables listed (Table 1).

When developing the scale, firstly the publication index was examined and variable pool was established. Later, structural characteristics related to the subjective welfare phenomenon have been established. Accordingly, subjective well-being has been regarded

as three-dimensional, with satisfaction from public services, social life, education and health services.

Additivity is a feature that must be on scales and there must be a minimum of 5 points for a scale to be additable. The data set is suitable for this purpose. Reliability and item analysis were applied using SPSS 20 statistical program. Then descriptive statistics, Cronbach Allfa and If Item Deleted Cronbach Alfa coefficients were calculated (Table 2 and 3).

The Cronbach's alpha coefficient is a general reliability coefficient that measures the strength, adequacy, and reliability of the measure of a phenomon questioned by a scale (Özdamar, 2016). The value varies between 0 and 1. If the Cronbach alpha value, close to 1, indicates that the scale has high reliability. According to the obtained value, the scale has a very high level of reliability (Table 2).

Table 2. Reliability Statistics

Cronbach's Alpha	Cronbach's Alpha Based on Standardized Items	N of Items
,924	,927	25

When Table 3 is examined, it can be seen that the items are significantly different from each other ($F_{24,1} = 40221,535$, $P < 0.001$). This result indicates that the items in the measure are of a structure that will describe at least two different sub-dimensions. The probability of nonadditivity is 0.520. Accordingly, the items in the scale are additive (Table 3).

Table 3. ANOVA with Friedman's Test and Tukey's Test for Nonadditivity

		Sum of Squares	df	Mean Square	Friedman's Chi-Square	Sig
Between People		65534,451	80	819,181		
	Between Items	965316,838	24	40221,535	648,531	,000
	Nonadditivity	25,740 ^a	1	25,740	,415	,520
Within People	Residual	119051,610	1919	62,038		
	Total	119077,350	1920	62,019		
	Total	1084394,188	1944	557,816		
Total		1149928,639	2024	568,147		

Principal Component Analysis (PCA)

Previously used indexing and taxonomy techniques did not provide a concrete and objective weighting system for variables. For this reason, the use of these techniques has been abandoned (Dinçer and Özasan, 2004). Principal component analysis is one of the most commonly used multiple analysis methods (Mainly, 1994; Joliffe, 2002). PCA is, in the broadest sense, a statistical method that makes it possible to summarize a number of features from a particular direction and to deduce from common qualities. This feature allows analysis of key components and the ability to extract, understand and identify common and basic self-contained information contained in a large and diverse set of data.

In PCA, it is preferable to identify factors or factors that account for at least 67% of the observed / original variance of findings in the data matrix (Özdamar, 2016). For this, it is required that the Kaiser-Meyer-Olkin Sample Proficiency Measurement statistic is above 0,50 ($KMO \geq 0.50$) (Field, 2000; Özdamar, 2016). Accordingly, the is scale provides the requirements for the KMO test (Table 4). The Bartlett sphericity test tests whether the answers given to the items are independent or related to each other. If the sphericity test is important ($p \leq 0.05$), it means that all or some of the substances have a significant correlation with each other, and that at least one factor structure exists on the scale, and it is considered that the scale is a specific measurement tool. If the sphericity test is insignificant ($p > 0.05$), it is decided that the items are independent of each other and that the scale is in the form of a questionnaire.(Özdamar, 2016). According to the results obtained, it was determined that the sphericity test is important (Table 4).

Table 4. KMO and Bartlett's Test

Kaiser-Meyer-Olkin Measure of Sampling Adequacy.		,894
	Approx. Chi-Square	2381,128
Bartlett's Test of Sphericity	df	300
	Sig.	,000

Table 5. Total Variance Explained

Component	Initial Eigenvalues			Extraction Sums of Squared Loadings		
	Total	% of Variance	Cumulative %	Total	% of Variance	Cumulative %
1	12,982	51,929	51,929	12,982	51,929	51,929
2	3,422	13,687	65,617	3,422	13,687	65,617
3	1,454	5,815	71,432	1,454	5,815	71,432
4	1,315	5,258	76,690	1,315	5,258	76,690
5	,963	3,853	80,543			
6	,908	3,633	84,176			
7	,685	2,739	86,915			
8	,608	2,431	89,346			
9	,419	1,676	91,022			
10	,360	1,439	92,461			
11	,324	1,295	93,756			
12	,278	1,112	94,867			
13	,229	,915	95,782			
14	,196	,786	96,568			
15	,182	,729	97,297			
16	,131	,524	97,821			
17	,109	,438	98,259			
18	,080	,319	98,577			
19	,067	,268	98,845			
20	,063	,252	99,097			
21	,060	,240	99,337			
22	,051	,206	99,543			
23	,051	,206	99,748			
24	,037	,148	99,896			
25	,026	,104	100,000			

Extraction Method: Principal Component Analysis.

RESULTS AND CONCLUSION

It is decided by looking at the eigenvalue whether a particular component is important. The statistical program used in the study determines this according to the Kaiser scale. If Eigenvalues are greater than 1 they do not considered as factors. Following the signing of the results of the statistical significance tests, indicating that the application of the analysis of the principal components is meaningful, four important principal components were obtained according to the analysis of the principal components applied to the correlation matrix for the variables, together with these four principal components accounting for 76.6% of the total variance (Table 5).

The first principal component alone is the basic component with the greatest variance explanatory rate, accounting for 51.9% of the variance. For this reason, the subjective welfare rankings of provinces are made according to this basic component. The weights of the variables in the formation of the first basic component and the direction of these weights are given separately in Table 6. When the weights of each variable in the first principal component explaining the subjective welfare dimension are examined, it is seen that 10 variables are negative and 15 variables are positive weights.

Table 6. Component Score Coefficient Matrix

	Component			
	1	2	3	4
Satisfaction with judicial services	-,093	,200	,058	-,118
Satisfaction with relatives	-,064	-,048	,011	,312
Satisfaction with education	-,053	,244	-,046	-,069
Satisfaction with friends	,013	-,101	-,050	,389
Satisfaction with public service	-,048	-,142	,308	,040
Satisfaction with monthly household income	-,045	,246	-,097	,013
Satisfaction with wages in working life	-,101	,185	,011	-,011
Satisfaction with job	,017	,138	-,056	,025
Satisfaction with the number of doctors and health personnel	,079	-,121	,149	-,034
Satisfaction with educational services	-,077	-,056	,289	-,018
Satisfaction with pensions	,083	-,056	,044	,044
Satisfaction with marriage	,089	-,081	-,156	,395
Satisfaction with medicine prices	,046	,057	-,286	,139
Satisfaction with medicine supply	-,002	-,053	-,096	,051
Satisfaction with personal health	,025	,180	-,193	,123
Satisfaction with health care	-,012	-,103	,257	,007
Satisfaction with social life	-,086	,350	-,113	-,102
Satisfaction with transportation services	,008	-,062	,210	-,021
Satisfaction with garbage and waste services	,214	-,093	-,072	,034
Satisfaction with sewerage services	,224	-,183	-,033	,138
Satisfaction with network water services	,208	-,109	-,027	-,007
Satisfaction with public transport services	,158	-,033	-,026	-,029
Satisfaction with the amount of green space	,126	,031	-,049	-,033
Satisfaction with disability services	,094	,125	-,106	-,041
Satisfaction with services for the sick and the poor	,102	,070	-,049	-,037

Extraction Method: Principal Component Analysis.

Rotation Method: Varimax with Kaiser Normalization.

Component Scores.

For each province, to obtain subjective welfare, the first principal component value was calculated and this value obtained by multiplying the values of the relevant variables by the value of the principal component was taken as the welfare level. By arranging these values according to their size order, the subjective welfare order of the provinces was established. Then, using these values, provinces were divided into 5 groups according to their development level. The first group expresses the lowest development while the fifth group expresses the highest development (Figure 1).

When the spatial pattern of the subjective welfare is examined, it is seen that the welfare generally declines from the western side to the welfare state regularly. However, differences can be seen in the neighboring provinces.

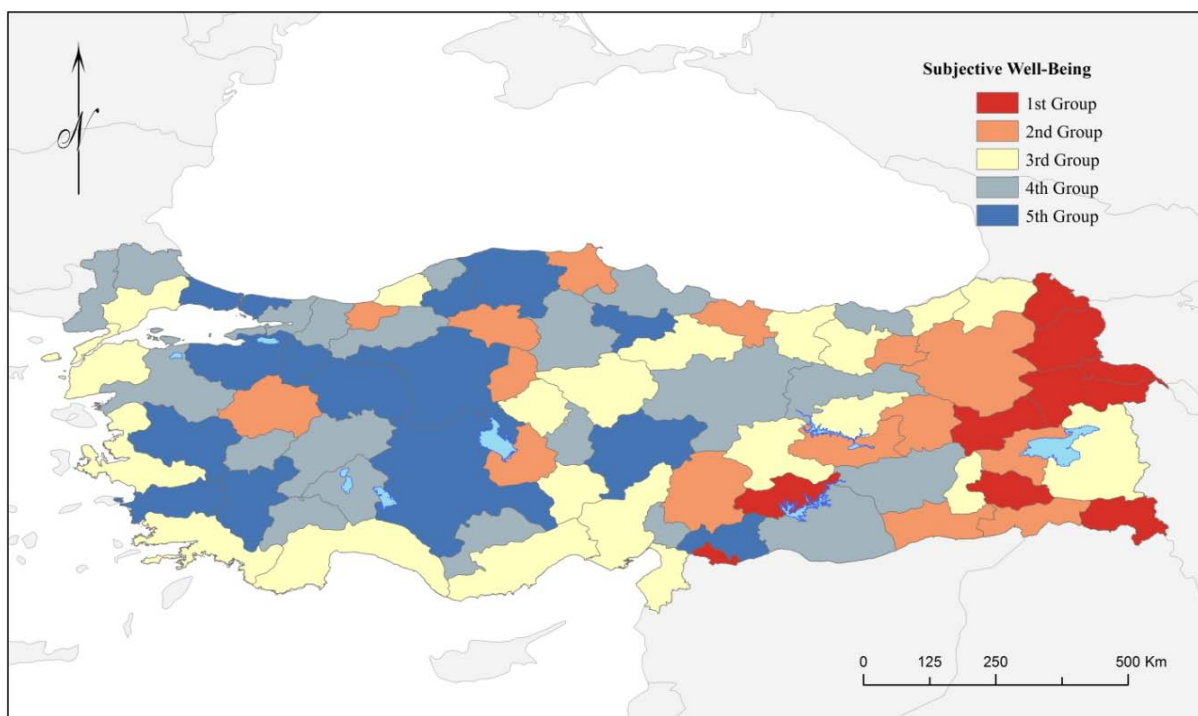


Figure 1. Subjective Well-Being Map of Turkey

When the correlation table for the first basic component was examined, it was determined that 10 of the variables considered had a negative correlation with subjective welfare and 15 of them had positive correlation values. Variables related to public services, which have the highest degree of relationship with subjective well-being. These variables are satisfaction with sewerage, garbage-waste, transportation, public transport, green space, help to the sick and poor, network water, and disability. When Figure 1 is examined, it is seen that the rate of satisfaction of public services in the lowest development group is also very low. Satisfaction with judicial services and public order services are variables that have a negative relationship with subjective well-being.

Health related variables determined to have a positive linear relationship with subjective welfare are personal health services, drug purchase procedures, and the number of doctors

and health personnel are sufficient. On the other hand, it is seen that there is a negative relationship with satisfaction with health services in general.

There are two variables taken into account in the evaluation of education and there is a negative relationship with the these. There is a higher level of subjective well-being in areas where both publicly offered educational services as well as the satisfaction rates of received education are low in general.

Income constitutes the most important variable group in socio-economic development and welfare studies. In this category, the subjective welfare is low, where the satisfaction from the monthly household income and the wages in the working life in general is high. On the other hand, it is seen that the subjective well-being is higher in the cases where the satisfaction rate from the work and the pension is high.

Satisfaction from social life is considered an important indicator of well-being in many studies. It also directly affects the happiness rate. It has been determined that subjective well-being is low in areas where relatives and social life satisfaction are high. On the other hand, it was determined that subjective well-being is high in areas where satisfaction with friends is high.

Inequality is one of the most important socio-economic problems in Turkey. In addition to income inequality, there are significant spatial differences in variables related to social indicators such as education and health. Subjective welfare is another variation where inequality is found. In this study, subjective well-being concept was defined, subjective well-being levels according to provinces were calculated and spatial distribution was evaluated. The outcomes will be guided in the planning of social policies and in the case of developmental practices.

REFERENCES

- Akçiş, Ö. 2015. Bir refah göstergesi olarak Türkiye’de mutluluğun mekânsal dağılışı. *Türk Coğrafya Dergisi*, (65), 69-76.
- Baker, J. L., and Grosh, M. E. 1994. *Measuring the effects of geographic targeting on poverty reduction* (Vol. 99). World Bank Publications.
- Camfield, L., and Esposito, L. 2014. A cross-country analysis of perceived economic status and life satisfaction in high-and low-income countries. *World Development*, 59, 212-223.
- Conceição, P., and Bandura, R. 2008. Measuring subjective wellbeing: A summary review of the literature. *United Nations Development Programme (UNDP) Development Studies, Working Paper*.
- Diener, E., Suh, E. M., Lucas, R. E., and Smith, H. L. (1999). Subjective well-being: Three decades of progress. *Psychological bulletin*, 125(2), 276.

- Dinçer, B., and Özaslan, M. 2004. İlçelerin sosyo-ekonomik gelişmişlik sıralaması araştırması. DPT. Bölgesel Gelişme ve Yapısal Uyum Genel Müdürlüğü. Ankara: DPT. *ekutup. dpt. gov. tr/bolgesel/gosterge/2004/ilce. pdf*.
- Easterlin, R. A. 2006. Life cycle happiness and its sources: Intersections of psychology, economics, and demography. *Journal of Economic Psychology*, 27(4), 463-482.
- Easterlin, R. A. 2006. The economics of happiness. *Economics*, 133(2).
- Field, A. 2000. Discovering statistics using SPSS for Windows: Advanced techniques for beginners, SAGE Publications.
- Fujii, T. 2008. How well can we target aid with rapidly collected data? Empirical results for poverty mapping from Cambodia. *World Development*, 36(10), 1830-1842.
- Henninger, N., and Snel, M. 2002. Where are the poor? Experiences with the development and use of poverty maps.
- Huppert, F. A. 2009. Psychological well-being: Evidence regarding its causes and consequences. *Applied Psychology: Health and Well-Being*, 1(2), 137-164.
- Hyman, G., Larrea, C., & Farrow, A. 2005. Methods, results and policy implications of poverty and food security mapping assessments. *Food Policy*, 30(5), 453-460.
- International Wellbeing Group 2006, *Personal Wellbeing Index*, 4th edition, Melbourne, Australian Centre on Quality of Life, Deakin University.
- Kahneman, D., and Krueger, A. B. 2006. Developments in the measurement of subjective well-being. *The journal of economic perspectives*, 20(1), 3-24.
- Kahneman, D. 2003. A perspective on judgment and choice: mapping bounded rationality. *American psychologist*, 58(9), 697.
- Özdamar, K. 2016. Eğitim, sağlık ve davranış bilimlerinde ölçek ve test geliştirme yapısal eşitlik modellemesi. *Eskişehir: Nisan*.
- Pavot, W., Diener, E. D., Colvin, C. R., and Sandvik, E. 1991. Further validation of the Satisfaction with Life Scale: Evidence for the cross-method convergence of well-being measures. *Journal of personality assessment*, 57(1), 149-161.
- Van Praag, B. M., Frijters, P., and Ferrer-i-Carbonell, A. 2003. The anatomy of subjective well-being. *Journal of Economic Behavior & Organization*, 51(1), 29-49.

Overcapacity of Lower-Level Municipalities In Metropolitan Region: Case of Bagcilar

Canan Külek¹, Selver Özözen Kahraman²

¹Department of Geography, Canakkale Onsekiz Mart University, Terzioğlu Campus, 17020, Turkey, canankulek@comu.edu.tr

²Department of Geography, Canakkale Onsekiz Mart University, Terzioğlu Campus, 17020, Turkey, sozozen@comu.edu.tr

ABSTRACT

Migration is an important factor that affects space and spatial capacity because of the huge number of residents, small-sized spaces in terms of surface area and large-sized spaces in terms of population especially Bagcilar. This study aims at revealing the relationship between space and resident population in Bagcilar and how they affect each other. Also it covers whether space gets enough population, and its carrying capacity via some parameters and indexes like person per square kilometer, person per the amount of park and green area, and stuff like that by comparing with international standards. Thus it finds out whether this space gets much more migrant population.

In this study, it was used statistical data that is obtained by some government agency such as Turkish Statistical Institute (TUIK), district municipality, the Ministry of National Education (MEB) and Ministry of Environment and Urbanization, and neighborhood map getting from the municipality. All data were showed on ArcGIS program. In the result of the study, findings were obtained that the municipality got enough migrant population, and there is no space on district for other new migrants. Also currently population needs social fields, and goes to the other districts having social fields to satisfy their needs.

INTRODUCTION

Migration which is a dynamic phenomenon has revealed the new terms. “Capacity” is the leading term that occurs with the concentration of the population and the narrowing of the space as a result of the intense migration to the city. Although the capacity has not a single meaning, it has meanings like “to keep, to hold, to carry” as the meaning of the world. In this study, the word of capacity that can be expressed as the carrying capacity has been used in the meaning of “a certain amount of food, habitat, water and vital structures, and the maximum level of population that can be met by an organism” (Türkkan, 2007).

When looked at the history of migration in Turkey, the number of those who leave their places with migration has gained the great momentum in 1950s (Tümertekin, 1977). The problem of slum emerged in big cities along with increased migration and urban sprawl

increased. The migrated population settled to different districts in Istanbul which was one of the cities heavily exposed to these problems and increased the population by squatting there. Bagcilar which was one of the districts living negative consequences of rapid and unplanned settlements with the increased migration was confronted with a consequences of the growing population in 1960s. Bagcilar district that improved with an irregular configuration has become one of the most infrastructure-strapped districts of Istanbul. Modern urban planning came into work with gained the status of district in 1992 in Bagcilar that this situation continued until 1992 (The Ministry of Environment and Urbanization, 2012).

There is a dynamic relationship between the industrial activities-space-slum (Tümertekin, 1997). Industrial activities that previously were in the city center spread around the city in time and has increased the settlements in this region. The number of slum increased a significant amount as a result of the increased settlements with migration.

The reasons for the emigration of the migrating population varies in time. According to a summarized article of Sağlam (Sağlam, 2006) from Fichter, 1960s that economic factors traditionally were effective drew migrants to cities by replacing the desire to live better. This factors were effective the migration decisions of migrants in Bagcilar district. Additionally, the desire to take advantage of the opportunities of Istanbul and be close to the center of the city were influential in the choice of Bagcilar of the migrants. Also, active industrial activities in Bagcilar, positioning in close proximity to residential areas of industrial activities within district and much more job opportunities because of this drew the migrant population here.

Cities has had to face many problems as a result of rapid and unplanned urbanization. Congestion experienced in cities as result of increased number of factories with effect of industrialization in the 1950s and located in the city center of these factories (Başdoğan and Manisa, 2015). The population densities were experienced in the districts of Istanbul where the population are not evenly distributed. In Bagcilar district which is one of these, overcapacity has experienced because of increased population density as result of narrower field of district and much more population. In addition to this, the narrowing of roads due to the increase of the vertical and horizontal growth has issued an invitation to the disruptions in transportation and traffic jams.

Field Study

Bagcilar, which is located on 41° 2' 44.3292" North and 28° 49' 28.9992" East, covers an area of 22 square kilometer. As seen on Figure 1, Bagcilar subprovince is in European side of Istanbul province. Neighbor subprovinces around it are Basaksehir, Esenler, Gungoren, Bahcelievler, and Kucukcekmece.

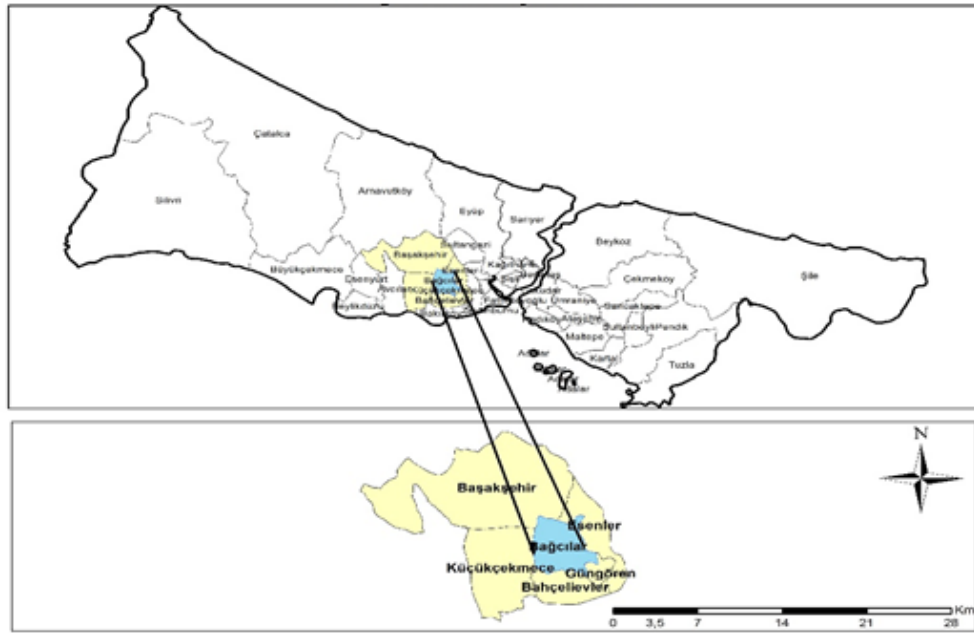


Figure 1. Bagcilar's Location Map in İstanbul

The population of Istanbul's districts is shown on Figure 2. Bagcilar is the third most crowded district of Istanbul with population of 751.510* (TUIK).

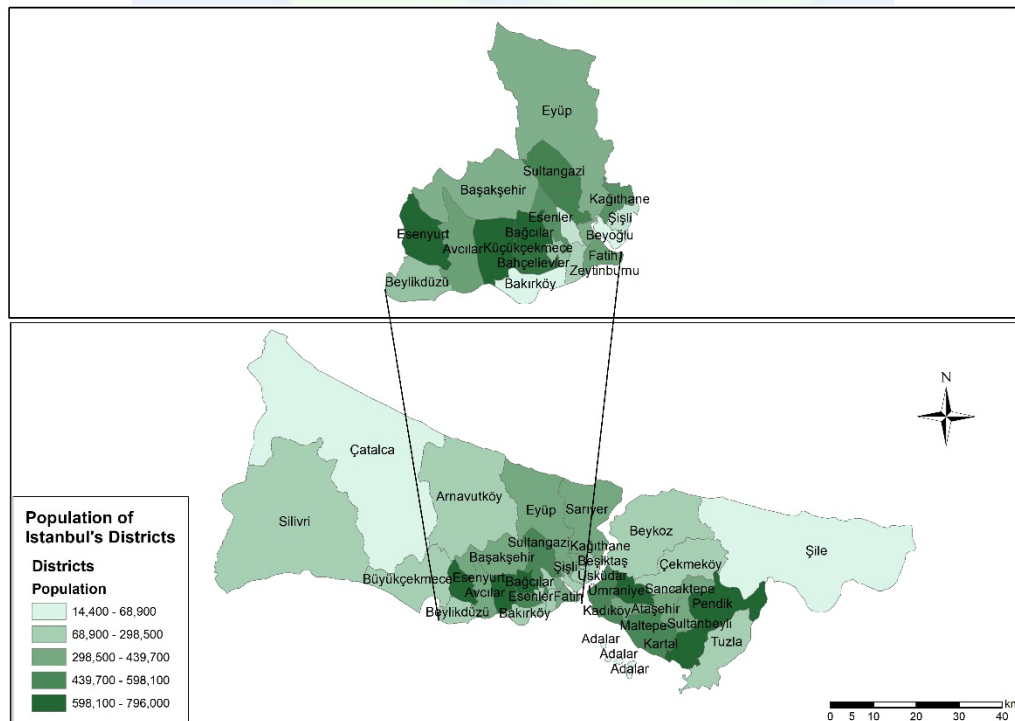


Figure 2. The Population of Istanbul's Districts (2016)

* (1)Esenyurt: 795.010, (2)Kucukcekmece: 766.609

Bagcilar was municipality with immigrants coming from Anatolia in 1992 while it was a neighborhood connected to Bakirkoy municipality. Bagcilar is today a district founded by immigrants (Ministry of Environment and Urbanization, 2012).



Figure 3. Bagcilar in 1960s and Nowadays (Source: Bagcilar Municipality Web Site)

Figure 4 shows the population of Bagcilar district according to years. Bagcilar's population was 9.688 when it was connected to Bakirkoy municipality. In the end of 2016, Bagcilar has become the third most populous district of Istanbul by reaching out to 751.510 people.

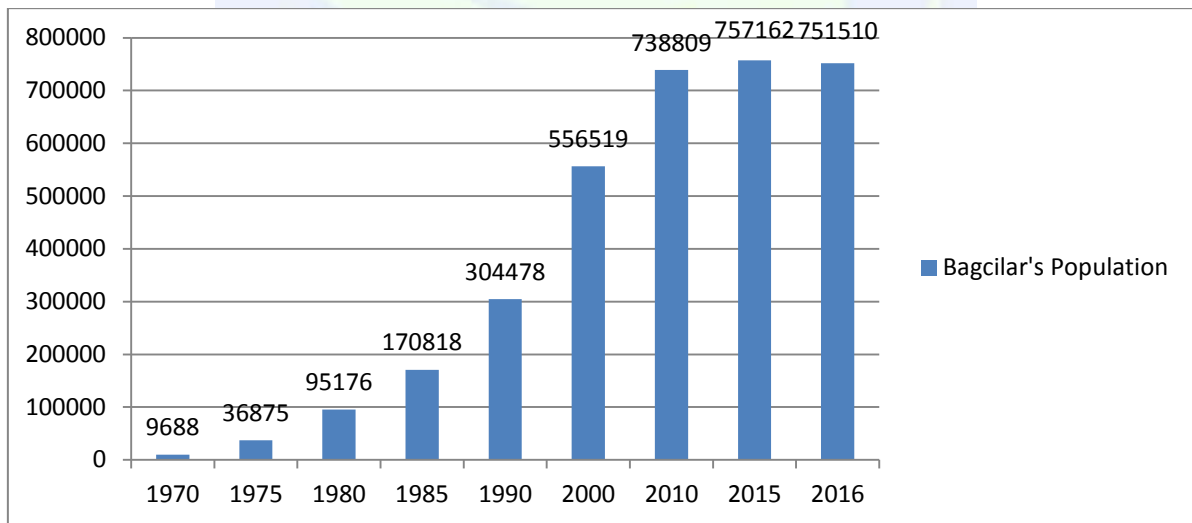


Figure 4. Bagcilar's Population by Years (TUIK)

As can be seen in Figure 5, when the largest quarter in terms of surface area of Bagcilar district that consist of 22 quarters in administrative structure is Mahmutbey, the most populous quarter in terms of population is Demirkapi (TUIK).

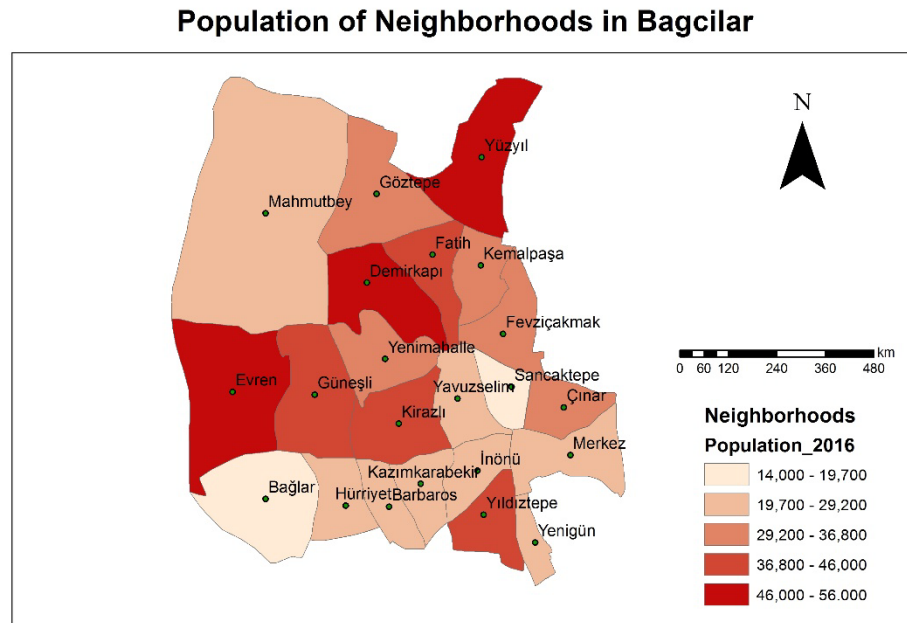


Figure 5. The Population of Neighborhoods in Bagcilar (2016)

METHOD

The study examines the relationship between population and surface area of Bagcilar district in Istanbul.

In this study, it was used statistical data that is obtained by some government agency such as Turkish Statistical Institute (TUIK), district municipality, the Ministry of National Education (MEB) and the Ministry of Health, and neighborhood map getting from the municipality and provincial map of Istanbul getting from General Command of Mapping (HGK), the proportion of green areas obtaining from Parks and Recreation Commission. All data were showed on ArcGIS program.

It was shown population of Bagcilar by using data obtained from the institutions, done the analysis of population density and land use belong to 2000, 2007 and 2016, examined Bagcilar district on the basis of quarters of it. Data were mapped with ArcMap program. Various analyses were applied.

RESULTS

Bagcilar that is the third most populous district of Istanbul with population of 751.510 has been allowed immigrants from every province of Turkey. Figure 6 shows the numbers of those who reside in Bagcilar according to the place of birth. The highest proportion in Bagcilar which has migrant population from each province is births Istanbul with 316.338. Bitlis with 21.665 people, Malatya with 20.727 people and Ordu with 19.160 follow in order with Istanbul. When looked as a region, those who come from Black Sea and East Anatolia region constitute the majority of migrants (TUIK).

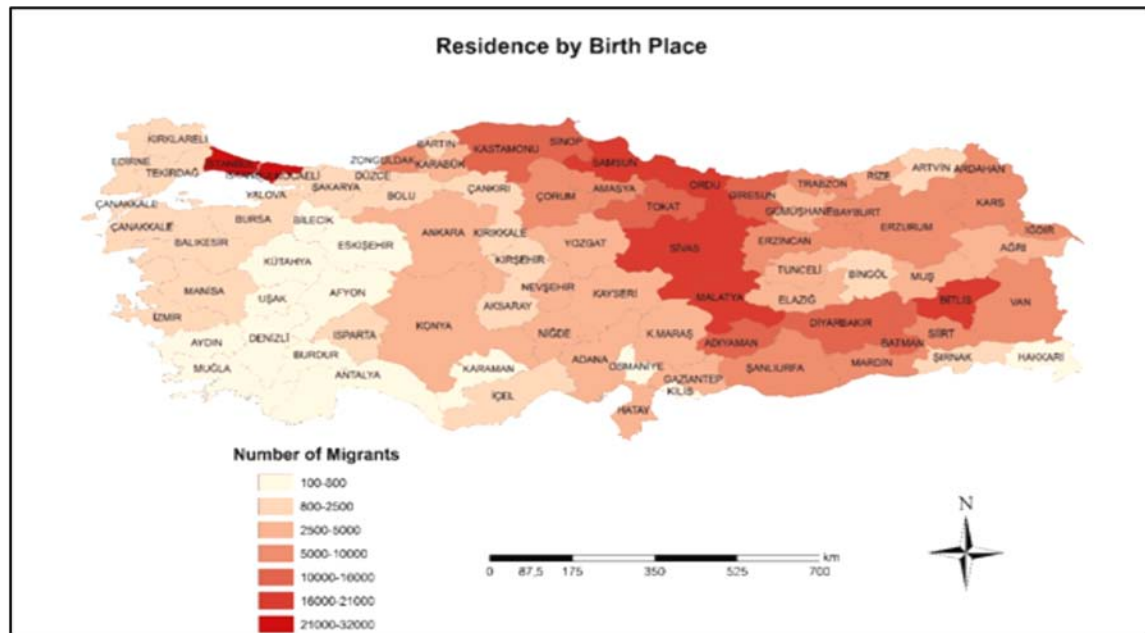


Figure 6. Number of Migrants by Birth Place in Bagcilar(2016)

Bagcilar ranks the fourth district among 39 districts of Istanbul in terms of population density when looked Bagcilar that migrants doesn't show regular distribution*. According to the population of 2016, the number of people per square kilometer is 34,160[†]. This number indicates that too many people have been living together in a small area. As a result of this, many problems based on population density has experienced in this district such as traffic congestion and so on.

Figure 7 illustrates the population densities in different years. The population density has increased in the years of 2007 and 2016 while this situation is less in 2000. Density increased much more in 2016. Density is accumulated in the quarters of Demirkapi, Fatih, Kazim Karabekir and Yuzyil in 2016. Quarters having the minimum density are Mahmutbey, Evren and Baglar. The reasons for this is the having large area of these quarters and the much more taking space of industrial area than residential area due to doing industrial activity in the region.

* (1)Bayrampasa: 39.133 per km², (2)Bahcelievler: 35.814 per km², (3)Güngören: 35.579 per km²

[†] It was obtained by using the formula of population density (per km²)

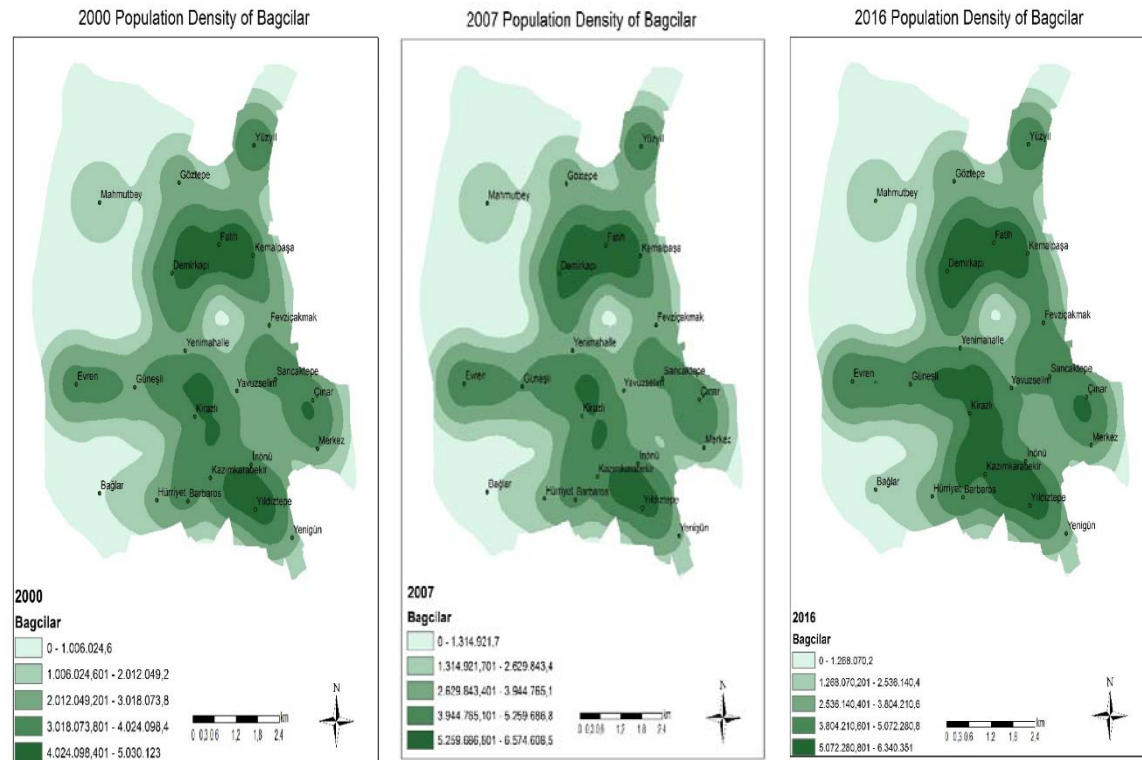


Figure 7. Population Densities of Bagcilar in 2000, 2007 and 2016

If looked from the viewpoint of land use to Bagcilar district, Figure 8 emerges. Accordingly, factories and industries exist on the western parts of the district, and residents exist on the eastern and center parts of it. In addition to this, when there are empty spaces in industrial area, there is no empty spaces in other parts of areas that have residential density. This also shows which quarters gathered immigrant population over the years. Proportionately residential area covers 60 %, plants or factories are 20%, other (empty space, cemeteries, car park) are 10 %, park and open spaces are 5%, foundations are 2,5 %, education areas are 2,5%.

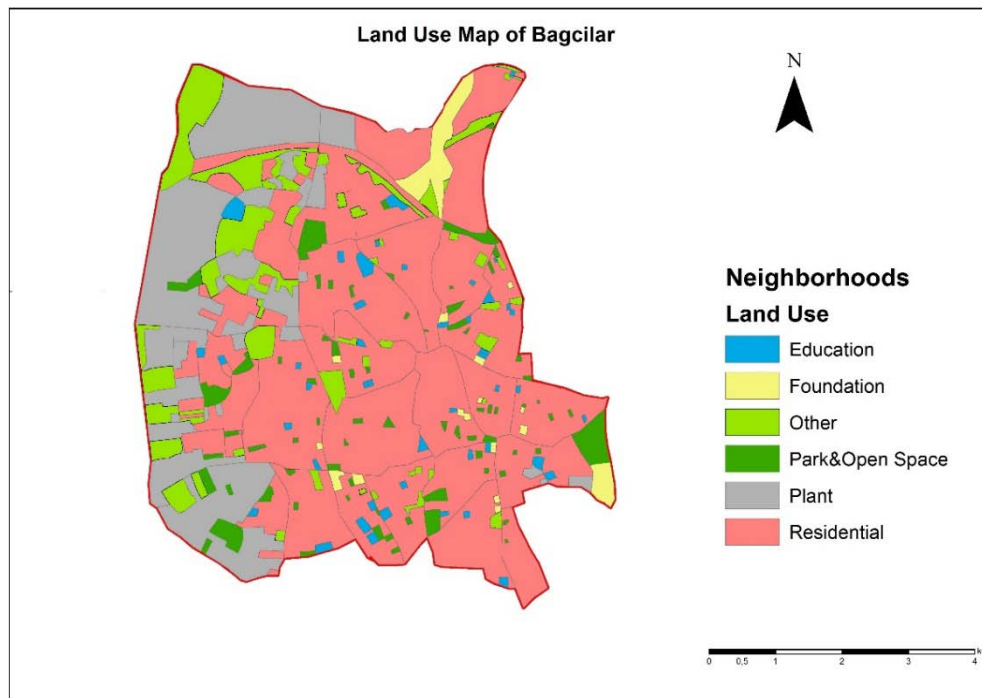


Figure 8. Land Use Map of Bagcilar, 2016

Lack or deficiency of space and social space that is one of the biggest problems in areas where the population density is high, shows itself in Bagcilar. According to the regulations of the Ministry of Environment and Urbanization, the amount of green area per capita should be at least 15 square meter. The amount of green area recommended by the World Health Organization is at least 9 square meter per capita. But this amount is 0,50 square meter in Bagcilar. This is far below the amount of green areas per capita in Bagcilar. The maximum amount of green areas per capita on the basis of quarters is 2,30 m² in center quarter. On this amount, the forest of the State Hospital has the huge impact. However, this amount also indicates how much remained below the standards. Much of the population per quarter also plays a role in this amount.

If examined the education rates of Bagcilar, there are 144 schools of private and public institutions, 153.802 students and 4.124 teachers in Bagcilar according to data of the district Ministry of National Education (2016). Those who want to school the private institutions have many preference. Parents who do not want to send them to private institutions are forced to send public institutions in district. This makes it possible to be made for capacity analysis. The number of students per classroom in all school types is 62, the number of students per teacher is 37. According to international standards, the number of students per teacher is 20 but the number in Bagcilar is below the ideal. This also indicates that the capacity has been exceeded in schools.

There are a state hospital in the center quarter and also health centers in all quarters of the district. Additionally, there are 54 public institutions and 57 private health institutions (Bagcilar Municipality). It can be said without question out of the capacity in this area. Because people can benefit from any hospitals due to the existence of hundreds health

institutions in the metropolitan regions like Istanbul. Similarly, being more private institutions doesn't create over in the field of health.

CONCLUSION

Bagcilar district that fed the migrant population in the background grew to reach as much as the size of a city over the years. It was experienced overcapacity in district because of small area but much population size of quarters. This caused an increase of the number of housing, an increase and accelerating of vertical growth in the quarters which doesn't have empty space. Apart from these, the dense number of students per teacher and classroom are the factor supporting this overcapacity. Similarly, no empty space due to the much amount of housing, narrowing of the roads and the failure to find a suitable place for the construction of social spaces has also created difficulties in meeting the need of residents for creation and social space, and caused the insufficiency of the green areas.

REFERENCES

- Bagcilar Municipality Web Site, <http://www.bagcilar.bel.tr/icerik/35/140/bagcilar-ve-parklar.aspx>
- Başdoğan, S, and Manisa, K. 2015. Endüstrileşme Sonrası Kentlerin Dönüşümü "Konut Odaklı Kentsel Dönüşüm Örneği "Merchant City - Glasgow". *Yapı Dergisi*, 404, July 2015, page 50-56
- Ministry of Environment and Urbanization, 2012. Bağcılar Meydanı Kentsel Dönüşüm Alanı Kentsel Dönüşüm Planlaması Ve Yönetimi Analitik Etüt Ve 1/5000 Ölçekli Nazım İmar Planı Plan Açıklama Raporu
- Ministry of National Education (MEB), <https://bagcilar.meb.gov.tr/>
- Sağlam, S. 2006. Türkiye 'de İç Göç Olgusu ve Kentleşme.
- TUIK, 2000 General Population Censuses, Ankara
- TUIK, 2016 Address Based Population Registration System Results, News Bulletin
- TÜİK, 2016 Birthplace of Turkish Citizens by District of Residence, Ankara
- TÜİK, 2016 Population by Subprovinces, Ankara
- TÜİK, 2007-2016 Population of Quarters of Bagcilar, Ankara
- Tümertekin, E. 1977. Türkiye'de İç Göçler Üzerine. *Review of the Geographical Institute of the University of Istanbul*, 22, 29-42.
- Tümertekin, E. 1997. *İstanbul İnsan Mekan*. Tarih Vakfı Yurt Yayınları. Page 81.
- Türkkan, S. 2007. *Yoğunlaşan Kent ve Yaşamında Kapasite Arayışları ve İstanbul'a Bakış*. Master Thesis, Istanbul Technical University.



HYDROLOGY

Evaluation of the Trace-Element in Goksu Delta Using GIS Techniques

Esra Deniz Guner¹, Senem Tekin², Galip Seckin³

¹Department of Environmental Engineering, Cukurova University, Balcalı Campus, 01330, Turkey. (e-mail eguner@cu.edu.tr)

² Department of Geology Engineering, Cukurova University, Balcalı Campus, 01330, Turkey. (e-mail senemtekin01@gmail.com)

³ Department of Environmental Engineering, Cukurova University, Balcalı Campus, 01330, Turkey. (e-mail gseckin@cu.edu.tr)

ABSTRACT

This study assessment water quality at Goksu Delta where is a major agricultural and wetland area in Turkey. Although delta is composed predominantly of agriculture, it has national and international significance. Delta is an ecologically important land as well as agricultural land. Alluvial soil structure provides fertile land for agriculture and is quite noteworthy in natural life. Especially water birds are an important point, delta chosen as the Ramsar field. Such an important area is very important in terms of monitoring of water quality and understaning of anthropogenic activities (especially agricultural) pressures. The purpose of these analyses was to determine the trace element concentration and distribution in the Goksu Delta. A total of 24 water wells were selected, 13 from the Goksu region and 11 from the Silifke region, to represent all the study areas. Water samples from the selected wells were collected on a monthly basis between May 2012 and April 2013. Using inductively coupled plasma- Optical Emission Spectrometry (ICP-OES), the concentration of trace element were measured in the Delta. Samples were collected from 24 separate groundwater wells between May 2012 and April 2013, and chemical water quality parameters were examined. Water quality maps of the study area were created using the Geographic Information Systems (GIS). GIS was applied to illustrate the trend of trace element in the Goksu groundwaters. These have been created to comprise the most decisive criteria used for the delineation of groundwater degradation in terms of agriculture or construction.

INTRODUCTION

The anthropogenic effects of the Goksu Delta are quite intense because of situated in the fertile alluvio-deltaic plains of the Goksu rivers (Turkey). Although the industry is not much, extensive and intensive agricultures activities are very dense. So the region is as ecologically important as economically important. The delta is special environmental protection area. It is also a RAMSAR site and an important wetland in terms of has many migrants birds. Goksu Delta constitute one of the most important main nesting zone in the

Mediterranean as “*Caretta caretta*”, “*Chelonia mydas*” and Nile turtle, for leaving their eggs. There are also 507 plant species, of which 10 are endemic species.

Demirel (2004), assessment of saltwater intrusion into a coastal aquifer in Mersin, Turkey. According to this study the history and development of saltwater intrusion up to the year 2000 in the region. To determined the wide of the seawater pollution in the aquifer used to mapping of chloride ion. The seawater intrusion extended about 500 m inland in the north direction. Evaluation of impact anthropogenic activities on the groundwater hydrology and chemistry in Tarsus coastal plain in Mersin using GIS technique (Güler et. al., 2012). With the helping GIS maps showing the spatial distribution of seawater of the groundwater samples in the area. The results of these study the deterioration in quality of groundwater resources responsible for anthropogenic activities especially excessive application fertilizers in agricultural areas in the area. Çobaner et al (2012) simulation of seawater intrusion in Goksu Delta with SEAWAT computer program. The simulation results indicate that reached a steady-state condition after 300.000 (822 years) days and saltwater intrusion reverted 500 m back towards the sea. Seckin et al. (2010) studied spatial and temporal changes of water quality parameters observed in 21 irrigation and observation wells, located in Göksu plain. The results demonstrate that the highest values found to be closed the sea so seawater intrusion. But they referenced water quality determination owing to seawater intrusion, widely used agricultural activity.

Approach for groundwater vulnerability mapping using the hydrochemical investigations is adopted. The geographic information system (GIS) was applied to illustrate the trend of groundwater contamination by seawater intrusion. These have been created to comprise the most decisive criteria used for the delineation of groundwater degradation due to seawater intrusion. These criteria's are represented by the total dissolved solids, hydraulic conductivity (EC) and hydrochemical parameters (Cl^- , SO_4^{2-} , NO_3^-), which have been used to characterize to seawater intrusion. The regions having low and highly groundwater vulnerability occupy 78.8%, 20.83% of total study area respectively, which designate to a deteriorated territory of groundwater quality, and needs special treatment and cropping pattern before use. However, the very highly groundwater vulnerability class occupies an area of about 8.3% of the total mapped area, which highlighted the need for certain management practices to prevent the saltwater intrusion from expanding further to the Goksu side.

MATERYAL AND METHODS

Goksu Delta is situated in the Mediterranean Sea region of Turkey. The study area is located between latitude $35^{\circ}35'$ N and longitudes $33^{\circ}17'$ E (Fig. 1a–d). The area is a delta plain, which is formed by Goksu River. The morphology in the study area is characterized by a wide flatness and it has an elevated from 0 to 5 m in height from the sea. To the west of the Goksu Delta has two lagoons which are Paradeniz and Akgol lagoons. The total area is about 15 000 ha which 226 km^2 is protection area. The study area is situated in a region with typical Mediterranean climate. Wet and mild winter combined with dry and hot summers are typical for the coastal zone around the Mediterranean Sea. The mean annual

precipitation is 1.8 mm. The major part of the rainfall occurs during November to February.

To characterize the entire field a total 24 water wells were examined, 13 of which are in Goksu and 11 of which are in Sıfıfke region. Water samples for trace-element analysis were obtained every month at the same time water temperature, electrical conductivity (EC), and pH were measured on site. Chemical components including Cl^- , SO_4^{2-} , HCO_3^- , NO_3^- , Na^+ , K^+ , Mg^{2+} , and Ca^{2+} were measured in the Environmental Chemistry Laboratory of Cukurova University. Samples were analyzed by Inductively Coupled Plasma (ICP) in accordance with American Society for Testing and Materials (ASTM).

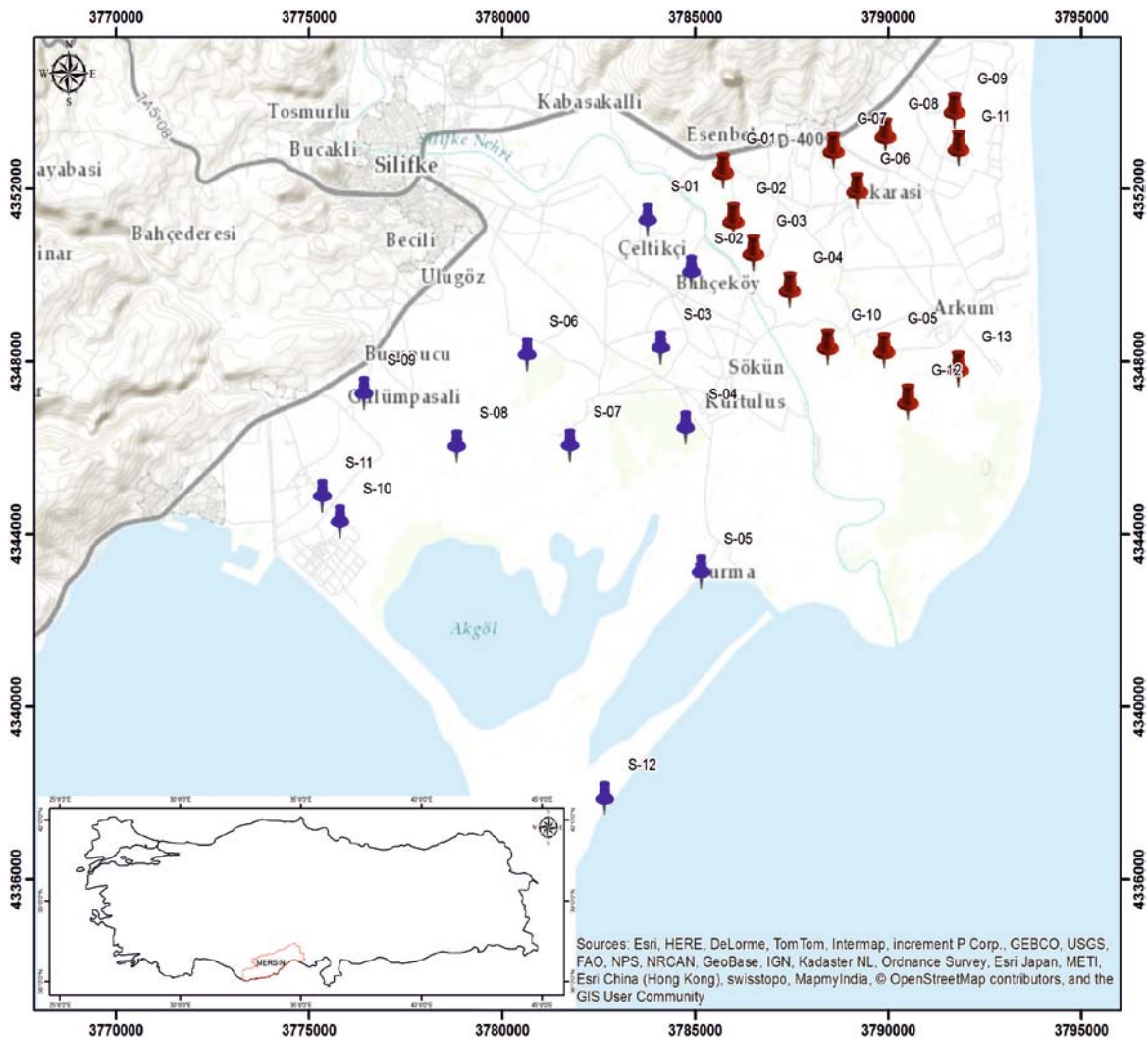


Figure 1. The location map of Goksu Delta area.

RESULT AND DISCUSSION

To assess water chemistry values under natural conditions, 24 samples of groundwater in the study area were collected during May 2011 and April 2012 from short-term groundwater observation wells and drinking wells with depth of 4–75 m. The water

samples of Goksu Delta were collected at two different sites Goksu and Silifke Plain. The pH value of river water is 7.82, indicated a weak alkaline characteristics. The TDS concentrations of delta groundwater are 1010.5 mg/l and 568.39 mg/l in two sampling sites Goksu and Silifke sites, respectively, belonging to the fresh water (TDS <1,000 mg/l). The cation Ca^{2+} , Mg^{2+} , and Na^+ , K^+ concentrations of delta groundwater are 60.91 and 64.23 mg/l; 45.67 and 32.25 mg/l; 233.89 and 148.5 mg/l; 12.72 and 5.51 mg/l in two sampling sites Goksu and Silifke, respectively. The order of abundance is $\text{Na}^+ > \text{Ca}^{2+} > \text{Mg}^{2+} > \text{K}^+$ according to annually concentration in Goksu Delta. The anion HCO_3^- , Cl^- , SO_4^{2-} and NO_3^- concentrations of delta groundwater are 278 and 230 mg/l; 347 and 209.9 mg/l; 214.6 and 173.9 mg/l; 12.3 and 12.7 mg/l in two sampling sites Goksu and Silifke, respectively. The order of their abundance is $\text{Cl}^- > \text{HCO}_3^- > \text{SO}_4^{2-} > \text{NO}_3^-$ according to annually concentration in Goksu Delta. The ion concentrations of Goksu Delta increased Goksu Plain.

Table 1. The annually chemical component concentrations of the groundwaters in the study area

Statistics	SKKY Nation Limit	Mean	Max	Min	SD
pH		7.82	8.19	7.5	0.2
EC ($\mu\text{S}/\text{cm}$)		1471.74	5677.5	265.57	1262.8
TDS (mg/l)		807.88	3941.3	156.61	821.98
Cl^- (mg/l)		284.22	1597.57	72.02	367.5
SO_4^{2-} (mg/l)		195.97	321.53	105.61	63.47
NO_3^- (mg/l)		12.49	13.34	12.06	0.35
Na^+ (mg/l)		194.75	880.11	19.51	217.85
Ca^{2+} (mg/l)		62.44	136.43	15.83	35.29
Mg^{2+} (mg/l)		39.53	125.64	13.4	26.23
K^+ (mg/l)		9.42	34.46	2.41	8.47

A hydrochemical investigation was conducted in the Goksu Delta to identify the hydrochemical characteristics and the salinity of groundwater. The results indicate that groundwater in the area is brackish and salinity. The vulnerability area map was compared with the regional hydrogeological setting of the Goksu Delta and it was found that the moderately and low vulnerability area. The Goksu Delta area can be roughly classified as moderately salinity. To estimated in aquifers salinity was used Cl^- ion concentration indicated that the Delta influence salinity.

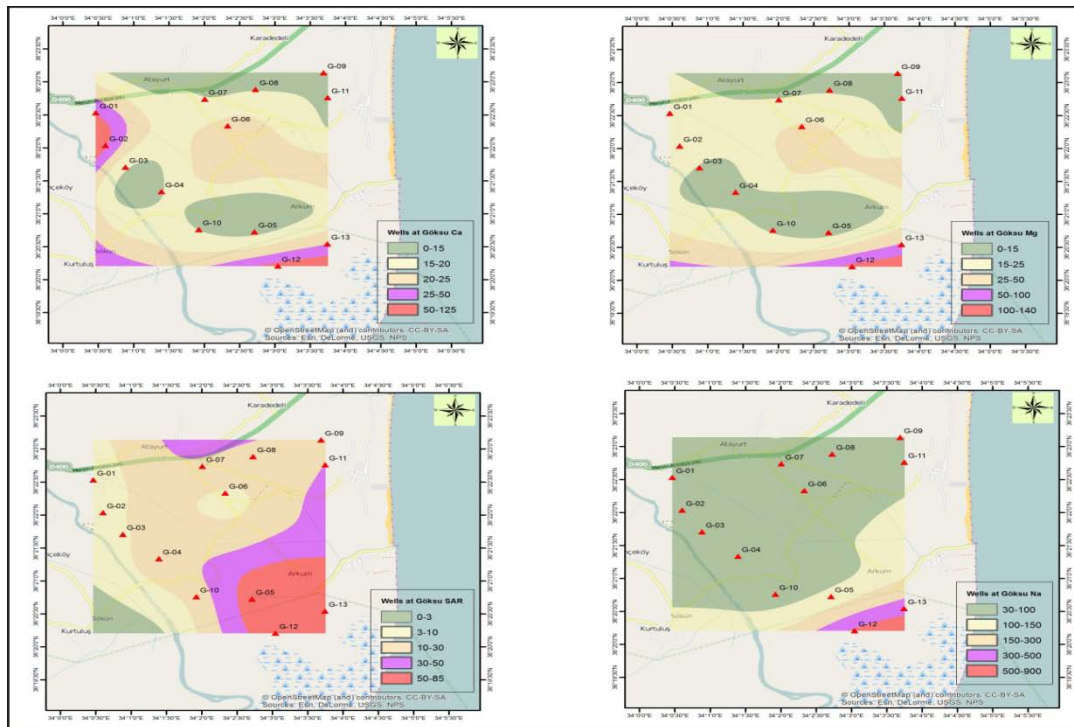


Figure 2. Trace-elements concentration (mg/l) contours in the well in Goksu Plain. (a) Ca^{2+} , (b) Mg^{2+} , (c) Na^+ , (d) SAR)

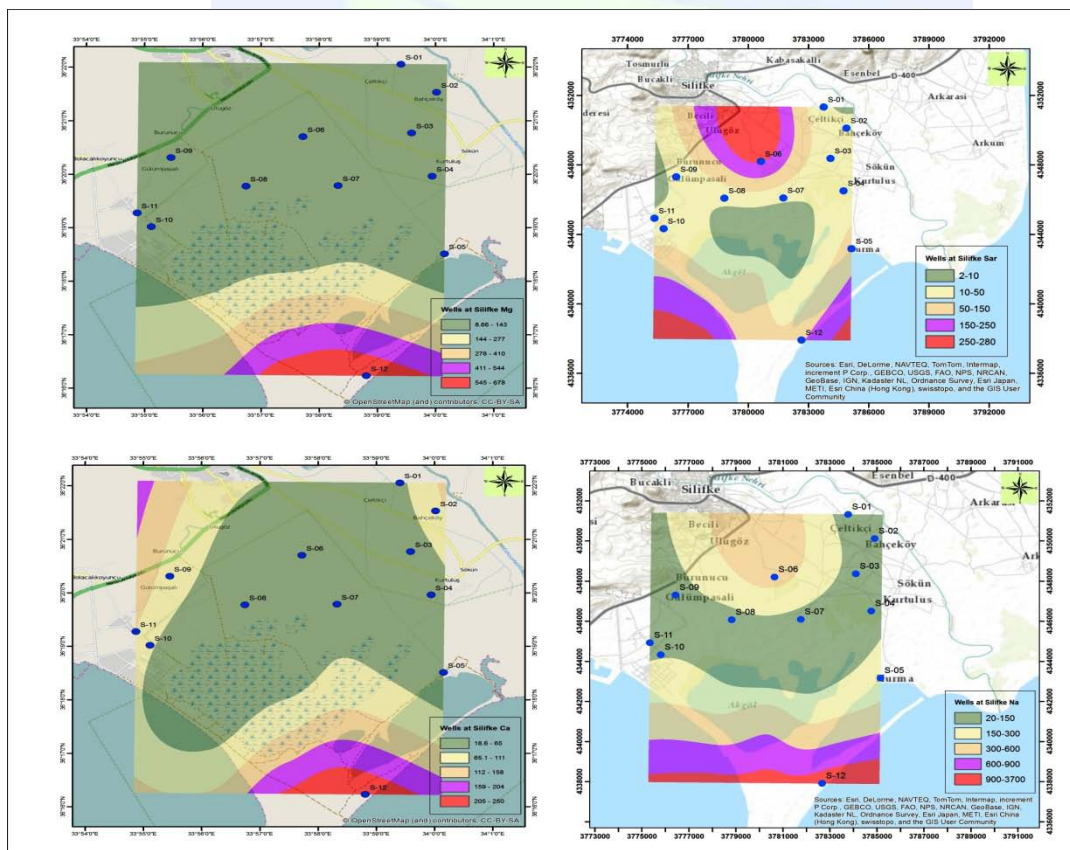


Figure 3. Trace-elements concentration (mg/l) contours in the well in Silifke Plain. (a) Ca^{2+} , (b) Mg^{2+} , (c) Na^+ , (d) SAR)

CONCLUSIONS

Groundwater is an indispensable resource for water supply for the Goksu Delta, for the agriculture. The objective was to characterize the physic-chemical properties of groundwaters in Goksu Delta. The alluvial aquifer in Goksu Delta shows predominance of Na^+ , SO_4^{2-} and Cl^- ions. The values of its ions in the coastal zone area due to seawater intrusion and agricultural activities. Following the this ions, Ca^{2+} and Mg^{2+} concentration levels have second plenty ions. This was caused by cation exchange reactions seawater intrusion increase Ca^{2+} and Mg^{2+} in addition to dissolution of carbonate minerals in the recharge area increases Ca^{2+} , Mg^{2+} and HCO_3^- contents.

REFERENCES

- Cobaner, M., Yurtal, R., Dogan A., Motz, L.H., 2012. Three dimensional simulation of seawater intrusion in coastal aquifers: A case study in the Goksu Deltaic Plain. *Journal of Hydrology* 464–465, 262–280.
- Demirel, Z., 2004. The history and evaluation of saltwater intrusion into a coastal aquifer in Mersin, Turkey. *Journal of Environmental Management* 70 (3): 275-282.
- Güler, C., Kurt, M.A., Alpaslan, M., Akbulut, C., 2012. Assessment of the impact of anthropogenic activities on the groundwater hydrology and chemistry in Tarsus coastal plain (Mersin, SE Turkey) using fuzzy clustering, multivariate statistics and GIS techniques. *Journal of Hydrology* 414, 435-451.
- Seckin, G., Yilmaz, T., Sari, B., Ersu, C.B., 2010. Groundwater hydrochemistry at the Mediterranean coastal plains—The case of Silifke, Turkey, *Desalination*, 253, 164-169.

ISGGG
2017

Flood Inundation Mapping for Tatlıçay (Çankırı)

Murat Ataol^{*1} and M. Murat Kale²

¹ Department of Geography, Çankırı Karatekin University, Uluşazı Campus, 18100, Turkey. e-mail: murat.ataol@gmail.com

² Department of Geography, Çankırı Karatekin University, Uluşazı Campus, 18100, Turkey. e-mail: muratkale@karatekin.edu.tr

ABSTRACT

The biggest flood natural disaster was took place at Çankırı in 1958. Results of 1958 flood were the death of 18 people in the city center and completely destroyed 300 houses. In this study, flood inundation mapping is made for Tatlıçay which passing through Çankırı city center. ArcGIS, HEC-GeoRAS and HEC-RAS software are used for flood analysis. The part of Tatlıçay that passes through Çankırı city center flows through the open artificial canal. Artificial channel has u-shape in geometry. Geometric measurements are taken along the channel. In this way, the digital terrain model is made even more sensitive. Scenario floods are created with HEC-RAS software and flood areas and water heights are calculated. Flood maps are formed with the obtained information. The roads and buildings to be affected by floods in each scenario have also been identified. In this study, an example has been tried to be prepared for disaster management depending on analyzes based on Geographic Information Systems (GIS). The results of this study can be dividing in two main groups. If 200 m³/s flow rate will be observed, over 467.000 m² of area in the city center can be under water. Same result is taken for 400 m³/s flow rate. In the case of 400 m³/s flow rate, over 769.000 m² of area can be under water.

INTRODUCTION

Flood is a natural process. Defined as the land that is not usually submerged, is covered by water mass (Ward, 1978). Trend analysis on natural disasters shows that the incidence of floods has been increasing in recent years (Berz, 2001; Kleinen and Petschel-Held, 2007). In different geography, floods often cause loss of life and property. Over 8.000 people have lost their lives as a result of flood events only in 2010 (EM-DAT, 2010).

After the earthquakes, the most disastrous natural disasters are floods in Turkey. Between 1955 and 2012, 1480 people lost their lives in the floods that took place in different places in Turkey (OSİB, 2015).

In this study Tatlıçay Basin which is located in Çankırı, is selected as a study area (Figure 1). The flood, which caused the biggest damage in Çankırı province, took place in 1958. 18

^{*} Corresponding Author

people lost their lives and 300 houses were destroyed in flood events that occurred due to sudden flow increase in Tatlıçay in May 1958 (Ersin, 1958).

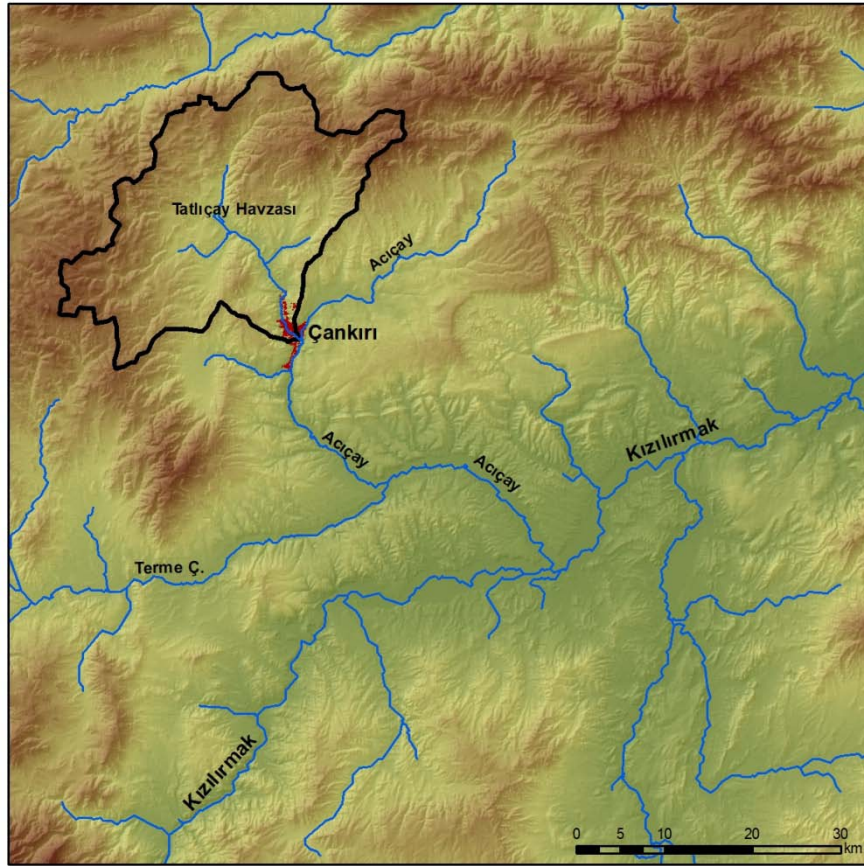


Figure 1. Tatlıçay Basin

Tatlıçay has a 672 km² basin area (Figure 1). River passes through the city center of Çankırı. The river forms one of the important arms of Kızılırmak by merging with Acıçay to the south of the city center and the Terme to the south. In this study, lower course of Tatlıçay is taken as an area to be analyzed. Flood analysis is carried out along the line of about 10 km from the section where it is merged with Aygır River in the north and the cut that it merged with Acıçay in the south.

MATERIALS AND METHOD

For flood analysis, flood bed and contour lines belonging to lower course of Tatlıçay are transferred to the GIS. After then digital terrain model is created. For this aim, 1: 25.000 scale topography maps (G31d3, G31d4, H31a1, H31a2) are used. Tatlıçay moves in an open channel in the city center of Çankırı. As a result of the channel measurements, it is determined that the channel has 17-20 meters wide and 5.2 meters deep. The dimensional information of the channel is also added to the digital terrain model. Thus, it is possible to determine exactly which phase of the increase of Tatlıçay will turn into a flood.

In this study, ArcGIS, HEC-GeoRAS and HEC-RAS software are used for flood analysis. The topographic data is prepared in the ArcGIS environment and transferred to the HEC-GeoRAS module. Cross-section lines are created in the HEC-GeoRAS module (Figure 2). Scenario floods are created with HEC-RAS software. Flood areas and water heights are calculated with HEC-RAS depending on previous inputs. Flood maps are formed with the obtained information.

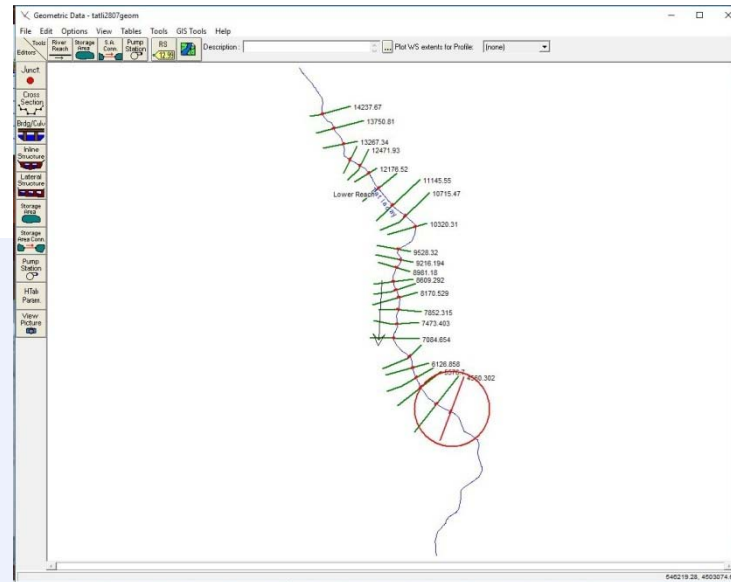


Figure 2. Cross section lines for lower course of Tatlıçay.

RESULTS

The artificial channel over Tatlıçay has 100 m² cross-sectional areas. Channel is capable of draining the water mass much above the average flow of the river. General Directorate of State Hydraulic Works (DSİ) has a stream gauging station over Tatlıçay. Number of station is D15-080 and station is located north of the study area. However, measurements were made only for 1965 and 1966 (Figure 3). According to time series at stream gauging station, the amount of flow seen in March and April is much more than other months. March average is 10.4 m³/s, and April average is 7 m³/s.

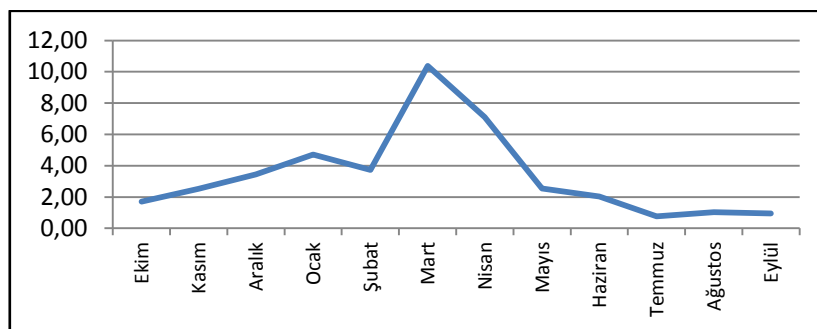


Figure 3. Monthly distribution of Tatlıçay flow rate (m³/s)

Due to the fact that only two years of current data is available for Tatlıçay, no calculations can be made about the frequency of flood repetition. With the HEC-RAS software, flood modeling is performed according to three different flow rates of $100 \text{ m}^3/\text{s}$, $200 \text{ m}^3/\text{s}$ and $400 \text{ m}^3/\text{s}$. It has been seen that the Tatlıçay canal is able to drain $100 \text{ m}^3/\text{s}$ of water flow without any overflow after modeling.

If a flow rate value will be $200 \text{ m}^3/\text{s}$, it is revealed that over 467.000 m^2 of area in the northern part of the city center can be flooded. It can be seen that over 60 buildings also directly affected by flood (Figure 4).

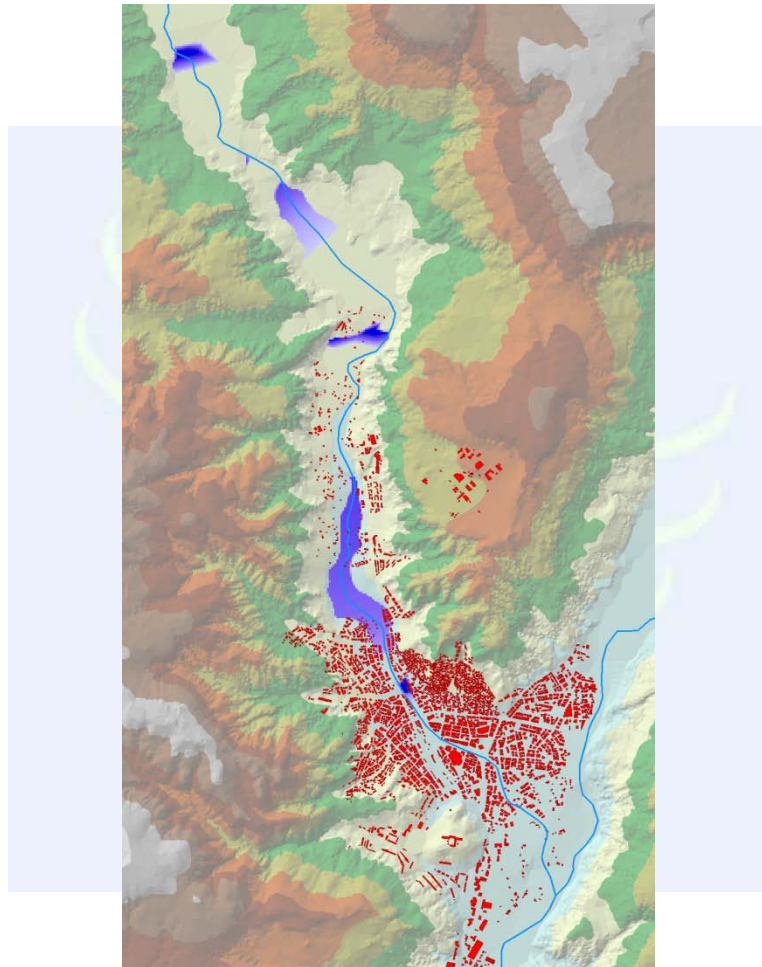


Figure 4. Flood inundation map of study area for $200 \text{ m}^3/\text{s}$ flow rate

When $400 \text{ m}^3/\text{s}$ flow rate will be seen, it is revealed that more central areas along the channel of Tatlıçay can be under water, starting from the north of the city center. The area to be flooded in the city center can be over $769,000 \text{ m}^2$. More than 150 buildings can be directly affected by floods (Figure 5).

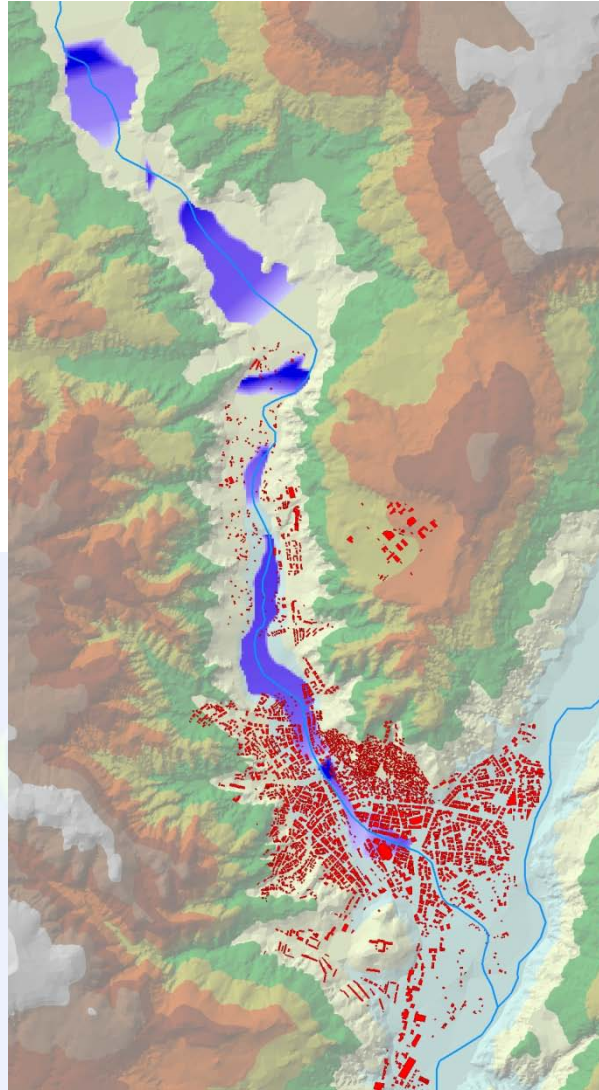


Figure 5. Flood inundation map of study area for 400 m³/s flow rate

CONCLUSIONS

In this study, flood maps are made for Tatlıçay passing through Çankırı city center for different flow rate conditions. Flood modeling studies require a high-resolution digital terrain model. Otherwise, calculations of what flood will occur after the current level in the stream bed do not reflect the reality. Because the part of Tatlıçay that passes through Çankırı city center flows through the artificial channel, it became possible to make the digital terrain model sensitive by the measurements made along this channel.

In this study, scenario floods are created with HEC-RAS software. After then, flood areas and water heights to be seen in these floods are calculated. In the modeling study, it is seen that the channel of Tatlıçay can carry 100 m³/s flow rate without leading to flood. When 200 m³/s flow rate will be observed, over 467.000 m² of area in the city center can be under water. Same result is taken for 400 m³/s flow rate. In the case of 400 m³/s flow rate, over 769.000 m² of area can be under water.

REFERENCES

- Berz, G., 2001. Flood disasters: lessons from the past-worries for the future. *Proceedings of The Institution of Civil Engineers-Water Maritime and Energy*, 148(1), 57-58.
- EM-DAT (Emergency Events Database), 2010. *OFDA/CRED International Disaster Database*, Universite Catholique de Louvain, Brussels, www.cred.be/emdat.
- Ersin, F., 1958. Çankırı'da selden 18 kişi öldü. *Milliyet Gazetesi*, 26 Mayıs 1958
- Kleinen, T. and Petschel-Held, G., 2007. Integrated assessment of changes in flooding probabilities due to climate change. *Climatic Change*, 81(3), 283-312.
- OSİB (Orman ve Su İşleri Bakanlığı), 2015. Ulusal Taşkın Yönetimi Strateji Belgesi ve Eylem Planı. Ankara.
- Ward, R. C., 1978. Floods - a geographical perspective. *Published by: Macmillan*.



Performance Analyses with LiDAR Data in Flood Modelling Using Remote Sensing and GIS in Artvin City

Hakan Celik^{*1}, H.Gonca Coskun¹, Necati Agiralioglu², Nuray Bas³ and Oyku Alkan¹

¹ Department of Geomatics, Istanbul Technical University, Ayazaga Campus, 34469, Turkey. e-mail: celikhakan@yahoo.com, oyku.alk@gmail.com, gonca@itu.edu.tr

² Engineering Faculty, Antalya Bilim University, Merkez Campus, 07190, Turkey. e-mail: necati.agiralioglu@antalya.edu.tr

³ 1st Regional Directorate, Turkey Electricity Transmission Company, Davutpasa, 34220, Turkey. e-mail: basn@gmail.com

ABSTRACT

The aim of this study is to analyze the performance of Airborne Light Detection and Ranging (LiDAR) in the hydrologic studies intended for flood modelling and to analyze the effects of spatial resolutions and vertical accuracy of Digital Terrain Models (DTMs) acquired with various technics on the resulting flood peak discharge values. Balci Stream Basin is selected as study area, lying within the boundaries of Borçka district of Artvin city in the northeast of Turkey. Types of data used in the study are as follows: LiDAR point cloud, GDEM-2 (Global Digital Elevation Model-2) from ASTER and DTED-2 (Digital Terrain Elevation Data-2) from 1/25 000 scale topographic maps, Ground Control Points (GCPs) derived from Global Positioning System (GPS) in the field study and finally LANDSAT 8 satellite image for determination of land use. TerraScan, TerraModeler and TerraPhoto softwares are used in laser point cloud filtering, classification, modelling and accuracy analysis; while ArcGIS, Surfer, Global Mapper and Erdas Imagine softwares are used for integration with Geographic Information System (GIS) and hydrologic modelling. Realizing the truth that the basic data for flood modelling is a highly accurate DTM; various LiDAR DTMs are created using different parameter combinations to find the best vertical accuracy in order to obtain the best representation of the topography of Balci Stream Basin, which has a very steep slopped and dense vegetated character. Several comparisons were executed among LiDAR, ASTER GDEM-2 and DTED-2 data and LiDAR came to the forefront with its capacity to produce bare earth model easily, extracting non-ground objects and with a vertical accuracy of 0.1855 m. Later on, in the hydrologic modelling phase; Flood Peak Discharge Values (Q_p) were calculated from these three different data types having different spatial resolutions and vertical accuracies, LiDAR DTM gave the nearest value to the reference. In addition, for ASTER GDEM-2 and DTED-2 data, Q_p could be moved away from the reference value and given exaggerated results as the spatial resolution and vertical accuracies decreased.

^{*} Corresponding Author

INTRODUCTION

It is very important to take the necessary precautions against flood risk before it happens. For this purpose, it is of utmost importance to reveal the topographic structure of the risky region with high accuracy by means of Digital Elevation Model (DEM) and Digital Terrain Model (DTM) obtained from terrestrial surveying, radar and satellite imagery, digital photogrammetry or from Light Detection and Ranging (LiDAR) as a new technology.

The two parameters; the drainage areas and the slopes of the water basins are the most important parameters for the hydrological studies. In order to obtain these parameters accurately, the topographic structure of the terrain needs to be determined very precisely in the digital environment. Highly inclined basins are present in many parts of our country, especially in the Eastern Black Sea region, and contain a wide variety of trees and plant species. It is very time consuming and costly to obtain 1: 1.000 or 1: 5.000 scale data in a wide area with such dense and complicated surface structure by in situ measurements using classical methods. In hydrological studies, the realistic determination of basin boundaries, area, and the slope and aspect conditions of sub-basins depends on the precision of the xyz values of the ground, so that the flood model can be accurately presented. With classical surveying methods, it is almost impossible to obtain these values in such steep sloped and dense vegetated areas.

When the data retrieval techniques for DEM and DTM production are reviewed within the scope of the geomatics science, five basic techniques come to the forefront:

- Classical ground survey,
- Digital Photogrammetry,
- LiDAR,
- Interferometric Synthetic Aperture Radar (InSAR) / Shuttle Radar Topography Mission (SRTM),
- Stereo satellite images.

Depending on the specific requirements of the flood modelling task, it is important to examine the characteristics of the different topographic data sets required for DTM generation and hydrological modeling in water basins.

LiDAR requires less terrain work and evaluation costs when compared with terrestrial surveying methods, satellite and radar imagery and digital aerial photogrammetry. This makes LiDAR an attractive technology for users who need digital elevation data with low cost, high point density, and referenced with the desired accuracy. Depending on these properties, LiDAR is complementary to some of the conventional technology, whereas replacing some of them. In many surveying applications, airborne LiDAR, which is a laser scanning technology from an aircraft or helicopter, is used in conjunction with digital cameras.

Traditional methods such as field surveying and photogrammetry can yield high-accuracy terrain data, but they are time consuming and labour-intensive. Moreover, in some situations, for example, in forested areas, it is impossible to use these methods for

collecting elevation data (Habib et al., 2005).

Compared with photogrammetry, one of the main competing technologies with airborne LiDAR in terms of accuracy, due to LiDAR's capability of canopy penetration, DEM generation from LiDAR data overcomes the limitations of photogrammetry for DEM generation in forested areas (Liu, 2008). Actually, the use of LiDAR for terrain data collection and DEM generation is the most effective way (Forlani and Nardinocchi, 2007) and is becoming a standard practice in the spatial science community (Hodgson and Bresnahan, 2004). There has been a significant increase in the use of LiDAR data for DEM generation over the last decade as more reliable and accurate LiDAR systems are developed (Sithole and Vosselman, 2003).

Airborne LiDAR systems are also capable of detecting multiple return signals for a single transmitted pulse (Wehr and Lohr, 1999; Reutebuch et al., 2005). Most LiDAR systems typically record first and last returns, but some are able to record up to six returns for a single pulse (Wagner et al., 2004; Lim et al., 2003). Multiple returns occur when a laser pulse strike a target that does not completely block the path of the pulse and the remaining portion the pulse continues on to a lower object. This situation frequently occurs in forested areas where there are some gaps between branches and foliage (Reutebuch et al., 2005). Recording multiple returns is quite useful for the topographic mapping in forested area or for the description of forest stand and structure (Sheng et al., 2003). It also makes the creation of a bare earth model possible, which is very important for hydrological studies. With the LiDAR point cloud data, the xyz value of each point is obtained directly, so terrain models such as DEM, DSM and DTM can be obtained at a high speed in data processing.

MATERIALS

Study Area

Balcı Stream Basin is selected as study area, lying within the boundaries of Borçka district of Artvin city in the northeast of Turkey (Fig. 1).



Figure 1. Study area

Data and the softwares used in the study

Types of data used in the study are as follows: LiDAR point cloud, orthophotos, DTED-2 (Digital Terrain Elevation Data-2) from 1/25 000 scale topographic maps, GDEM-2 (Global Digital Elevation Model-2) from ASTER and Ground Control Points (GCPs) derived from Global Positioning System (GPS) in the field study and finally LANDSAT 8 satellite image for determination of land use. TerraScan, TerraModeler and TerraPhoto softwares are used in laser point cloud filtering, classification, modelling and accuracy analysis; while ArcGIS, Surfer, Global Mapper and Erdas Imagine softwares are used for integration with Geographic Information System and hydrologic modelling.

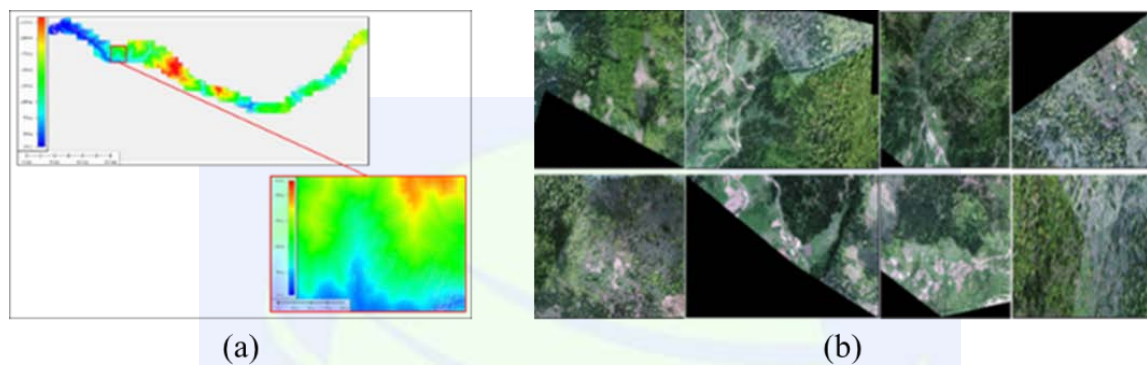


Figure 2. (a) Airborne LiDAR point cloud, (b) Orthophotos

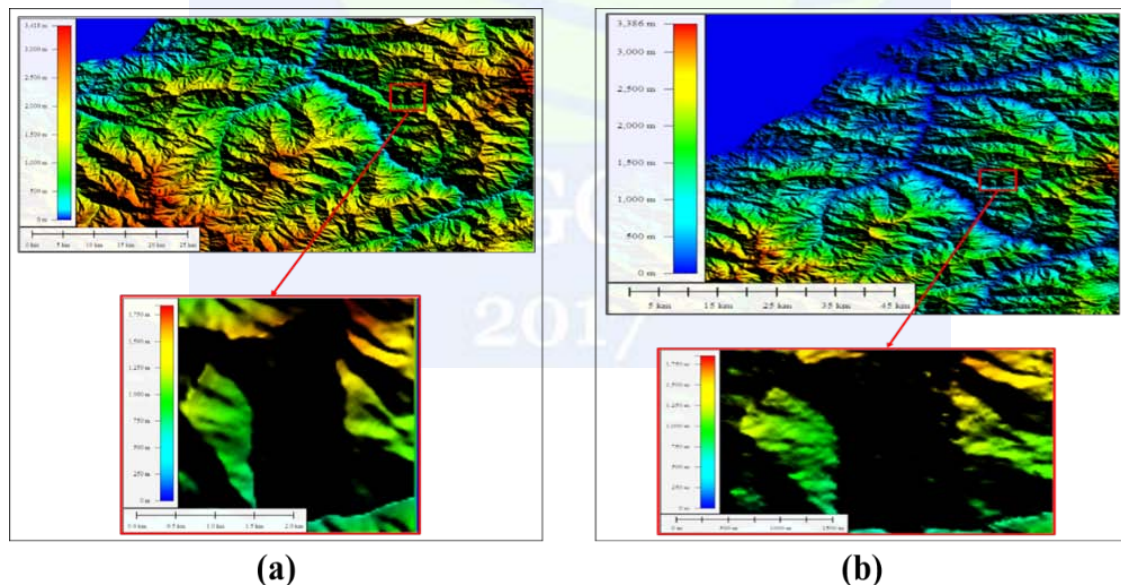


Figure 3. (a) DTED-2, (b) ASTER GDEM-2 data

METHODOLOGY

Lidar Data Classification

Terrain classes are determined by using TerraScan, TerraPhoto and TerraModel modules

included in Terrasolid LiDAR data processing software with unsupervised and supervised classification methods, by making use of orthophotos as visual reference. After completion of LiDAR data filtering process, the whole LiDAR point cloud package consists of 22 182 274 points has been completely filtered and classified (Fig. 4).

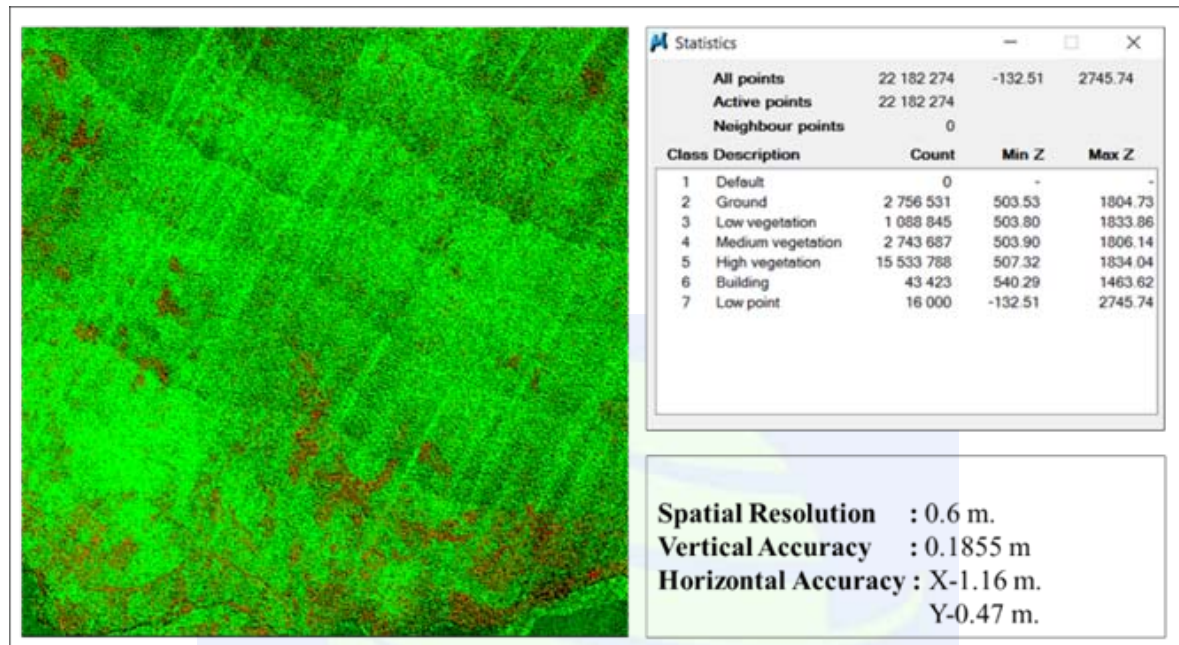


Figure 4. Completely classified LiDAR data.

Accuracy Analysis

The classified LiDAR data has been subjected to the accuracy analysis by using coordinates obtained from GPS survey performed in the study area. 16 different LiDAR DTM has been generated by extracting non-ground objects from the complete laser point cloud data with TerraModeler software to analyse the effects of filtering parameters to the accuracy. And the best vertical accuracy was found as 0.1855 m., while horizontal accuracy was found 1.16 m. in X axis and 0.47 m. in y axis. Spatial resolution of LiDAR data was found as 0.6 m. in all classes and 1.8 m. in only ground class (Fig. 4).

Comparison of Data Types

In this part of the study, LiDAR DTM has been compared with two other data, having different resolutions and vertical accuracies, which were DTED-2 and ASTER GDEM-2 elevation data, with respect to model accuracy and hydrologic modeling. The models were created using TerraModeler software and the vertical accuracies were calculated by using GCPs obtained with GPS field survey, as reference. As it was seen in Fig. 5, LiDAR DTM has the best point density and vertical accuracy.

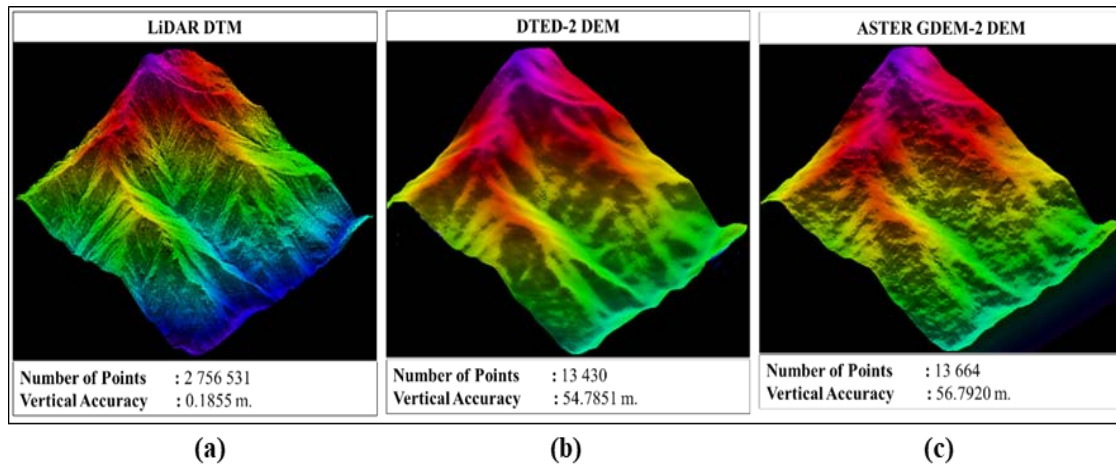


Figure 5. (a) LiDAR DEM, (b) DTED-2 DEM, (c) ASTER GDEM-2 DEM.

The comparison of the resolutions and vertical accuracies were shown in Table 1. The LiDAR DTM has got the best results with point number of 2 756 531, resolution of 1.8 m. and vertical accuracy of 0.1855 m.

Table 1. Data comparison results.

Ser.	Data	Number of points	Resolution (Grid Size) (m.)	Vertical Accuracy in RMSE (m.)
1	LiDAR DTM	2 756 531	1.8	0.1855
2	DTED-2 DEM	13 430	25.8	54.7851
3	ASTER GDEM-2 DEM	13 664	25.6	56.7920

While LiDAR data give better results in resolution and vertical accuracy, it is also best in hydrologic maps. Fig.6 gives us a visual perspective about how the drainage lines, pour points and sub-basins are composed in relief maps created with Erdas Imagine 2013. As it was seen in figure, basin drainage lines, pour points and sub-basins which are the basic inputs for hydrologic modelling, gave best results with LiDAR data and they gradually became poor as the resolution and vertical accuracy decreased with DTED-2 and ASTER GDEM-2 data.

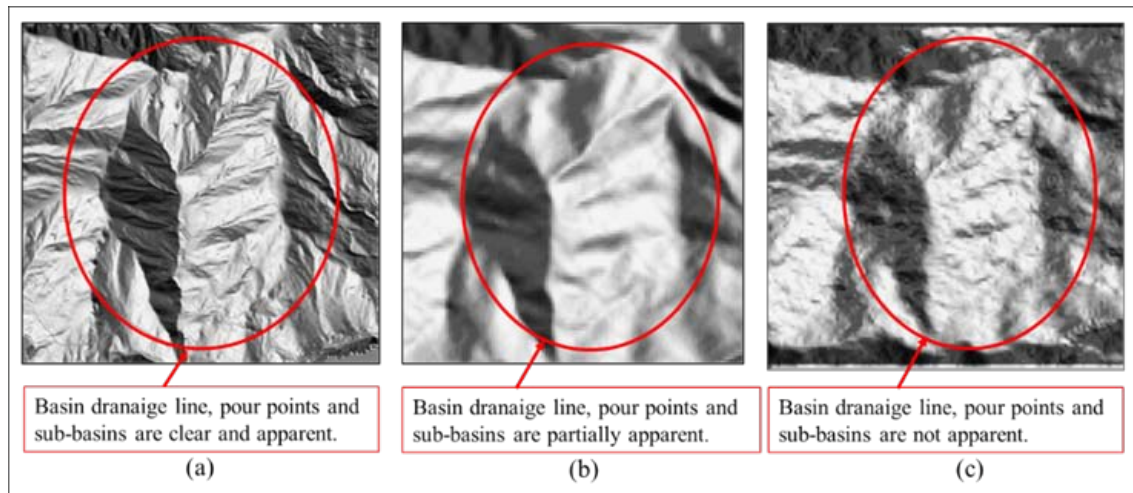


Figure 6. Relief maps created with Erdas Imagine 2013. (a) LiDAR DEM, (b) DTED-2 DEM, (c) ASTER GDEM-2 DEM.

Hydrologic Modelling

One of the most common problems in projecting river structures is the determination of the maximum flow in the stream. Since the Balçı Stream Basin is smaller than 5 km² and there is no Flow Observation Station (AGİ) and Automatic Meteorological Observation Station (OMGİ) installed on the basin, the Rational Method was used to calculate the hydrological model and calculate the flood peak discharge value. The rational method yields good results in small basins (0.5-5 km²) where the percentage of impermeable areas is large and the duration of rainfall is greater or equal to the Time of Concentration (T_c) of the basin.

The rational method can be explained as follows (Thompson, 2006): The flood peak discharge "Q", that the rainfall will bring to the basin sized as "A", at the intensity of the "i" multiplied by flow coefficient "C"

$$Q = C i A \quad (1)$$

Q: Flood peak discharge (m³/s), **i:** Rainfall intensity (mm/hr), **A:** Drainage area (m²), **C:** Flow coefficient (unitless).

The land cover and usage pattern (building, forest, meadow, road etc.) influence the infiltration potential and flow coefficient of the hydrologic model. For this reason, LANDSAT 8 multispectral (MS) satellite image is provided from USGS, having a spatial resolution of 30 m., dated 03.05.2013. Unsupervised and supervised classification have been done and land use patterns are determined. Since the flow coefficient takes different values according to the land use pattern in the basin, a single flow coefficient for the basin has been calculated by weighted average calculation. As a result, basin flow coefficient (C_b) was calculated and found as 0.4128.

The flood peak discharge values (Q_{p100}) were calculated for each of the three data types (LiDAR, DTED-2 and ASTER GDEM-2) using Equation (1) for return interval of 100 years. Rainfall Intensity "i" is taken from Turkey's Rainfall Intensity Book, dated 1987.

For LiDAR $Q_{p100}=0.4128 * (55/(1000*3600))*2830578 = 17.85 \text{ m}^3/\text{s}.$

For DTED-2 $Q_{p100}=0.4128 * (70/(1000*3600))*2830578 = 22.72 \text{ m}^3/\text{s}.$

For ASTER GDEM-2 $Q_{p100}=0.4128 * (75/(1000*3600))*2830578 = 24.34 \text{ m}^3/\text{s}.$

Analysis of the Differences in the Hydrologic Models with 3 Different Data Types

Hydrologic models were generated with three different data on the same basin and flood peak discharge values of 100 years return interval were reached. As a result, the importance of the resolution and the vertical accuracy of the three-dimensional model used in the hydrological model came in sight, therefore accuracy of the hydrologic model strongly related with how correctly the model reflects the details of the terrain.

As the result of the calculations, the LiDAR data gave the closest value to the value, measured in a similar basin (Kılıçlı Pond) before, which was taken as reference (Özdemir 1978). While LiDAR data generates a difference of %5.1 with the reference value, it was %20.8 in DTED-2 data and %29.5 in ASTER GDEM-2 data (Table 2).

As it was seen in Table 2, the flood peak discharge value increases as the resolution and vertical accuracy decreases and moves from the reference value and the value found by LiDAR.

Table 2. Comparison of flood peak discharge values calculated from different data types.

Flood peak discharge / Differences	Flood peak discharge measured in Kılıçlı Pond	Balı Stream Basin Flood peak discharge for 100 years return interval (m ³ /sn)					
		LiDAR DTM		DTED 2 DEM		ASTER GDEM DEM	
		Q _{p100}	Difference (%)	Q _{p100}	Difference (%)	Q _{p100}	Difference (%)
Flood peak discharge for 100 years return interval (m ³ /s)	18.8	17.85	-5.1	22.72	+20.85	24.34	+29.5
Spatial Resolution of Data (m)		1.8		25.8		25.6	
Vertical Accuracy of Data (m)		0,1855		54,7851		56.7920	

RESULTS & DISCUSSION

In this study, performance analyses of a new and effective technology, Light Detection and Ranging (LiDAR), was carried out for hydrological studies to be undertaken in order to take necessary precautions against the flood disaster which causes significant loss of lives and property every year in our country.

As a result of this study with LiDAR; unlike other existing DEM production techniques described in introduction section,

- Thanks to the GPS / INS system located on the same platform as the laser scanner, 3D data has been obtained directly, saving time to make the data 3D.

- Digital images are taken simultaneously with the laser points by means of digital camera mounted on the same flight platform with the laser scanner in airborne LiDAR systems. These images could be easily and quickly transferred to orthophotos with TerraPhoto software by means of position, orientation, and velocity parameters calculated by integrated GPS/INS system and these orthophotos had been used as a homogeneous visual reference during classification of the laser point cloud data, which was very essential for classification accuracy.

- Despite the fact that, it was very hard to get a DTM with the classical data acquiring technics and the accuracy of this DTM was low in such steep sloped and dense vegetated areas; making use of high penetration and multiple reflectance properties of the laser pulses, ground and other terrain details had been easily distinguished from each other, and a very sensitive DTM had been generated having a vertical accuracy of 0.1855 m.

- Thus, in cases there is no flow or precipitation station in the study area; hydrologic modelling could be performed with rational method and a flood peak discharge value has been obtained which is rather close to the values obtained by means of measurements.

CONCLUSION

DTM, generated with the LiDAR data with the spatial resolution of 1.8 m. and the vertical accuracy of 0.1855 m. is matched with the findings of Mason et al. (2010) about the data requirements for flood modelling. Resulted flood peak discharge calculations as part of hydrologic modelling was found strongly correlated with the spatial resolution and the vertical accuracy. Flood peak discharge values could be move away from the reference value and give exaggerated results as the spatial resolution and vertical accuracies decreased.

Because of all these above mentioned reasons, it was assessed that, usage of LiDAR technology in modelling river basins will make a significant contribution to hydrological and the flood risk analyzing studies

REFERENCES

- Habib, A., Ghanma, M., Morgan, M. ve Al-Ruzouq, R. (2005). Photogrammetric and LiDAR data registration using linear features. *Photogrammetric Engineering and Remote Sensing*, 71(6), 699-707.
- Hodgson, M. E. ve Bresnahan, P. (2004). Accuracy of Airborne Lidar-Derived Elevation. *Photogrammetric Engineering & Remote Sensing*, Number 3 / March 2004, pp. 331-339(9).
- Lim, K., Treitz, P., Wulder, M. ve Flood, B. S.-O. M. (2003). LiDAR remote sensing of forest structure. *Progress in Physical Geography*, 27(1), 88-106.

- Liu, X. (2008). Airborne LiDAR for DEM generation: some critical issues. *Progress in Physical Geography*, ISSN: 0309-1333.
- Mason, D. C., Schumann G. ve Bates, P. D. (2010). *Data Utilization in Flood Inundation Modelling. Flood Risk Science and Management*. Published Online: 15 Nov. 2010.
- Özdemir, H., (1978). *Uygulamalı Taşkın Hidrolojisi*, DSİ Basım ve Foto-Film İşletme Müdürlüğü Matbaası, Ankara, Shf 170-175.
- Reutebuch, S. E., Andersen, H.-E. ve McGaughey, R. J. (2005). Light detection and ranging (LIDAR): an emerging tool for multiple resource inventory. *Journal of Forestry*, 103(6), 286-292.
- Sanders, Brett F. (2007). Evaluation of on-line DEMs for flood inundation modeling. *Advances in Water Resources*, 30 (2007) 1831–1843.
- Sheng, Y., Gong, P. ve Biging, G. S. (2003). Orthoimage production for forested areas from large-scale aerial photographs. *Photogrammetric Engineering and Remote Sensing*, 69(3), 259-266.
- Sithole, G. ve Vosselman, G. (2003). Report: ISPRS Comparison of Filters. The Netherlands: Department of geodesy, Faculty of Civil Engineering and Geosciences, Delft University of Technology, ISPRS *Journal of Photogrammetry and Remote Sensing*, 59(1-2).
- Thompson, D.B. (2006). *The Rational Method*. Civil Engineering Department, Texas Tech University.
- Wagner, W., Ullrich, A., Melzer, T., Brieze, C. ve Kraus, K. (2004). From singlepulse to full-waveform airborne laser scanners: potential and practical challenges. *International Archives of the Photogrammetry, Remote Sensing and Spatial Information Sciences*, 35(B3).
- Wehr A. ve Lohr U. (1999). Airborne Laser Scanning, *ISPRS Journal*, Vol. 54, Issue 2/3.

TERKOS-Canal İstanbul Saltwater Intrusion Using Hybrid Geographic Information System-Analytical Solution

Khansaa A. Ahmed^{1*}, Abdüsselam Altunkaynak² and Hasan G. Elmazoghi³

PhD candidate, Department of Hydraulic and water resources, Istanbul Technical University, Ayazaga Campus, 34467, Turkey. E-mail: ahmedk@itu.edu.tr

Prof., Department of Hydraulic and water resources, Istanbul Technical University, Ayazaga Campus, 34467, Turkey. E-mail altunkay@itu.edu.tr

Associate Prof., Department of Civil Eng. University of Benghazi, Libya. E-mail: hasan.elmazoghi@uob.edu.ly

ABSTRACT

It is planned to build a massive navigational canal in Istanbul in order to link the Black Sea to the Marmara Sea. Construction of the newly proposed Canal Istanbul may have adverse effect on the nearby fresh water resources by encouraging seepage and salt water intrusion. This canal will built beside Terkos Lake which is one of the most important freshwater sources for Istanbul, (1-2 km) distance in between Canal Istanbul and Terkos Lake. Breaking of a saltwater way could cause a damage and contamination for the aquifer because saline water has a higher mineral content than freshwater, it is denser and has a higher water pressure. As a result, saltwater can push inland beneath the freshwater.

This study focused on the possibility of saltwater intrusion in the aquifer between the canal and the lake in order not to destroy the aquifer; analytical solution were used to simulate Terkos lake- Canal Istanbul intrusion using Ghyben-Herzberg, Glover analysis; A Geographical Information System (GIS) Geodatabase has been built for simulating the saltwater intrusion in case of canal construction.

Water level in Terkos lake is fluctuating; it is vary from +4.5 to -0.18, the results show there is no any serious problem as long as the lake level above mean sea level, but in case of the water level in the lake declined below mean sea level or equal; the saltwater will enter the aquifer and caused of freshwater pollution.

INTRODUCTION

Turkey government plans to build a massive navigational canal to link the Black Sea to the Marmara Sea. The canal will bypass the Bosphorus waterway that bisects Istanbul a rival to the Panama and Suez Canals. The new canal hopes to facilitate trade, reduce the

* Corresponding Author

possibility of shipping accidents and overcome the pressure through the Bosphorus. Although this canal may solve the Bosphorus dilemma, extensive studies surrounding this strategic waterway have to be prepared before its construction.

There are a total of 7 water basins supplying the drinking water demand in Istanbul. 4 of them reside in European side and the rest 3 of them are located in the Asian part of the Istanbul. Purposely use for drinking water, basins in the European side are Alibeykoy, Terkos, Sazlidere and lastly Buyukcekmece dams. Terkos Lake considered as one of the most crucial surface water resources of Istanbul city. Inevitably, as a result of increasing population, irregular urbanization over the Istanbul in the last 20 decades, qualities of the water basins have been reduced dramatically. All precautions taken and aggressive rules and regulations imposed did not prevent the water basins enough from environmental pollution (Çodur, 2004). The immediate threat of the canal on the freshwater resources in the area, especially Terkos Lake which is of a great importance has been considered as a highly significant national fresh water source in Istanbul by several authors (Yilmaz and Güleçal, 2012 and Kurt, 2015), its water is not only utilized for domestic water supply and recreation but also sustains important economic activities such as flower and vegetable growing, tourism and fishing. Its importance comes from being considered as a source of drinking water for an essential part of Istanbul (DAMOC, 1971). Construction of Canal Istanbul in the proposed site, (Figure. 1) breaks a salt water way in this area and may affect the fresh water of Terkos Lake through encouraging seepage of water in the aquifer system connecting Terkos Lake with the canal. According to the available water level measurements, the canal will always drain the nearby aquifer creating downward seepage from surface water of Terkos Lake into the aquifer system.

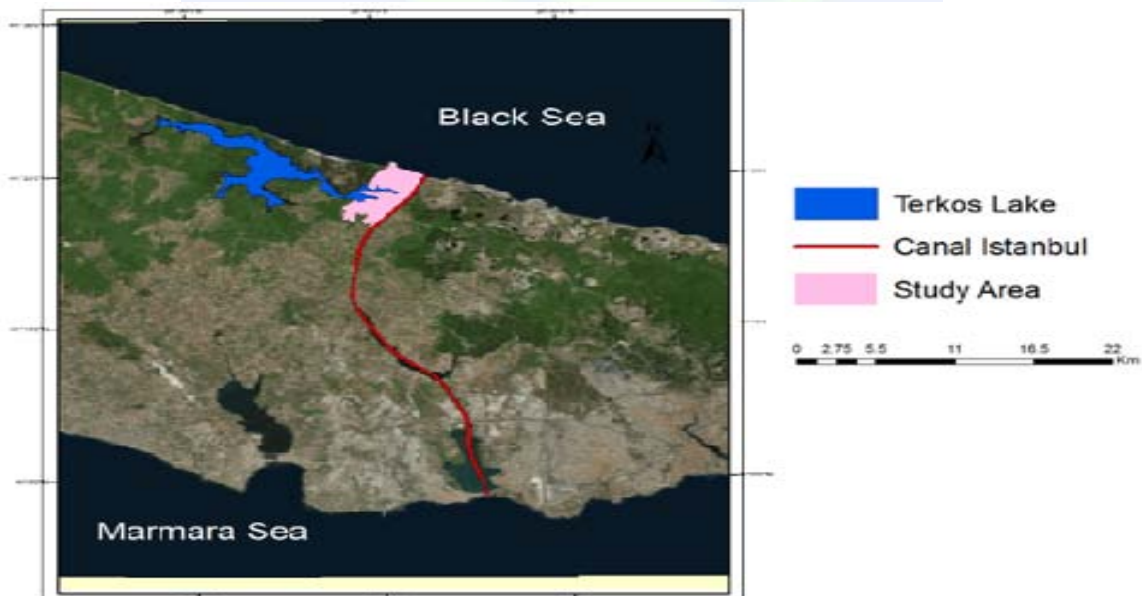


Figure 1. The proposed path of Canal Istanbul

DESCRIPTION OF THE STUDY AREA

The location of the study area was identified using Universal Transverse Mercator coordinate system (UTM) for the World Geodetic System (WGS 84) datum, Zone 35 for Istanbul. The upper left corner of the model area has the longitude and latitude values of $X= 636000$ and $Y= 4579000$ whereas the lower right corner has an $X= 645000$ and $Y= 4570000$ as shown in Figure. 1.

Terkos Lake:

Terkos Lake is 12 kilometers long and 5 kilometers wide. It is separated from the black Sea by a zone of sand dunes whose width varies between 0.25 kilometers and 3.7 kilometers, with an average of 2 kilometers. It is bordered on the south side by cliffs about 80 meters high; secondary rivers flow from that side into the lake. The major axis of Terkos Lake runs northeast-southwest along which flow two major rivers. Swampy areas are extensive in these two zones especially in the north in Istranca River Valley. The Black Sea beach is rectilinear with a berm of about 10 to 30 meters width. Along the Black Sea shore, the dune zone is bordered at the central part on the northwest and by small cliffs on the southwest. In the flat zone, dunes are about 10 meters in elevation. Active dunes have moved from the northwest to the southeast with a maximum displacement of about 350 meters over an 18-year period.

Aquifer systems and aquifer properties:

Aquifer properties were assigned based on the analysis of observation boreholes data (KGM, 2015). Five layers of the aquifer were taken into consideration depending on the lithological information of boreholes drilled in the study area. The properties and hydraulic conductivities (K) of the layers are shown in Table 1 (P. Dietrich, 2005).

Table 1 Aquifer properties

Layer	Average depth (m)	Properties	K (m/s)	Specific yield %	Porosity (%)
1	7	Silt	2.0×10^{-5}	8	34 – 61
2	4	Sand stone	6.0×10^{-6}	24	14 – 49
3	4	Silt stone	1.4×10^{-8}	12	21 – 41
4	20	Sand stone–Silt stone	3.0×10^{-6}	18	17 – 45
5	20	Silt stone	1.4×10^{-8}	12	21 – 41

Building the Geo-database:

Basic Concept of GIS is defined as a system for input, storage, manipulation, and output of geographically referenced data (Goodchild 1996). GIS provides a means of representing the real world through integrated layers of constituent spatial information (Corwin 1996). Geographic information can be represented in GIS as objects or fields. The object approach represents the real world through simple objects such as points, lines, and areas. The objects, representing entities, are characterized by geometry, topology, and non-spatial

attribute values (Heuvelink 1998). In hydrogeology, some examples of spatial objects are wells, piezometers, boreholes, galleries, and zones of protection. Attribute values of objects could be the number of a well, the ownership, and the diameter of a gallery or drain. The field approach represents the real world as fields of attribute data without defining objects; some examples are strata elevation, hydraulic head, and vulnerability zones. This approach provides attribute values in any location. In GIS, this distinction between objects and fields is often associated with vector data models and raster data models. The vector model represents spatial phenomena through differences in the distribution of properties of points, lines, and areas.

Geographic Information System (GIS) was used to input, store, retrieve, process and display spatial information in the form of maps or images including database which is linked to the mapping, ARC GIS 10.2 was utilized for the purpose of building the geodatabase. Figure 2. A digital elevation model (DEM) of 30 m resolution of the Advanced Space Borne Thermal Emission and Reflection (ASTER) on-board NASA satellite Terra was downloaded and GIS was used to process the digital elevation model (DEM) of the study area which in turn helped to define the boundary of the study area, Figure 3.

Saltwater Intrusion:

Coastal aquifers are highly sensitive to disturbances, inappropriate management of a coastal aquifer may lead to its destruction as a source for freshwater much earlier than other aquifers which are not connected to the sea. In many coastal aquifers, intrusion of seawater has become one of the major constraints imposed on groundwater utilization. As seawater intrusion progresses, existing pumping wells, especially those close to the coast, become saline and have to be abandoned. Also, the area above the intruding seawater wedge is lost as a source of natural replenishment to the aquifer (Bear, 1999). A complete model to describe saltwater intrusion should be three-dimensional, transient, and account for varied densities and for dispersion. Such a model, if any, is not only complicated, but requires also a lot of input data which are mostly not available. Even in areas rich in data it is never enough and the ever heard complaint of lack of data will remain forever. The modeler will have to learn the art of drawing acceptable conclusions and to indicate the range of their reliability from the available data. The most recent development in modeling is the coupling of the model with a geographic information system (GIS) for the input data and presentation of the model output. Where no comprehensive sophisticated model and/or computer capacity is available, or in the absence of sufficient knowledge or experience with such models, one can resort to simpler models. To evaluate the effects Canal Istanbul construction on saltwater intrusion, a two-dimensional cross-section model was developed using average hydrologic conditions. Analytical solutions, although not as powerful as numerical models, may be able to provide reasonable predictions of the risk of salt water intrusion. Simple analytical approaches which are physically based can be used to address local salt water intrusion issues. They play an important role to serve as instructional tools to present fundamental insights to clearly understand the trend of the salt water interface in coastal aquifers. Sophisticated numerical models cannot provide more accurate results without the support

of reliable input data. That is why it is often interesting to perform some preliminary calculations based on basic information and simplifying assumptions.

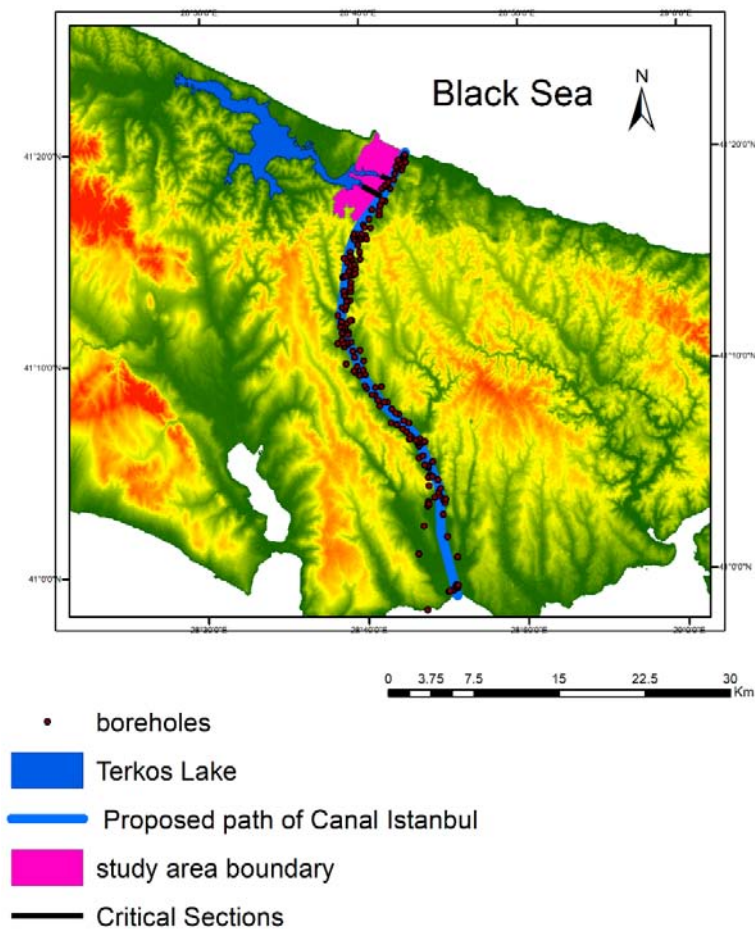


Figure 2. ARC GIS Geodatabase

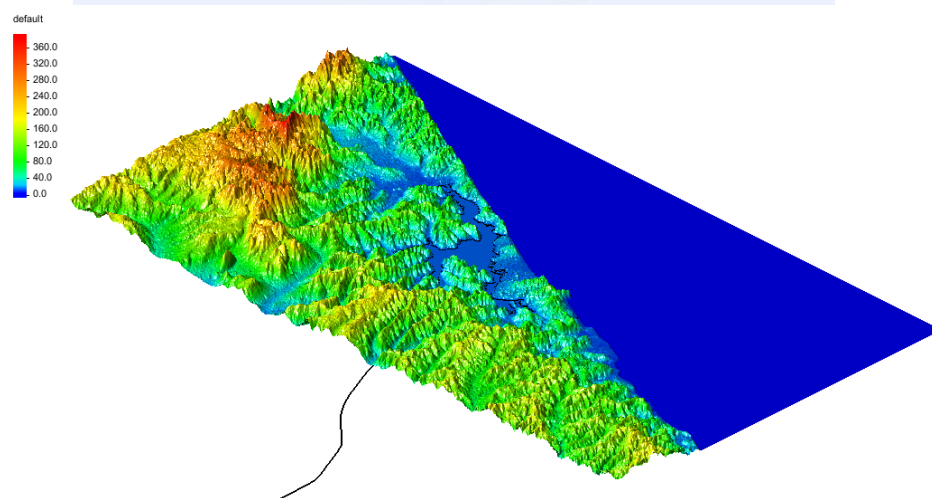


Figure 3. Digital Elevation Model for the study area

The analytical solutions made by Ghyben (1889) and Herzberg (1901), thus called the Ghyben-Herzberg relation, and the Glover (1959) equations for locating the position of the saltwater-freshwater interface in a coastal aquifer form the basis of the work presented in this section. The advantage of such analytical approaches is that they have fewer parameters and require a minimum of computational resources to provide reasonable recommendations for characterizing salt water intrusion in aquifers. Ghyben-Herzberg analytical solution to derive the position of the saltwater interface is reliant on a sharp interface assumption, however, Glover's (1959) analytical solution accounts for a transition zone between the two types of water near the shoreline.

Ghyben-Herzberg analysis:

This analysis assumes hydrostatic conditions in a homogeneous, unconfined coastal aquifer. Moreover, it assumes a steady salt-fresh water interface. An exact mathematical statement of the saltwater intrusion problem, assuming that an abrupt interface separates fresh water and saltwater, was presented by Ghyben-Herzberg relationship which can be introduced as:

$$Z = \frac{\rho_f}{\rho_s - \rho_f} \times h_f \quad (1)$$

Where:

Z = vertical position of the saltwater interface measured below the mean sea level, m.

ρ_f = density of the fresh water, kg/m³.

ρ_s = density of the salt water, kg/m³.

h_f = height of the fresh water table measured above mean sea level, m.

Using the fresh and saline water densities for typical sea water conditions at 20 °C, we have $\rho_f = 1000 \text{ kg/m}^3$ and $\rho_s = 1025 \text{ kg/m}^3$. Substituting these values in Eq. (1) yields that: $Z = 40 h_f$

For the black sea the salt water density is $\rho_s = 1018 \text{ kg/m}^3$. This would lead to the relation:

$$Z = 55.56 h_f$$

The validity of the Ghyben-Herzberg relationship was investigated by Bear and Dagan (1964). It shows reasonable estimates except that close to the coast the depth of the interface is greater than that predicted by the Ghyben-Herzberg relationship. It is important to note from the Ghyben-Herzberg relation that fresh-salt water equilibrium requires that the water table, or the piezometric surface (1) lie above sea level and (2) slope downward toward the sea. Without these conditions, seawater will advance directly inland (Todd, 2005).

Glover analysis

One of the simplest stationary interface solutions based on Dupuit assumption was proposed by Glover (1959) for confined flow, later extended by Van Der Veer (1977) to

include phreatic flow. The saltwater interface can be considered as a streamline and, its position can be determined as a function of the distance from the shoreline as follows:

$$Z = \sqrt{\left(\frac{\rho_f Q}{\Delta \rho K}\right)^2 + \frac{2\rho_f Q}{\Delta \rho K} X} \quad (2)$$

Z = vertical position of the saltwater interface measured below the mean sea level, m.

X = horizontal distance measured inland from the shoreline, m.

ρ_f = density of the fresh water, kg/m³.

$\Delta \rho = \rho_s - \rho_f$ = Difference between the density of the salt water and fresh water, kg/m³.

Q = constant total freshwater flow per unit length of shoreline, m³/s/m.

K = hydraulic conductivity of the aquifer, m/s.

The width of the region through which freshwater discharges to the sea is obtained for $Z = 0$ and is given by:

$$X_0 = \frac{\rho_f Q}{2\Delta \rho K}$$

The depth of the interface beneath the shoreline Z_0 occurs when $X = 0$ so that:

$$Z_0 = \frac{\rho_f Q}{\Delta \rho K}$$

Several scenarios were assumed for the Terkos Lake levels as (+4.5, +3.5, +2.5, +1.5 and +0.5 m) and the distribution of the hydraulic heads altogether with the seepage flow rates towards Istanbul canal were calculated by MODFLOW. These results were used to locate the corresponding position of the salt water interface for each lake level using the previous analytical solutions (i.e. Ghyben-Herzberg and Glover relationships). The results are given in Table (2) and Table (3) for Ghyben-Herzberg and Glover relationships, respectively. From the different scenarios, it is observed as the Terkos Lake levels decrease, a significant movement of the salt water interface would occur with a maximum extent of 1200 m when the Terkos Lake level is 0.5 m. This means that the saltwater will almost reach Terkos Lake. Hence, operation of Terkos Lake should not allow the lake level to reach such low levels. Figures 4,5.

Results

Table 2. Results of Ghyben-Herzberg relationship

Terkos Lake level (m)	Distance from canal X (m)	Height of fresh water a.m.s.l. h_f (m)	Height of salt water b.m.s.l. Z (m)	Seepage flow rate Q (m ³ /year)
4.50	1275	4,5	249,75	530000
	850	2,23	-123,76	
	425	0,867	-48,12	
	0	0	0	
3.50	0	3,5	-194,25	409000
	425	1,72	-95,46	
	850	0,76	-42,18	
	1275	0	0	
2.50	0	2,5	-138,75	289000
	425	1,23	-68,26	
	850	0,474	-26,30	
	1275	0	0	
1.50	0	1,5	-83,25	172000
	425	0,73	-40,51	
	850	0,28	-15,54	
	1275	0	0	
0.50	0	0,5	-27,75	56800
	425	0,242	-13,43	
	850	0,093	-5,16	
	1275	0	0	

Table 3. Results of Glover relationship

Terkos Lake level (m)	Distance from canal X (m)	Height of fresh water a.m.s.l. h_f (m)	Seepage flow rate Q (m ³ /year)	Hydraulic conductivity K (m/s)	Freshwater density ρ_f (kg/m ³)	Saltwater density ρ_s (kg/m ³)	Height of salt water b.m.s.l. Z (m)
4.50	1275	4,5	530000	0,0000305	1000	1018	-105,69
	850	2,23					-86,33
	425	0,867					-61,13
	0	0					-4,37
3.50	1275	3,5	409000	0,0000305	1000	1018	-92,83
	850	1,72					-75,82
	425	0,76					-53,67
	0	0					-3,37
2.50	1275	2,5	289000	0,0000305	1000	1018	-78,02
	850	1,23					-63,71
	425	0,474					-45,08
	0	0					-2,38
1.50	1275	1,5	172000	0,0000305	1000	1018	-60,18
	850	0,73					-49,14
	425	0,28					-34,76
	0	0					-1,42
0.50	1275	0,5	56800	0,0000305	1000	1018	-34,57
	850	0,242					-28,23
	425	0,093					-19,96
	0	0					-0,47

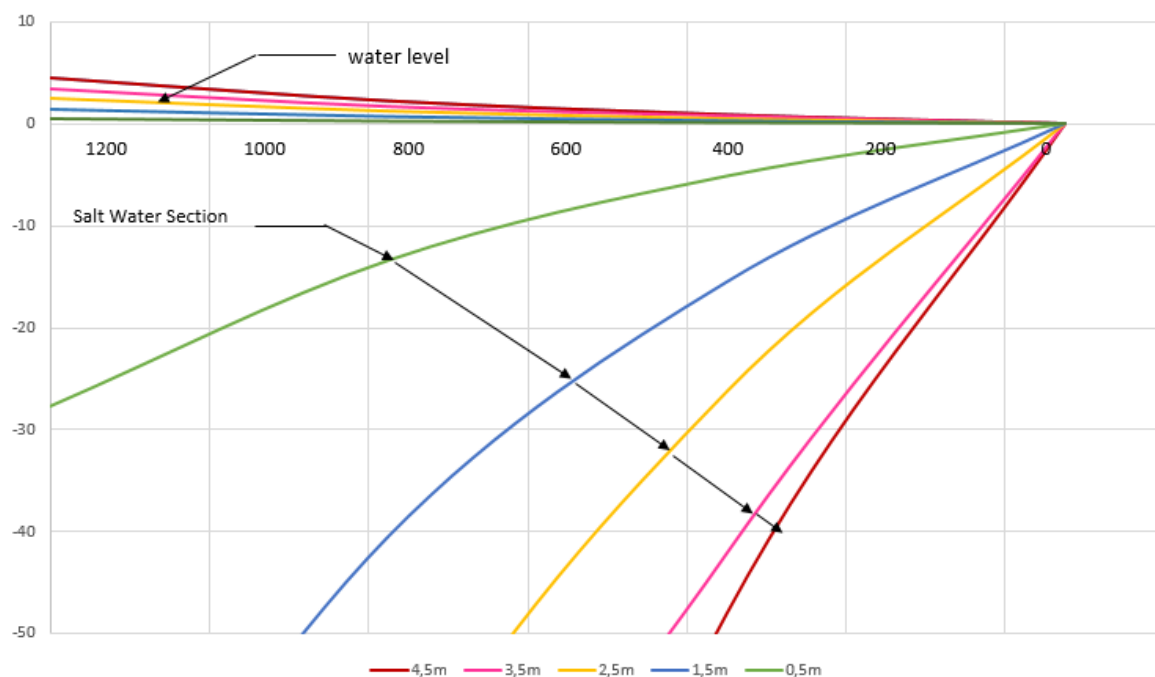


Figure 4. Ghyben-Herzberg saltwater interface

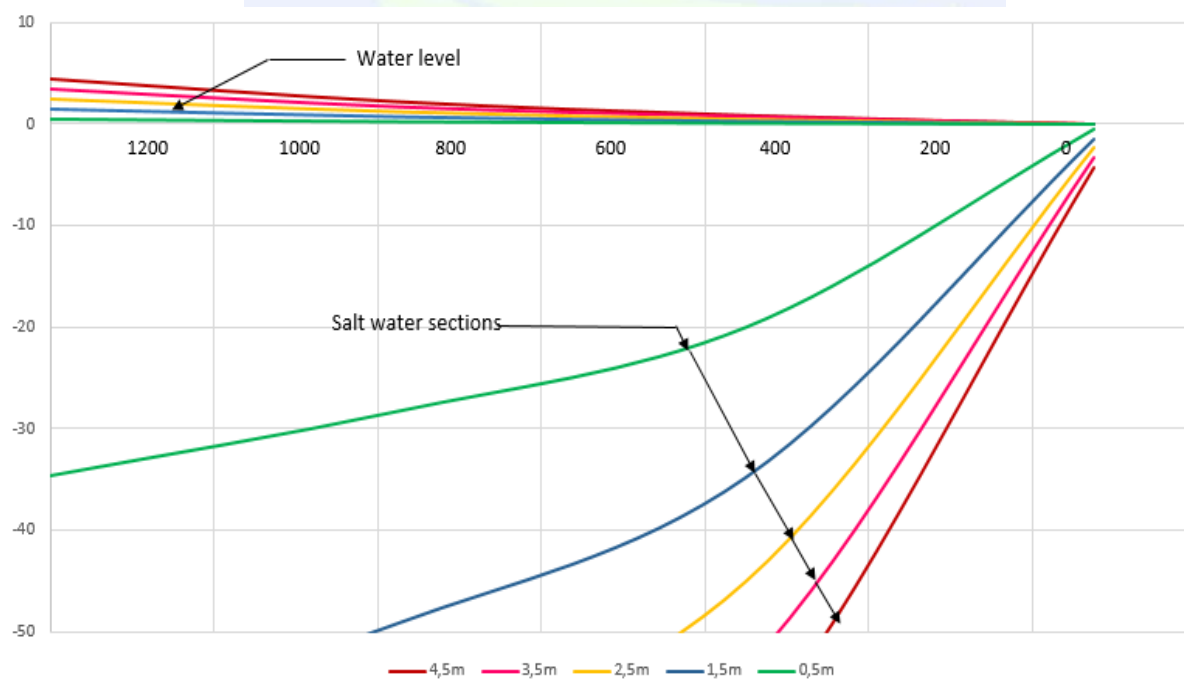


Figure 5. Glover saltwater interface

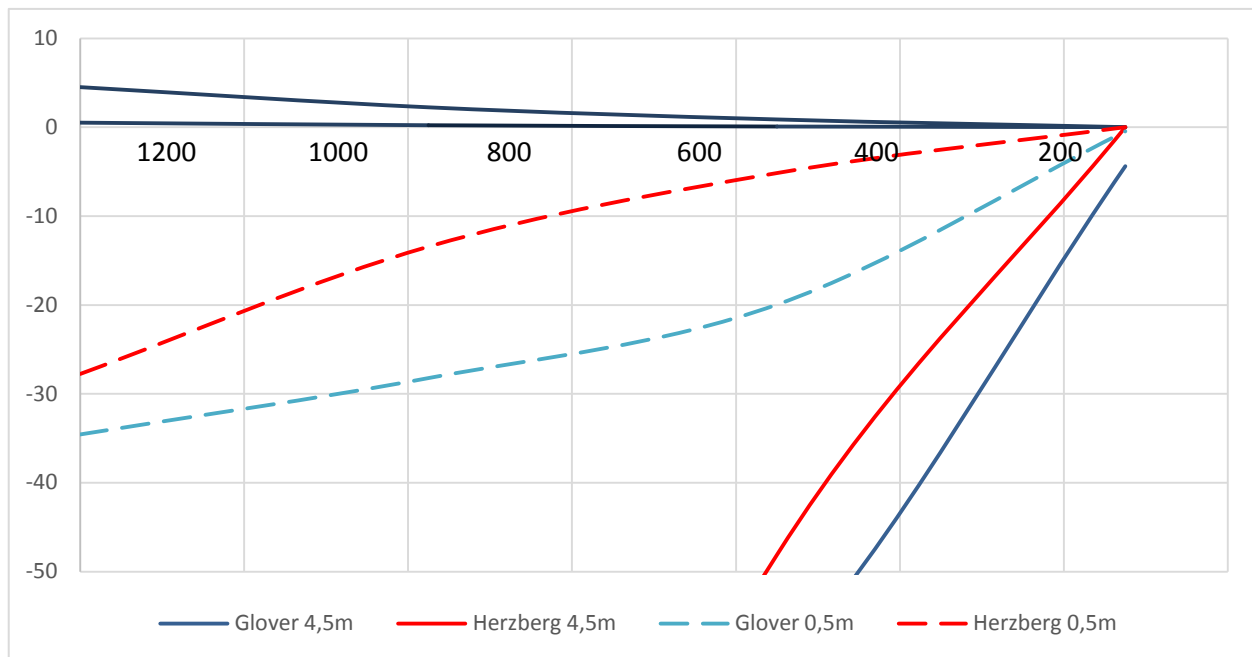


Figure 6. Saltwater intrusion comparison of Ghyben-Herzberg and Glover analytical methods for Terkos Lake levels of 4.5 m and 0.5 m.

Discussion and Recommendation:

For an essential project like Canal Istanbul has to be studied thoroughly, our study still in progress using numerical analysis solution by SEWAT GMS 10.2. the model will be 3-dimension, Transient, and multi sinario model starting by steady state conditions (current period) moving to excavation period and calculating the seepage amount of fresh water from the lake towards the canal. The third senario will be the transient flow calculations using numerical analysis and prepare the saltwater intrusion numerically.

From the analytical solution its clearly visible in Figure 6 that the interface location was presented in solid lines for the two cases with different outflow rate. For comparison, Glover's analytical solution is plotted as dash lines. There is a good agreement. A notable occurrence of salt water intrusion at Sections 1 and 2 is possible due to the lower water levels and the nature of the soil. The salt water intrusion could be explained by the formation of a wedge in such sections.

The study recommended that the most effective factor can play the role of saltwater intrusion is the water level in the lake, in case of water level in the lake declined below mean sea level the saltwater will enter the aquifer and cause aquifer destruction.

REFERENCES

Bear, J., and Dagan, G., Intercepting freshwater above the interface in a coastal aquifer, Intl. Assoc. Sci. Hydrology Publ. 64, pp. 154-181, 1964.

- Bear, Jacob. And others., 1999. Theory and Applications of Transport in Porous Media, Seawater Intrusion in Coastal Aquifers Concepts, Methods and Practice, SPRINGER-SCIENCE+BUSINESS MEDIA, B.V.632 p.).
- Corwin DL., 1996. GIS applications of deterministic solute transport models for regional-scale assessment of non-point source pollutants in the vadose zone. In: Corwin DL, Loague K (eds) Applications of GIS to the modelling of non-point source of pollutants in the vadose zone. Soil Sci Soc Am 48:69–100
- Çodur, A. D., 2004. İstanbul'un Mevcut Su Kaynakları, Su Kalitesi ve İçme Suyu Havzalarının Korunması' 04, İstanbul, 8-9 Ocak 2004, 2, 3-8.
- DAMOC (A Consortium)., 1971. "Master plan and feasibility report for water supply and sewerage for the Istanbul region, Volume I: General background studies".
- General Directorate of Highways (KGM)., 2015, Küçükçekme - karaburunara Km: 0 + 000-43 + 150 Corridor Geological - Engineering Geology and hydrogeological survey and report.
- Glover, R. E., 1959, The pattern of fresh-water flow in a coastal aquifer: Jour. Geophys. Research, v. 64, no. 4, p. 457-459.
- Goodchild MF., 1996. The application of advanced information technology in assessing environmental impacts. In: Corwin DL, Loague K (eds) Applications of GIS to the modelling of non-point source of pollutants in the vadose zone. Soil Sci Soc Am 48:1–17.
- Herzberg, A.D., Wasserversorgung einiger Nordseebaeder [The water supply of selected North Sea towns]. Z.F. Gas- beleuchtung und Wasserversorgung 44, 815–819, 842–844, 1901.
- Heuvelink GBM., 1998. Error propagation in environmental modelling with GIS. Taylor and Francis, London, UK
- P. Dietrich · R. Helmig · M. Sauter · H. Hötzl, J. Köngeter · G. Teutsch., 2005. Flow and Transport in Fractured Porous Media, Library of Congress Control Number: 2004117959 ISBN 3-540-23270-2 Springer Berlin Heidelberg New York.
- Todd, D.K., ve Mays, L.W., 2005. Groundwater Hydrology. John Wiley&Sons, Inc. Danvers, USA, 636 pp.
- Van der Veer, P., Analytical solution for steady interface flow in a coastal aquifer involving a phreatic surface with precipitation, J. of Hydrol., 34, 1-11. 1977.
- Yilmaz Neşe and Güleçal Yasemin., 2012. Phytoplankton community of Terkos Lake and its Influent streams, Istanbul, Turkey. Pak. J. Bot., vol 44 no(3): 1135-1140.



LAND USE

Assessment And Mapping of Spatial Variation of Soil Quality Around The Gulf of Edremit, Turkey

Cagan Alevkayali¹ and Sermin Tagil^{*2}

¹Department of Geography, Suleyman Demirel University, Cunur/ Isparta. email: cagan.alevkayali@sdu.edu.tr

²Department of Geography, Balikesir University, Cagis Campus, 10100, Turkey e-mail: stagil@balikesir.edu.tr

ABSTRACT

The quality of soil is one of the most important factor for achieving sustainable land use and an inhibitor to prevent land degradation. The objective of this study is to explore the soil quality and the influence factors of negative consequences of human activities around the Gulf of Edremit. Soil Quality Index (SQI), which is an effective method to assess the soil quality for any region, was used to determine the soil condition in the study area. The assessment of soil quality in this study is based on indicators and indices derived from some soil properties. Soil reaction, soil texture, soil depth, parent material, rock fragments, drainage and slope parameters has been used to generate SQI that is an important measure of land values. After, the study area was divided into a 3.0 x 3.0 km grid; samples have been collected using the systematic random method from soil pits at 0-30 cm depths that reflect the influence of anthropogenic activities. Field and laboratory research of soil has been conducted on samples from 100 pedological profiles taken with a professional soil probe. Soil texture and reaction were analyzed in the soil laboratory by using pH meter and Bouyoucos Hydrometer Method, and also Geographical Information Systems used to analyze both the spatial distribution of soil parameters and SQI model. Results showed that almost 4.07% of the study area was located in the high quality class, 75.65% was located in the moderate quality, and 21.28% was located in the low quality class of degradation. Soils of high quality and moderate quality were observed in plain and flat lands; but, at the same time, some parts of these areas were most affected places by urbanization. This demonstrates that the urbanization cause the pressure on high quality soils which are potential agricultural areas around the gulf.

INTRODUCTION

Climate and environmental changes in many places throughout the world and mainly in the Mediterranean Basin have been known to be resourced from social, financial and global inequalities (Butzer, 2005). Even though it is difficult to estimate in what aspect climate and environmental changes would be, it is possible to obtain information on the cause and

* Corresponding Author

dimension of their effects. Soil is one of the components, with which these effects can be observed the best; because it is the product of a complex process, in which horizons are created within a period with the interaction of components such as climate, vegetation, parent material and becomes the living space of plants and other organisms. Sarioglu and Dengiz (2012) express soil as a natural resource, which is necessary for human survival and welfare and for the continuity of terrestrial ecosystems. According to Balci (1996) soil is a natural mass, in which minerals and organic components are separated in horizons and which is different from the bedrock in terms of morphological, physical characteristics, structure, chemical characteristics and biological characteristics and which is unconsolidated. Therefore, soil has a determinant characteristic in terms of the continuity of the ecosystem.

In as much as being significant for the ecosystem, soil has the leading duty for agricultural production and development. Although soil is such a significant natural resource, it has been coming to an end due to the reasons such as intense agricultural operations, erosion, desertification and misuse of lands (Karabulut and Kucukonder, 2008). Thus, putting forth the soil quality within local or regional scale has gained importance.

The quality of soil is significant for measuring environmental sensitivity and for developing a sustainable planning approach based on these measurements. Presenting the “soil quality” in the vicinity of the Gulf of Edremit has been aimed in this study. In this framework, the soil quality in the vicinity of the Gulf of Edremit has scrutinized by presenting different quality classes with Geographical Information Systems (GIS) models and its quality levels have been tried to be presented.

MATERIAL AND METHOD

Study Area: The study area is the Gulf of Edremit, which is located in the north of the Aegean Region, and the watershed between Altinoluk in the north and Burhaniye subdistrict in the south has been accepted as the boundaries (Figure 1). The boundaries of the study area have been passed from the watershed, which contains the aforesaid subdistricts. The area has an approximate width of 1580 km²; whereas the Gulf of Edremit reaches from Babakale Cape to Ayvalik. Ida Mountains that surround the north of Edremit Plain and that reach 1774 metres, Eybek Mountain that summits at 1298 metres and Maya Hill on Madra Mountains at 1341 metres in the south are the most significant elevations (Gursoy, 2009; Uzun and Sonuncu, 2013).

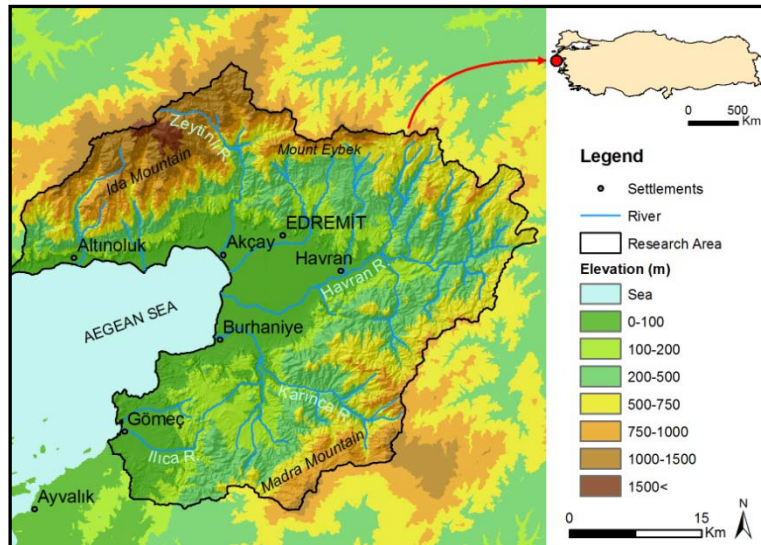


Figure 1. Location of study area

Data: Data that is used in this study have been obtained from geology map taken from MTA, the soil map which is prepared by the Republic of Turkey Ministry of Food, Agriculture and Livestock and from field work. The main material used in the analysis and data that belongs to all of the parameters except for the incline have been obtained from samples that were taken from sampling points, which were determined randomly with field works. 3x3 km grid method has been used while topographic samples were being taken. Sampling process has been made by taking four soil samples from 100 sampling points from four meter radius, by adopting the method for points that were not systematically chosen. Aerial distribution of these data has been made with the Inverse Distance Weighting (IDW) method.

Method: The Soil Quality Index (SQI) which is used in this study is a developed version of the model that was used in the project conducted by Kosmas et al (1999) in the framework of the United Nations Convention to Combat Desertification. This SQI has been defined as “the capacity of soil to sustain vegetative and animal production, to increase water-air quality and to enable life functions that are suitable for human health within natural or managed ecosystem” (Karlen et al., 1997). SQI model has been given in formula 1:

$$SQI = (Parent\ Material \times Rock\ Fragments \times Soil\ Depth \times Soil\ Texture \times Drainage \times Slope \times Soil\ Reaction)^{1/7} \quad (1)$$

While SQI was being calculated in this study, “soil reaction” value has been added to the model by us unlike the previous studies. Its reason is that a parameter that would represent chemical characteristic of soil was disregarded at the previous model.

Main Material: The characteristic of the bedrock that create the soil is the leading element for assessing the quality of soil (Kantarci, 2000). This relation of the soil with the bedrock has been assessed as it can be seen in Table 1 and included in the formula.

Table 1. The values used to define the parameters in the SQI formula.

Parent Material				Rock Fragments			
Quality	Descriptio	Material	Index	Quality	Descriptio	Fragments	Index
Very	Good	Shale, schist, basic,	1	Very	Very stony	>60	1
Moderat	Moderate	Limestone, marble,	1.7	Moderat	Stony	20-60	1.3
Very	Poor	Marl, piroclastic	2	Very	Slightly ston	<20	2
Soil Depth				Soil Texture			
Quality	Description	Depth	Index	Quality	Descriptio	Texture	Index
Very	Deep	>75	1	Very	Good	L,SCL,SL,LS,C	1
Moderate	Moderate	75-30	1.5	High	Moderat	SC,SiL,SiCL	1.2
Low	Shallow	15-30	2	Moderat	Poor	Si,C,SiC	1.6
Very Low	Very shallow	<15	3	Very	Very	S	2
Soil Reaction				Slope			
Quality	pH	Description	Index	Quality	Descriptio	Slope (%)	Index
Very	3-4	Extremely acid	4	Very	Very gentle	<6	1
Low	4-5	Strongly acid	2	High	Gentle	6-18	1.2
Moderat	5-6	Moderately acid	1.5	Moderat	Steep	18-35	1.5
Very	6-7	Slightly acid	1	Very	Very Steep	>35	2
Very	7	Neutral	1	Soil Drainage			
High	7-8	Slightly alkaline	1,3	Quality	Descriptio	Drainage	Index
Moderat	8-9	Moderately	1.5	Very	Good	Well	1
Low	9-10	Strongly alkaline	2	High	Moderate	Imperfectly	1.2
Very	10-11	Extremely	4	Very	Poor	Poorly d.	2

L: Loamy, SCL: Sandy clay loam, SL: Sandy loam, LS: Loamy sand, CL: SC: Sandy clay, SiL: Silt loam, SiCL:Silty clay loam Si:Silty, C:Clay, SiC: Silty Clay, S: Sand

Rock fragment cover: As well as rock fragment cover of soil can show the level of becoming soil, the plant nutrition strength changes in accordance with the level of rock fragment cover (Kantarci, 2000). The criteria that is assessed in the rock fragment cover of soil is that the more the rock fragment cover increases, the more the strength to resist erosion is (Table 1). Determination of rock fragment cover is based on counting stones that are larger than 2 mm at sampling points (Altinbas et al., 2008). It has been included in the system that the way of assessing rock fragment cover rate of the soil and surface in terms of SQI decrease the sensitivity of land degradation in the soil and increase it on the contrary (Table 1). Rock fragment cover samplings have been determined by visually counting by using a grid of 1 m² at land (Figure 2a).



Figure 2. Sampling processes; a) determination of rock fragment (1 m^2) b) measuring soil depth with 100cm auger c) glass electrode pH meter d) pH measurements of soil samples

Depth of Soil: The term of depth of soil represents the area from the top horizon of the soil to the lower section of the B horizon (Kantarci, 2000). When the distribution of soil depth in the land is taken into consideration, it is accepted that environmental sensitivity is more in areas where depth is less (Kosmas et al., 1999). The measurements of the soil depth has been determined in this study by making measurements directly at sampling points with a 100 cm Eijkelkamp steel soil auger with 30 mm radius (Figure 2b). The study carried out by Kosmas et al. (1999) has been taken into consideration while the depth of soil was being categorized (Table 1).

Soil Texture: Inorganic components in the soil create minerals or rock fragments of various size and shapes depending on dissolution (Altinbas et al., 2004). Proportional amount of ingredients at the dimension of sand, alluvium and clay that constitute soil are defined as the texture (granular structure) of soil (Kantarci, 2000). In order to create soil structure classes, samples taken from 30 cm depth at determined points in the land have been dried first and then granulated. After the granulation process is completed, a 2 cm griddle has been used to separate organic substances and large gravels. Bouyoucos hydrometer method has been used at the final stage so as to determine texture characteristics of the samples (Oberthurt et al., 2000). Hydrometer analyses have been carried out at Ege University Faculty of Agriculture Department of Soil Science and Plant Nutrition.

Drainage: The fact which is expressed as soil drainage is the relation between the water of soil and the plant growth. Soil's retention of water is related with the present drainage and texture characteristics of the soil (Kosmas et al., 1999). "High quality" in other words well drained soil means that the water in the soil drained rapidly, the lower sections of the soil is

lest moist and the surface is dry at plant growth period; whereas sections that are very close to the surface (30 cm) are moist and the wetness in the soil enable it to continue at the initial stages of plant growth in soil with medium drainage; on the other hand, soil with poor drainage is the soil whose all layers including the surface is moist and prevent plants to grow. Determinations on soil drainage have been found by way of observation in a non-pluvial period.

Slope gradient represents the angular proportion that is actually created by the incline. In terms of the soil, slope affects the erosion and soil formation. Considering that the classification in the study conducted by Kosmas et al. (1999) in the Lesvos is in conformity with the field, it has been taken into account while the maps were being classified. The slope map has been obtained by using digital elevation model (DEM).

Soil Reaction Other parameters that are used in determining quality index of soil are quite significant indicators with regards to soil. However, chemical characteristic of the soil is another element that is significant in terms of soil and that should be taken into account at land degradation process (Schoenholtz et al., 2000). When it is included in the soil quality index, it makes a contribution to the index with innovation and meaningfulness. As it can be seen in Figure 2b and 2c, soil reaction has been measured at soil-water suspension of 1:2,5 with a "Glass-Electrode" pH meter (Ardahanlioglu et. al., 2003).

RESULTS AND DISCUSSION

In terms of the characteristics of the parent material of the soil, soil that are formed on formations such as alluvium, conglomerate, agglomerate, basic rocks, schist, marble and shale is the most durable soil to land degradation; therefore that soil is "High Quality" in terms of quality index (Kosmas et al., 1999). Accordingly, soil of high quality that show the highest resilience against land degradation expand on plains and some sections of Ida Mountains (Figure 3a). On the other hand, units in the work area such as sand stone and pebble stone have been accepted as "medium quality." This kind of soil has been seen in the sides of the study area, in other words piedmonts as it can be seen in Figure 3a. Soil of "low" quality, which shows high level of sensitivity at the study area, have been accepted as soil that is formed on andesite, gneiss, granite, limestone and dacite (Kosmas et al., 1999). These formations are generally spread on high sections of Ida Mountains and Madra Mountain (Figure 3a). The fields that are most sensitive to land degradation are the regions in which Marn and Pyroclastic materials exist. Although these units are not suitable for plants to exist in the dry period that takes place particularly in the Mediterranean region, they are unresisting both for wind and for water erosion (Kosmas et al., 1999). These units have been seen only around Kuyucak and Hisarkoy on the Madra Mountain. The characteristics of the main material at the study area in terms of SQI has been determined as very high, high and medium quality at 58% rate and the remaining part has been determined as low and very low quality (Figure 3a).

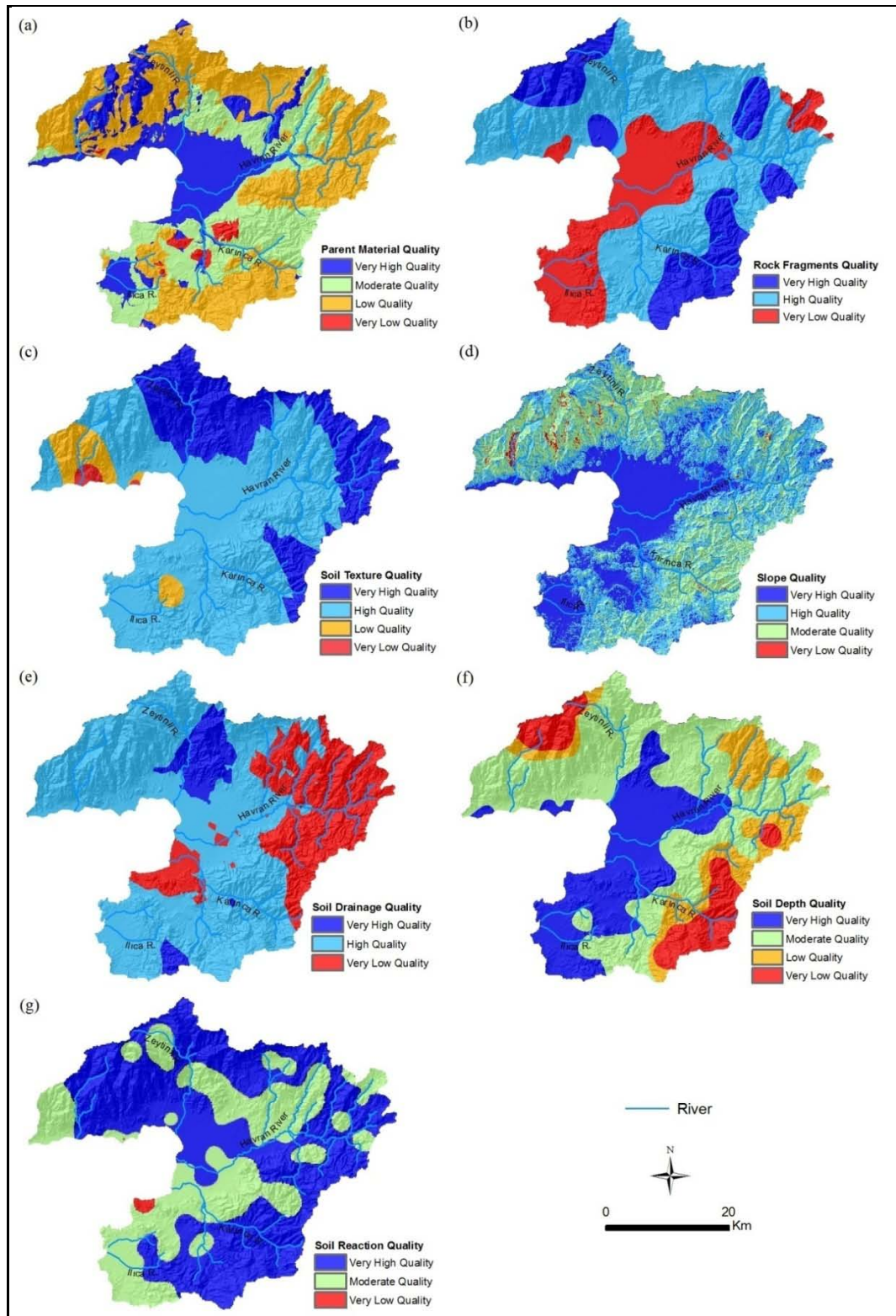


Figure 3. SQI Parameters: a) Parent Material Quality, b) Rock Fragment Quality, c) Soil Texture Quality d) Slope Quality e) Soil Drainage Quality, f) Soil Depth Quality, g) Soil Reaction Quality

Rock fragment cover characteristics are one of the parameters that are taken into account in terms of SQI. Rock fragment cover of the soil in other words aggregation level

of the soil in the Mediterranean region creates direct and indirect effects on the protection of the wetness of the soil for sensitivity, speed of surface flow, permeability level, surface erosion amount and the change of land cover (Kosmas et. 1999). The highest risk group for rock fragment cover values in the study area has been determined as the region where Havran Stream passes and low areas (Figure 3b).

Soil texture characteristics affect the permeability of soil and therefore water flow (Schaetzl and Thompson, 2015). In general sense, texture characteristics of soil give information on productivity situation of soil as well. It has been pointed that clay levels at the study area are high mainly at flat levels and sand rates are high in these areas. Thus, when the quality classes in terms of SQI are considered, it has been seen that a large part of the study area is located within the high quality group (Figure 3c). Grain size distribution is at balanced rates in the region in which Ilica Stream is located in particular has shown that the productivity of soil is quite good. These areas, which are expressed as high quality, are seen in narrow areas at the coastline at the northwest and a point at the south of the study area (Figure 3c). It has been understood that soil texture characteristics, which are assessed within SQI, make a positive effect that decrease sensitivity at the study field in general sense.

Slope is an important indicator of soil erosion in relation with topography (Kosmas et. 1999). Slope shows directly proportional effects on soil erosion. In addition, slope rates of land plays a significant role on drainage conditions of the soil. When the overall study area is considered it has been seen that incline levels are low in coastal sections and particularly Edremit Plain which is located at the center and these areas are taken as very high quality (Figure 3d). There is a narrow zone in Ida Mountains, which are located at the northwest, in which incline suddenly increases right behind the coast (Figure 3d). Areas similar to that have been defined as low quality. Sections of Ida Mountains and Madra Mountain, which are the high parts of the study field, which are eroded with valleys or steep slopes, have been represented with quite low quality (Figure 3d). Moreover, the region in which water catchment area of Karınca Stream exists on the Madra Mountain has been included in the low quality class (Figure 3d). Medium quality areas are mild sloped hills and hillsides that are located within plain bases of high sections (Figure 3d). When gradient of incline is assessed in terms of SQI, it is understood that it has a direct effect on the soil depth and therefore it plays a significant role within the system.

Soil drainage creates a compatible balance among water, soil and plant and plays a significant role for benefitting from these resources in the most efficient way (Tuncay, 2010). Soil drainage conditions in the study area have been determined from observations made at field works and in the framework of data that were obtained from structure analysis of soil (Kantarci, 2000). Due to drainage conditions being poor, water that comes with rain strengthens erosion by increasing surface flow rate. The field which has very high quality and in which soil drainage is the best within the study field is the region that falls within the lower sections of Zeytinli Stream (Figure 3e). When soil drainage characteristics are taken into assessment in terms of SQI, it has been seen that soil drainage conditions at the higher sections of Havran Stream are insufficient and these areas have been classified as “very low quality” (Figure 3e). Another area, in which drainage is poor,

is the region where Karinca Stream pours into the Aegean Sea (Figure 3e). It has been known that marshes and reed beds exist in the region as well. Drainage conditions at the study field have appeared to be medium quality in general sense. That situation is considered positive in terms of soil quality. Therefore, plant development in these areas has been accelerating.

Soil depth is defined as the term solum scientifically (Kantarci, 2000). Soil depth has significant effects on plants. For example, annual plants whose stem depth is not much can develop in surface or shallow areas (Altinbas et al., 2004). Another element for soil depth not being discussed independent from vegetation and climate conditions is that in areas where soil depth increases, there is a mutual benefit mechanism with vegetation. When soil quality classes in the study area are taken into account, it has been found that soil depth decreases from low plain sections towards high sections of mountainsides (Figure 3f). Based on this situation, decrease in the quality of soil has been the same. Even though this is an expected situation, the soil that is described as shallow is seen at wide areas within the study area and this can be qualified as the most significant problem of the quality of soil and the presence of soil in the region. A wide area in the study area appears to be in very low and low quality group when soil depth classes in terms of SQI are taken into consideration (Figure 3f). It has been pointed that soil of poor quality in terms of soil depth has been spread to wide areas in the region where Zeytinli Stream is located (Figure 3f). It has been known that these areas are quite important for olive production. Soil of quite poor quality, in other words shallow soil has been spread at the south of the study area in the region where the Madra Mountain is located (Figure 3f). Deep soils, whose extent is narrow within the study area is occupied with settlements and this shows that the situation for land degradation is at critical levels.

The reaction of soil is a significant parameter for affecting genetic development of soil as well as affecting physical, chemical and biologic characteristics of soil (Sariyildiz and Kucuk, 2004). Therefore, it has been added to the model. It is known that pH characteristics of soil have direct effects on the productivity of soil (Sarioglu and Dengiz, 2012). Taking pH measurements in the study in the framework of SQI has determined quality classes as in other parameters. Areas of very poor quality among these risk classes are seen in an area that is close to coastal section of Karinca Stream (Figure 3g). The reason for the situation to be created here is the pressure created by human factors as vacation homes are intense in the region. In addition, the effect of agricultural activities in these areas may cause the quality of soil to decrease. The areas of medium quality in the east and north of the study area are usually the areas where forests exist. With this respect, soil reaction values in these regions are within suitable limits for plants to develop and they are included in very high quality classes (Figure 3g). When the results obtained from measuring the reaction of soil in the study area are assessed in respect to soil quality, it has been found that the situation is quality throughout the region (Figure 3g). That means that there isn't significant chemical degradation in soil in the region. However, it must not be disregarded that soil reaction can show quicker changes when compared to other factors.

In general manner areas that have very high quality that are represented with a rate of 3% in terms of SQI are located on the plain base (Figure 4). The city of Edremit, which is the

biggest settlement area of the region, is located on this productive area is the leading conclusion that is pointed the most. When SQI values of the study area are taken into account, it has been seen that areas with medium quality has a wide range of 74% (Figure 4). Akcay, Burhaniye and Havran that are also significant settlements are located on these areas. It indicates that settlement areas are determined without considering the soil quality (Figure 4). When the extent of areas of very poor quality is taken into account, they are seen at the north of Altinoluk and at the high parts of Ida Mountains (Figure 4). The region, which is determined as the most intense place of areas of very poor quality, is the high parts of Madra Mountain. This shows that these areas are particularly sensitive to degradation. It has been found that areas of very poor quality are represented with a rate of 23% that should be taken into consideration (Figure 4). According to that, it is understood that the effect of the change in vegetation or climate quality at high parts would create irreversible conclusions with regards to soil. Determining soil at wide areas as medium quality has also indicated that the ground cover is at a sensible threshold.

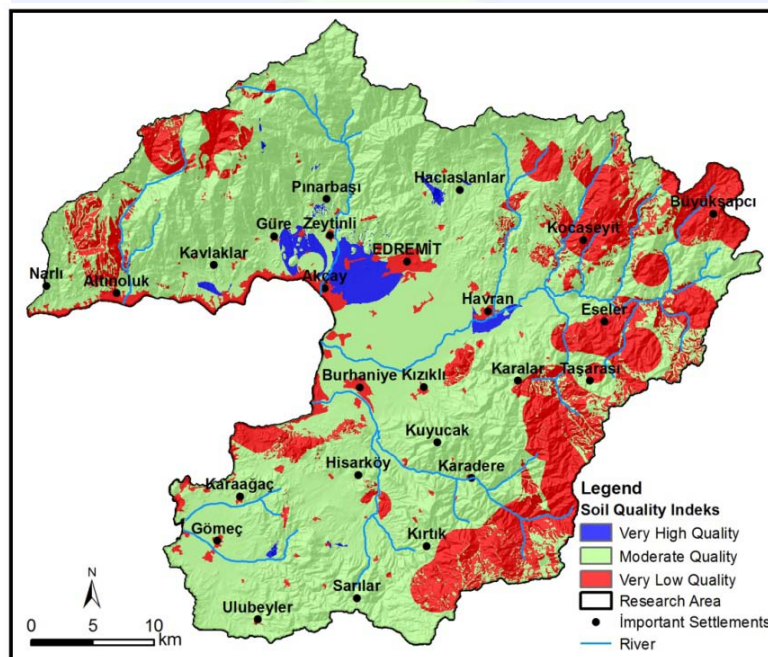


Figure 4. Soil-Quality Index Map

CONCLUSION

SQI has been used for determining soil quality at the study area. The studies, which were made by using soil quality index in the Mediterranean Region, have been stated to be quite important tools for fighting with land degradation, desertification and similar environmental problems (Kosmas et al., 1999). In accordance with the findings of SQI at the study area have indicated that the biggest problem is the settlements creating pressure on the regions where soil quality is high. It is known that settlements have many direct or indirect negative effects on the quality of soil (Pavao-Zuckerman, 2008; Pickett and Cadenasso, 2009). In accordance with analyses made in this study, these are problems that may be resourced from having low soil quality at high sections in other words

mountainsides. When the low level of soil quality and the high risk of erosion at mountainsides of the Mediterranean Basin are taken into account, the most efficient way to avoid from them is the continuity of vegetation (Dur'an Zuazo et al., 2006). Accordingly, in order to protect ground cover in the study area, it is necessary to protect vegetation. Moreover, it is necessary to take cautious decisions on the extent of settlements at plain base, where soil depth is high. Therefore, soil quality levels have been determined with this study and conclusions that can be used for continuity have been introduced.

REFERENCES

- Altinbas, U. Cengel, M. Uysal, H. Okur, B. Okur, N Kurucu, Y. and Delibacak, S. 2004. *Soil Science*. EU Faculty of Agriculture, University Publication No: 557, Bornova/Izmir.
- Ardahanlioglu, O. Oztas, T. Evren., S. Yilmaz H. and Yildirim, Z.N. 2003. Spatial variability of exchangeable sodium, electrical conductivity, soil pH and boron content in salt and sodium-affected areas Igridir plain (Turkey). *Journal of Arid Environments*, 54, 495-503.
- Balci, N. 1996. *Soil Conservation*, Istanbul University, University Publication No: 394. Istanbul.
- Butzer, K.W. 2005. Environmental history in the Mediterranean world: cross-disciplinary investigation of cause-and-effect for degradation and soil erosion. *Journal of Archeological Science*, 32; 1773-1800.
- Dur'an Zuazo V.H, Francia Mart'inez J. R., Rodr'iguez P.C.R., Mart'inez Raya A. and C'arceles R. B. 2006. Soil-erosion and runoff prevention by plant covers in a mountainous area (SE Spain): implications for sustainable agriculture. *Environmentalist*. 26: 309–319.
- Gursoy, B. 2009. *The study of hydrogeological data and GIS application of Edremit Plain*, Istanbul Technical University, Institute of Science, Unpublished master's thesis in the Department of Geological Engineering, Istanbul.
- Karabulut, M. and Kucukonder M. 2008. Soil erosion identification using GIS techniques in Kahramanmaras Plain and its vicinity. Kahramanmaras Sutcu Imam University, *Journal of Engineering Sciences*, 11(2), 14-22
- Karlen, D.L., M.J. Mausbach, J.W. Doran, R.G. Cline, Harris, R.E and Schuman, G.E. 1997. Soil quality: A concept, definition, and framework for evaluation. *Soil Science Society of America Journal*, 61 (1):4-10.
- Kantarci, D. 2000. *Soil Science*. Istanbul University Publication No. 4261, Istanbul.
- Kosmas, C., Kirkby, M. and Geeson, N., 1999. *Manual on: Key indicators of desertification and mapping environmentally sensitive areas to desertification*. European Commission Energy, Environment and Sustainable Development. EUR 18882:87.

- Oberthur, T., Goovaerts, P. and Dobermann, A., 1999. Mapping soil texture classes using field " texturing, particle size distribution and local knowledge by both conventional and geostatistical methods. *European Journal Soil Science*, 50, 457–479.
- Pavao-Zuckerman, M.A. 2008. The nature of urban soils and their role in ecological restoration in cities. *Restoration Ecology*, 16: 642–649.
- Pickett, S.T.A. and Cadenasso, M.L., 2009. Altered resources, disturbance, and heterogeneity: a framework for comparing urban and non-urban soils. *Urban Ecosystems*, 12: 23–44.
- Sarioglu, F.E. and Dengiz, O., 2012. Assessment of different parametric approaches in land evaluation studies. *Soil Water Journal*, 1(2), 82-87.
- Schoenholtz, S.H., Van Miegroet, H. and Burger, J.A., 2000. Physical and chemical properties as indicators of forest soil quality: Challenges and opportunities. *Forest Ecology and Management*, 138: 335-356.
- Uzun, A. and Somuncu, M., 2013. Using Remote Sensing Method to Evaluate the Change of the Land Cover/Land Use In Time In Madra Mountain. *Balıkesir University Social Sciences Journals*, 16, 1-21.



A Case Study on Comparison of the Classifiers provided by Google Earth Engine for Land Cover Identification

Naime Çelik¹, Mehmet Dikmen¹

¹*Department of Computer Engineering, Baskent University, Ankara, Turkey*

ABSTRACT

As the number of freely available geospatial data with higher spatial resolutions increases day by day, applications and processing tools begin to require more capabilities, thus, new methodologies evolve and new platforms emerge as a consequence. Google Earth Engine (GEE) is one of these platforms operating on cloud. It provides many readily available data sets as well as a platform for processing and visualization of geospatial data. In addition, GEE is freely available for research, education, and nonprofit use. This study explores classification algorithms and tools provided by the platform by using band combination of LiDAR Canopy Height Model and Rugosity with extracted principle components of hyperspectral image of same area. The LiDAR and hyperspectral image were collected by NASA Goddard's LiDAR, Hyperspectral and Thermal (G-LiHT) airborne imager and freely available for use under NASA's data and information policy. These two data were fused together to perform a land cover classification on the study area. For this purpose, various supervised and unsupervised classification algorithms were implemented and then compared by each other by assessing their validity. The results were obtained as a confusion matrix for each classifier and discussed thoroughly with respect to their performances for each cover type. We believe that this study will encourage other researchers to use GEE platform to take the advantage of accessing a large freely available data throughout the world and perform most state-of-the-art methods easily and efficiently to get fast results.

INTRODUCTION

Land cover classification and detection of land cover change over time is very essential for implementation of effective decision mechanisms. Various problems such as disasters, uncontrolled urban development, declining environmental quality, loss of basic agricultural land, destruction of important wetlands and reduction of habitats impact land cover and lead to increase in necessity of accurately identified land cover information. Increasing application areas and data diversity in geographical information systems and remote sensing upsurge the work done in this regard.

The Google Earth Engine (GEE) Project, established in 2009, has been available since 2010 with the petabytes of satellite data and tools for high performance analysis and

interpretation (Hancher, 2014). It has free use for research, education and non-commercial work (Padarian et al., 2015). GEE platform provides various classification algorithms. Shelestov et al. (2017) explained and compared the classification algorithms that exist in GEE (Support Vector Machine (SVM), Classification and Regression Tree (CART), Random Forests (RFs), GMO Max Entropy, Multi Class Perceptron, Naïve Bayes, Intersection Kernel Passive Aggressive Method (IKPamir), Winnow, Primal Estimated sub-Gradient Solver for SVM (Pegasos)). Ensemble of Neural Networks are not available and Shelestov et al. (2017) proposed one neural network classifier that performed the highest classification accuracy to present in GEE on the Landsat 8 satellite image.

Increasing use of LiDAR (Light Detection and Ranging) data and accessibility of it also has increased the studies in three-dimensional classification. One of these studies (Zou et al., 2016) applies the Object Based Image Analysis method using the intensity values of point data. In a different study performed by Teo & Huang (2016), features such as Intensity and Echo ratio of LiDAR, Grey Level Co-occurrence Matrix of LiDAR and texture of spectral image were used.

The goals of this research are, first to evaluate the potential use of GEE platform with LiDAR data products together with hyperspectral image derivatives on land cover identification, and second, to compare the results obtained from various classifiers provided by GEE and evaluate them.

MATERIALS & METHODS

Data

LiDAR data and Hyperspectral images collected by "NASA Goddard's LiDAR, Hyperspectral and Thermal" (G-LiHT) airborne imager were used in this study. The data tiles used for this study is obtained from webpages, ftp://fusionftp.gsfc.nasa.gov/G-LiHT/Loudon_Jun2015 and ftp://fusionftp.gsfc.nasa.gov/G-LiHT/Keen_Jun2014/. The first area of study is located in Loudon, New Hampshire with the acquisition date of 2015. The second is in Keene, New Hampshire with the acquisition date of 2014. Original horizontal coordinates of data were WGS 84 UTM Zone 19 and vertical coordinates were referenced to Earth Gravitational Model 1996 (EGM96). Horizontal coordinates were converted to WGS84 geographic coordinates for this study. According to Cook et al. (2013), during data acquisition, single-solution GPS-INS was used and real time differential correction was performed using OmniStar HP. Vertical offset bias occurs (<1m) for absolute accuracy of the LiDAR data due to lack of a base station.

Data acquisition specifications were indicated in detail by Cook et al. (2013) and shown in Figure 1. LiDAR data have spatial resolution of 0.24m between points in a scanline and 0.56m between scanline. Hyperspectral images have 114 bands, 15-8nm bandwidth, and their spatial resolution changes 1m to 10m depending on altitude. Radiometric resolution of hyperspectral images is 12bit (Cook et al., 2015).

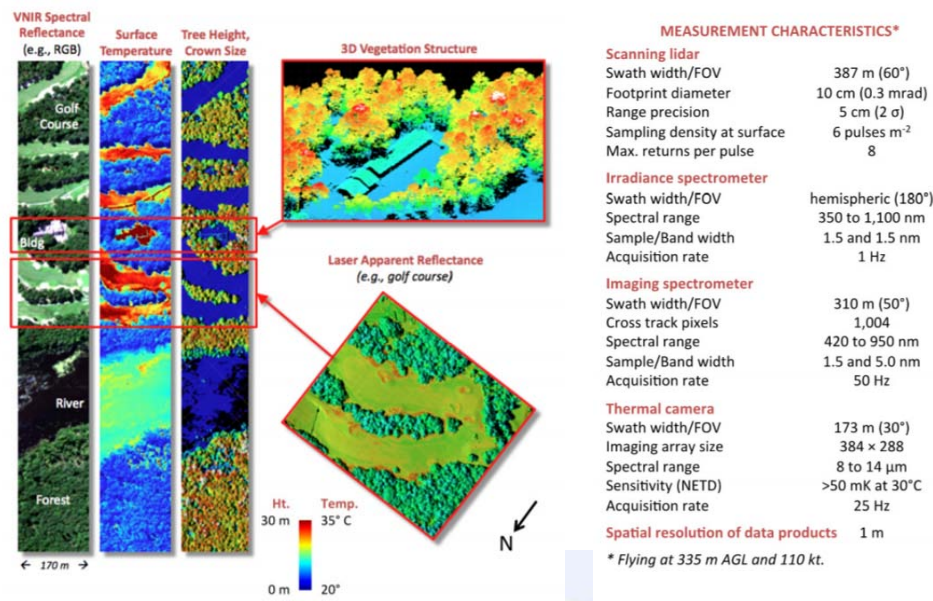


Figure 1. NASA Goddard's LiDAR, Hyperspectral and Thermal (G-LiHT) airborne imager and G-LiHT Data acquisition specifications (Cook et al., 2013)

The first area of study is in Loudon, New Hampshire covering about 385ha and the second is in Keene covering 143ha. Figure 2 shows study areas with hyperspectral images shown as a 55, 33, 16 color composite. LiDAR derivatives, Canopy Height Model (CHM) and Rugosity (standard deviation of height within an area equivalent to a 1/24 ac) were already available in the data repository (Cook et al., 2015). However, the rugosity image was recalculated to obtain the image with more detail based on CHM by using 3 by 3 rectangular kernel.

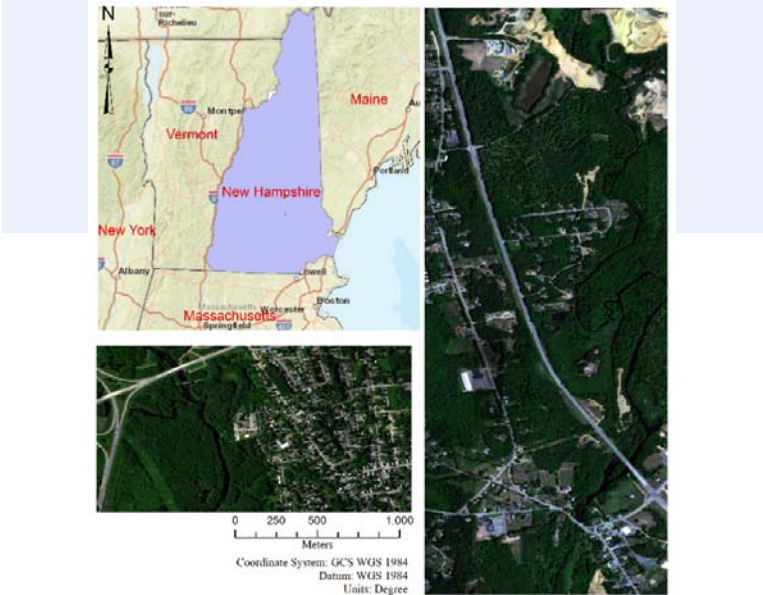


Figure 5. Area of study, Keene (right) and Loudon (left), New Hampshire

Table 1. Percent and Accumulative Eigen Values for Loudon

PCA	EigenValue	% of Eigen Values	Accumulative % of EigenValues
1	32487010.00	78.41	78.41
2	8461768.00	20.42	98.83
3	212465.50	0.51	99.34

Table 2. Percent and Accumulative Eigen Values for Keene

PCA	EigenValue	% of Eigen Values	Accumulative % of EigenValues
1	56373440.00	86.22	86.22
2	6565784.00	10.04	96.26
3	1400333.00	2.14	98.41
4	366207.90	0.56	98.97
5	253865.60	0.39	99.35

Reference Data

Reference data containing land cover classes of the study area was obtained by manually drawing each class. In Loudon, the study area classified into six classes: water, residential, grass, soil, road and forest. The area has disperse and tree dominant land cover state. Figure 3 shows reference data including those six classes. In Keene, five classes were identified as water, residential, grass, road and forest. In some areas, the pixels that were initially assigned as soil in the reference image corresponded 0.15 % of total image, which was negligible, thus, integrated into grass class. Therefore, Figure 4 shows the reference data including only those five classes. The reference image is in WGS84 Geographic Coordinate System (EPSG:4326). Although, all the processing was performed in this coordinate system, GEE platform displays maps in EPSG:3857, WGS 84 Pseudo-Mercator-Spherical Mercator (Google Earth Engine, 2016) as in Google Maps, OpenStreetMap and Bing.



Figure 3. Reference Image for Loudon and Hyperspectral Image of RGB = 55, 33, 16

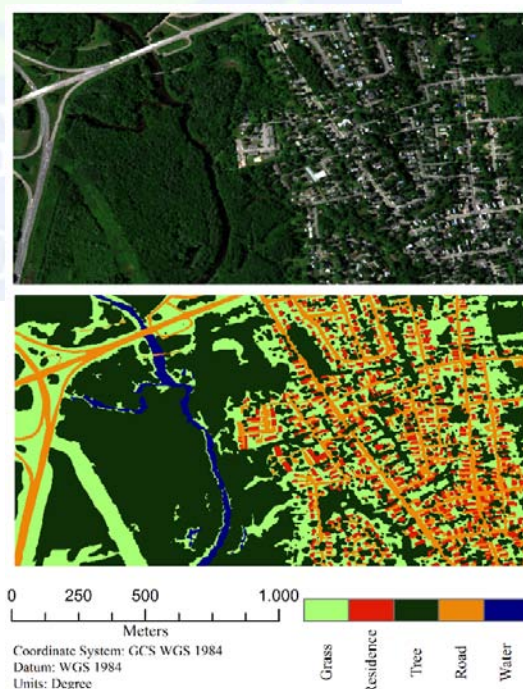


Figure 4. Reference Image for Keene and Hyperspectral Image of RGB = 55, 33, 16

METHODOLOGY

1. Feature Reduction: Principle Component Analysis and Creating Composite Bands

The feature reduction of hyperspectral image was performed by using ArcGIS software via Principle Components (PCs) Tool due to “Computation timed out” error appeared in GEE. GEE calculated PCA only with large tile scale parameters, which results disappearance of some of the small size classes such as residence during classification process. The number of PC images selected is 3 for Loudon and 5 for Keene, which corresponds to at least 99.34% of the total variance in the data (Table 1 and Table 2). Composite images were created by adding 2 more bands, namely CHM and Rugosity. As a result, a composite image with five bands for Loudon and a composite image with seven bands for Keene were obtained.

2. Classification

From GEE’s pixel based supervised classification methods, Classification and Regression Tree (CART), Random Forests (RFs), Minimum Distance (MD) with Mahalanobis distance and Support Vector Machine (SVM) were used in this study. In addition, two of the unsupervised classification (Clustering in GEE) methods were also utilized. Classification and Regression Tree (CART) classifier grows large classification tree by recursively partitioning data and by looking the lowest cross-validation estimate of error (regression tree) or the highest gain of entropy and it prunes tree (Guszcza, 2005). Random Forest (RF) is a widely used classifier by many (Padarian et al., 2015; Shelestov et al., 2017). It produces more than one classification and regression trees and the output classes become the most voted class by these trees. Minimum Distance (MD) classifier is offered with various distance functions in GEE and, in this study Mahalanobis distance was selected since it provided a higher accuracy compared to other metrics. In multi-feature space, the measure is used for minimizing the distance between classes and unknown pixels (Japan Association of Remote Sensing, 1996). Support Vector Machine (SVM) classifier separates classes with an optimal hyperplane (Awad M., Khanna R., 2015). From various kernels, radial basis function (RBF) was used in this work.

In addition to mentioned supervised classification methods, two of them were examined. These clusters use WEKA (Waikato Environment for Knowledge Analysis) implementations. CascadeSimpleKMeans selects best k number of classes and LVQ is a clusterer implementing Learning Vector Quantization algorithm (Weka, 2017).

3. Implementation in GEE

Classification was performed using GEE’s playground – a web based IDE – through a JavaScript (Google Earth Engine API, 2017) Code Editor which offers variety of geospatial analysis tools and visualization interface. The PC images and LiDAR derivatives were imported into GEE assets. In order to train classifiers, the reference data was sampled with 10,000 random points and uploaded as shp file.

Each classifier used in this study was trained based on the sampled point data and the trained classifiers were then used to classify whole study area. The resulted classified

image was post-processed with a morphological filter (focal mode) similar to median filter to reduce the noise caused by pixel-based classification. Figure 5 shows Random Forest classification result and the result of square kernel focal mode filter with radius 2 after 3 iterations.

Table 3 Test Consumer and Producer Accuracy
Supervised Classifiers In Loudon

	Random Forest	SVM (RBF)	CART	Minimum Distance
Classifier Training Total Accuracy	0.9546	0.8101	0.8294	0.7437
Test Consumer's accuracy (rows)				
Grass	0.7646	0.7666	0.7807	0.6872
Soil	0.8402	0.8211	0.8194	0.8304
Residence	0.6108	0.4822	0.5989	0.4261
Road	0.7970	0.8031	0.7642	0.8611
Tree	0.9693	0.9577	0.9649	0.9616
Water	0.6672	0.4456	0.5459	0.6186
Test Producer's accuracy (columns)				
Grass	0.8686	0.8226	0.8407	0.8652
Soil	0.7924	0.7497	0.7735	0.7264
Residence	0.6564	0.6264	0.6269	0.5636
Road	0.7526	0.6719	0.7263	0.5607
Tree	0.9256	0.9232	0.9319	0.9093
Water	0.9306	0.9074	0.9244	0.7962
Test overall accuracy:	0.8883	0.8683	0.8828	0.8570
Test Kappa:	0.8046	0.7696	0.7944	0.7499

Table 4 Test Consumer and Producer Accuracy
Supervised Classifiers In Keene

	Random Forest	SVM (RBF)	CART	Minimum Distance
Classifier Training Total Accuracy	0.9669	0.8396	0.8545	0.7800
Test Consumer's accuracy (rows)				
Grass	0.7894	0.8017	0.8028	0.7703
Residence	0.7428	0.7073	0.7213	0.6880
Tree	0.9580	0.9429	0.9514	0.9527
Road	0.8416	0.8487	0.8081	0.8346
Water	0.6895	0.4683	0.6580	0.2598
Test Producer's accuracy (columns)				
Grass	0.8619	0.8208	0.8314	0.7816
Residence	0.7086	0.6851	0.6954	0.5947
Tree	0.9070	0.9188	0.9140	0.9014
Road	0.8437	0.7827	0.8469	0.7403
Water	0.9671	0.9425	0.9444	0.9315
Test overall accuracy:	0.8724	0.8580	0.8671	0.8260
Test Kappa:	0.8041	0.7814	0.7958	0.7357

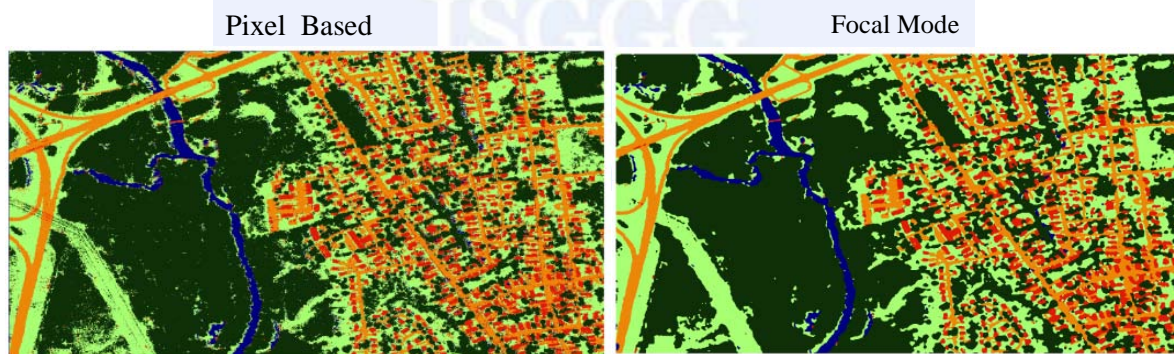


Figure 5. Pixel-based classification and applied focal-mode

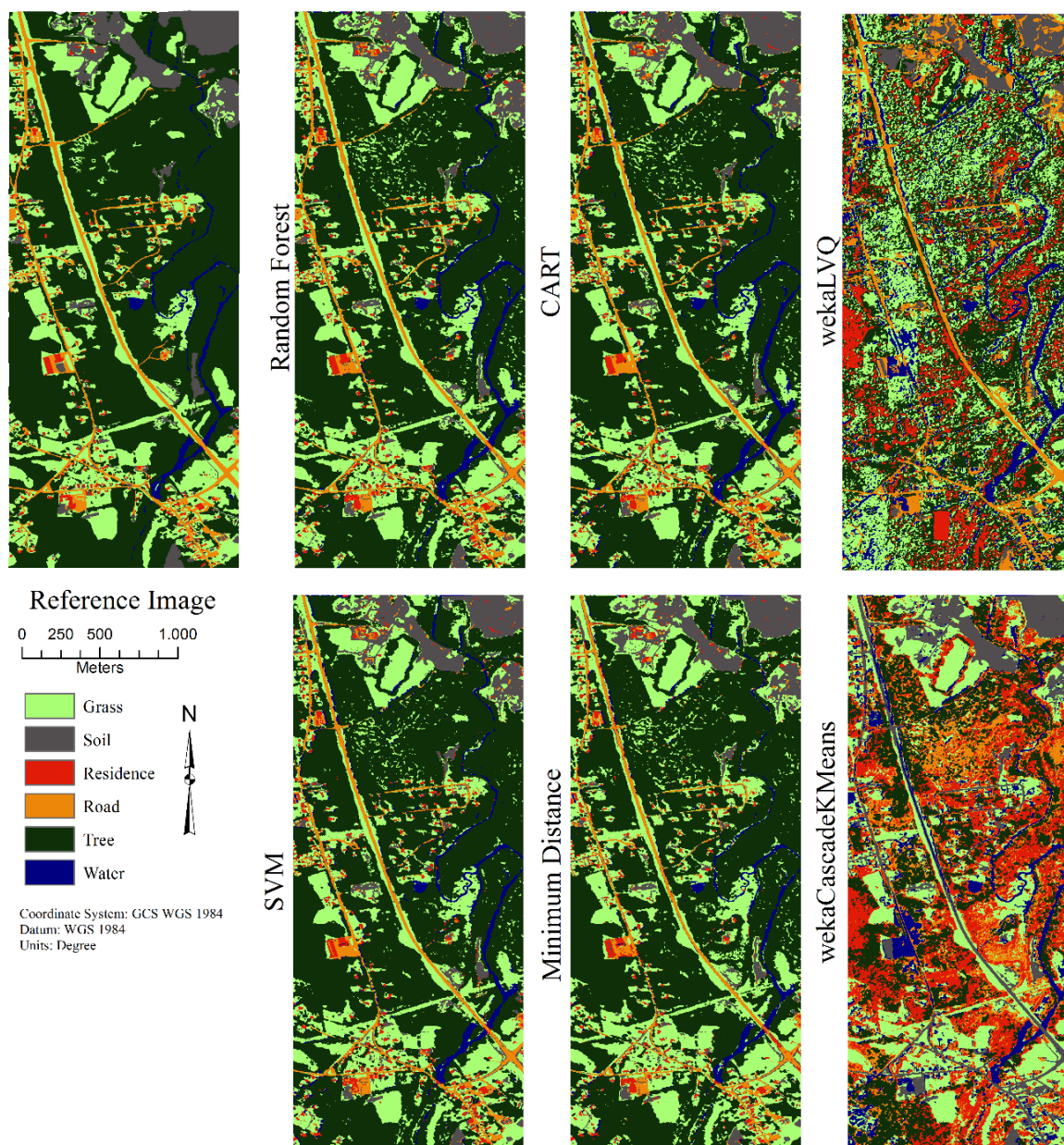


Figure 6. Supervised and Unsupervised classification results for Loudon

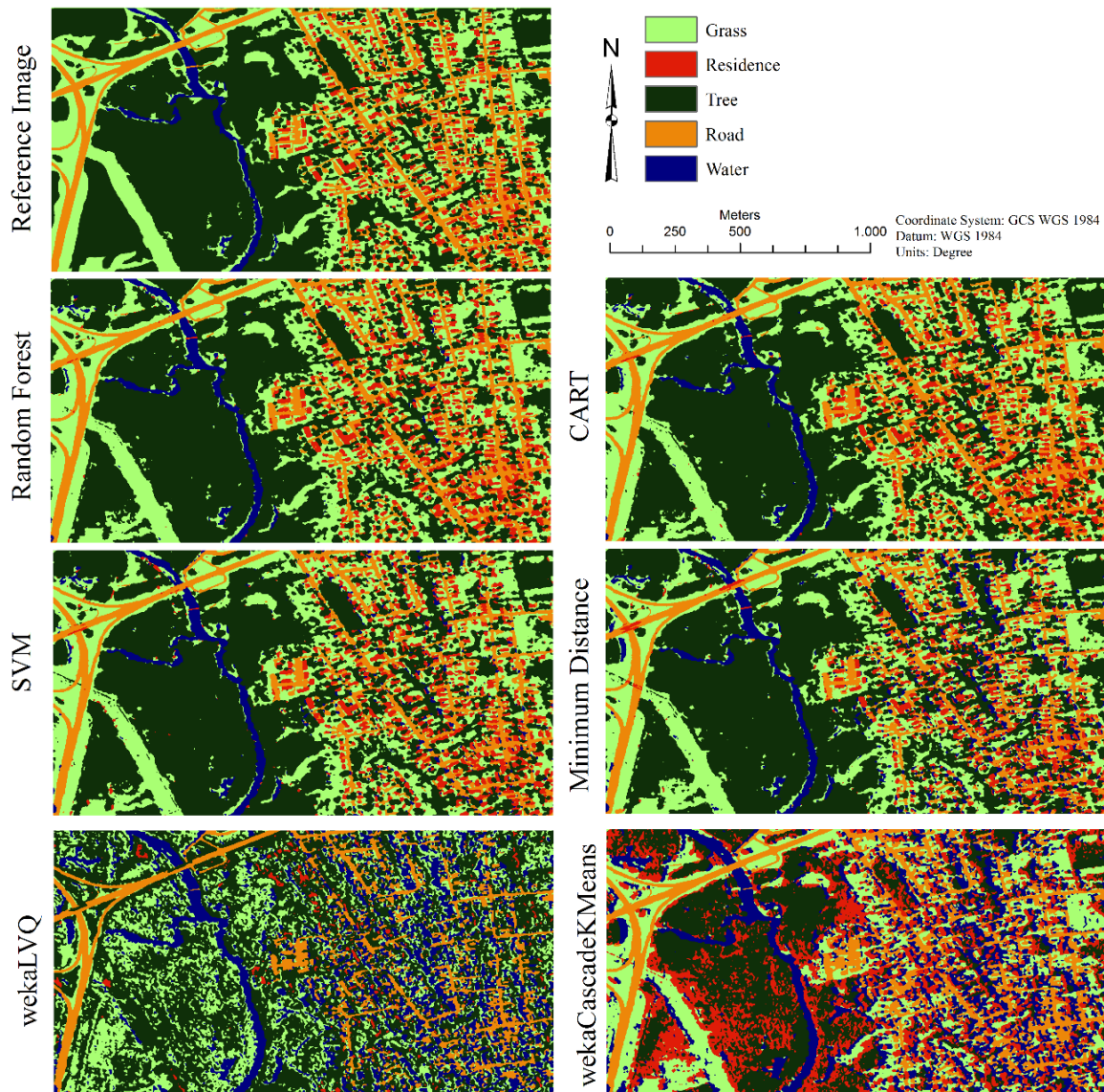


Figure 7. Supervised and Unsupervised classification results for Keene

RESULTS & DISCUSSION

$$\text{Producers accuracy} = \frac{\# \text{ of pixels correctly classified as Class } X}{\# \text{ ground reference pixels in Class } X} \quad \text{Equation 1}$$

$$\text{Consumer accuracy} = \frac{\# \text{ of pixels correctly classified as Class } X}{\text{total \# of pixels classified as Class } X} \quad \text{Equation 2}$$

$$\text{Overall accuracy} = \frac{\# \text{ pixels correctly classified}}{\text{total \# of pixels}} \quad \text{Equation 3 (Horning, 2004)}$$

$$\text{Kappa Coefficient} = \frac{N * d - q}{N^2 - q}$$

N = total # of pixels, k =# of classes
 d =total # of cases in diagonal cells of error matrix

$$q = x_{+j} * x_{i+}$$

$$x_{+j} = \sum_{i=1}^k x_{ij} \text{ (sum over all rows for columns)}$$

$$x_{+j} = \sum_{i=1}^k x_{ji} \text{ (sum over all columns for rows)}$$

Equation 4
(Lillesand et al., 2004)

Table 5. Random Forest Classifier Results with Different Band Combinations In Loudon

	PCA3B CHM Rugosity	PCA3B CHM	PCA3B Rugosity	PCA3B
Classifier Training Total Accuracy	0.9546	0.9551	0.9566	0.9425
Test Consumer's accuracy (rows)				
Grass	0.7646	0.7510	0.7933	0.7125
Soil	0.8402	0.8409	0.8458	0.8243
Residence	0.6108	0.6240	0.5642	0.4300
Road	0.7970	0.8142	0.8041	0.8355
Tree	0.9693	0.9703	0.9607	0.9402
Water	0.6672	0.5990	0.6674	0.5583
Test Producer's accuracy (columns):				
Grass	0.8686	0.8727	0.8466	0.7784
Soil	0.7924	0.7866	0.7881	0.7845
Residence	0.6564	0.6464	0.6625	0.5811
Road	0.7526	0.7342	0.7382	0.6176
Tree	0.9256	0.9200	0.9394	0.9125
Water	0.9306	0.9291	0.9317	0.9245
Test overall accuracy:	0.8883	0.8839	0.8914	0.8519
Test Kappa:	0.8046	0.7975	0.8081	0.7392

Table 6 Random Forest Classifier Results with Different Band Combinations In Keene

	PCA5B CHM Rugosity	PCA5B CHM	PCA5B Rugosity	PCA5B
Classifier Training Total Accuracy	0.9669	0.9618	0.9560	0.9423
Test Consumer's accuracy (rows)				
Grass	0.7894	0.7836	0.7484	0.5943
Residence	0.7428	0.7363	0.6054	0.5259
Tree	0.9580	0.9590	0.9013	0.8803
Road	0.8416	0.8360	0.8507	0.8090
Water	0.6895	0.6851	0.6293	0.6575
Test Producer's accuracy (columns):				
Grass	0.8619	0.8623	0.7382	0.7141
Residence	0.7086	0.7036	0.7039	0.6280
Tree	0.9070	0.9039	0.8891	0.7822
Road	0.8437	0.8386	0.7596	0.6890
Water	0.9671	0.9536	0.9675	0.9600
Test overall accuracy:	0.8724	0.8695	0.8207	0.7439
Test Kappa:	0.8041	0.8000	0.7233	0.6125

In order to evaluate the performance of the classifiers, error matrices were calculated for each classification method. Error matrices are widely used in remote sensing to assess omission and commission errors for individual classes and categories (Congalton & Green, 2008). GEE provides functions to calculate producer accuracy (Eq. 1), consumer accuracy (Eq. 2), overall accuracy (Eq. 3) and Kappa coefficient (Eq.4).

Table 3 shows consumer and producer accuracies for utilized supervised classifications and Figure 6 contains classified imaged for Loudon. From selected supervised classifiers, Random Forest classifier performed the finest results in overall test accuracy and kappa.

In Loudon, the existence of soil based roads over the study area made it difficult to differentiate them. As a consequence, accuracies of soil and road classes were obtained below 80%. Furthermore, yard areas of many houses have mixed soil and grass content. Table 4 shows accuracies for Keene and Random Forest classifier has the best performance among other classifiers as well.

In both areas of the study, classifiers have a tendency to classify the shadowed locations as water. This leads consumer accuracy of water to be low in opposed to producer accuracy. The best accuracy was obtained for trees, classified above 90% in both areas.

Table 7. Clusterer Results In Loudon

	Weka Cascade KMeans	Weka LVQ
Test Consumer's accuracy (rows)		
Grass	0.7385	0.2283
Soil	0.5616	0.8102
Residence	0.0031	0.0045
Road	0.0238	0.4516
Tree	0.9799	0.7377
Water	0.1910	0.1845
Test Producer's accuracy (columns):		
Grass	0.7730	0.2885
Soil	0.7432	0.4299
Residence	0.0355	0.0266
Road	0.0561	0.7026
Tree	0.3742	0.4749
Water	0.9324	0.9696
Test overall accuracy:	0.4687	0.4464
Test Kappa:	0.3245	0.1919

Table 8. Clusterer Results In Keene

	Weka Cascade KMeans	Weka LVQ
Test Consumer's accuracy (rows)		
Grass	0.7753	0.2394
Residence	0.0144	0.0354
Tree	0.9833	0.6605
Road	0.6540	0.7056
Water	0.0920	0.1060
Test Producer's accuracy (columns)		
Grass	0.5999	0.2157
Residence	0.0370	0.0061
Tree	0.4577	0.5858
Road	0.7662	0.6757
Water	0.9715	0.9792
Test overall accuracy:	0.5071	0.4622
Test Kappa:	0.3720	0.2130

Another experiment was also made to evaluate contribution of CHM and Rugosity on classification. Using Random Forest classifier, the resulted accuracies were investigated by excluding first Rugosity, then CHM and finally both. Table 5 and 6 demonstrates their impacts on classified accuracies. In Loudon, exclusion of CHM gives slightly better overall accuracy. However, in Keene, the same effect is not observed. Instead, overall accuracy falls down with the exclusion of CHM and the addition of Rugosity has minor impact on overall accuracy. It can be concluded that height can be seen as a major factor for identification of the classes in Keene.

After applying unsupervised classification methods, the classes were identified with respect to the reference class, which fits best to the clusterer result, by manual inspection. However, the results presented in Table 7 and 8 are not desirable due to the inconsistency in the number of pixels for different classes. Therefore, clustering algorithms may not be used solely for the land cover identification in the study areas chosen.

CONCLUSIONS

To explore GEE platform and classifiers provided, G-LiHT LiDAR derivatives and hyperspectral images were utilized to obtain land use identification in two areas of the study. In this platform, most of the studies were performed by using low-resolution data such as Landsat image. This study demonstrated that the platform also have potential in use with high-resolution data to test the most popular classification methods and many others with ease and efficiently.

The data used in this study was publicly shared so the one accessing with the link below can also run the code as well. The sample code contains Random Forest classification for Keene.

<https://code.earthengine.google.com/4e36b58775b742f532dcd73f4f81f932>

REFERENCES

- Awad M., Khanna R. (2015) Support Vector Machines for Classification. In: *Efficient Learning Machines*. Apress, Berkeley, CA
- Congalton, R. G., and Green, K.. *Assessing the Accuracy of Remotely Sensed Data: Principles and Practices*. Boca Raton, FL: CRC Press. 2008
- Cook, B., Corp, L., Nelson, R., Middleton, E., Morton, D., McCorkel, J., Montesano, P. (2013). NASA Goddard's LiDAR, Hyperspectral and Thermal (G-LiHT) Airborne Imager. *Remote Sensing*, 5(8), 4045-4066. doi:10.3390/rs5084045
- Cook, Bruce, and Larry Corp. *Metadata For Nasa Goddard's Lidar, Hyperspectral And Thermal (G-LiHT) Airborne Imager*. Nasa, 2015. ftp://fusionftp.gsfc.nasa.gov/G-LiHT/Loudon_Jun2015/metadata/Loudon_Jun2015_metadata.pdf.
- Google Earth Engine. "Projections | Google Earth Engine API | Google Developers." Google Developers, 9 Aug. 2016, developers.google.com/earth-engine/projections. Accessed 24 May 2017.
- Google Earth Engine API. "Earth Engine Code Editor | Google Earth Engine API | Google Developers." Google Developers. Last modified April 27, 2017. <https://developers.google.com/earth-engine/playground>.
- Guszcza, J., (2005). "predictive modeling techniques handouts.", Casualty Actuarial Society Sept. 2005, www.casact.org/education/specsem/f2005/handouts/cart.ppt. Accessed 25 May 2017.
- Hancher, M. (2014). *Planetary-Scale Geospatial Data Analysis with Google Earth Engine*. Retrieved from http://cega.berkeley.edu/assets/cega_events/76/5RS_Matt_Hancher.pdf
- Horning, N. (2004). *Overview of accuracy assessment of land cover products*. Retrieved from http://www.amnh.org/content/download/74332/1391258/file/AccuracyAssessmentOverview_Final.pdf
- Japan Association of Remote Sensing (1996). "11.6 Minimum Distance Classifier." 1999, wtlab.iis.u-tokyo.ac.jp/~wataru/lecture/rsgis/rsnote/cp11/cp11-6.htm.
- Lillesand, T. M., Kiefer, R. W. and Chipman, J. W. (2004) *Remote Sensing and Image Interpretation*, John Wiley, New York
- Padarian, J., Minasny, B., & McBratney, A. (2015). Using Google's cloud-based platform for digital soil mapping. *Computers & Geosciences*, 83, 80-88. doi:10.1016/j.cageo.2015.06.023
- Shelestov, A., Lavreniuk, M., Kussul, N., Novikov, A., & Skakun, S. (2017). Exploring Google Earth Engine Platform for Big Data Processing: Classification of Multi-Temporal Satellite Imagery for Crop Mapping. *Frontiers in Earth Science*, 5. Retrieved from <http://journal.frontiersin.org/article/10.3389/feart.2017.00017/full>
- Teo, T., & Huang, C. (2016). Object-Based Land Cover Classification Using Airborne Lidar and Different Spectral Images. *Terrestrial, Atmospheric and Oceanic Sciences*,

27(4), 491. Retrieved from http://tao.cgu.org.tw/index.php/articles/archive/space-science/item/download/2221_5b8b98b651a0bb07704a90d2450e8c7d

Weka,(2017) Retrieved from

<http://weka.sourceforge.net/doc.packages/cascadeKMeans/weka/clusterers/CascadeSimplerKMeans.html>

Zou, X., Zhao, G., Li, J., Yang, Y., & Fang, Y. (2016). 3D Land Cover Classification Based On Multispectral Lidar Point Clouds. *ISPRS - International Archives of the Photogrammetry, Remote Sensing and Spatial Information Sciences*, XLI-B1, 741-747. Retrieved from <http://www.int-arch-photogramm-remote-sens-spatial-inf-sci.net/XLI-B1/741/2016/isprs-archives-XLI-B1-741-2016.pdf>



Investigation of Normalized Difference Vegetation Index and Land Surface Temperature Using Remote Sensing Techniques for 20 years of Diyarbakir Province

Mehmet Tahir Kavak^{*}, Sabri Karadoğan²

¹Dicle University, Ziya Gökalap Faculty of Education, Department of Physics, 21280 Diyarbakir/Turkey

²Dicle University, Ziya Gökalap Faculty of Education, Department of Geography, 21280 Diyarbakir/Turkey

ABSTRACT

The relationship between vegetation and Land Surface Temperature (LST) using AVHRR (Advanced Very High Resolution Radiometer) for 17 years (1998-2014), NDVI for 20 years (1994-2014) over 94 % and cloud cover for 15 years of Diyarbakir are presented. It is found that the correlations between LST and Normalized Difference Vegetation Index (NDVI) depend on the season-of-year. For winter, the correlation between NDVI and LST is positive. Correlations between LST and NDVI decreased during the warm seasons. Thus temperature-related drought indices may only be used in the warm seasons from June to October, and should be used with caution during cold seasons in Diyarbakir. Since vegetation is high on April and May both month was also studied.

INTRODUCTION

Cloud cover can influence numerous important ecological processes including reproduction, growth, survival, and behavior, yet our assessment of its importance at the appropriate spatial scales has remained remarkably limited. If captured over large extent yet at sufficiently fine spatial grain cloud cover dynamics may provide key information for delineating a variety of habitat types and predicting species distributions.

The Normalized Difference Vegetation Index (NDVI) is a numerical indicator that uses the visible and near-infrared bands of the electromagnetic spectrum, and is adopted to analyze remote sensing measurements and assess whether the target being observed contains live green vegetation or not. NDVI has found a wide application in vegetative studies as it has been used to estimate crop yields, pasture performance, and rangeland carrying capacities among others. It is often directly related to other ground parameters such as percent of ground cover, photosynthetic activity of the plant, surface water, leaf area index and the amount of biomass. NDVI was first used by (Rouse Jr, Haas, Schell, & Deering, 1974) from the Remote Sensing Centre of Texas A&M University. Recently NDVI for Diyarbakir was also studied by (Kavak, Özdemir, Karadoğan, & Yılmaz A, 2015).

^{*} Corresponding Author

Generally, healthy vegetation will absorb most of the visible light that falls on it, and reflects a large portion of the near-infrared light. Unhealthy or sparse vegetation reflects more visible light and less near-infrared light see Figure 1. Bare soils on the other hand reflect moderately in both the red and infrared portion of the electromagnetic spectrum (Holm, Burnside, & Mitchell, 1987).

Moreover, the negative correlations between NDVI and LST are much stronger than those between NDVI and the brightness temperature. Therefore using daytime LST for drought monitoring should be more reasonable than using brightness temperature or nighttime LST (Sun & Kafatos, 2007).

Since we know the behavior of plants across the electromagnetic spectrum, we can derive NDVI information by focusing on the satellite bands that are most sensitive to vegetation information (near-infrared and red). The bigger the difference therefore between the near-infrared and the red reflectance, the more vegetation there has to be. The NDVI algorithm subtracts the red reflectance values from the near-infrared and divides it by the sum of near- infrared and red bands.

$$NDVI = \frac{NIR - RED}{NIR + RED}$$

This formulation allows us to cope with the fact that two identical patches of vegetation could have different values if one were, for example in bright sunshine, and another under a cloudy sky. The bright pixels would all have larger values, and therefore a larger absolute difference between the bands. This is avoided by dividing by the sum of the reflectances.

Theoretically, NDVI values are represented as a ratio ranging in value from -1 to 1 but in practice extreme negative values represent water, values around zero represent bare soil and values over 0.6 represent dense green vegetation

Land surface temperature is how hot the “surface” of the Earth would feel to the touch in a particular location. From a satellite’s point of view, the “surface” is whatever it sees when it looks through the atmosphere to the ground. It could be snow and ice, the grass on a lawn, the roof of a building, or the leaves in the canopy of a forest. Thus, land surface temperature is not the same as the air temperature that is included in the daily weather report. Present work used 1km high resolution AVHRR data from 1995 to 2014. Due to the satellite position 94% of Diyarbakır was studied Figure 2. Day measured average temperatures range from 14.20 degrees Celsius to 14.2 degrees Celsius.

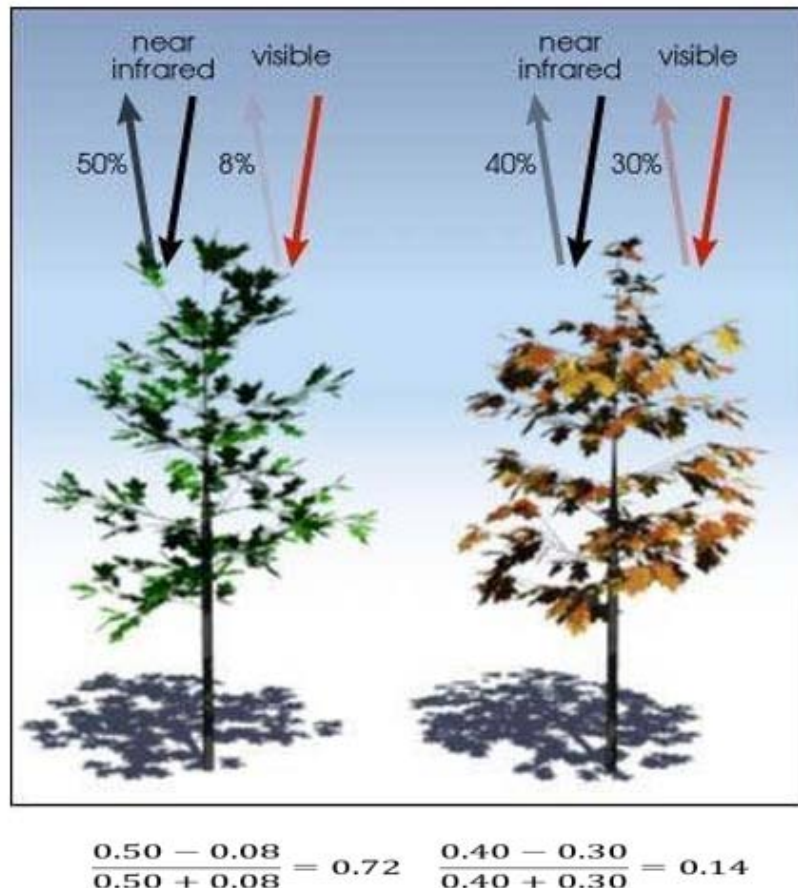


Figure 1. NDVI is calculated from the visible and near-infrared light reflected by vegetation. Healthy vegetation (left) absorbs most of the visible light that hits it, and reflects a large portion of the near-infrared light. Unhealthy or sparse vegetation (right) reflects more visible light and less near-infrared light. The numbers on the figure above are representative of actual values, but real vegetation is much more varied (Herring, 2000).

Night measured average temperatures range from -3.95 degrees Celsius to 22.2 degrees Celsius. Measured average NDVI from 0.14 to 0.43 and average cloud frequency from 8.4 to 62.7. Altitude plays a clear role in temperatures, with mountain ranges like the North American Rockies cooler than other areas at the same latitude (NASA, 2017). Scientists want to monitor how increasing atmospheric greenhouse gases affect land surface temperature, and how rising land surface temperatures affect glaciers, ice sheets, permafrost, and the vegetation in Earth's ecosystems.

Commercial farmers may also use land surface temperature maps like these to evaluate water requirements for their crops during the summer, when they are prone to heat stress. Conversely, in winter, these maps can help citrus farmers to determine where and when orange groves could have been exposed to damaging frost.



Figure 2. Study Area

MATERIAL AND METHOD

To conduct present work LST-D, LST-N and NDVI data from NOAA-AVHRR data was downloaded from (DLR) German Aerospace Center via the internet (<http://eoweb.dlr.de:8080/servlets/template/welcome/entryPage.vm>) Earth observation on the web interface (EOWEB). Cloud removal process was performed by DLR. AVHRR data was chosen since it has large swath width (3000km), spatial resolution(1km), spectral resolution (4-5 AVHRR channels), Temporal resolution(a daily image from DLR formed by using up to five acquisitions), availability (online), cost (free) and data processed (ready for analysis). Cloud data from <http://www.earthenv.org/>, the datasets integrate 15 years of twice-daily remote sensing-derived cloud observations at 1-km resolution using (Moderate Resolution Imaging Spectroradiometer) MODIS which explained by (Wilson & Jetz, 2016).

RESULTS

High temperature difference between day and night may be seen on figure 3. particularly on summer months.

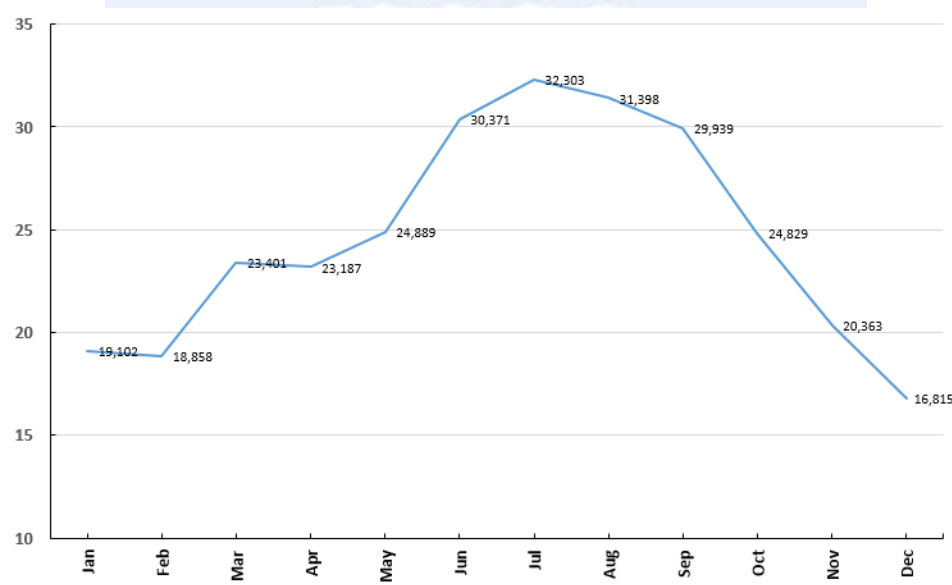


Figure 3. Temperature difference between day and night in °C.

Average LST (day-night), CC (Cloud Cover) and NDVI on figure 4. The behavior of cloud cover and LST's are normal as clouds hamper sun light to heat land. LST-D and NDVI increases significantly together from March to May and then vegetation decreases due to high temperature and seasonal harvest.

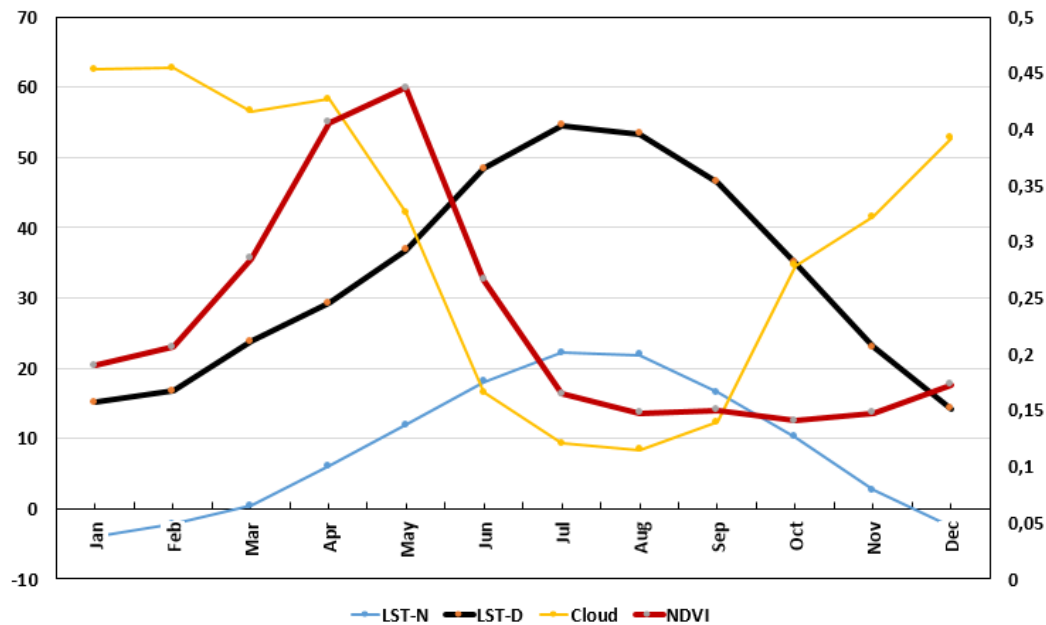


Figure 4. 20 years average LST (Day-Night) 15 years cloud and 20 years NDVI.

Figure 5 shows 20 years average LST and NDVI. An increase on NDVI as well as on LST. Increase on NDVI can be explained together with the development of irrigation technology in agriculture.

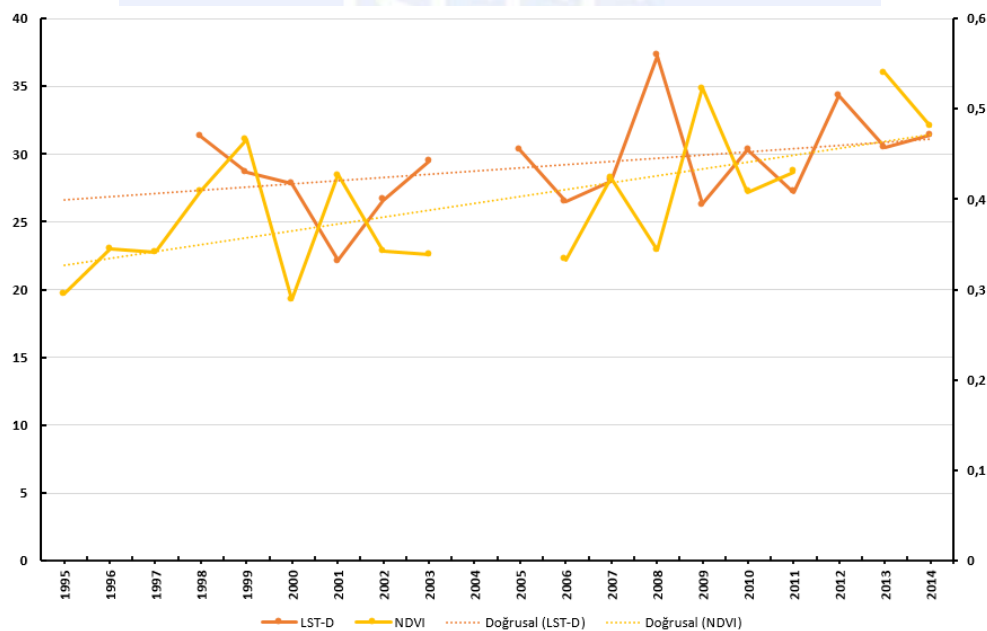


Figure 5. Variation of NDVI, LST (day) for April.

Again an increase on average NDVI as well as on LST for 20 years on figure 6. This can be explained together with the development of irrigation technology in agriculture.

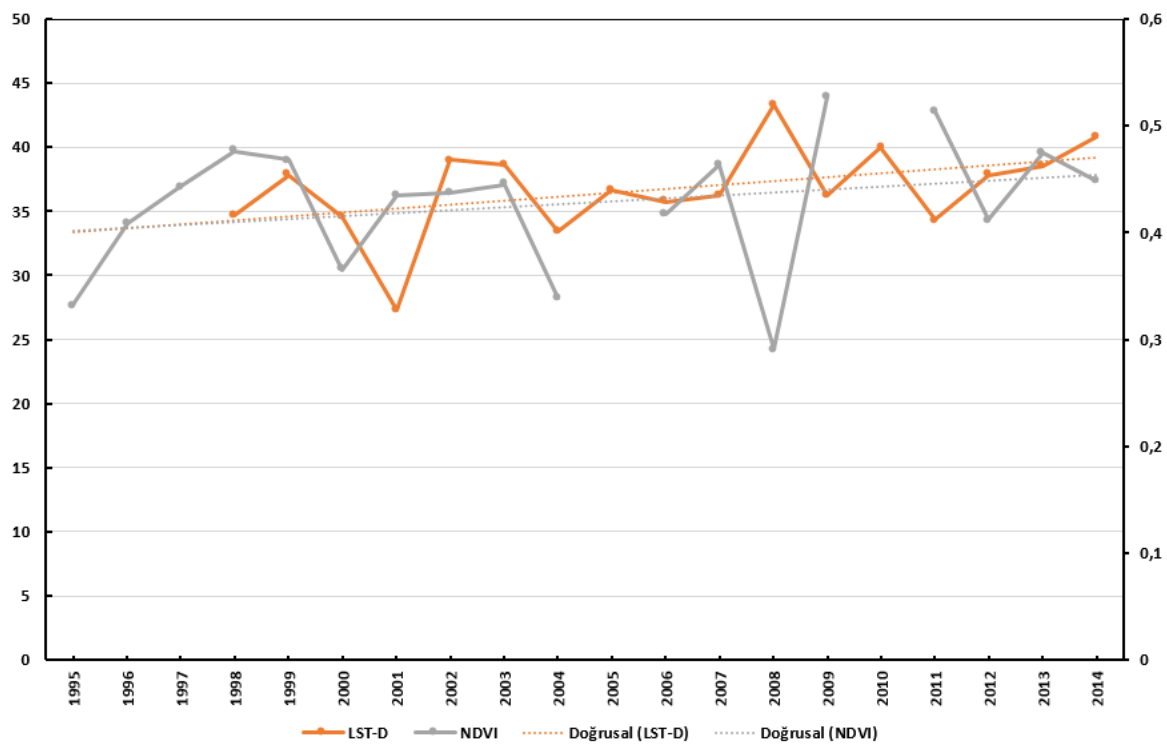


Figure 6. Variation of NDVI and LST (day) for May.

As a result of the analysis of the images we obtained in 1994 and 2014, the amount of green area is observed to vary depending on season or area usage. The months of April and May are the highest in NDVI. Although the tendency for NDVI to increase is linked to improved irrigation technologies in agriculture, it can be made more understandable by using more local and higher resolution satellite images (such as SPOT). In the light of this data, past product yield can be linked to this data to make forecasts, plans or models for the future. This study showed that remote sensing gave us a broad perspective on the region. This method is a very useful method that can be used for other purposes (eg agricultural) in other regions. In this regard, the Ministry of Agriculture retains the right to use SPOT images and bureaucratic obstacles are encountered in obtaining images. The bureaucratic obstacles must be removed in order for these images to be made available to universities for research purposes.

ACKNOWLEDGMENTS

Authors are grateful to the DLR-DFD (German Aerospace Center-German Remote Sensing Data Center) center for giving access to valuable SST data.

REFERENCES

- Herring, J. W. a. D. (2000). Measuring Vegetation (NDVI&EVI). Retrieved 24 August, 2017, from https://earthobservatory.nasa.gov/Features/MeasuringVegetation/measuring_vegetation_1.php
- Holm, A., Burnside, D., & Mitchell, A. (1987). The development of a system for monitoring trend in range condition in the arid shrublands of Western Australia. *The Rangeland Journal*, 9(1), 14-20.
- Kavak, M. T., Özdemir, G., Karadoğan, S., & Yılmaz A. (2015). Uzaktan Algılama Yöntemleri Kullanılarak Diyarbakır İlinin 20 yıl için Bitki Örtüsündeki Değişimin İncelenmesi. Paper presented at the Conference: 29. *Ulusal Tarımsal Mekanizasyon ve Enerji Kongresi*, Diyarbakır.
- NASA. (2017). Land Surface Temperature. Retrieved 24 August, 2017, from https://www.earthobservatory.nasa.gov/GlobalMaps/view.php?d1=MOD11C1_M_LSTD_A
- Rouse Jr, J. W., Haas, R., Schell, J., & Deering, D. (1974). *Monitoring vegetation systems in the Great Plains with ERTS*.
- Sun, D., & Kafatos, M. (2007). Note on the NDVI relationship and the use of temperature-related drought indices over North America. *Geophysical Research Letters*, 34(24).
- Wilson, A. M., & Jetz, W. (2016). Remotely sensed high-resolution global cloud dynamics for predicting ecosystem and biodiversity distributions. *PLoS biology*, 14(3), e1002415.



Designing Land Administration Data Infrastructure Supporting the Interoperability between Applications: Land Valuation Example for Turkey

Arif Cagdas Aydinoglu ^{*1}, Rabia Bovkir¹

¹Department of Geomatics Engineering, Gebze Technical University, 41400, Kocaeli, Turkey.
(aydinoglu; rbovkir)@gtu.edu.tr

ABSTRACT

Effective land information management is quite important issue for the governments in order to provide rightful housing, security of natural resources and food, public welfare and ultimately sustainable development and progress. To achieve sustainable land information management, primary needs are reliable and standardised data about topology, topography, and property. Once different datasets are produced interoperable way, various land related applications can be performed easily and reliably. Geographic Data Infrastructures (GDI) concept has emerged to solve the interoperability issues and develop geographic data production standards. Land valuation is a highly important concept for societies and governments especially for taxation, expropriation, market capitalization and economic activity purposes. In this study, for integrated operability and collaboration between different applications, parcel based real estate evaluation model was designed according to the national GDI requirements. Factors affecting the land value was considered into seven groups and evaluated separately. Then combined for determining the general value approximations in GIS environment.

INTRODUCTION

Effective land information management has significant importance to success sustainable development and progress. Governments have emphasis on the managing the land related information in order to provide rightful housing, security of natural resources and food, social order and public welfare. Definitive, reliable and comprehensive land administration infrastructures promote the geographic enablement and efficient information management (Williamson, 2005; Yomralioglu, 2011). Reliable and interoperable data about topology, topography, and property are the basic requirements for sustainable land information management. In addition, today's land management concept, demands land mapping, registration, and valuation functions as the parts of the land administration policy for better and effective development (Kalantari et al., 2005). In respect to this, applications like real estate valuation, rural-urban transformation, expropriation, land consolidation can be

* Corresponding Author

performed throughout the government agencies more efficiently with the standardised and interoperable data.

With growing technology, data can be obtained from various sources and manipulated in various software with different techniques (Aydinoglu and Yomralioglu, 2006). Therefore, interoperability and management of geographic data sets and services in different thematic applications has become an important requirement for meeting the needs. Recently governments and organizations put emphasis on producing and sharing interoperable geographic datasets, because only with the actual and interoperable geographic data governments can provide the opportunity of data sharing between various thematic applications. For the solution of the interoperability issues, Geographic Data Infrastructures (GDI) concept has emerged with the purpose of developing geographic data production and sharing standards (Budic *et al.*, 2004; Aydinoglu, 2009). Governments and geographic data organizations developed their own GDI to specify their standards and manipulate their data effectively throughout the different applications.

Real Estate valuation has always been a weighty matter for societies and governments for taxation, market capitalization and economic activity purposes (Yalpir, 2007). To achieve better valuation results, interoperability and reliability of the required data coming from different sources is as important as the determination of the method. Because of the intensively performed urban transformation applications, real estate valuation has increased its importance within the sector in Turkey as such in many other countries. Accessing real estate related data easily increases regional development and provide effective land policy implementation (Dawidowicz *et al.*, 2014). Therefore; if real estate related datasets can be obtained from national GDI, problems about data interoperability and access can be solved. Valuable and reliable real estate evaluations can be performed which can directly contribute to the social and economic development.

In this study, main purpose is to analyse the land administration infrastructure of Turkey in terms of the interoperable land management concept. Once the datasets have the same data structure and properties, they can be used effectively in any applications. In land administration concept, valuation extension model was designed within the national GDI to perform land valuation with standardised and interoperable data. For this purpose, a case study was implemented in Pendik to analyse the affectivity of the model and perform by using fuzzy logic approach and geographic analysis tools in GIS environment.

DATA ANALYSIS AND MODEL DESIGN

Real Estate is the immobile and tangible land with all natural and unmanned equipment affixed to land that are both below or above the ground like buildings, site improvements and natural resources (Appraisal Institute, 2001; IVSC, 2011; RICS, 2014). The legal definition according to Aclar and Cagdas (2008) with consideration of the Turkish Civil Law, real estate is the land subject to the ownership and substantive rights with independent sections registered separately in land registers. Valuation term can be used to refer to the estimated value or to refer to the preparation of the estimated value (IVSC,

2011). In reality, it is quite difficult to determine the exact value of real estate because of the many different factors that varies from person to person in terms of quality and quantity. However, due to the application needs or subjective expectations, it is possible to determine the estimated values of real estate by evaluating all the relevant factors. In this way, objective and subjective criteria are evaluated separately and unit values reflected to the whole real estate are determined (Bulut Nas, 2011).

The most general excepted factors affect the value of the real estate are determined according to the nationally and internationally accepted standards and academic researches (CMB, 2006; TDUB, 2011; IVSC, 2011, TKGM, 2011; RICS, 2014; TEGoVA, 2016; Yomralioglu 1993; Nisanci, 2005; Candas 2012; Yalpir et al., 2016). Determined and complied factors can be grouped into four basic categories as Legal Factors, Locational Factors, Physical/Zoning Factors and Socio-Economic Factors.

After determining the factors, data requirement analysis for these factors according to the INSPIRE and TUCBS data theme for evaluating the possibility to carry out real estate valuation within the national and international GDI. After the evaluation, it was determined that data themes corresponding most of the factors are available within both standards. Some of the factors cannot be provided in TUCBS because it is still developing. However, INSPIRE data themes are more detailed and comprehensive and almost all data factors can be obtained for real estate evaluation process.

According to determined criteria in Table.1, a real estate evaluation model was designed as an extension of Turkish National GIS (TUCBS). Designed model is associated with the land registry and cadastre data theme (TUCBS.TK) because real estate is a kind of spatial unit inside cadastre concept. *TK_TasinmazDeger* extension was added to the model as a subclass of *TK_Parsel* (Figure 1). *TK_TasinmazDeger* feature class is related with seven thematic factor groups relating to the real estate; EnvironmentalFactors, Utilization, Planning, PublicService, CulturalFactors, Transportation and SocialFactors which affect the real estate value (Figure 1).

Table 1. Factors effecting real estate value

LEGAL FACTORS	LOCATIONAL FACTORS	PHYSICAL/ZONING FACTORS
Ownership Status <ul style="list-style-type: none"> • Full Ownership • Joint Ownership 	Health Organizations <ul style="list-style-type: none"> • Healthcare Centres • Hospitals 	Building Geometry <ul style="list-style-type: none"> • Frontage Length • Frontage Number • Geometric Shape
Legal Restrictions <ul style="list-style-type: none"> • Mortgage • Easement • Annotation 	Educational Institutions <ul style="list-style-type: none"> • Primary-High School, University • Additional Courses 	Position in Cadastral Block
Legal Transactions <ul style="list-style-type: none"> • Land Amalgamation • Subdivision 	Governmental Agencies <ul style="list-style-type: none"> • Governorate/District • Governorate/Municipality • Courthouse 	Landscape <ul style="list-style-type: none"> • Mountain, Valley, Forest • Lake, River, Sea • City View
Zoning Status <ul style="list-style-type: none"> • TAKS/KAKS • Number of Allowed Floors • Building Layout • Allowed Construction Style 	Public Transportation <ul style="list-style-type: none"> • Airport • Terminal, Coach Station • Metro/Tram • Bus, Minibus • Port, Harbour, Pier • Under/Over Pass 	Road Condition <ul style="list-style-type: none"> • Access to Street • Road Connections • Highways, cross roads Parking Area
Taxation Current Market Value	Attraction Centres <ul style="list-style-type: none"> • City Centre • Town Square 	Industrial Zones
SOCIO-ECONOMIC FACTORS	Security Units <ul style="list-style-type: none"> • Police Station • Gendarmerie Station • Fire Station 	Unit Price and Cost Income (Rent, Business Income)
Population Density <ul style="list-style-type: none"> • Migration Rate • Age Distribution 	Underground, Ground, Aboveground Features <ul style="list-style-type: none"> • Slope • Ground Condition • Air Quality • Noise 	Traffic Density / Congestion Alternative Transportation
Social Stratification <ul style="list-style-type: none"> • Education Level • Income Rate • Unemployment Rate 	Shopping Centers <ul style="list-style-type: none"> • Mall, Market Square • Commercial Enterprise 	Cultural Centres <ul style="list-style-type: none"> • Cinema, Theatre • Historical / Touristic Places
Social Relations <ul style="list-style-type: none"> • Neighbourhood Relationships • Landlord/Tenant Status 	Deleterious Areas <ul style="list-style-type: none"> • Waste Discharge Zones • Treatment Facilities • Dump Sites • Swamp Areas • Natural Disaster Zones • Undeveloped Stream Areas 	<ul style="list-style-type: none"> • Infrastructure Services • Drinking / Tap Water • Natural Gas • Electricity • Sewage • Drainage
Environmental Status <ul style="list-style-type: none"> • Popular Neighbourhood • Building Density • Development Potential 	Green Space <ul style="list-style-type: none"> • Forest, Copse • Park, Playground • Picnic Side • Recreation Area 	

- Planning group includes data about planning conditions of real estate like building coverage ratio, floor area ratio, zoning status, allowed floor number, existing of parking area.

- Environmental Factors group includes data about environmental conditions of real estate such as existence of green space, distance to deleterious and unpleasant areas.
- Transportation group includes data about transportation facilities such as existence and type of the public transportation, density, distance to main roads.
- Utilization group includes data affecting the utilization such as slope, aspect and visibility.
- Cultural Factors group includes data about cultural facilities such as libraries, cinema and theatre centres, art galleries, conference halls.
- Public Services group includes data about proximity to public services and public facilities such as administrative facilities, education facilities, healthcare facilities, religious facilities and infrastructure opportunities.
- Socio-Cultural Factors group includes data about social status of real estate owners and neighbours. Related data can be average age, education level, income and population density.

Each class defining the factor groups uses the data sets coming from different geographic data themes in TUCBS and uses external data when necessary. It is expected that if data coming from different sources are converted into TK_TasinmazDeger data exchange format, these data can be used in the real estate valuation applications effectively. Detailed representation of TK_TasinmazDeger with its relations is shown in Figure 1.

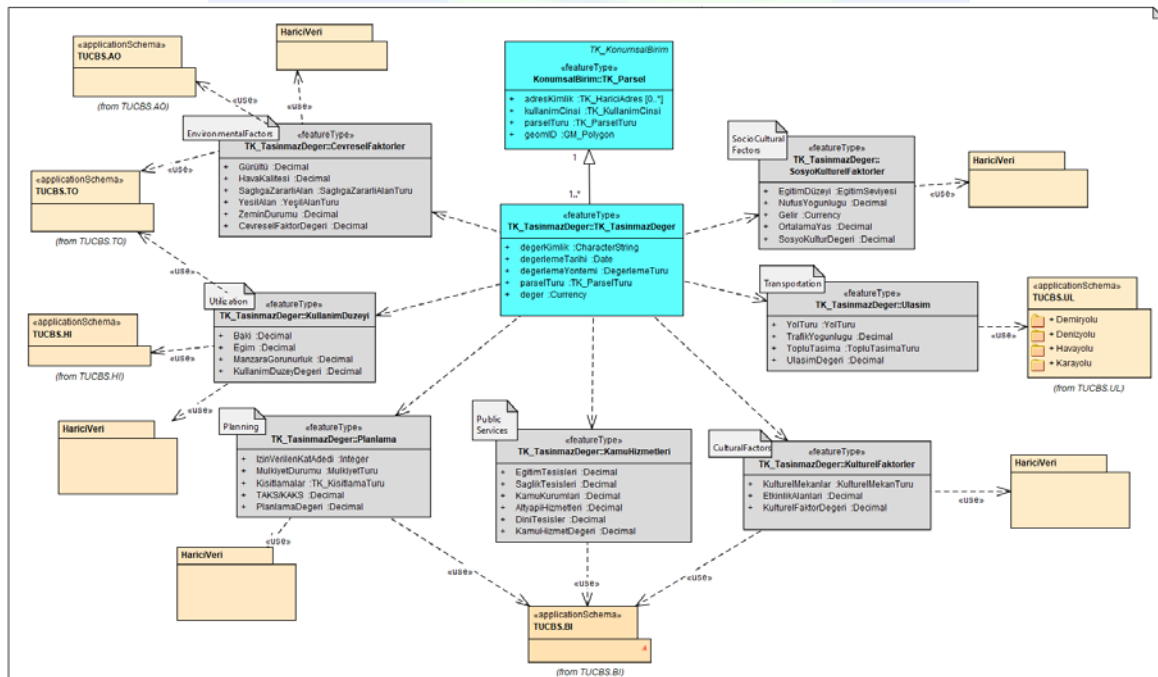


Figure 1. Detailed representation of TK_TasinmazDeger with its relations

CASE STUDY

Pendik district of Istanbul province was chosen as the study area for the application in Turkey. Pendik was chosen because as the study area because it has a large surface area (190 km²), urban and rural variety and 7.5 km of shoreline that provides a wide perspective. Available source data was gathered for study area and source dataset structures were transformed into related TUCBS data models for data interoperability by using ETL (Extract-Transform-Load) tools in HALE (Humboldt Alignment Editor). Schema mapping process was performed and all related attributes were mapped and transformation process was executed for transforming XSD files into GML format data.

After data transformation, ArcGIS software with its geographical analysis tools was used to implement the model and perform valuation calculations. Because information can be the form of verbal expressions such as large, small and little in fuzzy logic, it is an effective method for processing oral variables, which is very important for valuation process (Nedeljkovic, 2006). In addition, a lot of studies revealed that fuzzy logic approach is highly effective for real estate evaluation (Bagnoli and Smith, 1998; Hansen, 2003; Gonzalez and Formoso, 2006; Kusan et al., 2010; Bogataj et al., 2011; Hajnal, 2014; Sarip and Hafez 2015). That's why in this study for real estate evaluation process fuzzy logic is used with geographic analysis functions.

In this study, all factors are grouped in thematic factor groups rather than determining a specific range for each factor and these thematic factor groups evaluated in fuzzy logic. Firstly, raster datasets were produced by using geospatial analysis tools in GIS. According to the characteristics determined for each thematic factor, fuzzy membership functions were defined and applied. In this way, each pixel in the raster data receives different pixel values ranging from 0 to 1. Then, fuzzy overlay maps were created for each thematic factor group by using fuzzy overlay functions in ArcGIS program. Each thematic group gives an approach for evaluating and identifying the general situation of land in the point of different thematic perspectives (Figure 2).

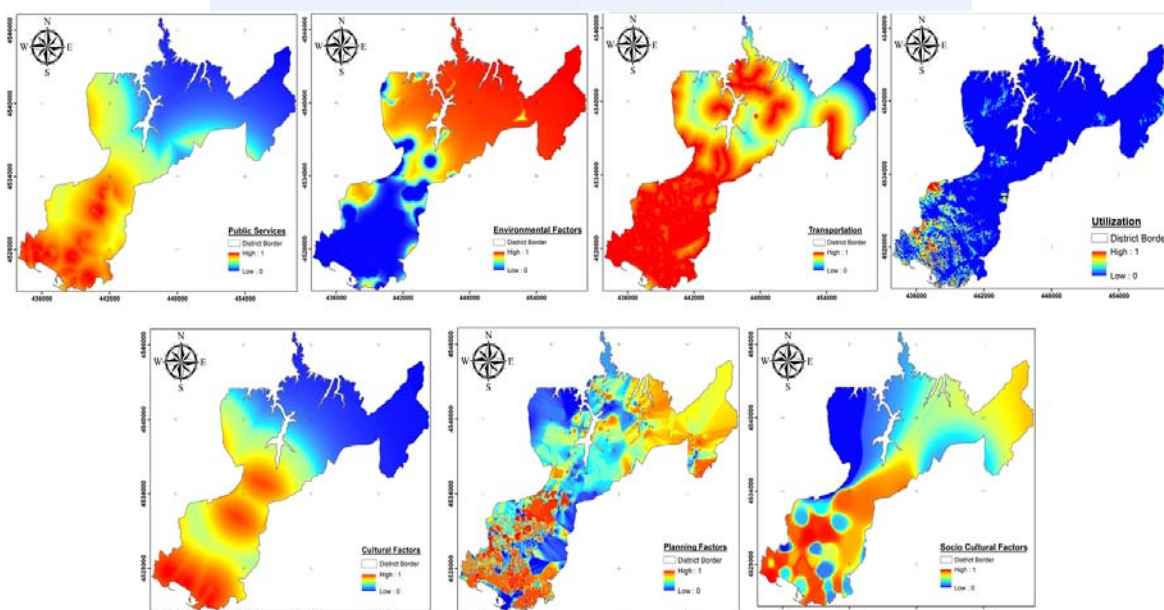


Figure 2. Fuzzy overlay maps for thematic factor groups

Value estimations can be calculated by combining the values of each thematic group. For the integration of these thematic data, their effects and weights over the process should be considered. For this purpose, weighted overlay analysis was performed. Related studies (Yomralioglu, 1993; Yomralioglu and Nisanci, 2004; Nisanci, 2005; Cakir and Sesli, 2013; Derinpinar, 2014; Yalpir and Bunyan Unel, 2016) were examined and analysed in detail. Weights of each factor group were determined after examining researches, statistics and questionnaire studies in Turkey (Table 2). Considering these weights, Weighed Sum overlay function was applied and weighted fuzzy overlay map was produced (Figure 3). Produced map demonstrates the value trends for the study area.

Table 3: Weights of the Thematic Groups

<i>Thematic Group</i>	<i>Weight</i>
<i>Planning</i>	0.82
<i>Environmental Factors</i>	0.78
<i>Transportation</i>	0.75
<i>Utilization</i>	0.70
<i>Cultural Factors</i>	0.68
<i>Public Services</i>	0.68
<i>Social Factors</i>	0.60

Fuzzy based weighted overlay operation gives a general evaluation approach for land valuation process. Produced maps from the analysis reflected close and logical tendency to the reality. It is seen that coastline and the area near the D100 highway have high values and the rural areas near to the Omerli Dam have low values (Figure 3). Also, near to the metro stations, Sabiha Gokcen Airport and attraction centers (shopping centers, cinema) have high values.

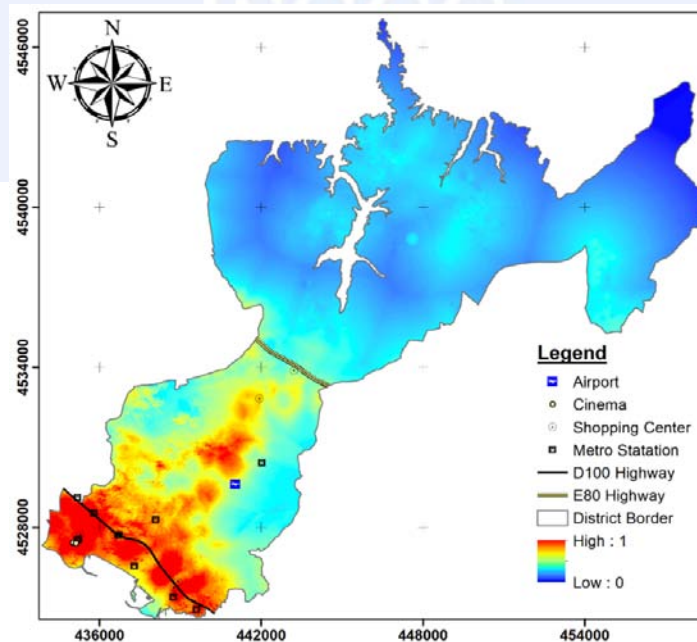


Figure 3. Weighted fuzzy overlay map

CONCLUSION AND DISCUSSION

Primary purpose of this study is to analyse the national land administration infrastructure for performing interoperable and reliable land related applications by using public data. Once the data interoperability is provided, stakeholder needs for different land related applications like expropriation, real estate valuation, taxation, rural-urban transformation, land consolidation are supposed to be met. For this purpose, TUCBS.TK model was improved and land valuation model was designed as an extension to provide a standardised and interoperable valuation model within national GDI.

After the designing the model, for analysing the operability of the designed model and performing a valuation process with standardised data within the TUCBS a case study in Pendik was performed. Source data sets which has different data structures was combined and transformed into TUCBS standard by using designed ETL tools. Designed land valuation model was implemented by using fuzzy logic and geographical analysis in GIS environment. Produced fuzzy weighted surfaces demonstrates the thematic pattern of land values in the study area. However, produced map is not an ideal valuation map that reflects the exact land parcel values. It represents the close and logical tendency to the real values and with future research, if advance statistical methods examine in detail with train data, more accurate values can be calculated. Also, if proposed model implemented as a collective software, an automated valuation process can be performed within national GDI.

REFERENCES

- Aclar A., Cagdas V., 2008. *Taşınmaz (Gayrimenkul) Değerlemesi*. 2nd Edition, HKMO Publication.
- Appraisal Institute, 2001. *The Appraisal of Real Estate*. Illinois: Appraisal Institute.
- Aydinoglu A. C., Yomralioglu T., 2006. Information Infrastructure Approach: Spatial Data Infrastructure Implementation Issues in Turkey. *XXIII. International FIG Congress*, CD, Munich, Germany, October 8-13.
- Aydinoglu, A.C., 2009. *Türkiye İçin Coğrafi Veri Değişim Modelinin Geliştirilmesi*. Thesis (PhD). Karadeniz Technical University.
- Bagnoli C., Smith H. C., 1998. The Theory of Fuzzy Logic and its Application to Real Estate Valuation. *Journal of Real Estate Research*, 16 (2), 169-199.
- Bogataj M., Tuljak Suban D., Drobne S., 2011. Regression-Fuzzy Approach to Land Valuation. *Central European Journal of Operations Research*, 19, 253-265.
- Budic, Z.N., Feeney, M.E., Rajabifard, A., Williamson, I., 2004. Are SDIs serving the needs of local planning? Case study of Victoria. *Environment and Urban Systems*, 28, 329-351.
- Bulut Nas B., 2011. *YSA ve DVM Yöntemleri ile Taşınmaz Değerlemesi için Bir Yaklaşım Geliştirme*. Master Thesis, Selcuk University.

- Cakir, P. and Sesli, A., 2013. Arsa Vasıflı Taşınmazların Değerine Etki Eden Faktörlerin ve Bu Faktörlerin Önem Sıralarının Belirlenmesi. *Electronic Journal of Map Technologies*, 5(3), 1-16.
- Candas, E., 2012. *Taşınmaz Değerlemesi İçin Mevzuat Altyapısının Modellenmesi*, Master Thesis, Istanbul Technical University.
- CMB (Capital Markets Board of Turkey), 2006. *Sermaye Piyasasında Uluslararası Değerleme Standartları Hakkında Tebliğ*. Ankara: Capital Markets Board of Turkey.
- Dawidowicz, A., Radzewicz, A., Renigier-Bilozor, M., 2014. Algorithm for purposes of determining real estate markets efficiency with help of land administration system. *Survey Review*, 46 (336), 189-204.
- Derinpinar, M. A., 2014. *Bulanık Mantık ile Coğrafi Bilgi Teknolojilerini Kullanarak Taşınmaz Değerlemesi: Sarıyer-Istanbul Örneği*, Thesis (MSc). Istanbul Technical University.
- Gonzalez M. A. S., Formoso, C. T., 2006. Mass Appraisal with Genetic Fuzzy Rule-based Systems. *Property Management*, 24 (1), 20-30.
- Hajnal I., (2014), "Continuous Valuation Model for Work-in-progress Investments with Fuzzy Logic Method", *Procedia Engineering*, 85, 206-213.
- Hansen H. S., 2003. A fuzzy Logic Approach to Urban Land-use Mapping. *The 9th Scandinavian Research Conference on Geographical Information Science, Espoo, Finland*, June 4-6.
- International Valuation Standards Council (IVSC), 2011. *International Valuation Standards*. London: International Valuation Standards Council.
- Kalantari, M., Rajabifard, A., Wallace, J., Williamson I., 2005. An Interoperability Toolkit for e-Land Administration. Expert Group Meeting on Incorporating Sustainable Development Objectives into ICT Enabled Land Administration Systems, 9-11 November 2005 Melbourne, Australia.
- Kusan, H., Aytekin, O., Ozdemir, I., 2010. The Use of Fuzzy Logic in Predicting House Selling Price. *Expert Systems with Applications*, 37, 1808-1813.
- Nedeljkovic, I., 2006. Image Classification Based on Fuzzy Logic. *Remote Sensing and Spatial Information Sciences*, 34, 1-6.
- Nisanci R., 2005. *Coğrafi Bilgi Sistemleri ile Nominal Değerleme Yöntemine Dayalı Piksel Tabanlı Kentsel Taşınmaz Değer Haritalarının Üretilmesi*. Doctorate Thesis, Karadeniz Technical University.
- Royal Institution of Chartered Surveyors (RICS), 2014. *Professional Valuation Standards*. London: Valuation Professional Group of the Royal Institution of Chartered Surveyors.
- Sarip, A.G., Hafez, M.B., 2015. Fuzzy Logic Application for House Price Prediction, *International Journal of Property Sciences*, 5(1), 24-30.

- TDUB (Turkish Appraisers Association), 2011. TUGDES (Turkey Valuation Standards) Draft Study.
- TEGoVA (The European Group of Valuers' Associations), 2016. *European Valuation Standards*. 8th Edition, Belgium: Gillis Printing.
- TKGM, 2011. *4th Component of Land Registry and Cadastre Modernization Project (TKMP): Determination and registration of real estate value*. Ankara: General Directorate of Land Registry and Cadastre.
- Williamson, I., 2005. A Land Administration Vision. Expert Group Meeting Incorporating Sustainable Development Objectives into ICT Enabled LAS, 9-11 November Melbourne.
- Yalpir S., 2007. *Bulanık Mantık Metodolojisi ile Taşınmaz Değerleme Modelinin Geliştirilmesi ve Uygulanması: Konya Örneği*. Doctorate Thesis, Selcuk University.
- Yalpir, S. and Bunyan Unel, F., 2016. Türkiye 'de ve Uluslararası Çalışmalarda Arsa Değerlemede Kullanılan Kriterlerin İrdelenmesi ve Faktör Analizi ile Azaltımı. *Afyon Kocatepe University Journal of Science and Engineering*, 16, 303-322.
- Yomralioglu, T., 1993. *A Nominal Asset Value-Based Approach for Land Readjustment and Its Implementation Using Geographical Information Systems*, Thesis (PhD). Newcastle University.
- Yomralioglu, T. and Nisanci, R., 2004. *Nominal Asset Land Valuation Technique by GIS*. FIG Working Week 2004, 22-27 May Athens.
- Yomralioglu, T., 2011. Dünya'da arazi yönetimi, *Sustainable Land Management Workshop in Turkey*, 26-27 May, Okan University, İstanbul.

Identification of Future Land-Use Conflict and Landscape Pattern in Denizli, Turkey

Sevgi Gormus¹, Serhat Cengiz², Sermin Tagil³

¹ Department of Landscape Architecture, Faculty of Forestry, Bartin University, 74200, Bartin, Turkey, sevgigormus@gmail.com

² Department of Landscape Architecture, Faculty of Fine Arts and Design, Inonu University, Malatya, Turkey, srhtcengiz@gmail.com

³ Department of Geography, Faculty of Arts and Sciences, Balikesir University, 10100 Balikesir-Turkey, stagil@balikesir.edu.tr

ABSTRACT

Denizli city is one of the nine cities in Turkey that has grown the most in economy and population in the last thirty years. The growing economic structure and position of the city have caused the population increase. It is envisaged that the new urban areas required due to population growth will develop on agricultural landscapes, archaeological landscapes and natural landscapes. The prediction of the risks that occur in spatial planning is now possible through various scenarios. Paul Zwick's Land Use Conflict Identification Strategy (LUCIS) is one of the goal driven Geographic Information Systems (GIS) models that produces a spatial representation of where agriculture, conservation, and urban land use suitability will be in future conflict and helps illustrate potential future alternative land-use scenarios. The overall goal of this research has to isolate and quantify future land-use conflict in Denizli and effectively create future land-use scenarios for future. Visualizing how land-use change was spatially distributed, and where competing land-use classifications will be in conflict, have been examined by using LUCIS for the future of Denizli.

INTRODUCTION

The cities, namely urban, are an attraction center for the better part of the world's population due to their economic opportunities. Hence, this fact leads to an increase in urban population. In this period, if there would be no remigration, it is foreseen that increase in population will gradually rise. Due to increased demand, growth in urban areas would bring along ecological problems and land-use conflict in future.

Land use conflict can be defined as a comparison on suitability of different land-use categories in a specific land area (Carr and Zwick 2007). Equal suitability metrics of a land area can also be referred as land use conflict. For a specific land use category, having a higher suitability metric than other categories imply that there is no conflict in the relevant land area. In this case, this land area maintains its actual land use. By means of this

approach, a potential land use conflict can be predicted for a whole region (Carr ve Zwick 2007).

The important thing is to be able to take measures against future land use conflicts. In order to accomplish this, future land use purposes should be modeled. In this scope, Geographic Information Systems (GIS) can be helpful tools for responding researches on landscape. Most of the important ecological issues can be revealed easily thanks to GIS. In addition, the Land Use Conflict Identification Strategy (LUCIS) is also a model which determines the land use conflicts in GIS environment. It's an overlapping technique for land use suitability through maps. The foundations of LUCIS models rest on an "ecological perspective" developed by McHarg. In the "map overlay method", a technique developed by McHarg within the framework of ecological planning approach, physical and social variables are included in decision making process by probing in terms of their economic benefits. This technique, in the later years, has been used a method in GIS for "suitability analyzes/suitability evaluation". Within the context of this model, suitable areas for urban settlement, agricultural activities and conservation are determined. While defining these areas, priority and suitability criteria are applied through decision support systems (Carr and Zwick, 2007).

The main aim of this study is to reveal land use conflicts that are critical for understanding how urban dynamics and ecosystems transform, and making policy for urban. In the study, land use scenarios in relation with agricultural areas, conservation areas and settlement areas are created. Potential conflicts between three land-uses in Denizli city are detected by using LUCIS model in the scope of these three use category. The conflicts between agricultural area, conservation area and settlement area are evaluated through a comparison with the Environmental Master Plan's land use planning. The results of this study allows shareholders to interactively choose areas for improvement in future in order to arrive a consensus on population planning activities and critical decisions that affect land use changes.

MATERIAL AND METHOD

The Study Area: Having a surface area of 11.868 km², Denizli province constitutes approx. 1.5% of Turkey and 18.5% of the Aegean Region. Denizli consists of 19 districts in total, including central districts Pamukkale and Merkezefendi (Figure 1). The study is confined in an area of 1135 km² which contains Merkezefendi and Pamukkale districts (the borders of new metropolitan municipality). In this area, there exists archeological landscapes, natural landscapes and agricultural landscapes such as Pamukkale travertine, Hierapolis and Laodicea ancient cities (Figure 1).

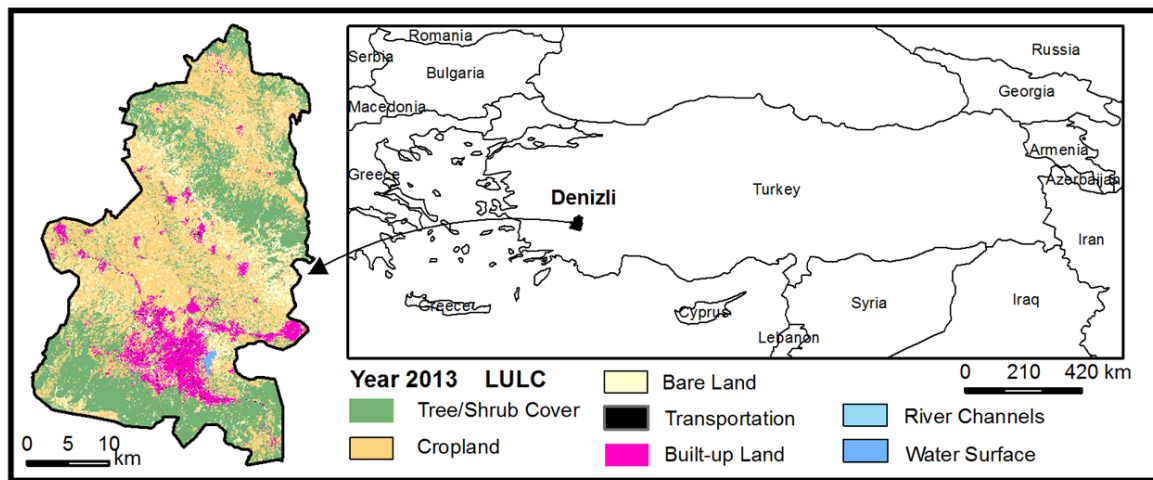


Figure 1. The geographical location of the study

The Data: In the study, LANDSAT 5 (1987), LANDSAT 7 (2000) and LANDSAT 8 (2013) images geographically (spatially) referenced according to WGS 84 (35 N) projection were used. Obtaining of data and numerical analyzes of them were conducted via various software in a numerical environment. The classifications were done within the scope of CORINE program. After determining the class of land-use and land cover to be used in classification, thanks to the object oriented classification method in eCognition software, the classification was performed. eCognition allows to classify with two main classification method. These methods utilize ‘nearest neighbor’ and ‘fuzzy membership’ functions. While the ‘nearest neighbor’ method defines the classes obtained via sample objects that should be decided on for each class by the user, the ‘fuzzy membership’ defines intervals of important characteristics for the areas in which the objects belong to a specific class or lie beyond a particular level (Oruç et al., 2007). Therefore, classification via eCognition software was particularly preferred since it makes enable to generate results in different levels due to its ability to reflect the characteristic of an object depending on level of its class hierarchy.

In the study, 1:25,000 scale Environmental Master Plan (2007), the Forest Management Plan (Denizli Regional Directorate of Forestry, 2014), roads, rivers, conservation areas, etc. were used for generating geographical and ecological variables and creating Digital Elevation Model (DEM) altitude and slope maps; TUIK (Turkish Statistical Institute) data were used for obtaining economic, infrastructural and demographical information; interviews with local government units, institutional data related with legal-administrative structure and legislation outputs were used for defining political variables.

Also, UTM (Universal Transverse Mercator) WGS 84 UTM Zone 36 N coordinate system was applied. When converting all numerical maps into raster format, the resolution of 15mx15m was preferred.

The Method: Unlike from traditional land-use suitability, LUCIS is a goal driven model (Carr and Zwick 2005). Based on three main type of land-use, the model generates

potential/prospective scenarios for landscape patterns in future. The reason for the strength of LUCIS is to show alternative land-use scenarios rested on priorities and conflicts of shareholders over land-use.

In the study, the LUCIS model is adapted in the context of change in landscape pattern (Figure 2). Affecting and affected land use according to analyze on change in landscape pattern were considered as baseline. These land uses are; agricultural areas (affected), conservation areas (affected) and urban settlement areas (affecting). Within the scope of the variables affected all three land uses (geographical, ecological, demographical, economic, political and infrastructure), for each of land use category, goals, aims and sub-aims were defined and then the suitability concept was developed accordingly. The maps of weighted rates (Table 1-3) obtained for agricultural areas, conservation areas and urban areas were modeled via ESRI ArcGIS 10.1 software Model Builder tool by using Weighted Overlay Analysis (figure 2).

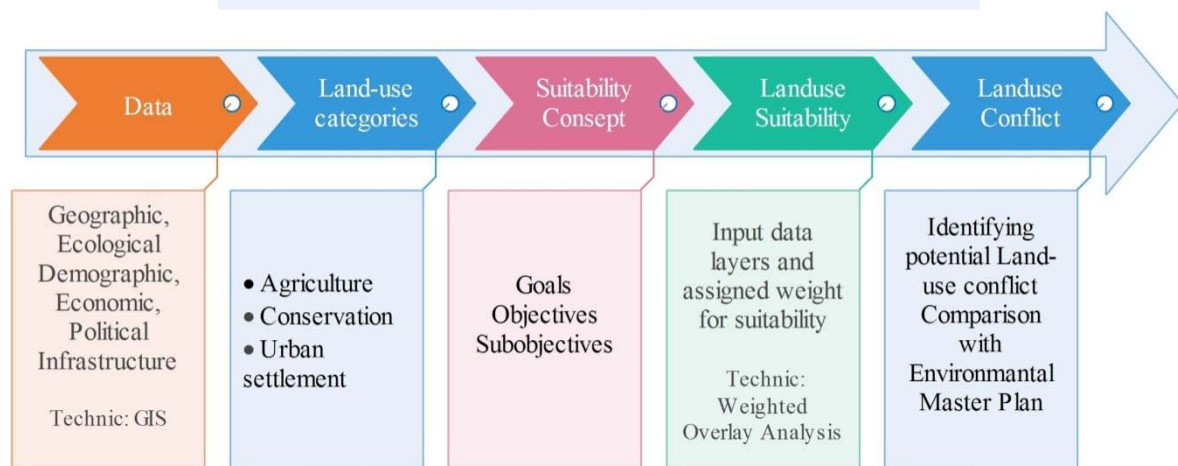


Figure 2. The stages of LUCIS Model (adapted from Carr and Zwick, 2007)

Table 1. Sub-criteria for suitability of urban settlement areas, and their weight rates.

Goal: YeGa: Suitable areas for settlement	
1. YeKo (L: .400): Determining suitable areas for housing	
1.1. YeKoa1 (L: .333): Physically suitable areas for housing	
1.1.1. YeKoa1a1 (L: .040): Soil	
1.1.2. YeKoa1a2 (L: .023): Slope	
1.1.3. YeKoa1a3 (L: .017): Altitude	
1.1.4. YeKoa1a4 (L: .081): Risk of landslide	
1.1.5. YeKoa1a5 (L: .077): Environmental problems	
1.1.6. YeKoa1a6 (L: .427): Seismicity	
1.1.7. YeKoa1a7 (L: .069): Distance to sources of pollution	
1.1.8. YeKoa1a8 (L: .265): Erosion risky areas	
1.2. YeKoa2 (L: .333): Economically suitable areas for housing	
1.2.1. YeKoa2a1 (L: .154): Proximity to highways	
1.2.2. YeKoa2a2 (L: .057): Distance to nearest urban cluster	
1.2.3. YeKoa2a3 (L: .032): Distance to railways	
1.2.4. YeKoa2a4 (L: .301): Distance to power lines	
1.2.5. YeKoa2a5 (L: .457): Distance to health centers	
1.3. YeKoa3 (L: .333): Socio-culturally suitable areas for housing	

1.3.1. YeKoa3a1 (L: .059): Distance to important places
1.3.2. YeKoa3a2 (L: .289): Distance to recreational areas
1.3.3. YeKoa3a3 (L: .476): Distance to city center
1.3.4. YeKoa3a4 (L: .176): Distance to sources of water
2. YeHs (L: .400): Suitable areas for service sector
2.1. YeHsa1 (L: .500): Physically suitable areas for service sector
2.1.1. YeHsa1a1 (L: .066): Slope
2.1.2. YeHsa1a2 (L: .292): Erosion risk areas
2.1.3. YeHsa1a3 (L: .516): Seismicity
2.1.4. YeHsa1a4 (L: .089): Altitude
2.1.5. YeHsa1a5 (L: .037): Soil
2.2. YeHsa2 (L: .500): Economically suitable areas for service sector
2.2.1. YeHsa2a1 (L: .250): Proximity to highways
2.2.2. YeHsa2a2 (L: .250): Distance to city center
2.2.3. YeHsa2a3 (L: .250): Distance to the nearest urban cluster
2.2.4. YeHsa2a4 (L: .250): Distance to intersections of highways
3. YeSa (L: .200): Suitable areas for industry sector
3.1. YeSaa1: Physically suitable areas for industry sector
3.1.1. YeSaa1a1 (L: .057): Slope
3.1.2. YeSaa1a2 (L: .248): Erosion risk areas
3.1.3. YeSaa1a3 (L: .550): Seismicity
3.1.4. YeSaa1a4 (L: .034): Altitude
3.1.5. YeSaa1a5 (L: .112): Soil
3.2. YeSaa2: Economically suitable areas for industry sector
3.2.1. YeSaa2a1 (L: .483): Proximity to highways
3.2.2. YeSaa2a2 (L: .088): Distance to city center
3.2.3. YeSaa2a3 (L: .157): Distance to the nearest urban cluster
3.2.4. YeSaa2a4 (L: .272): Distance to railways

Table 2. Sub-criteria for suitability of agricultural areas and their weight rates

Goal: TaGa Determining suitable areas for agriculture
1. TaTa1 (L: .750): TaGa Determining suitable areas for field agriculture
1.1. TaTa1a1 (L: .800): TaGa Determining physically suitable areas for field agriculture
1.1.1. TaTa1a11 (L: .182): Soil
1.1.2. TaTa1a12 (L: .098): Slope
1.1.3. TaTa1a13 (L: .239): Distance to sources of pollution
1.1.4. TaTa1a14 (L: .065): Irrigation conditions
1.1.5. TaTa1a15 (L: .039): Distance to sources of water
1.1.6. TaTa1a16 (L: .027): Actual land cover
1.1.7. TaTa1a17 (L: .351): Flood plain
1.1.7.1. TaTa1a12 (L: .200): Sloping areas
1.1.7.2. TaTa1a15 (L: .400): Distance to water
1.1.7.3. TaTa1a16 (L: .400): Land cover
1.2. TaTa1a2 (L: .200): Determining economically suitable areas for field agriculture
1.2.1. TaTa2a11 (L: .750): Distance to highways
1.2.2. TaTa2a12 (L: .250): Distance to the nearest urban cluster
2. TaHa1 (L: .250): Determining suitable areas for animal husbandry
2.1. TaHa1a1 (L: .359): Distance to pastures and meadows
2.2. TaHa1a2 (L: .124): Distance to market
2.3. TaHa1a3 (L: .517): Slope

Table 3. Sub-criteria for suitability of conservation areas and their weight rates

Goal: KoGa: Determining suitable areas for nature conservation
1. KoDo (L: .500): Determining suitable areas for nature conservation

1.1. KoDoa1 (L: .333): Bio-physical suitability for nature conservation
1.1.1. KoDoa1a1 (L: .119): Distance to nearest urban cluster
1.1.2. KoDoa1a2 (L: .119): Distance to highways
1.1.3. KoDoa1a3 (L: .027): Slope
1.1.4. KoDoa1a4 (L: .065): Distance to sources of pollution
1.1.5. KoDoa1a5 (L: .186): Distance to sources of water
1.1.6. KoDoa1a6 (L: .022): Actual land cover
1.1.7. KoDoa1a7 (L: .310): Erosion
1.1.8. KoDoa1a8 (L: .153): Distance to power lines
1.2. KoDoa2 (L: .333): Determining suitable areas in terms of biodiversity for nature conservation
1.2.1. KoDoa2a1 (L: .750): Distance to Flora and Fauna existence
1.2.2. KoDoa2a2 (L: .250): Distance to wildlife improvement area
1.3. KoDoa3 (L: .333): Suitability of area status for nature conservation
1.3.1. KoDoa3a1 (L: .429): Distance to nature conservation zones
1.3.2. KoDoa3a2 (L: .429): Distance to natural park
1.3.3. KoDoa3a3 (L: .143): Distance to afforestation areas
2. KoKu (L: .250): Determining suitable areas for cultural preservation
2.1. KoKua1 (L: .333): Determining bio-physically suitable areas for cultural preservation
2.1.1. KoKua1a1 (L: .500): Distance to nearest urban cluster
2.1.2. KoKua1a2 (L: .500): Distance to highways
2.2. KoKua2 (L: .667): Determining suitable areas in terms of area status for cultural preservation
2.2.1. KoKua2a1 (L: .500): Distance to archaeological site
2.2.2. KoKua2a2 (L: .500): Distance to special environmental protection areas
3. KoKt (L: .250): Determining suitable areas for cultural tourism
3.1. KoKta1 (L: .500): Determining bio-physically suitable areas for cultural tourism
3.1.1. KoKta1a1 (L: .089): Distance to nearest urban cluster
3.1.2. KoKta1a2 (L: .089): Distance to highways
3.1.3. KoKta1a3 (L: .035): Slope
3.1.4. KoKta1a4 (L: .246): Distance to sources of pollution
3.1.5. KoKta1a5 (L: .155): Distance to sources of water
3.1.6. KoKta1a6 (L: .385): Erosion
3.2. KoKta2 (L: .500): Determining suitable areas in terms of area status for cultural tourism
3.2.1. KoKta2a1 (L: .200): Distance to Pamukkale travertine and Hierapolis ancient city
3.2.2. KoKta2a2 (L: .200): Distance to Laodicea ancient city
3.2.3. KoKta2a3 (L: .200): Distance to tourism corridor
3.2.4. KoKta2a4 (L: .200): Distance to archaeological site
3.2.5. KoKta2a5 (L: .200): Distance to Denizli tourism region

RESULTS and DISCUSSION

Land Use: Seeking for getting a share from global economy within the globalization period has brought the concept of interurban competition in to the forefront. In this competition, the basic determinants are local capital/sources and knowledge of cities. At this point; it can be said that the cities which have ability to put their “equity/resource” and “indigenous” dynamics to global markets distinguish within the international and national urban network (Ozcan and Ozkan, 2010). In Denizli city, distribution trend of urban has developed in a sprawl and expansionist manner. In 1987, urban settlement areas following road path have created new centers by growing laterally from these paths in 2001, and then in the year of 2013 empty spaces between these centers have become urbanized. Until now, urban sprawl has mostly occurred on meadows, pastures and arid lands. However, when considering the topological limitations and the urban distribution trend on slightly inclined areas from past to present, it can be predicted that in future, the

urban distribution will develop on regionally important agricultural landscapes. This will not only lead to critical ecological results such as disappearing or dissolving agricultural landscapes, but also cause social problems in the medium and long term by degrading agricultural sector, constituting 16.7% of urban economy (TUIK, 2013).

It was observed that the variables (factors) that lead to urban sprawl and ramification have negatively affected agricultural lands (Figure 3). As a result of highway routes passing through plain lands and farmlands, the settlements, the commercial and industrial areas clustered around these routes have given rise to a loss in agricultural lands. Increasing transportation facilities has made greater housing, and around the three main transportation route; Ankara, Izmir and Antalya roads, there has been formed urban sprawl and fringes. When we analyze the total loss of agricultural lands between the years of 1987-2013, the total loss pattern is as following; 510 ha in the slums, 94 ha in the University area and its 1 km around, 1704 ha in the Industrial area and its 1 km around; 2207 ha in 1 km around highway route, 314 ha in the touristic area and its 1 km around. In both periods, it is seen that the most significant agricultural land loss occurred around highways and industrial areas (Figure 3).

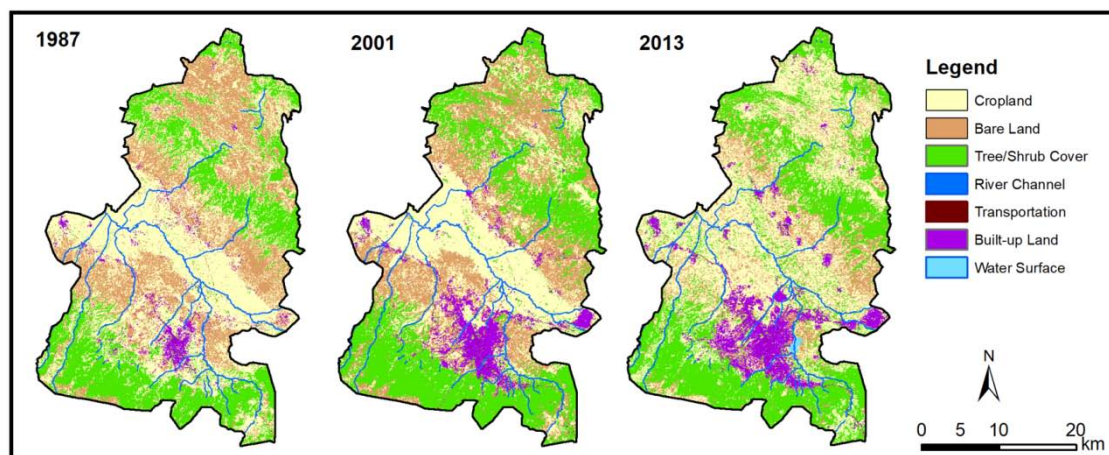


Figure 3. LULC change

Land Use Disputes: Land suitability and land use dispute data obtained through LUCIS model are of importance for Denizli city. Suitable lands for urban settlement significantly overlap with actual urban settlement of Denizli. However, it can be noticed that in more suitable lands for agriculture, housing is emerging as well. Also, agricultural lands overlapping with suitable lands for conservation areas should be considered as an important implication (Figure 4.) For agricultural lands, while (in terms of suitability) medium and high quality areas require less investment on fertilizers and food chemicals for a significant production, unsuitable areas with poor lands and steep slopes require high investment. Indeed, for settlement areas, moving from the most suitable areas to unsuitable ones, the pressure on ecosystem would increase.

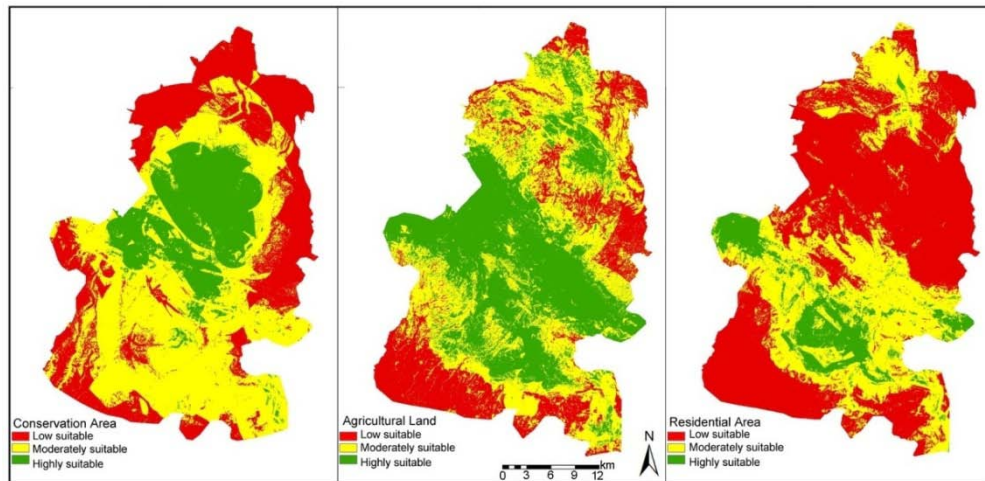


Figure 4. Suitability for settlement, agriculture and conservation areas

Based on land suitability and land use priority, the conflict between urban settlement, agricultural lands and conservation lands occurs at the rate of 16.7% (Figure 5). It is seen that conflicting lands will mostly expand towards particularly conservation lands and agricultural lands in the urban periphery. Nonetheless, the most part of the conflict has been experienced on agricultural lands (Table 4).

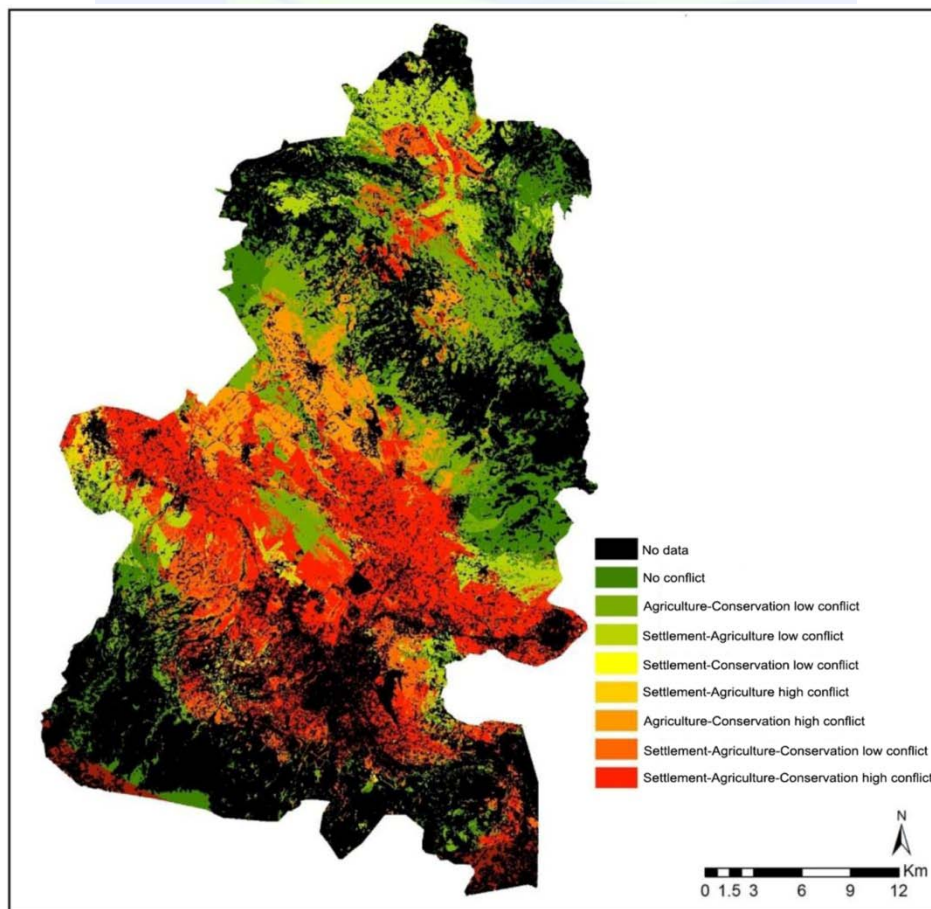


Figure 5. Land use disputes and conflict potential

Table 4. Areal rate of land use disputes

Dispute/Conflict intensity	Area (Km ²)	%
No conflict	126.805	11,288
No data*	485,626	43,231
Agriculture-Conservation low conflict	126,617	11.272
Agriculture-Conservation high conflict	62.645	5.577
Settlement-Conservation low conflict	0.605	0.054
Settlement-Agriculture-Conservation low conflict	48.959	4.358
Settlement-Agriculture-Conservation high conflict	188.658	16.795
Settlement-Agriculture low conflict	73.543	6.547
Settlement-Agriculture high conflict	9.869	0.879

*'No data' refers to masked areas (settlement, roads, water surfaces and conservation areas).

In accordance with the results of overlapping Denizli Environmental Master Plan with the dispute map (Table 5), the urban development area and proposed housing areas are designed on unsuitable lands. In addition, proposing an urban development area on the most conflicting areas regarding settlement, agriculture and conservation is an important threat to ecosystem service. It can be easily observed that perforation-separation and fragmentation processes which will occur on agricultural lands were not took into consideration in the Environmental Master Plan.

Table 5. Rate of land use conflicts in Environmental Master Plan

Potentially conflict areas	In Environmental Master Plan	Area (ha)	%
Housing development area	Settlement-Agriculture-Conservation high conflict	1215.42	29.24
Suitable areas for secondary housing settlement	Suitable areas in terms of settlement for secondary housing	67.82	1.63
Suitable areas for rural settlement	Suitable areas for rural settlement	6.79	0.16
Suitable areas for housing development	Suitable areas for housing development	51.55	1.24
Actual settlement suitable areas	Actual settlement suitable areas	16.72	0.40
Suitable areas for secondary housing settlement	Agriculture-Conservation low conflict	175.95	4.23
Suitable areas for secondary housing settlement	Agriculture-Conservation low conflict	8.22	0.20
Rural settlement areas	Agriculture-Conservation low conflict	82.91	1.99
Actual housing areas	Agriculture-Conservation low conflict	103.91	2.50
Dense housing area	Agriculture-Conservation low conflict	78.56	1.89
Rural settlements	Agriculture-Conservation high conflict	42.74	1.03
Housing development area	Agriculture-Conservation high conflict	1.66	0.04
Actual settlement areas	Agriculture-Conservation high conflict	2.29	0.06
Dense housing areas	Agriculture-Conservation high conflict	0.09	0.00
Housing development area	Settlement-Conservation low conflict	2.31	0.06
Actual housing areas	Settlement-Conservation low conflict	1.66	0.04
Secondary housing settlement	Settlement-Agriculture-Conservation low conflict	2.25	0.05
Urban development area	Settlement-Agriculture-Conservation low conflict	418.66	10.07
Rural settlements	Settlement-Agriculture-Conservation low conflict	16.15	0.39
Actual settlement area	Settlement-Agriculture-Conservation low conflict	251.03	6.04
Mass housing area	Settlement-Agriculture-Conservation low conflict	23.08	0.56
Secondary housing settlement	Settlement-Agriculture-Conservation high conflict	11.23	0.27
Rural settlements	Settlement-Agriculture-Conservation high conflict	178.97	4.31
Actual settlement area	Settlement-Agriculture-Conservation high conflict	647.21	15.57
Mass housing area	Settlement-Agriculture-Conservation high conflict	128.22	3.08
Secondary housing settlement	Settlement-Agriculture low conflict	78.84	1.90
Rural settlements	Settlement-Agriculture low conflict	50.94	1.23
Housing development area	Settlement-Agriculture low conflict	213.17	5.13
Actual housing area	Settlement-Agriculture low conflict	109.64	2.64
Mass housing area	Settlement-Agriculture low conflict	27.66	0.67
Secondary housing settlement	Settlement-Agriculture high conflict	0.06	0.00
Housing development area	Settlement-Agriculture high conflict	70.75	1.70
Rural settlements	Settlement-Agriculture high conflict	0.88	0.02
Actual settlement area	Settlement-Agriculture high conflict	63.48	1.53
Mass housing area	Settlement-Agriculture high conflict	6.52	0.16
		4157.33	100.00

CONCLUSION

In this study, within the scope of LUCIS model, the land use disputes were acquired by including distribution tendency of urban and the priorities leading this tendency to the suitability maps. This model provides usable results for making ecological urban planning decisions, and particularly areal information obtained by comparing relevant plans constitutes a critical basis for revising urban policies. Indeed, this argument is tested upon Denizli city. In fact, Denizli faces the threat of rapid land use change. In this study, in order to support community members and shareholders for determining the location and the degree of potential land use conflicts in future, getting quantitative data and visualizing, an adaptation of Carr and Zwick's LUCIS model were prepared. This was used to obtain multiple potential land use scenarios in future. Thanks to the resulted basic scenario, by revealing actual land use decisions are not ecological and sustainable, it is proved that land was considered merely a good and landscape functions were ignored. Also, comparative effects of agricultural, conservation or urban-centered land-use conflicts with the applicable decisions were highlighted by showing spatial importance of the conflict.

While the analytical products of this study provide information about future potential land-use conflicts, the obtained land-use scenarios have ability to suggest proposals for collaboration between shareholders, governmental institutions and development groups. The results of this study offers an opportunity to arrive a consensus on critical decisions affecting land-use change in urban and periphery landscape planning, and provides map-based data that allows planners and related parties to make their decisions interactively.

Acknowledgement: This study was conducted under the project "Landscape Pattern Ecological Process Interaction in Urban-Rural Belts: Denizli Case" (1130543-TOVAG-TUBİTAK). We thank to TUBİTAK (The Scientific and Technological Research Council of Turkey) for its support.

REFERENCES

- Carr, M and P. Zwick. 2007. *Smart Land-Use Analysis: The LUCIS Model*. Redlands, California: ESRI Press.
- Carr, M. and P. Zwick. 2005. "Using GIS Suitability Analysis to Identify Potential Future Land Use Conflicts in North Central Florida.". *Journal of Conservation Planning* 1: 58-73.
- ÇDP, 2007. Aydın-Muğla-Denizli Planlama Bölgesi 1/100.000 Ölçekli Çevre Düzeni Planı Revizyonu <http://www.csb.gov.tr/gm/mpgm/index.php?Sayfa=sayfaicerik&Id=486>, 08 November 2013.
- Denizli Regional Directorate of Forestry, 2014. *Forest Management Plans, 1:25,000*. Ministry of Environment and Urbanisation, Denizli Regional Directorate of Forestry, Denizli

- Oruc, M., Marangoz, M. and Karakis, S., 2007. Pan-Sharp Landsat 7 ETM+ Görüntüsü Kullanılarak Piksel-Tabanlı ve Nesne-Tabanlı Sınıflandırma Yaklaşımlarının Karşılaştırılması, UCTEA (Union of Chambers of Turkish Engineers and Architects) Chamber of Survey and Cadastre Engineers, *11th Turkish Scientific and Technical Congress Geomatics*. April 2007, Ankara.
- Ozcan, K., Ozkan, H.T., 2010. Denizli Kentinin Planlama Deneyimi, *Doğu Coğrafya Magazine*, 27, Denizli
- TÜİK, 2013. Turkish Statistical Institute, Database, <http://tuikapp.tuik.gov.tr/nufusmenuapp/menu.zul> 14 November 2013.



Preparation of Preliminary Survey Report with GIS in Land Consolidation Projects

Ela Ertunç¹, Tayfun Çay¹

¹ *Department of Geomatic Engineering, Selcuk University, Aleaddin Keykubat Campus, 42030, Turkey. e-mail: elaertunc@selcuk.edu.tr, tcay@selcuk.edu.tr*

ABSTRACT

Land consolidation, which is implemented in rural areas by terrain and land regulation, is one of the important means of increasing productivity in agricultural production and applied all over the world.

After a decision has been made to consolidate a rural area, the first thing to do is to study it in all aspects of this area in detail. For this reason, the land consolidation projects require a comprehensive preliminary survey, including future plans, as there is a general change in the settlement area, ie the village, as well as the economic and social structure of the village. In the land consolidation project, both the agricultural area and the subdivision of the village settlement are subject to change. So, first of all, the current situation of the village should be determined. Because all subsequent operations will be done according to the information and documents that will emerge from here.

Land consolidation processes carried out in the preliminary survey; general definition of the region should be made ,the structural and sociological status of the village should be investigated and the sources of production (such as agricultural land, climate of the region, topographic status of the land, distance of settlements) should be investigated. In addition, the use of cultivable land should be explored (such as the number of plots, parcel sizes, parcel shapes, spreads of parcels, area losses due to border and edge strips, production decline caused by road insufficiency), information which the trend of development in the social and rural areas information needs to be acquired.

The Geographical Information System was used for the preparation of preliminary survey reports in the Land Consolidation projects. Ownership survey for a example project has been in the GIS environment. This study demonstrates the usability of GIS in preparing preliminary surveys in land consolidation projects.

INTRODUCTION

The development of the agricultural infrastructure is of primary importance in order to make more income from the unit side and to make our country's agriculture competitively with the world by producing a product with high productivity. One of the most important

problems for improving the agricultural infrastructure is the size of the existing structural problems and the necessary legal arrangements to solve the problems and the completion of the lack of responsible institutions and the provision of financial resources (Kirmikil, 2010).

The most important of agricultural infrastructure problems in our country is that, in a great majority of agricultural enterprises, land is small parcels, scattered, and shapes are irregular and lack access network. This situation causes the farmers' families to produce smaller and more scattered agricultural land, and thus agricultural development is inadequate Land consolidation is the only solution to the get rid of this problem for business owners with fragmented and scattered land. (Arıcı, 1994).

An important aim of the land regeneration work for the reorganization of the agricultural area is to increase the agricultural yield. However, this activity is done on land that is essential to life and the land must be used in a sustainable way to meet the needs of future generations (İşcan, 2009).

Land consolidation, which is implemented in rural areas by land and land regulation, is one of the important means of increasing productivity in agricultural production. In order to increase agricultural production, unfavorably shaped land belonging to individuals and enterprise, which are divided into small pieces in small pieces, are shaped and planned according to the principles of modern agriculture management (Temel 2013).

With the integration and irrigation, people's living standards will change positively in economic and social terms and sustainable rural development will be provided. Land consolidation is not only to combine scatter parcels of, but also land use plan is implemented. (Sert ve ark., 2011).

The first thing to do after deciding on land consolidation in a rural area is to study it in all aspects of this area in detail Preliminary studies have a major role in modern land consolidation studies. For this reason, the study requires a comprehensive preliminary survey to include forward-looking planning, as there is a total change in the settlement area, ie the village, as well as the economic and social structure of the village. In the land consolidation project, both the agricultural area and the subdivision of the village settlement are subject to change. So, first of all, the current situation of the village should be determined. Because all subsequent operations will be done according to the information and documents that will emerge from here. So preliminary study reports will shed light on future work.

In the preliminary study report; The introduction of the study areas (Location, transportation status, ownership and cadastral status, topography and land status, agricultural structure and land use status, number of farmers, land fragmentation status and forms), the requirements for the cultural technical services and the necessary precautions to be taken, the estimated costs according to the alternatives of the project to be prepared, the reasons for the land consolidation, the property map and the decision document.

Geographical Information System (GIS) is an information system in which the spatial and vector data that provide the collection, storage, processing, display, analysis and output of non graphic-vektorial data are matched in the same environment (Timur, 2009).

One of the greatest advantages of GIS, which can be defined as a software and hardware component, is to provide the user with the functioning technology by combining graphics and non-graphical data. This system, which provides great convenience in accessing information, is being used effectively in spatial data processing fields (Yomralıoğlu, 1994).

Using data in the GIS has a lot of advantages compared to traditional methods. Information transfer with GIS has been accelerated. It makes storing and accessing data convenient. Increased work performance of people. It is used intensely by the institutions because it can be analyzed with GIS. It can help to move towards strategic decisions through analyzes made via GIS. Current information can be obtained from the system by renewing the information within the GIS (Altıntaş, 2017).

The Geographical Information System was used for the preparation of preliminary survey reports in the Land Consolidation projects. Ownership survey for a example project has been in the GIS environment. This study demonstrates the usability of GIS in preparing preliminary surveys in land consolidation projects.

MATERIALS & METHOD

Konya City, Çumra District, Üçhüyük Neighborhood, which is under continental climate effect, is chosen as research area (Figure 1). Üçhüyük Neighborhood takes its name from 3 hills surrounding it. Üçhüyük Neighborhood is 13 km to Çumra, 63ckm to Konya. The end date of the project for three large land consolidation projects is 20.10.2016. Initially the project was made by the Konya Agricultural Reformation Regional Directorate and after the TRBM was closed, the Konya Agricultural Provincial Directorate continued to work. Therefore, project data have also been provided by the provincial directorate of agriculture in Konya.

Project data has been transferred to ArcMap-10 program. The database of the AT1, AT2 lists from the Land Consolidation project data was created. The created database is transferred to the program as attribute information. After making necessary analyzes, maps were created and ownership etude which required for preliminary study report have been carried out.

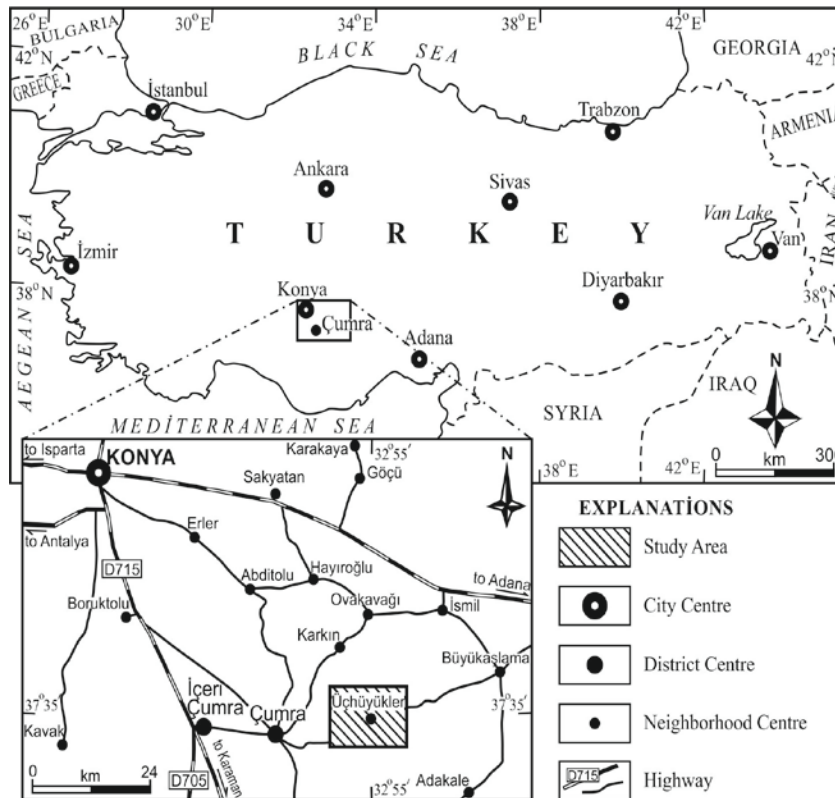


Figure 1. Study area Konya city Çumra district Üçhüyük Neighborhood

RESULTS & DISCUSSION

When a parcel is queried, the parcel's property information, business number, parcel number, title deed area, if there is shared or not, how many shareholding it has, whether it has facility plant, parcel position, parcel quality information is reached (Figure 2).

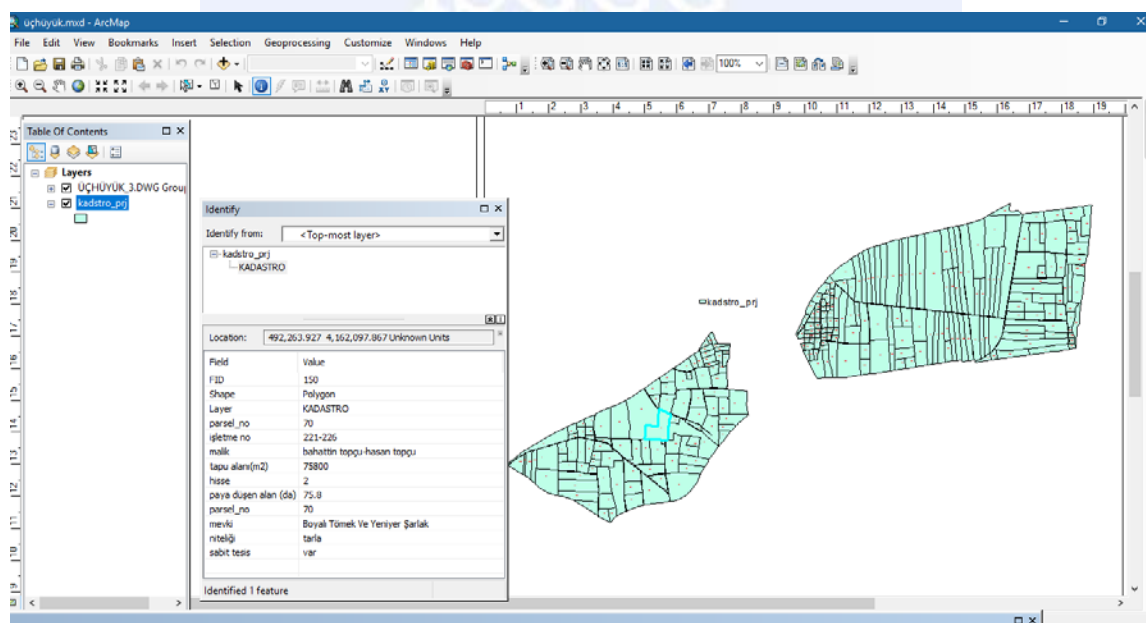


Figure 2. Screenshot of information about a parcel

The average parcel size in the project area is 33.04 da. 158 parcels are below the average parcel size and 107 parcels are above the average parcel size. (Figure 3.)

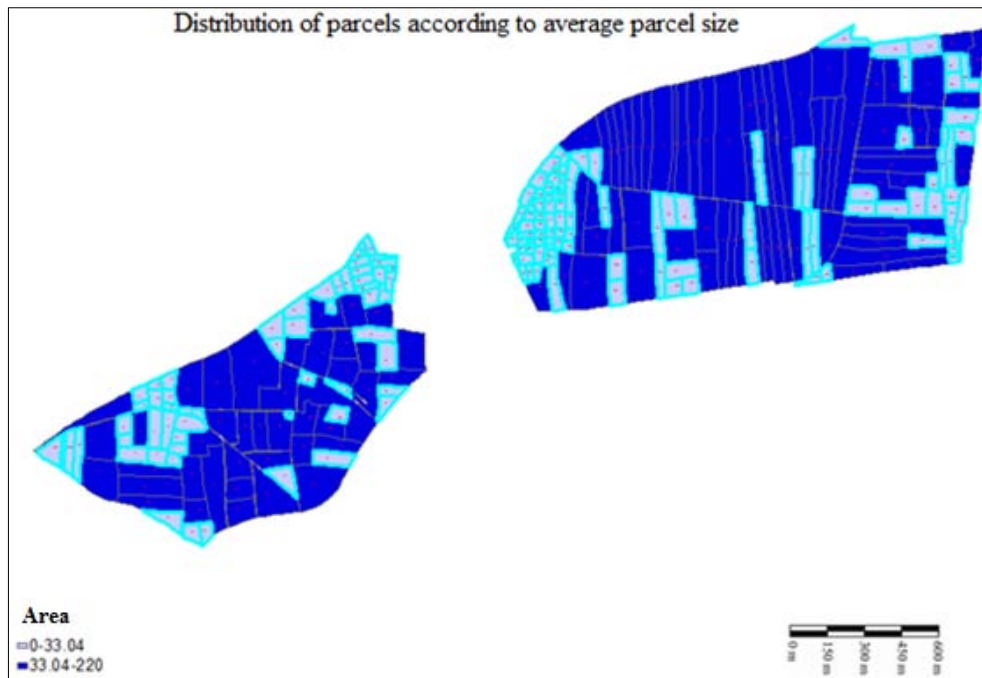


Figure 3. Distribution of parcels according to average parcel size

There are 265 cadastral parcels in the project. It is the only shareholder with 201 cadastral parcels and 64 cadastral parcels are shareholding. Distribution of shared parcels is seen Figure 4.

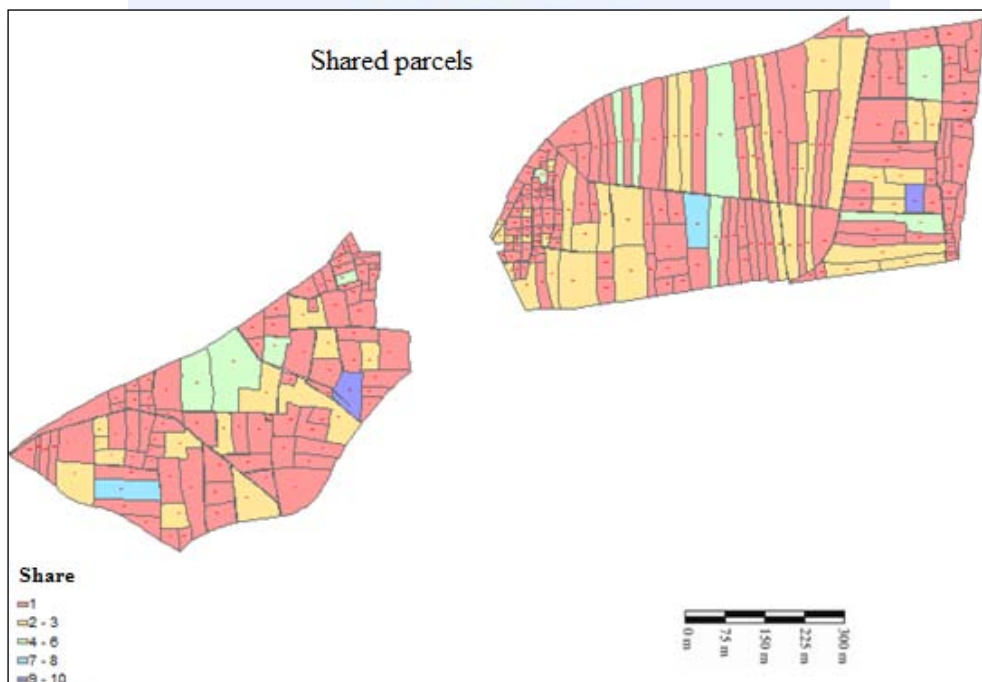


Figure 4. Distribution of shared parcels

Figure 5 shows the current situation of the enterprises in terms of the number of parcels they hold. Approximately 24% of the parcels in the project area are shared parcel.

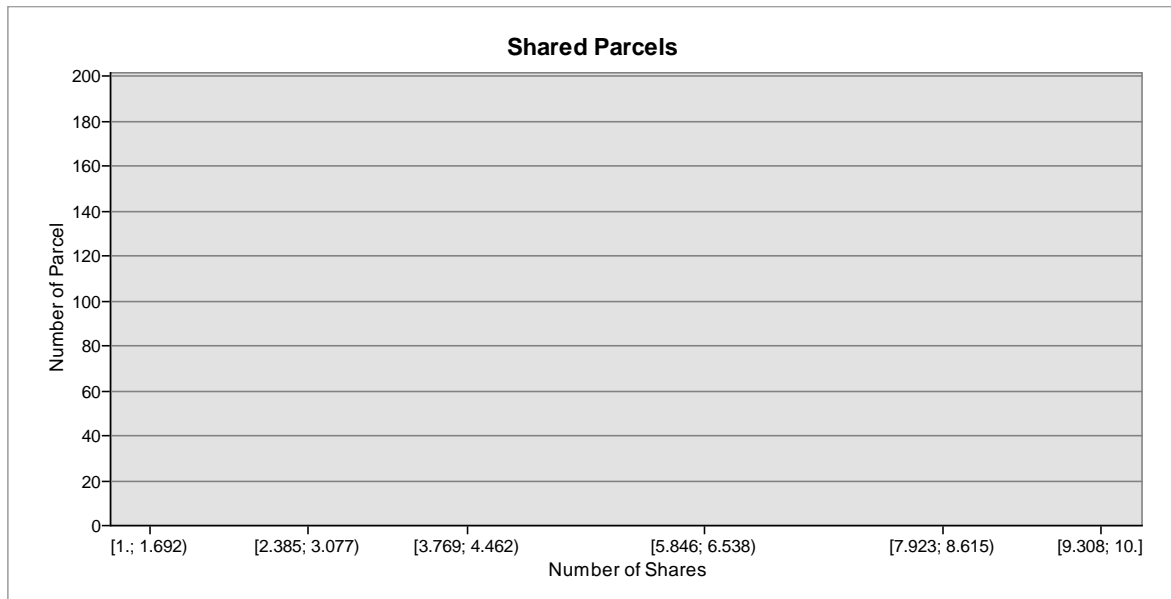


Figure 5. Number of parcels shareholding

When we examine the distribution of parcel sizes in Figure 6, parcels are usually between 0 and 5 da. There is only 1 parcel over 150 da.

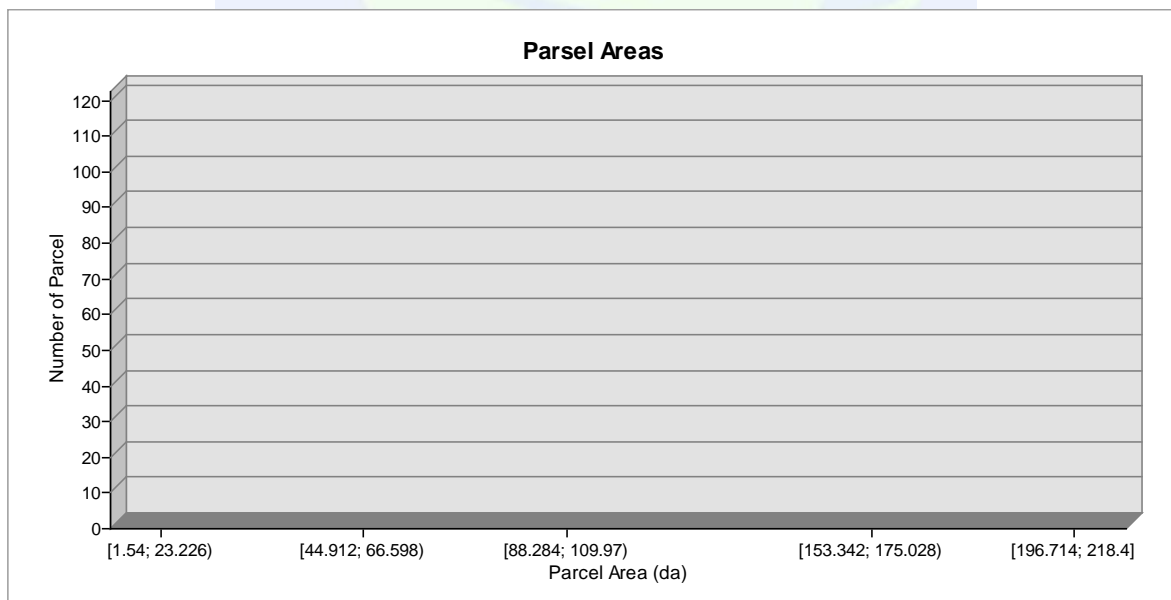


Figure 6. Distribution of parcel sizes by number of parcels

Figure 7 also shows the distribution of parcel sizes in the application area.

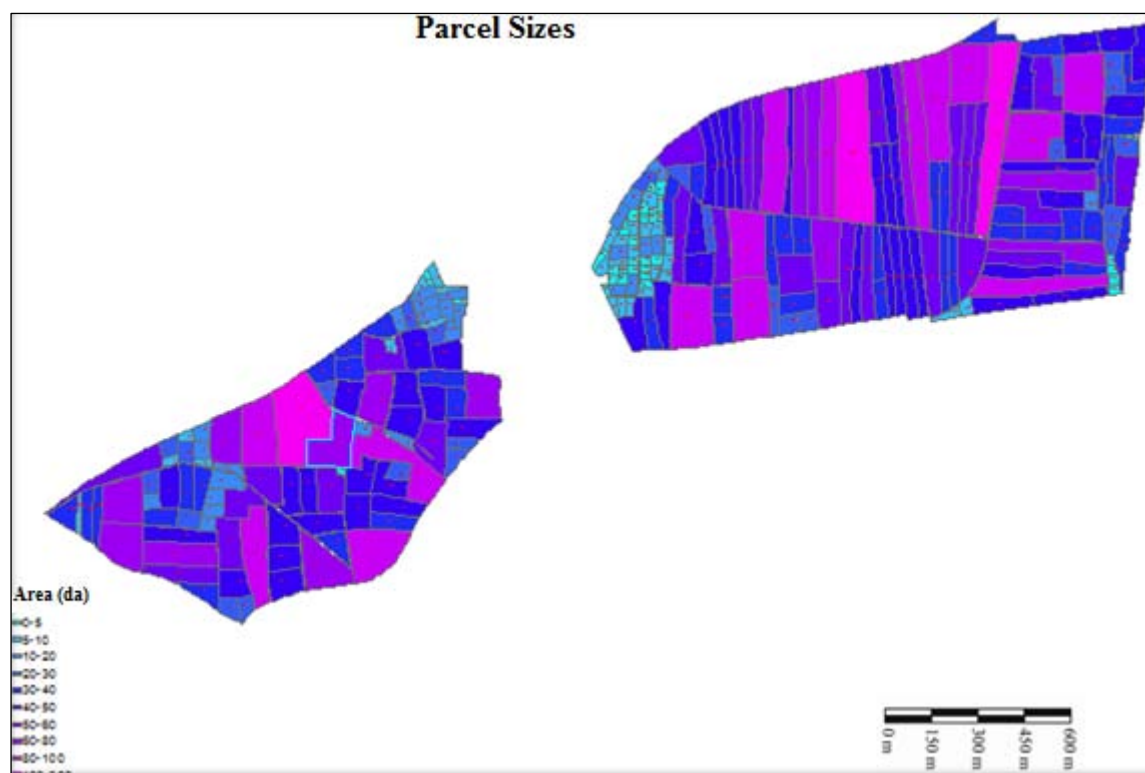


Figure 7. Distribution of parcel sizes

The parcel with the fixed facility on it is shown in Figure 8. Accordingly, 49 parcels in the project area have fixed facilities such as wells and electric wells.

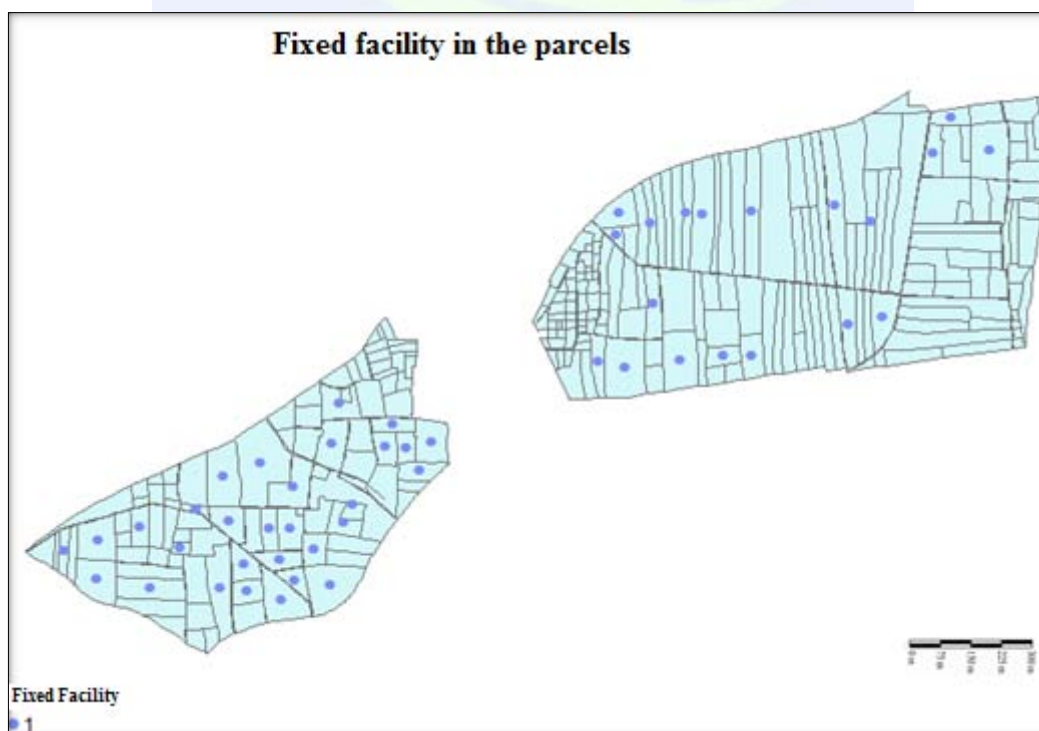


Figure 8. Map display of fixed facility in the parcels

Konya Çumra Üçhüyük neighborhood which application area, the land norms declared in the official gazette dated 30.03.1995 for the is 154 decare for dry agricultural land and 50 decare for irrigated agricultural land. Of the 265 cadastral parcels in the implementation plan, 53 are above the soil norm. 212 parcels are bigger than the land norm (Figure 9).

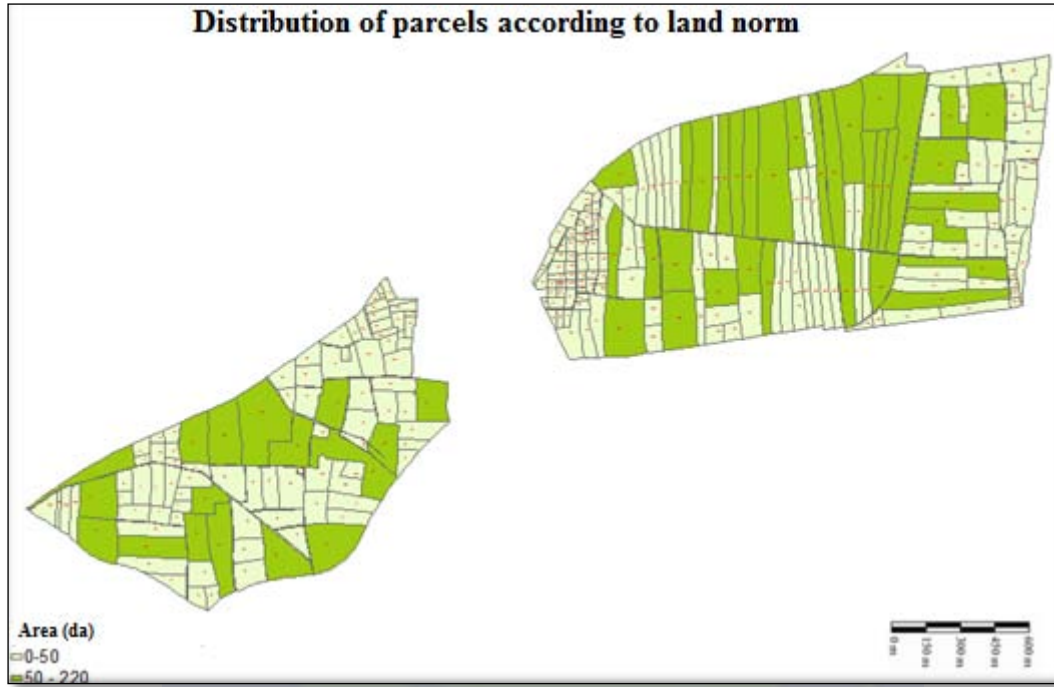


Figure 9. Distribution of parcels according to land norm

CONCLUSIONS

Land consolidation studies are taking a long time because they are comprehensive projects. Preliminary study reports have a major role in land consolidation studies because they shed light on future work. Due to these reasons, the preparation of the preliminary study reports is carried out in a short time and in detail by means of Geographic Information Systems, collecting all the information about a land together with their locations, storing them, making statistical evaluations, visualizing them in the virtual environment and testing their results.

The Geographic Information System is based on the questioning of the numerous databases that make up and the statistical and geographic analysis of them. For this reason, the use of GIS in land consolidation studies accelerates this process and is a fast and highly effective method of developing measures.

REFERENCES

Altıntaş, N.C.,2017. *Kent İçi Yol Yapım, Bakım ve Onarım İçin Coğrafi Bilgi Sistemleri İle Veri Tabanı Oluşturulması*, Pamukkale Üniversitesi, Fen Bilimleri Enstitüsü, Yüksek Lisans Tezi, Denizli

- Arıcı, İ., 1994. *Arazi Toplulaştırması, Uludağ Üniversitesi Ziraat Fakültesi Ders Notları* No: 60, Bursa 1994, 121s.
- İşcan, F., 2009. *Arazi Düzenleme Çalışmalarında Bulanık Mantık Uygulaması*, Doktora Tezi, Selçuk Üniversitesi Fen Bilimleri Enstitüsü, Konya.
- Kirmikil, M., 2010. *Sulama Proje Alanlarında Kırsal Aşan Geliştirilmesi İçin Arazi Toplulaştırması Rolünün GIS Destekli Analizi*, Uludağ Üniversitesi, Fen Bilimleri Enstitüsü, Doktora Tezi, Bursa.
- Sert, A., Ceylan, A.R., Vanlı, C., Karagöz, Ö. 2011. Arazi toplulaştırma Projelerinin Etüt Aşamasında Uydu Görüntülerinin Kullanılması “DSİ İzmir Küçük Menderes Havzası Ödemiş Ovası Örneği
- Temel, M., 2013. *Kırsal alanların Korunarak Kalkınmasında ve Planlanmasında Bir Araç Olarak Arazi Toplulaştırması: Avrupa Birliği Türkiye Karşılaştırması*, Yüksek Lisans Tezi, Gazi Üniversitesi Fen Bilimleri Enstitüsü, Ankara.
- Timur, S., 2009. *Coğrafi Bilgi Sistemleri Destekli Taşınmaz Değer Haritalarının Oluşturulması: İstanbul İli, Şişli İlçesi Örneği*, İstanbul Teknik Üniversitesi Fen Bilimleri Enstitüsü, Yüksek Lisans Tezi, İstanbul
- Yomralıoğlu, T., 1994. Kentsel bir Coğrafi Bilgi Sistemi Modelleme., *1 Ulusal Coğrafi Bilgi Sistemleri Sempozyumu*, Trabzon, 276-290

ISGGG
2017

A Study on Determination of Optimum Parcel Size in Land Consolidation

Tayfun Çay¹, Ela Ertunç¹

¹ Department of Geomatic Engineering, Selcuk University, Aleaddin Keykubat Campus, 42030, Turkey. e-mail: tcay@selcuk.edu.tr, elaertunc@selcuk.edu.tr

ABSTRACT

Our country, given its land and the climate of the region we live on is very favorable for agricultural production. In this case, it is obligatory to organize the agricultural space. Land consolidation is one of the most widely used methods of rural area management in the world and in our country. Land Consolidation projects have many benefits, including access to parcels, efficient use of water resources, consolidation of parcels, reduction of the costs of irrigation and drainage projects. Land consolidation in our country is carried out in accordance with the provisions of the "Law on Agricultural Reform of Land Regulation in Irrigation Areas" numbered 3083 and the provisions of the "Soil Conservation and Land Use Law" numbered 5403 and regulations and regulations based on these laws. Although the Land Consolidation projects in our country are carried out according to the provisions of two different laws, the steps of implementation are similar in general. The ministry in charge of the projects under both laws is the Ministry of Food, Agriculture and Livestock (GTHB).

In this study, the data of a land consolidation project completed by the Provincial Directorate of Agriculture in 20.10.2016 has been used. According to the supplementary law no. 6537 issued in 2014, which is one of the land consolidation legislation numbered 5403 for Soil Conservation and Land Use Law, the parcel sizes were compared after the consolidation of the selected project area according to the soil norm. In addition, the effectiveness of the land norm sizes determined by the Ministry and the determination of the optimum parcel size have been researched.

INTRODUCTION

In our country, the agricultural sector is one of the most important sectors, especially due to the increase in the population, the supply of industrial raw materials, employment and the contribution of the economy. Various policies have been developed and put into effect in order to ensure productivity and continuity in agriculture sector. Since 2000's, various changes have been made in agricultural policy instruments and structural transformations have taken place in the agricultural sector with different implementations coming with these policy changes. These structural transformations in the agricultural sector are

introduced in the 8th, 9th and 10th Development Plans. Especially in the EU harmonization process, the importance of the agriculture sector in terms of food safety is indisputable.

Land consolidation is one of the most effective land management approaches used to improve the agricultural sector, protect natural resources, and at the same time contribute to the development of rural areas all over the world and in our country.

Since 1973, land consolidation studies in Turkey have been carried out by different legislation and institutions. This brings with it the problems of implementation (Ülger ve Çay, 2012).

The legal basis for the land consolidation in Turkey is 3083 numbered Irrigation Lands Agricultural Reforms and 5403 numbered Soil Conservation and Land Use Laws. The methods and principles of land consolidation are regulated by the "Regulation on the Protection, Use and Land Consolidation of Agricultural Land" published in the Official Gazette dated 24 July 2009 (Ceylan ve ark, 2014).

Land consolidation works within the scope of Law No. 3083 are implemented by the General Directorate of Agricultural Reform of the Ministry of Food, Agriculture and Livestock. For the law numbered 5403, the implementing organizations; It is defined as the Ministry of Food, Agriculture and Livestock, Special Provincial Administrations (former), municipalities and villages, cooperatives operating in agricultural activities, associations such as associations and other public institutions. (Çağdaş, 2010).

The Land Conservation and Land Use Law (TKAKK) No. 5403, one of the land consolidation legislation, has been amended with the Supplementary Law No. 6537 issued in 2014. At the beginning of the amendments made with the Law No. 6537, the definitions of the terms "minimum agricultural land size" and "sufficient income agricultural land size" are added by adding the items (h) and (i)

Article 3 – In this law;

h) **(Changed: 30/4/2014-6537/3 art.)** Minimum agricultural land size: The minimum agricultural parcel size determined by the Ministry of Agriculture, where production efficiency and inputs are used rationally and economically, can not be achieved if the productivity obtained on an agricultural land, in other words, the agricultural land is further reduced,

i) **(Changed: 30/4/2014-6537/3 art.)** Sufficient income agricultural land size: Considering the regional differences, the provinces and county express the agricultural land sizes of sufficient income determined in the attached list (1) (Anonim, 2014-a).

Purpose of this Law; Protection of land, development, classification of agricultural land, determination of minimum agricultural lands and land sizes of sufficient income and determine the principles and procedures to ensure the planned use of agricultural lands and agricultural lands with adequate income in accordance with the environmental priority sustainable development principle.

Article 8 / A, added to Article 8 of Law No. 5403 by Law No. 6537, states that "Agricultural land sizes of provinces and county can not be subdivided or divided under the agricultural land sizes of sufficient income determined in the list (1). *This nature of the agricultural land shall be reported by the Ministry to the related title deed office for commentary.* "

MATERIALS & METHOD

Konya-Çumra-Üçhüyükler project data have used in the study. The end date of the project is 20.10.2016. Initially the projects were carried out by Konya Agricultural Reform Regional Directorate and after TRBM was closed, Konya Agriculture Province Directorate continued their work. Therefore, project data have also been provided by the provincial directorate of agriculture in Konya.

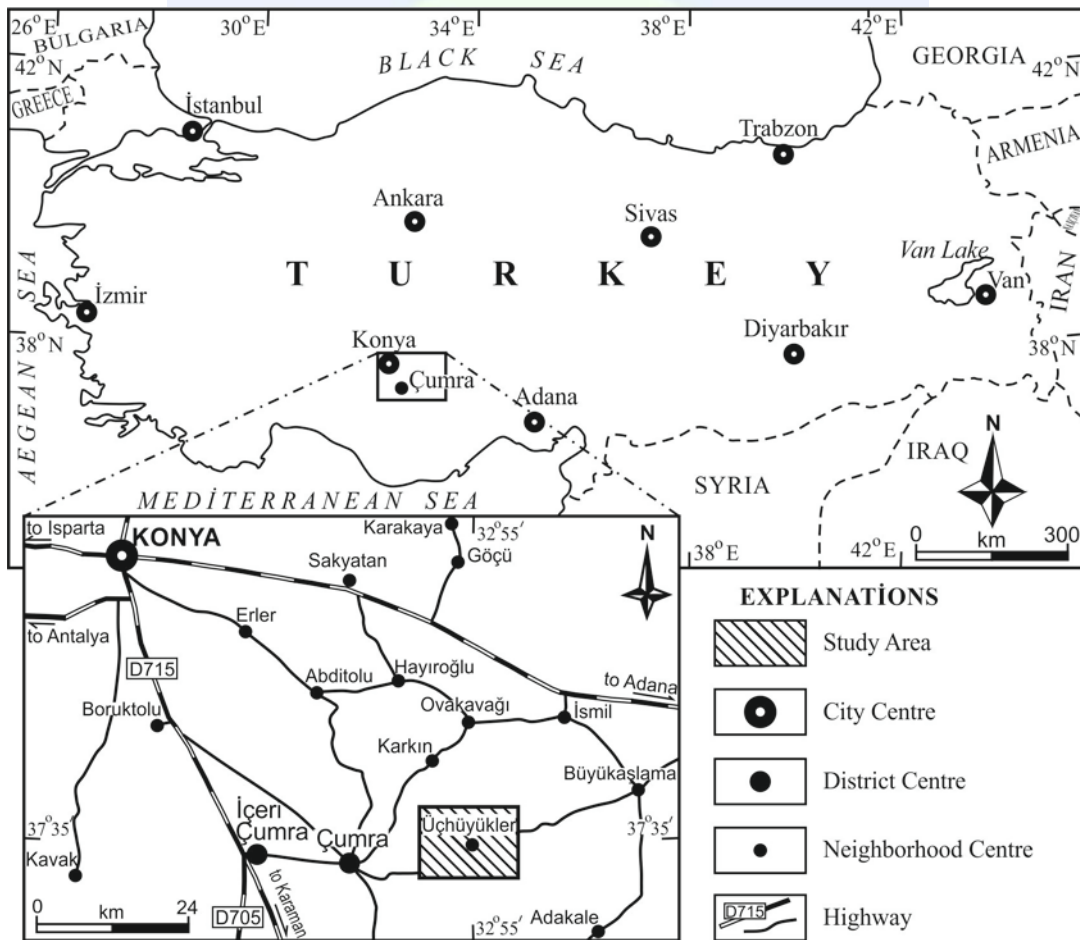


Figure 1. Study area

There are 265 cadastral parcels and 274 agricultural enterprises in the project area. The average parcel size before land consolidation is 33.04 da. After consolidation, the number of island parcels was 243 and the average parcel size is 36.06.



Figure 2. Üçhüyük cadastral state

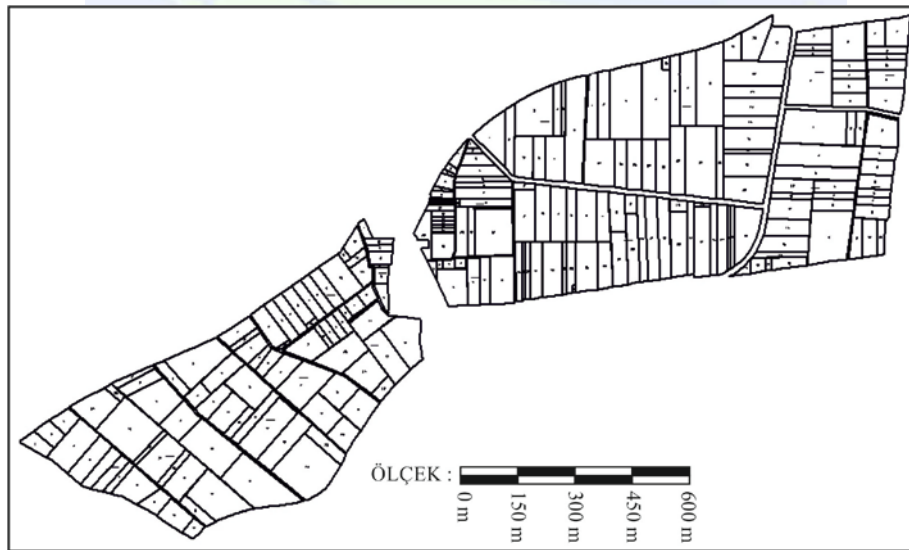


Figure 3. Üçhüyük Interview-based model parceling plan

RESULTS & DISCUSSION

The average parcel size before consolidation is 33.04 and the average parcel size after consolidation is 36.06. This rate is well above the average of 15 decares, which is Turkey's average (Anonim, 2014-b). In terms of average parcel size, there are bigger values than the average in Turkey. The reason for this is the large cadastral parcels in the study area.

Sufficient income agricultural land size refers to the land sizes separately determined for each province and county, considering the existing differences in terms of agricultural activity between the regions in the list attached to TKAKK. (URL 1). In the Konya Çumra

where we have working area, sufficient agricultural land sizes are 55 da for irrigated agricultural land, 200 da for dry agricultural land, and 10 da for planted farming land. When Çumra Üçhüyük land consolidation project data is analyzed, 274 enterprises are located in the current project and only 42 enterprise have over 55 da on land with irrigated agricultural land size. The remaining 232 farms do not have sufficient agricultural land size for irrigated land so that the amount of land is below 55 da. When the size of agricultural land with sufficient income declared by the Ministry is compared with the values in practice, it does not reflect the real situation.

CONCLUSIONS

The general aim of the amendments made with Law No. 6537 is to eliminate the existing shortcomings of the TTK in terms of preventing the disintegration of agricultural land. The concepts of minimum agricultural land size and sufficient income agricultural land size introduced by Law No. 6537 attract the attention as important innovations. Although the measures taken with the amendments made by Law No. 6537 are suitable to provide an indivisibility in legal terms, it is not enough when the existing land sizes are considered in our country.

At the project area Konya Çumra Üçhüyük land consolidation project, only 42 enterprises have more than 55 da for irrigated land with adequate income agricultural land size. The remaining 232 farms do not have sufficient agricultural land size for irrigated land so that the amount of land is below 55 da. However, it should be noted that there are some important errors and deficiencies of the regulations. The most important of these is that the land sizes stated as sufficient income do not reflect the current situation in the land.

REFERENCES

- Anonim, 2014. Toprak Koruma ve Arazi Kullanımı Kanununda Değişiklik Yapılması Hakkında Kanun, No:6537, *Resmî Gazete*, Ankara.
- Anonim, 2014. Tarım Arazilerinin Sürdürülebilir Kullanımı Çalışma Grubu Raporu, T.C. *Kalkınma Bakanlığı yayını*, No; 2860, Ankara, 9-10.
- Çağdaş, V. 2010. *Kırsal Toprak Düzenlemesi. Ders Notları*, Yıldız Teknik Üni., İstanbul
- Ülger, N. E., Çay, T., 2012. "An Assessment About Land Consolidation in Turkey". FIG Working Week 2012, Knowing to Manage the Territory, *Protect the Environment, Evaluate the Cultural Heritage*, 6-10 May 2012, Rome, Italy [http://www.fig.net/pub/fig2012/papers/ts02e/TS02E_ ulger_cay_5677.pdf](http://www.fig.net/pub/fig2012/papers/ts02e/TS02E_ulger_cay_5677.pdf) (Erişim: 15.08.14)
- Ceylan, F., Sayın, C.ve Özalp, M., 2014. "Türkiye'de İzlenen Arazi Toplulaştırması Politikalarının Sürdürülebilir Aile Çiftçiliği Modeline Etkileri", Ulusal Aile Çiftçiliği Sempozyumu, 30-31 Ekim, 2014, Ankara.
- URL 1 ,http://webftp.gazi.edu.tr/hukuk/dergi/19_1_3.pdf



METEOROLOGY AND CLIMATOLOGY

Trend Analysis Of The Zenith Tropospheric Delay Time Series

Emine Tanır Kayıkcı¹, Cansu Beşel^{*1}

¹Department of Geomatics Engineering, Karadeniz Technical University, 61080, Trabzon, Turkey. e-mail: cansubesel@ktu.edu.tr

ABSTRACT

Nowadays, climate change is one of the most important environmental problems and there are many scientific studies on adaptation to climate change. Zenith Tropospheric Delay (ZTD) have a great importance in climate change studies. Analyzes of Global Navigation Satellite System (GNSS) observations can be used to obtain the ZTD parameter representing the effect of weather conditions. In this study, trend analysis of time series of (IGS Repro1) ZTD data between 1995-2010 reprocessed in the framework of COST Action ES1206, GNSS4SWEC were performed. 19 IGS (International GNSS Service) stations were used in the study selected from Turkey and Europe. Simple Linear Regression Model and Mann-Kendall tests were used for trend analysis. The results obtained from these two tests were compared. In this way, evaluations were made on the climatic change that occurred in the last 15 years. According to Simple Linear Regression Model, an increasing trend was observed at IGS stations ANKR, EBRE and MAS1, a decreasing trend was observed at the IGS stations BRUS, GRAS. There was no significant trend in other stations. On the other hand, according to Mann-Kendall test, an increasing trends were observed at the IGS stations ANKR, EBRE and MAS1 stations. There was no significant trend in other stations.

INTRODUCTION

Climate involve statistics of average weather conditions consisting of temperature, humidity, precipitation, atmospheric pressure and other meteorological elements. Nowadays, climate is one of the most environmental issue. In this context, studies are doing about scientific side of climate change, climate change prevention and climate change adaptation (Demircan et al., 2016).

GNSS observations have an important place in climate studies because of the advantages of which provide. GNSS signals are exposed to tropospheric delay in atmosphere before reaching the receiver on Earth. This delay is generally converted to zenith orientation and obtained as Zenith Tropospheric Delay (ZTD) (Baldysz et al., 2016). Integrated Water Vapour (IWV) is obtained from ZTD data with the help of various conversion models.

* Corresponding author

Water vapour is one of the most significant factors affecting climate change and which increases about 60-70% of Earth's temperature (COST, 2012). Besides, water vapour has an importance place in the atmosphere and hydrological cycle. ZTD data inform about regional weather conditions (Jin et al., 2007; Demircan et al., 2016). Trend analysis of time series generated from ZTD indicates change of data in the used the time period. In this way, forecasts are made for the future.

In this study, trend analysis of time series of (IGS Repro1) ZTD data between 1995-2010 reprocessed in the framework of COST Action ES1206, GNSS4SWEC were performed. 19 IGS stations selected from Turkey and Europe were used in the study. Linear Regression Model and Mann-Kendall tests were used for trend analysis. The results obtained from these two tests were compared. In this way, evaluations were made on the climatic change that occurred in the last 15 years.

Methods

Trend analysis is a mathematical technique which makes a prediction relevant to the future by using past results through parametric and nonparametric methods (Yadav et al., 2015). In parametric methods, the actual value of the data in series is important and this value used in calculations. On the other hand, in nonparametric methods are used number of rows obtained by sorting from small to large or large to small. T-test and Linear regression model are some of parametric methods. Mann-Kendall test, Mann-Kendall Rank Correlation test, Spearman's Rho test, Sen's Slope methods and Sen's T test are non-parametric methods for trend analysis.

Simple Linear Regression Model

Simple linear regression as a linear function between independent (x) and dependent (y) variables. The time series expressing the time-dependent change of the data as:

$$y + v = a_0 + a_1x \quad (1)$$

where x is the independent variable, y is the data, a_1 is the slope, a_0 is the intersection constant, v is the correction parameter. Trend analysis is performed according to simple linear regression model (Öztürk and Şerbetçi, 1992; Bayazıt and Yeğen Oğuz, 2005).

Mann-Kendall Test

Mann-Kendall test is commonly used fields such as hydrology and climatology to determine trend in time series. This is a method recommended by World Meteorological Organization (WMO). Mann-Kendall test statistic;

$$S = \sum_{k=1}^{n-1} \sum_{j=k+1}^n \text{sgn}(x_j - x_k) \quad (2)$$

$$\text{sgn}(x_j - x_k) = \begin{cases} 1 & ; x_j > x_k \\ 0 & ; x_j = x_k \\ -1 & ; x_j < x_k \end{cases} \quad (3)$$

where x_j and x_k are the data while $k=1, \dots, n-1$, $j=i+1, \dots, n$ and S is the statistical factor, describes the character of linear trend.

Normalized Mann-Kendall statistic as;

$$Z = \begin{cases} \frac{S-1}{\sqrt{\text{Var}(S)}} & ; S > 0 \\ 0 & ; S = 0 \\ \frac{S+1}{\sqrt{\text{Var}(S)}} & ; S < 0 \end{cases} \quad (4)$$

where $\text{Var}(S)$ is the variance. Variance is computed by using the following equation,

$$\text{Var}(S) = \frac{n(n-1)(2n+5) - \sum_{i=1}^k t_i(t_i-1)(2t_i+5)}{18} \quad (5)$$

where n is the number of measurements, k is the number of groups of tied ranks, each with t_i tied observations.

The Mann-Kendall statistic Z is compared with the standard normal distribution table value (Z_{table}) with 95% confidence. H_0 is agreed, if $Z < Z_{table}$ there is no trend. In the opposite case, H_0 is rejected and there is trend. A positive value of S indicates an upward trend. A negative value of S indicates a downward trend (Mann, 1945; Kendall, 1975).

RESULTS AND DISCUSSION

In this study, trend analysis of time series of (IGS Repro1) ZTD data between 1995-2010 reprocessed in the framework of COST Action ES1206, GNSS4SWEC were performed. 19 IGS stations selected from Turkey and Europe were used in the study (URL- 1). Within scope of the work, one IGS station from Turkey *ANKR*, from Turkey, 18 IGS stations from Europe *BORI*, *BRUS*, *EBRE*, *GOPE*, *GRAS*, *GRAZ*, *HERS*, *JOZE*, *KIRU*, *LAMA*, *MASI*, *MATE*, *METS*, *PENC*, *POTS*, *REYK*, *WTZR* and *ZIMM* were used for trend analysis of ZTD data (Table 1). Within the work, first time series graphics of ZTD data for selected stations were plotted. Simple linear regression model and Mann-Kendall test were used in trend analysis. Applications of selected methods were performed by written programming codes in MATLAB. For each stations, generated trend graphics and the changes in ZTD were interpreted.

Table 1. Stations names and geographic coordinates

Station Code	Country	Latitude (degree)	Longitude (degree)	Elevation (m)
ANKR	Turkey	39.8875000	32.7583333	974.8
BOR1	Poland	52.1000000	17.0666667	124.0
BRUS	Belgium	50.7980556	4.3583333	158.3
EBRE	Spain	40.8208333	0.4922222	107.9
GOPE	Czech Republic	49.9136111	14.7855556	592.6
GRAS	France	43.7547222	6.9205556	1319.3
GRAZ	Austria	47.0669444	15.4933333	538.3
HERS	England	50.8672222	0.3361111	76.5
JOZE	Poland	52.0972222	21.0313889	141.4
KIRU	Sweden	67.8572222	20.9683333	391.1
LAMA	Poland	53.8922222	20.6697222	187.0
MAS1	Spain	27.7636111	-15.6330556	197.3
MATE	Italia	40.6488889	16.7044444	535.6
METS	Finland	60.2175000	24.3952778	94.6
PENC	Hungary	52.3791667	13.0658333	144.4
POTS	Germany	47.7894444	19.2813889	291.7
REYK	Iceland	64.1386111	-21.9552778	93.1
WTZR	Germany	49.1441667	12.8788889	666.0
ZIMM	Switzerland	46.8769444	7.4650000	956.4

In the preprocessing phase of data, it was observed that some of the stations have missing data. In other words, there is no data for some day(s) of the year. Thus, missing days are removed in this study.

According to simple linear regression model applied with eq(1), a_1 parameter which expresses slope of trend was calculated according to Least Square Estimation (LSE).

ANKR and BOR1 stations have trends that markedly increasing direction. On the other hand BOR1 and EBRE stations have trends that tending to increase. When a_1 coefficient values are considered which expresses the tendency and direction of trend, $a_1=0.2475$ for the ANKR station, $a_1=0.1807$ for the MAS1 station. On the other side, a_1 coefficient values of BOR1 and EBRE are positive but smaller. Thus, evaluated that the trend in BOR1 and EBRE stations is less obvious than the trend in ANKR and MAS1 (Figure 1).

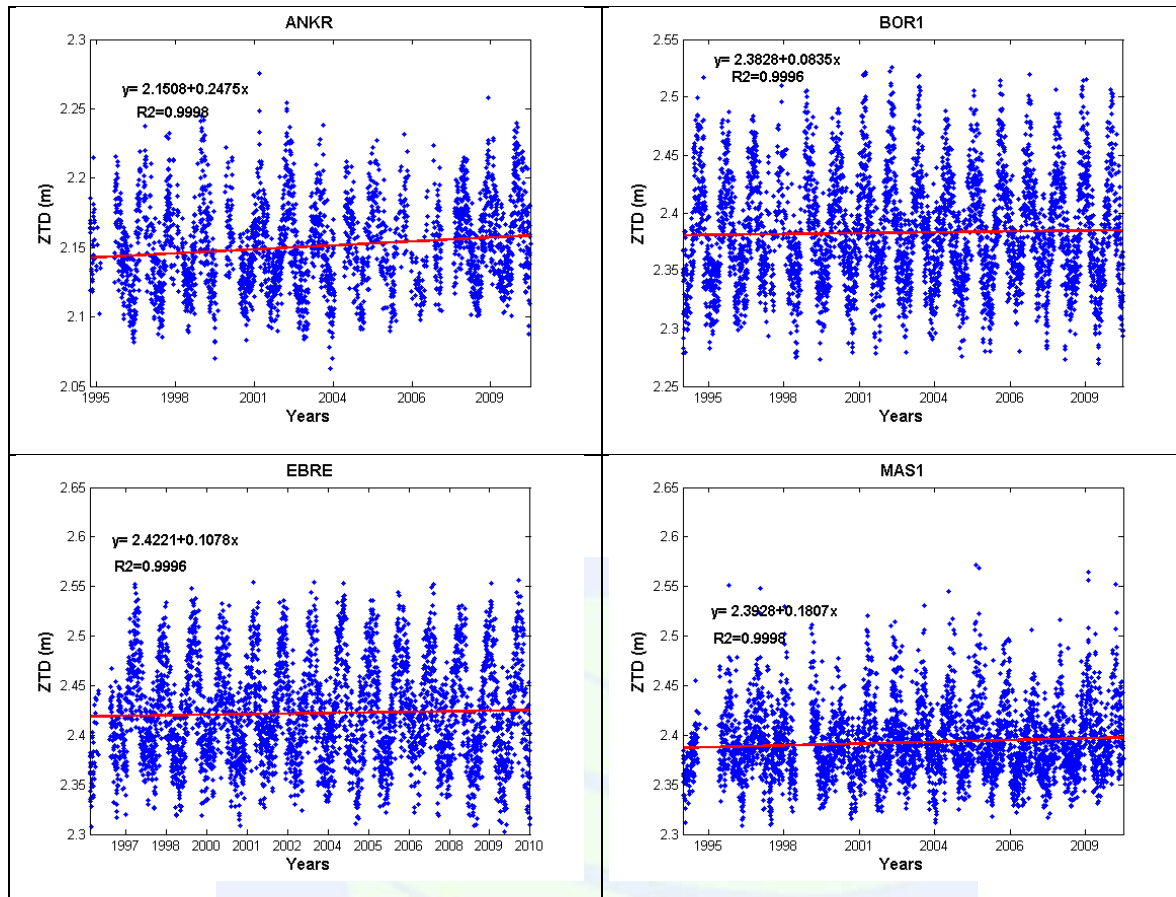


Figure 1. Simple linear regression trend graphics of ANKR, BOR1, EBRE and MAS1 stations

Among the stations used in the study, the BRUS and GRAS stations showed a trend of decreasing direction (Figure 2). There is no trend at other stations.

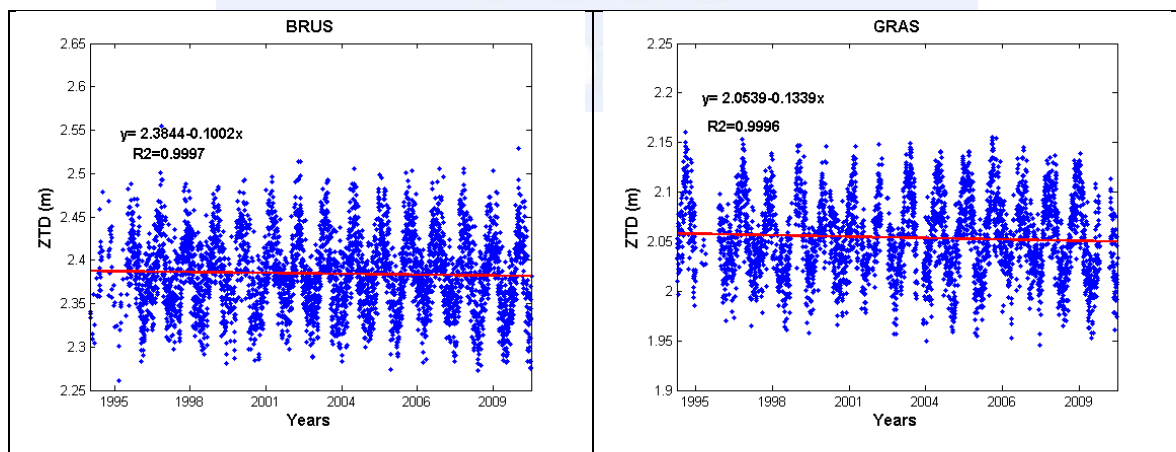


Figure 2. Simple linear regression trend graphics of BRUS and GRAS stations

The change in parameter of a_1 is shown in Figure 3. The colour scale was used to make a general assessment of the direction and magnitude of the trend at stations was. Value of a_1

between -0.1339 to 0.005 is red colour, 0.005 to 0.1078 is yellow colour, and 0.1078 to 0.2475 is green colour. The conclusions obtained from here are in great agreement with the trend graphs drawn separately for each station according to the simple linear regression model.



Figure 3. Slope of trend at IGS stations according to simple linear regression

According to Mann-Kendall test result, ANKR, EBRE and MAS1 stations have trends that increasing direction. There are no trends at other stations (Figure 4).



Figure 4. Mann-Kendall test result

The stations based trend analysis comparing Z test values calculated according to the Mann-Kendall test and Z_{table} value with 95% statistic confidence are shown in Table 2.

Table 2. Mann-Kendall test

Station Code	Normalized Mann-Kendall statistic (Z)	Standard normal distribution table value (Z) ($\alpha=0.05$)	Trend	Direction of trend
ANKR	7.6578	1.96	Trend	Upward
BOR1	1.7687	1.96	No Trend	-
BRUS	-2.3002	1.96	No Trend	-
EBRE	2.1397	1.96	Trend	Upward
GOPE	1.4549	1.96	No Trend	-
GRAS	-2.9557	1.96	No Trend	-
GRAZ	-0.9073	1.96	No Trend	-
HERS	-0.6723	1.96	No Trend	-
JOZE	-0.3171	1.96	No Trend	-
KIRU	1.6757	1.96	No Trend	-
LAMA	1.1883	1.96	No Trend	-
MAS1	4.3215	1.96	Trend	Upward
MATE	0.7774	1.96	No Trend	-
METS	0.544	1.96	No Trend	-
PENC	-1.4826	1.96	No Trend	-
POTS	0.5327	1.96	No Trend	-
REYK	1.5295	1.96	No Trend	-
WTZR	-1.3315	1.96	No Trend	-
ZIMM	0.2202	1.96	No Trend	-

CONCLUSIONS

Trend determination in long-term ZTD time series has great importance in monitoring climate change. Trend analysis of ZTD time series graphics or test values indicate how effective is the wet component of ZTD.

In this study, used Simple Linear Regression Model and Mann-Kendall test. Test results are shown in Table 3.

Table 3. Parametric and nonparametric test results

Station Code	Simple Linear Regression Model	Mann-Kendall Test
ANKR	+	+
BOR1	+	0
BRUS	-	0
EBRE	+	+
GOPE	0	0
GRAS	-	0
GRAZ	0	0
HERS	0	0
JOZE	0	0
KIRU	0	0
LAMA	0	0
MAS1	+	+
MATE	0	0
METS	0	0
PENC	0	0
POTS	0	0
REYK	0	0
WTZR	0	0
ZIMM	0	0

where "+" expresses the trend in increasing direction, "-" expresses the trend in decreasing direction and "0" indicates no trend. According to simple linear regression model, within the scope of stations used in work, there is a trend just in BOR1 (Poland) station which located in the Central Europe region. GOPE (Czech Republic), GRAZ (Austria), PENC (Hungary), WTZR (Germany) and POTS (Germany) are Central Europe region and noncoastal stations. There are no trends at these stations. LAMA (Poland) and JOZE (Poland) stations are coastal and it is seen that, there is no trend at these stations compared to the BOR1 (Poland) station. Trends in decreasing direction BRUS (Belgium) and GRAS (France) stations which located in West Europe region. Generally, it is seen that, the trends of the stations in the same geographical region are the same. According to Mann-Kendall test, there is trend at ANKR, EBRE and MAS1 stations and trend is increasing at these stations. On the other hand, there is no trend other station.

ACKNOWLEDGMENTS

We would like to acknowledge Dr. Olivier BOCK, IGN, France, for making the IWV data from IGS repro1 and ERA-Interim available. These data were prepared and quality checked in the framework of COST Action ES1206, GNSS4SWEC.

REFERENCES

- Baldysz, Z., Nykiel, G., Figurski, M., Szafranek, K. ve Kroszczyński, K., 2015. Investigation of the 16-year and 18-year ZTD Time Series Derived from GPS Data Processing, *Acta Geophysica*, 1103-1125.
- Baldysz, Z., Nykiel, G., Araszkiewicz, A., Figurski, M., ve Szafranek, K., 2016. Comparison of GPS Tropospheric Delays Derived from Two Consecutive EPN Reprocessing Campaigns from the Point of View of Climate Monitoring, *Atmos. Meas. Tech. Discuss.*, doi:10.5194/amt-2016-5, 1.
- Bayazıt, M. ve Yeğen Oğuz, E.B., 2005. *Mühendisler İçin İstatistik*, Birsen Yayınevi, İstanbul.
- Beşel, C. ve Tanır Kayıkçı, E., 2016. Meteorolojik Verilerin Zaman Serisi ve Tanımlayıcı İstatistiklerle Yorumlanması; Karadeniz Bölgesi Örneği, *TÜCAUM Uluslararası Coğrafya Sempozyumu*, Ekim, Ankara, Bildiriler Kitabı: 50-69.
- Beşel, C., 2017. *IGS İstasyonları Zenit Troposferik Gecikme Parametresi Zaman Serilerinde Trend ve Mevsimsel Etki Analizleri*, Yüksek Lisans Tezi, Karadeniz Teknik Üniversitesi, Fen Bilimleri Enstitüsü, Trabzon.
- Bevis, M., Businger, S., Herring, T.A., Rocken, C., Anthes, R.A. ve Ware, R.H., 1992. GPS Meteorology: Remote Sensing of Atmospheric Water Vapour Using The Global Positioning System, *Journal of Geophysical Research*, 97, D14, 15787– 15801.
- Bianchi, C.E., Mendoza, L.P.O., Fernandez, L.I., Natali, M.P., Meza, A.M. ve Moirano, J.F., 2016. Multi-year GNSS Monitoring of Atmospheric IWV over Central and South America for Climate Studies, *Ann. Geophys.*, 34, 623-639.
- Bosy, J., Rohm, W., Sierny, J. ve Kaplon, J., 2011. GNSS Meteorology, *International Journal on Marine Navigation and Safety of Sea Transportation*, 5, 79-83.
- Box, G.E.P. ve Jenkins, G.M., 1976. *Time Series Analysis Forecasting and Control*, Revised Edition, Holden Day Inc., ISSN 0130607746, California.
- COST, 2012. Memorandum of Understanding Fort He Implementation of a European Concerted Research Action, COST Action ES1206, Advanced Global Navigation Satellite Systems Tropospheric Products for Monitoring Severe Weather Events And Climate (GNSS4SWEC), European Cooperation in Science and Technology.
- Çeribaşı, G., 2015. *Karadeniz ve Sakarya Havzalarında Yağış Askıda Katı Madde Verilerinin Trend Analizi ile İncelenmesi*, Doktora Tezi, Sakarya Üniversitesi, Fen Bilimleri Enstitüsü, Sakarya.

- Demircan, M., 2016. Arabacı, H., Coşkun, M., Türkoğlu, N. ve Çiçek İ., Sıcaklıkların Aylık Dağılım Desenleri, *TÜCAUM 2016 Uluslararası Coğrafya Sempozyumu*, Ekim, Ankara, Bildiriler Kitabı: 98-105.
- Demircan, M., Tanır Kayıkçı, E. ve Zengin Kazancı, S., 2016. Comparison of Water Vapour Estimates in Ankara, Turkey, *9th European Conference on Radar in Meteorology and Hydrology (ERAD2016)*, Ekim, Antalya.
- Gocic, M. ve Trajkovic, S., 2013. Analysis of Changes in Meteorological Variables Using Mann-Kendall and Sen's Slope Estimator Statistical Tests in Serbia, *Global and Planetary Change*, 100,172-182.
- Guerova, G., 2013.Ground-Based GNSS Meteorology, Gfg Summer School, Potsdam, Almanya.
- Guerova, G., 2015.Exploitation of Ground-Based GNSS for Meteorology and Climate Studies in Bulgaria/South-Eastern Europe, FIG Working Week 2015 from the *Wisdom of the Ages to the Challenges of the Modern World Sofia, Bulgaria*, *Bildiriler Kitabı*: 1-8.
- Guerova, G., Ground Based GNSS Meteorology, [http://www.gfg2.eu/sites/gfg2.eu/files/guero va_gpsmet.pdf](http://www.gfg2.eu/sites/gfg2.eu/files/guero_va_gpsmet.pdf), 26 Ocak 2017.
- Gümüş, V., 2006.*Fırat Havzası Akımlarının Trend Analizi ile Değerlendirilmesi*, Yüksek Lisans Tezi, Harran Üniversitesi, Fen Bilimleri Enstitüsü Şanlıurfa.
- Hopfield, H.S., 1971.Tropospheric Effect of Electromagnetically Measured Range: Prediction from Surface Weather Data, *Radio Science*, 6, 357-367.
- Hopfield, H.S., 1972. Tropospheric Refraction Effects on Satellite Range Measurement, *APL Technical Digest*, 11, 11-19.
- Jin, S., Park, J., Cho, J. ve Park, P., 2007.Seasonal Variability of GPS-Derived Zenith Tropospheric Delay (1994-2006) and Climate Implications, *Journal of Geophysical Research*, 112, D09110, doi:10.1029/2006JD007772.
- Kalaycı, S. ve Kahya E., 1998. Susurluk Havzası Nehirlerinde Su Kalitesi Trendlerinin Belirlenmesi, *Tr. J. of Engineering and Environmental Science*, 22, 503-514.
- Kendall, M.G., 1975. *Rank Correlation Methods*, Charles Griffin, London.
- Kleijer, F., 2004. *Troposphere modeling and filtering for precise GPS leveling*, Delft University of Technology, Delft.
- Klos, A., Hunegnaw, A., Teferle, F.N., Abraha, K.E., Ahmed, F. ve Bogusz, J., 2016. Noise Characteristics in Zenith Total Delay from Homogeneously Reprocessed GPS Time Series, *Atmos.Meas.Tech.Discuss.*, 1-28,doi:10.5194/amt-2016-385.
- Lindenbergh, R., Keshin, M., Van der Marel, H. ve Hanssen, R., Combining Water Vapor Data from GPS and Meris, Delft Institute of Earth Observation and Space Systems, DelftUniversityofTechnology,<http://www.isprs.org/proceedings/XXXVI/part7/PDF/018.pdf> , 17 Ocak 2017.

- Longobardi, A. ve Villani P., 2009. Trend Analysis of Annual and Seasonal Rainfall Time Series in the Mediterranean Area, *International Journal of Climatology*, doi: 10.1002/joc.2001.
- Mann, H.B, 1945. Non-Parametric Tests Against Trend, *The Econ. Society*, 3, 245-259.
- Mann, S.P., 1995. *Statistics for Business and Economics*, Wiley, USA.
- Nychka, D., Ten Lectures on Statistical Climatology, <http://www.statmos.washington.edu/?p=42>, 8 Ekim 2013.
- Öztürk, E. ve Şerbetçi, M., 1992. *Dengeleme Hesabı, Cilt III*, KTÜ Basımevi, Genel Yayın No: 144, Fakülte Yayın No:40, Trabzon.
- Rocken C., Hove.,T.V., Johnson, J., Solheim, F., Ware, R., Bevis, M., Chiswell, S. ve Businger, S., 1994. GPS/STORM-GPS Sensing of Atmospheric Water Vapor for Meteorology, *Journal of Atmospheric and Oceanic Technology*, 12, 468-478.
- Tanır Kayıkçı, E., Zengin Kazancı S. ve Tornatore, V., 2016. Analysis of ZTD and IWV Time Series from GPS Reprocessing Campaign, *COST ES1206 sub-WG Workshop on Data Homogenisation*, Brüksel, Belçika.
- Tanır Kayıkçı, E., Tornatore, V. ve Zengin Kazancı S., 2017. Effect of Data Homogenization for Trend and Seasonal Signal Detection, *ES 1206 COST Action Final Workshop*, Şubat, Hollanda.
- URL-1, <ftp://cost1206homogen@ftp-as.oma.be>. 29 Mart 2016.
- Yadav, G., Mishra, N., Prashanthi, K. ve Chaturvedi, S., 2015. Air Pollution Trend Analysis Using Sen Estimator Method-a Survey, *International Journal of Science and Research*, 4,3, 71-76.
- Yong, W., Binyun, Y., Debao, W. ve Yanping, L., 2008. Zenith Tropospheric Delay from GPS Monitoring Climate Change of Chinese Mainland, *Education Technology and Training*, 2008 and 2008 International Workshop on Geoscience and Remote Sensing, ETT and GRS 2008, International Workshop on, 1, doi: 10.1109/ETTandGRS.2008.43.
- Yue, S., Zou, S. ve Whittemore, D., 1993. Non-parametric Trend analysis of Water Quality Data of Rivers in Kansas, *Journal of Hydrology*, 37, 61-80.
- Yücel, A. ve Topaloğlu, F., 1999. Adana İli Uzun Yıllık (1929-1990) Günlük Minimum, Ortalama ve Maksimum Sıcaklık Verilerinin Zaman Serisi Analizi ile İncelenmesi, *Turkish Journal of Agriculture and Forestry*, 23, Ek Sayı 4, 863-868.
- Zengin Kazancı, S., 2014. *Konumsal Enterpolasyon Yöntemlerinin Uygulanması Üzerine Bir Çalışma: Karadeniz Bölgesi Günlük Ortalama Sıcaklık Verileri Örneği*, Yüksek Lisans Tezi, Karadeniz Teknik Üniversitesi, Fen Bilimleri Enstitüsü, Trabzon.
- Zengin Kazancı, S., Tanır Kayıkçı, E. ve Tornatore, V., 2017. Comparison of Time Series Homogenization of IWV Estimates at IGS Stations, *COST ES1206 Sub-Working Group "Data Homogenisation": 2nd Workshop*, Ocak, Polonya.

Comparison of Areal Precipitation Estimation Methods in Akarcay Basin, Turkey

Emin Tas¹

¹Department of Civil Engineering, Afyon Kocatepe University, Ahmet Necdet Sezer Campus, 03200, Turkey.
emintas@aku.edu.tr

ABSTRACT

In this study, it is aimed to model spatial distribution of mean annual precipitation in Akarcay basin by using GIS techniques. In this context, point precipitation data of meteorological observation stations in and around Akarcay basin is used for spatial interpolation. As areal precipitation estimation methods, various deterministic and geostatistical interpolation methods are applied. Thiessen (T), inverse distance weighted (IDW), natural neighbor (NN), spline (S), radial basis functions (RBF), local-global polynomial interpolation (LPI-GPI) and Simple Kriging (SK) methods are practiced in this paper. Then, spatial interpolation techniques are compared with each other and optimal method for Akarcay basin is determined in terms of model performance test by performing cross validation. In this way, annual precipitation prediction in ungauged areas can be made, water potential of basin can be determined and similar subbasins in terms of precipitation can be identified. Performing spatial analysis of precipitation is crucial for decision makers in water resources planning and management works as reservoir operating, irrigation, water supply system, hydroelectric power generation, flood and drought forecasting.

INTRODUCTION

Precipitation is one of basic inputs in most hydrometeorology studies. Therefore, accuracy and reliability of areal precipitation estimation are crucial for success of water resources management. Because of precipitation is more changeable in terms of spatiotemporal than other many climatic variables, gauge-based observations are insufficient to represent areal precipitation. Due to economical, geographical and other constraints in especially mountainous areas, point observations are single-handedly inadequate to measure accurately amount of precipitation. For this reason, areal precipitation modeling may be necessary alongside of remote-sensed observations.

On spatial distribution of precipitation, a great deal of studies have done using various methods in many countries of the world. Ball and Luk (1998) stated that developing computer technology and hydroinformatics tools facilitated estimation models' application of precipitation, an important component of basin simulation process. It was emphasized that accurate and reliable real time prediction of spatial distribution of precipitation was

possible in Upper Parramatta catchment in Australia by using a GIS software (Arc Info). Saghafian and Bondarabadi (2008) investigated spatial distribution of precipitation in mountainous areas, which are insufficient in number and distribution of observation stations. In the southwest of Iran, validity of interpolation-extrapolation techniques was researched in mountainous areas using S, weighted moving average, Ordinary Kriging (OK) and Co-Kriging (CK) methods. Although S method was the most accurate method according to cross-validation in the study, it was pointed out that CK method showed better consistency with land topography. Wang et al. (2014) compared six different interpolation techniques (IDW, LPI, GPI, RBF, OK and Universal Kriging-UK) and evaluated by cross validation in Canada. LPI was optimal method in terms of results. Adhikary et al. (2016) used genetic programming and artificial neural networks (ANN) based OK methods to determine spatial distribution of precipitation and demonstrated that genetic programming based OK method gives more successful results than ANN based and conventional OK methods. Citakoglu et al. (2017) estimated spatial variability of seasonal precipitation by using Gaussian type semi-variogram based Kriging method. Monthly mean precipitation data of 200 meteorological observation stations located in Turkey were used in their paper. Chen et al. (2017) analyzed three different interpolation methods, principal component regression with residual correction (PCRR), IDW and multiple linear regression (MLR) in Fuhe river catchment in China at annual, daily and hourly time scales. Additionally, impact of rainfall interpolation methods was evaluated on results of a hydrologic model, HEC HMS. According to the study, PCRR is better than other methods.

Several studies have used auxiliary variable as particularly elevation data in interpolating spatial precipitation. Carrera-Hernandez and Gaskin (2007) applied spatiotemporal analysis of daily precipitation and temperature in the Basin of Mexico by using Kriging methods and stated that elevation as a secondary variable, increases performance of interpolation. Di Piazza et al. (2011) practiced different spatial interpolation techniques (IDW, linear regression, geographically weighted regression-GWR, ANN and Kriging) to complete missing data values of monthly precipitation time series for Sicily. In some techniques, elevation was model input as co-variable. A part of data set was included in the modeling, the other part was used in the validation to compare different techniques with model performances. In the study it was expressed that methods disused elevation have bigger error and OK method has the best performance. Bostan et al. (2012) modeled spatial distribution of mean annual precipitation of Turkey via MLR, OK, regression Kriging (RK), UK and GWR by using secondary data such as elevation, aspect and river density and studied the effects of secondary data on model performance. In order to compare performance of interpolation techniques, k-fold cross validation was used; data set was randomly divided into ten equal parts, 90% of each part being used as training data set (calibration) and the rest as test data set (validation). The predictions of the interpolation model established using the training data set were compared with the test data set in terms of various performance criteria. According to the validation results, UK was the most accurate method, MLR was found as the worst method. In addition, extrapolation of annual precipitation for eastern part of Turkey was carried out using observation stations located in western part of Turkey and it was stated that MLR, GWR and RK methods gave the best

results with close error values. It is also specified that auxiliary variables increase interpolation and extrapolation performance greatly. Gonga-Saholiariliva et al. (2016) carried out geostatistical estimation of daily monsoon rainfall by means of Ordinary CK (OCK) method, which uses elevation as an auxiliary variable in the Koshi river basin, a mountainous region of Nepal where precipitation is highly changeable. OCK results were compared with data sets produced by Aphrodite Project (Asian Precipitation-Highly Resolved Observational Data Integration Towards Evaluation of Water Resources) and it was mentioned that OCK grids (1 km resolution) have better match with observed values than Aphrodite grids (25 km resolution). It was also emphasized that OCK has advantage of higher product resolution.

In this study, ground based precipitation data of meteorological stations in and around Akarcay basin is inputted into spatial interpolation models. Various deterministic and geostatistical interpolation techniques are performed and compared by cross validation performance test. The main motivation of the paper is spatial precipitation modeling and prediction by using optimal method in Akarcay basin, a quite arid basin.

MATERIALS AND METHODS

Study Area and Data

This study is carried out for spatial interpolation of precipitation in Akarcay closed basin (Figure 1) which includes river basins of Eber and Aksehir Lakes in the western of Turkey. A large part of the basin is located within borders of Afyonkarahisar province. The basin has an area of 7993 km² and ranges in altitude from 905 to 2561 m with a mean elevation 1207 m and a mean slope % 10. Approximately 40% of the basin area is the plain area. Sultan mountains in southeast of the basin are important mountainous areas. The main land cover types are agricultural (% 42) and pasture (% 28). Mean annual runoff volume of the basin is 0,49 km³. Main river of the study basin is Akarcay whose average discharge is 6 m³/s (at outlet to Eber Lake) with a max observed stream flow 165 m³/s that is obtained from General Directorate of State Hydraulic Works of Turkey. The slope of main stream channel is % 2. Annual mean total precipitation and annual mean temperature are respectively about between 400-450 mm and 11 °C that are derived from meteorological stations of Turkish State Meteorological Service. Eber and Aksehir Lakes are ecologically wetlands of international importance and protected under the Ramsar Convention. Due to the basin has great agricultural importance and is faced with high drought risk, water resources planning and management studies are crucial in the basin.

Long term observed annual precipitation data of 26 meteorological stations (Table 1) located in and around study area is used as input for interpolation methods. DEM (Digital Elevation Model) is provided SRTM (Shuttle Radar Topography Mission) conditioned with HydroSHEDS data base whose spatial resolution is approximately 90 m (3 arc-sec). DEM is used to derive various layers related to basin characteristics as slope, aspect and river network by spatial analysis. Land cover data of the basin is taken from EEA (European Environment Agency) CORINE database and reclassified appropriately.

Table 1. Information and long term observed annual precipitation data of meteorological stations

Station		Altitude (m)	Annual precipitation (mm)						
No	Name		Min	Mean	Median	Max	Std. dev.	Skewness	Kurtosis
17190	Afyon	1034	238	435	445	679	92	0,22	0,10
17830	Aksehir	1010	264	610	613	943	134	0,20	0,35
4956	Bayat	1100	286	436	454	548	79	-0,40	-0,82
17796	Bolvadin	1018	212	391	380	746	83	1,07	4,15
5477	Cay	1020	334	526	511	751	99	0,30	-0,32
17862	Dinar	864	282	451	454	638	85	0,05	-0,47
4947	Dumlupinar	1250	428	521	493	669	90	0,96	0,01
17752	Emirdag	945	162	401	411	699	99	0,17	0,55
4777	Ihsaniye	1110	306	419	402	779	91	2,09	7,58
5128	Iscehisar	1100	255	385	398	518	72	0,00	-0,81
17794	Sandikli	1100	320	471	485	669	89	0,04	-0,89
5296	Sinanpasa	1130	344	542	534	760	99	0,13	-0,33
5650	Sultandagi	1020	300	516	513	697	112	-0,10	-1,17
5643	Suhut	1130	212	383	394	540	88	-0,29	-0,87
5827	Tuzlukcu	1000	194	321	320	489	86	0,22	-0,93
11006	Bozhoyuk	1155	264	403	408	530	62	-0,21	-0,39
11007	Cankurtaran	1525	423	662	654	940	134	0,25	-0,62
11012	Eber	975	215	347	349	514	72	0,16	-0,02
11002	Kocbeyli	1065	372	563	576	802	123	0,12	-0,94
11008	Kulak	1310	320	467	494	640	98	0,00	-1,34
11009	Maltepe	1000	246	399	410	524	75	-0,63	-0,39
11004	Selevir	1130	194	352	351	464	73	-0,15	-0,80
07009	Serban	1215	317	505	481	794	115	0,85	0,26
11005	Seydiler	1150	258	406	394	592	72	0,43	0,47
11001	Seyitler	1060	209	345	330	456	62	0,23	-0,79
11011	Taskopru	960	186	340	347	501	81	-0,12	-0,87

Interpolation Methods

Spatial interpolation of precipitation consists of three main parts as pre-process (dataset processing and GIS basement), modeling and post-process (efficiency criteria tests). In this paper, all stages are realized in GIS environment.

GIS is a crucial decision support system in numerous fields as well as water resources branch for collection, storage, compilation, selection by location, spatial analyses and presentation processes of data. ArcGIS used in this study, a software of ESRI (Environmental Systems Research Institute, California) is a GIS packaged software that can performed mapping, geographical analyses, data organization, data management and visualization operations by integrated interfaces (Icaga et al., 2016). ArcGIS includes many interpolation methods, some are quite flexible and can use different aspects of sample data. Others are more restrictive and require that the data actualize specific conditions. Each of these methods has typical parameter sets to calibrate model for a particular dataset and requirements for output prediction layer. Interpolation methods derives a continuous surface from sample points that are classified as deterministic (mathematical functions) and geostatistical (stochastic). In spite of deterministic methods are based on similarity extent of measured points and degree of smoothing; geostatistical techniques utilize statistical properties of measured points to quantify spatial autocorrelation and assess uncertainty of predictions. In addition, interpolation methods can be divided into two groups: local and global. While local techniques use measured points within neighborhoods in prediction, global ones consider entire dataset (ESRI, 2001). Deterministic interpolation methods are T, IDW, NN, S, RBF, LPI and GPI techniques; geostatistical method is SK used in this study. Interpolation models are optimized by performing manual calibration such as neighborhood, order and type of function searches and automatic calibration of parameters and semivariogram/covariance modeling. General expression of interpolation methods is;

$$P = \sum_{i=1}^N \lambda_i P_i \quad (1)$$

where P is predicted value of interpolation point; P_i is value of observation point i ; N is number of sample points and λ_i is weight for measured value at i th point.

Thiessen Polygons (T)

T approach (Thiessen, 1911) based on basin geometry and station locations defines the polygon area closer to an observation station and assumes that spatial precipitation on that area is represented by point measurement at the observation station.

Inverse Distance Weighted (IDW)

IDW (Watson and Philip, 1985) based on distance of each gauge from point where rainfall is estimated supposes that nearby points have most influence on interpolation point. Areal rainfall is estimated with weights being inversely proportional to square distance between observation points and given by;

$$P = \frac{\sum_{i=1}^N \frac{1}{d_i^2} P_i}{\sum_{i=1}^N \frac{1}{d_i^2}} \quad (2)$$

where P is predicted value of interpolation point; P_i is value of sample point i ; N is number of sample points and d_i is distance between interpolated and sample points.

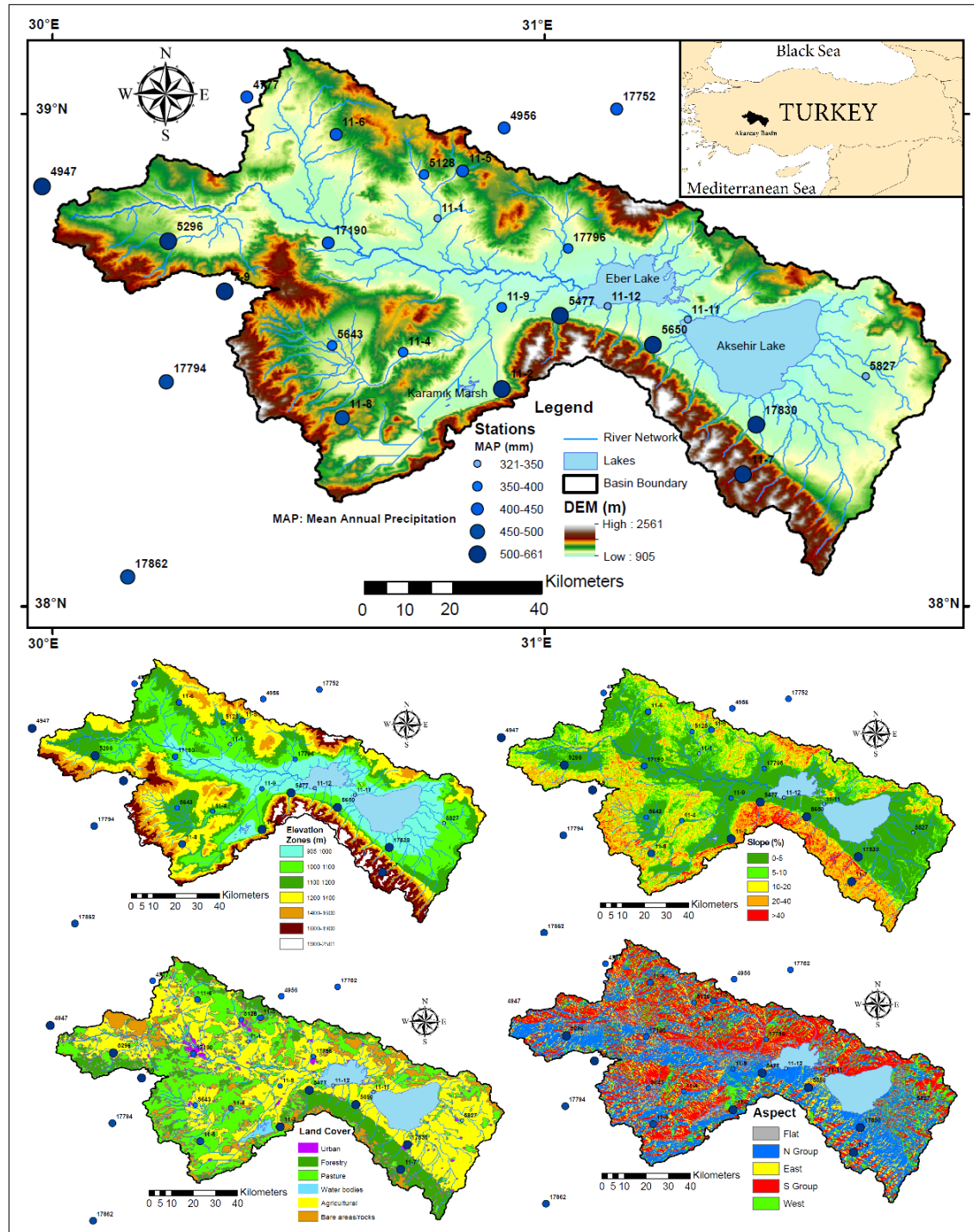


Figure 1. Geographical location-characteristics of study area and position of meteorological stations

Natural Neighbor (NN)

NN (Sibson, 1981), a local interpolation technique based on Voronoi polygons finds the closest subset of input samples to a query point and applies weights to them based on proportionate areas to interpolate a value.

Spline (S)

S method (Shaw and Lynn, 1972; Franke, 1982) uses a mathematical function that minimizes overall surface curvature. Like RBF, S method is also more convenient for gently varying surfaces due to basic minimum curvature technique, thin plate smoothing interpolation. In this study, regularized spline type is used.

Radial Basis Functions (RBF)

Unlike LPI and GPI, RBF interpolates a surface passed through each sample points as an exact interpolator while minimizing total curvature of surface. RBF is ineffective to predict surface values with high spatial variability in short distance. RBF can be locally sensitive to outliers. RBF is a form of ANN that can predict values above maximum and below minimum observed values compared with IDW, another exact interpolator. Whereas IDW never predict values above max or below min measured values (ESRI, 2001). Spline with tension as kernel function is utilized in this paper.

Local Polynomial Interpolation (LPI)

LPI uses points only within specified overlapping neighborhoods to estimate, for this reason LPI is more suitable to represent short range variation. LPI is sensitive to neighborhood distance that weights of sample points within defined neighborhood decrease based on distance (ESRI, 2001). Epanechnikov as kernel function is applied in this study.

Global Polynomial Interpolation (GPI)

GPI fits a smooth surface -which highly is susceptible to outliers, changes gradually and has global pattern- to sample points by a polynomial function. GPI uses whole dataset to predict in contrast to local interpolation methods, thereof GPI is useful to determine long range trends (ESRI, 2001).

Simple Kriging (SK)

Kriging is an advanced powerful geostatistical technique that is related to spatial distribution analysis of sample points as distinct from deterministic interpolation techniques. Kriging takes account of spatial correlation and statistical relationships between observation points differently from deterministic methods (Krige, 1951). Prediction error and probability output layers can be also obtained in Kriging family methods. There are data assumptions such as normal distributed, detrending and declustering in Kriging. For quantifying spatial structure of data (variography), Kriging fits a spatial dependence model by semivariogram and covariance analysis. SK, OK, CK, UK, RK, residual Kriging, moving window Kriging, indicator Kriging, disjunctive Kriging and Bayesian Kriging are different types of Kriging method. SK assumes a constant mean. Whenever trend is known, it forms the model for SK (ESRI, 2001). In this research,

transformation for normal distribution, trend removal by local polynomial interpolation (epanechnikov kernel function), declustering and semivariogram analysis are performed.

Cross Validation

Cross validation test (Isaaks and Srivastava, 1989), a statistical technique with residual evaluation is applied to assess accuracy and skill of interpolation models in terms of root mean square error (RMSE). It can be used to determine best spatial interpolation method. In cross validation (leave-one-out) test process, data values are eliminated one after another from observed data and then each data value (witness station observation) is predicted using remaining data and interpolation methods. For comparison of predicted and observed values, RMSE, standard deviation of prediction residuals is used to analyze the error originating from interpolation. RMSE, a performance criteria to measure strength of statistical relationship between observed and predicted values that is calculated as follows:

$$RMSE = \sqrt{\frac{1}{N} \sum_{i=1}^N (M_i - O_i)^2} \quad (3)$$

where M_i is the i th predicted value, O_i is the i th observation value and N is the total number of observations. In evaluation process of sensitivity and suitability of interpolation models, less RMSE value means better quality of prediction.

RESULTS AND DISCUSSION

Spatial precipitation prediction maps of interpolation methods are presented in Figure 2. Comparison results in terms of RMSE of interpolation methods are given in Table 2. RMSE values are changed between 53-107 mm that are about %10-20 of mean annual precipitation of stations. While SK, LPI, NN and RBF are given close error values, T has maximum RMSE.

Table 2. Cross validation performance test results of interpolation techniques used

Interpolation method	RMSE (mm)	Rank
SK	53	1
LPI	53	1
NN	57	2
RBF	59	3
IDW	81	4
S	87	5
GPI	92	6
T	107	7

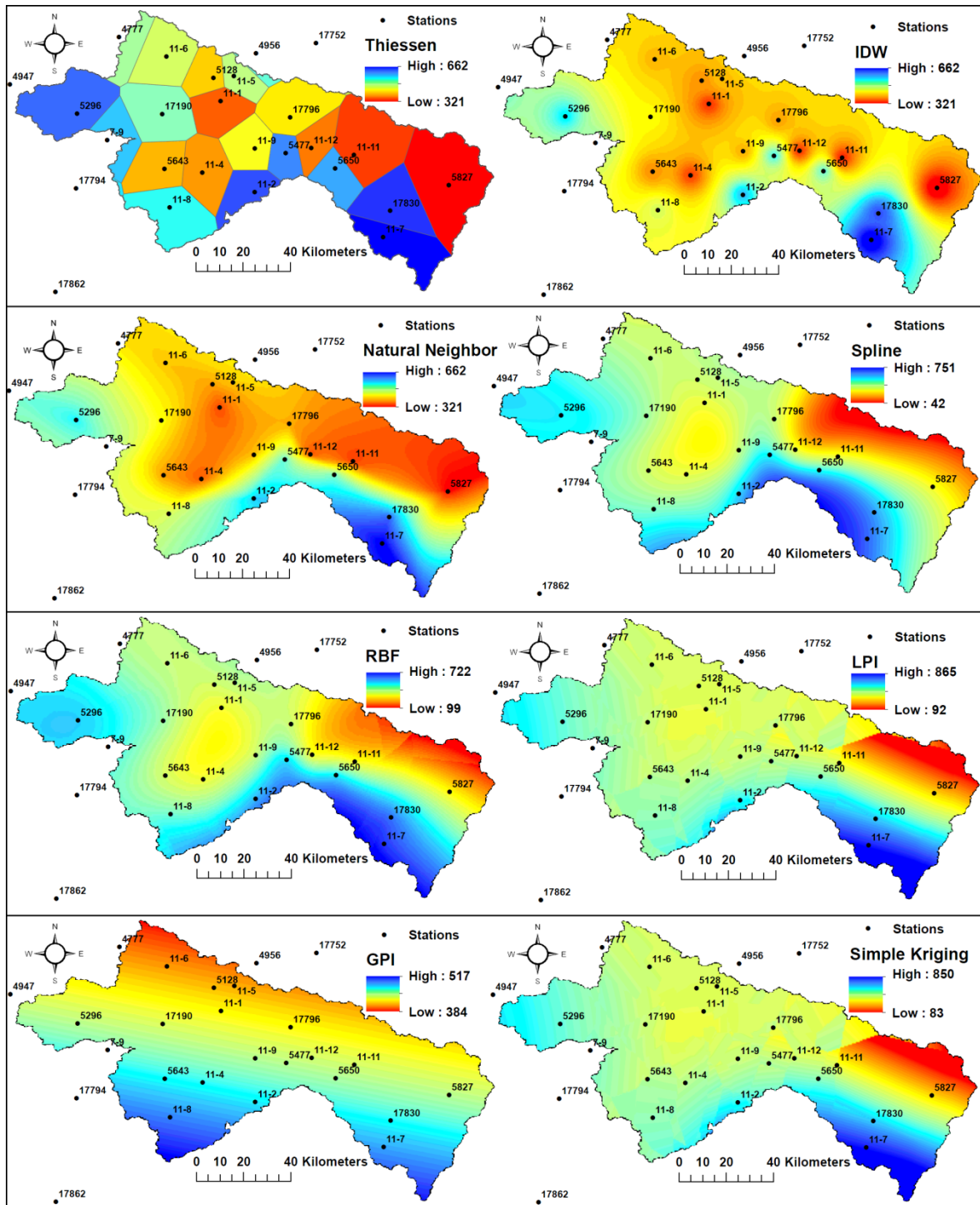


Figure 2. Spatial distributions of mean annual precipitation (mm) by interpolation methods used

CONCLUSION AND RECOMMENDATIONS

In this study, eight different interpolation methods (T, IDW, NN, S, RBF, LPI, GPI and SK) are considered to model spatial distribution of mean annual precipitation in Akarcay basin and evaluated by cross validation in terms of RMSE performance criterion. According to the results, best methods are SK and LPI with min RMSE (53 mm) and worst

method is T with max RMSE (107 mm) for mean annual precipitation in study area. NN and RBF with close RMSE values to SK and LPI can be used for spatial precipitation in the basin. The results show that SK, LPI, NN and RBF can be regarded as optimal interpolation models; it can be said that IDW, S, GPI and T have poor performance models for Akarcay basin.

It can be stated that interpolation accuracy is higher in lowlands due to more dense station network in comparison of highlands. When stochastic and deterministic methods with solid performance used in this paper are compared, it is seen that they have no clear advantages to each other in study area. When smooth transition between rainfall gauge locations is evaluated, all methods except T method have sufficiently smoothness. Only RBF, LPI and SK have sharp transitions in northeast of the basin.

In Akarcay basin, determination of spatial precipitation distribution is essential drought analysis, reservoir operating, irrigation and ecology of Eber and Aksehir Lakes. In addition, importance of precipitation spatiotemporal distribution for hydro-meteorological studies as hydrological modeling, climate change and land use effect is great. Accordingly, spatial distribution of other climatic variables such as air temperature can be analyzed. Temporal distribution of various hydro-meteorological factors can be considered. Effects of using auxiliary data such as elevation, vegetation and temperature on spatial interpolation performance can be searched. Univariate and multivariate analyses in precipitation spatial distribution can be compared. The performance of interpolation methods in spatial distribution of precipitation can be compared, evaluated and integrated with satellite based and radar products besides of ground based observations. The interpolation model performance can be enhanced by some techniques as updating, correction factor and downscaling. Furthermore, spatial interpolation performance of precipitation can be tested by using a hydrological model. The success of hydrological model is a very strong indicator of accuracy and robustness level of spatial precipitation, a basic input data for the model.

REFERENCES

- Adhikary, S. K., Muttil, N. and Yilmaz, A. G., 2016. Genetic programming-based Ordinary Kriging for spatial interpolation of rainfall. *J. Hydrol. Eng.*, 21 (2), -1--1.
- Ball, J. E. and Luk, K. C., 1998. Modeling spatial variability of rainfall over a catchment. *J. of Hydrol. Eng.*, 3 (2), 122-130.
- Bostan, P. A., Heuvelink, G. B. M. and Akyurek, S. Z., 2012. Comparison of regression and kriging techniques for mapping the average annual precipitation of Turkey. *Int. J. of Applied Earth Observation and Geoinformation*, 19, 115-126.
- Carrera-Hernandez, J. J. and Gaskin, S. J., 2007. Spatio temporal analysis of daily precipitation and temperature in the Basin of Mexico. *J. of Hydrology*, 336 (3-4), 231-249.

- Chen, T., Ren, L., Yuan, F., Yang, X., Jiang, S., Tang, T., Liu, Y., Zhao, C. and Zhang, L., 2017. Comparison of spatial interpolation schemes for rainfall data and applications in hydrological modeling. *Water*, 9: 342, 1-18.
- Citakoglu, H., Cetin, M., Cobaner, M. and Haktanir, T., 2017. Modeling of seasonal precipitation with geostatistical techniques and its estimation at un-gauged locations. *IMO Teknik Dergi*, 469, 7725-7745.
- Di Piazza, A., Lo Conti, F., Noto, L. V., Viola, F. and La Loggia, G., 2011. Comparative analysis of different techniques for spatial interpolation of rainfall data to create a serially complete monthly time series of precipitation for Sicily, Italy. *Int. J. of Applied Earth Observation and Geoinformation*, 13, 396-408.
- ESRI, 2001. *Using ArcGIS geostatistical analyst*. ESRI Press, Redlands, CA.
- Franke, R., 1982. Smooth interpolation of scattered data by local thin plate splines. *Computer and Mathematics With Applications*, 8 (4), 273-281.
- Gonga-Saholiariliva, N., Neppel, L., Chevallier, P., Delclaux, F. and Savean, M., 2016. Geostatistical estimation of daily monsoon precipitation at fine spatial scale: Koshi river basin. *J. of Hydrol. Eng.*, 21 (9), -1--1.
- Icaga, Y., Tas, E. and Kilit, M. 2016. Flood inundation mapping by GIS and a hydraulic model (HEC RAS): A case study of Akarcay Bolvadin subbasin, in Turkey. *Acta Geobalcanica*, 2 (2), 111-118.
- Isaaks, E. H. and Srivastava, R. M., 1989. An introduction to applied geostatistics. *Oxford University Press*, New York, 351-368.
- Krige, D. G., 1951. A statistical approach to some mine valuations and allied problems at the Witwatersrand, *MSc Thesis of the University of Witwatersrand*.
- Saghafian, B. and Bondarabadi, S. R., 2008. Validity of regional rainfall spatial distribution methods in mountainous areas. *J. of Hydrol. Eng.*, 13 (7), 531-540.
- Shaw, E. M. and Lynn, P. P., 1972. Areal rainfall estimation using two surface fitting techniques. *Hydro. Sci. Bull.*, XVII (4), 419-433.
- Sibson, R., 1981. A brief description of natural neighbor interpolation, V. Barnett (Ed.), *Interpreting Multivariate Data*, Wiley, Chichester, 21-36.
- Thiessen, A. H., 1911. Precipitation averages for large areas. *Monthly Weather Rev.*, 39 (7), 1082-1084.
- Wang, S., Huang, G. H., Lin, Q. G., Li, Z., Zhang, H. and Fan, Y. R., 2014. Comparison of interpolation methods for estimating spatial distribution of precipitation in Ontario, Canada. *Int. J. Climatol.*, 34: 3745-3751.
- Watson, D. F. and Philip, G. M., 1985. A refinement of inverse distance weighted interpolation. *Geo-Processing*, 2, 315-327.

Evaluating the impact of agricultural drought using MODIS sensor: A Case Study over the Aegean Region

Semra Kocaaslan Karamzadeh^{*1}, Nebiye Musaoğlu²

¹Department of Applied Informatics, Geographical Information Technologies Program, Istanbul Technical University, Ayazaga Campus, 34469, Turkey, (e-mail: kocaaslan@itu.edu.tr).

²Geomatics Engineering Department, Istanbul Technical University, Ayazaga Campus, 34469, Turkey, (e-mail: musaoglune@itu.edu.tr)

ABSTRACT

Drought, as the considerable affair brought by global climate change, is one of the most important environmental problems. It can affect large areas and has devastating effects on environmental, social and economic sectors. Remote sensing is an effective tool for finding, evaluating and refining convenient drought monitoring methods, by providing near real-time and accurate data throughout long-term periods, especially for large areas. Among many human-related sectors, which are adversely affected by drought, agriculture is the first and most vulnerable one. In this study, Aegean Region of Turkey has been selected as a case study of agricultural drought assessment in growing seasons (from May to October) of the time interval between 2007 to 2016. For this purpose, 16-day composite 250 m spatial resolution Normalized Difference Vegetation Index (NDVI) and 8-day composite 1 km spatial resolution Land Surface Temperature (LST) data derived from the Moderate Resolution Imaging Spectroradiometer (MODIS) sensor were compiled and the most common agricultural drought monitoring indices Vegetation Condition Index (VCI), Temperature Condition Index (TCI) and Vegetation Health Index (VHI) were applied. The results of applying the TCI, VCI and VHI to the drought-prone areas have been investigated for all months and years one by one in the mentioned region.

INTRODUCTION

Among the other environmental threats, drought is the most complicated one because of its nature. It can occur anywhere and anytime by illustrating the sign slowly and affecting large areas having devastating effects on environmental, social and economic sectors.

According to the literature, drought can be classified into four types depending on the parameters used. These are; (1) meteorological drought, which can be described as the amount of rainfall over a long period to remain below the average amount of precipitation belonging to that region, (2) agricultural drought, which can be occurred when the value of the soil moisture is lower than the required for growing and developing the plants, (3)

^{*} Corresponding Author

hydrological drought, which specifies a decrease in the amount of water in surface and underground water resources as a result of long-term insufficient precipitation, and (4) socioeconomic drought, which describes the effects of drought on living, agriculture, water resources and the industries benefiting from it (Wilhite and Glantz, 1985; Wilhite, 2008; Mishra and Singh, 2010).

Various tools and methods are in use for drought detection and monitoring. Traditionally, meteorological based drought indices have been used for drought monitoring with historical data. Additionally, these indices are mainly calculated from measurements of weather stations. However, when weather stations are scarce or not homogeneously distributed this approach gives unsatisfactory results (Rhee, 2010; Ji and Peters, 2003). Furthermore, apart from traditional meteorological based drought indices, satellite remote sensing with their wide spatial coverage and near real-time acquisition gives fast and reasonable results for drought analyses in recent years.

The most commonly used remote sensing based drought indices are certainly the Normalized Difference Vegetation Index (NDVI; Tucker, 1979) which was first applied to drought monitoring by Tucker and Choudhury (1987) utilized August-September from 1984-1986 using 4-km AVHRR data. In this way, different vegetation indices (VIs) were developed for drought monitoring and the Vegetation Condition Index (VCI; Kogan, 1990) is relied on by modifying NDVI. Kogan (1990) concluded that the VCI supplies an enhancement for analysis of vegetation conditions with weather impact, especially in non-homogeneous areas. On the other hand, he considered that only the VCI was not adequate for drought monitoring. Thus, in addition to the optical sensors, Land Surface Temperature (LST) parameters derived from thermal bands were also utilized to develop drought indices as the Temperature Condition Index (TCI; Kogan, 1995). Then, the Vegetation Health Index (VHI; Kogan, 1997) which rely on combination of VCI and TCI was developed.

This study focuses on evaluating agricultural drought impacts by using the Moderate Resolution Imaging Spectroradiometer (MODIS) satellite data over the Aegean Region of Turkey for ten years (2007-2016) growing seasons.

MATERIALS and METHODS

Study Area

The Aegean region, one of the most popular agricultural and industrialized regions of Turkey, considered as a case study area. The region is located in the west part of the country inside the Mediterranean climatic regime (Türkeş, 2011) and consist of eight cities named İzmir, Manisa, Aydın, Denizli, Muğla, Uşak, Kütahya, Afyonkarahisar as shown in Figure 1.

According to the Turkish Statistical Institute (TUIK) last year statistics, in the Aegean region, the total agricultural area is 2774259.5 ha that accounts for %11.67 of Turkey. In this region, cereals and other crop products (sown area and fallow land) cover 16.352.994 da (58.95%); vegetable gardens, fruits and Ornamental Plants Area cover 1.369.343 da

(4.94%), 8.134.488 da (29.32%) and 17.629 da (0.06%), respectively (Topçu and Ozkan, 2017). The statistics belong to previous years are shown in Table-1.

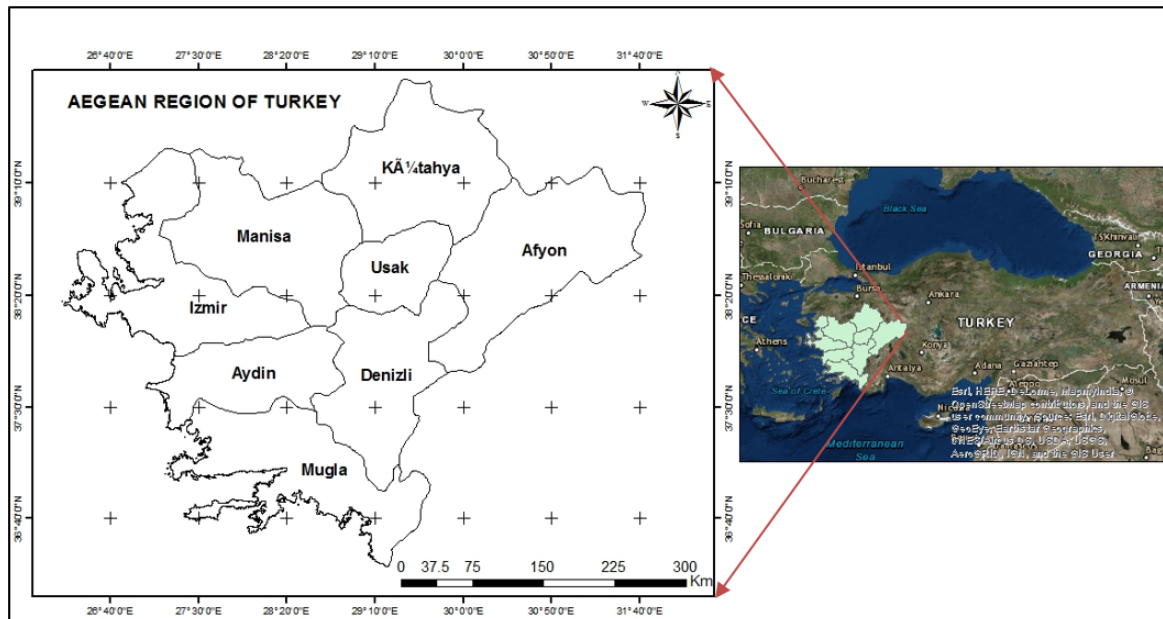


Figure 1. Location of the study area.

Table 1. The statistics of agricultural of the region compatible with research years (Source: Turkish Statistical Institute-TUIK, 2017).

Year	Area(ha)					
	Total	Cereals and other crop products		Vegetable gardens	Fruits, beverage and spices	Ornamental Plants
		Sown	Fallow land			
2007	2 925 786.1	1854 916.9	194 718.3	143 368.5	732 782.4	no data
2008	2 893 222.1	1 808 503.4	194 852.9	148 474.0	741 391.8	no data
2009	2 791 944.3	1 765 920.8	132 229.8	144 670.9	749 122.8	no data
2010	2 839 761.5	1 773 588.9	160 542.9	146 146.6	759 483.1	no data
2011	2 752 324.8	1 686 592.1	147 907.5	144 086.1	772 876.2	862.9
2012	2 799 935.8	1 702 213.3	171 252.9	145 348.1	780 028.3	1 093.3
2013	2 809 454.0	1 704 522.2	178 628.5	140 432.4	784 674.8	1 196.1
2014	2 784 683.0	1 689 871.1	166 809.0	138 775.9	787 701.5	1 525.5
2015	2 795 303.8	1 677 988.4	180 016.9	137 958.2	797 760.5	1 579.8
2016	2 774 259.5	1 635 299.4	186 814.1	136 934.3	813 448.8	1 762.9

[Land under permanent meadows and pastures are not included].

Remote Sensing Data

National Aeronautics and Space Administration (NASA)'s product MODerate Resolution Imaging Spectroradiometer (MODIS) satellite, which has 36 spectral bands (optical and

thermal) ranging in wavelength from 0.4 μm to 14.4 μm and at varying spatial resolution of 250 m, 500m and 1 km, was selected for this study. In the study, Terra-MODIS eight-day composite LST (MOD11A2, collection 5) and sixteen-day composite NDVI (MOD13Q1, collection 5) products spanning from 2007 to 2016 in the growing season periods (about April 23 through October 31) were used. Data specifications are shown in Table-2. The data sets were acquired from United States Geological Survey (USGS) Center for Earth Resources Observation and Science (EROS) using webmrt tool. A total of 120 images covering the growing seasons of 2007-2016 were reprojected from the Sinusoidal to World Geodetic System (WGS84).

Table 2. The satellite data basic specifications.

Satellite	Product name	Temporal resolution	Spatial resolution
MODIS/Terra	MOD13Q1 Vegetation indices (NDVI)	16-day composite	250 m
MODIS/Terra	MOD11A2 Land surface temperature (LST)	8-day composite	1000 m

The eight-day composite LST data was averaged into the sixteen-day composite, which matches the period of the NDVI data. 250m spatial resolution NDVI data was resampled to 1000 km spatial resolution in order to be compatible with LST data by using nearest neighbor resampling method that uses the values of the closest pixel to assign to the output pixel value. The sixteen-day composite NDVI data sets Julien date and the related time interval given as an example of 2007 year for the growing season from the beginning of May to the end of October in Table 3.

Table 3. 16-day composite data time used for this study (an exp.2007).

Julien Date	Time Interval
NDVI07_113	23 Apr 2007 - 08 May 2007
NDVI07_129	09 May 2007 - 24 May 2007
NDVI07_145	25 May 2007 - 09 Jun 2007
NDVI07_161	10 Jun 2007 - 25 Jun 2007
NDVI07_177	26 Jun 2007 - 11 Jul 2007
NDVI07_193	12 Jul 2007 - 27 Jul 2007
NDVI07_209	28 Jul 2007 - 12 Aug 2007
NDVI07_225	13 Aug 2007 - 28 Aug 2007
NDVI07_241	29 Aug 2007 - 13 Sep 2007
NDVI07_257	14 Sep 2007 - 29 Sep 2007
NDVI07_273	30 Sep 2007 - 15 Oct 2007
NDVI07_289	16 Oct 2007 - 31 Oct 2007

Drought indices

Normalized Difference Vegetation Index (NDVI) that uses the near-infrared (NIR) and visible (VIS) bands of the electromagnetic spectrum and analyzes whether the target being observed contains live green vegetation or not (Rouse, 1974; Tucker, 1979). It is defined as:

$$NDVI = \frac{R_{NIR} - R_{RED}}{R_{NIR} + R_{RED}} \quad (1)$$

where R_{NIR} and R_{RED} are the reflectances in the near infrared and red bands refer to the reflectance of MODIS band1 (620–670 nm) and band2 (841–876 nm), respectively (Huete et al., 2002). The values of this index range from -1 to + 1 according to being unhealthy to healthy vegetation conditions.

Vegetation Condition Index (VCI) was designed for definite improvement in the analysis of vegetation conditions especially in non-homogeneous areas while extracting the weather impact on vegetation while removing the ecosystem signal from the NDVI (Kogan, 1990). It is calculated with the following formula;

$$VCI = 100 * \frac{NDVI_i - NDVI_{min}}{NDVI_{max} - NDVI_{min}} \quad (2)$$

where $NDVI_i$ is absolute, $NDVI_{min}$ and $NDVI_{max}$ are multi-year minimum and NDVI values for each pixel, respectively. The VCI values vary between 0 and 100 (Kogan; 1990, 2001).

Temperature Condition Index (TCI) that uses land surface temperature (LST) derived thermal infrared bands. It is related with the altered response of vegetation to temperature and calculated using following equation;

$$TCI = 100 * \frac{LST_{max} - LST_i}{LST_{max} - LST_{min}} \quad (3)$$

where LST_i , LST_{min} and LST_{max} mean the absolute, minimum and maximum LST values for each pixel, respectively, calculated from multiyear time series data. While high temperature shows unfavorable or drought conditions, low temperature commonly shows favorable conditions (Kogan, 1995).

Vegetation Health Index (VHI) is based on the combinations between VCI and TCI and calculated using following equation;

$$VHI = \alpha * VCI + (1 - \alpha) * TCI \quad (4)$$

where α and $(1 - \alpha)$ is related to the weight of VCI and TCI from 0 to 1. If contributions of indices are unknown, it is commonly used as 0.5. VHI values similarly vary between 0 and 100. If VCI, TCI, and VHI values are larger than 70, that means the conditions are favorable and the vegetation is healthy. In contrary, if VHI values below 40, vegetation is stressed (Kogan, 1997; 2001).

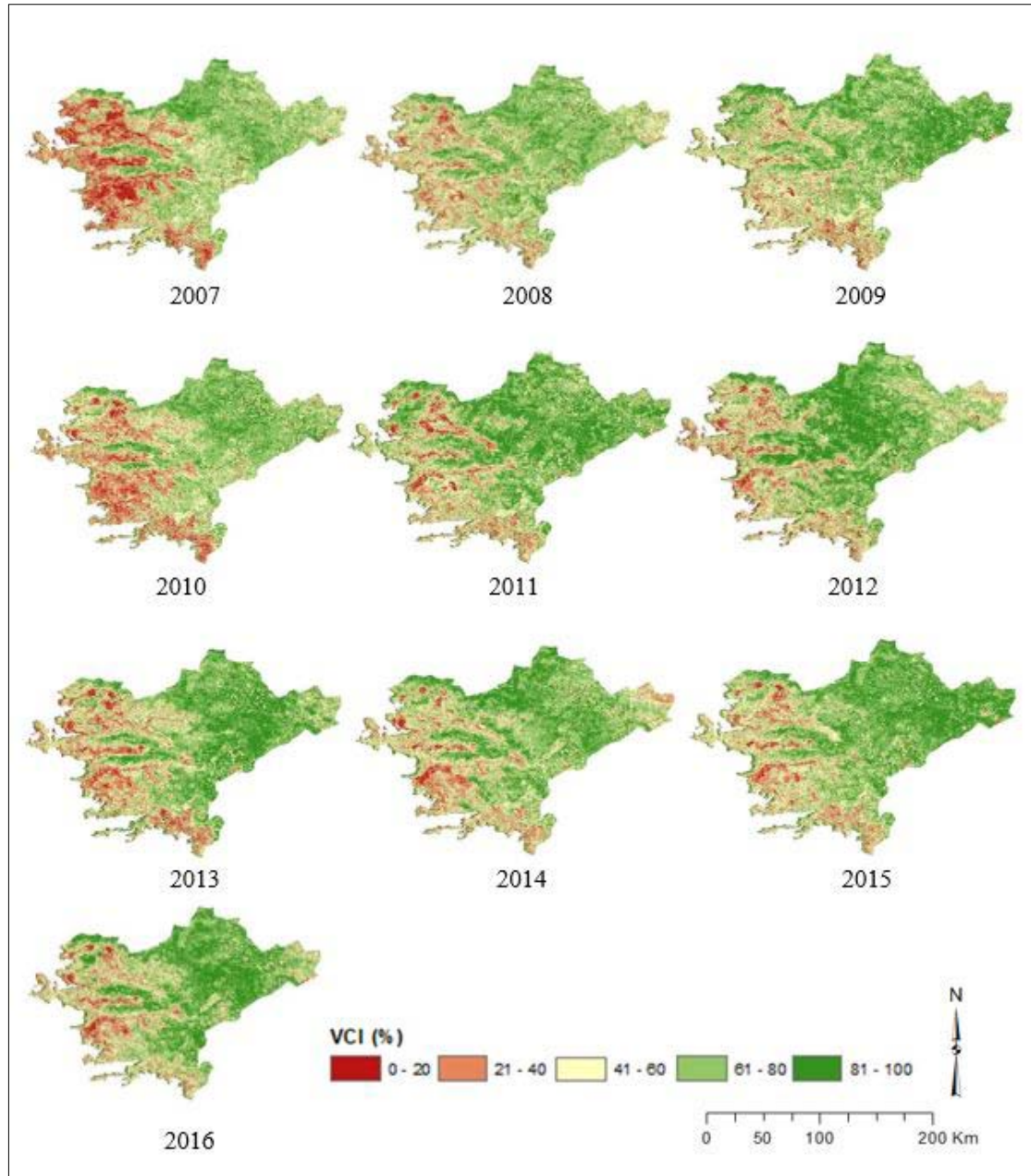


Figure 2. The results of VCI maps with 250m spatial resolution for 10 years (09 - 24 May 2007 to 2016).

RESULTS AND CONCLUSIONS

The study efforts to assess the spatio-temporal extent of agricultural drought over the Aegean Region of Turkey by using remote sensing based Vegetation Condition Index

(VCI), Temperature Condition Index (TCI) and Vegetation Health Index (VHI). For this purpose, MODIS sensor data, which is mostly utilized for drought monitoring research globally and regionally because of high temporal and wide spectral resolutions, was used.

The results of the VCI in the period of 2007 to 2016 of May are shown in Figure 2. As reflected in the results, drought impact has been observed in the years of 2007 and 2014 more than the others. All results have been confirmed by VHI indices as well. To illustrate this impact, 2007 and 2013 years' results are given in Figure 3.

In Figure 3, the Vegetation Health Maps of the growing seasons (beginning-May through end of October) of 2007 and 2013 were selected to represent the drought year and the non-drought year, respectively. The values below 40 that indicate drought-prone areas can be seen spatially distributed around Izmir, Manisa, Aydın and partly Usak in 2007 (with dark red colors).

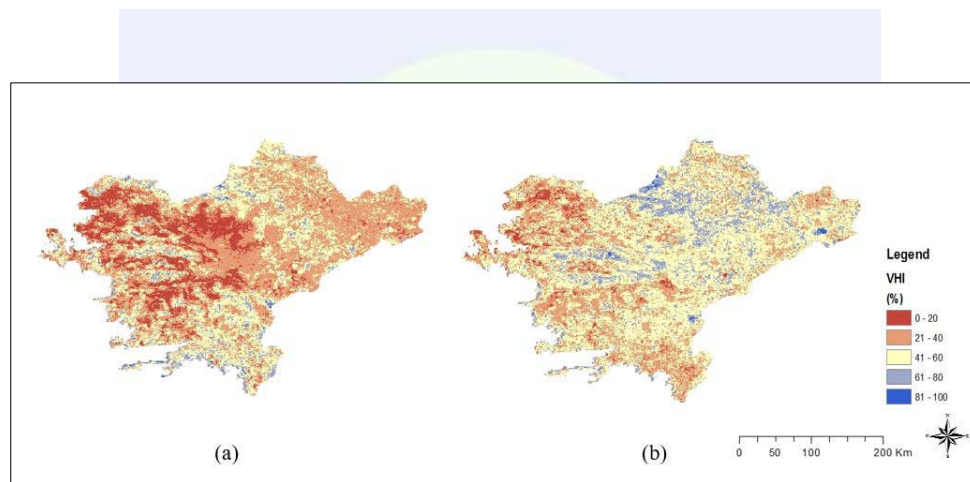


Figure 3. VHI maps produced by VCI and TCI with 1 km spatial resolution 09 - 24 May (a) 2007 as a drought year (b) 2013 as a normal year

It can be concluded that remote sensing based-methods can perform near real-time agricultural drought monitoring at appropriate spatial and temporal resolution. In addition, because MODIS data has only been available since 2000, another satellites data such as Landsat, AVHRR can be applied for observing historical drought conditions depending on coverage of area and sufficient spatial resolution.

In further research, amount of crop yield statistic might be used for validation compared with the results. Also, the correlation between remote sensing-based drought indices (VCI, VHI) and traditional station based-drought indices (SPI, PDSI etc.) might be investigated for more accurate outcomes.

REFERENCES

- Huete, A., Didan, K., Miura, T., Rodriguez, E.P., Gao, X. and Ferreira, L.G., 2002. Overview of the radiometric and biophysical performance of the MODIS vegetation indices. *Remote Sensing of Environment* 83:195–213.

- Ji, L. and Peters, A., 2003. Assessing vegetation response to drought in the northern Great Plains using vegetation and drought indices. *Remote Sensing of Environment* 87:85-98.
- Kogan, F.N., 1990. Remote sensing of weather impacts on vegetation in non-homogeneous areas. *International Journal of Remote Sensing* 11, 1405–1419.
- Kogan, F. N., 1995. Application of vegetation index and brightness temperature for drought detection. *Advances in Space Research* 15:91–100.
- Kogan, F.N., 1997. Global drought watch from space. *Bulletin of the American Meteorological Society* 78, 621–636.
- Kogan, F. N., 2001. Operational space technology for global vegetation assessment, *Society Bulletin of the American Meteorological Society*, 82(9), 1949–1964.
- Mishra, A. and Singh, V., 2010. A Review of Drought Concepts. *Journal of Hydrology* 391, 202–216.
- Rhee J., Im J., and Carbone G.J., 2010. Monitoring agricultural drought for arid and humid regions using multi-sensor remote sensing data. *Remote Sensing of Environment* 114: 2875-2887.
- Rouse, J. W., Haas, R. H., Schell, J. A., and Deering, D. W., 1974. Monitoring Vegetation Systems in the Great Plains with ERTS in Proceedings of the Third Earth Resources Technology Satellite-1 Symposium, Vol. 1, 48–62.
- Topçu, G.D., and Özkan, Ş.S., 2017. Türkiye ve Ege Bölgesi Çayır-Mera Alanları ile Yem Bitkileri Tarımına Genel Bir Bakış. *COMU Journal of Agriculture Faculty* 5 (1): 21–28.
- Tucker, C. J., 1979. Red and photographic infrared linear combinations for monitoring vegetation. *Remote Sensing of Environment* 8, 127–150.
- Tucker, C. J., and Choudhury, B. J., 1987. Satellite remote sensing of drought conditions, *Sensing of Environment* 23(2), 243–251.
- Türkeş, M., 2011. Akhisar ve Manisa Yörelerinin Yağış ve Kuraklık İndisi Dizilerindeki Değişimlerin Hidroklimatolojik ve Zaman Dizisi Çözümlemesi ve Sonuçların Çölleşme Açısından Coğrafi Bireşimi. *Coğrafi Bilimler Dergisi* 9 (1), 79-99.
- TUIK, 2017. Bitkisel Üretim İstatistikleri, http://www.tuik.gov.tr/PreTablo.do?alt_id=1001 retrieved 14 September 2017.
- Wilhite, D.A. and Glantz, M.H., 1985. Understanding the Drought Phenomenon: The Role of Definitions. *Water International* 10(3):111–120.
- Wilhite, D.A., 2008. Encyclopedia of Water Science, Second Edition, Volume I-II: Drought, Taylor & Francis Press, 215-217.

Temperature extremes in summer and winter seasons over the Mediterranean Coastlines of Turkey

Zahide Acar Deniz^{*1}, Barbaros Gönençgil²

¹Department of Geography, Canakkale Onsekiz Mart University, Terzioğlu Campus, Canakkale, Turkey 17020, Turkey. (e-mail: zdeniz@comu.edu.tr)

²Department of Geography, Istanbul University, 34459, Istanbul, Turkey (e-mail: barbaros@istanbul.edu.tr)

ABSTRACT

Extreme events are described with the maximum and minimum measurements of atmospheric variables that can be expected to occur at a certain place and time a long period of observations. The extreme events are affected by the measured physical attributes of weather or climatic variables or the vulnerability of social systems.

In this study, we determined extreme temperatures in both summer and winter seasons at the meteorological stations in the Mediterranean coastal areas of Turkey. In the study, the data of 16 meteorological stations for the daily maximum and minimum temperatures of the period from 1966-2015 were used.

In this paper, we examine the variation of regional extreme temperatures (tropical nights, summer days, frost and ice days) that would potentially be due to the heat-cold wave effects in Mediterranean coastlines of Turkey.

Spatial clustering has searched using the Arc-GIS statistical package. The association between station indices has obtained by calculating the Anselin Local Moran's I index. The Cluster and Outlier Analysis (Anselin Local Moran's I) tool describes concentrations of high values, concentrations of low values, and spatial outliers. Furthermore, we also plotted the winter and summer temperature trends during the last five decades. Our results are interpreted on the basis of frequency and intensity of extreme hot events increases while cold extremes decrease during the past ten years.

INTRODUCTION

Recent work outlined at IPCC's 2007 report has made striking impact on the climate studies which suggests that atmospheric greenhouse gases due to the human activities have been increasing since 1960's. In more recent report published 2012, Managing the risk of extreme events and disasters to advance climate change adaptation report (IPCC, 2012) recommend that the disaster risk management and climate change adaptation literature describe "extreme weather" and "extreme climate" events. Their relationship simply involves in "extreme impacts" and its disastrous consequences. Extremes are defined with

^{*} Corresponding Author

the maximum and minimum measurements of atmospheric variables that can be expected to occur at a certain place and time (Rohli and Vega, 2012) that established a long period of observations.

As well as this, the classification of extreme events, extreme impacts and disasters is affected by the measured physical attributes of weather or climatic variables or the vulnerability of social systems.

For example, Beniston et al. (2007) suggests that regional surface warming causes the frequency, intensity and duration of heat waves that increases over European continent. Also, the authors postulate that by the end of the twenty first century, especially central Europe countries will suffer the same number of hot days as are currently experienced in southern Europe. The intensity of extreme temperatures increases in southern Europe more rapidly than in central Europe.

Current studies also aim to explain the temperature anomalies in the Mediterranean region (Unkasevic and Tomic, 2009; Beniston et al., 2007; Baldi et al, 2006). Hertig et al. (2010) suggests that mostly insignificant trends for the 5th percentile of minimum temperatures in winter during the period 1961–1990. They have analyzed significant increases of the 5th percentile of minimum temperatures (marked with filled triangles) occurred mainly at stations in the central-northern Mediterranean area with values of more than 2°C in some cases (e.g. Palermo, Italy or Istanbul, Turkey). In addition, the 95th percentile of maximum temperature trend is recorded with mostly in the western Mediterranean area and such trend conversely decreases in the eastern Mediterranean region. While Turkey encompasses a large region in the eastern section of the Mediterranean basin, unfortunately there has been less published work on the extreme temperature conditions for the last three decades.

In this paper, we examine the variation of regional extreme temperatures (tropical nights, summer days, frost day and ice day indices) that would potentially be due to the heat and cold events in Mediterranean coastlines of Turkey. Furthermore, we also plotted the temperature indices trends during about the last five decades. Our results are interpreted on the basis of extreme hot temperature anomalies (in summer season) that would likely be owing to the northward migration of the monsoon circulation. Cold extreme events (frost and ice days) occur under the control of northern circulation.

DATA AND METHOD

The study area is spread southern part of Anatolian Peninsula, Turkey. The temperature records are collected based on daily maximum and minimum temperatures data provided by Turkish State Meteorological Service. Temperature data recorded from 16 stations in southern part of Turkey during the period of 1966- 2014 (Figure 1).

This paper concentrates on indices that refer to cold and warm extremes, i.e. which investigate the characteristics of the southern part of Turkey climate with respect to intense events and changes in the daily temperature. A list of the indices is shown in Table 1. The temperature indices describe warm and cold extremes in summer and winter seasons. As

well as this, a linear trend in the warm days and cold night is determined with Mann-Kendall rank correlation test.

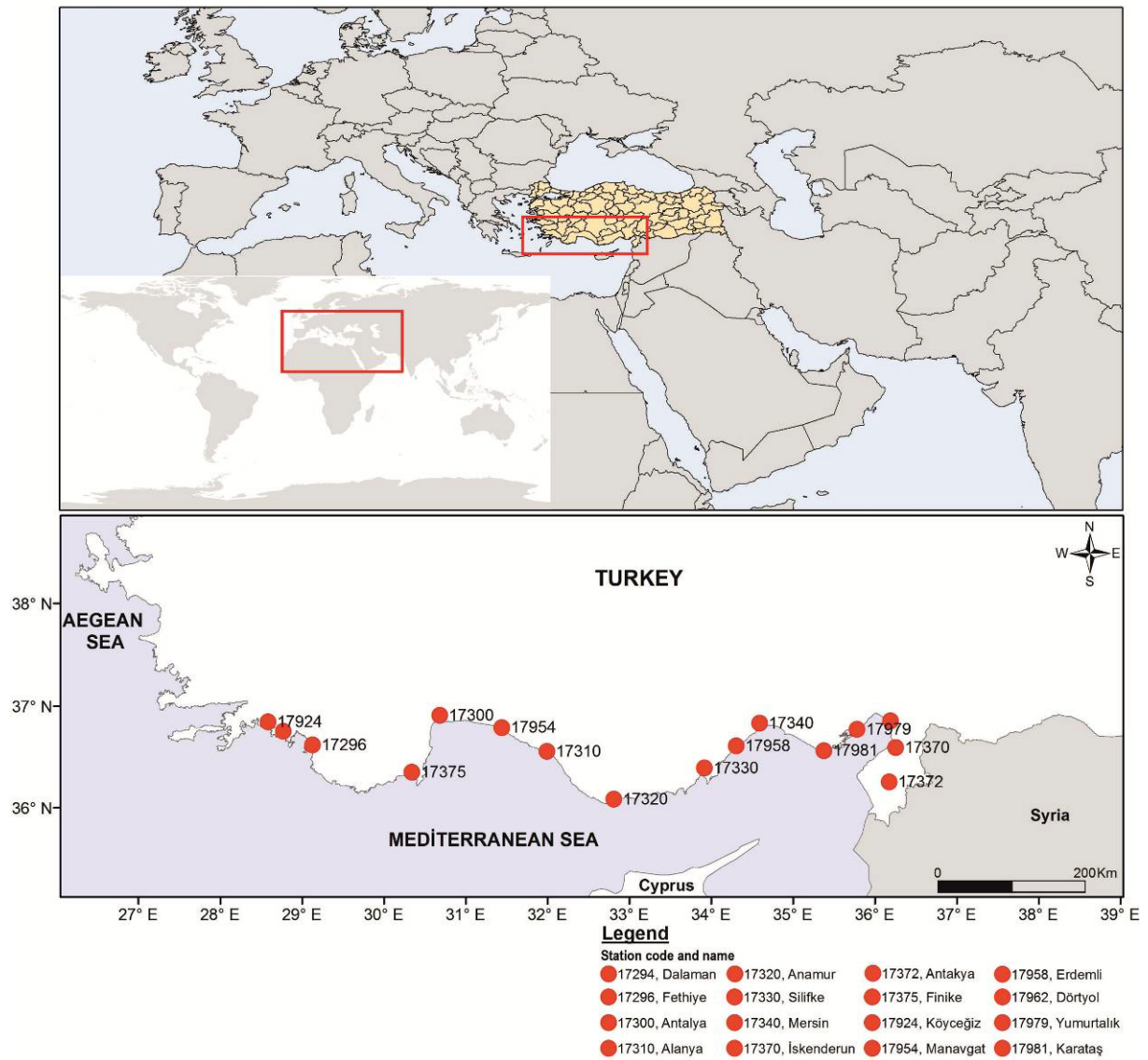


Figure 1. The geographical distribution of meteorological stations that provides temperature data used in this study.

Table 1. Definitions of the minimum and maximum temperature indices used in this study.

ID	Indicator name	Definitions	Units
TN	Tropical nights	Annual count of days when TN (daily minimum temperature) > 20°C.	Day
SD	Summer days	Annual count of days when TX (daily maximum temperature) > 25°C.	Day
FD	Frost days	Annual count of days when TN (daily minimum temperature) < 0°C.	Day
ID	Ice days	Annual count of days when TX (daily maximum temperature) < 0°C.	Day

The numbers of tropical nights, summer, frost and ice days are determined by specifying the threshold values for summer temperature change in Mediterranean region of Turkey. As well as this, the trends in the number of temperature indices are determined with Mann-Kendall rank correlation test. According to Mann-Kendall test τ is a value that indicates magnitude of the observations. The P statistic is calculated by;

$$P = \sum_{i=1}^{N-1} n_i$$

Mann Kendall test statistic τ is calculated as follows;

$$\tau = \frac{4P}{N(N-1)} - 1$$

The value of the test statistics is normal for all N values, larger than 10. The significance test is calculated as follows;

$$\tau_{(t)} = 0 \pm t_g \frac{(4N+10)}{9N(N-1)}$$

Where t_g value is the requested probability point in the normal distribution (two sided). a positive value of τ indicates an upward trend, a negative value of τ indicates a downward trend (Mann, 1945; Kendall, 1975). $u(t)$ and $u'(t)$ values are used to determine the trend in the time series. Similarly to the calculation of progressive rows of statistics $u(t)$, the retrograde rows of statistics $u'(t)$ are computed backwards starting from the end of series. $u(t)$ is significant at a desired level of significance, one can decide whether it is an increasing or decreasing trend depending on whether $u(t) > 0$ or $u(t) < 0$.

Spatial clustering has searched using the Arc-Gis statistical package. The association between station indices has obtained by calculating the Anselin Local Moran's I index. The Cluster and Outlier Analysis (Anselin Local Moran's I) tool describes concentrations of high values, concentrations of low values, and spatial outliers. Positive value means a perfect positive correlation, negative value means negative correlation. The zero displays exactly random spatial pattern.

RESULTS

This study focuses on observed trends in temperature indices in summer and winter seasons during 1966-2014 in Mediterranean coastline of Turkey.

Tropical Nights: Tropical nights (TN) represent the number of days with daily minimum temperature above 20 °C. The TN has steadily risen eastern part of study area. The numbers of TN reach average 75 to 87 days in Mersin, Karataş, İskenderun and Antakya stations (Figure 2).

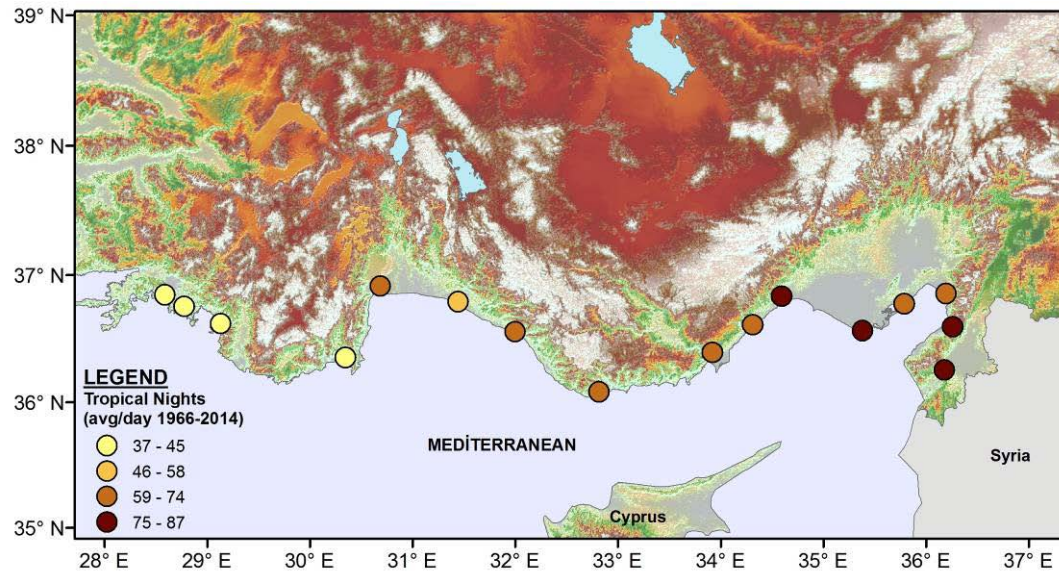


Figure 2. Spatial distribution of tropical nights in Mediterranean coastline of Turkey.

Summer Days: Summer days are corresponded to the days with maximum temperatures above 25°C. Generally, SD shows similar patterns for the distribution number of the days. The number of days varies between 90 and 92 in stations (Figure 3) that shows a homogeneous distribution for summer day index.

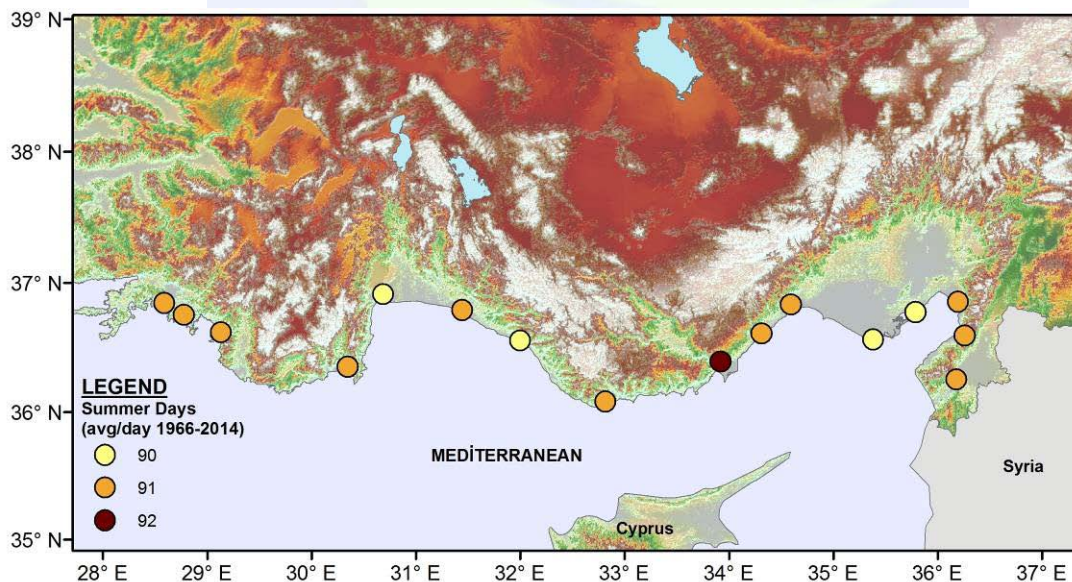


Figure 3. Spatial distribution of summer days in Mediterranean coastline of Turkey.

Frost Days: FD represents the number of days with minimum temperature below 0°C. The FD index shows quite a different distribution in the stations. The sum of the number of FD (1966-2014) ranged from 495 to 5 days (Figure 4). The numbers of FD has experienced less than 90 days in most of the stations the period of 1966-2014. This index is over 150

days at the station Antakya and Köycegiz. At these stations are frequently experienced frosty days in winter.

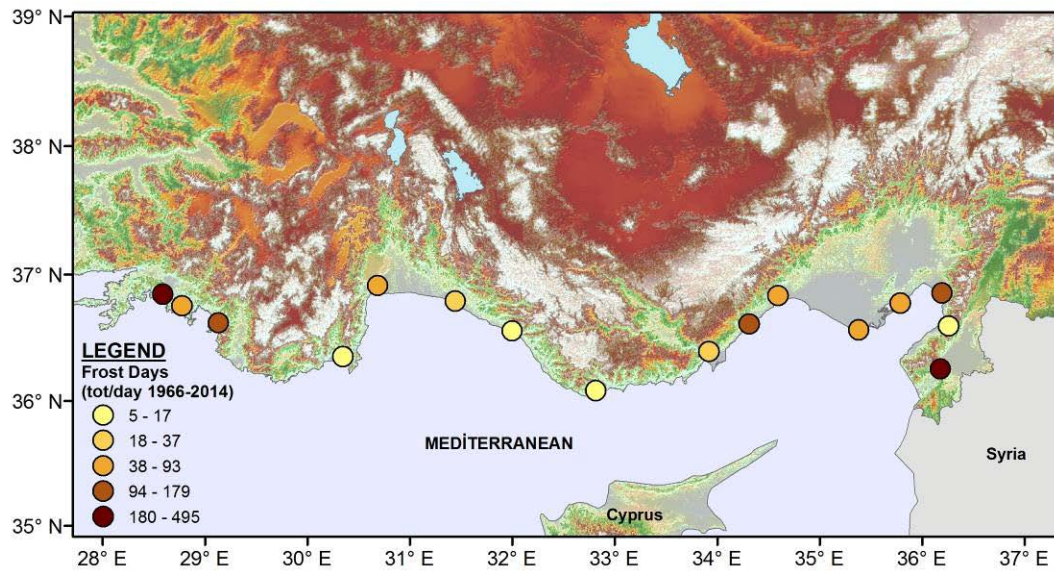


Figure 4. Spatial distribution of frost days in Mediterranean coastline of Turkey.

Ice Days: ID represents the number of days with maximum temperature below 0°C. The number of ice days, there is not any difference between the stations. Finike station has experienced icy days only one time in 50 years (Figure 5). Winter season is quite warm in the Mediterranean coastline stations.

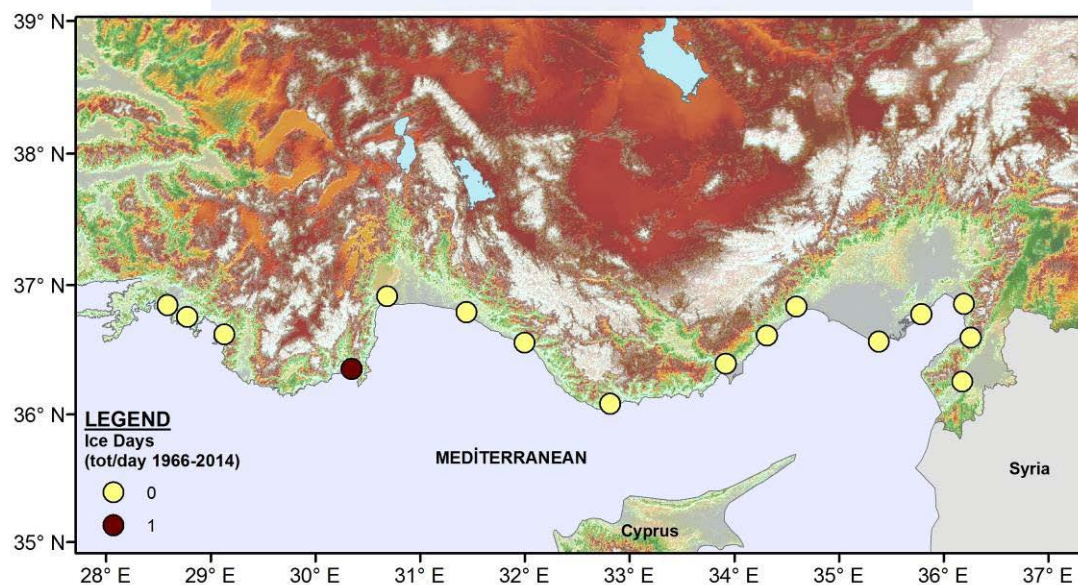


Figure 5. Spatial distribution of ice days in Mediterranean coastline of Turkey.

MANN-KENDALL TEST

The index Tropical nights (TN) displayed with positive trend at the stations, evidencing an overall increase in the annual number of days when the minimum temperature was higher than 20°C. In 1993 is the change point for the tropical night index. This index displays a statistically significant increase trend since 1994 (Figure 6).

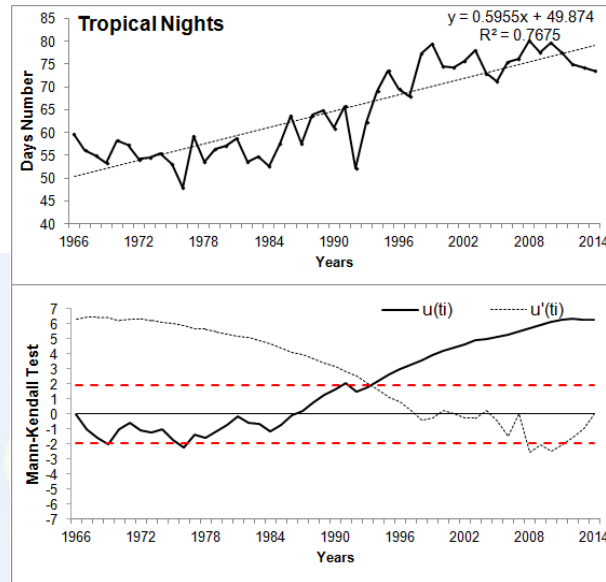


Figure 6. TN indices time series and Mann-Kendall statistics over Mediterranean coastline stations.

Summer maximum extreme variability for the SD index is calculated and illustrated Mann-Kendall tests over Mediterranean coastline stations of Turkey. The numbers of summer days in Mediterranean coastline during the 1966-2014 with linear regression is present in figure 7. There has been generally no-trends in summer day value. The warmest period and years have experienced in Mediterranean coastline such as, 1999 to 2006, 2008, 2010-2011 (Figure 7).

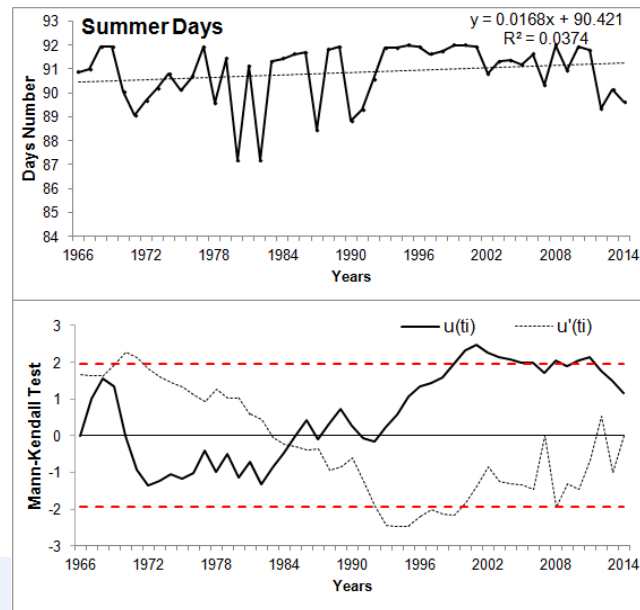


Figure 7. SD indices time series and Mann-Kendall statistics over Mediterranean coastline stations.

The index Frost Days showed with negative trends, showing that the annual number of days when the minimum air temperature was less than 0°C is decreasing (Figure 8). In 1983, severe cold weather has experienced in Mediterranean Coastline stations. Ice days have not experienced in the Mediterranean coastline region (except Finike). Therefore, any assessment for the ice day index could not made this section.

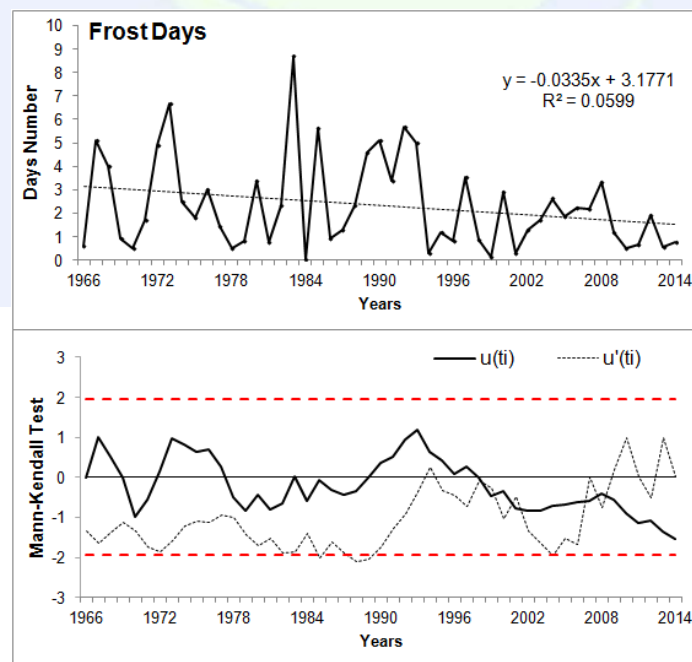


Figure 8. FD indices time series and Mann-Kendall statistics over Mediterranean coastline stations.

CLUSTER ANALYSIS

The Anselin Moran's I clustering analysis is applied to classify 16 stations to obtain homogeneous groups and resulting are displayed in figure 9 to figure 12.

Dalaman, Fethiye and Köycegiz stations are similar clustering extent. These stations display high positive. Iskenderun, Antakya and Karataş stations have significantly positive correlation. In this region, TN condition has been dominated by the similar features likes this Dalaman, Fethiye and Köycegiz. On the other hand, the other stations display nonsignificantly negative and positive value. This area has very different TN value than its neighbors (Figure 9).

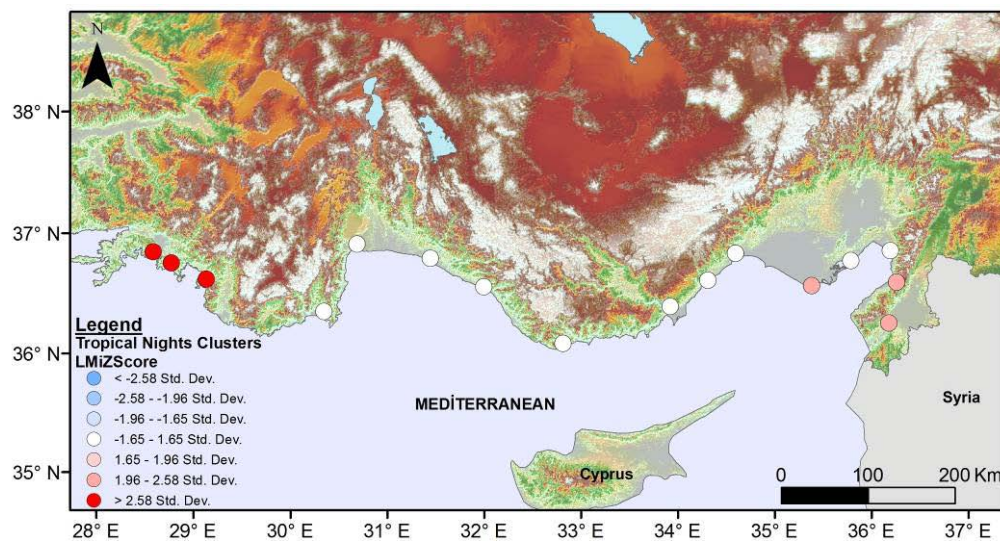


Figure 9. The results from scattering of Anselin Moran's I for TN indices.

All of the stations are similar clustering extent. These stations display nonsignificantly negative and positive value. Summer Days values in the neighborhood display similarity the overall the study area (Figure 10).

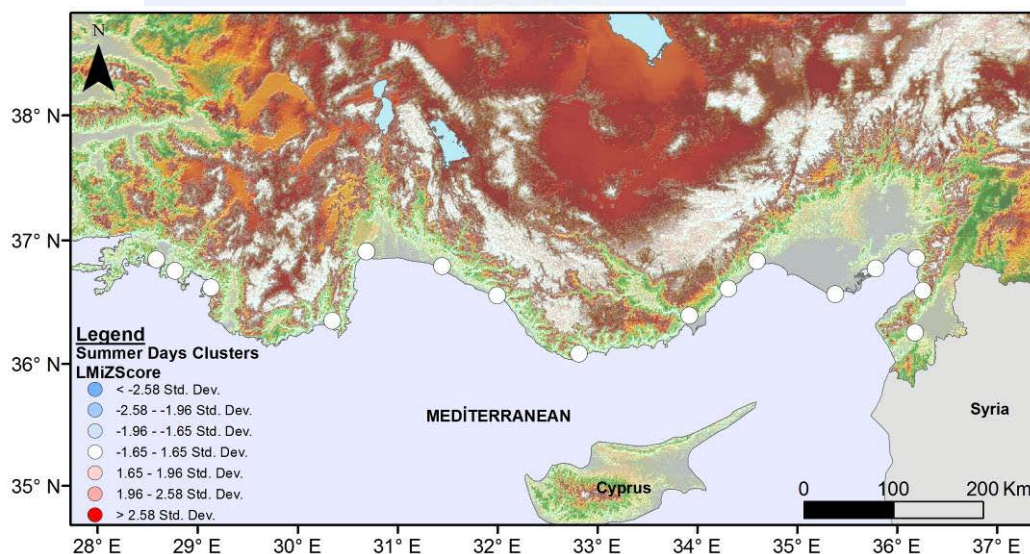


Figure 10. The results from scattering of Anselin Moran's I for SD indices.

All of the stations are similar clustering extent in the frost and ice day values. All of stations display nonsignificantly negative and positive value. Frost and ice day values in the neighborhood display similarity the overall the study area (Figure 11 and Figure 12). Exclusively, Finike station differs from the other stations in ice days. Statistically significant negative value indicates that the feature is surrounded by features with dissimilar values.

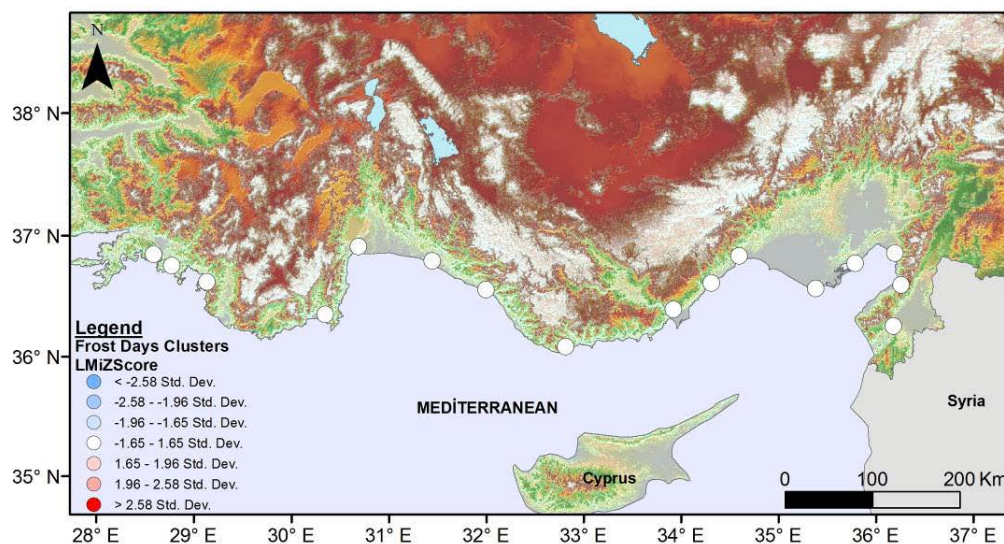


Figure 11. The results from scattering of Anselin Moran's I for FD indices.

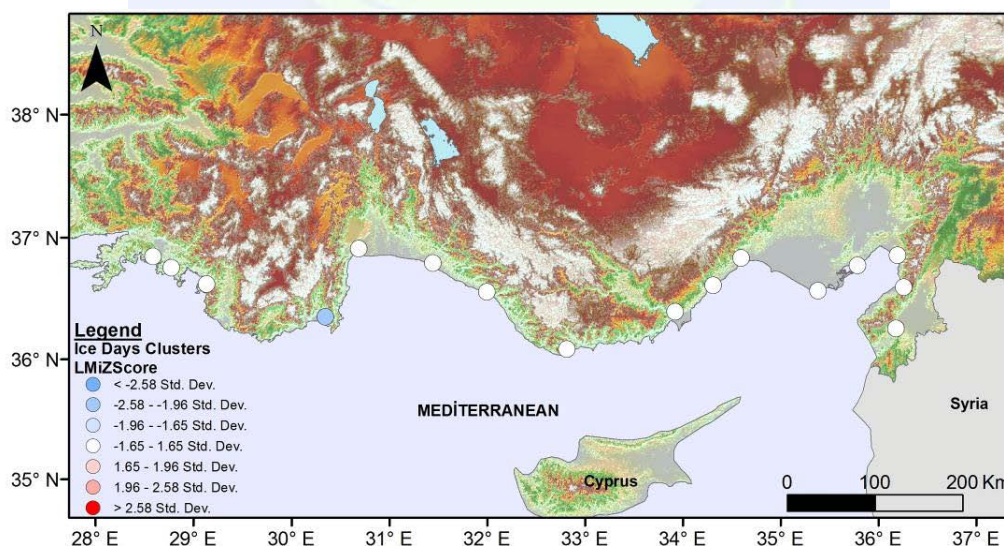


Figure 12. The results from scattering of Anselin Moran's I for ID indices.

CONCLUSIONS

Generally, physical and geographical factors controlling summer climatic conditions over the Mediterranean basin have identified latitude, longitude, interaction of land-sea and the most important general atmosphere circulation.

Based on temperature indices, the study is determined warming in minimum summer temperatures than that of maximum temperatures in most of stations. Significant increasing trend displays in TN. SD index shows a significant increase in some period or years, while the index included a generally downward trend. FD and ID indices show no-trend during 1966-2014 period. At the stations have not experienced remarkable frosty days except for some cold years such as; 1973, 1983, 1985, 1990 and 1992.

Tropical nights have a significant positive spatial autocorrelation with high cluster pattern in western and eastern part of study area. These areas shows similar characteristics with neighbouring stations. Dalaman, Fethiye and Köycegiz stations experienced a low number of tropical nights that this stations shows a different characteristic feature of Mediterranean Climate of Turkey. This area is open to the effects of the Etesian wind. Therefore, the low number of tropical nights when the refreshing effects of the wind is most important factor.

Antakya, Iskenderun and Karataş stations, where a high number of tropical nights are prominently affected from the southern circulation during summer season. The results of this section displayed that tropical nights from under influence of atmospheric circulation (etesian wind and the influence of the monsoon connected the southern circulation).

ACKNOWLEDGMENTS

We thank the Turkish State of Meteorological Office for providing the daily temperature data in Turkey.

REFERENCES

- Baldi, M., Dalu, G., Maracchi, G., Pasqui, I., & Cesarone, F. 2006. Heat waves in the Mediterranean: a local feature or o larger-scale effect?, *International Journal of Climatology*, 26, 1477-1487.
- Beniston, M., Stephenson, D.B., Christensen, O.B., Ferro, C.A.T., Frei, C., Goyette, S., et al. 2007. Future extreme events in European climate: an exploration of regional climate model projections, *Climate Change*, 81, 71-95.
- Hertig, E., Seubert, S., & Jaccobeit, J. 2010. Temperature extremes in the Mediterranean area: trends in the past and assessments for the future. *Natural Hazards and Earth System Sciences*, 10, 2039-2050.
- IPCC, 2007. Contribution of Working Group I to the Fourth Assessment Report of the Intergovernmental Panel on Climate Change, 2007, Solomon, S., D. Qin, M. Manning, Z. Chen, M. Marquis, K.B. Averyt, M. Tignorand H.L. Miller (eds.) Cambridge University Press, Cambridge, United King domand New York.
- IPCC, 2012. Managing the Risks of Extreme Events and Disasters to Advance Climate Change Adaptation. A Special Report of Working Groups I and II of the Intergovernmental Panel on Climate Change [Field, C.B., V. Barros, T.F. Stocker, D. Qin, D.J. Dokken, K.L. Ebi, M.D. Mastrandrea, K.J. Mach, G.-K. Plattner, S.K.

Allen, M. Tignor, and P.M. Midgley (eds.)]. Cambridge University Press, Cambridge, UK, and New York, NY, USA, 582 pp. ISBN 978-1-107-02506-6.

Kendall M. G. 1975. *Rank correlation methods*. Charles Griffin: London.

Mann H.B. 1945. Nonparametric tests against trend. *Econometrica*, 13, 245-259.

Rohli, R.V., & Vega, A.J. 2012. *Climatology*. Jones & Bartlett Learning LLC, 2th edition, ISBN 978-0-7637-9101-8.

Unkasevic, M., & Tosic, I. 2009. An analysis of heat waves in Serbia. *Global and Planetary Change*, 65, 17-26.





NATURAL HAZARDS AND MANAGEMENT

ISGGG
2017

Development of GIS-based Building Management Model for Natural Disasters

SinemTurhan^{*1}, R. Cüneyt Erenoğlu²

¹ Ankara Provincial Health Directorate, 112 Emergency Medical Services, 06105, Ankara, Turkey.e-mail: sinemtrhn@hotmail.com

² Department of Geomatics Engineering, Canakkale Onsekiz Mart University, Terzioğlu Campus, 17020, Canakkale, Turkey

ABSTRACT

There are many mass events around the world. One of these mass events is disasters. A disaster is a natural phenomenon that occurs suddenly, is difficult to prevent by people after it starts, and causes loss of life and property. The events that cause the loss of life and property created by people are considered as human disasters. Disasters affect countries economically, socially and psychologically. During these disasters, the most important point is measures to be taken during risk and crisis management. One of the things to be aware of when these precautions are taken is the number of individuals affected by these events. In disasters, there is a great loss of time during the detection of individual numbers. It provides assistance such as search and rescue, health care, housing, and food.

In this work, it is aimed to employ electronic infrared human counter used for commercial purposes to prevent this loss of time. The infrared human counter uses advanced image processing technologies to count people passing wherever they are. In stores, shopping centers, every kind of public area offers a complete, efficient, economical and quick solution due to its high accuracy and counting reports. These can be accessed anywhere in the world and instant recording of these data. This enables the creation of a building management model during extra-ordinary events that take place in the buildings in the targeted buildings. Using the artificial intelligence and artificial vision algorithms, the system can work without loss of performance in crowded entrances and exits, and also even shadowy environments. Persons close to each other can distinguish between persons who pass in different directions at the same time. With its flexible infrastructure, it has a high performance ratio with its fully multi-language interface, reporting pages and user-definable infrastructure that makes it possible to create panoramic images by combining images taken from multiple cameras at the same time.

By means of instantaneous transfer of the report data provided by this counter system to the GIS environment, a public institution and foundation building management model is designed so that the search and rescue activities can be successfully carried out efficiently after a possible natural disaster. Because the proposed building model allows the

^{*} Corresponding Author

identification of the numbers and locations of the individuals in the building at the moment of disaster, it is possible to determine the possible time losses in a concrete way. Finally, a workflow will be provided for the GIS-based building management model for natural disasters.

INTRODUCTION

Disasters are natural phenomena that cause unpredictable, often sudden, loss of life and property that has no clear time ahead. Disasters are classified into two categories; natural disasters and human-induced disasters. Natural Disasters: Rapid winds, earthquakes, sellers, fires, tsunami and coastal landslide, landslide, slip, avalanche, volcano eruption, drought (Kanlı and Ünal, 2004). These kinds of disasters are sudden, unpredictable, sudden occurrences of nature.

Disasters Caused by Human Deaths: Fires, explosions, mine accidents and explosions, environmental pollution, traffic accidents, radioactive rays, thermo-nuclear wars, wars (Sengezer and Kansu, 2001). These are situations in which people have somehow contributed in some way. Sometimes it suddenly occurs with time. The consciousness of people and their contribution influence the situation.

Disasters are a natural phenomenon. People who have had a nomadic life have passed into settled life over time. Especially, these harmless nature events have increased in the affects with the passing of established faults. The disaster that occurs in all the regions that are experienced varies according to the damages. In some regions earthquake is effective in some regions landslide, volcanic eruption, flood, etc. nature events are effective. Over time, with the increase in losses created by these effects, people have tried to find solutions to these unwanted, unexpected, and unusual effects of disasters. It has been noticed that the precautions to be taken before the disasters, the moment of disaster and the loss of the correct and quick intervention after the disaster are the least. In return, disaster management was needed.

Disaster management can be gathered in two stages: pre-disaster (risk management), disaster moment and after (crisis management). However, there are other classifications for disaster management stages in the literature. The most common is the classification that states that an ideal disaster management should cover three stages, defined as "pre-disaster, post-disaster and post-disaster" (Gökçe and Tetik, 2012).

Pre-disaster: aims to take necessary precautions in order to minimize disaster damage, to prevent them when possible, to enable effective emergency rescue and relief work when not possible, to spread disaster damage reduction studies at every stage of development and to educate people on these issues (Gökçe and Tetik, 2012).

During the disaster, the disaster management aims to ensure that the objectives of the disaster, to get information and transportation possibilities again, to save the maximum number of people, to protect the human life and property from the additional risks and risks that disasters may cause, to carry out all kinds of evacuation and evacuation, and destroying these homes if necessary, to ensure that communities affected by disaster meet

the vital needs as soon as possible and that life returns to normal as much as possible. The realization of these aims can be achieved by pre-disaster planning and preparatory work, when the organizations providing disaster services are effectively acted at the moment of disaster.

After the disaster, the disaster management aims to minimize the economic and social losses that the disaster may cause, or to correct the effects in the shortest time, and to provide a safe and developed new life environment for affected communities (Gülkan et al., 2003; Erkol and Evalliyurt, 2009)

We are aiming to use this work actively in all phases of disaster management mentioned above.

Some Disasters in Turkey; before 1944, natural disasters, and especially earthquakes, seem to extend to the ancient history of helping people. The first written example in this regard is seen in the Istanbul earthquake that took place on 14 September 1509. After this earthquake, which was reported to have killed 13,000 people, 109 mosques and 1,407 buildings had been destroyed, Ottoman Sultan II.Beyazit of the period donated 20 gold to the family in order to rebuild the house. In addition, 50.000 masters were recruited for the reconstruction of Istanbul after the earthquake, and men between 14 and 60 years of age were ordered to work in construction works. It is prohibited to build houses on the fill floors near the sea and the wooden carcass is encouraged to be built (Özalp, 2000)

The government of Republic of Turkey, the day after the earthquake of Niksar-Erbaa, Adapazari-Hendek, Tosya-Ladik, Bolu-Gerede, the death of 43 thousand 319 people, the injuries of 75 thousand people and the destruction of 200 thousand buildings, which took place on 26 December 1939 after the Great Erzincan earthquake, on July 18, 1944, the Law No. 4623 on Measures to be Taken Before and After the Earthquakes, arriving at the judgment that the problems that he had caused must only be solved by making a new house instead of being demolished and that some work should be done to reduce earthquake damages in our country. Measures such as the determination of earthquake hazard areas of the country, making certain special sanctions for the buildings to be constructed in these regions, preparation of aid and rescue programs in provinces and districts to be implemented in emergency situations and not allowing new residential areas without geological surveys have been introduced. the duties and responsibilities of both the administrator and the public have been described. Work in order to reduce natural disaster damages in the real sense in our country started with this law (Suna, 2000; Özalp, 2000)

1992 Erzincan earthquake; At 6.4 (M), 653 people lost their lives and 3850 people were injured. While 3200 housing units and 850 workplaces were heavily damaged, 12000 dwellings and 700 workplaces were moderately and slightly damaged (Şengezer, 1999).

1995 Dinar earthquake 6.2 (M) 90-100 people lost their lives and 170-230 people were wounded. 2727 houses were heavy, 1417 houses were medium, 2166 houses were few, 282 were heavy, 231 were medium, and 148 were slightly damaged (TMMOB, 1998).

1998 Adana-Ceyhan earthquake 5.9 (M) according to the earthquake 145 deaths and according to 06.07.1998 damages, 1113 houses and 11 workplaces were demolished, 9067

houses and 210 workplaces were damaged and 21051 houses and 581 workplaces were mild (Disaster Affairs General Directorate, 1998).

After two major earthquake disasters that took place on August 17 and November 12, 1999, disaster management and society were not adequately prepared and responsibility consciousness did not occur, and disruption, regret, helplessness and coordination disorder occurred after the disaster. After two massive earthquakes, where 18,000 citizens lost their lives, tens of thousands of citizens were hurt, 75,000 houses, 12,500 workplaces were destroyed, thousands of official buildings were destroyed or damaged, 150,000 families were left homeless and Turkey was in control of extraordinary situations (Ozturk, 2003), a more comprehensive system is needed.

An earthquake of 7.0 (M) size occurred on the morning of October 23, 2011 at 13.40, including the headquarters of the village of Tabanlı, connected to the Van center. Two weeks after this depression, a new earthquake of 5.7 (M) occurred in the town of Edremit, 16 kilometers from Van center, on Wednesday, November 9, 2011, at 21.20. After the main earthquake that came to the plaza, for a month, an average of 180 aftershocks had come to the scene. In total, more than 11 thousand aftershocks were recorded. Due to the earthquake, 644 people lost their lives and 1,966 people were injured. Erçis district was the most lost district. Approximately 187 thousand structures have been examined within the scope of damage assessment studies. Nearly ruined / severely damaged structure has been identified. Immediately after the earthquakes, the search and rescue operations began quickly and wrecked a total of 252 people. Due to the earthquake, 36,203 dwellings, 2,884 workplaces and 9,602 branches were destroyed or seriously damaged (Republic of Turkey Prime Ministry Disaster and Emergency Management Directorate, Ankara, 2014)

MATERIAL AND METHOD

It is understood that all these earthquakes and natural phenomena are caused by physical, economic, social and psychological losses. With our work, we aim to reduce all these losses especially physical and economic losses. During the calculations of individual numbers in the area affected by disasters, there is a huge loss of time. In addition, after the search and rescue operations in regions, high economic losses occur. It is aimed to use the electronic infrared person counters used for commercial purposes to prevent these losses coming to the square, by utilizing the geographic information system.

The infrared human counter uses the advanced image processing technology to count people everywhere. In shopping malls, shopping malls offer easy access to the system, which is connected to everywhere in the world with high accuracy rates in all kinds of private and public areas, counting reports, efficient, fast and economical service.

These counters were initially intended to be placed in public institutions. In this respect, the public institution;

- Which is intense between the hours,
- Which is the density in the floors,

- The density ratio at the inlet-outlet doors,
- The density ratio of the building on different dates,
- The intensity ratio of the building at different times,
- The busiest day of the week
- Peak hour of the week
- A monthly density average of the building,
- Comparison of desired date and time
- We can reach many places like the building corridor density ratio

All these data devices can be accessed with a continuous stream of data graphically displayed on the system to which they are connected. The system is vulnerable to modification. We also aim to reach the instantaneous data on the map by adding a Geographic Information System product to our system with our work. The administrator of the institution and those who deal with the system can access the instant data when they want for 24 hours.

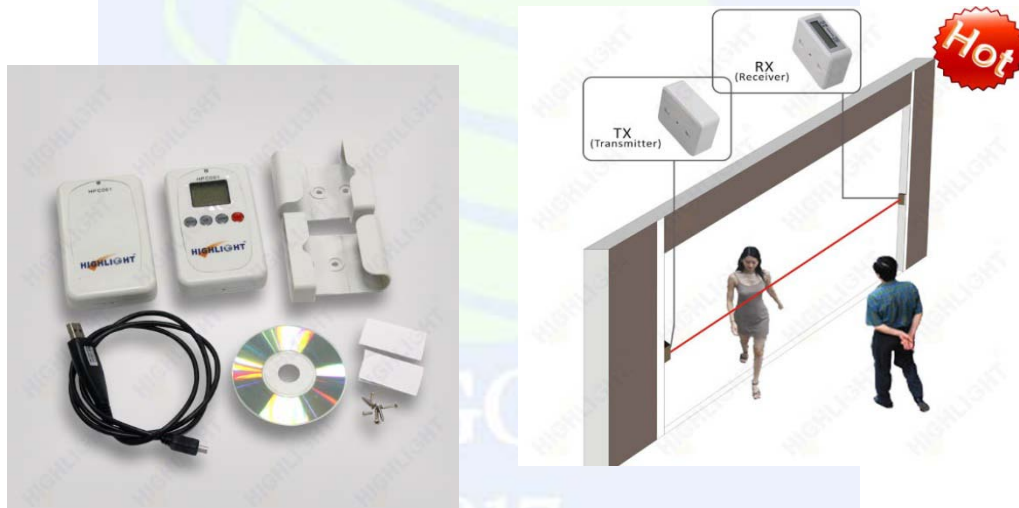


Figure 1. Person counter instruments and infrared people counting system (URL1, URL2)

RESULTS

In case of any disaster, it is planned to reach the number of persons on floor and building basis in the public Karum institutions in the city with the current data from the system. In this case, an earthquake, fire, etc. will prevent the search and rescue works in empty buildings, and the economic and human loss losses will be minimized by providing the appropriate number of assistance to that building.

- Accuracy rates of 95 percent are available.
- It works successfully inside and outside the building.
- We can place the devices where we want the appropriate spot.

- If there are more than one devices in the building, they can all be monitored via a single system.
- It counts people who are side-by-side properly,
- Easy to install
- In some models adults and children are separated.
- In general, most of the devices on the market are not affected by electricity interruption. This situation gives us an advantage during disasters.
- The crowd has been successful in counting people.

Due to these features, the device is suitable for use. The devices receive data from the sensors installed in the form of usage, which is stored in memory and served to the users on the network system.

For example, hospitals, schools, dormitories, some public institutions, etc., can be used in the study by placing the device in the corridor for the data of the entrance and exit doors and then for the data of the floors in the first place, transferring them from a single network to a map of the geographical information system, management model. Intervention aimed at the number of people affected by any earthquake, flood, fire, terror, etc. In empty buildings, time and economic loss will be tried to be avoided.



Figure 2. Directional Customer Counter (URL 3)

Another important element of this study is the geographic information system. Geographical Information Systems includes all kinds of data related to the earth by transferring them to the computer environment and storing, classifying, comparing with

each other, analyzing, updating and visualizing them as maps, graphics and tables as required by special programs used in these data . With this state, GIS is not merely transferring and storing various kinds of data in a computer environment. The most important feature that distinguishes GIS from other database systems is the storage of all data on earth according to their location and the possibility of various spatial associations between them, i.e. various analyzes. GIS provides the most important information that can be used in disaster related researches and disaster management studies (Demirci and Karakuyu, 2004). It allows these various analyzes and interrogations and provides all results and data for displaying in a map. GIS, which has such an effective place in disaster management, will provide easy and simple access to our work for us. The GIS program, which we will use to modify the device, will support the operation of the system.

DISCUSSION

Various methods are being developed and used in the world and our country to minimize disaster damage. At the beginning of these methods, it is necessary to put out the disaster danger situation of that region and make the existing plans accordingly. Geographic Information System (GIS) techniques are seen as a preferred tool in terms of reliable, fast and easy use in disaster reduction. The reason for using GIS in disaster management is to control destruction, to help reduce the damage caused by disaster, and to help protect lives and resources (Aydınoğlu et.al., 2009) We aim to benefit from the geographic information system as a support system in reducing the negative consequences of our work.

CONCLUSIONS

There are many mass events around the world. Disasters are at the beginning of these mass events. The occurrence of disasters cannot be clearly predicted in advance and cannot be given a definite time, so it is a difficult event to be prevented by people. Since they cause serious loss of life and property, trying to withdraw the most loss before and after the disaster by various solutions. When these solutions are sought, appropriate disaster management will not be done, or serious physical, economic, social and psychological losses will occur if the management style is not implemented in appropriate ways. We are aiming to reduce these losses with our work.

When implementing disaster management steps, the number of affected people is important. Often times these people cannot be predicted, so the disruptions and losses occur during management. A geographical information system based building management model for the number of people has been developed. With this management model, electronic scales used for commercial purposes will be placed in public institutions and organizations, instantaneous data will be taken on the basis of buildings and floors and these data will be transferred to the geographical information system and the number of active persons will be reached. With these numbers, it is aimed to provide services to the appropriate number of people with high data in areas such as health care, shelter service, food and clothing service, education service in search and rescue phase after disaster. In

this way, unnecessary economic, physical and time losses will be prevented.

REFERENCES

- Kanlı B.İ. and Ünal Y., 2004. Üst düzey planlama sistemi ve afet yönetimi ilişkileri. *İTÜ Dergisi/A* 3(1): 103-112.
- Şengezer B. and Kansu H., 2001. *Kapsamlı Afet Yönetimi*. YTÜ Basım Yayın Merkezi, İstanbul, pp. 132.
- Şengezer B., 1999. *Erzincan Depremi Hasar Analizi ve Türkiye’de Deprem Sorunu*. YTÜ Basım Yayın Merkezi, İstanbul.
- TMMOB, 1998. Dinar Depremi Raporu, Ankara
- Afet İşleri Genel Müdürlüğü, 1998. Adana – Ceyhan Depremi, Ön Rapor, Ankara.
- AFAD, 2011. Van Depremi Raporu
- Öztürk N, 2003. Türkiye’de afet yönetimi: karşılaşılan sorunlar ve çözüm önerileri. *Çağdaş Yerel Yönetimler* 12(4): 42-64.
- Özalp T., 2000. *TBMM Tutanak Dergisi*, 21. Dönem, 2. Yasama 60. Birleşimi.
- Aydinoglu A.C., Quak W., Yomralioglu T., 2009. Some Spatial Data Management Issues towards Building SDI, *International Workshop on Spatial Information for Sustainable Management of Urban Areas, FIG Commission 3 Workshop*, 24 February, Mainz, Germany.
- Demirci A., Karakuyu M., 2004. Afet yönetiminde Coğrafi bilgi teknolojilerinin rolü. *Doğu Coğrafya Dergisi* sayı 12.
- Suna H., 2000. *TBMM Tutanak Dergisi*, 21. Dönem, 2. Yasama 60.
- Gökçe O., Tetik Ç., 2012. *Teoride ve Pratikte Afet Sonrası İyileştirme Çabaları*. Başbakanlık Afet ve Acil Durum Yönetimi Başkanlığı Yayını, Ankara
- Gülkan P., Balamir M., Yakut A., 2003. *Afet Yönetiminin Stratejik İlkeleri: Türkiye ve Dünyadaki Politikalara Genel Bakış*. ODTÜ Afet Yönetimi Uygulama ve Araştırma Merkezi, Ankara, 61 s.
- URL1: <http://www.highlight86.com/hpc-person-counter-204.html>
- URL2: <http://www.highlight86.com/hpc-infrared-people-counting-66.html>
- URL3: <http://www.highlight86.com/hpc-directional-customer-counter-1073.html>

Monitoring Natural Disasters Using Geographical Information Systems: A Case Study of Kayseri

Abdurrahman Geymen¹

¹*Department of Engineering, Erciyes University, 15 Temmuz Campus, 38039, Kayseri, Turkey.
(ageymen@erciyes.edu.tr)*

ABSTRACT

Turkey is a country, where many natural disasters occur and loss of lives and properties emerge. In order to minimize those losses originating from natural disasters and to take measures, various methods and techniques are utilized. From the aspect of creating the position-based maps, the leading one among those methods and techniques is the Geographical Information System (GIS). In this study, by using the Geographical Information System technologies, it is aimed to obtain the natural disaster risks of Kayseri City and the web-based risk maps regarding those risks. During this study, for Kayseri city, the earthquake, landslide, rock fall, and avalanche maps to shed light to the policies for preventing the natural disasters and selecting the locations were prepared. Moreover, the study will also be guiding in terms of determining the natural disaster danger and risk status of Kayseri city, to prepare the base maps that city and region planners would need for revising the plans, and to convey true, fast, reliable, and momentary information to administrator in decision-maker position.

INTRODUCTION

Disasters are destructive natural events that occur abruptly, are unpreventable when they start, and cause loss of life and property (Olowu, 2010; Durduran ve Yağcı, 2015). Disasters not only cause loss of life and property, but also lead to huge material damage on agricultural fields (Yiğiter, 2008).

Geographical Information Systems (GIS) are the systems that collect, store, control, process, analyze and display earth-referenced data (Aranoff, 1989; Yomralıoğlu, 2000; Valacich and Christoph, 2010; Geymen, 2016). GIS is one of the most important technological tools that can help in the process of healing wounds caused by natural disasters (Konu, Mızrak ve Memeoğlu, 2015). GIS provides effective solutions in management systems before, after and during the disasters in Turkey as well (İlter ve Özkeser, 2007). There are many studies conducted regarding disasters in our country. A study by Turoğlu et al. (2010) sought answers for how today's technologies can be used as most efficiently as possible in performing interventions properly and quickly during and after possible disasters that can be experienced in Istanbul. They offered suggestions for identifying damaged areas in a rapid and right way by using GIS, making interventions in a

healthy way and minimizing losses of life and property caused by natural disasters (Turoğlu et al., 2010). Reis and Yomralıoğlu conducted a study in 2005 and suggested that "natural disaster" fact is the most essential environmental hazard in areas, such as Eastern Black Sea Region, receiving heavy rain and having a sloping topographic structure. They also suggested that, first of all, it is required to determine potential landslide sites at regional level, and then to determine the most appropriate urban development areas by taking these areas into consideration in order to reduce landslide risk and to plan proper settlement areas (Reis ve Yomralıoğlu, 2005). Furthermore in the study conducted by Yağcı and Durduran in 2015, analyses have been performed for the types of earthquakes occurred in Konya between the period of 2000 and 2011, the usage types of buildings and their resistance to earthquake intensity, the number of casualties caused by earthquakes, and to determine safe areas for homeless people injured during the earthquakes (Yağcı ve Durduran, 2015). A postgraduate study conducted by Özdilek in 2007, the real-time systems, one of today's most advanced disaster management technologies and their combinations with GIS are examined (Özdilek, 2007).

MATERIALS & METHODS

In Figure 1, some digital data are required to obtain maps for natural disasters such as avalanche, flood, rock fall, landslide and earthquake occurred in metropolitan area of Kayseri selected as study area. In the study, firstly the province, district and neighborhood borders obtained from Kayseri Metropolitan Municipality are transferred to the computer environment according to the specified object catalog. Afterwards data regarding natural disasters occurred in the province of Kayseri such as flood, rock fall, landslide, earthquake, avalanche and bereavement are received from the Provincial Disaster and Emergency Directorate of Kayseri and the data is processed on GIS database. It is ensured to make visual interpretation and have an opportunity to make a more efficient and quicker decision due to the characteristic of being expressed as geographical of tables and statistics.



Figure 1. Study area

RESULTS & DISCUSSION

Borders of district and neighborhoods in the province of Kayseri are taken as a base for ensuring the maps of natural disasters. Some spatial analyses are carried out by using ArcGIS 10.4 software and relevant maps are obtained.

First of all, the district layer of Kayseri province is displayed on the ArcGIS software and then density analyses are used to create maps for rock fall in Figure 2, and landslide in Figure 3. It was found that the rock fall is most densely seen in Melikgazi district and landslide is most densely seen in the district of Develi.

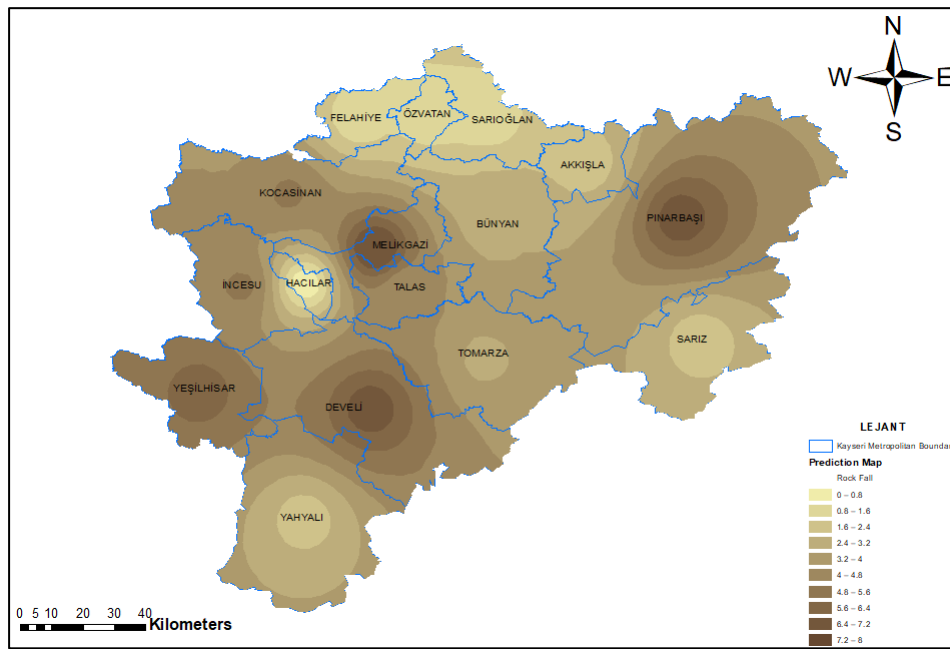


Figure 2. Areas that rock fall is the highest on a district base

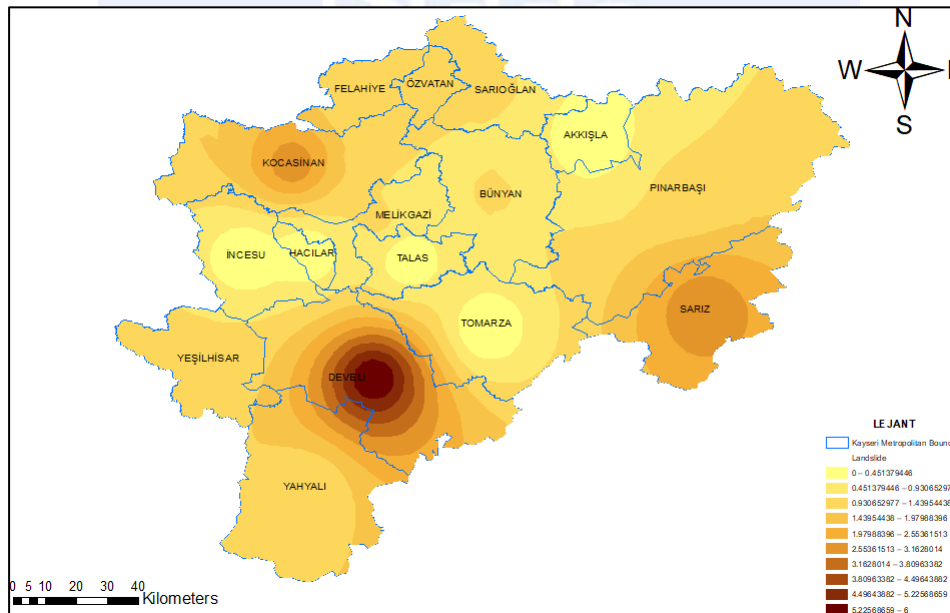


Figure 3. Areas that landslide is the highest on a district base

Secondly, the neighborhood layer of Kayseri is displayed on the ArcGIS software, an input layer is obtained to be used in density analysis by using Tools- Features - Polygon to Line instructions. Afterwards density analysis maps of disaster types related to the relevant neighborhoods are obtained by using the instruction 'Line Density' from Density section of the Spatial Analyst Tools.

These analyses performed on neighborhood basis showed that landslide disaster type was seen in 20 neighborhoods, rock fall and flood/deluge disasters were seen in 57 and 28 neighborhoods, respectively. Figure 4 shows flood/deluge disaster map on a neighborhood basis as an example. Moreover, it is observed that earthquake disaster is seen in Burhaniye and Kardeşler neighborhood of Bünyan district, Güneşli neighborhood of Kocasinan district. Bereavement and avalanche disasters are seen in Şen neighborhood of Akkışla district and Kayaönü neighborhood of Pınarbaşı district, respectively.

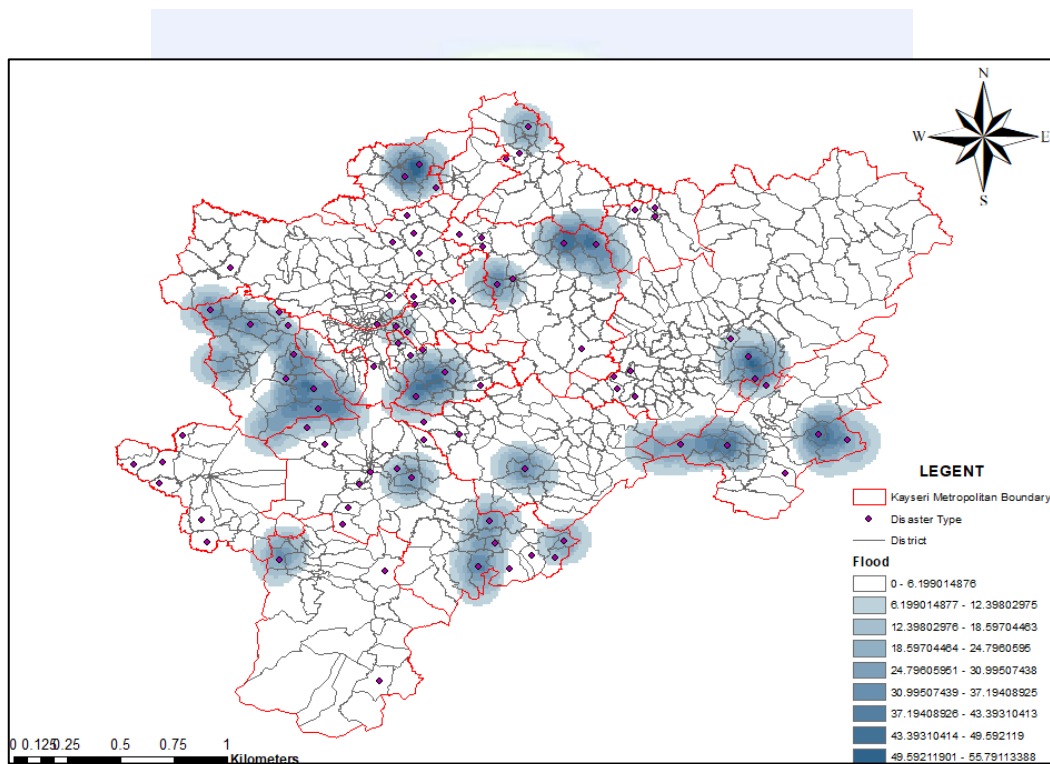


Figure 4. Flood/deluge disaster map on a neighborhood basis

CONCLUSIONS

Data on natural disaster is sustained from Kayseri Provincial Disaster and Emergency Directorate and processed on ArcGIS software and thus some spatial analyses are able to be conducted in the study. Two main purposes and the results obtained from these purposes are presented in the study:

- As a result of monitoring, examining, analyzing and assessing natural disasters seen in the province of Kayseri such as flood, rock fall, landslide, earthquake and bereavement by using GIS, mapping these disasters on a district and neighborhood basis.

- b. Within the frame of these results, it is aimed to forecast events such as disasters that can happen in the province of Kayseri by using GIS and to minimize damages, dangers, and losses of life and property which will be experienced during and after these disasters.

Both technology and all services provided by technology have the aim to serve humanity. Especially life safety and services related to that have first-degree importance. However, there should be planned, realized and prepared sources in advance in order to perform services especially during the disasters. For the most efficient management of these sources, information system usage is inevitable.

REFERENCES

- Aranoff, S., 1989. *Geographical information systems: a management perspective*. WDL Publications: Ottawa, Canada.
- Geymen, A., 2016. Software developments to ease the usage of urban information system in local municipalities, Selçuk *International Scientific Conference on Applied Sciences*, Antalya.
- İlter, H.B., Özkeser, İ., 2007. Coğrafi Bilgi Sistemleri ile Afet ve Acil Durum Yönetim Bilgi Sistemleri, *TMMOB Afet Sempozyumu*.
- Konu, A., Mızrak, Y., Memelioğlu, R.Y., 2015. Kentlerde Afet Yönetimi ve CBS'nin Rolü, *International Burdur Earthquake & Environment Symposium*.
- Olowu, D., 2010. The Hyogo Framework for Action and its Implications for Disaster Management and Education in Africa. *JAMBA: Journal of Disaster Risk Studies*, 3(1):303-320.
- Özdilek, O., 2007. *Gerçek Zamanlı CBS ile Afet Yönetimi Uygulama: Marmara Denizi için Gerçek Zamanlı Tsunami Uyarı Sistemi Değerlendirilmesi*, İstanbul Teknik Üniversitesi, Fen Bilimleri Enstitüsü Yüksek Lisans Tezi.
- Reis, S., Yomralıoğlu, T., 2005. Coğrafi Bilgi Sistemleri ile İl Ölçeğinde Afet Yönetim Amaçlı Planlama, *TMMOB Harita ve Kadastro Mühendisleri Odası 10. Türkiye Harita Bilimsel ve Teknik Kurultayı*, Ankara.
- Turoğlu, H., Döker, F., Bayrakdar, C., 2010. Afet sonrası müdahalede UZAL ve CBS teknolojilerinin İstanbul için önemi. *İstanbul'un Afetlerden Zarar Görebilirliği Sempozyumu*, İstanbul.
- Valacich, J., Christoph S., 2010. *Information Systems Today: Managing in the Digital World*, Prentice Hall.
- Yağcı, C., Durduran, S.S., 2015. Konya İlinde Olası Bir Afet Durumunda CBS ile Afet Yönetimi Afet Yönetimi, *Akademik Bilişim Konferansı*, Eskişehir.

- Yiğiter, N.D., 2008. *Planlamada Afet Bilgi Sistemi ve Yönetiminin Coğrafi Bilgi Sistemleriyle Modellenmesi: Adana Örneği*. Gazi Üniversitesi Fen Bilimleri Enstitüsü Yüksek Lisans Tezi.
- Yomralıoğlu, T., 2000. *Coğrafi bilgi sistemleri temel kavramlar ve uygulamalar*. Seçil Ofset: İstanbul.



Applying GIS and Multi Criteria Evaluation in Forest Fire Risk in Bakircay Basin

Sevki Danacioglu¹ and Sermin Tagil^{*2}

¹Department of Geography, Balikesir University, Cagis Campus, 10100, Turkey.

²Department of Geography, Balikesir University, Cagis Campus, 10100, Turkey e-mail: stagil@balikesir.edu.tr

ABSTRACT

Forest fire is one of the abiotic factors that have an effect on the forest ecosystem. Forest fires have significant local effects on soil degradation, soil erosion, natural habitat and biodiversity. However, since greenhouse gases have a significant share in gas emissions, forest fires have global impacts. Spatial analysis by GIS (Geographic Information System) provides a tool for accurately zoning the area with high potential risk of forest fire. Through GIS spatial analytical procedure, forest fire risk ranging from high to low is derived, according to its sensitivity to fire or fire-inducing capability. In this study, vegetation (vegetation type, vegetation density), topographic (elevation, slope, aspect, topographic wetness index), climatic (average precipitation of the warmest quarter, area solar radiation WH/m^2) and human-made (distance from settlements, distance from roads) parameters were used as causative factors of fire to determine the risk by using combination of GIS in spatial analysis and multi criteria evaluation in Bakircay Basin, Turkey. Each causative factor was classified and weighted according to its own fire sensitivity and fire-inducing potential. Spatial resolutions of these biophysical and human-made parameters were set as 30 meters. Protection measures for forest fires can be taken beforehand and the results of this study were very useful in determining the potential hotspots. In addition, this study also demonstrates the potential of multi criteria analysis integrated with GIS which is an effective tool in assessing “where and when” forest fires are likely to occur frequently.

INTRODUCTION

Fires, one of the abiotic factors that damage the forests, is one of the processes that cause considerable effects on the ecosystems (Food and Agricultural Organization [FAO], 2007). Forest fires, which lead to significant local effects such as soil degradation, soil erosion, natural habitat and biodiversity, have global impacts due to the fact that forests have a significant share in greenhouse gas emission (Chuvieco, 2008).

* Corresponding Author

Risk must be considered with a status of danger; not in the context of an ordinary probability or estimation concept. Accordingly, risk is not just a probability or estimate, but the possibility of emergence of a danger. (Ozmen, 2010). Within this framework, fire is a danger with its impacts on the ecosystem, and the possibility of emergence of a fire means the fire risk. According to FAO terminology, fire risk is the presence or activeness of any factor and the possibility of start of a fire (FAO, 1986).

Forest fires is a risk that affects all the forest ecosystem. Fires, directly or indirectly, have multidimensional; local, regional and global effects (Chuvieco et al., 2010). As a result of impacts observed specifically on a local scale, there are changes in soil conditions and the impact of rain drops on the ground change. Besides this, locally, the impermeable layer formed by the ashes of the burned material reduces the infiltration, and causes rain waters to move into surface flows, and this increases the erosion. If fire occurs in the areas where water resources are present, hydrological functions of the forests might be affected negatively (Kucukosmanoglu, 1995). According to Goldammer (1999), forest fires on a local scale impact the soil microbial processes, and may change the soil and plant structure and compound. Also, death of young plants depending on the increase of terrestrial radiation, extinction of nutrients and organic substances in the soil is another local effect of the forest fires on the ecosystem (Yildiz et al., 2010).

One of the most significant regional effects of the fires is the dispersion of aerosols and other chemical particles into the atmosphere. Aerosols and particles might affect the terrestrial radiation and atmosphere chemistry (Andreae and Merlet 2001), air quality (Hardy et al., 2001) and human health (Brauer 1999) negatively. Forest fires at regional and global scale might have an impact on the climate. Studies show that there is strong correlation between the climate and fire regime. It's known that destruction of dead and living vegetation of the forests by the forest fires leads to changes in climate features by causing; change on the average and extreme temperatures depending on the increase in ground solar radiation, earlier start of vegetation cycle, decrease of relative wetness, increase in the speed of air movements, reduction of interception and increase in evaporation (Cepel, 1975).

First, places with high risk of fire must be determined to be able to fight against forest fires. The areas with high risk in this respect are the fields where natural and human processes with an impact on the occurrence of forest fires exist together with certain priorities. Priority of factors changes on the basis of their capacity to have an impact on fire. In other words, determination of the areas with high risk of fire depends on a process requiring categorization of all factors by their degrees of effect and discussing them on a joint basis. In this respect, Multi Criteria Analysis Techniques (MCAT) are characterized as an ideal approach for determination of areas with high risk of fire, as it has a nature that allows analyzing multiple variables together by specified priority status (Prasad et al., 2009; Erdogan, 2012; Karabulut et al., 2013). Analysis capability of GIS, combination of MCAT approach provides a wide usage opportunity for solution of spatial problems.

The purpose of this study is to determine the fields where the possibility of occurrence of a fire is the highest in Bakircay Basin by using MCAT. In the study, danger analysis, which

is the first stage of fire risk analysis, was performed. In this direction, the study seeks an answer for the following question: Which fields have the highest risk of fire in Bakircay Basin?

MATERIAL AND METHOD

Study Area:

Bakircay River Basin is located in the northern side of Aegean Region, Bakircay area of Aegean Part, between the east longitudes 27°-28° and north latitudes 39°-40° at large (Figure 1). Length of the river, originating from Kocadag, named Bakircay upon entering in Kirkagac Plain by passing through Karakurt Strait of Gelenbe Stream, is 129 km. Supplied by Madra Mountain in north and Yunt Mountain in south throughout its linear flow, fed by many branches, Bakircay has a drainage basin area of 3356 km² according to the spatial analyses we performed.

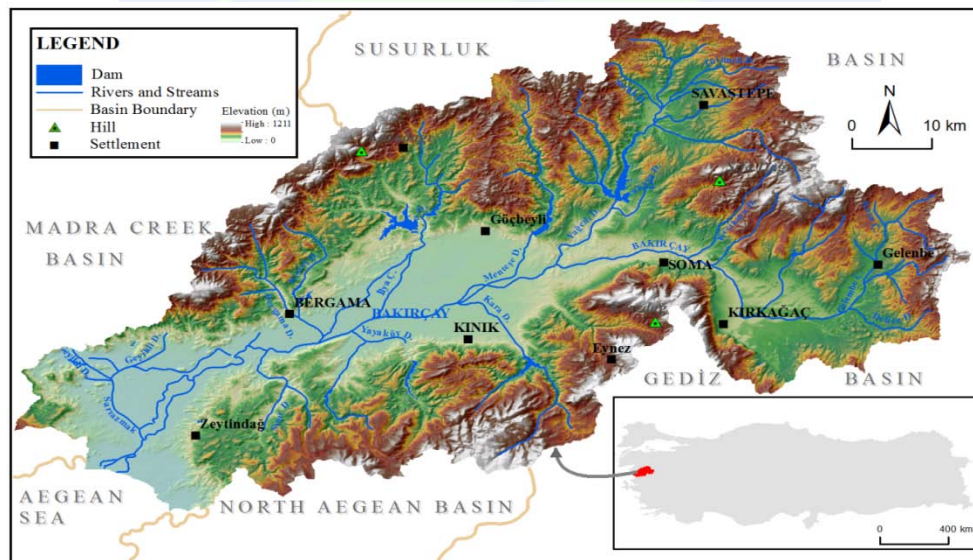


Figure 1. Location map of Bakircay basin

Data:

Data used in the model for fire risk analysis has been obtained from various organizations and institutions. Meta data of the primary and secondary data used in the study are as follows. 1:25,000 scaled digital vector topography maps generated by the General Command of Mapping (GCM) have ± 5 m vertical location accuracy in UTM ED 1950 projection system. Contour lines obtained from these 1:25,000 scaled topography maps were used at generation of Digital Elevation Model (DEM). DEM was generated at 30m x 30m spatial resolution. For determination of climatic characteristics and climate type of Bakircay Basin, measurement data of Akhisar, Dikili, Bergama and Soma meteorology stations (1998-2013) were assessed. Another primary data set used in the study is the

1:25,000 scaled vegetation maps procured from the Ministry of Forestry and Water Affairs. For human data, 1985 and 2013 population data of all settlements obtained from the Turkish Statistical Institute (TSI) was also included into the fire risk analysis process.

Method:

In this study, the factors with an impact on the fire risk at Bakircay Basin were determined by considering the methods developed by Prasad et al, (2009) and Erdogan, (2012). Determined variables and their weights by the capacity of creating a fire risk were displayed in Table 1. Fire risk analysis was performed in the Bakircay Basin by means of the formula provided below:

$$FR = 8 * Sc + 5 * (Cc + Dr + Ds) + 3 * (E + S + A + TWI + Sr + Ap)$$

Where FR - fire risk, Sc - species composition, Cc - crown closure; Dr - distance from roads, Ds - distance from settlements, E - elevation, S - slope, A - aspect, TWI - topographic wetness index, Sr - solar radiation and Ap - average precipitation.

Definition of the parameters employed for determination of the areas with fire risk and the methods used are as follows:

Vegetation Parameters consist of two parameters as Sc and Cc. In this context, vegetation features of the Bakircay Basin were obtained from the stand maps, and divided into risk groups by considering the flammability features. Categorization of groups was performed by considering the studies performed by Dimitrakopoulos and Papaioannou, (2001), Dinc Durmaz, (2004) and Kucuk, (2004). Fields with high vegetation per km² in Cc were determined to be the fields with high risk of fire.

Table 1. Risk Values and Criteria Weights of the Variables Used at Fire Risk Analysis.

Parameters	Classes	Risk Degree	Factors	Weight	Explanation
Sc	Other	EH	5	8	Sc, the flammability degree of the natural vegetation, is one of the significant factors that affect the fire behavior. Categorization of risk groups were performed by considering the studies performed by Dimitrakopoulos and Papaioannou, (2001), Dinc Durmaz, (2004) and Kucuk, (2004).
	Agriculture	H	4		
	Oak & Cedar	M	3		
	Black pine & Oak & Grass	L	2		
	Brutian pine - & Peanut pine	EL	1		
Cc (%)	0-10	H	5	5	Cc indicates the stand crown closure, because high stand crown closure means high flammability (Prasad et al., 2009).
	11-40	M	4		
	41-70	L	3		
	>70	EL	1		
E (m)	0-200	L	2		It has significant effects due to the fact that it shapes the behavior of wind, affects the precipitation received and the relationship with the surrounding lands
	201-400	EH	5		

	401-600	H	4	3	(Rothermel, 1983).
	601-800	M	3		
	801-1212	EL	1		
S (°)	0-5	EH	5		S is significant as burning occurs faster at sheer slopes and it affects the direction of fire (Kushla and Ripple, 1997). Such that, spreading speed of fire in areas with a slope of 55% or more is approximately four times more than the fields with a slope up to 5% (Rothermel, 1983).
	5.01-10	H	4		
	10.01-20	M	3	3	
	20.01-30	L	2		
	>30	EL	1		
A	Level	EH	5		A has a strong impact on the fire behavior as it causes variation in insolation.
	North	H	4		
	East	M	3	3	
	West	L	2		
	South	EL	1		
TWI	12.01-23	EH	5		Forest fires may be influenced by hydrogeological conditions (Conedera et al., 2003). Tdetermines the degree of wetness of an area and topographically, the areas with high soil wetness area the areas with low risk of fire (Moore et al., 1991).
	10.01-12	H	4		
	7.01-10	M	3	3	
	5.01-7	L	2		
	3-5	EL	1		
Sr (kW/m²)	417.11-475	EH	5		Sr is significant because fields with high solar radiation duration are more susceptible to a fire.
	476-550	H	4		
	551-625	M	3	3	
	626-700	L	2		
	701-805	EL	1		
Ap (mm)	31.01 - 33.1	EH	5		Ap is favorable for fires as it would increase the wetness values of the fuels on the surface of the lands with high precipitation.
	30.01 - 31	H	4		
	29.01 - 30	M	3	3	
	28.01 - 29	L	2		
	26.2 - 28	EL	1		
Dr (m)	>400	EH	5		While being favorable for fires by sectionalizing the progress of the fire, it provides the ambient conditions to lead to occurrence of human related fires due to the fact that people determine movement routes.
	301-400	H	4		
	201-300	M	3	5	
	101-200	L	2		
	0-100	EL	1		
Ds (m)	>2000	EH	5		Regions near the settlements are areas with high human-induced burn.
	1501-2000	H	4		
	1001-1500	M	3	5	
	501-1000	L	2		
	0-500	EL	1		

* **EH:** Extremelyhigh risk, **H:** High risk, **M:** Medium risk, **L:** Low risk, **EL:** Extremelylow risk,

Topographic Parameters consist of E, S, A and TWI. E, S and A were generated from DEM at 30-meter resolution. TWI, one of the parameters, was obtained according to the equation provided below:

$$(([\text{FA}] + 1) / ([\text{S}] + 1)) \cdot \text{Log}$$

Accordingly, FA (Flow Accumulation) indicates how much body of water flows through the unit area while S (Slope) indicates the flow speed of the water (Tagil, 2006). ArcGIS Hydrography Tool was used for performance of the analyses.

Climatic parameters consist of Sr and Ap. Sr is calculated at 1 W/m² unit by means of the solar radiation analysis included in the ArcGIS software. Huge majority of the forest fires in Turkey start between June and October, when dry summer takes place (Doganay and Doganay, 2003). In this context, the dates June 1-October 31 in 2013 were considered for calculation of the solar radiation values. Ap was calculated by using the amount of precipitation occurred in the hottest periods from 1999 to 2013 at Akhisar, Soma, Bergama and Dikili meteorological stations. Spatial modeling was performed by using kriging interpolation method.

Human parameters, Dr and Ds, were used. Settlement and road maps obtained from 1:25,000 topographic maps were used for calculation of the variables. Euclidean Distance function was used for distance analysis.

RESULTS AND DISCUSSION

Topographic parameters, one of the variables analyzed for determining the fields with risk of fire in the Bakircay Basin, are provided in Figure 2 (a). When the study area is inspected topographically, conversion of the elevation related vegetation from agricultural areas to the *Pinus Brutia* and *Pinus Pinea* increased the risk; however, reduction of human activities after a certain elevation caused the risk to fall. Therefore, the fact that 0-200-meter elevation gradient consists of a rather agricultural land in the basin base has led these fields to be considered within the group with relatively lower risk (34.7%). As it covers the areas where human factor is most intensely experienced, elevation gradient with the highest risk of fire was taken as 200-400-meters elevation gradient (31.6%). 400-600 meters are the fields where both pinus brutia and settlements are intense, and regarded as high risk zone (21.4%). After 600 meters it's considered to be the less risky zone as human activity component is less although pinus brutia, with flammability feature, is the common vegetation. Topographically, southern slopes where Sr is high were categorized as the parts with the highest risk of fire while northern slopes where low Sr and TWI are high were categorized as the parts with the lowest risk of fire in the Bakircay Basin (Figure 2.c). The study area being in the E-W direction causes wide areas to be covered by areas in North and South direction in general at site. 38.9% of the land consists of southern slopes. And this is a very high value in terms of fire risk. 16.4% of the remaining lands are covered by slopes in west direction with a high risk, 12% by slopes in east direction, which is regarded as medium risk, and 32.7% by slopes in north direction, which have relatively less risk. Delta area and plain base with high level of ground water in the study area are the

parts with high TWI and low risk of fire (3.2%). On the other hand, slopes with less TWI causes high risk of fire (33%). The fact that wetness is a restrictive factor against occurrence and spreading of fire has an impact on it (Figure 2.d).

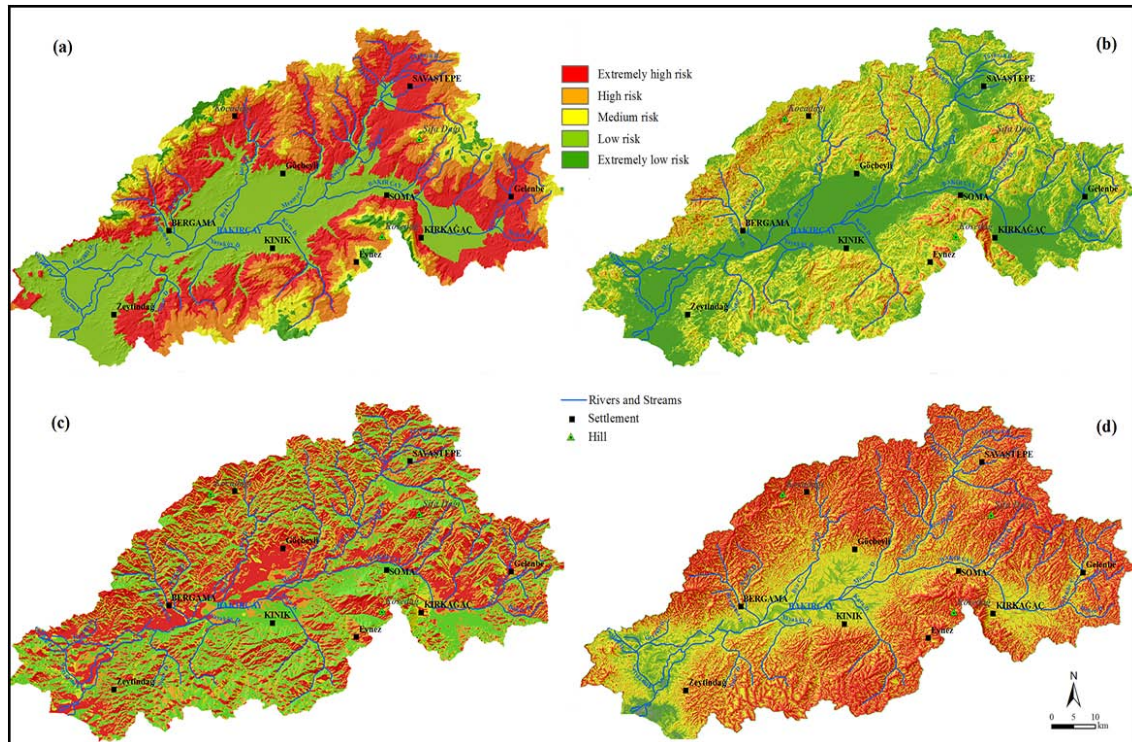


Figure 2. Fire risk maps in each variable a) elevation, b) slope, c) aspect, d) TWI.

Flammable material is defined as any material in or on the soil which may ignite and burn, available for burning and ignition (Omi, 2005). Flammable materials constitute a ground for start and spread of fire (Bilgili et al., 2001). Resistance of tree species against fire varies. When vegetations in the study area are categorized by their flammability capacities, forested lands with climax specie of the region, *Pinus Brutia* and *Pinus Pinea* species are the sites with the highest risk of fire (29.8%). On the other hand, the sites with the lowest risk of fire by stand type (6.4%) consists of surfaces such as settlement areas, stony areas, dune areas, water surfaces and mining areas (Figure 3.a). High Cc have flammable surfaces on which living and dead canopy layer with plenty of dry and dying materials, and so they are the areas with high risk of fire (Dinc Durmaz, 2004). The areas with the highest level of Cc (>71%) are the areas with the highest level of fire risk, and this areas cover 8.8% of the total study area. 75.5% of the basin has low risk in terms of Cc in general (Figure 3.b).

Another parameter that has an impact on the fire risk is the climatic factors. Sr and Ap were investigated as climatic parameters. In these areas, which cover 20.8% of the study area and where Sr is very high, so high is the risk of fire due to Sr, (Figure 4.a). On the other hand, areas with less risk are 63% and indicate that Sr in the basin might pose a risk in general. Study area is under the effect of continental air mass during the fire period from June to October. Thus, considering the precipitation values, the highest Ap value is

observed to be 33.1 mm. These sites, covering the upper course of Bakircay Basin, have relatively higher values than lower basin and thus lower risk of fire (46.2%). In the lower basin between Dikili and Bergama, the lowest summer precipitation is observed. Therefore, they are the riskiest areas in terms of fire risk. The areas with the highest risk stand out by 19,6% (Figure 4.b).

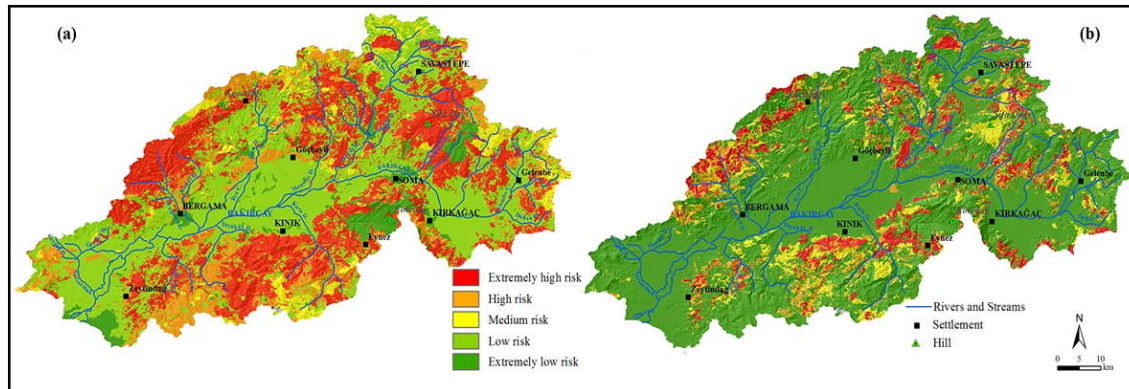


Figure 3. Fire risk maps in each variable a) flammabil species composition and b) stand crown closure.

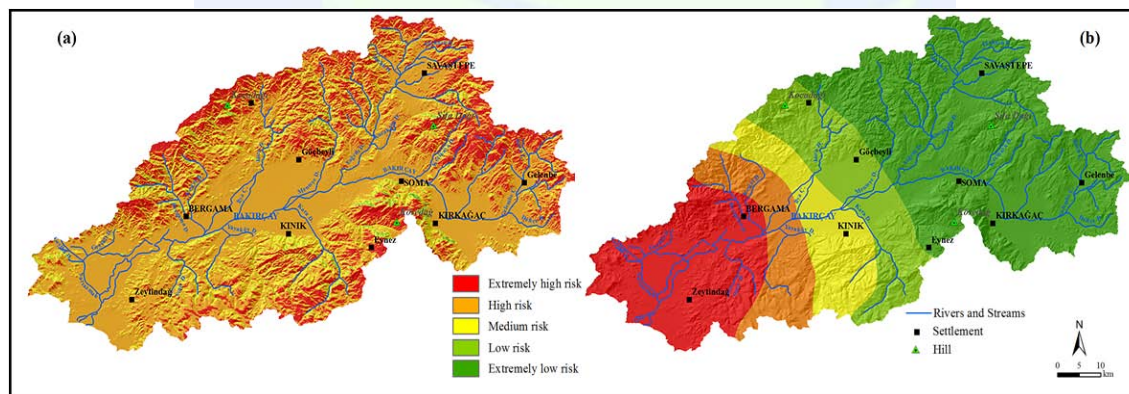


Figure 4. Fire risk maps in each variable a) solar radiation and b) average amount of precipitation during fire period (June-October).

The main cause of the forest fires is the human factor. Within human activities, Dr and Ds are investigated as the factors leading to fire risk (Chuvieco et al., 2003). The site with a distance less than 100 meters to the roads in the Bakircay Basin are areas with high risk of fire, and cover 12,6% of the study area (Figure 5.a). The decrease in road density accordingly decrease the risk of fire as moved from the basin towards the perimeter. On the other hand, a 500-meter risk limit was determined to cover all of 245 village/neighborhood and town settlements in the Bakircay Basin (Figure 5.b). Sites remaining outside the limit were considered to be areas with relatively lower risk of fire. In this context, 38.9% of the study area is of 500 m distance to the settlements at most and has

human related potential fire risk. Areas with high risk and the highest risk cover an area of 58.2%.

As a result, map of fire risk in the study area is provided in Figure 6. The areas with the highest level of fire risk were determined to be the forested lands on the high mountainous masses surrounding the basin base in the north and south (Figure 6). Those sites are the areas with the highest potential risk of fire both because they are close to the human interactions and due to the natural features they have. Since significant ecological destruction is to occur in case of a potential fire on these sites, they are characterized as the areas required to be prioritized during ecological risk analysis.

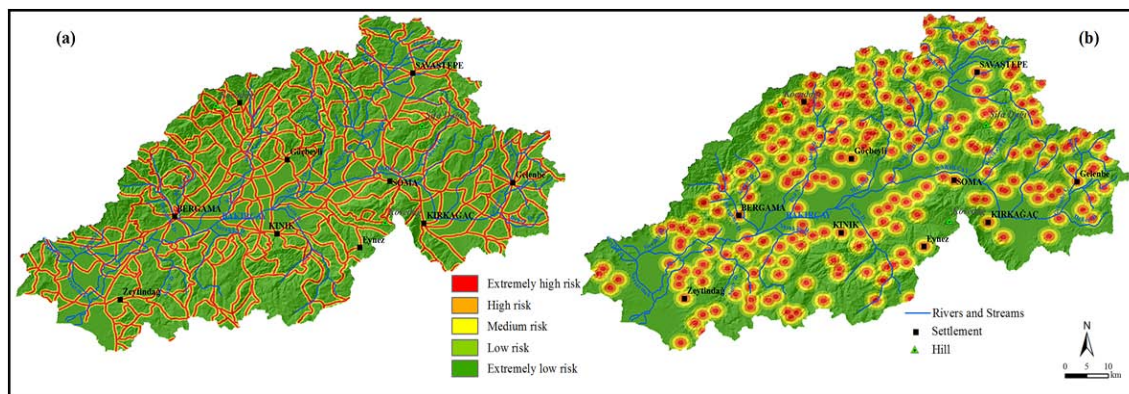


Figure 5. Fire risk maps in each variable a) distance from road and b) distance from settlements

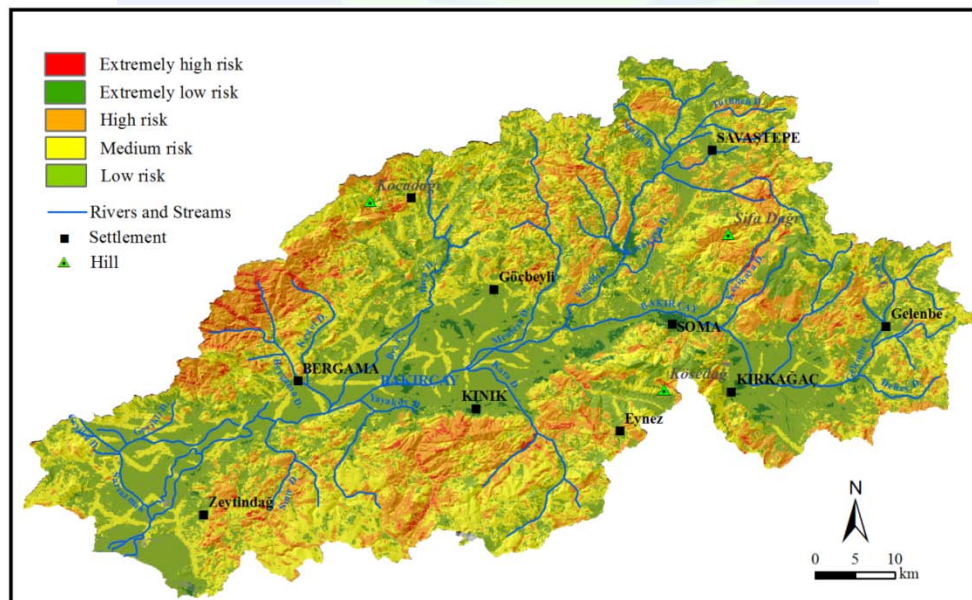


Figure 6. Fire risk map of bakircay basin.

The slopes connecting the high masses and the basin base to each other in the study area are included in the risky category. When land cover and usage features of these sites are investigated, it is observed that they are planted agricultural and maquis lands in general. It

is a fact that land is covered densely by the maquis affects the fire behavior significantly. Making a fire during agricultural activities in the planted agricultural areas affects the possibility of occurrence of a fire. In this respect, such areas have medium risk as they are areas with high level of human activities but relatively less ecological features. Lands in this class are included in areas where human factors stand out, from place to place in basin base. The areas, especially on the route of roads and also in the basin base where agricultural activities are performed are included in this category, which we might call 3rd degree risk areas.

Basin floors were identified as areas with low and lowest fire risk. Due to absence of natural vegetation, elevation, slope, exposure and high ground water level, these areas are included in the class of risk free areas. Although human activities prove to be intense in such areas, non-adjacency to the areas with ecological importance causes risk value of these areas to decrease.

Also, vicinity of Kosedag and Denisin on the south side of Soma are observed to have low risk in the study area since mining sites located on the high mountainous masses are not included into the analysis. Mining sites were considered within the scope of ecological risk analysis, in land cover and usage analysis. The fact that these areas have low risk at fire risk analysis is to lead to errors in ecological risk analysis. Thus, for the purpose of avoiding errors in analyses due to the inclusion of such areas, these areas are exempted from the fire risk analysis and included into ecological risk analysis.

CONCLUSION

In Mediterranean type ecosystems, which have an apparent summer dry cycle, fire affects ecosystem dynamics significantly. In this research, the sites with high risk of fire in the Bakircay Basin within the Mediterranean type ecosystem were determined. Topographic, vegetative, climatic and human parameters were considered for determination of fire risk. Fire risk maps obtained within the framework of these parameters are to help decision makers during management and planning works. As a result, this study demonstrates the potential of GIS technology. It is an exemplary study demonstrating integrated use of multi criteria analysis techniques, which is an effective tool in assessment of “where and when” forest fires might occur, and GIS.

REFERENCES

- Andreae, M. O. and Merlet, P. 2001. Emission of Trace Gases and Aerosols from Biomass Burning. *Global Biogeochemical Cycles*, 15, 955–966.
- Brauer, M. 1999. Health Impacts Of Biomass Air Pollution. In K. T. Goh, D. Schwela, J. G. Goldammer, & O. Simpson (Eds.), *Health Guidelines for Vegetation Fire Events—Background Papers* (p 189–254). Singapore: WHO.

- Bilgili, E., Saglam, B. and Baskent, E.Z. 2001. Fire Danger Rating And Geographical Information Systems In Fire Management Planning, *Kahramanmaraş Sutcu Imam University Journal of Engineering Sciences*, 4(2), 288-297.
- Chuvieco, E., Allgower, B. and Salas, J. 2003. Integration of Physical and Human Factors in Fire Danger Assessment. In E. Chuvieco (Ed.), *Wild Land Fire Danger Estimation and Mapping. The Role of Remote Sensing Data*. New Jersey: World Scientific.
- Chuvieco, E. 2008. Satellite Observation of Biomass Burning: Implications in Global Change Research. In: Chuvieco, E. (Ed.), *Earth Observation and Global Change*. Springer, New York, p.109–142.
- Chuvieco E, Aguado, I., Yebra, M., Nieto, H., Salas, J., Martin, M.P, Vilar, L., Martinez, J., Martin, S., Ibarra, P., de la Riva, J., Baeza, J., Rodriguez, F., Molina, J.R., Herrera, M.A.and Zamora, R. 2010. Development of a framework for fire risk assessment using remote sensing and geographic information system technologies. *Ecol Model*, 221,46–58.
- Cepel. N. 1975. Effects of forest fires on microclima and soil.Istanbul University,*Journal of the Faculty of ForestryB*, 25 (1).
- Conedera, M. Peter, L., Marxer, P., Forster, F., Rickenmann, D. and Re, L. 2003. Consequences of forest fires on thehydrogeological response of mountain catchments: a case study of the Riale Buffaga, Ticino, Switzerland.*Earth Surf. Process. Landf*. 28, 117–129.
- Dimitrakopoulos, A.P. and Papaioannou, K.K. 2001. Flammability assessment of mediterranean forest fuels. *Fire Technology*, 37, 143–152.
- Dinc Durmaz, B. 2004.*Effects of Stand Characteristics on Fire Potantial*. Unpublished Master's Thesis, KTUInstitute of Science, Trabzon.
- Doganay, H. and Doganay, S. 2003. Forest Fires and Measures to be Taken in Turkey . *Eastern Geographical Review* 11.
- Erdogan, M.A. 2012.*Generating Ecological Risk Analysis Method For Buyuk Menderes Basin*. Unpublished Doctoral Thesis, Istanbul Technical University, Institute of Science Department of Landscape Architecture.
- FAO. 1986. Wildland Fire Management Terminology. Report number 70.*FAO Forestry Paper*, Roma.M-99. ISBN 92-5-0024207.
- FAO. 2007. Fire Management-Global Assessment 2006. *A Thematic Study Prepared in the Framework of the Global Forest Resources Assessment 2005*. FAO, Rome.
- Goldammer, J. G. 1999. Forests on fire. *Science*, 284, 1782–1783.
- Hardy, C.C., Ottmar, R.D., Peterson, J.L., Core, J.E. and Seamon, P. (Eds.) 2001. Smoke management guide for prescribed and wild land fire: 2001 edition PMS 964 420-2. NFES 1279. Boise, ID: National Wildfire Coordination Group (226 p).

- Karabulut, M., Karakoc, A., Gurbuz, M. and Kızılelma, Y. 2013. Determination of forest fire risk areas using geographical information systems in Baskonus Mountain (Kahramanmaraş). *The Journal of International Social Research*, 6 (24), 171-179.
- Kushla, J. D. and Ripple, W.J. 1997. The role of terrain in a fire mosaic of a temperate coniferous forest. *Forest Ecology and Management*, 95, 97–107.
- Kucuk, O. 2004. *Determining and Mapping Fire Potential Based on Fuel Type and Fire Behavior*. Unpublished Doctoral Thesis. Karadeniz Technical University Institute of Science, Trabzon.
- Kucukosmanoglu, A. 1995. Relation between protecting water resources and forest fires. Istanbul University, *Journal of the Faculty of Forestry. B*, 45(2), 107-118.
- Moore, I.D., Grayson, R.B. and Ladson, A.R. 1991. Terrain based catchment partitioning and runoff prediction using vector elevation data. *Water Resources Research*, 27, 1177–1191.
- Omi, P.N. 2005. *Forest Fires: A Reference Handbook*. ABC-CLIO, Santa Barbara, CA.
- Ozmen, S. 2010. *Fire Risk Analysis and Production of Fire Risk Maps for Istanbul City*. Unpublished Master's Thesis. Yıldız Technical University Institute of Science., Istanbul.
- Prasad, V.K, Eaturu, A. and Badarinath, K.V.S. 2009. Fire Risk evaluation using multicriteria analysis a case study. *Environmental Modelling and Assessment*, 166(1-4), 223-239.
- Rothermel, R.C. 1983. *How to Predict The Spread and Intensity of Forest and Range Fires* (40 p). Gen.Tech.Rep.INT-143. USDA Forest Service. Intermountain Forest and Range Experiment Station.
- Tagil, S. 2006. Geomorphometric factors controlling landcover organization in Kazdag(İda) National Park: a GIS approach. *Journal of Geographical Sciences*, 4 (2), 37-47.
- Yildiz, O., Esen, D., Sarginci, M. and Toprak, B. 2010. Effects of Forest Fire on Soil Nutrients in Turkish Pine (*Pinus brutia*, Ten) Ecosystems, *Journal of Environmental Biology*, 31, 11-13.

UAV-ASSISTED LANDSLIDE ACTIVITY MONITORING: APPLICATIONS AND OPEN ISSUES

İrfan ZİREK¹ and R. Cüneyt ERENOĞLU²

¹ Canakkale Provincial Directorate of Disaster and Emergency Management Presidency, 17020, Canakkale Turkey. e-mail: irfandrsm@gmail.com

² Department of Geomatics Engineering, Canakkale Onsekiz Mart University, Terzioğlu Campus, 17020, Turkey, e-mail: ceren@comu.edu.tr

ABSTRACT

In this study, landslide development monitoring approach based on an unmanned aerial vehicle (UAV), data acquisition, data processing, analyzes and results were presented. The development of the landslide that took place in Saricaeli Village in Çanakkale Province were tracked and monitored by using a digital camera integrated UAV and a Global Positioning System (GPS) receiver. Three consecutive measurements were performed on May 2016, October 2016 and January 2017 and digital elevation models (DEM), digital terrain models (DTM), three dimensional models and orthomosaics were produced by using photogrammetry methods based on the aerial images. The displacements on the landslide were evaluated based on these datas.

INTRODUCTION

Landslides are natural events that are seen around the world and that have negative economic impacts and result in loss of lives. High slope, lack of stability of the ground, ground water and human effects are some of the factors that cause landslides. Data can be gathered easily in difficult weather and terrain conditions using digital cameras supported by Unmanned Aerial Vehicle (UAV). The fact that data collection is fast and less costly is an important reason for using this technique.

In this study, the studies the Global Navigation Satellite Systems (GNSS) and UAV techniques were evaluated in the landslide area that took place in 2012 in the Saricaeli Village in Çanakkale Province. The landslide observed over a year and the aerial images of the landslide area were at different campaigns. Ground control points (GCP) were established before taking aerial images and the coordinates of the ground control points were measured with the geodetic GNSS receiver. The aerial images were processed using photogrammetric techniques in order to create high accurate three dimensional digital models of the landslide.

Using the photogrammetry methods and software along the study, the DEMs, the DTMs, orthomosaics and three dimensional models of the landslide area were successfully created. Moreover, the area, volume and orientation of slip mass for the landslide were determined

and its development was monitored. Furthermore, some derives were obtained from digital elevation models such as surface gradient, slope orientation. Finally, the slope direction and accumulation area of the landslide were determined by examining the global cell relationships of the DTMs in the GRID form.

STUDY AREA

The Saricaeli Landslide is located at coordinates of $40^{\circ}7'14.48''$ N and $26^{\circ}26'0.94''$ E and altitude of the landslide is approximately 100 m above the sea level. The current activity of the Saricaeli Landslide is deep seated rotational slip. It is far 1 km from the Saricaeli Village Center and 7 km from the Çanakkale Province Center. The landslide extends over a horizontal distance of 150 m and lenght of it is 45 m.



Figure 1. The Saricaeli Landslide

METHODOLOGY

Data Acquisition

In data acquisition stage, a quad-rator UAV and a digital camera which is integrated on the UAV, a Global Positioning System (GPS) receiver and five GCPs were used. GCPs, which were used to transform coordinate systems, were located at upper side of the landslide. The GCPs and their locations were chosen to be easy to see. The coordinates of the GCPs were measured with the geodetic GPS receiver. After the coordinate measurement, flight mission was carried out. The flight height was 50 m and interval beetwen the locations, where the aireal images were recorded, were 5 m. The flight mission was carried out covering the whole landslide area, approximately 6000 m². Size of images are 4000x2250 pixels. Three consecutive measurements were performed on May 2016, October 2016 and January 2017.



Figure 2. Left – An Unmanned Aerial Vehicle, Right – A GPS Receiver

Data Processing

The procedure and the methodology were the same for all the campaigns so only the assesment of the first campaing was mentioned here.

In data processing stage, all the images taken by the UAV were opened by using a photogrammetry software. Camera alignment was performed after uploading the images. In this stage, the software searches and matches the common points on the images and it finds the camera position and orientation for each images and refines camera calibration parametres. As a result a sparse point cloud and a set of camera positions are formed by the software.

Next stage was to build dense point cloud. It was built based on the images and estimated camera positions. Based on the camera positions, the software calculates the depth informations for each camera to be combined into a single dense point cloud.

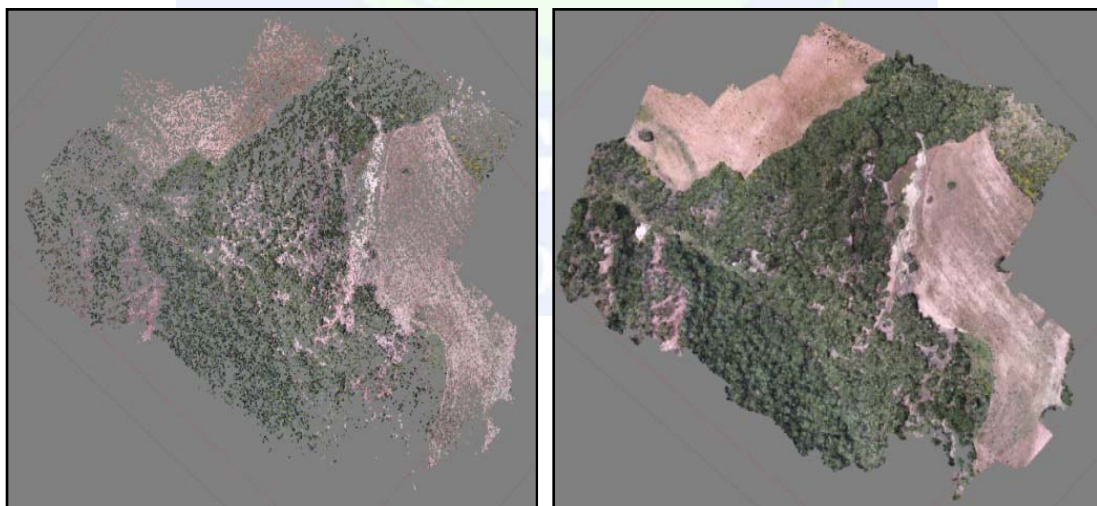


Figure 3. Left – Sparse Point Cloud, Right – Dense Point Cloud

3D polygonal mesh was built after the dense point cloud has been built. This mesh represents the object surface. It is built based on the sparse or the dense point cloud.

After all these operations were completed, the DEM, the DTM and the orthomosaic were produced. The DEM can be built based on the sparse point cloud, the dense point cloud or

the mesh but the DEM which is produced based on the dense point cloud gives the best result. The DEM shows the current situation of the landslide area and also objects like trees are represented in this model. This causes problems during analyzes. Therefore the DEM was not used in analyzes. To build the DTM which was used in analyzes, the dense point cloud should be classified to determine points that represent ground. To do this, the dense point cloud was classified automatically by using the software. There were also cases where the classification could not be done automatically. In these cases, the classification was done manually. The ground points in the dense point cloud were classified by using the colours related to ground. As a result the DTM was built in GRID form. The resolution of the DTM is approximately 7 cm.

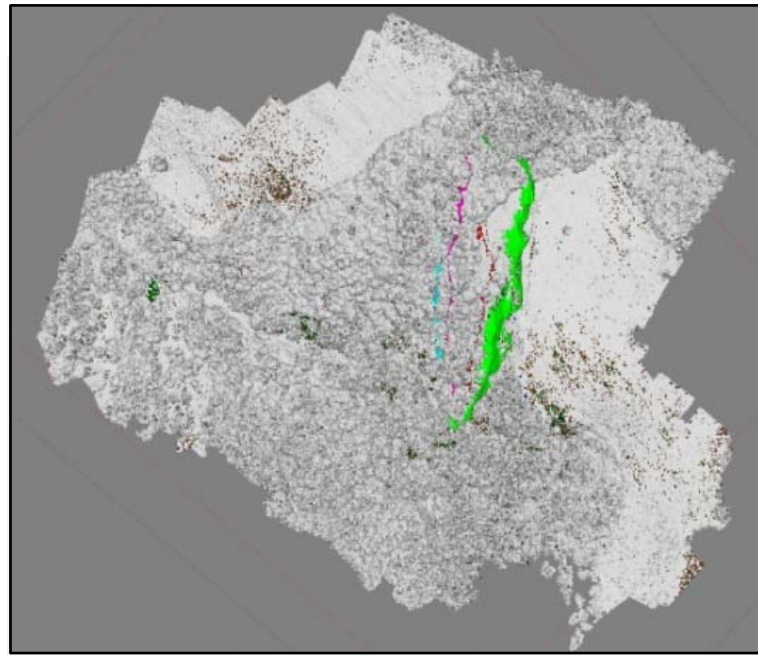


Figure 4. The Classified Dense Point Cloud

After the DTM has been built, a high-resolution orthomosaic was created based on aerial images. This data is very usefull when the detailed view of the landslide is needed. The resolution of orthomosaic is approximately 2 cm.

The produced DTM and orthomosaic have a geographic projection system and have a datum in World Geodetic System 1984 (WGS 1984). Datum transformation was performed by using the GCPs. Transformations to Universal Transvers Merkator (UTM) 6° Projection and International Terrestrial Reference Frame 1996 (ITRF96) Datum was done by using the coordinates of GCPs.

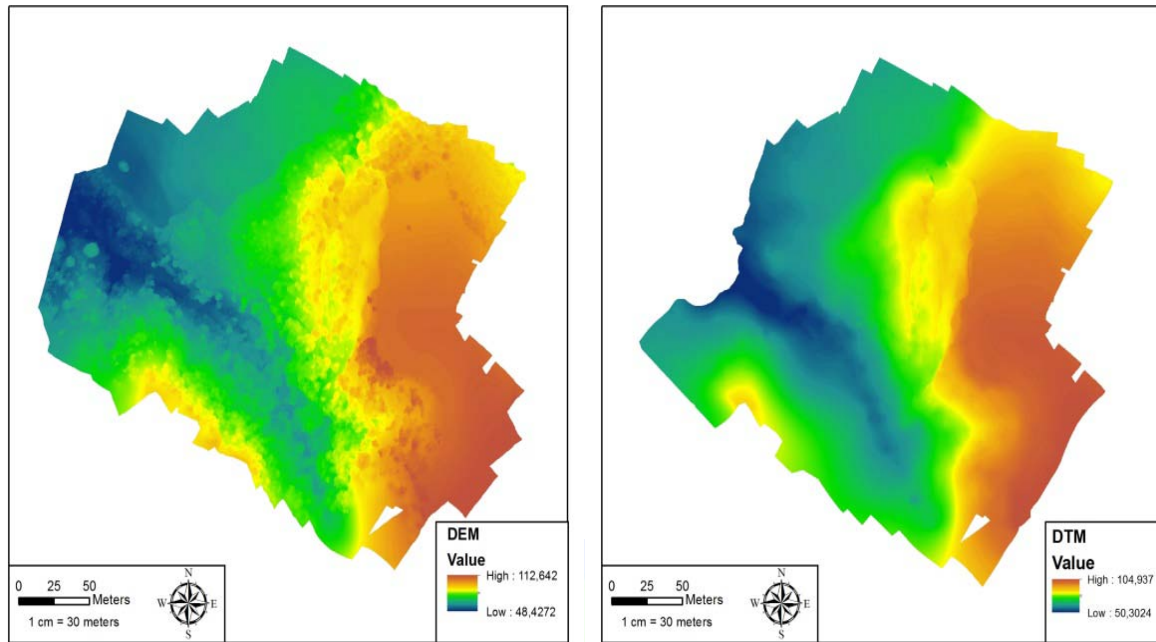


Figure 5. Left – Digital Elevation Model, Right – Digital Terrain Model

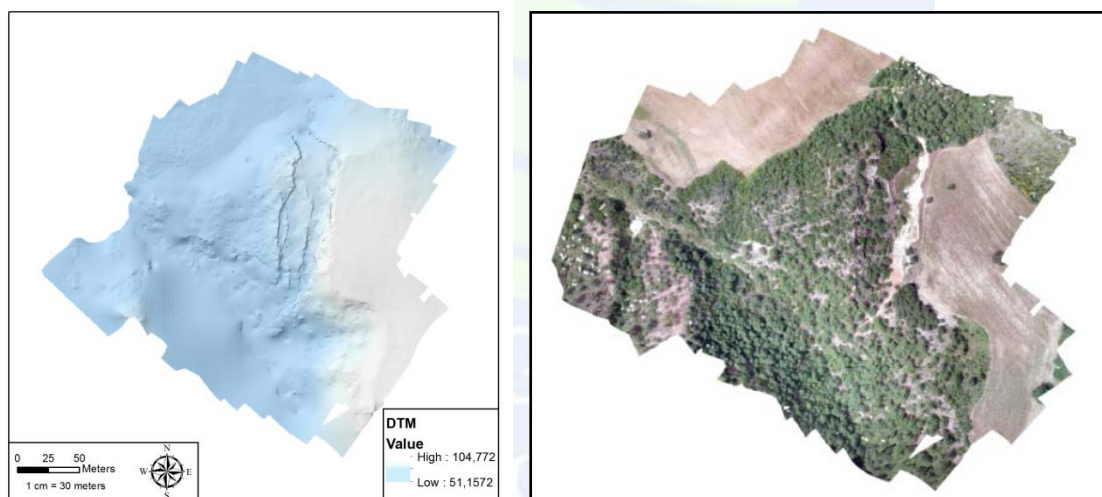


Figure 6. Left – Digital Terrain Model, Right – Orthomosaic

ANALYSIS

The produced datas were opened in a geographic information system (GIS) software. Before starting analyzes, the resolution of the DTM resampled to 50 cm. The analyzes without doing this did not give healthy results.

By examining the global cell relationships of the DTM, the slip direction and accumulation area of the landslide were determined. Before this operation, “Fill Sink” function was applied to the DTM to eliminate sink errors which may occur in the data. If a cell has less height value than the eight cells around it, the flow accumulation does not occur. Therefore sink errors should be eliminated.

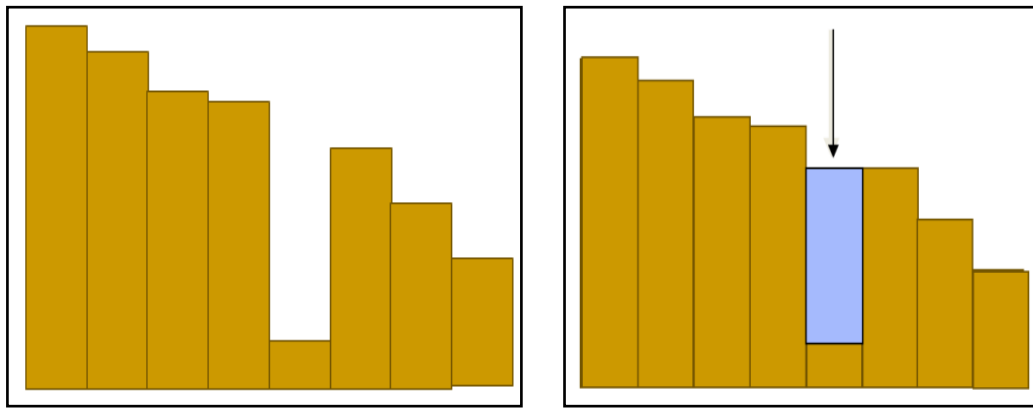


Figure 7. Fill Sink

After performing “Fill Sink” function on the data, the flow direction of the landslide was determined by using “Flow Direction” function. In this function, height values of the cells are compared to the eight neighbor cells. The flow will be to the cell which has less height value.

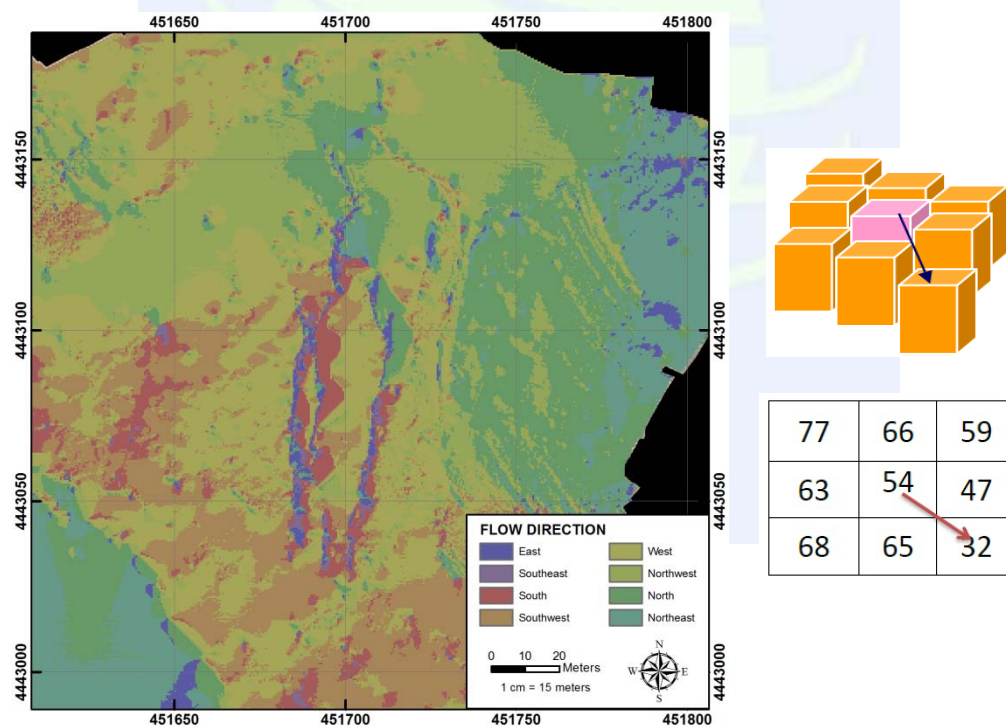


Figure 8. Flow Direction

Also the derivatives of the DTM like slope and aspect datas were produced in the GRID form. Their resolutions are 50 cm as well. Also contours were produced with equidistance of 50 cm.

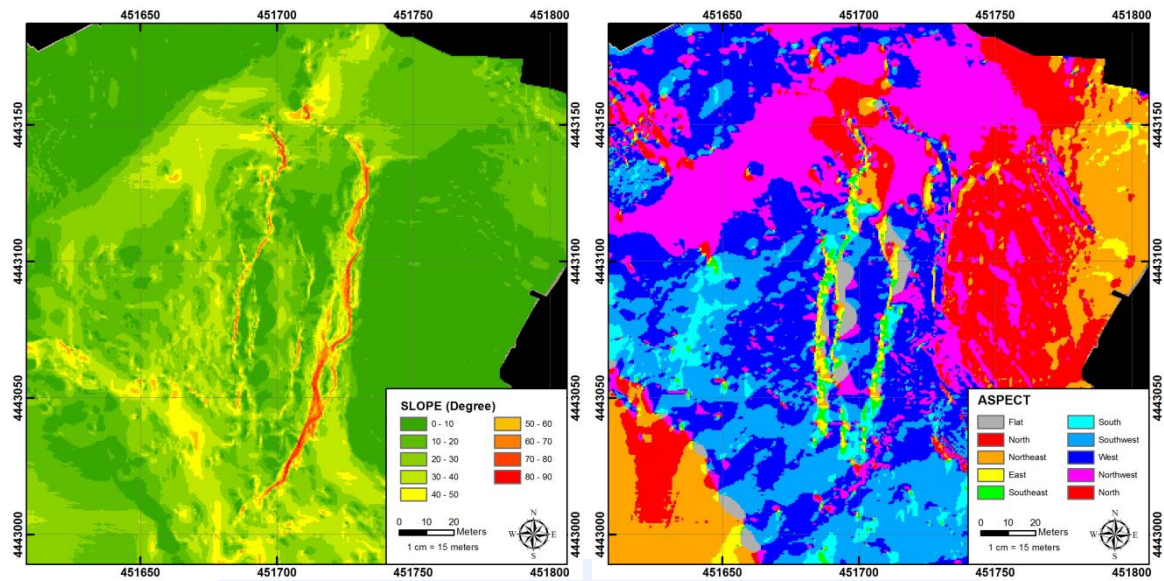


Figure 9. Left – Slope Map, Right – Aspect Map

To make comparison between the datas which were produced based on the collected and produced datas in different campaigns, a grid net, which has the same cell size and extend as the DTM, was built. The development of the landslide, the last situations of the natural objects in landslide area and displacements were monitored on this grid.



Figure 10. Landslide Progression, Left – Campaign 1, Middle –Campaign 2, Right – Campaign 3

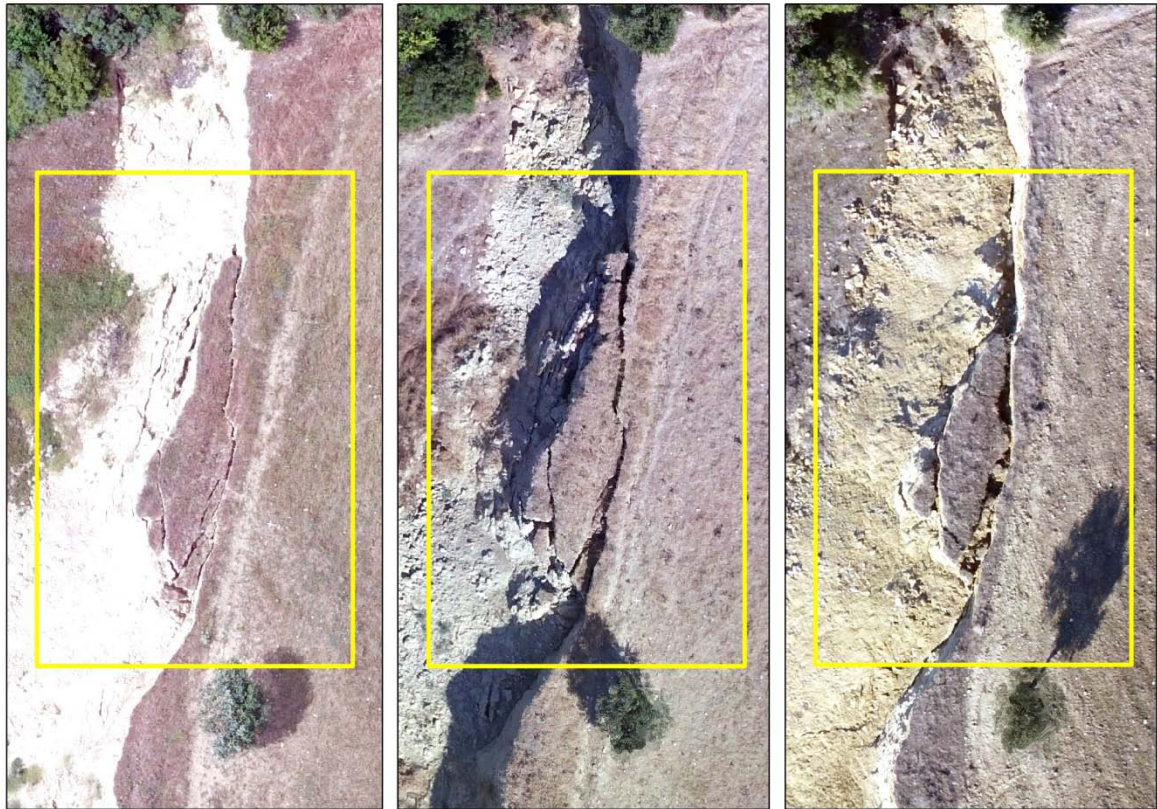


Figure 11. Landslide Progression, Left – Campaign 1, Middle – Campaign 2, Right – Campaign 3

CONCLUSION

Meteorological datas provided from the Meteorology Directorate in Çanakkale show us the amount of the precipitation between May 2016 - January 2017. The amount of the precipitation was high especially November 2016 and January 2017.

Table 1. The Amount of Precipitation per Month (kg/m²)

MONTH	PRECIPITATION in 2016 (kg/m ²)	PRECIPITATION 2017 (kg/m ²)
January	110.2	174.3
February	88.4	56.8
March	53.6	22.1
April	15.0	14.9
May	26.8	20.9
June	39.9	36.8
July	-	17.2
August	-	-
September	1.8	-
October	8.6	-
November	209.0	-
December	28.6	-

The ground in the study area is watery and the structure of the rocks composed of conglomerate-sandstone-mudstone intercalation observed in the study area consist of units that pass and do not pass ground and surface water. This, combined with the high slope factor, creates a suitable environment for the landslide development.

Based on the performed analyzes, detailed analysis of the orthomosaics, structural and environmental factors in the landslide area, it has been found that the landslide is continuously growing.

REFERENCES

Agisoft PhotoScan User Manual: Professional Edition, Version 1.2.

Fernandez T., Perez J. L., Cardenal F. J., Lopez A., Gomez J.M., Colomo C., Delgado J., Sanchez M., 2015, Use Of A Light UAV And Photogrammetric Techniques To Study The Evolution Of A Landslide, Jaen (Southern Spain), *The International Archives of the Photogrammetry, Remote Sensing and Spatial Information Sciences*, Volume XL-3/W3, 2015, 241-248.

Güreşçi, N. G., Seyrek, K., Sargın A. H., (2012). *Hydrological Applications With Geographic Information Systems*, Ministry of Forestry and Water Management, General Directorate of State Hydraulic Works, Department of Technology.

Niethammer U, James M. R., Travelletti J., Joswig M., 2010, UAV-based Remote Sensing of Landslides, *International Archives of Photogrammetry, Remote Sensing and Spatial Information Sciences*, Vol. XXXVIII, Part 5, 496-501.

Peterman V., 2015, Landslide Activity Monitoring With the Help Of The Unmanned Aerial Vehicle, *The International Archives of the Photogrammetry, Remote Sensing and Spatial Information Sciences*, Volume XL-1/W4, 2015, 215-218.

Trauth M. H., *MATLAB Recipes for Earth Sciences*, Springer, 2. Ed.

An Assessment of Disaster Management From The Viewpoint of Geographical Information System

Miraç N. Karakoç¹, Özcan Erdoğan²

¹Department of Disaster Medicine, Bezmialem Vakif University, Vatan Caddesi Campus, 34093, Turkey.
(e-mail: mnkarakoc@hotmail.com)

²Department of Disaster Management, Bezmialem Vakif Mart University, Vatan Caddesi Campus, 34093, Turkey. (e-mail: oordogan@bezmialem.edu.tr)

ABSTRACT

Geological structure of Turkey contains many natural disasters and the effects that they shall cause. Millions of our people face with the risk of being exposed to and suffering from the effects that natural disasters shall cause. The first step of responding to potential risks and making through them with minimum damages is to be prepared. All technological solutions must be considered to minimize the potential damages against the destructive effect of nature. Regardless of the natural disaster to occur, the preparations to be made shall always minimize any potential damage. Inter-regional differential land structures lead to the requirement of making a separate preliminary preparation for the risk born by each region. In the face of differences in lands structures and the risks that they pose, the contribution of the information to be saved the Geographical Information System in the disaster plans to be prepared for reasons such as risk of earthquake, landslide etc. is incontrovertible.

Emergency response plans against any potential disaster are primarily based on the time for arriving at disaster area for response. Faster people arrive at the disaster area, more important steps shall be taken for minimizing the losses of life and property. First of all, Geographical Information Systems must be studied for regions, then geographical systems must be created for the locally different areas, and information on these areas must be considered within the disaster planning. Using this information in the disaster management planning shall make serious contributions toward making quick and accurate decisions in the process of solution against the disaster occurred.

Risks to which Turkey is exposed regarding disasters require disaster management to be perfect. Presence of a specialized geographical information expert within emergency response units in the stage of Disaster management would be a substantially complementary solution for response to a disaster.

INTRODUCTION

Human life has become complicated due to the factors such as increased domestic population, complex and unplanned urbanization, etc. High-rise buildings and the settlements that are not suitable for the land structure and located at topographic risk zones comprise the factors being effective in increasing the possible losses in cases of disaster.

After each disaster suffered, it is understood that more efforts should be made in the action plans and for decreasing the damages from disaster.

The disasters and emergencies occurred lead to very severe financial losses in addition to the losses of life. Considering the investment in technology and man power as a financial burden and trying to keep up with the technology only with a time-dependent slow momentum lead to more damages. Time is the most precious thing while responding to a disaster or an emergency. Loss of life and property increases in direct proportion to the time elapses during the intervention. The interventions performed with missing data will cause unnecessary waste of time, money and man power.

The increase in the information types to be accessed has become one of the factors making it difficult to access the information correctly and timely. Having a good command of information and technology and using it properly for disaster recovery make up an important factor in minimizing any damages. Utilizing the conveniences brought by the technology at the right time and at an adequate level became inevitable in reaching a solution. Particularly when the conditions of the human life are considered, all available opportunities should be seized. Collecting the available data correctly, using the opportunities offered by the technology to assess them accurately as soon as possible, and the active role played by the specialists are all very important factors in reaching a conclusion by evaluating the processes together and correctly.

Regarding the disaster and emergency recovery, Geographic Information System is an important assistive technology used to measure, map and analyze the areas under the risk of disaster. In other words, GIS can be defined as an organization consisting of hardware, software and personnel components that fulfill the functions of collecting the geography-related graphical and non-graphical data from various resources as well as storing, processing, analyzing, managing and submitting them as a whole so as to meet the user needs (Çelik, et al., 1997). It makes serious contributions to disaster management planning in the phase of preparation against natural disaster. The fact that the natural disasters affect the geography shows how much all information and solutions to be obtained are needed. Minimizing all eventual losses can be possible by utilizing this technology properly and efficiently.

NATURAL DISASTERS AND THEIR EFFECTS

We can call the natural events that result in loss of life and property and are caused by natural phenomena briefly as Natural Disasters. Although human factor plays an important role in the loss of life and property caused by them, the main factor in their occurrence is the natural phenomena. Natural disasters are a reality of the earth, and the mankind must sustain their lives with these realities. Natural disasters emerge unexpectedly and affect the lives of all communities and living beings that live at the suffering area. They lead to the results that damage the general imperative means of life such as settlement, production, infrastructure, transportation and communication. While avoiding from the costs of the measures to be taken, the costs of the eventual results are heavier; however, adequate

measures cannot be taken in this regard. Natural phenomena are the inevitable behaviors of the earth. They are impossible to be prevented; however, mankind is able to prevent such events to turn into a disaster or minimize the damages as much as possible. Just taking steps that will not go beyond these natural phenomena and trying not to act superior to the nature are enough.

“The number of the deaths caused by natural disasters in 2015 was doubled (approx. 10 thousand people) compared to 2014. The number of deaths in this assessment was individually calculated by us through daily monitoring of all disasters around the world from the resources, and the following table was created (Table 1). As it is seen in the following table, the number of deaths caused by natural disasters was calculated to be 19,241 in 2015. (Ersoy, 2016).

Table 1. Deaths caused by natural disasters in year 2015

Disaster Type	Loss of Life
Earthquake	9640
Volcano	N.A.
Landslide	1147
Avalanche	341
Flood and Deluge	1751
Heavy Winter Conditions	38
Heavy Temperature Wave	4704>
Cyclone, Typhoon, Hurricane	884
Tornado	549>
Lightning	35
Dust Storm	8
Rip Current	~139
Meteor Fall	N.A.
<i>Total Loss of Life</i>	19,241

We can classify the natural disasters in three groups:

1. Terrestrial (Geological) Natural Disasters: Earthquake, landslide, rock fall, tsunami, volcanic eruption.
2. Atmospheric (Meteorological) Natural Disasters: Flood-overflow, excessive snow, avalanche, fog, frost, storm, lightning, drought.
3. Biological Natural Disasters: Epidemics, insect invasion.

The types of the natural disasters frequently occurring in our country are Geological and Meteorological natural disasters. Their rate of occurrence is as follows:

- Earthquake 61%,
- Flood 15%,
- Landslide 14%,
- Rock fall 5%,
- Fire 4%,
- Avalanche 1%.

THE CONCEPT OF DISASTER MANAGEMENT

Disaster Management is a very extensive management type that requires utilizing all institutions and organizations of the society as well as its resources for a common purpose so as to plan the activities to be carried out in the damage reduction, preparation, intervention and improvement phases of a disaster in order to prevent the disasters and decrease their damages (Kadioğlu and Özdamar 2006). As it is understood from the definition, disaster management should be conducted through the joint operation of many parameters.

It is not proper to limit the disaster management only to the interventions at the time of the disaster and taking steps in this direction to reduce the losses of life and property. Any preparation work to be made before disaster constitute the most important step in reducing the activities during and after the disaster and minimizing the loss of life and property. This means that disaster recovery starts not during the disaster, but before its occurrence; and it is the most effective recovery method.

Disaster Management is a management model that is achieved through the coordinated operation of 4 basic concepts (Figure 1). Disaster Management system is obtained by planning and managing each individual phase correctly and then, assessing them in a holistic manner. The correct structuring and management of each individual phase directly influence the whole and the result.

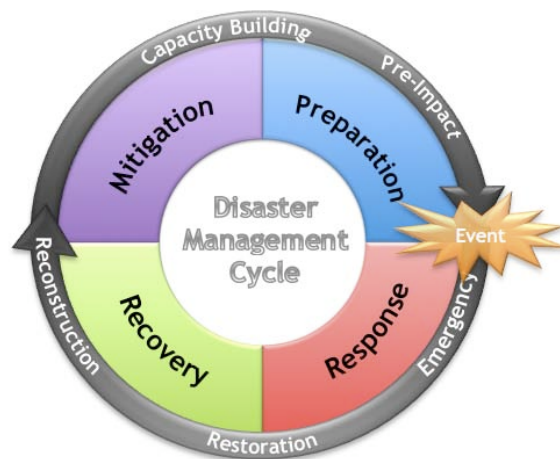


Figure 1. Disaster Management Cycle

1. Preparation

We can consider the preparation phase as the planning, training and implementation before and during the disaster. At this point, all risks are identified and set forth, and training and planning are ensured for those to be carried out during the disaster. All necessary planning is performed by taking measures against all hazards to arise from the disaster, and it is aimed to use the time in the most proper manner against all interventions. To that end, the personnel to be in charge during the disaster as well as their authority and responsibility are identified, organization chart is created and regular implementations and exercises are performed. All available technology, equipment and personnel should be availed in the preparation phase and their trainings should be followed up carefully. Those to be experienced during the disaster should be assessed by realizing various disaster scenarios, and all possible troubles should be identified earlier. Remember that each step from the bottom to the top unit of the management organization is very important. The most important step in minimizing the possible damages is that the organization reaches and responds to the tiniest point during the disaster.

2. Damage Reduction

Within the Disaster Management system, damage reduction should be assessed together with the subsequent preparation phase. The infrastructure to be created in the damage reduction phase constitutes the basis of the preparation part. The basic rule in damage reduction is to eliminate all risks that are possible to be prevented or to take measures to minimize them. All technological, scientific and technical R&D activities to be needed in such works should be evaluated. It is necessary to focus on technological solutions against unpredictable troubles and benefit from all available opportunities. The data to be obtained in a short time should be assessed again in a short time, thus they are ensured to make a contribution to planning and management. The legal regulations, organizational harmony and infrastructure works related to the damage reduction activities planned to be carried out as well as their implementation should also be remembered.

3. Intervention

Shortly, it means utilizing all personnel, equipment and resources to minimize the possible losses of life and property during a disaster. In the intervention phase, meeting all evacuation, food, drink and accommodation needs of the disaster victims should also be considered. The continuity of the communication and transportation networks should be ensured.

4. Improvement

In this phase, the basic purpose is to make efforts which restore the daily life after disaster to the condition before disaster. Providing temporary accommodation, meeting the needs, sustaining the education and health care systems and providing the disaster victims with

psychological rehabilitation are included in the important works in the improvement process. For the recovery to the normal life, making plans for the government institutions to return their normal activities and implementing them urgently are quite important in this phase.

DISASTER MANAGEMENT AND GEOGRAPHIC INFORMATION SYSTEM

Natural disaster management is a process which can be conducted correctly by combining many parameters. As the purpose is to protect the human life against the disasters and minimize the loss of life and property, the more accurate the available information and data are, the more correct the target to be achieved by the recovery is. When the phases before and after disaster are assessed, it is seen that the disaster management is a composition of works. It is the effort of the mankind to minimize the destructive effect of the nature, and this can be possible with a multi-phase disaster management system. It should be conducted under the joint responsibility of the institutions and organizations such as international organizations, states, local authorities, NGOs and universities. GIS is a correct technological infrastructure both as an international and as a local joint scientific field.

The term Geographic Information System embodies three words: Geography, information and system. Geography deals with all processes occurring on the earth and their properties. Information is in the heart of the geographic information system and mostly covers the storage and analysis of the data. Consequently, system is a structure which tells the network of relationships among the computer, data and human by asking questions and exploring new answers (Ludwig and Audet, 2000).

The most important property distinguishing the GIS from other database systems that it stores all data in relation to their space on the earth and enables to make a variety of spatial associations, i.e. several analyses among them. Thus, the GIS, which allows for various analyses and queries as well as enables to view all results and data in the form of a map associated with the area, constitutes the most important information system that can be used in the disaster-related researches and all works related to the disaster management (Demirci and Karakuyu 2004). As it is seen, the fact that the GIS has the meaning of a scientifically common language also makes the international information and data sharing easier. By assessing the data and information of the natural phenomena in a country, it is possible to evaluate the behaviors of those events in another country, to make risk analyses, to draw risk maps and to use them in all phases (Preparation, Damage Reduction, Intervention, Improvement) of disaster management.

We can group the contributions of the GIS to the Disaster Management under the following headings:

1. It Provides a Fast Information Flow:

The collaboration among the institutions is very important when creating the geographic database. Thus, the results obtained following the cooperation will be more clear and

available to use. In this regard, it is important that all parameters used should be standard. It is necessary for the institutions and organizations taking part and being in charge in the disaster management to access these data as well as share their works easily. The data being in the same format with the GIS are collected in a common base and stored in a manner where they can be used instantly by the organizations. Analyzes can be made by benefiting from these data at any time, and they can be instantly shared with other institutions and organizations.

2. It Provides Accurate and Effective Information Sharing:

As the GIS is technology-based, this increases the accuracy of the results such as maps, analyses, tables, etc. obtained from the data and information entered in the system and minimizes the margin of error. Likewise, the possibility to obtain the computer-based, instant printouts of these data saves a significant time in disaster management. Many different parameters are needed in disaster management and the ease of reaching them can positively affect the disaster recovery process.

3. Ease of Updating:

The change in the social conditions getting faster day by day is the most important reason for the requirement of updating the available data continuously. The first step for reaching the correct data and information is that the structural changes both in the urban and in the rural areas as well as the changes to the settlements are up to date. If the available data and information are missing or incorrect during the disaster, it may result in the chain of incorrect decisions and interventions in the management process. However, the operation of the GIS system on a common database with all institutions and organizations enables all users to receive the instant updates immediately.

4. It Provides Increased Efficiency:

In the disaster management, the human factor is one step forward no matter how advanced the technology you have. Assigning specialist people and directing these people with a correct planning ensure both to reach the correct data and to achieve it in a very short time. The fields of work and the distributions of tasks of the specialists are more clearly specified by using the GIS, thus everybody has adequate time to work in their fields of specialty. This prevents unnecessary labor loss and avoids the loss of time being the most important thing in disaster recovery. As the GIS system provides the time enabling to assign correct people at right places, this also increases the efficiency significantly.

CONCLUSION

Disaster recovery must be one of the primary national targets in our country which always faces with the disaster risk and was occasionally subject to severe losses of life and property. Due to its geographic location, the losses caused by all the natural disasters are

accordingly high. All technological opportunities should be used so as to struggle with such a great risk correctly and timely, and efforts should be made to develop them. Against these risks, Turkey should not only use the technology, but also develop this technology by adapting it to its conditions. Being an important technology in natural disaster recovery, GIS is a correct solution point for that purpose. Turkey should not only use the GIS, but also develop it against these risks. It should be developed according to our institutions, our communication system among the institutions and our natural disaster recovery system, opportunities enabling its use by the individuals should be provided and necessary trainings should be offered.

REFERENCES

- Çelik, M., Maraş, H. H., Ilgın, E.D., Üstün, 1997. M., Computer Aided Map Generation and Geographic Information Systems, *Geographical Information Systems Symposium*, 121-130.
- Demirci, A., Karakuyu, M. 2004. The Role of Geographic Information Technologies in Disaster Management, No. 12.
- Ersoy, Ş., 2016. Natural Disasters of the Year 2015 "World and Turkey". *Geological Engineering*. XII.
- Kadioğlu, M., Özdamar, E. (Editors) 2006. Basic Principles of Disaster Management. JICA Turkey Office Publications, No.1. *Disaster Management*. 10.
- Ludwig G., Audet R., 2000. GIS in Schools, ESRI Inc. GIS. 88.

ISGGG
2017



Biodiversity Mapping Using Landscape Complexity and Bird Species as Indicators by Remote Sensing and GIS

Onur Şatır^{*1}, Erşat Hüseyini¹ and Emel Baylan¹

¹Department of Landscape Architecture, Van Yuzuncu Yil University, 65090, Van, Turkey E-mail: osatir@yyu.edu.tr

ABSTRACT

Biodiversity of a region is directly depends on biotope variation and environmental comfort for the life. Biotope variation is caused landscape complexity and this situation is provided life condition for many various types of living organisms. In this research, biodiversity of the Bendimahi Basin that is located around Van Lake, was predicted using landscape complexity and bird species by a simple biodiversity index (SBI) in GIS environment. Research designed in three stages to be; Land use cover classification to define habitats in 30m spatial resolution, habitat definition of the birds using interactive open source spatial and literature based maps to weight the habitat priorities and fuzzification and weighting the all habitats in 300m spatial resolution. A biodiversity mapping model was developed using areal diversity of the biotope in a grid (%), priority degree of the biotope (defined from birds) and biotope variation in a grid (biotope count). Biodiversity map of the region was produced between 0 and 1 values in 300m spatial resolution. Mapping results showed that particularly wetland areas and diverse natural landscapes were richer than other places on biodiversity. Pure alpine areas was of the worst biodiversity degree in the region.

INTRODUCTION

Biodiversity is described shortly to be variety of the species in a Landscape (biome, basin, ecosystem etc.). Biodiversity is included three factors that are directly related each other as ecological variability (topography, land form, Land Use Cover etc.), climate variability, and interactions between species (Çetiner, 2010). Therefore, landscape complexity per area can be an indicator of the biodiversity. According to the Conception et al. (2008), Landscape complexity and biodiversity have a sigmoidal relationship in positive way, and if a landscape of an area has complex structure, biodiversity of the region can be higher than less complex landscapes (Figure 1).

^{*} Corresponding author

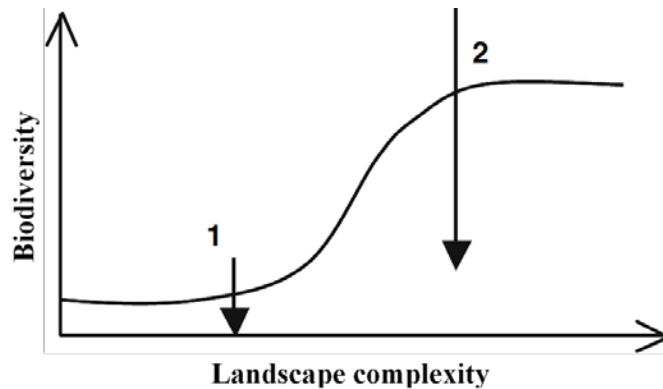


Figure 1. Biodiversity vs. Landscape complexity theoretical chart (“1” homogenous landscape, “2” complex landscape)

There are many biodiversity index directly related with living organisms in the world such as Red List Index (RLI) and Living Planet Index (LPI). Also satellite remote sensing techniques are allowed to monitor the landscape variation including biodiversity, vegetation and physical structure (Saatchi et al. 2008, Nagendra et al. 2010). A complex landscape is contains many different biotopes. However, all biotopes have various biodiversity capability. Only defining the landscape complexity is not enough to see the real biodiversity. For example, some landscape metrics like shannon’s landscape diversity index (SDI), is showed only habitat richness in a grid, but it is not identified species variability.

Nowadays, biotopes or habitats can be detected using appropriate remote sensing techniques easily (Şatır and Berberoğlu 2012). However defining biological capability of a biotope is needed in situ measurement or monitoring. In this point, bio indicators are commissioned. An effective bio indicator must be countable, easily obtainable, reliable, understandable and analytical (Gregory et al. 2003). In this point, birds are outshined in the literature because of their capability as a bio indicator. Variability of the birds in a region is indicated that there might be many food sources and habitats in a region, and this condition is provided living area for the life (plants, mammals etc.).

The purpose of the paper was to map the biodiversity considering habitat variability and bird species in GIS environment. In this extent, Land Use Cover (LUC) image of the study area was derived from a previous study using remotely sensed data.

STUDY AREA AND DATA

Bendimahi River Basin is a part of the Van Lake Basin that is located in Eastern Turkey. Total area is approximately 175194 ha. Typical terrestrial climate is dominant, and alpine climate and lands are stated in higher than 2200 m. Dominant LUC is grassland and rocky areas. Topography is variable and elevation range is 1645 – 4000 m (Figure 2).

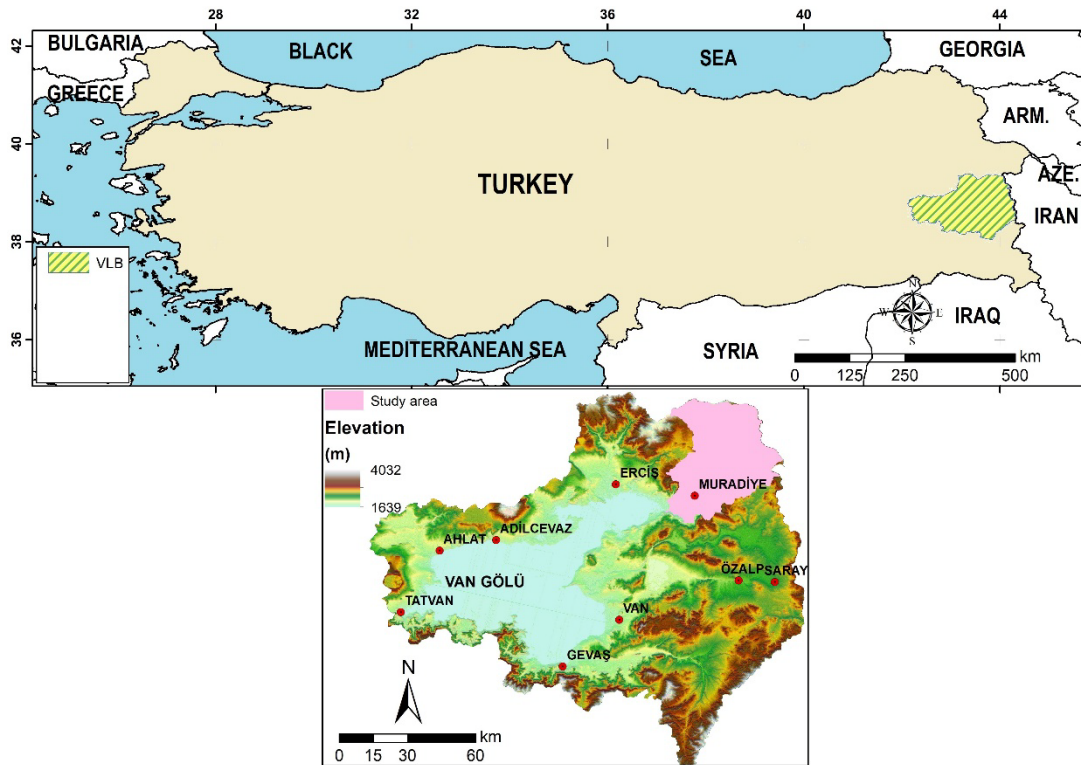


Figure 2. Location of the Bendimahi Basin (Study area)

The main dataset of the study was LUC map of the region that was produced from Multi-Temporal Landsat 8 dataset using object based classification approach. This LUC map was obtained from Şatır et al. (2017).

Another dataset was bird monitoring records. These records were integrated from Turkey's bird bank interactive database (TBB, 2015), Bird guide of Turkey (Eken and Çağlayan, 2005), Turkey and Europe Birds (Heinzel et al. 1995), and E-bird android application.

METHOD

In this study, a simple biodiversity index (SBI) was developed for the Bendimahi Basin. SBI are contained three main variables to be areal diversity of a habitat in a grid (A), priority of the habitat on biodiversity (P) and habitat variability in a grid (H). Simple model established as following:

$$SBI = A * P * H \quad (1)$$

Land use cover data was obtained from Şatır et al. (2017) with a very good accuracy ($\kappa = 0.92$) in 30m spatial resolution. LUC are included six main habitat as settlement, grassland, agriculture, bareground, rocky and mountain regions and wetland. All habitats were aggregated to 300X300m resolution and areal diversity of each habitat in per grid was calculated.

In second stage, total habitat counts in a grid was determined and priority of each habitat was derived from total bird species of habitats.

In this point we need to know the habitat priority and areal diversity of each habitat. In fuzzy form, habitat areal diversity in a grid was calculated as percent cover (%) (Figure 4).

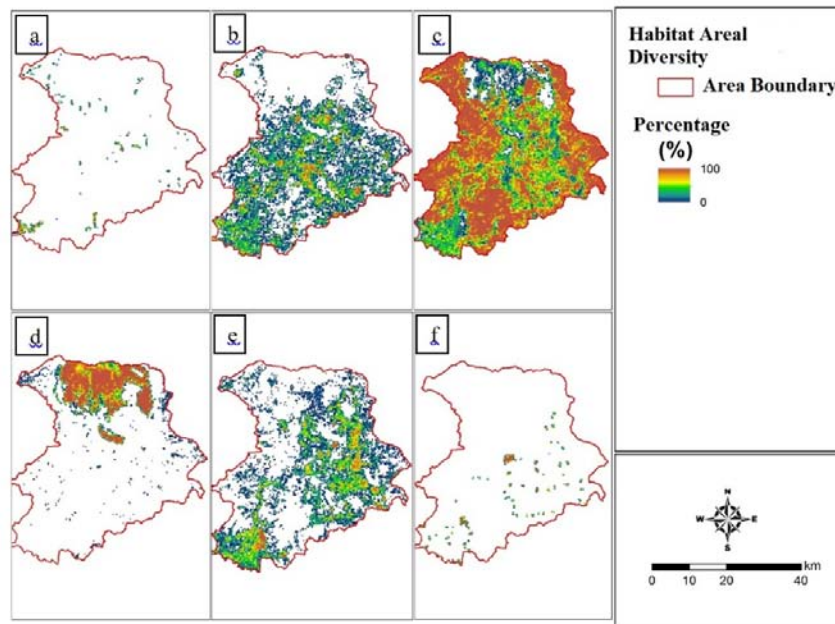


Figure 4. Areal diversity of the habitats (%) (a: wetlands, b: bareground, c: grassland, d: rock and mountainous areas, e: agriculture, f: settlement).

iii) Detecting the weights of habitats based on bird species; was the third stage. Bird species counts were obtained from various interactive and hardcopy sources for the each classified habitat. In total 147 bird species were integrated with the habitats that were existed in the study area (Table 2). Weights of the habitats were derived from bird species counts in each habitat.

Table 2. Distribution of the bird species in habitats and habitat weights for SBI.

Habitat name	Bird species count	Priority degree (weight)
Agriculture	38	0.16
Wetland	60	0.26
Grassland	24	0.11
Bareground	32	0.14
Rocky and mountainous landscape	40	0.17
Settlement	38	0.16
TOTAL	232*	1

* Some birds can be located more than one habitat so it is more than monitored bird's counts.

Model was created like equation (1), and SBI run using the user friendly raster model maker tools. SBI results are between 0 and 1, and “1” refers high biodiversity and “0” low biodiversity.

In the study area, the highest biodiversity was predicted around the wetlands and the fragmented sub-alpine regions. Whereas the lowest values were at the bareground and monotype grassland areas (Figure 5).

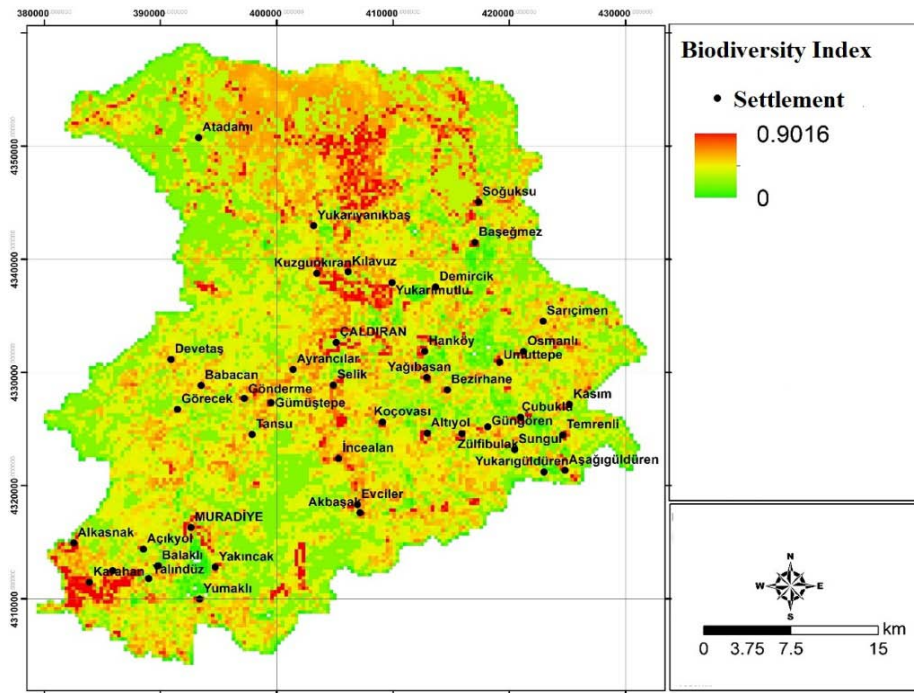


Figure 5. SBI values of the study area in 300m spatial resolution.

CONCLUSIONS

In conclusion; this research mentality was based on a positive relationship between landscape complexity and biodiversity. This was the preliminary results, and validation progress is still needed. For this study, field measurements of the bird species were used and according to the preliminary results, SBI has an impressive accuracy. Only LUC data and bird species according to the habitats were enough to create this simple model. Also this index was derived globally comparable result between 0 and 1. So that SBI values of the other regions can be used to identify the biodiversity difference, but same LUC classification scheme and same methodological procedure must be followed.

ACKNOWLEDGMENTS

We authors would like to thanks to the TUBİTAK project no: 214O392 for the financial and technical supports.

REFERENCES

- Bibby, C.J., 1999. Making the most of birds as environmental indicators. Oesrich: *Journal of African Ornithology*. 70(1): 81 – 88, DOI: 10.1080/00306525.1999.9639752.
- Concepcion, E.D., Diaz, M., Baquero, R.A., 2008. Effects of landscape complexity on the ecological effectiveness of agri-environmental schemes. *Landscape Ecology*, 23: 135 – 148.
- Çetiner, S., 2010. Biyoçeşitlilik nedir ne değildir? TarlaSera Dergisi, Kasım sayısı: 14 – 16.
- Eken, G., Çağlayan, E., 2005. *Türkiye Kuşları Rehberi*, Doğan Burda Dergi Yayıncılık ve Pzr. AŞ. İstanbul, p. 134.
- Gregory, R.D., Noble, D., Field, R., Marchant, J., Raven, M., Gibbpns, D.W., 2003. Using birds as indicators of biodiversity. *Ornis Hungarica*, 12 – 13: 11 – 24.
- Heinzel, H., Fitter, R., Parslow, J., 1995. *Türkiye ve Avrupa'nın Kuşları*, WWF, İstanbul. p. 384.
- Nagendra, H., Rocchini, D., Ghate, R., Sharma, B. and Pareeth, S. 2010. Assessing plant diversity in a dry tropical forest: comparing the utility of Landsat and IKONOS satellite images. *Remote Sensing*. 2 (2): 478 – 496.
- Saatchi, S., Buerman, H.T.S., Steege, S.M. and Smith, T.B., 2008. Modeling distribution of Amazonian tree species and diversity using remote sensing measurements. *Remote Sensing of Environment*, 112 (5): 2000 – 2017.
- Şatır, O. and Berberoğlu, S., 2012. Land use/cover classification techniques using optical remotely sensed data in landscape planning. In: Özyavuz, M. (Ed.), *Landscape Planning*. Intech, Croatia, pp. 21–54.
- Şatır, O., Alp, Ş., Bostan, P., Baylan, E., Yeler, O. and Aşur, F. 2017. *Van Gölü Havzası'ndaki Arazi Örtüsü ve Alan Kullanım Değişikliklerinin Yarım sırlık Süreçte Periyodik Olarak Belirlenmesi*. Proje Sonuç Raporu, Yüzüncü Yıl Üniversitesi Bilimsel Araştırma Projeleri Birimi, Münferit BAP projesi.
- TBB, 2015. Turkey Bird Bank, eKuşbank, interactive bird watching database for Van Region, <http://ebird.org/ebird/turkey/subnational1/TR-65?yr=all>, erişim tarihi; 15.09.2015.

Comparison of PCA and NLPCA Methods for Band Reduction of Hyperspectral Images

Hakan Kartal^{*1}, Ugur Alganci² and Elif Sertel^{1,2}

¹ Center for Satellite Communication and Remote Sensing (CSCRS), Istanbul Technical University, Ayazaga Campus, 34469, Turkey. e-mail: (hakan)@cscrs.itu.edu.tr

² Department of Geomatics Engineering, Istanbul Technical University, Ayazaga Campus, 34469, Turkey. e-mail: (alganci, sertele)@itu.edu.tr

ABSTRACT

In this study, two different dimension reduction methods namely Principle Component Analysis (PCA) and Non-Linear Principle Component Analysis (NLPCA) were applied to Indian pines hyperspectral test data acquired by AVIRIS airborne platform. The performance of each method was evaluated in terms of reconstruction errors and Support Vector Machine (SVM) classification accuracy. Results of the study demonstrated that hyperspectral data could be better represented with non-linear components compared to linear components. SVM classification of NLPCA using 4 components provided higher accuracy with %70, when compared to SVM classification of PCA which provided %68 accuracy using 4 components for the 16 LCLU classes defined in reference classification data. In addition, SVM classification accuracy tend to increase with increased number of components for both methods. Moreover, reconstruction of the data from NLPCA components resulted with less erroneous pixels than reconstruction from PCA components. Similarly, reconstruction efficiency increased with increased number of components for both methods. Lastly, the computation cost for NLPCA method is higher than the PCA method due to its complex structure thus, it is recommended to consider the processing performance and hardware requirements to apply the method in further studies.

INTRODUCTION

Hyperspectral sensors acquire images including hundreds of spectral bands with narrow wavelength ranges acquired from different wavelength portions of electromagnetic spectrum. Each pixel in image has a detailed and unique spectral signature that represents the spectral characteristics of the surface. This important property of hyperspectral images makes them to be appropriate data source for various application such as crop type identification, tree species determination, mineral identification, and thematically detailed land cover/use (LCLU) mapping (Melgani and Bruzzone, 2004; Chang, 2003; Chang 2007).

While high spectral resolution is important advantage for information extraction considering the valuable spectral information that could be obtained from different bands

for different land categories, high storage space and computing power requirements are regarded as the main disadvantages of hyperspectral data processing. Moreover, increase in the spectral bands brings out complexity in analysis performance. Hughes (1968) reported that classification accuracy decreases when the input information amount exceeds a certain threshold.

Therefore, dimension reduction for hyperspectral data is an important preliminary step before applying further image processing techniques in order to minimize these disadvantages and problems (Landgrebe, 2005). Dimension reduction methods aim to transform the high dimensional original data space to a lower dimension vector space with minimum loss of information.

Principal Component Analysis is a statistics based technique widely used in remote sensing applications that converts the data from high dimension vector space to low dimension vector space (Journaux et al., 2006). This method uses the eigenvalues and eigenvectors from the variance – covariance matrix of the data and defines linear shaped principal components that perpendicular to each other and oriented towards the regions where the variance is large (Abdi and Lynne, 2010). Non-Linear Principle Component Analysis (NLPCA) is a modified version of PCA that components are now defined with curves instead of linear lines. Components are calculated by use of auto associative neural networks in this approach (Kramer, 1991; Scholz, 2005).

The efficiency of PCA for representation of hyperspectral images in low dimension vector space has already been approved by recent studies (Lennon et al. 2002; Journaux et al., 2006). This study, additionally investigates the performance of NLPCA method in dimension reduction of hyperspectral images within comparison to PCA method. Comparisons were performed using reconstruction errors and classification accuracy values. Support Vector Machine (SVM) was selected as the classification method to investigate the classification accuracies of the data produced by NLPCA and PCA methods. SVM algorithm asserted to provide higher performance and accuracy in satellite image classification in several researches (Hermes et al., 1999; Melgani and Bruzzone, 2004).

In summary, this study investigates the efficiency of NLPCA and PCA methods in dimension reduction of hyperspectral images. Efficiency comparisons were performed by reconstruction errors and classification accuracy of the data. Processing time was also taken into account in order to discuss the efficiency – cost relationship for the methods.

DATA

The Indian Pines hyperspectral image data acquired by AVIRIS airborne platform in 1992 was used in this study. Data has a size of 145x145 pixels and consists of 220 spectral bands acquired between 400 – 2500 nanometer range of the electromagnetic spectrum. Image data is distributed with ground based reference data that consists of 16 classes (Baumgardner et al., 2015). Original hyperspectral data is presented in Figure 1 and class information of the reference data is given in Table 1.

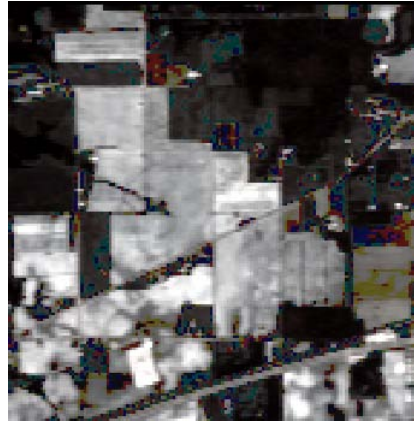


Figure 1. Original Indian Pines hyperspectral image.

Table 1. Class names and number of samples in the ground based reference data.

No	Class name (# of Samples)	No	Class name (# of Samples)
1	Alfalfa (46)	9	Oats (20)
2	Corn-notill (1428)	10	Soybean-notill (972)
3	Corn-mintill (830)	11	Soybean-mintill (2455)
4	Corn (237)	12	Soybean-clean (593)
5	Grass – pasture (483)	13	Wheat (205)
6	Grass-trees (730)	14	Woods (1265)
7	Grass-pasture-mowed (28)	15	Buildings-Grass-Trees-Drives (386)
8	Hay-windrowed (478)	16	Stone-Steel-Towers (93)

METHODOLOGY

Principal Component Analysis (PCA)

PCA method aims to express high dimensional data in a lower dimension space with minimum loss of information. Components can be derived from the eigenvalues and eigenvectors of variance-covariance matrix (Abdi and Williams, 2010). In other words, PCA can be explained as follows in order to relate it with NLPCA.

If Y is considered as the matrix defining the hyperspectral image data ($n \times m$, n : band amount in image data, m : total pixel amount in one band of the image), PCA factorizes the Y matrix in optimum way to form T ($n \times f$, f : component number) score matrix and E ($n \times m$) increment matrix. Process can be defined with following equation (Kramer, 1991):

$$Y = T P^T + E \quad (1)$$

Optimum factorization condition of Y matrix is satisfied when Euclid norm of E matrix is minimized. P ($m \times f$) matrix in Equation (1) represents the eigenvectors corresponding to biggest eigenvalue (f) in Y matrix (Kramer, 1991).

According to these information, PCA can be defined as a transformation function that transforms the original data space to f dimensional vector space. This transformation can be presented as Equation (2):

$$T = Y P \quad (2)$$

In Equation (2) Y represents a row in Y matrix while, T represents the coordinates of this row in f dimensional new vector space. In this form P represents the linear transformation coefficients (Kramer, 1991). Loosed information due to this transformation (E) can be regained with reconstruction process.

$$Y' = T P^T \quad (3)$$

$$E = Y - Y' \quad (4)$$

In Equation (3) and (4) Y' corresponds to coordinates of T component (gathered by transformation) in original data space Reconstruction error (E) can be derived by calculating the difference between Y and Y'. Euclid norm of the E will decrease with increment in component number (f).

Non – Linear Principal Component Analysis (NLPCA)

With a similar approach of PCA, NLPCA aims to transform the original data space to a lower dimension space. However, a non-linear transformation function is proposed in NLPCA method (Kramer, 1991) where PCA uses a linear function. Proposed transformation is described in Equation (5):

$$T = G(Y) \quad (5)$$

When Equation (5) is compared to Equation (2), G represents the coefficients of the non-linear transformation function which is represented by P (coefficients of linear transformation function) in Equation (2). Moreover, reconstruction function for PCA given in Equation (3) can be modified for NLPCA as presented in Equation (6):

$$Y' = H(T) \quad (6)$$

Where H represents the coefficients of reconstruction function and it consists of non-linear function coefficients likewise G.

The E matrix related to NLPCA transform is also calculated by use of Equation (4). The selection of G and H vector functions is performed according to the condition which minimizes the Euclidian norm of E matrix. Construction of the G and H functions can be performed by use of artificial neural networks that is defined in Equation (7):

$$V_k = \sum_{j=0}^{N_2} w_{ijk} \sigma(\sum_{i=1}^{N_1} w_{ij1} u_i + \theta_1) \quad (7)$$

Equation (7) defines the general form of forward feed artificial neural network which can be used to solve any form of non-linear equation with an acceptable approximation to desired accuracy (Cybenko,1989). N_1 defines the number of bands in original hyperspectral image while N_2 defines the number of intermediate layers that are composed of non-linear activation functions. w_{ijk} is the relative weight coefficient between i cell in k layer and j cell in $k+1$ layer.

Tangent sigmoid activation function was used in this study to obtain the non-linear components as outputs (Equation 8):

$$\sigma(x) = \frac{2}{1+e^{-2x}} - 1 \quad (8)$$

Tangent sigmoid function provides results between $[-1, 1]$ range which is suitable as an activation function in this study as normalized data inputs are used.

Support Vector Machine (SVM) Classification

SVM is a commonly used classification method in remote sensing applications (Alganci, Sertel, Ozdogan, & Ormeci, 2013; Melgani and Bruzzone, 2004; Huang, Davis, & Townshend, 2002). Main purpose of SVM is to transform the original data space into a bigger dimension space with use of kernel function and define the hyperplane which maximizes the distance between the samples collected from different land cover/use classes (Mountrakis, Im, and Ogole, 2011). In this research, reference class samples for 16 classes were selected over 3 data sets namely original hyperspectral image, PCA transformed images (2-3-4 components) and NLPCA transformed images (2-3-4 components). Then, SVM algorithm was applied on data sets, selecting the radial basis function as kernel.

RESULTS AND DISCUSSION

In this research, performances of PCA and NLPCA were evaluated by reconstruction and classification processes. Firstly, components derived from PCA and NLPCA transformations were reconstructed and compared with the original data in order to determine how efficiently transformed components preserve the original information. Reconstruction error can be calculated by counting the pixels that has different value from the original data and can be considered as a metric of data preservation success. Reconstruction errors were calculated for components (1-7) of PCA and NLPCA transformation and results were presented in Table 2.

Table 2. Reconstruction errors of PCA and NLPCA methods.

Number of Components	1	2	3	4	5	6	7
PCA	56019	14188	11527	10065	9932	9208	8563
NLPCA	37838	12585	10479	9994	9920	9912	9905

According to Table 2, NLPCA outperformed PCA in reconstruction process performed for the first 5 components by demonstrating lower reconstruction errors. While lower reconstruction error achieved for 5 components in NLPCA approach, it is clearly seen that reconstruction error values converged each other. Thus, it can be strongly asserted that NLPCA transform preserves the original information comparatively better than the PCA transform method for the first 5 components. While reconstruction errors keep improving in PCA approach, they are approximately same as the 5 components result in NLPCA approach for 6 and 7 components. This comparison show that NLPCA approach gives significantly better results when small number of components are used.

As a second comparison method; original image data, PCA transformed data (2-4 components) and NLPCA transformed data (2-4 components) were classified by use of SVM algorithm. Same sample set was used for whole classification process to prevent effects of sampling in results. Figure 2 presents the results of classification with reference class description.

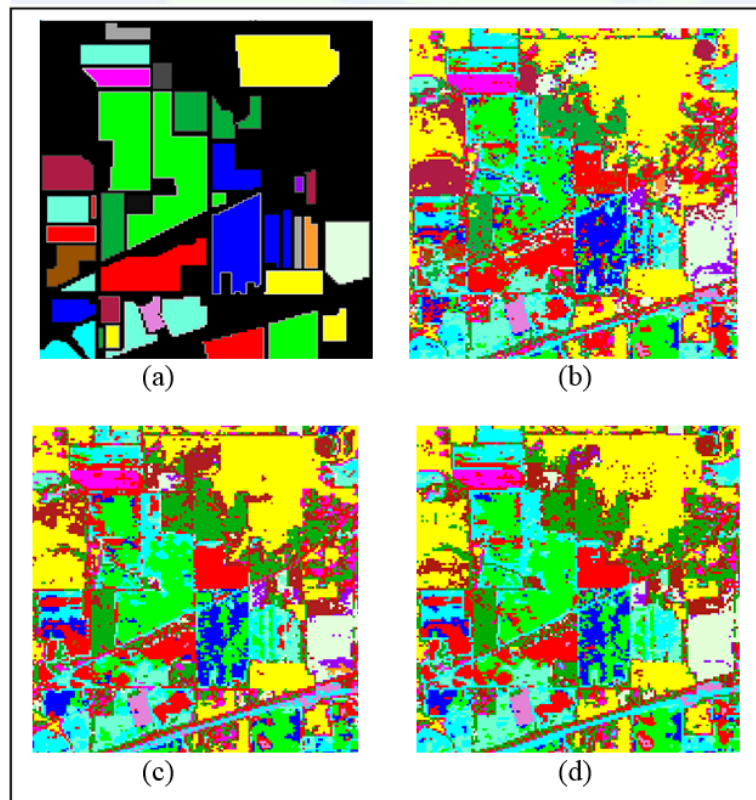


Figure 2. SVM classification results: reference classes (a), original image classification (b), 4 component NLPCA classification (c), 4 component PCA classification (d).

After classification process, accuracy assessment was performed for each classified image with same reference class data. Results of the accuracy assessment were given in Table 3. According to accuracy assessment, NLPCA again outperformed the PCA method with around 2-3% improvement and providing closer accuracy to original image classification results. Moreover, increasing the component number directly increases the accuracy of classification for both NLPCA and PCA methods.

Table 3. Overall accuracy and kappa results of SVM classification

Number of Components		2	3	4
PCA	Overall Acc.	58%	65%	68%
	Kappa	52%	60%	64%
NLPCA	Overall Acc.	61%	67%	70%
	Kappa	55%	63%	66%
Original Data	Overall Acc.	74%		
	Kappa	70%		

Another important factor to evaluate the efficiency of methods is the processing time. For this study, PCA transformation method required less time to produce components when compared to NLPCA method. PCA method required seconds to produce 4 components from original data while NLPCA needed hours to produce 4 components with a mid-range desktop computer. Time consumption of the NLPCA method is directly related to its iterative calculation steps. Reducing the iteration number reduced the time consumption but also reduced the classification accuracy.

CONCLUSIONS

Results of this study proved that, NLPCA method represents the original data better than PCA method. Dimension reduction with LPCA method resulted with better classification accuracies when compared to PCA method. Moreover, reconstruction from NLPCA transformed data was more successful than the PCA transformed data. However, NLPCA method consumed considerably much time to transform the data which is an important drawback of the method. Integration of deep learning techniques into NLPCA method is planned for further studies to overcome this drawback. A faster modified NLPCA method is anticipated by preparation of a training data set from several hyperspectral sensor data and deriving parameter weights from this training data set to be applied in transformation.

ACKNOWLEDGMENTS

The authors acknowledge D. Landgrebe, L. Biehl and M. Baumgardner from Purdue University for making hyperspectral data, which is used in this study, accessible.

REFERENCES

- Alganci, U., Sertel, E., Ozdogan, M., & Ormeci, C. (2013). Parcel-level identification of crop types using different classification algorithms and multi-resolution imagery in southeastern turkey. *Photogrammetric Engineering & Remote Sensing*, 79(11), 1053-1065.
- Abdi, H. and Williams, L.J., 2010. Principal component analysis. *Wiley interdisciplinary reviews: computational statistics*, 2(4), pp.433-459.
- Baumgardner, M.F., Biehl, L.L., Landgrebe, D.A. 2015. *220 Band AVIRIS Hyperspectral Image Data Set: June 12, 1992 Indian Pine Test Site 3*. Purdue University Research Repository. doi:10.4231/R7RX991C
- Melgani, F., and Bruzzone, L. 2004. Classification of hyperspectral remote sensing images with support vector machines. *IEEE Transactions on Geoscience and Remote Sensing* 42, 1778–1790.
- Chang, C.I., 2003. *Hyperspectral imaging: techniques for spectral detection and classification* (Vol. 1). Springer Science & Business Media.
- Chang, C.I. ed., 2007. *Hyperspectral data exploitation: theory and applications*. John Wiley & Sons.
- Cybenko, G., 1989. Approximation by superpositions of a sigmoidal function. *Mathematics of Control, Signals, and Systems (MCSS)*, 2(4), pp.303-314.
- Hermes, L., Friauff, D., Puzicha, J. and Buhmann, J.M., 1999. Support vector machines for land usage classification in Landsat TM imagery. In Geoscience and Remote Sensing Symposium, 1999. *IGARSS'99 Proceedings. IEEE 1999 International* (Vol. 1, pp. 348-350). *IEEE*.
- Huang, C., Davis, L. S., & Townshend, J. R. G. (2002). An assessment of support vector machines for land cover classification. *International Journal of remote sensing*, 23(4), 725-749.
- Hughes, G., 1968. On the mean accuracy of statistical pattern recognizers. *IEEE transactions on information theory*, 14(1), pp.55-63.
- Journaux, L., Tizon, X., Foucherot, I.N. and Gouton, P., 2006, June. Dimensionality reduction techniques: an operational comparison on multispectral satellite images using unsupervised clustering. In *Signal Processing Symposium, 2006. NORISIG 2006. Proceedings of the 7th Nordic* (pp. 242-245). *IEEE*.
- Kramer, M.A., 1991. Nonlinear principal component analysis using autoassociative neural networks. *AIChE journal*, 37(2), pp.233-243.

- Landgrebe, D.A., 2005. *Signal theory methods in multispectral remote sensing* (Vol. 29). John Wiley & Sons.
- Lennon, M., Mercier, G., Mouchot, M. and Hubert-Moy, L., 2001. Curvilinear component analysis for nonlinear dimensionality reduction of hyperspectral images. *Proc. SPIE Image and Signal Process. for Remote Sens. VII*, 4541, pp.157-169.
- Mountrakis, G., Im, J. and Ogole, C., 2011. Support vector machines in remote sensing: A review. *ISPRS Journal of Photogrammetry and Remote Sensing*, 66(3), pp.247-259.
- Scholz, M., Kaplan, F., Guy, C.L., Kopka, J. and Selbig, J., 2005. Non-linear PCA: a missing data approach. *Bioinformatics*, 21(20), pp.3887-3895.



Texture Based Classification of Hyperspectral Images with Support Vector Machines Classifier

Cigdem Serifoglu Yilmaz^{*1}, Esra Tunc Gormus² and Oguz Gungor³

¹Department of Geomatics, Karadeniz Technical University, 61080, Turkey. cigdemserifoglu.jdz@gmail.com

²Department of Geomatics, Karadeniz Technical University, 61080, Turkey. etuncgormus@gmail.com

³Department of Geomatics, Karadeniz Technical University, 61080, Turkey. oguzgungor@gmail.com

ABSTRACT

Hyperspectral images offer detailed colour information owing to their high spectral resolutions. These images are being used in many practical applications for better interpretation of the surface of the earth. One of the biggest disadvantages of this type of images is that they include repetitive information, which may be considered redundant for most classification applications. In such cases, it is more reasonable to reduce the data to minimize the computational load while increasing the classification accuracy. Another procedure that may be useful to increase the classification accuracy is the integration of complimentary data like texture information to the hyperspectral image to be classified. In this study, the Gabor and Grey Level Co-occurrence Matrix (GLCM) based texture information is exploited together with Principle Component Analysis (PCA). The performance of classification is evaluated with the Support Vector Machines (SVM) classifier to investigate whether or not the texture information is capable of increasing the classification accuracy. In this study texture information is used not only for increasing the classification accuracy, but also for analysing useful texture features according to their capability to classify different regions on hyperspectral images of different areas like urban, rural or suburban. In order to evaluate and compare the results with other studies, publicly available hyperspectral images are used in this study. Results show that texture information can improve classification performance over what is achieved by using spectral information or data itself.

INTRODUCTION

Land cover mapping is beneficial in many application areas. It facilitates the easier and comprehensive interpretation of the surface of the earth. Classification of remotely-sensed images is a common way of land cover mapping. Various image classification algorithms have been reported in the literature. The Artificial Neural Networks (ANN), Random Forest (RF), Rotation Forest (RTF) and Support Vector Machines (SVM) algorithms are

^{*} Corresponding Author

some of the state-of-the-art classifiers. Multispectral images are often used to create thematic maps owing to their advantages to enable the analysts to benefit from multiple wavelength intervals. However, classification of land cover features may not always be possible with multispectral images, especially in terrains with features having similar spectral characteristics. In such cases, it would be more reasonable to use hyperspectral images, which offer a huge number of spectral bands. This, of course, enables the easier separation of features with similar colours. The main disadvantage of hyperspectral images is that they mostly contain redundant information, which should be avoided for the sake of the ease of the processing. Principal Component Analysis (PCA) is a commonly-used data reduction method used in many remote sensing applications in order to reduce hyperspectral images to smaller-dimension ones that include majority of the image content. Lim et al. (2001), Radarmel and Shan (2002), Cheng et al. (2004), Fauvel et al. (2006), Du and Fowler (2007,2008) and Chen and Qian (2011) were just some of the researchers who used the PCA method on hyperspectral images. One other way to enhance the interpretability of the surface of the earth is to use texture information, which is helpful to identify objects or regions of interest in images (Haralick et al., 1973). In the literature, many studies utilized texture information to increase the interpretability of remotely-sensed images (Haralick et al., 1973; Wieszka et al., 1976; Permuter et al., 2006; Bau et al., 2010; Huo and Tang, 2011; Su et al., 2015; Mirzapour and Ghassemian, 2015; Imani and Ghassemian, 2016; Li et al., 2017).

The aim of this study is to increase the performance of the SVM classifier by means of the PCA transformation and texture features extracted from the Gabor and GLCM (Grey Level Co-occurrence Matrix). Detailed information about the used methodology and explanations of the used texture features are given in the following section.

TEXTURE EXTRACTION

The GLCM aims extracting texture information by means of the relationships among the grey values in an image (Tso and Mather, 2009; Akar, 2013). A GLCM contains the conditional-joint probabilities of all pairwise combinations of grey levels in an image (Clausi and Jernigan, 1998). Images with a number of homogenous areas include neighbouring pixel pairs having similar grey values. In such cases, similar grey values seem as relatively greater values gathered around the diagonals (Tso and Mather, 2009; Akar, 2013). Haralick et al. (1973) proposed a set of 14 textural features that can be derived from a GLCM. These features contain information regarding such textural characteristics as homogeneity, contrast, grey level linear dependencies, complexity of the image etc (Haralick et al., 1973). In this study, 8 of the textural features are used, which were given by Haralick et al. (1973) as;

- Mean: The local mean within the processing window.

- Variance:
$$\sum_{i=1}^{N_g} \sum_{j=1}^{N_g} (i - u)^2 p(i, j) \quad (1)$$

- Homogeneity:
$$\sum_{i=1}^{N_g} \sum_{j=1}^{N_g} \frac{1}{1 + (i - j)^2} p(i, j) \quad (2)$$

- Contrast:
$$\sum_{n=0}^{N_g-1} n^2 \left\{ \sum_{i=1}^{N_g} \sum_{j=1}^{N_g} p(i, j) \right\} \quad (3)$$

- Dissimilarity:
$$\sum_{n=0}^{N_g-1} n \left\{ \sum_{i=1}^{N_g} \sum_{j=1}^{N_g} p(i, j)^2 \right\} \quad (4)$$

- Entropy:
$$- \sum_{i=0}^{N_g-1} \sum_{j=0}^{N_g-1} p(i, j) \log(p(i, j)) \quad (5)$$

- Second Moment:
$$\sum_{i=0}^{N_g-1} \sum_{j=0}^{N_g-1} \{p(i, j)\}^2 \quad (6)$$

- Correlation:
$$\frac{\sum_{i=0}^{N_g-1} \sum_{j=0}^{N_g-1} (i, j) p(i, j) - \mu_x \mu_y}{\sigma_x \sigma_y} \quad (7)$$

where, $p(i, j)$ is the $(i, j)^{\text{th}}$ entry in the GLCM and N_g is the number of distinct grey levels in the quantized image (Haralick et al., 1973). μ_x and μ_y are the mean of the p_x , whereas σ_x and σ_y are the standard deviations of the p_y . Note that p_x is the marginal-probability matrix derived by summing the rows of the $p(i, j)$.

The Gabor filter is another widely-used texture extraction method. The aim of the Gabor filter is to extract edge information in a specific direction and scale. Mirzapour and Ghassemian (2015) stated that scale-direction filters $h_{s,d}(x, y)$ are obtained by using

$$h_{s,d}(x, y) = a^{-s} \phi(X, Y) \quad (8)$$

from a mother wavelet,

$$\phi(x, y) = \frac{1}{2\pi\sigma_x\sigma_y} \exp \left\{ -\frac{1}{2} \left(\frac{x^2}{\sigma_x^2} + \frac{y^2}{\sigma_y^2} \right) + 2\pi j U_h x \right\} \quad (9)$$

in which,

$$a = \left(\frac{U_h}{U_1} \right)^{\frac{1}{N_s-1}}$$

$$\sigma_x = \frac{(a+1)\sqrt{\ln 4}}{2\pi(a-1)U_h}$$

$$\sigma_y = \frac{\sqrt{\ln 4 - \left(\frac{\ln 4}{2\pi U_h \sigma_x} \right)^2}}{2\pi \tan\left(\frac{\pi}{2N_d}\right) \left[U_h - \frac{\ln 4}{U_h(2\pi \sigma_x)^2} \right]} \quad (10)$$

$$X = a^{-s} \left[(x - x_0) \cos\left(\frac{\pi d}{N_d}\right) + (y - y_0) \sin\left(\frac{\pi d}{N_d}\right) \right]$$

$$Y = a^{-s} \left[-(x - x_0) \sin\left(\frac{\pi d}{N_d}\right) + (y - y_0) \cos\left(\frac{\pi d}{N_d}\right) \right]$$

where, $s \in \{1, \dots, N_s\}$ and $d \in \{1, \dots, N_d\}$ are the scales and directions of wavelets, respectively. x_0 and y_0 define the centre coordinates of the filters. U_1 and U_h are the minimum and maximum centre frequency of filters, respectively (Mirzapour and Ghassemian, 2015).

Scale-direction filters are applied to images by employing sliding windows. Application of Gabor filters to a single-band image results in a feature vector with $N_d \times N_s$ elements for each pixel (Mirzapour and Ghassemian, 2015). Mirzapour and Ghassemian (2013,2015) stated that 4 directions and 6 scales are appropriate for most cases.

IMAGE CLASSIFICATION

The SVM algorithm, which is based on the statistical learning theory (Vapnik, 1995), is used in this study to classify the images. The SVM classifier aims to find the optimum hyperplane that maximizes the margin between classes (Tso and Mather, 2009). In cases where classes are linearly separable, the algorithm generates two parallel planes maximizing the margin between classes and the optimum hyperplane is placed in the middle of these parallel planes (Vapnik, 1995). However, in most cases, classes are not separated linearly. In such cases, the separability between classes is increased by projecting the data onto a higher-dimensional space by means of non-linear functions such as linear kernel function, polynomial function, radial basis function, sigmoid function etc. In this study, the radial basis function (RBF) is used with the SVM classifier. The RBF is given as;

$$K(x_i, x_j) = \exp(-g\|x_i - y_i\|^2) \quad (11)$$

where, g is the gamma term (ENVI Field Guide) and $\{x_i, y_i\}$ is the training set consisting of k training samples (x is an N -dimensional space and y is the classes' labels). Further information about the SVM classifier can be found in Vapnik (1995), Sherrod (2003), Oommen et al., (2008), Tso and Mather (2009), and Kavzoglu and Colkesen (2009).

EXPERIMENTAL DATA

In this study, the Indian Pine hyperspectral data is used, which was acquired by the AVIRIS sensor in 1992. The data has 220 spectral bands (145 x 145 pixels) with a spatial resolution of 20 m. The study area includes a mixture of forest and agricultural features. The dataset includes 20 water absorption bands (bands 104-108, 150-163 and 220), which should be discarded from the dataset to avoid their possible adverse effects to classification result. Visual examination of all bands of the dataset revealed that 37 of the bands (1, 57, 61, 75, 80, 89-91, 103-107, 143-147, 151, 152, 188-200) contained a huge amount of noise. These noisy bands were discarded from the dataset. As a result, 167 bands were decided to use. A false-colour image and ground truth map are shown in Figure 1. The study area consists of 16 land cover classes, which are given in Table 1. Note that the classes with few samples were ignored and only the classes shown in bold were used in this study.



Figure 1. False-colour image (left) and ground truth map (right) of the study area.

Table 1. Land cover classes with their number of samples.

Class	Samples	Class	Samples
Alfalfa	46	Oats	20
Corn-no till	1428	Soybean-no till	972
Corn-min till	830	Soybean-min till	2455
Corn	237	Soybean-clean	593
Grass-pasture	483	Wheat	205
Grass-trees	730	Woods	1265
Grass-pasture-mowed	28	Buildings-Grass-Tress-Drives	386
Hay-windowed	478	Stone-Steel-Towers	93

METHODOLOGY

In order to reduce the computational load, a PCA were performed to the 167-band dataset (HS=Hyperspectral Image). The PCA transformation enables the dataset to transform into another space in which the correlations between the transformed bands are minimized. The first principal component of the transformed image contains most of the total variance, which means that it may represent most of the details in the dataset. Hence, the GLCM and Gabor texture extraction procedures were conducted on the first principal component. Different combinations of the 167-band dataset, and GLCM and Gabor texture features were classified with the SVM algorithm to see if these texture extraction algorithms were able to increase the performance of the SVM classifier. Note that 150 training samples were used for each class to train the SVM classifier and the optimum parameters ($C=2^{15}$ and $\gamma=2^{-2}$) of the SVM were found with a two-fold cross-validation technique. The ENVI software was used to perform the GLCM texture extraction. The software uses eight features as the mean, variance, homogeneity, contrast, dissimilarity, entropy, second moment and correlation, which were aforementioned before. The software computes the GLCM features with three parameters; *processing window*, which was set to 11x11; *co-occurrence shift*, which was set to [0 1]; and *grey scale quantization levels*, which was set to 64. The Gabor filter was performed by using the MATLAB script developed by Haghighat et al., (2015). The script uses six parameters to operate; d_1 and d_2 , which are the factor of downsampling along rows and columns, were set to 4; u , which is the total number of scales, was set to 6; v , which is the number of orientations, was set to 4; m and n , which define the size of the image, were set to 145 and 145, respectively.

RESULTS AND DISCUSSION

Table 2 shows the classification results of different combinations. As seen in the table, the SVM algorithm classified the HS dataset with an accuracy of 77.45%. Classification of eight GLCM features gave an accuracy of 41.24%. As seen in the table, the classification of 24 Gabor features yielded an accuracy of 82.97%, which was higher than that of the HS data. Adding the GLCM features to the Gabor features did not increase the accuracy significantly. The classification of the combination of the HS data and GLCM features yielded almost the same accuracy as HS data itself. Compared to the accuracy of the HS, a significant accuracy increase was obtained when the HS, GLCM and Gabor features were combined. This combination resulted in an accuracy of 89.56%. The maximum classification accuracy (92.3%) was obtained by the classification of the combination of HS and Gabor features. As can be seen, the accuracy increase was most likely due to the addition of the Gabor features. The classified images are given in Figure 2.

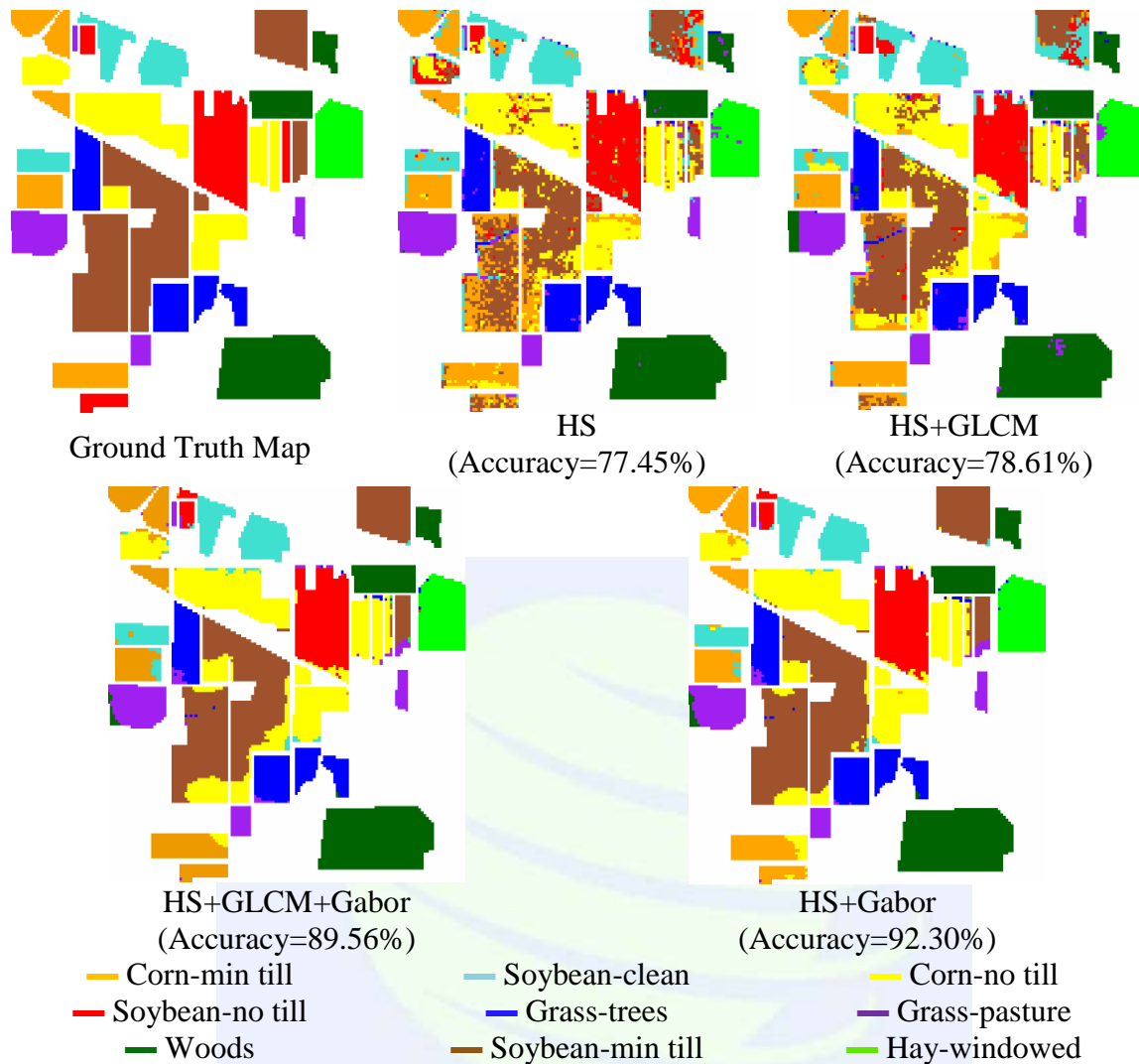


Figure 2. Ground truth map and classified images.

Table 2. Classification accuracies of different combinations.

Method	No. Features	Accuracy (%)
HS	167	77.45
GLCM	8	41.24
Gabor	24	82.97
GLCM+Gabor	32	79.67
HS+GLCM	175	78.61
HS+GLCM+Gabor	199	89.56
HS+Gabor	191	92.30

CONCLUSIONS

In this study, it is aimed to increase the performance of the SVM classifier by combining the HS data with texture information extracted from the GLCM and Gabor features. The results showed that adding the GLCM and Gabor features to the HS data increased the SVM accuracy by 15.6%, whereas combining the HS data with just Gabor features yielded an accuracy increase of 19.17%, which was the greatest increase achieved in this study. The parameters used by the SVM classifier have a direct effect on the classification

accuracy. Hence, much care should be taken to find optimum parameters for the SVM classifier. Future studies will focus on increasing the overall classification accuracy with less number of features.

ACKNOWLEDGMENTS

This study has been supported with the funding provided by Karadeniz Technical University BAP03 (Scientific Research Project) FBB-2017-5688 project under the title of 'Investigating the Effects of Dimensionality Techniques to the Classification of Hyperspectral Images'.

REFERENCES

- Akar, Ö., 2013. *Rastgele Orman Sınıflandırıcısına Doku Özellikleri Entegre Edilerek Benzer Spektral Özellikteki Tarımsal Ürünlerin Sınıflandırılması*, Doktora tezi, Karadeniz Teknik Üniversitesi, Fen Bilimleri Enstitüsü.
- Bau, T.C., Sarkar, S. and Healey, G., 2010. Hyperspectral region classification using a three-dimensional Gabor filterbank. *IEEE Transactions on Geoscience and Remote Sensing* 48 (9): 3457-3464.
- Chen, G. and Qian, S.E., 2011. Denoising of hyperspectral imagery using principal component analysis and wavelet shrinkage. *IEEE Transactions on Geoscience and Remote Sensing* 49 (3): 973-980.
- Cheng, X., Chen, Y.R., Tao, Y., Wang, C.Y., Kim, M.S. and Lefcourt, A.M., 2004. A novel integrated PCA and FLD method on hyperspectral image feature extraction for cucumber chilling damage inspection. *Transactions of the ASAE (American Society of Agricultural Engineers)* 47 (4): 1313.
- Clausi, D.A. and Jernigan, M.E., 1998. A fast method to determine co-occurrence texture features. *IEEE Transactions on Geoscience and Remote Sensing* 36 (1): 298-300.
- Du, Q. and Fowler, J.E., 2007. Hyperspectral image compression using JPEG2000 and principal component analysis. *IEEE Geoscience and Remote Sensing Letters* 4 (2): 201-205.
- Du, Q. and Fowler, J.E., 2008. Low-complexity principal component analysis for hyperspectral image compression. *The International Journal of High Performance Computing Applications* 22 (4): 438-448.
- ENVI Field Guide
- Fauvel, M., Chanussot, J. and Benediktsson, J.A., 2006. Kernel principal component analysis for feature reduction in hyperspectral images analysis. In *Signal Processing Symposium, NORSIG 2006. Proceedings of the 7th Nordic*, pp. 238-241.

- Haghighat, M., Zonouz, S. and Abdel-Mottaleb, M., 2015. CloudID: Trustworthy cloud-based and cross-enterprise biometric identification. *Expert Systems with Applications* 42 (21): 7905-7916.
- Haralick, R.M., Shanmugam, K. and Dinstein, I.H., 1973. Textural features for image classification. *IEEE Transactions on Systems, Man, and Cybernetics* SMC-3 (6): pp. 610-621.
- Huo, L.Z. and Tang, P., 2011. Spectral and spatial classification of hyperspectral data using SVMs and Gabor textures. In *Geoscience and Remote Sensing Symposium (IGARSS), 2011 IEEE International*, pp. 1708-1711.
- Imani, M. and Ghassemian, H., 2016. GLCM, Gabor, and morphology profiles fusion for hyperspectral image classification. In *Electrical Engineering (ICEE), 24th Iranian Conference on*, pp. 460-465.
- Kavzoglu, T. and Colkesen, I., 2009. A kernel functions analysis for support vector machines for land cover classification. *International Journal of Applied Earth Observation and Geoinformation* 11 (5): 352-359.
- Li, Q., Huang, X., Wen, D. and Liu, H., 2017. Integrating Multiple Textural Features for Remote Sensing Image Change Detection. *Photogrammetric Engineering & Remote Sensing* 83 (2): 109-121.
- Lim, S., Sohn, K.H. and Lee, C., 2001. Principal component analysis for compression of hyperspectral images. In *Geoscience and Remote Sensing Symposium 2001 (IGARSS'01)*, Vol. 1, pp. 97-99.
- Mirzapour, F. and Ghassemian, H., 2013. Using GLCM and Gabor Filters for Classification of PAN Images. *21st Iranian Conference on Electrical Engineering (ICEE)*, 14–16 May 2013.
- Mirzapour, F. and Ghassemian, H., 2015. Improving hyperspectral image classification by combining spectral, texture, and shape features. *International Journal of Remote Sensing* 36 (4): 1070-1096.
- Oommen, T., Misra, D., Twarakavi, N.K., Prakash, A., Sahoo, B. and Bandopadhyay, S., 2008. An objective analysis of support vector machine based classification for remote sensing. *Mathematical Geosciences* 40 (4): 409-424.
- Permuter, H., Francos, J. and Jermyn, I., 2006. A study of Gaussian mixture models of color and texture features for image classification and segmentation. *Pattern Recognition* 39 (4): 695-706.
- Rodarmel, C. and Shan, J., 2002. Principal component analysis for hyperspectral image classification. *Surveying and Land Information Science* 62 (2): 115.
- Sherrod, P.H., 2003. *Classification and regression trees and support vector machines for predictive modeling and forecasting*. DTREG program manual.

- Su, H., Sheng, Y., Du, P., Chen, C. and Liu, K., 2015. Hyperspectral image classification based on volumetric texture and dimensionality reduction. *Frontiers of Earth Science* 9 (2): 225-236.
- Tso, A. and Mather, P.M., 2009. *Classification Methods for Remotely Sensed Data*, Second Edition, ISBN: 978-1-4200-9072-7.
- Vapnik, V.N., 1995. *The Nature of Statistical Learning Theory*.
- Weszka, J.S., Dyer, C.R. and Rosenfeld, A., 1976. A comparative study of texture measures for terrain classification. *IEEE Transactions on Systems, Man, and Cybernetics* 4: 269-285.



Assessment of Transparency and Water Quality in the Bay of Bou-Ismaïl from Landsat Satellite Imagery

**Boufeniza Redouane Larbi¹, Bachari Houma Fouzia¹, Alsahli Mohammad², Bachari
Nour el Islam³, Toumi Yasser³, Benyoub Walid³, Benm'barek Ghania¹**

¹ National School of marine Science and coastal Management, university Campus Dely Brahim, Bois des cars, PB 19,16320, Algiers, Algeria.

²Geography Department, Kuwait University, POB 68168, Kaifan71962, Kuwait.

³University of sciences and technology Houari Boumedienne, Department of biology, BP 32 El Alia 16111 Bab Ezzouar Algiers.

ABSTRACT

The aim of this research was to develop empirical models to estimate and quantify variability of water transparency in Bou-Ismaïl Bay, using satellite bands for Landsat sensors. are followed using Landsat 5 Thematic Mapper (TM) scenes, Landsat 7 Enhanced thematic Mapper (ETM), and Landsat 8 Operational Land Imager (OLI). For this we persisted over synoptic and seasonal time scales over a 32-year time-series from 1984 to 2016 during the different months, to improve our understanding of coastal climate processes.

The process describes interannual variability, of secchi disc depth (SDD) , chlorophyll a (CHL a) and suspended particulate matter (SPM) the results showed that the good performance with R B G , and panchromatic bands , and the correlative analysis have a consistent and optimal shape for most processed images showing more or less reliable results.

INTRODUCTION

Various human activities such as hydrological transformations and terrestrial nutrient loading have had significant impacts on ecosystem health of water (Pereira et al., 2009; Roselli et al., 2009). Water clarity (or transparency), as the color of seawater and water quality are determined by the presence of materials in water such as chlorophyll a, And the suspended particulate matter. It is a common measure of water quality (Carlson, 1977).

Detection of changes in transparency of the water column is essential for understanding the responses of marine organisms to the availability of light. Water transparency models determine long-term geographic and depth distributions, while acute reductions cause

short-term stress, potentially mortality, and may increase the vulnerability of organisms to other environmental factors.

Several studies have shown that monitoring water clarity, which is well correlated with water quality, is a good way to manage water quality, however, it is impossible to monitor the clarity of water in a large area for long periods because of the expense and the time required (Nelson et al., 2002).

The use of satellite remote sensing is a cost-effective way of collecting the information needed for regional water quality assessments.

The objective was to establish multi-temporal analysis and use of remote sensing technology, in particular the integration of in situ measurements with remote sensing data (Al-Yamani, et al., 2004; Nezhlin, et al., 2007).

The goal of this study preliminarily tried estimating the water clarity, Chlorophyll-a and Suspended particulate matters in Bou - Ismail bay using Landsat series, also:

- To investigate the relationship between in situ measurements and reflectance or luminance variables of the bands;

STUDY AREA

Our study area corresponds to the Bay of Bou Ismail, which extends from the meridian of Mount Chenoua to the West ($2^{\circ} 25' E$ and $36^{\circ} 38' N$) to that of the Ras Acrata in the East ($2^{\circ} 55' E$ and $36^{\circ} 48' N$), the Mitidja plain to the south and the Mediterranean Sea to the north. It is located in the Wilaya of Tipaza, 30 km west of Algiers. The bay of Bou Ismail has an area of 509 km², with a coastline of more than 48 km. It is oriented from South East to North East (Figure 1).

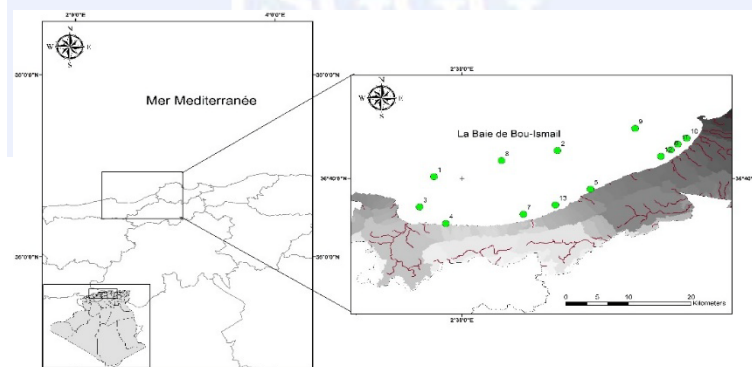


Figure 1. Satellite image of Bou-Ismaïl Bay.

DATA AND METHODS

Data processing in this study is divided into several stages and the process is shown in (Figure 2).

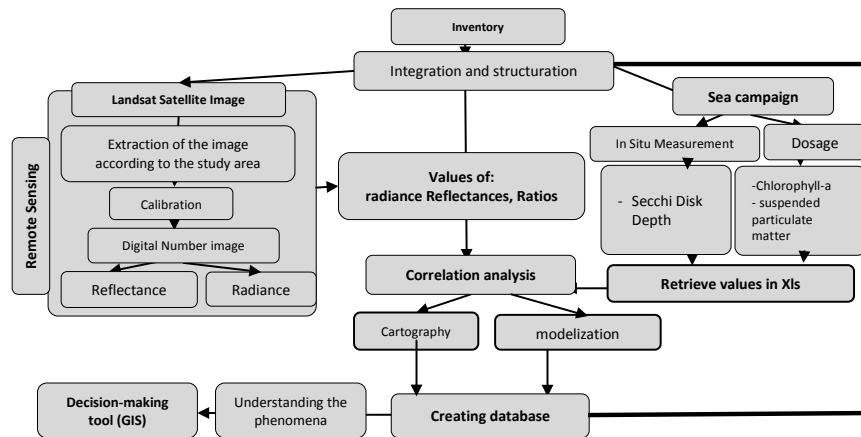


Figure 2. Structure and methodology of work

In situ measurements

Four sampling campaigns were conducted during periods of March, April and May 2016, includes 13 stations across the bay in a manner to cover the entire bay and especially the most affected by pollution zones and human activity. The choice of the sampling period was in the late summer when the water mass of the components are relatively constant. The samples are taken according to standardized techniques, using a shaped bottle “Niskin” type of five liters. The samples are stored at 4 ° C in coolers filled with cold accumulators and then they are sent to the laboratory to carry out the physicochemical analysis.

Secchi disc was used to measuring depth transparency. The analyzes are carried out using the methods described by (Rodier, et al., 2009): Suspended particulate matter (SPM) (membrane filtration), Chlorophyll-a (spectrophotometer).

Remote sensing data

The images download correspond to the various sensors of the Landsat series. An archive of 68 Landsat (TM, ETM, and OLI) daytime images covering the central coast of Bou-Ismaïl Bay was acquired, spanning the time period from May 27, 1984 to May 19, 1996. All images were visually inspected for cloud and fog, however, arrangement of the images by year-month-day (Table 1) and taking a climatological approach to their analysis allows dominant and/or recurrent features within an annual cycle to be characterized. All images treated are devoid of clouds in the marine part of the study area.

The images selected for the assessment of water quality in Bou Ismaïl Bay were high quality cloudless images during the period (Table 1).

Table 1. Date and sensors of Images processed

Date of Images processed	Sensors	Date of Images processed	Sensors	Date of Images processed	Sensors
27/05/1984	TM	18/11/2004	ETM	04/08/2012	ETM
16/09/1984	TM	04/12/2004	ETM	02/10/2013	OLI
27/03/1985	TM	05/01/2005	ETM	03/11/2013	OLI
12/04/1985	TM	21/01/2005	ETM	06/01/2014	OLI
01/03/1987	TM	09/02/2006	ETM	23/02/2014	OLI
24/08/1987	TM	19/07/2006	ETM	11/03/2014	OLI
09/09/1987	TM	11/01/2007	ETM	01/07/2014	OLI
20/11/1990	TM	28/02/2007	ETM	24/12/2014	OLI
29/07/1995	TM	20/06/2007	ETM	09/01/2015	OLI
14/08/1995	TM	03/04/2008	ETM	21/08/2015	OLI
15/03/1998	TM	09/08/2008	ETM	29/08/2015	OLI
05/11/1999	ETM	21/03/2009	ETM	22/09/2015	OLI
25/02/2000	ETM	08/05/2009	ETM	16/10/2015	OLI
06/10/2000	ETM	24/05/2009	ETM	09/11/2015	OLI
11/02/2001	ETM	13/09/2009	ETM	11/12/2015	OLI
16/04/2001	ETM	16/11/2009	ETM	27/12/2015	OLI
21/05/2002	ETM	12/06/2010	ETM	05/02/2016	OLI
15/12/2002	ETM	31/08/2010	ETM	13/02/2016	OLI
05/03/2003	ETM	02/10/2010	ETM	24/03/2016	ETM
06/04/2003	ETM	07/02/2011	ETM	17/04/2016	OLI
12/08/2003	ETM	28/04/2011	ETM	03/05/2016	OLI
11/06/2004	ETM	25/01/2012	ETM	19/05/2016	OLI
13/07/2004	ETM	19/07/2012	ETM		

All processed images are arranged in tables of data organized according to the type of sensor, the period (date) and season (Table 2).

Table 2. Characteristic of images processed

Type of Landsat satellite	Number of downloading images	Number of images treat	Parameters treated	Corrections applied
TM	11	11	SPM, CHL, SDD	Radiance, reflectance
ETM+	37	37	SPM, CHL, SDD	Radiance, reflectance
OLI	20	20	SPM, CHL, SDD	Radiance, reflectance

Image processing

Radiance calibration

At-sensor radiances measured at a wavelength region is stored in Digital Numbers (DNs) .and DN values have no unit and any physical connotation; therefore, need to be converted to radiance (Ghulam, 2010).

$$L_{\lambda} = \left(\frac{LMAX_{\lambda} - LMIN_{\lambda}}{QCALMAX - QCALMIN} \right) * (QCAL - QCALMIN) + LMIN_{\lambda} \dots \dots (1)$$

Where L_{λ} the cell value as radiance, LMIN and LMAX is are the spectral radiances for each band at digital numbers 1 and 255. DN is the pixel DN value, λ is the wavelength,

QCALMAX-QCALMIN are the minimum and maximum values quantified for a pixel corresponding to LMIN and LMAX.

Reflectance Calibration

According to (USGS, 2016), the reflectance calibration of the satellite image is similar to the luminance conversion, 16-bit integer values in the product level 1, can also be converted to Top of Atmosphere (TOA) reflectance. The following equation is used to convert the level values 1 to DC TOA reflectance (Eq. 2):

$$\rho_{\lambda}' = M_{\rho} * Qcal + A_{\rho} \dots \dots \dots (2)$$

Or : ρ_{λ}' is TOA Planetary spectral reflectance, uncorrected for solar angle. (No unit), M_{ρ} is reflectance multiplicative scale factor for the band, A_{ρ} is additive reflectance scale factor for the band. ρ_{λ}' is converted to the true TAO reflectance According to the following formula (Eq. 3):

$$\rho_{\lambda} = \frac{\rho_{\lambda}'}{\sin(\theta)} \dots \dots \dots (3)$$

Or ρ_{λ} is TOA the true reflectance after calibration, θ is elevation angle of the sun.

Statistical analysis

Statistical techniques have been used to investigate the correlation between spectral bands or band combinations and the desired water quality parameters (Ritchie et al., 1976; Verdin, 1985; Lathrop and Lillesand, 1986; Baban, 1993; Allee and Johnson, 1999; Nelson et al., 2003).

Calibrated satellite images from the in situ measured data provide a quantitative and continuous information on the aquatic environment and can be used to estimate with reasonable approximation, the factors affecting water quality (Houma, et al., 2004; Muelle, 2000),

Correlation

Most of the samples were taken on the same day of Landsat overpass as previous studies suggested that ground observations coinciding with the image yield the best calibrations (Kloiber et al. 2002), however, other studies concluded that a few days difference (3 to 10 days) between satellite overpass and ground sampling does not pose a problem (Wu et al. 2010). In our work Landsat satellite images were downloaded and respectively with an interval of ± 3 days between the imaging and sampling date.

The procedures for estimating the measured parameters (depth transparency, suspended particulate matter and chlorophyll a in the Bay of Bou-Ismaïl, Through Landsat satellite imagery are carried out using correlation tests and Regression statistics on the reflectance and radiance values of the spectral bands.

The choice is made on the best fit, which corresponds, to the R2, which tends towards the one. We also correlate the spectral bands of the same sensor to each other, in order to find in which band the satellite information relating to the seawater parameter is located.

RESULTS

After processing and analysis of satellite data and data from campaigns at sea, we counted many families of results, that allowed us to map the measured parameters, to trace histogram and which led us to create a basic digital and scalable GIS data.

The advantage of this result is to determine which are the specific bands to determine the different transparency parameters of the water.

Radiance values

During the correlation of the values of the parameters measured in situ with the radiance and reflectance values recovered by remote sensing, we have taken into consideration that the offshore stations (1,2,8,9) which are far from being influenced by the terrigenous and The sources of pollution in order to eliminate any disturbance

The colors in the following tables, meaning, Blue: high positive values; Green: high negative values; Yellow: low values.

Between TM bands

Table 3. Correlation between Landsat TM spectral bands.

	B1	B2	B3	B4	B5	B6	B7
B1	1,00	-0,12	0,08	-0,61	-0,69	0,37	-0,24
B2	-0,12	1,00	0,64	0,57	0,71	-0,71	0,19
B3	0,08	0,64	1,00	0,52	0,58	-0,76	0,30
B4	-0,61	0,57	0,52	1,00	0,89	-0,63	0,59
B5	-0,69	0,71	0,58	0,89	1,00	-0,80	0,49
B6	0,37	-0,71	-0,76	-0,63	-0,80	1,00	-0,40
B7	-0,24	0,19	0,30	0,59	0,49	-0,40	1,00

The radiance values of the bands (B2, B3, B4, B5) are strongly correlated with each other and vary in the same direction (table 3), inversely with the thermal band (B6) which represents a strong inverse correlation with respect to them, which means a relationship of dependence between the radiance values.

Between ETM bands

Table 4. Correlation between Landsat ETM spectral bands

	B1	B2	B3	B4	B5	B6-1	B6-2	B7	B8
B1	1,00	0,54	0,76	0,78	0,52	0,33	0,54	0,73	0,58
B2	0,54	1,00	0,85	0,53	0,08	-0,16	-0,07	0,49	0,63
B3	0,76	0,85	1,00	0,83	0,53	0,19	0,36	0,77	0,76
B4	0,78	0,53	0,83	1,00	0,81	0,23	0,50	0,81	0,67
B5	0,52	0,08	0,53	0,81	1,00	0,45	0,66	0,66	0,39
B6-1	0,33	-0,16	0,19	0,23	0,45	1,00	0,92	-0,03	0,51
B6-2	0,54	-0,07	0,36	0,50	0,66	0,92	1,00	0,23	0,61
B7	0,73	0,49	0,77	0,81	0,66	-0,03	0,23	1,00	0,28
B8	0,58	0,63	0,76	0,67	0,39	0,51	0,61	0,28	1,00

The linear correlation of the bands B1, B3, B4, B8 represents a dependence between the radiance values that vary in the same direction, so they correlate strongly positively with each other (table.4), inversely with the thermal bands (B61-B62) Which represents a low correlation with respect to them, which means an independence relation between the radiance values.

Between OLI bands and in situ measurements

Table 5. Correlation between Landsat OLI spectral bands and in situ measurements

	B1	B2	B3	B4	B5	B6	B7	B8	B9	B10	PDS (m)	SPM (mg/l)	CHL a (µg/l)
B1	1.00	0.80	0.63	0.74	0.56	0.54	0.51	0.58	0.03	-0.03	-0.49	0.50	-0.64
B2	0.80	1.00	0.93	0.93	0.84	0.67	0.66	0.89	0.35	0.53	-0.68	0.70	-0.53
B3	0.63	0.93	1.00	0.92	0.84	0.66	0.66	0.92	0.31	0.70	-0.57	0.56	-0.57
B4	0.74	0.93	0.92	1.00	0.93	0.86	0.85	0.87	0.15	0.56	-0.44	0.47	-0.66
B5	0.56	0.84	0.84	0.93	1.00	0.93	0.92	0.84	0.09	0.70	-0.43	0.36	-0.47
B6	0.54	0.67	0.66	0.86	0.93	1.00	0.99	0.65	-0.19	0.49	-0.24	0.13	-0.55
B7	0.51	0.66	0.66	0.85	0.92	0.99	1.00	0.62	-0.16	0.50	-0.25	0.12	-0.50
B8	0.58	0.89	0.92	0.87	0.84	0.65	0.62	1.00	0.18	0.75	-0.60	0.58	-0.59
B9	0.03	0.35	0.31	0.15	0.09	-0.19	-0.16	0.18	1.00	0.26	-0.24	0.45	0.34
B10	-0.03	0.53	0.70	0.56	0.70	0.49	0.50	0.75	0.26	1.00	-0.34	0.26	-0.17
PDS (m)	-0.49	-0.68	-0.57	-0.44	-0.43	-0.24	-0.25	-0.60	-0.24	-0.34	1.00	-0.81	0.13
SPM (mg/l)	0.50	0.70	0.56	0.47	0.36	0.13	0.12	0.58	0.45	0.26	-0.81	1.00	-0.27
CHL a (µg/l)	-0.64	-0.53	-0.57	-0.66	-0.47	-0.55	-0.50	-0.59	0.34	-0.17	0.13	-0.27	1.00

The linear correlation, the bands B2, B3, B8 with Secchi disc depth (SDD) represents a dependency between the values of radiance which vary in the opposite direction, so they are highly negatively correlated (Table 5). the chlorophyll values are inversely correlated with the visible bands (R,G,B) and the bands B6, B7, B8, therefore it has a dependence which varies in the opposite direction.

According to the correlation analysis of radiances values TM band, ETM, and OLI each of them and through this, we found that almost all of satellite information of the seawater is concentrated in the first strips and especially the strips of the visible (R; G; B). This indicating a strong positive correlation between the first satellite band and also a strong negative correlation to the thermal bands so provide contributions and quantify the relationship with the dominant values of radiance.

Also the highest radiance values correspond to the stations which present pollution anomalies (Oued Mazafran, Oued el Nadour) may explain reflect information about the presence of the compositions in suspension in the shallow water column.. It is apparent that higher radiance values are observed on winter time than on the summer and autumn period.

Reflectance values

Several studies have shown a strong relationship between the Landsat series (TM, ETM, and OLI) data and ground clarity observations of water and chlorophyll (Brown, et al., 1977; Lillesand, et al., 1983; Lathrop, et al., 1986; Cox, et al., 1998).

The target reflectance represent potentially useful information about the state of water. The greater the amount of total suspended particulate matter (SPM) in the water, the murkier it appears and the higher the measured turbidity. The reflectance values found for each Landsat band, after atmospheric correction. Such values represent the spectral characteristics of Bou-ismail bay in different season.

According to the results obtained in Table 6, the choice of the ratios is applied to the bands, which have a strong correlation with the parameters measured in situ, The regression equations most suited to the processing of the parameters are summarized in the following (Table 1).

Table 6. Regression models and Determination Coefficients (R^2)

parameters	Independent (Landsat OLI Bands)	R^2	Regression equations
Chlorophyll-a Chl (a)	Band 4/band2	0,7056	Chl (a) = -24,801*(Band 4/band2) + 12,028
	Band 2/band4	0,7207	Chl (a) = 5,2332*(Band 2/band4) - 10,775
	Band 1/band4	0,6929	Chl (a) = 3,2511*(Band 1/band4) - 7,7875
Suspended particulate matter (SPM)	Band 1/band 2	0,5486	SPM = -2657,5*(Band 1/Band2) + 3301,5
	Band 2/band 1	0,6065	SPM = 4312,9*(Band 2/Band1) - 3498,8
	Band 3/band 1	0,459	SPM = 1566,5*(Band 3/Band1) - 723,77
secchi disc depth (SDD)	Band1/ band2	0,6339	SDD= 123,06* (Band1/ band2) - 135,52
	Band2/band1	0,4380	SDD= -157,87* (Band2/ band1) + 144,1
	Band2/band3	0,4955	SDD= 26,964* (Band2/ band3) - 30,88

Regression equations relating Landsat data to Ocean Color parameters are given in Table 6 which give results of bivariate models analyses show better R^2 . Among the regression models, we choose the best models for each ocean color parameter and estimate.

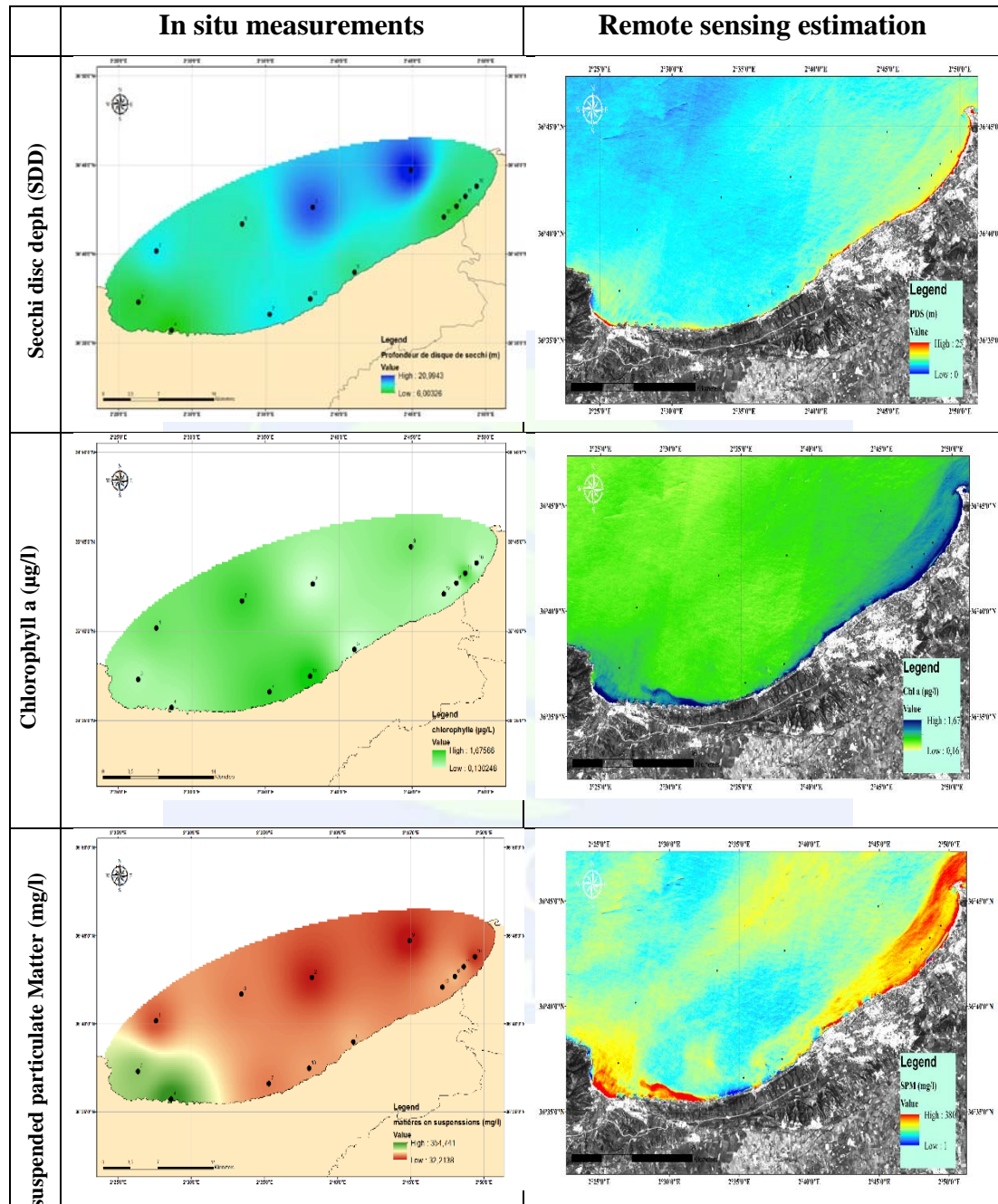


Figure 3. Mapping of measured and estimated parameters

The values of the in situ measurements are correlated with the reflectance values extracted from the image 2016-05-19 and which corresponds to the sampling days closest, to 16 and 22 May 2016 with 13 stations distributed over the entire bay. Ocean color parameters from the image. Chl-a, SPM and SDD was mapped with using Landsat-8 OLI, it has around 60% accuracy.

CONCLUSION

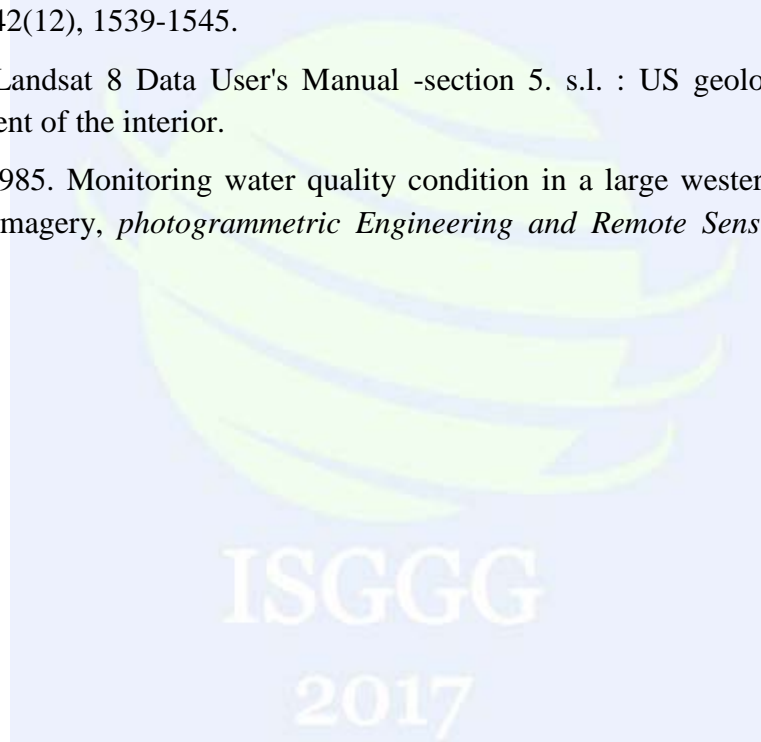
From these results, we can notice that the color and quality of the marine waters of Bou-Ismaïl Bay is characterized by a marked deterioration during the period 1984-2016, it is mainly due to human activities and terrestrial inputs. Faced with this situation is the direct consequence of the disappearance of several spaces. We tested various regression models using combinations of bands, and generated maps with best model. The regression models and maps showed acceptable correlation and accuracy, This work allows the constitution a basic georeferenced data integrated into a geographic information system. We confirmed that the visible bands (R.G.B) are the most useful in our study. All treatments and analysis and the correlative study allows us to create models which facilitates the task of calculating radiance, reflectance, in a specific area. While emphasizing the limitations of the method and the estimation errors in the colors followed and the water quality of Bou-Ismaïl Bay was penalized by the low spatial resolution of Landsat images (15 m) to our disposition. It will be interesting in the future to use high spatial resolution images. also the number of sampling stations must more important to have more reliable results.

REFERENCES

- Allee, R. J., & Johnson, J. E., 1999. Use the satellite imagery to estimate chlorophyll-a and Secchi disc depth of bull Shoals Reservoir, Arkansas, USA, *International Journal Of Remote Sensing*, 20(6), 1057-1072.
- Al-Yamani, F., Bishop, J., Ramadan, E., 2004. *Oceanographic atlas of Kuwait's waters*. Kuwait Institute for Scientific Research, Kuwait. Al-Husiani M, Al-Ghadban A.
- Baban, S, M, J., (1993). Detecting water quality parametres in the Norfolk Broads, UK, Using Landsat imagery, *International Journal of Remote Sensing*, 14(7), 1247-1267.
- Brown, D., Warwich, R., Skaggs, R., 1977. Lake condition in east central Minnestoa. Rept, Minnestoa Land Managgment information system, center for Urban and regional affairs, 5022.
- Cox, R.M., Forsythe, R. D., & Vaughan, G. E., 1998. Assessing water quality in the Catawba River reservoirs using Landsat thematic Mapper Satellite data, I, Lake and res, manage, 14,404-416.
- Ducrot, D., 2005. Méthode d'analyse et d'interprétation d'image de télédétection multi-sources, extraction de caractéristiques du paysage. s.l. : INP Toulouse, p. 167. memoire de recherches.
- Gower, J., 2006. Remote Sensing of the Marine Environment: Manual of Remote Sensing, 3. *The American Society for Photogrammetry and Remote Sensing*, Bethesda, Maryland, USA, pp. 338.
- Gabr, S., Ghulam, A., Kusky, T. 2010. Detecting areas of high-potential gold mineralization using ASTER data. *Ore Geology Reviews*, 38(1), 59-69.ai,

- F.C., Lee, C.F. and Zhang, X.H., 2001. GIS-based geo-environmental evaluation for urban land-use planning: a case study. *Engineering Geology* 61, 257–271.
- Houma, F., et al. 2004. Correlative Study of Physicochemical Parameters and Satellite Data IRS1C For Characterizing Aquatic Pollution. Application in Oran Bay: s.n., Vol. 17/4.
- Herrmann, S. and Osinski, E., 1999. Planning sustainable land use in rural areas at different spatial levels using GIS and modelling tools. *Landscape and Urban Planning* 46 (43): 93-101.
- Kallio, K., Kutser, T., Hannanem, T., Koponen, S., Pulliainen, J., Vepsäläinen, J., et al. (2001). Retrieval of water quality from airborne imaging spectrometry of various lake in different seasons, *Science of Total Environment*, 268, 59-77.
- Kloiber, S.M., Brezonik, P.L., Olmanson, L.G., Bauer M.E., 2002. A procedure for regional lake water clarity assessment using Landsat multispectral data. *Remote Sensing Environ* 82(1), 38-47.
- Koponen, S., Pulliainen, J., Kallio, K., & Hallikainen, M. 2002. Lake water quality classification with airborne hyperspectral spectrometer and simulation MERIS data. *Remote Sensing Environment*, 79, 51-59.
- Koponen, S., Pulliainen, J., Serrvoma, H., Zhang, Y., Hallikainen, M., Kallio, K., et al. 2001. Analysis on the feasibility of multisource remote sensing observation for chl-a monitoring in Finnish lakes. *Science of the Total Environment*, 268, 95-106.
- Lathrop, R. G., & Lillesand, T. M., 1986. Utility of thematic Mapper to assess water quality in southern green bay and west central Lake Michigan, *Photogram, Engng, Remote Sens* 52, 671-680.
- Leboeuf, A., Samson, M. P., Paquet, A. 2015. *Guide to Interpreting Satellite Image Mosaics Landsat*. s.l. : National Forestry, pp. 2-11. Ministry of Forests, Wildlife and Parks, Forestry Sector.
- Lillesand, T.M., & al., 1983. Use Landsat data to predict the trophic state of Minnesota lake, *Photogram Engng, Remote Sensing*, 49, 219-229.
- Muelle, J.L. . 2000. SeaWIFS Algorithm for the Diffuse Attenuation Coefficient K(490) using Water -Leaving Radiances at 490 and 555nm SeaWIFS Postlaunch Calibration and validation Analyses, Part 3, in: Seawifspostlanch Technical Report, 11, 2000.
- Nelson, S. A. C., Soranno, P. A., Cheruvilil, k. S., Batzli, S.A., & Skole, D. L., 2003. Regional Assessment of lake water clarity using remote sensing, *J Limnol.* 62(Suppl.1), 27-32.
- Nezlin, NP., Polikarpov, IG. et Al-Yamani, F. 2007. Satellite-measured chlorophyll distribution in the Arabian Gulf: Spatial, seasonal and interannual variability. *International Journal of Oceans and Oceanography*: 2, pp. 139–156.

- Pulliainen, J., Kallio, K., Eloheimo, K., Koponen, S., Servomaa, H., Hannanem, T., et al. 2001. A semi –operative approach to lake water quality retrieval from remote sensing data, *Science of Total Environment*, 268, 79-93.
- Pereira, P., De Pablo, H., Vale, C., Franco, V., & Nogueira, M. 2009. Spatial and seasonal variation of water quality in an impacted coastal lagoon (Óbidos Lagoon, Portugal). *Environmental monitoring and assessment*, 153(1), 281-292.
- Rodier, J, Legube, B, Merlet, N. 2009. *L'Analyse de l'Eau*. 9è édition. Dunod Paris. 1579p
- Roselli, L., Fabbrocini, A., Manzo, C., & D'Adamo, R. 2009. Hydrological heterogeneity, nutrient dynamics and water quality of a non-tidal lentic ecosystem (Lesina Lagoon, Italy). *Estuarine, Coastal and Shelf Science*, 84(4), 539-552.
- Teillet, P, M., 1986. Image correction for radiometric effects in remote sensing of suspended sediments in surface waters , *photogrammetric Engineering and Remote Sensing*, 42(12), 1539-1545.
- USGS. 2016. Landsat 8 Data User's Manual -section 5. s.l. : US geologicalsurvey, US département of the interior.
- Verdin, J P., 1985. Monitoring water quality condition in a large western reservoir with Landsat imagery, *photogrammetric Engineering and Remote Sensing*, 51(3), 343-353.



Wetland Mapping Using Sentinel-1 SAR Data

Gordana Kaplan^{1*}, Ugur Avdan¹

¹Earth and Space Sciences Institute, Anadolu University, Iki Eylul Campus, 26555, Turkey
(kaplangorde@gmail.com; uavdan@anadolu.edu.tr)

ABSTRACT

Mapping and monitoring wetlands is critical for planning ecosystem management and sustainable regional development. Remote Sensing has proven to be a useful application in wetland management over the last few decades. Number of Earth observation satellites is growing with the development of the Remote Sensing. In this paper, the potential of the recently launched Sentinel-1 SAR (Synthetic Aperture Radar) satellite for mapping and monitoring wetlands was investigated. For this purpose, one Sentinel-1 image downloaded from the Copernicus Open Access Hub and one WorldView-2 image were used. As a study area in this paper, one of the biggest wetlands of Turkey that lies on the Sakarya River, and it is located 30-40 km south of Sivrihisar, Balıkdami wetland, has been chosen. After the data have been calibrated, terrain corrected and filtered, visual inspection with different scenarios have been applied in order to estimate the different combination of VV and VH polarizations. For the accuracy assessment high resolution WorldView-2 image and field work data have been used. The results show that the combination of the two polarization increase the accuracy against the use of single polarization. The results are significant for the wetland remote sensing since SAR images can be used when meteorological conditions do not allow acquirement of optical data.

INTRODUCTION

Wetlands provide huge number of environmental and socioeconomic benefits such as their ability to store floodwaters and improve water quality, providing habitats for wildlife and supporting biodiversity, as well as aesthetic values (Ji 2007). The complex hydrology of wetlands controls the source, amount, and temporal and spatial distribution of sediment and nutrient movements, and influences distribution of flora and fauna (Ustin 2004). The loss of wetlands has gained considerable attention over the past few decades (Ji 2007), more than 50% since 1900 (WWAP 2003). Remote sensing technology has proven to be a useful and frequent application in monitoring and mapping wetlands (Adam et al. 2010; Bartlett and Johnson 1985; De Roo et al. 2008; Klemes 2014; Zhao et al. 2006). Remote sensing techniques are often less costly and time-consuming for large geographic areas. Over the years, different sensors and data have been used for wetland monitoring such as optical sensors, LiDAR data (Huang et al. 2014), DEM (Li and Chen 2005), and

* Corresponding Author

microwave data (Moser et al. 2016; Morandeira et al. 2016; White et al. 2015), as well as their combination (Rodrigues and Souza 2011; Ruan et al. 2007) have been used for wetlands monitoring.

However, Synthetic Aperture Radar (SAR) data have the unique abilities to penetrate vegetation cover and are sensitive to wet soil and flooded conditions that may exist beneath a canopy (Bourgeau-Chavez et al. 2009). A combination of wavelengths, polarization, or incidence angles provides the most useful information about the wetland and have the best ability to effectively map wetlands (Bourgeau-Chavez et al. 2009).

Currently available SAR data are of three different wavelengths: L-band (≈ 23 cm wavelength); C-band (≈ 5.7 cm wavelength); and X-band (≈ 3.5 cm wavelength). In sub-tropical regions, longer wavelengths such as L-band are more useful than C-band or X-band. C-band is best for discriminating emergent wetlands from agricultural and herbaceous uplands (Bourgeau-Chavez et al. 2001).

The latest SAR satellite developed by the European Space Agency, Sentinel-1, is an imaging radar satellite at C-band consisting of a constellation of two satellites, Sentinel-1A and Sentinel-1B. Their main cover applications are: monitoring sea ice zones and the arctic environment; Surveillance of marine environment; Monitoring land surface motion risks; Mapping of land surfaces: forest, water and soil, agriculture; Mapping in support of humanitarian aid on crisis situation (Attema et al. 2008; Torres et al. 2012).

In this paper, an investigation of Sentinel-1 abilities for mapping and monitoring wetlands was made. For this purpose, visual inspection of the different polarization combination has been made. For the accuracy assessment high-resolution WorldView-2 pan-sharpened image was used. As a study area, Balikdami wetland located in the Anatolian part of Turkey has been selected.

MATERIALS AND METHODS

Study Area

As a study area in this paper, Balikdami wetland which is located in the Anatolian part of Turkey, in the Eskisehir province, has been selected (Figure 1). The area of the wetland Balikdami is approximately 1.470 km² and it is 140 km away from the city Eskisehir. The area has been chosen for its special, unique and rich flora and fauna. In this area, also known as bird paradise, more than 235 different bird species can be found. It is known that this area has been losing its value since 1980s.

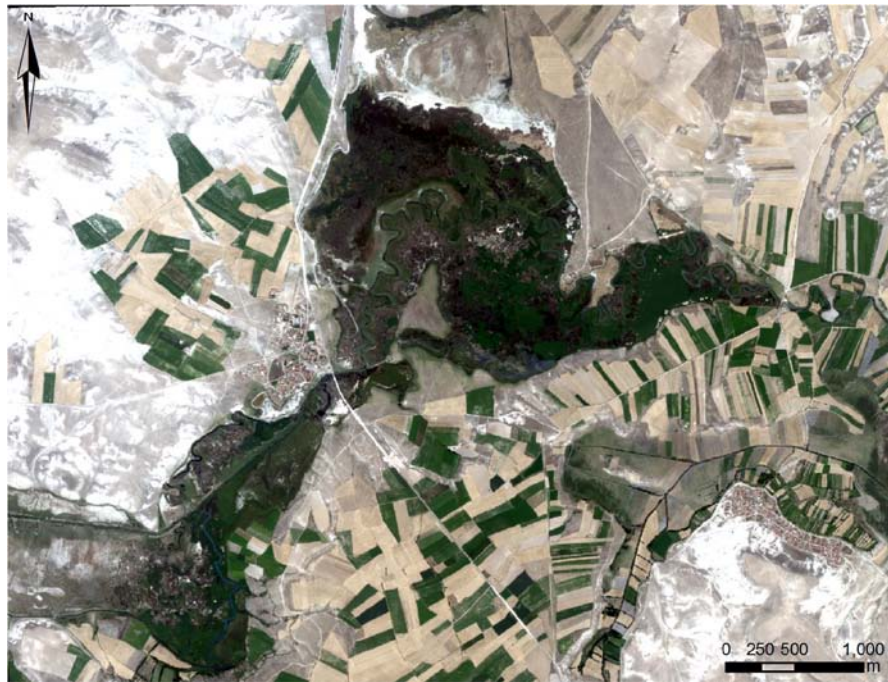


Figure 1. WorldView-2 satellite image (RGB: 432) – Balıkdami Turkey

Materials

In this paper the capability of Sentinel-1 for mapping wetlands was investigated. For that purpose, a single date Ground Range Detected (GRD) Interferometric Wide (IW) swath Sentinel-1 image from 30 August 2016 over the Balıkdami wetland in Turkey, was downloaded from the Copernicus Open Access Hub for free. Details about the used image are given in Table 1.

Table 1. Sentinel-1 image specifications

<i>Specification</i>	<i>Sentinel-1 image</i>
Acquisition date	30 August 2016
Imaging mode	IW
Imaging frequency	C-band
Polarization	VV-VH
Coordinate system	Ground range
Bits per pixel	16
Pixel spacing rg x az m	10x10

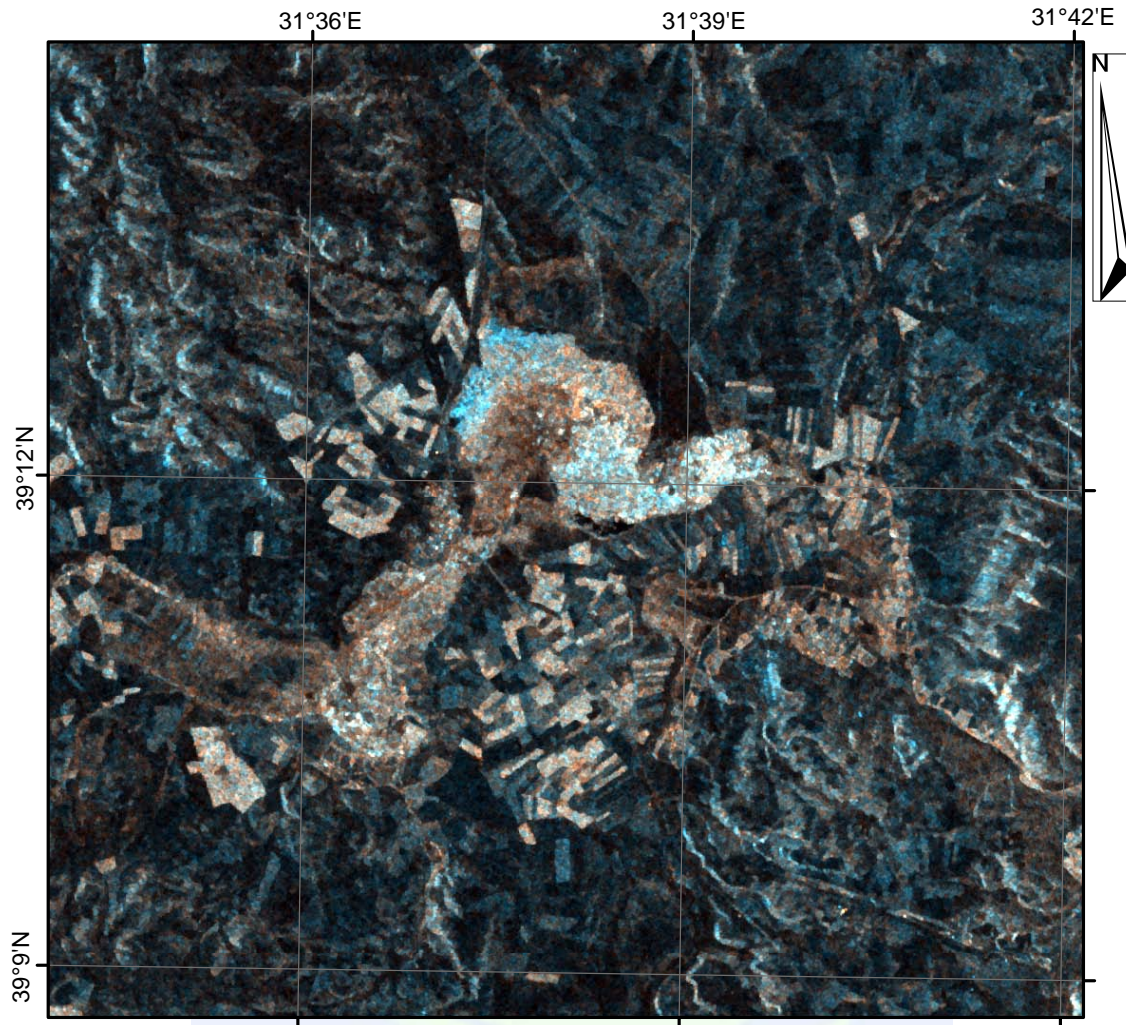


Figure 2. Sentinel-1 composite image (VV, VH, (VV+VH)/2)

For the accuracy assessment, WorldView-2 high-resolution optic satellite image acquired on 16 August 2016. The resolution of the multispectral bands is 1.84 m, but it has been increased to 0.48 m with pan-sharpening techniques.

Methods

The Sentinel-1 image has been pre-processed before its application. After the download of the image, radiometric and terrain calibration, as well as speckle reduction has been performed. The product has been filtered with Lee Sigma filter 5x5 window size. For the terrain correction a Range Doppler Terrain Correction with a digital elevation model of 30 m has been used. The pre-processing has been performed in the SNAP software by ESA using the Sentinel-1 toolbox. The digital number values have been converted into backscattering values in decibel (dB) scale following Equation 1.

$$\beta_{db}^{\circ} = 10 * \log_{10}(\beta^{\circ}) \quad (1)$$

Where β° is the digital number value of the image, and β_{db}° is the backscattered value in dB.

Also the WorldView-2 satellite image used for the accuracy assessment in this paper has been preprocessed. The resolution of the image has been increased to 0.48 m with fusing the multispectral bands with the panchromatic band. For this purpose, the Intensity-Hue-Saturation method has been used.

The IHS technique is one the most commonly used techniques for image fusion. The technique used in this study, called Modified IHS resolution merge, combines high-resolution panchromatic data with lower resolution multispectral data. The tool integrated into Erdas IMAGINE provide an implementation of the method proposed by Y. Siddiqui (Siddiqui 2003).

Different combination of the available variables has been made and compared. First, an inspection of the single polarizations, VV, VH has been made. Afterwards, combinations of the polarization have been performed as in (Abdikan et al. 2016). The details about the combination are given in Table 2.

Table 2. Variable combinations details

Combination	Variables
1	VV
2	VH
3	VV;VH
4	$(VV+VH)/2$
5	VV;VH; $(VV+VH)/2$
6	VV;VH; $(VV-VH)$
7	VV;VH; $(VV+VH)/2$; $(VV-VH)$; (VV/VH)

Considering the variables in Table 2, a visual inspection comparing the different SAR images with the high-resolution optic image has been made.

RESULTS

In this paper, different polarization combinations have been studied in order to investigate the abilities of Sentinel-1 for mapping and monitoring wetlands areas. After the SAR images have been preprocessed, seven different combinations have been observed for wetland monitoring and have been compared with a high-resolution optical satellite image. The results showed that using single polarization cannot separate wetlands from vegetated areas and shadow. Also, a two-band combination, did not showed good results in separating wetlands from the other areas. In the scenarios where three or more bands were combined, vegetated areas and wetland areas can be separated one from another. The SAR images were compared to a WorldView-2 pan sharpened satellite image (Figure 3) taken in

the same period as the Sentinel-1 image. For the accuracy assessment of the pan-sharpening, statistical analyses have been made and they are presented in Table 2.

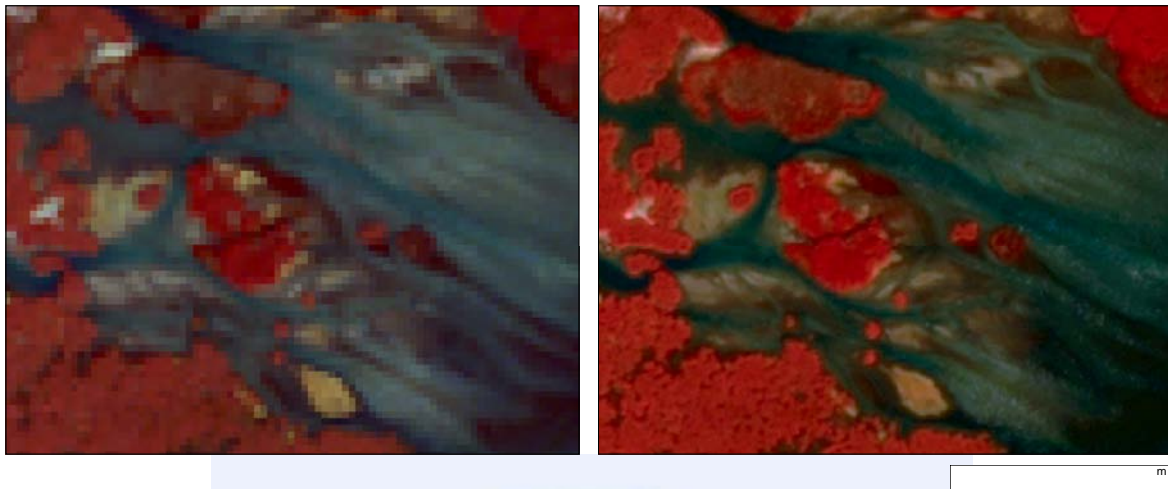


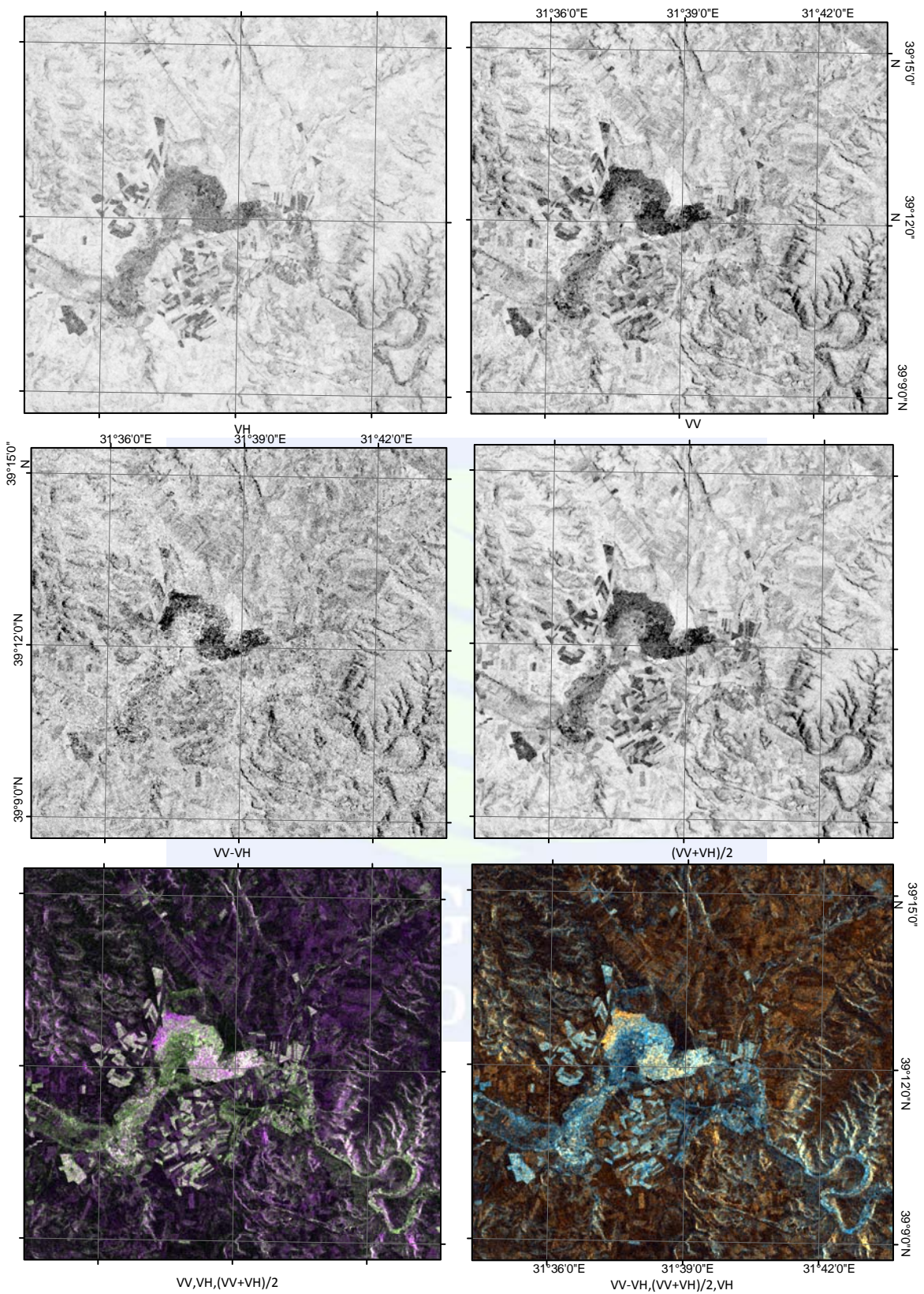
Figure 3. WorldView-2 pan-sharpening results: Left – 1.84 m resolution; Right – IHS pan-sharpening methods results

Table 2. IHS pan-sharpening results

Band	Mean	Std Dev	RMSE	MSE	CC	UIQI	RASE	ERGAS
Avg	-33.181	-51.970	39.889	2274.493	0.957	0.879	2.467	1.716

CONCLUSIONS

In this paper a visual inspection of Sentinel-1 SAR imagery was made in order to inspect its ability in separating wetland areas from the other areas. It can be concluded that with combination of more than three bands of the given variations, wetland areas can be separated from vegetated areas as well as from shadows. Since in this paper only visual inspection has been made, for future studies classification of the images as well as accuracy assessment should be made.



Appendix A. Different combinations for wetland observation

ACKNOWLEDGMENTS

This study was supported by Anadolu University Scientific Research Projects Commission under the grant no: 1705F121.

REFERENCES

- Abdikan, S., F. Sanli, M. Ustuner, and F. Calò. 2016. Land Cover Mapping Using SENTINEL-1 SAR Data. *ISPRS Int. Arch. Photogramm. Remote Sens. Spat. Inf. Sci.* 757-761.
- Adam, E., O. Mutanga, and D. Rugege. 2010. Multispectral and hyperspectral remote sensing for identification and mapping of wetland vegetation: a review. *Wetlands Ecology and Management* 18 (3):281-296.
- Attema, E., M. Davidson, N. Floury, G. Levrini, B. Rosich, B. Rommen, and P. Snoeij. 2008. Sentinel-1 ESA's new European radar observatory. Paper read at Synthetic Aperture Radar (EUSAR), 2008 7th European Conference on.
- Bartlett, D. S., and R. W. Johnson. 1985. Remote-Sensing for Ecological Assessment of Wetlands. *Estuaries* 8 (2b):A7-A7.
- Bourgeau-Chavez, L., E. Kasischke, S. Brunzell, J. Mudd, K. Smith, and A. Frick. 2001. Analysis of space-borne SAR data for wetland mapping in Virginia riparian ecosystems. *International Journal of Remote Sensing* 22 (18):3665-3687.
- Bourgeau-Chavez, L. L., K. Riordan, R. B. Powell, N. Miller, and M. Nowels. 2009. Improving wetland characterization with multi-sensor, multi-temporal SAR and optical/infrared data fusion. In *Advances in geoscience and remote sensing*: InTech.
- De Roeck, E. R., N. E. C. Verhoest, M. H. Miya, H. Lievens, O. Batelaan, A. Thomas, and L. Brendonck. 2008. Remote sensing and wetland ecology: a South African case study. *Sensors* 8 (5):3542-3556.
- Huang, C. Q., Y. Peng, M. G. Lang, I. Y. Yeo, and G. McCarty. 2014. Wetland inundation mapping and change monitoring using Landsat and airborne LiDAR data. *Remote Sensing of Environment* 141:231-242.
- Ji, W. 2007. *Wetland and water resource modeling and assessment: a watershed perspective*: CRC Press.
- Klemas, V. V. 2014. Advances in Coastal Wetland Remote Sensing. *2014 Ieee/Oes Baltic International Symposium (Baltic)*.
- Li, J. H., and W. J. Chen. 2005. A rule-based method for mapping Canada's wetlands using optical, radar and DEM data. *International Journal of Remote Sensing* 26 (22):5051-5069.
- Morandeira, N. S., F. Grings, C. Facchinetti, and P. Kandus. 2016. Mapping Plant Functional Types in Floodplain Wetlands: An Analysis of C-Band Polarimetric SAR Data from RADARSAT-2. *Remote Sensing* 8 (3).

- Moser, L., A. Schmitt, A. Wendleder, and A. Roth. 2016. Monitoring of the Lac Bam Wetland Extent Using Dual-Polarized X-Band SAR Data. *Remote Sensing* 8 (4).
- Rodrigues, S. W. P., and P. W. M. Souza. 2011. Use of Multi-Sensor Data to Identify and Map Tropical Coastal Wetlands in the Amazon of Northern Brazil. *Wetlands* 31 (1):11-23.
- Ruan, R. Z., X. Z. Feng, and Y. J. She. 2007. Fusion of Radarsat SAR and ETM plus imagery for identification of fresh water wetland - art. no. 675221. *Geoinformatics 2007: Remotely Sensed Data and Information, Pts 1 and 2* 6752:75221-75221.
- Siddiqui, Y. 2003. The modified IHS method for fusing satellite imagery. Paper read at ASPRS 2003 Annual Conference Proceedings.
- Torres, R., P. Snoeij, D. Geudtner, D. Bibby, M. Davidson, E. Attema, P. Potin, B. Rommen, N. Floury, M. Brown, I. N. Traver, P. Deghay, B. Duesmann, B. Rosich, N. Miranda, C. Bruno, M. L'Abbate, R. Croci, A. Pietropaolo, M. Huchler, and F. Rostan. 2012. GMES Sentinel-1 mission. *Remote Sensing of Environment* 120:9-24.
- Ustin, S. 2004. vol. 4: *Remote sensing for natural resource management and environmental monitoring*.
- White, L., B. Brisco, M. Daboor, A. Schmitt, and A. Pratt. 2015. A Collection of SAR Methodologies for Monitoring Wetlands. *Remote Sensing* 7 (6):7615-7645.
- WWAP, U. 2003. UN World Water Development Report: Water for People. *Water for Life*.
- Zhao, W. J., Z. N. Gong, H. L. Gong, X. J. Li, S. M. Zhang, and L. Jing. 2006. Using remote sensing to research Beijing wetlands dynamics. *Science in China Series E-Technological Sciences*:97-107.

ISGGG
2017



Modeling of Urban Transportation Network by Linear Programming

Elif Ergin^{*1} and R.Cüneyt Erenoğlu²

¹Master Programme of Geographical Information Technologies, Graduate School of Natural and Applied Sciences, Çanakkale Onsekiz Mart University, Terzioğlu Campus, 17020, Çanakkale, Turkey. e-mail: erginelif91@gmail.com

²Department of Geomatics Engineering, Çanakkale Onsekiz Mart University, Terzioğlu Campus, 17020, Çanakkale, Turkey. e-mail: ceren@comu.edu.tr

ABSTRACT

Geographic Information Systems (GIS) have been used in many different disciplinary applications and studies in recent years. In this study, models were developed to adjust the costs of firm and satisfaction of passengers in urban transportation planning and integrated into GIS. For this purpose, passenger boarding graphics and reports according to stops, line voyage report, elaborate passenger boarding report, instant vehicle tracking and instant route tracking systems have been studied in detail. Thus, the number of stops in Çanakkale, the distances in the stop intervals, the density of passengers (for each stop), bus routes, fleet size, capacities, bus service frequency, fuel consumption for each bus, the demands of passengers and firm have been evaluated. The obtained data are modeled by the linear programming approaches. While the models were being created, linear programming was employed for simultaneous multi-objective validation. Then the existing situation was evaluated with the created models and the regression analyzes were made. When comparing the results, there is no need for a part of 103 buses of the 21 lines that actively work in the city of Çanakkale and the others can be reduced in the frequency of the bus service. As a result, it is seen that the appropriate bus service times and stop intervals for passengers were determined and the firm increases the gain. Thus, while the transportation plan and the tariff regulations are made so as to meet the demand of the passengers, an effective decision support system is presented to the firms and managers at the same time. As a result of the contribution of GIS, the transfer and evaluation and analysis of these spatial and non-spatial data are carried out easily. Finally, the proposed approach will make public transportation more attractive in terms of passengers.

INTRODUCTION

A geographic information system (GIS) is a computer system for capturing, storing, querying, analyzing, and displaying geospatial data. Geospatial data, or geographically referenced data, describe the locations and characteristics of spatial features (Horner and Grubestic, 2001). The ability of GIS handle and process geospatial data distinguishes GIS

^{*} Corresponding Author

from other information systems. It also establishes GIS as a technology important to geoscientists, cartographers, environmental engineers, and urban and regional planners (Lu, 2003). The GIS based transportation system got many advantages which include analytical capabilities, visual power, efficient data storage, integration of spatial database, and capabilities for spatial analysis (Sarsam and Motasher, 2015).

In the assessment of Canakkale urban transportation, the data which were obtained from Canakkale Private Public Buses database were processed and analyzed. The number of vehicles and their capacities were evaluated between 2013 and 2016 in the office work. Accordingly, when the current vehicle situation in 2013 was examined 81 buses are 7-meters with a capacity of 46 passengers, 7 buses are 9-meters with a capacity of 66 passengers and 10 buses are 12-meters with a capacity of 104 passengers. There are 98 vehicles in total. In 2013, the vehicle that leaves the garage in the morning is 84. By the year 2016, the number of cars leaving the garage increased to 94. The numbers of vehicle and capacities were revised remarkably in 2017. Currently, there are 45 buses are 7-meters with a capacity of 46 passengers, 7 buses are 9-meters with a capacity of 66 passengers and 50 buses are 12-meters with a capacity of 104 passengers. Thereby, the increase of vehicle capacity is 47% and the increase of public transport capacity is 60% between 2013 and 2016. However, the increase of the daily vehicle is 13%; current status can not bear the expenses. When the each of the bus lines is examined with GIS databases containing real-world information in Canakkale, it is seen that these lines have very long and complicated routes. The survey results show that local residents complain about the extended time of the travel time in the vehicle and the complexity of the lines. All of these factors are dissuading from public transport.

This paper studied passenger flows intensity and transportation within the city of Canakkale. The expectation and satisfaction of passengers are the most important elements of urban transportation system. It has been detected that investors have increased the number of vehicles, their routes and bus stop numbers in order to satisfy the increased demand for transportation over time. Nevertheless, both passengers and investors were not able to make the desired profit. In this context, bus stops and bus rotations have been determined for a pilot zone where was chosen. Subsequently, these have been assigned on digital map of Canakkale by using Geographic Information Systems. Data which were obtained in case study were transferred to GIS databases. Thus, density maps have been created with the numbers of passengers for each bus stop and bus intervals. The mathematical model of the problem has been created by using linear programming. It is planned that the analyzes will be a decision support system for managers.

LINEAR PROGRAMMING MODEL

Linear programming (LP or linear optimization) is a mathematical method for determining a way to achieve the best outcome (such as maximum profit or lowest cost) in a given mathematical model for some list of requirements represented as linear relationships.(Kumar at all,2014)

$$\text{Max/Min } z = \sum_{j=1}^n c_j x_j \quad (1)$$

Subject to

$$\sum_{j=1}^n a_{ij} x_j \begin{cases} \leq \\ = \\ \geq \end{cases} b_i, \forall i = 1, \dots, m \quad (2)$$

$$x_j \geq 0, \forall j = 1, \dots, n \quad (3)$$

z : value of overall performance measure

x_j : level of activity j ($j=1, \dots, n$)

c_j : performance measure coefficient for activity j

b_i : amount of resource i available ($i=1, \dots, m$)

a_{ij} : amount of resource i consumed by each unit of activity j

Decision Variables: x_j

Parameters: c_j, a_{ij}, b_i

A Linear programming problem can be expressed in the following standard form:

$$\text{Max/Min } z = c_1 x_1 + c_2 x_2 + \dots + c_n x_n \quad (4)$$

Subject to

$$\left. \begin{aligned} a_{11}x_1 + a_{12}x_2 + \dots + a_{1n}x_n &\leq b_1 \\ a_{21}x_1 + a_{22}x_2 + \dots + a_{2n}x_n &\leq b_2 \\ \cdot &\quad \cdot \quad \dots \quad \cdot \quad \cdot \\ \cdot &\quad \cdot \quad \dots \quad \cdot \quad \cdot \end{aligned} \right\} \quad (5)$$

$$a_{m1}x_1 + a_{m2}x_2 + \dots + a_{mn}x_n \leq b_m$$

$$\left. \begin{array}{l} x_1 \geq 0 \\ x_2 \geq 0 \\ \dots \\ x_n \geq 0 \end{array} \right\} \quad (6)$$

Objective functions: overall performance measure

$$c_1x_1 + c_2x_2 + \dots + c_nx_n \quad (7)$$

Constraints:

$$a_{i1}x_1 + a_{i2}x_2 + \dots + a_{in}x_n \leq b_i, \forall i = 1, \dots, m \quad (\text{Functional constraints}) \quad (8)$$

$$x_j \geq 0, \forall j = 1, \dots, n \quad (\text{Nonnegativity constraints}) \quad (\text{Turkay, 2016}) \quad (9)$$

STUDY AREA AND APPLICATION

The city of Canakkale is located between 40°9'16" north latitudes and 26°24'19" east longitudes. In this paper, the region where the passenger density is highest is examined. It have been studied only the case of one direction as from SSK to Bolge Traffic. This direction goes to the center of Canakkale. Figure 1 illustrates the location of study area in Canakkale.

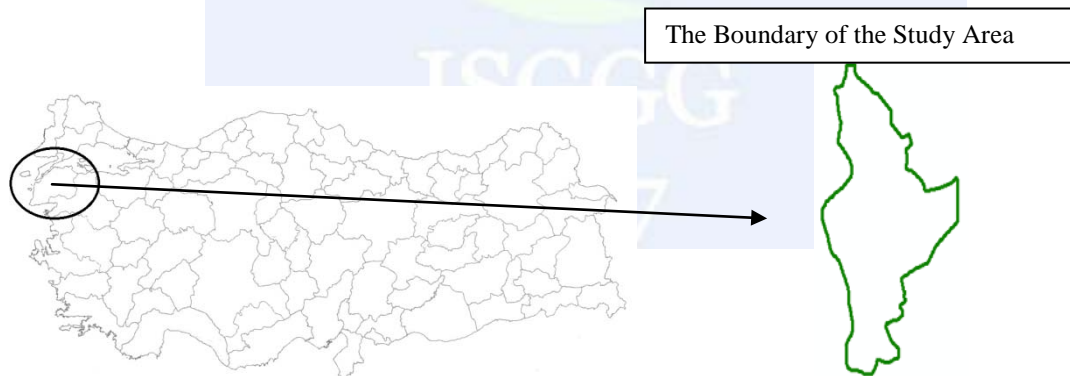


Figure 1. A Study Area from Canakkale

The decision variables of mathematical model have been made of the number of each bus travel. The system constraints have been created by taking into consideration that the total capacity of 6 bus routes shouldn't be less the total passenger demands and the each bus the total time (240min) in the region. While it was creating mathematical model, it was considered range from 8:00 am to 12:00 pm as a time constraint.

The system constraints;

$$S_i * C_i \geq K_i \quad (10)$$

S_i : The frequency for each i^{th} bus routes

C_i : The values of capacity for each bus type

K_i : The passenger demands of each route (Alp 2008).

Time constraints;

$$\left. \begin{aligned} \sum_{i=1}^6 t_i X_{i1} &\leq T * N_1 \\ \sum_{i=1}^6 t_i X_{i2} &\leq T * N_2 \\ \sum_{i=1}^6 t_i X_{i3} &\leq T * N_3 \end{aligned} \right\} \quad (11)$$

t_i : The travel time for i^{th} bus routes

X_{ij} : The number of travel which has i^{th} bus routes for j^{th} bus type

T : Total time (240min)

N_i : The total number of i^{th} bus type.(Uludağ, 2010)

Travel constraints;

$$\sum_{j=1}^3 X_{ij} \leq F_i, \forall i = 1, \dots, 6 \quad (12)$$

X_{ij} : The number of travel which has i^{th} bus routes for j^{th} bus type

F_i : The total travel number for i^{th} bus routes

Objective function;

$$\text{Max } z = \sum_{i=1}^6 \sum_{j=1}^3 C_i X_{ij} \quad (13)$$

$$x_{ij} \geq 0, \forall j = 1, \dots, 6 \text{ and } \forall j = 1, \dots, 3 \quad (14)$$

The information about an each route is shown as bus route, headway, travel time, number plate and bus capacity in Figure 2.

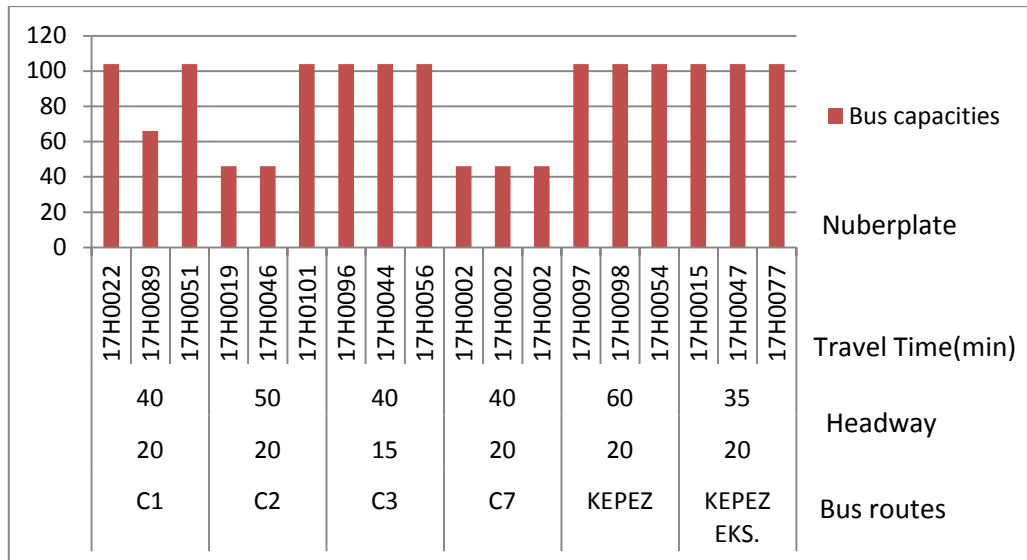


Figure 2. The information of the bus routes

It have been utilized from Automatic Toll Collection and Vehicle Tracking System in order to attain the number of the passenger boarding per a day in July (Figure 3).

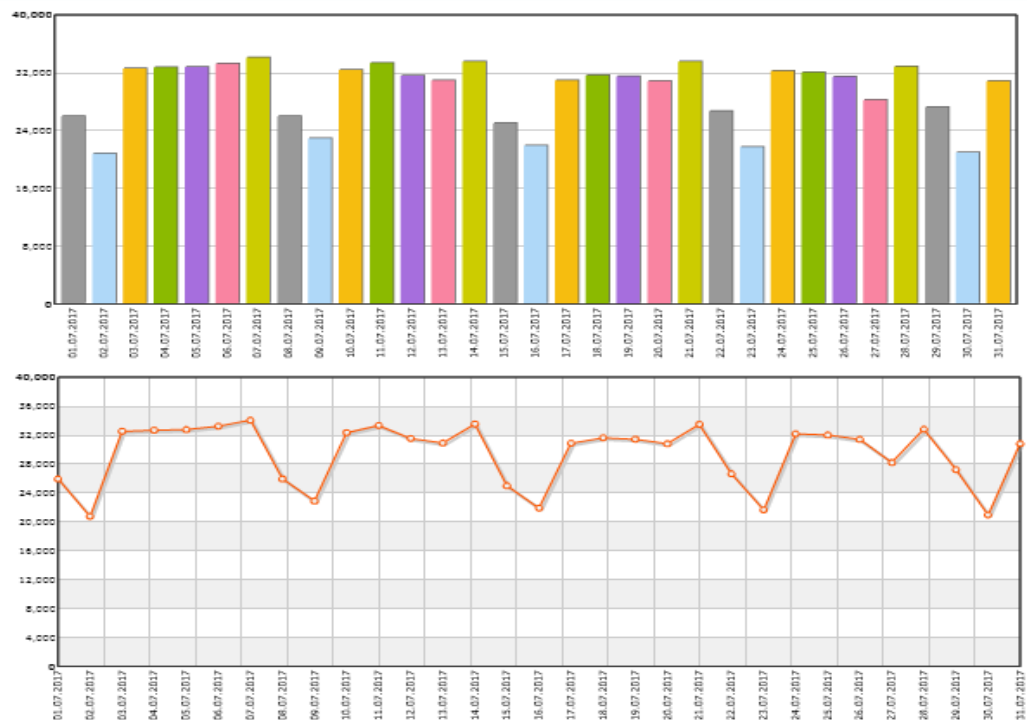


Figure 3. The Passenger Boarding Graphics of the July

The passenger flows were determined during the period between 08:00 am and 08:00 pm which are divided into 3 time periods (08:00 am - 12:00 pm, 12:00 pm - 04:00 pm and 04:00 pm - 08:00 pm) on 14 July 2017. Simultaneously, the weighted average of the

number of passengers was taken so that passenger flows intensity was detected between the intervals of the two stops for a time from 9:30 am to 10:00 am and from 13:30 to 14:00 and from 17:30 to 18:00 in the study area. The dataset have been created by the means of collected information. Afterwards, these dataset have been transferred to database by using GIS. Then, the density analyses were performed with the aid of ArcGIS Spatial Analyst Toolbox.

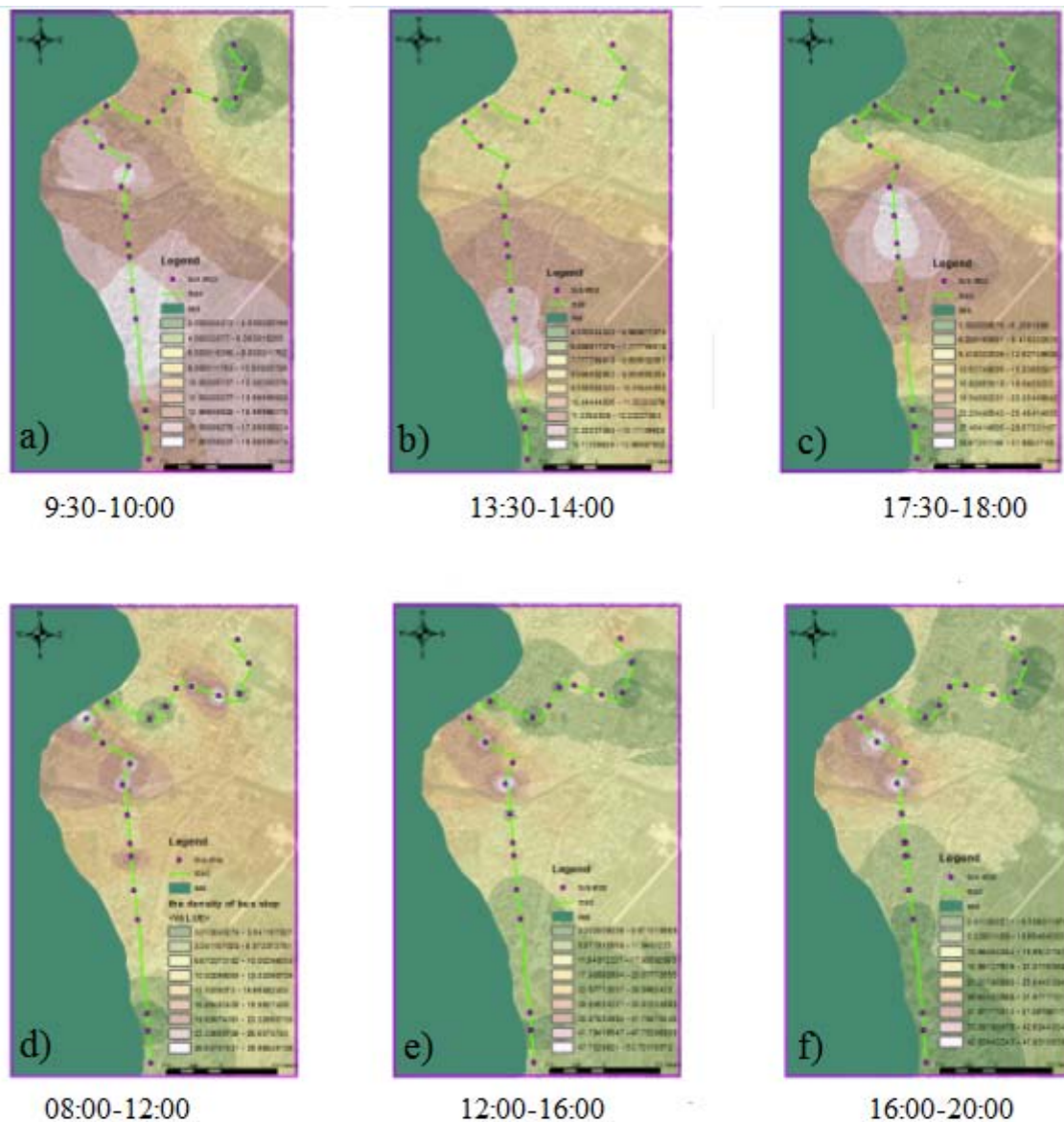


Figure 4. The density of bus intervals (a,b,c) and bus stops (d,e,f)

Figure 4 shows that the passenger flows intensity of the two bus stops interval for C1 which was chosen as an example has the enormous demands. The same analyses have been done for each bus routes and bus stops in this region.

The mathematical model in the study has been solved by using LINGO. At the end of the solution, the number of travel which has 6 bus routes for 3 bus type has been obtained. The results are shown in the Table 1.

Table 1. The result of the model

Variable	Value	Variable	Value	Variable	Value	Variable	Value	Variable	Value	Variable	Value
X11	15	X21	13	X31	18	X41	10	X51	12	X61	12
X12	0	X22	0	X32	0	X42	0	X52	0	X62	0
X13	0	X23	0	X33	0	X43	0	X53	0	X63	0

CONCLUSIONS

In this study, data have been attained with the aid of Automatic Toll Collection and Vehicle Tracking System and case studies. According to created map, the demands of the passengers have been seen where passenger has high density. Thus, the distribution passengers for each bus routes have been analyzed. Afterwards, the number of travel for bus routes with different capacities has been obtained by the means of the created linear programming model. Consequently, the methods of the linear programming have quite solutions with Geographic Information Systems.

REFERENCES

- Alp S.,2008. An Application and Modelling of Intercity Passenger Transportation by Bus with Linear Goal Programming. *PhD Thesis. Marmara University, Institute of Social Sciences: Istanbul.*
- Horner M. and Grubescic T.,2001. A GIS-based planning approach to locating urban rail terminals. *Transportation*. 28:55-77.
- Kumar A., Singh M. and Kumar Shrivastava B.,2014.Optimization of Inventory System: A Case Study of Haldiram Bread Industry. *International Journal of Engineering Research and Applications*. Vol. 4, Issue 2(Version 1), February 2014,pp.468-473.
- Lu X., 2003. A New approach for Web-GIS based collaborative transportation planning system design. *Proceedings, the International Conference on Computer Supported Cooperative Work in Design*. P637-642
- Sarsam S. and Motasher R.,2015. Using GIS-based travel potential data for alignment design of Baghdad Subway. *American Association for Science and Technology*.2375-3803.
- Turkay M., 2016. INDR 262 Optimization models and mathematical programming, Linear Programming Models.
- Uludağ N., 2010. Bulanık optimizasyon ve doğrusal hedef programlama yaklaşımları ile otobüs hatlarının modellenmesi. *Pamukkale Üniversitesi, Fen Bilimleri Enstitüsü, Doktora Tezi, İnşaat MühendisliğiAnabilim Dalı, Denizli*

Site Selection of Solid Waste Landfill Using Geographical Information System: A Case Study for Artvin City Center

Halil Akıncı¹, Kazım Onur Demirarslan^{*2}

¹ Faculty of Engineering, Department of Geomatics Engineering, Artvin Çoruh University, Artvin, TURKEY.
(E-mail: hakinci@artvin.edu.tr)

² Faculty of Engineering, Department of Environmental Engineering, Artvin Çoruh University, Artvin, TURKEY.(E-mail: onurdemirarslan@artvin.edu.tr)

ABSTRACT

Solid wastes are one of the environmental problems that arise due to accelerated and unplanned urbanization today. The sum of the stages from the collection to the disposal of solid wastes is called waste management and is generally the responsibility of local governments. Problems such as air, soil, and water pollution arise from the poor management of solid wastes, threatening human health. One of the common methods used for the disposal of solid wastes is regular storage. In regular storage, waste is buried in pre-prepared and environmentally controlled areas in a controlled manner, and the associated environmental and human health hazards are minimized. However, the process of site selection for regular storage of solid wastes is quite troublesome. The site selection criteria include many factors such as proximity to settlement areas, ease of access, distance from historical and cultural sites, wind direction, and topographic conditions. The eastern Black Sea region in Turkey is very complicated in terms of both topography and natural environment. Particularly in Artvin, selected as the study area, it is very difficult to identify locations even for settlement, and this difficulty also negatively affects the identification of areas for depositing solid wastes. For the purpose of this study, a suitability map showing possible landfill sites with a potential life of 20 years was produced for Artvin city center using the ArcGIS 10.2 program. Seven parameters including slope, land use capability classes, distance from settlement areas, distance to roads, distance to rivers and dam lakes, and distance from the national parks were considered in the study. After removing all the forest and pasture areas, the generated suitability map was categorized into five classes ranging from very high to very low. The produced suitability map indicated that there was only one suitable area for solid waste landfill with a moderate degree and this outcome can be associated with the high coverage of forests, very steep terrain and poor connection to existing roads in the study area.

* Corresponding Author

INTRODUCTION

Along with developments such as industrialization, rapid population growth, change of urbanization and consumption habits, as well as the scarcity of natural resources such as energy and raw materials in the world, rational use of resources has become a necessity and causing the environment to be rapidly polluted. As a result of industrialization and urbanization, many environmental problems such as the damage of public areas and rivers, air pollution, water pollution and solid waste generation occur. It is seen that the amount of industrial production processes and the amount of waste increasing more than the population has a significant share in this pollution. The amount of waste materials, the types and the effects on the environment reach dangerous extent (Akdoğan & Güleç, 2007; Yılmaz & Bozkurt, 2010). Looking at the definition of the solid waste, it defined as the solid matter and treatment mud which should be disposed regularly, wanted by its producer to be removed and in terms of peace of society and protection of environment (Gökçe et al., 2015). One of the most important problems in urban areas has been the management of solid wastes. Solid wastes included in the existing pollution, in case they are not disposed of, transform into environmental pollution, which is the first thing to be noticed by the people living in cities. The effects of solid wastes on the environment can be biological, chemical and physical. Diseases such as leprosy, cholera, dysentery, tuberculosis, rabies, malaria, which can be transmitted directly or via vectors, are examples of biological problems; Leachate and gasses in garbage storage areas can cause chemical and biological problems (Demirarslan & Demirarslan, 2016). These wastes leading to environmental pollution are mainly; food waste, paper-cardboard, plastic, nylon, metal-tin, glass, leather, bone, rubber, stone-soil, wood, textile, garden wastes and fine grained garbage (Demirbağ & Güngörmüş, 2012). It is called as solid waste disposal to have these wastes processed through various physical, chemical and biological processes according to the type and characteristics, until the end product is obtained, without causing adverse effects on environment and human health (Özaydın Şenol, 2017). Commonly used methods for the disposal of solid wastes; regular storage, wild storage, composting, incineration, pyrolysis and recycling. Regular storage is one of the most commonly used methods. Stored solid wastes are stored taking precautions in order not to harm the ground and ground waters or atmosphere (Gülmez, 2016).

In this study, it was planned to select a solid waste landfill site of Artvin Provincial Center, which is located in the easternmost part of Turkey's Eastern Black Sea Region and has a different geographical and climatic structure. In this study, the regular landfill site selection for Artvin city centre, which could have a life of 20 years, was determined using the ArcGIS 10.2 program. Seven parameters consisting of slope, land use capability class, distance to road, distance to river and dam lakes, distance to residential areas and distance to national park were used in the study.

MATERIAL AND METHOD

Artvin province, the study area, is between 40,35 and 41,32 northern latitudes and between 41,07 and 42,00 eastern longitudes and is located on an area of 7367 square kilometers.

The industry sector is quite low level in the province. Enterprises operating in the industrial sector have a structure predominantly of food, mining and forestry products, which act mainly to utilize the natural resource potential of the province. There are no organized industrial zones in Artvin (Demirarslan et al., 2017). For this reason, only household solid wastes are created in the province center.

Study Area Population Projection

It is envisaged to design a 20-year storage facility in order to be able to regularly store solid wastes from the field in the study area. The amount of solid waste after 20 years must be calculated in order to plan the installation. For this reason, a 20-year population projection was made for the study area.

While making the population projections, Provincial Bank Method, Arithmetic Increase Method and Geometric Increase Method are used and the population after 20 years is calculated by taking the average of the results. Population change in Artvin city center is given in Figure 1.

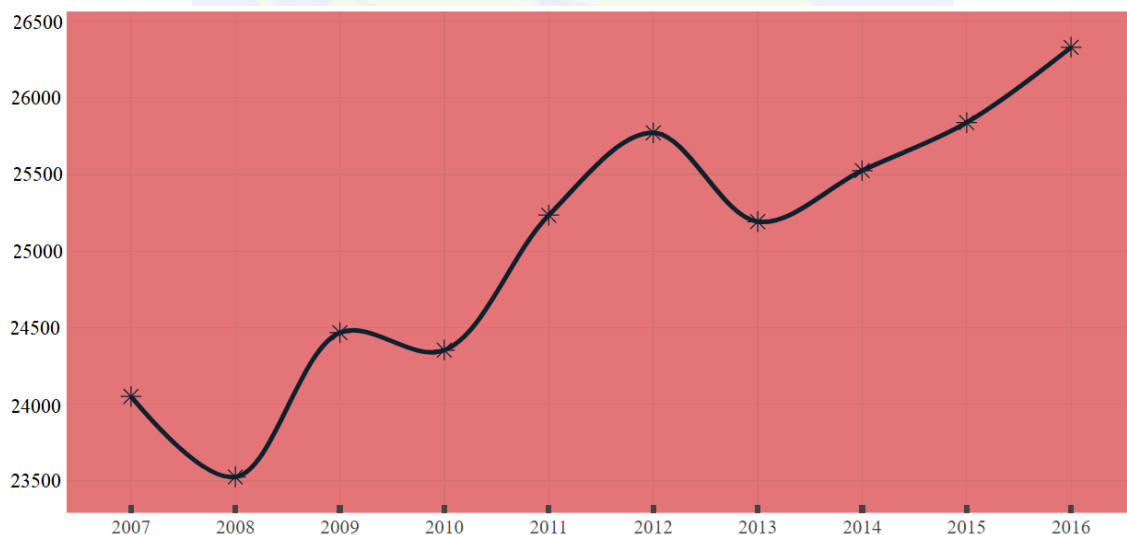


Figure 1. Population exchange of Artvin (2007-2016)

By taking the averages of the population projections made with all three methods, 20-year population data for the study area were obtained (Table 1). The amount of waste produced per person in the province of Artvin was found to be 1,002 kg/person per day according to the "Average Municipal Waste Amount per Person" of the Statistical Institute of Turkey (TUIK, 2017). The amount of waste by years in light of this data is given in Table 1.

Table 1. Population and waste projection of the study area

Year	Polulations	Waste amount (kg/day)	Waste amount (kg/year)
2019	28817	28875	10539241
2020	29280	29338	10708452
2021	29752	29812	10881199
2022	30234	30294	11057359
2023	30725	30786	11237054
2024	31227	31289	11420529
2025	31739	31803	11608026
2026	32262	32327	11799181
2027	32796	32862	11994603
2028	33342	33408	12194048
2029	33899	33967	12397881
2030	36468	36541	13337442
2031	35050	35120	12818715
2032	35644	35715	13036080
2033	36251	36324	13258200
2034	36872	36946	13485318
2035	37507	37582	13717313
2036	38156	38232	13954672
2037	38819	38897	14197273

According to Table 1, at the end of the 20th year, 14197273 kg (14197.273 tons) of waste is created annually. Although solid wastes vary in density, they are reported in the literature as 700-1000 kg/m³ after being compacted in landfills (UNEP, 2017). If the value of 850 kg/m³ is taken as average, the annual amount of garbage in 2037 can be found to be approximately 16703 m³. Regular storage landfills are large structures with heights ranging from 10 m to 150 m (Gao, et al., 2018). According to this, when the height of waste to be stored is selected as 10 m, a storage area of 1670 m² is needed.

Landfill Area Selection

In this study, seven parameters consisting of slope, land use capability class, distance to road, distance to river and dam lakes, distance to residential areas and distance to national park were used in the stage of landfill area selection.

One of the most important parameters used in solid waste landfill area selection is the distance to residential areas. Various environmental problems arise in storage areas near residential areas. Especially, because of bad smell and noise, storage areas are required to be away from the residential areas. In the manual of "Designing, Site Selection and Saving of Wild Storage Areas of Regular Storage Areas", prepared by the Municipalities Union Waste Commission of Turkey, in 2014 (TBB, 2014; Baran et.al. 2015, 2015), it is required that II. and III. class regular storage facilities are at least 250 m away from settlements. For this reason, buffer zones are formed around the settlement areas in the study area and these zones are scored between 1-10 points according to the distance (Table 2).

On the other hand, solid waste regular storage areas should not be made in agricultural lands. For this reason, digital soil maps of the study area were obtained from the General Directorate of Agricultural Reform and the land use capability classes (LUCC) map of the area was produced using land use capability classes. There are no I. and II. class agricultural lands in the study area. It is not appropriate to build a storage area in III. and IV. class lands due to soil characteristics. For this reason, VII. and VIII. class lands in the study area are designated as suitable storage areas (Table 2).

In order to ensure that the solid waste regular storage areas are not located both in flood areas and to be located in a distance not to affect surface waters (such as rivers and lakes) in terms of pollution, the distance parameters to rivers and dam reservoirs have also been used in the study. Buffer zones were created around the rivers and dam lakes and areas nearest to the surface waters were scored 0 and the farthest areas were scored 10 (Table 2).

Table 2. The main and sub-criteria used in the study

Criteria	Weight	Sub-criteria	Score
Distance to settlements (m)	0.3393	0-250	1
		250-500	2
		500-750	3
		750-1000	4
		1000-2000	5
		2000-3000	6
		3000-4000	7
		4000-5000	8
		5000-6000	9
		6000-8461	10
LUCC	0.2597	No Data	0
		3	1
		4	1
		6	6
		7	9
		8	10
Distance to rivers (m)	0.1308	0-100	0
		100-200	1
		200-300	2
		300-400	3
		400-500	4
		500-1000	6
		1000-2000	7
		2000-3000	8
		3000-4000	9
		4000-5724	10
Distance to dam lakes (m)	0.1308	0-250	0
		250-500	1
		500-750	2
		750-1000	3
		1000-2000	4
		2000-5000	6
		5000-10000	7
		10000-15000	8
		15000-20000	9
		20000-24247	10

Table 2. Cont.			
Distance to roads (m)	0.0721	0-100	10
		100-200	9
		200-300	8
		300-400	7
		400-500	6
		500-1000	5
		1000-2000	4
		2000-3000	3
		3000-4000	2
		4000-9846	1
Slope (°)	0.0423	0-10	10
		10-20	8
		20-30	7
		30-40	6
		40-50	5
		50-60	4
		60-70	3
		70-80	2
		80-89.55	1
Criteria	Weight	Sub-criteria	Score
Distance to protected sites (Hatila national park) (m)	0.0249	0-250	0
		250-500	1
		500-750	2
		750-1000	3
		1000-2000	4
		2000-5000	6
		5000-10000	7
		10000-20000	8
		20000-30000	9
		30000-32774	10

Slope is one of the important parameters in the selection of solid waste landfill areas. Since the slope of the land directly affects the construction and excavation costs, areas where the slope is high are not preferred for site selection. For this reason, in the study, Digital Elevation Model (DEM) of Artvin Central District was produced first by using the contour lines included in the digital topographic maps of 1 / 25.000 scale, and then the slope map of the study area from DEM in ArcGIS environment was obtained. The slope of the study area ranges from 0 to 89.55 degrees. The generated slope map was then divided into 9 classes with 10° intervals, and these classes were scored as 10 points for areas where slope is low (0-10°) and 1 for areas where slope is very high area (80-89.55°) (Table 2).

One of the important parameters to be taken into account when choosing a solid waste storage area is the proximity to the road. Regular storage areas should be located at a location accessible by alternative roads in all weather conditions and should not be located too far from existing road networks to avoid expensive construction of the link roads. For this reason, buffer zones were formed around the roads in the study area and 10 points were given to the areas nearest to roads (0-100m) and 1 point to the areas farthest from roads (4000-9846m) (Table 2).

Protected areas such as national parks and archaeological sites are not suitable areas for solid waste disposal areas. For this reason, buffer zones were formed around the Hatila National Park within the study area, giving 0 points to the nearest places (0-250 m) to the national park and 10 points to the farthest places (30-32.77 km) (Table 2).

Thus, the sub-parameters and scores used in the study were determined. The weights of the main parameters were determined by pairwise comparisons according to the AHP method (Table 3). Judgments in the pairwise comparison matrix were determined by examining expert opinions and similar studies in the literature. The consistency ratio (CR) of the pairwise comparison matrix is calculated as 0.067.

Tablo 3. The pairwise comparisons matrix and weights of main criteria

Criteria	P1	P2	P3	P4	P5	P6	P7	Weights
P1	1	2	3	3	5	7	9	0.3393
P2		1	3	3	4	6	8	0.2597
P3			1	1	3	4	5	0.1308
P4				1	3	4	5	0.1308
P5					1	3	4	0.0721
P6						1	3	0.0423
P7							1	0.0249
P1: Distance to settlements, P2: LUCC, P3: Distance to rivers, P4: Distance to dam lakes, P5: Distance to roads, P6: Slope, P7: Distance to protected sites (national park) $\lambda_{max} = 7.5309, CI = 0.088, CR = 0.067$								1.000

RESULTS

Seven criteria were determined in the determination of the location of landfill site of the study area, and these criteria were weighted against the pairwise comparison method used in AHP and then the solid waste storage area suitability map of the study area was produced in ArcGIS 10.2 software by using these weights. The suitability map produced was classified into five different classes to show very high, high, moderate, low and very low suitable areas (Figure 2). As can be seen in the suitability map in Fig. 2, 4 areas were identified for the solid waste storage area. There are no high level suitable areas where solid wastes can be stored in the study area. The main reasons for this are; the fact that a large part of the land is covered with forest, the slope being is very high in the area general and transportation problems.

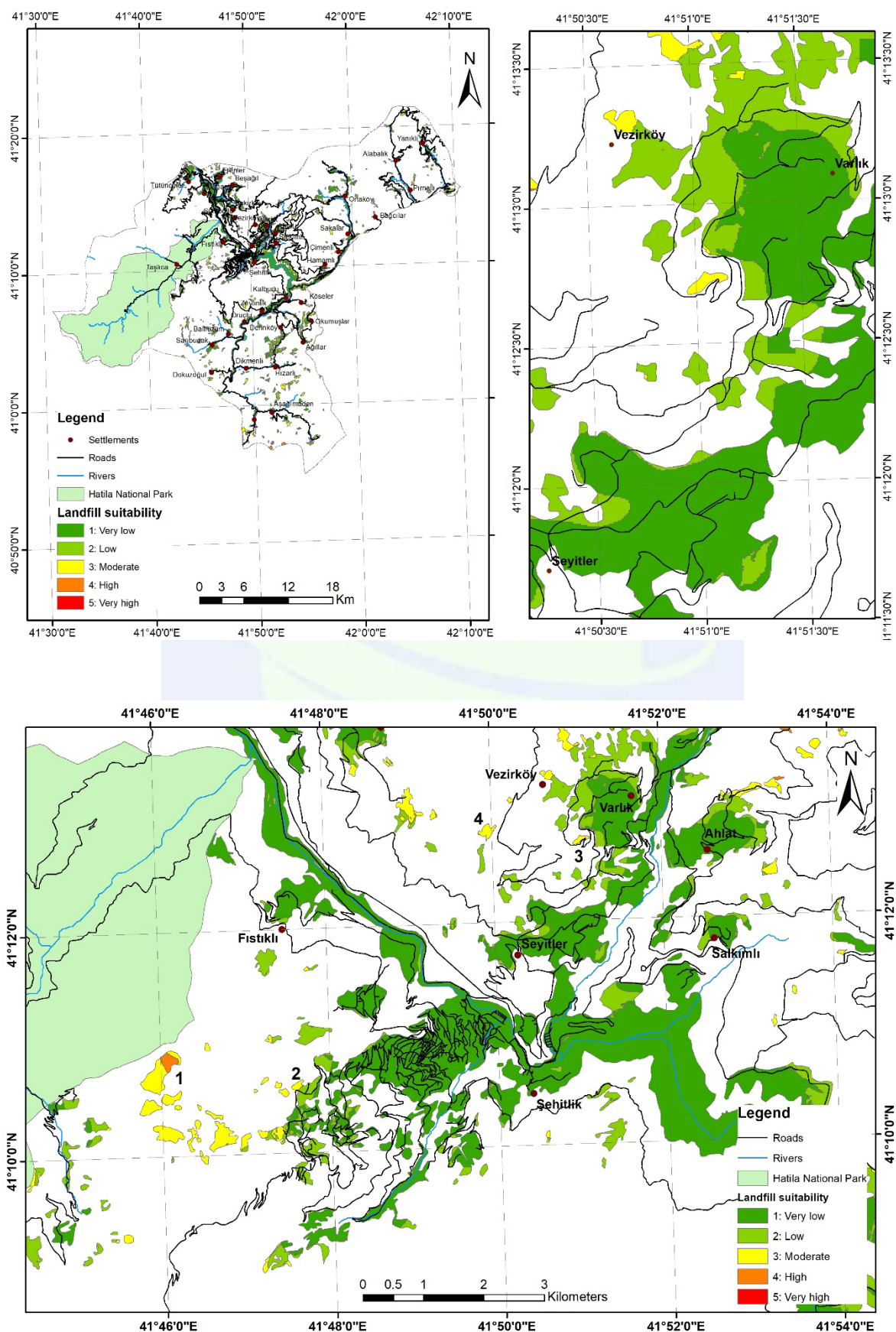


Figure 2. Solid waste storage area compliance map

When the area indicated by the number 1 and determined as highly suitable in the suitability map in Fig. 2 is examined, it is understood that the area is 150 m closer to Hatila National Park which has the national park status and that there is no connection to the neighboring roads. This area is not preferred, especially if the area in question is selected, due to new road works causing problems in terms of both economic and environmental. Area number 2, shown in the suitability map in Fig. 2, is a medium level suitable area in terms of solid waste storage. When this area is examined, the proximity to the city center stands out. However, no suitable way to reach this point, and also the mountain houses in the vicinity which are used more actively in summer, makes this area impractical. Again, areas 3 and 4, which are medium level suitable areas, are more suitable areas than areas 1 and 2. The passage of the high voltage line near the area 4, 7923m from the city center, makes it impossible to use this area. Area 3 is at a distance of 9542 m from the city center. Also, link roads are available to here and there are no settlements nearby. A research was conducted by going to area 3 and it was determined that the area belonged to the Treasury and the Village Legal Entity. In addition, it has been determined that a road passes right by the area and Artvin city center has an area of sufficient size (about 19,000 m²) to store solid wastes. Other medium level suitable locations seen in the map in Fig. 2 are ignored because of the difficulty of transportation, the distance from the city center and also other factors (topographical, energy transmission line, etc.).

CONCLUSIONS

In this study, suitable areas for 20 years long solid waste landfill facility for Artvin city center which is the easternmost of the Eastern Black Sea Region have been determined. In the study, the population projections were made according to the Provincial Bank Method, the Arithmetic Increase Method and the Geometric Increase Method, and the averages of the results were taken and the population after 20 years was calculated. The population of the province center of Artvin in 2037 was calculated as 38819 people and the amount of solid waste collected was found to be 141972.73 tons / year. When the density of the solid waste is considered as 850 kg / m³, the annual amount of garbage in the year 2037 is calculated to be approximately 16703 m³. It has been determined that 1670 m² of storage space will be needed when the height of waste to be stored is 10 m. In this study, seven parameters consisting of slope, land use capability class, distance to road, distance to river and dam lakes, distance to residential areas and distance to national park were used in the stage of landfill area selection. The weights of the main parameters were determined by a pairwise comparison according to the AHP method in accordance with expert opinions. Sub-parameters were again scored in the range of 1-10 points in accordance with expert opinions. Using these weights and scores, a map of the solid waste storage area of the study area was produced in ArcGIS environment. According to the suitability map created, 4 points where the solid waste storage area can be constructed in the study area are determined. First area was removed from consideration because of the proximity to the national park and the lack of connection with the existing roads, and the second area due to the distance from the roads and the houses used as summer houses in the vicinity. Area number 4 was removed from selection due to the high voltage line passing nearby. Thus,

area number 3 was concluded to be more suitable for solid waste storage. However, the geological and hydrogeological characteristics of the area must be examined in order to make the final decision.

REFERENCES

- Akdoğan, A., Güleç, S., 2007. Sürdürülebilir Katı Atık Yönetimi ve Belediyelerde Yöneticilerin Katı Atık Yönetimiyle İlgili Tutum ve Düşüncelerinin Analizine Yönelik Bir Araştırma. *H.Ü. İktisadi ve İdari Bilimler Fakültesi Dergisi*. 25(1), 39-69.
- Baran A., Arıkan, O.A., Yıldız Ş., Demir İ., Sarı, H., Altınbaş, M., Balahorli, V. 2015. Katı Atık Düzenli Depolama Tesisleri İşletimi El Kitabı, İSTAÇ, Teknik Kitaplar Serisi.
- Demirarslan, K.O., Aydın, E., Aydın, M.A., 2017. Artvin Çoruh Üniversitesi Seyitler Yerleşkesinin Güz Dönemi Katı Atık Karakterizasyonu, *Doğal Afetler ve Çevre Dergisi*, 3(2), 77-86.
- Demirarslan, K.O., Demirarslan, D. 2016. Kentlerde Yeni Yerleşim Alanlarının Gelişimi ve Katı Atık Sorunu: İzmit Yahyakaptan Mahallesi Örneği, *Doğal Afetler ve Çevre Dergisi*, 2(2), 108-120.
- Demirbağ, B.C., Güngörmüş, Z., 2012. Bireylerin Evsel Katı Atık Yönetimine İlişkin Bilgi ve Davranışları, *Gümüşhane Üniversitesi Sağlık Bilimleri Dergisi*, 1(3), 127-137
- Düzenli Depolama Sahalarının Tasarımı, Yer Seçimi ve Vahşi Depolama Alanlarının Islahı, Türkiye Belediyeler Birliği Atık Komisyonu, 2014, Ankara, <http://www.tbb.gov.tr/download.php?dosya=storage/catalogs/0864274001399277406.pdf&dosyaAdi=duzenli-depolama-sahalarinin-tasarimi-yer-secimi-ve-vahsi-depolama-alarinin-islahi>.
- Gao, W., Bian, X., Chen, Y., (2018). Effects of one weak interlayer on seismic response of municipal solid waste landfill. *Environmental Vibrations and Transportation Geodynamics*, Editors: Bian, X., Chen, Y., Ye, X., Springer.
- Gökçe., G. F., Kırık Aydemir, K.P., Hasanoğlu, P. Özbay, M. 2015. Katı Atık Düzenli Depolama Sahalarının ve Vahşi Depolama Alanlarının Islahı ve Bitkilendirilmesi, *Düzce Üniversitesi Bilim ve Teknoloji Dergisi*, 3, 258-271.
- Gülmez, M., 2016. Yerel yönetimlerde kentsel katı atık yönetimi - Derince Belediyesi örneği, Yüksek Lisans Tezi, Gebze Teknik Üniversitesi Fen Bilimleri Enstitüsü.
- Özaydın Şenol B., 2017. Evsel Katı Atık Toplama, Taşıma ve Bertarafı İş Kolunda Çalışanların Sağlık ve Güvenlik Şartlarının İncelenmesi, Yüksek Lisans Tezi, İş Sağlığı ve Güvenliği Yüksek Lisans Programı, İstanbul Gedik Üniversitesi.
- TUİK, 2017. <https://biruni.tuik.gov.tr/medas/?kn=119&locale=tr>,

UNEP, 2017. United Nations Environment Programme, 2.4 Topic g: Waste characterization, http://www.unep.or.jp/Ietc/ESTdir/Pub/MSW/RO/Latin_A/Topic_g.asp

Yılmaz, A., Bozkurt, Y., 2010. Türkiye’de Kentsel Katı Atık Yönetimi Uygulamaları Ve Kütahya Katı Atık Birliği (KÜKAB) Örneği. *Süleyman Demirel Üniversitesi İktisadi ve İdari Bilimler Fakültesi Dergisi*. 15(1), 11-28.



A GIS-Based Landfill Site Selection Approach Using Spatial Multi-Criteria Decision Making Methods

Dogus Guler^{*1}, Tahsin Yomralioglu²

¹Department of Geomatics Engineering, Istanbul Technical University, Istanbul, Turkey. gulerdo@itu.edu.tr

²Department of Geomatics Engineering, Istanbul Technical University, Istanbul, Turkey. tahsin@itu.edu.tr

ABSTRACT

Decision-making is a process that starts with the problem of detection and covers activities that are carried out up to the recommendation. All decision-making processes start with the diagnosis and identification of a decision problem. The ability of data storage, management, administration and analysis of Geographical Information Systems (GIS) is a great support in the course of problem definition. The spatial multi-criteria analysis is sharply distinguished from traditional multi-criteria decision-making methods due to its geographical component. Spatial multi-criteria analysis requires not only the values of alternatives but also their geo-references, unlike traditional multi-criteria decision-making methods. Spatial multi-criteria analysis can be considered as the process of reaching the final decision by combining and transforming the geo-data used as input. Data is processed to enable decision making using GIS and multi-criteria decision-making methods. Analytic Hierarchy Process (AHP), which is one of the multi-criteria decision-making methods, is a general measurement theorem. It has been used in broadly in many various decision and planning projects. The rationality of the AHP; to focus on the problem-solving goal, to develop an integrated model of the relationship and effects of the problem, to know and experience those who have dominant and prior influence among the relations in the structure, to reach the best agreement by permitting among the differences. As an example of spatial multi-criteria decision-making methods, the site selection analysis of solid waste landfill site has been carried out using AHP and GIS methods for Istanbul province in Turkey. A total of 11 factors were used in the study, under the two main classification parts like environmental and economic. Environmental factors; land use, geology, settlement areas, surface waters, population density, airports and protected areas. Economic factors are a slope, solid waste transfer stations, land values, and highways. The identified factors are separated by sub-criteria according to the appropriateness of solid waste landfill site, and values are assigned. As a result of the study, using the power of GIS functionality, the digital data sets leading to the decision-makers were created.

^{*} Corresponding Author

INTRODUCTION

Today, in order for societies to carry out a qualified lifestyle, the needs, methods and principles are determined first and they are tried to be applied with the most appropriate resources, techniques and methods in the most appropriate way according to their targets. Urban solid waste management, which has an important place in environmental services in this context, is a serious issue in the whole world. Geographical Information Systems (GIS) is one of the most important technological tools used to solve environmental problems and has an effective role in processes where spatial information is directed (Yomralioğlu, 2000). The urgent solution of environmental problems has been understood more in recent years and much effort has been made to produce realistic solutions to the problems. Instead of material-minded thoughts, studies involving multi-criteria methods are seen (Hokkanen and Salminen, 1997). In developing countries, the increase of human population and related human activities accelerated urbanization (Sumathi et al., 2008). As a result of increasing population, change of consumption patterns, economic growth, change of income, urbanization and industrialization, solid waste production and diversity have increased (Ngoc and Schnitzer, 2009). Waste management and waste disposal alternatives are a complex process involving decision makers and related parties. Choosing the most suitable landfill site; administrative constraints and regulations, as well as physical process conditions and environmental, economic, health and socio-cultural effects (Sadek et al., 2006; Yıldırım, 2012).

In the work done by Monsef (2015), an alternative landfill site for the Red Sea, a rapidly growing tourist area in recent years, has been identified by using GIS and AHP methods. Different criteria such as transportation routes, airports, surface waters and residential areas were used in the study. As a result of the study, three alternative landfill sites were identified. In the study carried out by Djokanovic et al. (2016), a complex process, the determination of the landfill site, has been evaluated from the viewpoint of geological engineers. In this study, alternative landfill sites for Pancevo region of Serbia were identified using GIS and AHP methods. As a result of the study, it was determined that 62% of the region was unsuitable and 12% was very suitable. Nascimento et al. (2017) used MCDM and GIS methods to conduct a study within the US state of California. 61 landfill sites in the area were evaluated. Using the developed model, 61% of the landfill sites are found to be in suitable and very suitable classes.

MATERIALS AND METHOD

In this study, a region covering the administrative borders of Istanbul, which is the most populous province of the country, located in the northwest of Marmara region of Turkey, was selected as a study area. The same limits were used for all criteria used in the spatial analysis. Figure 1 shows the elevation map of Istanbul, which was selected as a study area.

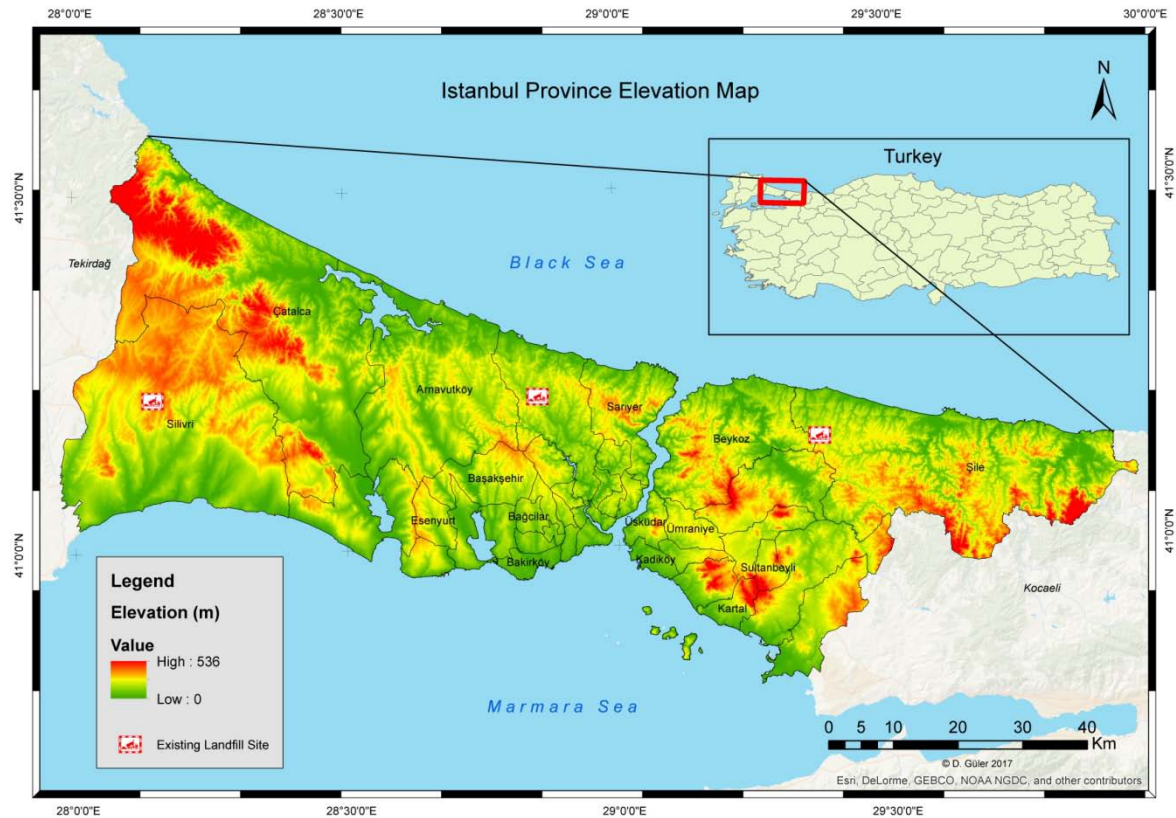


Figure 1. Istanbul province elevation map (Guler, 2016).

In the study conducted, the criteria used in the AHP method were evaluated by the literature survey together with the restrictions specified in the country's regulation. In addition, the criteria to be used were determined considering the characteristics of the study area. 11 criteria were used in the study, with two main categories, environmental and economic (Guiqin et al., 2009; Şener et al., 2010; Donevska et al., 2012; Vasiljevic et al., 2012; Yal and Akgün, 2013; Shahabi et al., 2014; Baba et al., 2015; Yıldırım and Güler, 2016). Environmental factors; land use, geology, settlement areas, surface waters, population density, airports and protected areas. Economic factors are a slope, solid waste transfer stations, land values, and highways. Values are assigned in the range of 0 to 5 to meet the standard for all criteria. The appropriate AHP hierarchy model created in the study is shown in Figure 2.

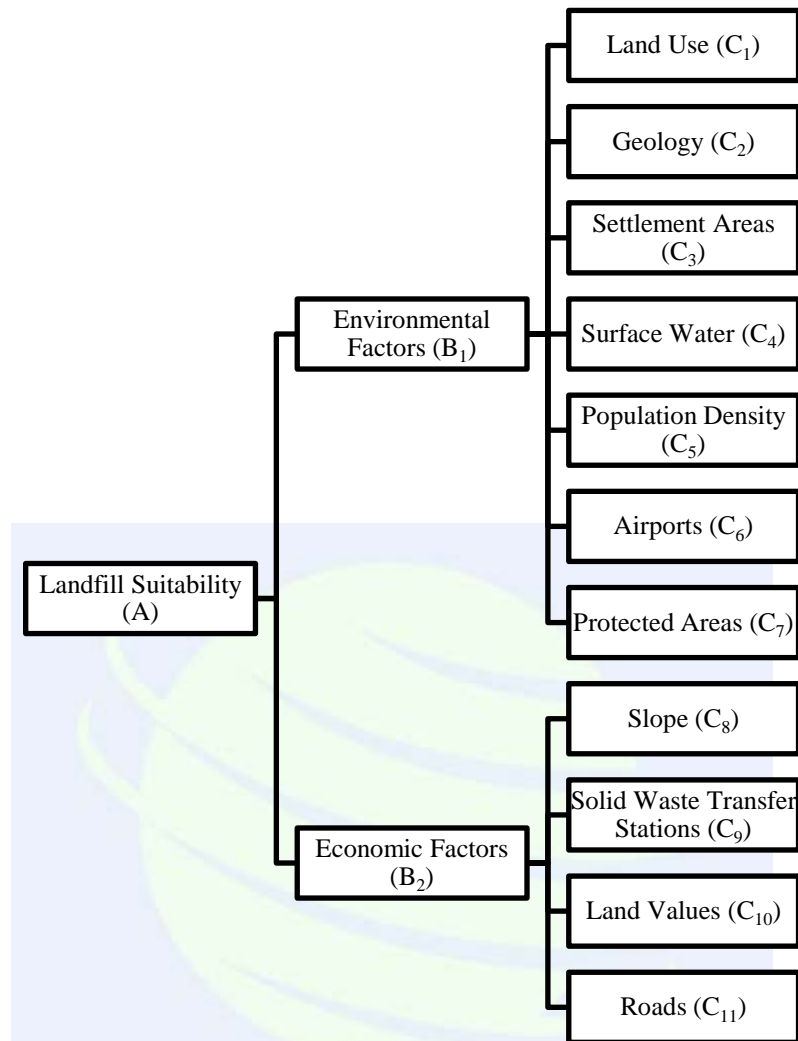


Figure 2. Hierarchy model of landfill suitability.

The geological data for Istanbul was obtained from Orr & Associates, Australia. Data containing population density was obtained from Istanbul Metropolitan Municipality (IMM). The existing airports in Istanbul for the airport criteria and the coordinate information for the new airport planned for operation in 2018 were obtained via Google Maps and the layer to be used was created by transferring to the GIS environment. Spatial data for protected areas in Istanbul were obtained from the General Directorate of Nature Conservation and National Parks. The slope classes were formed by analyzing the digital elevation model of ASTER fitting in GIS. Data on solid waste transfer stations in Istanbul have been obtained from IMM Waste Management Directorate. Information including land values was created by processing and adapting the data shared by the Revenue Administration. Data for roads have been obtained from the EU project named Trans-Tools. In the study, each set of geographic data corresponding to each criteria was produced separately and subjected to spatial analyzes. The weight matrix for the criterion is shown in Table 1.

Table 1. Criteria weights of all factors.

Goal A	Hierarchy B	Hierarchy C	W
A	B1	C1	0.10477125
		C2	0.08172525
		C3	0.13240050
		C4	0.14761500
		C5	0.04514850
		C6	0.11738175
	B2	C7	0.12095775
		C8	0.13515775
		C9	0.06337700
		C10	0.02935350
		C11	0.02211175

Since the Consistency Ratios (CR) obtained in the comparison matrices formed in the AHY are below the desired value of 0.10 in the theorem, the calculated weights can be evaluated and used significantly.

The "Model Builder" module included in the ArcGIS software used in the study has created a model for the landfill site. The model is prepared according to the instructions used in the study. Different studies will be able to perform site selection with different criteria using the same model.

RESULTS

In this study, using the 11 criteria, the most suitable alternative landfill site for Istanbul was selected. With the help of GIS-enabled spatial analysis, result maps in raster data format have been produced. In the study, the pixel size was taken as 30X30 meters. Areas obtained as a result of analysis; classified as unsuitable, less suitable, appropriate and very appropriate. In the light of legal restrictions, 80% of the study area is classified as unauthorized area. 1% of the study area is not suitable, 4% is less suitable, 13% is suitable and 2% is very suitable. As a result of the evaluations, the most suitable area in terms of land use and environmental conditions was determined as Silivri district of Istanbul near E-80 highway and Çerkezköy districts. The presence of a highway near the area will also reduce costs for solid waste transported from stations. The area is far away from settlements. Figure 3 shows the current Silivri Yemen Landfill Site opened in 2016 near the area indicated by number 1. As it is aimed to find alternative sites for the future, area 1 has a high degree of suitability when the other existing fields lose their function.

A total of three landfill sites are currently operating in Istanbul. These are Kömürcüoda on the Anatolian side and Odayeri and Silivri Seymen on the European side. The landfill sites that are in use are made to service by choosing the location according to the environmental and legal features in the construction years. Whether or not the existing landfill sites are included in, the appropriate areas found in the results obtained in the study are also examined. İstanbul-Odayeri landfill site is located within the appropriate region obtained as a result of the work. The Silivri Seymen landfill site is in the forest area from the

characteristics of land use in operation. For this reason, there are areas classified as unauthorized areas in the study. The current site is located at a very short distance to the appropriate areas obtained in the study. The landfill site in Kömürçüoda is also located in the forested area like Silivri Seymen and is not allowed. The area where the landfill site is located in Kömürçüoda very close to the less appropriate classification obtained in the study.

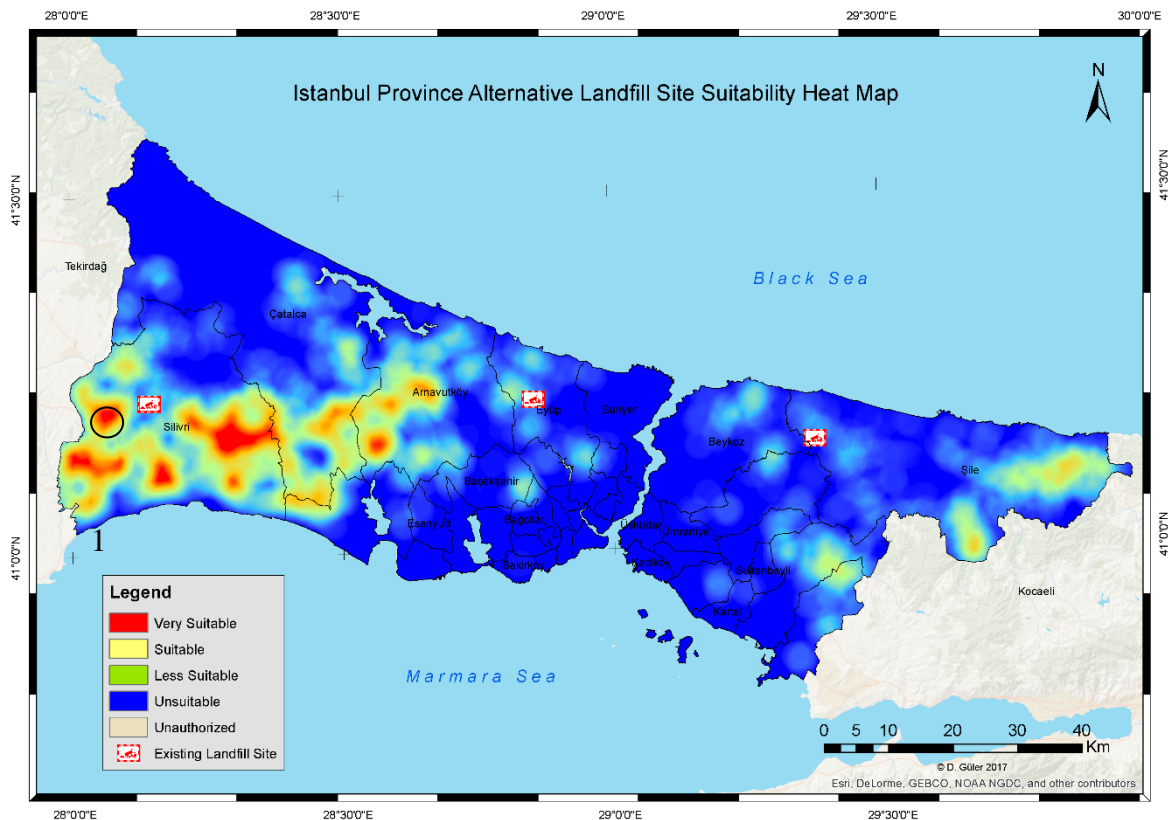


Figure 3. Istanbul province alternative landfill site suitability heat map (Guler, 2016).

The pixel values of the data used in the study and the pixel size according to the studies in the literature were chosen as 30X30 meters. Analysis results were obtained by transforming the data of the criteria of highways, airports, solid waste transfer stations and protected areas in the vector data format into raster data of 30-meter pixel size. The model was resampled and the model was resumed by selecting the pixel size 100X100 meters. When the result data generated by the model is examined, it is seen that the classification values generated by the 30-meter pixel size are very close to the 100-meter pixel result of the percentages in the study region.

In the AHP approach, environmental criteria were calculated at 75% and economic criteria at 25%. These weights determined by examining the studies in the literature were changed in the name of model analysis and the results were also re-evaluated. Considering the creation of an economic scenario, the environmental criteria were taken into consideration as 25% and the economic criteria as 75%, and the weights of the sub-criteria were

recalculated. The model was reworked by recalculating the weights and yielding results for the economic scenario.

CONCLUSIONS

Today, with the rapid population growth, the urbanization process is accelerating and it is seen that the amount of solid waste in social consumption is increased as a natural result. In order to solve the environmental problems that arise in this context, regular storage, which is one of solid waste disposal methods, is preferred. However, the most appropriate location for this purpose is a complex and difficult positional problem for decision makers. In this study, alternative location selection analyzes of the landfill site were carried out with effective analysis capacities of geographic information systems. By creating a dynamic model with GIS based, it is possible to provide faster and more accurate results. The province of Istanbul is taken as an example and the suitability of the existing landfill sites by the output obtained from the model is examined. It can be seen that in case of work to be done, it can be beneficial by arranging the created model according to the working region or the properties of the data to be used. It has once again been confirmed that GIS is an important tool in solutions to environmental problems with its large volume geographical availability. The GIS-integrated AHP has been found to be an effective decision support method, particularly for the detection of landfill sites.

REFERENCES

- Baba, M.E., Kayastha, P., Smedt, F.D., 2015. Landfill site selection using multi-criteria evaluation in the GIS interface: a case study from the Gaza Strip, Palestine. *Arabian Journal of Geosciences*, 8, 7499-7513.
- Djokanovic, S., Abolmasov, B., Jevremovic, D., 2016. GIS application for landfill site selection: a case study in Pancevo, Serbia. *Bulletin of Engineering Geology and the Environment*, 75, 1273-1299.
- Donevska, K.R., Gorsevski, P.V., Jovanovski, M., Pesevski, I., 2012. Regional non-hazardous landfill site selection by integrating fuzzy logic, AHP and geographic information systems. *Environmental Earth Sciences*, 67, 121-131.
- Guiqin, W., Li, Q., Guoxue, L., Lijun, C., 2009. Landfill site selection using spatial information technologies and AHP: A case study in Beijing, China. *Journal of Environmental Engineering*, 90, 2414-2421.
- Guler, D., 2016. Alternative Landfill Site Selection Using Analytic Hierarchy Process And Geographic Information Systems: A Case Study Istanbul (*In Turkish*), Master Thesis, Istanbul Technical University, Dept. of Geomatics, Istanbul, Turkey.
- Hokkanen, J., Salminen, P., 1997. Choosing a solid waste management system using multicriteria decision analysis. *European Journal of Operational Research*, 98, 19-36.

- Monsef, H.A., 2015. Optimization of municipal landfill siting in the Red Sea coastal desert using geographic information system, remote sensing and an analytical hierarchy process. *Environmental Earth Sciences*, 74, 2283-2296.
- Nascimento, V.F., Yesiller, N., Clarke, K.C., Ometto, J.P.H.B., Andrade, P.R., Sobral, A.C., 2017. Modeling the environmental susceptibility of landfill sites in California. *GIScience & Remote Sensing*, 1-21.
- Ngoc, U.N., Schnitzer, H., 2009. Sustainable solutions for solid waste management in Southeast Asian countries. *Waste Management*, 29, 1982-1995.
- Sadek, S., E Fadel, M., Freiha, F., 2006. Compliance factors within a GIS -based framework for landfill siting. *International Journal of Environmental Studies*, 63, 71-86.
- Shahabi, H., Keihanfard, S., Ahmad, B.B., Amiri, M.J.T., 2014. Evaluating Boolean, AHP and WLC methods for the selection of waste landfill sites using GIS and satellite images. *Environmental Earth Sciences*, 71, 4221-4233.
- Sumathi, V.R., Natesan, U., Chinmoy, S., 2008. GIS-based approach for optimized siting of municipal solid waste landfill. *Waste Management*, 28, 2146-2160.
- Şener, Ş., Şener, E., Nas, B., Karagüzel, R., 2010. Combining AHP with GIS for landfill site selection: A case study in the Lake Beyşehir catchment area (Konya, Turkey). *Waste Management*, 30, 2037-2046.
- Vasiljevic, T.Z., Srdjevic, Z., Bajcetic, R., Miloradov, M.V., 2012. GIS and the Analytic Hierarchy Process for Regional Landfill Site Selection in Transitional Countries: A Case Study From Serbia. *Environmental Management*, 49, 445-458.
- Yal, G.P., Akgün, H., 2013. Landfill site selection utilizing TOPSIS methodology and clay liner geotechnical characterization: a case study for Ankara, Turkey. *Bulletin of Engineering Geology and the Environment*, 73, 369-388.
- Yıldırım, Ü., Güler, C., 2016. Identification of suitable future municipal solid waste disposal sites for the Metropolitan Mersin (SE Turkey) using AHP and GIS techniques. *Environmental Earth Sciences*, 75, 101.
- Yıldırım, V., 2012. Application of raster-based GIS techniques in the siting of landfills in Trabzon Province, Turkey: a case study. *Waste Management & Research*, 30, 949-960.
- Yomralıoğlu, T., 2000. Geographical Information Systems Basic Concepts and Applications (*In Turkish*). Seçil Ofset, Trabzon.

Design and Development of a Spatial Advertisement Tax System

Hicret Gürsoy Sürmeneli^{*1}, H. Ebru Çolak² and Mehmet Alkan¹

¹ Department of Geomatics Engineering, Yildiz Technical University, Davutpasa Campus, 34220, Turkey. e-mail: hsurmen@yildiz.edu.tr

² Department of Geomatics Engineering, Karadeniz Technical University, Kanuni Campus, 62080, Turkey

ABSTRACT

The advertising method that is most connected with urbanization is outdoor advertising which involves the publicity of products in various forms such as billboards, posters, screens, totem, zeppelin as well as through the press organs in the city. In addition, advertising elements are considered a part of city furniture. Therefore the design and implementation of outdoor advertisement should be aesthetically, environmentally and culturally aware to preserve the historical and cultural particularities of the areas and prevent pollution. The most important feature that distinguishes the advertising elements from the city furniture is that it is rented by the relevant municipality to obtain advertising revenue. However, there is no standard in advertising revenue collection and archiving systems of related municipalities in Turkey. The geographical locations of the advertising elements are not available in the municipal databases. The problems also arise in the control part of the advertisement elements with the declaration given for getting advertisements. For this purpose, this study aimed to bring a different perspective to archiving the advertisement data and monitoring the advertisement tax. All parameters were found to respond to positional queries and were visualized on the map. Considering all these problems, a database design has been realized in which spatial queries can be made by integrating advertising elements and tax. An interface that works integrated with ArcGIS is designed by Using C # programming language. Through the designed database, it is possible to display in which region the number of the advertisement element is found. Finally, the list of taxpayers with tax debts can be displayed by entering text in any of the fields. The results not only show the tax amount owed by a specific taxpayer, but also give the total tax debt and the number of people that have not paid their tax.

INTRODUCTION

From the past to the present, throughout the course of history, humans have been arranging the environment that surrounds them, building up villages, towns and cities. Meanwhile, cultural structure of societies has also been reflected to the cities. Big cities have become the symbols of civilizations. Each society has exhibited its own culture in the city through architectural works of art. Worldwide, changing technologies, altering lifestyles and

^{*} Corresponding Author

therefore the alternating social structure gave way to a variety of urbanization phenomena depending on such socio-economic issues as industrialization, migration and rapid population growth (Korkmaz, 2001). Phenomena of urbanization that change over time can be exemplified with, namely, the Agora, Forum, city squares in the Middle Ages, city squares in the Renaissance, the Baroque city squares and modern squares (Susmus, 1999). In order to build cities that meet the lifestyle of modern societies, designers tend to make research and offer their services to match the needs. For this reason, urban spaces are not merely public spaces open to people but also areas used by urban dwellers for recreational, entertainment and socialization purposes (Kuang et al, 2013). Various studies have been conducted in order to define and most effectively use these spaces. These studies priorly targeted the detection and classification of city squares, as well as their aesthetic conformity with the city and the identification of the issues encountered in city squares and communal areas (Kılıc, 2001; Korkmaz, 2001; Susmaz, 1999; Moughtin, 1992; Holden, 1996). The subsequent studies were directed towards more specific subjects rather than general public areas. In this respect, studies involved with the functionality of urban squares for children, elderly and people with disabilities or with the most convenient use of green spaces, recreational areas, historical artefacts in urban squares were adopted later on (Ocak, 2006; Ergen, 2000; Yavas, 2002; Curran, 1983).

The urban elements that facilitate life and express certain amount of aesthetics in these defined urban areas are the city furniture. City furniture should be known by people, have the quality to meet the physical requirements and serve for safety and comfort of people using them (Altıncekic and Koc, 2003). Additionally, city furniture can also be defined as service equipment and structures placed in all outdoor urban spaces with specific functions targeting the users (Hacıhasanoglu, 1991). For this reason, they can be regarded as a whole as systems produced according to certain standards and conditions that aim to serve for the people in the city, facilitate urban life and can be live, dynamic, meet the needs and provide information (Akyol, 2006). Researchers have carried out certain studies for the production of city furniture according to the needs of urban dwellers, their classification, the material used for them, their position at the city squares and their aesthetic conformity with the surrounding area (Akyol, 2006; Hacısalihoglu, 1991; Durmus, 2008; Surmeneli, 2015).

Especially the improper positioning of the advertising elements and information boards has caused positive and negative impacts both on the aesthetics of the cities and the people living in cities (Kartal, 1978). Some of the universities including Brunel, Monash and Nottingham conducted researches on the impact of the roadside and pavement positioning of advertising elements such as large billboards on the drivers and pedestrians. According to researches, more than 10% of accidents are caused by illuminated signs on crossroads or roadsides (Young et al., 2009; Edquist et al., 2010; Crundall et al. 2005; Wallace, 2003; Norgate, 2012). Outdoor venues play a significant role in reflecting the social and cultural structure of a society (Isbir, 1991). Advertisements and promotional elements displayed in various places of the city should constitute a whole with the urban life. Furthermore, advertising should be designed to feature the urban identity without disrupting the urban pattern. Advertising elements of different colours and sizes cause visual pollution resulting

in unhealthy and irregular urbanisation (Yomralioglu and Uzun, 1995). For this reason, advertising elements that are a component of city furniture should be placed correctly on city squares, roadsides and pavements (Surmeneli, 2015).

The advertising method most connected with urbanization is outdoor advertising, which involves publicising products through media such as billboards, posters, screens, totems and zeppelin. Advertising elements that are part of the city furniture consist of fixed and non-fixed road panels, banners, billboards, electric poles, wall roof advertisements, Light-emitting diode and unlit signs, cloth banners and bulletins. The design and implementation of outdoor advertising should be aesthetically, environmentally and culturally aware to preserve the historical and cultural particularities of urban areas and to prevent pollution.

In Turkey, advertisement activities have a commercial dimension for municipalities, which are responsible for the administration of tax revenue. Advertisements generating important income are taxable under the law. The determination, tracking and management of this revenue are extremely important for municipalities. In Turkey, the current relevant regulation ('Regulation on Advertisements and Promotions') needs further revision, as the regulation is insufficient for taxation of advertising elements. In addition, it is necessary to create the visual maps of the existing advertisement elements to determine their optimal positions and to track them easily. While the Directorate of Urban Design controls the advertising elements, advertising taxes are collected by the Directorate of Revenue in Istanbul Metropolitan Municipality. There is no common database system between the two departments. Moreover, a geographical information system (GIS)-aided archiving system is not available.

This study aimed to bring a different perspective to archiving the advertisement data and monitoring the advertisement tax. For this purpose, a positional database based on a geographical information system was created using the advertisement and tax data from a district of Istanbul, Turkey. All parameters were found to respond to positional queries and were visualized on the map.

ADVERTISING ELEMENTS

Advertising elements consist of fixed and non-fixed road panels, banners, billboards, electric poles, wall roof advertisements, Light-emitting diode and unlit signs, cloth banners and bulletins. In Turkey, advertisement activities have a commercial dimension for municipalities, which are responsible for the administration of tax revenue. Advertisements generating important income are taxable under the law. This tax constitutes a significant source of income for municipalities to provide services for their citizens such as urban planning, building construction, transportation, infrastructure and mapping (Geymen and Yomralioglu, 2010). Therefore, the determination, tracking and management of this revenue are extremely important for municipalities. In Turkey, the current relevant regulation ('Regulation on Advertisements and Promotions') needs further revision, as the regulation is insufficient for taxation of advertising elements. In addition, it is necessary to create the visual maps of the existing.

Advertisement elements to determine their optimal positions and to track them easily. While the Directorate of Urban Design controls the advertising elements, advertising taxes are collected by the Directorate of Revenue in Istanbul Metropolitan Municipality. There is no common database system between the two departments. Moreover, a geographical information system (GIS)-aided archiving system is not available. So many problems have been identified in Istanbul Metropolitan Municipality such as the low quality of data and services, slowness, and the concerns about the accuracy of the information and date updated that there is an urgent need for a new system to handle better the recording and use of information. For this purpose, geographical information systems will be used in the framework of Regulation on Advertisements and Promotions rules that define ads elements in outdoor area, which are part of the city furniture and which provide income to the country's economy. It will also be determined by the geographical coordinates of the most suitable advertising area so as not to damage the aesthetic texture of the city. A design has been realized which aims to implement the advertising signboards in a way that will create an integrity in terms of visual aesthetics. In addition, all the parameters were found to respond to positional queries and were visualized on the map.

DESIGN AND DEVELOPMENT OF SYSTEM: A CASE OF ADVERTISING ELEMENTS

The design phase consists of requirements analysis, determination of the study area, determination of data, determination of data types and design. An analysis of the requirements is the first phase of the design and development of a database. This phase involves the determination of the requirements for data collection and queries to create an appropriate database structure (Alkan and Bulut, 2010). They are listed in the order of the items to be used below in accordance with the determined purpose.

- The size and type of the advertising board.
- The location of the hanging advertising signs and their photographs.
- A digital base map of the study area.
- The current unit price list.
- The amount of tax payable by taxpayers.
- Querying and displaying the advertising signs in a specific region on the map.

Displaying the fixed advertising signs on the screen and the map.

Study Area

In this study, Istiklal Street in Beyoglu (Figure 1) was chosen as the study area to design and develop a GIS database. For the creation of the GIS database, Istiklal information related to the location of buildings and road names were obtained from the GIS laboratory in Yildiz Technical University. The attributes of the fixed signboards on the main section of Istiklal Street were obtained from Istanbul Metropolitan Municipality Directorate of Revenue. In addition, the photographs of all signs and buildings in the study area were taken. The attribute data of the advertising signs were matched with the position data of the buildings, and then converted from Excel to DXF (Drawing eXchange Format – file

extension for a graphic image often used with AutoCAD). All the photographs were transferred to the GIS.

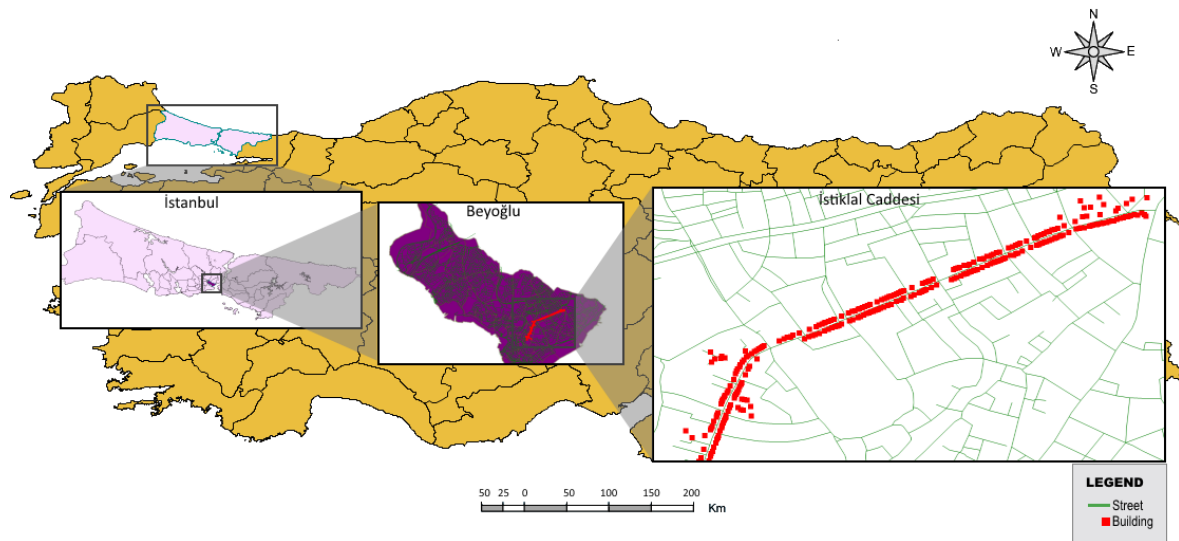


Figure 1. Study area

Determination of Data and Data Types

Geometry types of point, line and polygon can be used in the representation of city furniture. For example, city furniture, which has a closed area such as parks and stations, pools, is represented by a type of polygon geometry. Some city furniture are represented by point geometry type such as Advertisement elements, Electrical poles and bouquets. Finally, elements such as boundary barriers can be represented in the database by line geometry type. Fixed advertising elements will be displayed on the map according to our designed models. This is because it is difficult to determine the location of moving advertising elements such as brochures. The locations of the advertising elements will be marked on the map by their geographical coordinates. The advertising elements will be stored in the point geometry type in the database. A photograph of each advertising element will also be displayed on the map. In addition, the full addresses of the advertising elements will be placed in the database.

Implementation of Design

This package was situated in the following five packed: Locations subject to advertisement tax, Address data, Taxpayers data, Accrual system, Tax credit system. In these packets, many different data were stored in several classes using attribute information such as the AdvertisementLocation ID, Geographical Coordinates, Address ID, AdvertisementWorkPlaced ID, TaxPayer ID and AdvertisemenetLocationPhoto ID. The AdvertisemenetLocation class that allows geo-coordinates of ad elements placed in squares to be shown on the map. The full addresses of the advertising elements are kept in the address class. AdvertisemenetLocationPhoto class which will display the photo of the advertising elements on the map. It is the TypeofActivity class in which the types of

advertising elements (board, digital led, etc.) are kept. The municipality responsible for the advertising element is the *AdvertisemenetLocation* class and *AdvertisemenetTaxTable* class where the information of the organizations is kept. Finally, it consists of *Accural* classes in which legislation or legislation that constitutes the basis for placing advertising elements in the outdoor is included. The classes were located at the ends of the relationship between 0 .. * 1 .. * 1 and were represented by the multitude of expressions. Figure 2 presents the main packages in the database design with their relationships.

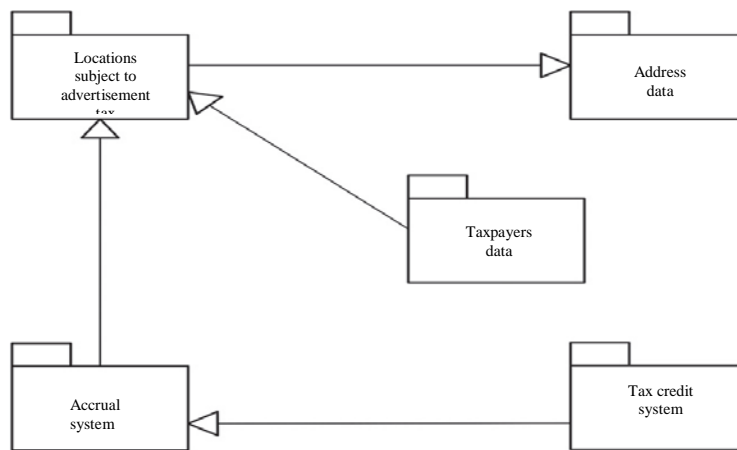


Figure 2. Overview of database design

Development of the Interface Design

On the basis of the results of requirement analysis, the database design was created using an entity-relationship (ER) model. A relationship between the attribute and spatial data was established over the 'Object_id' (available in all tables). The attribute queries were carried out by way of SQL. When spatial data were involved in the query, ArcMap was used. Some of the important queries for design are given in Figures 3 and 5. These queries help municipalities easily monitor and manage the data. In this study, the application interface was designed using the C# programming language in the MS Visual Studio (Microsoft Visual Studio) development environment. Windows Forms were utilised to create user interface elements. MS SQL Server was chosen as the database management tool. The application data model designed.

TESTING THE DESIGN

The proposed application allows displaying the advertising elements in a specified area (Beyoglu, Hüseynaga) according to the type of advertisement. Demonstration of advertisement signs and tax debts for business places which have the same activity in a region. The produced map is presented in Figure 3.

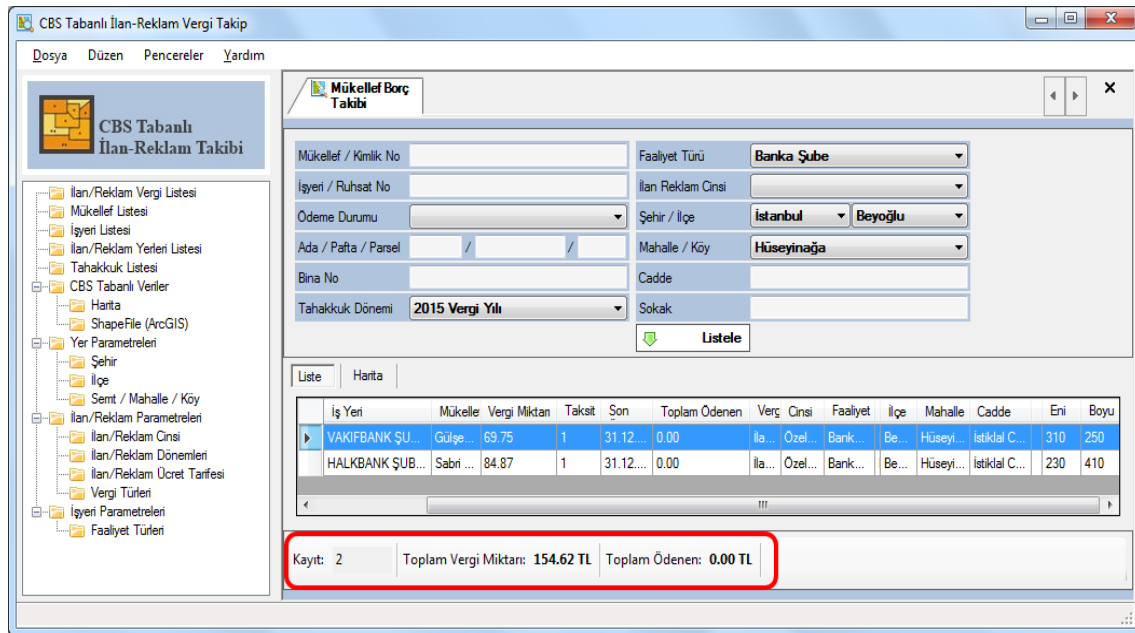


Figure 3. Representation of advertisement sign of the same activity in a region.

In the second example, a subtype of the advertising elements on a street was selected and a query was made. There are 10 DigitalLEDs on that street. Displayed on the map of signs classified by the type of advertisement in a specific region. The produced map is presented in Figure 4.

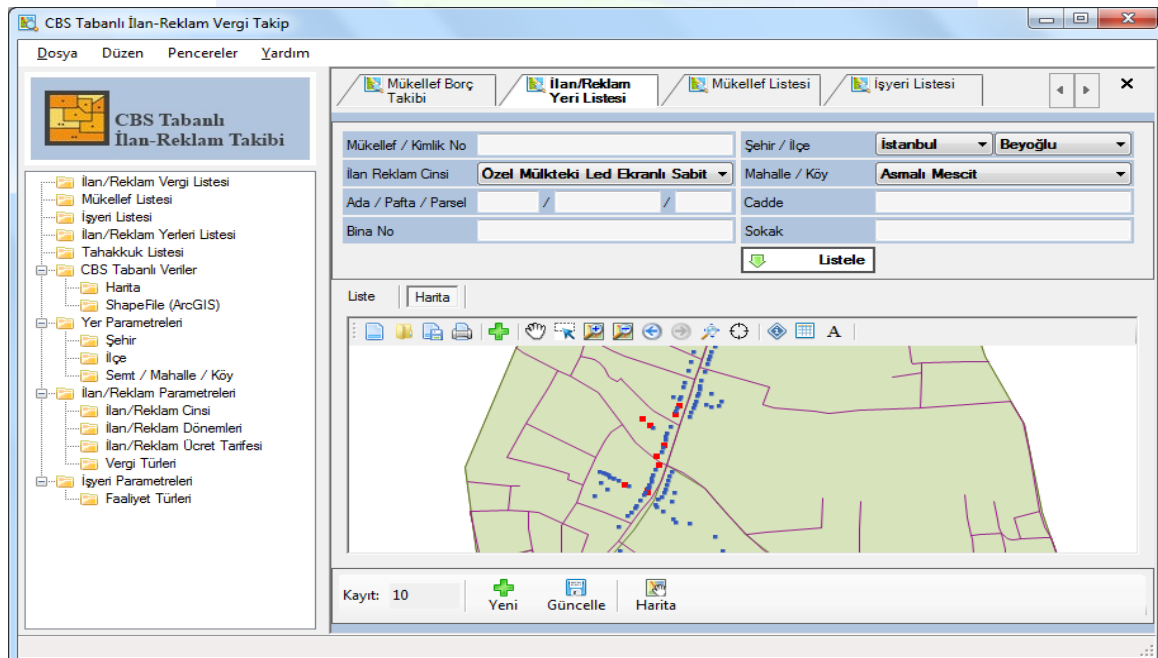


Figure 4. Light-emitting diode advertising displays in Asmalı Mescit.

In the last example, a photo of any selected advertising elements such as sign can be displayed (Figure 5).

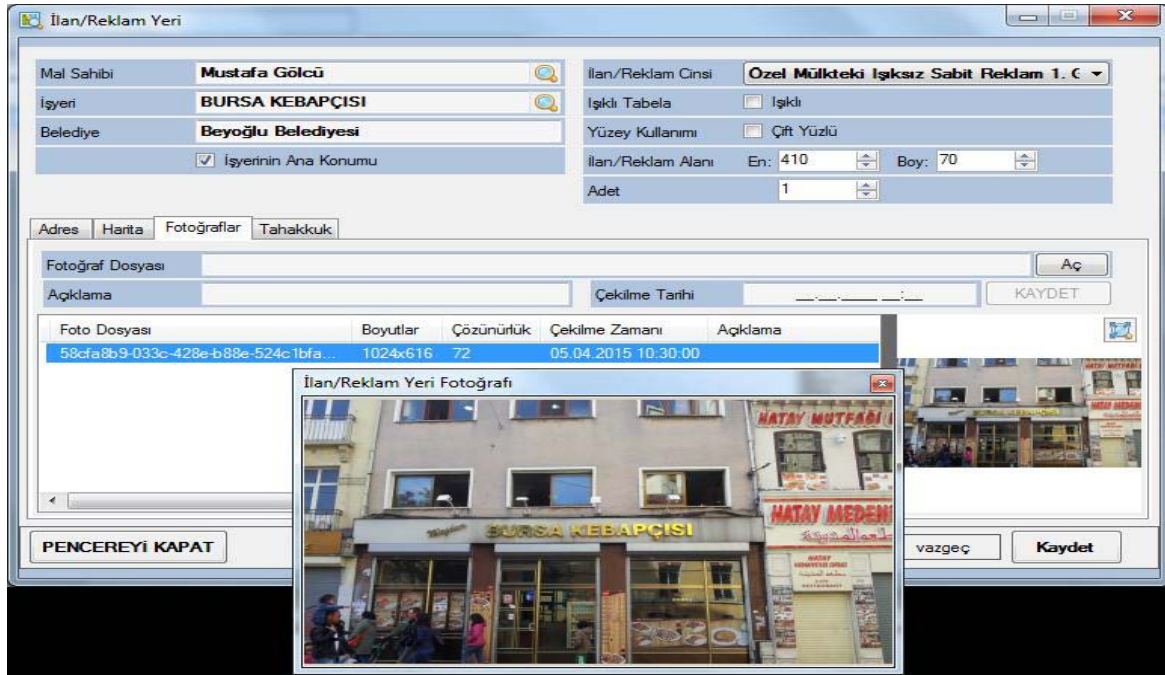


Figure 5. Displaying the photograph of the advertising sign on the screen.

RESULTS AND RECOMMENDATIONS

The city furniture is the smallest part of the city that should be in an aesthetic harmony with the city. Studies related to urban furniture have been examined within the scope of our studies. In our studies, a design has been realized for the advertising elements which are part of the urban furniture in the direction of the existing data. The first objective of this study was to reduce the problems regarding the monitoring of the advertising tax payments. The second purpose of the design is to display the advertising elements on the map with photos and geographical coordinates. In addition, the design can be query according to the region, street and advertising elements. The analysis results obtained by system design and application in this study are given below.

- The system used by the municipality is difficult to control signboard data and check the tax. This situation is also causing time loss. But, with this designed system, all the advertising signboard data will be kept in the system in a totally. It will also be able to respond to many queries.
- It is also possible to display all the advertisement signs on the map by associating the advertisement sign data with the current map. This will ensure that the location and address of the boards will be correctly and quickly detected.
- Organizations that need signboard data for a particular area have to wait a long time due to the current system when they request data to the municipality. Apart from official correspondence, the selection of the requested data from the existing system causes both the need for more staff and the waste of time. However, the designed system allows field or street-based interrogation for signage data. So that in a very short time the desired data is obtained in a more healthy way.

- Advertising signs with photos of the declaration during the application can be kept in a system designed with matched ad spaces. When a query is made, the location of the advertisement is shown both on the map and the photograph where the hanging is showed can be displayed on the screen.
- In addition, the billboard can be photographed and transferred to the system. In this way, it is possible to check the correctness of positioning by comparison with the photographs given on the front or the accuracy of information given to the brain (without light, without light etc.).
- Finally there is no standard among the regulations. Different standards are applied by each municipality. In this case, the advertising elements disturb the integrity in terms of elements.

Some things need to be evaluated for the paper that can be done in the continuation of this study is available. These particulars are given below.

- In this study it is only intended to be questioned on the map, maintaining a database of advertising elements. However, the design can be elaborated further and all city furniture can be kept in a common database and questioned.
- In addition, city furniture is placed by different institutions with different regulations. Each institution has different methods to keep the city furniture with its own data. This situation both damages the aesthetics of the city and makes data sharing between the institutions difficult.
- For this purpose, a unique legislation for all city furniture should be established. City furniture should be placed in the areas in accordance with the legislation to be formed. In addition, city furniture maps should also be created.

REFERENCES

- Akyol, E., 2006. *Kent mobilyaları tasarım ve kullanım süreci*. MSc thesis, Istanbul Technical University Graduate School of Natural and Applied Sciences, Istanbul Turkey.
- Altincekic, H., and Koc, H., 2003. Peyzaj tasarımında kent mobilyaları ve kalite beklentileri. *II.Uluslararası Kent Mobilyaları Sempozyumu*, Istanbul, Turkey.
- Crundall, D., Loon, E.V., and Underwood, G., 2005. Attraction and Distraction of Attention with Roadside Advertisements. *Accident Analysis and Prevention*, 38 (2006) pp. 671–677.
- Durmus, C., 2008. *İstanbul kent mobilyaları üzerine bir araştırma*. MSc thesis, Yıldız Technical University Graduate School of Natural and Applied Sciences, Istanbul Turkey.
- Edquist, J., Horberry, T., Hosking, S. and Johnston, I., 2010. Effects of Advertising Billboards During Simulated Driving. *Applied Ergonomics*.

- Gursoy Surmeneli, H., 2015. *Implementation and design of geographic information system for tracking advertisement tax system*, MSc thesis, Yildiz Technical University Graduate School of Natural and Applied Sciences, Istanbul Turkey (in Turkish).
- Hacıhasanoglu, I., 1991. Kent mobilyaları. *Teknografik Matbaacılık*, İstanbul, Turkey.
- Norgate, Sarah H., 2012. Accessibility of urban spaces for visually impaired pedestrians. *Proceedings of the Institution of Civil Engineers-Municipal Engineer*, 165(4): pp. 231-237.
- Young, Mark S., Mahfoud, Janina M., Stanton, Neville A., Salmon, Paul M., Jenkins, Daniel P., Walker and Guy H., 2009. Conflicts of interest: the implications of roadside advertising for driver attention. *Transportation Research Part F*.
- Wallace, B., 2003. Driver distraction by advertising: genuine risk or urban myth. *Proceedings of the Institution of Civil Engineers-Municipal Engineer*, Volume 156(3): 185-190.
- Alkan M and Bulut G 2010. GIS and remote-sensing-based urban information system design and development: a case study for Kozlu, Zonguldak. *Scientific Research and Essays* 5(19): 2889–2899.
- Geymen A and Yomralioglu T 2010. Spatial data-based e-municipality applications. *Proceedings of the Institution of Civil Engineers – Municipal Engineer* 163(2):77–88, <http://dx.doi.org/10.1680/muen.2010.163.2.77>.
- Korkmaz, Y., 2001. *Kentsel açık alanların kullanıcılar tarafından değerlendirilmesi: Beşiktaş örneği*. MSc thesis, Istanbul Technical University Graduate School of Natural and Applied Sciences, Istanbul Turkey.
- Moughtin, C., 1992. Urban design: street and square. *Department of Architecture and Planning, University of Nottingham Press*, United Kingdom.
- Susmus, Y., 1999. *Kentsel mekanda estetik değerler*. MSc thesis, Istanbul Technical University Graduate School of Natural and Applied Sciences, Istanbul Turkey.
- Kılıc, A., 2001. *Kentsel açık alanların kullanıcılar tarafından değerlendirilmesi: Kadıköy iskele meydanı ve yakın çevresi*. MSc thesis, Istanbul Technical University Graduate School of Natural and Applied Sciences, Istanbul Turkey.
- Yomralioglu T and Uzun B (1995) İlan ve reklam gelirlerinin arttırılması. *Belediye Dergisi* 12: 36–40 (in Turkish).
- İsbir EG (1991) Kentleşme ve çevre sorunları. *Anadolu Üniversitesi Yayınları*, Eskişehir, Turkey (in Turkish).
- Kartal, K. (1978). “Kentleşme ve insan”. *Türkiye ve Orta Doğu Amme İdaresi Enstitüsü Yayınları*, Ankara.
- Krier, E., 1998. Urban Space. *Academy Edition*, London, England.
- Curran, R.J., 1983. *Architecture and the urban experience*, Van Nostrand Reinhold Company.

- Yavaş, H., 2002. *Özürlülerin kentsel mekanda hareketliliği*. MSc thesis, Istanbul Technical University Graduate School of Natural and Applied Sciences, Istanbul Turkey.
- Ergen, S., 2000. *Sokakların çocuk oyun alanı olarak kullanılabilirliğine ilişkin bir yöntem denemesi: Süleymaniye örneği*. MSc thesis, Istanbul Technical University Graduate School of Natural and Applied Sciences, Istanbul Turkey.
- Ocak, E., 2006. *Istanbul'daki tarihi parkların günümüz kullanım işlevleri açısından irdelenmesi*. MSc thesis, Istanbul Technical University Graduate School of Natural and Applied Sciences, Istanbul Turkey.
- Holden, R., 1996. *International landscape design*. Laurence King, London, England.



Determining Parameters Affecting Residential Real Estate Value and Their Significance Level Using AHP Method: The Case Study of Artvin

Ayşe Yavuz Özalp^{*1} and Halil Akıncı¹

¹*Department of Geomatics Engineering, Artvin Çoruh University, 08100, Artvin, Turkey.
(ayavuzozal@artvin.edu.tr; hakinci @artvin.edu.tr)*

ABSTRACT

In this study, it is aimed to define parameters affecting residential real estate value and their degree of significance in Artvin city center possessing limited landed property and zoning area because of its steep topographical terrain by using one of the widely used methods, Analytic Hierarchy Process (AHP). In identifying suitable parameters for residential real estates selected as the subject of this study, we utilized the list of parameters already determined for all property types within “Land Valuation” prepared as the 4th component of the Land Registry and Cadastre Modernization Project initiated by the General Directorate of Land Registry and Cadastre in 2008. Out of approximately 80 parameters, 41 of them were chosen for this study and an expert group currently working on real estate and appraisal processes in Artvin was consulted to determine parameters and their degrees of significance. A total of 25 parameters -with 14 structural and 11 spatial- were identified as effective on the value of real estates in Artvin. Then, the weights of these efficient parameters were estimated and applied to the sample residential real estates sold in Artvin city center in 2015. The results of valuation for the sample houses were examined with their actual sale prices.

INTRODUCTION

Real estate related activities, such as leasing, sale and purchase, taxation, expropriation, nationalization, privatization and banking, which play significant roles in the economy of a country, are based on being aware of the values of immovable properties (Yılmaz and Demir, 2011; Yalpir, 2014; Emek and Öztürk, 2015). Real estate valuation is the identification of the potential value of a real estate, a real estate project or rights and benefits of the real estate on the day of its appraisal, based on independent and objective measures (Yılmaz and Demir, 2011).

Nevertheless, it is a fact that the real estate market is heterogeneous both for the real estate and for the buyers/sellers and every real estate has some distinctive characters. These distinctive characters result in a different value and pricing of the real estate (Yayar and Demir, 2014). As is known, immovable properties are classified as land and residence

^{*} Corresponding Author

(such as housing, working place etc). Within this scope, residential properties are observed to be the most transacted properties in Turkey when immovable properties are considered as an investment (Türkay, 2015). A total of 1341000 houses were sold in 2016, while in 2015 it was 1289000 (TurkStat, 2017). Therefore, in this study we have focused on residential real estate.

Houses, as symbols of cities, have the characteristics of a cultural artifact in the process of urbanization (Uysal and Yiğit, 2016). Houses are not only shelters but also a relatively profitable investment tool. At the same time, the right to housing is one of the most fundamental human rights.

At this point, a realistic prediction of real estate sales prices is important for buyers/sellers and for those who want to invest in real estate (Bin, 2004); however, it is quite difficult to predict the exact value of a residential real estate because it includes a variety of features (environmental, spatial, structural, quality of materials used inside a house, etc.) that are difficult to measure and gather information about. Consequently, establishing the parameters involved in determining the value of residential real estate and their degree of importance have recently been the subject of many studies (Bin, 2004; Yılmaz, 2010; Yalpir, 2014). Examining these studies reveals that there is no standard for the selection of parameters and their application.

In this context, several scientific and institutional research studies have been carried out in recent years; however, as yet there is no sound basis. One of these studies was the Land Registry and Cadastre Modernization Project (LRCMP) initiated by the General Directorate of Land Registry and Cadastre in 2008 with the support of the World Bank. The Land Valuation Component is regarded as the fourth part of the relevant project. In 2011, a report was published focusing on the work aimed at determining the parameters affecting the value of real estate, according to its type and designating specific standards for this (GDLRC, 2014). Within the scope of the same project, pilot implementations were carried out in Mamak, Ankara and Fatih, Istanbul. It is very important that these studies are extended throughout the country, since it is well known that the parameters affecting the value of real estate are shaped in line with local features.

In this study, our aim was to determine the parameters affecting the value of residential properties in the case study of Artvin Province and their significance level, taking into consideration the parameters of real estate for residential purposes specified within the scope of the LRCMP, using the Analytic Hierarchy Process (AHP) method. In this context, the parameters, which were defined in accordance with the topography and residential features of Artvin Province, were scored by a group of experts who were engaged in housing appraisal for this province, so as to determine the parameters and weights that are effective on housing and subsequently develop a model for their appraisal. This model was applied to 66 residential real estate that were put up for sale in 2015 in Artvin city center and, as the final step of this study, testing its accuracy.

MATERIALS AND METHODS

Determining Parameters Affecting Residential Real Estate Value

The accuracy and consistency of the appraisal studies depend on the accurate construction of the model, which relies on the accurate determination of parameters affecting the value, as well as of their impacts. Therefore, it can be said that the most important step in the real estate appraisal process is the selection of the parameters affecting the value of the real estate and their impact levels.

This study seeks to determine the parameters affecting the value of residential real estate in Artvin city center and their degree of significance, by applying the Analytic Hierarchy Process (AHP). The parameters to be used in this study are selected from the list of parameters already determined for each property type within “Land Valuation Component” prepared as the 4th component of the Land Registry and Cadastre Modernization Project (LRCMP) initiated by the General Directorate of Land Registry and Cadastre in 2008. This project lists approximately 80 parameters that may be influential on the value of the real estate (GDLRC, 2014). In two pilot implementations conducted within the scope of this particular project, a total of 48 parameters were used in Fatih, Istanbul for residential real estates and 46 parameters were used in Mamak, Ankara (GDLRC, 2014).

Likewise, taking into consideration the geographical features and physical structure of Artvin, which was selected as the case study for the present research, 41 parameters are found to be applicable to this study. According to this, the parameters concerning the distance to the sea, subway/metrobus/suburbs/trolleys, shanty settlement and solid waste disposal area were excluded due to the scope of this study. Thus, a total of 41 parameters - 18 of them being structural and 23 of them being environmental- were determined (Table 1).

Table 1. Parameters determined for residential real estate in LRCMP

Structural Parameters (SP_i)			
		SP15 occupancy permit	EP11 distance to elementary school
SP1 position of the flat	SP16 independent unit gross open area		EP12 distance to high school
SP2 type of heating	SP17 number of floors	EP13 distance to university	
SP3 floor	SP18 ownership share	EP14 area of storage space	
SP4 direction of frontage	Environmental Parameters (EP_i)		EP15 slope
SP5 physical condition of the building	EP1 parking area	EP16 distance to bazaar	
SP6 age of the building	EP2 neighborhood	EP17 distance to market place	
SP7 floor area	EP3 development level	EP18 distance to shopping mall	
SP8 number of balconies	EP4 distance to city center	EP19 distance to mosque	
SP9 elevator	EP5 road/street	EP20 distance to hospital	
SP10 number of rooms	EP6 position of the plot	EP21 distance to cultural areas	
SP11 independent hall	EP7 main road facade	EP22 distance to recreation areas	
SP12 number of facades	EP8 distance to main road	EP23 facility management	
SP13 en-suite bathroom	EP9 street width		
SP14 facade material	EP10 distance to bus station		

Determining Weights of Parameters Affecting the Value of Residential Real Estate by Using AHP

The value of real estate is affected by local characteristics and the social and economic structure of the appraisal area, together with the structural and environmental features of the area. Thus, as stated by Kauko (2002), it is important to obtain the opinions of real estate appraisers, who are familiar with the area, in determining the factors and impact levels affecting value. Within this context, 41 parameters, which were understood to be effective on housing, were scored by a group of 10 real estate appraisers working in Artvin and having examined Artvin's real estate market in depth, and the parameters and weights affecting the value, were identified using the AHP method.

The Analytic Hierarchy Process (AHP), one of the Multi-Criteria Decision Analysis (MCDA) methods, is a theory of measurement through pairwise comparisons and relies on the judgments of experts to derive priority scales (Yalpir, 2014). It can be thus said that the AHP is an appropriate method for studies of real estate value, in which many objective criteria are required for consideration in the process of appraisal identification, and is widely used research on real estate (Kryvobokov and Williamson, 2007; Yilmaz, 2010; Yalpir, 2014). In scoring, the preference scale suggested by Saaty is used and a pairwise comparison matrix is created (Saaty, 1980).

In this present study, a three-step application was conducted to determine the parameters and weights influencing the value of real estate. In the first step, by taking the geographical and physical features of Artvin city center into account, the appraisers group scored the 41 parameters listed on a scale of 0-100 with regard to their impact on residential real estate. Analyzing the parameter scores obtained, the group took 16 parameters, the main score for which remained below 50, and excluded these from the study. The study then continued using the remaining 25 parameters.

In the second step, the remaining 25 parameters were divided into two groups according to their qualities as structural and environmental parameters (14 structural and 11 environmental), and the group of appraisers scored these parameters in accordance with the 9-unit scale and pairwise comparisons (Saaty, 1980). Thus, the pairwise comparison matrixes for both the structural parameters (Table 2) and the environmental parameters (Table 3) were created to determine the weights of parameters according to the AHP method. It was found out that the structural parameters are five times important than environmental parameters when these groups were compared. The weights of the structural and environmental parameters were thereby found to be 0.8333 and 0.1667, respectively. The consistency of the pairwise comparisons was analyzed as the final stage of step two. According to this, the consistency rates (CR) for structural and environmental parameters were found to be 0.0665 and 0.0846, respectively. These comparisons are considered to be sensitive in a consistent and acceptable manner, as the CR values that were calculated were found to be less than 0.10 (Saaty, 1980).

Table 2. Pairwise comparison matrix of the structural parameters

0.8333	SP1	SP2	SP3	SP4	SP5	SP6	SP7	SP8	SP9	SP10	SP11	SP12	SP13	SP14	Weights
SP1	1	1	2	3	3	3	3	4	5	5	7	7	9	9	0.1788
SP2	1	1	2	3	3	3	3	4	5	5	7	7	8	8	0.1768
SP3	1/2	1/2	1	2	2	2	2	3	4	4	5	5	7	7	0.1186
SP4	1/3	1/3	1/2	1	1	1	1	2	3	4	6	6	7	7	0.0860
SP5	1/3	1/3	1/2	1	1	1	1	2	3	3	5	5	6	6	0.0792
SP6	1/3	1/3	1/2	1	1	1	1	2	3	3	5	5	6	6	0.0792
SP7	1/3	1/3	1/2	1	1	1	1	2	3	3	5	5	6	6	0.0792
SP8	1/4	1/4	1/3	1/2	1/2	1/2	1/2	1	2	2	4	4	5	5	0.0528
SP9	1/5	1/5	1/4	1/3	1/3	1/3	1/3	1/2	1	2	4	4	5	5	0.0432
SP10	1/5	1/5	1/4	1/4	1/3	1/3	1/3	1/2	1/2	1	4	4	5	5	0.0395
SP11	1/7	1/7	1/5	1/6	1/5	1/5	1/5	1/4	1/4	1/4	1	2	3	4	0.0224
SP12	1/7	1/7	1/5	1/6	1/5	1/5	1/5	1/4	1/4	1/4	1/2	1	3	3	0.0195
SP13	1/9	1/8	1/7	1/7	1/6	1/6	1/6	1/5	1/5	1/5	1/3	1/3	1	2	0.0132
SP14	1/9	1/8	1/7	1/7	1/6	1/6	1/6	1/5	1/5	1/5	1/4	1/3	1/2	1	0.0117

Max. eigenvalue (λ_{\max}) = 15.3567

n=14

Random index (RI) = 1.57

Consistency index (CI) = $(\lambda_{\max} - n)/(n-1) = 0.10436$ Consistency ratio (CR) = $CI/RI = 0.0665$.

Table 3. Pairwise comparison matrix of the environmental parameters

0.1667	EP1	EP2	EP3	EP4	EP5	EP6	EP7	EP8	EP9	EP10	EP11	Weights
EP1	1	2	2	3	3	5	5	7	8	8	9	0.2410
EP2	1/2	1	1	2	2	3	4	6	7	7	8	0.1595
EP3	1/2	1	1	2	2	3	4	6	7	7	8	0.1595
EP4	1/3	1/2	1/2	1	1	2	3	5	6	7	7	0.1083
EP5	1/3	1/2	1/2	1	1	2	3	5	6	6	7	0.1066
EP6	1/5	1/3	1/3	1/2	1/2	1	2	4	5	5	6	0.0729
EP7	1/5	1/4	1/4	1/3	1/3	1/2	1	4	5	5	6	0.0610
EP8	1/7	1/6	1/6	1/5	1/5	1/4	1/4	1	3	4	5	0.0365
EP9	1/8	1/7	1/7	1/6	1/6	1/5	1/5	1/3	1	2	3	0.0226
EP10	1/8	1/7	1/7	1/7	1/6	1/5	1/5	1/4	1/2	1	2	0.0181
EP11	1/9	1/8	1/8	1/7	1/7	1/6	1/6	1/5	1/3	1/2	1	0.0140

Max. eigenvalue (λ_{\max}) = 12.2774

n=11

Random index (RI) = 1.51

Consistency index (CI) = $(\lambda_{\max} - n)/(n-1) = 0.12774$ Consistency ratio (CR) = $CI/RI = 0.0846$

In the third and final step of the study, the attributes of the parameters (sub-parameters), for which the weights were already determined, were scored on a scale of 0-5 by the same group of appraisers. Table 4 shows the sub-parameters as well as the number of residential real estates (n) classified within each sub-parameter.

Taking the local conditions of Artvin into consideration, the weights of the parameters affecting the value of the residential real estate (W_i) as well as the scores of their sub-parameters (S_i) were identified, and a real estate value estimation model (1) was specified for Artvin city center.

$$Score_{AHP} = [0.8333 * ((S_{SP1} * W_{SP1}) + (S_{SP2} * W_{SP2}) + (S_{SP3} * W_{SP3}) + (S_{SP4} * W_{SP4}) + (S_{SP5} * W_{SP5}) + (S_{SP6} * W_{SP6}) + (S_{SP7} * W_{SP7}) + (S_{SP8} * W_{SP8}) + (S_{SP9} * W_{SP9}) + (S_{SP10} * W_{SP10}) + (S_{SP11} * W_{SP11}) + (S_{SP12} * W_{SP12}) + (S_{SP13} * W_{SP13}) + (S_{SP14} * W_{SP14}))] + [0.1667 * ((S_{EP1} * W_{EP1}) + (S_{EP2} * W_{EP2}) + (S_{EP3} * W_{EP3}) + (S_{EP4} * W_{EP4}) + (S_{EP5} * W_{EP5}) + (S_{EP6} * W_{EP6}) + (S_{EP7} * W_{EP7}) + (S_{EP8} * W_{EP8}) + (S_{EP9} * W_{EP9}) + (S_{EP10} * W_{EP10}) + (S_{EP11} * W_{EP11}))] \quad (1)$$

Table 4. Scores of sub-parameters

parameters	sub-parameters	score	n	parameters	sub-parameters	score	n
SP1	front	5	46	EP1	parking garage	5	10
	back side	3	20		parking lot	4	48
SP2	centrally heated	5	65	EP2	absent	0	8
	stove-heated	1	1		Çarşı	5	7
SP3	room heater	2	0		Orta	3	13
	top floor	4	11		Çayağzı	3	8
SP4	below of the top floor	5	12		Dere	2	10
	Intermediate floor	4	38	EP3	Çamlık	4	10
SP5	ground floor	2	2		Balcıoğlu	3	8
	Basement floor	1	3		Yeni Mahalle	3	10
SP6	south, south east, south west	5	18		good	5	23
	east, west	4	35	EP4	medium	3	30
SP7	north east, northwest	2	11		poor	1	13
	north	1	2	EP5	0-500	5	2
SP8	great	5	38		500-1000	4	3
	well	4	15	EP6	1000 – 1500	3	10
SP9	medium	3	8		1500 - 2000	2	21
	uncared	1	5	EP7	2000 – 3000	1	22
SP10	0 (new)	5	43		> 3000	1	8
	1-5	4	6	EP8	road	5	18
SP11	6-10	3	3		street	3	48
	11-15	2	4	EP9	corner	5	50
SP12	16-20	2	5		intermediate	3	16
	≥ 21	1	5	EP10	present	5	9
SP13	0-60	1	1		absent	2	57
	61-80	2	3	EP11	0-100	5	30
SP14	81-100	3	16		100-200	4	6
	101-120	4	14	EP12	200-300	3	8
SP15	121-149	5	24		300-500	2	4
	≥ 150	5	8	EP13	> 500	1	18
SP16	≥ 2	5	37		Single lane one way	2	8
	1	3	28	EP14	Double lane two way	5	58
SP17	absent	0	1		0-100	5	45
	present	5	54	EP15	100- 200	5	10
SP18	absent	0	12		200-300	4	6
	2	2	1	EP16	300-400	3	2
SP19	3	4	20		400-500	2	-
	4	5	37	EP17	>500	1	3
SP20	≥ 5	4	8		0-400	5	35
	independent hall	5	64	EP18	400-800	4	19
SP21	dependent hall	2	2		800-1200	3	7
	1	1	6	EP19	1200-1600	2	2
SP22	2	4	51		>1600	1	3
	3 and 4	5	9				
SP23	1	2	42				
	≥ 2	5	24				
SP24	uninsulated overcoat	2	16				
	Insulated overcoat	5	50				

Case Study

In this section of the study, the model was applied to and tested in Artvin city center. There are a total of seven neighborhoods in the city center area, comprising Balcıoğlu, Çamlık, Çarşı, Çayağzı, Dere, Orta and Yeni Mahalle. Therefore, the material for this study constitutes residential real estates sold in 2015 on the basis of these seven neighborhoods. Firstly, this sales data were obtained from Artvin Directorate of Land Registry for the period between January 1, 2015 and December 31, 2015. According to this data, total of 584 real estate properties (house, office, land, plot etc.) were sold in the city center. As stated by several researchers (Yahşi, 2007; Türkay, 2015), the sales prices registered by Land Registry Directorates are lower than their market value. Therefore, the real estates offered for sale, which were used for residential purposes to include every neighborhood and were able to reach its actual sales value, were selected. Accordingly, the accuracy of the studies will be affected by the use of these registered values, which do not reflect the market. Therefore, in this study, the use of actual sales prices obtained from the residential real estate buyers/sellers through face-to-face interviews was preferred. In this context, a total of 66 residences were selected in proportion to the number of residences put up for sale in each neighborhood, and the data on 25 parameters for each residential real estate detailed above was collected from the relevant institutions and organizations.

In this context, the numbers of the cadastral islands, parcels and independent units (flat), the dates of sales, sales prices and the type of real estates sold were obtained from the Artvin Directorate of Land Registry. Next, the cadastral and the city maps for the study area were accessed from the Artvin Directorate of Cadastre and from the Municipality of Artvin, respectively. The data regarding the environmental parameters was identified from these maps. The distances of the real estate from facilities such as schools and the city center were calculated in meters, based on the roads currently used, which are digitized in the city maps by using ArcGIS 10.2 GIS software. The structural characteristics of the residential real estates were obtained from the Occupancy Permits accessed from the Municipality of Artvin, and from *in situ* observations.

By using all the data acquired, the AHP scores of each residence were calculated using the formula (1) stated above. Then, the sales value of each house, equivalent to AHP unit price, was ascertained by dividing the actual sales prices into the calculated AHP scores (actual sales prices / AHP score). The Pope test was applied for the acquired values, revealing that 3 of the residential values from the data set were found to be incompatible and were accordingly removed from the study. The remaining data set, consisting of 63 residential real estates, were randomly selected and 25 of these were re-ordered as a sample set, while 38 of them were re-ordered to be an appraisal set. Subsequently, the estimated sales prices of the appraisal set were determined using the data acquired from the study sample set (Table 5).

Table 5. Analyzing results for appraisal set with appraisal level and appraisal uniformity

No	Actual Sales Prices	Valuation Prices	Ratio (%)	Ratio-median	No	Actual Sales Prices	Valuation Prices	Ratio (%)	Ratio-median
1	105000.00	131509.96	125	0.2367	20	90000.00	104505.53	116	0.1454
2	75000.00	76167.69	102	0.0002	21	150000.00	127927.05	85	0.1630
3	130000.00	125649.27	97	0.0493	22	120000.00	144936.12	121	0.1920
4	135000.00	152215.12	113	0.1117	23	120000.00	138223.04	115	0.1361
5	135000.00	134403.16	100	0.0202	24	150000.00	148529.64	99	0.0256
6	115000.00	149778.18	130	0.2866	25	165000.00	157322.44	95	0.0623
7	110000.00	142789.21	130	0.2823	26	145000.00	157322.44	108	0.0692
8	110000.00	135676.45	123	0.2176	27	205000.00	160060.02	78	0.2350
9	120000.00	132394.19	110	0.0875	28	170000.00	144653.17	85	0.1649
10	155000.00	152459.16	98	0.0322	29	165000.00	157166.81	95	0.0633
11	100000.00	127997.79	128	0.2642	30	145000.00	147323.55	102	0.0002
12	140000.00	153728.92	110	0.0823	31	160000.00	144433.88	90	0.1131
13	125000.00	143188.88	115	0.1297	32	135000.00	143111.07	106	0.0443
14	115000.00	141137.47	123	0.2115	33	160000.00	149541.20	93	0.0812
15	105000.00	144706.22	138	0.3624	34	185000.00	143899.81	78	0.2380
16	155000.00	133625.04	86	0.1537	35	130000.00	141501.77	109	0.0727
17	159000.00	159172.25	100	0.0147	36	150000.00	136567.76	91	0.1053
18	140000.00	140893.42	101	0.0094	37	180000.00	148710.02	83	0.1896
19	135000.00	151691.65	112	0.1078	38	225000.00	165857.04	74	0.2787
Median		Arithmetic Average		Weighted Average		COV		COD	PRD
1.0158		1.0432		1.0144		0.13		13.05	1.03

At this point, it is important to control at what rate the estimated sales values reflect the specified actual sales values. Consequently, a ratio study, as applied in the literature (Yılmaz, 2010; Yılmaz and Demir, 2011; IAAO, 2013; Kim and Kim, 2016), was used. A ratio study is a general concept to evaluate the appraisal success in sales-based studies (Yılmaz and Demir, 2011). In order to measure the success of the appraisal study conducted within the scope of this study, the appraisal level and appraisal uniformity were analyzed. The **appraisal level** is the ratio of the value estimated through the AHP to the actual sales value, thus revealing how close the estimated value is to the sales value. Central tendency measurements, which were calculated as median, arithmetic and weighted averages, are used to determine the appraisal level. **Appraisal uniformity** indicates the consistency of the estimated values. In other words, it indicates that at what rate the real estates, of which the appraisal was made, gets closer to their sales values and in which direction the deviation from the sales values lie. In determining the appraisal uniformity, the coefficient of dispersion (COD), coefficient of variation (COV) and price related differential (PRD) are used.

In this context, after analyzing the appraisal models from the perspectives of the appraisal level and uniformity, it can be concluded that the appraisal level is acceptable and uniformity has been achieved, due to the fact that the analyzed data is at the same standard as that set by the IAAO (2013); the COD values under the title of Single-family

residential- Older or more heterogeneous areas are between the range of 5-15; central tendency measurements are between the range of 0.90-1.10; and PRD value is between the range of 0.98-1.03. In conclusion, the appraisal model can be said to be usable as a result of the rate study.

FINDINGS AND RESULTS

According to the overall examination of the results, 25 out of 41 parameters (Table 1), which were determined by taking into consideration the estimated parameters for residential real estates within the scope of the LRCMP, were determined to be effective on Artvin-specific real estates. These 25 parameters were analyzed in two groups, as structural and environmental, and their weights were determined in accordance with expert opinions. Accordingly, the three most important structural parameters out of 14 (Table 2) were found to be as follows: position of the flat (SP1; 0.1788), type of heating (SP2; 0.1768) and floor (SP3; 0.1186), respectively; while, the three least important parameters were facade materials (SP14; 0.0097), en-suite bathroom (SP13; 0.0110) and number of facades (SP12; 0.0195), respectively. Likewise, the three most important environmental parameters out of 11 (Table 3) were parking area (EP1; 0.2410), neighborhood and development level (EP2-EP3; 0.1595) and distance to city center (EP4; 0.1083) respectively; while the three least important parameters were distance to elementary school (EP11; 0.0140), distance to bus station (EP10; 0.0181) and distance to main road (EP9; 0.0226), respectively. As stated in several studies (Yusof and Ismail, 2012; Ayan and Erkin, 2014; 2015; Daşkıran, 2015), the parameter of distance to city center is reported to be one of the most significant parameters affecting property values. Likewise, the floor parameter, one of the most significant of structural parameters (the storey on which the flat is situated), is among the most important parameters affecting property value in many studies in the literature (Mirasyedi, 2006; Kryvobokov and Wilhelmsson, 2007; Daşkıran, 2015). In contrast, for this study an en-suite bathroom was in the three least important structural parameters; nevertheless, in other studies it has been identified as one of the most significant. Additionally, when Table 3 is analyzed, it can be seen that the impact of parameters such as distance to elementary schools/hospitals/bus station/main road were found to have less influence on residential values. The reason of this may be that Artvin is a small city and reinforcements are located at an accessible distance.

When the structural and environmental parameters are compared, structural parameters are found to be 5 times more important than the environmental parameters ($W_{\text{structural}} = 0.8333$, $W_{\text{environmental}} = 0.1667$); however, in a study by Yalpir (2014), environmental features (0.70) were reported to be more important than structural features (0.30). In this context, it is recognized that each parameter affects the determination of house prices of each province in a different way. This also emphasizes the importance and necessity of carrying out city-based studies.

In the second step of this study, the real estate appraisal model, which was created using the weights and attribute scores of parameters affecting the residential property values in the Artvin case study, was analyzed. In this model, the AHP values of the residential real

estates are determined to be in the range of 2.1535-4.7116, and that 1 AHP score is about TRY 35369.25 when the study sample set is considered. The estimated sales values of an appraisal set (38 houses) were calculated using this value (Table 5). When Table 5 is analyzed, the ratio of appraisal prices/actual sales prices are found to vary between 74% and 138%, and its average is 104%. Likewise, the total of the actual sales prices and the total of the appraisal values are found to be TRY 5314000.00 and TRY 5390776.41, respectively. It can be seen that the values are quite close to each other and the same situation was observed in the study of Yılmaz (2010). In conclusion, the test results of this study can be considered acceptable in terms of the appraisal level and appraisal uniformity in accordance with the standards set by the IAAO (2013), and therefore, the appraisal model can be used.

CONCLUSIONS

In this study, the structural and environmental parameters affecting residential real estate values and their degree of significance in Artvin city center have been determined using the AHP method. In identifying these parameters, we have utilized the list of parameters determined within the Land Registry and Cadastre Modernization Project, initiated by the General Directorate of Land Registry and Cadastre in 2008. Thus, a total of 25 parameters -with 14 structural and 11 environmental- have been identified as effective on the value of residential real estate in Artvin. Subsequently, the weights of these efficient parameters were estimated by consulting a group of experts. Thus, a real estate value estimation model was created for Artvin city center and the estimated sales values of selected real estates were calculated using the weights computed. When the estimated sales values and actual sales prices were compared, the values were observed to be quite close to each other. This situation shows that the appraisal model can be used for Artvin city center. In this context, it is quite significant to expand the real estate appraisal studies by developing them, which were firstly initiated by General Directorate of Land Registry and Cadastre in 2008, of which infrastructure and standards were tried to be settled, however, not built on a solid ground yet, and to designate real estate value maps by urgently determining the parameters affecting the residential value and their significance level on an urban basis, and to serve them all studies which require value. Therefore, the results of this study on the management of the real estate market, could be informative for all actors in the sector, such as real estate owners, real estate agencies and specialists.

REFERENCES

- Ayan, E. and Erkin, H.C., 2014. Hedonic modeling for a growing housing market: valuation of apartments in complexes. *Int. Journal of Economics and Finance*. 6(3): 188-199.
- Bin, O., 2004. A prediction comparison of housing sales prices by parametric versus semi-parametric regressions. *Journal of Housing Economics*. 13, 68-84.

- Daşkıran, F., 2015. Denizli kentinde konut talebine etki eden faktörlerin hedonik fiyatlandırma model ile tahmin edilmesi. *Uluslararası Sosyal Araştırmalar Dergisi*. 8(37): 850-857.
- Emek, M.L. and Öztürk, S., 2015. Taşınmazların satış suretiyle devrinde piyasa fiyatlarının kullanılmamasının kamu gelirleri üzerine etkisi: Adıyaman ili Gölbaşı ilçesi örneği. *International Journal of Social Science*. 39p. 529-539.
- GDLRC., 2014. The Land Registry and Cadastre Modernization Project (LRCMP) Case Study Report, Ankara.
- IAAO., 2013. Standard on ratio studies. International Association of Assessing Officers, ISBN 978-0-88329-208-2.
- Kauko, T. J., 2002. Modelling the locational determinants of house prices: neural network and value tree approaches. PhD thesis, Utrecht, Utrecht University.
- Kim, B. and Kim, T., 2016. A study on estimation of land value using spatial statistics: focusing on real transaction land prices in Korea. *Sustainability* 8, 203, doi:10.3390/su8030203, 1-14.
- Kryvobokov, M. and Wilhelmsson, M., 2007. Analysing location attributes with a hedonic model for apartment prices in Donetsk, Ukraine. *International Journal of Strategic Property Management*. 11(3): 157-178.
- Mirasyedi, A., 2006. An investigation of factors affecting the housing prices case of Üsküdar. Master's Thesis, Istanbul Technical University.
- Saaty, T. L., 1980. *The Analytic Hierarchy Process: Planning, Priority Setting, Resource Allocation*, McGraw-Hill Comp., New York.
- TürkStat., 2017. Population Registration System based on addresses <https://biruni.tuik.gov.tr/medas/?kn=95&locale=tr> Accessed 25 January 2017.
- Türkay, İ., 2015. Gayrimenkul alım ve satımının vergisel boyutları. *Vergi Dünyası Dergisi*. <http://vergialgi.net/makaleler/gayrimenkul-alim-ve-satiminin-vergisel-boyutlari/>
- Uysal, D. and Yiğit, M., 2016. Determinants of housing demand in Turkey (1970-2015): An empirical study. *Journal of Selcuk Uni Vocational School of Social Sciences*. 19(1): 185-209.
- Yahşi, E., 2007. *Housing valuation and examination of the factors affecting the housing prices by using regression analyse*. Master's Thesis, İstanbul Technical Universty.
- Yalpir, S., 2014. Forecasting residential real estate values with AHP method and integrated GIS. In conference proceedings of *People, Buildings and Environment 2014*, an international scientific conference, Kroměříž, Czech Republic, pp. 694-706, ISSN: 1805-6784.
- Yayar, R. and Demir, D., 2014. Hedonic estimation of housing market prices in Turkey. *ERU. Journal of Economics and Administrative Sciences*. 43, 67-82.

- Yılmaz, A., 2010. *Çok ölçütlü karar destek sistemleri ile taşınmaz değerlendirme ve oran çalışması*. Master's Thesis, Yıldız Technical University.
- Yılmaz, A. and Demir, H., 2011. Çok ölçütlü karar destek sistemleri ile taşınmaz değerlendirme ve oran çalışması. *TMMOB HKMO 13. Türkiye Harita Bilimsel ve Teknik Kurultayı*, Ankara, April 18-22.
- Yusof, A. and Ismail, S., 2012. Multiple regressions in analysing house price variations. *Communications of the IBIMA*, DOI: 10.5171/2012.383101.



Spatial Analyses of Accessibility of Urban Transportation Network for Istanbul

Baris Besol^{*1}, Hande Demirel¹

¹Department of Geomatics Engineering, Istanbul Technical University, Ayazaga Campus, 34469, Turkey. e-mail: (besol, demirelha, varolber)@itu.edu.tr

ABSTRACT

Transportation is one of the most important factors that effects our life in every manner and there are also a lot of factors that effecting transportation. Once these factors are identified, using developed methods and GIS, these factors can be analyzed and problems can be discovered thus solutions could be achieved. In this paper, the robustness of the transport network is analyzed via accessibility indicators. Within this study, this robustness is tested via a selected scenario where disruption of the road network due to natural disasters, maintenance or accidents is analyzed and vulnerability is determined on a selected study area in Istanbul, where twelve districts of Istanbul is included. As the network data, the Open Street Map (OSM) is used, which is open source. Furthermore, population statistics per district is utilized that is received from TUIK. Only the main roads have been selected from OSM for analysis and transportation capacities are defined as equal. Using re-edited road data, information about nodes has been derived with setting Arc-Node structure in network analysis. Origin- Destination (OD) matrix is calculated and robustness of the network is determined. The accessibility of road has been tested. As a result of this research, 520km road and 382km² area in test area have been analyzed and accessibility is determined.

INTRODUCTION

Transportation is a challenge for metropolitan cities such as Istanbul. Demand for transportation is high. For obtaining economic development and regional integration, the traffic networks should be designed efficiently and less costly. However, transportation system affects the land use, and changes the eco-social environment. Economic globalization and regional integration require the support of efficient traffic networks to reduce factor costs (Wang, 2017). There are different ways of transportation including roads, seaways, railways, and airways. A physical access to personal possessions, target locations or services is commonly defined as transportation, while it means a relative flexibility to reaching a determined point or are, in the fields of geography and urban

^{*} Corresponding Author

economics. Social planners use this term as individual's capability to use services and opportunities. (Mavoa, 2012). The main 'product' of a transport system is accessibility.

A city's transportation system affects the comfort of travelling and the development of the city. Thus, by improving the social quality, it makes the city more appealing to tourists. To offer a better transportation service to the individuals, the road network must be in equilibrium with the population density. To measure the accessibility is a demanding request because it is hard to meet the people's needs in transportation (Acheampong, 2015; Van, 2015). When accessibility is calculated, the environmental and economic factors are usually taken into account (Murray, 1998). Accessibility is calculated according to these factors and the distances between roads.

In this study, the accessibility of Istanbul urban transportation network is calculated with using open-source geo-data, where only the accessibility on the roads is studied. OpenStreetMaps' (Haklay, 2008) are used and only the main transportation network and crucial roads are determined and used in this project. Additionally, the determined roads are generalized in order to be processed. Origin destination (O-D) flows from traffic counts in a road network are calculated with a one-stage network observer named accessibility (Chen, 2009). We calculated the shortest distance between two different points using O-D COST matrix. Due to the transportation capacity on the test area is not known, all capacities assumed equal in the process. The data gathered from TUIK are district-based. That reduces the precision of this study. Individual's travel behaviors are affected by the population in the business and residential areas in a settlement zone (Etminani-Ghasrodashti, 2016). Population data is used to detect the popularity of different regions. Especially in big metropolises such as Istanbul, there are traffic problems in over-crowded areas. In the calculations, it is assumed that the denser population leads to a worse road accessibility.

The aim of this study is to test robustness of the network, where one scenario is designed for the test. Disruption of the road network due to natural disasters, maintenance or accidents is selected as a scenario and vulnerability is determined on a selected study area that covers twelve districts of Istanbul.

STUDY AREA AND DATA

Twelve districts those have a high density of population and road network in Istanbul are chosen as the study area. The area is 382 km². The road network is denser at some zones compared to the others. Those differences allowed the study to carry out different scenarios. The total length of the road network is 520 km. In order to obtain more precise and systematic results, the district is divided into 1 km x 1 km grid network. Study area and center points of the grids are presented in Figure 1. Besides, the districts and the road network obtained from OSM are shown in figure 2.



Figure 1. Study area and center point of grids.

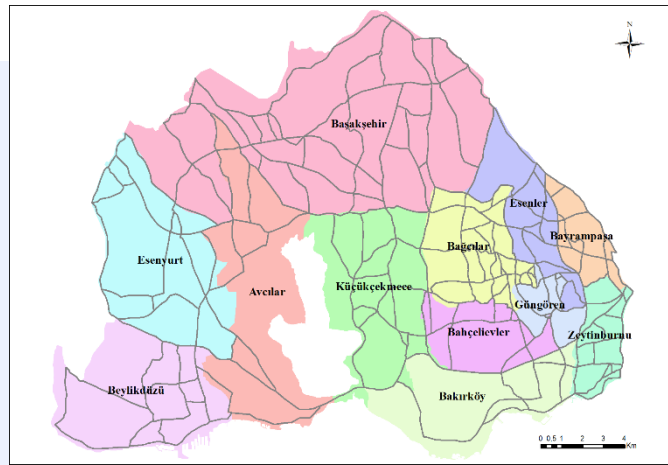


Figure 2. The districts and the road network.

METHODOLOGY

The OD cost matrix used in calculations computes the shortest distance between selected origin and destination points and detects the length of the route. Because all the road capacities and traffic densities are assumed equal, the drivers are thought to choose the shortest road.

To calculate the accessibility, the area is divided into grids. The total number of grids is 298. The shortest distances between the centers of every 2 different grids are calculated. Therefore, the accessibilities of every grid is calculated. Apart from these calculations, the population values of every grid are taken into account and the population data is introduced as a parameter in the accessibility analyses.

After every grid's accessibilities are calculated, some roads are assumed unusable and new accessibilities are calculated. These processes are made with and without using the population data. Therefore, the effects of an unused road on a test area are detected. Since the population data is district-based, the population values of grids are calculated proportionally with the number of grids in a district. Figure 3. Represents the population values of grids. The darkest areas are the most intensely populated areas which are harder to

reach than less populated areas. Table 1 shows the district based populations and the population per grid.

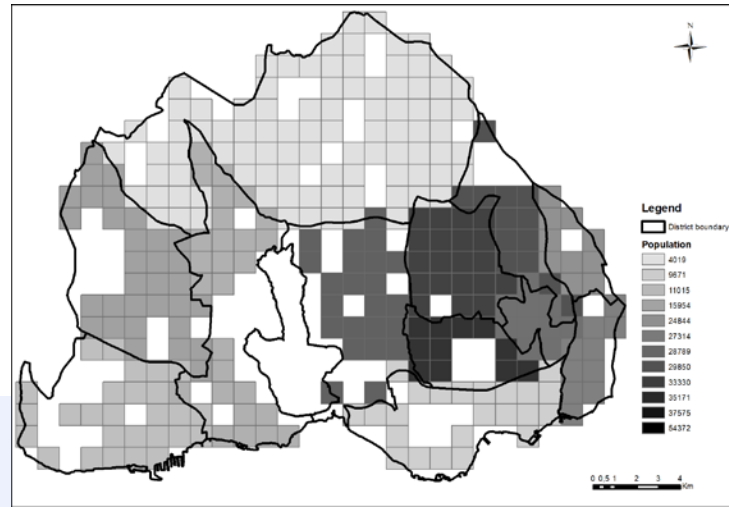


Figure 3. Population of grids.

Table 1. Population of grids and districts.

Districts	Population of Districts	Number of Grids	Population per Grids
Basaksehir	369810	92	4020
Bakirkoy	222437	23	9671
Beylikduzu	297420	27	11016
Avcilar	430770	27	15954
Esenyurt	795010	32	24844
Bayrampasa	273148	10	27315
Zeytinburnu	287897	10	28790
Gungoren	298509	10	29851
Kucukcekmece	766609	23	33331
Esenler	457231	13	35172
Bagcilar	751510	20	37576
Bahcelievler	598097	11	54372
Total	5548448	298	

RESULTS AND DISCUSSION

Following the methodology described, shortest distances between every two different grid is calculated with OD cost matrix and the sum of those values gives the grid's accessibility. Figure 4a. represents the shortest distances. It can be seen in the figure that the

accessibility reduces as moving away from the center of the grid. Additionally, the results with the population included can be seen on Figure 4b. Because the population is calculated approximately, the calculations are made with new coefficients. These coefficients are distributed proportionally to make the most populated grid value to be half of the least populated grid value. Thus, with the population effect, the accessibility is reduced in the most densely populated areas.

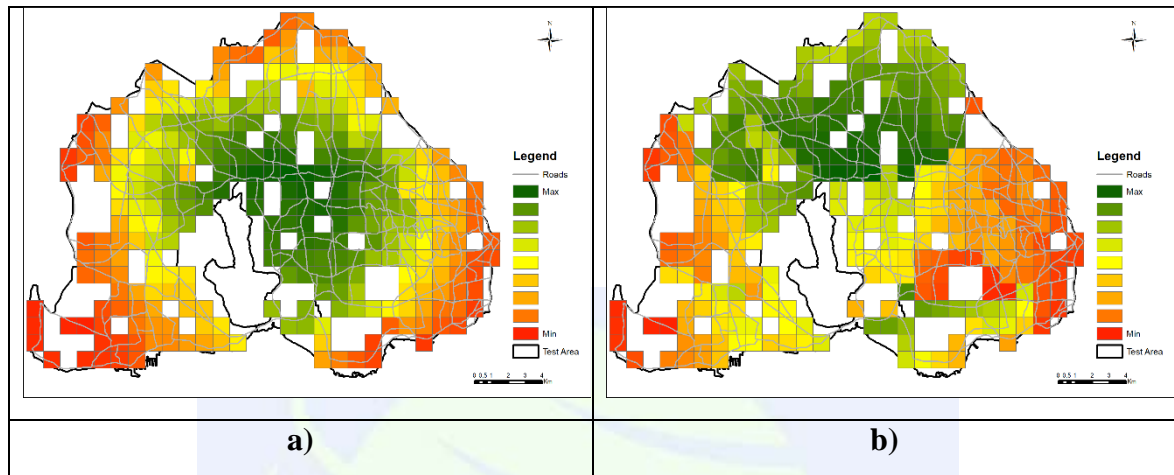


Figure 4. Results of accessibility.

The effect of a removed road to the grids' accessibility is investigated. The calculations are made by removing two different roads one by one. The results are obtained from the shortest distances calculated with and without the population effect. The achieved results should be handled cautiously, where the results depend upon the assumptions pre-described in this manuscript.

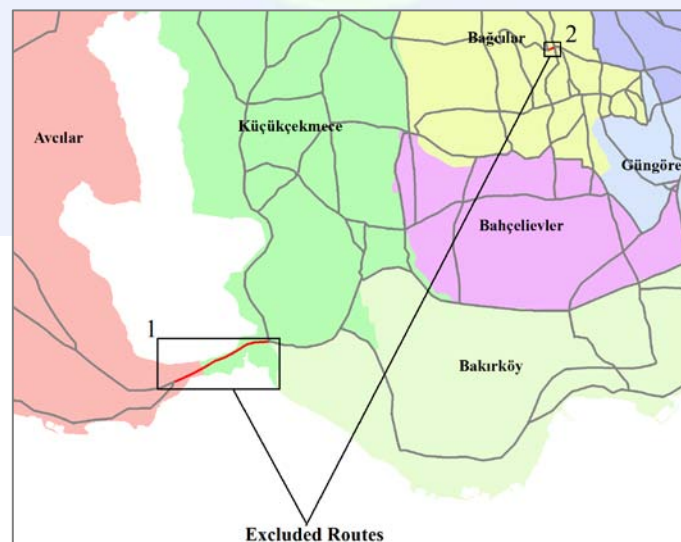


Figure 5. Excluded routes.

Figure 5. shows the removed roads. Road 1 is an important road that has no alternative in the network. Road 2 is a road with an alternative in it's area. This situation weakens the importance of the road 2.

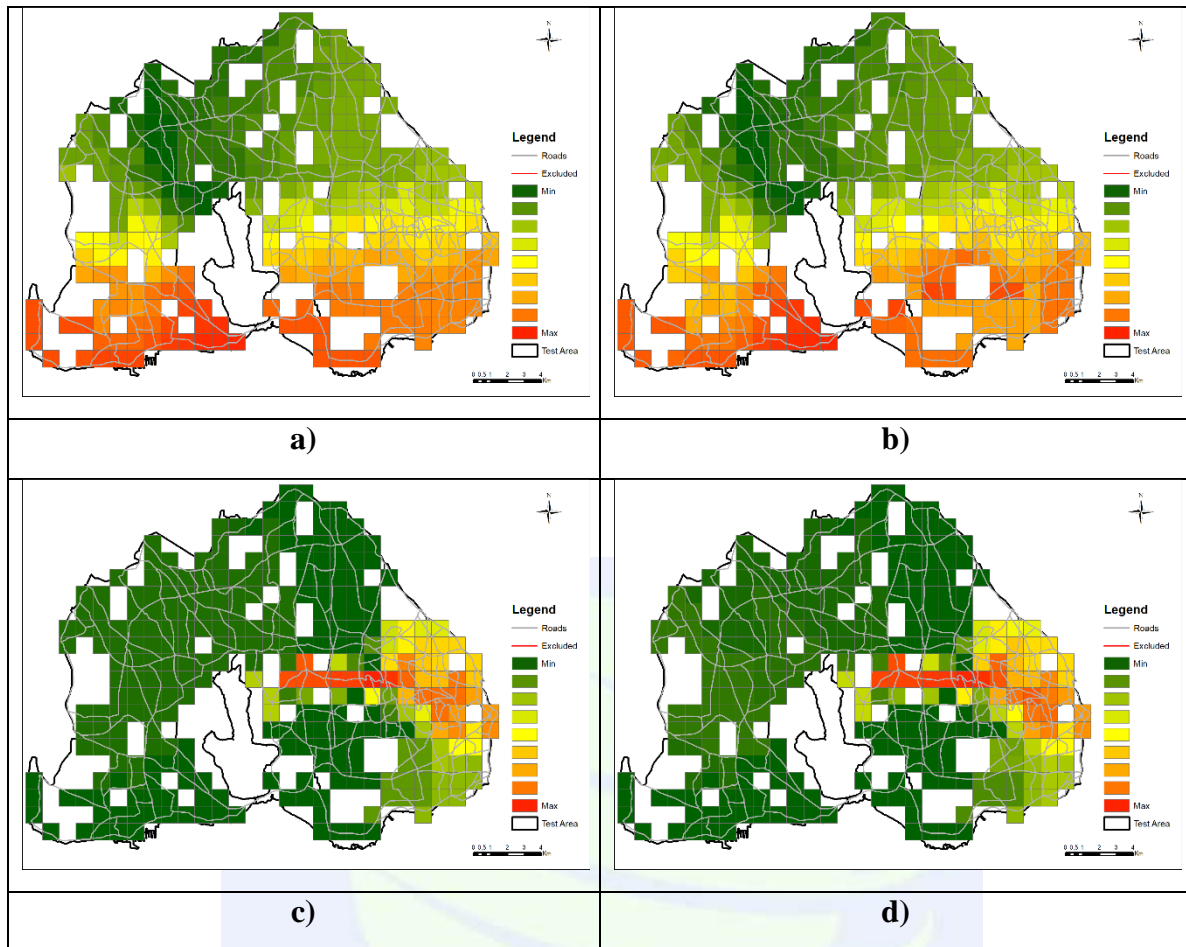


Figure 6. Result of vulnerability.

The system's response to road 1 being taken off is shown on Figure 6a. The red grids show the most vulnerable areas and the green grids show the least vulnerable areas. Also, figure 6b. illustrates the results of road 1 being removed with population effect included. The response of the neighborhood of the removed road is affected most highly.

On the road 2, similar to road 1, the effect is steadily decreased moving from the center to the other zones. This is demonstrated on Figure 6c. With the population effect, the results are illustrated on Figure 6d.

Table 2. Results of extra distance.

	Extra Distances (km)	Extra Distances (%)	Max Distance (km)	Min Distance (km)	Unaffected Number of Grids
1	73492.1	5.75	221.2	0	13
2	328.6	0.025	64.4	0	113

Table 2 shows the system's change. These results show the extra distances, most, least and non-affected grid numbers when roads 1 and 2 are excluded from the system. The accessibility reduced proportionally with the extra distances. The decrease in accessibility is %5.75 and %0.025 respectively, when road 1 and road 2 were taken off from the transportation network.

CONCLUSIONS

In this study, by using shortest distances calculated with OD cost matrix the accessibility values are determined. To make a more comprehensive result, every grid in the grid network should be evaluated and critical elements should be identified. There are many reasons that affect the operational accessibility. The results show that accessible areas are both central and less populated regions. Besides, the critical importance of a road can be calculated with the extra distances, in the case of that road being eliminated from the system.

ACKNOWLEDGMENT

The authors would like to thank to Turkish Statistical Institute for sharing 1km*1km population data of the study area.

REFERENCES

- Acheampong, R.A. and Silva, E., 2015. Land use–transport interaction modeling: A review of the literature and future research directions. *Journal of Transport and Land Use*, 8(3).
- Chen, A., Chootinan, P. and Recker, W., 2009. Norm approximation method for handling traffic count inconsistencies in path flow estimator. *Transportation Research Part B: Methodological*, 43(8), pp.852-872.
- Etminani-Ghasrodashti, R. and Ardeshiri, M., 2016. The impacts of built environment on home-based work and non-work trips: An empirical study from Iran. *Transportation Research Part A: Policy and Practice*, 85, pp.196-207.
- Haklay, M. and Weber, P., 2008. Openstreetmap: User-generated street maps. *IEEE Pervasive Computing*, 7(4), pp.12-18.
- Mavoa, S., Witten, K., McCreanor, T. and O'sullivan, D., 2012. GIS based destination accessibility via public transit and walking in Auckland, New Zealand. *Journal of Transport Geography*, 20(1), pp.15-22.
- Murray, A.T., Davis, R., Stimson, R.J. and Ferreira, L., 1998. Public transportation access. *Transportation Research Part D: Transport and Environment*, 3(5), pp.319-328.

- Van Wee, B., 2015. Toward a new generation of land use transport interaction models. *Journal of transport and land use*, 8(3).
- Wang, Z., Xu, G., Bao, C., Xu, J. and Sun, F., 2017. Spatial and economic effects of the Bohai Strait Cross-Sea Channel on the transportation accessibility in China. *Applied Geography*, 83, pp.86-99.





Analysis of Landscape Changes For A Sustainable Urban Decision Making

Anıl Akın¹, Gül Atanur¹

¹*Department of Regional and Urban Planning Department, Bursa Technical University, Yıldırım Campus, 16330, Turkey.*

ABSTRACT

Urbanization is a major driving force of landscape change besides, this change is neither uniform nor constant. Geographical and historical trends should be considered as well as planning scenarios that shape the urban forms.

This study aims to analyse landscape change in terms of sustainability by considering the land use decisions such as master development and environmental plans in Bursa, Turkey. In this frame, subjected study focused on the aforementioned plans plus remotely sensed data between the period of 1924 and 2013. Analyses of urban landscape change are maintained by the comparison of Central Metropolitan Planning Zone plans and land use land cover map acquired by classification of remotely sensed data. Comparisons and assessments were made within GIS (geographical information system). Considerable change was observed especially between the years of 1975-2010. The commercial and industrial areas, mainly housing, have expanded more than 100% between the years 1976 and 2005. Until 2015, 113 km² agricultural area was shifted for urban use. Also, 10 km² area was degraded for agricultural use from the forest areas. The factors such as topography, transportation network, slope and decisions on urban policy were the dominant factors of the spatial growth pattern for the defined time periods. The greater agricultural land loss was observed when development was restricted by the steeper slopes.

The results confirmed that the urbanized landscapes are highly dynamic, complex and multifunctional. Therefore, detailed inventories of landscape conditions and monitoring of change trends are urgently needed in for the sustainability of urbanization.

INTRODUCTION

Urbanization is one of the most pressing environmental issues of our time. Many countries are about to enter an era in which not only the urban population is greater than the rural population, but also the lands occupied by urban expansion compete with the lands for agriculture. Therefore, the main objective of this study is to contribute to the improvement of the sustainable urban planning by integrating multi-temporal- spectral remotely sensed

data with the historic municipality maps to better deal with multi-dimensional components of urban areas.

Landscape monitoring datasets are scarce for many parts of the earth's surface. In situ data is not always available and often have limitations. Earth observation data from spaceborne, airborne and ground-based sensors have a major role to play in improving monitoring systems by providing several types of information. The various phases of environmental policy require up-to-date and synoptic spatial information at various spatial scales on the state of the environment and the extent and magnitude of environmental and policy impacts over larger areas. So, urban observation is well suited for this as a large number of data set relevant to environmental policy can be remotely detected with the integration of municipality maps. Moreover, remote sensing permits repeated and consistent assessment and monitoring of the environment (De Leeuw et al., 2010). It is therefore a powerful tool for monitoring landscape status and change. Change analysis is a fundamental part of any monitoring system providing the mechanism for determining whether policies and actions are having the desired effect. They are also designed to communicate simple and clear messages to decision makers (UNEP, 2013). Land use/ land cover (LU/LC) change in urban areas can contribute to improved management of existing and potential development areas and can also be useful to identify landscape fragmentation and degradation to focus efforts to produce a set of effective land-cover/use scenarios that meet the needs of the urban community. For the study, different dated remotely sensed data and municipality maps such as environmental layout plans (1/100.000), master development plan for the metropolitan area (1/25000) and complete city and immediate plans (1/25000) were compared and overlaid in order to evaluate physical change and policy decisions over the city. Change detection was performed on considering the recent dated images such as 1979 satellite image and 1976 city map in the GIS (Geographical Information Systems) environment. The rate of loss/gain of main land use/land cover classes were identified.

The land use of the Bursa City is intensive and is dominated by agricultural, urban and tourism activities. The use of urban and rural landscaping has varied and therefore cultural landscapes have changed in an unsustainable manner. It is concluded that in order to be able to put forward sustainable urban development strategies, the changes in land use/cover and conflict between the planning scenarios and anthropogenic effects should be analyzed.

MATERIAL AND METHOD

The main materials of the study comprises Bursa Regional maps including: (i) 1/25000 scaled City Plans for the year 1976; (ii) 1/5000 scaled Master Development Plans for the year 1990; (iii) 1/25000 scaled Master Development plan for the metropolitan area for the year 2005 and different dated remotely sensed data including 1979 Corona air photo, 1989 SPOT satellite data and 2013 RapidEye with the 10 m spatial resolution. Different dated and resolutions of data were used for the study area. Therefore, a precise rectification was performed by considering the 2013 RapidEye image and the resolution were resampled to a common cell size of 10 m.

Bursa city and the near environment were subjected to the study. Bursa is located in the southeast of Marmara Region between $28^{\circ} 10'$ and $30^{\circ} 10'$ north latitudes and $40^{\circ} 40'$ and $39^{\circ} 35'$ east longitudes (Anonymous, 2007)(Figure 1). The city of Bursa is the fourth most populated city in Turkey with a population of 2.8 million, of which 1.7 live in the metropolitan municipality.

Bursa is facing with the rapid urban change with the intensive urban regeneration studies that cause the irreversible landscape changes. This subversive process constitutes the main motivation of the study. The reflections of change over time and space were analyzed via city plans and remotely sensed data in the GIS environment. Firstly, all city maps were registered to the UTM WGS 84 coordinate system and rectification was performed according to the orto-rectified remotely sensed data. Traditional digitizing process for the city maps was performed. The areas of LULC classes including current settlement, commercial, industrial, public, potential development area, parks, recreation, forest, zoo, woodlands, cemetery and agriculture were calculated. For the remotely sensed data, supervised classification was performed for the subjected classes.

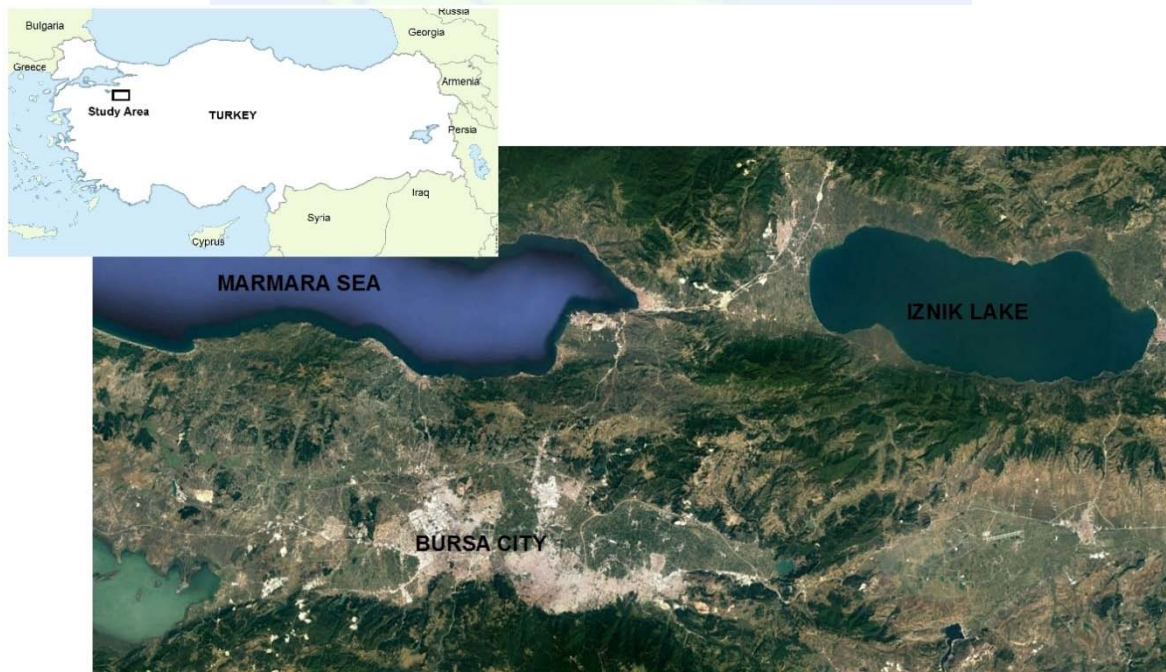


Figure 1. Study Area

After generating the thematic data, some classes were combined and finally three main classes including urban, open area and agriculture were acquired. Urban class was masked out from the classification images for further analysis in order to evaluate comparatively urban development of the Bursa City. The quality and the quantity of urban, open area and agriculture classes were calculated. The city plans are evaluated in three main stages. The first stage displayed the increase of the sizes that are subject to planning. Second stage determined the increase of the urban area uses. The third stage included the comparison of

the separate plans with the remotely sensed data and the analysis of the urban change. However, the quality and the quantity of change was calculated by considering two city maps (1976 and 2005) and remotely sensed data (1979 and 2013). 1968 and 1990 maps and images were only used for the visual interpretation of the urban development trend.

RESULTS

The urban change of the Bursa city was evaluated with the different dated and sourced data in terms of urban sustainability. 1976 complete city and immediate area plan was prepared in the process when Bursa plain was threatened by rapid urbanization, industrialization and shanty establishments and aimed to preserve Bursa Plan which has a high agricultural value. When 1976 plan is compared to Piccinato's Plan, it is seen that the increase in urban area continues by spreading towards east, west, north and northwest (Figure 2)(Atanur, 2011). Piccinato plan was prepared in 1968 and has significantly affected the macro form of the Bursa City. This plan was only used for the evaluation of the urban development due to lack of satellite images belongs to 1960's.

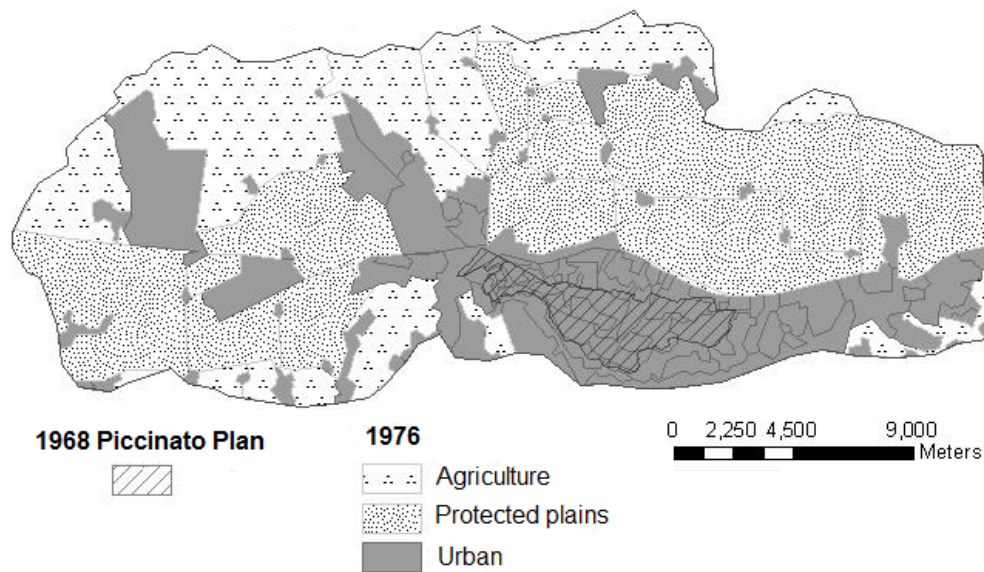


Figure 2. Comparison of the 1968 and 1976 city maps (Atanur, 2011).

The digitization was performed on the 1976 and 2005 city maps. 1979 urban class was masked out from the supervised classification data. The overlay analysis of the mentioned data was given in the fig.3.

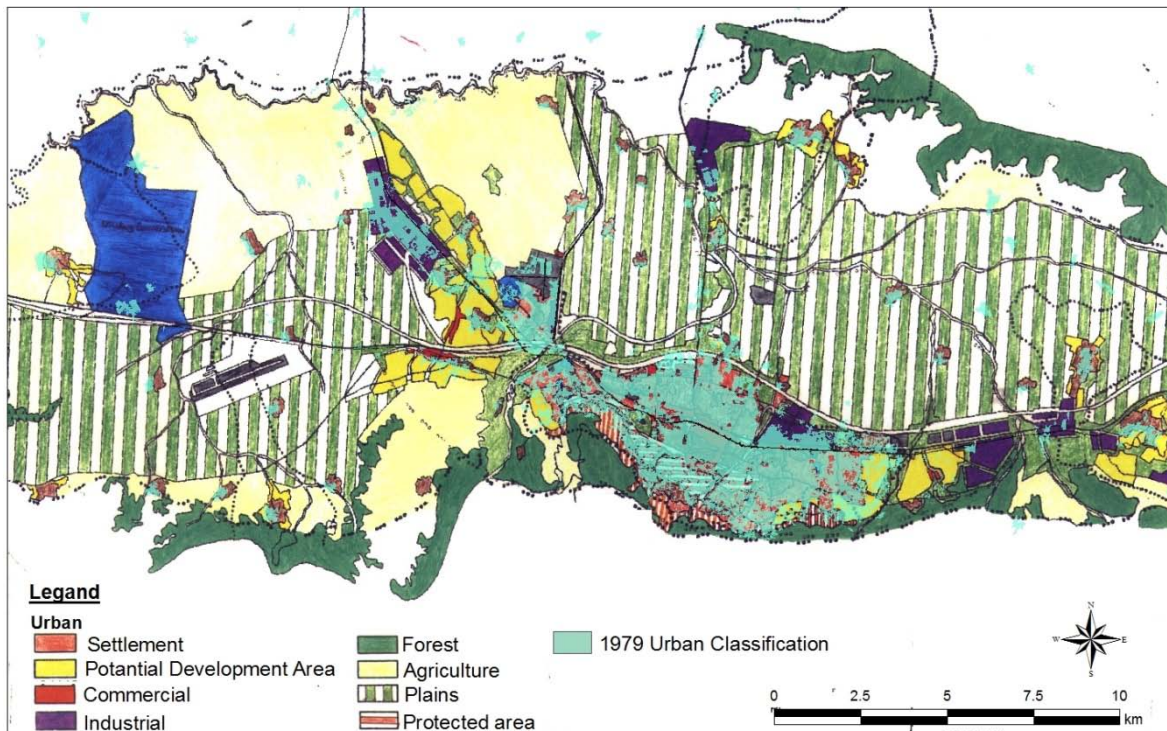


Figure 3. Comparison of the 1976 city map via 1979 urban class.

After the year 1976, a 1/5000 scaled Master Development Plan was prepared in 1981 and was revised in 1990 (Figure 4) and 1995.

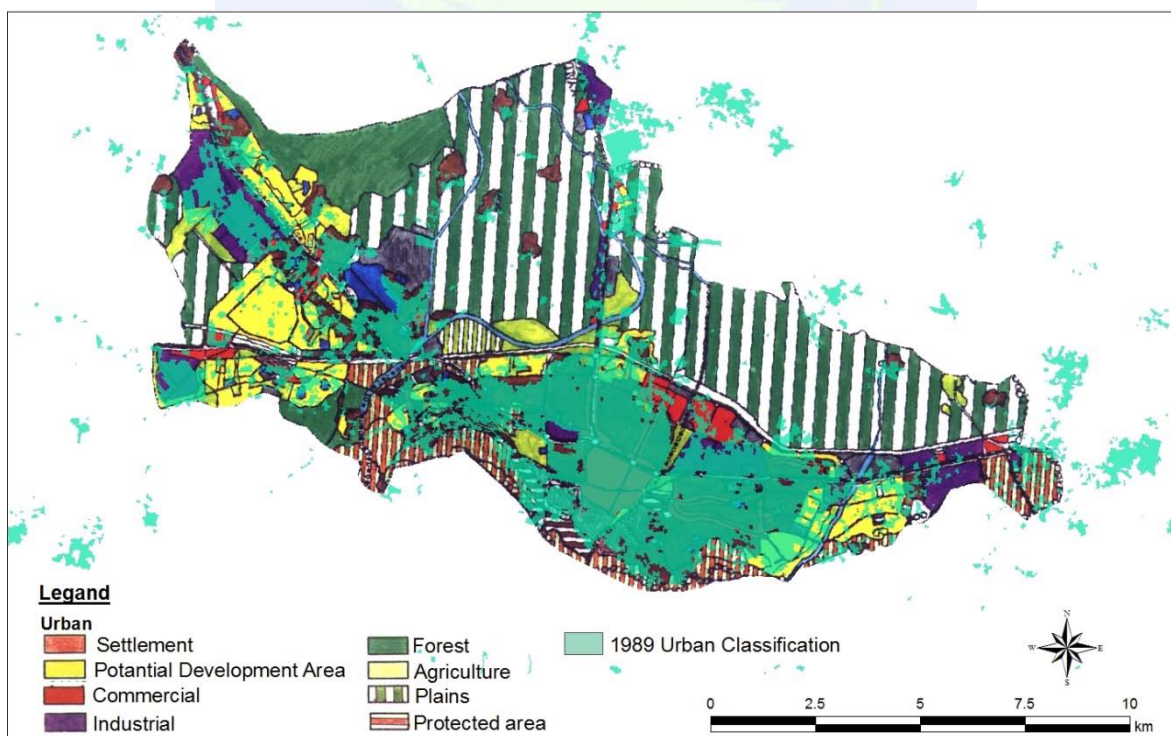


Figure 4. Comparison of the 1990 city map via 1989 urban class.

Master Development Plan for the year 2005 was prepared for the six metropolitan zones. Absolute and marginal agricultural grounds were not identified and natural sources were not protected. The plan was applied without the decision of a Ground Commission (İlkme, 2009) and still in use. Therefore, 2013 urban map was overlaid with the 2005 master plan (Figure 5).

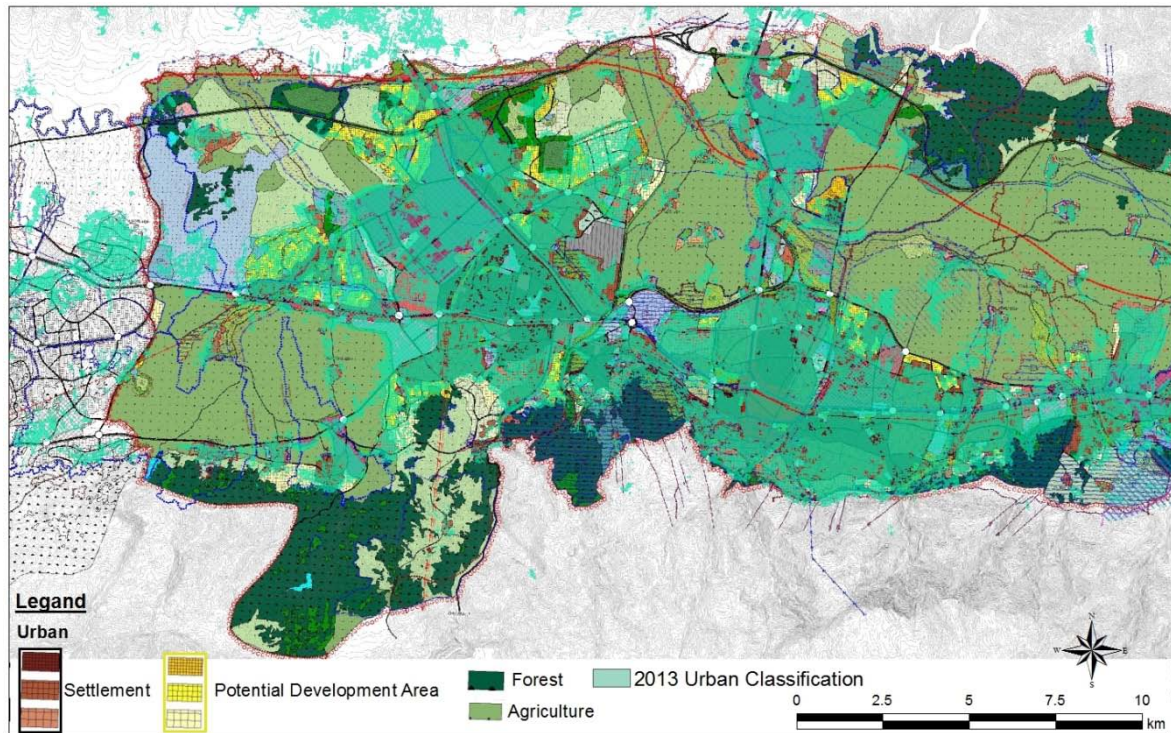


Figure 5. Comparison of the 2005 city map via 2013 urban class

Table 1. Comparison of the LU/LC classes

LULC (ha)		1976	1979	2005	2013
Total Urban	Current Settlement				
	Commercial		3648		15704
	Industrial	6844		28838	
	Public (healt/education)				
	Potantial Development Area		-		-
Open Area	Parks				
	Recreation				
	Forest	3489	3041	9568	7949
	Zoo				
	Woodlands				
	Cemetery				
Agriculture		17897	32585	15323	18361

After the overlay analysis for urban change, comparison of the city maps with the classification data was performed (Table 1)(Atanur, 2011; Akın 2016). For the comparison, three main LU/LC class was evaluated. The study is mostly focused on the urban development. However, degradation of the natural lands and cultivated areas such as green areas and agricultural lands are also important in order to evaluate the effect of the urban growth.

The most considerable change was observed on the urban class. 1976 and 2005 maps are also includes the potential urban development areas. 1979 and 2013 classification maps present the active urban use. However, this difference is an effective way of comparison. In other words, 28838 ha area was calculated as urban for the year 2005. The active urban use for the year 2013 is calculated as 15704 ha. Despite the potential urban development areas in the 2005 plan, the city could not reach the planned urban scenario. Even though eight years difference, plenty of potential urban area was reserved for the future. This is one of the main drivers of the future urban sprawl and very typical in Turkish cities (Akın, 2016; Erdoğan, 2011; Atanur, 2011). Congruently, 1979 urban use could not reach the planned urban scenario. Agricultural lands were mostly occupied with the urban. This explains the decrease in agricultural areas between the years of 1976-2013. In the 1976 map, plain areas were determined as protected lands, however, 2013 urban classification maps indicated that the city is growing through these productive plains. Macroform of the city is still under the effect of Piccinato Plan. The slope of the Uludağ Mountain restricts the urban development and a natural zone for the urban sprawl. However, the greater agricultural land loss was observed when development was restricted by the steeper slopes. Therefore, the city witness to organic growth and has a linear structure.

The difference of the agricultural lands between the city maps and classification data is due to the potential urban areas. There is 14688 ha difference between the 1976-1979 time periods. In the complete city and immediate area plan of 1976, 1368 ha area was reserved for the potential urban. Finally, there was an increase in the open area for the 1976-2013 time periods. New green and woody areas such as university campus, botanic garden and zoo, contributed to the urban green.

CONCLUSIONS

In the 20th century, Bursa has been faced with the rapid urbanization movements due to developed industrialization opportunities. Nowadays, Bursa is an industrial center of attraction with the extensive automotive and textile sectors. The city has a strategic and geographic importance due to closeness of the other developed industrial centers such as İstanbul and Kocaeli. Besides, İstanbul Environmental Layout Plan and Osmangazi Bridge transportation route will increase the pressures on Bursa city for industry-centered use and accelerate the LU/LC degradation.

Commercial and industrial areas, mainly housing, have expanded more than 100% between the years 1976 and 2005. The same expansion is observed in the use of open spaces defined in the plans. While the areas reserved for agriculture and public use have

decreased. The comparison of planned and actual urban use have clearly emphasized that, plenty of new urban areas are reserved for the potential urban growth which is actually more than required. Also new spreading centers were observed during the 1979-1990 time period. Besides, protected lands which are described as natural protected areas were occupied with the urban use for the 1990-2013 time periods. Productive plains and agricultural lands were determined as the most degraded land uses for the 1968-2013 time periods. Degradation of landscapes due to rapid urban growth or urban sprawl is a common problem all over the world and this is especially true in developing/new developing countries such as Turkey. So, it is important to track and monitor temporal landscape changes in order to develop more sustainable, objective, rational and effective urban policy decisions.

In this frame, the study evaluated various data types for the different time periods and detected the conflicts between planned and existing urban uses. Also the quality and the quantity of the landscape changes degraded by the urban were emphasized. Remotely sensed data enables to monitor temporal changes of landscapes all over the world. We hope this study will help to develop more sustainable planning decisions for the Bursa city and other cities.

REFERENCES

- Atanur, G., 2011. The effects of urban expansion on cultural landscapes – Case study of Bursa. *Scientific Research and Essays*.6(20):4185-4194.
- Berberoglu, S., Akin, A., Clarke, K.C., 2016. Cellular automata modeling approaches to forecast urban growth for Adana, Turkey: A comparative approach.153:11-17.
- De Leeuw, J., Georgiadou, Y., Kerle, N., De Gier, A., Inoue, Y., Ferwerda J., Smies, M., Narantuya D., 2010. The Function of Remote Sensing in Support of Environmental Policy. *Remote Sensing*. 2(7):1731-1750.
- Erdoğan, N., 2011. *İzmir İli Örneğinde Peyzaj Değişim Senaryolarına Yönelik Modelleme Yaklaşımı*: Clue-S. Ege Üniversitesi, Peyzaj Mimarlığı Anabilim Dalı, Doktora Tezi.
- İlkme, M., 2009. Planning problems experienced in Bursa. *Solutions to the Bursa Symposium*, March 2009, Bursa.1-9.
- Oguz., H, 2012. Simulating Future Urban Growth in the City of Kahramanmaraş, Turkey from 2009 to 2040. *Journal of Environmental Biology*. 33:381-386.
- UNEP, 2013. United Nations Environmental Programme-World Conservation Monitoring Centre (UNEP), “Review of the use of remotely-sensed data for monitoring biodiversity change and tracking progress towards the aichi biodiversity targets”.

Development of a New Silhouette Analysis Tool for Urban Planning Applications

Sebahat Temuçin Kılıçer^{*1}, Çetin Cömert² and Halil Akıncı¹

1 Department of Geomatics Engineering, Artvin Coruh University, Seyitler Campus, 08100, Turkey. (e-mail: stemucin@artvin.edu.tr)

2 Department of Geomatics Engineering, Karadeniz Technical University, Kanuni Campus, 61000, Turkey.

ABSTRACT

3D city models are digital models of urban areas that represent terrain surfaces, sites, buildings, vegetation, infrastructure and landscape elements as well as related objects belonging to urban areas. 3D city models support presentation, exploration, analysis, and management tasks in a large number of different applications such as urban planning, disaster management, facility management, logistics, security, telecommunication, location-based services, real estate portals as well as urban-related entertainment and education products and 3D spatial analysis. Silhouette analysis, one of 3D spatial analysis, is important for urban and landscape planning. Silhouette analysis is especially used to protect the silhouette of historical buildings in cities. ArcGIS is one of the most popular software in GIS market. It has "3D Analyst Tools" with functions such as construct sight lines, intervisibility, line of sight, skyline, shadow, viewshed and visibility analysis. However, 3D Analyst Tools does not have a function that will create a silhouette view of 3D buildings. In this study, a silhouette analysis tool is developed using python programming language for ArcGIS software. The silhouette analysis tool creates silhouette view of the buildings in 3D city model. This newly developed silhouette analysis tool calculates the maximum height floor number of new buildings and analyses whether the new buildings will distort the silhouette of the historical or cultural buildings.

INTRODUCTION

In general, Geographic Information Systems (GIS), defined as "the whole of software and hardware elements designed for spatial database management" (Masry and Lee, 1988), are widely used in location-based decision making processes to solve complex social, economic and environmental problems around the world. Apart from the display and presentation of spatial data, GIS, thanks to the two-dimensional (2D) and three-dimensional (3D) data modeling, query and analysis functions support decision makers on making the most appropriate decisions in various fields such as tourism, environment,

^{*} Corresponding Author

energy, agriculture, forestry, transportation, disaster and emergency management, vehicle tracking, urban planning, urban management and land-use practices.

2D maps, produced by representing spatial data in a 2D plane, are used as a base in many studies using GIS. However, it is observed that 2D spatial data and analyzes performed on these data are inadequate in applications related to noise estimation models (Kluijver and Stoter, 2003), air pollution models, flood models, geological models (Van Wees vd., 2002) and real estate market (Stoter and Zlatanova, 2003; Stoter and Ploeger, 2003); (Stoter and Zlatanova, 2003). The increase in demand for 3D database in applications, parallel to the development in hardware and computer graphics, has led to focus be on the third dimension in the spatial data model (Zlatanova vd, 1998). In this way, "3D City Models" were produced in the computer environment by representing the objects such as energy transmission lines, lighting columns, roads, trees and buildings located on the land. 3D spatial modeling and analysis together with the expansion of application areas where 3D urban models are used, have become important research topics in the field of GIS today.

There are many studies in the literature which contribute to the planning and management of urban areas using 3D city models. In a study conducted by Sadek et al. (2002), a 3D city model was created for city planners to use for 3D visualization of cities. In another study Czerwinski et al. (2007) conducted, noise analysis and noise emission calculations were performed for buildings modeled as 3D in North Rhine-Westphalia, the city with the highest population in Germany. With the ViSuCity project designed by Ban et al. (2011), a web-based interactive viewer was designed to support sustainable urban and environmental planning. Lamberti et al. (2011) have worked on lighting streets and avenues using the 3D city model (Mao, 2011). Schulte and Coors (2008) developed an application in the field of disaster management by simulating the flood with 3D designed buildings. Lee and Zlatanova (2008) have worked on 3D modeling of buildings and 3D topological analyzes to determine appropriate evacuation routes in situations where people should be evacuated urgently, such as fire.

Noise analysis, air pollution analysis, network analysis, shadow analysis, visibility analysis and silhouette analysis as well as spatial analysis etc. can be presented as examples in which 3D GIS applications are needed. Visibility analysis, has been used in the GIS applications since the 1970s (Yang vd., 2007). Visibility analysis is widely used in applications like urban planning, environmental regulation, landscape planning and identification of ares for base stations, wind turbines and solar energy systems.

The silhouette analysis included in the visibility analysis has great importance in terms of protecting city architecture in urban planning and making the appropriate decisions in the production of development plans. Güney et al. (2012) have provided two separate silhouette definitions in their studies. In the first, the silhouette is defined as "the line and horizon that the earth and the sky meet; representation of this in a painting or in another art form". In the latter, silhouette is defined as "the draft of one building or a series of buildings or other objects seen in the skyline". Urban silhouette or city silhouette can be described as an image of buildings in urban areas seen from one point. In the literature, there are various studies that produce the silhouettes of buildings in the urban areas. For

example, there is a study of by Nasar and Terzano (2010) that compares silhouettes of natural and urban areas through digital photos. There have been studies for the protection of silhouettes of Kuala Lumpur by Yusoff et al. (2014) using a 3D urban model. In a study conducted by Czyńska (2015), the impact of high-rise structures in urban areas on historical structures have been studied. In the study made by Tafahomi et al. (2016), silhouettes studies have been made on the buildings in the city of Mashhad, Iran's second-largest city. Tavernor and Grassner (2010) studied the visual impact of the towers in London on the Waterloo Bridge and the St. Paul's Cathedral. Akdag et al. (2010) examines the impact of high-rise buildings located on the Zincirlikuyu-Maslak road in Istanbul on the silhouette change of the Bosphorus. Güney et al. (2012) in their studies, emphasizing the importance of urban silhouettes in the planning of urban areas, developed a 3D city model of the work area that was established by setting a pilot region around Levent district of Istanbul. The visibility of the work area was examined from key points of the city such as, Bosphorus Bridge, Fatih Sultan Mehmet Bridge, Harem and Çamlıca Hill, and various 3D analyzes were performed.

Although today widely used GIS softwares -with commercial or open source- make it possible to perform various analyses with their 3D analysis functions, they remain insufficient in respect to carrying out the silhouettes analyses. The inadequacy of the silhouette analysis leaves unanswered questions such as "which buildings distort the silhouette, and which do not, where and how much high the building should be constructed so that the silhouette does not distort, and how the silhouette changes when viewed from different points". The availability of a software that enables urban silhouette analyzes during the planning of urban areas and development plans will help decision makers to make correct decisions by finding answers to such questions.

ArcGIS software provides many functions and modules such as data entry, processing, query, analysis, and presentation and it is widely used all over the World. ArcGIS software can represent data as 3D and provides various spatial analysis with its "3D Analyst" module. The visibility analysis sub-module of the 3D Analyst module; has various functions used in visibility analysis such as construct sight lines, intervisibility, line of sight, observer points, sun shadow volume, viewshed, visibility, skyline, skyline barrier and skyline graph. Many of these analysis functions usually allow the determination of areas that can be seen or not be seen from a point, taking into account the land surface, 3D building models or other 3D objects. It is not possible to create silhouette views of 3D buildings or calculate how high should be the buildings to be newly constructed and how many floors they should have not to distort the silhouette of buildings with historical or cultural importance by using such analysis functions above. In this study, it is aimed to design and implement a new module that enables the analysis of silhouettes in ArcGIS software using the Python programming language.

METHODOLOGY

In this study, the following steps were followed in order to develop a module that has the ability to perform silhouette analysis using the 3D city model.

- Producing the building layer and Digital Elevation Model (DEM) of a sample study area,
- Producing 3D building models with CityEngine program,
- Transfer of 3D building models to ArcGIS environment,
- Development of the silhouette analysis module with Python programming language and with the PyScripter program,
- Designing the toolbar for the silhouette analysis module with the ArcGIS Python Add-In Wizard program and integrating it into the ArcGIS program,
- Producing a silhouette view of the buildings in the study area using the developed silhouette analysis module and obtaining the analysis messages.

The operations listed above are discussed and explained under four main headings: i) producing 3D building models of the sample study area with CityEngine program, ii) developing a silhouette analysis module that will perform silhouette analysis using the Python programming language for the buildings produced in 3D model, iii) designing a toolbar to integrate the developed silhouette analysis module into ArcGIS software, iv) Finally, demonstration of the operating principle of the silhouette analysis module and the analysis outputs with a sample application.

3D Building Model Production

Firstly, DEM of the study area was created and 2D building layers in DXF format were obtained in order to perform silhouette analysis in the ArcGIS program. The DEM used in the study is produced by using the contour lines on 1/1.000 scale maps. The number of floor attribute has been added to the building layers converted into ESRI Shape format and floor number of all buildings are entered in the table of attributes. Then 3D building models belonging to the building layers of the study area are produced with CityEngine v. 2015.2 program by using the floor numbers. In CityEngine program, after the completion of the production of 3D models, the data need to be exported in order to make spatial analysis. Therefore, the produced 3D building model is exported in multipatch data structure for use in ArcGIS environment.

Development of Silhouette Analysis Module

ArcGIS program allows to be extended by using object-oriented programming language Python. ArcGIS program presents its users IDLE Editor together with desktop GIS software. However, in this study PyScripter editor is considered to be more practical and required codes for silhouette analysis are encoded. With the silhouette analysis module developed within the scope of this study, silhouette views of a certain points which will be

determined by the users and certain buildings on a sight line in 3D urban areas can be produced. In addition, a silhouette analysis is carried out between the building where the silhouette is to be preserved and the building to be constructed by selecting the building which is important for preserving the silhouette. With this analysis, the maximum height of the building and the maximum numbers of floor can be calculated so that the new building does not distort the silhouette of the preserved building. Thus, by applying a silhouette analysis when building a new building in urban areas, the silhouette condition of the new building can be interpreted both visually and numerically.

Toolbar Design for Silhouette Analysis Module

The ArcGIS Python Add-In Wizard program allows you to design toolbars easily. In this study, a tool bar named "Silhouette" shown in Figure 1 for silhouette analysis module was designed and presented in ArcMap program for use.

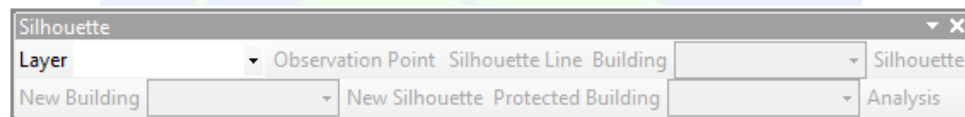


Figure 1. Silhouette toolbar

Application

In this study, in order to produce 3D building models belonging to the region where silhouette analysis will be made, 17 different building models were produced in different structures as block models of the Lod 1 level according to the DEM and CityGML standards. The 3D building models created using the 2015.2 version of CityEngine program are shown in Figure 2 in ArcGIS 10.2 program view. The building, which is mentioned as a new building in the silhouette analysis of the produced 3D building models and whose silhouette condition will be evaluated, is shown in red color.

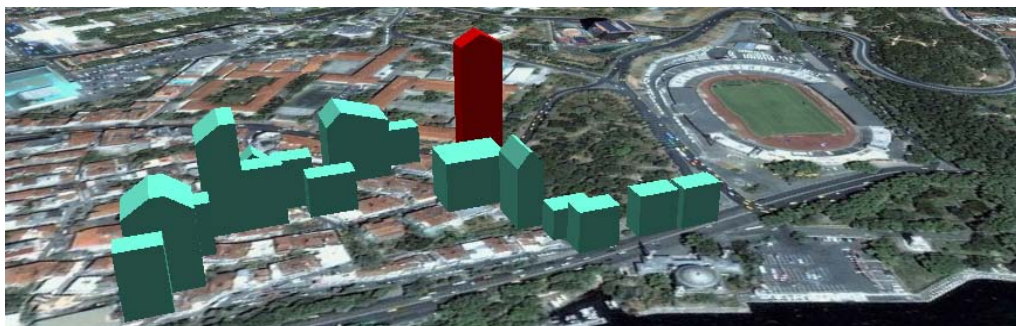


Figure 2. 3D building models in ArcGIS 10.2 software

With this application, only silhouette view of existing buildings and silhouette view of existing buildings together with new building are produced on a certain point and a determined silhouette line. In addition, the building which is important for preserving its silhouette of existing buildings is selected by the user and a silhouette analysis is performed between the building where the silhouette is to be preserved and the new building to be built. With this analysis, it is evaluated whether the silhouette of the new building distorts the existing building that should be preserved.

If the new building does not distort the silhouette of the preserved building, an information message is presented that the new building does not distort the silhouette of the preserved building. If the new building distorts the silhouette of the preserved building, an analysis is performed between the new building and the preserved building. Thus, in order to prevent the new building from distorting the preserved building silhouette, the maximum building height required and the maximum number of floors that can be constructed are calculated and these values are presented with another information message. The process steps of the silhouette analysis module are explained below.

1. The user uploads the DEM into the map window using the combo box named Layer in the toolbar (Figure 1).
2. The user then uses the Observation Point button in the toolbar to determine the point to be observed where the user stands (Figure 3).
3. The user specifies the silhouette line in the sight area using the Silhouette Line button in the toolbar (Figure 3).
4. The user selects the building layer in the multipatch format, from which the silhouette will be produced according to the determined silhouette line.

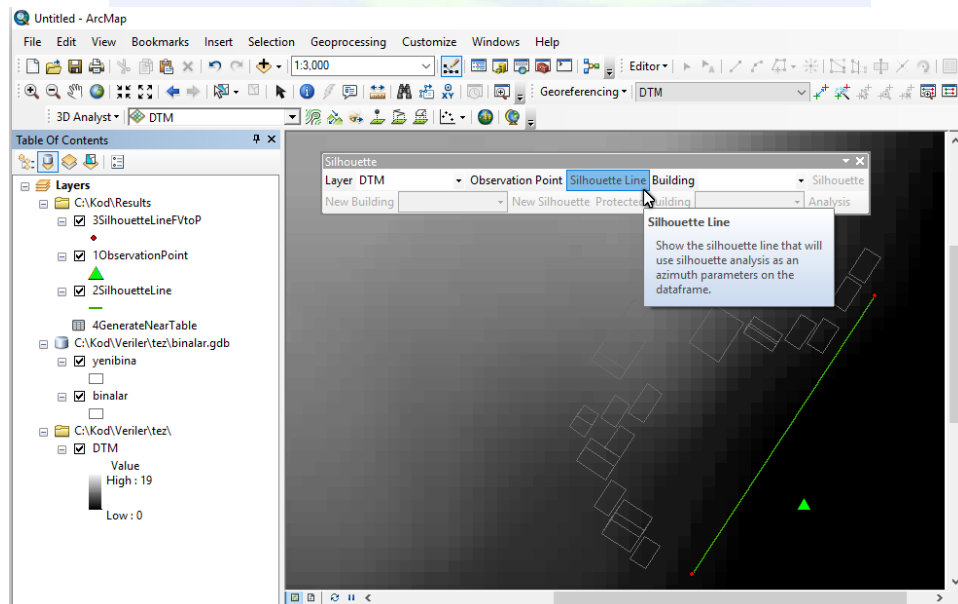


Figure 3. Determination of Observation Point and Silhouette Line

5. A SVG format silhouette view of existing buildings are produced using the Silhouette button in the toolbar and displayed as a new window on the screen (Figure 4).

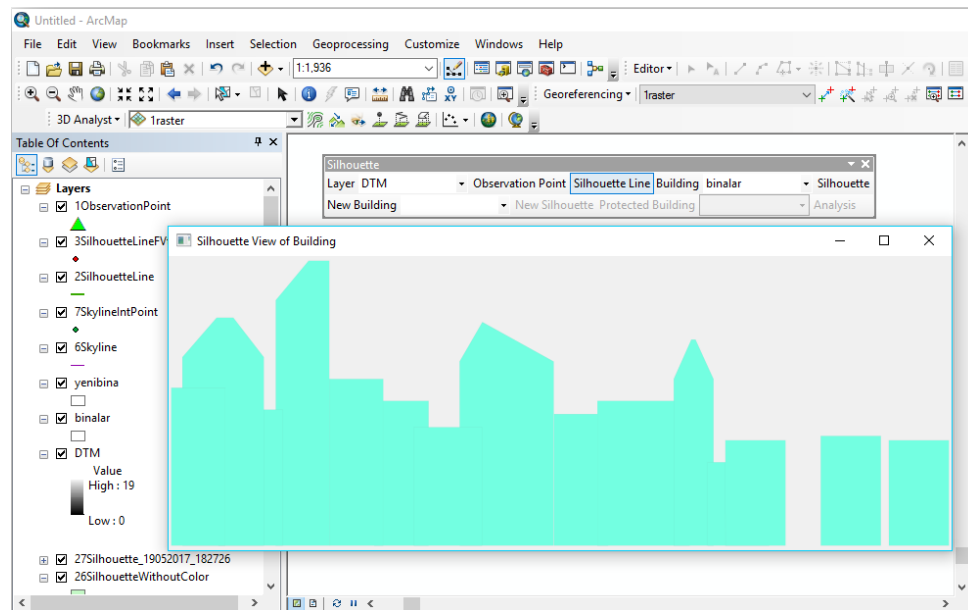


Figure 4. Silhouette view of existing buildings in silhouette line

6. The new building layer in the multipatch format is selected using the combo box named New Building.
7. A silhouette view of the new building to be constructed and existing buildings is created and displayed using the button named NewSilhouette (Figure 5).
8. The building that is to be preserved is selected using the combo box named Protected Building.

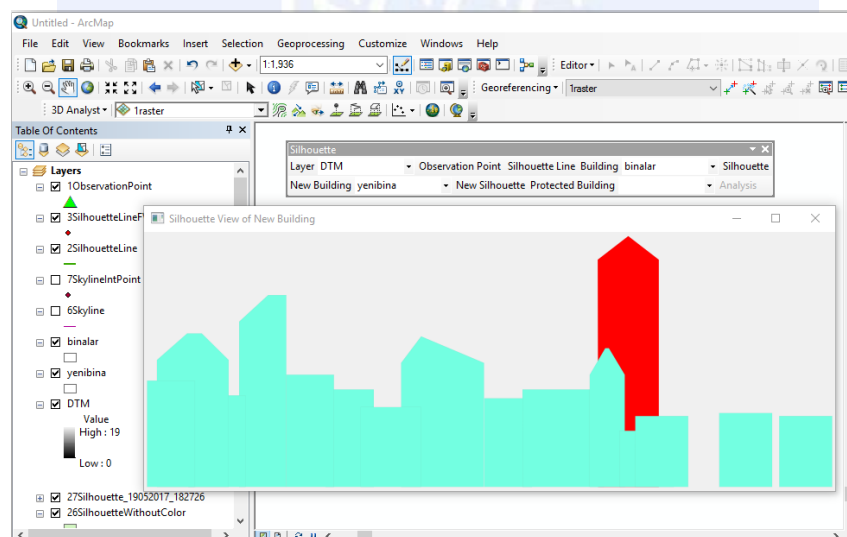


Figure 5. Silhouette view of new building and existing building

9. The building to be constructed and the silhouette of the building to be preserved are evaluated in terms of silhouette by using the button named Analysis. If the new building does not distort the silhouette of the preserved building, an information message indicating that the silhouette is not distorted is displayed. If the silhouette is distorted, the maximum building height and maximum floor number that the new building should have to comply with the silhouette of the preserved building is calculated and displayed on the screen in an information message (Figure 6).

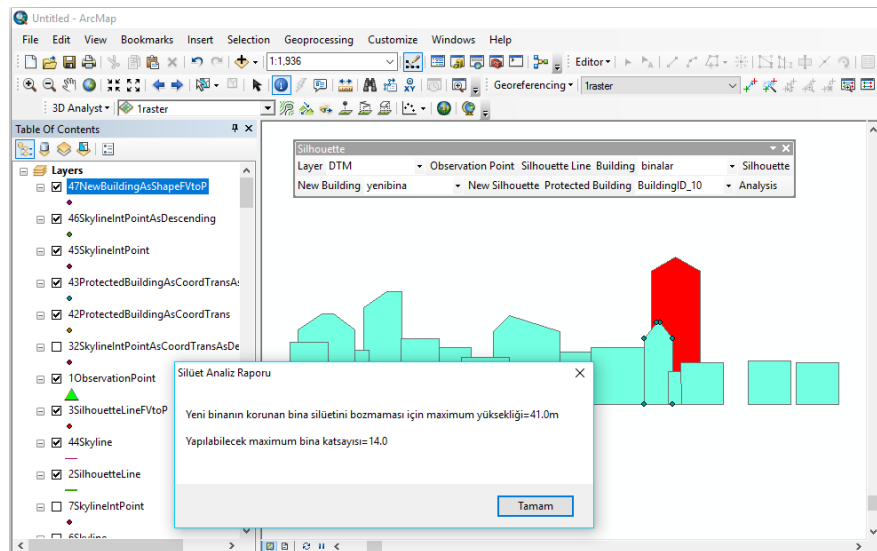


Figure 6. Silhouette analysis message

RESULTS

In this study, a new silhouette analysis module has been developed which determines silhouette impact of new buildings that are planned to be built in the same area. The module generates a silhouette view of the buildings that are within a certain field of view from the observation point. Thus, it is aimed to solve the problems arising from the urban silhouette distortion seen in the urban planning process and the implementation of the development plans.

Silhouette analysis module, was developed using the Python programming language to be run in ArcGIS GIS software. The 3D buildings used in the study are modeled according to CityGML standards so that it will work in LoD 1 detail level. Because as the LoD level increases, architectural details such as the roof structures, building textures, wall details and balconies of the building models will also increase. Therefore, the detail points of the multipatch geometry type will also increase. Thus, repetition of the point coordinates on the surface sections representing the multipatch object will both cause problems in determining the point to be used in the process phases and slow down the developed module in terms of performance. The difference in the visibility analysis functions provided by ArcGIS from the developed silhouette analysis module and the work done in the literature using these functions is explained in the following parts.

By using the visibility analysis functions of ArcGIS software, various visibility analyzes can be performed in 3D urban areas. However, the analysis of the presented functions and

the analysis of silhouette situation in urban areas requires both a large number of procedural steps and parameters, and the obtained result is visually interpreted, as well. Visibility analysis functions offered by ArcGIS software can be manufactured only with similar graphic images to the silhouette. Through visual interpretation of the graphics it can be determined whether the silhouette is distorted or not. From these graphs, information such as, the height or the floor number of buildings that are visible, can not be reached from the point where observation is made. From the graphs generated, it can be determined how many objects from how many angles and distances are visible from the observation point. In the literature, there are some silhouette studies conducted by using the visibility analysis functions provided by ArcGIS software. For example; in the study conducted by Güney et al. (2012), the 3D city model of Levent district of Istanbul was produced and both the visual skyline analysis and the temporal skyline analysis of the study area were performed. In the study, visual skyline analysis and silhouette change was analyzed using 3D city models of 1999 and 2008 of Levent district. In the same study, the visual impact of the high-rise buildings constructed, was evaluated by the Levent district's temporal skyline analysis developed from four important points of the city such as the Bosphorus Bridge of Istanbul, Fatih Sultan Mehmet Bridge, Harem and Çamlıca Hill. Similar to another study conducted by Yusoff et al. (2014), studies on preservation of Kuala Lumpur's silhouette by using ArcGIS software. After completing 3D city model production, silhouette views of existing buildings were produced from 3 different observation points through ArcGlobe program. Then, three new buildings to be built are produced from the same observation point and viewpoint. In this way, the impact of the new buildings on the city silhouette were evaluated.

When the results of the studies and the 3D analysis functions used are evaluated, the diversity of the analysis of the visibility analysis presented and the lacking of completion of analysis of data produced in ArcGIS software in a single platform (ArcMap, CityEngine, ArcScene and ArcGlobe) make it difficult to use the software in silhouette studies. Therefore, only the visual impact of the models can be evaluated with the studies made in the context of silhouette analyzes. Through the skyline analyses mentioned as silhouette analysis, only limited spatial information is available. Apart from these, since different silhouettes will be formed from different observation points, so as the observation point changes, the workload will increase and analyzes will need to be recollected.

CONCLUSIONS

3D urban model production, data representation and spatial query and analysis, are active research areas in GIS. In this study, silhouette analyzes, one of the visibility analyzes, were examined using 3D building models. Whether in the planning process of urban areas or in the process of granting licenses to newly built buildings in the implementation of development plans, there is a need for the production of silhouette views of urban areas and monitoring of changes in the urban silhouette. Current GIS softwares used today do not provide direct functions for silhouette analysis, but it allows the generation of silhouette-like graphics with the visibility analysis functions they have. In addition, the

functions provided by the existing GIS softwares are inadequate in determining how new buildings will affect the silhouettes of the buildings required to be preserved and the existing buildings, and determining the maximum heights and number of floors of the new buildings intended for the preservation of the silhouette. In this study, a silhouette analysis module that can perform silhouette analysis on 3D building models was developed. The developed module generates a silhouette view of a 3D buildings from a standing point which is a point of observation that can be determined by the user from the screen and calculates the maximum height and number of floors that the new buildings should have not to distort the silhouette. The silhouette analysis module has been designed and developed to be simple and functional so that users of the development directorates of the municipalities can easily use it without too much technical knowledge requirement. Through the developed silhouette analysis module, silhouette views of mega cities such as Istanbul can be produced and the temporal change in the silhouette can be analyzed. Moreover, the impact of the new buildings to the silhouette can be determined for the preservation of historical heritage in these big cities through the developed module. For example, if such a module had existed, silhouette analyses of the 16/9 towers in Zeytinburnu could have been performed while the project was still in plan phase before construction and it would not cause the deconstruction of the towers due to damage to the silhouette. Therefore, it is considered that the developed module will make a significant contribution to the municipalities.

REFERENCES

- Akdag, S.G., Cagdas, G. and Guney, C., 2010. Analyzing the Changes of Bosphoru Silhouette, *Proceedings of the 28th Conference on Education in Computer Aided Architectural Design in Europe*, September 15-18, Zürich, Switzerland, 815-823.
- Ban, Y., Jakobsson, P., Kjell Dahl, L., and Ranhagen, U., 2011. Visualization in ViSuCity, a tool for sustainable city planning, *Proceedings of SIGRAD 2011. Evaluations of Graphics and Visualization-Efficiency, Usefulness, Accessibility, Usability*, November 17-18, KTH, Stockholm, Sweden, 105-109.
- Czerwinski, A., Sandmann, S., Stöcker-Meier, E. and Plümer, L., 2007. Sustainable SDI for EU noise mapping in NRW – best practice for INSPIRE, *International Journal of Spatial Data Infrastructures Research*, 2, 90-111.
- Czyńska K., 2015. *Impact of Tall Buildings on the Attractiveness of Urban Landscape-On the Example of Selected European Cities*, Norway Grants, 131-144.
- Güney, C. Girginkaya, S.A., Çağdaş, G. and Yavuz, S., 2012. Tailoring a Geomodel for Analyzing an Urban Skyline, *Landscape and Urban Planning*, 105, 160-173.
- Kluijver, H.de. and Stoter, J., 2003. Noise mapping and GIS: optimising quality and efficiency of noise effect studies, *Comput. Environ. and Urban Systems*, 27(1), 85-102.

- Lamberti F., Sanna A., Ramirez E., (2011). Web-based 3D visualization for intelligent street lighting, In *Proceedings of the 16th International Conference on 3D Web Technology (Web3D '11)*, June 20-22, Paris, France.
- Lee J., and Zlatanova S., 2008. *A 3D data model and topological analyses for emergency response in urban areas*, *Geospatial Information Technology for Emergency Response*, ISPRS Book Series, Taylor&Francis, London, 143-168.
- Mao, B., 2011. *Visualisation and Generalisation of 3D City Models*, PhD Thesis, K.T.H., Stockholm.
- Masry, S.E. and Lee, Y.C., 1988. *An Introduction to Digital Mapping*, Department of Surveying Engineering publication, UNB, Canada.
- Nasar, J.L. and Terzano, K., 2010. The Desirability of Views of City Skylines After Dark, *Journal of Environmental Psychology*, 30, 215-225.
- Sadek, E.S.S.M., Ali. S.J.B.S., Rosdi, B. and Kadzim, M.R.B.M.D, 2002. *The Design and Development of a Virtual 3D City Model*, 1-12.
- Schulte, C. and Coors, V., 2008. Development of a CityGML ADE for dynamic 3D flood information, In *Proceedings Joint ISCRAM-CHINA and GI4DM Conference on Information Systems for Crisis Management*, Harbin, China.
- Stoter, J.E. and Ploeger, H.D., 2003. Registration of 3D objects crossing parcel boundaries, FIG Working week 2003, April, Paris.
- Stoter, J. and Zlatanova, S., 2003. 3D GIS where are we standing?, *ISPRS Joint Workshop on Spatial, Temporal and Multi-Dimensional Data Modelling and Analysis*, October 2-3, Quebec city, Canada.
- Tafahomi, R., Hosseini, S.M.S.A., Lamit, H. ve Burshri, A., 2016. Application of GIS Method to Identify Urban Silhouette Form Case study: Mashhad city in Northeast of Iran, *Planning Tech*, 1-8.
- Tavernor, R. and Gassner, G., 2010. Visual Consequences of the Plan: Managing London's Changing Skyline, *City, Culture and Society*, 1, 99-108.
- Van Wees, J.D., Versseput, R.W., Simmelink, H.J., Allard, R.R.L. and Pagnier, H.J.M., 2002. *Shared Earth system models for the dutch subsurface*, Netherlands Institute of Applied Geoscience TNO-National Geological Survey, The Netherlands.
- Yang, P.P., Putra, S.Y. and Li, W., 2007. Viewsphere: a GIS Based 3D Visibility Analysis for Urban Design Evaluation, *Env. and Planning B: Planning and Design*, 34, 971-992.
- Yusoff, N.A.H., Noor, A.M. and Ghazali, R., 2014. City skyline conservation: sustaining the premier image of Kuala Lumpur, *Procedia Environmental Sciences*, 20, 583-592.
- Zlatanova, S., Painsil, J. and Tempfli, K., 1998. 3D object reconstruction from aerial stereo images, *6th international conference in Central Europe on computer graphics and visualization '98*, February 9-13, Plzen-Bory, Czech Republic.

Recognising Building Patterns in Topographic Maps with HDBSCAN Clustering Algorithm

Kadir Sahbaz^{*1} and Melih Basaraner¹

¹ Division of Cartography, Department of Geomatic Engineering, Yildiz Technical University, 34220 Esenler Istanbul, Turkey

ABSTRACT

In topographic maps, meaningful groups of buildings form various patterns. Those buildings are generalized in a way as to retain significant pattern characteristics during contextual generalization. One of the main problems in this process is that those patterns are not available in datasets. For this reason, they need to be recognised with appropriate approaches. In this context, clustering methods in data mining are used quite commonly. So, this paper investigates the effectiveness of relatively new Hierarchical Density-Based Spatial Clustering of Applications with Noise (HDBSCAN) algorithm for recognising building patterns based on several geometric and structural characteristics. HDBSCAN uses unsupervised learning to find clusters of a dataset. In experimental tests, urban blocks were created by means of road networks as a topological constraint for buildings. Visual evaluation of the results indicated that HDBSCAN had some potential for discovering collinear and curvilinear building patterns, especially in well-structured urban blocks according to Gestalt factors. In case of u-shaped and unstructured building patterns, the results were not sufficiently successful.

INTRODUCTION

Cartographic generalization is responsible for reducing complexity in a map in a scale reduction process, emphasizing the essential while suppressing the unimportant, maintaining logical and unambiguous relations between map features, and preserving aesthetic quality (Weibel 1995). As a part of topographic map generalization, building generalization is a complex operation due to the complexity of the spatial configuration of buildings (Li et al. 2004, Basaraner and Selcuk, 2008, Yan et al., 2008). A group of buildings constitute various patterns depending on their distribution characteristics. Those patterns of buildings are generalized with contextual generalization operators (Basaraner and Selcuk, 2008). The critical issue with respect to the generalization is to extract meaningful patterns from topographic datasets. One of the most common methods within this scope is to apply clustering methods offered by data mining community.

^{*} Corresponding Author

Different approaches for recognizing building patterns exist in cartography and GIScience literature. Minimum spanning tree (MST) is used for pattern recognition intensively (Zahn 1971). Regnauld (1996) employs this technique to detect building clusters for map generalization. However, building patterns recognized with this technique do not meet the needs except some tree-like clusters. Allouche and Moulin (2005) obtain different clusters of buildings with Kohonen's self-organizing maps (SOM) approach by setting different distance thresholds in order to provide multiple representations of the same data set at different scales. Yan et al. (2008) use Delaunay triangulation to detect topological adjacency relations of buildings and generated 2-building groups firstly, and then constructed larger, intermediate groups according to a set of rules. After aggregation and separation of intermediate groups owning common buildings, final groups were created which can be used as a basis for generalization. Cetinkaya et al. (2015) compare four clustering algorithms, Minimum Spanning Tree (MST), Density-Based Spatial Clustering Application with Noise (DBSCAN), CHAMELEON and Adaptive Spatial Clustering based on Delaunay Triangulation (ASCDT) to extract groups from a building dataset based on proximity. Their findings show that DBSCAN and ASCDT are superior to the other two methods. Deng et al. (2017) present a comparative analysis of nine typical building grouping approaches, including three approaches that only consider proximity principle and six approaches that consider multiple grouping principles. Those approaches are gathered under four categories: natural principle-based, partition-based, graph-based, and region merging approaches. Although the previous efforts produce some solutions to the building pattern recognition problem, none of them works perfectly. Therefore, this paper investigates the effectiveness of Hierarchical Density-Based Spatial Clustering of Applications with Noise (HDBSCAN) algorithm in the building pattern recognition based on several characteristics of buildings.

IDENTIFICATION OF BUILDING PATTERNS

Principles

Various criteria are taken into account to identify patterns in maps. In this respect, Gestalt principles describing human visual perception of groupings of objects have a guiding role (Li, 2007). There are six principles that can be utilized for grouping the building features (Deng, 2017): (1) Proximity: Objects that are close together appear to form a group; (2) Similarity: Objects of similar size, shape, and orientation are more likely perceived as a group; (3) Continuity: Oriented objects tend to be regarded as a whole when regularly aligned with each other; (4) Connectedness: Connected or overlapping objects can easily form a group; (5) Closure: Objects tend to be grouped together if they are parts of a closed figure. (6) Common region: Objects in same region tend to be grouped together.

Geometric and structural characteristics of buildings

Regarding Gestalt principles, a number of characteristics that are of geometric and structural nature can be defined for buildings. Both geometric and structural characteristics derived

by means of coordinates or metric properties of features; however, structural characteristics, describing shape, need meaning for the interpretation of a geometry. Location (x,y), size and orientation and nearest road distance are main geometric characteristics of buildings. Shapes of buildings are measured with various indices such as convexity, rectangularity, squareness, circularity and elongation (Burghardt and Schmid, 2010; Basaraner and Cetinkaya, 2017).

Typology of building patterns

Building patterns can be defined in a hierarchy, considering Gestalt principles (Figure 1). At the top level, the building clusters consisting of spatially close features with similar geometric (e.g. spacing, size, orientation), structural (i.e. shape) properties take place. At an intermediate level, the building clusters are distinguished as linear alignments and nonlinear clusters in terms of ‘group shape’. In general, the linear alignments appear to be more elongated and their constituent buildings can be organized by a linear path, while the nonlinear ones appear to stretch in two dimensions. At a finer level, the linear alignments are subdivided into collinear, curvilinear, and align-along-road patterns; the nonlinear clusters consist of grid-like and unstructured patterns (Zhang et al., 2012).

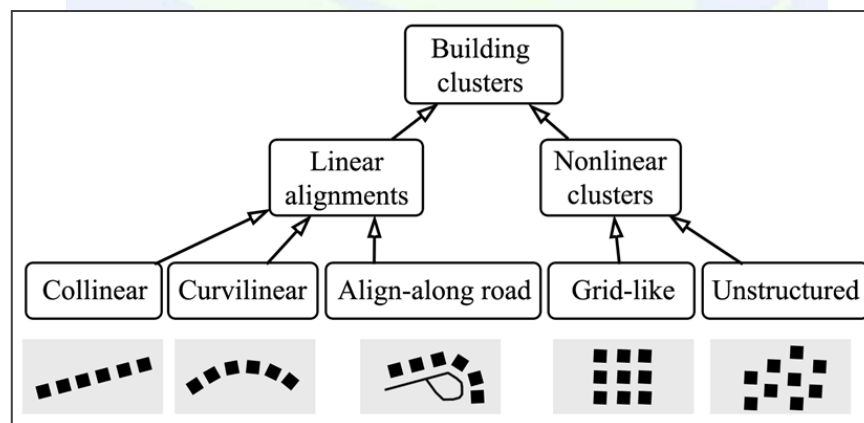


Figure 1. Typology and illustration of building patterns (Zhang et al., 2012)

HDBSCAN CLUSTERING ALGORITHM

Density plays an important role in statistics and data mining. Therefore, density-based clustering is one of the prominent approaches in cluster analysis. It works by identifying “dense” clusters of points, allowing it determine outliers in the data. DBSCAN is the most well-known density-based clustering algorithm (Ester et al. 1996). DBSCAN transforms the space according to density, then identifies for dense regions as clusters. All points are not forced to have a cluster. DBSCAN determines non-globular clusters well, however, variable density clusters become a problem. HDBSCAN extends DBSCAN which can handle variable density clusters. DBSCAN uses single-linkage clustering (Campello, Moulavi and Sander 2013). Thus, a point may act as a bridge between two clusters by

accident, such that they are characterised as a single cluster. HDBSCAN avoids this by transforming the space according to the density/sparsity. For this purpose, it calculates core distance denoted as $core_k(x)$, which is point x 's distance from its k th nearest neighbor. Then, it defines new metric based on $core_k(x)$, called mutual reachability distance (MRD) denoted with $d_{mrd-k}(a, b)$. MRD is defined as follows:

$$d_{mrd-k}(a, b) = \max \{core_k(a), core_k(b), d(a, b)\}$$

where $d(a, b)$ is the original distance, defined by *metric* parameter in HDBSCAN, between a and b (Figure 2).

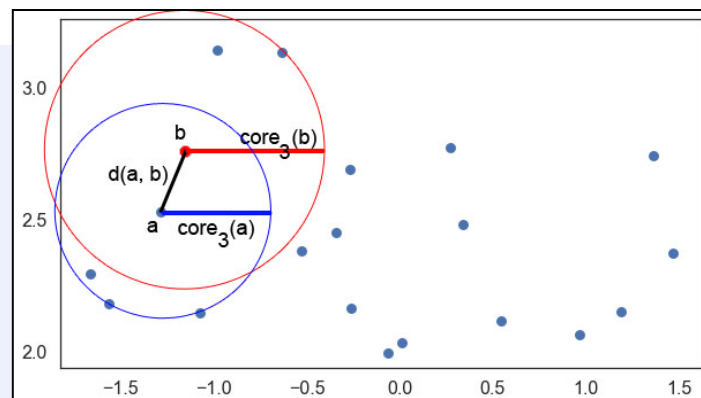


Figure 2. Mutual reachability distance for $k=3$ (a, b : core points)

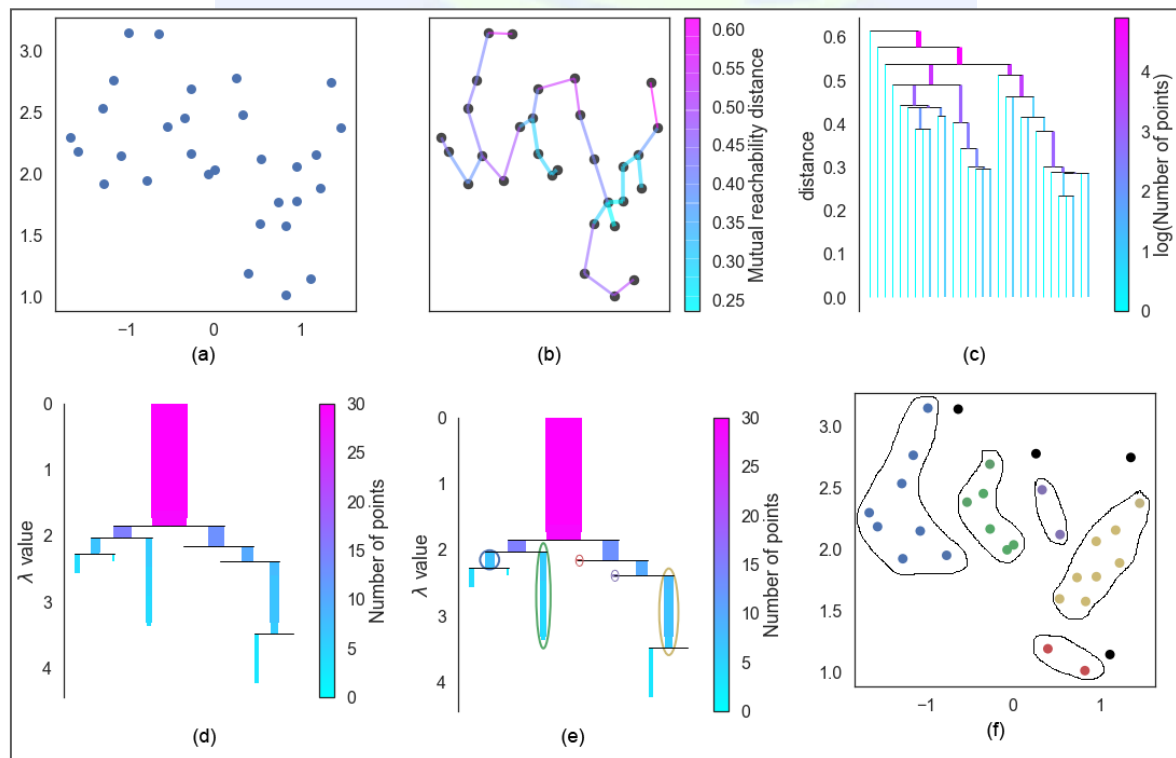


Figure 3. HDBSCAN main steps

Briefly stated, HDBSCAN works as follows: (i) transform the space using so-called mutual reachability distance metric, (ii) generate minimum spanning tree of the MRD weighted graph (Figure 3(b)), (iii) build a cluster hierarchy of connected points (Figure 3(c)), (iv) condense the cluster hierarchy based on minimum cluster size which is principal parameter of the algorithm (Figure 3(d)), and (v) select the stable clusters (Figure 3(e), 3(f)). The algorithm has two main parameters that affect the results substantially: minimum cluster size and minimum sample. The former states minimum number of points to be included in a cluster. The latter is the number of samples (points) in a neighbourhood for a point to be considered a core point.

GENERAL STRATEGY

Our strategy, briefly, is to (i) generate blocks based on roads, (ii) compute several geometric and structural characteristics (attributes) of buildings (iii) use these characteristics in the HDBSCAN algorithm as inputs (by applying normalization when more than one attribute is used).

Urban blocks were generated to restrict clustering operation from topological aspect. Otherwise, the buildings within different blocks would have possibility to be included in same cluster. Therefore, buffering operation was applied taking road width into account. There are many characteristics that can be included in clustering process but using too many characteristics make the process very complex. So, in this study it was limited with several geometric and structural characteristics. In this context, location (x, y), i.e. building's center of gravity, size, i.e. area of building and orientation, i.e. direction angle of long axis of minimum area bounding rectangle (MABR) of a building were used as geometric characteristics while convexity, i.e. the ratio of the area of a building to the area of its convex hull and elongation, i.e. the ratio of the length of the MABR's short axis to long axis as structural characteristics. In the experimental study, various combinations of these characteristics were used in the clustering in order to understand their influence on the results. In addition, statistics about the obtained clusters were given.

EXPERIMENTAL STUDY

Data and Software

A large-scale topographic dataset was used in experimental tests. A QGIS add-in was developed with Python to carry out experimental study.

Implementation

Three sample blocks were selected for the experiments. At the beginning, urban blocks were generated through road network as mentioned above. Geometric and structural characteristics were then computed. After that, the parameters for HDBSCAN algorithm were determined in the following way. The minimum cluster size value is set to 2 and the minimum sample value is set to 1 since a building pattern contains at least two buildings and it is sufficient to have at least one building nearby so that a building can form a cluster.

Finally, the following combinations of characteristics (attributes) were experimented in the clustering process: (i) location, (ii) location, size, (iii) location, elongation, (iv) location, orientation, (v) location, convexity, (vi) location, size and orientation, (vii) location, size, elongation, orientation. Min-max normalization was applied when multiple attributes were used. Location parameter is used in every scenario since proximity has a significant role in finding groups of buildings from geographic and cartographic aspects (Basaraner and Selcuk, 2008).

RESULTS AND DISCUSSION

Depending on the parameters, different clustering results were obtained and shown in Table 1 for the selected blocks. These clusters were evaluated visually and three clustering results and statistics which give the optimum result in this regard were presented in detail in Figure 4 and Table 2, respectively.

It was observed that the sizes of the clusters were very large when the location parameter was used alone (Table 1(a1)). This makes sense only in case that the buildings in a cluster were approximately same in size and same in shape (as in Block 322 in Figure 4). In those blocks, it became largely possible to reveal linear and curvilinear patterns successfully.

In every scenario, when another parameter used in addition to “location”, clustering results were affected negatively in the blocks consisting of buildings with similar/close attribute values (as in Block 139 and 322 in Table 1) because the normalization process seriously increases the standard deviation of these values.

When typologically assessed, linear and curvilinear building patterns were quite successfully determined when we considered the above criteria. It was thought of as a coincidence that building patterns aligned along the road were successfully identified, e.g. in block 322 and partly in block 83 (Figure 4) because the clustering process does not contain any information about the alignment of buildings along the roads. This was particularly owing to the regular arrangement of buildings along the roads.

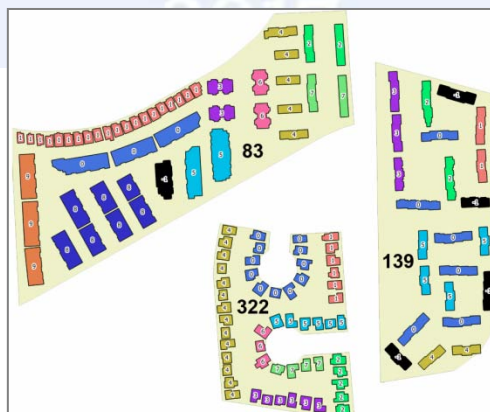


Figure 4. Sample clustering results. Buildings with same colour/number represent a cluster except black buildings (with the number -1) which are outliers and not assigned to any cluster by the algorithm.

Table 1. Clustering results obtained by using different combinations of buildings characteristics. Buildings with same colour represent a cluster except black ones which shows outliers. n_{bld} : number of buildings, n_{cls} : number of clusters, n_{out} : number of outliers.

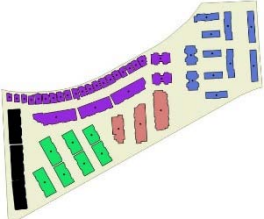


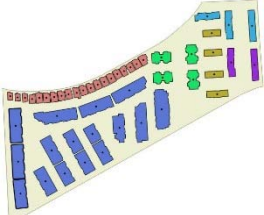


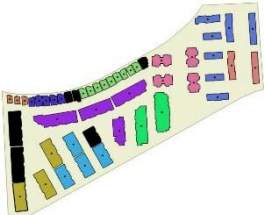
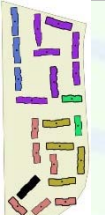

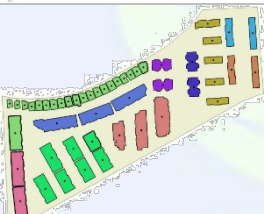

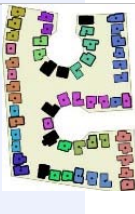
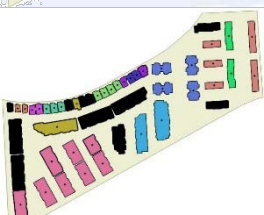
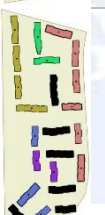

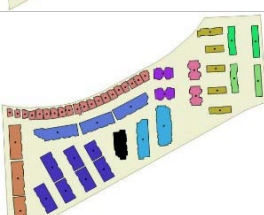
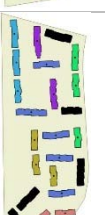

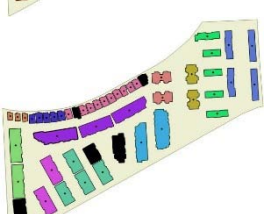


Block Characteristics	Block 83 $n_{bld}: 49$	Block 139 $n_{bld}: 23$	Block 322 $n_{bld}: 55$
<i>Location</i>	 (a1) $n_{cls}: 4$ $n_{out}: 3$	 (a2) $n_{cls}: 6$ $n_{out}: 2$	 (a3) $n_{cls}: 8$ $n_{out}: 0$
<i>Location, Size</i>	 (b1) $n_{cls}: 6$ $n_{out}: 0$	 (b2) $n_{cls}: 6$ $n_{out}: 4$	 (b3) $n_{cls}: 18$ $n_{out}: 9$
<i>Location, Elongation</i>	 (c1) $n_{cls}: 10$ $n_{out}: 6$	 (c2) $n_{cls}: 5$ $n_{out}: 1$	 (c3) $n_{cls}: 14$ $n_{out}: 8$
<i>Location, Orientation</i>	 (d1) $n_{cls}: 10$ $n_{out}: 0$	 (d2) $n_{cls}: 7$ $n_{out}: 3$	 (d3) $n_{cls}: 14$ $n_{out}: 6$
<i>Location, Convexity</i>	 (e1) $n_{cls}: 12$ $n_{out}: 11$	 (e2) $n_{cls}: 5$ $n_{out}: 6$	 (e3) $n_{cls}: 16$ $n_{out}: 11$
<i>Location, Size, Orientation</i>	 (f1) $n_{cls}: 10$ $n_{out}: 1$	 (f2) $n_{cls}: 6$ $n_{out}: 5$	 (f3) $n_{cls}: 16$ $n_{out}: 7$
<i>Location, Size, Elongation, Orientation</i>	 (g1) $n_{cls}: 12$ $n_{out}: 5$	 (g2) $n_{cls}: 6$ $n_{out}: 4$	 (g3) $n_{cls}: 17$ $n_{out}: 9$

Table 2. Statistical results of sample blocks presented in Figure 4 (std: standard deviation).

Block	Cluster	n_{bid}	Size (m ²)				Orientation (degree)				Elongation				Convexity			
			min	max	mean	std	min	max	mean	std	min	max	mean	std	min	max	mean	std
Block 83		49	95.7	1340.9	456.9	337.57	2	121	85.1	41.23	0.20	0.82	0.51	0.17	0.85	1.00	0.96	0.04
83	0	3	983.9	1177.5	1070.1	98.55	8	28	18.7	10.07	0.30	0.34	0.32	0.02	0.92	0.98	0.96	0.03
83	1	20	95.7	181.7	150.5	24.27	93	121	107.1	11.27	0.51	0.82	0.67	0.06	0.94	0.99	0.97	0.02
83	2	2	476.2	504.2	490.2	19.80	93	94	93.5	0.71	0.20	0.26	0.23	0.04	0.94	1.00	0.97	0.04
83	3	2	472.7	479.5	476.1	4.81	2	3	2.5	0.71	0.62	0.62	0.62	0.00	0.86	0.86	0.86	0.00
83	4	5	287.1	415	325.4	55.45	3	4	3.2	0.45	0.31	0.35	0.33	0.02	0.90	1.00	0.97	0.04
83	5	2	1057.1	1340.9	1199.0	200.68	93	93	93.0	0.0	0.29	0.37	0.33	0.06	0.95	0.96	0.95	0.01
83	6	2	483.7	486.5	485.1	1.98	90	93	91.5	2.12	0.65	0.66	0.66	0.01	0.85	0.86	0.85	0.01
83	7	2	462.6	501.4	482.0	27.44	93	93	93.0	0.00	0.20	0.25	0.23	0.04	0.92	1.00	0.96	0.06
83	8	7	507.4	818.2	680.2	107.85	119	120	119.14	0.38	0.41	0.69	0.51	0.09	0.98	0.98	0.98	0.00
83	9	3	826.6	989.1	933.9	92.97	93	96	94.0	1.73	0.35	0.42	0.37	0.04	0.97	0.98	0.97	0.01
Block 139		23	333.5	536.6	439.5	66.88	0	164	65.0	48.51	0.21	0.36	0.29	0.05	0.87	0.94	0.92	0.02
139	0	6	464.2	536.6	489.9	25.42	0	45	90.0	17.71	0.21	0.28	0.26	0.02	0.89	0.94	0.91	0.02
139	1	2	416.2	473.6	444.9	40.59	90	93	91.5	2.12	0.25	0.29	0.27	0.03	0.93	0.94	0.94	0.01
139	2	2	519.1	533.5	526.3	10.18	90	93	91.5	2.12	0.21	0.22	0.21	0.01	0.87	0.90	0.89	0.02
139	3	3	391.8	494.2	449.9	52.60	90	93	92.0	1.73	0.25	0.29	0.27	0.02	0.9	0.91	0.91	0.01
139	4	2	364.5	372.3	368.4	5.52	3	39	21.0	25.46	0.33	0.35	0.34	0.01	0.92	0.94	0.93	0.01
139	5	4	357.9	367.8	362.2	5.07	90	93	91.5	1.73	0.33	0.35	0.34	0.01	0.91	0.94	0.92	0.01
Block 322		55	126.5	201.3	165.3	19.67	0	175.0	75.3	65.23	0.46	0.94	0.76	0.11	0.87	1.00	0.94	0.04
322	0	11	140.4	193.1	165.5	18.50	0	175	109.3	76.27	0.54	0.92	0.75	0.13	0.88	1.00	0.93	0.04
322	1	6	135.6	184.1	163.3	15.66	3	4	3.5	0.55	0.46	0.94	0.73	0.17	0.90	0.95	0.93	0.02
322	2	5	166	201.3	181.6	13.51	3	5	3.6	0.89	0.64	0.76	0.70	0.05	0.87	0.97	0.91	0.04
322	3	6	136.4	192.3	163.5	22.72	81	172	113.2	45.69	0.64	0.91	0.81	0.1	0.88	1.00	0.95	0.04
322	4	14	126.5	185.2	158.5	20.73	4	173	72.1	67.45	0.60	0.92	0.78	0.1	0.90	1.00	0.96	0.03
322	5	6	137.9	191.3	166.9	19.63	4	111	81.7	38.67	0.58	0.88	0.79	0.11	0.90	0.98	0.95	0.03
322	6	3	130.7	198.1	173.0	36.85	31	144	91.3	56.89	0.66	0.84	0.77	0.1	0.88	0.98	0.92	0.06
322	7	4	153.7	183.5	165.15	12.84	94	164	112.0	34.67	0.66	0.85	0.76	0.08	0.88	0.96	0.93	0.04

CONCLUSIONS

This paper presented an approach for revealing building patterns from large-scale topographic maps, mainly for use in cartographic generalization. In this context, relatively new HDBSCAN clustering algorithm was employed. Several geometric and structural characteristics of buildings were selected and used as inputs in the clustering algorithm. In the study, at first, blocks were created by means of roads to prevent clustering process from producing topologically incorrect patterns. After that the geometric characteristics (location, size and orientation) and the structural characteristics (convexity and elongation) were computed.

Experimental study showed that the linear and curvilinear patterns were obtained quite successfully when appropriate parameters were used. In case of u-shaped patterns, the

results were unsatisfactory; however, location parameter produced relatively less worse results when used alone. Therefore, it appears that this kind of patterns requires incorporating more specific characteristics into the clustering process. Clusters extracted from the unstructured patterns did not produce meaningful results. Besides, it seems that normalization process can increase or decrease the effect of some characteristics in some cases when a few characteristics were used together.

Future works will possibly focus on applying clustering algorithm by assigning a weight to each characteristic of buildings. In addition, successive clustering might offer some potential in this context.

REFERENCES

- Allouche, M. K., and B. Moulin, 2005. Amalgamation in cartographic generalization using Kohonen's feature nets. *International Journal of Geographical Information Science* 19 (8-9), 899-914.
- Basaraner, M., and Cetinkaya, S., 2017. Performance of shape indices and classification schemes for characterising perceptual shape complexity of building footprints in GIS. *International Journal of Geographical Information Science* 31(10), 1952-1977.
- Basaraner, M., and Selcuk, M., 2008. A structure recognition technique in contextual generalisation of buildings and built-up areas. *The Cartographic Journal* 45(4), 274-285.
- Burghardt D, Schmid S., 2010. Constraint-based evaluation of automated and manual generalised topographic maps. In: Gartner, G. (ed.) *Cartography in Central and Eastern Europe. Lecture Notes in Geoinformation and Cartography*. Berlin: Springer, 147-162.
- Campello, R.J.G.B., Moulavi, D., and Sander, J., 2013. Density-based clustering based on hierarchical density estimates. Pei, J., Tseng, V.S., Cao, L., Motoda, H., and Xu, G. (eds.) *Advances in Knowledge Discovery and Data Mining (PAKDD 2013)*. Berlin: Springer, 160-172.
- Cetinkaya, S., Basaraner, M., and Burghardt, D., 2015. Proximity-based grouping of buildings in urban blocks: a comparison of four algorithms. *Geocarto International* 30 (6), 618-32.
- Deng, M., Tang, J., Liu, Q., and Wu, F. 2017. Recognizing building groups for generalization: a comparative study. *Cartography and Geographic Information Science*. <http://dx.doi.org/10.1080/15230406.2017.1302821>.
- Ester, M., Kriegel, H., Sander, J. and Xu, X., 1996. A density-based algorithm for discovering clusters a density-based algorithm for discovering clusters in large spatial databases with noise. *Proceedings of the Second International Conference on Knowledge Discovery and Data Mining*. Portland, Oregon: AAAI Press, 226-31.

- Li, Z., Yan, H., Ai, T. and Chen, J., 2004. Automated building generalization based on urban morphology and Gestalt theory. *International Journal of Geographical Information Science* 18 (5), 513-534.
- Regnauld, N., 1996. Recognition of building clusters for generalization. In: Kraak M.J., Molenaar, M. (eds.) *Advances in GIS Research II*, London: Taylor&Francis, 185-98.
- Weibel, R., 1995. Map generalization in context of digital systems. *Cartography and Geographic Information Science* 22(4), 716-36.
- Yan, H., Weibel, R., and Yang, B., 2008. A multi-parameter approach to automated building grouping and generalization. *Geoinformatica* 12(1), 73-89.
- Zahn, C. T., 1971. Graph-theoretical methods for detecting and describing gestalt clusters., *IEEE Transactions on Computers* C-20(1), 68-86.
- Zhang, X., Ai, T. and Stoter, J., 2012. Characterization and detection of building patterns in cartographic data: two algorithms. In: Yeh, A.G.O., Shi, W., Leung Y., and Zhou, C. (eds.) *Advances in Spatial Data Handling and GIS*. Berlin: Springer, 93-107.



An Overview of Mobile LIDAR Systems and Their Usability in Corridor Mapping Studies

Barış Süleymanoğlu^{*1}, Metin Soycan²

¹ Department of Surveying Techniques, Yildiz Technical University, Davutpasa Campus, 34220, Turkey. e-mail: bariss@yildiz.edu.tr

² Department of Surveying Techniques, Yildiz Technical University, Davutpasa Campus, 34220, Turkey email: soycan@yildiz.edu.tr

ABSTRACT

Mobile LIDAR systems is currently one of the most popular topic in the LIDAR industry and evolving measuring technology. These systems can be integrated on Mobile platforms to provide highly accurate 3D point data for different application areas. Mobile LIDAR systems consist of many different subsystems such as IMU, GNSS, laser scanner, camera and control units. In this study, detailed information provided about Mobile LIDAR technologies and detailed information about positioning, scanning and imaging devices used in these systems and how to integrate these devices into Mobile LIDAR system. In addition, the advantages and disadvantages of these systems compared to the airborne LIDAR , terrestrial LIDAR, photogrammetry and classical measurement methods are explained. In this study, it is aimed to test the possibilities of using Mobile LIDAR systems for corridor mapping, inventory mapping. For this purpose, Mobile LIDAR data collected from urban area was used. As a result of this work road surface geometry, including the road shoulder, and all objects on, above or near that surface, like road sides, road markings, trees, traffic lights, traffic signs, crash barriers were extracted.

INTRODUCTION

High-precision maps contains 3-dimensional, highly detailed and highly accurate data. These maps have been developed to create the map infrastructure required by autonomous car technology. They require a detailed knowledge of the road in order to ensure safely and comfortably drive. These road knowledge:

- Road inclination and curve information
- Road lane boundaries, strip geometry and speed limit
- Precise locations of traffic signs and signs

These maps are much more detailed maps than the classic navigation maps. For this

^{*} Corresponding Author

reason, advanced measurement methods are needed for the creation of these maps. Mobile LIDAR systems has become one of the most important measuring systems used in the creation of these maps (<https://www.mercedes-benz.com>).

MOBILE LIDAR SYSTEMS

Mobile LIDAR systems (MLS) have emerged as an important mapping technology developed in recent years. Mobile LIDAR systems are installed in vehicles and scan the profile on a certain line so that high accuracy three-dimensional point clouds from surrounding objects can be obtained. The data obtained with this system provides information such as trees, buildings, bridges, traffic signs and signposts, energy transmission lines, road lanes and road geometry. In addition, MLS systems can be customized for different tasks by being mounted on different types of moving vehicles. All of these features make this system an indispensable part of the road-related work (Kukko (2012)).

Figure 1 shows the mobile LIDAR system mounted on the vehicle and the components forming this system. Mobile LIDAR systems is a complex measuring system consisting of a combination of different systems. These systems mobile platform, positioning and navigation component, laser scanners, digital cameras and control systems(Computer, Data Storage Devices). As mentioned above, Mobile LIDAR systems can be used with different measuring platforms to adapt to changing working areas. Position of mobile vehicle determined by positioning and navigation component. Positioning and navigation component consist of Global Navigation Satellite System(GNSS), Inertial Measuring Unit(IMU), Distance Measurement Indicator(DMIs). The GNSS system is the basic tool for positioning system. GNSS system gives position information in centimeter level in WGS-84 system. Inertial Measurement Unit(IMU) provides location and attitude of mobile vehicle. DMI measures wheel rotation and calculates travelled distance. Camera systems are used to visualize the point cloud data obtained by MLS. The point cloud can be colored(RGB) with the data obtained with the camera systems. Computer and data storage systems are used in the storage and processing of data obtained with the MLS system ((Olsen (2013), (Puente (2013)).

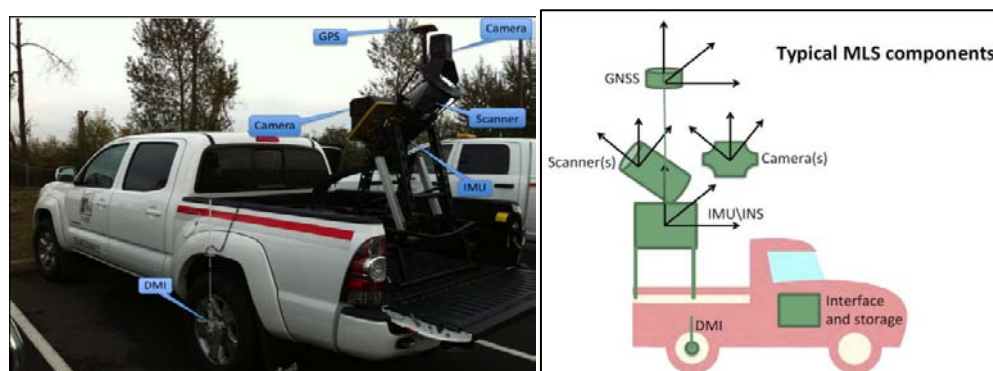


Figure 1. Mobile LIDAR System mounted on vehicle (Williams (2013) and system component ((Olsen (2013)

Mobile LIDAR systems have some advantages over other systems (especially Airborne LIDAR System) as part of road inventory applications. These systems provide good visibility of the road surface and vertical view of the road. High density point cloud data can be obtained with this system and this system is best captured on the ground surface and surrounding objects because it is close to the ground surface and the objects on this surface (Olsen (2013)). The calculation of the coordinates of any object within MLS data is called geo-referencing (Guan (2016)). Figure 2 contains the formula used to calculate a point p in the object obtained by MLS and the information of the parameters in this formula.

$$\begin{bmatrix} X_P \\ Y_P \\ Z_P \end{bmatrix}^M = \begin{bmatrix} X_{GNSS} \\ Y_{GNSS} \\ Z_{GNSS} \end{bmatrix}^M + R_{IMU}^M(\omega, \varphi, \kappa) \cdot \left(R_S^{IMU}(\Delta\omega, \Delta\varphi, \Delta\kappa) \cdot r_p^S(ad) + \begin{bmatrix} L_X \\ L_Y \\ L_Z \end{bmatrix}_S^{IMU} - \begin{bmatrix} L_X^G \\ L_Y^G \\ L_Z^G \end{bmatrix}_{GNSS}^{IMU} \right)$$

X_P, Y_P, Z_P	Location of the target P in the mapping frame.
$X_{GNSS}, Y_{GNSS}, Z_{GNSS}$	Location of GNSS antenna in the mapping frame.
$R_{IMU}^M(\omega, \varphi, \kappa)$	Rotation matrix between IMU and mapping frame, $(\omega, \varphi, \kappa)$ are the roll, pitch and yaw of the sensor with respect to the local mapping frame. These values are provided by the IMU system.
$R_S^{IMU}(\Delta\omega, \Delta\varphi, \Delta\kappa)$	Rotation matrix between the laser scanner and IMU, $(\Delta\omega, \Delta\varphi, \Delta\kappa)$ are the boresight angles which align the scanner frame with IMU's body frame. Those values are determined by the system calibration.
$r_p^S(ad)$	Relative position vector of Point P in the laser scanner coordinate system, a and d for scan angle and range measured and returned by the laser scanner.
L_X, L_Y, L_Z	Lever-arm offsets from the navigation and IMU origin to the laser scanner origin. These values are determined by system calibration or measurement.
$L_X^{(G/I)}, L_Y^{(G/I)}, L_Z^{(G/I)}$	Lever-arm offsets from the IMU origin to the GNSS origin. These values are determined by system calibration or measurement.

Figure 2. Equation and parameters used in geo-referencing MLS data (Guan (2016))

MOBILE LIDAR SYSTEM IN CORRIDOR MAPPING AND ROAD INVENTORY

Mobile LIDAR data can be used in various road inventory information extraction applications. These applications can basically divided into 3 category.

- Extracting the path geometry
- Extracting road surface features (road lane information and cracks on the road)
- Extracting pole-like objects around the road (such as traffic signs and signposts)

The geometrical design parameters of the roads are needed when renovation or editing work on the old roads is to be carried out. However, most of the time this data is not available. Extracting of the path geometry by using MLS data is needed in such cases.

For this purpose, a number of path recognition and extraction algorithms have been developed. These algorithms basically work in 3 different ways (Guan (2016)).

- Algorithms using the geometric properties of the path
- Algorithms that use LIDAR data features as well as path geometry
- Algorithms that use extra data sources(Photogrammetry, Airborne LIDAR)

Different approaches have been developed in the derivation of the road geometry as mentioned above. Some algorithms extract the road surfaces directly while others detect the road edges and extract the road geometry. With the algorithms directly extracting the

road surface from the LIDAR data, the road lane information is obtained directly from the point cloud data. The processing time is very long in these algorithms. An example of these algorithms is the Hough transformation algorithm developed by Takashi and Kiyokazu (2006) or weighted least-square linear fitting algorithm developed by Yuan et al. (2010). Another way is to extract the road surface by detecting the road edges. These algorithms are based on the extraction of road information by detecting the road edges instead of determining complete road surface to increase the calculation efficiency. These algorithms use altitude difference, altitude change, mean values calculated from point cloud data (Yoon and Crane (2009)). Some algorithms that detect road surfaces use properties of path geometry as well as LIDAR data properties such as point distribution, intensity, and laser beam return information.

Road surfaces include information such as road signs, roger covers, sewer wells and grills. In particular, road signs have important functions in traffic management systems, steering drivers and pedestrians, and informing autonomous vehicles about the road. This is why it is very important to extract this information. The intensity features of the LIDAR data is used to extract this information. For this purpose, image processing algorithms such as hough transformation and morphology are used (Guan (2016).

Finally, it is an important process to extract pole-like objects such as electric poles, traffic signs and lamp poles. Traffic signs and signpost are made up of highly reflective surfaces. Chen et. al(2007) used intensity value to detect traffic signs and signposts

MATERIAL AND METHODS

In this study, it is aimed to extract some geometrical features of the road surface, to drawn the as-built maps of the road and its surroundings and to carry out the processes of classification of powerlines with Mobil LIDAR data. The data used in this study was obtained from a specific region of the Isparta-Antalya highway with the Riegl WMX-450 MLS system. This system is seen in Figure 3. The technical specifications of this system are shown in Table 1.



Figure 3. RIEGL VMX-450 (9)

Table 1. RIEGL VMX-450 technical specifications

Effective Measurement Rate	1.1 MHz
Max. Measurement Range	
natural targets $p \geq 10 \%$	140 m
natural targets $p \geq 80 \%$	220 m
Minimum Range	1.5 m
Accuracy	8 mm
Precision	5 mm
Max. Effective Measurement Rate	1100 000 meas./sec
Line Scan Speed	Up to 400 lines/sec

In this study, approximately 700 m of the data obtained from Isparta-Antalya highway was used. Figure 4 shows the data used in this study. Table 2 contains statistical information about the study area shown in Figure 4. As can be seen from the table, very dense point cloud data is obtained with the MLS system. The point cloud data includes the road surface, traffic signs and signposts, trees, certain corners of buildings and powerlines. All these data provide valuable information that will form the basis for the editing, management and updating of structures of roads and their surroundings. Global mapper 18.1 and NetCAD software were used in this study.

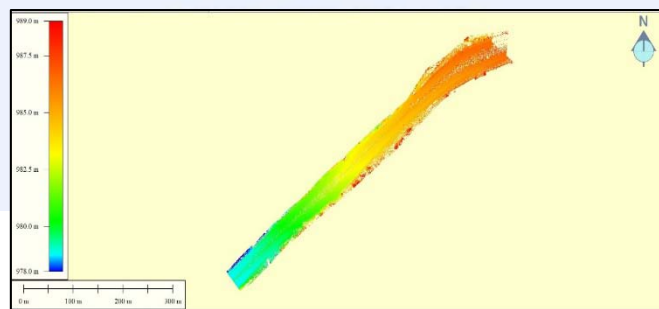


Figure 4. Test area

Table 2. Statistical Values of Test Area

Point count	7.689.576
Point Density	170.70 samples/m ²
Min. Elevation	969.245 m
Max. Elevation	1050.994

Figure 5. Profile section of road surface

673

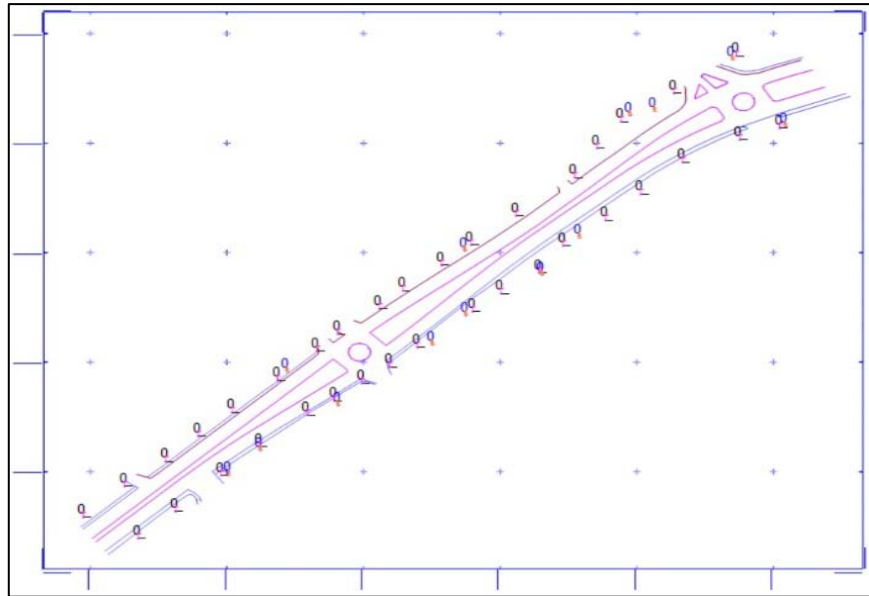


Figure 6. As-built maps from MLS data

Finally, powerline extraction from MLS data was performed. The Lidar module of the Global Mapper software used for this study. First, the ground data of the study area needs to be determined, then the power lines can be extracted. For this purpose, work area is divided into user defined parts. Ground points are determined separately for each part. Threshold values are used to determine the ground points. To increase the accuracy of the detected ground points, the expected height and slope change parameters for the work area are entered. Since these parameters vary according to the study area, it is necessary to make experiments in order to reach optimum values. After the optimum parameters for the ground data were determined for our study area, the process of extracted the powerlines was started. Since the powerline are flat surfaces covering small areas, high density point cloud data is needed to be accurately detected. The aim here is to find linear patterns between the points above the ground. For this purpose, the minimum height value on the ground on which powerlines are located must be specified first. Once these linear dots are detected, threshold values are used to determine whether they follow random dots or a specific pattern. For our study area, these parameters were tested one by one and the most optimum values were determined. Figure 7 shows powerlines that automatically extracted from work area.

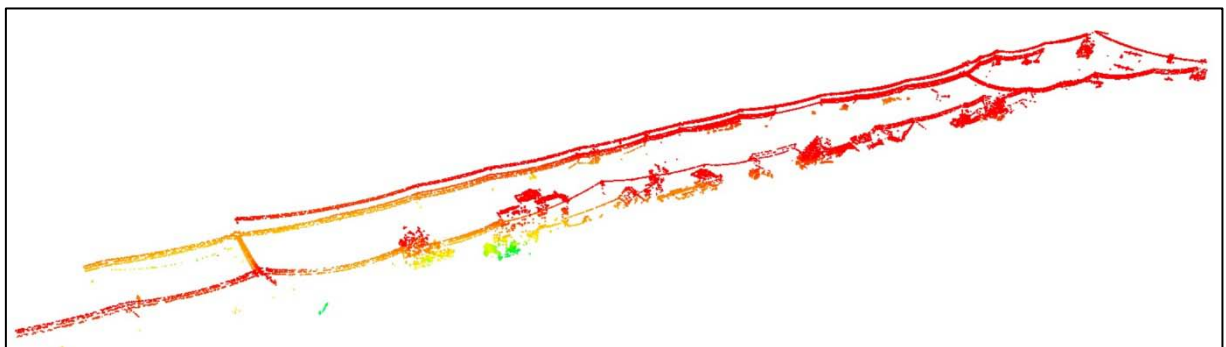


Figure 7. Powerlines of work area

CONCLUSION

Based on the information above and our study, it has been found that Mobile LIDAR Systems have a significant potential for extracting road inventory information in terms of security, efficiency, flexibility and data density. Moreover, it has been shown that these algorithms produce erroneous results at different ratios. Accordingly, errors were encountered in the powerline classification study conducted within the scope of this study. Some objects such as trees and buildings are incorrectly classified. It has been seen that comparative studies of the advantages and disadvantages of software or programs should be tested in order to determine best algorithm or software to extract the objects of the road and its surroundings. Furthermore, during the as-built study the data obtained by MLS alone were not sufficient. Especially in specific applications such as as-built, it is seen that in addition to the MLS system, the data obtained by different measurement methods (Photogrammetry, Airborne LIDAR) can be used as supportive features.

REFERENCE

- Kukko, Antero, et al. "Multiplatform Mobile laser scanning: Usability and performance." *Sensors* 12.9 (2012): 11712-11733.
- Williams, Keith, et al. "Synthesis of transportation applications of Mobile LIDAR." *Remote Sensing* 5.9 (2013): 4652-4692.
- Olsen, Michael James. *Guidelines for the use of Mobile LIDAR in transportation applications*. Vol. 748. Transportation Research Board, 2013.
- Puente, I., et al. "Review of Mobile mapping and surveying technologies." *Measurement* 46.7 (2013): 2127-2145.
- Duffell, C. G., and D. M. Rudrum. "Remote sensing techniques for highway earthworks assessment." *Site Characterization and Modeling*. 2005. 1-13.
- Guan, Haiyan, et al. "Use of Mobile LIDAR in road information inventory: a review." *International Journal of Image and Data Fusion* 7.3 (2016): 219-242.
- Chen, Xin, et al. "Next generation map making: geo-referenced ground-level LIDAR point clouds for automatic retro-reflective road feature extraction." *Proceedings of the 17th ACM SIGSPATIAL International Conference on Advances in Geographic Information Systems*. ACM, 2009.
- Teo, T. A., & Chiu, C. M. (2015). "Pole-like road object detection from Mobile LIDAR system using a coarse-to-fine approach". *IEEE Journal of Selected Topics in Applied Earth Observations and Remote Sensing*, 8(10), 4805-4818.
- http://www.riegl.com/uploads/tx_pxpriegldownloads/DataSheet_VMX-450_2015-03-19.pdf
- Takashi, O. and Kiyokazu, T., 2006. Lane recognition using on-vehicle LIDAR. In: *IEEE intelligent vehicle symposium*, 13–15 June, Tokyo. IEEE, 540–545.

- Yuan, X., Zhao, C., and Zhang, H., 2010. Road detection and corner extraction using high definition LIDAR. *Information Technology Journal*, 9, 1022–1030.
- Yoon, J. and Crane, C.D., 2009. “Evaluation of terrain using LADAR data in urban environment for autonomous vehicles and its application in the DARPA urban challenge”. In: *Proceedings of ICROS-SICE international joint conference*, 18–21 August, Fukuoka. SICE, 641–646.
- Chen, Y., Zhao, H., and Shibasaki, R., 2007. A mobile system combining laser scanners and cameras for urban spatial objects extraction. In: *Proceedings of IEEE conference on machine learning and cybernetics*, 19–22 August, Hong Kong, 3. IEEE, 1729–1733.

<https://www.mercedes-benz.com/en/mercedes-benz/next/connectivity/high-precision-maps-for-self-driving-cars>



Use of GIS in some issues of landscape planning

Cumhur Güngöroğlu

*Department of Forest Engineering, Karabük University, Demir-Çelik Campus, 78050, Turkey.
(cumhurgungoroglu@karabuk.edu.tr)*

ABSTRACT

*GIS can be used in the different issues of the environmental planning process. Especially, GIS is very useful applied for the landscape planning in the process of getting, processing, developing, analyzing, visualizing and mapping of data. The aim of this study is to present the application areas of GIS in landscape planning studies used in different purposes. Firstly, the application areas of GIS have been taken as examples from a study based on European Landscape Typology applied in Turkey. In another study, the role of GIS in the analysis of landscaping measurements based on the patch, unit and diversity of the spatial pattern of the cypress (*Cupressus sempervirens* L.) forest is considered. At the classification of landscape types for first example study was used LANMAP recommended across Europe for landscape classification. The layers in LANMAP are overlayed to each stage according to GIS-based hierarchical order. Different layers are used in each stage respectively. Totally, three layers are used to classify the landscape in this study. In another study, spatial pattern analyze of cypress forest biotopes in the National Park Köprülü Kanyon was realized by measuring of area, density and diversity metrics. The Patch Analyst application, which is compatible with GIS studies, was used to calculate the landscape metrics in this study.*

INTRODUCTION

One of the most important challenges Landscape ecologists face is that it is not possible to provide landscape data at various scales with existing analytical tools. The collection of consistent data at different scales and features is difficult, time consuming and expensive. Large data volumes have also complicated the operation at the same time, making integration more difficult. Fortunately, most of these difficulties have come to the fore of most of these difficulties with the availability of computer-based systems to process geographic or spatial data, called 'geographic information systems' (Haines-Young, *et al.* 1993). To assess the structure and functioning of the landscape are used spatially dispersed ecological data on various spatial and temporal scales. The best planning of a landscape requires knowledge of its structural and functional characteristics. Landscape planning aims generally to sustainable development by creating planning principles that will enable future generations to live in an ecologically environment. Regarding to the design this approach it has been developed a planning system based on analytical processes. Planning

objectives will be derived from scientifically based analysis and normative goals (Pietsch, 2012; von Haaren, 2004). As an information technology, GIS can help to improve the landscape planning process and to use the results in the future for existing information systems (Arnold *et al.* 2005; Lang and Blaschke, 2007). The areas where GIS is used in the landscape planning process are identified below:

1. provide a database structure for efficiently storing and managing landscape data over large regions (Pietsch, 2012);
2. enable aggregation and disaggregation of data between regional, landscape and plot scales (Burnett and Blaschke, 2003);
3. provide priority areas, ecologically sensitive or suitable areas for conservation (Fairbanks and Benn, 2000; Orsi and Geneletti, 2010);
4. support spatial statistical analysis of ecological distributions (Wagner and Fortin, 2005);
5. capabilities to extract, improve and integrate remote-sensing information into planning process (Burnett and Blaschke, 2003);
6. provide input data/parameters for ecosystem modelling, valuing and characterizing ecosystem services and functions (Diaz-Varela *et al.* 2009);
7. design methods and its applications (e.g. decision support systems, agent-based modeling) (Volk *et al.* 2010) and;
8. representation of the results (e.g. visualization techniques, animations, simulations) (Lerouge *et al.* 2017; Pietsch, 2012).

The power of GIS in landscape planning stems from the fact that data from any combination of different layers of data can be used to solve a specific problem. In addition, when problems change, the data can be processed in different ways to address different issues in a highly flexible manner. With the ability to process spatial information in the form of a map important, GIS can also store non-geographic attribute information that can be associated with various map features in a type of database management system. This data can also be used to access map information (Haines-Young, *et al.* 1993).

Study 1: European Landscape Typology applied in Turkey

With the European Landscape Convention (ELC) is aimed the preservation, management and promotion of the planning of European landscapes at the organisation of European cooperation (CoE, 2006). ELC provides countries that are developing and protecting their landscapes with principles, strategies, guidance and instruments (Butler and Berglund, 2014). LANMAP is suggested as a coherent landscape classification system for the European scale the context of the ELC (Wascher *et al.*, 2005). The aim of this study is to present the application areas of GIS during the applicability of the European approach to landscape classification studies at the local scale (Turkey, Çakırlar basin) within the context of the LANMAP.

Study 2: GIS in the analysis of landscaping measurements based on the spatial pattern of the cypress (*Cupressus sempervirens* L.) forest

Landscape is made up of the area patches of parts (patches). Abiotic factors, vegetation and land-use-based characteristics are mainly attributed to the formation of these landscape parts. These properties make up ecologically homogeneous units with the values they have at a certain scale (Pickett *et al.*, 1999). In this study, the analysis of the spatial pattern of the cypress biotops (*Cupressus sempervirens* L.) distributed in Köprülü Kanyon National Park was carried out by landscape measurements based on patch, unit and diversity metrics. In this way, it is aimed to analyze the landscape structure of unit and class levels of cypress biotopes.

METHODOLOGY

Study Sites

The study site 1 is the Çakırlar drainage basin, where is located to adjoining Antalya city centre. The study site 2 is the natural cypress forests of the Köprüçay basin which is located on the Antalya province boundaries of Köprülü Kanyon National Park (Figure 1).

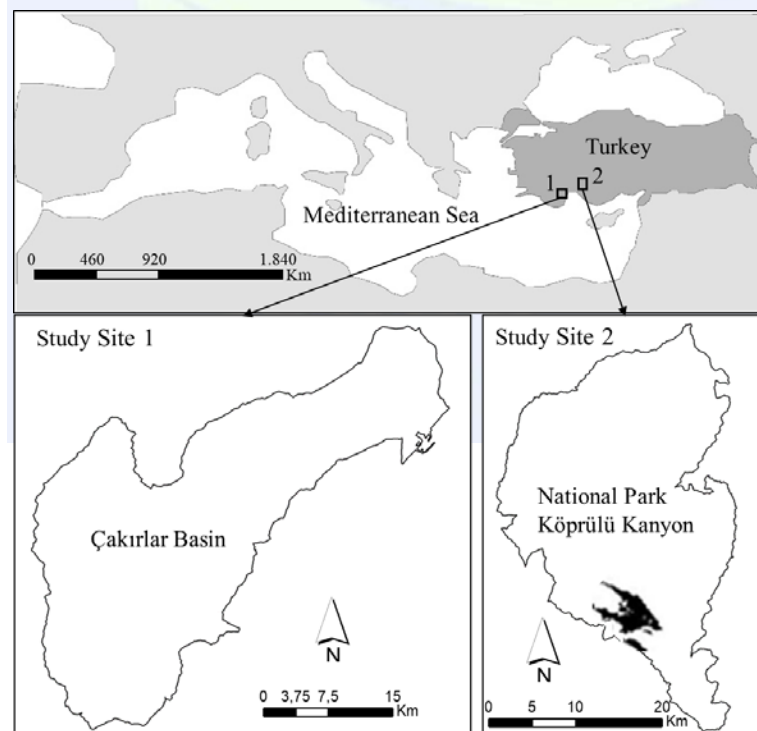


Figure 1. Location of study sites

European Landscape Typology applied in Turkey

Landscape types are grouped hierarchically in four stages (Figure 2). The whole of the study area is characterized by the climate type – Mediterranean – in the first stage. Five

altitude ranges were used as a layer for the second stage. Five bedrock classes were used for the third stage. Finally, nine land-cover types were used at the fourth stage. The classification of altitude used the same classes as LANMAP (Mücher *et al.*, 2003). The maps of parent materials and land cover were classified more specifically to refer to the study site. GIS-based overlapping methods have been used to overlay the stages. All of the maps have been produced with a 20×20 m raster cell size. Güngöroğlu (2017) was used for the material and method of this study.

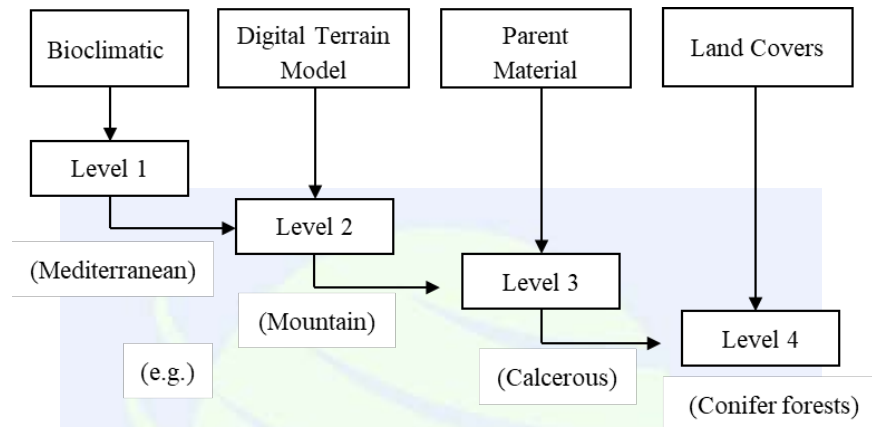


Figure 2. Hierarchical classification of landscape types

GIS in the analysis of landscaping measurements based on the spatial pattern of the cypress (*Cupressus sempervirens* L.) forest

Biotope types formed in a hierarchical structure by Güngöroğlu (2010) were used as material (patches) in this study. The hierarchical levels for analysis of cypress biotope types is given below.

1. Cypress Forests (*Cupressus sempervirens*) (Landscape Level)

1.1 Pure cypress forests on deep and narrow valley hillsides (Class Level)

1.1.1 On the hillsides with less insolation impact (Unit Level)

1.1.2 On the hillsides with many insolation affects

1.2 Mixed cypress forests on deep and narrow valley hillsides

1.2.1 Cypress dominated calabrian pine (*Pinus brutia* T.) forests

1.2.2 Cypress dominated calabrian pine and oaks forests

1.2.3 Calabrian pine dominated cypress forests

1.2.4 Calabrian pine dominated cypress and oaks forests

1.3 Cypress forests on the upper slopes of the valleys, open to cold air streams

1.3.1 Cypress dominated calabrian pine mixed forests

1.3.2 Calabrian pine dominated cypress mixed forests

The classification codes used to construct biotope types are the basis for the systematic classification of cypress landscapes. This basis is shown as the reduction of the complex structure of the landscape in the present case, thanks to the model-like systematically formed shapes (Knickrehm and Rommel, 1995). In this study, cypress forests were classified and mapped by GIS supported remote sensing methods in three hierarchical layers (landscape, class, unit) based on homogeneous characteristics of each layer for vegetation, habitat and land uses. Güngöroğlu and Sabuncu (2008) investigated surface characteristics of slopes, elevation and elevation of cypress forests according to the mixture of tree species. In their study, it is stated that all cypress forest types spread on very sloping and in steep terrain.

RESULTS

European Landscape Typology applied in Turkey

All layers are overlaid in hierarchical order. Eighteen landscape units are classified at the third level (Figure 3). MK is the biggest unit in this classification with a surface area of 3771.27 ha. On the other hand, LK is the smallest unit with a surface area of 22.13 ha. There are 120 patches related to landscape units. The smallest patch is 4.099 ha and the biggest patch is 3075.044 ha. The average patch width is 197.888 ha. There are 101 landscape units classified at the fourth level (Figure 3).

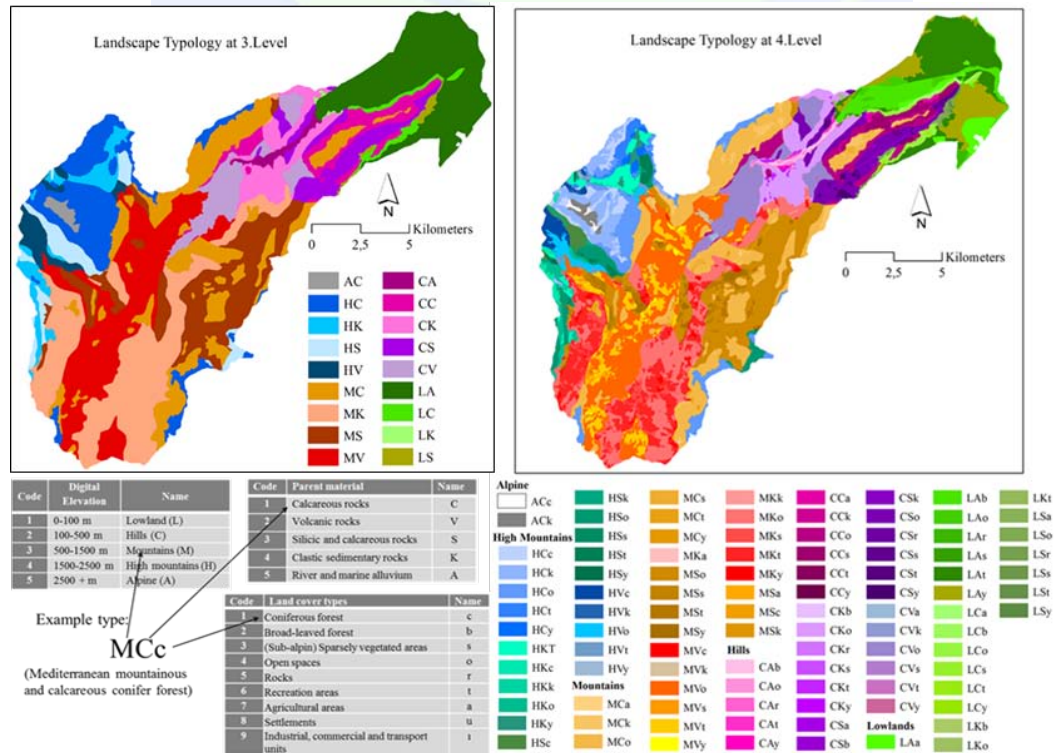


Figure 3. Coding landscape types and their classification at different levels

GIS in the analysis of landscaping measurements based on the spatial pattern of the cypress (*Cupressus sempervirens* L.) forest

The polygons of the biotope types are combined at the unit and class level (Figure 4). The number of polygons (patches) (NP) and size of area (SA) of unit and class level biotopes were determined. Metric values of the spatial structure analysis of landscape created by cypress biotope types are also shown in Table 1. When these data are examined, it is seen that the Shannon Diversity Index (SDI) values are higher in the classes with higher tree species diversity. Compared to the mixed service forests in the deep and narrow valley hillsides (1.2), understand that the pure cypress forests (1.1) are more fragmented regarding to NP (Table 2), SA, average mean size of cypress biotopes at the unit level (AMU) and standard deviation of mean size between unit-level cypress biotope types (SDMU) values (Table 1). The total class area of the cypress forests on the upper slopes of the valleys (1.3), which is open to the cold airstreams, is closer to the pure cypress forests, but with a smaller NP compared to them. It is also remarkable that the average unit size of this class code is higher than the other classes, and the unit size variation coefficient is also lower than the other. This can be explained by limiting the environmental conditions of this class to a wide range of environmental conditions (Güngöroğlu, 2010). This class is limited at high altitudes, sunny aspects and steep terrain. Linear similarities between the values of AMU and SDMU of pure and mixed forests have been noted which are located in the deep and narrow valley hillsides. It can be interpreted that these two classes coexist in a mosaic in the same environmental growth conditions and that especially the exposition, sloping and altitude play an important role in their local distribution (Güngöroğlu, 2010).

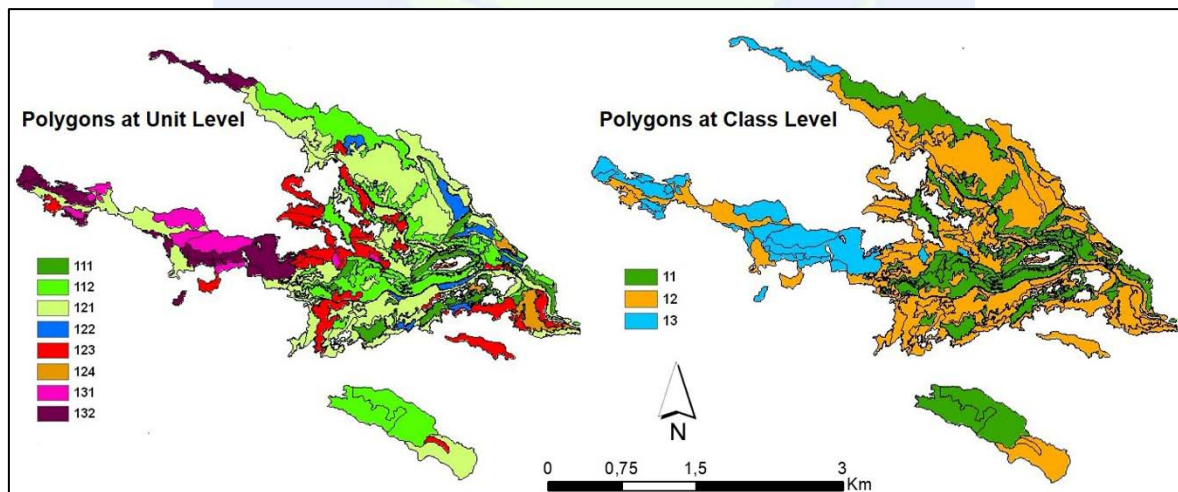


Figure 4. Dissolve of cypress biotopes at unit and class level

Table 1. Metric values of landscape spatial pattern

Level of Analysis	SDI	AMU	NP	SDMU	SA
1.1 - Landscape	0,5408	5,0663	32	11,6019	162,1213
1.2 - Landscape	0,8478	8,9436	55	20,7993	491,8972
1.3 - Landscape	0,6920	11,8331	11	17,9497	130,1645
All units - Landscape	1,6749	8,0019	98	18,1071	784,1829
All classes - Landscape	0,9165	13,7573	57	39,5596	784,1661

Table 2. Number of polygons at hierarchical levels

Class Code	Unit	Class
1.1	32	26
1.2	55	27
1.3	11	4

DISCUSSION

While the landscaping units by LANMAP methodology are being identified, the comparison of unit numbers and widths emerges as a point to be considered. It appeared sliver polygons which are less than <0.01 ha. Although it is possible that there can be 30 units by number of layer polygons in the first-level classification and 270 units in the second-level classification, given the combination of environmental factors, in reality, there are 18 units in the first-level classification and 101 units in the second-level classification. This similar situation has been encountered with classifications at European level (Mücher *et al.*, 2010). The study area includes partial forms of high mountainous areas in particular. When the parent materials in the partial form are added, large and small units start to appear from the third level. Later, it is determined that land-cover types related to land-use conditions, which the third level serves, provide an irregular large and small distribution. It is understood that a variety of land-cover types play an important role in the number of units in local classification of landscapes with LANMAP methodology. Therefore, grouping land-cover types suitably according to the structural properties of land-use types enables higher content characterization at the local level.

Deep valley hillsides reveal a pattern in which the cypress is spreading purely and mixedly. Pure cypress biotopes are distributed in smaller areas and partly in mixed cypress forests which are a more complete unity than pure biotopes. Care should be taken to ensure that the largest units in these two classes are narrowed down due to human use and that their fragmentation does not increase, particularly regarding to the protection of cypress genetic resources. In addition, habitat functions such as hiding, reproduction and nutrition of wild animals are higher than smaller units. Open mixed cypress forests to cold air flows are more uniq in terms of fragmentation, number of units, and area size than other classes. However, these areas are more precisely limited in terms of the site conditions for the growing and they have a narrower area width in terms of total area. In this respect, they are highly sensitive to external influences.

CONCLUSIONS

It is also understood in two studies that GIS is a useful tool for gathering, analyzing and evaluating different environmental conditions that are geographical distributed. It has a capability to find homogeneous areas, where different factors bring together, provides an assessment of their number and spatial extent. It has also been found to play an important role in establishing the ecological characteristics to be considered in terms of planning and management.

REFERENCES

- Arnold, V., Lipp, T., Pietsch, M., Schaal, P., 2005. Effektivierung der kommunalen Landschaftsplanung durch den Einsatz Geographischer Informationssysteme, *Naturschutz und Landschaftsplanung* Heft 11, S. 349.
- Burnett, C., Blaschke, T., 2003. A multi-scale segmentation/object relationship modelling methodology for landscape analysis. *Ecological Modelling* 168, 233–249.
- Butler, A., Berglund, U., 2014. Landscape Character Assessment as an Approach to Understanding Public Interests within the European Landscape Convention, *Landscape Research*, 39(3), 219-236.
- Council of Europe (2006). Landscape and sustainable development: challenges of the European Landscape Convention. Challenges of the European Landscape Convention. Council of Europe Publishing, 213 S. Available at <https://rm.coe.int/CoERMPublicCommonSearchServices/DisplayDCTMContent?documentId=090000016802f24d2> (accessed 30.11.2015)
- Diaz-Varela, E. R., Marey-Pérez, M. F., Rigueiro-Rodriguez, A., Álvarez-Álvarez, P. 2009. Landscape metrics for characterization of forest landscapes in a sustainable management framework: potential application and prevention of misuse. *Annals of forest science* 66 (3), 1-10.
- Güngöroğlu, C. 2017. Applicability of European Landscape Typology in Turkey (Çakırlar Watershed Case/Antalya). *Landscape Research* (in Press).
- Güngöroğlu, C. 2010. *Entwicklung eines Biotopkartierungsverfahrens für die Türkei mit Hilfe von GIS- und Fernerkundungstechnik (Fallbeispiel Nationalpark Köprülü Kanyon)*. Dissertation zur Erlangung des Dokortitels, angenommen von: Georg-August-Universität Göttingen, Fakultät für Forstwissenschaften und Waldökologie. 265 S.
- Güngöroğlu, C., Sabuncu, R., 2008. Threatened Cypress Forest Ecosystems in the Mediterranean Region, EFE, R. et al (ed.) "Natural Environment and Culture in the Mediterranean Region", *Cambridge Scholars Publishing*, S. 131-148

- Haines-Young, R., Green D.R., Cousins, S., 1993. Landscape ecology and spatial information systems. Haines-Young, R., Green D.R., Cousins, S. (ed.) *Landscape Ecology and GIS*. Taylor & Francis, 3-8 pp.
- Fairbanks, D.H.K., Benn, G.A., 2000. Identifying regional landscapes for conservation planning: a case study from KwaZulu-Natal, South Africa. *Landscape and Urban Planning* 50, 237-257.
- Knickrehm, B., Rommel, S., 1995. Biotoptypenkartierung in der Landschaftsplanung. *Natur und Landschaft*, 70. Jg., Heft 11, S. 519-528.
- Mücher, C.A., Bunce, R.G.H., Jongman, R.H.G., Klijn, J.A., Koomen, A.J.M., Metzger, M.J., & Wascher, D.M. (2003). Identification and Characterisation of Environments and Landscapes in Europe (Alterra report 832), Wageningen, Alterra.
- Mücher, C.A., Klijn, J.A., Wascher, D.M., & Schaminée J.H.J. (2010). A new European landscape classification (LANMAP): a transparent, flexible and user-oriented methodology to distinguish landscapes. *Ecological Indicators*, 10, 87–103.
- Lang, S., Blaschke, T., 2007. *Landschaftsanalyse mit GIS*, UTB Verlag, 404 S.
- Lerouge, F., Gulinck, H., Vranken, L., 2017. Valuing ecosystem services to explore scenarios for adaptive spatial planning. *Ecological Indicators* 81, 30-40.
- Orsi, F., Geneletti, D., 2010. Identifying priority areas for Forest Landscape Restoration in Chiapas (Mexico): An operational approach combining ecological and socioeconomic criteria. *Landscape and Urban Planning* 94, 20–30.
- Pickett, S.T.A., Wu, J., Cadenasso, M. L., 1999. Patch dynamics and the ecology of disturbed ground: a framework for synthesis. Walker, L.R. (ed.) *Ecosystems of Disturbed Ground*, Elsevier, Amsterdam, 707-722
- Pietsch, M., 2012. GIS in Landscape Planning. In: Ozyavuz, M. (Ed.), *Landscape Planning*. InTech, pp. 55–84. www.intechopen.com/books/landscape-planning/gis-inlandscape-planning
- Volk, M., Lautenbach, S., van Delden, H., Newham, L.T.H., Seppelt, R., 2010. How Can We Make Progress with Decision Support Systems in Landscape and River Basin Management? Lessons Learned from a Comparative Analysis of Four Different Decision Support Systems. *Environmental Management* 46, 834–849.
- von Haaren, C., 2004. *Landschaftsplanung*, Eugen Ulmer Verlag, Stuttgart, 528 S.
- Wagner, H.H., Fortin, M.J., 2005. Spatial analysis of landscapes: concepts and statistics. *Ecology* 86 (8), 1975–1987
- Wascher, D.M., Groom, G., Mücher, C.A., Kindler, A., 2005. Recent developments in mapping Europe's landscapes. In Wascher, D.M. (Ed.), *European Landscape Character Areas – Typologies, Cartography and Indicators for the Assessment of Sustainable Landscapes* (pp. 5 – 31). Final ELCAI Project Report, *Landscape Europe*.

Use of SENTINEL-1 Data In Oil Spill Surveillance And Modeling

Niyazi Arslan^{*1}, R. Cuneyt Erenoglu²

¹ Department of Geomatics Engineering, Cukurova University, 01950 Ceyhan, Adana, Turkey. e-mail: narслан@cu.edu.tr

² Department of Geomatics Engineering, Canakkale Onsekiz Mart University, 17100, Canakkale, Turkey email: ceren@ceren.edu.tr

ABSTRACT

A consistent surveillance and modeling of oil spills which is taken place from ships, offshore platforms and accidents is very important in terms of public safety, urban modelling and environmental protection. It is also necessary to detect spillage, spread from the source to nearby coastal areas. In this context, Sentinel-1 data was processed for detection and monitoring of oil spills which have received great interest due to wide-area coverage, day and night availability and usage in all weather conditions. In this study, the oil spill incident was investigated at the İlica and Paşa ports that are the most of the favorite beaches of Çeşme occurred in December 18, 2016. A simple and relatively quick approach for oil spill detection has been employed to VV polarized Sentinel-1 imagery before and after the incident. Moreover, the obtained results are discussed taking into account oil spill area. The processing steps for the oil spill detection were carried out using Sentinel Application Platform (SNAP). The results indicate that the Sentinel-1 data can be used efficiently for oil spill detection. In the future study, a semi-automatic or automatic strategy based on the relevant methodology will be developed for detection of oil spill with timely and cost effectively.

INTRODUCTION

A consistent surveillance and modeling of oil spills which is taken place from ships, offshore platforms and accidents is very important in terms of public safety and environmental protection (Lawal *et al.* 2016; Caruso *et al.* 2013; Gade *et al.* 2013; Hua *et al.* 2010; Topouzelis *et al.* 2009; Migliaccio *et al.* 2005; Noriega, 2005; Del Frate and Salvatori, 2004; Alpers and Melsheimer, 2004; Jackson and Apel, 2001; Fiscella *et al.* 2000; Hovland *et al.* 1994)

^{*} Corresponding Author

In this study, the oil spill incident was investigated at the İlica and Paşa ports that are the most of the favorite beaches of Çeşme occurred in December 18, 2016. A simple and relatively quick approach for oil spill detection has been employed to VV polarized Sentinel-1 imagery before and after the incident. The processing steps for the oil spill detection were carried out using Sentinel Application Platform (SNAP). The results indicate that the Sentinel-1 data can be used efficiently for oil spill detection.

SEA VESSEL INCIDENT

While the cargo ship in motion was manoeuvring to avoid hitting the fishing boat, it hit on the rocks near the Fener Island, Cesme, Turkey (Figure 1). It has led to the greatest environmental disaster in the history of Cesme.



Figure 1. Location map of the study area, A snapshot from the coast after Sea Vessel Incident on December 18, 2016 in Ildir Bay, Izmir, Turkey

Oil was leaked to the sea due to the torn in the body of the ship. When the situation is reported, the crew arriving at the region has set a barrier to prevent leakage of the oil on board. However, due to the weather conditions, the rescue of the ship and environmental clean-up work could not be started. Figure 2 shows the photograph indicating the slick of the oil spill on the sea surface that was taken from the coast of Ildir Bay (Izmir, Turkey) after sea vessel incident on December 18, 2017.

After the storm, the leaking oil from the ship was quickly taken under control. When a 100 person cleaning work was carried out, 30 ton of 50 tons of oilslick were cleaned. The city of Çeşme has returned at the brink of a much greater catastrophe. Even though the barriers around the ship controls the oil spill, it exploded in the second storm on December 22th causing a new pollution spreading 50 tons of fuel oil. Starting at 10:00 am on December 27th, the ship was able to be unloaded from the rocks as a result of 12 hours of work. Then, the ship was towed to safe region between the south of Fener Island and the west of Celebi Island, and it was anchored here for conducting an investigation. Two officials from the Marine Accidents Investigation Commission, established under the Undersecretariat for Maritime Affairs, came in and started work to ensure both damage detection and safe return of the ship to our territorial waters.

A commercial ship hit the rocky place, the fuel oil leaking into the sea as it landed spread over a large area. A team of 80 people, including divers, and municipal teams started to work against extreme pollution, on the sea and on the shore, respectively. However, it is

estimated that nearly 130 tonnes of fuel oil leaked as a result of the accident. Nearly 40 tonnes of oil has spread rapidly due to storms and sea currents. The main motivation here is to develop a method based on SAR data so that the oil slick can be monitored with high accuracy both temporally and spatially to prevent hazardous environmental disaster.

METHODOLOGY

Sentinel-1 is a team suite consisting of two conjugate satellites with C band SAR imaging which is a successor to ESA's ERS and ENVISAT satellites.³³ ENVISAT was launched in 2002 with 10 instruments aboard and at eight tons is the largest civilian Earth observation mission. Two Sentinel-1 satellites in the same orbit help to increase the imaging frequency as the temporal resolution is reported to be 12 days.

Table 1. Technical specifications of Sentinel-1A

Imaging type	Center Frequency	Resolution Range x Azimuth (m)	Reflection Angle	Frame Size (km)
StripMap	λ :18 cm, FRQ:5.405 GHz	5 x 5	20-45	80
Interferometric WS		5x 20	>25	240
Extra WS		25 x 40	>20	400
Interferometric WS		25 x 80	-	240
Wave (WM)		20 x 5 / 20 x 20	23/36.5	20 x 20

The pulse of the electromagnetic energy is transmitted by the antenna with the horizontal or vertical. The Sentinel-1A is a dual polarization SAR system. The polarization is possible in 4 different combinations for sending and receiving radiation as follows:

- HH-horizontal sending / horizontal receiving,
- VV-vertical sending / vertical receiving,
- HV-horizontal sending / vertical receiving,
- VH- vertical sending / horizontal receiving

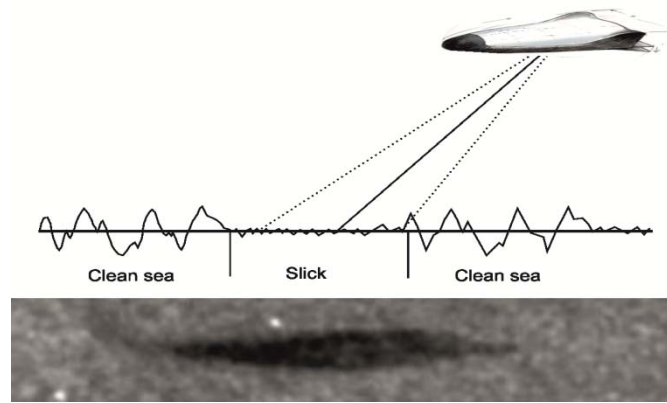


Figure 2. Dampening effect of oil spill

MATERIAL AND ANALYSIS

Sentinel-1A data were used from the monitoring of the oil spill after the sea vessel incident on Dec 18, 2017 in Ildır Bay, Izmir, Turkey. The data acquired by Sentinel-1A can be used for the surveillance of the marine environment such as ship detection and oil spill monitoring in case of an emergency situations. The Sentinel-1A data were acquired at Ground Range Detected (GRD) processing level and in the Interferometric Wide (IW) swath with dual polarization VV+VH mode.

Table 2. The list of Sentinel-1A data

Date (Month, Day, Year)	Time	Product type	Mode	Polarization
12.14.2016	16:06:48.901	GRD	IW	VV+VH
12.19.2016	16:15:17.886	GRD	IW	VV+VH
12.20.2016	04:14:51.333	GRD	IW	VV+VH
12.25.2016	04:23:16.849	GRD	IW	VV+VH
12.26.2016	16:06:48.562	GRD	IW	VV+VH
12.31.2016	16:15:17.476	GRD	IW	VV+VH
01.01.2017	04:14:49.902	GRD	IW	VV+VH
01.07.2017	16:06:47.026	GRD	IW	VV+VH
01.12.2017	16:15:15.981	GRD	IW	VV+VH
01.13.2017	04:14:49.417	GRD	IW	VV+VH
01.19.2017	16:06:46.547	GRD	IW	VV+VH
01.24.2017	16:15:15.713	GRD	IW	VV+VH
01.25.2017	04:14:49.167	GRD	IW	VV+VH
01.30.2017	04:23:14.689	GRD	IW	VV+VH

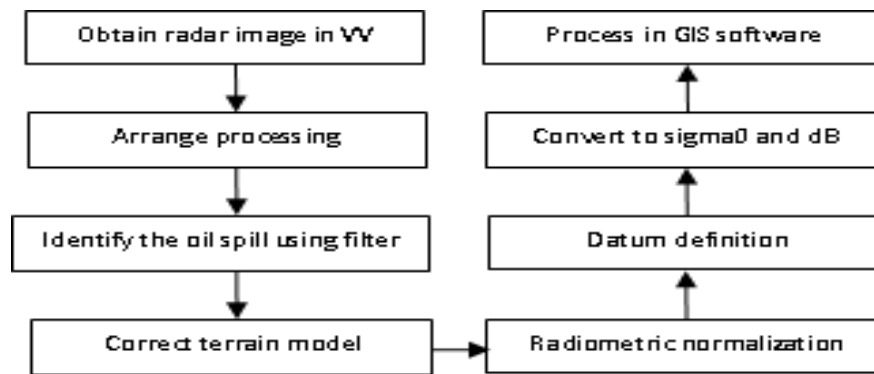


Figure 3. The work flow used in the study

RESULTS

Oil spill is one of the environmental hazard that have a damaging effect on the coastal environment. Coastal data should be analyzed to determine the extent of oil spill along coastal waters and likely spread directions will be affected. For this purpose, the Sentinel-1A IW GRD products were chosen for the period before and after the ship incident. Five interesting cases have been chosen for monitoring the following stages of oil spill around the Ildir Bay where the ship's accident occurred and the immediate vicinity:

Case 1. Clean sea data before the accident.

Case 2. The ship incident and oil spread on 12.18.2016.

Case 3. Barriers preventing faster spread of oil shredded due to bad weather conditions on 12.22.2016.

Case 4. Removal of the ship from the rocks and cleaning work on 12.27.2016.

Case 5. The ship left Ildir Bay on 01.21.2017.

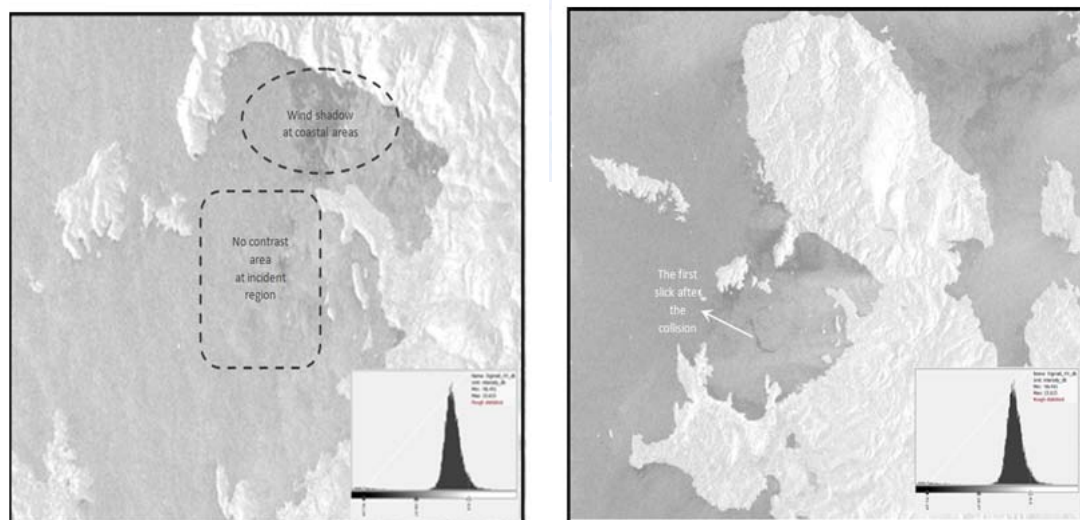


Figure 4. The 2nd result from the data acquired on 12.20.2016 between Case 2 and Case 3 and the 3rd result from the data acquired on 12.25.2016 between Case 3 and Case 4

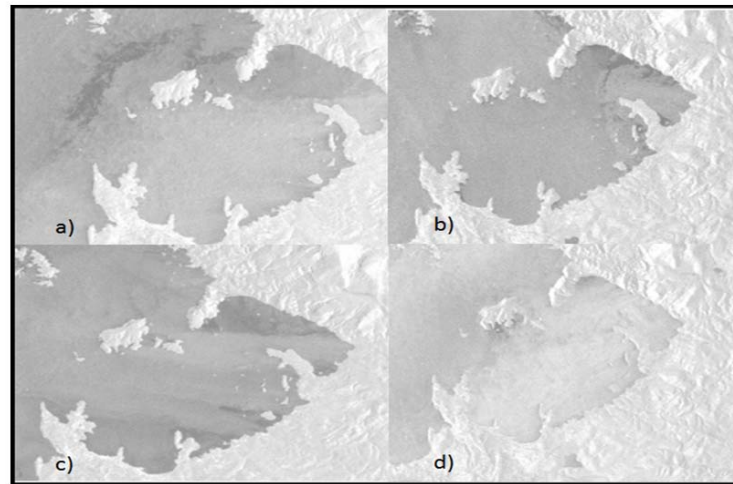


Figure 5. The results from the data acquired on: a) 01.01.2017, b) 01.07.2017, c) 01.13.2017, and d) 01.19.2017

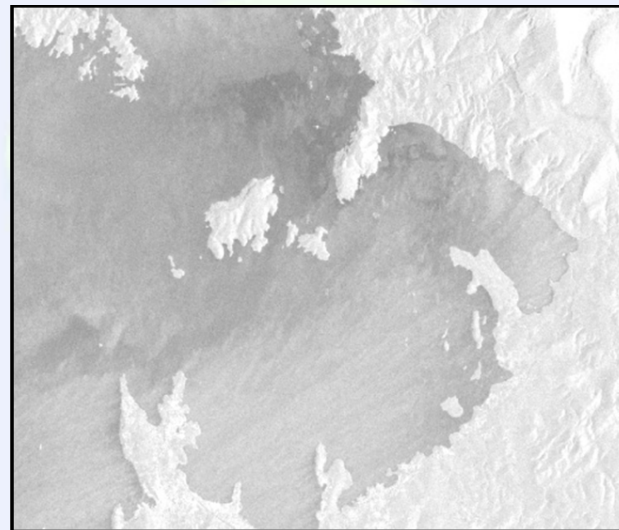


Figure 6. The result from the data acquired on 01.25.2017

CONCLUSION

Satellite-based remote sensing is an effective tool for emergency situations where it is not possible to perform fast and effective on-site measurements. There are different satellite missions to monitor the Earth. One of this mission is Sentinel 1 SAR platform that can be used to detect oil spill monitoring. Monitoring of the direction and magnitude of spilled oils, on the surface of the sea, especially due to accidents involving marine vessels, is very important in terms of ecosystem and environmental effects. In this study, SAR satellite images were used to determine the efficiency of oil spill detection. It is an effective tool for emergency situations. SAR satellite images were used to determine the efficiency of oil spill detection. The oil spill area can be identified by using Sentinel 1A data using VV polarized images. Different scenarios, such as weather events and marine waves, should be taken into account in the analysis for monitoring oil spills.

ACKNOWLEDGMENTS

This study was supported by Cukurova University, Scientific Research Projects Coordination Unit [grant number FBA-2017-8601].

REFERENCE

- Caruso, M.J., Migliaccio, M., Hargrove, J.T., Garcia-Pineda, O. and Graber, H.C., 2013. Oil spills and slicks imaged by synthetic aperture radar. *Oceanography* 26(2):112–123
- Del Frate F., Salvatori L., 2004. Oil spill detection by means of neural networks algorithms. A sensitivity analysis. Geoscience and Remote Sensing Symposium, 2004. IGARSS '04. Proceedings. IEEE International. pp. 1370-1373.
- Fiscella B., Giancaspro A., Nirchio F., Pavese P., Trivero P., 2000. Oil spill detection using marine SAR images, *International Journal of Remote Sensing* 21: 18, 3561-3566.
- Gade, M., Byfield, V., Ermakov, S., Lavrova, O., Mitnik, L., 2013. Slicks as Indicators for Marine Processes, *Oceanography* 26(2), 138-149.
- Hovland H., Johannessen J., Digranes G., 1994. Slick detection in SAR images. Nansen Environmental and Remote Sensing Center.
- Hua B., Xiaofeng W., Fulong M., 2010. Cascade SVM based OilDetection in SAR images. IEEE.
- Jackson C., Apel J., 2004. NOAA Synthetic Aperture Radar Marine User's Manual. U.S. Department of Commerce.
- Migliaccio, M., Nunziata, F., and Buono, A., 2015. SAR polarimetry for sea oil slick observation. *International Journal of Remote Sensing* 36:12,3243-3273.
- Lawal, A.D., Radice, G., Ceriotti, M., Makarfi, A.U., 2016. Investigating SAR Algorithm for Spaceborne Interferometric Oil Spill Detection. *International Journal of Engineering and Technical Research (IJETR)*, Vol.4 issue 3, pp. 2454-4698.
- Alpers W., Melsheimer C., 2004. Rainfall. Synthetic Aperture Radar Marine User's Manual. Cap.17. NOAA.
- Noriega L., 2005. Multilayer Perceptron Tutorial. School of Computing. Staffordshire University.
- Topouzelis K., Stathakis D., Karathanassi V., 2009. Investigation of genetic algorithms contribution to feature selection for oil spill detection. *International Journal of Remote Sensing* 30, pp. 611-625.

SPONSORS



ÇANAKKALE ONSEKİZ MART ÜNİVERSİTESİ



T. C. ÇANAKKALE VALİLİĞİ



ÇANAKKALE BELEDİYESİ



KEPEZ BELEDİYESİ



GEOTEKNİK GEODEZİ ALETLERİ LTD. ŞTİ.



KALE HOLDİNG A.Ş.